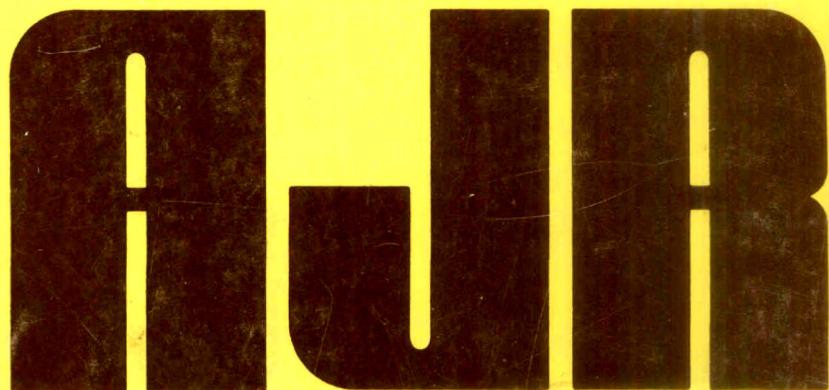


~~6~~ Doc 16 8/93

Cuk-HO3508-34-P024168



34



American
Journal of
Roentgenology



May 1991



PICTURE PERFECT

IF YOUR MAMMOGRAPHY EQUIPMENT ISN'T
THE "PICTURE" OF EFFICIENCY,

YOUR PRODUCTIVITY AND PERFORMANCE WILL BE OUT OF FOCUS!

For over 40 years, specially-dedicated S & S x-ray equipment and accessories have been improving Radiologists' efficiency and productivity. Specially-dedicated mammography equipment includes:

MOBILE MOTORIZED VIEWERS

Hold Mammography radiographs for random access recall and viewing within 7 seconds! Individual on-off light switches control divided viewing areas.

MODELS:

MV810-170: 10 viewing areas for 170 8x10" films

MV 1824-272: 16 viewing areas for 272 18x24cm films
MV2430-204: 12 viewing areas for 204 24x30cm films

S & S MAMMOGRAPHY ILLUMINATORS:

The standard for illumination excellence. Surface or recessed mounting is available for 1 to 6 banks—1 over 1 up to 6 over 6. Individual on-off light controls for each viewing section reduce glare and prevent spill-over. Single or two tier models for straight or angulated viewing include:

MODELS:
147000: Series for 8x10/
18x24cm films
146000: Series for 24x30cm
films

MAMMOGRAPH-SIZED VERTIFILE:

Doubles capacity over conventional drawer files. Adjustable partitions. Available with or without sliding door closures.

MODELS:

871: 1 shelf (2 doors)
14x30x13½"
873: 3 shelves (6 doors)
14x30x37¾"
876: 6 shelves (12 doors) 14x30x74½"

ADD-ON MOVING GRID BUCKY SYSTEM:

Converts existing non-Bucky mammography equipment. Improves contrast and micro-calcification visibility. Eliminates grid lines. Reduces scattered radiation.

MODELS:

MB-12: for 18x24cm film
MB-24: for 24x30cm film

See your local x-ray dealer or call S & S directly for Picture Perfect mammography equipment and our expanded line of radiological equipment and accessories.

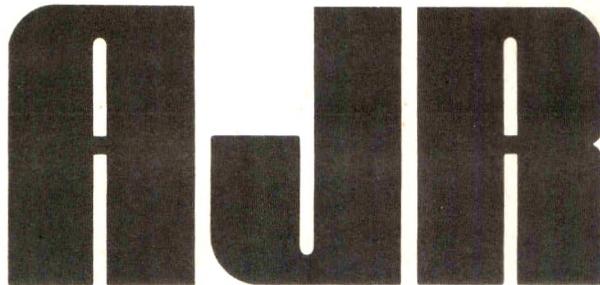


S & S X-RAY PRODUCTS, INC.

1101 Linwood Street, Brooklyn, NY 11208

TOLL FREE: 800/347-XRAY ■ NY STATE: 718/649-8500 ■ FAX: 718/257-0219

Acc 16 8
93



American Journal of Roentgenology
Diagnostic Imaging and Related Sciences

Editor-In-Chief Robert N. Berk, *La Jolla, California*
University of California, San Diego
School of Medicine and Medical Center

Editor Emeritus Melvin M. Figley, *Seattle, Washington*

P 24468

Associate Editor Saskia von Waldenburg Hilton, *San Diego, California*

Consulting Editor Michael S. Huckman, *Chicago, Illinois*

Statistician Charles C. Berry, *San Diego, California*

Editorial Board

John R. Arberg
Ithamar Aviad
Mark E. Baker
Lawrence W. Bassett
Michael A. Bettmann
Felix S. Chew
N. Reed Dunnick
David K. Edwards
Ronald G. Evens
David S. Feigin
Sandra K. Fernbach
Richard H. Gold
William R. Hendee

John R. Hesselink
Charles B. Higgins
Melvyn T. Korobkin
Faye C. Laing
Thomas L. Lawson
Robert G. Levitt
Bruce L. McClellan
Richard P. Moser
Albert A. Moss
Jeffrey H. Newhouse
Donald L. Resnick
Stewart R. Reuter
Charles A. Rohrmann, Jr.

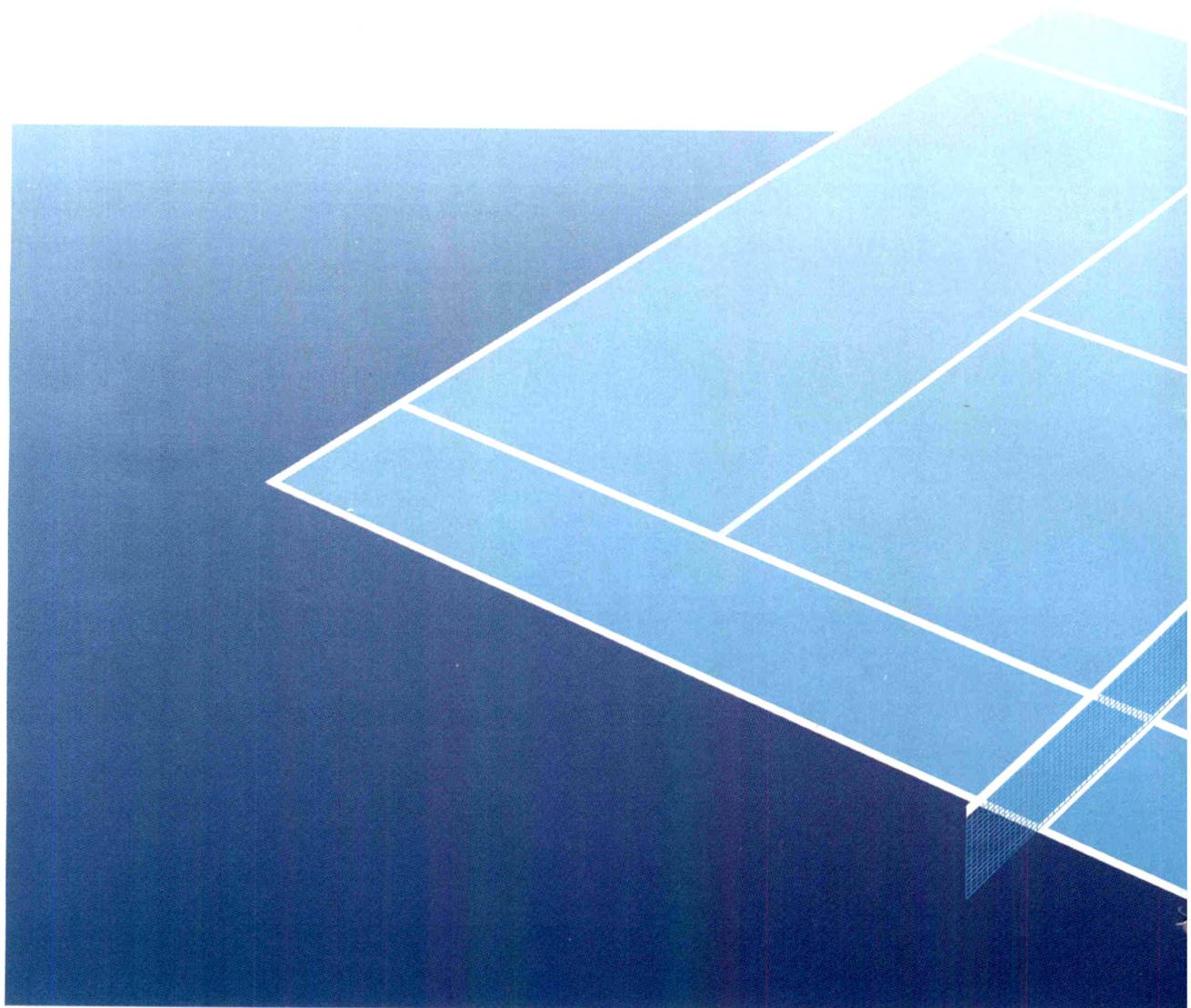
Peter M. Ronai
Sjef H. J. Ruijs
Stuart S. Sagel
David J. Sartoris
Stefan C. Schatzki
William P. Shuman
Edward A. Sickles
Barry A. Siegel
David D. Stark
Edward T. Stewart
Murali Sundaram
Eric vanSonnenberg
Robert K. Zeman

Editorial Staff: Margaret Levene, *managing editor*; Katie L. Spiller, Barbara Rose, Barbara L. Halliburton, and Janine Anderson, *manuscript editors*; Nancy Rydbeck, *office manager*; Sheri Smith, *administrative assistant*; Linda J. Waggoner, *administrative secretary*.

AJR, AMERICAN JOURNAL OF ROENTGENOLOGY (ISSN 0361 803X) is the official journal of the American Roentgen Ray Society and is published monthly by Williams & Wilkins, 428 E. Preston St., Baltimore, MD 21202. Annual dues include \$50 for journal subscription. Second-class postage paid at Baltimore, MD, and at additional mailing offices. Postmaster, send address changes (Form 3579) to AJR, 428 E. Preston St., Baltimore, MD 21202. Subscription rates \$125 (\$180 foreign); institutions \$135 (\$190 foreign); in training \$25 (\$80 foreign); single copy \$18 (\$22 foreign). Airmail rates furnished on request. Indexed by Current Contents and Index Medicus. Copyright © 1991 by American Roentgen Ray Society.



SIEMENS



Matchpoint!
1 Tesla impact in
450 square feet

AJR Guidelines for Authors

Address new and revised manuscripts, correspondence, and classified ads to the Editor:

AJR Editorial Office
2223 Avenida de la Playa, Suite 103
La Jolla, CA 92037-3218
Telephone: (619) 459-2229; FAX: (619) 459-8814

Inquiries regarding subscriptions, display advertising, reprints, or permission to republish AJR material should be addressed to the publisher:

The Williams & Wilkins Co.
428 E. Preston St.
Baltimore, MD 21202 Telephone: 1-800-638-6423

The AJR publishes original contributions to the advancement of medical diagnosis and treatment. Submitted manuscripts should not contain previously published material and should not be under consideration for publication elsewhere. Papers dealing with neuroradiology should be addressed to: American Journal of Neuroradiology, Dept. of Diagnostic Radiology, 1653 W. Congress Pkwy., Chicago, IL 60612. At the discretion of the AJR Editor, AJNR articles that are of interest to the general reader may be republished in the AJR. Neuroradiologic papers sent to the AJR will be forwarded to the Editorial Office of the AJNR.

Manuscript decisions are based on peer review. Reviewers receive manuscripts without title pages to ensure an unbiased review. Statements made in the article, including changes made by the Editor or manuscript editor, are the responsibility of the author and not of the AJR or its publisher. Authors will be sent the edited manuscript, galley proof, and proofs of illustrations. If the corresponding author will be unavailable to review galleys, arrangements should be made for a coauthor or colleague to read and return the proof.

The following guidelines are based on instructions set forth in the **Uniform Requirements for Manuscripts Submitted to Biomedical Journals** (*Ann Intern Med* 1988;108:258-265). Articles will be edited, however, to conform to the individual style of AJR.

General Guidelines for Major Papers

Abstract. Clearly state (in 200 words or less) the purpose, methods, results, and conclusions of the study. Include actual data.

Introduction. Briefly describe the purpose of the investigation and explain why it is important.

Methods. Describe the research plan, the materials (or subjects), and the methods used, in that order. Explain in detail how disease was confirmed and how subjectivity in observations was controlled.

Results. Present results in a clear, logical sequence. If tables are used, do not duplicate tabular data in text, but do describe important trends and points.

Discussion. Describe the limitations of the research plan, materials (or subjects), and methods, considering both the

purpose and the outcome of the study. When results differ from those of previous investigators, explain the discrepancy.

AUTHOR'S CHECKLIST

For priority handling, complete the following checklist, sign the copyright form on the reverse side of this page, and include both with the manuscript.

Two copies of the manuscript (the original and a photocopy) and two complete sets of figures are submitted. One copy has been retained by the author.

If appropriate, AJR Guidelines for case reports, technical notes, pictorial essays, or letters to the Editor have been followed. (See page A17.)

The manuscript, including references, figure legends, and tables, is typed double-spaced on 8½ × 11 in. (21.6 × 27.9 cm) nonerasable paper. Right-hand margins are not justified.

All manuscript pages are numbered consecutively beginning with the abstract. Authors' names do not appear on the manuscript pages.

The manuscript is organized as follows: title page, blind title page (title only), abstract, introduction, methods, results, discussion, acknowledgments, references, tables, figure legends, and figures.

Informed consent has been obtained from patients who participated in clinical investigations. If experiments were performed on animals, authors complied with NIH guidelines for use of laboratory animals.

Use of unfamiliar acronyms and abbreviations is kept to a minimum. When abbreviations are used they are defined at first mention, followed by the abbreviation in parentheses.

Metric measurements are used throughout, or the metric equivalent is given in parentheses.

Names and locations (city and state only) of manufacturers are given for equipment and nongeneric drugs.

Title Page

The following information is given: title of article; names and complete addresses (including zip code) of all authors; current addresses of authors who have moved since study; acknowledgment of grant or other assistance. The corresponding author is clearly identified, and a current address, phone number, and FAX number are given.

A blind title page is included in each copy of the manuscript, giving only the title (without the authors' names) for use in the review process.

Abstract

An abstract of approximately 200 words concisely states the purpose, methods, and results of the study in one paragraph. Actual data are included. Conclusions are stated in a second, summary paragraph.

No abbreviations or reference citations are used.

References

_____ References (not to exceed 35) are typed double-spaced starting on a separate page and are numbered consecutively in the order in which they appear in the text.

_____ All references are cited in the text and are enclosed in brackets and typed on line with the text (not superscript).

_____ Unpublished data are not cited in the reference list, but are cited parenthetically in the text, for example, (Smith DJ, personal communication), (Smith DJ, unpublished data). This includes papers submitted, but not yet accepted, for publication.

_____ Papers presented at a meeting are not cited in the reference list, but are cited parenthetically in the text (e.g., Smith DJ et al., presented at the annual meeting of the American Roentgen Ray Society, May 1990). After first mention, use (Smith DJ et al., ARRS meeting, May 1990).

_____ Inclusive page numbers (e.g., 333–335) are given for all references.

_____ Journal names are abbreviated according to *Index Medicus*.

_____ Style and punctuation of references follow the format illustrated in the following examples (all authors are listed when six or fewer; when seven or more authors, the first three are listed, followed by "et al."):

Journal article

1. Long RS, Roe EW, Wu EU, et al. Membrane oxygenation: radiographic appearance. *AJR* 1986;146:1257–1260

Book

2. Smith LW, Cohen AR. *Pathology of tumors*, 6th ed. Baltimore: Williams & Wilkins, 1977:100–109

Chapter in a book

3. Breon AJ. Serum monitors of bone metastasis. In: Clark SA, ed. *Bone metastases*. Baltimore: Williams & Wilkins, 1983:165–180

Tables

_____ Each table is typed double-spaced on a separate page without vertical or horizontal rules; each has a short, descriptive title. Tables do not exceed two pages in length and contain at least four lines of data.

_____ Tables are numbered in the order in which they are cited in the text.

_____ Abbreviations are defined in an explanatory note below each table.

_____ Tables are self-explanatory and do not duplicate data given in the text or figures.

_____ All arithmetic (percentages, totals, differences) has been double checked for accuracy, and tabular data agree with data given in the text.

Figures and Legends

_____ Two complete sets of original figures are submitted unmounted in labeled envelopes.

_____ Figures are clean, unscratched, 5 × 7 in. (13 × 18 cm) glossy prints with white borders. A separate print is submitted for each figure part.

_____ All figure parts relating to one patient have the same figure number.

_____ Each figure is labeled on the back with the figure number and an arrow indicating "top." For black-and-white figures, labeling is done on a gummed label, which is then affixed to the back of the print. Never use labels on color figures, but write figure number on the back lightly in pencil. Never use ink on front or back of any figures.

_____ Author's names are not written on the backs of figures.

_____ Only removable (rub-on) arrows and letters are used on the figures. Symbols are uniform in size and style and are not broken or cracked.

_____ Images are uniform in size and magnification.

_____ Line drawings are done in black ink on a white background. They are professional in quality, and all use the same size type. (Only glossy prints are acceptable.)

_____ Written permission has been obtained for use of all previously published illustrations (and copies of permission letters are included), and an appropriate credit line is given in the legends.

_____ Legends are typed double-spaced, and figure numbers correspond with the order in which the figures are cited in the text.

Transfer of Copyright Agreement, Conflict of Interest Acknowledgment, Certification of Coauthors, and Exclusive Publication Statement

Complete copyright to the article entitled: _____

is hereby transferred to the American Roentgen Ray Society (for United States government employees to the extent transferable), effective if and when the article is accepted for publication in the *American Journal of Roentgenology*. In the case of the authors who are officers or employees of the United States government, the American Roentgen Ray Society recognizes that works prepared by officers or employees of the United States government as part of their official government duties are in the public domain.

Authors reserve all proprietary rights other than copyright, such as patent rights and the right to use all or part of this article in future works of their own. The authors retain the right of replication, subject only to crediting the original source of publication and receiving written permission from the publisher.

Authors guarantee that this manuscript contains no matter that is libelous or otherwise unlawful, invades individual privacy, or infringes any proprietary rights.

Authors understand that they will receive no royalty or other compensation from the American Roentgen Ray Society or the publisher.

Authors guarantee that the editor has been or will be informed of any proprietary or commercial interest or conflicts of interest the authors may have that relate directly or indirectly to the subject of this article.

All authors certify that they have made substantive and specific intellectual contributions to the article and assume public responsibility for its content.

Finally, the authors certify that none of the material in this manuscript has been published previously or is currently under consideration for publication elsewhere.

First author/date

Second author

Third author

Fourth author

Fifth author

Sixth author

This agreement must be signed by all authors in order for the manuscript to be published.

Case Reports

A case report is a brief description of a special case that provides a message that transcends the individual patient.

Format. There is no abstract. The introduction should be a short paragraph giving the general background and the specific interest of the case. No more than one case should be described in detail (similar ones can be mentioned briefly in the discussion). Emphasis should be on the radiologic aspects; clinical information must be limited to that necessary to provide a background for the radiology. The discussion should be succinct and should focus on the specific message and relevance of radiologic methods. A review of the literature is not appropriate.

Length. Maximum of five double-spaced, typewritten pages, including the references but not the title page or figure legends.

References. Maximum of eight.

Figures. Maximum of four, unless the text is shortened accordingly. Legends must not repeat the text.

Tables and Acknowledgments. Not appropriate in case reports.

Technical Notes

A technical note is a brief description of a specific technique or procedure, modification of a technique, or equipment of interest to radiologists.

Format. No abstract, headings, or subheadings are required. If headings are used, they should be a combination of "Case Report," "Materials and Methods," "Results," and "Discussion." A brief one-paragraph introduction should be included to give the general background. Discussion should be limited to the specific message, including the uses of the technique or equipment. Literature reviews and lengthy case reports are not appropriate.

Length. Maximum of five double-spaced, typewritten pages, including the references but not the title page or figure legends.

References. Maximum of eight.

Figures. Maximum of two, unless the text is shortened accordingly.

Tables and Acknowledgments. Not appropriate in technical notes.

Pictorial Essays

A pictorial essay is an article that conveys its message through illustrations and their legends. Unlike other AJR articles, which are based on original research, pictorial essays serve primarily as teaching tools, like exhibits at a scientific meeting. They are not encyclopedic book chapters. The abstract should be a short, introductory paragraph.

Length. Maximum of four double-spaced, typewritten pages, including the references but not the title page or figure legends.

References. Maximum of four.

Figures. Maximum of 30 figure parts. Number should be as few as necessary to convey the message of the paper.

Tables and Acknowledgments. Not appropriate in pictorial essays.

Letters to the Editor and Replies

Letters to the Editor and Replies should offer objective and constructive criticism of published articles. Letters may also discuss matters of general interest to radiologists. Do not end a letter with a hand-written signature.

Format. All letters should be typed double-spaced on nonletterhead paper, with no greeting or salutation. Name and affiliation should appear at the end of the letter. Titles for letters should be short and pertinent. The title for a reply is simply "Reply."

Length. Maximum of two double-spaced, typewritten pages, including references.

References. Maximum of four.

Figures. Maximum of two.

Tables and Acknowledgments. Not appropriate in Letters to the Editor and Replies.

Opinions, Commentaries, and Perspectives

Opinions, commentaries, and perspectives are special articles dealing with controversial topics or issues of special concern to radiologists.

Format. Include a title page but no abstract. Headings may be used to break up the text.

Length. Maximum of five double-spaced, typewritten pages.

References. Maximum of five.

Tables and Figures. Maximum of four.

Computer Page Articles

Articles published on the computer page deal with practical computer applications to radiology.

Format. Include a title page and an abstract.

Length. Maximum of eight double-spaced, typewritten pages.

References. Maximum of five.

Figures and Tables. Maximum of five. Computer printouts are not acceptable. Figures must be submitted as 5 × 7 in. glossy prints.



MR vascular image demonstrating an arteriovenous malformation

MR

Get the most complete picture.

Now you can easily perform comprehensive, routine vascular imaging studies with MR.

GE's new multi-sequence vascular package (MVP) makes it possible.

Paired with our standard shielded gradients (which virtually eliminate gradient-induced artifacts), this package offers the most complete range of MR vascular acquisition methods available—including:

- **2D phase contrast.** For directional and velocity information, without contrast injections.
Excellent for head, carotids, portal and hepatic veins.
- **3D phase contrast.** Providing high-resolution imaging of slow flow in tortuous vessels and intracranial arteries.
- **3D time-of-flight.** For a faster exam, well-suited for capturing the Circle of Willis, arterial/venous malformations, and other small volumes of fast flow.
- **2D time-of-flight.** Offering venous or arterial selection—for quick evaluation of occlusions and slow flow in the carotids, as well as venous evaluation in the legs and pelvis.
- **And 2D phase contrast with cine acquisition.**
Allowing assessment of alterations in hemodynamic conditions during the cardiac cycle with the Cine Plus option.

For more information on GE's MR multi-sequence vascular package (MVP), call 1-800-433-5566.



2D phase contrast



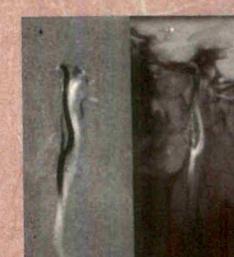
3D phase contrast



3D time-of-flight



2D time-of-flight



2D phase contrast with cine



GE Medical Systems

AJR Business and Subscriber Information

The American Roentgen Ray Society

AJR, American Journal of Roentgenology, is published monthly to disseminate research on current developments in the radiologic sciences and commentary on topics related to radiology. It is published by the American Roentgen Ray Society, 1891 Preston White Dr., Reston, VA 22091; (703) 648-8992. Inquiries regarding society business, the annual ARRS meeting, and membership should be addressed to the Society at the above address.

Correspondence Concerning the AJR

Correspondence regarding display (not classified) advertising, subscriptions, address changes, reprints, and permission requests should be addressed to Williams & Wilkins, 428 E. Preston St., Baltimore, MD 21202; (301) 528-4000.

Correspondence regarding editorial matters and classified advertising should be addressed to Editorial Office, AJR, 2223 Avenida de la Playa, Ste. 103, La Jolla, CA 92037-3218; telephone (619) 459-2229; FAX (619) 459-8814. For information on manuscript submission, see Guidelines for Authors, pages A3-A5.

Subscriber Information

Subscription requests and inquiries should be sent to Williams & Wilkins, 428 E. Preston St., Baltimore, MD 21202. ARRS annual dues include \$50 for journal subscription. Subscription rates are as follows: nonmembers, \$125/year (\$180 foreign); institutions, \$135 (\$190 foreign); nonmember in-training, \$25 (\$80 foreign). Single copies of the Journal may

be purchased for \$18 (\$22 foreign). Airmail rates will be furnished on request.

Call toll-free, 1-800-638-6423 (in Maryland call 1-800-638-4007), with subscription questions or problems. Please have the mailing label from your latest issue available when you call.

If a subscriber receives a damaged copy of the *AJR* or fails to receive an issue, the subscriber should notify Williams & Wilkins (428 E. Preston St., Baltimore, MD 21202) within 60 days of publication (90 days for foreign subscribers) and that issue will be replaced.

Change of address information should be sent to Williams & Wilkins, 428 E. Preston St., Baltimore, MD 21202. Allow 90 days for address changes.

Copyrights, Permissions, and Reprints

The American Roentgen Ray Society holds the copyright for all material published in the *AJR*. No part of this publication may be reproduced without permission from the ARRS. Requests for such permission should be addressed to Williams & Wilkins, 428 E. Preston St., Baltimore, MD 21202.

For reprints of a particular article, please contact the author designated in the footnotes for that article.

Indexes

The *AJR* provides volume and yearly indexes (subject and author) in the June and December issues each year. *AJR* articles are also indexed in *Current Contents*, *Index Medicus*, and the cumulative index published by *Radiology*.

Anaphylaxis Associated with Latex Allergy During Barium Enema Examinations

Dennis R. Ownby¹
 Michael Tomlanovich²
 Nancy Sammons²
 Judith McCullough¹

During the interval from January 1989 to March 1990, signs and symptoms of anaphylaxis developed in six patients during barium enema examinations in our institution. In all six cases the symptoms of anaphylaxis began during the procedure, usually within 10 min of starting the examination. The principal manifestation of anaphylaxis was severe hypotension, usually accompanied by edema and urticaria. The symptoms were considered potentially life threatening in all patients, and one patient died despite prompt recognition of the anaphylactic nature of the reaction and resuscitative efforts. Serum samples were obtained within a few hours of the reaction in two patients and at autopsy in the fatal case: all three samples showed elevated concentrations of mast cell tryptase, demonstrating the systemic release of anaphylactic mediators. In vitro tests demonstrated the presence of immunoglobulin E antibodies specific for latex allergens in five of the six cases. Further in vitro inhibition tests confirmed the specificity of the antibodies for latex allergens and demonstrated that similar allergens were found in both raw latex, latex gloves, and catheter balloons. Only one patient was willing to undergo a skin test, and her skin test was positive for extracts of latex products.

After considering multiple possibilities, we conclude that the reactions associated with barium enemas observed in these six patients are most probably the result of latex allergy.

AJR 156:903-908, May 1991

Barium enema examinations are normally considered to be very safe diagnostic procedures with rare fatalities resulting from rectal or vaginal perforations [1]. Previous reports have estimated that allergic reactions during barium enemas occur at a rate of less than two per one million examinations [2]. In January 1989, a patient at our institution died during a barium enema examination with symptoms typical of anaphylaxis: generalized itching, urticaria, wheezing, and cardiorespiratory arrest [3]. Between January 1989 and March 1990, we evaluated five additional anaphylactic reactions during barium enemas. Multiple possible causes were considered for the reactions, including allergy to a component of the barium suspension, allergy to a contaminant of the barium suspension, vasovagal reactions, and allergiclike reactions due to the nonimmunologic release of inflammatory mediators.

Evaluation of these cases indicates that the reactions were most likely allergic and that latex was the allergen most likely to have provoked the anaphylactic reactions. In all cases, the rectal catheter used included a latex balloon designed to aid barium retention, and reactions in two patients began before any barium was administered. The results of our studies were furnished to Food and Drug Administration investigators and to those companies requesting the information before the recall of some rectal catheters.

Case Reports

Patient 1 has previously been reported [3]. She was a 49-year-old woman who had no

Received December 7, 1990; accepted after revision January 7, 1991.

¹ Division of Allergy, Department of Medicine, Henry Ford Hospital, 2799 W. Grand Blvd., Detroit, MI 48202. Address reprint requests to D. Ownby.

² Division of Risk Prevention, Department of Quality Assessment, Henry Ford Hospital, 2799 W. Grand Blvd., Detroit, MI 48202.

0361-803X/91/1565-0903
 © American Roentgen Ray Society



history of previous barium studies. During a routine physical examination, occult blood was found on stool examination and a barium enema was ordered. The patient was allergic with current atopic dermatitis, asthma, and allergic rhinitis. Her asthma had been well controlled, and she had no history of adverse reactions to rubber products. She was not taking any beta-blocking medications.

A single-contrast colonic examination was started with Sol-o-pake (E-Z-EM, Inc., Westbury, NY) administered via a Cath Cuff (Multi-Med Industries Inc., Southfield, MI). The catheter was positioned and the balloon inflated without difficulty. A few minutes after barium infusion was started, the patient complained of feeling warm and itchy. She also complained of tightness in her chest. The examination was stopped while the patient used her albuterol inhaler. The generalized pruritus and erythema intensified and the dyspnea increased, prompting a call for immediate emergency department assistance. When the emergency department physician arrived, the patient was still conscious but gasping for breath. While resuscitation was started with IV fluids and epinephrine, the patient became unconscious and suffered cardiac arrest. Resuscitation efforts with intubation, IV epinephrine, and cardiopulmonary resuscitation were unsuccessful.

Autopsy findings were consistent with anaphylaxis as the cause of death including severe mucous plugging of the bronchi, pulmonary edema, and emphysema. No evidence was found of other cardiac or pulmonary disease. Examination of the colon disclosed no abnormality and no tears or perforations. A blood sample also was obtained during the autopsy.

Patient 2 was a 32-year-old woman with recurrent abdominal pain. She had no history of adverse reactions to rubber but did have active atopic dermatitis. She had previously had an upper gastrointestinal examination without difficulty. An air-contrast examination was started with Liquid Polibar (E-Z-EM, Inc.) and a prepackaged infusion set (Super XL, E-Z-EM, Inc.). After administration of approximately 500 ml of suspension, the patient began to complain of itching and burning of the eyes. Facial urticaria, periorbital edema, and hypotension were noted. She was successfully resuscitated with intramuscular aqueous epinephrine and IV diphenhydramine. She was admitted to the hospital for observation. A blood sample was obtained 1 month later.

Patient 3 was a 25-year-old woman with a recent exacerbation of her previously diagnosed Crohn disease. Because of the exacerbation, she had been taking oral prednisone 35 mg per day for the preceding month. Previous barium enema examinations had been well tolerated. She, too, had active atopic dermatitis. A few minutes after placement of the rectal catheter (Super XL), but before any barium was administered, the patient began to complain of nausea. The examination was halted. Diaphoresis and facial flushing developed, followed by generalized pruritus and facial swelling. Blood pressure was initially only weakly palpable but after subcutaneous epinephrine, the blood pressure improved to 80/50 mm Hg. The blood pressure later stabilized at 112/75 mm Hg. Within the first hour after the onset of the reaction, the patient had required 0.8 mg of subcutaneously administered epinephrine, 100 mg of IV diphenhydramine, and 125 mg of IV methylprednisolone. The patient was admitted to the hospital for observation. A blood sample was obtained approximately 3 hr after the event.

Patient 4 was a 78-year-old woman with multiple medical problems including recurrent abdominal pain. A previous barium enema had been uneventful. She gave a history of adverse reactions to multiple medications, but none of these had been specifically documented. She had had previous, uneventful, abdominal surgery. During the examination she complained that her face suddenly became numb, and massive facial edema, including swelling of the tongue, was noted. Treatment was instituted with intramuscular diphenhydramine and IV methylprednisolone. The glossal swelling resolved in several

days. The patient had received approximately 500 ml of Polibar Plus (E-Z-EM, Inc.) before the onset of the reaction, but no air had been instilled. A blood sample was obtained several months later when skin testing was performed.

Patient 5 was a 42-year-old woman with chronic abdominal pain and a history of asthma and allergic rhinitis. Because of a history of recurrent abdominal pain, the patient underwent an air-contrast colonic examination with Polibar and a Super XL infusion set. During the examination periorbital edema developed and the patient felt nauseated, but it was possible to complete the examination. Vital signs remained stable and the edema resolved 30–40 min after she was given 50 mg of oral diphenhydramine. No colonic abnormalities were identified. A blood sample was obtained several weeks later.

Patient 6 was a 62-year-old woman with a history of recurrent pain in the right lower quadrant. She also gave a history of allergy to common inhalant allergens. Less than a minute after insertion of the enema tip (Super XL) and inflation of the balloon, the patient became nauseated and vomited. A few minutes later the patient felt better, and the barium infusion was started using Liquid Polibar Plus. Within 2–4 min the patient complained of generalized pruritus and became poorly responsive. Blood pressure was palpated at 60/0 mm Hg. She responded to resuscitation efforts including IV dopamine, methylprednisolone, diphenhydramine, and subcutaneous epinephrine. Oxygen by mask and IV fluids also were given. A blood sample was obtained approximately 3 hr after the event.

During follow-up interviews, no specific risks could be identified for these patients. None had a history of adverse reactions during radiologic procedures. Only patient 4 had prior surgery, and she was the only patient with a history of adverse reactions to drugs. None of the patients were health care workers or employed in industrial settings with latex contact. Five of the six patients, however, had common forms of allergic disease, including three patients with active atopic dermatitis. All of the patients with atopic dermatitis indicated that they sometimes used rubber gloves to protect their hands during housework.

Materials and Methods

Controls

Sera from four nonatopic adults, a pool of sera from donors having negative in vitro tests for allergen-specific immunoglobulin E (IgE) to common allergens, and serum from a patient with an IgE myeloma having a total IgE concentration of 96,000 µg/l served as controls for the in vitro testing. Additional controls included 20 sera known to contain detectable quantities of IgE specific for common inhalant allergens. Three women, one nonatopic and two atopic, served as control subjects for the skin testing.

Materials

Ammoniated latex concentrate (raw latex) was obtained from Killian Latex (Akron, OH). Latex products included surgical gloves (Triflex, Travenol Laboratories, Deerfield, IL) and balloons from rectal catheters designed for barium administration (Cath Cuff). The catheter balloons used were from the same lot as the one used in the examination of patient 1. A commercial vegetable gum product (sodium carrageenan), a component common to all of the diagnostic barium products associated with our patients' reactions, was obtained from the manufacturer (E-Z-EM, Inc.). A commercial short ragweed extract (Hollister-Stier Laboratories, Downers Grove, IL) served as a control in inhibition experiments.

Extract Preparation

Extracts of the latex products were made by cutting the latex into approximately 0.5-cm-wide strips and then extracting the strips overnight in phosphate-buffered saline at a ratio of 1 g of latex to 5 ml of saline, resulting in 1:5 weight to volume (w:v) extracts. The ammoniated latex concentrate was centrifuged. The clear supernatant was dialyzed against phosphate-buffered saline and considered undiluted. One gram of the vegetable gum preparation was dissolved in 150 ml of phosphate-buffered saline and considered undiluted. All extracts were filtered through 0.22- μ m filters.

Skin Tests

Extracts of the latex concentrate and the surgical glove were diluted in saline containing phenol (0.4%) for skin testing. The skin of the patient and three female control subjects were tested by the prick and then by the intradermal routes. Results were read 15 min after injection. A positive control of histamine phosphate (Lilly, Indianapolis, IN) was used at 1 mg/ml for prick tests and 0.1 mg/ml for intradermal tests.

Tryptase Assays

Assays of human mast cell tryptase were performed by using a previously described assay [4, 5]. Values of less than 5 ng/ml are normal, values between 5 and 10 ng/ml are indeterminate, and values greater than 10 ng/ml are indicative of systemic release of mast cell mediators.

IgE Measurements

Total serum concentrations of IgE were measured by an enzyme-linked immunosorbent assay (ELISA) as previously reported [6].

Radioallergosorbent tests (RAST) for latex-specific IgE were performed by using disks coated with latex (*Hevea brasiliensis*, Pharmacia Diagnostics, Piscataway, NJ). Fifty microliters of the patient's serum was diluted into 500 μ l of buffer and mixed with each disk overnight at room temperature. After washing, radiolabeled anti-human IgE (Pharmacia Diagnostics) was added to each disk. Results are reported as the percentage of the mean counts bound by duplicate patient samples to the mean counts bound by the negative control pool. As previously reported, values of greater than 300% are considered positive for allergen-specific IgE [7].

ELISAs, similar to previously reported ELISAs, were developed to detect IgE specific for latex or for the vegetable gum [6]. Briefly, microtiter strips (Microstrips PS, ICN Flow, Costa Mesa, CA) were coated with extracts of the latex products at 1:100 w:v dilutions or a 1:50 dilution of the vegetable gum mixture overnight at room temperature. The strips were then blocked with 5% fetal calf serum in phosphate-buffered saline. After six washes, 50- μ l aliquots of the serum samples were added to triplicate well sets. After overnight incubation followed by six washings, biotinated, affinity-purified goat antihuman IgE (Kirkegaard-Perry Labs, Gaithersburg, MD) was added to each well. The quantity of antihuman IgE bound was quantified by the sequential addition, with interspersed washings, of an avidin-alkaline phosphatase conjugate (Sigma Chemical, St. Louis, MO) and the enzyme substrate. The resulting density was measured in a microtiter plate reader (Titertek Multiscan, ICN Flow). Results are expressed as the ratio of the mean absorbance of triplicate patient wells to the mean of control wells containing the negative serum pool. Values greater than the mean plus two standard deviations above the mean of the negative pool were considered positive (>140%).

Inhibition Studies

The antigenic specificity and relevance of the IgE measured in the RAST and ELISAs were evaluated by using inhibition studies. Detection of allergen-specific IgE antibodies is based on the ability of the antibodies to bind to an allergen chemically attached to a solid support (solid-phase allergen). If a serum containing IgE antibodies specific for an allergen is mixed with an aqueous solution of the same allergen, some of the specific antibodies will bind to the allergen in the fluid phase. If this treated serum is then assayed for the quantity of allergen-specific IgE, less antibody will become bound to the solid-phase allergen, because some of the specific antibodies have already bound to the fluid-phase allergen. The degree of decreased binding to the solid phase can be expressed as an inhibition percentage. Assuming that the serum dilution is kept constant, there will be a consistent relationship between increasing amounts of the allergen incubated with the serum and the percentage of inhibition observed. For this study, aliquots of patients' serum were incubated with experimentally determined dilutions of the latex product extracts before measuring the quantity of latex-specific IgE in the serum. Short ragweed extract was used as a control for nonspecific inhibition. The percentage of inhibition in the RAST was calculated as the mean counts per minute (cpm) observed for the serum without the inhibitor minus the mean cpm with the inhibitor divided by the cpm without the inhibitor times 100. Inhibition in the ELISA was calculated in a similar fashion except that optical density units rather than cpm were used. Greater than 25% inhibition was considered significant [8].

Results

The results of the patients' studies are shown in Table 1. The RAST values presented are the mean values from two separate assays. Values were positive in the first three patients and negative in the last three, whereas the ELISA results were positive in patients 1, 2, 4, and 5. The highest RAST value was from the fatal case, and the highest ELISA value was found in patient 4. Control samples from nonatopic persons were consistently negative in both the RAST and ELISA, and the 20 sera containing IgE to other allergens were all negative in the latex ELISA. The IgE myeloma sample also was negative in the ELISA. Total serum IgE concentrations were above the normal range in four of the six patients.

None of the patients' sera produced positive reactions in the ELISA for vegetable gum-specific IgE. All of the control sera also were negative in the vegetable gum ELISA.

Patient 4 was the only patient willing to undergo a skin test. Intradermal skin tests were positive with 1:2000 w:v extracts with both the latex concentrate and the surgical glove. The wheal diameters were 15 mm and 16 mm, with flare diameters of 50 mm and 46 mm for the latex concentrate and the surgical glove, respectively. There was no reactivity to the negative control. The patient's arm remained edematous and pruritic for 8 days after the testing. None of the three control subjects showed any reactivity to 1:200 w:v concentrations of the same latex extracts.

Tryptase measurements were clearly positive in patients 3 and 6, the only two patients in whom blood samples were obtained within a few hours of the reactions. The value of 8.1 ng/ml in the sample obtained at autopsy from patient 1 is in the indeterminate range.

TABLE 1: Summary of Six Patients with Anaphylaxis During Barium Enemas

Patient Number	Reaction ^a	Age (yr)	RAST ^b (%)	ELISA ^c (%)	Total IgE ^d ($\mu\text{g/l}$)	Tryptase ^e (ng/ml)
1	Death	49	4800 3610	340	6480	8.1
2	U, E, HT	32	520 500	148	816	ND
3	N, F, HT	25	610 690	112	552	18.8
4	E	78	180 140	1740	110	ND
5	E	42	140 130	337	110	ND
6	N, V, HT	62	170 120	96	372	29.3

^a Symptoms during the reactions: U = urticaria, E = edema, HT = hypotension, N = nausea, F = flushing, V = vomiting.

^b Radioallergosorbent test (RAST) results as a percentage of the negative control, >300% is positive, values from two separate assays.

^c Enzyme-linked immunosorbent assay (ELISA) results as a percentage of negative control, >140% is positive.

^d Reference interval 12–240 $\mu\text{g/l}$, divide values by 2.4 to yield IU/ml.

^e Reference concentrations: normal, <5 ng/ml; indeterminate, 5–10 ng/ml; positive, >10 ng/ml. ND = not done.

Table 2 and Figure 1 present the results of inhibition experiments designed to test the specificity of the *in vitro* assays. In experiment 1, the serum of patient 1 was used in the RAST assay with extracts of the surgical glove. Three increasing dilutions of the glove extract produced decreasing levels of inhibition. The latex concentrate also inhibited to a similar degree. In experiment 2, extracts of the catheter balloon produced inhibition similar to that observed in the first experiment. The ragweed extract produced insignificant inhibition. The figure illustrates the results of three separate ELISA inhibition experiments with the serum from patient 4. The experiments were performed with strips coated with an extract of the catheter balloon. Increasing quantities of the balloon extract produced progressively more inhibition in a clear dose-responsive fashion in three separate experiments, for experiment 3 ($r = .996$). The ragweed extract did not produce significant inhibition in these experiments.

Discussion

The clinical signs of the reactions observed in these patients were consistent with those of anaphylaxis and not with those

of vasovagal reactions. The fact that the reactions were observed during several months at different practice sites, with different support staff, and with different staff radiologists made a single procedural problem unlikely. Similarly, the reactions had occurred with different barium products, and with different lots of each product, making it unlikely that the reactions were due to a single contaminant in one lot of product. The water supplies at each site also were checked for contamination and none was found.

Previous reports of allergic reactions during barium enemas have focused on possible sensitivity to components of the barium suspension such as methyl paraben, or on drugs administered as part of the examination, such as glucagon [2, 9–13]. The possibility of the allergen coming from the apparatus used to administer the barium is just beginning to be realized [14].

Barium suspensions commonly contain barium sulfate, si-

TABLE 2: Results of Inhibition Studies with Radioallergosorbent Test (RAST)

Experiment Number	Inhibitor	Dilution (w/v)	Percentage Inhibition
1	Surgical glove	1:5	60.9
	Surgical glove	1:50	52.0
	Surgical glove	1:500	12.0
	Latex concentrate	1:100	64.5
2	Catheter balloon	1:20	60.4
	Catheter balloon	1:200	58.7
	Ragweed	1:100	6.4

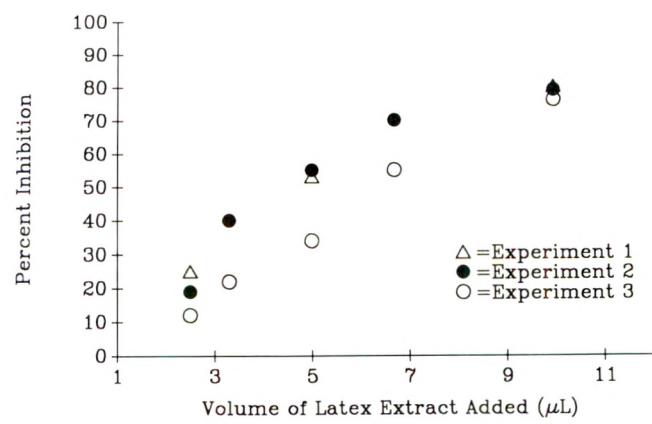


Fig. 1.—Dose-dependent inhibition of immunoglobulin E binding to latex is shown by increasing quantities of latex extract in enzyme-linked immunosorbent assay with serum of patient 4.

methicone, surface-active agents, vegetable gums, pectin, sorbitol, and preservatives. Preparations designed for both upper and lower gastrointestinal tract examinations also contain natural and artificial flavorings and sweeteners. Barium sulfate and simethicone are chemically and immunologically inert. The surface-active agents, sorbitol, and pectin are also relatively immunologically inert. Allergic reactions to vegetable gums have been reported [15], but skin testing of reactive patients with barium preparations has failed to produce positive responses [9, 11]. Patient 1 had also undergone skin testing with three individual vegetable gums found in barium preparations approximately 2 years before the fatal barium enema, and she showed no evidence of sensitivity at that time. Our inability to detect IgE binding to the vegetable gum preparation common to all of the barium preparations used in these six patients also suggests that vegetable gums were not the causative allergen. Methylparaben has also been reported as a sensitizing agent [16]; however, according to the manufacturer, none of the barium preparations used in our patients contained methylparaben.

Several reports have raised the possibility that glucagon may be the cause of some reactions because glucagon is commonly administered IV before barium enema studies [2, 13, 17]. Glucagon was not administered in any of our six cases, nor were any other drugs administered as part of the examinations. We could not find any reports of proved allergy to glucagon.

In contrast to the limited information on other potential allergens, latex allergy has been well documented as a cause of systemic allergic reactions [18–24]. Reports of latex-induced anaphylaxis have included a variety of medical care settings such as donning surgical gloves, contact between surgical gloves and patients' tissues, vaginal examinations, and rectal manometry [18–23]. The use of rubber gloves for hand protection and contraceptive devices such as condoms and diaphragms are other potential settings of latex contact. At least one case of a systemic allergic reaction caused by contact with a condom has been reported [23].

The observation that patient 3 had a moderately severe reaction after insertion of the rectal catheter and inflation of the balloon, but before the instillation of any barium, suggests that the apparatus was the source of the allergen and not the barium suspension. Patient 6 also developed initial symptoms after catheter insertion and before barium administration. In some patients, balloon cuffs were inflated immediately after positioning the catheter, which may have increased the patient's exposure to latex.

Further evidence for the allergic nature of the reactions is the elevated serum concentration of mast cell tryptase found in three of the patients [5]. Although the tryptase concentration in patient 1 is not in the clearly positive range, the lower value could be the result of rapid circulatory collapse (Schwartz L, personal communication). These elevated tryptase concentrations confirm that release of mast cell mediators occurred during the reactions.

On a practical basis, it is impossible to exclude totally the possibility that some of the observed reactions resulted from allergens other than latex or from nonallergic mechanisms.

The combination of detectable latex-specific IgE in five of six patients and the elevation of serum tryptase concentrations in all of the patients for whom serum samples were obtained shortly after the onset of the reactions strongly suggest that the reactions were IgE-mediated anaphylaxis and that latex was the causative allergen. Consistent with other reports of latex allergy, our patients were likely to have histories of atopic disease (especially atopic dermatitis), frequently had elevated concentrations of serum IgE, and five of the six had positive in vitro tests for latex-specific IgE antibody [18–24]. The RAST used in this study has been successfully used in previous studies to detect latex-specific IgE [19, 21, 23, 24]. In this study, both the RAST and ELISA appeared to detect IgE specific for allergens from latex products. The specificity of each assay was confirmed by the inhibition produced by latex and not by unrelated (ragweed) extracts. Furthermore, sera with IgE to other common allergens were negative in the latex ELISA. Nonspecific binding was not observed with the IgE myeloma serum. The RAST and ELISA tests for latex-specific IgE antibodies did not produce totally concordant results, suggesting that they may be detecting antibodies of slightly different specificities. However, the fact that the same latex catheter balloon extract produced similar inhibition in each assay is evidence of substantial allergen cross-reactivity. Latex allergy does not explain all reactions to diagnostic barium sulfate, because at least one allergiclike reaction to ingested barium has been reported [25].

The potential risks of medical products to latex-sensitive persons should lead to several preventive efforts. Patients with histories suggestive of rubber allergy should be evaluated before procedures involving substantial contact with latex, and efforts should be made to limit the latex contact of sensitive individuals. Manufacturers of latex products also should be encouraged to attempt to reduce the allergenicity of their products. Finally, the possibility of allergic origin should be considered when instituting therapy for adverse reactions occurring when patients are undergoing procedures involving latex contact.

ACKNOWLEDGMENTS

The authors thank the members of the Department of Radiology, Henry Ford Hospital, for their cooperation with these studies.

REFERENCES

- Rimarenko S, Finkel L, Taff ML, et al. Fatal complications related to diagnostic barium enema. *Am J Forensic Med Pathol* 1988;9:78–84
- Gelfand DW, Sowers JC, DePont KA, Summer TE, Ott DJ. Anaphylactic and allergic reactions during double contrast studies: is glucagon or barium suspension the allergen? *AJR* 1985;144:405–406
- Feczko PJ, Simms SM, Bakirci N. Fatal hypersensitivity reaction during a barium enema. *AJR* 1989;153:275–276
- Wenzel S, Irani AM, Sanders JM, Bradford TR, Schwartz LB. Immunoassay of tryptase from human mast cell. *J Immunol Methods* 1986;86:139–142
- Alter SC, Schwartz LB. Tryptase: an indicator of mast cell-mediated allergic reactions. In: Spector SL, ed. *Provocative challenge procedures: background and methodology*. Mount Kisco, NY: Futura Publishing, 1989: 167–183
- Rowe MS, Bailey J, Ownby DR. Evaluation of the cause of nasal and ocular symptoms associated with lawn mowing. *J Allergy Clin Immunol*

Review Article

Colorectal Cancer: Cross-sectional Imaging for Staging of Primary Tumor and Detection of Local Recurrence

Ruedi F. Thoeni¹

This review describes the use of cross-sectional imaging in the staging of colorectal carcinoma and detection of local recurrence. The contributions of CT, MR imaging, and sonography are discussed and illustrated. Colorectal carcinoma is the second most common tumor in the United States and the most common cancer in the gastrointestinal tract. The prognosis for patients with this neoplasm is closely related to the extent of tumor at the time of diagnosis. Accurate noninvasive preoperative assessment of tumor stage by one or a combination of radiologic techniques would enable appropriate treatment to be planned in each case. Also, determination of possible tumor recurrence would permit effective monitoring of success of therapy and surgical intervention for recurrent disease before widespread metastasis occurs.

Nearly two decades have passed since CT was introduced as a cross-sectional imaging technique. Since then, CT has been used to detect and stage many tumors, including primary and recurrent colorectal neoplasms, and has been joined by MR imaging, transrectal sonography, monoclonal antibody imaging, and positron emission tomography. Although many reports have been published on the subject of imaging colorectal tumors by using modern technology, very few studies invoke an in-depth assessment of the value of the various imaging techniques. A review of the large body of literature reveals many conflicting reports on the effectiveness of the various methods. This has resulted largely from early, overly enthusiastic conclusions claiming high success rates for each new imaging technique.

It is difficult to compare investigations on CT and MR imaging, whether performed alone or in combination, for

detection of primary and recurrent disease, mainly because of the great variations in the types of scanners used, the scanning methods, and the methods of administering contrast agents. Even the diagnostic criteria, the study populations, and the analyses of the data vary greatly.

Nevertheless, the importance of an in-depth analysis of the effectiveness of these new technologies for evaluating patients with colorectal cancer is emphasized by the fact that colorectal neoplasm is the second most common tumor in the United States and the most common cancer in the gastrointestinal tract. Each year, 155,000 new cases are seen [1], and in a large percentage of these cases colonic and hepatic surgery is performed each year for palliation or possible cure. Widely published data indicate the importance of screening for colorectal cancer after the age of 40 [2] and improved survival rates for patients in whom colorectal cancer is detected at an early stage [3]. Prognosis for patients with this neoplasm is closely related to the extent of tumor at the time of diagnosis. The Dukes classification, a surgical-pathologic staging system for colorectal cancer, has been the most widely used classification, but many modifications have been introduced since the seminal article appeared in 1932 [4]. Today, the most commonly used classification is the Astler-Coller version [5] modified by Turnbull [6], who introduced stage D (Table 1). Under this modified version, the overall 5-year survival rate is about 50% (stage A, 81–85%; stage B, 64–78%; stage C, 27–33%; stage D, 5–14%) [2, 3, 7]. The TNM system introduced in 1954 [8] never gained the popularity of the modified Dukes classification, but in recent years, its use has increased because it more clearly defines extent

Received September 17, 1990; accepted after revision November 13, 1990.

¹Department of Radiology, University of California, San Francisco, Box 0628, 505 Parnassus Ave., San Francisco, CA 94143-0628.

TABLE 1: Surgical-Pathologic Staging (Modified Dukes Classification)

Stage	Description
A	Limited to mucosa
B1	Extension into, but not through, the muscularis propria
B2	Extension through muscularis, no nodes
C1	Limited to bowel wall, positive nodes
C2	Extension through bowel wall, positive nodes
D	Distant metastases

Note.—This staging system represents the Astler-Coller version [5] of the Dukes classification [4], as modified by Turnbull [6].

of tumor within and beyond the bowel wall. Generally, there is a consensus that the most important prognostic factor is the presence or absence of lymph node invasion, but malignant fixation of colorectal tumor through direct invasion of adjacent tissue also appears to be an important sign. In one study, the 5-year survival rate in patients with fixed Dukes B rectal carcinoma was 44%, whereas with mobile C lesions it was 63% [9].

Accurate noninvasive preoperative assessment of tumor stage based on one or a combination of radiologic techniques allows appropriate treatment to be planned in each case. Also, precise determination of possible tumor recurrence permits effective monitoring of success of therapy and surgical intervention for recurrent disease before widespread metastases are present. Such an aggressive approach has been shown to improve survival even in patients with recurrent disease [10]. The following paragraphs analyze the effectiveness of the various imaging techniques for local extent of primary and recurrent colorectal neoplasms. They do not address the detection of distant metastases such as metastases to the liver.

Preoperative Staging of Colorectal Tumor

In many institutions, flexible sigmoidoscopy combined with a well-performed barium enema is used in place of colonoscopy alone for safe, cost-effective, complete, and accurate examination of the colon in patients with a positive occult blood test [11], and barium enema and/or colonoscopy is used in patients with suspected or known colorectal carcinomas. However, even though these methods can detect tumor with a sensitivity of over 90%, they cannot assess local, regional, and distant extent to enable staging of a neoplasm. High sensitivity and high specificity for tumor extent and nodal involvement are essential for any imaging method to provide useful information on the stage of tumor. Debate continues as to which imaging method or combination of methods should be used for the most effective preoperative staging.

CT

CT together with transrectal sonography provides better evaluation of tumor stage than manual examination, barium enema, and fiberoptic techniques do. Both CT and sonography may image a colorectal cancer as a discrete mass or focal wall thickening, but this is a nonspecific finding and

TABLE 2: CT Staging of Primary or Recurrent Colorectal Tumor [13]

Stage	Description
I	Intraluminal mass without thickening of wall
II	Thickened wall (>0.6 cm) or pelvic mass, no invasion or extension to sidewalls
IIIa	Thickened wall or pelvic mass with invasion of adjacent structures but not to pelvic sidewalls or abdominal wall
IIIb	Thickened wall or pelvic mass with extension to pelvic sidewalls and/or abdominal wall without distant metastases
IV	Distant metastases with or without local abnormality

requires further exploration. Early reports suggested CT findings of local extent and regional spread of tumor correlated well with surgical and histopathologic findings, and accuracy rates between 77% and 100% (sensitivity rates ranging from 54% to 100% and specificity rates from 93% to 100%) [12–16] were reported. A special CT staging method was introduced to correlate as much as possible with Dukes classification (Table 2) [13]. Because of the high accuracy rates, these early studies suggested CT should be used routinely as a preoperative staging procedure. Later studies showed much lower accuracy rates (41–64%), largely owing to low sensitivity for detection of lymph node metastases (22–73%) and of local tumor extent (53–77%) [17–23]. Lymph node metastases were not separately analyzed in some of the earlier studies, which tended to have more advanced stages in their series. A more recent study [22] demonstrated that staging accuracy increased from 17% for Dukes B lesions to 81% for Dukes D lesions. Insufficient spatial resolution to detect small perirectal or pericolonic tumor infiltration and a high prevalence of metastatic foci in lymph nodes smaller than 1.5 cm in diameter caused these lower detection rates.

Refinement of CT techniques, such as colonic preparation, prone positioning of the patient, and air distension of the rectum [24], have increased the accuracy of assessing local tumor extent by CT. Also, lowering the threshold for diagnosing lymph node metastases improved sensitivity for detecting lymph node metastases, but such an approach decreased specificity.

MR Imaging

At present, MR imaging appears to have overall the same limitations as CT [25–28], but multiplanar imaging may offer special advantages. An early investigation [27] showed CT and MR imaging were equally effective in staging. Particularly, local tumor extent was well shown on T1-weighted images (e.g., 600/20/2 [TR/TE/excitations]) (Fig. 1) [27, 28]. Direct invasion of tumor into bone or muscles such as the levator ani or piriformis muscle (Fig. 2) may be better shown by MR imaging [27, 29]. However, the depth of tumor infiltration in the bowel wall and the presence of metastatic foci in lymph nodes cannot be accurately determined by MR imaging. An overall staging accuracy of 74–79% was found, but only small MR imaging series have been reported [26–29]. Also, preliminary results with endorectal coils in 10 patients [30] have

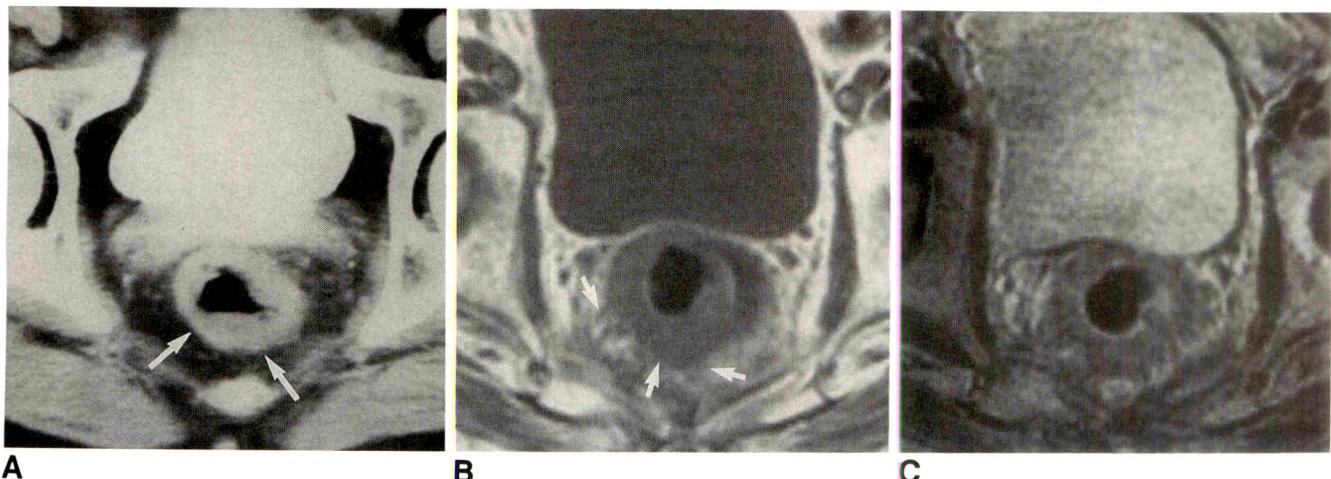


Fig. 1.—Patient with surgically proved rectal carcinoma and perirectal fat invasion, Dukes stage B2 or T3N0M0.

A, CT scan shows marked thickening of rectal wall (arrows), but no definite extension of tumor beyond bowel wall can be seen.

B, T1-weighted spin-echo MR image (600/20/2) shows marked thickening of rectal wall with perirectal infiltration of tumor into fat (arrows).

C, On T2-weighted spin-echo MR image (2000/70/2), perirectal extension of tumor is difficult to detect.

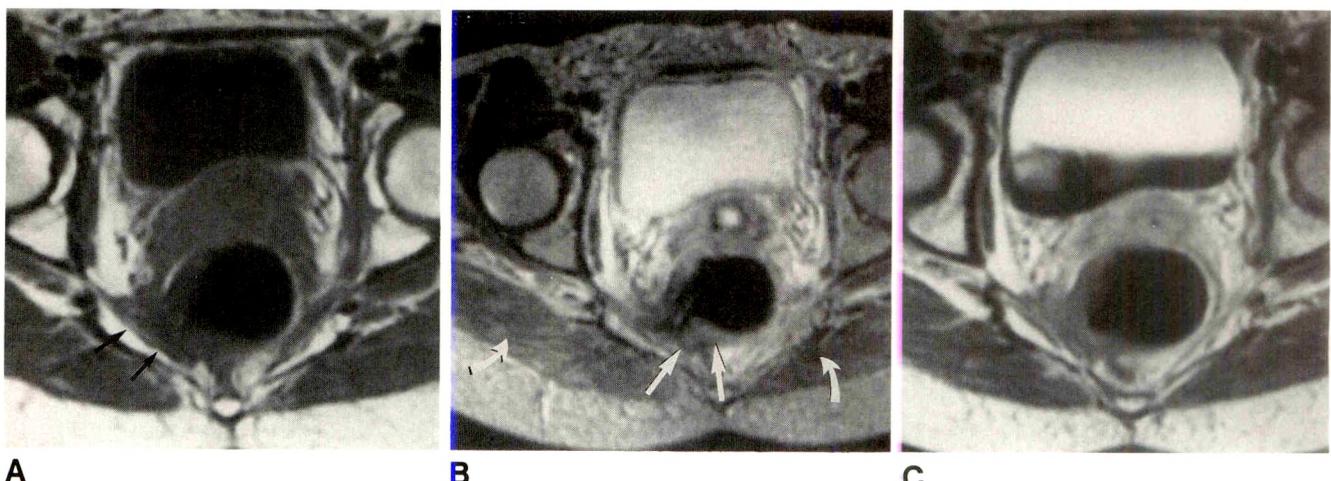


Fig. 2.—Patient with rectal carcinoma invading piriformis muscle and three perirectal nodes, Dukes stage C2 or T3N1M0, proved by surgical resection.

A, T1-weighted MR image (600/20/2) shows thickening of rectal wall on left with extension into left piriformis muscle (arrows).

B, On T2-weighted image (2500/80/2), tumor shows higher signal intensity (straight arrows) than gluteus muscle (curved arrows).

C, T1-weighted image after administration of gadopentetate dimeglumine shows enhancement of tumor in rectal wall and in extension to piriformis muscle when compared with A. Lymphadenopathy was not seen in any sequence.

shown great promise for assessment of local tumor extension, but detection of lymphadenopathy, even though superior to MR imaging with a body coil, was limited.

Sonography

Although transabdominal sonography may be used to assess the presence or absence of liver metastases, transrectal sonography is used increasingly to detect the depth of tumor infiltration and local adenopathy in patients with rectal carcinomas. Its advantage lies in its ability to distinguish the normal layers of the bowel wall and to visualize disruption of one or more of these layers by tumor. With this method, sensitivities of 67–96% have been reported for assessing perirectal

spread [17, 21, 29], but the presence of regional lymph node metastases is detected less well (sensitivity, 50–57%) [17, 31]. The broad range of sensitivities of transrectal sonography for detection of tumor extent in and through bowel wall emphasizes the operator dependence of this method. Endoscopic sonography has expanded the application of sonographic methods to the entire colon [32, 33]. Although sonography of the colon and rectum appears promising, valid and comprehensive clinical trials remain necessary.

Role of Cross-sectional Imaging for Preoperative Staging

On the basis of currently available results, routine CT staging is not recommended for primary colorectal tumors.

CT should be reserved for those patients in whom locally extensive or widespread disease is suspected. If extensive local spread of tumor is shown by CT, these patients can be treated with radiation therapy alone or can be irradiated and later undergo tumor resection, if feasible.

Although the presence or absence of lymphadenopathy is not a significant clinical problem, if a colonic resection is planned, the decision on local tumor excision by surgery or colonoscopy cannot be based on CT findings because of CT's poor sensitivity for possible adenopathy. CT may be used to guide fine-needle aspirations of suspected metastases and assess complications such as perforation with abscess formation. Transrectal sonography may be used to determine local tumor extent; however, currently it is doubtful that sonographic diagnosis can be used for management of patient [17] because up to 14% of patients with primary tumors confined to the rectal wall have regional lymph node metastases. While transrectal sonography frequently can detect regional lymph nodes and is superior to CT at this task, it cannot predict the histology of the visualized lymph nodes. MR imaging may be beneficial in determining involvement of the levator ani if coronal views and images enhanced with gadopentetate dimeglumine have been obtained. If involvement of the levator ani is demonstrated, an anterior resection is not indicated and an abdominoperineal resection is needed. It is possible that endorectal coils and contrast-enhanced MR imaging, particularly MR lymphangiography, could improve staging of colorectal tumors. Whether MR imaging may offer other advantages over CT in patients with primary colorectal cancer is uncertain, and more comprehensive studies are needed.

Imaging of Recurrent Colorectal Tumor

CT and MR imaging have been used extensively to detect the presence or absence of recurrent colorectal cancer, and a general consensus has been reached that both methods have merit inasmuch as each enables detection of recurrence at a time when carcinoembryonic antigen titers are normal and/or symptoms are absent [34, 35]. Their value is particularly great in patients who have had total abdominoperineal resection and colostomies. Colonoscopy in patients with curative resections and ileocolic or colorectal reanastomoses has been shown to be successful for detection of recurrence at the anastomoses. Follow-up studies in patients with potentially curative resection of recurrent tumor have demonstrated an average of 38 months without symptoms, compared with an average survival of 8 months in patients without resection of recurrent tumor [36-38]. Although today CT and MR imaging are accepted methods for detecting recurrent colorectal tumor, the debate on the appropriate timing of these imaging tests is ongoing and has gained importance owing to the high cost of frequent imaging in these patients.

Several investigations have shown that the stage, histology, and site of primary tumor at the time of diagnosis are most predictive of eventual relapse [38, 39]. Anastomotic recurrence occurs mostly after anterior resection and usually is related to residual tumor outside the colorectal wall that

grows into the suture site. The prevalence of endoluminal recurrence (3.3%; reported range, 0.3-15.0%) and metachronous lesions (1.3%) is low, and the prevalence of extra-luminal disease in these patients at the time of detection is relatively high (up to 50%) [40]. Therefore, routine follow-up colonoscopy, although valuable for early detection and re-resection for cure, must be considered an adjunct to follow-up history taking, physical examination, carcinoembryonic antigen levels, guaiac testing for occult blood, and cross-sectional imaging.

CT

Early studies established the usefulness of CT in determining the presence of local recurrence and metastases to lymph nodes, liver, peritoneal cavity, and retroperitoneum [41, 42]. As with results for primary tumors, very high accuracy rates were reported initially for detection of locally recurrent tumor (sensitivity, 93-95%) [43, 44], but more recent investigations indicate accuracy rates ranging from 69% to 88% [18, 19, 34, 45]. Most errors in interpretation result from the inability to detect microscopic invasion of perirectal or pericolonic fat, to assess the presence or absence of metastatic foci in normal-sized lymph nodes (even if a diameter of 1 cm or less was used for normal), and to visualize local tumor at the anastomotic site.

In patients who had undergone abdominoperineal resection, some studies suggested that streaky densities or a clean operative bed suggest fibrosis, whereas the presence of a mostly globular mass favors the diagnosis of tumor recurrence [46]. However, several other studies indicated that one can expect to see a mass of soft-tissue density in the early postoperative period due to granulation tissue, hemorrhage, edema, and/or fibrosis [42, 47-49]. Also, postirradiation changes can produce the appearance of streaky densities or a presacral mass [2, 20]. Serial CT scans obtained within 28 months of surgery established that persistence of a mass for up to at least 24 months after abdominoperineal resection may be normal [2]. Performing a baseline CT study 2-4 months after surgery frequently demonstrates the presence of a mass. A study at 4-9 months often reveals decrease in size and better definition of margins. In the absence of symptoms and raised carcinoembryonic antigen titers, such a change in a mass should not result in concern for local tumor recurrence. However, any enlargement of a mass, with or without invasion of adjacent structures and with or without appearance of lymphadenopathy or perineal soft-tissue density, should be considered suggestive of recurrence and percutaneous biopsy is indicated [19, 48, 49].

MR Imaging

It is possible to detect and stage presacral masses with MR imaging. Initial reports suggested that fibrosis after surgery with or without irradiation had a low signal intensity on both T1- and T2-weighted sequences (Fig. 3), whereas tumor recurrence had a higher signal intensity on T2-weighted images (Fig. 4) [50-55]. It was concluded that MR imaging was superior to CT at distinguishing between fibrosis and recur-

Fig. 3.—Patient with total abdominoperineal resection for rectal carcinoma 2 years before and with absence of tumor recurrence proved by biopsy and follow-up.

A, T1-weighted MR image shows an area of very low signal intensity (arrows) in presacral space.

B, On T2-weighted image, presacral mass (arrows) remains of low signal intensity, suggesting presence of scar tissue.

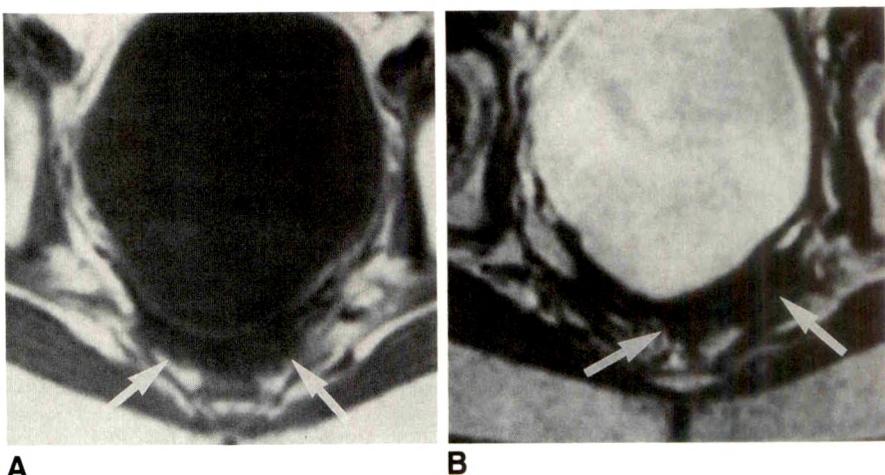
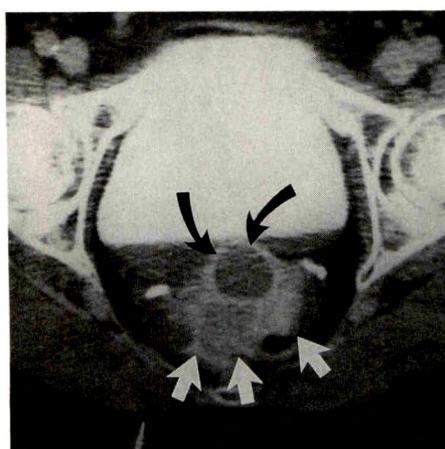
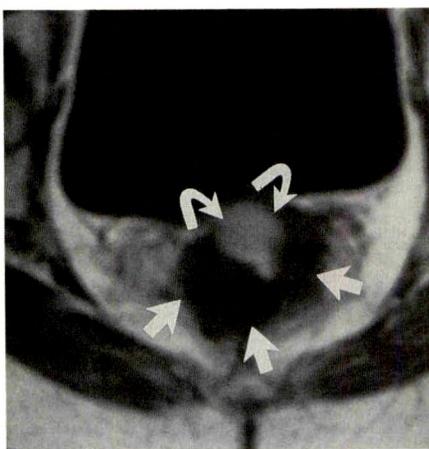
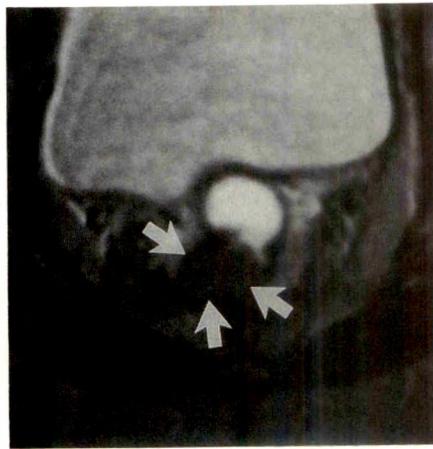
**A****B****A****B****C**

Fig. 4.—Patient with biopsy-proven recurrent rectal carcinoma after total abdominoperineal resection.

A, CT shows a mass (straight arrows) representing recurrent rectal tumor and a cystic-appearing area (curved arrows) representing obstructed cervix filled with fluid and blood.

B, T1-weighted spin-echo MR image (700/20/2) shows a mass of signal intensity (straight arrows) similar to that of muscle. Area of high signal intensity (curved arrows) adjacent to it represents fluid in cervix.

C, T2-weighted spin-echo MR image (2500/70/2) shows mass (arrows) to be of higher signal intensity than muscle but not as high as could be expected from tumor. Recurrent tumor with desmoplastic reaction (see text) was suspected and confirmed by CT-guided biopsy.

rent tumor, and the hope was raised that MR imaging could eliminate the need for percutaneous biopsies. However, more recent studies have demonstrated that it is very doubtful whether MR imaging can distinguish among recurrent tumor, fibrosis, and inflammation [27, 56, 57].

One study, using long TR/long TE (T2-weighted) sequences, examined the value of MR imaging in distinguishing among early fibrosis (1–6 months after first treatment), tumor or late fibrosis (more than 12 months), and recurrent tumor [56]. On T2-weighted images, tumor recurrence is diagnosed on the basis of high signal intensity, whereas scar or fibrosis has low signal intensity. The authors found that early fibrosis after treatment had higher signal-intensity values than late fibrosis, probably owing to increased vascularity, edema, and the presence of immature mesenchymal cells in granulation tissue. Radiation-induced necrosis and postsurgical inflammatory reaction also can contribute to an increase in signal

intensity on T2-weighted images. The increase in tissue fluids seen in granulation tissue and necrosis caused by radiation renders distinction between early fibrosis and tumor recurrence difficult or even impossible. However, late fibrosis and tumor recurrence could be clearly distinguished from one another [56]. Other studies found similar results [51, 55, 57], but a more recent study showed that the accuracy of MR imaging in differentiating between radiation damage and residual/recurrent tumor varied with the primary site. It was excellent for cervical carcinoma but suboptimal for rectal carcinoma [58]. The best investigation yet to appear on this topic was published by de Lange et al. [59], who compared MR imaging results with histologic sections from tissue obtained during radical pelvic exenteration or extensive partial resection of a mass in patients with suspected recurrent rectosigmoid carcinoma. They found that the signal intensities on T2-weighted images do not permit prediction of the his-

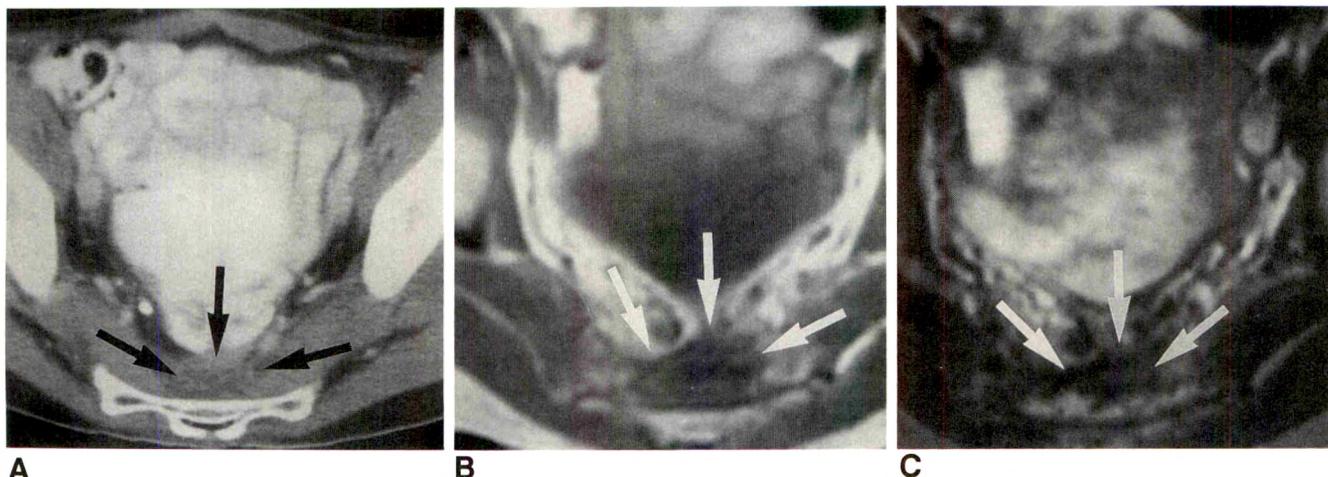


Fig. 5.—Patient with total abdominoperineal resection, 14 months after surgery and radiation therapy for Dukes stage C2 rectal carcinoma. Biopsy proved absence of tumor recurrence.
A, CT scan shows a poorly defined area (arrows) in presacral space.
B, T1-weighted MR image shows the same area (arrows) is of intermediate signal intensity.
C, T2-weighted image shows presacral region (arrows) is of intermediate signal intensity. Recurrence of tumor cannot be distinguished from fibrosis with granulation tissue.

tologic diagnosis of the lesion in question. High signal intensity was found in areas of viable tumor, tumor necrosis, benign inflammation, and edematous tissue. Because desmoplastic reaction is a common host response to many benign and malignant processes including tumors of the colon and rectum, areas of low signal intensity on T2-weighted images also were nonspecific, and the differential diagnosis included tumor-induced fibrosis and nonneoplastic, benign fibrotic tissue (Fig. 5). However, MR imaging can depict a presacral mass accurately and demonstrates its extent well. If such a mass consists mainly of desmoplastic tissue with only small strands of tumor tissue interspersed, even a percutaneous biopsy may show only fibrous tissue and no malignant cells. In these cases, a definitive diagnosis needs to be obtained by surgical removal of the mass or biopsy at laparotomy.

Role of Cross-sectional Imaging of Recurrent Colorectal Tumor

Like CT, MR imaging is a sensitive method for detecting masses after colorectal surgery, but its specificity is not improved over that of CT. Whereas CT cannot distinguish a benign from a malignant process based on attenuation coefficients and morphologic appearance in these patients, MR imaging cannot base such a distinction on signal intensity. CT also may be more helpful in evaluating anastomoses in patients with suture material and in patients with multiple clips from lymphadenectomies because susceptibility artifacts may be prominent in the high magnetic field. For overall screening to detect nonlocal recurrence, CT may be more valuable than MR imaging, but more studies are needed to determine the efficacy of these procedures and their possibly complementary natures. A multiinstitutional, multitechnique prospective study on the use and effectiveness of these imaging techniques is eagerly awaited [60].

While advances in MR imaging such as contrast-enhanced sequences, endoluminal coils, and fast imaging may improve results with this technique, newer techniques such as monoclonal antibody imaging and positron emission tomography after IV injection of ^{18}F -fluorodeoxyglucose demonstrate very promising results and may prove to hold the key to the accurate detection of tumor stage and distinction of recurrent rectal cancer from scar [61].

REFERENCES

- Silverberg E, Boring CC, Squires TS. Cancer statistics, 1990. *CA* 1990;40(1):9-26
- Kelvin FM, Maglione DT. Colorectal carcinoma: a radiologic and clinical review. *Radiology* 1987;164:1-8
- Zinkin LD. A critical review of the classifications and staging of colorectal cancer. *Dis Colon Rectum* 1983;26:37-43
- Dukes CE. The classification of cancer of the rectum. *J Pathol* 1932;35:323-332
- Astler VB, Coller FA. The prognostic significance of direct extension of carcinoma of the colon and rectum. *Ann Surg* 1954;139:846-851
- Turnbull RB Jr. The no-touch isolation technique of resection. *JAMA* 1975;231:1181-1182
- Nauta R, Stablein D, Holyoke D. Survival of patients with stage B2 colon carcinoma: the gastrointestinal tumor study group experience. *Arch Surg* 1989;124:180-182
- Denoix PF. Monograph no. 4. Paris: French Ministry of Public Health National Institute of Hygiene, 1954
- Durdey P, Williams NS. The effect of malignant and inflammatory fixation of rectal carcinoma on prognosis after rectal excision. *Br J Surg* 1984;71:787-790
- Sugabaker PH, Kemeny N. Management of metastatic cancer to the liver. *Adv Surg* 1989;22:1-56
- Barry MJ, Richter JM. Effect of work-up strategy on the cost effectiveness of fecal occult blood screening for colorectal cancer (abstr). *Gastrointest Endosc* 1984;30:141
- Dixon AK, Fry IK, Morson BC, Nichols RJ, Mason AY. Pre-operative computed tomography of carcinoma of the rectum. *Br J Radiol* 1981;54:655-659
- Thoeni RF, Moss AA, Schnyder P, Margulis AR. Detection and staging of

- primary rectal and rectosigmoid cancer by computed tomography. *Radiology* **1981**;141:135-138
14. Zaunbauer W, Haertel M, Fuchs WA. Computed tomography in carcinoma of the rectum. *Gastrointest Radiol* **1981**;6:79-84
 15. Grabbe E, Lierse W, Winkler R. The perirectal fascia: morphology and use in staging of rectal carcinoma. *Radiology* **1983**;149:241-246
 16. Van Waes PF, Koehler PR, Feldberg MA. Management of rectal carcinoma: impact of computed tomography. *AJR* **1983**;140:1137-1142
 17. Holdsworth PJ, Johnston D, Chalmers AG, et al. Endoluminal ultrasound and computed tomography in the staging of rectal cancer. *Br J Surg* **1988**;75:1019-1022
 18. Thompson WM, Halvorsen RA, Foster WL, et al. Preoperative and postoperative CT staging of rectosigmoid carcinoma. *AJR* **1986**;146:703-710
 19. Freeny PC, Marks WM, Ryan JA, et al. Colorectal carcinoma evaluation with CT: preoperative staging and detection of postoperative recurrence. *Radiology* **1986**;158:347-353
 20. Cohan RH, Silverman PM, Thompson WM, et al. Computed tomography of epithelial neoplasms of the anal canal. *AJR* **1985**;145:569-573
 21. Rifkin MD, Ehrlich SM, Marks G. Staging of rectal carcinoma: prospective comparison of endorectal US and CT. *Radiology* **1989**;170:319-322
 22. Balthazar EJ, Megibow AJ, Hulnick D, et al. Carcinoma of the colon: detection and preoperative staging by CT. *AJR* **1988**;150:301-306
 23. Adalsteinsson B, Glimelius B, Graffman S, et al. Computed tomography in staging rectal carcinoma. *Acta Radiol* **1985**;26:45-50
 24. Megibow AJ, Zerhouni EA, Hulnick DH, et al. Air insufflation of the colon as an adjunct to computed tomography of the pelvis. *J Comput Assist Tomogr* **1984**;8:797-800
 25. Hodgman CG, MacCarty RL, Wolff BG, et al. Preoperative staging of rectal carcinoma by computed tomography and 0.15T magnetic resonance imaging: preliminary report. *Dis Colon Rectum* **1986**;29:446-450
 26. Guinet C, Buy J-N, Sezuer A, et al. Preoperative assessment of the extension of rectal carcinoma: correlation of MR, surgical, and histopathologic findings. *J Comput Assist Tomogr* **1988**;12(2):209-214
 27. Butch RJ, Stark DD, Wittenberg J, et al. Staging rectal cancer by MR and CT. *AJR* **1986**;146:1155-1160
 28. De Lange EE, Gechner RE, Edge SB, Spaulding CA. Preoperative staging of rectal carcinoma with MR imaging: surgical and histopathologic correlation. *Radiology* **1990**;176:623-628
 29. Guinet C, Buy JN, Ghossain MA, et al. Comparison of magnetic resonance imaging and computed tomography in the preoperative staging of rectal cancer. *Arch Surg* **1990**;125:385-388
 30. Chan TW, Milestone B, Kressel HY, Schnall M, Daly J, Rosato E. MR imaging of rectal carcinoma using an endorectal coil (abstr). In: *Book of Abstracts. Ninth Annual Scientific Meeting and Exhibition*. Berkeley, CA: Society of Magnetic Resonance in Medicine, **1990**:305
 31. Hildebrandt U, Feifel G. Preoperative staging of rectal cancer by intrarectal ultrasound. *Dis Colon Rectum* **1985**;28:42-46
 32. Fukuda M. Endoscopic sonography. In: *Ultrasound annual*. New York: Raven, **1986**:141-170
 33. Takemoto T, Aibe T, Fuji T, et al. Endoscopic ultrasonography. *Clin Gastroenterol* **1986**;15:305-319
 34. McCarthy SM, Barnes D, Deveney K, et al. Detection of recurrent rectosigmoid carcinoma: prospective evaluation of CT and clinical factors. *AJR* **1985**;144:577-579
 35. Kelvin FM, Korobkin M, Breiman RS, et al. Recurrent rectal carcinoma in an asymptomatic patient. *J Comput Assist Tomogr* **1982**;6(1):186-188
 36. Bühler H, Seefeld U, Deyhle P, et al. Endoscopic follow-up after colorectal cancer surgery. *Cancer* **1984**;54:791-793
 37. Barkin JS, Cohen ME, Flaxman M, et al. Value of routine follow-up endoscopy program for the detection of recurrent colorectal carcinoma. *Am J Gastroenterol* **1988**;88:1355-1360
 38. Stulc JP, Petrelli NJ, Herrera L, et al. Anastomotic recurrence of adenocarcinoma of the colon. *Arch Surg* **1986**;121:1077-1080
 39. Olson RM, Perencevich P, Malcolm AW, et al. Patterns of recurrence following curative resection of adenocarcinoma of the colon and rectum. *Cancer* **1980**;45:2969-2974
 40. Barkin JS, Cohen ME, Flaxman M, et al. Value of a routine follow-up endoscopy program for the detection of recurrent colorectal carcinoma. *Am J Gastroenterol* **1988**;88:1355-1360
 41. Ellert J, Kreel L. The value of CT in malignant colonic tumors. *J Comput Assist Tomogr* **1980**;4:225-240
 42. Husband JE, Hodson NJ, Parsons CA. The use of computed tomography in recurrent rectal tumors. *Radiology* **1980**;134:677-682
 43. Moss AA, Thoeni RF, Schnyder P, Margulis AR. Value of computed tomography in the detection and staging of recurrent rectal carcinomas. *J Comput Assist Tomogr* **1981**;5:870-874
 44. Adalsteinsson B, Glimelius B, Graffman S, Hemmingsson A, Pahlman L, Rimsten A. Computed tomography of recurrent rectal carcinoma. *Acta Radiol* **1981**;22:669-672
 45. Chen YM, Ott DJ, Wolfman N. Recurrent colorectal carcinoma: evaluation with barium enema examination and CT. *Radiology* **1987**;163:307-310
 46. Lee JKT, Stanley RJ, Sagel SS, et al. CT appearance of the pelvis after abdomino-perineal resection for rectal carcinoma. *Radiology* **1981**;141:737-741
 47. Reznek RH, White FE, Young JWR, et al. The appearances on computed tomography after abdomino-perineal resection for carcinoma of the rectum: a comparison between the normal appearances and those of recurrence. *Br J Radiol* **1983**;56:237-240
 48. Kelvin FM, Korobkin M, Heaston DK, et al. The pelvis after surgery for rectal carcinoma: serial CT observations with emphasis on nonneoplastic features. *AJR* **1983**;141:959-964
 49. Adalsteinsson B, Pahlman A, Glimelius B, et al. Computed tomography in early diagnosis of local recurrence of rectal carcinoma. *Acta Radiol* **1987**;28:41-46
 50. Johnson JR, Jenkins JPR, Isherwood I, et al. Quantitative magnetic resonance imaging in rectal carcinoma. *Br J Radiol* **1987**;60:761-764
 51. Krestin GP, Steinbrich W, Friedmann G. Recurrent rectal cancer: diagnosis with MR imaging versus CT. *Radiology* **1988**;168:307-311
 52. Blum L, Kressel HY, de Roos A, et al. MR imaging differentiation of fibrosis versus recurrent colorectal carcinoma in the pelvis: quantitative assessment. *Radiology* **1988**;169(P):167
 53. Gomberg JS, Friedman AC, Radecki PD. MRI differentiation of recurrent colorectal carcinoma from postoperative fibrosis. *Gastrointest Radiol* **1986**;11:361-363
 54. Glazer HS, Lee JKT, Levitt RG, et al. Radiation fibrosis: differentiation from recurrent tumor by MR imaging (work in progress). *Radiology* **1985**;156:721-726
 55. Krestin VG, Steinbrich W, Friedmann G. Rezidivdiagnostik der Rektumkarzinome: Vergleich CT/MR. *ROFO* **1988**;148:28-33
 56. Ebner F, Kressel HY, Mintz MC, et al. Tumor recurrence versus fibrosis in the female pelvis: differentiation with MR imaging at 1.5T. *Radiology* **1988**;166:333-340
 57. Rafto SE, Amendola MA, Gefter WB. MR imaging of recurrent colorectal carcinoma versus fibrosis. *J Comput Assist Tomogr* **1988**;12(3):521-523
 58. Sugimura K, Carrington BM, Quivey JM, Hricak H. Postirradiation changes in the pelvis: assessment with MRI imaging. *Radiology* **1990**;175:805-813
 59. De Lange EE, Fechner RE, Waneko HJ. Suspected recurrent rectosigmoid carcinoma after abdominoperineal resection: MR imaging and histopathologic findings. *Radiology* **1989**;170:323-328
 60. Moss AA. Imaging of colorectal carcinoma. *Radiology* **1989**;170:308-310
 61. Schlag P, Lehner B, Strauss LG. Scar or recurrent cancer. *Arch Surg* **1989**;124:197-200

Book Review



Practical Echocardiography and Doppler. By Mark J. Monaghan. New York: Wiley & Sons, 176 pp., 1990. \$69.50

Applications of echocardiography have grown tremendously in the past years, and this technique has become a major diagnostic tool in clinical cardiology. Many comprehensive textbooks on Doppler echocardiography are available, but there is still always a need for a concise and brief text that centers on the practical applications of the technique. Monaghan, with his significant experience as an echocardiographer and his long teaching background, has helped fill this need with this condensed and practical guide. The book's high quality and concise style reveal how carefully he has worked to assemble this text.

The first chapter offers a review of the basic physics of echocardiography, including the fundamentals, stressing the basics of instrumentation and image processing. In the second chapter, the author presents comprehensive images of the most common two-dimensional image planes and practical approaches to obtain excellent M-mode and two-dimensional images. In the third chapter, related to analyzing ventricular function, the author presents most of the basic M-mode formulas used for calculating volumes and ejection fraction, but does not illustrate the use of the two-dimensional images for analyzing ventricular function, an approach recently endorsed by the American Society of Echocardiography and one that would help the novice echocardiographer who used the bidimensional mode when the M-mode cannot be used.

The rest of the book concerns specific clinical applications of echocardiography and is divided into sections on mitral valve disease, aortic valve disease, cardiomyopathies, coronary artery disease, pericardial effusion, and intracardiac masses. All the sections have

examples of the most common findings in all of these diseases. The chapter on congenital heart disease deals with only the most common forms of cardiac anomalies, with no reference to the more complex congenital heart lesions. The last chapter is about Doppler imaging, and the author explains the basic principles, normal findings, and the most abnormal patterns of disturbed flow observed in some diseases. Additionally, some common flow calculations, pressure estimation theory, and a few comments about color Doppler imaging are provided.

One of the major strengths of this book is its economy of price and space; the author packs a considerable deal of practical information into clearly written and succinct text and figures with remarkably little overlap of information among various chapters. One of the book's weaknesses is a lack of emphasis on the integration of pulsed- and continuous-wave Doppler imaging into cardiac practice and almost a total lack of inclusion of information about color Doppler imaging.

We recommend this book to beginning cardiologists and sonographers who want to begin performing and interpreting two-dimensional and Doppler echocardiography and need a quick start-up reference handy.

Paulo Golebiovski
David J. Sahn
*University of California, San Diego, Medical Center
San Diego, CA 92103*

P 24468

Factors Affecting the Development of Pneumothorax Associated with Thoracentesis

Vassilios Raptopoulos^{1,2}
 Lawrence M. Davis^{1,3}
 Grace Lee^{1,4}
 Cynthia Umali¹
 Robert Lew⁵
 Richard S. Irwin⁶

This study is a retrospective survey of the variables that may influence the development of pneumothorax after thoracentesis. In a 30-month period, a computer search of hospital records identified 342 thoracenteses, of which 154 were done with conventional techniques by the clinical services, and 188 were done with sonographic guidance. Other factors surveyed included the patients' age, sex, underlying pulmonary disease, and overall clinical condition; the size of the effusion; the type of tap (diagnostic or therapeutic); the amount and type (exudate or transudate) of fluid acquired; and the size of the needles used. The technique used was the most significant single risk factor affecting the development of pneumothorax (18% for clinical vs 3% for sonography-guided thoracenteses). The incidence of pneumothorax decreased when a smaller amount of pleural fluid was aspirated (mean, 246 ml aspirated from patients who did not vs 472 ml from those who did develop pneumothorax) and when thin needles were used (4% pneumothorax with 20-gauge or smaller and 18% with larger than 20-gauge needles). The other factors surveyed did not influence the development of pneumothorax.

Our results show that sonography-guided thoracentesis is complicated by pneumothorax significantly less often than is thoracentesis done with conventional techniques. Use of the smallest possible needle and aspiration of the smallest possible amount of fluid will also result in fewer cases of pneumothorax.

AJR 156:917-920, May 1991

Received August 27, 1990; accepted after revision November 16, 1991.

¹ Department of Radiology, University of Massachusetts Medical Center, 55 Lake Ave. N., Worcester, MA 01655.

² Present address: Department of Radiology, Beth Israel Hospital and Harvard Medical School, 330 Brookline Ave., Boston, MA 02215. Address reprint requests to V. Raptopoulos.

³ Present address: Department of Medicine, Worcester Memorial Hospital, 119 Belmont St., Worcester, MA 01605.

⁴ Present address: Department of Radiology, Johns Hopkins Hospital, 600 N. Wolfe St., Baltimore, MD 21205-2191.

⁵ Department of Pharmacology, University of Massachusetts Medical School, Worcester, MA 01655.

⁶ Division of Pulmonary Medicine and Critical Care, University of Massachusetts Medical Center, Worcester, MA 01655.

0361-803X/91/1565-0917
 © American Roentgen Ray Society

In a recent randomized, prospective study from our institution, Grogan et al. [1] showed that, compared with other methods, sonography-guided thoracenteses were associated with significantly fewer complications, including pneumothorax. That study took place under specific circumstances, limited to presumed low-risk patients who were cooperative, spontaneously breathing, and had substantial amounts of free-flowing pleural fluid. The purpose of this study was to see if Grogan's findings apply to a broader range of patients and to see if other factors favor the development of pneumothorax in patients having thoracentesis.

Materials and Methods

In this study we included all thoracenteses recorded in the computerized listings of hospital procedures and the records of the sonography section of the Department of Radiology. The search identified 342 pleural taps, of which 154 were performed by clinical physicians and 188 by radiologists. The hospital records and the radiographs and sonograms done before, during, and after the procedures were reviewed.

The variables surveyed included patients' age, sex, underlying pulmonary disease, and clinical condition; method used; size of the effusion; type of tap (diagnostic or therapeutic); amount and type (exudate or transudate) of fluid acquired; and needle size used.

The patients' ages ranged from 18 to 94 years (mean, 62 years); 187 were men and 155

were women. They had no underlying disease ($n = 103$), or they had diffuse pulmonary disease ($n = 32$), focal pulmonary disease such as pneumonia ($n = 136$), or pulmonary manifestations of cardiovascular disease such as pulmonary edema ($n = 50$). No data were available in 21 patients. The patients' clinical condition was considered critical ($n = 79$) or not critical ($n = 242$) depending on whether or not they were in an intensive care unit. No data were available on 21 patients.

One hundred fifty four conventional thoracenteses were performed by clinical physicians. In 106 cases, the pleural effusion was localized clinically, whereas in 48, the effusion was localized by sonography and the thoracentesis performed later by clinicians. Sonography-guided thoracenteses were done by radiologists with sonographic guidance in the department or at the bedside ($n = 188$). In both groups, the needle was inserted by physicians in training in over 90% of the cases.

The amount of pleural fluid was estimated by three investigators who reviewed the patients' chest radiographs without knowledge of the tapping method used or the outcome of the procedure. A consensus based on the following guidelines was recorded: Grade 1 = blunting of the costophrenic angle on the frontal view, or layering of fluid on the lateral decubitus film of less than 5 mm, measured at the midthorax; Grade 2 = obliteration of less than 1/3 of the ipsilateral diaphragm on upright chest radiograph, or layering of fluid on the lateral decubitus film of 5 mm to 1 cm; Grade 3 = obliteration of greater than 1/3 of the diaphragm, or greater than 1 cm of layering on the lateral decubitus film. Half grades were given when observers disagreed or when the particular amount was judged to fall between grades. For statistical purposes, the effusions also were divided into Small = grades 0–1.5 ($n = 216$); and Large = grades 2–3 ($n = 126$).

The amount of fluid aspirated in milliliters was recorded in 307 cases. No data were available on 35 taps. Analysis of the pleural fluid revealed a transudate in 211, an exudate in 23, and blood in 35 thoracenteses. No information was available about 73 pleural taps. The thoracenteses were characterized as diagnostic ($n = 234$) when stated as such and 100 ml or less of fluid was aspirated and as therapeutic ($n = 106$) when the intent was to aspirate as much fluid as possible for symptomatic relief or when more than 100 ml of fluid was aspirated. The needles used were classified as small (equal to or smaller than 20-gauge, used in 194 taps) and large (larger than 20-gauge, used in 134 taps).

The size of pneumothorax was estimated according to the method of Rhea et al. [2]. The pneumothoraces were then graded as follows: grade 1 = small pneumothorax, estimated to be smaller than 10% ($n = 18$); grade 2 = medium pneumothorax estimated between 10% and 30% ($n = 8$); grade 3 = large pneumothorax, estimated to be greater than 30% ($n = 6$). Grade 0 meant uncomplicated, that is, no pneumothorax ($n = 310$). Critical pneumothorax was defined as when a chest tube was inserted for treatment ($n = 14$). The number of radiographs taken until resolution or, if first, until discharge from the hospital was recorded ($n = 115$).

Data were analyzed with a commercially available software program: CSS (Complete Statistical System, StatSoft, Inc., Tulsa, OK). For multiway frequency tables, we used the Spearman R t-test to assess the relationship between variables with a level of significance set at $p \leq .05$. For confirmation, the standard Pearson χ^2 was used, and for small sample size, the Yates correction or the V² test was used [3]. Because the discriminations obtained from both tests were similar, only the Spearman R t-test results are reported. We used Student's t test and analysis of variance (ANOVA) to compare the averages of continuous variables among categories. We also used multiple linear regression analyses with dummy variates for categories of nominal variables to find regression models. In parallel, we used stepwise multiple logistic regression analysis to evaluate candidate predictors of the binary outcome, pneumothorax [4].

Results

During a 30-month period, 342 thoracenteses were performed: 154 with the clinical and 188 with the sonography-guided method. Pneumothorax occurred in 32 (9%): 27 (18%) in the clinical and five (3%) in the sonography-guided group. This difference was statistically significant ($p < .0001$) and, comparing the two methods, a sevenfold increased risk was estimated for the clinical taps. The occurrence of critical pneumothoraces (pneumothorax requiring chest tube) was significantly more frequent with the clinical than with the sonography-guided method (7% vs 2%, $p < .009$). Of the 154 clinical taps, the occurrence of pneumothorax was not different in the clinically localized and performed taps (19%), compared with the sonographically localized but clinically performed taps (15%).

Age, sex, underlying pulmonary disease, critical clinical condition, and the type of pleural fluid had no significant effect on occurrence of pneumothorax after thoracentesis. The mean age of the patients who did not and of those who did develop pneumothorax was 62 and 66 years, respectively. Pneumothorax occurred in 10% of men and in 9% of women, in 8% of patients without and 11% of those with underlying pulmonary disease. In the latter group, the incidence of pneumothorax was not different among the patients with focal (7%) or diffuse (12%) lung disease or pulmonary edema (8%). Similarly, pneumothorax did not occur more commonly when taps were performed in critically sick patients, many under assisted respiration (9% for patients in the intensive care unit vs 10% for patients not in intensive care). Furthermore, no difference was seen in occurrence of pneumothorax when the pleural fluid was transudate (9%) or exudate (7%), and when exudate was or was not hemorrhage (6% and 9%, respectively). These five variables (age, sex, pulmonary disease, clinical condition, and type of pleural fluid) had no significant effect on the development of pneumothorax when considered separately in patients tapped with the clinical or the sonography-guided group. However, when the method used for each of these variables was considered, the differences favored sonographic guidance.

The occurrence of pneumothorax after thoracentesis was not affected by the amount of fluid present in the pleural cavity, but was affected by the amount of fluid aspirated and the size of needle used. In addition, the method used in patients grouped under each of these variables was associated with significant differences in occurrence of pneumothorax, again favoring sonographic guidance. The estimated amounts of pleural effusion were comparable in patients who did not and did develop pneumothorax (mean grade of 1.48 vs 1.73; range 0–3), and occurrence of pneumothorax was not significantly different on effusions estimated as small (i.e., fluid obscuring less than 1/3 of the diaphragm) or large (8% vs 12%). However, pneumothorax developed more frequently in patients with either small or large effusions when the taps were performed with the clinical, rather than the sonography-guided method (18% vs 3% for small, $p = .0001$; and 14% vs 2% for large effusions, $p = .012$).

Occurrence of pneumothorax was significantly higher in

therapeutic than in diagnostic taps (18% vs 6%, $p = .001$), and the mean volume of fluid aspirated was significantly greater in taps associated with than in those not associated with pneumothorax (472 ml vs 246 ml, $p = .006$). Compared with clinical thoracentesis, the sonography-guided method was associated with significantly lower occurrence of pneumothorax in both diagnostic (2% vs 13%, $p \leq .0019$), and therapeutic taps (4% vs 21%, $p = .048$). This was also the case for "dry" or "near-dry taps," that is, less than 5 ml of pleural fluid aspirated (3% in sonography-guided vs 17% in clinical taps, $p = .049$).

Use of a large needle (i.e., larger than 20-gauge) was associated with higher occurrence of pneumothorax than when a small needle was used (18% vs 4%, $p = .00019$). This was also the case when the effusions were small (17% for large vs 4% for small needle, $p = .0015$) or large (16% for large vs 5% for small needle, $p < .05$), and when the thoracentesis was done with the sonography-guided (14% for large vs 2% for small needle, $p < .005$) but not with the clinical method (25% for large vs 16% for small needle).

The increased risk from the clinical compared with the sonography-guided method is also demonstrated by the higher grade of pneumothorax (mean grade of .28 vs .04; range, 0-3, $p < .0001$) and the larger number of follow-up chest radiographs (mean number of 0.70 vs 0.06 additional studies per tap; $p < .001$) and chest tubes (mean number of 0.080 vs 0.005 tubes per tap; $p = .004$), required with the clinical method. Once pneumothorax did develop, however, the method used did not have a different effect on the grade of pneumothorax (mean grade of 1.6 for both methods; range, 1-3) or the number of chest radiographs and chest tubes in taps performed with one or the other method (mean number of four vs two chest radiographs and mean number of 0.4 vs 0.2 chest tubes per pneumothorax occurring with the clinical or sonography-guided method). The increase in cost from follow-up chest radiographs and chest tubes alone was estimated to be an average of \$128 for every thoracentesis performed with the clinical method, as opposed to \$5 for every sonography-guided tap.

Multiple regression analysis showed that the method of thoracentesis was the dominant significant factor ($p = .00757$) for the development of pneumothorax. When tested with three other important variables, including the amount of effusion (small or large), type of tap (diagnostic or therapeutic), and size of needle (small or large), these factors were not significant after controlling for method. This was the case when the thoracentesis method was considered with any combination of these three variables. When the method was excluded from the analysis, both the type of tap ($p = .0434$) and size of needle ($p = .015$) but not the effusion size were significant in the development of pneumothorax. This was the case when all possible combinations of these three variables were tested. Multivariate analysis by logistic regression confirmed these findings.

Discussion

In this retrospective survey of patients undergoing thoracentesis, the incidence of pneumothorax was significantly

influenced by the method used: sonographic guidance was superior to conventional pleural taps. These results are in agreement with those from the prospective, randomized study of Grogan et al. [1], which included only patients at low risk to develop or to be seriously affected from the development of pneumothorax. Also, the occurrence of pneumothorax in our study is similar to previous accounts in which the one or the other method was used [5-10].

The disadvantage of a retrospective study such as this is the difficulty in controlling for extraneous factors, but ethical considerations posed restrictions to the prospective, randomized design of Grogan et al. [1]. As these two studies were done in the same institutions, at approximately the same time, many of the extraneous factors were similar. Viewed together, many of the weaknesses of the two studies are counterbalanced.

For the development of pneumothorax, our results showed no contribution from age, sex, underlying pulmonary disease, critical clinical condition, or the type of fluid aspirated. Interestingly, the amount of effusion present did not affect the occurrence of pneumothorax. Conversely, pneumothorax occurred more frequently as the amount of pleural fluid aspirated increased. This may be due to rapid changes in pressure in the pleural space while fitting reexpansion of the underlying lung lags behind. As expected, larger needles were associated with higher incidence of pneumothorax.

One subgroup of patients had clinical pleural taps performed after sonographic localization of the fluid, but not under sonographic guidance. In these taps, the occurrence of pneumothorax was not different from that in the rest of the clinical taps, although it was significantly higher than that in the sonography-guided taps. Kohan et al. [11] also found that the occurrence of pneumothorax was not reduced with remote sonographic localization. This may be related to a change in position of the fluid over time and change in the patient's position, and the ultimate reliance on physical examination for the selection of the tap site. Furthermore, the occurrence of pneumothorax in our clinically performed taps was not different for small or for large effusions. Assuming a large effusion is easier to localize, one would expect a higher rate of pneumothorax in small effusions. These findings suggest that there may be no significant room for improvement of the conventional techniques, and that the advantage of sonographic guidance probably lies in the synchronous direct visualization of the pleural fluid during thoracentesis.

Other technical differences, such as training and experience, also may play a role. Sonographers are used to percutaneous needle placements, and it may be easier to train and closely supervise a relatively small group of radiologists to perform a procedure in a consistent manner than to work with a much larger group of physicians in various clinical disciplines. Although Grogan et al. [1] tried to control this factor prospectively by providing similar instructions to radiology and medical personnel and by ensuring house physicians were competent to perform the procedure, the difference in occurrence of pneumothorax among the two groups remained significant.

Our results show sonography-guided thoracentesis to be

safer than a conventional pleural tap, and it does not appear to increase the cost substantially. The extra expense from additional chest radiographs and required chest tubes alone was estimated at \$123 per patient having conventional thoracentesis, which is almost comparable to the additional cost of chest sonography. Therefore, a strong case could be made in favor of sonography, proclaiming safety and comfort without significant increase in cost. In a busy clinical service, however, the logistics of such a routine may be substantial and, for low-risk patients, it is reasonable to wait for future studies to confirm our results.

At a minimum, we recommend sonography-guided thoracentesis for patients whose clinical condition may be jeopardized by the development of pneumothorax, such as critically sick patients and patients with severe lung disease or who are on respiratory assistance. In addition, when single-needle passage does not provide sufficient fluid for diagnostic tests, we suggest that taps be repeated under sonographic guidance. Moreover, we advocate use of the smallest possible needle and aspiration of the smallest possible amount of fluid, even for therapeutic taps, irrespective of the method used, but especially when sonographic guidance is not used.

ACKNOWLEDGMENT

We are grateful for the dedication of our radiology residents.

REFERENCES

1. Grogan DR, Irwin RS, Channick R, et al. Complications associated with thoracentesis: A prospective, randomized study comparing three different methods. *Arch Intern Med* **1990**;150:873-877
2. Rhea JT, DeLuca SA, Greene RE. Determining the size of pneumothorax in the upright patient. *Radiology* **1982**;144:733-736
3. Rhoades HM, Overall JE. A sample size correction for Pearson chi-square in 2x2 contingency tables. *Psychol Bull* **1982**;91:418-423
4. Dixon W, Brown M, Engelma L, et al. *BMDP statistical software*. Berkeley, CA: University of California Press, **1985**
5. Collins TR, Sahn SA. Thoracentesis: clinical value, complications, technical problems, and patient experience. *Chest* **1987**;91:817-822
6. Seneff MG, Corwin RW, Gold LH, Irwin RS. Complications associated with thoracentesis. *Chest* **1986**;90:97-100
7. Schroeder SA, Marton KI, Strom BL. Frequency and morbidity of invasive procedures: report of a pilot study from two teaching hospitals. *Arch Intern Med* **1978**;138:1809-1811
8. Harnsberger HR, Lee TG, Mukuno DH. Rapid, inexpensive real-time directed thoracentesis. *Radiology* **1983**;146:545-546
9. O'More PV, Mueller PR, Simeone JF, et al. Sonographic guidance in diagnostic and therapeutic interventions in the pleural space. *AJR* **1987**;149:1-5
10. Hirsch JH, Rogers JV, Mack LA. Real-time sonography of pleural opacities. *AJR* **1981**;136:297-301
11. Kohan JM, Poe RH, Israel RH, et al. Value of chest ultrasonography versus decubitus roentgenography for thoracentesis. *Am Rev Respir Dis* **1986**;133:1124-1126

Prevalence of Air Bronchograms in Small Peripheral Carcinomas of the Lung on Thin-Section CT: Comparison with Benign Tumors

Keiko Kuriyama¹
 Ryuhei Tateishi²
 Osamu Doi³
 Masahiko Higashiyama³
 Ken Kodama³
 Etsuo Inoue¹
 Yoshifumi Narumi¹
 Makoto Fujita¹
 Chikazumi Kuroda¹

Despite improved techniques—such as bronchoscopy and percutaneous needle biopsy—to evaluate pulmonary nodules, there are still many cases in which surgical resection is necessary before carcinoma can be differentiated from benign lesions. The present study was undertaken to determine if the presence of an air bronchogram or air bronchiogram (patent visible bronchus or bronchiole) is useful in distinguishing small lung cancers from benign nodules. Thin-section chest CT scans were obtained in patients with 20 peripheral lung cancers less than 2 cm in diameter (18 adenocarcinomas, one squamous cell carcinoma, and one large cell carcinoma) and 20 small benign nodules (eight hamartomas, seven tuberculomas, two foci of aspergillosis, one focus of cryptococcosis, one chronic focal interstitial pneumonitis, and one plasma cell granuloma). The images were compared with regard to the patency of any bronchus or bronchiole within the lesions. After surgical resection, the specimens were inflated with agar and sectioned transversely to correlate gross morphology and low-power histologic sections with the CT appearance. An air bronchogram or air bronchiogram was seen in the tumors on 65% of CT scans and 70% of histologic sections. Benign nodules had a patent bronchus or bronchiole on CT scans and histologic sections in only one case (5%).

These findings suggest that the presence of an air bronchogram in a lung nodule is a useful finding to help differentiate adenocarcinomas from benign lesions.

AJR 156:921–924, May 1991

CT has been shown to be an effective means of detecting calcification and fat in peripheral lung nodules [1–3]. In peripheral lung cancers, thin-section CT reveals spiculation, lobulation, pleural retraction, and convergence of peripheral vessels [4]. Additionally, CT provides excellent contrast resolution between air-containing bronchus and airless lung; hence, an air bronchogram is nicely demonstrated. We undertook the present study to determine if the presence of an air bronchogram or air bronchiogram is useful in distinguishing small lung cancers from benign nodules.

Materials and Methods

Patients in whom a new or enlarging solitary pulmonary opacity was detected on routine chest radiographs were selected for study. If the lesions were stable on a 1-week follow-up radiograph, thin-section CT was performed with a GE 9800 (1.5-mm section) or Toshiba TCT 900S (sequential 2-mm sections at one breath hold) scanner; images were reconstructed with an edge-enhancing algorithm. Nodules scanned on the Toshiba TCT 900S scanner were also reconstructed in sagittal, coronal, and oblique planes with real-time multiplanar reconstruction software. If the CT features of the lesion were considered to be indeterminate in distinguishing benign and malignant lesions [2, 3], a histologic diagnosis was obtained within 2 weeks. When cancer was not confirmed by transbronchial brushing or percutaneous needle biopsy, surgical resection was undertaken within 2 months, based on thin-section CT findings

Received September 7, 1990; accepted after revision November 30, 1990.

Presented at the annual meeting of the American Roentgen Ray Society, Washington, DC, May 1990.

¹ Department of Diagnostic Radiology, The Center for Adult Diseases, Osaka, 3 Nakamichi, 1-chome, Higashinari-ku, Osaka 537, Japan. Address reprint requests to K. Kuriyama.

² Department of Pathology, The Center for Adult Diseases, Osaka, Osaka 537, Japan.

³ Department of Surgery, The Center for Adult Diseases, Osaka, Osaka 537, Japan.

0361-803X/91/1565-0921\$00.75 © American Roentgen Ray Society

of fine spiculations, lobulation, pleural retraction, and convergence of peripheral vessels [4]. Noncalcified nodules without CT findings suggestive of cancer were managed conservatively.

We evaluated high-resolution thin-section CT scans of 20 lesions in 19 other patients seen between 1986 and 1989 who had surgically proved primary lung cancers less than 2 cm in diameter. The lesions included 18 adenocarcinomas (15 papillary, three acinar), one squamous cell carcinoma, and one large cell carcinoma, according to the classification [5, 6]. The tumor size ranged from 5 to 20 mm (mean, 16 mm). Thin-section CT images of 20 surgically proved benign nodules were also reviewed, including eight hamartomas, seven tuberculomas, two foci of aspergillosis, one focus of cryptococcosis, one chronic focal interstitial pneumonitis, and one plasma cell granuloma. These lesions were considered indeterminate on thin-section CT, were false positive on preoperative cytologic examination, and/or had enlarged on 1-month follow-up chest radiographs despite antibiotic treatment.

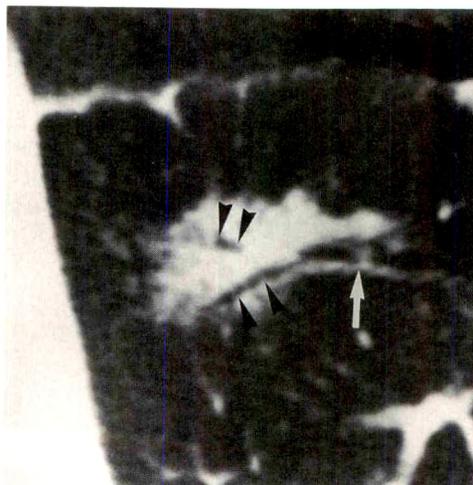
All 40 lesions were surgically resected within 2 months of the CT examination. After excision, inflated lung specimens were prepared by injecting a 1% agar solution through the leading bronchi. The specimens were sectioned transversely where the bronchus entered the lesion to provide optimal correlation with the CT images.

Pathologic specimens were examined to determine the patency of any bronchus or bronchiole in the lesion and the degree of aeration of the alveolar space within the lesions.

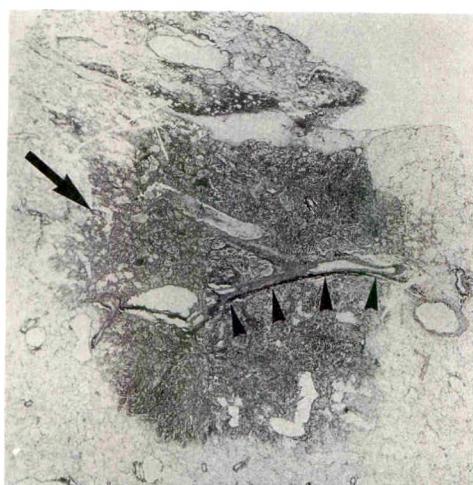
Results

On thin-section CT images, an air bronchogram and/or bronchiogram was seen in 13 (72%) of 18 patients with adenocarcinoma (Figs. 1–5). No air bronchogram was seen in the single cases of squamous cell carcinoma, large cell carcinoma, or poorly differentiated papillary adenocarcinoma.

Histologic sections revealed a patent bronchus or bronchiole in 14 (78%) of 18 patients with adenocarcinomas and was not observed in other histologic types of lung cancers. In five cases, CT findings and histologic evidence disagreed as to the presence or absence of an air bronchogram. An air bronchogram noted on thin-section CT correlated with normal or slightly dilated bronchi or a bronchiole surrounded by tumor cells seen pathologically (Figs. 1–3). Thin-section CT could demonstrate a patent bronchial tree larger than 1.5 mm



A



B



A



Fig. 1.—45-year-old man with well-differentiated papillary adenocarcinoma (19 × 19 mm) in right lower lobe.

A, Preoperative thin-section CT scan shows an air bronchogram (arrow) running into lesion and a branching lucency within lesion (arrowheads). Fluffy density is seen in periphery of lesion.

B, Low-power photomicrograph of histologic section shows lesion is a well-differentiated papillary adenocarcinoma with patent bronchus and bronchiole (arrowheads). Bronchioloalveolar type of growth pattern is observed in peripheral area (arrow).

Fig. 2.—72-year-old man with well-differentiated papillary adenocarcinoma (13 × 13 mm) in left upper lobe.

A, Preoperative thin-section CT scan shows relatively well-defined homogeneous nodule with air bronchiogram (arrowheads) located adjacent to interlobar fissure (arrow).

B, Low-power photomicrograph of histologic section shows lesion is a well-differentiated papillary adenocarcinoma. A patent bronchiole that does not contain cartilage in its wall is observed in periphery (arrowheads).

Fig. 3.—51-year-old woman with well-differentiated papillary adenocarcinoma (19 × 18 mm) in right upper lobe.

A, Preoperative thin-section CT scan shows an air bronchogram (arrowheads) and small round lucency (black arrow) in lobulated nodule with indented pleura (white arrow).

B, Low-power photomicrograph of histologic section shows lesion is a well-differentiated papillary adenocarcinoma with patent bronchiole (arrows). Central fibrosis and solid tumorous area are surrounded by bronchioloalveolar cell growth pattern in periphery.

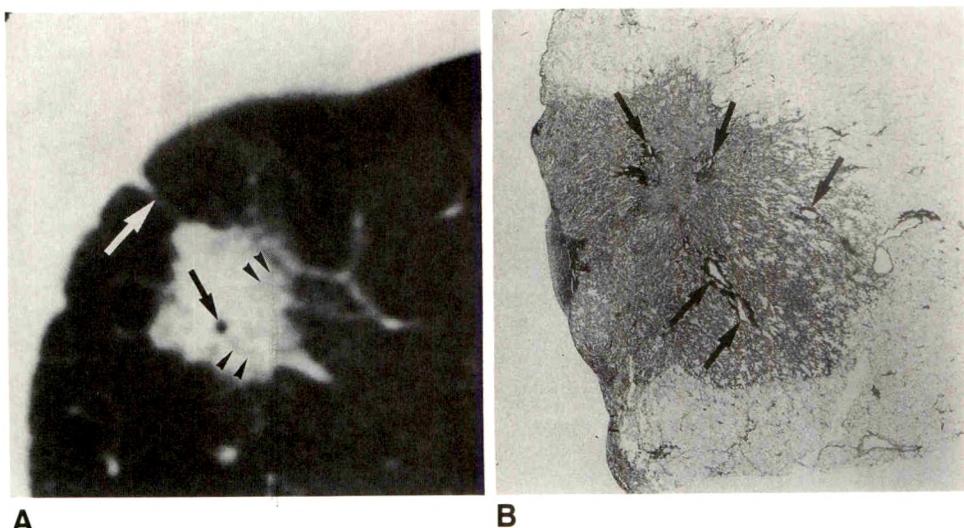


Fig. 4.—46-year-old man with well-differentiated papillary adenocarcinoma (20 × 12 mm) in right upper lobe. Preoperative thin-section CT scan shows an air bronchogram running into lesion (arrowheads) with indented pleura (arrow).

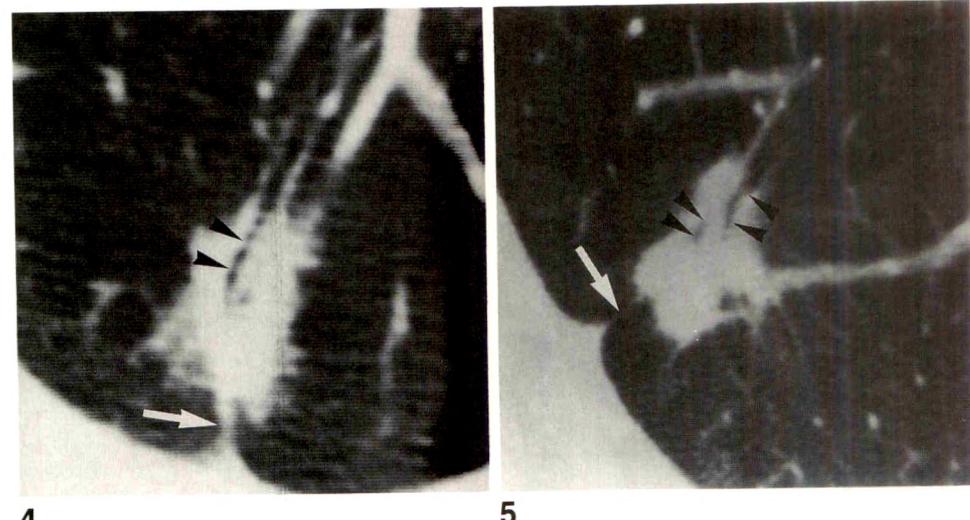


Fig. 5.—56-year-old man with well-differentiated papillary adenocarcinoma (18 × 14 mm) in right lower lobe. Preoperative thin-section CT scan shows an air bronchogram (arrowheads) in lobulated nodule with indented pleura (arrow) and convergence of peripheral vessels.

(spatial resolution of thin-section CT by phantom study); however, it was impossible to differentiate peripheral bronchi from an ectatic bronchiole (Fig. 2). Small bronchi could be distinguished from ectatic bronchioles by histologic features. The epithelial layers of terminal and respiratory bronchioles were seen to be replaced by cancer cells in well-differentiated adenocarcinomas on pathologic study (Figs. 1 and 3).

Of the benign nodules, an air bronchogram was seen in only one case of chronic focal interstitial pneumonitis. In this instance, the patent bronchus was surrounded by airless lung with markedly thickened alveolar interstitium inflated by lymphocytes. In the other 19 benign nodules, an air bronchogram was not seen on either CT images or histologic sections (Figs. 6 and 7).

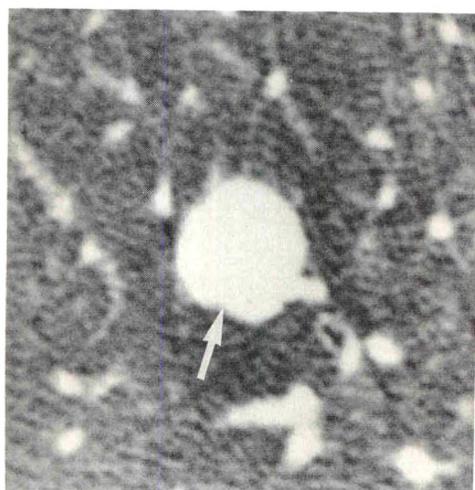
Discussion

An air bronchogram is an important radiologic sign of air-space consolidation in which the normally invisible bronchial air column becomes visible because of contrast with sur-

rounding tissues [7]. Two situations must exist for an air bronchogram to be identified: the bronchus must contain air (it cannot be occluded completely at its origin) and the surrounding lung parenchyma must have reduced air content or be airless [8]. Although most commonly seen in the presence of air-space consolidation, a severe degree of interstitial lung disease can also cause an air bronchogram [9].

It is accepted that lung cancer of the bronchioloalveolar cell type may produce air bronchograms on radiographs or CT scans [10–12]. Previous reports have also suggested the presence of pseudocavitations in small peripheral bronchioloalveolar cell carcinoma, which may represent air bronchograms in cross section [13]. However, air bronchograms have been considered uncommon in other types of lung cancer [14, 15].

In this study, 72% (13/18) of the adenocarcinomas demonstrated air bronchograms when examined by thin-section CT scanning. This unexpected finding may have some diagnostic value in suggesting carcinoma as a likely cause of a pulmonary nodule.



6



7

Fig. 6.—44-year-old woman with hamartoma (13 × 11 mm) in right upper lobe. Preoperative thin-section CT scan shows smooth-edged nodule (arrow) without air bronchogram. Computer printout indicated no evidence of cavity, calcium, or fat in lesion.

Fig. 7.—56-year-old man with alcoholic cirrhosis associated with aspergiloma (20 × 16 mm) in left upper lobe. Preoperative thin-section CT scan shows nodule (arrow) without air bronchogram in emphysematous lung.

Our study suggests that when an air bronchogram or bronchiogram is detected in a small peripheral lung nodule, suspicion of malignancy should be high. Further study of sufficient numbers of lung cancers of other types is needed to determine if the presence of these findings suggests adenocarcinoma specifically.

REFERENCES

- Siegelman SS, Zerhouni EA, Leo FP, Khouri NF, Stitik FP. CT of the solitary pulmonary nodule. *AJR* 1980;135:1-13
- Siegelman SS, Khouri NF, Leo FP, Fishman EK, Braverman RM, Zerhouni EA. Solitary pulmonary nodules: CT assessment. *Radiology* 1986;160:307-312
- Siegelman SS, Khouri NF, Scott WW Jr, et al. Pulmonary hamartoma: CT findings. *Radiology* 1986;160:313-317
- Kuriyama K, Tateishi R, Doi O, et al. CT-pathologic correlation in small peripheral lung cancers. *AJR* 1987;149:1139-1143
- World Health Organization. World Health Organization histologic typing of lung tumours, 2nd ed. *Am J Clin Pathol* 1982;77:123-136
- Schraufnagel D, Peloquin A, Paré JAP, Wang N. Differentiating bronchioalveolar carcinoma from adenocarcinoma. *Am Rev Respir Dis* 1982;125:74-79
- Fleischner FG. The visible bronchial tree: a roentgen sign in pneumonic and other pulmonary consolidations. *Radiology* 1948;50:184-189
- Fraser RG, Paré JAP, Paré PD, Fraser RS, Genereux GP. *Diagnosis of diseases of the chest*, vol. 1, 3rd ed. Philadelphia: Saunders, 1988:468-472
- Reed JC, Madewell JE. The air bronchogram in interstitial diseases of the lungs. A radiological-pathological correlation. *Radiology* 1975;116:1-5
- Shapiro R, Wilson GL, Yesner R, Shuman H. A useful roentgen sign in the diagnosis of localized bronchioalveolar carcinoma. *AJR* 1971;114:516-524
- Hill CA. Bronchioalveolar carcinoma: a review. *Radiology* 1984;150:15-20
- Dock VW, Grabenwöger F, Pinterits, Bardach G. Das bronchioalveolare Karzinom. *ROFO* 1986;145:510-514
- Kuhlman JE, Fishman EK, Kuhajda FP, et al. Solitary bronchioalveolar carcinoma: CT criteria. *Radiology* 1988;167:379-382
- Theros EG. Varying manifestations of peripheral pulmonary neoplasms: a radiologic-pathologic correlative study. *AJR* 1977;128:893-914
- Fraser RG, Paré JAP, Paré PD, Fraser RS, Genereux GP. *Diagnosis of diseases of the chest*, vol. 3, 3rd ed. Philadelphia: Saunders, 1988:1342-1367

CT Evaluation of Solitary Pulmonary Nodules: Value of 185-H Reference Phantom



Stephen J. Swensen¹
Gordon F. Harms¹
Richard L. Morin¹
Jeffrey L. Myers²

The pulmonary nodule CT reference phantom is widely used in the evaluation of nodules 2 cm or less in diameter. It is used to detect benign patterns of calcification that are not visible on thin-section CT scans. Since 1986, the reference nodules have been manufactured with a nominal composition of 185 H. The multicenter study published in 1986 used nodules with a nominal composition of 264 H, 100 H more than the threshold value reported by Siegelman et al. in 1980. In the multicenter study, one of 37 nodules diagnosed as benign with the phantom proved to be malignant. The purpose of this study was to determine the misdiagnosis rate with the 185-H phantom and to ascertain whether the malignant tumors predicted to be benign actually contained calcification. We retrospectively reviewed 296 cases in which examinations had been performed with the 185-H nodules since 1986. Eighty-five nodules were diagnosed as benign by comparison to the reference phantom. These 85 contained no visible calcification on thin-section CT scans. Ten of the 85 cases were shown to be malignant tumors. Eight were diagnosed as having a high probability of benignity. Two were diagnosed as having a moderate probability of benignity. Calcium was present in the tissue of all six nodules available for review. Fifty-nine of the 85 nodules were still clinically indeterminate at the time of this review.

Even if all of the clinically indeterminate nodules are benign, the misdiagnosis rate would be significantly higher than in most previous studies. Although analysis by using the reference phantom with 185-H nodules may indicate a high probability of benignity, close radiologic follow-up is necessary.

AJR 156:925-929, May 1991

The pulmonary nodule CT reference phantom is widely used in the evaluation of small nodules. It simulates transaxial anatomy of the thorax and is produced with materials that are equivalent to tissue with respect to X-ray attenuation properties [1, 2]. The nominal (nom.) composition of the original reference nodules described by Zerhouni et al. [1] in 1983 was 164 H. This was based on the 164-H threshold described by Siegelman et al. in 1980 [3]. The validity of the CT reference phantom was tested in a large multicenter CT phantom study described in 1986 [2]. For this trial, 264-H (nom.) reference nodules were used. This was 100 H higher than the previously described threshold, and it was used as a safety measure because of the variety of hardware and software used in the study and because the Pfizer/ASE 500 scanner tended to overestimate, disproportionately, the CT numbers of smaller nodules [2].

Since the CT reference phantom became available commercially in 1986, it has contained nodules of different sizes, each with a nominal composition of 185 H. The nominal composition of 185 H was chosen to add a margin of safety to the 164-H threshold [3]. The nominal composition was lowered from 264 H in order to increase the percentage of calcified nodules diagnosed as benign with the reference phantom. To our knowledge, no study has exclusively evaluated the 185-H (nom.) CT reference phantom nodules [4-7]. To explore the outcome of nodules diagnosed

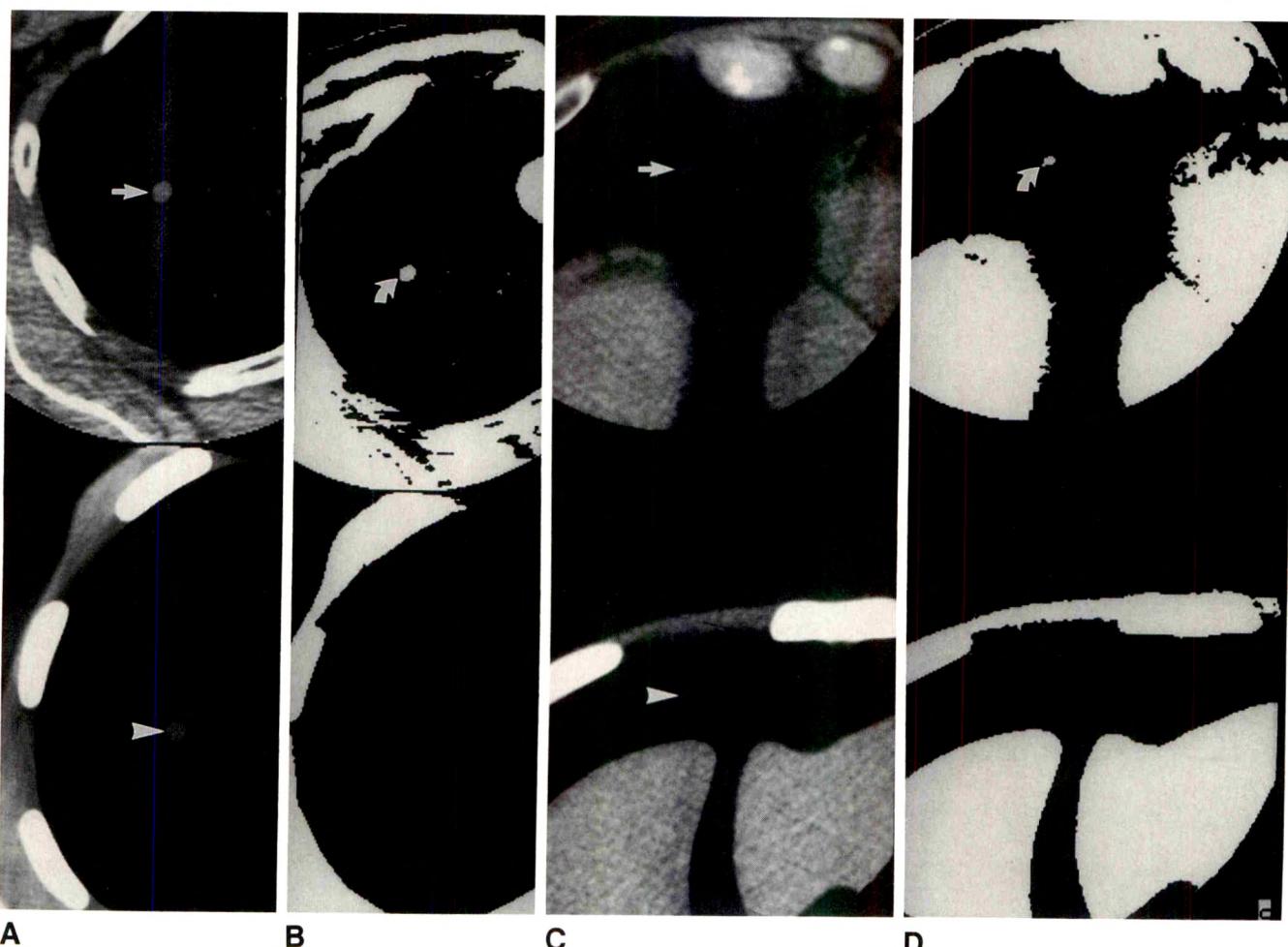
Received October 1, 1990; accepted after revision December 3, 1990.

Presented at the annual meeting of the American Roentgen Ray Society, Washington, DC, May 1990.

¹ Department of Diagnostic Radiology, Mayo Clinic and Mayo Foundation, 200 First St. S. W., Rochester, MN 55905. Address reprint requests to S. J. Swensen.

² Section of Surgical Pathology, Mayo Clinic and Mayo Foundation, Rochester, MN 55905.

0361-803X/91/1565-0925
© American Roentgen Ray Society



as benign by this system, we undertook a retrospective study of patients examined with the 185-H (nom.) CT reference phantom nodules.

Materials and Methods

Between September 1986 and April 1990, 296 pulmonary nodules were examined with the CT reference phantom. The reference phantom study was ordered at the discretion of the referring clinician. The examinations were performed with Picker 1200 SX (Highland Heights, OH) and GE Medical Systems CT 9800 (Milwaukee, WI) CT scanners. The CT reference nodules used were the commercially available 185-H (nom.) nodules (Computerized Imaging Reference Systems, Inc., Norfolk, VA).

The reference phantom was assembled to match the patient's anatomy and scanned with an identical technique. Studies of the phantom were performed immediately after examining the patient in order to minimize temporal variations in scanner performance. The reference phantom was placed in the gantry in the same position the patient had been in during scanning. CT scanning parameters consisted of 130 kVp, 140 mA, 2-sec scan, 512 × 512 pixel matrix, 20- and 48-cm circles of reconstruction, standard reconstruction algorithm, and 1.5-mm or 2.0-mm slice thickness. Scanner uniformity and Hounsfield unit calibration were checked daily. No patient received iodinated contrast material IV in the 24 hr before the CT scan.

The 296 consecutive examinations were independently reviewed

retrospectively by two thoracic radiologists without knowledge of the final diagnosis. All CT examinations resulting in a benign diagnosis or with a disparity in the retrospective diagnosis were reviewed again.

For the purpose of this discussion, calcification, when used in the context of the reference phantom, is defined as the presence of pixels in the patient's nodule that were of greater CT number than those for the reference phantom nodule when appropriately scanned.

The nodule was classified as having a high probability of benignity [2] if it met the following criteria: (1) The edge of the nodule could be smooth or lobulated. If the nodule edge was spiculated, it could not be classified as having a high probability of benignity. (2) The pattern of calcification had to be benign (i.e., central, laminated, or diffuse). If the calcification was centrally located within the nodule, at least 10% of the cross-sectional area had to be calcified. (3) This benign pattern of calcification had to be present on at least two sections through the nodule.

If a spiculated nodule had a benign pattern of calcification on three or more CT scans and was 1.5 cm or less in diameter, it was classified as having a moderate probability of benignity.

In order to determine the density of the patient's nodule, the scans of the patient's nodule and the reference phantom were displayed simultaneously. The display-window width was narrowed to 1 H and the display-window level was raised to the highest Hounsfield-unit level of a pixel contained within the reference phantom nodule. If more than 10% of contiguous pixels in the cross-sectional area of the image of the patient's nodule remained visible, the nodule was considered calcified. If the patient's nodule disappeared before the highest Hounsfield value of a pixel of the reference phantom nodule



Fig. 1.—Three representative cases of nodules diagnosed as high probability of benignity by using CT reference phantom.
A and B, 61-year-old woman with 12-mm breast adenocarcinoma metastasis.

C and D, 30-year-old man with 6-mm fibrosarcoma metastasis.

E and F, 53-year-old woman with 12-mm primary bronchial carcinoid. Upper images are 2-mm CT scans of patient. Lower images are 2-mm CT scans of reference phantom with nodule of appropriate size (arrowheads). A, C, and E are at normal window settings for soft tissue. There is no visible calcification in patients' nodules (straight arrows in A, C, and E). B, D, and F are at a window width of 1 H and window level at which reference phantom's densest pixel is visible. Accordingly, the reference nodule is no longer visible on these images (lower images in B, D, and F). Therefore, by definition, pixels seen in corresponding scan of patient are calcified. There is a benign pattern of pixels in patients' nodules that is denser than reference phantom (curved arrows in B, D, and F).

nodule. The diameter and the edge characteristics of the patient's nodule were evaluated at window settings for lung.

Pathology reports and slides from selected cases were retrieved from the surgical pathology files and were reviewed by one of us. von Kossa stains for calcium were done in all tumor cases.

Results

Of the 296 nodules studied, 175 had lower attenuation values than the reference phantom nodule did and were considered radiologically indeterminate. In four cases there was disagreement regarding a benign diagnosis by CT. Each case had approximately 10% of the cross-sectional area calcified. All four nodules were classified as indeterminate. One hundred twenty-one nodules were diagnosed as benign by CT examination. Of the 121 nodules, 36 were visibly calcified in a benign pattern on 2-mm sections, and 85 were benign by comparison with the reference phantom alone. The 85 nodules diagnosed as benign by comparison with the reference phantom alone were the focus of this study and will be referred to as reference-benign nodules. All of the reference-benign nodules contained central or diffuse calcification. None were laminated.

Fifty-nine of the 85 reference-benign nodules were still clinically indeterminate at the time of this review. Two have increased in size in 5–42 months of observation. Nineteen have not changed in size between 1 and 2 years of observation. Thirty-eight nodules have been followed up for less than 1 year.

Sixteen of the 85 reference nodules have been shown to be benign. Eleven had no growth during at least a 2-year period of radiologic follow-up. Five were resected via thoracotomy: four were fungal granulomas and one was a hamartoma.

So far, 10 of the 85 reference-benign nodules have been shown to be malignant (Table 1). Eight of the 10 had a CT diagnosis of high probability of benignity (Fig. 1). Two were diagnosed as having a moderate probability of benignity.

The difference in maximum pixel value (H) between the phantom and the patient's nodule for the benign and malignant groups is given in Table 2. No significant difference (t test, $p > .10$) was found between these groups.

Tissue slides were available for review from five of the eight malignant nodules diagnosed as having a high probability of

TABLE 1: Reference-Benign Nodules Later Proved Malignant^a

Sex	Age (yr)	Nodule Size (mm)	Diagnosis
High Probability of Benignity			
M	30	6	Fibrosarcoma metastasis ^b
F	81	6	Breast adenocarcinoma metastasis ^b
F	71	10	Small-cell adenocarcinoma ^{c,d}
F	53	12	Bronchial carcinoid ^c
F	70	20	Well-differentiated lymphocytic lymphoma ^{c,d}
F	61	10	Breast adenocarcinoma metastasis ^{c,d}
		12	Breast adenocarcinoma metastasis ^{c,d}
M	73	10	Bronchogenic squamous cell carcinoma ^{c,d}
Moderate Probability of Benignity			
F	51	10	Bronchogenic adenocarcinoma ^c
M	70	10	Papillary adenocarcinoma ^{c,d}

^a Edge characteristics of all lesions with a high probability of benignity were smooth and round. Of lesions with a moderate probability of benignity, one was spiculated and round and one was smooth with marked lobulation.

^b Diameter increase 100% or greater in less than 1 year and appearance of additional nodules.

^c Thoracotomy.

^d Calcium noted on histologic sections.

was reached or if less than 10% of contiguous pixels remained visible, the patient's nodule was considered uncalcified and, therefore, radiologically indeterminate. With these criteria, no nodule was considered to be of the same attenuation as the reference phantom

TABLE 2: Hounsfield Unit Difference Between Phantom and Patient's Nodule (Highest Pixel Value)

Reference-Benign and Clinically Benign		Reference-Benign and Clinically Malignant	
Patient	H Difference	Patient	H Difference
1	33	1	19
2	72	2	11
3	22	3	11
4	69	4	11
5	24	5	37
6	32	6	25
7	25	7	31
8	111	8	41
9	47	9	58
10	27	10	69
11	24	Average	31
12	28		
13	21		
14	73		
15	44		
16	43		
Average	43		

benignity and one case diagnosed as having a moderate probability (Table 1). Each contained calcification. Intratumoral calcium was identified in all three primary carcinomas examined. The microcalcifications were confined to areas of tumor necrosis in two and consisted of psammoma bodies in one. The lymphoma surrounded an encompassed calcified bronchial cartilage. The metastatic breast adenocarcinomas each contained dystrophic calcification in areas of necrosis.

Four of 16 benign lesions were also reviewed, including three necrotizing granulomas and a single chondroid hamartoma. All showed histologic evidence of calcification.

Discussion

The evaluation of a solitary pulmonary nodule is challenging and complex. In large part, the evaluation is a radiologic workup [8–12]. A primary goal is to maximize the detection of benign calcification without misinterpreting dense tissue or calcification in a cancer as benign [11]. CT, with its superior contrast sensitivity, has been shown to be useful in detection of calcification [1–10, 13, 14].

In 1980, Siegelman et al. [3] reported the use of CT for the evaluation of solitary pulmonary nodules. They concluded that nodules with representative CT numbers of 164 H or higher were benign. To control for inter- and intra-CT scanner attenuation values for pulmonary nodules of the same density [15, 16], Zerhouni et al. [1] developed a standard reference phantom for quantitative CT analysis of pulmonary nodules. Several studies have shown CT density and the CT reference phantom to be accurate and useful in the evaluation of pulmonary nodules [1–7, 13, 14]. The large multiinstitutional study [2] used a reference phantom nodule with a nominal composition of 264 H, 100 H higher than the original threshold reported by Siegelman et al. [3] and the prototype reference

phantom [1]. No study to date has looked exclusively at the 185-H (nom.) reference phantom nodule [1, 2, 4–7].

In our study, we found that eight (9%) of the 85 nodules diagnosed as having a high probability of benignity were actually malignant. This is the largest series reported. A significantly higher rate of misdiagnosis was found than in most previous reports [1, 2, 4–7]. Zerhouni et al. [2] reported that one (3%) of 37 reference-benign nodules proved malignant. Huston and Muhm [4] reported that only one (3%) of 33 reference-benign nodules was a cancer. Jones et al. [5] found one cancer (9%) among 11 reference-benign nodules, and Ward et al. [6] identified no malignant tumors in their series of 19 reference-benign nodules. Each of these studies includes scans obtained before 1986, when the 185-H (nom.) reference nodules became available (Drury B, personal communication).

Fifty-nine of the 85 reference-benign nodules in this study are still clinically indeterminate and are being managed with observation. It is conceivable that some of these reference-benign, clinically indeterminate nodules may ultimately prove to be malignant as well.

The 185-H (nom.) CT reference phantom pushes CT technology to the limit. Approximately one third of pulmonary nodules in this study with no visible calcium on thin-section CT were predicted to be benign. Calcium was present in each of the reference-benign nodules for which tissue was available for review, both in those later proved to be benign and in those proved to be malignant. This indicates that the reference phantom is sensitive in the detection of calcium. Unfortunately, calcium occurs naturally in a small percentage of lung cancers [2, 11]. It may be that the remarkable ability of CT to detect small amounts of calcium has reached a point of diminishing return.

Although on average the nodules correctly determined to be benign with CT differed more from the reference phantom (43 H vs 31 H), there was a great deal of overlap and no significant difference between the benign and malignant groups. If the decision threshold (185 H [nom.]) had been raised to eliminate those malignant nodules that were interpreted as benign, then at least 13 of the 16 known benign nodules also would have been declared indeterminate. These data suggest that the range of values in disease overlaps that of benign cases and within these boundaries a clinical compromise must be reached between sensitivity and specificity.

It is important for physicians who use the CT reference phantom to understand that a significant number of nodules diagnosed as having a high probability of benignity will ultimately prove to be malignant. Even though most will still be benign, these nodules should be considered indeterminate and closely followed up [1, 2]. These data indicate the need for meticulous attention to proper CT scanning techniques and to interpretation criteria.

ACKNOWLEDGMENT

Special thanks to Elias Zerhouni for his suggestions regarding the study.

REFERENCES

1. Zerhouni EA, Boukadoum M, Siddiki MA, et al. A standard phantom for quantitative CT analysis of pulmonary nodules. *Radiology* **1983**;149:767-773
2. Zerhouni EA, Stitik FP, Siegelman SS, et al. CT of the pulmonary nodule: a cooperative study. *Radiology* **1986**;160:319-327
3. Siegelman SS, Zerhouni EA, Leo FP, Khouri NF, Stitik FP. CT of the solitary pulmonary nodule. *AJR* **1980**;135:1-13
4. Huston J III, Muhm JR. Solitary pulmonary nodules: evaluation with a CT reference phantom. *Radiology* **1989**;170:653-656
5. Jones FA, Wiedemann HP, O'Donovan PB, Stoller JK. Computerized tomographic densitometry of the solitary pulmonary nodule using a nodule phantom. *Chest* **1989**;96:779-783
6. Ward HB, Pliego M, Diefenthal HC, Humphrey EW. The impact of phantom CT scanning on surgery for the solitary pulmonary nodule. *Surgery* **1989**;106:734-738
7. Fastro JF, Newell JD. Quantitative computed tomography evaluation of benign solitary pulmonary nodules. *J Comput Tomogr* **1987**;11:103-106
8. Swensen SJ, Jett JR, Payne WS, Viggiano RW, Pairolo PC, Trastek VF. An integrated approach to evaluation of the solitary pulmonary nodule. *Mayo Clin Proc* **1990**;65:173-186
9. Khouri NF, Meziane MA, Zerhouni EA, Fishman EK, Siegelman SS. The solitary pulmonary nodule: assessment, diagnosis, and management. *Chest* **1987**;91:128-133
10. Webb WR. Radiologic evaluation of the solitary pulmonary nodule. *AJR* **1990**;154:701-708
11. Mahoney MC, Shipley RT, Corcoran HL, Dickson BA. CT demonstration of calcification in carcinoma of the lung. *AJR* **1990**;154:255-258
12. Huston J III, Muhm JR. Solitary pulmonary opacities: plain tomography. *Radiology* **1987**;163:481-485
13. Siegelman SS, Khouri NF, Leo FP, Fishman EK, Braverman RM, Zerhouni EA. Solitary pulmonary nodules: CT assessment. *Radiology* **1986**;160:307-312
14. Proto AV, Thomas SR. Pulmonary nodules studied by computed tomography. *Radiology* **1985**;156:149-153
15. McCullough EC, Morin RL. CT-number variability in thoracic geometry. *AJR* **1983**;141:135-140
16. Levi C, Gray JE, McCullough EC, Hattery RR. The unreliability of CT numbers as absolute values. *AJR* **1982**;139:443-447

Book Review



Cardiovascular Application of Doppler Ultrasound. Edited by Abdul-Majeed Salmasi and Andrew N. Nicolaides. New York: Churchill Livingstone, 368 pp., 1989. \$150

This book, written by several contributors, reviews the application of Doppler ultrasound in cardiovascular disease. It is addressed to radiologists, cardiologists, surgeons, and clinicians dedicated to patients with cardiovascular disease. The authors only partially have accomplished their goal of publishing state of the art in the field. The book does not describe the use of ultrasound and Doppler imaging in important areas such as intraoperative assessment of coronary artery disease. The use of the technique in the postoperative period for patients with acquired and congenital heart diseases, in which this method plays an important role, is not mentioned.

The book is divided into three parts. In the first part (chapters 1–7), five chapters describe the physical and technical aspects of ultrasound and Doppler imaging comprehensively. The chapters contain important basic information about the technical and instrumental factors that significantly influence the results of using the technique.

In the 10 chapters of the second part, the authors describe the cardiac applications of Doppler ultrasound. They describe the basic principles on which the technique is based for assessing ventricular and valvular malfunction. Two chapters discuss the study of congenital heart disease through Doppler ultrasound. One of the chapters is dedicated to the diagnosis of cardiovascular conditions in the newborn. It describes the diagnosis of patent ductus arteriosus, coarctation of the aorta. It does not describe the use of Doppler imaging in the diagnosis of hypoplastic left ventricle and total anomalous venous connection. In the second chapter dedicated to congenital heart disease, the authors describe the use of Doppler imaging in the detection of valvular disease and shunts, particularly ventricular septal defect. This chapter is quite limited. It does not describe the application of this technique for the diagnosis of the vast majority of congenital malformations. It lacks information on the use of Doppler echocardiography in determining the blood-flow pattern in certain cardiac malformations such as tetralogy of Fallot, double-outlet right

ventricle, and univentricular atrioventricular connection. Even more, it does not consider the application of color Doppler imaging in the assessment of blood-flow patterns after repair of congenital heart disease. The chapters dedicated to diagnosis of valvular malfunction in mitral, aortic, tricuspid, and pulmonic valves are well illustrated. The chapter on prosthetic valvular malfunctioning is incomplete. It does not describe the use of color Doppler imaging in the detection of malfunction of the valves currently in wide use.

The third part of the book includes 8 chapters devoted to arterial and recent venous applications of Doppler ultrasound. The text has a very limited discussion of color duplex imaging, and its chapters are incohesive. The chapter on stenosis of the internal carotid artery contains multiple criteria for spectral interpretation; unfortunately, the new criteria used by the authors are not discussed until the end of the chapter, and the table that summarizes these criteria contains typographic errors. The discussion of peripheral arterial disease presents data from both duplex scanning and Doppler indexes, such as the ankle pressure index, again with little attention to color duplex imaging. The chapter on venous thrombosis is limited, failing to present any data or discussion of duplex scanning for evaluation of venous compressibility.

The audience of this book will find good information about technical aspects of Doppler ultrasound. The clinical evaluation is good for the diagnosis of valvular disease, but it is incomplete in other areas, particularly congenital conditions, and deficient in exploration of peripheral vascular disease.

Benigno Soto
Susan A. Mulligan
University of Alabama at Birmingham
Birmingham, AL 35233

Pictorial Essay

Imaging of the Azygos Lobe: Normal Anatomy and Variations

Josep Mata,¹ José Cáceres, Xavier Alegret, Pilar Coscojuela, and José Angel De Marcos

We describe the normal appearance of the azygos lobe on plain radiography and CT. Several findings are presented that, to our knowledge, have not been previously reported, such as the inferior prolongation of the fissure, the apparent intrapulmonary path of the right brachiocephalic vein and superior vena cava seen on the anteroposterior chest radiograph, and the visible fissure on the lateral chest radiograph.

The azygos lobe is a normal variant that is found in 1% of anatomic specimens and on about 0.4% of chest radiographs. It occurs when the right posterior cardinal vein, one of the precursors of the azygos vein, fails to migrate over the apex of the lung and penetrates it instead, carrying along pleural layers that entrap a portion of the right upper lobe. Several

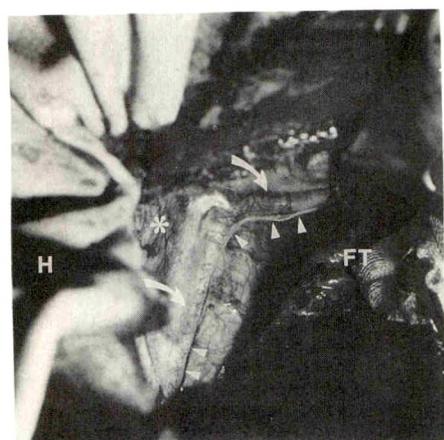


Fig. 1.—Photograph of surgical findings. Azygos arch (arrows); mesoazygos (asterisk); inferior prolongation of fissure (arrowheads). H = head, FT = foot.

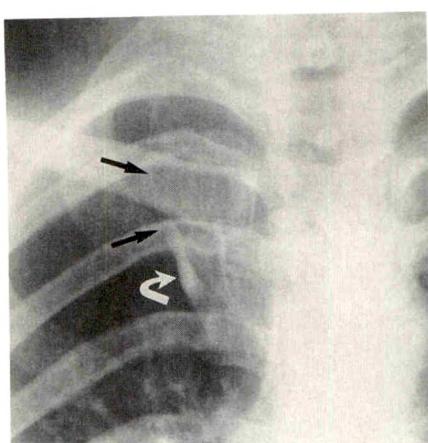


Fig. 2.—A, Azygos fissure is visible as a fine line (straight arrows) with right convexity on chest radiograph. Azygos vein is visible in lowermost part of fissure (curved arrow). B, Trigone is better seen (solid arrow) on linear tomogram. Azygos vein is not visualized at its usual position (open arrow).

Received October 1, 1990; accepted after revision November 29, 1990.

Presented in part at the annual meeting of the American Roentgen Ray Society, Washington, DC, May 1990.

¹ All authors: Servicio de Radiodiagnóstico, Hospital de Sant Pau, Facultad de Medicina, Universidad Autónoma, Avda. S. Antonio M. Claret, 167, 08025 Barcelona, Spain. Address reprint requests to J. Mata.

theories have been advanced to explain this abnormal migration, but exactly why this occurs is not known [1, 2].

The abnormally located vessel indents the lung and its overlying parietal and visceral pleural layers. Two folds of parietal and two folds of visceral pleura form a mesenterylike structure, containing in its lowermost portion the azygos arch (Fig. 1). Between this fissure (mesoazygos) and the mediastinum lies a portion of the right upper lobe. The enclosed lung is not an independent segment and its bronchial and arterial supplies arise from the apical or posterior segments of the right upper lobe [1, 2].

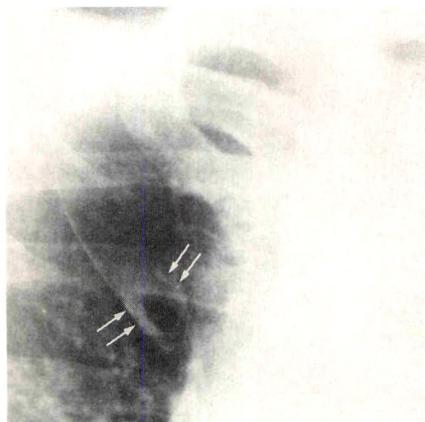
Plain Film Findings

The azygos lobe is usually well seen on the chest radiograph, where it is limited by a fine, convex (relative to the mediastinum) line that crosses the apex of the right lung (Fig. 2). The upper portion of the fissure has a triangular shape

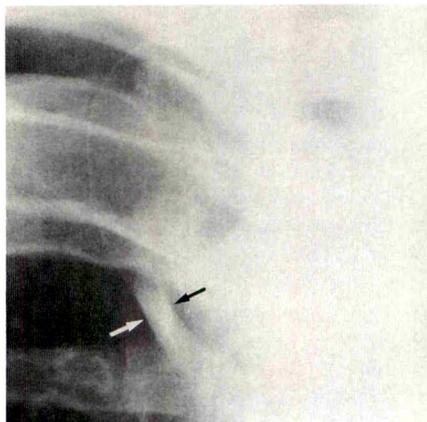
(trigonum parietale), which corresponds to a small amount of extrapleural areolar tissue between the parietal layers of pleura. The azygos vein is visible in the lowermost part of the fissure, as a tear-shaped shadow [2, 3]. Occasionally it may adopt a tubular or semicircular appearance (Fig. 3). The azygos arch is not visible at its usual location, at the junction of the trachea with the main bronchus [3].

According to its size, the azygos lobe has been classified into three types [1]: In type A, the trigonum parietale is located in the lateral aspect of the pulmonary apex; in type B, the mesoazygos has a vertical path; and in type C, the trigonum is located medially.

On the lateral view the azygos arch is situated higher than normal. The lung that penetrates behind the superior vena cava (SVC) renders its posterior wall visible (Fig. 5) [2]. The azygos fissure can be seen as a fine vertical line (Fig. 6). The whole azygos arch can occasionally be seen on conventional tomograms (Fig. 7).

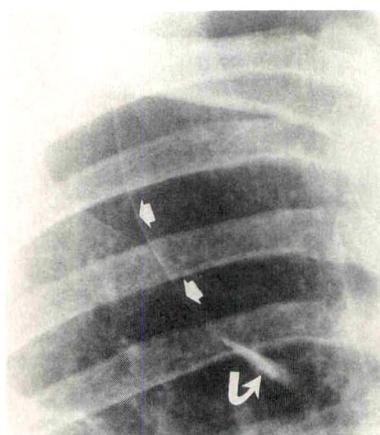


A

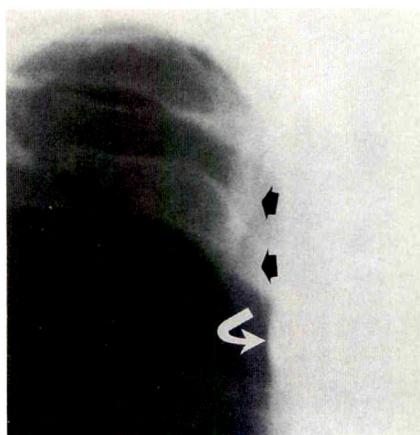


B

Fig. 3.—A, Azygos vein may have a semicircular appearance on plain films when the whole arch is visible (arrows). **B**, Azygos vein may appear as a tubular structure (arrows) when only posterior segment of azygos vein arch is seen.



A



B

Fig. 4.—A and B, On plain films, size of azygos lobe may vary markedly and can encompass much of right upper lobe (**A**) or be very small (**B**). Fissure = straight arrows, azygos vein = curved arrows.

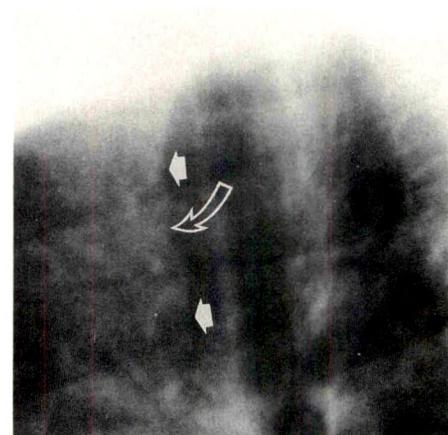


Fig. 5.—On lateral radiograph, lung that penetrates behind superior vena cava (SVC) makes posterior wall of SVC visible (solid arrows), except for area in which azygos vein ends (open arrow).

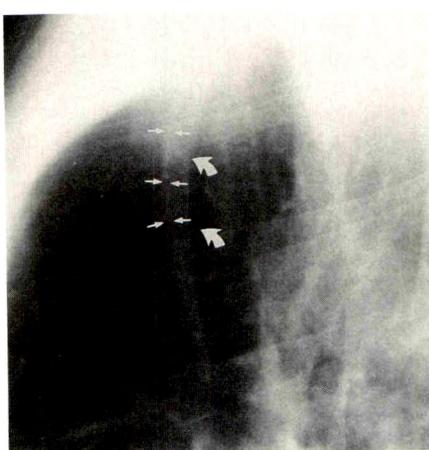
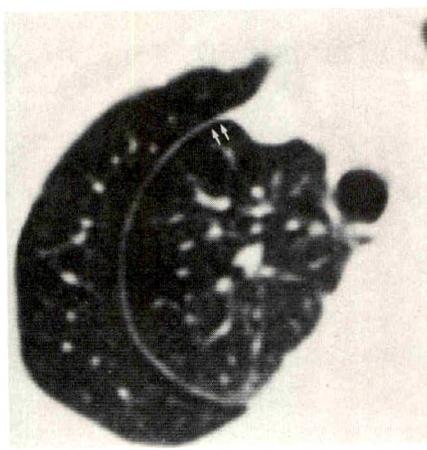
**A****B**

Fig. 6.—A, Lateral chest radiograph. Azygos fissure is visible as a fine vertical line (straight arrows) in front of posterior wall of superior vena cava (curved arrows).

B, CT scan shows that anterior portion of azygos fissure (arrows) is tangential to beam on lateral view.

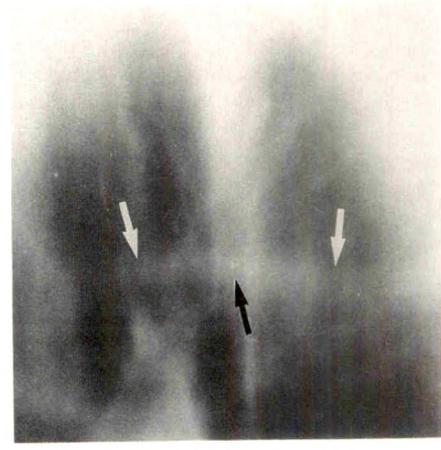


Fig. 7.—Linear tomogram obtained in lateral position shows azygos arch (arrows) clearly.

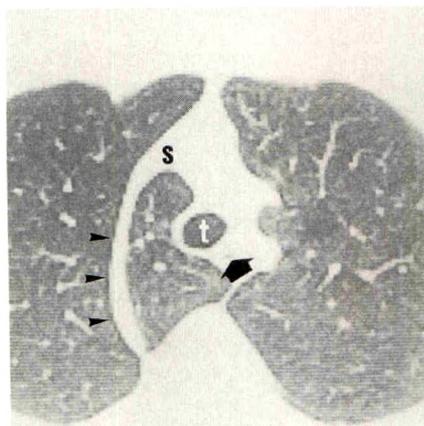
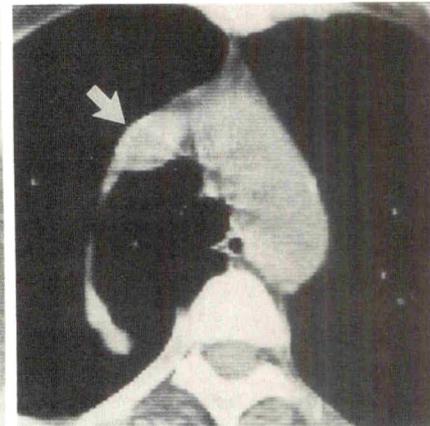
**A****B**

Fig. 8.—A, CT scan. Lung penetrates deeply behind superior vena cava (s) and trachea (t), contacting medial wall of esophagus (arrow). Azygos arch-arrowheads.

B, Mediastinal window setting in another patient shows elliptical shape of superior vena cava (arrow) and its oblique axis.

CT Findings

The azygos lobe causes important morphologic changes in the superior mediastinum. CT shows the deep penetration of the lung behind the SVC and the trachea, occasionally contacting the medial wall of the esophagus and the descending aorta. The SVC adopts an elliptical shape and its major axis is oriented obliquely toward the left (Fig. 8) [4]. These changes are not specific and can be seen occasionally in patients without azygos lobes.

The fissure is clearly visible and its morphology depends on the size of the lobe. It is C-shaped in larger lobes and straight or slightly undulated when the lobe is small. In the latter case, it may be seen as a double line on the chest radiograph (Fig. 9) [4]. The fissure ends anteriorly at the right brachiocephalic vein (RBV) and SVC, and posteriorly at the lateral aspect of the vertebral body near the location of the right superior intercostal vein.

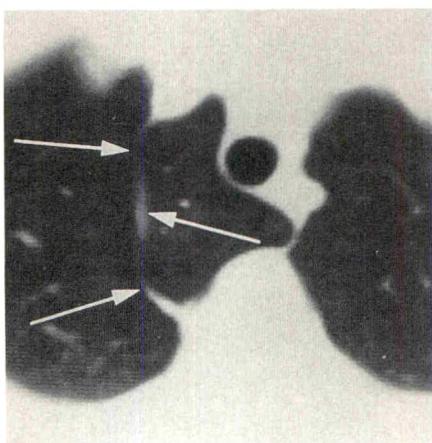
The azygos vein is seen as a thicker structure following the

same path as the fissure. The position of the arch is higher than when it follows an intramediastinal course [4]. The vein ends in the SVC and occasionally in the RBV (Fig. 10). In some patients, the undulated appearance of the posterior portion of the azygos arch may simulate a pulmonary nodule (Fig. 11) [4].

By using high-definition CT scan slices, we have found that the fissure does not terminate at the level of the azygos arch, but continues caudally, becoming shorter and ending at the mediastinal portion of the ascending azygos vein. This can be seen on the anteroposterior chest radiograph (Fig. 12).

RBV-SVC Complex

In some patients with an azygos lobe, the great right mediastinal veins can be seen on the anteroposterior chest radiograph. They are visible as tubular structures that follow an oblique course through the azygos lobe toward the me-

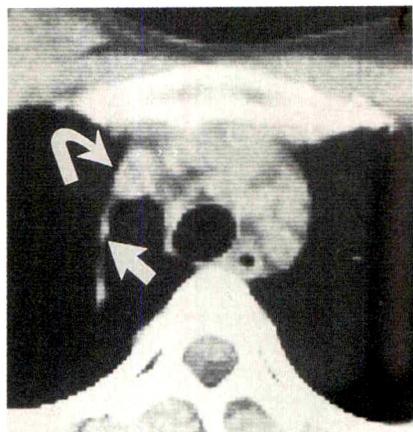


A



B

Fig. 9.—*A* and *B*, Undulation of azygos fissure (*A*, arrows) on CT scan, which appears as a double line (*B*, arrows) on chest radiograph, mimics a double azygos lobe.



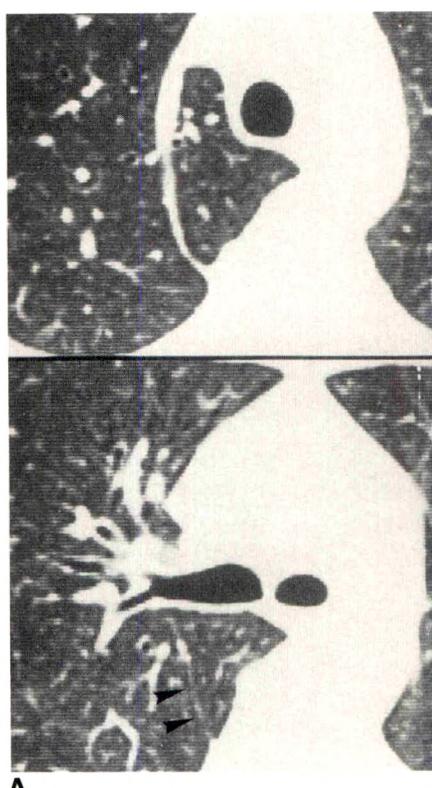
10



11

Fig. 10.—CT scan of azygos vein (straight arrow) draining into right brachiocephalic vein (curved arrow).

Fig. 11.—Undulation of azygos vein, which on a caudal CT scan simulates a pulmonary nodule (arrow). Pulmonary pseudonodule is due to undulation of posterior portion of azygos vein arch.



A



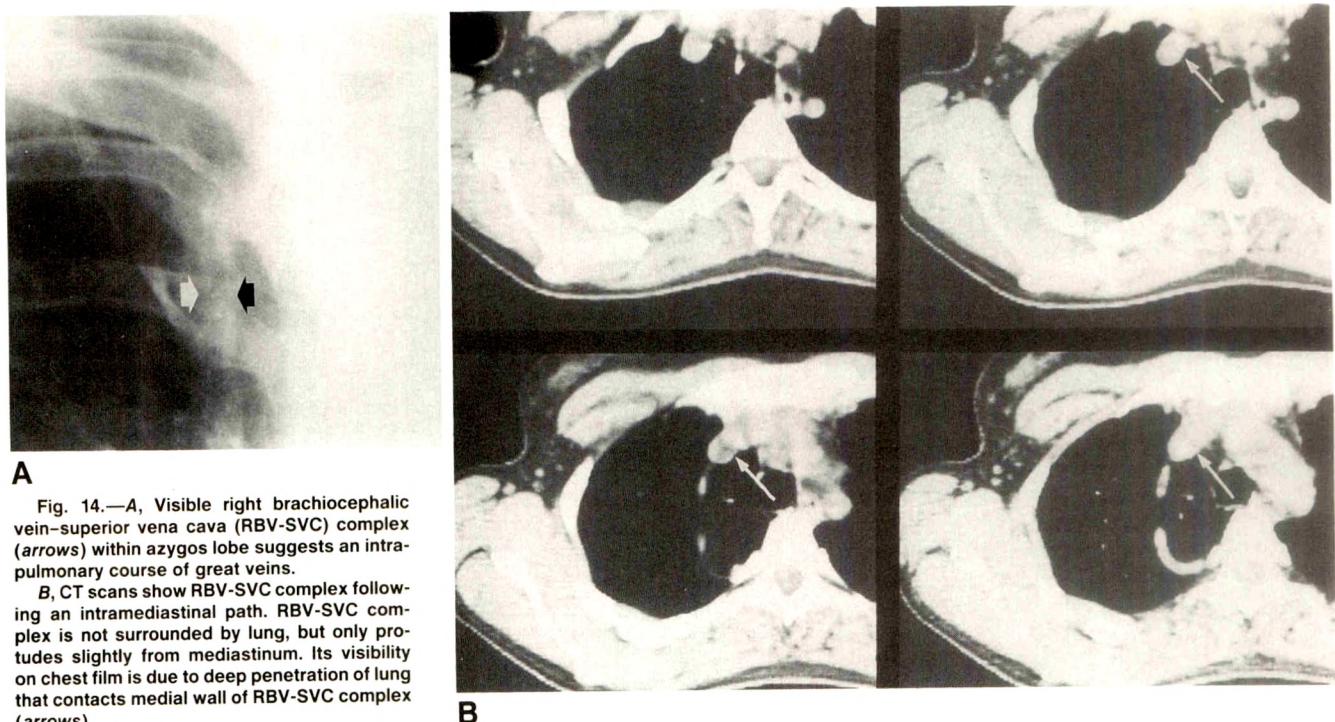
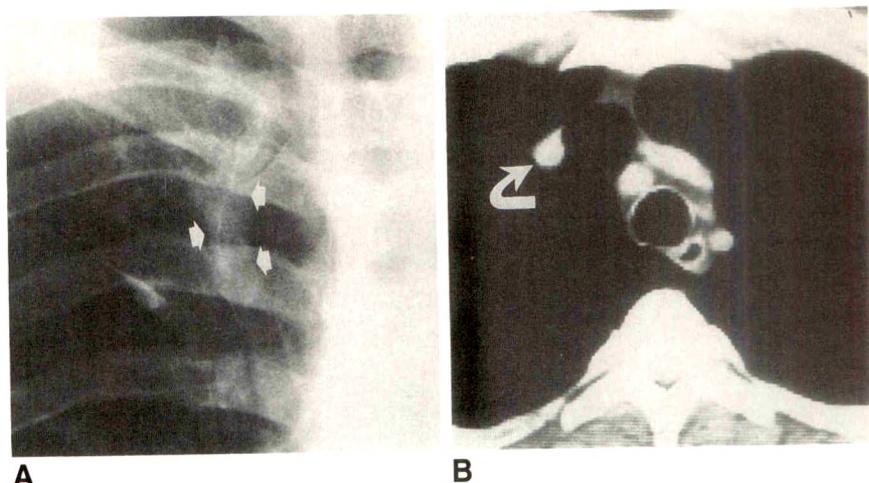
B

Fig. 12.—*A*, High-definition CT scans at supra- and infracarinal levels. Fissure (arrowheads) continues caudally, becoming shorter until it ends at mediastinum.

B, Fissure (straight arrow) is visible on chest radiograph. Azygos vein = curved arrow.

Fig. 13.—A, Chest radiograph shows a tubular structure (arrows) following an oblique course within azygos lobe.

B, CT scan shows right brachiocephalic vein (arrow) following an intrapulmonary course. (Reprinted with permission from Mata et al. [5].)



A

Fig. 14.—A, Visible right brachiocephalic vein—superior vena cava (RBV-SVC) complex (arrows) within azygos lobe suggests an intrapulmonary course of great veins.

B, CT scans show RBV-SVC complex following an intramedastinal path. RBV-SVC complex is not surrounded by lung, but only protrudes slightly from mediastinum. Its visibility on chest film is due to deep penetration of lung that contacts medial wall of RBV-SVC complex (arrows).

diastinum. A true intrapulmonary path is rare (Fig. 13) [5]. More often, the RBV-SVC complex follows an intramedastinal course, as is demonstrated by CT. In these cases, visibility of the RBV-SVC complex on the chest radiograph is due to the changes in the upper mediastinum brought about by the azygos lobe. This deep penetration of the lung medially, contacting the posterior and medial walls of the RBV-SVC complex, simulates an intrapulmonary course of these veins (Fig. 14).

We believe that the appearance of the RBV and SVC on the chest radiograph in patients with an azygos lobe reflects the variable relationship between these veins and their mediastinal attachments. In this regard, the intrapulmonary RBV, which is considered an isolated anomaly, would be the ex-

treme end of a spectrum of changes in which the intramedastinal course of the RBV-SVC complex would be the opposite extreme. Between these extremes are all possible pathways, some of which are visible on the anteroposterior chest radiograph (Fig. 15).

It should be pointed out that in some patients with an azygos lobe and a prominent RBV-SVC complex on CT scans, the chest radiograph appears normal and the veins are not visible (Fig. 16). That may be explained by the lenticular shape that the RBV-SVC complex adopts, which makes visualization of these veins difficult on anteroposterior radiographs. It may also reflect the difficulty of translating the findings from the supine CT scan to the upright chest radiograph.

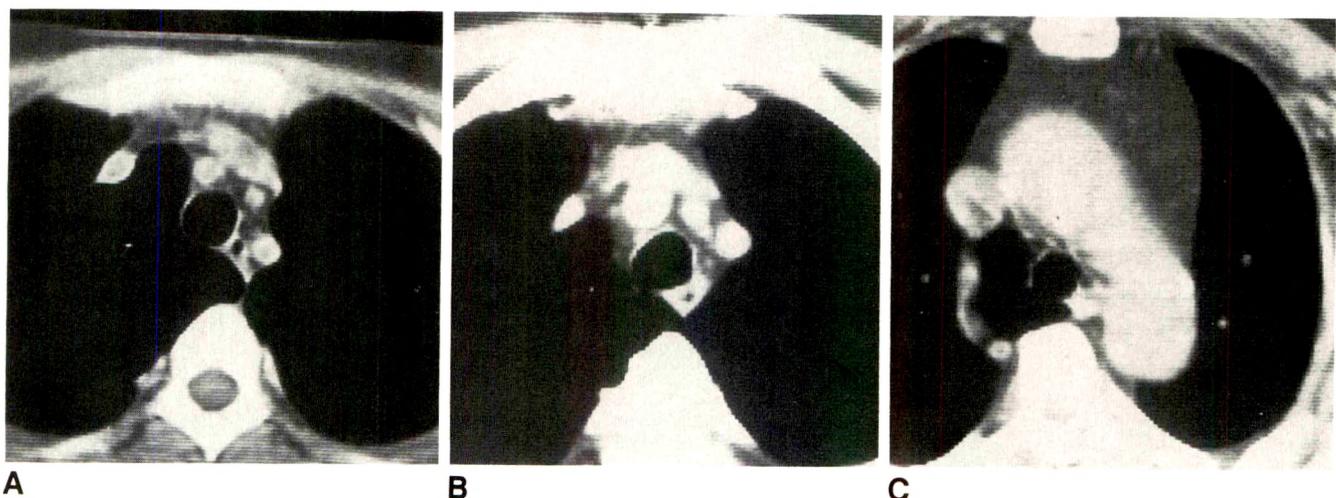


Fig. 15.—A-C, CT scans in three different patients show great variability that exists between right brachiocephalic vein-superior vena cava complex and its mediastinal attachments in patients with azygos lobe.

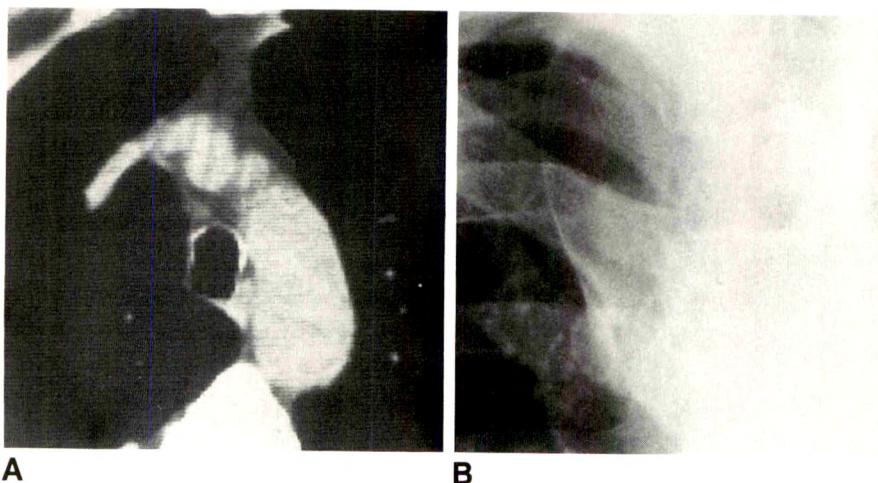


Fig. 16.—A and B, Prominent right brachiocephalic vein-superior vena cava complex on CT scan (A) is not visible on chest radiograph (B), possibly because of lenticular shape of veins, which do not cast a shadow on conventional radiograph.

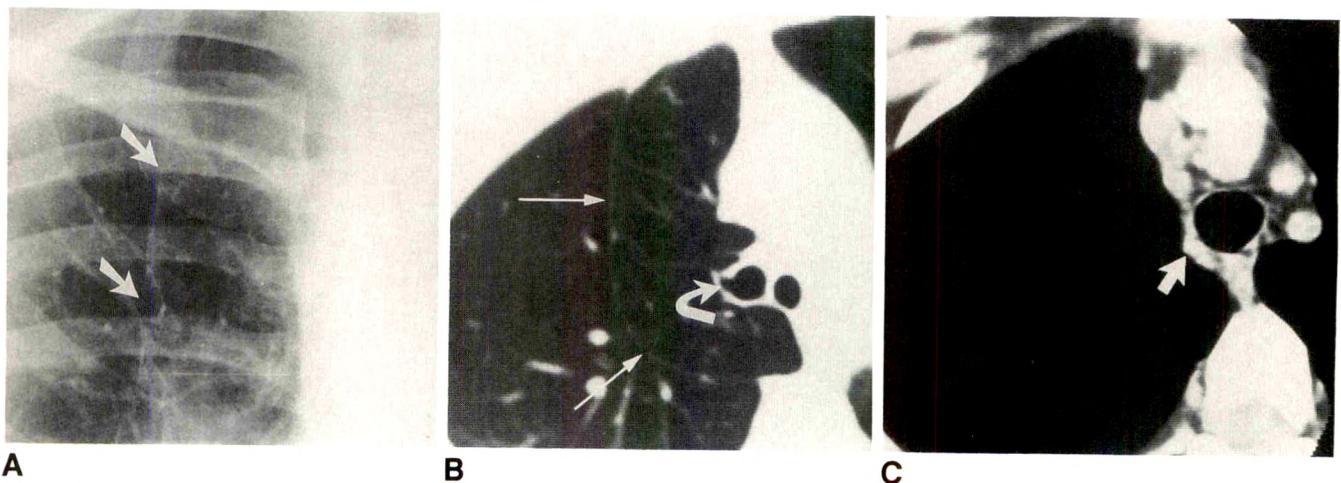


Fig. 17.—A, Radiograph of supernumerary fissure (arrows) simulating an azygous fissure. B, CT scan at level of bifurcation shows a tracheal bronchus (curved arrow). Anomalous fissure (arrows) ends in anterior chest wall. C, Cranial CT slice shows azygous arch (arrow) at its normal location.

False Azygos Lobe

The azygos fissure may be simulated by lines that occupy a similar position, such as scars, walls of bullae, displaced fissures, supernumerary fissures (Fig. 17). In such cases, identification of the azygos vein in its normal position, at the crotch (the angle between the trachea and the right bronchus), suggests the correct diagnosis [3]. This sign may fail, as the azygos arch is usually not visible on upright films [3]. If the question arises, CT may be helpful in excluding an azygos lobe by demonstrating the azygos vein at its normal location and identifying the underlying disease.

REFERENCES

1. Boyden EA. The distribution of bronchi in gross anomalies of the right upper lobe, particularly lobes subdivided by the azygos vein and those containing pre-arterial bronchi. *Radiology* **1952**;58:797-807
2. Heitzman ER. *The mediastinum: radiologic correlations with anatomy and pathology*, 2nd ed. Berlin: Springer-Verlag, **1988**:229-233
3. Felson B. The azygos lobe: its variation in health and disease. *Semin Roentgenol* **1989**;24:56-66
4. Speckman JM, Gamsu G, Webb WR. Alterations in CT mediastinal anatomy produced by an azygos lobe. *AJR* **1981**;137:47-50
5. Mata JM, Cáceres J, Llauger J, Palmer J. CT demonstration of intrapulmonary right brachiocephalic vein associated with an azygos lobe. *J Comput Assist Tomogr* **1990**;14:305-306

Plans for Radiology Centennial Celebration in 1995

John P. Tampas¹

The centennial year of the discovery of the X-ray, 1995, will be an opportunity for radiologists and other members of the radiologic community to tell the American public about the accomplishments of medical radiation science during 100 years of amazing progress.

The vehicle for the yearlong events planned for 1995 is Radiology Centennial, Inc. (RCI), an organization created for that purpose and sponsored by nearly 40 national societies, most of the leading companies in the field of radiology, and several federal agencies. RCI was organized in 1989 by the late Glen Hartman and others, working initially through the Intersociety Commission of the American College of Radiology. It is a not-for-profit corporation with directors named by each sponsor. It has been granted tax-exempt status by the Internal Revenue Service.

One of the earliest decisions made by RCI organizers is that the centennial celebration be a public one. It will be used as a framework for telling the story of modern radiology and remembering the achievements of its pioneers. Thus, the projects and committees are organized with two objectives. One is the creation of projects and events for the radiologic community. The other is public education for the entire nation. The RCI has named 11 committees to organize and carry out its activities.

RCI has projected a total expenditure of approximately \$3 million for its entire program. The RCI Industry Committee has received pledges of half of that from companies serving the radiologic community. A similar amount will be raised by solicitation from radiologists and their coworkers and societies.

The two management committees of the RCI are the Executive and Budget groups. The Executive Committee will be headed by President John P. Tampas of Burlington, VT. The Budget and Finance Committee is led by Robert Hattery, Jr., of Rochester, MN, RCI treasurer.

The Books Committee has projected the publication of five volumes about the history of radiology in this country and this century. Three volumes, one each on diagnosis, therapy, and basic radiation science, will be composed of contributed papers and are intended for the serious scholar. One book will be written by a science writer for general audiences and will trace the development of radiology. The fifth volume will be written for children, also by a science writer. All will be published by the beginning of 1995. Peter R. Almond of Louisville, KY, is the committee chairman.

The Exhibits Committee is working on exhibits to be used in various settings during the centennial year. In particular, a traveling exhibit is being designed that can be presented at the major radiologic society meetings during 1995. Many of the artifacts donated by the American Institute of Radiology to the Smithsonian Institution may be used in this traveling exhibit. The committee is also exploring the possibility of working with one or more museums on temporary exhibits. Also, it is preparing a set of simple exhibits that can be made available to radiology departments and practices for their own use during the centennial year. J. Frank Wilson of Milwaukee, WI, is

chairman of the Exhibits Committee.

The Industry Committee is composed of senior representatives of companies that have been members of the radiology family. It has two tasks: to coordinate the participation of companies and their employees in centennial projects and events and to coordinate the contributions that will help to support RCI activities. R. Barnes Parsons of Rochester, NY, is chairman of the committee.

The Lecture Series Committee has the task of working with participating societies to arrange suitable lectures and presentations at radiologic meetings during 1995. The committee will also develop slides and other speaking aids to help radiologists and coworkers make presentations in their communities during 1995. Beverly Wood of Los Angeles, CA, is the chairwoman of this committee.

The Radiology Art Committee will address the possibility of having exhibitions of art about radiology, radiology as an art form, and art by radiologists. Douglas MacEwan of Winnipeg, Manitoba, and A. Everette James, Jr., of Nashville, TN, are cochairmen. The Commemorative Stamp Committee will work with the U.S. Postal Service to encourage the issue of a radiology centennial stamp during 1995. Helen Redman of Dallas, TX, is chairwoman of the stamp group.

The Honors and Awards Committee will develop a series of honors suitable to the centennial and to those who participate in its activities. B. G. Brogdon of Mobile, AL, is the committee chairman. The International Relations Committee has the task of coordinating RCI projects with national centennial celebrations in other countries. For instance, German radiologists are planning recognition events. This committee, with Martin Donner of Baltimore, MD, as chairman, will recommend any RCI participation in other national events.

The Media Committee has the primary role of communicating about radiology and the importance of its history to the public. It will undertake a series of media relations efforts, including production of material for newspapers, magazines, television news and feature syndicates. It will also produce one or more videotapes suitable for use by television stations or interested groups. It will work with the Lecture Series Committee in developing support material for radiologists and others to use. A second task for this committee is the development of a teaching module about radiation science and medical radiology to be used in junior high school science classes. This effort could have the most lasting effect of any centennial activity. Anne Osborn of Salt Lake City, UT, is chairwoman of the media committee.

The members of the committees, subcommittees, and work groups have been chosen from those designated by the sponsoring societies and, recently, from volunteers. Many others will be needed to fill out committee ranks as more activities get under way. The American College of Radiology is providing the secretariat.

On behalf of radiology and its national organizations, participating companies, and other groups, RCI has been created and has been charged with the several missions defined here. The story of radiology, its past, its present, and its future, is worth the telling.

¹ President, Radiology Centennial, Inc., American College of Radiology, 1891 Preston White Dr., Reston, VA 22091.

Perspective

The Economic Implications of Radiologic Screening for Colonic Cancer

David W. Gelfand¹ and David J. Ott

Cancer of the colon and rectum is the second most common of the potentially lethal cancers, exceeded only by carcinoma of the lung. Relatively little progress toward decreasing the mortality rate from colonic cancer has been made in recent years, and it may be appropriate to examine the available means of screening asymptomatic persons for this disease. This presentation discusses the epidemiology and development of colonic cancer, the available means for its detection, and the economic implications of strategies for screening an asymptomatic population.

Epidemiology

Approximately 150,000 cases of colorectal cancer are diagnosed annually in the United States, resulting in an estimated 60,000 deaths [1]. The probability of a United States citizen developing colorectal cancer during their lifetime approximates 6%, and 3% are likely to die of the disease [2]. It is a disease of the elderly, with the median age at diagnosis of approximately 70 years [3, 4]. In persons 30–34 years of age, the annual incidence is only three per 100,000, whereas for persons 85 years or older, the annual incidence is 532 per 100,000 [4]. Colorectal cancers account for 15% of all malignancies and 13% of cancer deaths [1]. The total cost of colorectal cancer annually in the United States is estimated to be \$10 billion, of which \$2.5 billion represents actual medical costs [4].

Any program for systematic detection of colorectal cancer must be governed by assumptions about the natural history

of the disease and its curability when found in the early and later stages of development. The 5-year survival rate for early, localized colonic cancer is 87% and for rectal cancer is 79% [4]. This may be compared with an approximate 40% 5-year survival rate in patients with more advanced stages of the disease, when it is more typically first detected [4, 5].

Pathogenesis

Most colorectal cancers are thought to develop from preexisting areas of dysplasia or from adenomas. Development of clinically evident carcinoma of the colon is believed to undergo the following sequence of events: (1) development of adenoma or dysplasia, (2) growth of the dysplastic region or the adenoma to a critical mass of approximately 5 mm, and (3) invasion into the submucosa and lamina propria. Most authorities believe that the majority of colorectal cancers develop from preexisting adenomas and that the removal of adenomatous polyps potentially prevents the development of colorectal cancers [6, 7]. What remains unknown is the precise percentage of carcinomas developing from adenomatous polyps and the percentage of adenomatous polyps that may be expected to undergo malignant transformation.

Fecal Occult Blood Test

Four methods are available for detecting colorectal cancer in the context of a screening program: (1) examination of the

Received October 15, 1990; accepted after revision November 20, 1990.

¹Both authors: Department of Radiology, Bowman Gray School of Medicine, 300 S. Hawthorne Rd., Winston-Salem, NC 27103. Address reprint requests to D. W. Gelfand.

stool for blood, (2) rigid or flexible sigmoidoscopy, (3) radiologic examination of the colon, and (4) colonoscopy. Occult blood in the feces is usually detected with the common guaiac test, which detects a breakdown product of hemoglobin. Fecal occult blood testing is the most widely used means of detection of colorectal cancer and is both the least expensive and the least accurate method. Multiple samples are required, and red meat and foods with peroxidase activity may not be ingested for several days before each test. Even with full dietary compliance and acquisition of multiple stool samples, the fecal occult blood test will fail to detect the vast majority of colorectal adenomas and up to 50% of carcinomas [8]. In addition, a substantial number of false-positive results are generated, requiring radiologic or colonoscopic examination to exclude carcinoma. The most damning aspect of the use of fecal occult blood testing as the basic screening method for colorectal cancer is that when used alone it fails to detect 30–50% of malignant lesions.

Sigmoidoscopy

Sigmoidoscopy is now widely performed with flexible instruments of 35 or 60 cm length. Sigmoidoscopy with the 35-cm-long instrument requires approximately 5 min and will detect about 80% of those polyps seen with the 60-cm-long sigmoidoscope. The shorter instrument views the entire sigmoid colon in only 13% of the examinations. The 60-cm-long sigmoidoscope requires 8–10 min for examination and will view the entire sigmoid colon in approximately 80% of patients if the colon has been well cleansed [9]. However, only approximately 40% of colorectal cancers potentially lie within reach of even the 60-cm-long instrument. As an example, in a recent review of 174 colorectal carcinomas in our own institution, 77 (44%) were in the sigmoid colon and rectum [10], and it can be assumed that many of these would not be reached during sigmoidoscopy with some combination of 35-cm-long and 60-cm-long instruments.

Sigmoidoscopy may be used to supplement fecal occult blood testing in programs designed to screen for colorectal cancer. The current recommendation of the American Cancer Society suggests a combination of annual testing for fecal occult blood supplemented by sigmoidoscopy every 3–5 years. However, this combination of examinations is not inexpensive, and full compliance with the requirements of both fecal occult blood testing and sigmoidoscopy is unlikely in most patients being screened for colorectal neoplasms. More importantly, the combination of these two examinations is likely to fail to detect approximately $\frac{1}{3}$ to $\frac{1}{4}$ of all colorectal cancers in patients being screened. Despite the widespread availability of both sigmoidoscopy and fecal occult blood testing and their advocacy by the American Cancer Society for screening for colorectal cancer, little progress has been made in the early detection and cure of colorectal cancer in the United States in recent years.

An effective screening method for colorectal cancer must examine the entire colon and have a high accuracy for detecting any colorectal malignant tumor harbored by the patient at the time of screening. A further function of such a screening

examination would be to detect colorectal adenomas with the view of removing them as prophylaxis against future development of colorectal carcinoma. The two examinations currently available that can detect a neoplasm anywhere in the colon are the barium enema examination and colonoscopy. Each of these examinations has advantages and disadvantages as compared with the other. Both examinations could be the basis of a screening program for detection of colorectal cancer.

Barium Enema

The radiologic examination, or barium enema, has excellent accuracy in the detection of malignant lesions. Review of 19 English-language radiologic publications of the past decade (1980–1989) on the detection of colorectal cancer by barium enema shows that 15 of the 19 investigations had a radiologic sensitivity of 90–100% for detection of colorectal cancer, with a median sensitivity of 94% [11–29]. The radiologic literature indicates that there is little or no difference between single- and double-contrast barium examinations for detection of cancer [19]. Both examinations also exhibit similar sensitivity for the detection of polypoid lesions 1 cm or larger [11, 12]. However, the double-contrast examination appears to have greater sensitivity for lesions smaller than 1 cm. Typical sensitivities recorded in the recent radiologic literature are 95% sensitivity for detection of carcinoma, 80–95% for detection of polyps 1 cm or larger, and 50–85% for detection of polypoid lesions smaller than 1 cm.

The barium enema is less costly than colonoscopy, with an average reported cost of \$188 (range, \$144–\$240) [26, 30–34]. Complications and mortality rates in patients having barium enemas are reasonably low. Three published reviews with a total of 283,500 patients indicate a perforation rate of 1:10,000 and a mortality rate of 1:50,000 [35–37].

Colonoscopy

Colonoscopy is advocated by gastroenterologists as useful for screening for colorectal cancer. The endoscopic approach has the advantage of allowing biopsy of any suspicious lesion and removal of most polypoid adenomas during the diagnostic procedure. The preparation for colonoscopy is approximately as strenuous as that required for preparing the colon for barium enema. However, the examination is sufficiently painful for most patients that sedative and amnestic drugs must be administered in conjunction with the procedure.

Unfortunately, relatively few data on the accuracy of colonoscopy are available. Data that are available come from two sources: comparisons with lesions seen at barium enema examination and the recorded completion rate of colonoscopic examinations. Comparisons of colonoscopic polyp detection to lesions seen at barium enema have yielded fairly consistent results. Approximately 10–20% of colorectal lesions apparently are missed by colonoscopy [38–42]. Failure to diagnose these neoplasms is mostly due to failure to examine the right side of the colon to the cecum. For example, Thoeni and Menuck [38] found that 13% of adenomatous

polyps seen radiologically were undetected at colonoscopy. Three percent were missed in areas of the colon traversed by the instrument, whereas 10% were located in areas never reached by the colonoscope. This observation correlates well with the known rate of incomplete colonoscopies. The largest review to date indicates that approximately 25% of attempted complete colonoscopies fail to reach the cecum. However, there are reports of failure rates as high as 45% [43]. As a general rule, the average percentage of the colon unseen at colonoscopy is approximately half the percentage of incomplete colonoscopies [44].

The cost of colonoscopy has averaged approximately three times that of the barium enema during the past two decades. For diagnostic colonoscopy, excluding any cost of biopsies, published fees have averaged \$555 (range \$423-\$750) [26, 30-34]. More importantly, the high complication and mortality rates of colonoscopy probably preclude the use of this instrument as a primary screening method for colorectal carcinoma in asymptomatic persons. In a recent review of 100,773 diagnostic colonoscopies reported in the literature, hemorrhage and perforation occurred in 1:3600 and 1:600 examinations, respectively, and the mortality rate was 1:5000 [45]. According to published reports, the complication and mortality rates of colonoscopy have not been falling as greater experience with the instrument has been gained.

The additional costs and complications of colonoscopy as compared with the radiologic examination of the colon can be put into perspective if one considers the effect of substituting colonoscopy for the barium enema in the approximately 5 million barium enema examinations currently performed in the United States annually, most of which are performed for the detection or exclusion of colonic neoplasm [46]. Based on the conservative figures for the average cost of colonoscopy and barium enema stated above, the additional direct expense for colonic examinations would be increased by approximately \$1.75 billion annually if all examinations were initially performed by colonoscopy. Furthermore, approximately 10,000 additional colonic perforations and 1000 additional fatal complications attributable to colonoscopy would occur annually [47].

Screening Strategies

Available screening tests for colorectal cancer have been evaluated for cost-effectiveness by David M. Eddy, of the Center for Health Policy Research and Education of Duke University, using a mathematical model that synthesizes available indirect evidence, because sufficient direct evidence is not available [48, 49]. The estimations incorporate judgments and data concerning the following: (1) incidence rates of colorectal cancer, (2) natural history of colorectal cancer, (3) distribution of colorectal cancer, (4) sensitivity of available tests, (5) stage-specific survival rates, (6) death from other causes. Eleven possible screening strategies that use various combinations of fecal occult blood testing, sigmoidoscopy, barium enema examination, and colonoscopy were evaluated for their projected cost-effectiveness.

The results of Eddy's investigation can be presented in the

form of a graph (Fig. 1) that plots the discounted net financial cost in dollars (which considers inflation and the time value of money) on the x-axis against the decrease in probability of death from colorectal cancer on the y-axis. This graph demonstrates that the most cost-effective strategies are those that use the barium enema examination to examine the entire colon every 3 to 5 years, supplemented by a yearly fecal occult blood test. These prove to be considerably more cost-effective than strategies involving use of colonoscopy. This is primarily a function of the three times greater average cost of colonoscopy vs the barium enema examination. The estimates arrived at by Eddy suggest that the most cost-effective of the 11 strategies, involving a barium enema every 5 years and fecal occult blood testing yearly, is projected to be as effective or more effective in decreasing the probability of a death by cancer as is screening mammography at approximately the same annual cost [49, 50].

Several conclusions are drawn by Eddy from the data summarized here. First, screening for carcinoma of the colon and rectum can be both effective and cost-effective if the screening strategy is carefully chosen. Second, although the common use of the fecal occult blood test alone is simple and convenient, strategies that use examination of the entire colon are more than twice as effective in the detection of colonic cancer, although at higher cost. Third, strategies that examine the entire colon also have a far greater ability to detect adenomas and thus are more effective at preventing the development of malignant tumors. Fourth, considering the slow growth of the typical colonic carcinoma, a 3- to 5-year examination interval for barium enema or colonoscopy preserves approximately 90% of the effectiveness of annual examinations, greatly decreasing cost and inconvenience. Fifth, if a periodic barium enema examination is used as the screening method, routine sigmoidoscopic examination adds very little to the effectiveness of the strategy while greatly

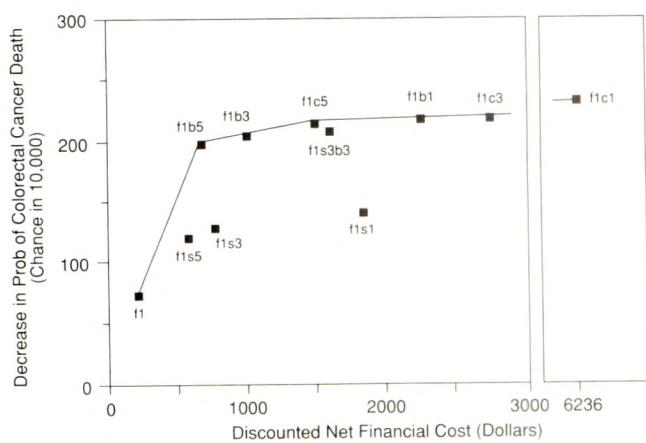


Fig. 1.—Cost-effectiveness of 11 colorectal cancer screening strategies, based on an average-risk 50-year-old man, from age 50 to 75. Discounted net financial cost in dollars is plotted on x-axis against decrease in probability of death from colorectal cancer on y-axis. f = fecal occult blood test, s = flexible sigmoidoscope, b = barium enema, c = colonoscopy, 1 = every year, 3 = every 3 years, 5 = every 5 years. (Redrawn from Eddy [49].)

increasing costs. Sixth, although colonoscopy and barium enema examination have comparable abilities to detect colonic malignant tumors, colonoscopy costs approximately twice as much as the barium enema examination even when the necessity for reexamination of a minority of patients with colonoscopy is considered. Finally, it can be added that the barium enema is an order of magnitude safer.

Screening of persons at high risk for colorectal cancer is likely to be particularly cost-effective. It has been found, for example, that patients with first-degree relatives (parents and siblings) with a history of colonic cancer have at least twice the chance of developing colorectal cancer as the general population, and approximately half of all colorectal cancers occur in such high-risk persons [51]. Screening of such asymptomatic high-risk persons is therefore likely to be twice as cost-effective as screening the general population. Stated in another way, the cost per additional year of life expectancy for screening a high-risk person is half that for the general population.

Recommendation

Based on the age-incidence of colonic adenomas and colorectal cancer, an appropriate screening strategy would be examination of the colon by barium enema examination every 5 years commencing at age 40–50, supplemented by a yearly test for fecal occult blood, to be continued through the remaining life of the person. This strategy is particularly appropriate for high-risk persons with a family history of colorectal cancer. In high-risk persons, the strategy is likely to be several times as cost-effective in decreasing the probability of death from cancer than are current mammographic screening programs. A similar screening strategy for the population as a whole would be less cost-effective, but still at least as cost-effective as mammographic screening. On the basis of these calculations, initial screening programs for high-risk persons based on the radiologic examination of the colon should be instituted to collect the data necessary to verify (or disprove) these projections.

In conclusion, the medical community currently finds itself at somewhat of an impasse regarding screening methods for colorectal cancer. As seen from several viewpoints, it is apparent that the present screening strategy suggested by the American Cancer Society is one of the least effective and least cost-effective of the many possible screening strategies. Accordingly, there has been relatively little impact by fecal occult blood testing and sigmoidoscopy on the overall death rate from colorectal cancer. Radiologists should take the initiative in more thoroughly exploring use of the radiologic examination of the colon as an effective means of screening for colorectal cancer that is reasonable in cost, far safer than any alternative method of examining the entire colon, and universally available.

REFERENCES

- Silverberg E, Lubera JA. Cancer statistics, 1989. CA **1989**;39:3–20
- Seidman H, Mushinski MH, Gelb SK, Silverberg E. Probabilities of eventually developing and dying of cancer: United States, 1985. CA **1985**;35:36–56
- Bresalier RS, Kim YS. Malignant neoplasms of the large and small intestine. In: Slesinger MH, Fordtran JS, eds. *Gastrointestinal disease*, vol. 2, 4th ed. Philadelphia: Saunders, **1989**:1519–1560
- Dodd GD. Epidemiology and economic impact of colon cancer. In: Gelfand DW, Laufer I, eds. *Colonic cancer: diagnosis in an era of cost containment*. Reston, VA: American College of Radiology, **1991**
- Fleischer DE, Goldberg SB, Browning TH, et al. Detection and surveillance of colorectal cancer. JAMA **1989**;261:580–585
- Muto T, Bussey HJR, Morson BC. The evolution of cancer of the colon and rectum. Cancer **1975**;36:2251–2270
- Gilbertson VA, Nelms JM. The prevention of invasive carcinoma of the rectum. Cancer **1978**;41:1137–1139
- Songster CL, Barrows GH, Jarrett DD. Immunochemical detection of fecal occult blood—the fecal smear punch-disc test: a new non-invasive screening test for colorectal cancer. Cancer **1980**;45:1099–1102
- Sivak MV. Flexible sigmoidoscopy. In *Gastroenterologic endoscopy*. Philadelphia: Saunders, **1987**
- Gelfand DW, Chen YM, Ott DJ. Radiologic detection of colonic neoplasms: benefits of a systems-analysis approach. AJR **1991**;156:303–306
- Ott DJ, Chen YM, Gelfand DW, Wu WC, Munitz HA. Single-contrast vs. double-contrast barium enema in the detection of colonic polyps. AJR **1986**;146:993–996
- Gelfand DW, Chen YM, Ott DJ. Detection of colonic polyps on single-contrast barium enema study: emphasis on the elderly. Radiology **1987**;164:333–337
- Ott DJ, Scharling ES, Chen YM, Wu WC, Gelfand DW. Barium enema examination: sensitivity in detecting colonic polyps and carcinomas. South Med J **1989**;82:197–200
- Ott DJ, Gelfand DW, Wu WC, Kerr RM. Sensitivity of double-contrast barium enema: emphasis on polyp detection. AJR **1980**;135:327–330
- Kelvin FM, Gardiner R, Vas W, Stevenson GW. Colorectal carcinoma missed on double contrast barium enema study: a problem in perception. AJR **1981**;137:307–313
- Bloomfield JA. Reliability of barium enema in detecting colonic neoplasia. Med J Aust **1981**;1:631–633
- Kaude JV, Harty RF. Sensitivity of single contrast barium enema with regard to colorectal disease as diagnosed by colonoscopy. Europ J Radiol **1982**;2:290–292
- Thoeni RF, Petras A. Detection of rectal and rectosigmoid lesions by double-contrast barium enema examination and sigmoidoscopy. Radiology **1982**;142:59–62
- Johnson CD, Carlson HC, Taylor WF, Weiland LP. Barium enemas of carcinoma of the colon: sensitivity of double- and single-contrast studies. AJR **1983**;149:1143–1149
- Thoeni RF, Venbrux AC. The value of colonoscopy and double-contrast barium-enema examinations in the evaluation of patients with subacute and chronic lower intestinal bleeding. Radiology **1983**;146:603–607
- Fork FT, Lindstrom C, Ekelund G. Double contrast examination in carcinoma of the colon and rectum. Acta Radiol Diagn **1983**;24:177–188
- Beggs I, Thomas BM. Diagnosis of carcinoma of the colon by barium enema. Clin Radiol **1983**;34:423–425
- Myllyla V, Paavansalo M, Laitinen S. Sensitivity of single and double contrast barium enema in the detection of colorectal carcinoma. Fortschr Geb Rontgenstr Nuklearmed Erganzungsband **1984**;140:393–397
- Baker SR, Alterman DD. False-negative barium enema in patients with sigmoid cancer and coexistent diverticula. Gastrointest Radiol **1985**;10:171–173
- Brekkan A, Kjartansson O, Tulinius H, Sigvaldason H. Diagnostic sensitivity for x-ray examination of the large bowel in colorectal cancer. Gastrointest Radiol **1983**;8:363–365
- Feczkó PJ, Halpert RD. Reassessing the role of radiology in hemoccult screening. AJR **1986**;146:697–701
- Jensen J, Kewenter J, Haglind E, Lycke G, Svensson C, Ahren C. Diagnostic accuracy of double-contrast enema and rectosigmoidoscopy in connection with faecal occult blood testing for the detection of rectosigmoid neoplasms. Br J Surg **1986**;73:961–964
- Hallman JR, Howland WJ, Wolf BH. Retrospective review of the sensitivity of barium enema examination in a community hospital setting. Ohio St Med J **1986**;82:126–130

29. Bolin S, Franzen L, Nilsson E, Sjodahl R. Carcinoma of the colon and rectum. *Cancer* **1988**;61:1999-2008
30. Barry JM, Mulley AG, Richter JM. Effect of workup strategy on the cost-effectiveness of fecal occult blood screening for colorectal cancer. *Gastroenterology* **1987**;93:301-310
31. Ott DJ, Gelfand DW, Chen YM, Munitz HA. Colonoscopy and the barium enema: a radiologic viewpoint. *South Med J* **1985**;78:1033-1035
32. Bradeau ML, Eddy DM. The workup of the asymptomatic patient with a positive fecal occult blood test. *Med Decis Making* **1987**;7:32-46
33. England WL, Halls JJ, Hunt VB. Strategies for screening for colorectal carcinoma. *Med Decis Making* **1989**;9:3-13
34. Eddy DM, Nugent FW, Eddy JF, et al. Screening for colorectal cancer in a high-risk population: results of a mathematical model. *Gastroenterology* **1987**;92:682-692
35. Masel H, Masel JP, Casey KV. A survey of colon examination techniques in Australia and New Zealand with a review of complications. *Australas Radiol* **1971**;15:140-147
36. Gardiner H, Miller RE. Barium peritonitis: a new therapeutic approach. *Am J Surg* **1973**;125:350-352
37. Han SY, Tishler JM. Perforation of the colon above the peritoneal reflection during the barium-enema examination. *Radiology* **1982**;144:253-255
38. Thoeni RF, Menuck L. Comparison of barium enema and colonoscopy in the detection of small colonic polyps. *Radiology* **1977**;124:631-635
39. Thoeni RF, Petras A. A double-contrast barium-enema examination and endoscopy in the detection of polypoid lesions in the cecum and ascending colon. *Radiology* **1982**;144:257-260
40. Fork FT. Double contrast enema and colonoscopy in polyp detection. *Gut* **1981**;22:971-977
41. Laufer I, Smith NCW, Mullens JE. The radiological demonstration of colorectal polyps undetected by endoscopy. *Gastroenterology* **1976**;70:167-170
42. Leinicke JL, Dodds WJ, Hogan WJ, et al. A comparison of colonoscopy and roentgenography for detecting polypoid lesions of the colon. *Gastrointest Radiol* **1977**;2:125-128
43. Aldridge MC, Sim AJW. Colonoscopy findings in symptomatic patients without x-ray evidence of colonic neoplasms. *Lancet* **1986**;2:833-834
44. Gelfand DW, Wu WC, Ott DJ. The extent of successful colonoscopy: its implication for the radiologist. *Gastrointest Radiol* **1979**;4:75-78
45. Habr-Gama A, Waye JD. Complications and hazards of gastrointestinal endoscopy. *World J Surg* **1989**;13:193-201
46. Johnson JL, Abernathy DL. Diagnostic imaging procedure volume in the United States. *Radiology* **1983**;146:851-853
47. Ott DJ. Complications and costs of radiologic and endoscopic examinations of the colon. In: Gelfand DW, Laufer I, eds. *Colonic cancer: diagnosis in an era of cost containment*. Reston, VA: American College of Radiology, 1991
48. Eddy DM. Benefits and costs of screening for colorectal cancer. In: Gelfand DW, Laufer I, eds. *Colon cancer: diagnosis in an era of cost containment*. Reston, VA: American College of Radiology, 1991
49. Eddy DM. Screening for breast cancer. *Ann Intern Med* **1989**;111:389-399
50. Eddy DM. Screening for colorectal cancer. *Ann Intern Med* **1990**;113:373-384
51. Guillen JG, Neugot AI, Forde KA, Waye JD, Treat MR. Colonic neoplasms in asymptomatic first-degree relatives of colon cancer patients. *Am J Gastroenterol* **1988**;83:271-273

Countdown to Discovery

Ronald L. Eisenberg¹ and Philip C. Goodman²

The Radiology Centennial, Inc., is preparing a variety of activities for the celebration of the 100th anniversary of Roentgen's 1895 discovery of X-rays (see p. 938). This is the first of a series of short articles describing some important and some curious events that occurred 100 years ago. In addition to describing the activities of Roentgen and other pioneers in physics that led to this epochal discovery, these articles will describe other major advances in medicine during that period and give the reader some understanding of what was happening throughout the world in politics, new inventions, the arts, and daily life.

As the final decade of the 19th century began, the Industrial Revolution was in full swing. In the United States, the long tradition of fear of monopoly and the astonishing growth of big business after the Civil War led to congressional passage of the Sherman Antitrust Act, designed to combat the new corporate conglomerates. Benjamin Harrison was in the White House after defeating Grover Cleveland in an election in which Harrison lost the popular vote but was victorious in the electoral college. Only 1 year before, more than 2000 residents of western Pennsylvania died in the catastrophic Johnstown flood. With the addition of Idaho and Wyoming as the 43rd and 44th states, the United States population reached 63 million. Two thirds of its citizens lived in rural communities, down from 90% a half century earlier. Average life expectancy jumped to more than 42 years.

New inventions were being developed rapidly. In 1890, peanut butter was invented by a physician in St. Louis, the first aluminum saucepan was produced, and unsweetened condensed milk was introduced commercially. Many American communities now required all milk to be pasteurized, a procedure some dairy interests fiercely attacked as "unnatural." In Toronto, a local pharmacist opened a small plant to manufacture carbonated water for sale to drugstores as a mixture for fruit juices and flavored extracts, calling his product Canada Dry ginger ale. A Manila brewer introduced San Miguel beer, and Thomas Lipton entered the tea business to ensure that supplies of tea were available at low cost for his 300 grocery shops. The first commercial dry-cell battery was introduced under the name Ever Ready [1].

In the world of medicine, rubber gloves were used for the first time during surgery at Johns Hopkins Hospital in Baltimore. The first tetanus and diphtheria antitoxins were produced in Berlin by the bacteriologist Emil von Behring. In New York, a new law required physicians to apply prophylactic drops to the eyes of newborn infants to combat the blindness caused by gonococcal infection. Other notable achievements were the construction of the first entirely steel-framed building in Chicago and the founding of the Daughters of the American Revolution in Washington, DC [1].

In events around the world, Bismarck was dismissed by Kaiser Wilhelm II in Germany, Cecil Rhodes became premier of Cape Colony (South Africa), Luxembourg separated from the Netherlands, the first general election was held in Japan, and the Swiss government introduced social insurance [2]. Two World War II heroes, Dwight D. Eisenhower and Charles de Gaulle, were born in 1890, one year after the birth of Adolph Hitler. The Indian leader Sitting Bull was killed in the Sioux uprising.

In the arts, Ibsen wrote *Hedda Gabler*, Tolstoy penned *The Kreutzer Sonata*, William James wrote *The Principles of Psychology*, and the first moving picture shows appeared in New York. Cézanne painted *The Card Players*, and Vincent Van Gogh ended his life at age 37. 1890 saw the first performances of Tchaikovsky's *Sleeping Beauty*, Richard Strauss's *Death and Transfiguration*, Borodin's *Prince Igor*, and Pietro Mascagni's *Cavalleria Rusticana* [2].

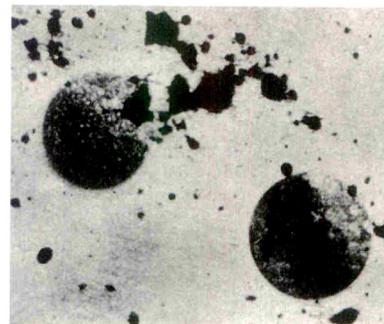


Fig. 1.—X-ray shadow picture, A. W. Goodspeed, February 22, 1890. (Courtesy of Burndy Library.)

In Philadelphia, Professor Arthur W. Goodspeed of the University of Pennsylvania was demonstrating the properties of a Crookes cathode-ray tube to William Jennings, a photographer. Next to the tube, Jennings had stacked several unexposed photographic plates, on top of which were two coins, reportedly his fare for the Woodland Ave. trolley. When Jennings later developed the plates, some were mysteriously fogged, and one showed two dark round disks as well as the usual tracing of electric sparks on the negative (Fig. 1). This curious shadowgraph could not be explained, and so the plates were filed away and forgotten for 6 years. At that time, Goodspeed and Jennings recreated the events of that night and grasped the magnitude of the observation that they had failed to make [3].

Half a world away, Ludwig Zehnder, an assistant physicist in Würzburg, Germany, was using black cloth to cover a vacuum tube to eliminate the disturbing light emanating from the cathode. He hoped to detect fluorescence of the screen not only nearby but also at some distance from the tube. When Zehnder turned the current on, he noticed a momentary flash where the remote screen was lying, but the tube was immediately punctured. Zehnder felt terribly upset and was willing to replace the tube at his own expense. His professor, however, consoled Zehnder with the prophetic remark, "Many more tubes will have to be punctured before all their mysteries are solved." Five years later, Zehnder, while making no claim to the discovery of X-rays, recalled the incident [4].

Zehnder's professor was a 45-year-old man from Lennep, a small town on the lower Rhine, who had assumed the prestigious post as director of the new Physical Institute of the University of Würzburg on October 1, 1888. Ironically, the professor had begun work at the university 18 years before, but his inadequate formal education had precluded his appointment to a salaried position on the faculty.

Five years later, after 20 years of intense scientific research and a newfound interest in the property of gases under high vacuum, this professor became a household word virtually overnight. Unlike several others with similar experiences, he was able to appreciate the significance of his observation and design a brilliant series of experiments to explain the phenomenon. Thus, Hugo Münsterberg's observation that "chance favors the prepared mind" was well proved by Wilhelm Conrad Roentgen and his discovery of "a new kind of ray."

REFERENCES

- Trager J. *The people's chronology*. New York: Holt, Rinehart & Winston, 1979
- Grun B. *The timetables of history*. New York: Simon and Schuster, 1979
- Brecher R, Brecher E. *The rays: a history of radiology in the United States and Canada*. Baltimore: Williams & Wilkins, 1969
- Kraft E. W. C. Roentgen: his friendship with Ludwig Zehnder. *NY State J Med* 1973;73:1002-1008

¹ Department of Radiology, Louisiana State University Medical Center, 1501 Kings Highway, Shreveport, LA 71130. Address reprint requests to R. L. Eisenberg.

² Department of Radiology, San Francisco General Hospital, 1001 Potrero Ave., San Francisco, CA 94110.

Sonography of the Gallbladder: Significance of Striated (Layered) Thickening of the Gallbladder Wall



Sharlene A. Teeffey¹
Richard L. Baron¹
Stephen A. Bigler²

Sonographic identification of thickening of the gallbladder wall that consists of multiple striations (alternate hypoechoic and hyperechoic layers) has been considered strong evidence of the presence of acute cholecystitis. We studied 27 patients in whom sonograms showed striated thickening of the gallbladder wall to determine the diagnostic significance of this finding. Striations were classified as focal or diffuse. Sonograms were correlated with pathologic findings in 16 patients and with clinical diagnoses and laboratory findings in 11. Patients were categorized as having cholecystitis with or without gangrene or edema of the gallbladder wall unrelated to gallbladder disease. Striated thickening of the gallbladder wall was due to cholecystitis in 10 patients, and all 10 had gangrenous changes at surgery or at pathologic examination. Striations were focal in eight of these patients and diffuse in two. Striated thickening of the gallbladder wall was due to edema of the wall unrelated to gallbladder disease in 17 patients. Causes included congestive heart failure ($n = 4$), renal failure ($n = 5$), liver disease (hepatic failure [$n = 1$], hepatitis [$n = 6$]), ascites ($n = 2$), hypoalbuminemia ($n = 3$), pancreatitis ($n = 1$), blockage of the lymphatic/venous drainage of the gallbladder ($n = 2$), and prominent Rokitansky-Aschoff sinuses ($n = 1$). More than one abnormality was present in five patients. Striations were focal in 11 of these patients and diffuse in six.

The sonographic finding of striated gallbladder wall thickening is no more specific for cholecystitis than the observation of gallbladder wall thickening by itself, and it may occur in a variety of diseases. However, in the clinical setting of acute cholecystitis, the presence of striations suggests gangrenous changes in the gallbladder. The extent of the striations (focal or diffuse) is not useful in predicting the cause of the striated gallbladder wall thickening.

AJR 156:945-947, May 1991

Several reports indicate that sonographic evidence of gallbladder wall thickening may be due to a variety of disorders not directly related to gallbladder disease [1-7]. However, a recent report suggests that gallbladder wall thickening consisting of multiple striations (alternate hyperechoic and hypoechoic layers) is indicative of the presence of acute cholecystitis [8]. We studied 27 patients with striated thickening of the gallbladder wall on sonograms to determine the diagnostic significance and specificity of this finding.

Materials and Methods

We reviewed the reports of 7300 nonobstetric sonograms obtained at Seattle Veterans Affairs Medical Center between July 1986 and February 1990. Sonograms of 128 patients in whom the sonograms were reported to show gallbladder wall thickening were reviewed. In 27 of these, sonography showed gallbladder wall thickening with a striated appearance. Striations were defined as sonolucent bands separated by echogenic zones forming layers in the gallbladder wall. All 27 patients were men between 30 and 81 years old.

Clinical records were reviewed to determine the presence of abnormalities known to cause gallbladder wall thickening (congestive heart failure, renal failure, hepatitis, cirrhosis, ascites,

Received September 21, 1990; accepted after revision December 26, 1990.

¹ Department of Radiology, University of Washington School of Medicine, Seattle, WA 98105. Address reprint requests to S. A. Teeffey, Seattle Veterans Affairs Medical Center, 1660 S. Columbian Way, Seattle, WA 98108.

² Department of Pathology, University of Washington School of Medicine, Seattle, WA 98105.

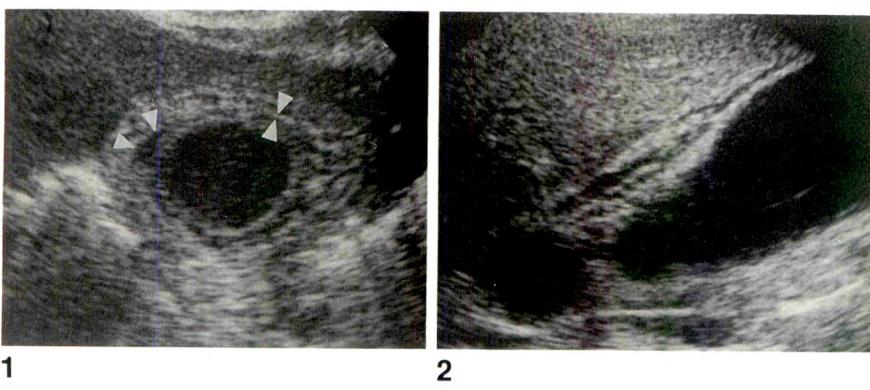


Fig. 1.—75-year-old man with pancreatitis who underwent cholecystectomy. Sonogram shows diffuse striations as multiple hypoechoic layers (arrowheads) separated by echogenic zones. Histologic examination of gallbladder showed a well-preserved mucosa and no evidence of wall inflammation; however, serosa was thickened and had appearance of granulation tissue. Striations were thought to be due to reactive changes in serosa from pancreatitis.

Fig. 2.—41-year-old man who underwent cholecystectomy. Histologic examination of gallbladder revealed gangrenous changes. Sonogram shows focal, striated thickening of gallbladder wall adjacent to hepatic surface.

and hypoalbuminemia). If the patient had a cholecystectomy, cholecystostomy, or autopsy, the pathologic findings in the gallbladder were determined. Histologic slides of the gallbladder were reviewed. Gangrenous cholecystitis was diagnosed if there was coagulative necrosis in addition to severe, acute, or chronic inflammation.

All sonograms were performed in real time by using an ATL (Advanced Technology Laboratories, Bellevue, WA) Ultramark 8 scanner ($n = 22$) or a Diasonic DRF 400 scanner (Diasonics Corp., Milpitas, CA) ($n = 5$).

Static images from the sonographic studies were reviewed for the presence of gallbladder wall thickening greater than 3 mm and for the presence of striations in the wall (multiple hypoechoic layers separated by echogenic zones) (Fig. 1) [8]. A determination was made of whether the striations were focal or diffuse.

Sonographic findings were correlated with pathologic findings after cholecystectomy, cholecystostomy, or autopsy in 16 of the 27 patients. In the other 11 patients, sonographic findings were correlated with the clinical diagnoses and laboratory findings. Patients were placed into one of two groups: (1) those with cholecystitis with or without gangrene or (2) those with edema of the gallbladder wall unrelated to gallbladder disease.

Results

Striated thickening of the gallbladder wall was due to cholecystitis in 10 patients, nine of whom underwent cholecystectomy. Histologic examination of the gallbladder revealed gangrenous changes in all nine patients. Acute inflammation was present in seven of these patients and chronic inflammation in two. The tenth patient had operative placement of a cholecystostomy tube at which time gangrenous changes were observed. No patient had cholecystitis without gangrenous changes. Striated thickening of the gallbladder wall was focal (Fig. 2) in eight of the patients with gangrenous cholecystitis and diffuse in two. Gallbladder wall thickening ranged from 5 to 12 mm.

Striated thickening of the gallbladder wall was due to edema of the wall unrelated to gallbladder disease in 17 patients. Review of the clinical records of six of these patients showed multisystem disease including congestive heart failure ($n = 4$), renal failure ($n = 3$), ascites ($n = 2$), and hypoalbuminemia ($n = 2$). More than one abnormality was present in three patients. Pathologic examination of the gallbladder in one of these patients with profound hypoalbuminemia showed no evidence of cholecystitis. Follow-up of four patients from 2

months to 2 years supported these clinical findings and showed no evidence of interval development of biliary tract disease. The sixth patient died of unrelated causes 11 days after the sonographic study, and an autopsy was not performed.

Striated thickening of the gallbladder wall was due to hepatitis in six patients. Four had clinical and laboratory evidence of alcoholic hepatitis and two of viral hepatitis (Figs. 3A and 3B). Follow-up of patients from 4 months to 2 years supported these clinical findings and showed no evidence of interval development of biliary tract disease.

Pathologic correlation was available in five patients with edema of the gallbladder wall unrelated to gallbladder disease. In three of these cases, findings at autopsy did not reveal the gallbladder wall abnormalities noted at sonography. Clinical diagnoses in these three cases included renal and hepatic failure, hepatic venoocclusive disease, and cholangiocarcinoma remote from the gallbladder. Autopsy performed three to 16 days after the sonograms revealed a normal gallbladder in these three cases. In the two remaining cases, clinical, operative, and pathologic correlation suggested unusual causes of striated thickening of the gallbladder wall. The first patient had pancreatitis (Fig. 1). The second patient with chronic renal failure and hypoalbuminemia (1.6 g/dl) underwent cholecystectomy for suspected cholecystitis. At surgery, the gallbladder wall showed moderate edema. Histologic examination of the gallbladder showed preservation of the mucosa, prominent Rokitansky-Aschoff sinuses, a thickened muscularis, and no evidence of inflammatory changes.

Striated thickening of the gallbladder wall was focal in 11 of the patients with edema of the gallbladder wall unrelated to gallbladder disease and diffuse in six. Gallbladder wall thickening ranged from 4 to 14 mm.

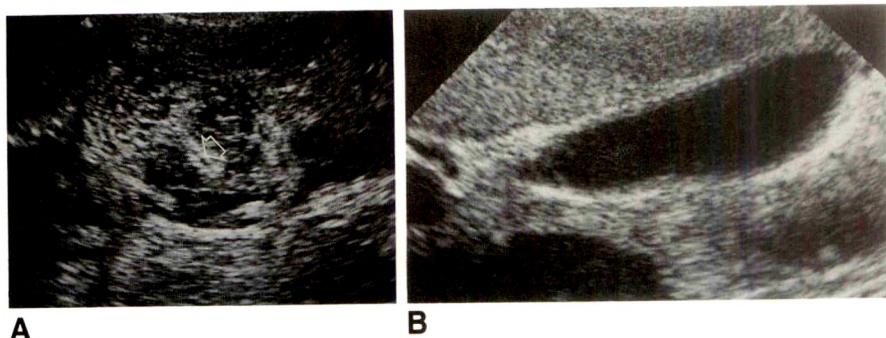
Discussion

Although it is well known that the finding of gallbladder wall thickening on sonography may be due to many causes, both biliary and nonbiliary, a recent report suggests that sonographic evidence of striations or layering of the gallbladder wall is a sign of acute cholecystitis [8]. Our study shows that this finding is suggestive of acute gangrenous cholecystitis (10 of 10 patients with cholecystitis). However, in patients without clinical evidence of acute cholecystitis, striated thick-

Fig. 3.—35-year-old man with viral hepatitis, type A.

A, Sonogram shows marked, diffuse gallbladder wall striations. Gallbladder lumen (arrow) is compressed by thickened gallbladder wall.

B, Sonogram shows resolution of wall thickening 1 month later.



ening of the gallbladder wall may be seen in a variety of abnormalities, including congestive heart failure, renal failure, liver disease (hepatitis), ascites, hypoalbuminemia, pancreatitis, blockage of the lymphatic and/or venous drainage of the gallbladder, and prominent Rokitansky-Aschoff sinuses. The extent of the striations (focal or diffuse) was not helpful in determining the cause of the striated gallbladder wall thickening because focal striations were present in the majority of patients with gangrenous cholecystitis (eight of 10 patients) and edema of the gallbladder wall unrelated to gallbladder disease (11 of 17 patients).

Although there was no sonographic-pathologic correlation in 11 cases, follow-up from 2 months to 2 years showed no evidence of primary gallbladder disease in 10 of these cases. The 11th patient died of unrelated causes 11 days after the sonogram. An autopsy was not performed, but there was no clinical evidence of biliary tract disease. Although the diagnosis of acute cholecystitis may have been overlooked in these cases, our patients had no evidence for this and had other diseases known to cause gallbladder wall thickening. In three other cases, sonographic gallbladder wall abnormalities were not evident at autopsy. We believe that this discrepancy was due to the time interval between the sonogram and autopsy (3–16 days) and the use of alcohol to prepare the histologic specimen. Alcohol, a dehydrating agent, is known to remove fluid from edematous organs. We can only speculate that the striations were due to hepatic and renal failure in one of these cases, and due to blockage of the venous and/or lymphatic drainage of the gallbladder in the other two patients with hepatic venoocclusive disease and cholangiocarcinoma. In two additional cases, pathologic correlation suggested unusual causes of striated thickening of the gallbladder wall. We again had to speculate that the striations were due to reactive changes in the serosa in the patient with pancreatitis, and due to wall edema, Rokitansky-Aschoff sinuses, and a thickened muscularis in the patient with renal failure and hypoalbuminemia.

We cannot readily explain why edema alone causes striated thickening of the gallbladder wall in patients without evidence of primary gallbladder disease, whereas in acute cholecystitis, the appearance correlates with gangrene. In uncomplicated acute cholecystitis, inflammation is limited primarily to the submucosal layer of the gallbladder wall, whereas in gangre-

nous cholecystitis, coagulation necrosis often involves all layers of the gallbladder wall. Perhaps in patients with gangrenous cholecystitis it is the full thickness involvement of the wall that produces the striations observed at sonography. Likewise, in patients with edema of the gallbladder wall unrelated to gallbladder disease, it may be the relatively even distribution of the fluid throughout the layers of the wall that produces the striations observed at sonography. Further studies with close sonographic-histologic correlation are necessary to confirm these speculations.

In conclusion, the sonographic finding of gallbladder wall thickening with striations may be due to several pathologic processes unrelated to primary disease of the gallbladder. However, in the clinical setting of acute cholecystitis, the presence of striations suggests that the patient has acute gangrenous cholecystitis.

ACKNOWLEDGMENTS

The authors acknowledge Cheryl Colacurcio for her sonographic expertise and John D. Harley for editorial assistance.

REFERENCES

- Shlaer WJ, Leopold GR, Scheible FW. Sonography of the thickened gallbladder wall: a non-specific finding. *AJR* 1981;136:337–339
- Ralls PW, Quinn MF, Juttner HV, Halls JM, Boswell WD. Gallbladder wall thickening: patients without intrinsic gallbladder disease. *AJR* 1981;137:65–68
- Wegener M, Borsch G, Schneider J, Wedmann B, Winter R, Zacharias J. Gallbladder wall thickening: a frequent finding in various nonbiliary disorders—a prospective ultrasonographic study. *JCU* 1987;15:307–312
- Fiske CE, Laing FC, Brown TW. Ultrasonographic evidence of gallbladder wall thickening in association with hypoalbuminemia. *Radiology* 1980;135:713–716
- Laudanna AA, Ferreyra NP, Cerri GG, Bettarello A. Thickening of the gallbladder wall in alcoholic hepatitis verified by ultrasonographic examination. *Scand J Gastroenterol* 1987;22:521–524
- Maresca G, DeGaetano AM, Mirk P, Cauda R, Federico G, Colagrande C. Sonographic patterns of the gallbladder in acute viral hepatitis. *JCU* 1984;12:141–146
- Juttner HV, Ralls PW, Quinn MF, Jenney JM. Thickening of the gallbladder wall in acute hepatitis: ultrasound demonstration. *Radiology* 1982;142:465–466
- Cohan RH, Mahony BS, Bowie JD, Cooper C, Baker ME, Illescas FF. Striated intraluminal gallbladder lucencies on US studies: predictors of acute cholecystitis. *Radiology* 1987;164:31–35

Videotape Review



RSNA Today, Vol. 4, No. 3. Oak Brook, IL: The Radiological Society of North America, 1990. \$55; by subscription, 6 issues annually at \$185 for RSNA members and \$225 for nonmembers (VHS videotape)

A night at the movies with the Marx Brothers it's not. However, with a little popcorn and 1 hour, you can learn about color flow Doppler imaging, superomedial oblique fissures, Alzheimer disease, and polyplanar endorectal sonography. A few pages in a journal would suffice for the oblique fissures. On the other hand, the video format is ideal for some areas of radiology, such as real-time sonography.

Lincoln Berland gives a dynamic, articulate review of color flow Doppler imaging, with specific abdominal applications and great labeling (I'm a stickler about arrows). After covering technological principles, Dr. Berland explores stenosis of the mesenteric and renal arteries, arterial venous fistulas, aneurysms in small vessels, and pseudoaneurysms. In addition, he discusses portal venous disorders, abnormal pulsation of the portal vein in congestive heart failure, spontaneous and surgical portosystemic shunts, and portal hypertension. Miscellaneous applications are mentioned: clarifying confusing anatomy, hepatic lesions, other neoplasms such as hypernephroma, and inflammatory conditions such as cholecystitis and appendicitis. Although not as detailed as a series of articles in *Seminars in Interventional Radiology* (March and September 1990 issues) or the

book *Duplex Sonography* edited by Grant and White (Springer-Verlag, 1988), this part of the videotape is a sound overview of a difficult field.

Unfortunately, I am not as positive about the segment on endorectal sonography. As guest editor, William Casarella states, "Polyplanar endorectal ultrasound is not new; has had limited experience in rectal carcinoma; and the results, while encouraging, are not conclusive." I find this segment rushed, poorly labeled, and difficult to fathom.

In the other major segment, Ajax E. George and B. Leonard Holman review the CT and MR findings of temporohippocampal tissue loss in Alzheimer disease and single-photon emission CT findings of perfusion loss in the temporoparietal region. This is an excellent compilation of material otherwise scattered in the literature.

At \$55 (or a subscription cost of \$185 for six tapes), this video night at the movies may be expensive for one person alone, but it is ideal for a group or a radiology department.

Lee B. Milner
Bluefield Regional Medical Center
Bluefield, WV 24701

Pictorial Essay



Sonography of Focal Lesions of the Spleen

Christian Goerg,¹ Wolf B. Schwerk, and Konrad Goerg

The sonographic appearances of benign and malignant splenic lesions in 154 patients are illustrated. Sixty-six of the 154 patients had malignant splenic lesions; 55 of these had malignant lymphoma and 11 had splenic metastatic lesions. The lesions were hypoechoic in 64 cases (97%), including all cases of malignant lymphoma, and were hyperechoic in two. Eighty-eight patients had benign splenic lesions; findings included cysts, infarcts, abscesses, hemangiomas, and calcifications.

Sonography plays a major role in the detection of diseases of the spleen [1–4]. The purpose of this essay is to illustrate

the sonographic features of an assortment of splenic lesions based on our experience with 154 patients with proved diseases involving the spleen.

Malignant Splenic Lesions

In 66 of our 154 patients the final diagnosis of metastatic involvement of the spleen was made on the basis of sonographic appearance, clinical data, and follow-up sonograms obtained after treatment. The malignant splenic masses were

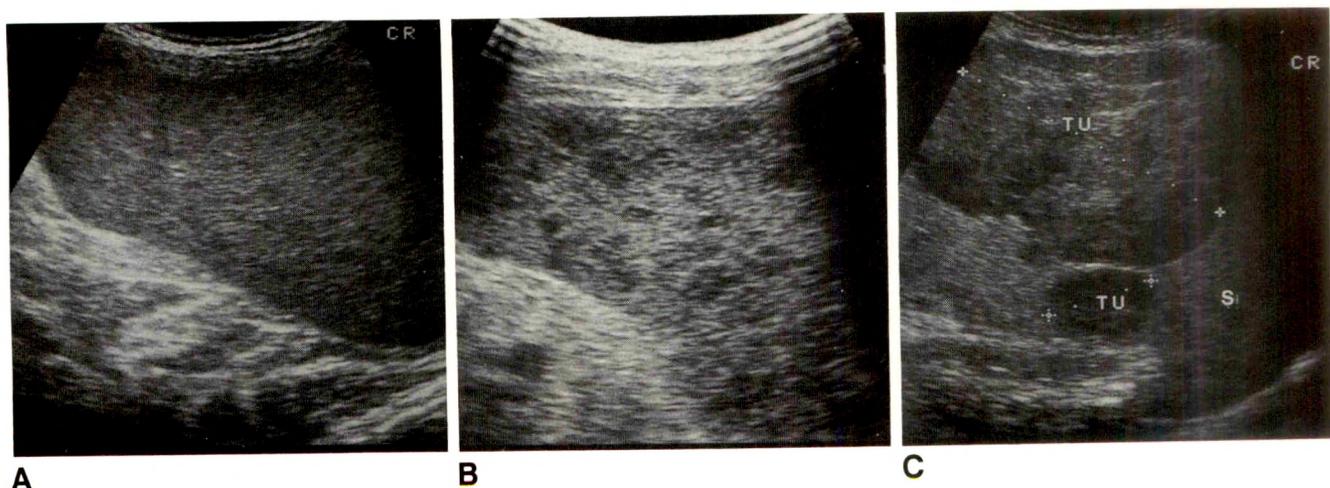


Fig. 1.—Malignant lymphoma (three patients).

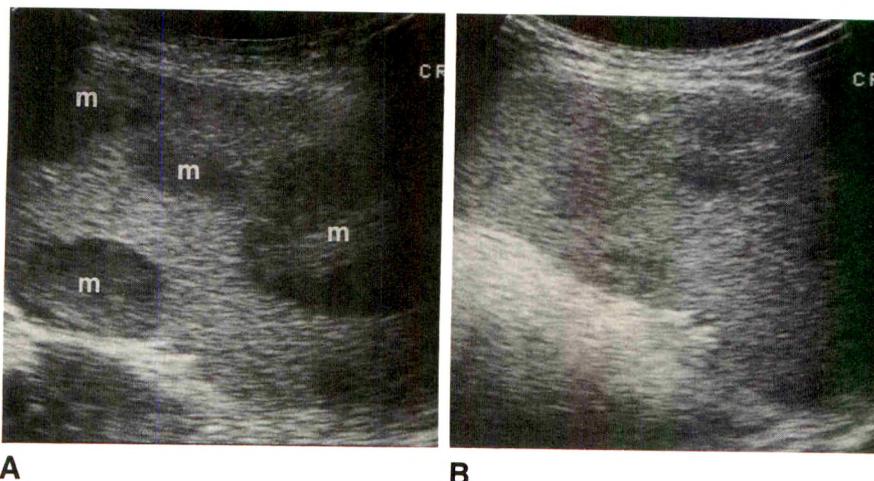
A, Sonogram in a patient with non-Hodgkin lymphoma of low-grade malignancy shows diffuse inhomogeneity of spleen with hypoechoic lesions smaller than 1 cm in diameter.

B, Sonogram in a patient with Hodgkin disease shows small, focal, nodular, hypoechoic lesions larger than 1 cm in diameter.

C, Sonogram in a patient with non-Hodgkin lymphoma of high-grade malignancy shows large, focal, nodular, hypoechoic lesions (TU). S = spleen.

Received July 9, 1990; accepted after revision October 24, 1990.

¹ All authors: Department of Internal Medicine, Philipps-University, Baldingerstrasse, D-3550 Marburg, Germany. Address reprint requests to C. Goerg.

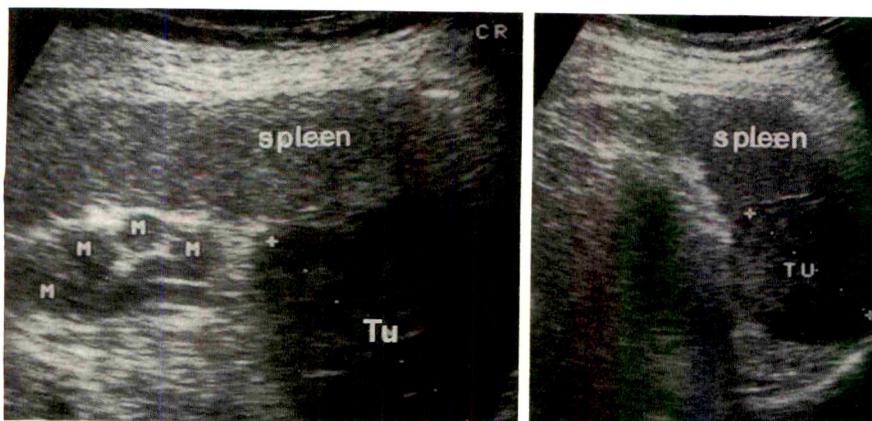


A B

Fig. 2.—Malignant lymphoma.

A, Initial sonogram in a patient with high-grade non-Hodgkin lymphoma shows large, rounded, hypoechoic lesions (m).

B, Sonogram 30 days after initiation of chemotherapy shows splenic inhomogeneity with nearly complete regression of lesions.



A B

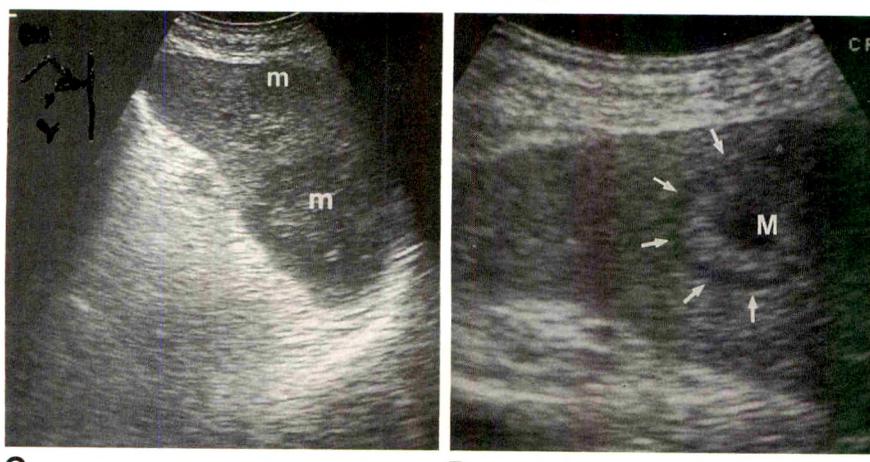
Fig. 3.—Splenic metastases.

A, Sonogram in a patient with breast carcinoma shows an intrasplenic hypoechoic metastasis (Tu) confirmed by splenectomy. Note abdominal metastases (M) in splenic hilum.

B, Sonogram in a patient with colonic carcinoma shows round, well-delineated splenic lesions (TU). Splenectomy revealed solitary metastasis of spleen.

C, Sonogram in a patient with malignant melanoma shows multiple hypoechoic metastases (m) of the spleen, confirmed at autopsy.

D, Sonogram in a patient with colonic carcinoma with diffuse liver metastasis shows splenic lesions (M) with a hypoechoic rim (arrows) and central liquefied area. Autopsy revealed splenic metastasis.



C

D

hypoechoic in 64 cases (97%). Two patients had hyperechoic metastasis.

Malignant lymphoma (Figs. 1 and 2) was the most frequent cause of splenic infiltration in our patients. These lesions were hypoechoic in all cases. Hypoechoic splenic lesions in patients with malignant lymphoma are virtually certain to be neoplastic because of the purity of other types of focal splenic lesions.

Consequently, verification by fine-needle biopsy is usually unnecessary. Splenic lesions with increased echogenicity are unusual in patients with lymphoma, and histologic confirmation is recommended. Diffuse splenic involvement with hypoechoic lesions smaller than 1 cm in diameter was found in 18 (33%) of 55 patients with malignant lymphoma.

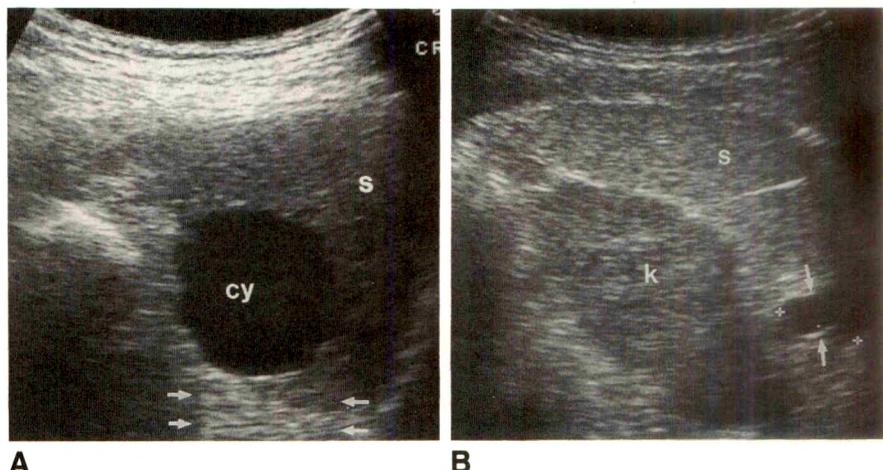
Different sonographic patterns of lymphoma could be dis-

Fig. 4.—Splenic cysts.

A, Sonogram shows round, discretely bounded, solitary, echo-free, "liquid" lesion with marked echo enhancement in distal parenchyma (arrows) due to lack of attenuation through fluid. CT confirmed splenic cyst (cy).

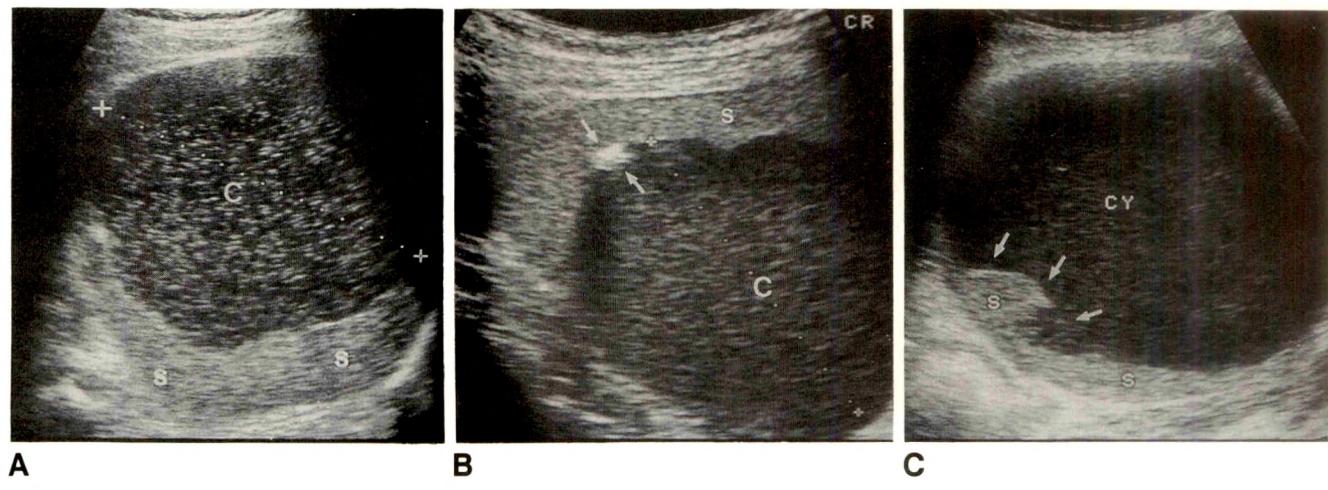
B, Sonogram in a patient with serologically confirmed *Echinococcus* shows a small, septated hydatid cyst (arrows). k = kidney.

s = spleen.



A

B



A

B

C

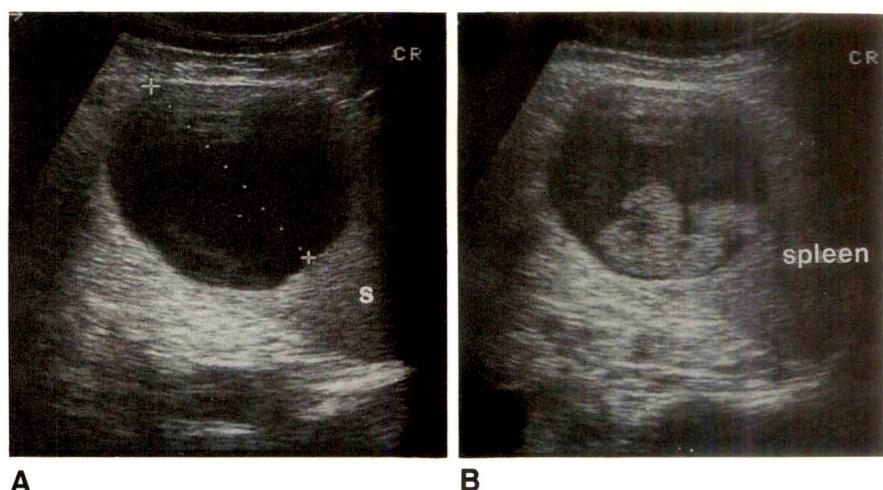
Fig. 5.—Splenic cysts.

A, Sonogram in a patient with pain in left upper quadrant shows irregularly delineated cystic lesion (c) within floating internal echoes. Fine-needle aspiration revealed blood cell aggregates. Surgery confirmed dysontogenetic cyst.

B, Sonogram in an asymptomatic patient with no anamnestic trauma shows large, well-delineated cystic lesion (c) with floating internal echoes and small borderline calcification (arrows). Fine-needle aspiration showed blood. CT confirmed splenic cyst with intracystic bleeding.

C, Sonogram in a patient with anamnestic trauma 1 year before and pain in left upper quadrant shows large, irregularly delineated (arrows) cystic lesion (CY). Splenectomy revealed pseudocystic organized hemorrhage from intrasplenic rupture.

s = spleen.



A

B

Fig. 6.—Splenic cyst.

A, Initial sonogram shows large echo-free cyst with echo enhancement in distal area. s = spleen.

B, Sonogram 3 years later shows echoes at bottom of cyst, probably caused by hemorrhage.

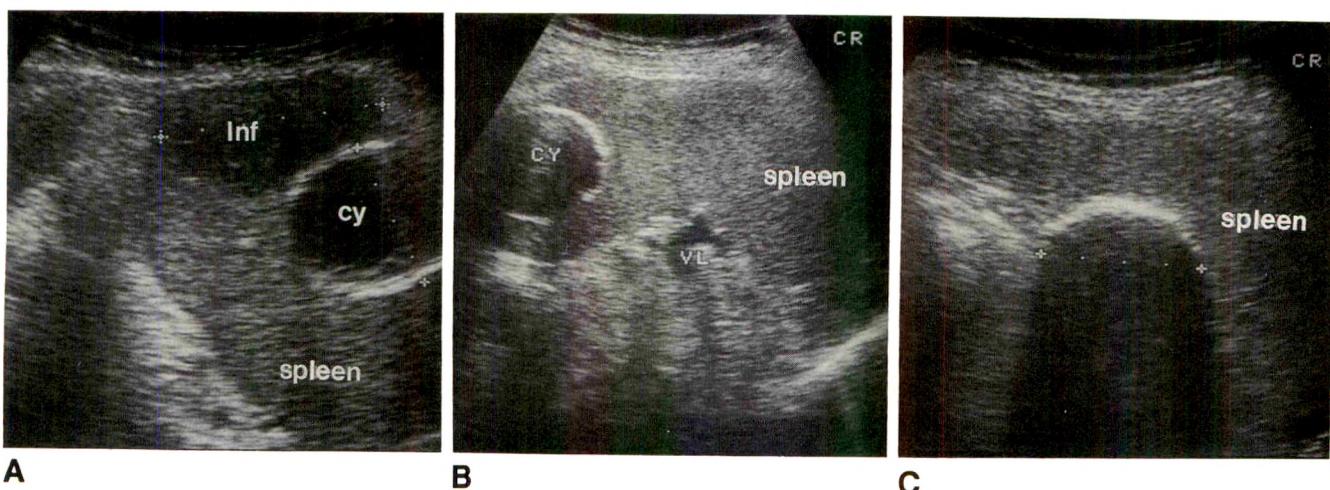


Fig. 7.—Splenic cysts

A, Sonogram in a patient with chronic myeloid leukemia and acute pain in left upper quadrant shows hypoechoic, irregularly delineated lesion caused by splenic infarction (Inf) beneath an echo-free, well-demarcated, strongly bounded splenic cyst (cy). Infarct was confirmed when complete healing was found at follow-up examination.

B, Sonogram shows cystic lesion (CY) with incomplete border calcification. VL = splenic vein.

C, Sonogram shows complete border calcification with distal shadowing. CT confirmed splenic cyst.

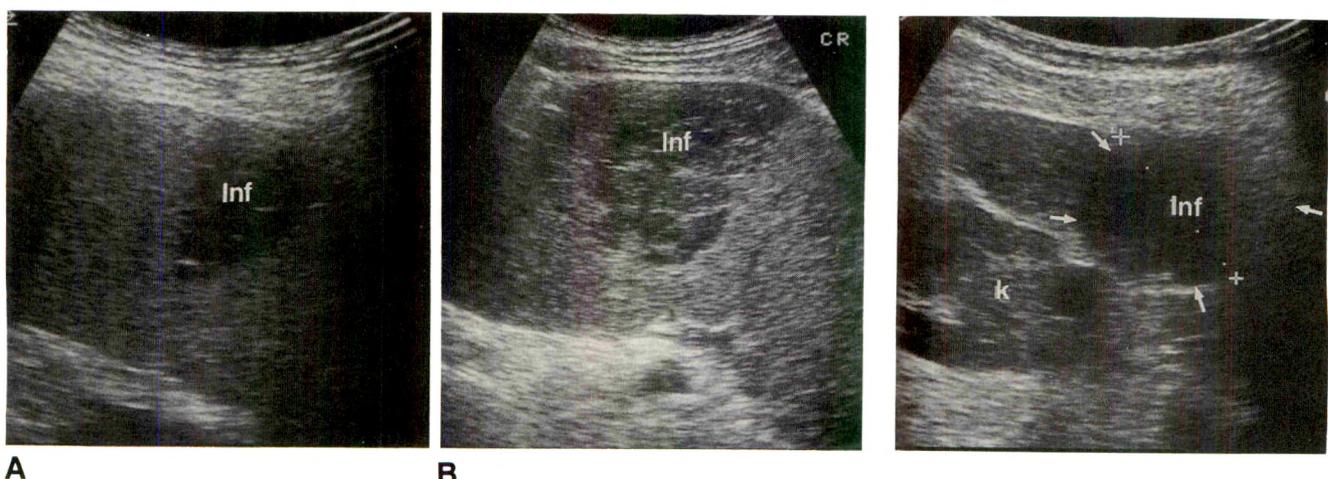


Fig. 8.—Splenic infarcts.

A, Sonogram in a patient with myeloproliferative disease and acute pain in left upper quadrant shows a wedge-shaped hypoechoic lesion. Complete healing at follow-up examination confirmed splenic infarct (Inf).

B, Sonogram in a patient with myeloproliferative disease and diffuse abdominal pain shows a predominantly round, hypoechoic lesion. Patient died of blast crisis. Autopsy confirmed splenic infarct (Inf).

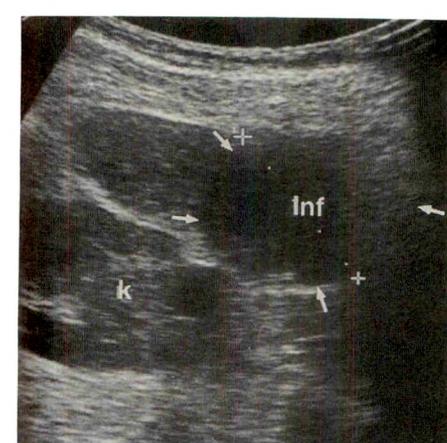


Fig. 9.—Splenic infarcts. Sonogram in a patient with endocarditis and septic infarcts of the brain and testis shows rounded, smoothly delineated, partly echo-free intrasplenic lesion (arrows). Infarct was confirmed by diagnostic and therapeutic fine-needle biopsy, which revealed necrosis and superinfection in infarcted area (Inf). Complete healing of infarction was seen 9 months after primary diagnosis. k = kidney.

tinguished. Patients with high-grade non-Hodgkin lymphoma had focal lesions larger than 3 cm in diameter. Those with low-grade non-Hodgkin lymphoma and Hodgkin disease had focal and diffuse destruction of the splenic parenchyma. Lesions smaller than 3 cm in diameter were typical for non-Hodgkin lymphoma of low-grade malignancy.

Splenic metastases (Fig. 3) are rare. Primary tumors include the lung, breast, stomach, and ovary. As in malignant lym-

phoma, splenic metastases are predominantly hypoechoic. Liver metastases often have a hypoechoic rim; this was seen in only one of our patients with splenic metastases. It is even impossible to make a specific diagnosis solely on the basis of the appearance of a hypoechoic lesion on sonography. In most cases follow-up sonograms are helpful in clarifying the cause of the lesion. Biopsy or surgery may be necessary if the nature of the lesion influences treatment.

Fig. 10.—Splenic abscess. Sonogram in a patient with severe septic disease of unknown origin shows a large hypoechoic splenic lesion. Sonographically guided percutaneous puncture confirmed the presence of an abscess (a). s = spleen.

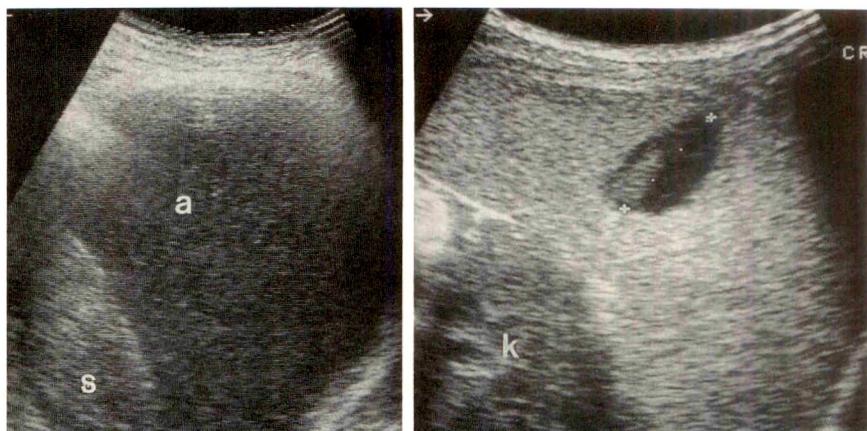


Fig. 11.—Splenic abscess. Sonogram in a patient with fever shows a small, rounded, hypoechoic lesion. Pus was aspirated by fine-needle puncture. k = kidney.

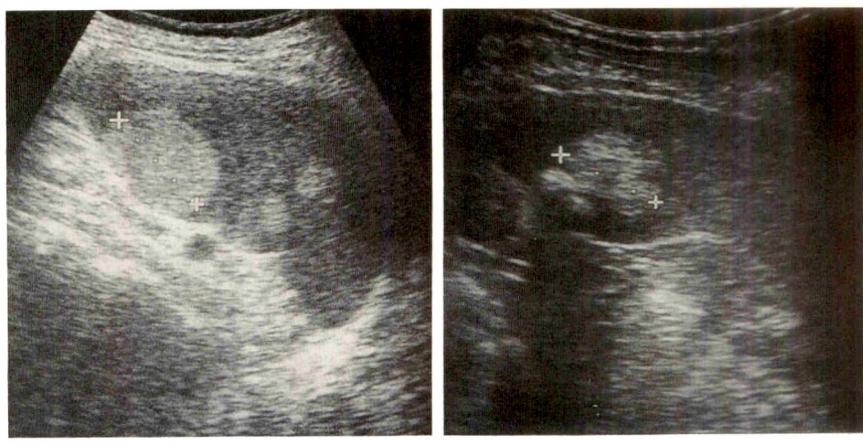
10

11

Fig. 12.—Splenic hemangioma.

A, Sonogram in an asymptomatic patient shows multiple, sharply marginated, hyperechoic lesions. Contrast-enhanced CT confirmed splenic hemangioma.

B, Sonogram in an asymptomatic patient shows rounded, well-margined, hyperechoic lesion with shadowing caused by calcification. Enhanced CT confirmed splenic hemangioma.



A

B

Benign Splenic Lesions

Sonographic diagnosis of cysts (Figs. 4–7) usually presents no problem. Solitary or multiple splenic cysts are mostly asymptomatic. Acquired cysts can be the result of trauma or parasitic infection such as with *Echinococcus*. Occasionally the differential diagnosis may be difficult because of internal echogenicity associated with bleeding or necrosis, which can occur in patients with infarcts, traumatic intrasplenic rupture, or abscesses. If an abscess is suspected on the basis of clinical symptoms, diagnostic and therapeutic puncture of the lesion is indicated.

Infarcts (Figs. 8 and 9) may cause focal splenic lesions. These occur mainly in patients with myeloproliferative disease and septic endocarditis. In the acute stage, a wedge-shaped, irregularly delineated hypoechoic lesion with a high tendency to heal on its own is typical.

Splenic abscesses (Figs. 10 and 11) are considered rare. The high mortality rate associated with delayed diagnosis makes the need for prompt detection and early therapy clear. Their various sonographic appearances include an anechoic

pattern, a mainly fluid pattern with a few nonreverberatory echoes, or a complex solid pattern. Hematomas, cysts, and occasionally infarcts are known to present with a variety of sonographic appearances similar to those of abscess collections. Percutaneous fine-needle aspiration guided by sonography is a safe diagnostic procedure to establish the diagnosis.

Hemangiomas. (Fig. 12) of the spleen present as focal, well-margined, solitary or multiple, predominantly hyperechoic tumors. Occasionally calcifications are seen.

REFERENCES

1. Goerg C, Schwerk WB. Splenic infarction: sonographic patterns, diagnosis, follow-up, and complications. *Radiology* 1990;174:803–807
2. Mittlestaedt CA. Ultrasound of the spleen. *Semin Ultrasound* 1981;11:233–240
3. Goerg C, Schwerk WB, Goerg K, Havemann K. Sonographic patterns of the affected spleen in malignant lymphoma. *JCU* 1990;18:569–574
4. Solbiati L, Bossi MC, Belotti E. Focal lesions in the spleen: sonographic patterns and guided biopsy. *AJR* 1983;140:59–65

Book Review



Fuch's Principles of Radiographic Exposure, Processing and Quality Control, 4th ed. By Quinn B. Carroll. Springfield, IL: Thomas, 380 pp., 1990. \$39.75

This text is designed to teach radiologic technologists the physics and instrumentation needed to select correct techniques, process film, and diagnose simple malfunctions in equipment. The illustrations are excellent, and the material is covered thoroughly. A history of films is a pleasant introduction to the chemistry of film exposure and development.

The image quality of radiographs is divided into visibility and recognizability; visibility includes contrast factors, and recognizability includes resolution factors. This dichotomy continues throughout the text. Chapters 5 through 13 are included in the visibility section and include amperage, kilovoltage, filtration, patient components, grids, intensifying screens, and films. Geometrical factors make up the recognizability sections. Chapters 14 through 22 cover focal spot size and geometry. The end of the text, chapters 28 through 34, concerns film processing, processing quality control, and radiographic quality control. Much new material has been added to this fourth edition, often without deleting outdated material. An example is an excellent chapter on automatic processors, which has been added without removing material on hand development and tank processing in the preceding chapter. Except for a short chapter on magnification, no computation is required. All computations for techniques have been reduced to charts and general concepts, rather than formulas.

Little consideration is given to the dose of radiation received by the patient. When the current public interest in doses received during radiographic imaging is considered, it is surprising not to have a separate chapter on this subject, so that technologists could be instructed how to answer patients' questions and could be aware of the exposure cost mistakes can generate. In chapters on collimation and low kilovoltage, the avoidance of unnecessary exposure to radiation is discussed, but little emphasis is given throughout the text to dose control as a factor in radiography.

Most of the text is illustrated with bone radiographs. Some chest radiographs are used in chapters on subject contrast, and one page of illustrations accompanies the discussion of abdominal imaging with contrast media. Contrast media is presented primarily as a vehicle for introducing material of greater atomic number into the patient. The enhancement from characteristic radiation is described as a shift in the proportion of photoelectric effect to Compton scattering between patients with and without contrast media. Because of the difference in emphasis in this text compared with that in texts written for radiologists, I often felt like Alice in Wonderland, where everything was not quite right. The effort of the author to simplify explanations

and "include only physics topics which relate directly to radiographic technique" often necessitated confusing explanations that required several pages to clarify. For example, image latitude was called "long (optical density) scale," and statements that the eye cannot see less than a 30% change in optical density, instead of a 30% change in amperage, required decoding. This text should not be used as a reference, as many explanations are clarified by later, nonindexed text. For example, the statement in the first chapter that contrast depends on the mix of energies in the X-ray beam and that no contrast would be possible with a monoenergetic beam is corrected and clarified in subsequent chapters.

A single chapter on plane tomography, fluoroscopy, digital fluoroscopy, and CT may introduce these techniques, but it certainly does not cover them at all thoroughly. Included in this chapter is a discussion of stereo imaging, which is presented not as a historical technique but as one that is as useful as plane tomography.

Five short chapters (23–27) review material in earlier chapters but do not present new material. In fact, this text could be improved by removing outdated material and repetitive explanations. The resulting reduction of 20% could be filled with new material on dosimetry, fluoroscopic equipment, contrast imaging (such as gastrointestinal and genitourinary imaging), and mammography. Questions at the end of each chapter would help technologists who are preparing for registry examinations.

Although the layout and proofreading of this text are satisfactory, I was confused by the poor sentence structure and context. Pronoun references were often ambiguous, and extraneous phrases and sentences were not removed.

However, these caveats should not discourage a potential technologist from purchasing this text. It contains a great deal of material necessary for good radiologic imaging, and it is written at a level that makes it easy to read. The plentiful diagrams and illustrations make it a good buy for learning radiation technology or for reviewing for examinations. This book is not intended to instruct radiologists or physicists preparing for board examinations, and it should not be used for this purpose. Radiologists or physicists who are teaching technologists should consider this book as a potential text.

Carolyn Kimme-Smith
University of California, Los Angeles School of Medicine
Los Angeles, CA 90024-1721

Case Report

Giant Esophageal Ulcer Due to Clinoril

Marc S. Levine,¹ Robin D. Rothstein,² and Igor Laufer¹

Drug-induced esophagitis is an increasingly frequent cause of acute odynophagia in adults. Affected persons typically have a history of ingesting their medication with little or no water immediately before going to bed. Prolonged exposure of the esophageal mucosa to a variety of capsules or tablets is thought to cause a focal contact esophagitis, manifested by one or more areas of shallow ulceration in the upper or midesophagus. In the past, endoscopy has been advocated as the primary technique for diagnosing this condition. More recently, double-contrast esophagography also has been recognized as a valuable technique for demonstrating these superficial ulcers [1, 2]. Occasionally, the length of the ulcers may be several centimeters or more [1, 2]. However, we recently encountered a patient in whom double-contrast esophagography showed a giant esophageal ulcer due to ingestion of Clinoril (sulindac), a nonsteroidal antiinflammatory drug (NSAID) that rarely has been implicated as a cause of drug-induced esophagitis.

Case Report

A 36-year-old man who had been in good health had acute onset of odynophagia. He denied smoking, drinking, or drug abuse but did indicate that during the past week he had begun treatment with Clinoril for occasional arthralgias. On the night before he became symptomatic, he ingested one Clinoril tablet with only a small amount of water immediately before going to bed. The next morning, he had

substernal chest pain and odynophagia so severe that he could barely swallow his saliva. Double-contrast esophagography 2 days later showed a giant (7×2 cm) esophageal ulcer below the level of the carina that had a longitudinal orientation in relation to the long axis of the esophagus (Fig. 1A). The crater of the ulcer had irregular margins. No evidence of a hiatal hernia or gastroesophageal reflux was found at fluoroscopy. Endoscopic examination 1 day later confirmed the presence of a giant ulcer in the midesophagus with erythema of the surrounding mucosa. The distal esophagus appeared normal. Biopsy samples from the ulcer margin and brushings from the ulcer base revealed acute and chronic inflammatory cells without evidence of viral inclusions, fungi, or tumor. No organisms (i.e., herpes or cytomegalovirus) were isolated on viral cultures of specimens from the esophagus. Blood tests for antibodies to human immunodeficiency virus also were negative. A tentative diagnosis of Clinoril-induced esophagitis was made.

The patient was advised to stop taking Clinoril and was treated with cimetidine and sucralfate. He had a dramatic clinical response and became asymptomatic within 3 days of treatment. Endoscopy repeated 2 months later showed a residual ulcer in the midesophagus that had decreased significantly in size. Biopsy samples and brushings again revealed acute and chronic inflammatory cells without evidence of viral or fungal infection or tumor. Esophagography repeated 4 months later showed a long, shallow depression with smooth borders in the same location as the original ulcer (Fig. 1B). Because the patient was still asymptomatic, it was uncertain whether this represented an active ulcer or an ulcer scar. Subsequent endoscopy confirmed the presence of a shallow depression in the midesophagus with relatively abrupt margins and normal overlying mucosa. Biopsies revealed normal squamous epithelium compatible with a reepithelialized ulcer scar.

Received November 26, 1990; accepted after revision December 27, 1990.

¹ Department of Radiology, Hospital of the University of Pennsylvania, 3400 Spruce St., Philadelphia, PA 19104. Address reprint requests to M. S. Levine.

² Department of Medicine, Hospital of the University of Pennsylvania, 3400 Spruce St., Philadelphia, PA 19104.

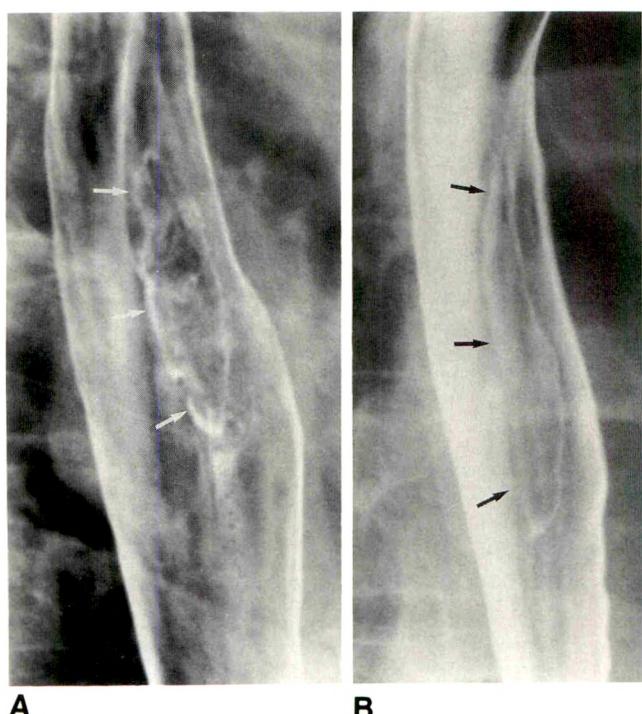


Fig. 1.—Giant esophageal ulcer due to ingestion of Clinoril (sulindac).
A, Initial double-contrast esophagogram shows 7 × 2 cm ulcer (arrows) in midesophagus below level of carina. Note irregular margins of ulcer.
B, Esophagogram obtained 6 months later shows long, shallow depression with smooth borders (arrows) at site of previous ulcer. Endoscopy showed this was an ulcer scar with a reepithelialized pit or depression.

Discussion

Drug-induced esophagitis has become a relatively common entity in today's pill-oriented society. The medications implicated in about half the reported cases are antibiotics, usually tetracycline or doxycycline. Other less frequent causes include potassium chloride, quinidine, emepromium bromide, ferrous sulfate, alprenolol hydrochloride, ascorbic acid, theophylline, and cromolyn sodium. Although it is well known that aspirin and other NSAIDs can cause erosive gastritis and gastric ulcers, these drugs rarely have been implicated in the development of esophagitis. However, our patient had acute odynophagia due to NSAID-induced esophagitis after ingesting Clinoril (sulindac). On review of the recent literature, we found that esophagitis or even esophageal strictures occasionally may be caused by a variety of NSAIDs, including aspirin, phenylbutazone, Indocin (indomethacin), Motrin (ibuprofen), Naprosyn (naproxen), Feldene (piroxicam), and Clinoril [3–5]. Some authors have postulated that these drugs may exacerbate esophagitis in patients with preexisting gas-

troesophageal reflux disease, increasing the risk of stricture formation [3, 4].

Whatever the offending agent, on double-contrast esophagography, drug-induced esophagitis is usually manifested by a solitary ulcer, several discrete ulcers, or a cluster of tiny ulcers in the midesophagus near the level of the aortic arch or left main bronchus [1, 2]. However, our patient had a giant esophageal ulcer approximately 7 cm long (Fig. 1A). Other causes of giant esophageal ulcers include quinidine, nasogastric intubation, Crohn disease, Behcet syndrome, and ulcerative carcinomas. With the worsening worldwide epidemic of AIDS, the possibility of a giant esophageal ulcer due to cytomegalovirus esophagitis in an AIDS patient also should be included in the differential diagnosis [6]. However, endoscopic biopsies, brushings, and cultures for cytomegalovirus and blood tests for antibodies to human immunodeficiency virus were negative in our patient. Ultimately, the correct diagnosis was suggested by the temporal relationship between ingestion of Clinoril and the onset of esophagitis. Thus, NSAIDs should be recognized as another cause of drug-induced esophagitis, and, more specifically, ingestion of Clinoril should be included as a possible cause of giant esophageal ulcers.

In our patient, esophagography repeated 6 months later showed a long, shallow depression with smooth borders in the same location as the original ulcer (Fig. 1B). Because the patient was asymptomatic, it was unclear whether this represented an active ulcer or an ulcer scar. However, subsequent endoscopy confirmed the presence of a reepithelialized pit or depression at the site of the previous ulcer. Radiologists therefore should be aware that healing of a giant esophageal ulcer occasionally may lead to the development of a smooth, well-defined pit or depression that can be mistaken for the crater of an active ulcer.

REFERENCES

1. Creteur V, Laufer I, Kressel HY, et al. Drug-induced esophagitis detected by double-contrast radiography. *Radiology* 1983;147:365–368
2. Bova JG, Dutton NE, Goldstein HM, Hoberman LJ. Medication-induced esophagitis: diagnosis by double-contrast esophagography. *AJR* 1987;148:731–732
3. Coates AG, Nostrand TT, Wilson JAP, Elta GH, Agha FP. Esophagitis caused by nonsteroidal antiinflammatory medication. *South Med J* 1986;79:1094–1097
4. Semble EL, Wu WC, Castell DO. Nonsteroidal antiinflammatory drugs and esophageal injury. *Semin Arthritis Rheum* 1989;19:99–109
5. Heller SR, Fellows IW, Ogilvie AL, Atkinson M. Non-steroidal anti-inflammatory drugs and benign oesophageal stricture. *Br Med J* 1982;285:167–168
6. Balthazar EJ, Megibow AJ, Hulnick D, Cho KC, Berenbaum E. Cytomegalovirus esophagitis in AIDS: radiographic features in 16 patients. *AJR* 1987;149:919–923

Case Report

CT Appearance of Retrograde Jejunoduodenogastric Intussusception: A Rare Complication of Gastrostomy Tubes

Andrew Weber¹ and Scott Nadel

Retrograde intussusception is an antiperistaltic telescoping of a more distal bowel lead point, the intussusceptum, through a portion of more proximal bowel, the intussuscipiens. A review of the world literature, including 103 cases of retrograde intussusceptions dating back to 1682 (Fabricius) reported by Akehurst [1], revealed only four cases of retrograde jejunoduodenogastric intussusception. Diagnoses were made by upper gastrointestinal series, and a gastrostomy tube was implicated as the inciting factor in each case [2–4]. We report the fifth case of retrograde intussusception as a complication of a gastrostomy tube and describe the characteristic features of the first such case to be diagnosed by use of CT.

Case Report

A 78-year-old woman with multiinfarct dementia and a history of a duodenal ulcer had an acute onset of hematemesis. Physical examination showed a gastrostomy tube with a mature entrance site and no evidence of a mass. An abdominal radiograph obtained at admission showed no evidence of free air or obstruction. During the next 18 hr, the patient's increasing WBC count and increasing abdominal distress prompted a CT examination. The balloon tip of the gastrostomy tube was closely applied to the anterior abdominal wall along the distal aspect of the greater curvature of the stomach. Marked gastric distension was associated with a reniform soft-tissue mass that occupied most of the antrum (Fig. 1A) and was contiguous with a rounded mass with eccentric fat in a target configuration in the second part of the duodenum (Fig. 1B), as well as a sausage-shaped

soft-tissue mass with central fat in a markedly expanded third and fourth part of the duodenum (Fig. 1C). A coiled-spring appearance was present on an inferior section through the horizontal duodenum (Fig. 1D). No oral contrast material was present in the distal small bowel.

An upper gastrointestinal series with water-soluble contrast material showed the typical appearance of an intussusception, with a large jejunal lead mass causing an antral filling defect and the trailing jejunal intussusceptum outlined by contrast material in the duodenum, giving a classic coiled-spring appearance. There was complete obstruction at the level of the horizontal duodenum.

At laparotomy, a long segment of jejunum was intussuscepted through the duodenum into the gastric lumen. Manual reduction failed, and 27 cm of intussuscepted jejunum, including a devitalized, ischemic lead point, were resected with primary duodenal-jejunal anastomosis at the ligament of Treitz. The existing untethered gastrostomy tube was replaced with a fixed version after intraoperative evaluation documented easy antegrade and retrograde mobility. The patient recovered uneventfully.

Discussion

Gastrointestinal intussusceptions in adults are uncommon and are generally antegrade with a demonstrable cause in over 90% of cases [5]. Retrograde intussusceptions are extremely rare, usually occurring as a complication of gastric surgery and long intestinal tubes, or less commonly in association with an inflammatory or neoplastic process [1, 6].

Received October 3, 1990; accepted after revision November 20, 1990.

¹ Both authors: Department of Radiology, Box 3808, Duke University Medical Center, Duke Hospital North on Erwin Rd., Durham, NC 27710. Address reprint requests to A. Weber.

AJR 156:957–959, May 1991 0361–803X/91/1565–0957 © American Roentgen Ray Society

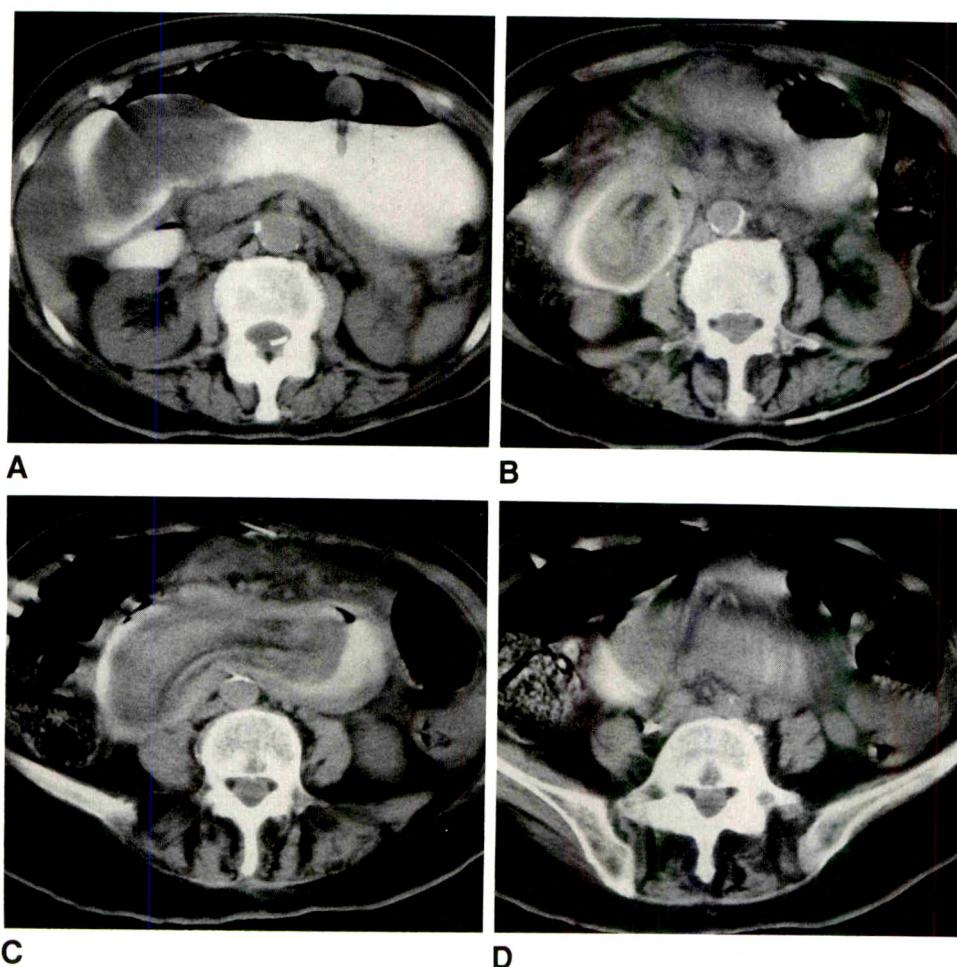


Fig. 1.—A, CT scan shows gastric distension with gastrostomy tube balloon in satisfactory position, but not fixed to anterior abdominal wall, and reniform antral filling defect representing jejunal lead point.

B, Target lesion composed of rounded soft-tissue mass with eccentric intussuscepted mesenteric fat and surrounded by contrast material in vertical portion of duodenum.

C, Sausage-shaped mass with central fat in third and fourth portions of duodenum.

D, Coiled-spring appearance in inferior section of distended horizontal portion of duodenum.

Diagnosis may be suspected on the basis of plain abdominal films, but is usually documented by an upper gastrointestinal series and less often by endoscopy [7]. A single case of CT-diagnosed jejuno-gastric intussusception after Billroth II partial gastrectomy has been reported [8].

The four prior cases of retrograde jejunoduodenogastric intussusceptions and the case reported all had mobile gastrostomy tubes. Prior studies have reviewed gastrostomy complications and have documented several cases of distal tube migration with various levels of duodenal obstruction related to gastrostomy tube balloons [2, 4, 9]. A proposed mechanism of retrograde jejunoduodenogastric intussusception links active peristalsis against the intraluminal balloon with inadequate fixation at the skin surface, resulting in migration through the pylorus and beyond the ligament of Treitz. Subsequent attempts at withdrawal with the balloon inflated result in retrograde telescoping of the jejunum back through the duodenum and into the gastric lumen. In each case, including the one reported here, episodes of migration and manual tube withdrawal were documented. Clinical presen-

tation was confusing in each case, and in no case was intussusception suspected. Clinical features varied and included symptoms and signs of obstruction as well as hematemesis, melena, and elevated WBC count.

Relatively insensitive plain film findings of intussusception have been described and include soft-tissue mass, decreased colonic gas and fecal content, and small-bowel ileus [7]. The classic coiled-spring appearance of luminal contrast studies in intussusception is well known. Merine et al. [10] reported CT findings in nine patients with enteroenteric intussusception. Four characteristic features were described among the patients, including: (1) a soft-tissue mass with an eccentrically placed fatty area of attenuation that represents the intussusception and intussuscepted mesentery, the so-called "target lesion", (2) a reniform or bilobed mass that reflects intussusception and surrounding thickened bowel wall, (3) a sausage-shaped mass with alternating areas of low and high attenuation, and (4) a coiled-spring appearance resulting from coating of ensheathing layers of intussusception by contrast material. Surgical-pathologic correlation from resected specimens

showed ischemic changes in intussusceptions that had a reniform appearance on CT.

Each of the four patterns was present in this patient, and furthermore, pathologic correlation supports the hypothesis that intussusceptions with a reniform configuration reflect ischemic changes and warrant more urgent surgical attention. The fixed anatomy of the duodenum in concert with the axial nature of CT and the extensive nature of the intussusception determine the distinctive appearance of retrograde jejunoduodenogastric intussusception. Because patients with gastrostomy tubes are often debilitated and clinical presentations may be confusing and nonspecific, a CT scan may be requested early in the evaluation of abdominal complaints in these patients. Radiologists must be aware of the CT appearance of the rare retrograde jejunoduodenogastric intussusception as a complication of unsecured gastrostomy tubes, because the radiologist may often be the first to suggest the diagnosis and thereby expedite prompt surgical therapy.

REFERENCES

1. Akhurst AC. Retrograde intussusception: report of case and review of 193 cases in literature. *Br J Surg* **1955**;43:207-213
2. Hopens T, Schwesinger WH. Complications of tube gastrostomy: radiologic manifestations. *South Med J* **1983**;76:9-12
3. Lamont A, Rode H. Retrograde jejunoduodenogastric intussusception. *Br J Radiol* **1985**;58:559-561
4. Haws EB, Sieber WB, Kiesewetter WB. Complications of tube gastrostomy in infants and children. *Ann Surg* **1966**;164:284-288
5. Agho FP. Review: intussusception in adults. *AJR* **1986**;146:527-531
6. Brume J, Meehan SE, Pringle R. Retrograde jejunogastric intussusception. *Br J Clin Pract* **1985**;10:408-410
7. White S, Blane C. Intussusception: additional observations on the plain radiograph. *AJR* **1982**;139:511-513
8. Leyman P, Ponette E, Marchal G, Vercruyssen J, Timmermans G, Ceulemans R, et al. Computed tomography of acute jejunogastric intussusception. *J Comput Assist Tomogr* **1989**;13:531-534
9. Vade A, Jafri SZH, Agha FP, Vidyasagar MS, Coran AG. Radiologic evaluation of gastrostomy complications. *AJR* **1983**;141:325-330
10. Merine D, Fishman EK, Jones B, Siegelman SS. Enterointeric intussusception: CT findings in nine patients. *AJR* **1987**;148:1129-1132

Book Review



Wolf-Heidegger's Atlas of Human Anatomy, 4th ed. Edited by Hans Frick, Benno Kummer, and Reinhard Putz. New York: Karger, 600 pp. 1990. \$100

It is difficult to think of a much less exciting or "romantic" type of book to review than an atlas of human anatomy. The topic already has been dealt with both in exquisite detail and in stark simplicity by numerous highly competent authors, and, realistically, there is nothing new about the subject that needs discussing. And yet it is exactly the romantic aspect of this atlas that is its major strength and distinguishing feature. Specifically, I refer to the extraordinary drawings that grace this book. These illustrations do much more than simply demonstrate human anatomy—they celebrate it. Their vivid colors and beautiful detail lead the reader to browse through this atlas for the simple pleasure of viewing them.

Unfortunately, the editors intend this book to do more than grace a coffee table. They state that the book is designed to serve as a dissection guide for medical students and as a ready source of relevant anatomic information for practicing physicians. Several features make it unlikely that it will accomplish either goal. The use of *Nomina Anatomica* terminology, although theoretically justifiable, is cumbersome and confusing, particularly for American-trained medical students and physicians, and will certainly limit use of this atlas.

The editors have elected to place the drawings in the center of the page and to place the labels for the specific anatomic structures in parallel columns flanking the drawings. The labels are connected to the appropriate organs, muscles, nerves, and so forth by very thin

dashed lines. Following these lines requires concentration, but it is not an insurmountable problem. However, at times, two separate structures are located along the same dashed line. This does come close to being an insurmountable problem and most certainly is an unnecessary difficulty imposed on the reader.

The conventional radiographs that appear throughout the text are generally of poor quality and do nothing to enhance readers' appreciation of the regional anatomy. The CT scans and MR images are technically better and at times are helpful, providing a different anatomic perspective. I am, however, mystified by the editors' choice of pairing supine axial MR images of the thorax with prone axial drawings showing the anatomy at the same "slice" level; this is needlessly confusing and discourages readers from comparing and learning from the two images.

This atlas contains many wonderful works of art, but the art required of the reader to make it work is much too great for the book to be of clinical use. Readily available standard texts such as *Grant's Atlas of Anatomy* and *Gray's Anatomy* do the "job" less elegantly but better, and are less expensive, to boot.

Stuart A. Groskin
SUNY Health Science Center at Syracuse
Syracuse, NY 13210

Inverted Colonic Diverticulum: Air Contrast Barium Enema Findings in Six Cases

Seth N. Glick¹

A polypoid elevation of the colonic wall was identified on air contrast barium enema in six patients. The abnormality in each case was found to be an inverted colonic diverticulum. Inverted diverticula appeared as broad-based, smooth, sessile polyps measuring 1.5–2.0 cm. In five of the six patients a characteristic central umbilication and/or evidence of barium within the polyp could be identified. The diagnosis was confirmed in three patients by demonstrating an everted diverticulum replacing the suspected lesion. In the remaining three patients, two of whom had normal findings on colonoscopy, the diagnosis was strongly suggested by the presence of barium extending into the substance of the mass.

Additional radiologic maneuvers or a second study may permit accurate diagnosis if the possibility of inverted diverticulum is considered. However, even when the diverticulum cannot be demonstrated, a central umbilication or barium within a smooth intraluminal projection should suggest inverted diverticulum and prevent unnecessary endoscopy or inadvertent diverticulectomy.

AJR 156:961–964, May 1991

The distinction between colonic diverticula and polyps on air contrast examination is usually readily apparent. On rare occasions, a diverticulum may be responsible for an intraluminal projection on barium enema, resulting in diagnostic confusion. One cause of such an abnormality is an inverted diverticulum. The head of the diverticulum may prolapse into the lumen of the diverticulum and extend into the lumen of the colon. Alternatively, the base of the diverticulum may invaginate into the lumen, acting as the lead point of minimal intussusception. This phenomenon may also be observed at endoscopy, and in two cases inadvertent diverticulectomy has been performed [1, 2].

Only two previous examples of inverted colonic diverticulum have been described in the radiologic literature [3, 4]. However, their occurrence may be more frequent than is currently recognized. Six patients with an inverted diverticulum were identified in a 1-year period. Radiologic features that should permit a specific diagnosis or suggest this diagnostic possibility were identified in these cases. Unnecessary colonoscopy or even inadvertent diverticulectomy can be avoided.

Materials and Methods

During a 1-year period, six patients, all of whom had occult blood in the stools, had intraluminal elevations on air contrast barium enema that were subsequently confirmed to represent inverted colonic diverticula. In four cases the abnormality simulated a mucosal mass with or without ulceration, and in the remaining two cases a mural lesion was suggested. No other lesions were identified in any of the patients. However, multiple diverticula were present in all of the patients. The patients were four women and two men ranging in age from 65 to 72 years, except for one 27-year-old man.

Colonoscopy was performed in three, and no colonic disease was identified in any of these patients. The presence of diverticula was not mentioned in any of the reports.

Received October 15, 1990; accepted after revision November 29, 1990.

¹ Department of Diagnostic Radiology, Hahnemann University Hospital, Broad and Vine Sts., Philadelphia, PA 19102. Address reprint requests to S. N. Glick.

0361-803X/91/1565-0961
© American Roentgen Ray Society

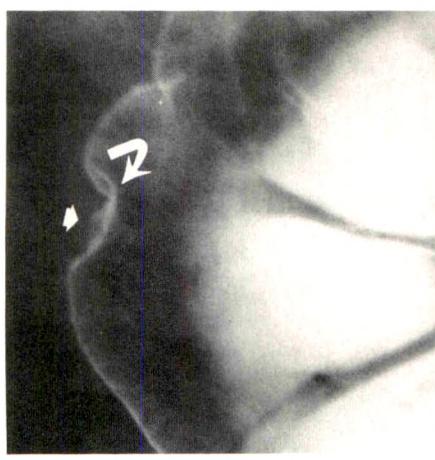
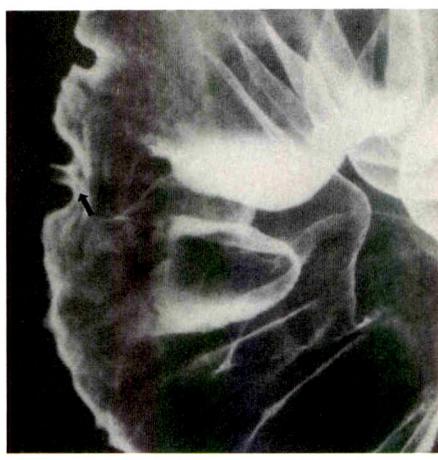
**A****B**

Fig. 1.—*A*, Smooth, broad-based intraluminal projection (curved arrow) on lateral wall of distal ascending colon shows a central collection of barium (short arrow) suggesting ulceration.

B, Increasing distension with air causes partial obliteration of lesion, and a small diverticulum (arrow) is noted within center of defect.

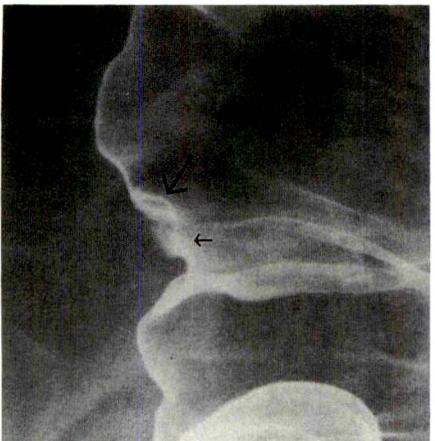
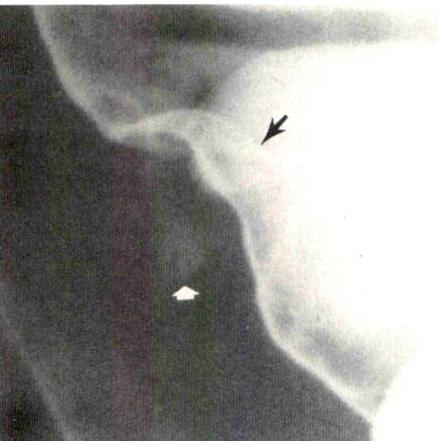
**A****B**

Fig. 2.—*A*, A 2-cm, flat, sessile polyp (large arrow) is shown on lateral wall of mid ascending colon. Lobulated contour suggests a mucosal plaque. Lack of spiculation weighs against diagnosis of diverticulitis. A central umbilication (small arrow) simulating an ulcer and characteristic of inverted diverticulum is noted.

B, After additional air insufflation, a faint collection of barium (white arrow) is seen adjacent to polypoid mass (black arrow).

Results

All of the filling defects were between 1.5 and 2.0 cm in diameter (average, 1.8 cm). Five of the six were located in the mid to distal ascending colon; four of these were on the lateral wall and one was on the medial wall. The sixth case was on the superior wall of the distal transverse colon.

Five of the lesions appeared as smooth-surfaced, broad-based, sessile polyps. Four of these five had central umbilications simulating ulcerations. In the fifth, demonstration of faint barium density within the filling defect initially suggested a calcified lesion, but inverted diverticulum also was considered. In two of the four with central umbilication, inverted diverticulum was suspected. A positive diagnosis was made by further insufflation of air, which produced eversion of the diverticulum in one patient (Figs. 1A and 1B) and barium within the body of the polyp in the other (Figs. 2A and 2B). In the patient whose findings initially suggested a calcified polyp, further insufflation resulted in eversion of the diverticulum (Figs. 3A and 3B). A review of the films of two patients who had normal endoscopic findings after a report of polyps on barium enema (both radiologic examinations were performed

early in the series) revealed the characteristic umbilication in a smooth, broad-based defect.

The sixth patient had a smooth intraluminal filling defect that appeared on a lateral decubitus radiograph to have a short, thick stalk similar to a lipoma (Figs. 4A and 4B). Findings on colonoscopy were normal, and a second barium enema showed a large diverticulum at the site of the previous polyp (Fig. 4C).

Discussion

The diagnostic problems created by diverticula in the detection of polypoid disease of the colon are well known [3, 5, 6]. Several radiologic features that facilitate the discrimination of these lesions have been reported [5]. These criteria are directly or indirectly related to the extraluminal and saccular nature of a diverticulum as opposed to the space-occupying intraluminal polyp. However, on occasion a diverticulum may appear as a polypoid filling defect. Inspissated stool in a diverticulum may produce such a defect, and differentiation may be difficult [7]. If a part of the lesion can be identified as

Fig. 3.—A, A smooth, broad-based elevation is present on superior surface of distal transverse colon (curved arrow). A faint ring-shaped density (open arrow) that suggests calcification is identified within lesion.

B, Further insufflation of air resulted in elimination of abnormality and barium filling diverticulum (arrow).

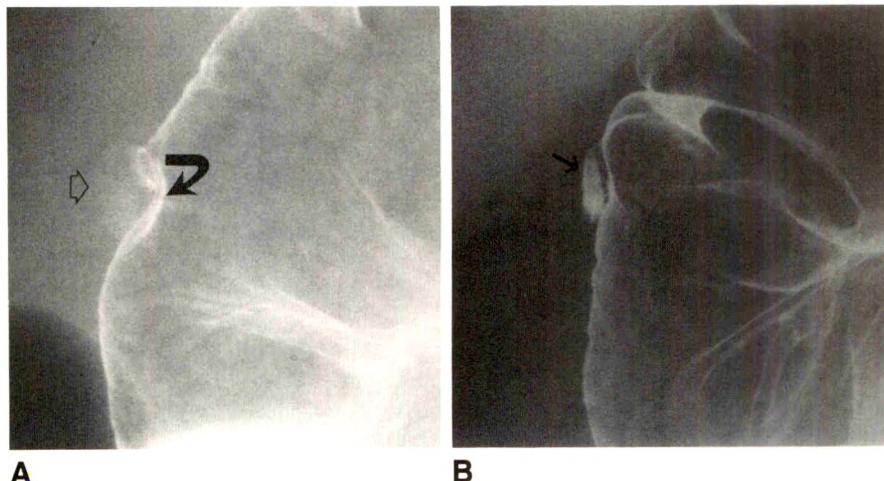
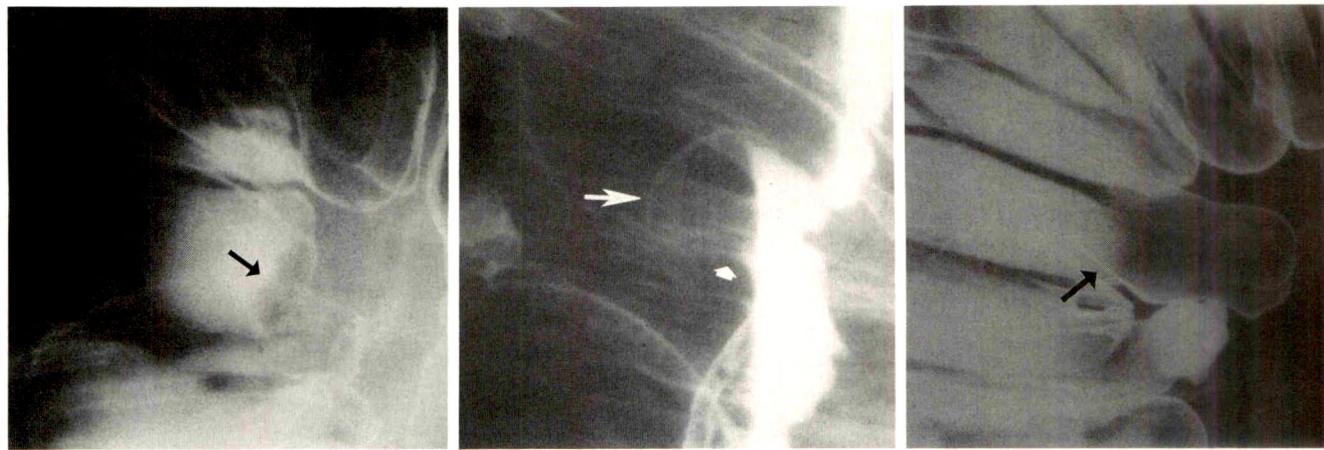
**A****B****A****B****C**

Fig. 4.—A, A 1.8-cm, smooth, broad-based polyp (arrow) with slight lobulation is noted on medial wall of distal ascending colon. "Lesion" appears as a lucency in barium pool.

B, Lateral decubitus film again shows polyp as a barium-coated structure (long arrow) with suggestion of a short thick stalk (short arrow) merging imperceptibly with head.

C, A barium enema performed 2 days after endoscopic findings were normal shows a large diverticulum (arrow) at site of polyp.

projecting beyond the lumen when viewed in tangent, the diagnosis may be suggested. In addition, the ring of barium within the diverticulum surrounding the stool may be nonuniform in thickness when viewed en face owing to incomplete obliteration of the diverticular orifice by the stool.

Another polypoid manifestation of a diverticulum is inversion of the diverticulum into the lumen. This phenomenon has been described with Meckel diverticula [4] and appendiceal intussusception [8]. However, information on inverted colonic diverticula is limited. Freeny and Walker [4] reported the first case in the radiologic literature. A 3-cm, smooth cecal mass was present on two separate barium enema studies. Surgery was required for diagnosis. Keller et al. [3] demonstrated a case in which an inverted diverticulum appeared as a small (1 cm), smooth, sessile filling defect that was misinterpreted as a polyp. After endoscopy with normal findings, a second barium enema showed a diverticulum at the site of the pre-

vious "lesion." In retrospect, a small wisp of barium could be identified outside the lumen.

References to this entity in the endoscopic literature are equally uncommon. Shah and Mazza [9] reported a 1-cm, sessile sigmoid polyp whose surface color was similar to that of the adjacent normal mucosa. The lesion was soft and easily indented. Dimpling during probing at the site of invagination was described; unlike the similarly soft lipoma, radiating folds also were visible at the site of indentation. They concluded that this represented an inverted diverticulum. Schuman [2] reported the endoscopic removal of a "submucosal" sigmoid polyp, which on pathologic examination proved to be a diverticulum. Although the patient was not treated, no complications occurred as a result of the diverticulectomy. Ladas et al. [1] performed a polypectomy on a 2-cm pedunculated sigmoid polyp that had a thick stalk and a red surface similar to the adjacent mucosa. The pathologic specimen indicated

that the polyp was a diverticulum. The patient was treated with bowel rest and antibiotics, and no evidence was found of free intraperitoneal air or clinical complications.

In this study, six cases of inverted diverticulum were identified in a 1-year period. All of the cases were proved or strongly suggested by the radiologic observations. None of the cases had pathologic confirmation, because no polypoid lesions were identified at colonoscopy and no patient required surgery to verify a persistent lesion.

Inverted diverticula were characterized by a 1.5- to 2.0-cm, broad-based, smooth elevation with a central umbilication and/or evidence of barium beyond the confines of the mucosa. The size of the filling defect may be disproportionate to the size of the diverticulum because invagination of the adjacent wall may contribute to the defect. One case had a short thick stalk that merged imperceptibly with the head, suggesting a lipoma. When an abnormality with this appearance is identified in the presence of other diverticula, the possibility of inverted diverticulum should be considered. Three of the cases were initially misdiagnosed as polyps. However, after a review of the films revealed the distinctive features, the remaining three cases were recognized and confirmed. Additional insufflation of air resulted in eversion of the diverticulum or evidence of barium in the lesion. Interestingly, all of the cases were proximal to the splenic flexure, with five located in the ascending colon. This is in contrast to the more frequent location of diverticula in the sigmoid colon. This may be related to segmental variations in mural structure, motility patterns, and intraluminal pressures. However, the numbers are too small to derive any conclusions.

Recognition of inverted colonic diverticulum on barium enema may prevent unnecessary endoscopy. Even when this diagnosis cannot be confirmed, radiologic features may suggest this possibility and alert the endoscopist, thereby preventing diverticulectomy. Although no complications have been reported from this procedure, the potential for bleeding or perforation remains. Finally, awareness of the entity may be useful in resolving radiologic-endoscopic discrepancies. Careful review of the barium enema or, when necessary, a second study may permit accurate diagnosis and result in appropriate management.

REFERENCES

1. Ladas SD, Prigouris SP, Pantelidaki C, Raptis SA. Endoscopic removal of inverted sigmoid diverticulum—is it a dangerous procedure? *Endoscopy* **1989**;21:243-244
2. Schuman BM. Endoscopic diverticulectomy in the sigmoid colon. *Gastrointest Endosc* **1982**;28:189-190
3. Keller CE, Halpert RD, Feczkó PJ, Simms SM. Radiologic recognition of colonic diverticula simulating polyps. *AJR* **1984**;143:93-97
4. Freemy PC, Walker JH. Inverted diverticula of the gastrointestinal tract. *Gastrointest Radiol* **1979**;4:57-59
5. Htoo AM, Bartram CI. The radiological diagnosis of polyps in the presence of diverticular disease. *Br J Radiol* **1979**;52:263-267
6. Baker SR, Alterman DD. False-negative barium enema in patients with sigmoid cancer and coexistent diverticula. *Gastrointest Radiol* **1985**;10:171-173
7. Ott DJ, Kerr RM, Gelfand DW. Colonic diverticula with stool simulating polyps. *Gastrointest Endosc* **1987**;33:252-254
8. Berk RN, Lasser EC. *Radiology of the ileocecal area*. Philadelphia: Saunders, **1975**:162-171
9. Shah AN, Mazza BR. The detection of an inverted diverticulum by colonoscopy. *Gastrointest Endosc* **1982**;28:188-189

Yersinia Terminal Ileitis: Sonographic Findings in Eight Patients

Takayuki Matsumoto¹
 Mitsuo Iida¹
 Teruo Sakai²
 Yutaka Kimura²
 Masatoshi Fujishima¹

To determine the sonographic features of *Yersinia* terminal ileitis, we analyzed the sonograms of eight patients with acute terminal ileitis. Bacteriologic or serologic confirmation of *Yersinia enterocolitica* infection was available in six patients. In the other two, the clinical course and radiologic findings were compatible with the diagnosis. Radiographs and endoscopy showed edematous mucosa with small elevations in the terminal ileum in all the patients. Sonograms showed thickening of the wall of the ileum in all eight patients and enlarged mesenteric lymph nodes in six patients.

Although the number of the patients is small, our experience suggests that sonography can be useful for the detection of acute terminal ileitis caused by *Yersinia*.

AJR 156:965-967, May 1991

Yersinia enterocolitica is a well-known cause of terminal ileitis with mesenteric adenitis [1]. The infection frequently occurs in Western Europe, Scandinavia, Canada, and Japan.

The radiologic and endoscopic findings [2, 3] of this disease have been described. The aim of our study is to analyze the sonographic features in eight patients with this condition.

Materials and Methods

From August 1989 to July 1990, we encountered eight patients whose clinical courses and findings obtained by barium follow-through examinations suggested acute *Yersinia* terminal ileitis. In all of the patients, sonography, colonoscopy, and barium follow-through examination of the small intestine were performed within 7 days of each other.

The patients comprised five men and three women 11–28 years old (mean, 18 years). Right-sided lower abdominal pain was the most frequent complaint; the next most frequent complaints were diarrhea and nausea. Positive C-reactive protein and leukocytosis were noted in seven patients and accelerated erythrocyte sedimentation rate in five. Serum antibody titers against *Y. enterocolitica* were elevated in six of the patients; in three, fecal cultures also revealed this organism.

Barium follow-through examinations of the small intestine were performed 2–8 days (mean, 5 days) after the onset of symptoms. In all patients, edema and small nodular elevations in the distal part of the ileum were shown on radiographs (Fig. 1). In seven of the eight patients, smooth filling defects, which were larger than nodular elevations, were noted (Fig. 2).

Colonoscopy, performed 4–15 days (mean, 7 days) after the onset of symptoms, revealed small nodular elevations in the terminal ileum (seven patients) and edema (six patients). In one patient, the terminal ileum could not be visualized endoscopically because of the redundant colon.

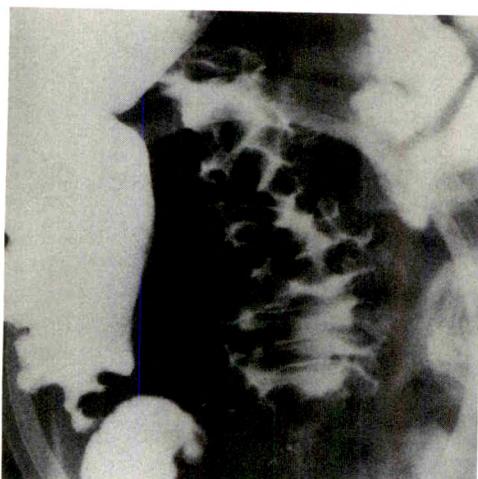
All sonographic examinations were performed with T-shaped 3.5-MHz convex-array and 7.5-MHz linear-array transducers (EUB-410, Hitachi, Tokyo). The time interval between the onset of symptoms and the sonograms ranged from 2 to 10 days (mean, 5 days). Before the study, all the patients were asked to point to the site of pain. Transverse scans of the right lower quadrant were made with the convex-array transducer, and compression was gradually

Received September 26, 1990; accepted after revision November 29, 1990.

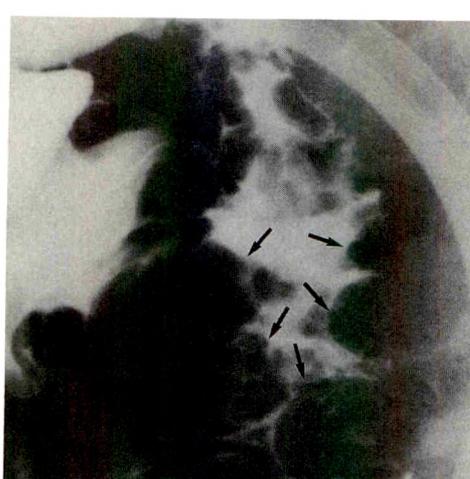
¹ Second Department of Internal Medicine, Faculty of Medicine, Kyushu University, Maidashi 3-1-1, Higashi-ku, Fukuoka 812, Japan. Address reprint requests to T. Matsumoto.

² Division of Surgery, Kimura Hospital, Chiyo 2-13-19, Hakata-ku, Fukuoka 812, Japan.

0361-803X/91/1565-0965
 © American Roentgen Ray Society

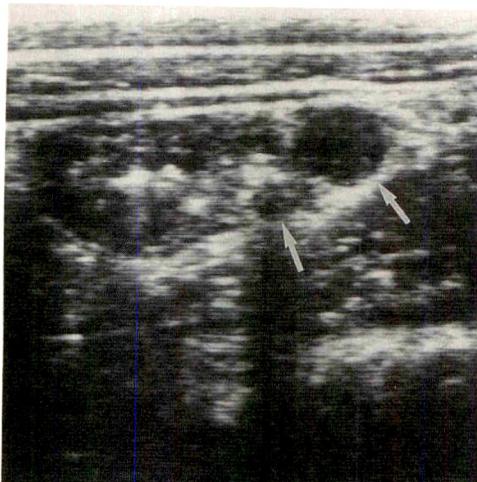


1

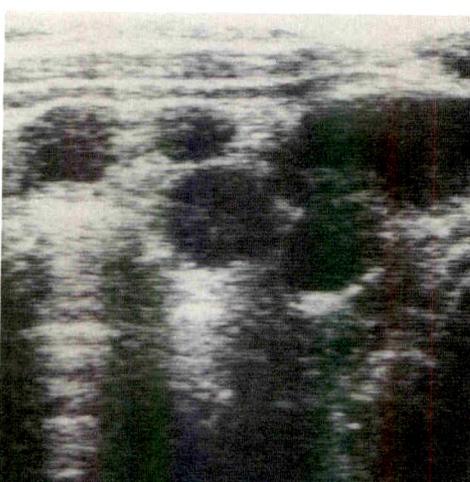


2

Fig. 1.—16-year-old girl with pain in right lower quadrant. Barium follow-through examination shows thickened folds and nodular elevations of terminal ileum, diagnosed as *Yersinia* terminal ileitis.



A



B

Fig. 2.—23-year-old man with right-sided abdominal pain and diarrhea. Barium follow-through examination shows smooth filling defects in terminal ileum (arrows).

increased until all gas, which was detected in half of the patients, was expressed from the ascending colon and the cecum to the hepatic flexure. If any abnormalities were found, the probe was changed to the linear-array transducer, and the compression study was repeated. The radiologist was aware of the patients' symptoms, but was not given any other information.

Results

During the sonographic examinations, none of the patients experienced severe abdominal pain or abdominal discomfort, though some had mild discomfort. Sonographic abnormalities were identified in all of the patients.

Mural thickening of the bowel in the right lower abdomen was detected in all patients (Figs. 3A, 4, and 5). The wall was always hypoechoic and was 7–10 mm thick. In addition, the thickened wall was divided into two layers: an outer hypoechoic layer and an inner layer composed of small, round,

hypoechoic spots (Fig. 4). The former conformed to the edematous mucosa detected by endoscopy and radiography, and the latter to the small nodular elevations seen on these studies. In six of the patients, enlarged lymph nodes were detected also (Fig. 3). They were round or oval, sharply demarcated hypoechoic masses 7–21 mm in diameter. The number of lymph nodes ranged from three to six per patient.

With antibiotic therapy, all the patients became asymptomatic within 2 weeks after the onset of symptoms. Follow-up sonograms, obtained 4 weeks after the initial examination in four patients, revealed no abnormalities.

Discussion

In two of the eight patients included in this study there was no bacteriologic or serologic evidence of *Y. enterocolitica* infection. However, the self-limiting clinical course and the

Fig. 4.—26-year-old woman with pain in right lower quadrant. Sonogram shows thickened wall of terminal ileum and round, hypoechoic areas in mucosa (arrows), which conform to small elevations seen on radiograph.

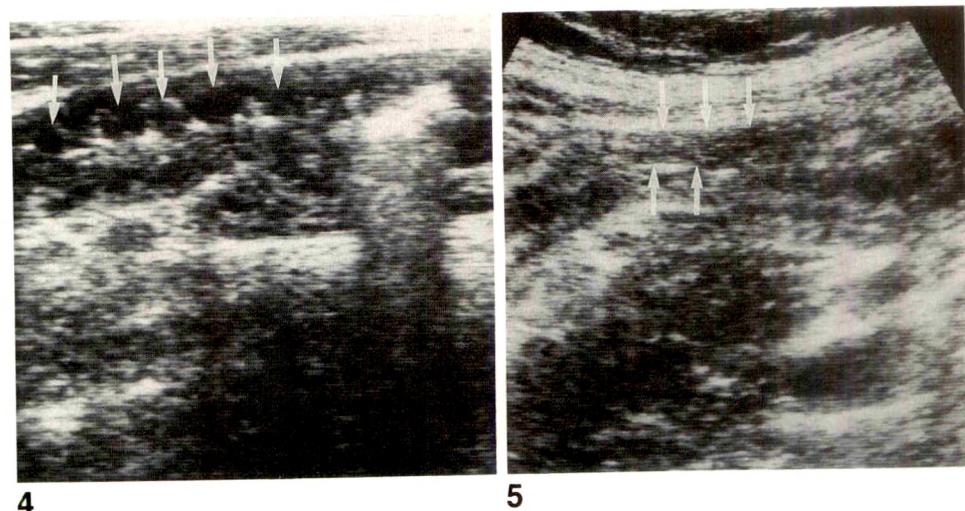


Fig. 5.—13-year-old boy with pain in right lower quadrant. Sonogram shows thickened wall (arrows) of terminal ileum.

radiographic or endoscopic findings were characteristic of the disease.

In all eight patients, sonograms showed thickening of the terminal ileum. This was believed to have been caused by the edema noted on the radiographs or during endoscopy.

The use of sonography in detecting bowel wall thickening has been reported [4]. Puylaert [5] reported sonographic findings of 14 patients with terminal ileitis; fecal cultures revealed *Y. enterocolitica* in eight of these. In his report, the terminal ileum was 4–6 mm thick, which is less than that in the present study (7–10 mm). This difference may be due to differences in the stage of infection. The sonograms in our patients were obtained within relatively short intervals (from 2 to 10 days) after the onset of symptoms.

Enlarged mesenteric lymph nodes, ranging from 7 to 21 mm in diameter, were found on sonograms in six of our eight patients. Although the size and the echogenicity of the lymph nodes detected in the present study were similar to those reported by Puylaert [5], we found fewer lymph nodes per patient. This may be because we did not use an intraoperative linear-array transducer, which allows deep penetration into the pelvis [6].

Acute appendicitis was highly suspected from the clinical

features in our patients. The sonographic findings of an inflamed appendix, characterized by targetlike aspects on the transverse view that consist of a hypoechoic lumen, a hyperechoic inner ring, and a hypoechoic outer ring [6–8], are different from those of terminal ileitis [5]. In addition, lymph node enlargement is not so evident in acute appendicitis.

REFERENCES

1. Winblad S, Nilehn B, Sternby NH. *Yersinia enterocolitica* (*Pasteurella X*) in human enteric infections. *Br Med J* 1966;2:1363–1366
2. Ekberg O, Sjöström B, Brahme F. Radiological findings in *Yersinia* ileitis. *Radiology* 1977;123:15–19
3. Matsumoto T, Iida M, Matsui T, et al. Endoscopic findings in *Yersinia enterocolitica* enterocolitis. *Gastrointest Endosc* 1990;36:583–587
4. Bluth EI, Merritt CRB, Sullivan MA. Ultrasonic evaluation of the stomach, small bowel, and colon. *Radiology* 1979;133:677–680
5. Puylaert JBCM. Mesenteric adenitis and acute terminal ileitis: US evaluation using graded compression. *Radiology* 1986;161:691–695
6. Puylaert JBCM. Acute appendicitis: US evaluation using graded compression. *Radiology* 1986;158:355–360
7. Schwerk WB, Wichtrup B, Rothmund M, Rüschoff J. Ultrasonography in the diagnosis of acute appendicitis: a prospective study. *Gastroenterology* 1989;97:630–639
8. Jeffrey RB, Laing FC, Lewis FR. Acute appendicitis: high-resolution real-time US findings. *Radiology* 1987;163:335–338



Book Review



Control of Radon in Houses. Recommendations of the National Council on Radiation Protection and Measurements. (NCRP Report No. 103.) Bethesda, MD: National Council on Radiation Protection and Measurements, 90 pp., 1989. \$15

For those readers who have little extra reading time available, do not bother with this report; for those readers with extra time, read something else.

The title of this report implies a working guide to radon mitigation in homes. The preface states, "It is intended that this report would be useful to home owners, to individuals involved in marketing services to reduce radon and radon decay products in houses, and to the scientific community interested in control techniques for radon and radon decay products." I suggest that a report from the National Council on Radiation Protection and Measurements (NCRP) will be of little help to these people. An excellent report on this same topic is available from the Environmental Protection Agency (EPA): *Radon Reduction Techniques for Detached Houses* (EPA/625/5-87/019). The EPA report is much more complete and should be used rather than the NCRP report.

As a final comment, the NCRP report suggests that one of three acceptable methods of radon mitigation is "the combination of unipolar space charging and enhanced convection." The EPA report gives one short paragraph to this method and suggests that a number of problems exist. I note this point because the chairman of the committee that prepared the NCRP report is an author on all the cited references on the unipolar space charging method. I wonder about the possible scientific bias of that committee.

Michael J. O'Brien
University of Washington
Seattle, WA 98195

Pictorial Essay

CT of AIDS-Related Lymphoma

Ronald R. Townsend¹

A spectrum of CT findings in patients with AIDS-related lymphoma (ARL) is illustrated herein. When a solid mass anywhere in the body is encountered in a patient with AIDS, lymphoma must be considered in the differential diagnosis. Although the CT findings alone generally are not enough for a specific diagnosis of lymphoma, this frequently will be suggested as the most likely diagnosis, facilitating further workup. CT-guided biopsy is useful in providing tissue diagnosis in many cases.

Initial reports of AIDS described opportunistic infections and Kaposi sarcoma in young homosexual men. More recently, AIDS has been recognized in other populations of patients, and many other clinical manifestations of AIDS have been identified. Although infectious diseases remain by far the most common manifestations of AIDS, several tumors also have been associated with this syndrome. An increased frequency of non-Hodgkin lymphoma in AIDS patients was recognized as early as 1982. The diagnosis of one of several relatively undifferentiated forms of non-Hodgkin lymphoma in a person with serologic evidence of human immunodeficiency virus (HIV) infection fulfills current criteria of the Centers for Disease Control (CDC) for the diagnosis of AIDS. These forms include small noncleaved, large, immunoblastic, and undifferentiated cell types. Hodgkin disease also occurs in patients infected with HIV, but whether this is a manifestation of AIDS is controversial, and Hodgkin disease currently is not found in the CDC criteria for diagnosis of AIDS.

Both non-Hodgkin lymphoma and Hodgkin disease tend to produce aggressive and atypical features in patients with

AIDS as compared with other patients. At the time of clinical presentation, advanced disease (stage III or IV) with extranodal involvement is common. Primary CNS lymphoma, rare before AIDS, is seen much more commonly in this setting.

Abdomen

ARL in the abdomen may be manifested in visceral organs, lymph nodes, bowel, omentum, retroperitoneum, or abdominal wall [1, 2]. The aggressive nature of the disease in these patients is often manifested as multiple sites of abdominal involvement.

Liver

Focal hepatic masses of lymphoma are much more common in AIDS patients than in the non-AIDS population. The appearance may vary from one or a few large low-attenuation masses (Fig. 1) to more than 100 smaller masses (Fig. 2). Hepatomegaly is common in patients with AIDS, and occasionally a large liver may harbor lymphoma without focal lesions evident on CT [2]. Fortunately, this appears to be uncommon.

Spleen

Focal splenic lesions are also seen more commonly in ARL than in lymphoma without AIDS (Fig. 3). Single or multiple low-attenuation foci may be present. Other causes of focal

Received October 17, 1990; accepted after revision November 29, 1990.

¹ Department of Radiology, San Francisco General Hospital, 1001 Potrero Ave., San Francisco, CA 94110. Present address: Department of Radiology, Box C-277, University of Colorado Health Sciences Center, 4200 E. 9th Ave., Denver, CO 80262. Address reprint requests to R. R. Townsend.

AJR 156:969-974, May 1991 0361-803X/91/1565-0969 © American Roentgen Ray Society

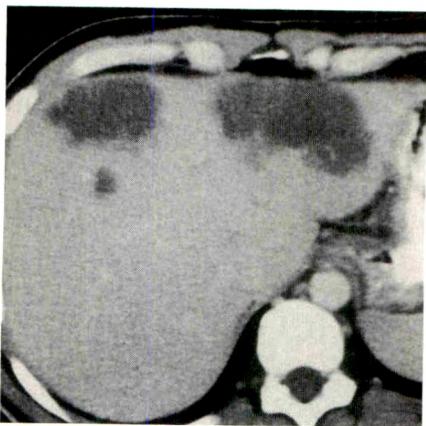


Fig. 1.—CT scan of hepatic undifferentiated non-Hodgkin lymphoma. Three low-attenuation foci of lymphoma are seen anteriorly in liver.

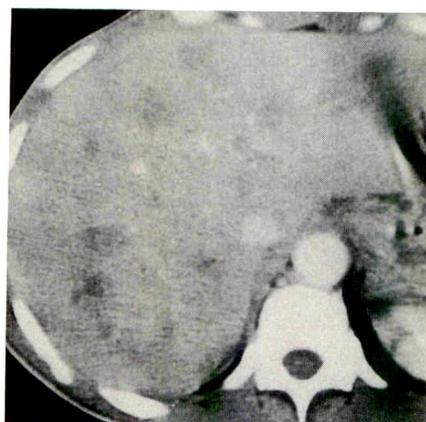


Fig. 2.—CT scan of hepatic non-Hodgkin lymphoma. Many low-attenuation lesions 0.5–2.0 cm in diameter are seen throughout an enlarged liver.

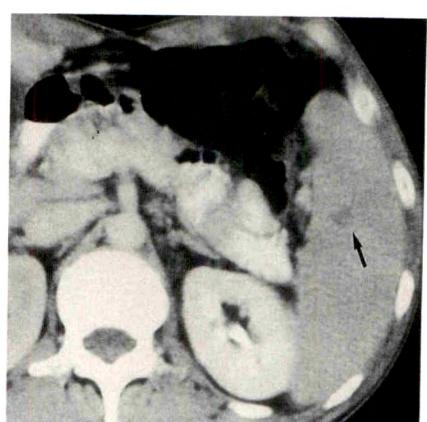


Fig. 3.—CT scan of splenic immunoblastic lymphoma. A solitary 1-cm low-attenuation focus of lymphoma is evident in spleen (arrow).

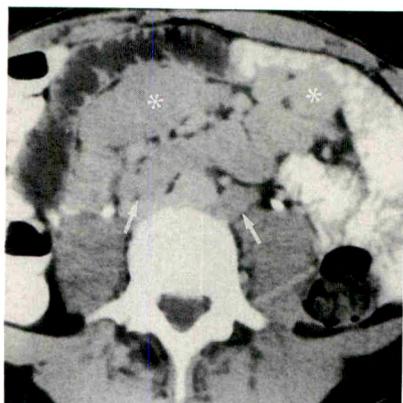


Fig. 4.—CT scan of nodal non-Hodgkin lymphoma. Extensive mesenteric (asterisks) and retroperitoneal (arrows) adenopathy are seen.

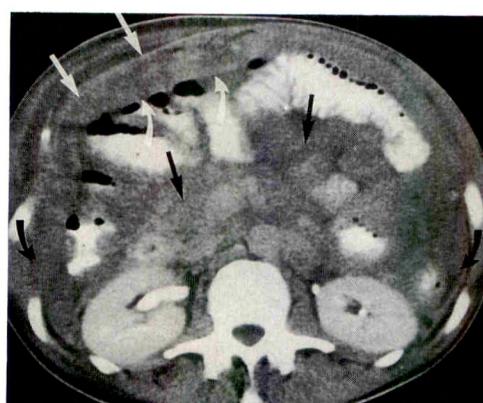


Fig. 5.—Peritoneal lymphomatosis—undifferentiated non-Hodgkin lymphoma.

A, CT scan shows enlarged infiltrated omentum (anterior margin of omentum = straight white arrows; posterior margin of omentum = curved white arrows). Mesentery (straight black arrows) is infiltrated, and pericolic gutters are filled with lymphomatous tissue (curved black arrows). (Reprinted with permission from Haskal et al. [3].)

B, Sonogram (transverse midabdomen) shows thickened omentum (between cursors). Results of sonographically guided biopsy with an 18-gauge core needle indicated non-Hodgkin lymphoma.

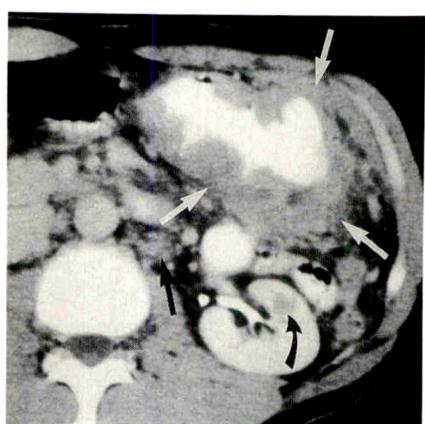
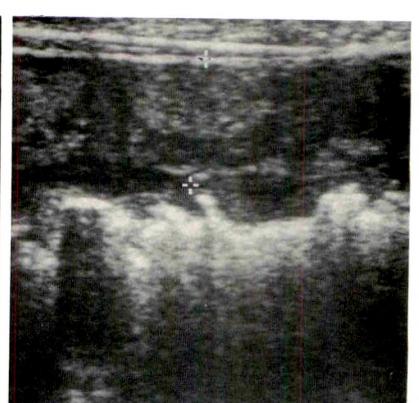


Fig. 6.—CT scan of gastric immunoblastic lymphoma. Grossly thick-walled contrast-filled stomach (outer margin of stomach, white arrows), retroperitoneal adenopathy (straight black arrow), and renal lesion (curved black arrow) are seen.

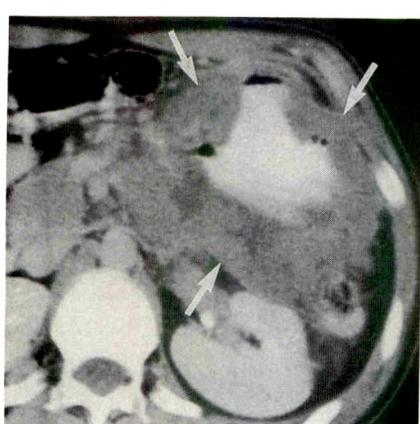


Fig. 7.—CT scan of jejunal small noncleaved cell non-Hodgkin lymphoma shows large mass of lymphoma (arrows) with central contrast and air, reflecting communication with jejunal lumen.

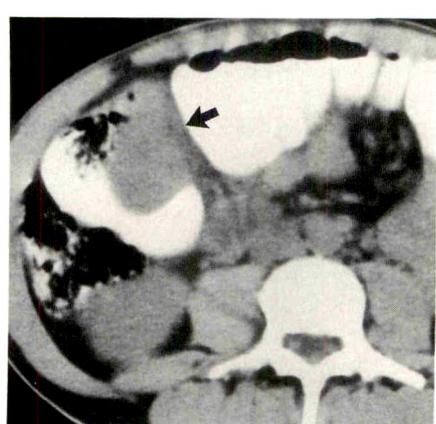


Fig. 8.—CT scan of colonic non-Hodgkin lymphoma shows intramural mass of lymphoma near hepatic flexure (arrow). Diagnosis was by sonographically guided fine-needle aspiration.

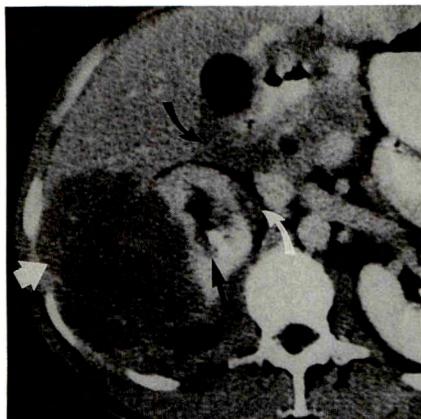


Fig. 9.—CT scan of renal/hepatic non-Hodgkin lymphoma shows large mass of lymphoma bridging anatomic planes between liver and right kidney (straight white arrow). Lymphoma also infiltrates renal sinus (straight black arrow), renal capsule (curved white arrow), and caudate lobe of liver (curved black arrow).

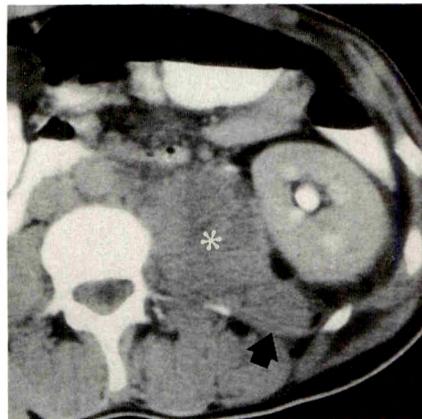


Fig. 10.—CT scan of psoas non-Hodgkin lymphoma shows that left psoas (asterisk) and quadratus lumborum (arrow) muscles are enlarged by lymphoma.

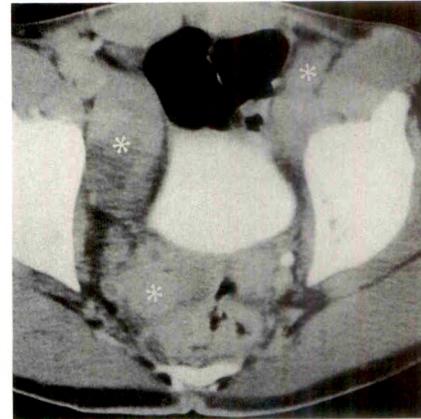


Fig. 11.—CT scan of pelvic adenopathy in Hodgkin disease. Multiple enlarged nodes (asterisks) are seen here and were evident throughout lower abdomen.

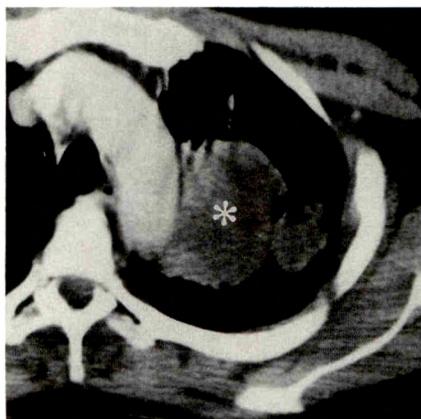


Fig. 12.—CT scan of pulmonary immunoblastic lymphoma shows large parenchymal mass of lymphoma in left side of chest (asterisk).

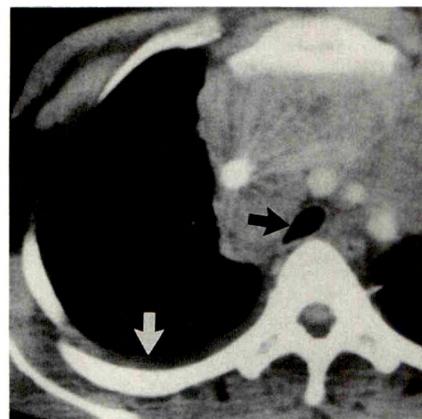


Fig. 13.—CT scan of mediastinal high-grade non-Hodgkin lymphoma. Large superior mediastinal mass surrounds and posteriorly displaces trachea (black arrow) and contrast-filled great vessels. Airway is compromised. A right-sided pleural effusion is also present (white arrow).

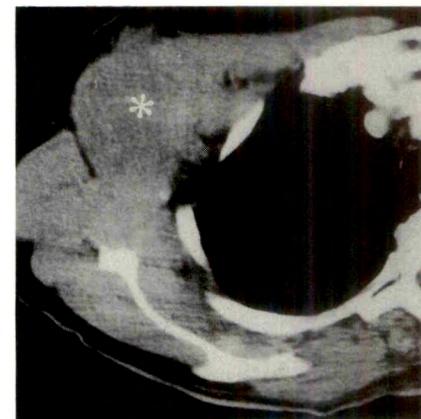


Fig. 14.—CT scan of right-sided axillary/chest wall immunoblastic lymphoma (asterisk) in patient who also had abdominal adenopathy.

splenic lesions in AIDS include mycobacterial or fungal infection, infarcts, and bacterial abscesses. Although it is preferable because of potential bleeding complications to perform biopsies of other masses if they exist, focal splenic masses can be aspirated successfully with a 22-gauge needle. Splenomegaly is quite common in AIDS and is not predictive of involvement with lymphoma.

Lymph Nodes

Adenopathy, especially retroperitoneal and mesenteric, is a common manifestation of abdominal ARL (Fig. 4). Such adenopathy also may be seen with Kaposi sarcoma and mycobacterial infection, however. Small (<1.5 cm) retroperitoneal lymph nodes in patients with AIDS commonly reveal only reactive hyperplasia at biopsy, so suspicion of neoplasm or specific infection is limited to patients with larger nodes,

nodes in other locations, or large clusters of smaller nodes. If nodes have low-attenuation centers, mycobacterial infection, rather than lymphoma, is likely. Biopsy is necessary for definitive diagnosis.

Omentum

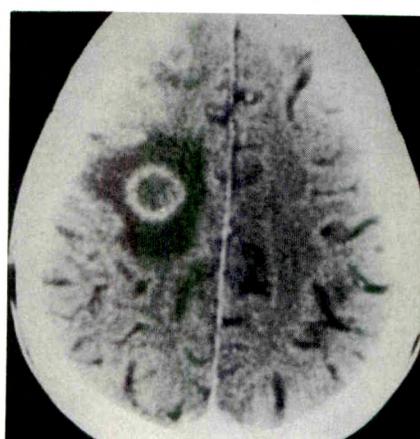
The omentum may be grossly infiltrated with lymphoma as one manifestation of peritoneal lymphomatosis (Fig. 5). This diffuse involvement of the peritoneal cavity with lymphoma illustrates well the aggressive nature of ARL and is associated with a poor prognosis.

Gastrointestinal Tract

Focal masses of ARL may be seen in the stomach (Fig. 6), small bowel (Fig. 7), or colon (Fig. 8). Masses in the gastroin-



Fig. 15.—CT scan of left-sided chest wall non-Hodgkin lymphoma (arrow). This was the only focus of disease at presentation.



A

Fig. 16.—Primary lymphoma of right cerebral hemisphere.

A, Contrast-enhanced CT scan shows ring-enhancing lesion with surrounding edema. This appearance is indistinguishable from toxoplasmosis.

B, Unenhanced CT scan shows slightly increased attenuation in lesion, which suggests lymphoma.

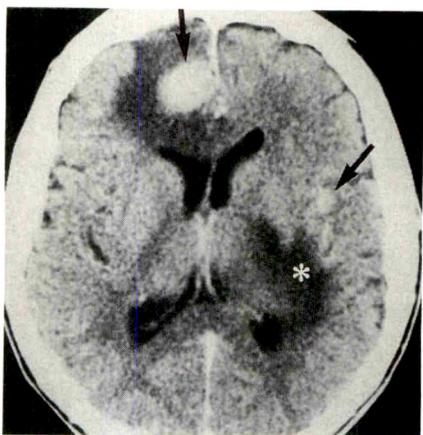
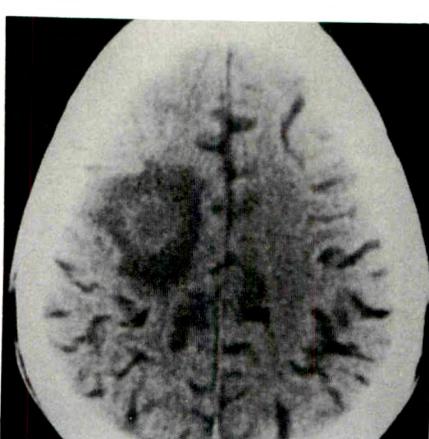


Fig. 17.—CT scan of multifocal CNS lymphoma with edema shows homogeneously enhancing lesions (black arrows). Edema (asterisk) of left hemisphere was related to additional lesions on adjacent images.

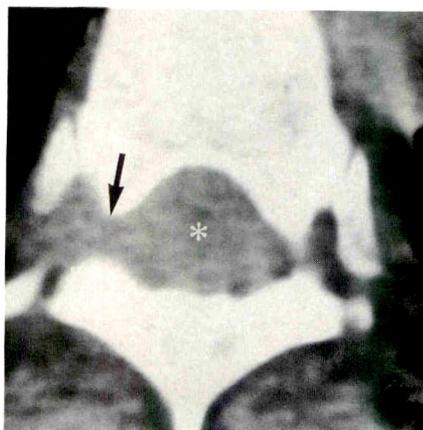


Fig. 18.—Myelogram CT scan of epidural non-Hodgkin lymphoma shows that soft-tissue mass (asterisk) totally fills spinal canal, obliterating thecal sac and extending out through neural foramen on right (arrow). Thoracic spine disease occurred several months after initial presentation with abdominal disease.

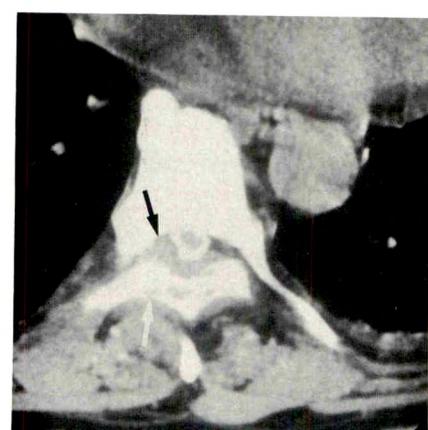


Fig. 19.—Myelogram CT scan of epidural non-Hodgkin lymphoma with bone erosion shows that abnormal epidural tissue (black arrow) effaces thecal sac and erodes vertebral posterior elements (white arrow = bone erosion).

testinal tract may be isolated findings, but evidence of disease elsewhere is common.

Kidney and Retroperitoneum

Focal masses of ARL in the kidney are not as common as in the liver or spleen. One or more renal masses may be seen (Fig. 9). Masses may be sharply circumscribed or may infiltrate into the renal sinus or surrounding tissues.

A grossly enlarged psoas muscle may represent a primary manifestation of ARL (Fig. 10). With infiltration of surrounding fat, findings may mimic a psoas inflammatory process.

Pelvis

Gross pelvic adenopathy is common in AIDS-related Hodgkin disease or non-Hodgkin lymphoma (Fig. 11).

Thorax

ARL in the chest may have a variety of manifestations, including pulmonary parenchymal infiltrate/mass (Fig. 12), mediastinal adenopathy or mass (Fig. 13), pleural effusion (Fig. 13), hilar adenopathy, axillary mass or adenopathy (Fig. 14), chest wall mass (Fig. 15), or cardiac mass. In a recent small series, pleural effusion and parenchymal lung disease were the most common thoracic radiologic manifestations of

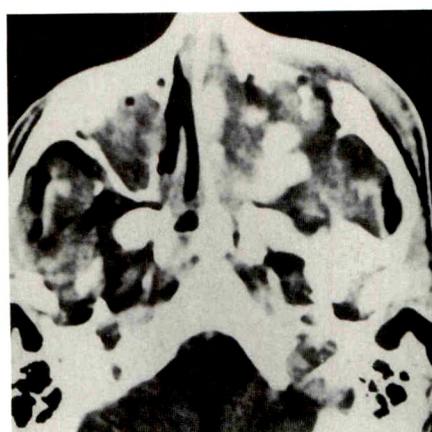
**A****B**

Fig. 20.—CT scans of left-sided maxillary/facial non-Hodgkin lymphoma. Right maxillary sinusitis. **A**, Soft-tissue windows show that both maxillary sinuses and left nasal cavity are filled with soft tissue.

B, Bone windows better illustrate sinus opacification bilaterally (asterisks) as well as destruction of walls of left maxillary sinus (black arrows). Lymphoma infiltrates face on left (white arrow) in this patient, who also had diffuse abdominal lymphoma.

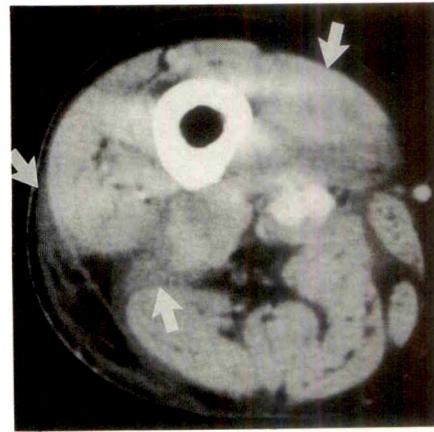


Fig. 21.—CT scan of right thigh shows immunoblastic lymphoma (arrows) infiltrating muscles and fat planes.



Fig. 22.—CT scan of osseous non-Hodgkin lymphoma. Multiple lytic lesions in ileum in a patient with diffuse disease involving liver and bone marrow.

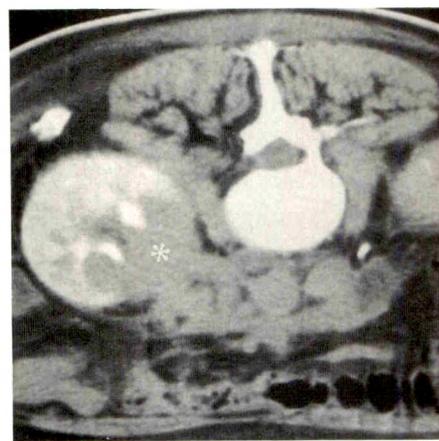
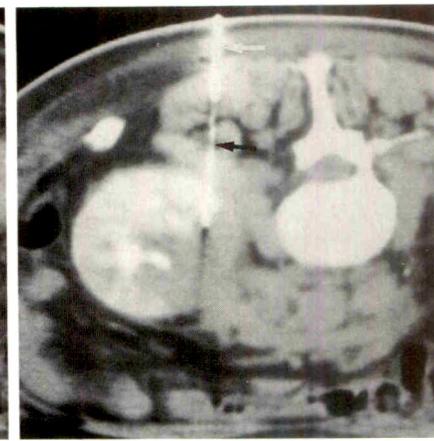


Fig. 23.—**A** and **B**, CT scans of renal non-Hodgkin lymphoma obtained with patient prone show mass (asterisk) of non-Hodgkin lymphoma infiltrating left renal sinus/pelvis and placement of needle for biopsy for diagnosis. 22-gauge needle (black arrow) has been inserted through 18-gauge needle (white arrow), a technique more commonly used in lung.

**B**

ARL [4]. This contrasts with mediastinal and hilar adenopathy as the most common thoracic findings in young nonimmuno-compromised lymphoma patients.

Central Nervous System

Brain

Primary CNS lymphoma is a rare entity in immunocompetent patients. In patients with AIDS it is much more common. Unfortunately, clinical findings and findings on CT scans are often nonspecific. ARL in the brain may present as a ring-enhancing lesion with surrounding edema, identical in appearance to the much more common toxoplasmosis lesion

(Fig. 16A). A lesion that is intrinsically high density on unenhanced CT (Fig. 16B) is more likely to be lymphoma than a lesion without this appearance. A homogeneously enhancing mass (Fig. 17) is more characteristic of lymphoma than toxoplasmosis. Multiple lesions are common with either process. If the corpus callosum is infiltrated, lymphoma is most likely. In most cases, CT findings are not enough for a definite diagnosis [5]. One clinical approach is to treat presumptively for toxoplasmosis (which is much more common than lymphoma) and to perform biopsies on those patients who do not respond to the toxoplasmosis treatment. MR imaging may help distinguish lymphoma from toxoplasmosis in some cases.

Spine

Epidural masses of ARL may cause neurologic deficit as a result of cord compression (Figs. 18 and 19). The epidural mass may represent local extension of a paraspinous mass (e.g., large psoas mass).

Face

Patients with AIDS commonly have opacified paranasal sinuses related to infectious sinusitis. Soft tissue filling the sinuses and infiltrating through the facial bones is a rare manifestation of ARL (Fig. 20).

Extremities

A new palpable soft-tissue mass of the extremities in a patient with AIDS may be the result of reactive adenopathy, inflammation, Kaposi sarcoma, or lymphoma. Masses infiltrating through the muscles and subcutaneous tissues of the extremities suggest lymphoma (Fig. 21).

Bones

Multifocal lytic bone lesions associated with disseminated ARL have been an uncommon finding during imaging (Fig.

22). Bony erosion related to an adjacent soft-tissue mass may be seen (Fig. 19).

CT-Guided Biopsy

For most masses identified by CT, tissue diagnosis can be obtained by using CT or sonographically guided percutaneous biopsy (Fig. 23). Although the diagnosis of non-Hodgkin lymphoma by fine-needle aspiration is somewhat controversial, the technique can be successful in patients with AIDS [2, 6]. Obtaining a larger sample of tissue by using a core biopsy needle (18 gauge or larger) will be necessary in some cases. Open surgical biopsy occasionally will be needed to make a diagnosis of non-Hodgkin lymphoma, but is the rule for diagnosis of Hodgkin disease.

REFERENCES

1. Nyberg DA, Jeffrey RB Jr, Federle MP, Bottles K, Abrams DI. AIDS-related lymphomas: evaluation by abdominal CT. *Radiology* 1986;159:59-63
2. Townsend RR, Laing FC, Jeffrey RB Jr, Bottles K. Abdominal lymphoma in AIDS: evaluation with US. *Radiology* 1989;171:719-724
3. Haskal ZJ, Lindan CE, Goodman PC. Lymphoma in the immunocompromised patient. *Radial Clin North Am* 1990;28:885-899
4. Sider L, Weiss AJ, Smith MD, VonRoenn JH, Glassroth J. Varied appearance of AIDS-related lymphoma in the chest. *Radiology* 1989;171:629-632
5. Lee Y-Y, Bruner JM, Tassel PV, Libshitz HI. Primary central nervous system lymphoma: CT and pathologic correlation. *AJR* 1986;147:747-752
6. Bottles K, McPhaul LW, Volberding P. Fine-needle aspiration biopsy of patients with acquired immunodeficiency syndrome (AIDS): experience in an outpatient clinic. *Ann Intern Med* 1988;108:42-45

Pictorial Essay

Anatomic Variants and Artifacts in ERCP Interpretation

David J. Gulliver,¹ Peter B. Cotton,² and John Baillie²

ERCP is a complex diagnostic procedure requiring manual dexterity, careful attention to endoscopic and radiographic technique, and correct interpretation of the resulting images. Not surprisingly, the procedure is associated with many potential pitfalls. Many of these are related to normal anatomic pancreatic and biliary variants and to artifacts associated with the examination itself. Knowledge of these variants and artifacts is necessary to perform procedures and interpret the results effectively. Our discussion and illustrations are based on a retrospective review of approximately 1300 ERCP studies performed at a single center during a 2-year period.

Anatomic Variants

Pancreatic duct variants are relatively common and usually do not cause diagnostic difficulty when the examination is of high technical quality. Pancreas divisum (Fig. 1) is easily recognized when the ventral portion is completely opacified, but a partially filled ventral duct can be mistaken for a main pancreatic duct obstructed by a stricture. The key to avoiding this pitfall is recognition of a ventral pancreatic duct by its small caliber. In cases of doubt, pancreas divisum may be confirmed by contrast injection into the dorsal pancreatic duct (Fig. 1B). A further source of difficulty with pancreas divisum is overinjection of the ventral portion causing acinar filling, which is very common if this anomaly is not anticipated. The risk of filling the acini is increased when the fluoroscopic image is not of optimal quality.

Anular pancreas is distinctive when the pancreatic duct is completely opacified, as the pancreas encircles the second part of the duodenum before passing to the left. It is an

uncommon anomaly, often associated with duodenal stenosis/atresia and other congenital anomalies [1]. Biventral pancreas (two small duct systems each the size of the ventral portion in pancreas divisum) and pancreatic hypoplasia are both rare. A bifid pancreatic duct (usually in the tail or body) (Fig. 1B) and unusually tortuous pancreatic ducts generally do not cause difficulty. However, the pancreatic duct in the head of the pancreas may take a steep downward course to the papilla, paralleling the common bile duct (Fig. 2). In this circumstance a partially filled pancreatic duct can be confused with the bile duct on fluoroscopy. The main pancreatic duct is occasionally narrowed at its junction with the accessory duct; it is important not to misinterpret this normal variant as a duct stricture [2]. The pancreatic duct may also have a slight fusiform dilatation just before entering the papilla [3].

Biliary variants are numerous. The hepatic ducts show considerable variability; a segmental (accessory) right hepatic duct, which usually drains into the common hepatic duct (Fig. 3) or cystic duct, is particularly common. When the right and left hepatic ducts have a low union (Fig. 2), the common hepatic duct may be "absent," with the cystic duct draining into the right main hepatic duct. The termination of the cystic duct is highly variable, with drainage into virtually any part of the biliary tree. The common hepatic artery or its branches can produce vascular indentations, most frequently in the common bile duct (Fig. 4).

The gallbladder has many anatomic variants. When only partially filled, a high gallbladder (Fig. 5) may be confused with a cavity in the liver. The gallbladder may have a low position, even reaching the true pelvis. Unusual shapes of the gallbladder (e.g., Phrygian cap, gallbladder diverticulum, septated/

Received October 24, 1990; accepted after revision November 29, 1990.

¹ Department of Radiology, Box 3808, Duke University Medical Center, Durham, NC 27710. Address reprint requests to D. J. Gulliver.

² Division of Gastroenterology, Duke University Medical Center, Durham, NC 27710.

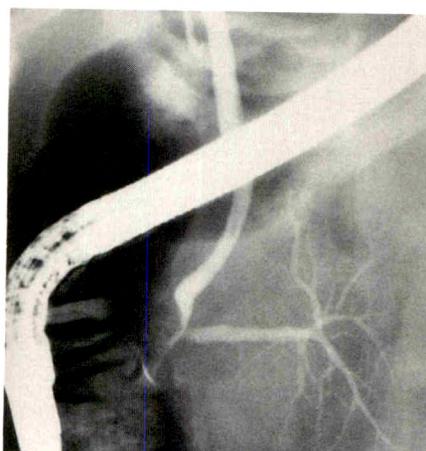
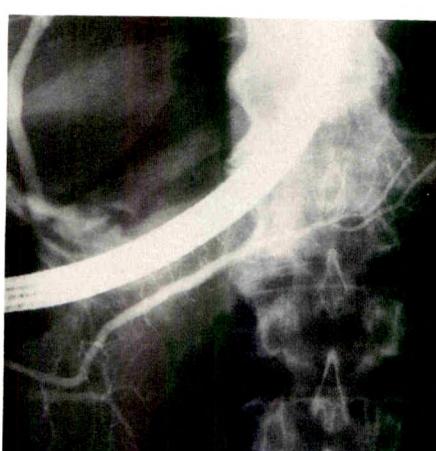
**A****B**

Fig. 1.—*A*, ERCP after injection of ventral pancreas and bile duct shows pancreas divisum. In most cases of pancreas divisum, ventral portion is smaller than in this case, with a duct caliber significantly less than that of dorsal duct. Duct caliber is a useful differentiating feature in cases of doubt.

B, ERCP after injection of dorsal duct shows moderate changes of pancreatitis and an incidental bifid duct in pancreatic tail. An unusual feature of this case is that contrast material is still present in ventral duct at the time of dorsal duct injection.

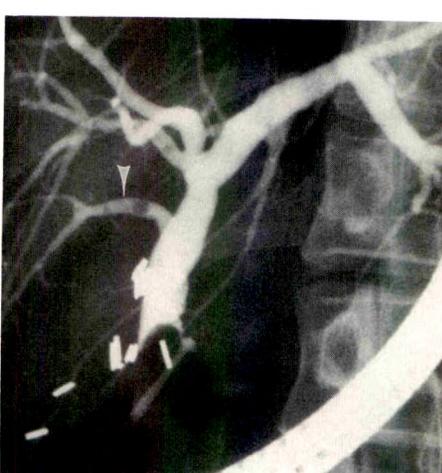
**2****3**

Fig. 2.—ERCP shows low union of right and left hepatic ducts (cystic duct is not visualized). Also in this case, pancreatic duct takes a steep downward course to papilla, almost paralleling bile duct; this may result in a partially filled pancreatic duct being mistaken for bile duct.

**4****5**

Fig. 3.—ERCP shows segmental (accessory) right hepatic duct (arrowhead) draining into common hepatic duct. Gas bubbles in biliary tree are due to a previous cholecodochoduodenostomy. A balloon-tipped catheter has been used to cannulate the cholecodochoduodenostomy.

Fig. 4.—ERCP shows vascular impression on common bile duct caused by hepatic artery (arrow).

Fig. 5.—ERCP shows high position of gallbladder in front of liver. Cystic duct (arrowhead).

hourglass gallbladder) do not usually cause diagnostic difficulty at ERCP if the organ is completely opacified. If in doubt, delayed films taken after rolling the patient prone and supine (to mix contrast material and bile) and oblique films should

resolve the question. Multiple gallbladders (prevalence, approximately 1:4000) may cause confusion; abdominal sonography and CT may fail to define this unusual anatomy (Janson J, Gulliver D, unpublished data). Absence of the gallbladder

is rare and usually is associated with other congenital anomalies [1].

The confluence of the common bile duct and pancreatic duct usually forms a short common channel within the duodenal wall. However, the ducts may not meet until they drain through the papillary orifice, and occasionally they have separate orifices into the duodenum. Duodenal diverticula may cause difficulty in interpreting the radiographs, especially when filled with contrast material (Fig. 6). However, this is not usually a problem if the diverticula are noted during endoscopy.

Artifacts

ERCP artifacts may be caused by endoscopic equipment (e.g., pressure from the cannula or endoscope distorting the

distal bile duct), contrast material injected outside the ductal systems, nonpancreaticobiliary calcifications, bowel gas overlying the area of interest, incomplete filling of ducts, and unintentional injection of air.

Pancreatic duct artifacts are commonly caused by inadvertent contrast injection in an inappropriate location. Misdirected or traumatic cannulation may be followed by submucosal injection of contrast material into the duodenal wall (this may also be seen in the wall of the bile duct). Unintentional cannulation of a pancreatic duct side branch followed by contrast injection can lead to branch duct rupture and contrast extravasation (Fig. 7).

Contrast material in the stomach or duodenum usually is a problem only if it obscures the area of interest, but contrast material lying between two gastric rugal folds may mimic a pancreatic duct. A calcified abdominal lymph node or renal calculus overlying the pancreas may be mistaken for a con-

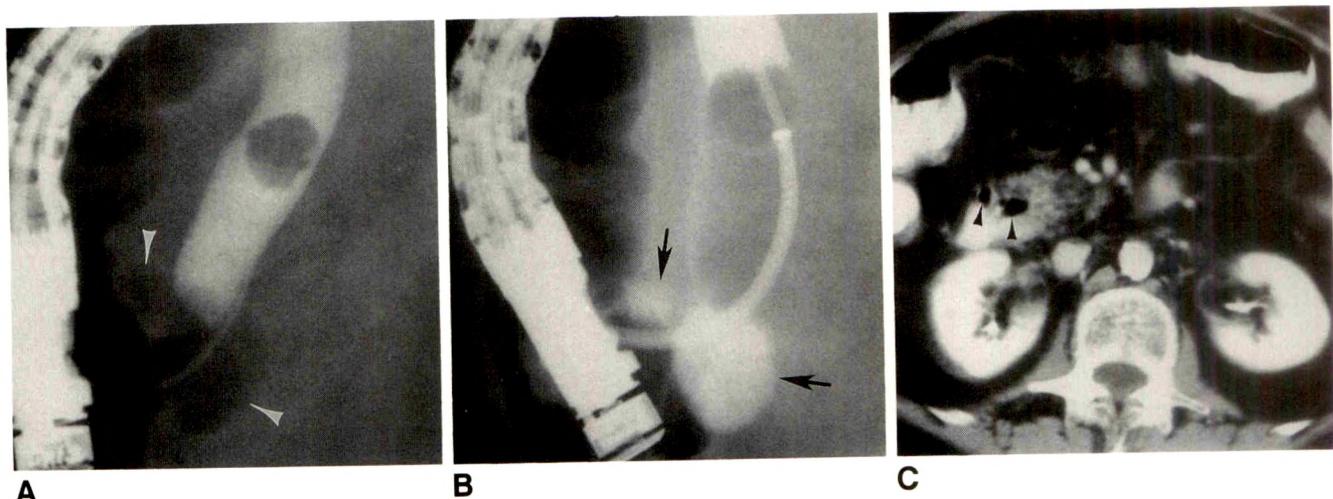


Fig. 6.—*A*, ERCP shows duodenal diverticula. Arrowheads indicate two gas-filled periampullary diverticula. An incidental common duct stone is noted. *B*, ERCP obtained later in examination shows duodenal diverticula filled with contrast material (arrows). Air is noted in bile duct distal to balloon. *C*, CT scan shows two gas-filled diverticula (arrowheads) anteromedial to contrast-filled duodenal second part.

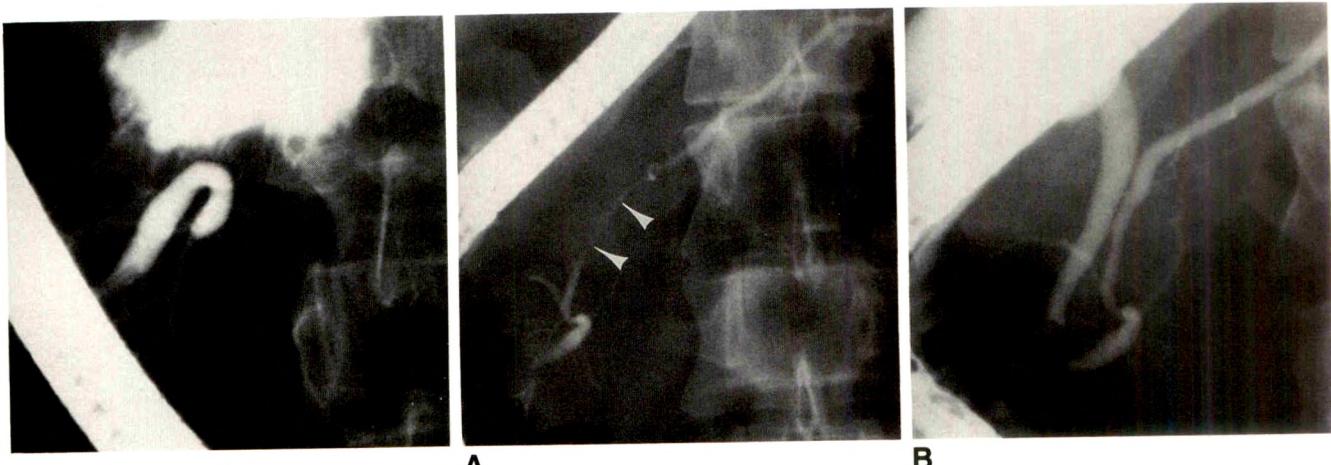


Fig. 7.—ERCP shows extravasated contrast material after inadvertent catheter placement into a pancreatic branch duct.

Fig. 8.—*A*, ERCP shows underfilling of pancreatic duct at head/body junction, mimicking a ductal stricture (arrowheads). *B*, ERCP obtained later in examination shows complete filling of duct, which excludes a stricture.

trast-filled cavity or pseudocyst; this is one of the many reasons for obtaining a plain film before each ERCP study.

Overlying bowel gas may be mistaken for gallstones in the gallbladder or biliary tree; this problem can usually be resolved by obtaining oblique films.

Pancreatic duct underfilling is a frequent cause of erroneous diagnosis of ductal stricture or obstruction, usually when the tail has not been opacified. With the patient in the prone position, contrast material must travel "uphill" to fill the tail, which requires the use of slightly greater injection pressure. For this reason a stricture or obstruction in the pancreatic body or tail should not be diagnosed unless there is adequate branch duct filling in the head and body, indicating that injection pressure has been sufficient. It is also worth noting that underfilling may also produce a "pseudostricture" in the head/body region (Fig. 8).

Inadvertent injection of a small volume of air into the pancreatic duct produces bubbles that are usually easily recognized as such and do not cause a diagnostic problem (Fig. 9). However, if enough air is injected before the contrast material (owing to insufficient flushing of the catheter), the duct in the tail (and even the body) may fill with air. This air may not be obvious on fluoroscopy. As a result, the endoscopist may inappropriately exert greater injection pressure to "fill the tail," causing overinjection and acinar filling (Fig. 10). Pancreatic acinarization not only decreases the diagnostic quality of the pancreatogram, but also carries increased risk of pancreatitis after ERCP.

Opacification of the biliary tree is gravity dependent. Contrast material, which is denser than bile, will fill dependent ducts preferentially. Thus, in the prone patient (the usual position for ERCP), ducts in the left lobe and anterior segment of the right lobe fill first, whereas in the supine position, contrast material tends to fill the posterior segment of the right lobe.

Injection of air into the biliary tree is a common problem; multiple air bubbles can make it difficult or impossible to

exclude choledocholithiasis. However, there are several methods to help differentiate stones from air bubbles. Bubbles tend to cluster together and conform to the shape of the duct and other bubbles. Bubbles can sometimes be flushed out of the duct by advancing the catheter tip past them and injecting contrast material, or may be identified by piercing them with the catheter during fluoroscopy. Tilting the fluoroscopy table may also be helpful as bubbles tend to rise more than calculi. As a last resort, trawling the common bile duct with a balloon catheter usually will resolve the issue if one can be inserted without prior sphincterotomy.

Injection of contrast material that is too dense, particularly into a dilated duct, may obscure small calculi. It is our opinion that dilute contrast material (e.g., Conray 30%, Squibb, New Brunswick, NJ) is preferable when calculi are suspected, especially in a dilated common duct [4]. If dense contrast material is already present, this can be "flushed out" with more dilute contrast material to improve visualization.

A contracted biliary sphincter may mimic a stricture or calculus of the distal bile duct. Less commonly, these appearances may also involve the adjacent pancreatic duct (Fig. 11). The absence of abnormality is recognized by the transient nature of these appearances and by the lack of upstream dilatation.

Streaming of contrast material in the bile duct refers to contrast material flowing along the dependent wall of a dilated duct rather than completely filling the lumen. This effect causes an illusion of normal caliber when the duct is dilated (Fig. 12); further contrast injection shows the true size of the duct.

During endoscopic biliary stenting procedures for tight strictures, mucosal tears or false passages may result in contrast extravasation; one of the less common forms is lymphatic filling (Fig. 13). Biliary lymphatics characteristically pass inferomedially from the liver hilum and consist of multiple narrow, tortuous channels [5].

Renal excretion of contrast material from ERCP or a prior

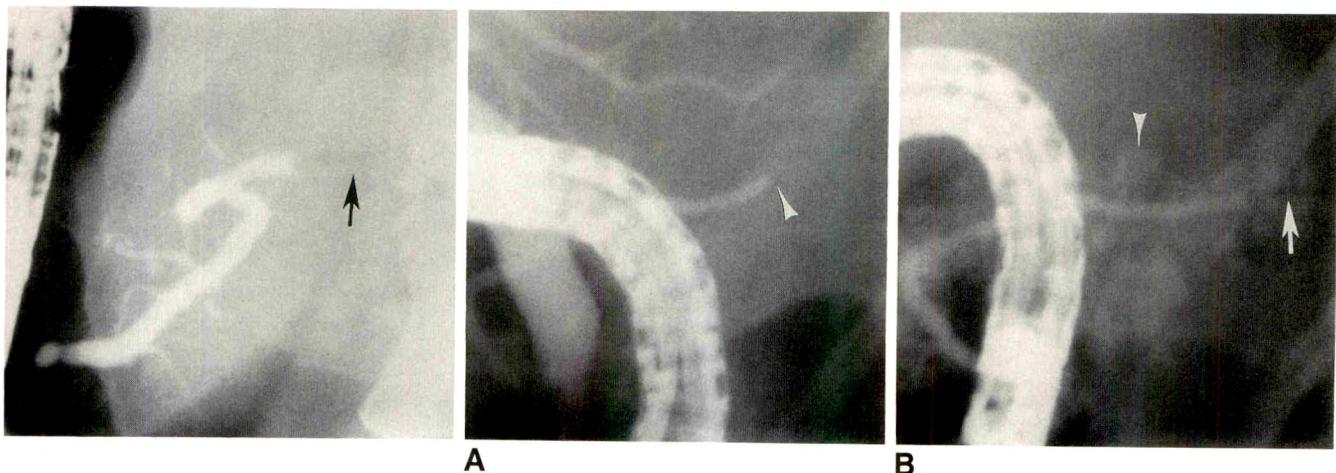


Fig. 9.—ERCP shows injected gas in pancreatic duct, resulting in a double-contrast appearance (arrow).

Fig. 10.—A, ERCP shows gas inadvertently injected into pancreatic duct mimicking an abrupt stricture (arrowhead). B, ERCP after continued injection of contrast material shows acinar filling of pancreatic head and body (arrowhead). In this radiograph, injected gas can be seen in main pancreatic duct (arrow).

Fig. 11.—A and B, Radiographs obtained at the same ERCP examination after removal of endoscope show sphincter action of ampullary sphincter that should not be confused with an ampillary stricture. Patient has had a cholecystectomy.

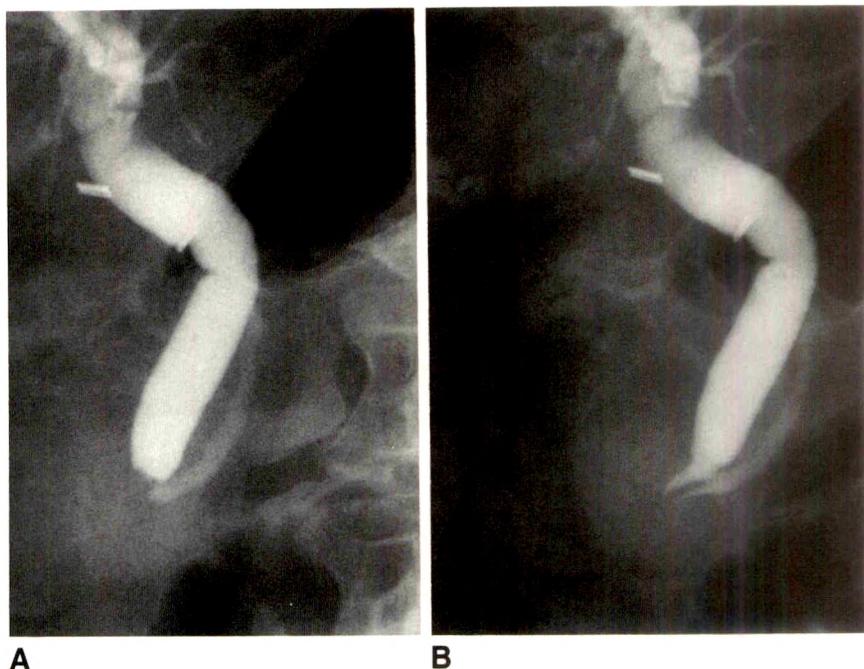
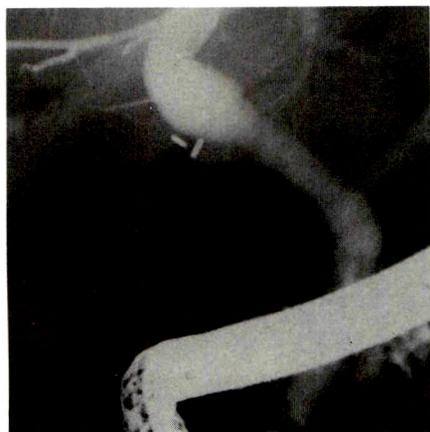
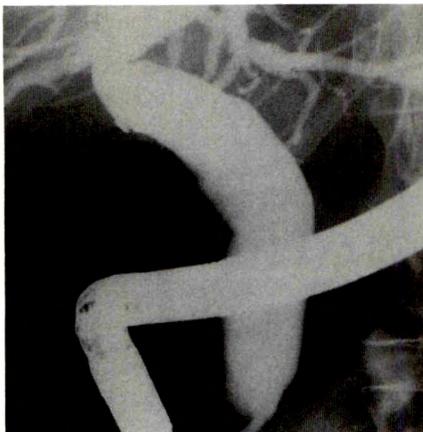
**A****B****A****B**

Fig. 12.—A, ERCP shows streaming of contrast material in bile duct, giving a false impression of a nondilated duct.

B, ERCP after complete biliary opacification confirms biliary dilatation.

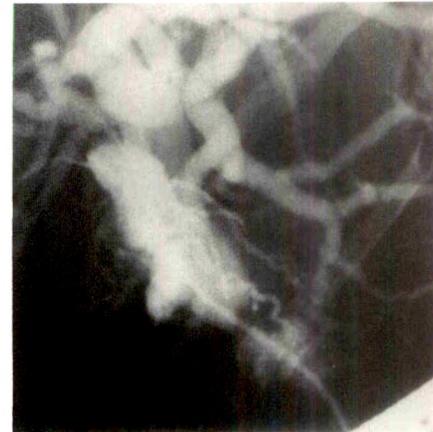


Fig. 13.—ERCP shows opacification of biliary lymphatics during difficult negotiation of a tight malignant common hepatic duct stricture.

diagnostic contrast study may cause sufficient opacification of the right renal collecting system and upper ureter to be visible at ERCP. This may occasionally be misinterpreted as an abnormality of the biliary tree or pancreatic ductal system. Similarly, contrast material lying within the duodenal bulb may occasionally be misinterpreted as a partially filled gallbladder.

Conclusions

There are many potential artifacts and anatomic variants that cause diagnostic difficulty or confusion at ERCP. Careful attention to technique is essential to eliminate those artifacts

(e.g., injection of air into the bile duct or pancreatic duct) caused by the procedure. Fluoroscopic equipment should be of high quality so that potential interpretation problems, such as filling the acini of the pancreas with contrast material, can be rectified or avoided.

Oblique or lateral radiographs are extremely valuable for decreasing the number of interpretative problems caused by artifacts, for example, overlying calcifications or bowel gas mimicking a pancreatic or biliary abnormality. Oblique and lateral radiographs also are useful for further assessing an abnormality seen on ERCP and to determine its exact anatomic relationship to the biliary tree or pancreatic duct.

Like most complex procedures, ERCP can be time-consuming. Consequently, the ideal situation of having an experienced radiologist available to assist at every ERCP study is rarely realized in practice, and most examinations are performed by gastroenterologists without specialized radiologic training. However, examination quality can be optimized if a radiologic technician with expertise in ERCP is present at the examination and responsible for image quality. In addition, all ERCP radiographs should be reviewed and formally reported by a radiologist with an interest in ERCP to minimize interpretive error.

REFERENCES

1. Hand BM. Anatomy and embryology of the biliary tract and pancreas. In: Sivak MV, ed. *Gastroenterologic endoscopy*. Philadelphia: Saunders, 1987:599-618
2. Fink AS, Perez de Ayala V, Chapman M, Cotton PB. Radiologic pitfalls in endoscopic retrograde pancreateography. *Pancreas* 1986;1:180-187
3. Stewart E, Vennes J, Geenen J. *Atlas of ERCP*. St. Louis: Mosby, 1977
4. Cotton PB. Problems in ERCP interpretation. In: Margulis AR, Gooding CA, eds. *Diagnostic radiology 1988*. San Francisco: Radiology Research and Education Foundation, University of California at San Francisco, 1988:505-510
5. Turner MA, Cho SR, Messmer JM. Pitfalls in cholangiographic interpretation. *RadioGraphics* 1987;7:1067-1105

Radiology Outreach Foundation



The Radiology Outreach Foundation (ROF) is a nonprofit corporation whose goal is to help disadvantaged countries improve their health care by providing radiology equipment, books, consultation, education, and training to their practitioners. This assistance is on an application basis that is independent of political, ethnic, or religious orientation of the grantee. It depends on the need of the people and the ability of the ROF to meet that need. The ROF is approved by the U.S. Internal Revenue Service as a tax-exempt organization. It is endorsed by the following radiologic societies: American Association of Women Radiologists, American College of Radiology, American Roentgen Ray Society, Association of University Radiologists, Radiological Society of North America, Society of Chairmen of Academic Radiology Departments, Society for Pediatric Radiology, European Society of Pediatric Radiology.

All donations to the ROF are tax deductible. Persons who would like to contribute financially to the ROF, would be interested in being a visiting professor, would like to send books or journals to any of the institutions supported by the ROF, or would like further information about the ROF should write to Charles A. Gooding, M.D., President, Radiology Outreach Foundation, 3415 Sacramento St., San Francisco, CA 94118 USA.

Subcapsular Hepatic Necrosis in Liver Transplantation: CT Appearance



Jean-Paul Abécassis¹
Denis Pariente¹
Vincent Hazebroucq¹
Didier Houssin²
Yves Chapuis²
André Bonnin¹

Eleven cases of subcapsular hepatic necrosis were found in 47 hepatic transplantation patients who underwent CT examination between the second and 14th postoperative day. CT examinations of all 11 cases showed nonenhancing hypodense subcapsular areas with irregular contours in the liver. Major vessels were free of obstruction. Anatomic correlation, possible in one case, confirmed the diagnosis. Size disproportion between the graft and the recipient abdominal cavity reduced hepatic blood flow and caused abnormal pressure points. One or both of these factors could result in ischemia in subcapsular areas and explain the subcapsular necrosis.

Although it has good prognosis without treatment, subcapsular hepatic necrosis is important to recognize to avoid confusion with liver necrosis after vascular thrombosis.

AJR 156:981-983, May 1991

Imaging techniques improve the prognosis of orthotopic liver transplantation by enabling early detection of complications. CT scanning, performed routinely in the postoperative period, resulted in the discovery of subcapsular hepatic necrosis, a common lesion without clinical manifestations.

Subjects and Methods

Between April 1987 and July 1989, 47 patients (14 female/33 male, aged 15–62 years) were prospectively examined with CT (CE 12000, CGR, Paris) after liver transplantation.

All patients underwent examination between the second and the 14th postoperative day. Images of 10-mm-thick contiguous sections of the entire liver were obtained before and after injection of iodinated contrast material. Two bolus injections of 60 ml of contrast material were administered manually through a central venous catheter; the first injection was administered at the top of the liver and the second one at the level where the portal vein divides. Additional images of 5-mm-thick sections of abnormal areas were obtained, for some patients, at the end of the examination.

Hepatic artery and portal vein patency were assessed by duplex sonography and/or CT. Anatomic-radiologic correlation was available in one patient who died of intraabdominal bleeding 4 days after the CT examination.

Results

Received October 10, 1990; accepted after revision November 13, 1990.

¹ Service de Radiologie A, Hôpital Cochin, 27 rue du Faubourg Saint-Jacques, 75014 Paris, France. Address reprint requests to J.-P. Abécassis.

² Clinique Chirurgicale, Hôpital Cochin, 27 rue du Faubourg Saint-Jacques, 75014 Paris, France.

0361-803X/91/1565-0981
© American Roentgen Ray Society

Subcapsular hepatic necrosis was noted in 23% of the patients (11/47). It was characterized by the presence of a low-density region in the liver on unenhanced CT scans. No enhancement was noticed after injection of contrast material, but the lesion was better delimited (Fig. 1). Its inner border was irregular, whereas the outer border was sharply defined by the hepatic capsule. The lesions were located in the subcapsular parenchyma, in contact with the diaphragm, mainly in the posterosuperior part of the right hepatic lobe. In two cases, the necrosis occurred also at the anterior surface of the liver (Fig. 2). Its thickness was less than 3 cm

and its width never exceeded one third of the hepatic circumference. Deep hepatic parenchyma was normal, and the distribution of the necrosis could not be correlated with vascular segmental anatomy. Major vessels were free of obstruction; duplex sonography, performed to assess vascular patency, failed to detect the small necrotic areas.

All hepatic transplantation patients have abnormal liver function tests in the first 2 weeks after surgery. We found no significant modification in results of these tests that could be attributed to the subcapsular necrosis.

No specific clinical symptom could be identified; some patients had a normal clinical course while others had fever due to an extrahepatic source of infection or to rejection.

In 10 of the 11 cases, the size of the subcapsular hepatic necrosis decreased on successive CT examinations (Fig. 1) until complete resolution occurred. In one case, the pathologic studies showed an irregular subcapsular band of necrotic tissue (Fig. 3).

Discussion

Although, to our knowledge, it has not been reported in the radiologic literature, subcapsular hepatic necrosis is a relatively well known anatomic-pathologic entity, described by several authors [1, 2], but mostly by Russo and Yunis [3]. Studying 53 hepatic allografts, Russo and Yunis found five cases of subcapsular necrosis and illustrated a macroscopic appearance identical to our anatomic and CT findings.

The absence of clinical and laboratory manifestations could be related to the small amount of hepatic parenchyma involved. Sonography failed to detect subcapsular hepatic necrosis because lesions are small and their echogenicity is close to that of normal parenchyma. Technical difficulties, such as the distance between the probe and the lesion or the small size of the acoustic window, also play a role in the failure of sonography in these cases.

CT signs of subcapsular hepatic necrosis are typical, allowing differentiation from lesions producing an intrahepatic or

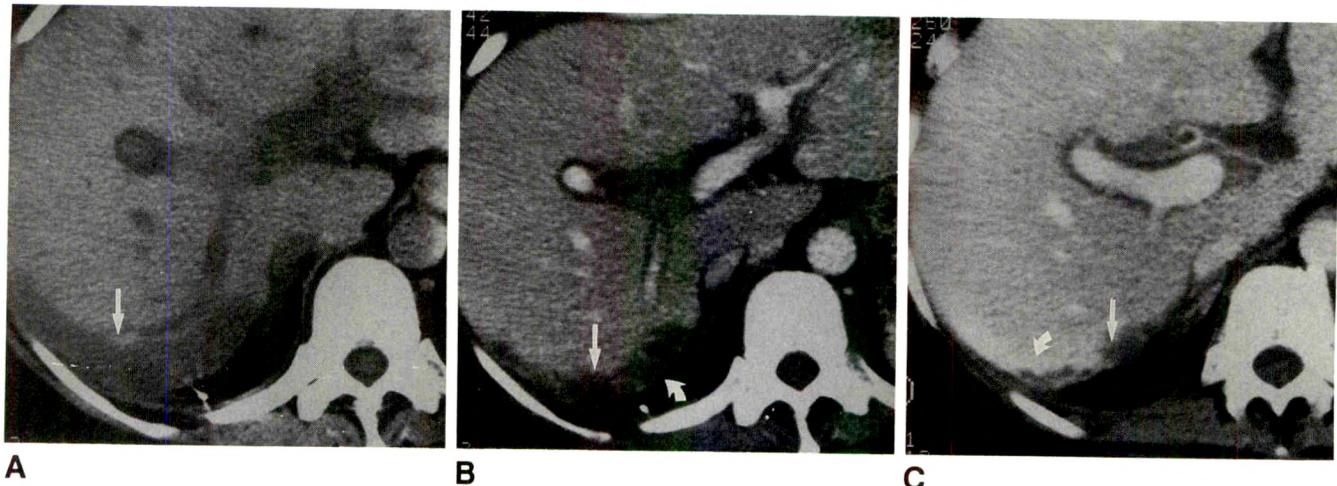


Fig. 1.—Subcapsular hepatic necrosis in 49-year-old woman 12 days after transplantation.
A, Unenhanced CT scan shows low-attenuation region in posterior part of liver (arrow).
B, Enhanced CT scan shows irregular inner border (straight arrow); outer border is hepatic capsule (curved arrow).
C, 27 days after transplantation, CT scan shows spontaneous reduction of size of lesion (straight arrow); note enhancing border (curved arrow) of normal hepatic parenchyma. Follow-up CT scan, obtained several months later, showed complete resolution of subcapsular necrosis.

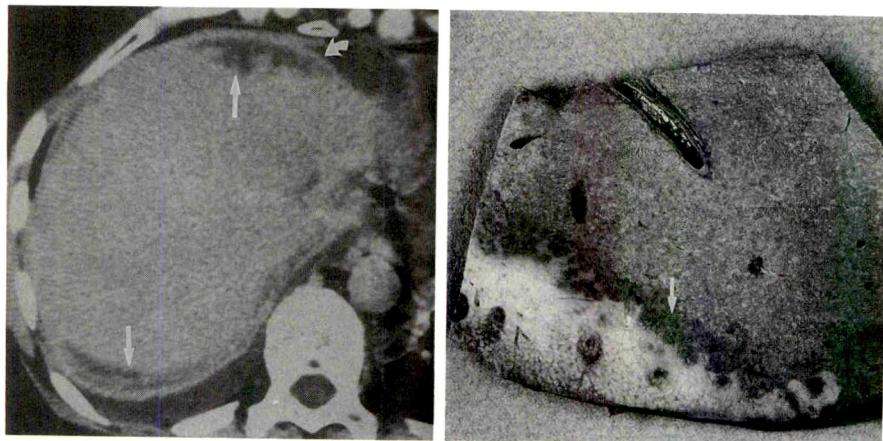


Fig. 2.—CT scan of 51-year-old woman, 8 days after transplantation: a 5-mm-thick section shows association of anterior and posterior subcapsular hepatic necrosis (straight arrows). Note hepatic capsule (curved arrow).

Fig. 3.—Autopsy specimen of liver transplant in 46-year-old man, 7 days after transplantation: macroscopic examination shows subcapsular white infarct with irregular necrosis (arrow).

perihepatic low density soon after transplantation. Pleural effusion is posterior to the diaphragmatic crus and is often associated with lung atelectasis. Free abdominal fluid lies anterior to the diaphragmatic crus and is crescent-shaped (after transplantation, both pleural and abdominal effusions may be posterior and medial to the liver due to hepatic ligament severance). Abdominal fluid collections have well-defined inner margins and sometimes have a specific density (hematoma). Hepatic subcapsular hematoma is a lenticular hyperdensity with regular margins; the underlying hepatic parenchyma is compressed but normal. Intrahepatic collections, such as biloma or liver abscess, involve deep parenchyma and are round. Liver necrosis has a segmental distribution. In acute rejection, no parenchymal abnormality is identified.

The lesions resolved without specific treatment during the first year. However, time of resolution could not be established more precisely, because follow-up CT scans were obtained at long intervals after the first examination.

The pathophysiology of subcapsular hepatic necrosis is not clearly established. The main hypothesis is that it is a result

of the size disproportion between the graft and the recipient's abdominal cavity. When the abdomen is closed, this disproportion is responsible for a reduction in blood flow from the hepatic artery and portal vein to the graft [4]. This disproportion also causes abnormal pressure points in the subcapsular hepatic parenchyma that is in contact with the diaphragm. The combination of these two factors could lead to subcapsular hepatic necrosis. Other causes, such as prolonged time for revascularization, trauma during organ procurement, or hypotension in the postoperative period, cannot be ruled out.

REFERENCES

1. Wight DGD. Pathology of liver transplantation (other than rejection). In: Calne RY, ed. *Liver transplantation*. New York: Grune & Stratton, 1983:293
2. Weinberg AG, Bolande RP. The liver in congenital heart disease. *Am J Dis Child* 1970;119:390-394
3. Russo PA, Yunis JY. Subcapsular hepatic necrosis in orthotopic liver allografts. *Hepatology* 1986;4:708-713
4. Houssin D, Fratacci M, Dupuy P, et al. One week of monitoring of portal and hepatic arterial blood flow after liver transplantation using implantable pulsed Doppler micropores. *Transplant Proc* 1989;1:2277-2278

Book Review



Duplex Scanning in Vascular Disorders. By D. Eugene Strandness, Jr. New York: Raven, 256 pp. 1990. \$85

Dr. Strandness's book contains much more than the title implies. It is more than a discussion of the applications of duplex sonography in vascular disorders. It is a discussion of the mechanics of blood flow in normal and disease states and of the clinical aspects and methods of diagnosing vascular disease, and it has some comments on treatment also. The role of sonography as a diagnostic technique is placed in perspective among other diagnostic techniques, both from a historical development point of view and from its relevance as compared with clinical methods for assessing vascular disease. Within the category of duplex sonography, Doppler imaging is the technique primarily discussed. Much of this book is written in the first person, because, to a great extent, it is a presentation of the author's clinical experience and extensive investigations over the past 20 years.

The book is composed of 11 chapters, written by Dr. Strandness, and an appendix on physics and instrumentation, written by Kirk W. Beach. The first chapter, "Historical Aspects," describes the development of vascular sonography from continuous-wave to duplex imaging and is especially interesting because Dr. Strandness has played a major role in developing this field. Chapter 2, "Traditional Methods of Patient Examination," provides a clinical perspective for the role of sonography in the investigation of vascular disease. Using the lower extremities as the clinical example, Strandness describes the different approaches to the diagnosis of acute vs chronic arterial and venous disease.

Chapters 3, 4, and 5 discuss the hemodynamics of normal, stenotic, and occluded arteries and veins. Variations of blood-flow velocity under different physiologic and pathologic conditions and how such changes cause variations in the Doppler waveform are presented. Vascular disease in specific sites—the extracranial arteries, the peripheral arteries in the lower extremities, the renal arteries, the mesenteric and portal systems, and the lower-extremity deep venous system—are covered in chapters 6–10. The chapters discuss the clinical findings, the various non-Doppler diagnostic tests (so as to put the benefit of sonography in perspective), and then the sonographic findings and their significance. The last chapter is devoted to color Doppler imaging. It briefly presents the benefits that color provides over spectral Doppler imaging; the illustrations are primarily of carotid and vertebral artery disorders.

The chapters on the extracranial arterial system and the arteries and veins of the lower extremities are the longest and most thorough, suggesting that these are the topics of greatest interest to the author. Unfortunately, color Doppler imaging is presented as a separate chapter. It would have been better to integrate color applications into each of the clinical chapters.

Technically the book is well done, with clear illustrations, though occasionally the inking on some angiograms is too light. The color Doppler images are well reproduced.

The detail with which topics are discussed varies considerably. On certain points, the author goes into considerable and appreciated discussion. At other times, he makes a brief comment without elaborating, perhaps presuming knowledge on the part of the readers. Sometimes he makes what appears to be a strongly felt statement without explaining his reasons.

In order to help the reader recall a previously presented topic that is being elaborated on in a subsequent chapter, the key points are summarized briefly so that the reader does not have to refer to the previous chapter to refresh his or her memory. This is done in a manner that will not offend the knowledgeable but will be appreciated by the neophyte.

Though appendixes often are not read, this one should be. It concisely describes with effective illustrations the basic physical principles governing sonography, including Doppler sonography, and provides explanations of the operation of various different types of probes and scanners.

As a radiologist, I enjoyed reading this book because it places the role of sonography in the workup of vascular disorders in perspective while providing background information on and clinical insights into vascular disorders that I do not find frequently in the radiologic literature. However, this is not a book that I would suggest for learning the basic techniques and interpretive skills needed to perform vascular studies.

M. Leon Skolnick
Presbyterian-University Hospital
Pittsburgh, PA 15213

Lacunae: A Urographic Finding in Chronic Obstructive Uropathy

Lee B. Talner¹
 Judith A. W. Webb^{1,2}
 David H. Dail³

Lacunae, small spaces in the renal sinus that communicate with the caliceal fornices, have been mentioned rarely in the radiologic literature. These lesions have been reported to opacify during excretory urography in patients with current or previous urinary obstruction. Lacunae have been presumed to form in response to urine extravasation through the fornices, but there has never been gross anatomic or histologic proof of their existence.

In two patients with obstructive uropathy, urographic-pathologic correlation confirmed the existence and nature of lacunae. On excretory urography, the appearance is likely to be confused with papillary necrosis.

AJR 156:985-988, May 1991

Urographic findings suggesting papillary necrosis were seen in two adults with obstructive uropathy. In both cases, autopsy findings showed intact medullary tissue and papillae. The radiologic findings were explained on the basis of cystic spaces in the renal sinus that communicated with the caliceal fornices.

Similar urographic findings, called lacunae, were shown previously in two children with obstructive uropathy [1, 2]. However, no cases have been corroborated pathologically. The radiologic-pathologic correlation in our two patients is presented to draw attention to this potentially confusing appearance.

Case Reports

Case 1

A 53-year-old man who was receiving chemotherapy for metastatic melanoma had lethargy, urinary frequency, and right inguinal lymphadenopathy. Results of laboratory examination showed renal failure (blood urea nitrogen, 44 mg/dl; serum creatinine, 5.5 mg/dl). Excretory urography showed bilaterally dilated pelvicaliceal systems and upper ureters with no opacification of the distal ureters. Multiple small pools of contrast material were seen adjacent to the caliceal fornices (Fig. 1A). Renal function continued to deteriorate, and the patient died 6 days after admission. Postmortem examination confirmed hydronephrosis and hydroureter due to obstructing tumor around the ureters. The renal papillae were intact, but small spaces communicating with the caliceal fornices were present (Fig. 1B). These pockets extended toward the renal sinus fat and were surrounded by myxomatous change and inflammatory infiltrate and did not have an epithelial lining (Fig. 1C).

Case 2

A 61-year-old woman had a large pelvic mass due to advanced endometrial carcinoma. Serum creatinine level was normal. Excretory urography showed delayed excretion of contrast medium on the left side with caliectasis but no pelvic dilatation. The left ureter was never seen. Multiple pockets filled with contrast material were present in the pericaliceal regions (Fig. 2A). The right kidney was normal. Left retrograde ureteropyelography showed encase-

Received October 9, 1990; accepted after revision November 15, 1990.

Presented at the annual meeting of the Society of Uroradiology, Vancouver, B.C., September 1990.

¹ Department of Radiology, University of California, San Diego, La Jolla, CA 92093. Address reprint requests to L. B. Talner, Radiology Department (H-756), UCSD Medical Center, 225 Dickinson St., San Diego, CA 92103.

² Present address: Department of Radiology, St. Bartholomew's Hospital, QE II Block, West Smithfield, London EC1A 7BE, England.

³ Department of Pathology, University of California, San Diego, La Jolla, CA 92093. Present address: Department of Pathology, Virginia Mason Clinic, 1100 Ninth Ave., P. O. Box 900, Seattle, WA 98111-0900.

0361-803X/91/1565-0985
 © American Roentgen Ray Society

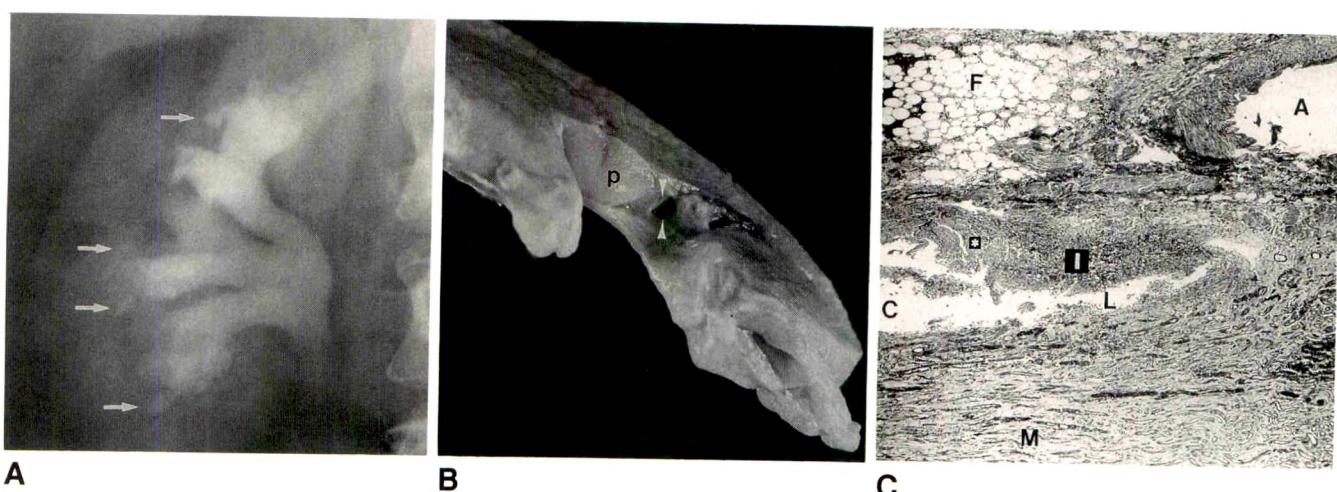


Fig. 1.—Case 1: Obstructive hydronephrosis due to ureteral encasement by metastatic melanoma.

A, Excretory urogram shows lacunae (arrows) as round or oval sharply marginated pockets of contrast material contiguous with caliceal fornices. (Reprinted with permission from Talner [3].)

B, Photograph of transverse slice from kidney in A shows opening of lacuna (arrowheads) adjacent to normal papilla (p).

C, Coronal histologic specimen shows relation of lacuna to caliceal fornix. F = renal sinus fat, A = interlobular artery, C = calix, L = lacuna, M = medulla. Note myxomatous change (asterisk) and inflammatory cell infiltrate (I) adjacent to lacuna. (H and E, original magnification $\times 40$)

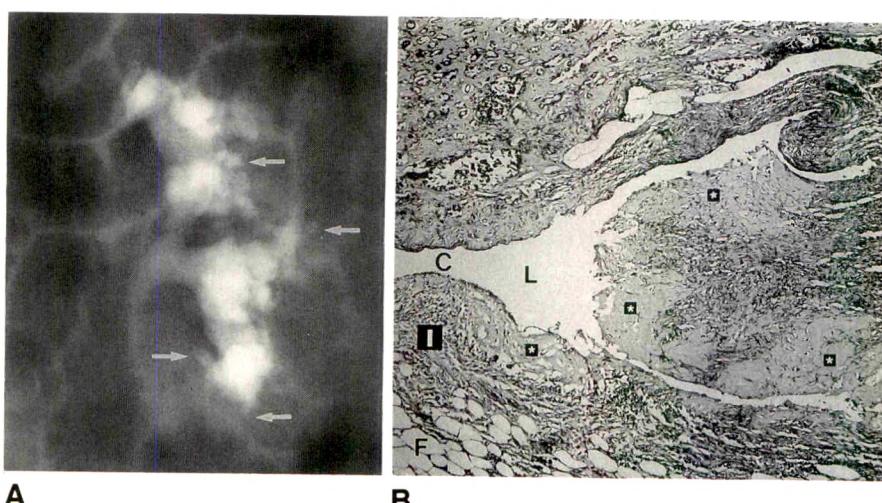


Fig. 2.—Case 2: Hydronephrosis due to ureteral obstruction from metastatic uterine adenocarcinoma.

A, Excretory urogram 2 hr after injection of contrast material shows several lacunae (arrows).

B, Coronal histologic specimen shows connection of lacuna (L) to caliceal fornix (C). Extensive myxomatous change (asterisks) and minimal inflammatory cell infiltrate (I) are seen next to lacuna. F = renal sinus fat. (Trichrome, original magnification $\times 60$)

ment of the upper half of the ureter extending to the ureteropelvic junction. Chemotherapy was begun, but the patient's condition deteriorated, and she died 10 days later. At postmortem examination, the left renal pelvis and ureter were encased by tumor. The microscopic findings (Fig. 2B) were similar to those in Case 1.

Discussion

In both patients, we initially interpreted the urographic findings as papillary necrosis. Only after examining the macroscopic and microscopic autopsy findings was it clear that the papillae and medullary tissues were intact. The cavities were beside the papilla and communicated with the caliceal fornix.

Frank papillary ulceration with necrosis, as a feature of obstructive renal damage, has been observed experimentally

in the unipapillary kidney of rabbits and the crest kidney of dogs with ureteral occlusion [4–6]. In the multipapillary kidney of pigs, necrosis of the papillary tip was found in the early stages of complete ureteral obstruction, but papillary cavities were not described in the chronic stages [7].

It is difficult to find proof in the literature that obstruction, in the absence of infection, diabetes, or other conditions predisposing to papillary necrosis, causes papillary necrosis [8, 9]. Virtually all reported cases of papillary necrosis associated with obstruction had evidence of current or past infection [9]. Certainly pyonephrosis often is associated with frank necrotizing papillitis. If obstruction alone causes papillary necrosis in humans, it must be exceedingly rare [8, 9].

Ransley [1] suggested that lacunae represent abnormal tissue spaces in the renal sinus related to urine extravasation from fornical rupture. Our findings support his hypothesis.

Fig. 3.—Peripelvic urinomas in patient with acutely obstructing ureteral calculus.

A, Excretory urogram shows oval circumscribed collections of contrast material (arrows) adjacent to several calices.

B, Excretory urogram (with abdominal compression) obtained 1 week after passage of stone shows peripelvic urinomas are no longer opacified. Urinoma is a localized urine extravasation that may be reabsorbed if urine leakage ceases or become encapsulated if leakage persists.

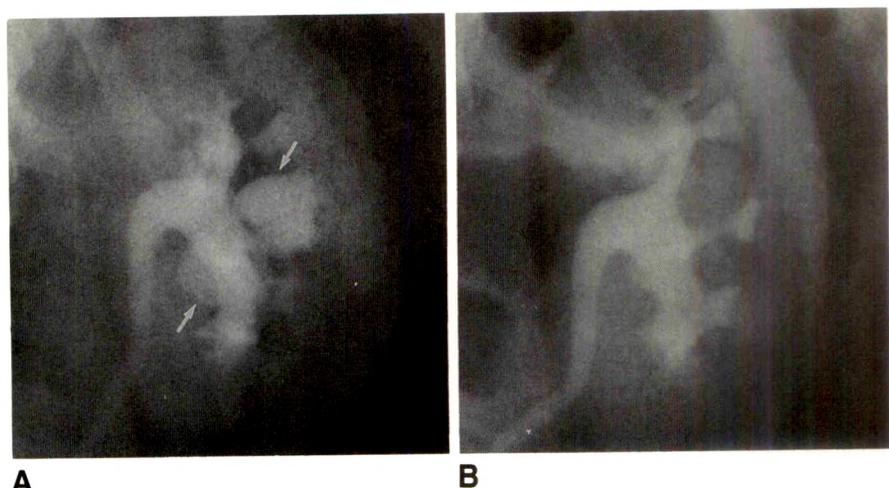
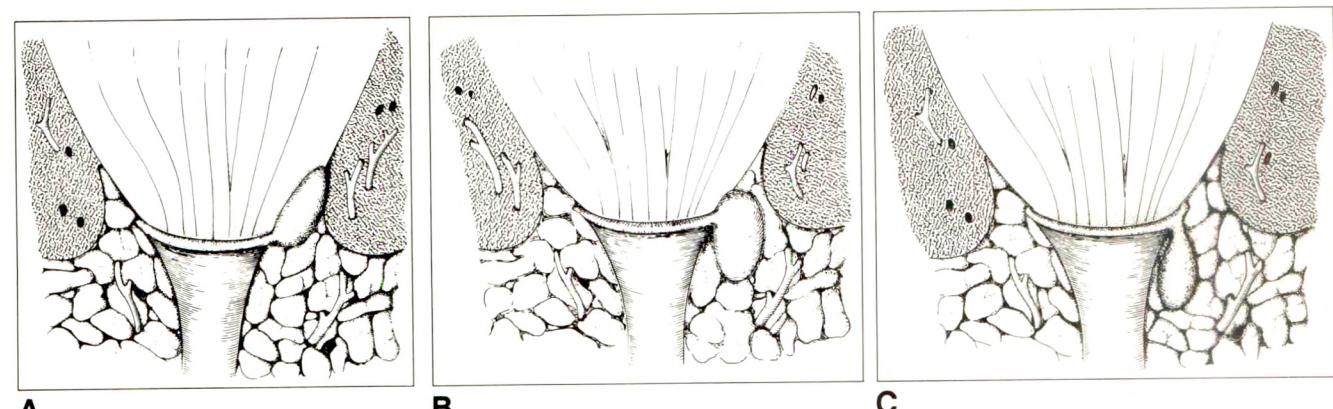
**A****B****A****B****C**

Fig. 4.—A-C, Drawings show relationship of lacuna to calix. Because renal sinus sometimes extends beyond caliceal fornix toward renal surface, lacunae may develop peripheral to fornix (A), at same level as fornix (B), or closer to renal hilum than to fornix (C).

Cystic spaces in the pericaliceal fat communicated with the caliceal fornix, and the tissues around the lacunae were laced with myxomatous degeneration and inflammatory infiltrate (Figs. 1C and 2B). These are known responses of adipose tissue to urine leakage.

Ransley [1] also suggested that in chronic obstruction, lacunae may become epithelialized and retain their connection to the caliceal fornix, even after obstruction is relieved. Histologically, the lacunae in our patients were not epithelialized and had not developed a fibrous wall, but it might take several weeks or months for this to develop.

Barbaric and Frank [10] and Friedenberg et al. [11] described somewhat larger, localized peripelvic urine collections in the renal sinus of patients with acute obstruction. These renal sinus urinomas may seal over to form pseudocysts or may be reabsorbed and disappear (Fig. 3). They may or may not opacify on urography, depending on whether the communication with the pelvicaliceal system is patent. Presumably their pathogenesis is similar to that of lacunae.

It has been postulated that pyelovenous communications at the caliceal fornices develop by a similar mechanism.

Weakening and rupture of the caliceal fornix are thought to produce communicating cysts in the renal sinus, which then rupture into venous channels [12].

Because the renal sinus extends somewhat beyond the caliceal fornix toward the surface of the kidney [13], tears of the fornix may lead to lacunae in different positions (Fig. 4). Lacunae may be peripheral to the fornix, at the same level as the fornix, or central to the fornix (i.e., closer to the renal hilum).

Lacunae central to the fornix are visible on urography without overlap from a papilla and should be easiest to diagnose correctly. On the other hand, lacunae farther out in the kidney are more likely to overlap one or more papillae and thereby resemble papillary necrosis. The position of lacunae relative to the papillary tips is key in differentiating them from the cavities of central papillary necrosis. In central papillary necrosis, the cavity lies within the papilla, whereas a lacuna, by definition, lies outside the papilla. Although on any single projection lacunae in front of or behind the papilla might project directly over the papilla, they would not be expected to do so on all projections. Diagnostic difficulty is most likely

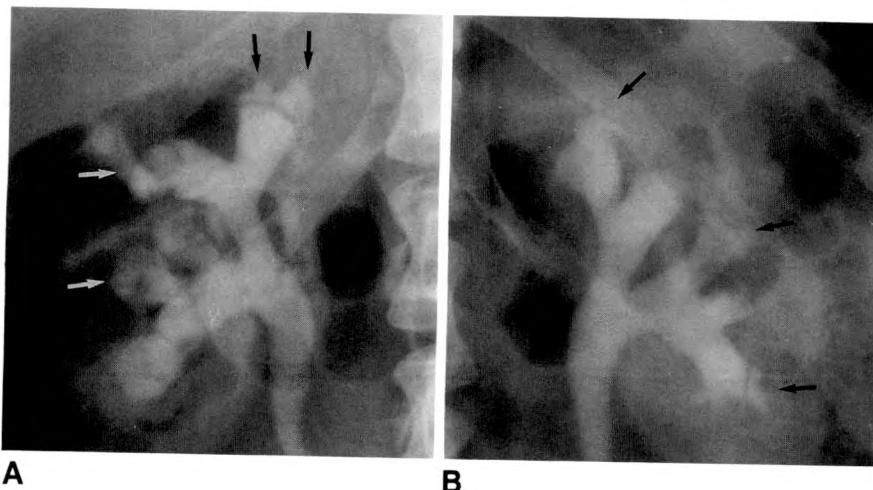


Fig. 5.—27-year-old man in whom obstructive renal failure at age 21 was caused by urethral stricture.

A and B, Excretory urograms with abdominal compression of right (A) and left (B) kidneys show well-circumscribed contrast collections (arrows) of various sizes and shapes in papillary regions. Findings suggest papillary necrosis rather than lacunae because each contrast pool appears centered on a calix. Nevertheless, the diagnosis is uncertain. Pathologic confirmation was not available.

to occur when necrosis occurs at the periphery of a papilla, with tracts of contrast material extending out from the region of the caliceal fornix.

Figure 5 illustrates a case in which the diagnosis is uncertain. Inasmuch as lacunae may easily be confused with papillary necrosis on urography, and as proof of their existence has been lacking, it is conceivable that lacunae have been interpreted erroneously as papillary necrosis.

Medullary sponge kidney, another condition that could be confused with lacunae on urography, is characterized by cystic dilatation of the collecting tubules and papillary ducts. At urography these are seen as multiple pools and streaks of contrast material that, unlike lacunae, lie within the papilla.

There is potential overlap in the urographic appearance of caliceal diverticula and lacunae. The typical caliceal diverticulum is a solitary, rounded cavity peripheral to an upper pole calix. It should present no difficulty in differential diagnosis, especially if the neck of the diverticulum is visible. In patients with Beckwith-Wiedemann syndrome or Laurence-Moon-Biedl syndrome, and rarely in other patients, caliceal diverticula may be multiple and simulate lacunae closely. The absence of a history of obstruction should suggest the correct diagnosis. Caliceal diverticula are always lined by transitional epithelium because they develop from an embryologic flaw in the branching process of the ureteral bud.

REFERENCES

- Ransley PG. Opacification of the renal parenchyma in obstruction and reflux. *Pediatr Radiol* 1976;4:226-232
- Aaronson IA, Cremin BJ. Urinary tract obstruction: general considerations. In: *Clinical paediatric uroradiology*. Edinburgh: Churchill-Livingstone, 1984:173-189
- Talner LB. Urinary obstruction. In: Pollack HM, ed. *Clinical urography*. Philadelphia: Saunders, 1990:1535-1628
- Strong KC. Plastic studies in abnormal renal architecture. V. The parenchymal alterations in experimental hydronephrosis. *Arch Pathol Lab Med* 1940;29:77-119
- Sheehan HL, Davis JC. Experimental hydronephrosis. *Arch Pathol Lab Med* 1959;68:185-225
- Muirhead EE, Vanatta J, Grollman A. Papillary necrosis of the kidney. A clinical and experimental correlation. *JAMA* 1950;142:627-631
- Hodson CJ, Craven JD, Lewis DG, Matz LR, Clarke RJ, Ross EJ. Experimental obstructive nephropathy in the pig. *Br J Urol* 1969;41[Suppl]:5-20
- Davidson AJ. Chronic parenchymal disease. In: Pollack HM, ed. *Clinical urography*. Philadelphia: Saunders, 1990:2277-2288
- Eknayon G, Qunibi WY, Grissom RT, Tuma SN, Ayus JC. Renal papillary necrosis: an update. *Medicine (Baltimore)* 1982;61:55-73
- Barbaric ZL, Frank IN. Peripelvic renal pseudocyst due to obstruction. *AJR* 1977;129:1097-1098
- Friedenberg RM, Moorehouse H, Gade M. Urinomas secondary to pyelo-sinus backflow. *Urol Radiol* 1983;5:23-29
- Low IA, Matz LR. Haematuria and renal fornecal lesions. *Br J Urol* 1972;44:681-691
- Narath PA. The hydromechanics of the calyx renalis. *J Urol* 1940;43:145-176

Pictorial Essay



MR Imaging of the Seminal Vesicles

Eduardo Secaf,^{1,2} Regina N. Nuruddin,^{1,3} Hedvig Hricak,¹ R. Dale McClure,⁴ and Barbara Demas¹

MR imaging (0.35 and 1.50 T) was used to assess the appearance of the seminal vesicles. The size and signal intensity of normal seminal vesicles vary with the age of the subject. In general, on T2-weighted images, the signal intensity of normal seminal vesicles is lower than that of fat in prepubertal children, similar to or higher than that of fat in adults, and similar to or lower than that of fat in patients older than 70 years of age. Endocrine and radiation therapy will influence the size and signal intensity of the seminal vesicles. The purpose of this essay is to illustrate the spectrum of seminal vesicle disease, including congenital anomalies, inflammation, and neoplastic disease. Although MR imaging is helpful in depicting seminal vesicle abnormalities, it does not allow differentiation of benign from malignant disease, distinction of hemorrhage due to tumor invasion from postbiopsy changes, or distinguishing between glandular obstruction due to tumor infiltration and mechanical compression.

Radiologic evaluation of the seminal vesicles by using either CT [1] or transrectal sonography provides information about the seminal vesicles' presence, size, and tumor invasion. Seminal vesiculography, although an invasive procedure involving cannulation of the vas deferens, is still often used for a detailed analysis of their architecture [1, 2]. The potential value of MR imaging in the evaluation of the seminal vesicles has been reported [2, 3]. This essay illustrates MR findings

in both normal subjects and patients with a variety of pathologic conditions.

Normal Seminal Vesicles

The seminal vesicles are androgen-dependent accessory glands with a complex relationship between size and chronologic age. This is reflected by a wide range in their size and signal intensity on MR images. The signal intensity of the seminal vesicles can be compared with the signal intensities of the three adjacent tissues: muscle, fat, and urine. On T1-weighted spin-echo (SE) images, the signal intensity of the normal adult seminal vesicles is similar to or slightly higher than that of skeletal muscle and always higher than that of urine (Fig. 1). On T2-weighted images, the glands show a range of signal intensities that range from lower than, similar to, or higher than the signal intensity of urine or fat. In general, in prepubertal patients, the signal intensity of the seminal vesicles is lower than the signal intensity of urine or fat (Fig. 2). In patients younger than 70 years old, the seminal vesicles are of similar or higher signal intensity than that of fat (Fig. 3), and in patients older than 70 years of age they have a signal intensity similar to or lower than that of fat. Exceptions, however, can be found in each age group. The convolutions of the seminal vesicles and the low-signal intensity capsule [4] are best seen on T2-weighted images, but can be seen on the T1-weighted images when contrast medium is used.

Received July 27, 1990; accepted after revision November 30, 1990.

¹ Department of Radiology, University of California, San Francisco, School of Medicine, Box 0628, 505 Parnassus Ave., San Francisco, CA 94143-0628. Address reprint requests to H. Hricak.

² Present address: Department of Radiology, University of São Paulo, Brazil.

³ Present address: Department of Radiology, University Malaya, Kuala Lumpur, Malaysia.

⁴ Department of Urology, University of California, San Francisco, School of Medicine, San Francisco, CA 94143-0628.

AJR 156:989-994, May 1991 0361-803X/91/1565-0989 © American Roentgen Ray Society

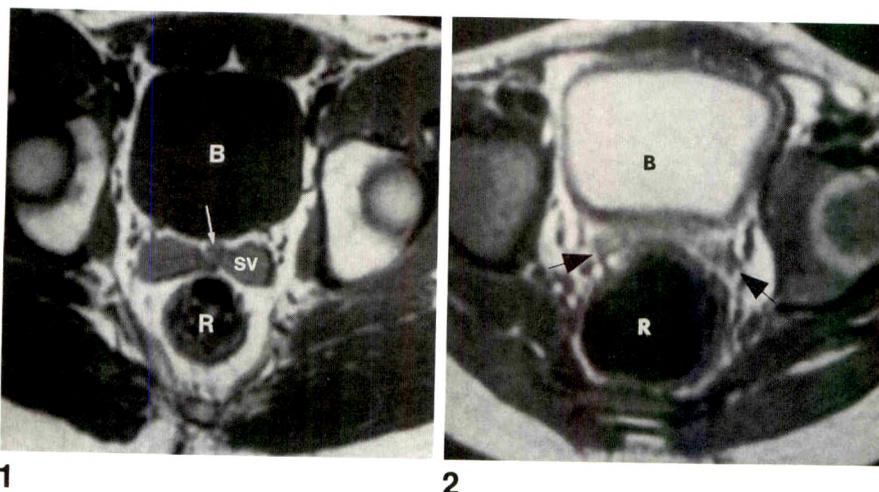


Fig. 1.—Normal seminal vesicles. Axial, 1.5-T, T1-weighted (SE 700/20) MR image. Signal intensity of seminal vesicles (sv) is higher than that of urine within urinary bladder (B) and similar to that of muscle. arrow = ductus deferens, R = rectum.

Fig. 2.—Normal seminal vesicles in a 5-year-old boy. Axial, 1.5-T, T2-weighted (SE 2500/70) MR image shows small, low-signal-intensity seminal vesicles (arrows). B = urinary bladder, R = rectum.

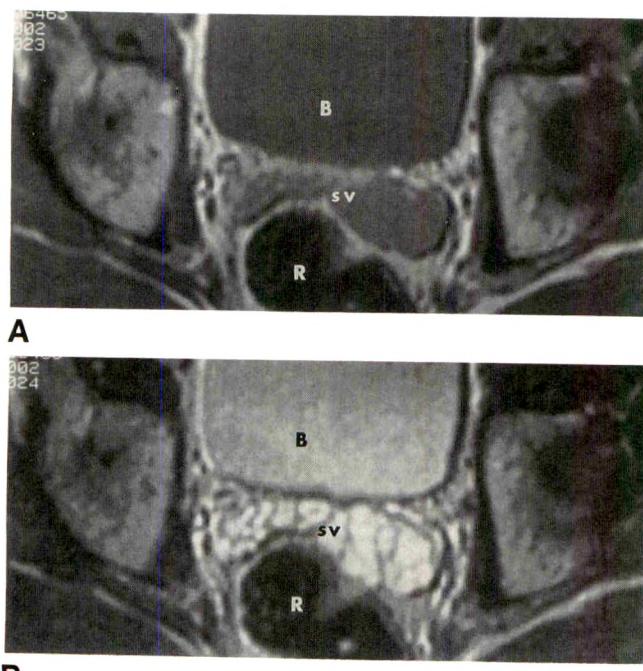


Fig. 3.—Asymmetric size of normal seminal vesicles.
A and B, Axial, 1.5-T, T1-weighted (A, SE 700/20) and T2-weighted (B, SE 2500/70) MR images show difference in size of seminal vesicles (sv). Glandular convolutions and signal intensity are, however, symmetrical. B = urinary bladder, R = rectum.

After injection of gadopentetate dimeglumine, the wall of the seminal vesicles enhances, and their convoluted appearance can be seen on T1-weighted images (Fig. 4).

The normal seminal vesicle measures 4.5 to 5.5 cm in length and 2 cm in width [4]. Because of their oblique course, the length of the seminal vesicles is usually underestimated in any cross-sectional orthogonal plane of imaging. In prepubertal boys, the seminal vesicles are small. The seminal vesicles tend to be wider in the fifth and sixth decades, probably owing to stasis and distension associated with the common occurrence of benign prostatic hyperplasia and sub-

sequent ejaculatory duct compression. The seminal vesicles decrease in size after the age of 70 years. In each age group, however, a wide range of measurements exists.

Asymmetry of seminal vesicle size can be seen among normal subjects. Although asymmetric in size, the signal intensity is symmetric on both T1- and T2-weighted images (Fig. 3). The location of the seminal vesicles, cephalic to the prostate between the bladder anteriorly and the rectum posteriorly, is readily displayed. The angle between the seminal vesicles and the horizontal plane (normally 50° to 60°) varies according to the degree of distension of the bladder and rectum. After abdominoperineal resection, the position and the orientation of the seminal vesicles changes to fill the void (Fig. 5).

Disease of the Seminal Vesicles

Congenital Anomalies

Agenesis.—The absence of seminal vesicles is best shown on transaxial T1-weighted images (Fig. 6). The vesicoprostatic venous plexus within the rectovesical pouch should not be mistaken for small glands.

Cysts.—The proximity of the cyst to the seminal vesicles, their lateral location, and separation from the prostate are important factors in diagnosis (Fig. 7). Signal intensity on either T1- or T2-weighted images varies depending on the fluid characteristics. The fluid is often proteinaceous, rendering different signal intensities depending on its concentration. When hemorrhage is present within the cyst, the fluid's signal intensity depends on the age of the bleeding.

Arteriovenous malformation.—Demonstration of large ectatic vessels adjacent to the lateral wall of the seminal vesicles indicates an arteriovenous malformation (Fig. 8).

Endocrine Therapy

After estrogen therapy or bilateral orchectomy, the seminal vesicles are diminished in size, and on T2-weighted images they show abnormally low signal intensity (less than that of fat but greater than that of skeletal muscle, Fig. 9).

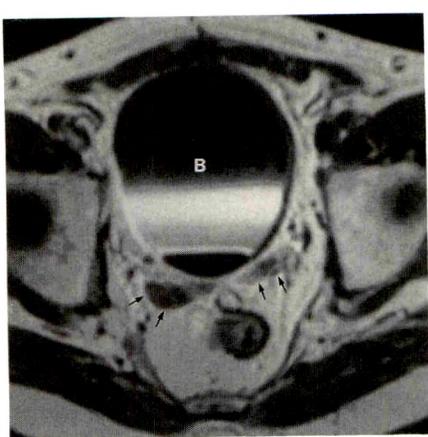


Fig. 4.—Normal seminal vesicles on gadopentetate-dimeglumine-enhanced axial, 1.5-T, T1-weighted (SE 550/20) MR image. Wall of seminal vesicle is enhanced, whereas fluid remains of low signal intensity. Convoluted appearance of normal glands (arrows) is therefore seen on T1-weighted image. Note layering of contrast medium in urinary bladder (B).

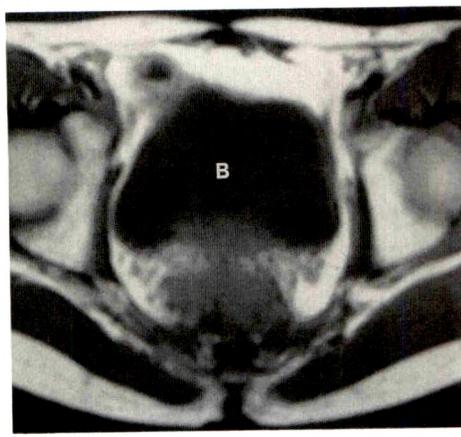
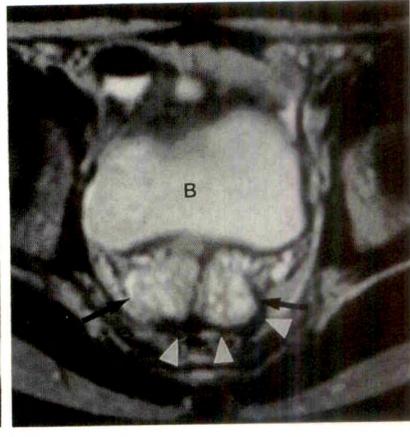
**A****B**

Fig. 5.—Location of seminal vesicles after abdominoperineal resection.

A and **B**, Axial, 1.5-T, T1-weighted (**A**, SE 700/20) and T2-weighted (**B**, SE 2500/70) MR images show posterior location of otherwise normal glands (arrows). Arrowheads = postsurgical scar tissue, **B** = urinary bladder.

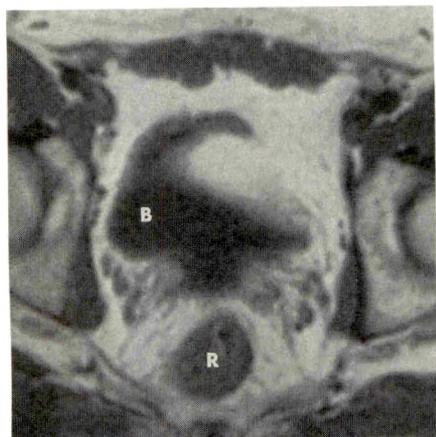
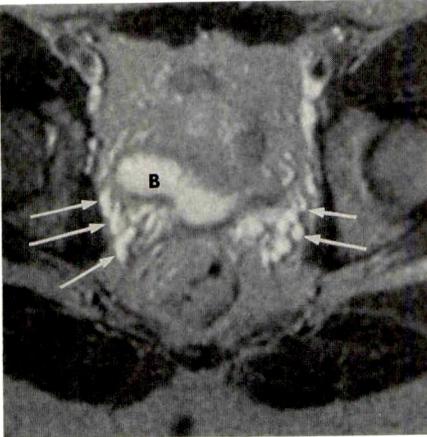
**A****B**

Fig. 6.—Seminal vesicle agenesis.

A and **B**, Axial, 1.5-T, T1-weighted (**A**, SE 700/20) and T2-weighted (**B**, SE 2500/70) MR images show absence of seminal vesicles between urinary bladder (B) and rectum (R). Vesicoprostatic venous plexus (arrows) should not be mistaken for small seminal vesicles.

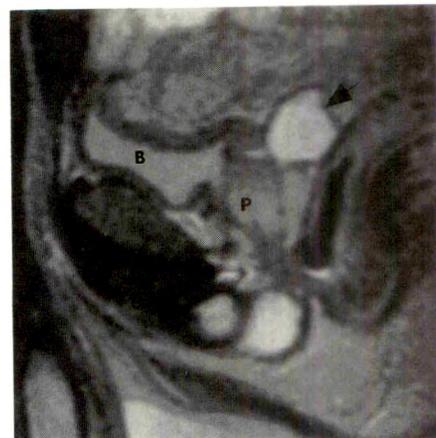


Fig. 7.—Seminal vesicle cyst. Sagittal, 1.5-T, T2-weighted (SE 2500/70) MR image shows high-signal-intensity cyst (arrow) at base of prostate (P). Note separation of cyst from prostate. **B** = urinary bladder.

Radiation Effects

The effect of radiation therapy on seminal vesicles depends on the patient's age, the duration of the treatment, and the dose applied. When the radiation dose to the seminal vesicles exceeds 5000 cGy, changes can be seen on MR images. The hallmark of radiation injury is the appearance of small, symmetric glands that remain hypointense on T2-weighted images. Their intensity, however, is usually higher than the signal intensity of skeletal muscle (Fig. 10). In patients younger than 40 years old, we found the MR appearance of seminal vesicles

to be normal when the radiation dose did not exceed 4500 cGy.

Inflammatory Disorders

The MR imaging appearance of inflammatory changes depends on the course of the disease. Patients with seminal vesiculitis are usually referred for imaging evaluation in the subacute phase, often after antibiotic treatment has failed.

Subacute inflammation.—The seminal vesicles are often enlarged. On T1-weighted images, the signal intensity may

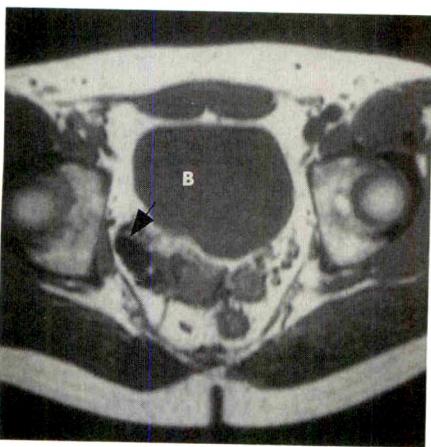
**A****B**

Fig. 8.—Arteriovenous malformation.

A and **B**, Proton-density-weighted (SE 2000/20) transaxial (**A**) and coronal (**B**) MR images show large ectatic vessels (arrows) near seminal vesicles.



Fig. 9.—Effect of endocrine therapy on appearance of seminal vesicles. Axial, 0.35-T, T2-weighted (SE 2000/80) MR image shows small low-signal-intensity seminal vesicles (arrows) in this 60-year-old man. **B** = urinary bladder.

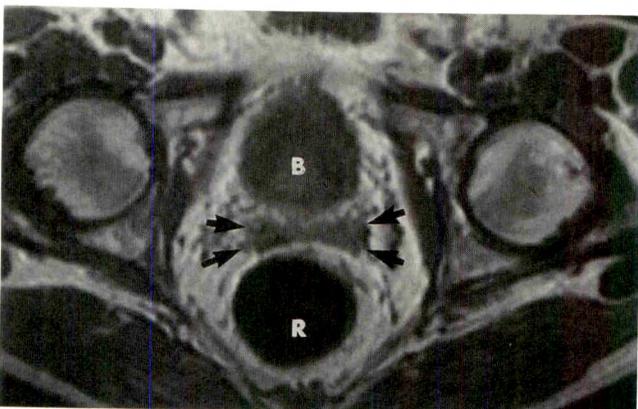
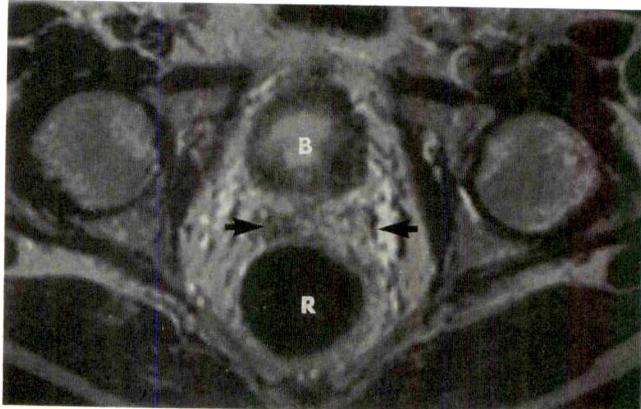
**A****B**

Fig. 10.—Effect of radiation therapy on appearance of seminal vesicles.

A and **B**, Axial, 1.5-T, proton-density-weighted (**A**, SE 2500/20) and T2-weighted (**B**, SE 2500/70) MR images show symmetric, small seminal vesicles (arrows), which remained hypointense on T2-weighting. This patient's total radiation therapy dose exceeded 5000 cGy. **B** = urinary bladder, **R** = rectum.

be normal or, as hemospermia often accompanies seminal vesicle infection, can be high. On T2-weighted images, signal intensity varies depending on the chronicity of the disease and the presence of bleeding (Fig. 11).

Chronic inflammation.—MR imaging reveals bilaterally or unilaterally small seminal vesicles with signal intensity lower than normal on both T1- and T2-weighted images.

Neoplasia

Primary.—A benign tumor appears as a sharply marginated mass arising from the seminal vesicles. The seminal vesicle lateral to the tumor may be normal or obstructed. A schwannoma of the right seminal vesicle is shown (Fig. 12). Primary malignant tumors of the seminal vesicles are rare and are not illustrated here.

Metastases.—The most common form of neoplasia affecting the seminal vesicle is invasion by prostatic carcinoma. Invasion may result from direct tumor spread in a contiguous fashion, or tumor infiltration may follow the course of the ejaculatory ducts. Seminal vesicles invaded by tumor may be enlarged (Fig. 13) or small (Fig. 14). Tumor invasion can be global (involving the entire gland, Figs. 13 and 14) or segmental (Fig. 15). Invaded seminal vesicles show low signal intensity on T2-weighted images. Obstruction of the seminal vesicles in the presence of adjacent tumor may be due to extrinsic compression of the ejaculatory ducts by tumor bulk or may be caused by direct tumor invasion of the ejaculatory ducts. MR imaging is not useful for distinguishing between the two causes (Fig. 16). Similarly, it is difficult to differentiate hemorrhage due to previous biopsy (Fig. 17) from hemorrhage caused by tumor invasion (Fig. 15) with MR. In spite of those difficulties, MR imaging is considered a valuable tool in the assessment of seminal vesicle invasion, with a reported overall 78% accuracy, 72% sensitivity, and 84% specificity [3].

Fig. 11.—Subacute inflammation.

A and *B*, Axial, 1.5-T, T1-weighted (*A*, SE 700/20) and T2-weighted (*B*, SE 2500/70) MR images show enlarged seminal vesicles (arrows), which are of high signal intensity on both T1- and T2-weighted images. Findings indicate hemorrhage. *B* = urinary bladder.

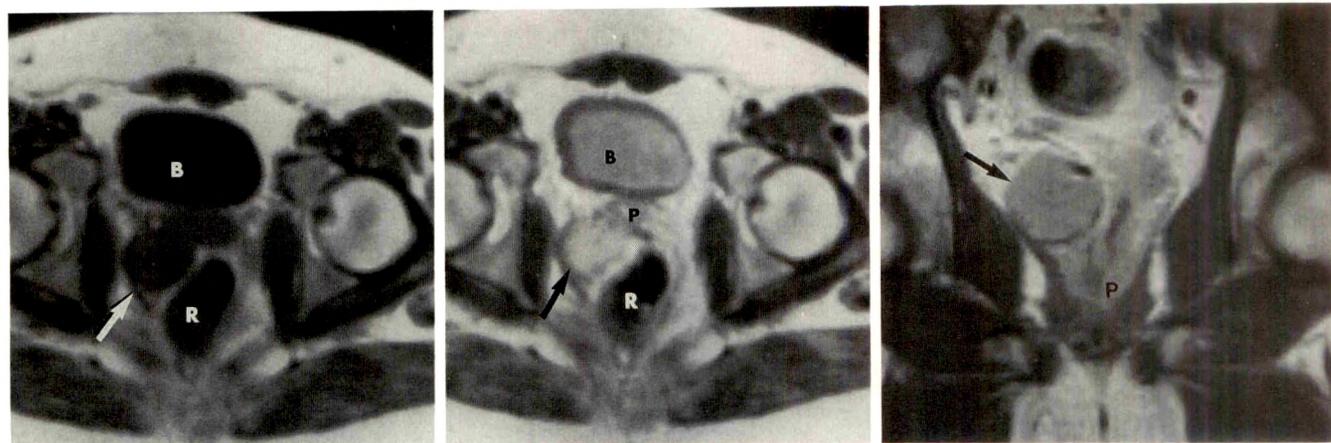
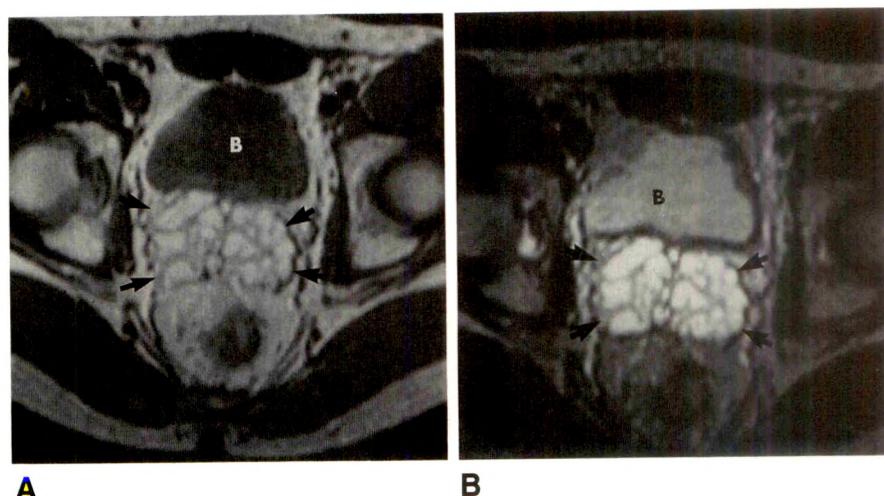
**A****B****C**

Fig. 12.—Seminal vesicle schwannoma.

A-C, Axial, 0.35-T, T1-weighted (*A*, SE 500/30), T2-weighted (*B*, SE 2000/60), and coronal T2-weighted (*C*, SE 2000/60) MR images show sharply outlined tumor (arrow) of right seminal vesicle that displaces rectum (*R*) and abuts base of prostate (*P*). Tumor has low signal intensity on T1-weighted image (*A*), and signal intensity homogeneously increases on T2-weighted images (*B* and *C*). *B* = urinary bladder.

Fig. 13.—Seminal vesicle invasion by prostatic carcinoma. Axial, 1.5-T, T2-weighted (SE 2500/70) MR image shows enlarged, low-signal-intensity right seminal vesicle. Note normal size and signal intensity of left seminal vesicle (arrow). *B* = urinary bladder, *R* = rectum.

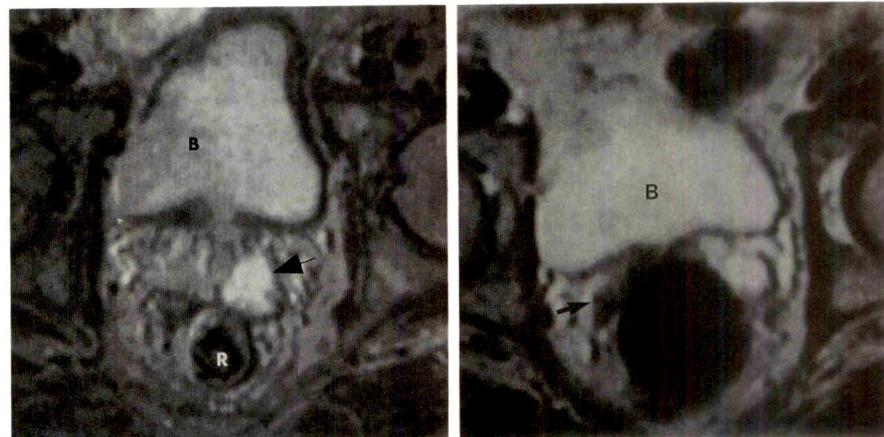
**13****14**

Fig. 14.—Seminal vesicle invasion by prostatic carcinoma. Axial, 1.5-T, T2-weighted (SE 2500/70) MR image shows small, low-signal-intensity right seminal vesicle (arrow), normal left seminal vesicle, and urinary bladder (*B*).

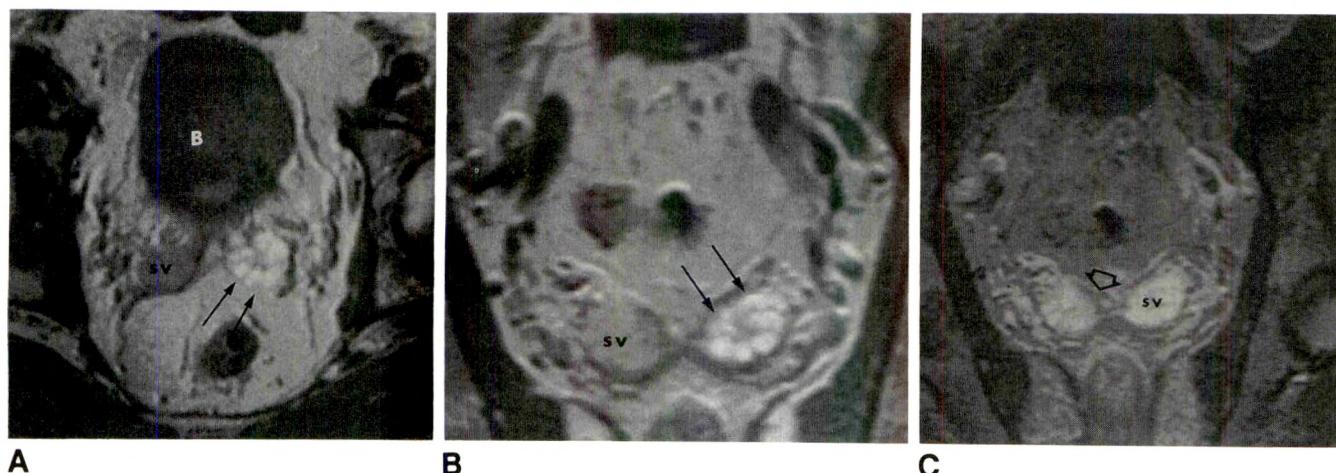


Fig. 15.—Tumor invasion of seminal vesicles (sv).

A-C, Axial (A) and coronal (B), 1.5-T, T1-weighted (SE 700/20), and coronal (C), 1.5-T, T2-weighted (SE 2500/70), MR images show high signal intensity of left seminal vesicle (solid arrows). Note low-signal-intensity area in medial segment of right seminal vesicle (open arrow). Tumor invasion as a cause of bleeding in left seminal vesicle and segmental tumor invasion of right seminal vesicle were confirmed at surgery.



Fig. 16.—Seminal vesicle obstruction due to invasion of ejaculatory ducts by prostatic cancer. Axial, 1.5-T, T2-weighted (SE 2500/70) MR image shows seminal vesicles (sv) are enlarged but are of normal signal intensity. Tumor invasion as a cause of obstruction was proved at surgery. B = urinary bladder, R = rectum.

Fig. 17.—Hemorrhage from biopsy. A and B, Coronal, 1.5-T, proton-density (A, SE 2500/20) and T2-weighted (B, SE 2500/70) MR images show high-signal-intensity area (open arrow). Distal end of right seminal vesicle (solid arrow) is normal. At surgery, hemorrhage was confirmed to be due to biopsy. B = urinary bladder, P = prostate.

REFERENCES

1. Silverman PM, Dunnick NR, Ford KK. Computed tomography of the normal seminal vesicles. *Comput Radiol* 1985;9:379-385
2. McClure RD, Hricak H. Magnetic resonance imaging: its application to male infertility. *Urology* 1986;27:91-98
3. Bezzi M, Kressel HY, Allen KS, et al. Prostatic carcinoma staging with MR imaging at 1.5T. *Radiology* 1988;169:339-346
4. Morris HB. *Human anatomy: the urogenital system*, 11th ed. New York: McGraw-Hill, 1942

Stones and Infection in Renal Caliceal Diverticula: Treatment with Percutaneous Procedures



James H. Ellis¹
 Stephanie K. Patterson¹
 L. Paul Sonda²
 Joel F. Platt¹
 Steven E. Sheffner¹
 Edward J. Woolsey^{1,3}

Percutaneous treatment of symptomatic caliceal diverticula has expanded the application of uroradiologic intervention. To assess the safety and efficacy of these procedures, we have reviewed our experience with percutaneous management of 12 symptomatic caliceal diverticula, 10 with stones and two infected. Nine stone-bearing diverticula were punctured directly with subsequent tract dilatation, nephroscopic stone extraction, and cavity obliteration (six with fulguration and drainage and three with drainage alone). One case was approached indirectly by puncturing a distant calix, dilating the diverticular neck, and flushing the stones into the collecting system for extraction. This cavity was not treated. Two infected diverticula were punctured directly for drainage and obliteration (one by fulguration and one by tetracycline sclerosis). Complete stone extractions were accomplished in all 10 cases. In eight with clinical follow-up ranging from 4 months to 6 years, one stone has recurred and seven patients are asymptomatic. Follow-up uograms were available in eight of 10 patients in whom cavity obliteration was attempted; in six (75%) of eight, nonvisualization of the diverticulum indicated successful obliteration. Only one major complication (urinoma requiring drainage) occurred.

We conclude that percutaneous procedures are safe and effective in treating infected or stone-bearing caliceal diverticula. Direct diverticular puncture for access and diverticular fulguration for cavity obliteration is our preferred technique.

AJR 156:995–1000, May 1991

Caliceal diverticula are found on 0.21 to 0.45% of excretory uograms [1, 2]. The true prevalence is most likely greater, because some diverticula are visualized only by retrograde pyelography [2]. Most caliceal diverticula are asymptomatic. Symptoms occur when there is urinary stasis leading to infection and calculi.

Until recently, the treatment of symptomatic caliceal diverticula has been surgical. However, newer techniques for percutaneous access to the kidney and extraction of stones can be applied to the treatment of infected or stone-bearing caliceal diverticula [3–7]. We report our experience in percutaneous treatment in 12 patients with symptomatic caliceal diverticula.

Subjects and Methods

Subjects

Twelve patients (three men, nine women), ranging from 24 to 64 (mean, 40.5) years old, were referred to our institution for treatment of stone-bearing or non-stone-bearing infected caliceal diverticula. Histories at presentation included recurrent urinary tract infections in two patients, flank pain in two, both urinary tract infection and flank pain in five, gross hematuria in two, and mild flank pain and occasional hematuria in another. Two patients had had a renal abscess surgically drained, apparently arising within the caliceal diverticula. Four patients had had pyelolithotomies of the ipsilateral kidney at other institutions, but it is not known if the diverticula contained stone at the time of the previous procedures. Two patients had had extracorporeal shock-wave lithotripsy (ESWL) of their stone-bearing diverticula without satisfactory passage of fragments.

Received September 11, 1990; accepted after revision November 20, 1990.

Presented in part at the annual meeting of the American Roentgen Ray Society, Washington, DC, May 1990.

¹ Department of Radiology (B1D520), University Hospital, University of Michigan Medical Center, Box 0030, 1500 E. Medical Center Dr., Ann Arbor, MI 48109-0030. Address reprint requests to J. H. Ellis.

² Department of Surgery, Section of Urology, University of Michigan Medical Center, Ann Arbor, MI 48109.

³ Present address: Radiology Ltd., Tucson, AZ 85716.

0361-803X/91/1565-0995
 © American Roentgen Ray Society

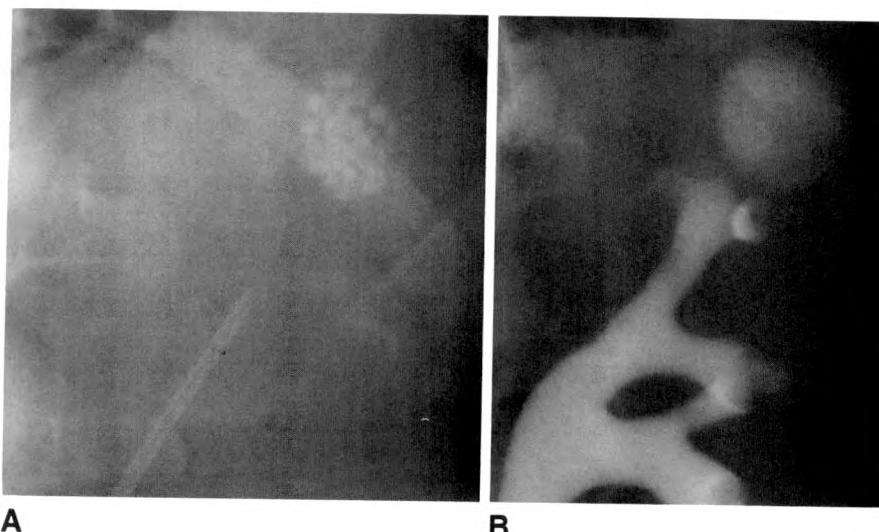


Fig. 1.—A, Plain film shows cluster of 25 small stones.

B, Retrograde pyelogram shows that stones are contained in a caliceal diverticulum arising from upper pole of left kidney.

Preprocedure Studies

Each patient had a retrograde or antegrade pyelogram obtained immediately before the procedure to evaluate renal anatomy. Ten of the 12 diverticula were found in the left kidney, and two occurred in the right kidney. Eight were located in the upper pole, three in the midpole, and one in the lower pole. Others have also noted that upper pole calices are the most frequent sites of both diverticula and diverticular stones [1, 2]. More than half of our diverticula arose from posterior calices. All were Type I diverticula (arising from a minor calix) by the criteria of Wulfsohn [8].

The diverticula ranged in size from 8 by 10 mm to 25 by 48 mm. Stones were present in 10 diverticula and ranged in size from 2 to 27 mm. Four diverticula contained single stones; the rest had as many as 25 stones (Fig. 1). One patient had an incidental ipsilateral second diverticulum, which did not contain stone and was not treated.

Procedures

All procedures were performed under fluoroscopic guidance after the patient had given informed consent. Local anesthesia and IV analgesia (meperidine, midazolam, or diazepam) were administered.

Eleven patients received direct punctures into the caliceal diverticulum. In two patients, an intercostal approach between the 11th and 12th ribs was required. One patient with an upper pole stone-bearing diverticulum had had an indirect puncture into the lower pole collecting system performed at another hospital and was sent to our institution with a drainage catheter already in the renal pelvis.

The nine nephrostomy tracts placed directly into stone-bearing diverticula were dilated with balloon catheters ranging in size from 24-French to 30-French. The indirect access tract was dilated to 26-French. The tracts into the two infected diverticula were dilated to either 12-French with manual dilators or 30-French with a balloon catheter.

Access to the neck of the diverticula in the 11 directly punctured cases was attempted on entry and was successful in three cases, leading to placement of safety wires. One of these cases was the infected diverticulum in which the access tract was dilated to only 12-French and no nephroscopy was performed. In the eight remaining cases, the safety wire was coiled in the diverticula and the diverticular neck was sought via nephroscopy after tract dilatation and, where applicable, stone extraction. In five of these patients, nephroscopy was successful in directing a guidewire through the diverticular neck under direct visualization, aided in some cases by the retrograde

injection of methylene blue. The diverticular neck in the patient treated via the indirect approach was catheterized by using fluoroscopy.

Methods used for stone extraction were rigid nephroscopy with forceps and ultrasonic lithotripsy, flexible nephroscopy with baskets, and simple suction with catheters. Of the 10 patients with stone-bearing diverticula, complete extraction was accomplished in a single sitting at the time of the original puncture in six. One patient who underwent ESWL after an initial nephrostomy into the diverticulum for drainage had all of his fragments removed at a single subsequent nephroscopy. One patient required two nephroscopic procedures to remove stone, and one patient required three procedures. The patient who had the indirect approach had had one pelvic stone extracted at the other institution. At our center, attempts to enter the diverticulum with a flexible nephroscope were unsuccessful both before and after dilatation of the diverticular neck with an 18-French balloon catheter. However, at the time of the second nephroscopy, three stones fell out of the upper pole diverticulum into the renal pelvis when the patient was in the reverse Trendelenburg position and were retrieved with forceps and basket. The remaining seven stones were flushed out of the upper pole diverticulum with contrast agent infused via catheter (Fig. 2) and then suctioned out with a catheter attached to a syringe.

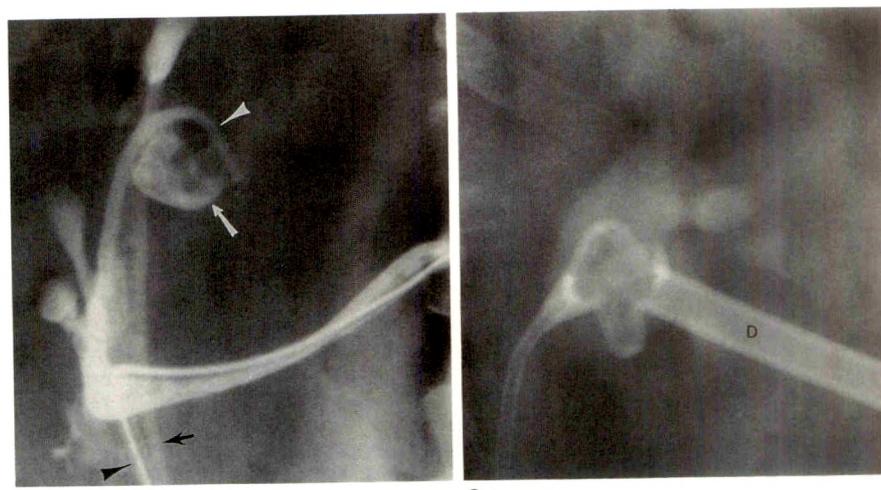
In the nine cases in which access to the diverticular necks was obtained, the necks were dilated with balloon catheters ranging in size from 18-French to 30-French. Depending on whether or not we achieved access to the diverticular neck, we left a large Malecot catheter in either the diverticulum (three cases) or the renal pelvis (eight cases) (Fig. 3) for drainage and cavity obliteration in all but the indirectly approached case in which no attempt was made to obliterate the diverticulum. After allowing the tract to mature for 2–4 days, we attempted diverticular obliteration with Bugby electrodes endoscopically in six of the 10 stone-bearing and one of the infected diverticula. After fulguration, drainage catheters were not replaced, which allowed the cavity and tract to close, except in one case in which drainage was continued with an 8-French nephrostomy tube for 2 days before tube removal. Tetracycline for sclerosis was infused twice in aliquots of 7 ml each, separated by 9 days, into the other infected diverticulum. This volume was chosen to fill but not distend the diverticulum and was left in place for 5 min before aspiration.

Follow-up

In eight patients, clinical and radiologic follow-up of the involved kidney was available (range, 4 months to 6 years; mean, 16 months).

Fig. 2.—Lateral pyelogram of case with indirect approach. Cluster of stones (white arrow) surrounded by contrast material is identified within diverticulum. Angled catheter (white arrowhead) has been manipulated into diverticulum for flushing of stones from cavity via contrast injection. Note angulation required to enter diverticulum, making nephroscopy impossible. Ureteral catheter (black arrow) and safety catheter containing guidewire (black arrowhead) are present.

Fig. 3.—Pyelogram shows stenting of caliceal diverticulum with 24-French Malecot catheter after stone extraction and dilatation of diverticular neck. Wings of Malecot positioned within renal pelvis. 8-French extension lies within ureter as protection against loss of access if tube is partly withdrawn inadvertently. Diverticulum is not opacified because it is filled by stent, but approximate location along course of tube is marked (D).



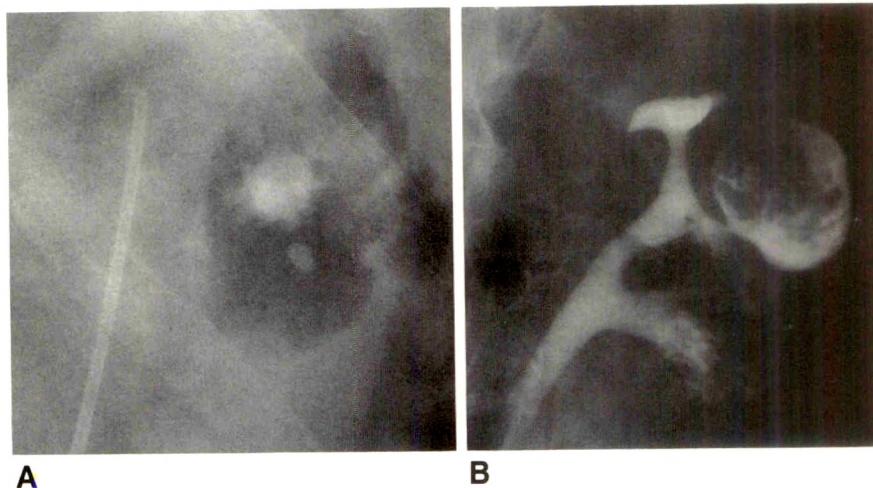
2

3

Fig. 4.—Caliceal diverticulum containing stone and transitional cell carcinoma.

A, Plain film shows stone material in right kidney (within diverticulum).

B, Retrograde pyelogram shows soft-tissue mass representing transitional cell carcinoma within opacified diverticulum.



A

B

Two patients were lost to follow-up, and one had an interval nephroureterectomy for transitional cell carcinoma. One patient has not yet reached the 4-month follow-up period.

Results

Stone Extraction

Complete stone extractions were accomplished in all 10 stone cases. One of the patients was found at the time of stone extraction to have a well-differentiated transitional cell carcinoma in the diverticulum in addition to the stone (Fig. 4). The mass had been visualized as a filling defect on a previous retrograde pyelogram and had increased in size on the retrograde pyelogram performed immediately before puncture. However, this enlargement was attributed to thrombus in this patient, who had presented with gross hematuria. The stone was removed via nephroscopy and excisional biopsy of the mass was performed. The patient subsequently elected to have a nephroureterectomy with excision of the drainage tract because of the possibility of tract seeding.

Most stones were found to be mixtures of calcium oxalate monohydrate and hydroxyapatite. None of the stones were composed of cystine or uric acid.

Infected Diverticula

In the infected diverticula, cultures of aspirated contents showed no growth in one patient and minimal growth of *Proteus* organisms in the other. Both patients had been treated with antibiotics before the procedures.

Complications

Minor complications included hemorrhage during the initial effort in three patients. This obscured the nephroscopic field and led to performance of the procedure in two stages. No transfusions were required. One of the patients who underwent an intercostal puncture developed a pneumothorax but did not require chest tube placement. One patient experienced transient hypertension and tachycardia during the procedure. One patient had mild extravasation of irrigant from the diverticulum; she experienced pain with fulguration, which obligated a second sitting to complete.

Our only major complication was a urinoma from perforation of the renal pelvis with resultant pain and fever, which lengthened the patient's hospital stay. The problem resolved with IV antibiotics and catheter drainage of the urinoma.

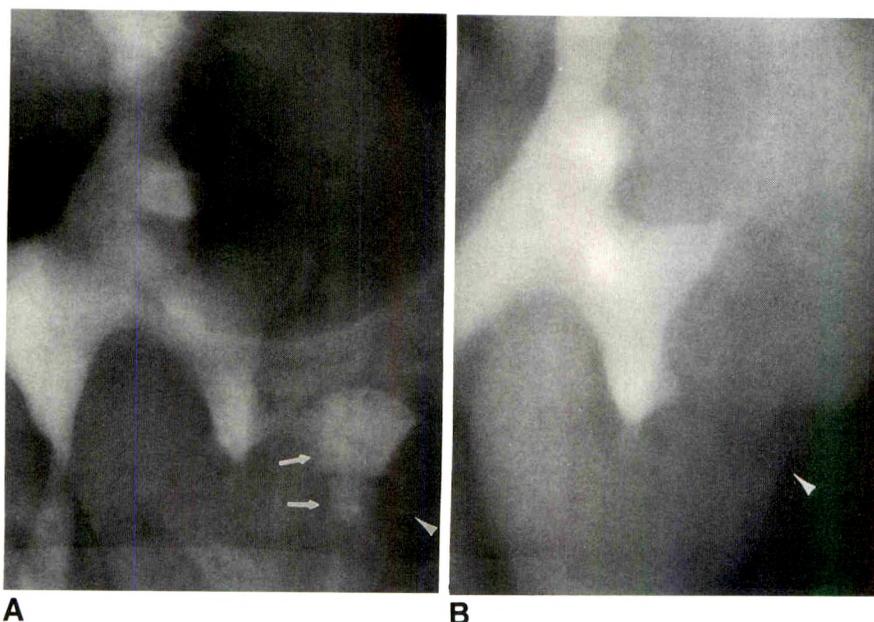


Fig. 5.—Successful obliteration of caliceal diverticulum by percutaneous techniques.

A, Preprocedure excretory urogram shows lobulated caliceal diverticulum (arrows). Stone material is obscured by contrast material. Overlying parenchymal thickness is reduced (arrowhead), typical for diverticula.

B, Follow-up tomogram during excretory urography at 13 months shows nonvisualization of diverticulum. Focal loss of overlying renal parenchyma (arrowhead) again is seen.

Follow-up

In six patients in whom cavity obliteration was attempted by fulguration and in whom follow-up is available, nonvisualization of the diverticulum on careful follow-up excretory urography indicated successful obliteration (Fig. 5); this non-visualization represented a change from preprocedural excretory urograms, which had shown the diverticula. One of these patients is asymptomatic but takes prophylactic antibiotics to prevent recurrent urinary tract infections; the others are entirely free of symptoms.

One patient who underwent only catheter drainage of her diverticulum has had recurrence of her flank pain. Excretory urography 30 months after the procedure showed a persistent cavity in which stone has recurred. In the patient who underwent tetracycline sclerosis, the cavity persists on follow-up studies but the patient has remained asymptomatic.

The patient who was found to have transitional cell carcinoma has been free of any evidence of tumor recurrence.

Discussion

We were able to treat successfully 12 symptomatic caliceal diverticula, 10 of which contained stones, with percutaneous techniques. In those patients in whom fulguration with a Bugby electrode was performed and follow-up is available, no stones have recurred and the diverticula are no longer seen on excretory urography. Two diverticula are known to persist: one infected diverticulum in which tetracycline was used as the sclerosing agent, and one stone-bearing diverticulum in which tube drainage only was used. In the latter case, stone has recurred 30 months after the procedure.

Although we were successful in extracting stones in a patient whose caliceal diverticulum had been approached indirectly elsewhere, we prefer, as do others [3, 6], to puncture the involved diverticulum directly. The two major advan-

tages of direct puncture are the ability to use the rigid nephroscope and the ability to treat the diverticular abnormality without accessing the diverticular neck, should this prove to be difficult.

The ability to use rigid nephroscopy is a distinct advantage of the direct-puncture approach. The better optics and larger irrigation channel of the rigid instrument are unquestionably beneficial in one-stage procedures for immediate visualization of the renal anatomy and stone if present, particularly in the presence of the bleeding that accompanies puncture and tract dilatation. Irrigation flow is much less through the smaller channels of the flexible nephroscope, and flow is further reduced when one channel is occupied with an instrument [9]. The rigid scope admits larger extraction instruments, and the ultrasonic lithotripsy available with the rigid scope is much more efficient in stone disintegration than the electrohydraulic lithotripsy of the flexible scope, especially for larger stones. Several other difficulties with the flexible nephroscope have been described [9].

For stone extraction or cavity fulguration with the indirect approach, the neck of the diverticulum must be located and the scope passed through it, a task that may be difficult or impossible, as we discovered in our indirectly approached case, even with balloon dilatation of the diverticular neck (Fig. 2). This difficulty is avoided when the direct approach is chosen.

Ideally, with a direct diverticular puncture, the original guidewire and safety guidewire are inserted through the diverticular neck into the renal collecting system as a precaution against loss of access [3]. However, when access to the neck is not possible before tract dilatation, both wires can be coiled within the diverticulum. Lang and Glorioso [6] reported the successful use of a single guidewire in diverticular stone extractions when access to the neck was not obtained before dilatation. We have found it easy to place the second guidewire within the diverticulum and value the security it provides.

In our series, traumatizing the lining by stenting with a large-caliber nephrostomy tube followed a few days later by fulgurating with a Bugby electrode proved to be successful in obliterating the cavity, whereas stenting alone was not in a single case. In contrast, Hulbert et al. [3] reported successful diverticular obliteration in five stone cases using a direct approach and nephrostomy drainage for 2 weeks, without fulguration, believing that the trauma of dilatation and ensuing formation of granulation tissue around the tube is sufficient to obliterate the cavity. The same group reported the use of fulguration to obliterate a large caliceal diverticulum because it was thought that only part of the lining might be traumatized by the percutaneous access and because shrinkage of the diverticulum might be retarded by the firm, supporting renal parenchyma [4]. Obliteration of an infected diverticulum has been successfully accomplished with percutaneous drainage and stenting in one case [5], but was unsuccessfully attempted with percutaneously injected absolute alcohol in an infected diverticulum with an occluded neck [7]. Indirect approaches without fulguration have not been successful in cavity obliteration [3].

Unfortunately, no single center has enough cases for a well-controlled study comparing various modifications of percutaneous treatment of caliceal diverticula. Currently, we briefly attempt to access the neck of the diverticulum fluoroscopically upon entry, but it is often easier to place a wire across the neck nephroscopically after stone removal, aided by retrograde injection of methylene blue. After balloon dilatation of the diverticular neck, the neck is stented with a 24-French Malecot catheter. After the tract matures, typically in 48 hr, we proceed to fulguration of the diverticulum and its neck. If no problems occur, we remove all tubes immediately after fulguration, but occasionally we have left a small nephrostomy tube in place for access and/or tube injections to assess cavity shrinkage.

We recommend fulguration rather than stenting alone because we believe something should be done directly to the epithelium within the diverticular cavity to incite scar formation. Stenting alone might only scarify the diverticular neck. The natural history of a diverticulum whose neck is isolated from the collecting system is unknown; theoretically the residual cavity could become infected. A randomized study would be needed to compare the efficacy of fulguration vs stenting alone. However, fulguration under direct vision is easily controlled and adds no morbidity and very little time to the procedure. Furthermore, we usually remove all tubes after fulguration and the patient can be discharged tube-free. In contrast, we discontinued our attempts at sclerosis with tetracycline after a single case because of the technical difficulties in calculating dosage and the potential hazards of extravasation or entry of tetracycline into the collecting system.

We believe that careful inspection with nephroscopy and fluoroscopic contrast injection with spot films should be done before fulguration. One should look for a flattened renal papilla and observe the anatomy of the neck. It is reasonable to fulgurate caliceal diverticula, as they are lined with nonsecretory endothelium [8]. However, should the presumed caliceal diverticulum be in fact a hydrocalix, fulguration of the tract

and portions of the cavity could lead to obstruction of the draining collecting ducts. The result could be focal renal parenchymal loss or redevelopment of the cavity and infection leading to abscess formation. We have percutaneously extracted stone from a patient not included in this series who appeared to have a caliceal diverticulum on initial retrograde pyelogram, but which looked like a calix on nephrostomy tube injection.

A limitation of our study is that radiologic follow-up was limited to excretory urography. We are satisfied that, in those patients with follow-up urograms, at least the necks were obliterated because the diverticula had been identified on preprocedural excretory urography, and we feel that retrograde pyelography would not be useful. CT or sonography would be necessary to assess any residual cavity within the parenchyma, but this information is not available in our series or that of Hulbert et al. [3].

ESWL has replaced percutaneous nephrolithotomy in at least 90% of patients with nondiverticular renal calculi [10], but it has not been widely used in the treatment of diverticular calculi because the stone fragments may not pass through the narrow diverticular neck [11]. Psihramis and Dretler [12] have recently reported their experience with ESWL for treating 10 patients with diverticular calculi. Although all stones were completely fragmented in one or two treatments, only two patients had passed all stone fragments after a minimum follow-up period of 3 months. Three patients (30%) had persistent symptoms. Although we have successfully treated one diverticular stone with ESWL alone despite a narrow neck, two other diverticula (included in this series) treated with ESWL were referred for percutaneous stone extraction because of the inability of fragments to drain.

Although primary use of ESWL for diverticular calculi has been proposed both for its low morbidity and the possibility of applying it in centers without extensive experience in percutaneous techniques [12], we believe that primary percutaneous nephrolithotomy is the optimal approach unless specific contraindications supervene. Percutaneous techniques have the advantage of treatment of the diverticulum at the same time as removal of the stone. Elimination of the underlying abnormality will reduce the chance of recurrent stones or infection. We have had no recurrences of stone in any patient who had successful cavity obliteration, but stone did recur in one of the two cases in which the cavity was not obliterated. Furthermore, some complications of ESWL are best treated with percutaneous techniques, so that it may be unwise to use ESWL for complex cases in which percutaneous techniques are not readily available. Two of our patients required percutaneous diverticular stone extraction when fragments failed to pass after ESWL.

ESWL may be appropriate initial therapy in cases in which a percutaneous approach would be difficult. For example, a disadvantageous position such as a diverticular location centrally near the renal vessels or high under the ribs increases the risks of hemorrhage or pneumothorax. Percutaneous techniques can be used later if ESWL fails. The most important factor that would lead us away from percutaneous treatment is the size of the diverticulum. Smaller diverticula are more difficult to puncture and to coil wires within. We suc-

cessfully treated a diverticulum measuring 8 by 10 mm and believe that in experienced hands, favorably positioned diverticula as small as 6 or 7 mm might be treated. If wires cannot be coiled in the diverticulum or advanced through its neck, then the technique described by Glanz et al. [13] for difficult caliceal stones could be attempted. This involves puncturing the far wall of the cavity and anchoring guidewires in the adjacent renal parenchyma.

We conclude that percutaneous nephrostomy and nephroscopy provide a safe alternative to an open procedure for the treatment of infected or stone-bearing diverticula. Whenever possible, obliteration of the cavity should be attempted to reduce the chance of recurrence of symptoms.

REFERENCES

1. Middleton AW Jr, Pfister RC. Stone-containing pyelocaliceal diverticulum: embryologic, anatomic, radiologic and clinical characteristics. *J Urol* **1974**;111:2-6
2. Timmons JW Jr, Malek RS, Hattery RR, DeWeerd JH. Caliceal diverticulum. *J Urol* **1975**;114:6-9
3. Hulbert JC, Reddy PK, Hunter DW, Castañeda-Zúñiga W, Amplatz K, Lange PH. Percutaneous techniques for the management of caliceal diverticula containing calculi. *J Urol* **1986**;135:225-227
4. Hulbert JC, LaPointe S, Reddy PK, Hunter DW, Castañeda-Zúñiga W. Percutaneous endoscopic fulguration of a large volume caliceal diverticulum. *J Urol* **1987**;138:116-117
5. Kremers PW, Beckmann CF, Bihrlie W, III. Percutaneous balloon dilatation in treatment of infected pyelocaliceal diverticulum. *Urology* **1988**;32:29-32
6. Lang EK, Glorioso LW. Multiple percutaneous access routes to multiple calculi, calculi in caliceal diverticula, and staghorn calculi. *Radiology* **1986**;158:211-214
7. Ramchandani P, Soulen RL, Kendall AR, Davis JA. Percutaneous management of a pyelocaliceal diverticular abscess. *J Urol* **1985**;133:81-83
8. Wulfsohn MA. Pyelocaliceal diverticula. *J Urol* **1980**;123:1-8
9. Lange PH, Reddy PK, Hulbert JC, et al. Percutaneous removal of caliceal and other "inaccessible" stones: instruments and techniques. *J Urol* **1984**;132:439-442
10. Bush WH, Gibbons RP, Lewis GP, Brannen GE. Impact of extracorporeal shock wave lithotripsy on percutaneous stone procedures. *AJR* **1986**;147:89-93
11. Smith TP, Castañeda-Zúñiga WR, Darcy MD, Cragg AH, Hunter DW, Amplatz K. Current trends in the management of urinary stones. *Acta Radiol* **1988**;29:145-150
12. Psihramis KE, Dretler SP. Extracorporeal shock wave lithotripsy of caliceal diverticula calculi. *J Urol* **1987**;138:707-711
13. Glanz S, Laungani GB, Gordon DH, Macchia RJ, Sclafani JA. Percutaneous removal of renal caliceal calculi: an alternative approach. *Urol Radiol* **1986**;8:40-43

Vaginal Reconstruction with Rectus Abdominis Myocutaneous Flap: CT Findings

Steven J. Willing^{1,2}
 Steven H. Pursell³
 Scott R. Koch^{1,4}
 Gordon R. Tobin⁵

The distally based rectus abdominis myocutaneous flap is used in a new technique for vaginal reconstruction after pelvic exenteration for malignant disease. We identified 27 patients who underwent this procedure, of whom eight had a total of 14 postoperative CT scans and two CT-directed biopsies. The myocutaneous flap appeared as a unilateral arcuate band of soft tissue extending from the linea alba to the rectal fascia or sacrum. Additional CT findings included asymmetric thinning of the ventral abdominal wall (7/8), fluid collections (2/8), vaginal breakdown (1/8), presacral soft-tissue thickening (6/8), and tumor recurrence (3/8).

The postoperative CT scan reflects the altered anatomy produced by the surgery. Complications and recurrent disease can be recognized as deviations from the normal postoperative appearance.

AJR 156:1001-1004, May 1991

Pelvic exenteration for locally advanced or recurrent malignant disease has been shown to improve survival and in some cases to effect a cure [1]. In order to decrease morbidity and improve patients' acceptance and quality of life, numerous techniques for vaginal reconstruction were developed. One of the more successful techniques has been the bilateral gracilis myocutaneous flap reported by McCraw et al. [2] in 1976. Its resultant CT findings were described by Epstein et al. [3] in 1987.

In 1988, Tobin and Day [4] reported their initial results with a distally based rectus abdominis myocutaneous flap for vaginal reconstruction. In this procedure, a myocutaneous flap is constructed from the cephalic portion of the rectus abdominis, the superior epigastric artery is ligated, and the flap is rotated around its inferior epigastric vascular pedicle and passed through a peritoneal incision into the pelvis (Figs. 1-3). The advantages of this technique are shortened operative time, improved graft survival, and better obliteration of the pelvic dead space. Patients who have undergone this procedure have a unique postoperative CT appearance, which we describe here.

Materials and Methods

We identified 27 patients who had pelvic exenteration with rectus abdominis myocutaneous flap reconstruction in the past 6 years, of whom eight patients had a total of 14 postoperative CT scans and two CT-directed biopsies. The patients ranged in age from 23 to 82 years old (median age, 45 years) at the time of the procedure. Five patients had squamous carcinoma of the cervix, one had adenocarcinoma of the cervix, one had squamous carcinoma of the vagina, and one had transitional cell carcinoma of the bladder. The time from original diagnosis to exenteration ranged from 1 month to 8 years. Six patients had complete exenteration with vaginal reconstruction, one had an anterior exenteration (sparing the rectum) with vaginal reconstruction, and one had exenteration with a rectus abdominis patch but no neovagina was constructed. Six patients were initially treated with radiation, and one patient was treated

Received September 5, 1990; accepted after revision November 21, 1990.

Presented as a scientific exhibit at the annual meeting of the American Roentgen Ray Society, Washington, DC, May 1990.

¹ Department of Diagnostic Radiology, University of Louisville, Louisville, KY 40202.

² Present address: Department of Diagnostic Radiology, University of Alabama at Birmingham, Birmingham, AL 35233. Address reprint requests to S. J. Willing.

³ Department of Gynecologic Oncology, University of Louisville, Louisville, KY 40202.

⁴ Present address: Department of Diagnostic Radiology, Emory University, Atlanta, GA 30322.

⁵ Department of Plastic and Reconstructive Surgery, University of Louisville, Louisville, KY 40202.

0361-803X/91/1565-1001

© American Roentgen Ray Society

initially with both radiation and hysterectomy. One patient was treated initially with exenteration followed by postoperative irradiation.

Fourteen postoperative abdominopelvic CT scans were reviewed. Four scans were obtained in the first postoperative month in two patients. One of these patients and six additional patients had follow-up examinations ranging from 2 to 17 months after surgery.

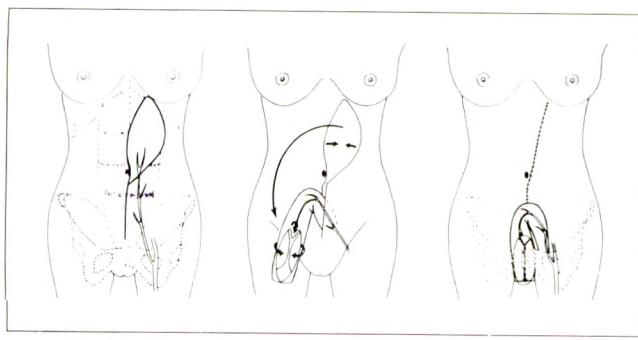


Fig. 1.—A, Myocutaneous flap is created, based on inferior epigastric vascular pedicle.
B, Skin of flap is wrapped to form neovagina.
C, Flap with neovagina is passed into pelvis and secured to perineum; laparotomy and donor site closed.

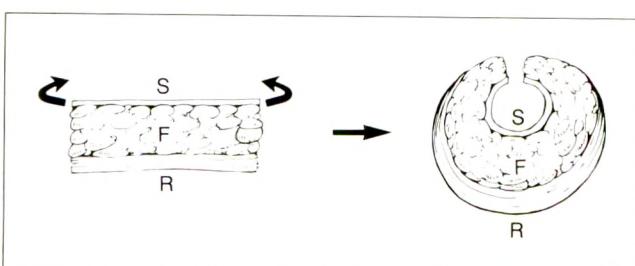


Fig. 2.—Cross section of flap illustrates how myocutaneous flap is wrapped to form neovagina. S = skin, F = subcutaneous fat, R = rectus abdominis muscle.

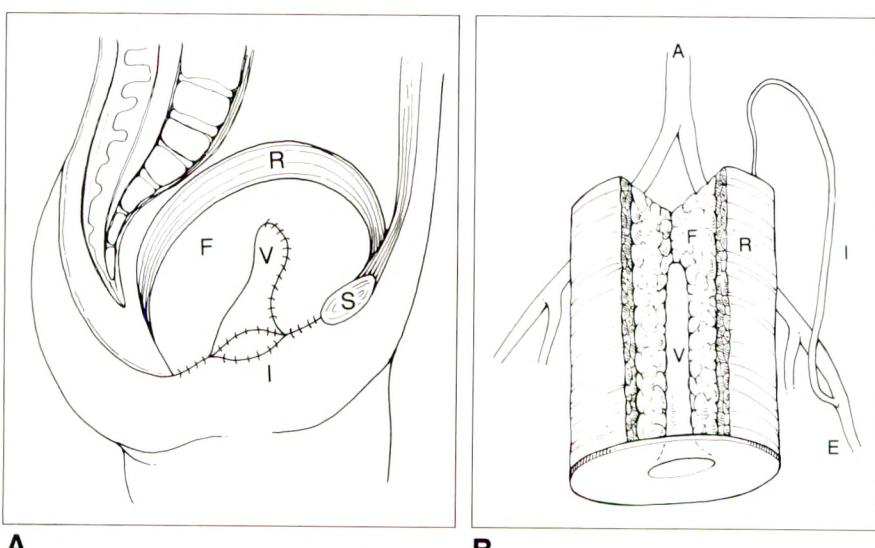


Fig. 3.—A, Sagittal view of reconstructed pelvis. I = neointroitus, S = pubic symphysis.
B, Cut-away view of reconstructed pelvis, viewed from perineum. A = aorta, E = external iliac artery, I = inferior epigastric artery.
R = rectus abdominis graft, F = subcutaneous fat, V = neovagina.

Results

Normal Postoperative Appearance

The muscular flap most often is seen as a unilateral arcuate band of soft tissue extending from the linea alba to the sacrum (Fig. 4) or, in the case of anterior exenteration, to the perirectal fascia (Fig. 5). It may be situated on either side of the pelvis. The flap may also lie in a more posterior position, anterior to the sacrum and nearly midline in position (Fig. 6). The cutaneous graft forms the neovagina, completely encircled by a layer of fat (Fig. 5). As reported after gracilis reconstruction, air may be seen in the neovagina and is a normal finding. Intravaginal air, when present, permits visualization of both inner and outer walls. Otherwise, the inner walls are apposed and only the outer wall is visible. The skin forming the neovagina is redundant, and tends to collapse into a linear or "Y" configuration.

Seven of the eight patients exhibited asymmetric thinning of the ventral abdominal wall at the graft donor site (Fig. 7A). Here the posterior rectus fascia forms the remaining abdominal wall support. This area is at risk for hernia formation, but the reported prevalence is only about 3% [5]. No hernias were present in this select group of patients.

Presacral soft-tissue thickening was seen in six patients (Fig. 6). This is usually attributable to the muscular flap. Only one of the six had recurrent tumor in the presacral space. In this case, the early postoperative scans showed a thin, smooth band of presacral soft tissue, which had thickened markedly 4 months later.

Abnormal CT Findings

One obese patient had a superficial abdominal wound separation that healed uneventfully. Another patient had a pelvic fluid collection during the first postoperative month that resolved spontaneously (Fig. 8A); however, she subsequently died of recurrent tumor. Breakdown of the neovagina oc-

Fig. 4.—23-year-old woman with squamous cell carcinoma of vagina. CT scan obtained in first month after surgery shows curvilinear band of soft tissue from linea alba to sacrum (arrows) due to muscular graft.

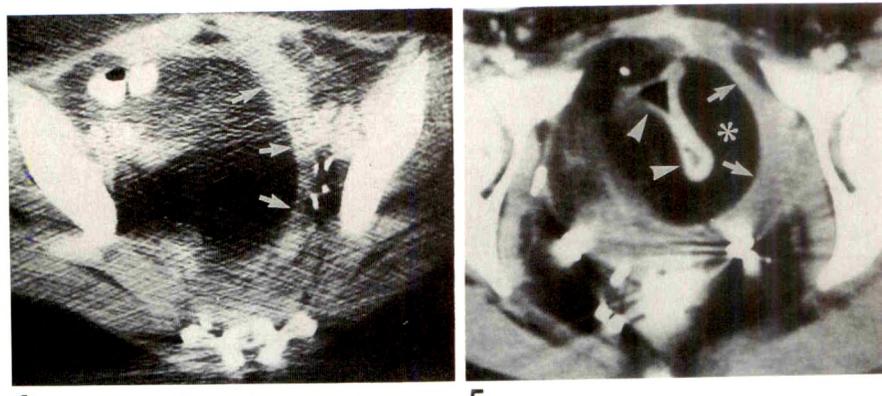


Fig. 5.—34-year-old woman with carcinoma of cervix, 6 months after anterior exenteration and reconstruction. CT scan shows rectus abdominis forming a soft-tissue band from linea alba to rectal fascia (arrows), surrounding neovagina. Neovagina is formed by grafted skin (arrowheads) surrounded by subcutaneous fat (asterisk).

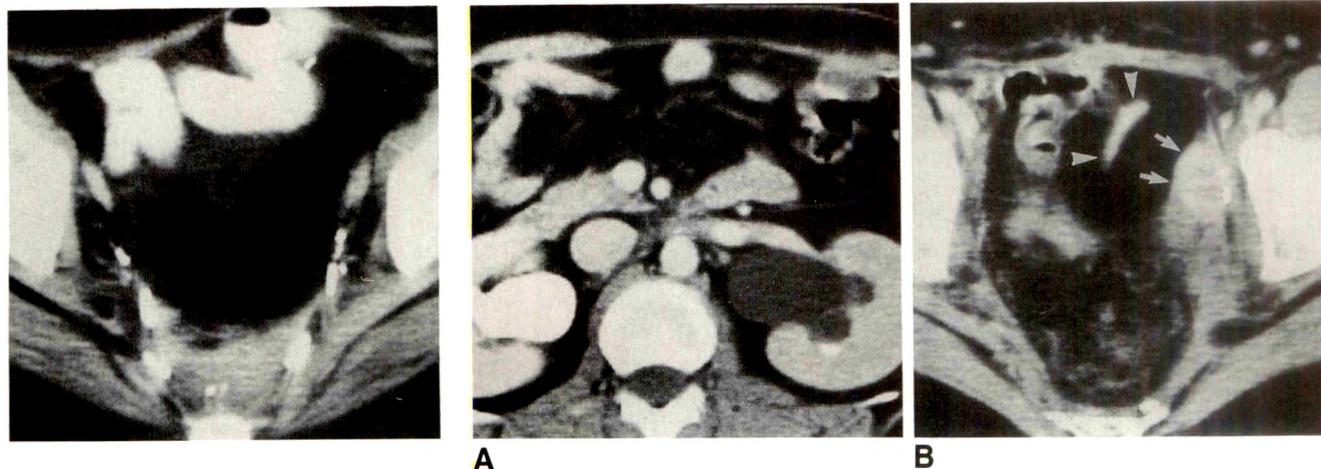


Fig. 6.—54-year-old woman with squamous carcinoma of cervix, 17 months after exenteration and reconstruction. CT scan shows presacral, midline band of soft-tissue density due to muscular patch.

Fig. 7.—**A**, 32-year-old woman with adenocarcinoma of cervix. CT scan obtained 10 months after exenteration and reconstruction shows a normal graft donor site. There is asymmetric thinning of left abdominal wall due to removal of rectus abdominis. Left kidney is hydronephrotic.

B, Biopsy-proved recurrent tumor (arrows) causes convex bulge on normally concave inner border of muscular flap. Note neovagina (arrowheads) surrounded by fat.

curred in one patient, indirectly identifiable on CT as a large extraperitoneal collection of free air in the pelvis.

Postoperative abscess occurred in one patient. This patient had a postoperative course complicated by small-bowel obstruction and jejunal perforation leading to a large abscess containing air and fluid in the anterior perihepatic space.

Pathologically confirmed tumor recurrence was identified in three patients. In the first case, follow-up scans showed omental tumor mass and a heterogeneous pelvic soft-tissue mass lateral and posterior to the flap extending to the piriformis muscles and sacrum (Fig. 8B). The second patient developed a focal soft-tissue mass altering the normal crescentic inner margin of the myocutaneous flap 10 months after reconstruction (Fig. 7B). A CT-guided needle biopsy was diagnostic for recurrent tumor. In the third case, recurrent pelvic tumor was visible as a soft-tissue mass with central low attenuation abutting the wall of the neovagina.

Discussion

Although pelvic exenteration can significantly improve the survival rate (up to a 50% 2-year survival rate) for patients with gynecologic malignant tumors, it is not without morbidity. The loss of pelvic soft tissue allows bowel herniation into the pelvis with the danger of fistulization and obstruction. If further radiotherapy is required, bowel may be in the therapy field. The loss of sexual function affects the patient's postoperative quality of life and acceptance of the procedure. In order to address these issues, pelvic soft-tissue packing and vaginal reconstruction have been performed by using a variety of techniques. The bilateral gracilis myocutaneous flap has commonly been used; however, the distally based rectus abdominis myocutaneous flap has certain advantages and is finding increasing acceptance. These advantages include improved graft survival and shortening of the operative time.

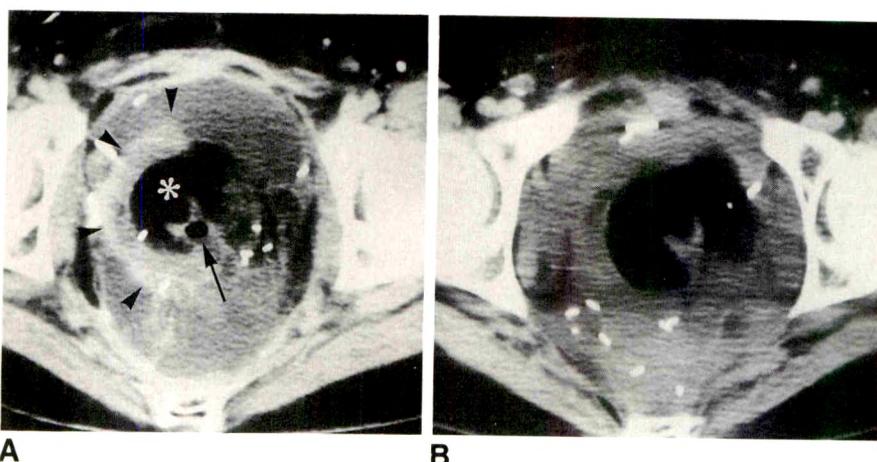


Fig. 8.—A, 50-year-old woman with squamous carcinoma of cervix. CT scan obtained in first postoperative month shows pelvic fluid collection surrounding graft. This resolved spontaneously. Note air in neovagina (arrow), rectus abdominis (arrowheads), and layer of subcutaneous fat (asterisk).

B, CT scan obtained 6 months later. Note marked increase in amount of presacral soft tissue.

The procedure begins with the design of a 10- to 12-cm-wide ellipse of skin beginning below the costal margin and extending a few centimeters below the umbilicus. The caudal end is extended into the laparotomy incision to allow a single closure. After the skin incision, the cephalic margin of the rectus abdominis is transected and the superior epigastric artery is ligated. A tube is created with the cutaneous portion of the graft to form a neovagina. The cephalic end is left open, to form the new introitus. The completed pouch is passed through a peritoneal incision into the pelvis, and the rectus fascia is closed to prevent hernia. Care is taken throughout to preserve the inferior epigastric vascular pedicle supplying the graft.

In Tobin and Day's series, there was complete graft survival in 18 of 20 patients. The remaining two had partial losses that were successfully revised. In these two, the paddles had been extended above the costal margin. Subsequently, the cephalic extent of the paddle was limited to just below the costal margin. No hernias or postoperative infections occurred in the series. Interestingly, patients who resumed sexual activity reported successful orgasms even though the neovagina is insensate. Our series of CT evaluations in this group yielded the following observations. (1) The muscular flap appears as a band of soft-tissue density abutting the pelvic side wall or sacrum. (2) The neovagina exhibits a doughnut

configuration of subcutaneous fat with inner cutaneous lining. (3) The graft donor site can be seen in most patients as unilateral thinning of the rectus sheath. (4) Presacral soft-tissue thickening can be a normal postoperative finding. (5) Recurrent tumor appears as a soft-tissue mass altering the normal configuration of the reconstructed pelvis, possibly with abnormal enhancement or tissue inhomogeneity. (6) Familiarity with the normal postoperative appearance is necessary both for the detection of recurrence and to avoid a falsely positive diagnosis.

REFERENCES

1. Morley GW, Lindenauer SM. Exenterative therapy for gynecologic malignancy: an analysis of 70 cases. *Cancer* **1976**;38:581-586
2. McCraw JB, Massey FM, Shanklin KD, Horton CE. Vaginal reconstruction with gracilis myocutaneous flaps. *Plast Reconstr Surg* **1976**;58:176-183
3. Epstein DM, Arger PH, LaRossa D, Mintz MC, Coleman BG. CT evaluation of gracilis myocutaneous vaginal reconstruction after pelvic exenteration. *AJR* **1987**;148:1143-1146
4. Tobin GR, Day TG. Vaginal and pelvic reconstruction with distally based rectus abdominis myocutaneous flaps. *Plast Reconstr Surg* **1988**;81:62-70
5. Kroll SS, Pollock R, Jessup JM, Ota D. Transpelvic rectus abdominis flap reconstruction of defects following abdominal-perineal resection. *Am Surg* **1989**;55:632-637

Case Report

Pancreatitis Causing Focal Caliectasis

Michael Fishman¹ and Lee B. Talner

Pancreatitis commonly involves the pararenal compartments, although it does not usually extend into the kidney. The perinephric fasciae are thought to provide an effective barrier to the spread of pancreatic enzymes toward or into the kidney [1–3]. We report a patient with focal caliectasis of the right kidney resulting from intrarenal extension of the inflammatory process. The history and imaging findings suggested a primary renal process rather than pancreatitis, and the correct diagnosis was not considered preoperatively. To our knowledge, focal caliectasis from pancreatitis has not been described previously.

Case Report

A 57-year-old man had a 5-week history of hematuria and a 3-day history of right flank pain. The patient was a known alcoholic without a history of pancreatitis. On physical examination, right-sided costovertebral angle tenderness was noted. Epigastric pain and tenderness were absent. Serum amylase and lipase levels were elevated on admission but became normal within several days.

Urinalysis revealed moderate pyuria and hematuria. No bacteria were seen or cultured. The plain abdominal radiograph showed no opaque stones. Excretory urography (Fig. 1A) showed focal caliectasis in the right upper pole with attenuated infundibula thought most likely to be due to peripelvic cysts. No signs of ureteral obstruction were seen. CT performed immediately after urography with no additional contrast material showed poorly marginated soft tissue encasing the infundibula of the right upper pole (Fig. 1B). Minimal streaky densities were present in the perinephric space. The pancreas was not enlarged. The CT findings were interpreted as peripelvic inflam-

mation of uncertain cause. The possibility of reaction to extravasated urine subsequent to a recently passed stone was considered. The patient was treated for 2 weeks with oral antibiotics.

Three weeks after the original urogram and CT, continued right flank pain and hematuria prompted a second CT examination (Figs. 1C and 1D). Increased perinephric and new posterior pararenal fascial soft-tissue and fluid densities were noted. The soft-tissue process in the renal sinus also had enlarged. A new 1.5-cm cystic mass was seen anterior to the inferior vena cava. Again the pancreas was not enlarged. Interpretation still centered on a renal inflammatory process or, less likely, an infiltrating tumor. The possibility of pancreatitis causing the renal and pararenal abnormalities was considered unlikely because of the absence of abdominal pain, the normal amylase level, and the normal appearance of the pancreas on CT.

Exploratory surgery was performed 2 weeks after the second CT examination because of persistent pain and microscopic hematuria. The serum amylase level was not measured preoperatively. The cystic mass anterior to the inferior vena cava was resected, and a nephrectomy was performed.

The pathologist reported focal regions of fat necrosis in the renal sinus and, to a lesser extent, in the perinephric fat. This was accompanied by an inflammatory infiltrate in the pericaliceal (sinus) fat and subepithelial layers of the upper pole calices. The papillae in the upper pole were minimally flattened. The renal parenchyma was normal except for mild interstitial inflammation. The mass anterior to the inferior vena cava was interpreted as an inflammatory, hemorrhagic "cyst" with areas of fat necrosis. The amylase content of the cyst fluid was not measured. No evidence of malignancy was found. Pancreatitis or reaction to extravasated urine was suggested as the most likely cause.

The patient was well until 12 months later, when he was readmitted with typical clinical, laboratory, and CT findings of acute pancreatitis.

Received October 17, 1990; accepted after revision December 13, 1990.

¹ Both authors: Department of Radiology, University of California, San Diego, Medical Center, 225 Dickinson St., San Diego, CA 92103 and Veterans Affairs Medical Center, La Jolla, CA 92041. Address reprint requests to L. B. Talner at UCSD Medical Center.

AJR 156:1005–1006, May 1991 0361–803X/91/1565–1005 © American Roentgen Ray Society

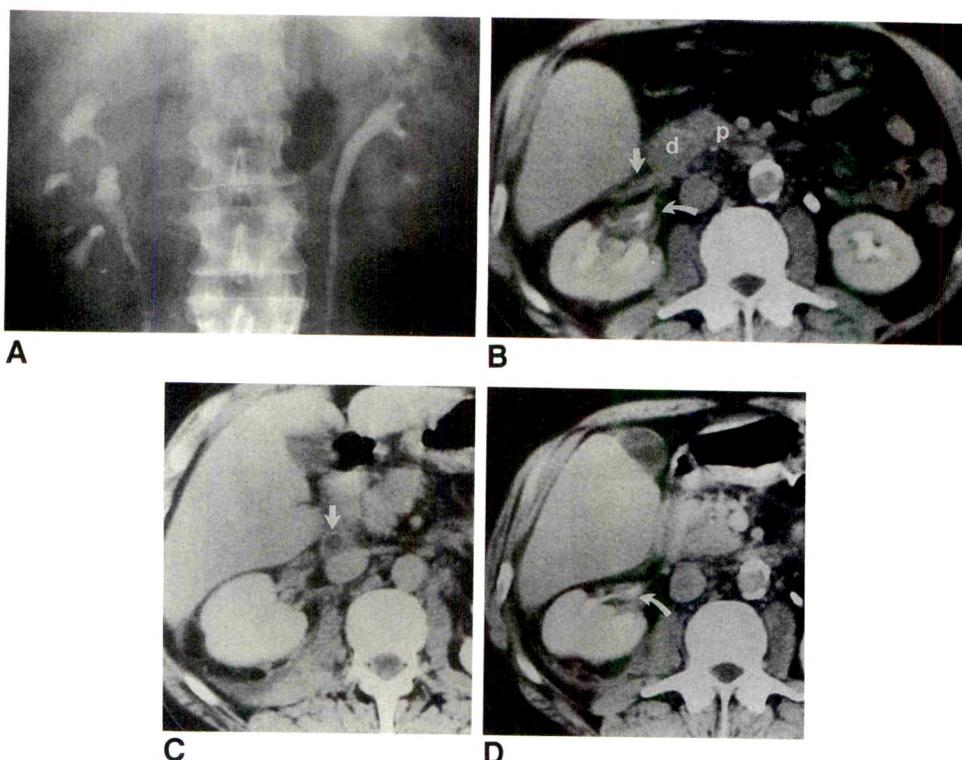


Fig. 1.—*A*, 5-min excretory urogram shows focal caliectasis in right upper pole. Corresponding infundibula are narrowed.

B, CT scan obtained immediately after *A* with no additional contrast material shows a soft-tissue mass (curved arrow) encasing upper portion of bifid renal pelvis and right-upper-pole infundibulum. Minimal anterior pararenal fascial thickening is present (straight arrow). Pancreas (*p*) is not enlarged. Duodenum (*d*).

C and *D*, Enhanced CT scans obtained 3 weeks after *B*. Scan at more cephalic level (*C*) shows 1.5-cm mass (arrow) with low central attenuation anterior to inferior vena cava. Posterior pararenal fluid is present. Scan (*D*) at level similar to *B* shows persistence of soft-tissue mass (arrow) encasing right-upper-pole infundibulum. Increased perinephric and posterior pararenal soft-tissue stranding are present.

Review of the histology with the pathologist, in light of the new information, left no doubt that focal caliectasis was caused by spread of pancreatic inflammation.

Discussion

Dissection of pancreatic enzymes along fascial planes is well known [1, 2, 4]. Most commonly, the spread is from the pancreas anteriorly into the lesser sac. The next most common pathway is posterior into the anterior pararenal space with extension into the leaves of the posterior perinephric fascia [1, 2, 4]. CT findings of anterior and posterior pararenal fascial thickening, sometimes containing fluid, surrounding an otherwise normal kidney produce the classic halo sign [5]. Although the perinephric fascia is often infiltrated, usually it is not penetrated.

Scattered reports of penetration of pancreatic inflammation into the perinephric space, producing strandlike densities on CT, have been published [4, 6–8]. Morehouse et al. [8] described six patients with pancreatitis in whom the inflammatory process compressed or encased the right ureter, causing hydronephrosis. In all the reported cases, the perinephric involvement by pancreatic enzymes was accompanied by thickening of the anterior and posterior pararenal tissues, producing a typical halo sign.

Rarely, a large pancreatic inflammatory process or pseudocyst may compress or even invade the kidney [7, 8]. Usually this occurs on the left side as a complication of a pseudocyst of the pancreatic tail. The mass effect on the kidney may be profound.

Our patient is unique in that the original CT scan (Fig. 1B) showed direct extension of the inflammatory process into the

perinephric space with little thickening of the anterior pararenal fascia. Pathologic findings were consistent with the CT findings. It is possible that the fascial envelope in this patient was incomplete or more porous than usual.

Pancreatitis is an intriguing disease because its initial manifestations (e.g., fluid or inflammation in the pleura, mediastinum, or pelvis) may occur in sites remote from the pancreas. In our patient, the symptoms appeared to be primarily renal, and the abnormalities on the initial and even subsequent imaging studies were centered on the renal sinus. If the correct diagnosis had been suggested earlier, nephrectomy might have been avoided.

REFERENCES

1. Siegelman SS, Copeland BE, Saba GP, Cameron JL, Sanders RC, Zerhouni EA. CT of fluid collections associated with pancreatitis. *AJR* 1980;134:1121–1132
2. Raptopoulos V, Kleiman PK, Marks S, Snyder M, Silverman PM. Renal fascial pathway: posterior extension of pancreatic effusions within the anterior pararenal space. *Radiology* 1986;158:367–374
3. Myers MA, Whalen JP, Peele K, Berne AS. Radiologic features of extraperitoneal effusions. *Radiology* 1972;104:249–257
4. Mendez G, Isikoff MB, Hill MC. CT of acute pancreatitis: interim assessment. *AJR* 1980;135:463–469
5. Susman N, Hammerman AM, Cohen E. The reno halo sign in pancreatitis. *Radiology* 1982;142:323–327
6. Feuerstein IM, Zeman RK, Jaffe MH, Letitia CR, David CL. Perirenal cobwebs: the expanding CT differential diagnosis. *J Comput Assist Tomogr* 1984;8:1128–1130
7. Guerrier K, Persky L. Pancreatic disease simulating renal abnormality. *Am J Surg* 1970;120:46–49
8. Morehouse HT, Thornhill BA, Alterman DD. Right ureteral obstruction associated with pancreatitis. *Urol Radiol* 1985;7:150–152

Technical Note

Retrograde Replacement of Internal Double-J Ureteral Stents

Joseph W. Yedlicka, Jr.,¹ Richard Aizpuru, David W. Hunter, Wilfrido R. Castañeda-Zúñiga, and Kurt Amplatz

The ability of internal double-J ureteral stents to maintain ureteral patency has been well documented [1–3]. However, these stents often need to be changed or removed. The techniques of retrograde cystoscopic manipulation and percutaneous antegrade placement or removal of these stents have been described [1–8]. We present a simple technique for retrograde removal or exchange of internal ureteral stents by using a right-angle snare/catheter system, under fluoroscopic control, that to our knowledge has not been previously reported.

Materials and Methods

Through a Foley or standard angiographic catheter, a guidewire is advanced into the bladder. Female patients are in the dorsal lithotomy position; male patients are supine. The Foley or angiographic catheter is then exchanged for an angled guiding catheter (6-French) to be used with a right-angle snare (Microvena Corporation, Vadnais Heights, MN; Fig. 1A). Under multiangled fluoroscopic guidance, the bladder end of the double-J stent is encircled with the snare loop (Fig. 1B). The guiding catheter is then advanced in order to close the snare loop on the stent. With the stent firmly grasped, the entire assembly is then carefully withdrawn a short distance through the urethra (Fig. 1C), and the end of the stent grasped with a clamp. The proximal end of the ureteral stent is still either within the renal pelvis or in the proximal ureter. A stiff guidewire is then inserted into the exteriorized end of the stent and advanced until the guidewire is coiled within the renal pelvis. The stent is then completely removed, leaving the guidewire in place (Fig. 1D). Next, the tapered end of a standard, appropriate-length, 10-French double-J stent (Cook,

Bloomington, IN; Medi-tech, Watertown, MA; Fig. 1E) is advanced in a retrograde fashion over the guidewire and positioned so that the proximal pigtail is formed in the renal pelvis. The stent stiffener is removed, leaving the guidewire and pusher in place. The wire is then partially withdrawn so that the floppy end of the wire is across the junction between the pusher and the stent. The pusher is then slowly advanced with a gentle rotating motion; the floppy end of the wire allows the distal pigtail portion of the stent to spontaneously re-form within the bladder (Fig. 1F). The pusher is removed, and a Foley catheter is placed into the urinary bladder for a follow-up cystogram to confirm proper stent positioning and patency. If necessary, the stent position can be adjusted, repeating the steps described here.

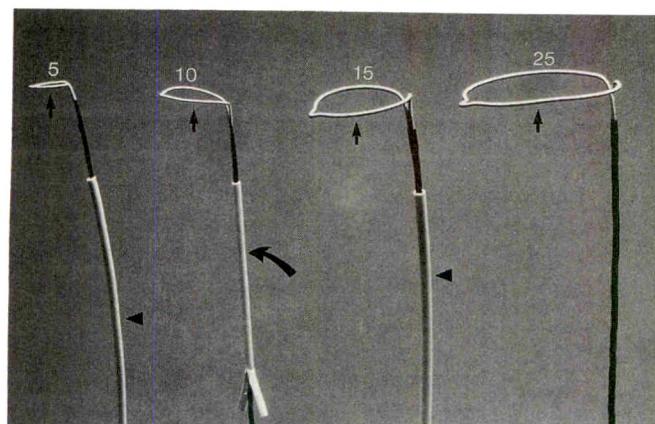
Results

Ureteral stent removals or exchanges were successfully performed in 21 of 22 female patients and two of two male patients during the past 2 years. The majority of these patients had malignant ureteral obstruction. In the single unsuccessful case, manipulation of the snare within the urinary bladder was limited by massive tumor ingrowth that necessitated cystoscopic removal of the occluded stent. We have had no complications except for minor transient hematuria in five cases. In two patients, the new stent was inadvertently pushed too far up the ureter. Both were quickly and easily repositioned (see Discussion). The procedure was very easy to perform, even for inexperienced operators. The average time for retrieval or exchange of the internal ureteral stents was less than 25 min per case; fluoroscopic time averaged 2–5 min.

Received November 6, 1990; accepted after revision December 11, 1990.

¹ All authors: Department of Radiology, Box 292 UMHC, University of Minnesota Hospital and Clinic, 420 Delaware St. S.E., Minneapolis, MN 55455. Address reprint requests to K. Amplatz.

AJR 156:1007–1009, May 1991 0361–803X/91/1565–1007 © American Roentgen Ray Society



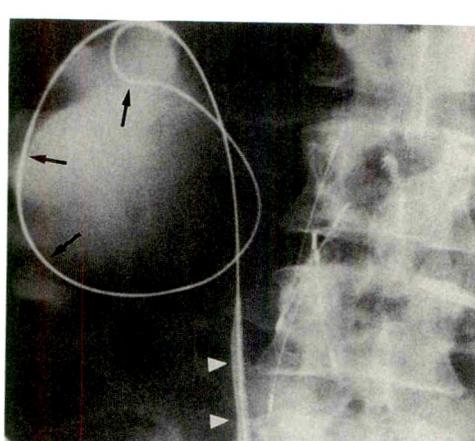
A



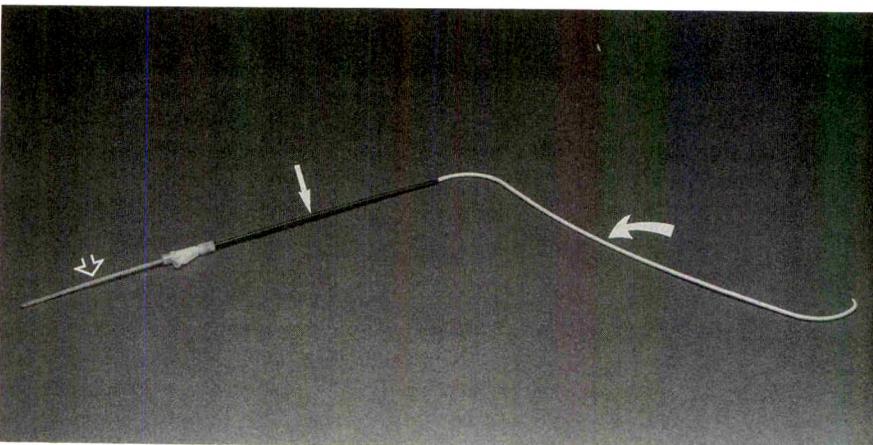
B



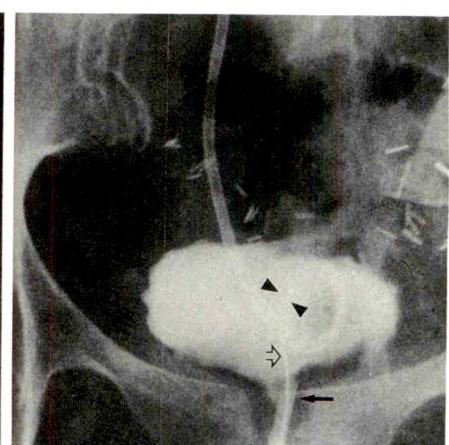
C



D



E



F

Discussion

Internal double-J ureteral stents have been widely used to maintain ureteral patency [1-3].

Antegrade approaches for removal and exchange of these stents have been described [4-6]. However, this is technically more difficult, is much more painful and psychologically demanding for the patient, and requires placement of a large catheter through a percutaneous tract with all the attendant

risks and complications of that procedure. Retrograde cystoscopic removal or exchange is widely used but usually requires general or epidural anesthesia and the use of a surgery or cystoscopy suite [1-3, 7, 8]. The retrograde approach with a right-angle snare/catheter system is easy to perform (even for inexperienced operators) and can be done in any fluoroscopy room. The patient's discomfort is minimal (small catheters) and the procedure is usually completed in 20-25 min. This technique is best suited for retrograde ma-

A, Right-angle nitinol snares. Snare loops are 5, 10, 15, and 25 mm (straight arrows). Guiding catheters (arrowheads), "cheater" (curved arrow).

B, A right-angle snare (arrow) through a 6-French guiding catheter has been inserted in a retrograde fashion into urinary bladder. Note distal pigtail of occluded internal ureteral stent (arrowheads).

C, 6-French guiding catheter advanced to close snare loop (arrow), enabling removal of occluded ureteral stent (arrowheads) through urethra.

D, After guidewire (arrows) was coiled in renal pelvis (contrast material is from a previous CT examination), old stent (arrowheads) was removed, leaving wire in place.

E, 10-French double-J ureteral stent set (Cook Co.) pusher (straight solid arrow), stiffener (open arrow), and double-J stent (curved arrow).

F, After inner stiffener had been removed, pusher (solid arrows) was used to advance distal end of stent (arrowheads) into bladder over floppy end of guidewire (open arrow). Note that guidewire is only slightly beyond stiffener-stent junction.

nipulation in females because a longer urethra and prostate enlargement in males may make this procedure more difficult and uncomfortable. At our institution, we perform this procedure on those male patients in whom cystoscopy is difficult or fails and in those male patients at high risk when anesthesia is used.

The most difficult part of the procedure is getting the snare loop around the lower end of the stent. Fluoroscopy in two planes is critical, and the new, more maneuverable snare system, although it has not improved our ability to complete the procedure successfully, has markedly reduced the time required. The only other slightly tricky part of the procedure is pushing the lower pigtail out of the urethra into the bladder.

In two patients, the new stent was inadvertently advanced too far into the ureter. In one patient, a small angioplasty balloon was advanced over the wire into the stent and the stent pulled into the bladder. In the other patient, the lower end of the stent was still in the bladder; it was grasped with the snare and easily repositioned.

In conclusion, we believe that the retrograde transurethral approach with a right-angle snare/catheter system under

fluoroscopic guidance is the procedure of choice for exchange or removal of internal double-J ureteral stents in female patients and also may be useful in selected male patients.

REFERENCES

1. Hepperlen TW, Mardis HK, Kammandel H. Self-retained internal ureteral stents: a new approach. *J Urol* **1978**;119:731
2. VanAarsdal KN, Pollack HM, Wein AJ. Ureteral stenting. *Semin Urol* **1984**;2:180-186
3. Smith AD. Percutaneous ureteral surgery and stenting. *Urology* **1984**;23:37-42
4. LeRoy AJ, Williams HJ, Segura JW, Patterson DE, Benson RR. In-dwelling ureteral stents: percutaneous management of complications. *Radiology* **1986**;158:219-222
5. Boren SR, Dotter CT, McKinney M, Rosch J. Percutaneous removal of ureteral stents. *Radiology* **1984**;152:230-231
6. Mitty HA, Train JS, Dan SJ. Placement of ureteral stents by antegrade and retrograde techniques. *Radiol Clin North Am* **1986**;24:587-600
7. Hezmall HP, Flechner SM, Sandler CM. Controlled endoscopic retrieval of ectopic ureteral catheters using fluoroscopic guidance. *Urology* **1985**;25:613-615
8. Smith AD. Retrieval of ureteral stents. *Urol Clin North Am* **1982**;9:109-112

Book Review

Orthopedic Radiology. A Practical Approach. By Adam Greenspan. Philadelphia: Lippincott, 640 pp., 1988. \$225

This textbook is intended for all physicians interested in the medical imaging of orthopedic diseases. Its primary audience is medical students and residents in diagnostic radiology and orthopedic surgery. The author is an eminent radiologist who has a wealth of experience in this area. The introductory chapter, "The Role of the Orthopedic Radiologist," is a practical overview emphasizing the importance of the "tailored" radiologic workup of patients who have orthopedic diseases. The author appropriately recognizes the importance of the plain radiograph as the first imaging study, which frequently will preclude the need for "high tech" techniques such as CT or MR. This concept is not as widely recognized as it should be and is particularly important in this era of cost-consciousness related to health care expenditures.

Thereafter, the book is divided into six parts: trauma, arthritides, tumors and tumorlike lesions, infections, metabolic and endocrine disorders, and congenital and developmental anomalies. Within each part, the number of chapters varies from two to seven. A detracting feature is the format for the references. All the references are given in a list at the end of the book rather than having a list of appropriate ones at the end of each chapter. In addition, the references are arranged alphabetically according to the last name of the first author and are not cited in the text.

A disproportionate amount of the text is devoted to trauma. The author discusses the topic according to the affected site, that is, upper limb: shoulder girdle and elbow; upper limb: distal forearm, wrist, and hand; lower limb: pelvic girdle and proximal femur; lower limb: knee; lower limb: ankle and foot; and spine. Throughout this section, the author liberally uses a triad that consists of a concise drawing of how the patient is positioned to obtain the radiograph, a high-quality radiograph, and a useful line drawing that depicts the pathologic findings and identifies the major anatomic landmarks.

Arthritides, tumors, infections, metabolic disorders, and congenital anomalies are treated in a more cursory fashion than trauma is. When the targeted audience is considered, however, the coverage is reasonable. Throughout, the quality of the illustrations is superb. In addition to the copious, clearly labeled line drawings, many algorithms are used. A number of these are overly simplistic, however. Several unusual (although not unique) features of this book include (1) a segment at the conclusion of each chapter entitled "Practical Points to Remember"—a useful summary of the important teaching points of that chapter—and (2) the option of purchasing, separately, a slide atlas that is based on the material in the book.

The medical literature currently contains numerous texts on orthopedic radiology. Consequently, more comprehensive books are available devoted solely to specific topics such as trauma (*Radiology of Skeletal Trauma* by Rogers), arthritis (*Arthritis in Black and White* by Brower), and bone tumors (*Bone Tumors* by Mirra). Several encyclopedic texts also are available (*Diagnosis of Bone and Joint Disorders* by Resnick and Niwayama and *Edeiken's Roentgen Diagnosis of Diseases of Bone* by Edeiken, Dalinka, and Karasick). Nevertheless, this text by Greenspan serves a useful intermediary function. It should be included in the library of residency training programs and located conveniently near the alternator where films from the emergency department and orthopedic clinic are interpreted.

Richard P. Moser
Pennsylvania State University
The Milton S. Hershey Medical Center
Hershey, PA 17033

Review Article

Condensing Osteitis of the Clavicle: A Rare but Frequently Misdiagnosed Condition

Adam Greenspan,^{1,2} Eugenio Gerscovich,¹ Robert M. Szabo,² and Joseph G. Matthews II²

Condensing osteitis of the clavicle is a benign, often painful disorder, marked by bony sclerosis at the sternal end of the clavicle. It can be mistaken for other abnormalities such as Friedrich disease, bone island, osteoid osteoma, sternoclavicular osteoarthritis, and even a metastasis and osteosarcoma. Clinical, radiologic, scintigraphic, and histologic features of this condition are discussed and a brief overview of the treatment is provided. Three histologically proved cases are added to the 13 previously reported in the literature. Recognition of condensing osteitis of the clavicle may avoid the occasional unnecessarily aggressive diagnostic approach taken to search for a malignant tumor.

Condensing osteitis of the clavicle is a benign, often painful disorder of unknown cause, marked by bony sclerosis of the sternal (medial) end of the clavicle with no involvement of the sternoclavicular joint. It is a rare lesion, thought by many investigators to be degenerative or traumatic in origin [1–4]. In the 17 years since its identification as a distinct entity by Brower et al. [5], who termed it "condensing osteitis" in two young women, only scattered reports have appeared in the literature. The condition is frequently misdiagnosed by radiologists and surgeons alike, occasionally resulting in unnecessary, extensive clinical and radiologic investigation. This is particularly the case because condensing osteitis of the clavicle radiologically resembles a sclerotic metastatic lesion, and patients may be subjected to intensive workup in the search

for a primary malignant tumor. Furthermore, the painful swelling of the sternoclavicular joint found in this disorder is a common physical finding that raises sternoclavicular arthritis, joint sepsis, or chronic osteomyelitis as diagnostic possibilities. The term *condensing osteitis* is a poor designation and a misnomer because inflammation is not a component of this lesion. *Posttraumatic clavicular sclerosis*, as suggested by Jurik and Möller [6], may be more appropriate, although a history of trauma is not invariably given.

The purpose of this article is to review the clinical, radiologic, scintigraphic, and histopathologic features of condensing osteitis of the clavicle and to discuss the differential possibilities.

Review of the Literature

Since its first description, 25 cases have been reported in the literature, but only 13 have been pathologically proved. We are adding three new histologically proved cases, bringing the total to 16. It is noteworthy that all patients with proved histopathology are women, mostly in their fourth and fifth decades (age range, 26–63 years) [1–4, 7–9]. Twelve patients had a history of pain, ranging from 7 months to 4 years, nine had a swelling or mass in the region of the sternoclavicular joint, and only two patients were asymptomatic, with the

Received October 5, 1990; accepted after revision November 14, 1990.

¹ Department of Radiology, University of California, Davis, Medical Center, 2516 Stockton Blvd., Sacramento, CA 95817. Address reprint requests to A. Greenspan.

² Department of Orthopaedic Surgery, University of California, Davis, Medical Center, 2516 Stockton Blvd., Sacramento, CA 95817.

AJR 156:1011–1015, May 1991 0361–803X/91/1565–1011 © American Roentgen Ray Society

lesion disclosed serendipitously. Twelve patients recalled some traumatic episode in the past, ranging from definite injury to occupational or sport-related stress.

Lesions identified as condensing osteitis of the clavicle that may not represent the same entity described by Brower and colleagues also have been reported. For example, the seven cases of clavicular lesions in children reported by Appel et al. [10] were marked by periosteal reaction, osseous destruction, bony expansion of most of the clavicle, and extraclavicular lesions, as well as histologic demonstration of inflammation. The consensus is that this is probably a form of chronic osteomyelitis. It is of particular interest that the erythrocyte sedimentation rate was elevated in all patients in the report, and technetium-99m methylene diphosphonate (MDP) scanning in two patients showed increased activity in other locations in addition to the affected clavicles. Moreover, treatment with antibiotics improved the clinical and radiologic course of four of the seven patients, but partial resection of the involved clavicle did not alter the course in one patient. Likewise, in our opinion, the six cases of chronic inflammatory hyperostotic and sclerotic changes of the clavicle reported by Jurik and Möller [6] probably represent the same entity or an entity similar to that described by Appel et al. [10]. Finally, the three cases in children identified as "condensing osteitis" in a report by Jones et al. [11] in all likelihood reflect a low-grade staphylococcal osteomyelitis.

Clinical Features

The clinical signs and symptoms of condensing osteitis consist of pain and local swelling and tenderness, usually localized to the medial end of the involved clavicle but sometimes radiating to the supraclavicular fossa and ipsilateral shoulder. Pain is usually present for several months before diagnosis [12] and may be intermittent or steady; it is usually mild, but at times may be intense. Abduction or forward elevation of the shoulder, in particular, aggravates the pain, but range of motion seldom is limited. A firm, fusiform, variably tender swelling eventually appears in the region of the medial third of the clavicle. Overlying skin changes suggesting infection or inflammation are absent. Generally, tenderness on palpation is mild, and in one case the swelling was painless [9]. The majority of the patients recall no acute traumatic episode, but mechanical (occupational or sport-related) stress

at the sternoclavicular joint has been implicated [1, 4, 7, 8]. Laboratory studies, including alkaline phosphatase levels, are usually normal; only on occasion have the erythrocyte sedimentation rate and WBC count been reported to be mildly elevated [8]. Cultures of biopsy specimens are consistently negative.

Radiologic Features

The radiologic and scintigraphic findings in condensing osteitis of the clavicle are distinctive and characteristic. Plain films typically reveal a homogeneously dense sclerotic patch in the medial end of the clavicle, usually limited to the inferior margin. The medial end of the clavicle may be slightly expanded, but a joint space abnormality, periosteal reaction, and bone destruction are all absent (Figs. 1A-C, 2A, and 2B). The sternoclavicular joint is invariably spared [1, 7, 9, 13]. CT scanning shows various degrees of obliteration of the marrow cavity and occasional swelling of the adjacent soft tissues (Fig. 2C). On radionuclide bone scan, a significant focal increase in tracer uptake is noted, corresponding to the area of sclerosis (Fig. 2D). Gallium scans and indium-labeled WBC scans are normal [8]. An additional radiologic finding, an associated osteophyte (usually on the inferomedial margin of the medial end of the clavicle), has been observed by several authors [1, 3, 4, 14].

Pathophysiology

Brower et al. [5] hypothesized that the hyperostotic response of the clavicle was probably a reaction to abnormal mechanical stress (a history of repeated episodes of heavy lifting); this was supported by histologic evidence of trabecular reinforcement and periosteal reaction. Although other investigators [1-4, 7, 8] have agreed with the concept of this pathomechanism, a history of repetitive trauma is not consistently reported; for example, in 11 cases reviewed by Outwater and Oates [9], none had a history of direct trauma, and occupational or athletic stress was implied in only two cases. Also, the expected features of a stress-induced bone reaction, such as periosteal reaction or scintigraphic or plain-film findings indicating an evolving lesion and complete resolution after conservative management, were absent in several of the reported cases. It is likely that condensing osteitis of



Fig. 1.—A, Condensing osteitis of clavicle. A 40-year-old woman had a 4-year history of right sternoclavicular joint pain. Plain radiograph shows a sclerotic lesion in lower portion of sternal end of clavicle.

B, Trisprial tomogram shows slight expansion of inferior aspect of clavicular head and sclerosis.

C, CT scan through sternal ends of clavicles shows a dense sclerotic focus obliterating marrow cavity. Diagnosis of condensing osteitis of clavicle was confirmed by incisional biopsy.

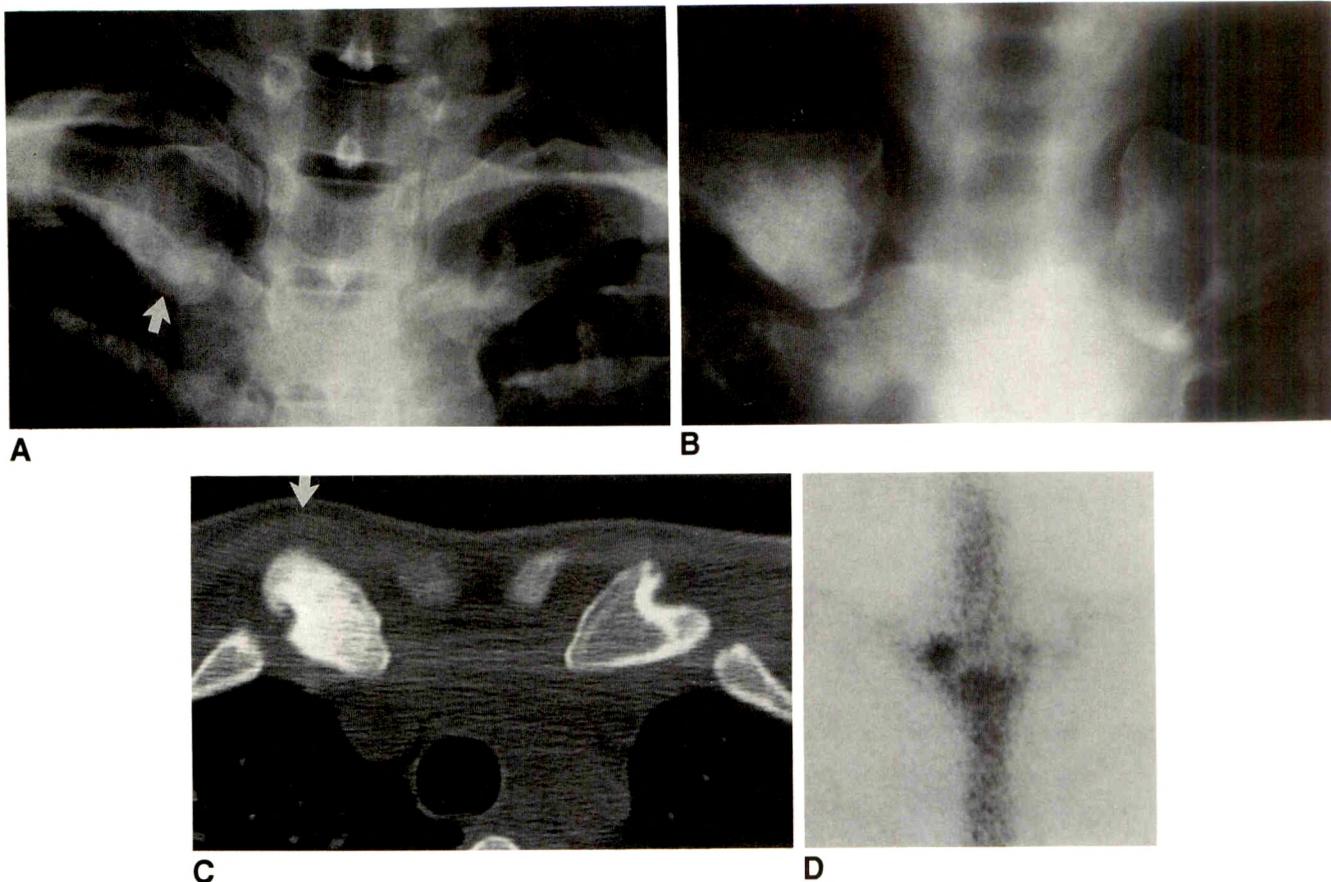


Fig. 2.—**A**, Condensing osteitis of clavicle. A 30-year-old woman had severe pain in right sternoclavicular region after she lifted a heavy object. Plain radiograph shows a sclerotic lesion in inferior aspect of right clavicular head (arrow).

B, Trispiral tomogram shows irregular borders of lesion better. Cranial (superior) aspect of clavicle is not affected. Subchondral bone at sternoclavicular joint is intact.

C, CT scan through sternal ends of clavicles shows homogeneous sclerosis of right clavicular head and soft-tissue swelling adjacent to it anteriorly (arrow).

D, Scintigram obtained after injection of 15 mCi (555 MBq) of 99m Tc-methylene diphosphonate shows increased uptake of tracer localized to sternal end of right clavicle. Diagnosis of condensing osteitis of clavicle was established by excisional biopsy.

the clavicle represents a low-grade osteonecrosis; in fact, some investigators have proposed that Friedrich disease (ischemic necrosis of the medial end of the clavicle) and condensing osteitis are either the same or pathologically closely related entities [6, 9, 15].

The histopathology of condensing osteitis of the clavicle in several reported cases is marked by an increased amount of normal-appearing bone associated with obliteration of the marrow spaces. In addition, the cancellous bone is more abundant and thicker because of reinforcement of the preexisting trabeculae [4, 7, 8] (Figs. 3A and 3B). Some authors report marrow fibrosis associated with features of osteonecrosis [3, 7, 8]. These foci of fibrosis and necrotic bone may be attributed to a low-grade, nonspecific ischemic process, such as that occurring in osteitis condensans illi [16]. In short, as Jurik and coworkers noted [6, 15], the histopathologic findings of condensing osteitis of the clavicle combine rarefaction, fibrosis, and sclerosis in a patchy distribution, but sclerotic changes predominate, as they did in our three patients.

Differential Diagnosis

Several entities should be differentiated from condensing osteitis of the clavicle. Among the conditions that can mimic

condensing osteitis are Friedrich disease, bone island (enos-tosis), osteoid osteoma, fibrous dysplasia, sternoclavicular osteoarthritis, chronic osteomyelitis, cleidometaphyseal osteomyelitis, pyarthrosis, sternocostoclavicular hyperostosis, sclerotic metastasis, and osteosarcoma.

Friedrich Disease

Ischemic necrosis of the medial end of the clavicle is a rare disorder, usually affecting children and adolescents; only 22 cases have been reported since its original description by Friedrich in 1924 [17]. Clinically, the signs and symptoms may be similar to those of condensing osteitis, lasting from several weeks up to several years, and may include associated soft-tissue swelling and tenderness [18]. In pediatric and adolescent patients, however, the duration of symptoms may be shorter and the relationship to trauma more apparent [9]. The cause of the disorder has been attributed to trauma or embolism of a nutrient bone artery, resulting in vascular compromise of the medial end of the clavicle.

The radiologic and histologic similarity of Friedrich disease to condensing osteitis [3, 7–9] has led some authorities to believe that no significant differences exist between these entities [1, 19]. Yet osteosclerotic changes in Friedrich disease involve the entire medial head of the clavicle, often

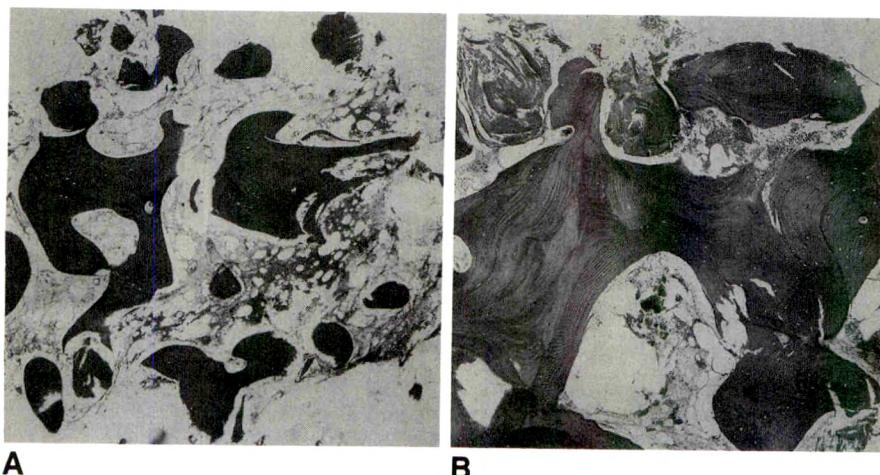


Fig. 3.—Histopathology of condensing osteitis.

A, Low-power photomicrograph reveals thickened, reinforced bony trabeculae. (H and E, $\times 40$)

B, Higher power photomicrograph shows trabecular sclerosis and arcuate cement lines of mature, lamellar bone. Few foci of marrow fibrosis are noted. (H and E, $\times 50$)

(Courtesy of M. J. Klein, New York, NY.)

A

B

associated with subchondral irregularities and focal radiolucencies and a notchlike defect in the articular surface [19-21]. Necrotic bone is the hallmark of Friedrich disease, together with fibrosis of the marrow spaces and haversian system, with empty lacunae.

Bone Island (Enostosis)

This benign, invariably asymptomatic condition of developmental origin is marked by a focus of cortical bone in the spongiosa. It exhibits a typical radiologic image with its spiderlike appearance, its margins forming a "brush effect," and its highly characteristic radiating bony streaks intimately blending into the normal trabeculae of the host bone [22]. In 90% of cases, scintigraphy shows no significant increase in activity of the tracer at the site of the lesion [23]. The clavicle is an unusual location for a bone island.

Osteoid Osteoma

The typical clinical complaint in this benign osteoblastic lesion is pain that is more severe at night and promptly relieved by salicylates (aspirin). Radiologic examination shows a radiolucent lesion (*nidus*) surrounded by reactive, sclerotic bone; occasionally, a central calcification is present in the *nidus*. The clavicle is a rare site for it [24].

Fibrous Dysplasia

The monostotic form of this disorder rarely affects the clavicle; the femoral neck, for example, is a much more common site. In reported cases, the clavicle was more diffusely involved, exhibiting a typical ground-glass appearance; moreover, the cortices were thinned, and the bone showed mild expansion [25, 26].

Osteoarthritis of Sternoclavicular Joint

This is a difficult diagnosis to exclude [20, 27]. It may be, as Brower et al. [5] suggested, that condensing osteitis of the clavicle is a degenerative phenomenon. However, the common signs of this process, joint-space narrowing, osteo-

phyte formation, and subchondral cysts, are absent in condensing osteitis.

Osteomyelitis and Septic Arthritis of Sternoclavicular Joint

Infectious processes at the sternoclavicular joint may present similarly to those of condensing osteitis [28]. However, a history of IV drug abuse is usually elicited, and common radiologic findings in septic arthritis and osteomyelitis, including bone destruction, periosteal reaction, and joint-space narrowing, are not seen in condensing osteitis. Indium-111 and gallium-67 scans are positive. Chronic recurrent multifocal osteomyelitis is a disease that mainly affects children and adolescents. It has a prolonged, fluctuating course with exacerbations, sometimes with low-grade fever; the erythrocyte sedimentation rate is elevated, and the WBC count is normal [29]. A number of bones may be affected, but the lesion is frequently localized to the clavicle. Radiologically, the lesions are characterized by lytic destruction surrounded by sclerosis, and periosteal reaction may be present [30, 31]. Cleidomastophyseal osteomyelitis (chronic symmetric plasma cell osteomyelitis) is an unusual syndrome, which, unlike chronic recurrent multifocal osteomyelitis, is infrequent in children and adolescents. It is marked by symmetric lesions of the tubular bones and clavicle in association with hyperostosis. Its histopathology exhibits chronic inflammatory cells with plasma cells [32].

Pyarthrosis of Sternoclavicular Joint

The lesion of pyarthrosis can mimic condensing osteitis, especially in the type of infection seen in IV drug users, because the sclerotic foci may appear in the clavicle adjacent to the sternoclavicular joint [1]. Radiologic evidence of sternoclavicular joint space narrowing and adjacent bone destruction are helpful in the differential diagnosis, as are abnormal laboratory findings.

Sternocostoclavicular Hyperostosis

This entity has only recently been described [32, 33]. In addition to other structures, it affects the medial end of the clavicle, where sclerotic changes are observed. It consists of

hyperostosis of the clavicle, sternum, and upper anterior ribs, associated with ossification of intervening soft tissues. It is usually bilateral and often accompanied by pustular lesions of the palms and soles (pustulosis palmaris et plantaris). The condition is more common in older patients, particularly men, and is seen more frequently in Japan [34, 35]. Radiologically, it appears as symmetric sclerosis of the medial portions of the clavicles, involving the sternum and costal cartilages [36, 37].

Metastasis

The lesion of condensing osteitis may mimic a metastatic tumor. This was the situation in a case reported by Kruger et al. [8], in which numerous screening tests for localization of a primary malignant tumor were performed by the initial investigators before the correct diagnosis of condensing osteitis was made.

Osteosarcoma

The clavicle is rarely the primary site of this malignant tumor [24]. Moreover, the aggressive bone destruction, periosteal reaction, and soft-tissue mass usually encountered in osteosarcoma distinguish it from condensing osteitis.

Treatment

Patients who have slight or no pain may not require treatment. When symptoms are so severe that treatment is indicated, nonsteroidal antiinflammatory medications have proved effective in relieving the pain [1, 8, 12]. In patients in whom excisional biopsy of the sclerotic medial third of the clavicle was performed, complete relief of symptoms followed [1, 4, 8].

It is recommended that an excisional or, preferably, incisional biopsy be performed in all patients unless pain is insignificant and the clinical presentation strongly supports the diagnosis of condensing osteitis. Patients in whom the lesion is refractory may require excision of the medial third of the clavicle as a last resort.

In summary, condensing osteitis of the clavicle, although rare, should be part of the differential diagnosis of sclerotic lesions at the sternal end of the clavicle, particularly in young and middle-aged women. Recognition of this process may avoid an unnecessarily aggressive diagnostic approach, and in particular, spare the patient a potentially long and mistaken search for an underlying primary neoplasm.

REFERENCES

- Cone RO, Resnick D, Goergen TG, Robinson C, Vint V, Haghghi P. Condensing osteitis of the clavicle. *AJR* 1983;141:387-388
- Duro JC, Estrada P, Ribas D, Bartrons S, Rotes-Querol J. Condensing osteitis of the clavicle (letter). *Arthritis Rheum* 1981;24:1454-1455
- Teates CB, Brower AC, Williamson BRJ, Keats TE. Bone scans in condensing osteitis of the clavicle. *South Med J* 1978;71:736-738
- Solovjev M. Ostitis condensans claviculae. *Fortschr Geb Roentgenstr Nuklearmed Erganzungsband* 1976;125:375-376
- Brower AC, Sweet DE, Keats TE. Condensing osteitis of the clavicle: a new entity. *AJR* 1974;121:17-21
- Jurik AG, Möller BN. Inflammatory hyperostosis and sclerosis of the clavicle. *Skeletal Radiol* 1986;15:284-290
- Franquet T, Lecumberri F, Rivas A, Inaraja L, Idoate MA. Condensing osteitis of the clavicle: report of two new cases. *Skeletal Radiol* 1985;14:184-187
- Kruger GD, Rock MG, Munro TG. Condensing osteitis of the clavicle: a review of the literature and report of three cases. *J Bone Joint Surg [Am]* 1987;69-A:550-557
- Outwater E, Oates E. Condensing osteitis of the clavicle: case report and review of the literature. *J Nucl Med* 1988;29:1122-1125
- Appel RG, Oppermann HC, Becker W, Kratzat R, Brandeis WE, Willich E. Condensing osteitis of the clavicle in childhood: a rare sclerotic bone lesion. *Pediatr Radiol* 1983;13:301-306
- Jones MW, Carty H, Taylor JF, Ibrahim SK. Condensing osteitis of the clavicle: does it exist? *J Bone Joint Surg [Br]* 1990;72-B:464-467
- Weiner SN, Levy M, Bernstein R, Morehouse H. Condensing osteitis of the clavicle: a case report. *J Bone Joint Surg [Am]* 1984;66-A:1484-1486
- Stewart CA, Siegel ME, King D, Moser L. Radionuclide and radiographic demonstration of condensing osteitis of the clavicle. *Clin Nucl Med* 1988;13:177-178
- Abdelwahab IG, Hermann G, Ramos R, Klein MJ, Kenan S, Lewis MM. Osteitis condensans of the left clavicle (OCC): case report 623. *Skeletal Radiol* 1990;19:387-389
- Jurik AG, De Carvalho A, Graudal H. Sclerotic changes of the sternal end of the clavicle. *Clin Radiol* 1985;36:23-25
- Numaguchi Y. Osteitis condensans illi, including its resolution. *Radiology* 1971;98:1-8
- Friedrich H. Über ein noch nicht beschriebenes, der Pertheschen Erkrankung analoges, Krankheitbild des sternalen Clavikelendes. *Dtsch Z Chir* 1924;187:385-398
- Drewes J, Günther D. Morbus Friedrich. *Fortschr Geb Roentgenstr Nuklearmed Erganzungsband* 1982;136:213-214
- Levy M, Goldberg I, Fischel RE, Frisch E, Maor P. Friedrich's disease: aseptic necrosis of the sternal end of the clavicle. *J Bone Joint Surg [Br]* 1981;63-B:539-541
- Köhler A, Zimmer EA. *Borderlands of the normal and early pathologic in skeletal roentgenology*, 3rd ed. New York: Grune & Stratton, 1968:9, 164-165
- Fischel RE, Bernstein D. Friedrich's disease. *Br J Radiol* 1985;48: 318-319
- Greenspan A, Steiner G, Knutzon R. Bone island (enostosis): clinical significance and radiologic-pathologic correlations. *Skeletal Radiol* (in press)
- Go RT, El-Khoury GY, Wehbe MA. Radionuclide bone image in growing and stable bone island. *Skeletal Radiol* 1980;5:15-18
- Smith Y, Yappa F, Watson RC. Primary tumors and tumor-like lesions of the clavicle. *Skeletal Radiol* 1988;17:235-246
- Franklin JL, Parker JC, King HA. Nontraumatic clavicle lesions in children. *J Pediatr Orthop* 1987;7:575-578
- Smith J, McLachlan DL, Huvos AG, Higginbotham NL. Primary tumors of the clavicle and scapula. *AJR* 1975;124:113-123
- Kier R, Wain SL, Apple J, Martinez S. Osteoarthritis of the sternoclavicular joint: radiographic features and pathologic correlation. *Invest Radiol* 1986;21:227-233
- Mollan RA, Craig BF, Biggart JD. Chronic sclerosing osteomyelitis. *J Bone Joint Surg [Br]* 1984;66-B:583-585
- Björksten B, Gustavson KM, Eriksson B. Chronic recurrent multifocal osteomyelitis and pustulosis palmo-plantaris. *J Pediatr* 1978;93:227-231
- Solheim LF, Paus B, Liverud K, Stoen E. Chronic recurrent multifocal osteomyelitis: a new clinicoradiological syndrome. *Acta Orthop Scand* 1980;51:37-41
- Björksten B, Boquist L. Histopathological aspects of chronic recurrent multifocal osteomyelitis. *J Bone Joint Surg [Br]* 1980;62-B:376-380
- Resnick D. *Bone and joint imaging*. Philadelphia: Saunders, 1989:657
- Resnick D. Sternoclavicular hyperostosis. *AJR* 1980;135:1278-1280
- Inoue M, Kudo T. Sterno-costo-clavicular hyperostotic syndrome with pustulosis palmaris et plantaris. *Kanto J Orthop Trauma* 1977;8:299-302
- Sonozaki H, Furusawa S, Seki H, Kurokawa T, Tateishi A, Kabata K. Four cases with symmetrical ossification between the clavicle and the first ribs of both sides. *Kanto J Orthop Trauma* 1974;5:244-247
- Rosenthal L, Burke PL. A radionuclide and radiographic diagnosis of sternoclavicular hyperostosis. *Clin Nucl Med* 1986;11:322-324
- Sokoloff L, Gleason IO. The sternoclavicular articulation in rheumatic diseases. *Am J Clin Pathol* 1954;24:406-414

Radiologic-Pathologic Conferences of the Massachusetts General Hospital

Chondrosarcoma

Felix S. Chew¹ and David G. Disler

A 69-year-old woman had an abdominal mass and pain in the right lower extremity. A radiograph of the pelvis showed a 15-cm soft-tissue mass with an underlying lesion in the right iliac wing (Fig. 1). CT showed two growth patterns within the tumor, an indolent, lobular, intraosseous expansion of the iliac cortex and a rapidly aggressive extension into the soft tissues with a sunburst pattern of periosteal reaction. The intraosseous tumor tissue was partially calcified; the extraosseous tumor tissue was uncalcified and heterogeneous. MR showed discrete regions in the soft-tissue mass of high and low signal intensity on both T1- and T2-weighted images. Hemipelvectomy was performed. The final pathologic diagnosis was chondrosarcoma with hyaline and myxoid regions, extensive necrosis, and hemorrhage. Regions of both high and low histologic grade were present.

Chondrosarcoma is a primary bone tumor composed of malignant cells and chondroid matrix [1] thought by most authorities to arise from preexisting hyaline cartilaginous lesions such as enchondroma or osteochondroma. On plain radiographs the lesions are radiolucent and destructive, with cartilaginous tumor replacing bone. The matrix is often mineralized, with rings-and-arcs calcifications (corresponding to enchondral ossification of lobules of hyaline cartilage), or with amorphous or punctate calcifications (corresponding to calcification of tumor tissue). Attenuation of uncalcified lesions is similar to that of water. Low-grade lesions have slow, eccentric growth that conforms generally to the shape of the host bone; dense calcification is frequent. High-grade lesions have permeated bone destruction (from tongues

of tumor growing along haversian systems), cortical breaks, concentric growth in the soft tissues, and sometimes central necrosis [2]. Sunburst periosteal reaction extending from the cortical surface results from fragments of active periosteum leaving streamers of bone as the tumor expands. Chondrosarcomas are avascular or hypovascular. The tumors are often heterogeneous, with low-grade or even benign lobules of mature ossifying hyaline cartilage adjacent to high-grade myxoid regions that have less mature chondroid matrix and greater cellularity. Hyaline regions have bright signal on T2-weighted MR images, whereas myxoid regions may have dark or intermediate signal [3].

Although rare, chondrosarcoma is the second most common primary bone tumor in adults older than 30. Approximately 25% arise in the pelvis. Growth is sometimes slow, and local recurrences after surgery may not be manifest for 5–10 years. Adequate treatment requires complete surgical removal of the tumor. Long-term survival is related to tumor grade.

REFERENCES

1. Hudson TM. *Radiologic-pathologic correlation of musculoskeletal lesions*. Baltimore: Williams & Wilkins, 1987:153–175
2. Rosenthal DI, Schiller AL, Mankin HJ. Chondrosarcoma: correlation of radiological and histological grade. *Radiology* 1984;150:21–26
3. Cohen EK, Kressel HY, Frank TS, et al. Hyaline cartilage-origin bone and soft-tissue neoplasms: MR appearance and histologic correlation. *Radiology* 1988;167:477–481

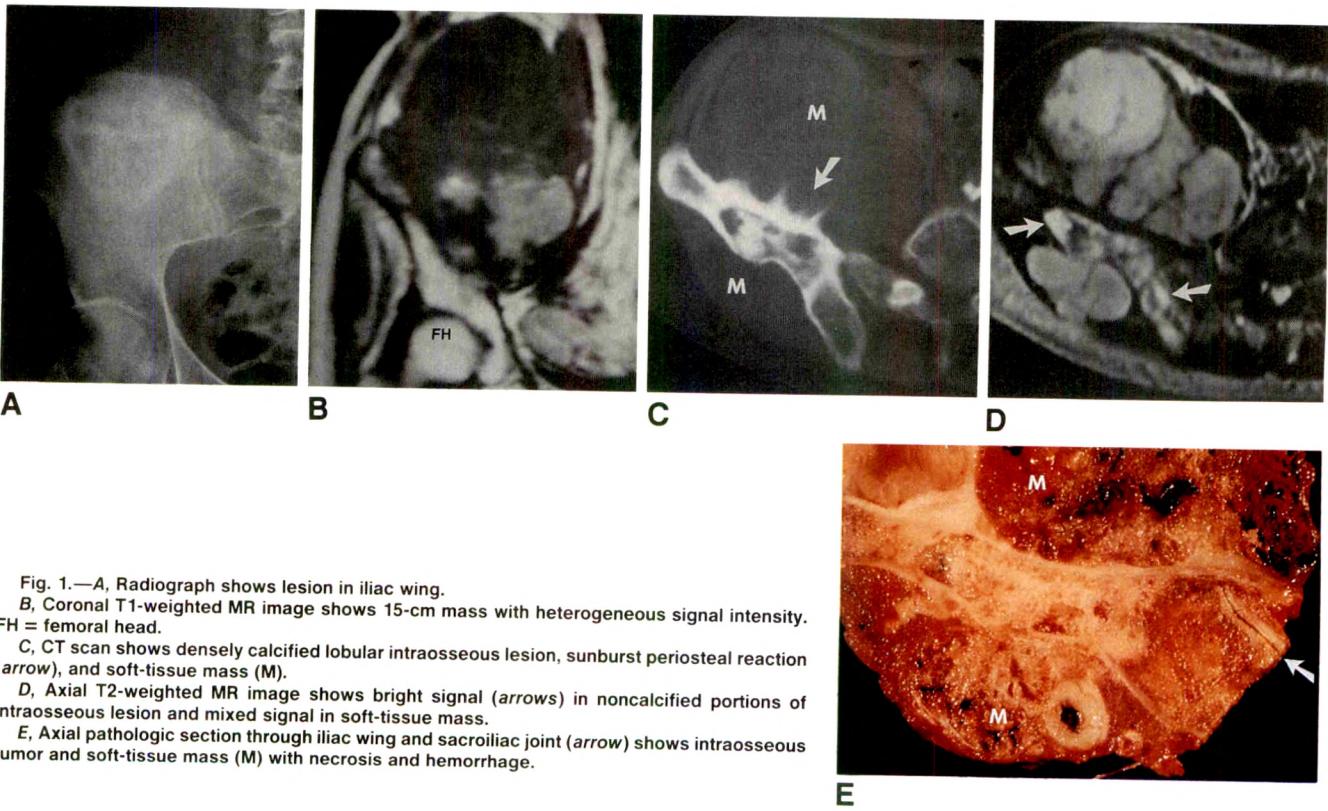


Fig. 1.—A, Radiograph shows lesion in iliac wing.

B, Coronal T1-weighted MR image shows 15-cm mass with heterogeneous signal intensity.

FH = femoral head.

C, CT scan shows densely calcified lobular intraosseous lesion, sunburst periosteal reaction (arrow), and soft-tissue mass (M).

D, Axial T2-weighted MR image shows bright signal (arrows) in noncalcified portions of intraosseous lesion and mixed signal in soft-tissue mass.

E, Axial pathologic section through iliac wing and sacroiliac joint (arrow) shows intraosseous tumor and soft-tissue mass (M) with necrosis and hemorrhage.

From the weekly radiologic-pathologic correlation conferences conducted by Jack Wittenberg. Pathology editor: Andrew E. Rosenberg. Radiology editors: William E. Palmer, Daniel P. Barboriak, Daniel I. Rosenthal, Felix S. Chew.

¹All authors: Department of Radiology, Massachusetts General Hospital and Harvard Medical School, 32 Fruit St., Boston, MA 02114. Address reprint requests to F. S. Chew.

Fibrous Dysplasia vs Adamantinoma of the Tibia: Differentiation Based on Discriminant Analysis of Clinical and Plain Film Findings

Johan L. Bloem¹
 Roy O. van der Heul²
 Herman M. Schuttevaer¹
 Dirkjan Kuipers¹

Differentiation between benign fibrous dysplasia and malignant adamantinoma of the tibia is challenging because of the impact the diagnosis has on the choice of treatment (none or extensive surgery). The histologic and pathologic similarities of the lesions and the controversial relationship between fibrous dysplasia, osteofibrous dysplasia, and adamantinoma complicate the matter. We found a large overlap of histologic features in lesions considered either fibrous dysplasia or osteofibrous dysplasia on the basis of the radiologic findings. The purpose of this study was to determine the value of the plain radiograph of the lower leg in combination with clinical findings to differentiate the benign from the malignant condition. The clinical symptoms, radiographs, and histologic slides of 46 patients with fibrous dysplasia and 22 with adamantinoma in the tibia were reviewed retrospectively. In only one of 12 patients with radiologic or histologic characteristics of osteofibrous dysplasia were both radiologic and histologic criteria for the diagnosis present. A linear discriminant analysis was performed on six clinical (age, spontaneous pain, pain after trauma, swelling only, pain and swelling, and bowing deformity) and 25 radiologic signs. Fibrous dysplasia and its variant osteofibrous dysplasia could be identified correctly in 87% (40 of 46 patients) and adamantinoma in 95% (21 of 22 patients) by using the patient's age and four radiologic signs. When results from the discriminant analysis of a randomized subgroup of patients (32) were used on the other subgroup (36 patients), fibrous dysplasia was correctly identified in 84% (21 of 25) and adamantinoma in 82% (nine of 11). Fibrous dysplasia is more prevalent than adamantinoma in a young patient, when radiographs show a ground-glass appearance and anterior bowing and when there is no multilayered periosteal reaction and moth-eaten destruction.

When radiologic signs and the patient's age are combined, fibrous dysplasia and adamantinoma can be discriminated in a high percentage of patients.

AJR 156:1017-1023, May 1991

The tibia is one of the preferential sites of fibrous dysplasia, a benign skeletal developmental anomaly of bone-forming mesenchyma [1-4]. A related condition called osteofibrous dysplasia or ossifying fibroma is found exclusively in the tibia or fibula [5-7]. Adamantinoma is a rare malignant neoplasm of bone that is typically found in the tibia [8-11].

Differentiation between these three lesions is important in planning therapy. Because fibrous dysplasia and adamantinoma both have large amounts of fibrous stroma, radiologic and histologic differentiation between the two is difficult [1, 4, 9-13]. The matter is further complicated by the fact that the relationship between fibrous dysplasia, osteofibrous dysplasia, and adamantinoma is controversial [5-7, 12, 13]. The purpose of this study is to determine if clinical or radiologic features can be used to differentiate the two benign disorders from adamantinoma.

Materials and Methods

We reviewed the files of the Registry of the Netherlands Committee on Bone Tumors, which contained 7500 files on patients at the time of the study. Although most new patients

Received March 30, 1990; accepted after revision November 20, 1990.

¹ Department of Radiology, Bldg. I, C2-S, University Hospital Leiden, Rijnburgerweg 10, 2333 AA Leiden, the Netherlands. Address reprint requests to J. L. Bloem.

² Department of Pathology, University Hospital Dijkzicht Rotterdam, Dr. Molewaterplein 4, 3015 GD Rotterdam, the Netherlands.

0361-803X/91/1565-1017
 © American Roentgen Ray Society

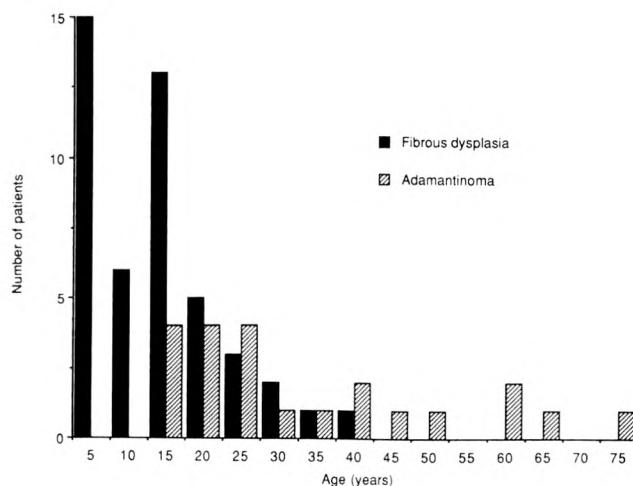


Fig. 1.—Graph shows age distribution of 46 patients with fibrous dysplasia and 22 patients with adamantinoma.

with bone tumors in the Netherlands are referred to this committee for diagnosis, the true prevalence is not reflected in the files because less troublesome cases are treated without consultation. Before osteofibrous dysplasia was described as a separate entity [5-7], this diagnosis was included in the cases of fibrous dysplasia. Distinction between the two was made at the subsequent review for this study. Seventy-two patients were identified with a histologic diagnosis of either adamantinoma (22 patients) or fibrous dysplasia (50 patients) in the tibia. Four of the patients with fibrous dysplasia were excluded because of extensive polyostotic disease (three patients) or the presence of McCune-Albright syndrome (one patient). Six patients were included with lesions in both the ipsilateral fibula and tibia.

Twenty-six males and 20 females had fibrous dysplasia of the tibia. The only patient with a lesion manifesting both the histologic and radiologic criteria of osteofibrous dysplasia was, for analysis, included among the fibrous dysplasia group. The adamantinoma group had eight males and 14 females. The mean age of patients with fibrous dysplasia was 12 years (range, 1-37 years), and of patients with adamantinoma, 23 years (range, 10-71 years) (Fig. 1). The clinical presentation was not recorded in two patients with fibrous dysplasia. Patients with fibrous dysplasia presented with spontaneous pain (12 patients), pain after trauma (16 patients, nine of whom had a fracture), swelling only (nine patients), pain and swelling (six patients), or a bowing deformity (one patient). The following distribution of clinical signs was found in patients with adamantinoma: pain only in seven patients, pain after trauma in four patients (three of whom had a fracture), swelling only in six patients, and pain and swelling in five patients. The average duration of symptoms was 6 months (range, 0-78 months) in patients with fibrous dysplasia ($n = 44$) and 31 months (range, 0-200 months) in patients with adamantinoma ($n = 22$).

The diagnoses were made by consensus by the Netherlands Committee on Bone Tumors, consisting of at least two pathologists, two radiologists, and two orthopedic surgeons. All members of this committee have extensive experience in the field of bone tumors. In each case, the diagnosis was based on histopathology, plain film radiographs, and clinical evaluation. The histologic material was obtained by surgery in 38 patients with fibrous dysplasia and by biopsy in eight patients. Pathologic material after resection was available in all 22 patients with adamantinoma. The histologic material was reviewed again by one of the authors. The osteoblast activity was graded arbitrarily on a three-point scale as low, intermediate, or high.



Fig. 2.—10-year-old girl with adamantinoma and painful swelling. Lateral radiograph shows anterior bowing. Tumor is multilobulated, contains intralesional opacifications, and extends into cortex. Tumor is confined within newly formed cortex (ballooning). This is one of four patients with adamantinoma in whom extensive fibrous stroma was found.

Characteristic findings indicative of fibrous dysplasia included fibrous stroma consisting of myxofibrous tissue and woven bone [1-4]. The presence of woven bone trabeculae rimmed by cuboidal active osteoblasts (graded as high osteoblast activity on our three-point scale) and small bands of lamellar bone in the periphery (zonal architecture) was considered to be consistent with osteofibrous dysplasia [5-7]. The histologic diagnosis of adamantinoma was made when epithelial-like cells arranged in palisading nests and strands of cells were identified [9, 11-14].

In the 46 patients with fibrous dysplasia, histologic studies showed a marked range of remodeling activity. This varied from a near absence of osteoblasts and osteoclasts (low osteoblast activity) to the presence of a large number of osteoblasts and osteoclasts (high activity), and from a pure woven bone pattern to a combination of woven and lamellar bone. In four patients with adamantinoma, large fields with fibrous stroma were encountered (Fig. 2).

Follow-up data were available on 29 patients (17 with fibrous dysplasia and 12 with adamantinoma). Follow-ups ranged from 5 months to 22 years. The mean follow-up time was 4.5 years for patients with fibrous dysplasia and 9.6 years for those with adamantinoma.

Clinical characteristics analyzed included age and presenting symptoms (spontaneous pain, pain after trauma, swelling only, pain and swelling, and bowing deformity). Anteroposterior and lateral radiographs of the lower leg were reviewed by two radiologists in conference. Although the observers were aware that the patients had either fibrous dysplasia or adamantinoma, the final diagnosis was not available to them. The radiologic features analyzed are listed in Table 1. Type of bone destruction was classified according to Lodwick [15]. In order to discriminate anterior bowing from an expansive lesion involving the anterior cortex, bowing was defined as a deformity of the posterior cortex of the tibia on a lateral radiograph.

A linear discriminant analysis using all the clinical and radiologic signs was performed to determine the feasibility of discriminating fibrous dysplasia from adamantinoma. We also performed a discriminant analysis based on selected signs. This subset of signs, derived

TABLE 1: Radiologic Findings in Fibrous Dysplasia and Adamantinoma of the Tibia

Finding	No. (%)	
	Fibrous Dysplasia (n = 46)	Adamantinoma (n = 22)
Fracture	9 (20)	3 (14)
Anterior bowing ^a	11 (24)	1 (5)
Additional lesion(s) in the fibula	6 (13)	1 (5)
Multifocal lesions in tibia	5 (11)	4 (18)
Lesion(s) in diaphysis only	43 (93)	20 (91)
Lesion(s) in diaphysis and metaphysis	2 (4)	2 (9)
Lesion(s) in metaphysis and epiphysis	1 (2)	0
Eccentric localization	23 (50)	12 (55)
Central localization	23 (50)	10 (45)
Geographic destruction ^a	46 (100)	20 (91)
Local moth-eaten destruction ^a	0	2 (9)
Predominantly osteolysis	3 (7)	2 (9)
Osteolysis with ossification or septation ^a	10 (22)	17 (77)
Ground-glass pattern ^a	14 (30)	0
Ground glass with ossification or septation ^a	19 (41)	3 (14)
Smooth margin	22 (48)	9 (41)
Lobulated margin	24 (52)	13 (59)
Sclerotic margin	27 (59)	9 (41)
Regular cortical destruction	46 (100)	21 (95)
Irregular cortical destruction	0	1 (5)
Intracortical localization	6 (13)	2 (9)
No periosteal new bone formation	3 (7)	4 (18)
Single-layered lamellar periosteal reaction	10 (22)	2 (9)
Multilayered lamellar periosteal reaction ^a	1 (2)	5 (23)
Ballooning	32 (70)	11 (50)

^a Significantly different for fibrous dysplasia and adamantinoma ($p < .05$).

from the literature, included pain after trauma, age, ground-glass appearance with and without densities, multilayered periosteal reaction, moth-eaten destruction, anterior bowing, skip lesions in tibia, and additional lesions in fibula [1, 2, 4, 8–11, 16–18]. The results subsequently were tested by randomizing the patients into two subsets and applying the discriminating functions derived from one group to the other.

Results

Eight of the 68 lesions were located in the ventral cortex of the tibia. The average age of these patients was 13 years (range, 4–17 years). Because of localization and age, a radiologic diagnosis of osteofibrous dysplasia instead of fibrous dysplasia was considered. However, the osteoblastic activity in these patients was graded high in only one. In two of the eight patients 14 and 15 years old, a histologic diagnosis of adamantinoma was made easily. One of these patients had low osteoblastic activity, the other had intermediate osteoblastic activity. The osteoblastic activity in the remaining five patients was intermediate in two and low in three (Fig. 3). In four other patients, high osteoblastic activity, such as occurs in osteofibrous dysplasia, was found. One of these was the patient with infantile pseudarthrosis. In the other three patients, a radiologic diagnosis of fibrous dysplasia instead of osteofibrous dysplasia was made because the lesions were located within the marrow cavity and cortex instead of the anterior tibial cortex. The ages of these three patients were 3, 13, and 24 years. Thus, in only one of these patients with radiologic or histologic characteristics of osteofibrous dyspla-



Fig. 3.—15-year-old girl with intracortical fibrous dysplasia and pain of 1 month's duration. Lateral radiograph shows a small lesion with well-defined margins in anterior cortex. No periosteal reaction was found. Histologic examination showed low osteoblastic activity.

sia were both the histologic and radiologic criteria in accordance with the diagnosis of osteofibrous dysplasia. This patient was included in the analysis of patients with fibrous dysplasia.

The radiologic findings are listed in Table 1 and are illustrated in Figs. 2–10. The patients who had fractures were part of the group of patients with pain after trauma (Fig. 4).

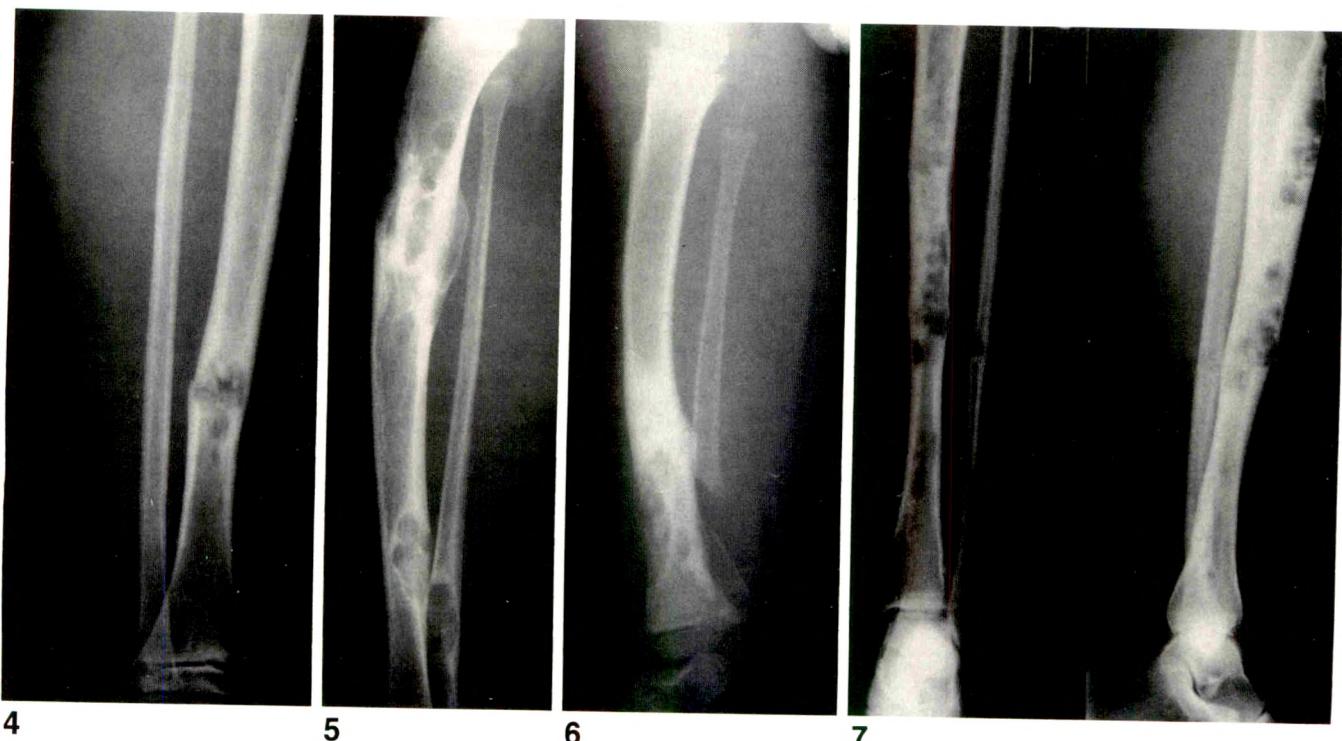


Fig. 4.—9-year-old boy with fibrous dysplasia who had a fracture after minor trauma. Lateral radiograph shows a lobulated, osteolytic lesion with an oblique fracture, located centrally in diaphysis.

Fig. 5.—7-year-old girl with fibrous dysplasia and acute onset of pain in lower leg. Lateral radiograph shows two lesions in tibia and one in fibula. Lesion in proximal part of tibia is central; lesion in distal part of tibia is eccentric. All three lesions are osteolytic with marked septation. Lesions are expansive and involve cortical bone. Anterior bowing of tibia is present.

Fig. 6.—1-year-old infant with pseudarthrosis and bowing deformity of lower leg. Lateral radiograph shows a defect in fibula with narrowing of marrow canal and tapering of both ends. Lesion in tibia is cystic and is characterized by anterior bowing and valgus deformity (*not shown*). Diameter of tibia is enlarged by callus formation. Tibial fracture is consolidated but still visible. Histologic diagnosis was fibrous dysplasia.

Fig. 7.—19-year-old woman with adamantinoma who had pain after trauma. Lateral radiograph shows multiple lobulated osteolytic lesions in both tibia and fibula. Lesion in proximal part of tibia is eccentric; lesions in midshaft and distal part of tibia are central. Cortical bone is thinned at endosteal side. Periosteal bone formation resulted in an intact neocortex, which confines lesions.

One of the patients with a bowing deformity (Figs. 2 and 5) had infantile pseudarthrosis (Fig. 6). Neither this patient nor his family had stigmata of neurofibromatosis. No tumor, but cellular fibrous tissue with woven bone rimmed by osteoblasts, was found. Lamellar bone was present in the periphery. The osteoblastic activity was graded as high.

Patients with fibrous dysplasia could be identified in 89% (41 of 46 patients) and patients with adamantinoma could be identified in 95% (21 of 22) of cases when age, presenting symptoms, and all 25 radiologic signs (Table 1) were subjected to a discriminant analysis. Five patients with fibrous dysplasia and one with adamantinoma were not identified correctly. The one patient with histologic and radiologic signs of osteofibrous dysplasia was identified as having fibrous dysplasia and not adamantinoma. Fibrous dysplasia was identified correctly in 84% of cases (21 of 25) and adamantinoma in 73% (eight of 11) when all radiologic and clinical signs used in a discriminant analysis on a randomized subset of patients (32 patient) subsequently were evaluated on the other subset (36 patients).

When our selected signs (pain after trauma, age, ground-glass appearance with and without densities, multilayered

periosteal reaction, moth-eaten destruction, anterior bowing, skip lesions in tibia, and additional lesions in fibula) were used, fibrous dysplasia was identified correctly in 87% (40 of 46) and adamantinoma in 95% (21 of 22). Six patients with fibrous dysplasia and one with adamantinoma were not identified correctly. Use of the results from the discriminant analysis of one of the randomized patient groups (32 patients) on the other (36 patients) yielded the following results: fibrous dysplasia was correctly identified in 84% (21 of 25) and adamantinoma in 81% (nine of 11).

The five signs with the greatest impact on making a diagnosis were, in order of decreasing importance, age, ground-glass appearance with or without ossification or septation (in favor of fibrous dysplasia), multilayered lamellar periosteal reaction (in favor of adamantinoma), moth-eaten destruction (in favor of adamantinoma), and anterior bowing (in favor of fibrous dysplasia). The other radiologic and clinical signs were not important in differentiating fibrous dysplasia from adamantinoma.

None of the patients with adamantinoma had distant metastases on conventional chest radiographs at the time of presentation. Later, metastases developed in the lung in three

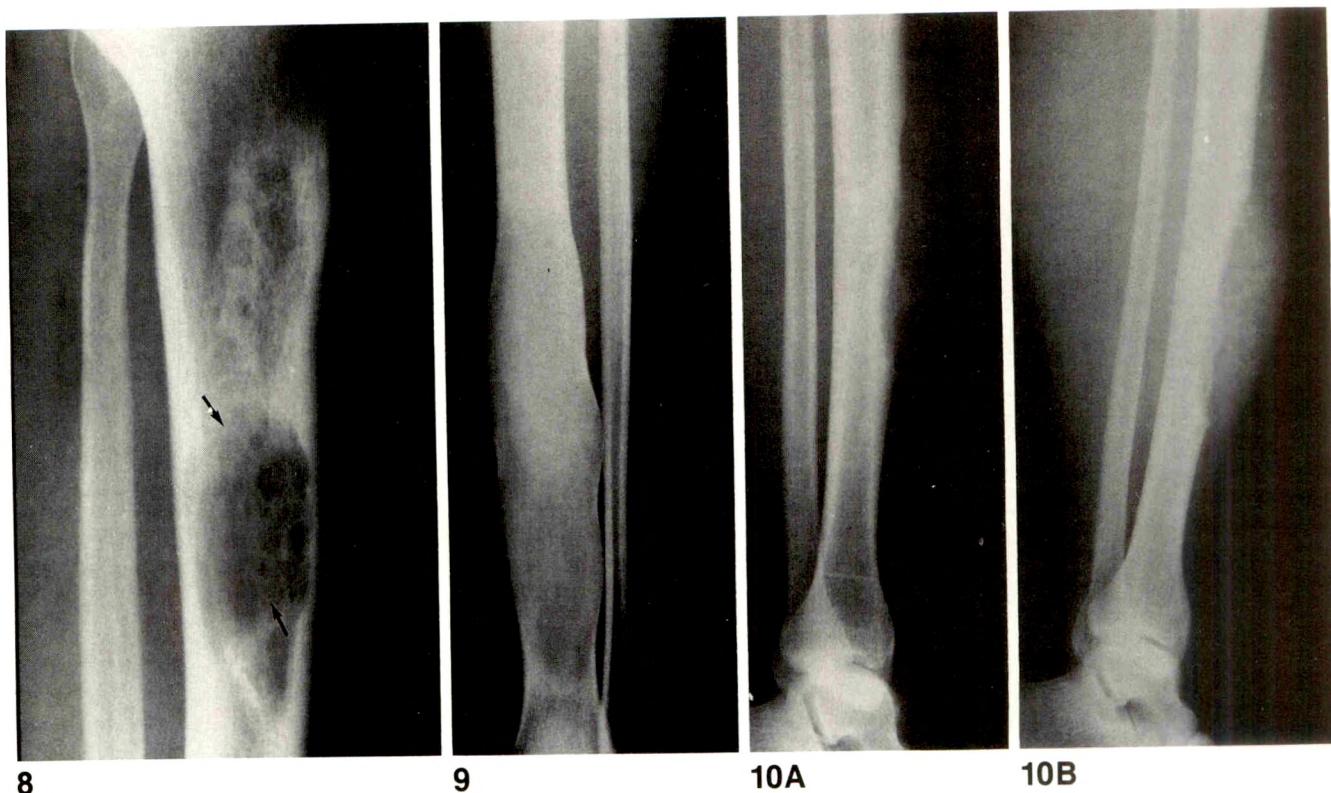


Fig. 8.—61-year-old man with adamantinoma and pain in tibia of 2 month's duration. Lateral radiograph shows intramedullary osteolytic lesion and endosteal thinning of cortex. Although bone destruction is partly geographic, especially in proximal and most distal parts, a local area with moth-eaten destruction can be seen (arrows).

Fig. 9.—37-year-old man with fibrous dysplasia and pain in lower leg for 18 months. Anteroposterior radiograph shows typical ground-glass appearance. Endosteal scalloping is present. Newly formed cortex (ballooning) confines lesion.

Fig. 10.—34-year-old woman with an adamantinoma and pain in lower leg for 3 months.

A, Lateral radiograph shows a large expansive intracortical lesion and scalloping of endosteal margin of cortex. Intralesional calcifications can be seen.
B, Radiograph 8 months later shows enlargement of tumor and soft-tissue extension.

patients, and osseous and lymph node metastases developed in another one. In one patient, a solitary liver metastasis was found. In these five patients, at least one metastasis was proved histologically. The disease-free interval in these five patients ranged from 6 to 13 years.

Discussion

Differentiation between fibrous dysplasia and adamantinoma may be difficult when the two conditions are confined to the tibia because their radiologic appearance is similar. Histologic findings for the two entities may be similar and, according to some authors, may even be related [1, 4, 9–11, 16].

Fibrous dysplasia may be monostotic (70–80%) or polyostotic (20–30%); only 2–3% of polyostotic cases are associated with endocrinopathy such as the McCune-Albright syndrome [1–3]. Any bone may be affected, but the tibia is one of the most frequently involved bones. Others are the rib, femur, craniofacial bones, and humerus [1, 4]. The true prevalence of fibrous dysplasia is not known because the lesion may be asymptomatic and thus may escape detection. The

relation of fibrous dysplasia to osteofibrous dysplasia, also called ossifying fibroma, and adamantinoma is controversial [5–8, 13, 19]. The name osteofibrous dysplasia [16] is preferred to ossifying fibroma [7] because it better reflects the relation with fibrous dysplasia and does not cause confusion with ossifying fibroma of the mandible and maxilla, which is a nonrelated entity [20, 21]. Osteofibrous dysplasia has been described as a bone-forming lesion located in the ventral, intracortical area of the tibial shaft with histology different from fibrous dysplasia [5, 6, 19]. Contrary to fibrous dysplasia, the formed, woven bone trabeculae in osteofibrous dysplasia are rimmed by cuboidal osteoblasts.

In our patients, radiologic signs of osteofibrous dysplasia or ossifying fibroma (eight patients) and histologic evidence of high osteoblastic activity of osteofibrous dysplasia (five patients) were combined in only one patient. In lesions considered radiologically to be fibrous dysplasia or osteofibrous dysplasia, a marked remodeling activity was found; overlap was large and no basic difference was seen. Although osteoblastic rimming is not a feature of classic fibrous dysplasia, plump, elongated cells rimming woven bone and layering of lamellar bone can be found in fibrous dysplasia [22]. We think that ossifying fibroma or osteofibrous dysplasia is not a well-

defined entity [7, 8, 19] but an active variant of fibrous dysplasia, an opinion shared by other authors [5, 6, 13].

The prevalence of adamantinoma is estimated to be 0.1% of primary bone tumors [8]. A less frequently used synonym is malignant angioblastoma. Typically, adamantinoma is found in the tibia, but the tumors may occasionally be found at other sites [9]. Although the histology of adamantinoma is reminiscent of that of ameloblastoma of the jaw, sometimes called adamantinoma of the jaw, no evidence has been reported that suggests a relationship between adamantinoma of the tibia and ameloblastoma of the jaw [8–11]. Usually fibrous dysplasia and adamantinoma have clearly different histologic features. However, large fields of fibrous stroma (like those that occur in fibrous dysplasia or osteofibrous dysplasia) may mask adamantinomous tissue [12, 13]. We encountered this problem in four of our patients. The diagnosis of adamantinoma could be made with confidence in these patients because we included in this study only patients with ample material available for histologic examination. Immunohistochemistry and electron microscopic demonstration of cytokeratins is helpful in identifying adamantinoma, especially in equivocal cases [14].

Depending on the signs used, fibrous dysplasia could be identified correctly in 84% and adamantinoma in 73–82% of our patients. We used discriminant analysis and evaluated the classification on an independent sample. These results were obtained by combining the clinical and radiologic signs. The most important signs that suggest a diagnosis of fibrous dysplasia over adamantinoma are, in order of decreasing importance, young age, presence of ground-glass appearance with or without additional opacifications, absence of multilayered periosteal reaction and moth-eaten destruction, and presence of anterior bowing.

Our patients who had fibrous dysplasia were usually younger than those who had adamantinoma; all patients with fibrous dysplasia were less than 38 years old, and 46% of them were 10 years old or younger. This is in accordance with the age distribution reported by Gibson and Middlemiss [16]. The peak occurrence of fibrous dysplasia is reported to be between the ages of 10 and 15 years, and patients with polyostotic fibrous dysplasia or osteofibrous dysplasia are even younger [1, 4, 8, 19]. The ages of our patients with adamantinoma were more or less equally distributed over the second to fifth decades. The peak occurrence of adamantinoma is reported to be between ages 11 and 30, but the reported range in the literature is between 3 and 74 years [9, 13].

A ground-glass appearance with or without intralesional opacifications frequently was found in fibrous dysplasia (72%, Fig. 9), but it also was encountered in adamantinoma (14%). Conversely, a mostly osteolytic appearance, with or without intralesional opacifications, was definitely present more often in adamantinoma (86%) than in fibrous dysplasia (28%).

Reports on anterior bowing in patients with fibrous dysplasia are, in contrast to those on bowing deformity of the femur, rather sparse [16]. In our patients, anterior bowing was found in about one quarter of patients with fibrous dysplasia (24%, Fig. 5). However, the presence of anterior bowing in one of

the patients with an adamantinoma (Fig. 2) warrants some constraint in using this criterion.

The presence of infantile or congenital pseudarthrosis, which was present in one of our patients (Fig. 6), allows the exclusion of adamantinoma from the list of differential diagnoses [4, 17]. As was the case in our patient, on histologic examination, the area of pseudarthrosis may not contain tumorous tissue but only fibrous tissue with increased osteoblastic activity.

Although patients with fibrous dysplasia more often had additional lesions in the fibula (13%, Fig. 5) than did patients with adamantinoma (5%, Fig. 7), these additional lesions were a relatively insignificant sign in differentiating between the two lesions. In their review of the literature, Moon and Mori [9] also found simultaneous localizations of adamantinoma in the tibia and fibula in 5% of their 200 reviewed patients. Solitary adamantinoma of the fibula may occur [18].

Entirely intracortical localizations were seen in both fibrous dysplasia (Fig. 3) and in adamantinoma (Fig. 10). This sign is also not important in differentiating fibrous dysplasia from adamantinoma.

No metastases were found on chest radiographs of our patients at presentation. Because metastases develop late in the course of adamantinoma, the absence of metastases does not assist in making a differential diagnosis [11, 12, 23, 24].

The role of CT and MR imaging in differentiating fibrous dysplasia from adamantinoma is probably limited, considering the histology of both lesions. Involvement of cortical bone is demonstrated exquisitely well with both cross-sectional techniques [25–27]. The signal intensities of fibrous dysplasia are low on T1-weighted images and variable on T2-weighted images [26, 28]. We found in four patients that the signal intensity of adamantinoma is similar to that of other tumors and not specific (unpublished data).

When no endocrine symptoms or obvious polyostotic fibrous dysplasia is found, the radiograph of the lower leg is used to assist in differentiating fibrous dysplasia from adamantinoma. When the selected signs described in this study are combined, the two disorders can be correctly identified in a high percentage of patients. However, the most important discriminating signs can occur in both lesions; therefore, a large biopsy to allow a histologic diagnosis often will be necessary. A histologic diagnosis of adamantinoma, with or without radiologic support, solves the diagnostic dilemma. The impact of a combined radiologic and histologic diagnosis of fibrous dysplasia on management depends on the level of confidence and clinical symptoms. When a histologic diagnosis of fibrous dysplasia cannot be supported by the radiologic diagnosis, further action, such as obtaining follow-up studies or performing a new biopsy or sometimes even a resection, will be necessary.

ACKNOWLEDGMENTS

We thank the Netherlands Committee on Bone Tumors and the referring physicians for their cooperation. Statistic analysis was done by Roland Brand.

REFERENCES

- Feldman F. Tuberous sclerosis, neurofibromatosis, and fibrous dysplasia. In: Resnick D, Niwayama G, eds. *Diagnosis of bone and joint disorders*, 2nd ed. Philadelphia: Saunders, 1988:4033-4073
- Harris WH, Dudley HR, Barry RJ. The natural history of fibrous dysplasia. *J Bone Joint Surg [Am]* 1962;44-A:207-233
- Lichtenstein L, Jaffe HL. Fibrous dysplasia of bone. *Arch Pathol Lab Med* 1942;3:777-816
- Wilner D. Fibrous dysplasia of bone. In: Wilner D, ed. *Radiology of bone tumors and allied disorders*. Philadelphia: Saunders, 1982:1443-1581
- Campbell CJ, Hawk T. A variant of fibrous dysplasia (osteofibrous dysplasia). *J Bone Joint Surg [Am]* 1982;64-A:231-236
- Nakashima Y, Yamamoto T, Fujiwara Y, Kotoura Y, Mori E, Hamashima Y. Osteofibrous dysplasia (ossifying fibroma of long bones). *Cancer* 1983;52:909-914
- Kempson RL. Ossifying fibroma of the long bones. *Arch Pathol Lab Med* 1966;82:218-233
- Mirra JM. Adamantinoma and osteofibrous dysplasia. In: Mirra JM, ed. *Bone tumors*. Philadelphia: Lea & Febiger, 1989:1203-1233
- Moon NF, Mori H. Adamantinoma of the appendicular skeleton—updated. *Clin Orthop* 1986;204:215-237
- Resnick D, Kyriakos M, Greenway GD. Tumors and tumor-like lesions of bone: imaging and pathology of specific lesions. In: Resnick D, Niwayama G, eds. *Diagnosis of bone and joint disorders*, 2nd ed. Philadelphia: Saunders, 1988:3616-3889
- Wilner D. Adamantinoma of long bones. In: Wilner D, ed. *Radiology of bone tumors and allied disorders*. Philadelphia: Saunders, 1982:2387-2410
- Weiss SW, Dorfman HD. Adamantinoma of long bone: an analysis of nine new cases with emphasis on metastasizing lesions and fibrous dysplasia-like changes. *Hum Pathol* 1977;8:141-153
- Schajowicz F, Santini-Araujo E. Adamantinoma of the tibia masked by fibrous dysplasia. *Clin Orthop* 1989;238:294-301
- Mori H, Yamamoto S, Hiramatsu K, Miura T, Moon NF. Adamantinoma of the tibia: ultrastructural and immunohistochemical study with reference to histogenesis. *Clin Orthop* 1984;190:299-310
- Lodwick GD. Radiologic concepts. In: Hodes PJ, Lodwick GS, eds. *Atlas of tumor radiology: the bone and joints*. Chicago: Year Book Medical, 1973:1-83
- Gibson MJ, Middlemiss JH. Fibrous dysplasia of bone. *Br J Radiol* 1971;44:1-13
- Resnick D. Additional congenital or heritable anomalies and syndromes. In: Resnick D, Niwayama G, eds. *Diagnosis of bone and joint disorders*, 2nd ed. Philadelphia: Saunders, 1988:3540-3595
- Sowa DT, Dorfman HD. Unusual localization of adamantinoma of long bones. *J Bone Joint Surg [Am]* 1986;68-A:293-296
- Campanacci M, Laus M. Osteofibrous dysplasia of the tibia and fibula. *J Bone Joint Surg [Am]* 1981;63-A:367-375
- Waldron CA. Fibro-osseous lesions of the jaws. *J Oral Maxillofac Surg* 1985;43:249-262
- Eversole LR, Leider AS, Nelson K. Ossifying fibroma: a clinicopathologic study of sixtyfour cases. *Oral Surg Oral Med Oral Pathol* 1985;60:505-511
- Krandsdorf MJ, Moser RP, Gilkey FW. From the archives of the AFIP: fibrous dysplasia. *RadioGraphics* 1990;10:519-537
- Schneider H, Enderle R. Zur Differentialdiagnose eines metastasierenden Adamantinoms der Tibia und Fibula. *Arch Orthop Trauma Surg* 1979;94:143-149
- Cohn BT, Brahms MA, Froimson A. Metastasis of adamantinoma sixteen years after knee disarticulation. *J Bone Joint Surg [Am]* 1986;68-A:772-776
- Daffner RH, Kirks DR, Gehweiler JA, Heaston DK. Computed tomography of fibrous dysplasia. *AJR* 1982;139:943-948
- Dominguez R, Saucedo J, Fenstermacher M. MRI findings in osteofibrous dysplasia. *Magn Reson Imaging* 1989;7:567-570
- Zeanah WR, Hudson TM, Springfield DS. Computed tomography of ossifying fibroma of the tibia. *J Comput Assist Tomogr* 1983;7(4):688-691
- Utz JA, Krandsorf MJ, Jelinek JS, Moser RP, Berrey BH. MR appearance of fibrous dysplasia. *J Comput Assist Tomogr* 1989;13(5):845-851

Medicine in American Art

The Gross Clinic

Stefan C. Schatzki¹

The Gross Clinic is the best-known painting by Thomas C. Eakins, one of America's most important artists, who was born in Philadelphia in 1844. Except for a few years of study in Europe, his entire life was spent in his native city. Between 1870 and the early years of the 20th century, Eakins painted many important works covering a wide range of subjects. He was particularly well known for his insightful portraits, which has led art historians to consider him the "American Rembrandt." In addition, his oeuvre included distinctive depictions of rowing and other sporting scenes and various genre scenes. This great, innovative artist based all his work on an intimate knowledge of anatomy and was one of the first to use photography to study human and animal movement.

In 1875, secure in his ability as an artist, Eakins decided to produce a major painting for the 1876 Philadelphia Centennial Exhibit. Earlier (before and after his European sojourn), Eakins had attended anatomy lectures at Jefferson Medical School. In addition, he had attended the surgical demonstrations of Professor Samuel Gross, who was perhaps the leading surgeon in the country at that time. Gross was a heroic figure, and as the first president of the Jefferson Alumni Association, had asked the alumni in 1871 to help the school obtain portraits of its faculty. Perhaps hoping to stimulate future commissions, Eakins decided to produce a monumental portrait of Jefferson's most famous alumnus.

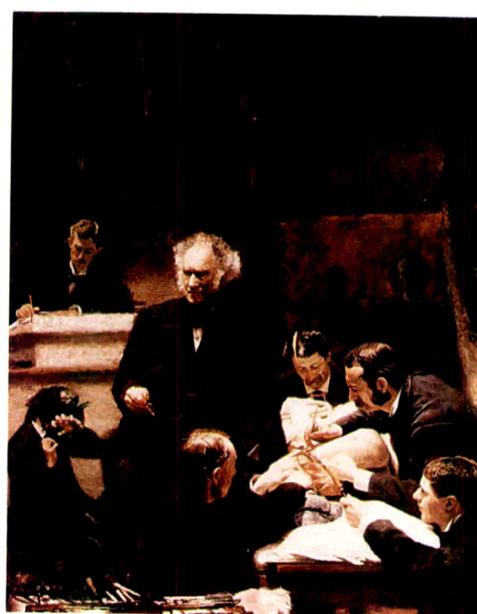
This huge painting, which demonstrates the removal of a tumor from a patient's thigh, emphasizes Gross's dual role as surgeon and educator. The painting is clearly centered on Dr. Gross, who is not only participating in the operation, as seen by the scalpel held in his bloody hands, but also is detached somewhat from the surgery, as a professor or lecturer might be. The light is focused on Dr. Gross's extraordinary head, making this one of America's most important portraits. All the details of the painting are carefully constructed. The assistants are specific, important Philadelphia surgeons, as is the recorder. The students who fill the theater and closely watch and listen to Dr. Gross are portraits of specific people, including an Eakins self-portrait. Only one woman is present, covering her eyes to shut out the proceedings. She is presumably the mother or wife of the patient, as it was customary to have a member of the family present when surgery was carried out on a charity patient.

The painting was not accepted for the centennial exhibit, perhaps because of the shock produced by the realistic details of the surgery. However, several years later, the Jefferson Alumni Association did buy the portrait, and Eakins subsequently painted insightful portraits of many faculty members

of the three Philadelphia medical schools. Despite its importance, "*The Gross Clinic*" was not exhibited outside Jefferson Medical School for more than 100 years, until the major Eakins exhibition in 1982 at the Philadelphia Museum of Art and the Museum of Fine Arts in Boston.

Eakins was responsible for oil-painting instruction at the Pennsylvania Academy of Fine Arts for many years. He thus became a major influence in the history of American-painting education. The anatomic knowledge that Eakins taught and the techniques he used with art students had many similarities to anatomic instruction given medical students at the time. He emphasized the importance of anatomic reality, regularly using live models and frequently requiring his students to dissect in order to understand anatomic detail. As noted earlier, he used photography to understand movement and muscular function. His techniques were largely responsible for the important place that the Pennsylvania Academy of Fine Arts held in art instruction during the late 19th century.

Although not fully appreciated throughout much of his life, Eakins was recognized as one of the major influences in American painting by the time he died in 1916.



Thomas C. Eakins (1844–1916). *The Gross Clinic, A Portrait of Dr. Samuel Gross*, 1875. Oil on canvas, 244 × 200 cm. Jefferson Medical College, Thomas Jefferson University, Philadelphia.

¹ Department of Radiology, Mount Auburn Hospital, 330 Mount Auburn St., Cambridge, MA 02238.

Pictorial Essay

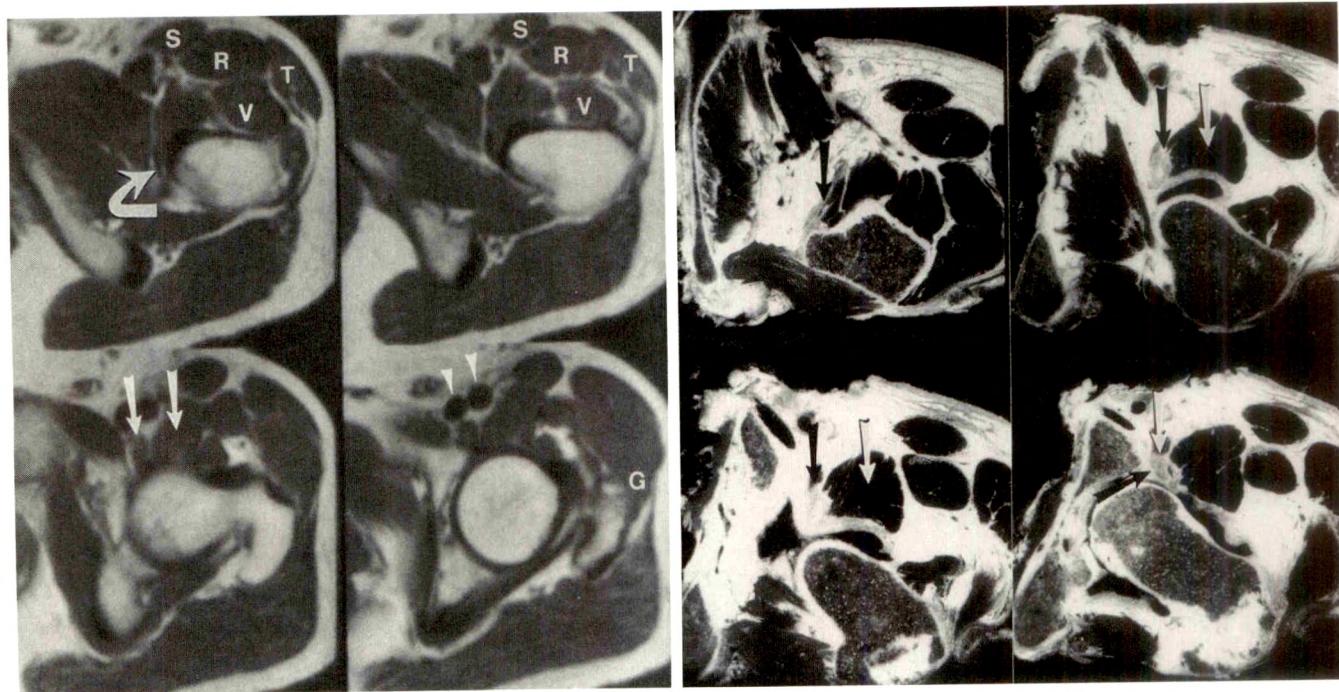


MR Appearance of the Distended Iliopsoas Bursa

Datla G. K. Varma,¹ William R. Richli, Chusilp Charnsangavej, Barry I. Samuels, Edmund E. Kim, and Sidney Wallace

The purpose of this essay is to illustrate the MR appearance of the distended iliopsoas bursa. The bursa must be recognized on MR scans to avoid confusing it with malignant neoplasms and other lesions.

The iliopsoas bursa is the largest bursa around the hip joint (average size, 6 × 3 cm) and is situated beneath the musculotendinous portion of the iliopsoas muscle, in front of the hip joint capsule and lateral to the femoral vessels [1, 2]. It can



A

B

Fig. 1.—*A*, Normal iliopsoas bursa. T1-weighted MR images (600/20) of 10-mm-thick contiguous sections obtained in a caudal to cephalic direction on a 1.5-T General Electric unit in a 65-year-old patient without iliopsoas bursal distension. Note intermediate-intensity iliopsoas muscle complex (straight arrows). Low-intensity iliopsoas tendon is seen at its insertion into lesser trochanter of femur (curved arrow). Normal iliopsoas bursa is collapsed. Signal void is identified in anterior femoral vessels (arrowheads). *S* = sartorius, *R* = rectus femoris, *T* = tensor fasciae latae, *V* = vastus intermedius, *G* = gluteus medius.

B, Photographs of cadaver sections approximately 3-mm thick. Iliopsoas muscle tendon complex (arrows) corresponds to MR images in *A*. Contrast material doped with India ink has been injected into hip joint.

Received September 19, 1990; accepted after revision November 14, 1990.

¹ All authors: Department of Diagnostic Radiology, Box 57, The University of Texas M. D. Anderson Cancer Center, 1515 Holcombe Blvd., Houston, TX 77030. Address reprint requests to D. G. K. Varma.

AJR 156:1025-1028, May 1991 0361-803X/91/1565-1025 © American Roentgen Ray Society

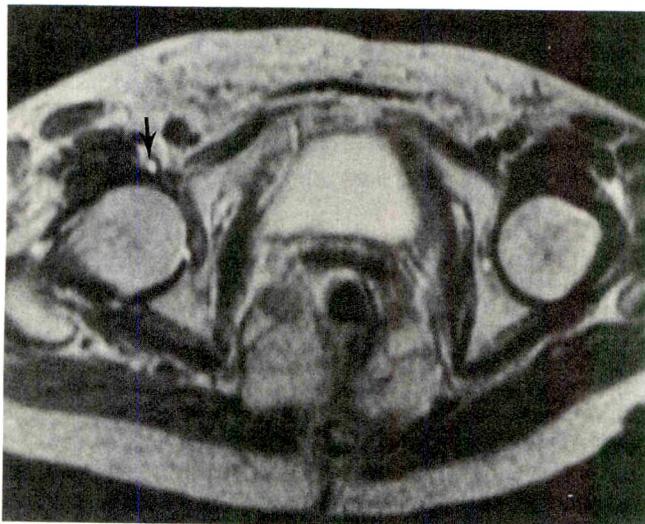


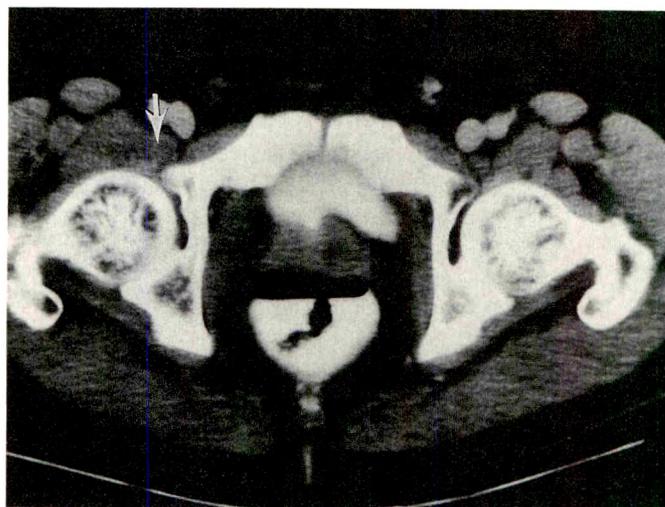
Fig. 2.—76-year-old woman with endometrial carcinoma and no hip pain. Axial T2-weighted MR image (2200/80) shows minimal distension of right iliopsoas bursa with fluid (arrow).

be found in about 98% of subjects and communicates with the cavity of the hip joint in about 15% of cases [1, 2]. The communication may be congenital or acquired. If acquired, it may be due to friction produced by the iliopsoas tendon on the bursa with resultant synovial thinning and small synovial tears [1].

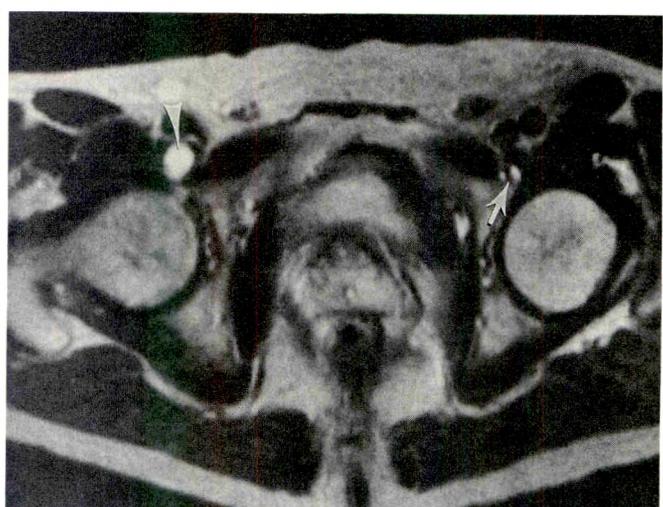
The normal iliopsoas bursa is collapsed. Distension of the bursa is usually caused by overproduction of synovial fluid in an arthritic hip leading to increased intraarticular pressure and extension of fluid into the potential space of the bursa. Age-related synovial villous proliferation of the bursal lining may lead to fluid overproduction and bursal distension [3]. The distension may be minimal or marked with extension of the bursa into the pelvis along the iliopsoas muscle.

MR Imaging

The iliopsoas bursa separates the iliopsoas tendon from the articular capsule of the hip joint. The normal iliopsoas bursa is collapsed. The iliopsoas muscle tendon complex anterior to the collapsed bursa is well delineated on MR images. The muscle is visualized as a structure of intermedi-



A

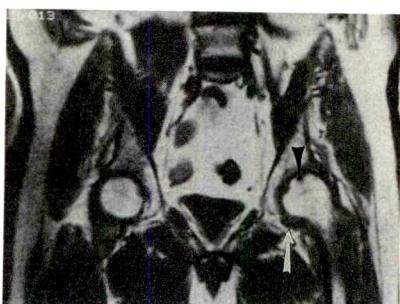


B

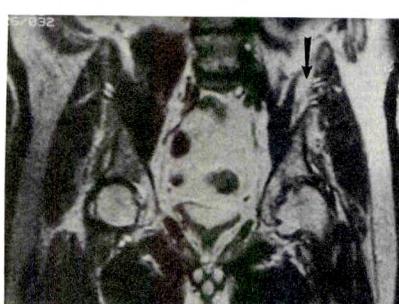
Fig. 3.—65-year-old patient with a history of bladder carcinoma.

A, CT scan shows incidental right iliopsoas bursal fluid collection (arrow) posterior to femoral artery and vein. Patient did not have hip pain.

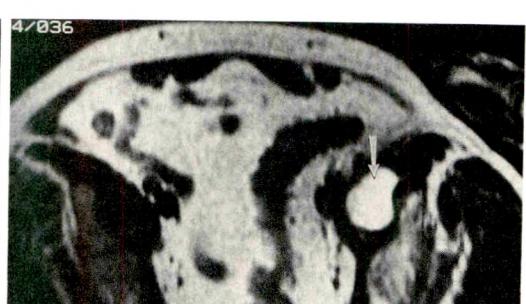
B, Axial T2-weighted MR image (2000/80) corresponding to CT scan. Note right-sided bursal fluid collection (arrowhead) and small biloculated left-sided bursal fluid collection (arrow).



A



B



C

Fig. 4.—69-year-old man with a history of spinal tuberculosis and osteoarthritis who had left hip pain.

A, Coronal T1-weighted MR image (600/20) shows fluid within hip joint (arrow) and cystic degenerative changes in femoral head (arrowhead).

B, Corresponding T2-weighted MR image (2000/80). High intensity is noted within fluid and degenerative cysts. Note cephalic extension of fluid into pelvis (arrow). Aspiration of fluid did not reveal any acid-fast bacilli.

C, Axial T2-weighted MR image (2000/80) reveals high-intensity bursal fluid extension into pelvis along left iliopsoas muscle (arrow).

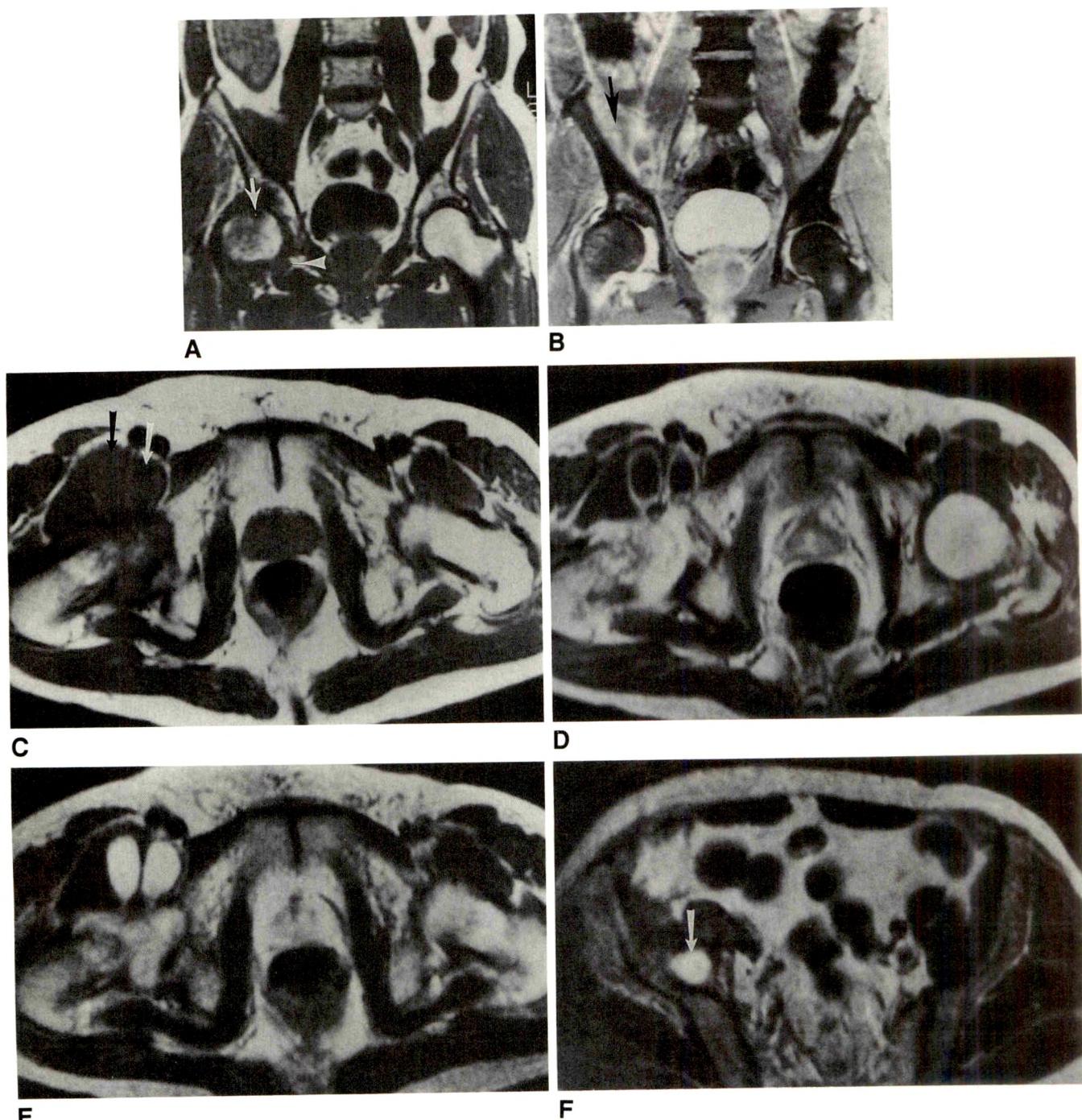


Fig. 5.—64-year-old man with a history of melanoma and osteoarthritis of right hip who had right hip pain.

A, Coronal T1-weighted MR image (700/20) reveals degenerative cyst (arrow) and fluid in right hip joint (arrowhead).

B, Coronal multiplanar gradient-recalled acquisition in the steady state MR image (250/10/60° flip angle) reveals corresponding high-intensity changes and pelvic extension (arrow). Effusion in right hip joint and possible small effusion in left hip joint are identified.

C, Axial T1-weighted MR image (600/20) reveals low-intensity biloculated right iliopsoas bursal fluid collection (arrows).

D, Enhanced T1-weighted MR image (650/20) confirms fluid within distended bursa. Fluid does not enhance.

E, Axial T2-weighted MR image (2200/80) reveals high-intensity biloculated distended bursa.

F, Axial T2-weighted MR image (2200/80) reveals pelvic extension of fluid into right iliopsoas sheath (arrow). Sonographically guided fluid aspiration revealed synovial fluid, which was negative for malignancy. Injection of contrast material into bursa did not reveal any communication with hip joint space.

ate signal intensity on routine T1-weighted (e.g., 600/20 [TR/TE]) or T2-weighted (e.g., 2000/80) spin-echo images; the tendon, at its insertion in the lesser trochanter of the femur, is visualized as a low-intensity structure (Fig. 1).

Various degrees of distension by synovial fluid of the iliopsoas bursa may be seen on MR images. The distension may be minimal and detected incidentally in asymptomatic patients in whom there are no radiologic findings of hip joint disease

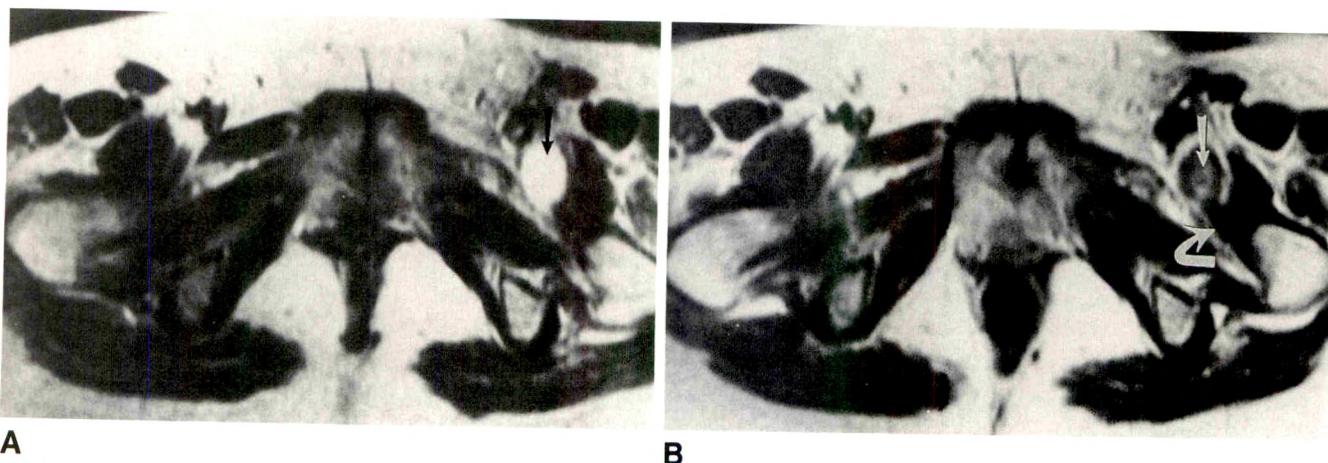
**A****B**

Fig. 6.—47-year-old woman with recurrent sarcoma.

A, Axial T2-weighted MR image (2200/80) reveals high-intensity focus of abnormality in left proximal thigh (arrow) posterior to femoral vessels.

B, Enhanced T1-weighted MR image (600/20) reveals an enhancing solid mass in left thigh (straight arrow), surgically confirmed to be a recurrent sarcoma. Note low-intensity iliopsoas tendon (curved arrow) medial to solid tumor.

(Figs. 2 and 3). In patients with degenerative hip joint disease, MR images may reveal bursal distension with extension of the bursa into the pelvis along the iliopsoas muscle (Figs. 4 and 5). The distended bursa has signal characteristics on MR images that are similar to those of water, and associated hip joint effusion or degenerative changes may be visualized. The fluid in the bursa may be biloculated. Gadopentetate dimeglumine-enhanced MR imaging further aids in distinguishing the distended bursa from other lesions (Figs. 5 and 6).

Discussion

Iliopsoas bursa distension in association with disease has been described in trauma, osteoarthritis, avascular necrosis, rheumatoid arthritis, synovial chondromatosis, pigmented villonodular synovitis, gout, and pyogenic infection [2–4]. Patients may have an asymptomatic groin mass or symptoms related to compression of neighboring structures. Bursal dis-

tension may extend into the pelvis along the iliopsoas muscle and result in compression or displacement of the colon, ureters, and urinary bladder [3].

The differential diagnosis of an enlarged iliopsoas bursa includes inguinal or femoral hernia, neoplasm, lymphadenopathy, undescended testis, hematoma, psoas abscess, femoral aneurysm, and arteriovenous fistula [3]. The clinical symptoms of iliopsoas bursal distension may mimic these conditions, and, as such, accurate imaging analysis to evaluate the distension is required.

REFERENCES

1. Chandler SB. The iliopsoas bursa in man. *Anat Rec* 1934;58:235–240
2. Armstrong P, Saxton H. Ilio-psoas bursa. *Br J Radiol* 1972;45:493–495
3. Binek R, Levinsohn ME. Enlarged iliopsoas bursa: an unusual cause of thigh mass and hip pain. *Clin Orthop* 1987;224:158–163
4. Cohen JM, Hodges CS, Weinreb JC, Muschler G. MR imaging of iliopsoas bursitis and concurrent avascular necrosis of the femoral head. *J Comput Assist Tomogr* 1985;9:969–971

Interobserver and Intraobserver Variations in Sonographic Renal Length Measurements in Children

Alan E. Schlesinger¹
 Ramiro J. Hernandez¹
 J. Michael Zerin¹
 Terri I. Marks¹
 Robert C. Kelsch²

Sonographic measurement of renal length is used commonly to evaluate growth of the kidneys in children. However, no previous studies have been performed to determine the degree of interobserver and intraobserver variability in such determinations. We measured the interobserver and intraobserver error in sonographic measurements of renal length obtained independently by three experienced imagers in 21 children (41 kidneys). The mean interobserver variation between any two imagers ranged from 3.87 to 5.49 mm. The mean intraobserver variation was 0.87 to 3.61 mm.

The observed variability in sonographic measurement of renal length is comparable to the expected annual increase in length of the kidneys during childhood (2.2–5.7 mm per year). Therefore, caution is suggested when using sonography to evaluate renal growth in children during a year's time.

AJR 156:1029–1032, May 1991

Measurement of renal length has become an integral part of the renal sonographic examination in children. Normal standards have been developed for renal length in children as a function of weight, height, body surface area, and age. Sequential measurements of renal length over time have been used to determine if renal growth is appropriate during a specified interval. The reproducibility of these measurements has not been investigated formally. We prospectively evaluated the interobserver and intraobserver variability in sonographic measurements of renal length.

Materials and Methods

The study group consisted of 21 consecutive children (41 kidneys) referred for renal sonographic examination. One patient had unilateral renal agenesis. No attempt was made to exclude patients with renal disease, as we tried to simulate the typical spectrum of patients who come to a pediatric sonography department for renal evaluation. The age range of the patients was 3 months to 15 years (median, 5 years).

Images were obtained by using a real-time scanner (Acuson, Mountain View, CA) with a 5.0- or 3.5-MHz sector transducer. Three experienced imagers each obtained two separate longitudinal views of each kidney and measured maximal renal length. Each observer first examined the kidneys thoroughly from different angles with the patients in various positions and with the patients using breath-holding techniques if possible to determine the best method of obtaining an image representing the maximal renal length. Two consecutive images were then obtained with this same technique, and the renal lengths were measured by using electronic calipers on the scanner. The observers had no knowledge of one another's results. All of the examinations were done within a 30-min period.

The data were analyzed separately for the right and left kidneys. The mean of the two separate measurements of renal length obtained by a given observer was used for that observer's measurement of kidney length. The mean renal length, standard deviation (SD), and standard error were calculated for the 21 right kidneys and the 20 left kidneys for each observer. A repeated measures analysis of variance (ANOVA) [1] was performed to compare

Received August 20, 1990; accepted after revision November 14, 1990.

¹ Department of Radiology, The University of Michigan Hospitals, 1500 E. Medical Center Dr., Ann Arbor, MI 48109. Address reprint requests to A. E. Schlesinger, Mott Children's Hospital, Section of Pediatric Radiology, Room C3123/0252, 1500 E. Medical Center Dr., Ann Arbor, MI 48109-0252.

² Department of Pediatrics, The University of Michigan Hospitals, 1500 E. Medical Center Dr., Ann Arbor, MI 48109.

0361-803X/91/1565-1029
 © American Roentgen Ray Society

TABLE 1: Descriptive Statistics of Renal Length Measured by Three Observers

Observer	Right Kidney			Left Kidney		
	Range (mm)	Mean (mm)	SD (mm)	Range (mm)	Mean (mm)	SD (mm)
1	54.4–110.7	78.7	14.8	46.7–121.7	79.2	17.6
2	51.0–107.1	77.3	14.0	51.2–122.9	79.4	17.6
3	46.6–103.7	75.9	13.1	48.3–122.2	81.1	16.6

Note.—SD = standard deviation.

TABLE 2: Standard Error of Renal Length Measurements by Three Observers

Observer	Right Kidney (mm)	Left Kidney (mm)
1	3.22	3.93
2	3.06	3.94
3	2.85	3.71

the mean renal length measurement of the three observers in each of the 41 kidneys. This parametric test was used after confirming normality and uniformity of variance.

Interobserver and intraobserver variability were then evaluated by analyzing the difference in individual measurements for each kidney. This was performed between observers (interobserver variability) and between the two separate measures for each kidney by the same observer (intraobserver variability). The mean of the difference between the measurements of the individual kidneys and the SD were calculated for the right and left kidneys. The absolute value of the difference between the two measurements was used to calculate the mean and SD, as we were concerned only with the magnitude of the difference between the measurements and not which measurement was larger. The intraclass correlation (a measure of interobserver variability) [2] also was calculated for the measurements by the three observers.

Results

The range, mean, and SD of the measurements of renal length made by the three observers are summarized in Table

1. The standard error, an evaluation of precision, was comparable for the three observers (Table 2). Each observer showed similar precision in measurement of the right kidney compared with the left kidney. A repeated measures ANOVA of the data showed no significant difference between the mean for the three different observers ($p = .7751$).

The variability of the measurements of individual kidneys was then analyzed for interobserver and intraobserver error. The range of disagreement in measurements of each of the kidneys between any two of the observers (with the mean and SD) is shown in Table 3. The range, mean, and SD of the variation in the two separate measurements of renal length for each observer (intraobserver error) is shown in Table 4. Scatterplots graphically display the two measurements of renal length for each observer (Fig. 1). The intraclass correlation, a measure of interobserver variability for the three observers, was -0.49 .

Discussion

Sonographically determined renal length has been used routinely to evaluate both renal size and interval renal growth over time. However, no studies of the variability of renal lengths measured sonographically are available.

Before the development of sonography, measurements of renal length were obtained from radiographs obtained during excretory urography [3, 4]. Potential causes for inaccuracy included changes in renal size due to swelling of the kidney

TABLE 3: Interobserver Error for Sonographic Measurements of Renal Length

Observers	Right Kidney			Left Kidney		
	Range (mm) ^a	Mean (mm) ^b	SD (mm) ^b	Range (mm) ^a	Mean (mm) ^b	SD (mm) ^b
1–2	-6.8, +9.3	3.87	2.39	-10.3, +7.7	4.13	3.04
1–3	-9.5, +11.8	5.49	3.27	-10.4, +10.1	5.00	3.57
2–3	-9.0, +17.9	4.90	4.02	-13.3, +8.0	4.71	3.52

^a First observer's measurement – second observer's measurement.

^b Calculated from absolute value of differences between observers. SD = standard deviation.

TABLE 4: Intraobserver Error for Sonographic Measurements of Renal Length

Observer	Right Kidney			Left Kidney		
	Range (mm) ^a	Mean (mm) ^b	SD (mm) ^b	Range (mm) ^a	Mean (mm) ^b	SD (mm) ^b
1	-2.3, +3.2	0.87	0.83	-19.8, +6.2	2.96	4.36
2	-8.0, +7.4	2.19	2.02	-7.0, +7.2	2.88	2.23
3	-9.0, +3.3	1.98	1.91	-7.2, +23.0	3.61	5.01

^a First measurement – second measurement.

^b Calculated from absolute value of difference between measurements. SD = standard deviation.

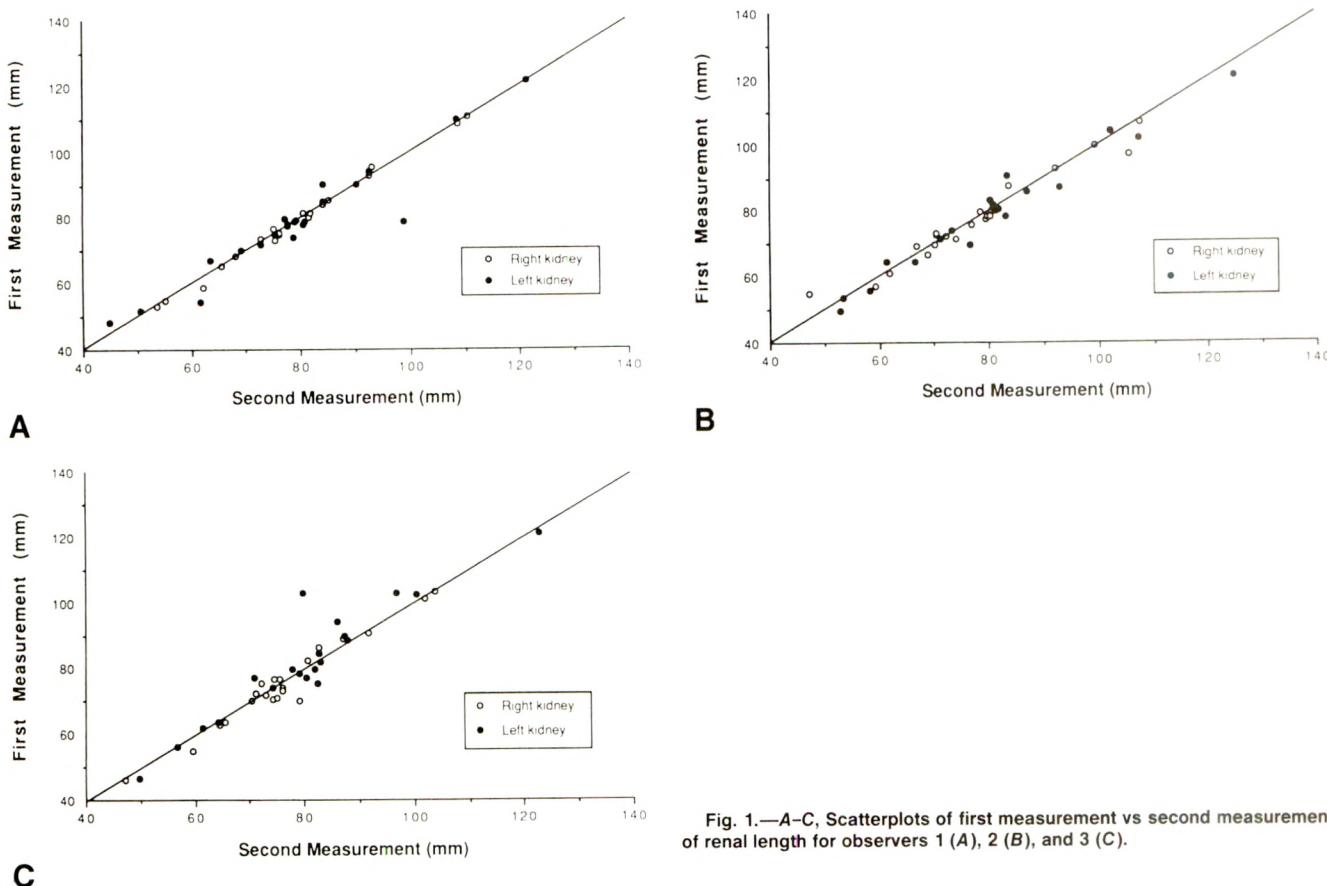


Fig. 1.—A–C, Scatterplots of first measurement vs second measurement of renal length for observers 1 (A), 2 (B), and 3 (C).

from the osmotic effect of the iodinated contrast material, variable magnification, changes in the angle of the kidney with respiration, differences in centering of the image, and measurement errors [5–7].

Sonography essentially has replaced excretory urography in a majority of cases in which imaging of the kidneys is necessary in children. Normal standards for renal length and/or volume have been determined for preterm infants [8–11], full-term neonates [9–12], infants [13], and older children [14–18]. These data are used to determine if a given patient's renal length is appropriate for age, weight, height, body surface area, or gestational age. Measurements of renal length on follow-up sonograms also are used to determine if renal growth in the interval between examinations has been appropriate.

Our data show that correlation of measurements between observers was good when the sample of 41 kidneys was analyzed as a whole. However, when each kidney was analyzed individually, the variability in the sonographic measurement of renal length was sizable, both between two separate observers (interobserver variability) and between two separate measurements by a single observer (intraobserver variability). The mean of the variability between the two measurements of an individual kidney by any two observers ranged from 3.87 to 5.49 mm (SD, 2.39–4.02). In individual kidneys, discrepancies as large as 17.9 mm were seen between observers. The mean intraobserver variability ranged from 0.87 to 3.61 mm (SD, 0.83–5.01). Intraobserver errors as large as

23.0 mm were encountered in individual kidneys. The intraobserver error was greater in the measurement of the left kidney than in that of the right for all three observers. The interobserver error between any two of the three observers was comparable for the right and left kidneys. The intraclass correlation is a measure of interobserver variability in the measurement of the individual kidneys. The intraclass correlation value approaches 1.0 if there is perfect agreement among the measurements of the individual kidneys by the observers. A value below zero implies poor correlation in these measurements. The intraclass correlation of –0.49 in our series implies a relatively high degree of interobserver variability in the measurement of individual kidneys.

To aid in estimating an acceptable level of variability in renal length measurement, we calculated the expected increase in renal length during 1 year. A formula for estimating renal length has been derived from data on renal length obtained from excretory urograms of 262 children between birth and 14.5 years of age [4]:

$$y = (0.589x + 6.198) - 0.013x^2$$

where y = renal length in centimeters and x = age in years. When this equation is used, the calculated renal growth during 1 year ranges from 2.2 to 5.7 mm during the first 14 years of life. Therefore, the expected rate of renal growth in a year is comparable to the potential error in sonographic measurement of renal length (Fig. 2).

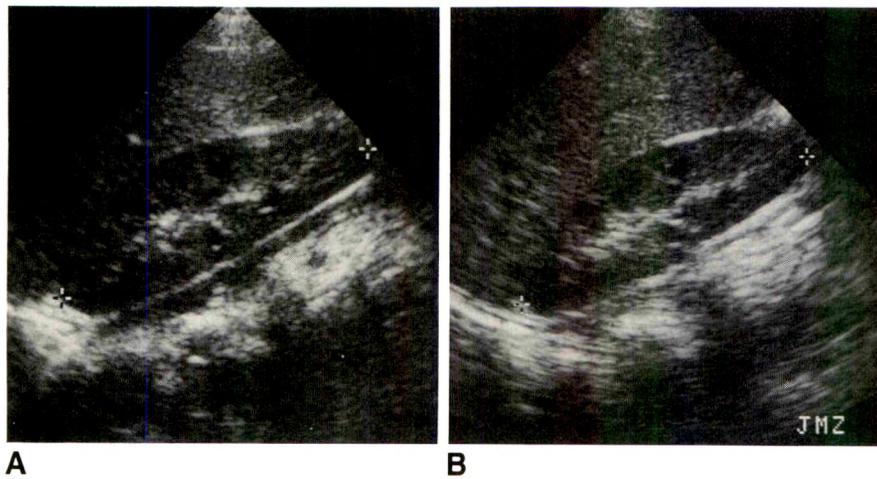


Fig. 2.—A and B, Longitudinal views obtained by two separate observers of right kidney in a 6-year-old girl. Measured length was 84.1 mm for observer 1 (A) and 80.4 mm for observer 2 (B) (interobserver error is 3.7 mm). Both images are of excellent quality without obscuration of kidney by bowel gas. Expected annual growth of a child's kidney from 5 to 6 years of age is 4.4 mm.

Our measurement of intraobserver variation may have been biased by the manner in which we obtained the two measurements of each observer. By obtaining two consecutive renal lengths, the second measurement may have been biased by the first. However, we think that the alternative method of obtaining two measurements at different times might also have introduced potential sources of bias as there may have been varying degrees of difficulty in obtaining an image portraying the maximal renal length due to changes in distribution of bowel gas or actual changes in renal length due to differing degrees of hydration. These biases would probably have overestimated intraobserver error, whereas the potential bias in our method of data collection would tend to underestimate intraobserver variability. Therefore, the substantial variability we observed may be a conservative estimate of potential intraobserver variability.

It would be of interest to know if interobserver or intraobserver variability was related to overall renal length. If the error is a constant percentage of overall length, the absolute magnitude of the error would increase with increasing renal length and patient's age. On the other hand, greater difficulty in obtaining reproducible images of maximal renal length in younger children who are unable to cooperate might lead to a larger absolute magnitude of error in younger children. Inspection of the scatterplots of our data does not suggest an obvious disproportionate magnitude of intraobserver variability at any particular renal length. However, our data base is too small to statistically analyze the degree of variability as a function of overall renal length or patient's age.

The possible sources of variability in sonographic measurement of renal length include difficulty in obtaining an adequate image because of bowel gas, selection of a longitudinal section that is not through the maximal longitudinal dimension of the kidney, and improper placement of the cursors of the electronic calipers. Determination of the degree that each of these potential sources of error contributes to the variability we report is not possible from our data. Change in axis of the kidney is a potential source of error in measurement of renal length from radiographs obtained during excretory urography. This does not affect renal length determination in sonography because the length is measured along the longitudinal axis of the kidney regardless of its relationship to the longitudinal axis of the body.

In conclusion, our data show that significant interobserver

and intraobserver error occurs in sonographic measurements of renal length. The calculated variability in length is sizable when compared with the expected normal renal growth in children during a year. Therefore, caution is suggested when sonographic measurements of renal length are used to determine if the renal growth in a 1-year interval in children is appropriate.

REFERENCES

1. Kleinbaum DG, Kupper LL, Muller KE. *Applied regression analysis and other multivariable methods*, 2nd ed. Boston: PWS-KENT, 1988:387-415
2. Fleiss JL, Shrout PE. The effects of measurement errors on some multivariate procedures. *Am J Public Health* 1977;67:1188-1191
3. Eklof O, Ringertz H. Kidney size in children: a method of assessment. *Acta Radiol* 1976;17:617-625
4. Curranino G, Williams B, Dana K. Kidney length correlated with age: normal values in children. *Radiology* 1984;150:703-704
5. Wolpert SM. Variation in kidney length during the intravenous pyelogram. *Br J Radiol* 1965;38:100-103
6. Hernandez RJ, Poznanski AK, Kuhns LR, McCormick TL. Factors affecting the measurement of renal length. *Radiology* 1979;130:653-656
7. Farrant P, Meire HB. Ultrasonic measurement of renal inclination: its importance in measurement of renal length. *Br J Radiol* 1978;51:628-630
8. Schlesinger AE, Hedlund GL, Pierson WP, Null DM. Normal standards for kidney length in premature infants: determination with US. *Radiology* 1987;164:127-129
9. de Vries L, Levene MI. Measurement of renal size in preterm and term infants by real-time ultrasound. *Arch Dis Child* 1983;58:145-147
10. Chiara A, Chirico G, Barbarini M, De Vecchi E, Rondini G. Ultrasonic evaluation of kidney length in term and preterm infants. *Eur J Pediatr* 1989;149:94-95
11. Fitzsimons RB. Kidney length in the newborn measured by ultrasound. *Acta Paediatr Scand* 1983;72:885-887
12. Holloway H, Jones TB, Robinson AE, Harpen MD, Wiseman HJ. Sonographic determination of renal volumes in normal neonates. *Pediatr Radiol* 1983;13:212-214
13. Blane CE, Bookstein FL, DiPietro MA, Kelsch RC. Sonographic standards for normal infant kidney length. *AJR* 1985;145:1289-1291
14. Rosenbaum DM, Korngold E, Teele RL. Sonographic assessment of renal length in normal children. *AJR* 1984;142:467-469
15. Dinkel E, Ertel M, Dittrich M, Peters H, Berres M, Schulte-Wissermann H. Kidney size in childhood: sonographic growth charts for kidney length and volume. *Pediatr Radiol* 1985;15:38-43
16. Moskowitz PS, Carroll BA, McCoy JM. Ultrasonic renal volumetry in children. *Radiology* 1980;134:61-64
17. Haugstvedt S, Lundberg J. Kidney size in normal children measured by sonography. *Scand J Urol Nephrol* 1980;14:251-255
18. Han BK, Babcock DS. Sonographic measurements and appearance of normal kidneys in children. *AJR* 1985;145:611-616

Case Report



Anomaly of the Descending Aorta: A Case of Persistent Double Dorsal Aorta

Augustin G. Formanek,¹ Kenneth M. Weisner,² and Patrick E. Lantz³

Although developmental abnormalities of the aortic arch, either isolated or associated with heart defects, have been described, few reports deal with anomalies of the descending aorta. Recently we examined a child with a complex congenital heart defect in whom an aortogram showed a rare, persistent double dorsal aorta, later verified at autopsy. We report this experience to promote awareness of developmental anomalies of the descending thoracic aorta and to emphasize the unique features as seen with angiography and MR imaging.

Case Report

A 2.5-year-old boy was examined with echocardiography and angiography. A complex congenital heart defect was diagnosed, including dextrocardia of indeterminate type, endocardial cushion defect with a common atrioventricular valve, double-outlet venous ventricle with the aorta anterior to the pulmonary artery, and pulmonic stenosis; anomalous pulmonary venous return was suspected also. After the first admission, the patient was readmitted several times for supraventricular tachycardia. He also was treated for bacterial meningitis and received prophylactic antibiotics because of asplenia. Systemic-to-pulmonary artery shunting was found on MR images when he was 5 years old. However, progressively worsening congestive heart failure ensued despite treatment with digoxin, furosemide, and captopril for afterload reduction. The patient died at the age of 5.5 years after undergoing a second catheterization.

During the second catheterization, an aortogram showed a right aortic arch with a right-sided descending aorta and a patent systemic-

to-pulmonary artery shunt. Surprisingly, no arterial branching was seen from the large main dorsal aorta distal to the origin of the aberrant left subclavian artery (Fig. 1A). However, a narrow ascending artery was evident, running craniad, parallel, and to the left of the main descending aorta. This artery started below the diaphragm and terminated in the upper mediastinum above the tracheal bifurcation. From this ascending counterpart of the dorsal aorta, segmental bilateral branches originated, corresponding to typical intercostal arteries (Fig. 1B). The artery terminated as an arborization with slightly tortuous small branches toward both hilar portions of the lungs, with subsequent opacification of small central pulmonary artery branches. These terminal branches of the left dorsal aorta were interpreted as bronchial arteries with collateral blood supply toward the pulmonary functional arterial bed. In addition, an arterial supply to the left lower lung from below the diaphragm was seen. Because the abdominal part of the aorta was not included in the cinearteriogram, neither the origin of the ascending trunk supplying the intercostal arteries nor the origin of the accessory artery for the left lung could be identified.

Autopsy confirmed all of the anatomic findings of the intrinsic heart defect shown by angiography. Additional findings included partial anomalous pulmonary venous return into the right superior vena cava, persistent left superior vena cava, bilaterally trilobate lungs, incomplete rotation of the colon with asplenia, and retroaortic left renal vein. The accessory dorsal aorta gave rise to intercostal arteries and then joined the main aorta at the level of the renal arteries (Fig. 1C).

Discussion

Although the complicated developmental events during formation of the definite aortic arch [1] may account for the great

Received November 26, 1990; accepted after revision January 7, 1991.

¹ Department of Radiology, Bowman Gray School of Medicine, 300 S. Hawthorne Rd., Winston-Salem, NC 27103. Address reprint requests to A. G. Formanek.

² Department of Pediatrics, Bowman Gray School of Medicine, 300 S. Hawthorne Rd., Winston-Salem, NC 27103.

³ Department of Pathology, Bowman Gray School of Medicine, 300 S. Hawthorne Rd., Winston-Salem, NC 27103.

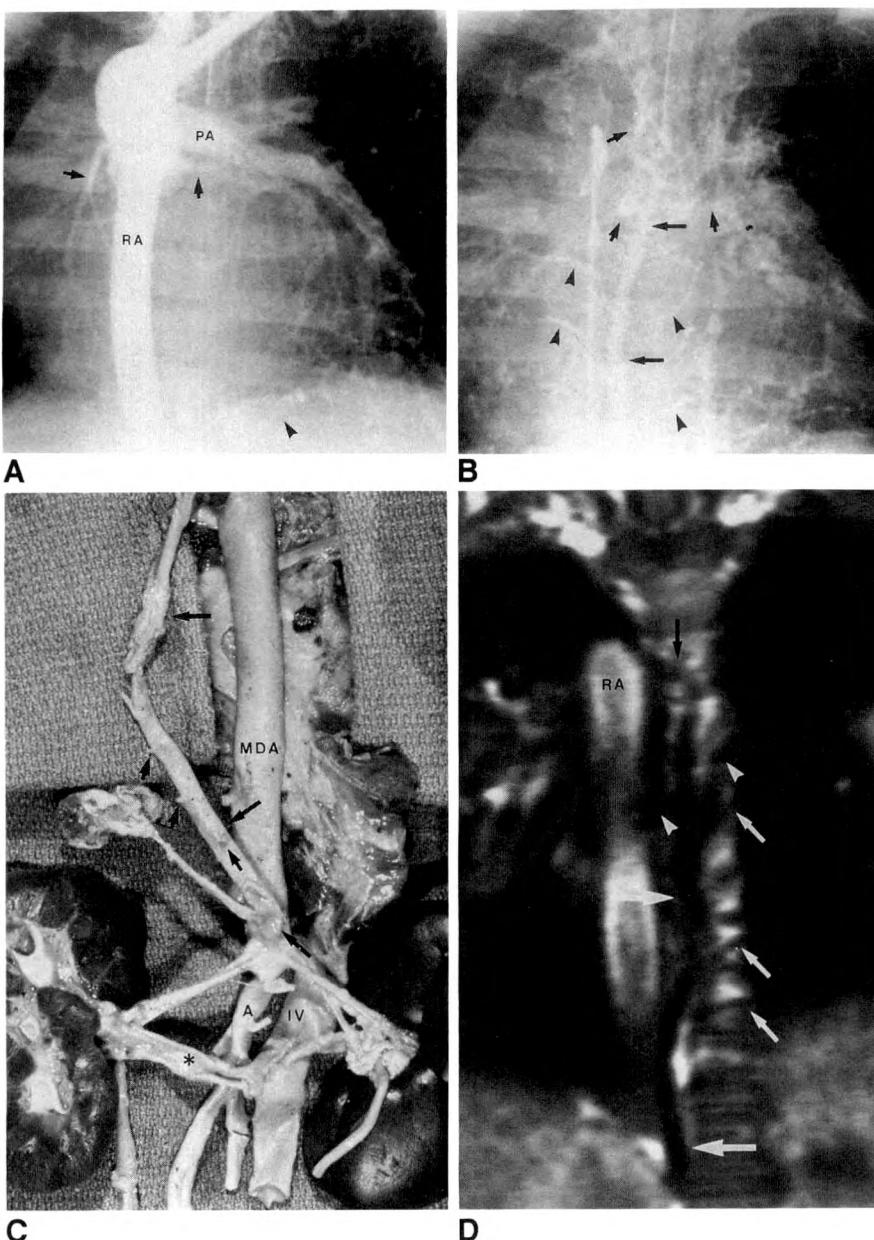


Fig. 1.—Double dorsal aorta.

A, Early-phase retrograde aortogram shows right aortic arch and right-sided descending aorta (RA) with aberrant left subclavian artery. No other branches take off distal to arch vessels from main descending aorta (right and left coronary arteries, arrows). Via a central shunt, left pulmonary artery (PA) is visualized. In addition, separate systemic artery supplies lower lobe of left lung (arrowhead).

B, Later-phase retrograde aortogram shows that when contrast medium cleared from main descending trunk, a slightly tortuous artery coursing to left of right aorta from below diaphragm is filled in caudocranial direction (long arrows). Typical intercostal arteries branch from it bilaterally (arrowheads). It ends with several branches toward hila of lungs (short arrows).

C, Autopsy specimen viewed from behind shows lack of intercostal arteries from main (right) limb of descending aorta (MDA). Origin of left-sided, posterior, smaller limb of double dorsal aorta (long arrows) is just above renal arteries. Short portions of several intercostal arteries are marked (short arrows). Because of abdominal heterotaxia, abdominal aorta (A) and inferior vena cava (IV) are on same side. Asterisk = left retroaortic renal vein.

D, Coronal spin-echo MR image (8-mm slice) shows slightly tortuous vessel (large white arrows) parallel and to left of large right-sided aorta (RA). Vessel gives off intercostal arteries (small white arrows) and bronchial arteries (arrowheads) and terminates with branch toward upper right thorax (highest intercostal artery, black arrow). This "common intercostal dorsal trunk" is carbon copy of left-sided part of double dorsal aorta shown in **B**.

variety of aortic arch anomalies, the formation of the future descending aorta is simple: in accordance with the fundamental bilateral symmetry of the body, the arteries and veins initially constitute a paired symmetric system [2]. Right and left primitive aortae, whose longest descending portions pass along the dorsal aspect of the gut, are in the earlier stages plexiform vessels that distribute blood from the heart to the embryonic tissues, yolk sac, and chorion by segmental plexuses [2]. The paired dorsal aortae initially run the entire length of the embryo but soon fuse to form a single aorta just distal to the branchial arches [3], which represent the anlage for the eventual aortic arch. Therefore, for the future thorax, the right-sided dorsal aorta supplies the right intercostal arteries, whereas the left-sided intercostal arteries originate from the left dorsal aorta.

In the case of persistent bilateral dorsal aorta, the unilateral origin of the paired arterial branches from the corresponding ipsilateral aorta, including the intercostal arteries, also might be expected to persist. However, based on the findings in our patient and on the four reports concerning double descending aorta [4–7], this is not always the case. Basically there are two types of this anomaly. There is either complete separation of the two dorsal aortae, similar to our case and two others [4, 5], or a double-lumen descending aorta is present with a central dividing septum from the level just below the ductal ligament to the aortic bifurcation [6, 7]. In the former situation, the bilateral intercostal arteries (our patient and one other [4]) and the visceral branches [5] take off from only one descending aorta, and only blindly ending rudimentary openings for the intercostal and visceral arteries

may be present in the opposite aorta [5]. In the situation of double aorta with the dividing septum, the paired arterial branches originate from the corresponding ipsilateral trunks, whereas the unpaired arteries originate from only one aorta [6, 7]. In only one of the four reported patients was the double dorsal aorta diagnosed *in vivo*. This patient had agenesis of the left kidney and multiple bony abnormalities [4]. In the other three patients, the aortic abnormality was an incidental finding at autopsy.

The explanation for the occurrence of the aberrant anatomy of the descending aorta is difficult. Obviously, as mentioned earlier, branch budding may occur from both dorsal aortae, but the opposite instead may be true: only one of the two original primitive trunks has the potential to supply bilateral branches for symmetric organs. In our patient, even the bronchial arteries represented the terminal arborization of the persistent left dorsal aorta. We wonder if it is possible that budding from one of the primitive dorsal aortae inexplicably was prevented, necessitating persistence of the other dorsal aorta supplying all the necessary branch vessels. Also, it is unclear why the common intercostal trunk, in the case of complete separation (not septation), originates below the diaphragm and ascends into the thorax, as in our patient and one other [4]. Most likely the persisting duplex dorsal aorta is an anomaly *per se* and is asymptomatic; it is not a complication, even for open-heart surgery with extracorporeal circulation, because the retrograde inflow of blood is not jeopardized.

Good contrast angiography will always show the double dorsal aorta: the parallel, vertical, second smaller trunk supplying the bilateral intercostal arteries is characteristic.

MR imaging may also contribute to the diagnosis (Fig. 1D). The persisting or accessory left dorsal aorta in our patient on the coronal MR images was interpreted originally as the azygous vein. In retrospect, however, the unmistakable features of the midline left aorta were present despite the small size. These characteristics include, specifically, its origin and progressive craniad tapering (the azygous vein should progressively increase in its caliber), the bilateral segmental origins of the intercostal arteries (the left-sided intercostal veins drain into the hemiazygous vein), and the terminal arborization (the azygous vein ends in the superior vena cava after passing over the right bronchus).

REFERENCES

1. Barry A. The aortic arch derivatives in the human adult. *Anat Rec* **1951**;111:221-238
2. Hamilton WJ, Mossman HW. *Human embryology: prenatal development of form and function*, 4th ed. Baltimore, MD: Williams & Wilkins, 1972: 261-264
3. Moore KL. *The developing human: clinically oriented embryology*. Philadelphia, PA: Saunders, 1988:291
4. Eibach VE, Walter E. Einseitige Nierenagenesie, kombiniert mit Aorta duplex persistens und Skeletanomalien. *ROFO* **1978**;129:386-387
5. Mosquera JE, Micarelli R. Aorta doble. *Rev Fac Cien Med Univ Nac Cordoba* **1975**;33:89-94
6. Trubnikov GV, Naimark DA, Nalobina MS, Kolomnec AY. A case of double aorta with renovascular hypertension. *Klin Med (Mosk)* [Rus] **1977**;55:138-141
7. Hristova M, Cenova V, Gegova A. A rare case with a double aorta descendens in an adult man. *Eksp Med Morfol [Bul]* **1985**;24:44-49

Book Review



Trauma of the Spine. CT and MRI. By B. Wimmer, E. Hofmann, and A. Jacob. New York: Springer-Verlag, 90 pp., 1990. \$89.50

This concise text is organized into three chapters. Chapter 1, "Basic Considerations," includes epidemiology and statistics, anatomy, biomechanical aspects and fracture classification, symptoms, and advantages and limitations of CT and MR studies. A description of "the motion segment" and 4.5 pages devoted to a discussion of fracture stability and classification are included. An excellent overview of the numerous classifications of fractures and the implications for stability is presented. The large number and complexity of the described classifications, however, lead the authors to state, "We therefore relinquish the idea of a classification of fractures of the lower cervical spine and limit ourselves to a statement as to stability." A summary of the authors' conclusions on the roles of imaging studies is included in this chapter.

In chapter 2, "Bone Injuries," the various regions of the cervical and thoracolumbar spine are considered. The mechanism of injury and the plain film and CT findings are discussed for each lesion. Most illustrations are CT scans, with some reformatted images, but plain films and MR images are included.

Chapter 3, "Injuries of the Intervertebral Disk and Neural Tissues," includes injuries to the disks, neural tissues, and meninges. MR images predominate, with additional CT scans and myelographic CT scans. Finally, the book ends with an appendix, which is actually one of the strengths of this text. It covers, in outline form, general principles of examination. Guidelines for the use of the various techniques, including functional evaluation and the sequence of examinations in elective, urgent, and life-threatening situations, are presented.

This book is short, only 90 pages and 72 illustrations, and this may be viewed as either an advantage or a disadvantage. Three-dimen-

sional CT scans are not included. As an overview, the text is exactly the right length, providing a quick reference with excellent, well-chosen illustrations. If more depth is necessary, 118 references are listed, several as recent as 1988.

As noted, the advantages of this text are its concise format and well-chosen illustrations and its coverage of the entire spine. The text is clearly written, without the difficulties in style that may occur when a book is written by authors for whom English is a second language. The large number of MR images is outstanding. Disadvantages include the lack of depth and the inability to include multiple illustrations of a particular condition. These can be provided in a longer text, such as the excellent book *The Radiology of Acute Cervical Spine Trauma* by Harris and Ediken-Monroe. That text is, however, limited to examination of the cervical spine. The textbook by Gehweiler, Osborne, and Becker, *The Radiology of Vertebral Trauma* covers the entire spine but lacks MR images and CT scans.

In summary, the brevity, clear style, good organization, and excellent-quality CT scans and MR images make *Trauma of the Spine* a good reference for the practicing clinician or resident in radiology, orthopedics, or neurosurgery. Additional consultation can be sought as necessary.

Barbara N. Weissman
Brigham and Women's Hospital
Harvard Medical School
Boston, MA 02115

Case Report

Primary Lymphoma of the CNS in an Infant with AIDS: Imaging Findings

P. Douek,¹ Y. Bertrand,² V. A. Tran-Minh,¹ J. D. Patet,³ G. Souillet,² and N. Philippe²

CNS lymphoma is a common complication of human immunodeficiency virus-1 (HIV-1) infection in adults, in whom more than 400 cases of AIDS-related non-Hodgkin lymphoma have been reported [1]. Only isolated cases of primary lymphoma occurring in children with HIV-1 infection and detected by CT have been reported [2, 3]. However, the World Health Organization estimates that during the past decade about 500,000 cases of AIDS occurred in women and children, and that during the 1990s AIDS will kill approximately 3 million women and children worldwide [4]. We report a case of CNS lymphoma in a 6-month-old infant with HIV-1 infection. The temporal lobe lesion was detected by transfontanellar sonography and diagnosed on the basis of CT-guided needle biopsy.

Case Report

A 6-month-old girl was admitted for fever and somnolence. Her mother was an IV drug user, and both the child and her mother were seropositive for HIV-1. Neurologic examination revealed axial rigidity and a mild right hemiparesis. The child had a normal head circumference of 40.5 cm and normal developmental milestones. Moderate hepatomegaly and maculopapular skin rash were noted. Findings on ophthalmoscopy were normal. Electroencephalography showed mild asymmetry between the right and left hemispheres. Cultures of CSF were negative for bacteria, fungi, and mycobacteria. Immunologic data showed reverse helper lymphocyte/suppressor lymphocyte ratio, hypergammaglobulinemia, positive P24 antigenemia, and a low level of anti-P24 antibodies. Serology was negative for Epstein-Barr virus.

Sonography showed a round hyperechoic mass in the left temporal lobe (Fig. 1A). The mass was isodense on unenhanced CT. After administration of contrast medium, the mass enhanced irregularly with a ringlike pattern, surrounded by an ill-defined hypodense region (Fig. 1B). Axial T1-weighted MR images showed the mass to have a poorly defined, low signal intensity (Fig. 1C). On coronal T2-weighted images (2000/120 [TR/TE]), the mass had a persistently low-signal core in a large area of highly intense signal (Fig. 1D). CT-guided needle biopsy of the temporal mass disclosed immunoblastic lymphoma of the brain. Chest radiography, abdominal sonography, and bone marrow biopsies showed no evidence of lymphoma apart from that in the CNS. The infant's clinical state improved under chemotherapy, but sonography, CT, and MR showed that the lymphoma did not regress completely. The infant died 2 months after initiation of therapy. The cause of death was believed to be AIDS-related encephalopathy. Autopsy was not performed.

Discussion

Primary CNS lymphoma is rare in immunocompetent children, but it has been diagnosed more frequently in immunocompromised persons [5]. It usually occurs in children infected with Epstein-Barr virus. In our case, serology for Epstein-Barr virus was negative.

Although CNS lymphoma has been seen in adults and older children, its presence in a 6-month-old child is unique. Sonography was the screening imaging technique used to examine this infant, who had neurologic symptoms. It showed a non-specific hyperechoic mass. Hemorrhage, abscess, and tumor

Received October 30, 1990; accepted after revision January 7, 1991.

¹ Department of Pediatric Radiology, UFR Lyon-Nord and Hôpital Debrousse, 29 rue Soeur Bouvier, F.69322 Lyon Cedex 05, France. Address reprint requests to V. A. Tran-Minh.

² Department of Hematology, Hôpital Debrousse, 29 rue Soeur Bouvier, F.69322 Lyon, France.

³ Department of Neurosurgery, Clinique Charcot, 51-53 rue Commandant Charcot, F.69110 Sainte Foy Les Lyon, France.

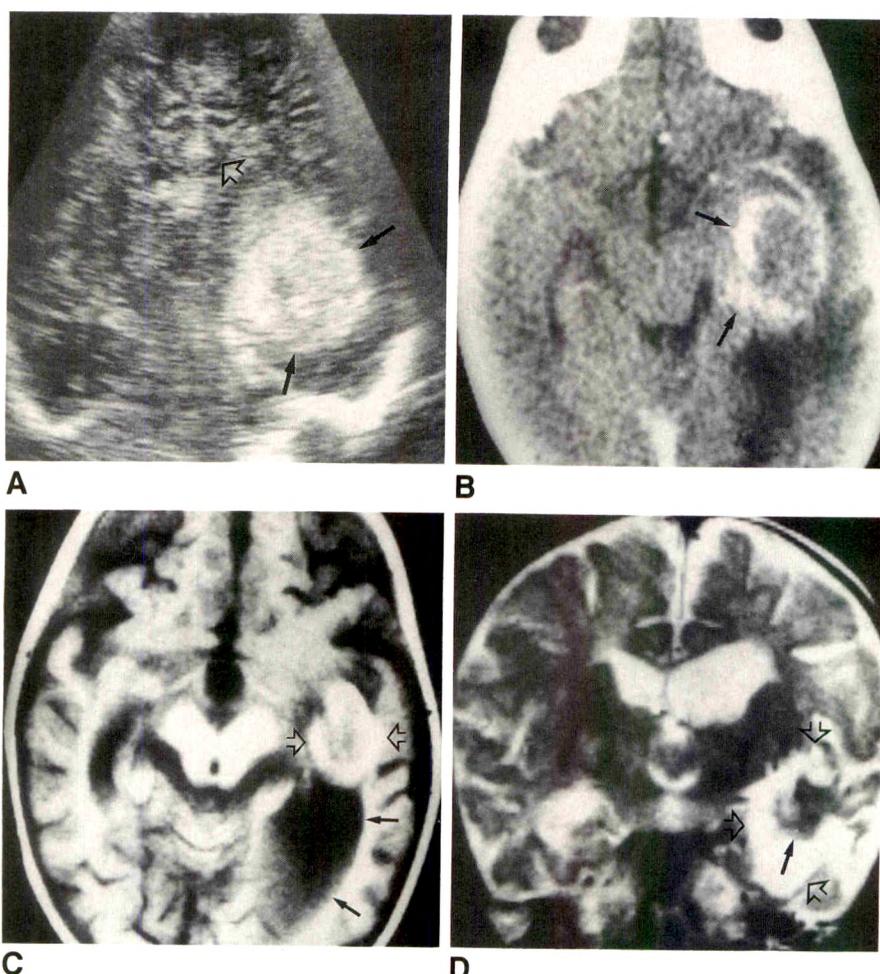


Fig. 1.—A, Coronal sonogram shows a hyper-echoic mass (solid arrows) displacing left lateral ventricle medially (open arrow).

B, CT scan obtained after contrast administration shows peripheral enhancement (arrows) of mass.

C, Axial T1-weighted (620/20) MR image shows mild dilatation of left occipital horn (solid arrow) behind mass (open arrows).

D, Coronal T2-weighted (2000/120) MR image through mass shows hypointense center (solid arrow) and hyperintense periphery (open arrows).

were considered. CT and MR also were nonspecific for lymphoma. In previous reports [6, 7], lymphoma, especially immunoblastic tumors, most often appears on CT as a hyperdense mass enhancing homogeneously after infusion of contrast medium. Less frequently, as in our case, lymphoma is isodense with a ring enhancement that simulates bacterial, fungal, or toxoplasmic abscess. Double-dose contrast CT with delayed scans may show additional lesions, because CNS lymphomas in adults with AIDS are typically multicentric. In our case, the tumor was isolated.

In CNS lymphoma, MR studies typically show a supratentorial periventricular mass that is isointense or hypointense on T1-weighted images. On T2-weighted images, the central tumor core is isointense or hypointense relative to adjacent edema. The signal intensity reflects the relative amount of edema and microscopic perivascular extension of tumor [8]. In our case, signal intensity was increased around the tumor, which had low signal on T2-weighted images. Other tumors occurring in childhood or adolescence, such as primitive neuroectodermal tumors, may have a similar appearance on MR.

In patients infected with HIV-1 or those who are seropositive for HIV, lymphoma is the most likely clinical diagnosis for a mass in the brain. On the other hand, toxoplasmosis is the most common cause of space-occupying lesions of the brain

in adults infected with HIV-1. Neither imaging technique is able to distinguish between lymphoma and brain abscess due to toxoplasmosis. Thus, CNS biopsy under CT guidance is useful before initiating chemotherapy, as was done in this patient.

REFERENCES

- Haskal ZJ, Lindan CE, Goodman PC. Lymphoma in the immunocompromised patient. *Radiol Clin North Am* 1990;28:885-899
- Epstein LG, Sharer LR, Oleske JM, et al. Neurologic manifestations of human immunodeficiency virus infection in children. *Pediatrics* 1986;78:678-686
- Epstein LG, Di Carlo FJ, Joshi VV, et al. Primary lymphoma of the central nervous system in children with acquired immunodeficiency syndrome. *Pediatrics* 1988;82:355-363
- Chin J. Current and future dimensions of the HIV/AIDS pandemic in women and children. *Lancet* 1990;336:221-224
- Belman AL, Diamond G, Dickson D, et al. Pediatric acquired immunodeficiency syndrome: neurologic syndromes. *Am J Dis Child* 1988;142:29-35
- Poon T, Matoso I, Tchertkoff V, Weitzner I, Gade M. CT features of primary cerebral lymphoma in AIDS and non-AIDS patients. *J Comput Assist Tomogr* 1989;13:6-9
- Jack CR, O'Neill BP, Banks PM, Reese DF. Central nervous system lymphoma: histologic types and CT appearance. *Radiology* 1988;167:211-215
- Zimmermann RA. Central nervous system lymphoma. *Radiol Clin North Am* 1990;28:697-721

Diagnosis of Cerebral Metastases: Double-Dose Delayed CT vs Contrast-Enhanced MR Imaging

Patricia C. Davis¹
 Patricia A. Hudgins
 Susan B. Peterman
 James C. Hoffman, Jr.

For patients suspected of having cerebral metastases, double-dose delayed CT (DDD-CT) has proved significantly more sensitive than CT scans obtained immediately after administration of a lesser dose of iodinated contrast material. Previous reports confirm the advantages of postcontrast MR imaging over contrast-enhanced CT, but data comparing DDD-CT and contrast-enhanced MR have not been reported. This study describes comparative imaging results in 23 patients who had contrast-enhanced MR imaging to clarify equivocal findings on DDD-CT studies. Contrast-enhanced MR demonstrated more than 67 definite or typical parenchymal metastases, T2-weighted MR revealed more than 40, while DDD-CT revealed only 37 typical metastatic lesions. Three patients had five or fewer lesions on DDD-CT and lesions "too numerous to count" on MR. The frequency of equivocal or unconvincing lesions was similar on DDD-CT (11) and contrast-enhanced MR (10). On T2-weighted images, we noted a substantially higher number of equivocal lesions (19), fewer definite metastases, and a number of definite metastases that had no corresponding lesion on the enhanced studies, confirming the inability of T2-weighted imaging to specifically identify cerebral metastases. In one case, multiple tiny lesions on T2-weighted images were not apparent on DDD-CT scans and were recognized only in retrospect on contrast-enhanced MR images.

In this series, MR with enhancement proved superior to DDD-CT for lesion detection, anatomic localization of lesions, and differentiation of solitary vs multiple lesions. Cost-benefit considerations precluded a comparison between the two techniques in all patients suspected of having cerebral metastases. Given the complexities of the cost of imaging procedures and the benefits of therapy, it is not possible to state that all patients suspected of having cerebral metastases should undergo contrast-enhanced MR imaging. At this time, given our protocol for evaluating metastatic disease, contrast-enhanced MR should be performed in patients with equivocal or solitary lesions on DDD-CT, particularly when surgical resection of a metastatic focus is considered.

AJNR 12:293-300, March/April 1991; AJR 156:1039-1046, May 1991

Cerebral metastases account for up to 40% of brain neoplasms in adults [1] and are identified in up to 5% of patients with fatal malignancies. Detection of these metastases has received much attention in recent years, particularly with the development of paramagnetic contrast agents, such as gadopentetate dimeglumine, for use with MR imaging. Many studies attest to the improved sensitivity and specificity of contrast-enhanced MR relative to routine contrast-enhanced CT and to unenhanced MR for a variety of CNS lesions, including both primary and metastatic neoplasms [2-10].

CT performed with a high dose of iodinated contrast (74-84.6 g l) and delayed scanning (double-dose delayed CT [DDD-CT]) significantly improves the sensitivity and specificity of cerebral metastatic disease detection [11-13]. In a study by Shalen et al. [11], delayed images afforded more information in 67% of cases; moreover, false-negative studies would have occurred in 11.5% of the patients if just a routine scan immediately after contrast administration had been obtained.

Earlier studies [2-10] comparing MR with contrast-enhanced CT for accuracy in

Received August 9, 1990; revision requested September 7, 1990; revision received October 15, 1990; accepted October 16, 1990.

¹ All authors: Department of Radiology, Division of Neuroradiology, Emory University School of Medicine, 1364 Clifton Rd., N.E., Atlanta, GA 30322. Address reprint requests to P. C. Davis.

0361-803X/91/156:1039-1046\$00.75
 © American Roentgen Ray Society

detecting cerebral metastases suggest a significant advantage of the MR technique; however, these studies generally compared immediate postcontrast CT scans with unenhanced or contrast-enhanced MR. As pointed out by Sze et al. [10], little is known of comparative sensitivity and specificity of DDD-CT vs contrast-enhanced MR. Since mid 1988, we have recommended confirmatory contrast-enhanced MR for all patients suspected of having cerebral metastasis who have had equivocal or solitary lesions on DDD-CT. Comparative findings from 23 patients who underwent both examinations within a short period of time form the basis of this report.

Materials and Methods

From September 1988 until December 1989, 22 patients underwent contrast-enhanced MR imaging for follow-up of DDD-CT studies considered equivocal for presence, number, and/or anatomic definition of cerebral metastasis. One additional study was performed earlier during the phase 3 FDA trials for gadopentetate dimeglumine. The group included 11 men and 12 women ranging in age from 34 to 72 years (mean, 55.9 years). Primary malignancies included lung (nine), breast (five), unknown (four), renal (two), melanoma (two), and plasma cell myeloma (one).

After obtaining informed consent, cerebral CT was performed in all patients suspected of having cerebral metastatic disease by using a bolus of 200 ml of iodinated contrast (diatrizoate dimeglumine and diatrizoate sodium; Angiovist-370 [Berlex, Wayne, NJ] or Hypaque 76 [Winthrop, Des Plaines, IL]; 74 g organically bound iodine) followed by a 1-hr delay before scanning. No patient had significant adverse sequelae after contrast administration, although patients who failed to receive a full contrast dose or who did not complete the DDD-CT protocol because of motion, instability, renal compromise, history of allergic reaction, or allergic reaction were excluded from this study. Twenty-one CT scans were acquired in the axial plane with 5-mm collimation in the posterior fossa and 10-mm collimation to the vertex (Philips LX or TX-60 [Shelton, CT], GE 9800 HiLite [Milwaukee, WI], or Picker Synerview 1200SX [Highland Heights, OH]). Two scans were obtained with sequential 7-mm collimation (Technicare 2010, Solon, OH). Scan angles varied from 0–15° relative to Reid's base line. All studies were photographed on soft-tissue and bone windows.

A follow-up postcontrast MR examination was recommended for any patient with equivocal or atypical lesions on DDD-CT scans, for patients with a solitary lesion who might be candidates for neurosurgical resection, and for patients with lesions that were equivocal or inadequately defined for confident therapeutic planning in the opinion of our referring physicians. Contrast-enhanced MR examinations were performed at a mean time of 9.3 days after the DDD-CT study (range, 0–43 days). Scans were obtained with a variety of magnets and field strengths (0.5 T, 12 cases, Philips [Shelton, CT]; 1.0 T, two cases, Siemens [Erlangen, Germany]; or 1.5 T, nine cases, Philips [Shelton, CT]), beginning with a multislice noncontrast T1-weighted scout sagittal sequence (TR </= 600, TE </= 30). After obtaining informed consent, gadopentetate dimeglumine was administered intravenously in a dose of 0.1 mmol/kg over 1–2 min. T2-weighted axial scans with 6–10-mm slice thickness were obtained first after contrast administration (1699–3700, 25–50, and 90–100/1–2) (TR/TE/excitations) followed by one or more T1-weighted postcontrast sequences (433–800, 15–30/1–2) using 4–10-mm slice thickness. Postcontrast sequences were delayed 14 min or more after contrast administration in 20 of the 23 patients. The mean delay between contrast administration and the last T1-weighted sequence was 22

min (range, 4–60 min). The MR imaging protocol used in this study is given in Table 1. In one patient, no T2 sequence was acquired owing to limited scanning time available; one MR study was suboptimal because of patient motion; one patient had additional sequences based on the phase 3 FDA investigation protocol for Magnevist; and one patient's first postcontrast T1-weighted scan was erroneously obtained with a TE of 50.

To reduce the possibility of bias in interpreting the scans, a retrospective blinded evaluation of the studies was made by at least two experienced neuroradiologists. These physicians were aware that the patients were thought to have cerebral metastases, but they were otherwise blinded to clinical findings and follow-up studies. Three groups of studies (DDD-CT, T2-weighted MR, and T1-weighted pre- and postcontrast MR) were presented to the observers in random order as independent examinations over several months and remote from the time of actual scan acquisition and interpretation. Two or three evaluators recorded by consensus the presence, number, and location of typical or convincing (definite) intraparenchymal metastatic lesions (supra- vs infratentorial); dural or meningeal metastases; bone metastases; equivocal lesions; and other abnormalities present (infarct, surgical sites). More than seven lesions in a given distribution were rated as too numerous to count. Patient follow-up included review of radiologic studies for evidence of disease progression and clinical status on last examination.

Results

A comparison of metastatic lesions detected on DDD-CT, T2-weighted MR, and pre- and postcontrast MR examinations is charted in Table 2. Two patients had one or more hemorrhagic or melanotic lesions, diagnosed on the basis of high signal intensity on T1-weighted MR images or marked hypointensity typical of hemoglobin breakdown products on T2-weighted images.

Contrast-enhanced MR revealed additional intraparenchymal lesions as compared with DDD-CT in nine of 23 patients (Fig. 1). In only one patient were metastases seen best on T2-weighted images, and they were recognized only in retrospect on contrast MR studies (Fig. 2). These multiple tiny foci were recognizable but subtly hypointense on noncontrast T1-weighted images at 0.5 T, and paramagnetic contrast enhancement rendered them nearly isointense with normal parenchyma on enhanced T1-weighted images. Of 11 patients with only one definite or one suspicious lesion on DDD-CT, one had dural disease only on MR, four had two or more

TABLE 1: MR Protocol for Suspected Cerebral Metastases

1. Obtain informed consent for paramagnetic contrast administration.
2. Start intravenous line with long tubing.
3. Position patient in magnet.
4. Obtain scout multislice T1-weighted sagittal image.
5. Obtain precontrast axial T1-weighted sequence *only* if hemorrhage is suspected.
6. Administer contrast and flush intravenous tubing.
7. Obtain axial T2-weighted sequence, 6 mm or less slice thickness, minimum interslice gap.
8. Obtain postcontrast axial T1-weighted sequence, minimum TE </= 30, TR < 800, slice thickness </= 6 mm.
9. If #8 reveals two or more typical metastases, stop scanning. Continue T1 scans to 20–30 min after contrast injection if one or no lesions are detected on first T1 contrast-MR sequence. If needed, use other imaging planes and T1 sequences to better demonstrate lesions anatomically.

TABLE 2: Comparative No. of Lesions Detected in 23 Patients: Double-Dose Delayed CT, Contrast-Enhanced MR, and T2-Weighted MR^a

	Double-Dose Delayed CT	Contrast-Enhanced MR	T2-Weighted MR
Supratentorial intraaxial metastases	27	35 ^b	17
Infratentorial intraaxial metastases	10	26 ^b	14 ^c
Total intraaxial metastases	37	61 ^b	31 ^c
Equivocal intraaxial metastases	11	10	19
Meningeal/dural metastases	0	3	2
Bone lesions (no. of patients)	3	3	3

^a One MR study was significantly degraded by motion, and in one patient no T2 sequence was performed.

^b Three patients had numerous (more than seven) lesions on contrast-enhanced MR that were not apparent on double-dose delayed CT and that were underestimated on T2-weighted MR. Of these, one had numerous lesions both supra- and infratentorially. One patient had multiple contiguous lesions on MR and only one lesion on double-dose delayed CT.

^c One patient had numerous infratentorial lesions on T2-weighted MR that were recognizable only in retrospect on contrast-enhanced MR; only one infratentorial lesion was detected on double-dose delayed CT.

typical metastases on contrast MR, and two had equivocal findings on both DDD-CT and contrast MR. One solitary lesion was mislocalized as intraparenchymal on DDD-CT, but was clearly an extraaxial dural and bone-based lesion on MR. One patient had two typical metastases on DDD-CT and only one lesion on contrast MR. In this patient, enhanced T1-weighted images were erroneously obtained with a prolonged echo time (500/50; 0.5 T). Repeat T1-weighted images, acquired after the error was recognized (60 min after contrast administration) failed to reveal additional lesions. In no other patient were more metastases found by DDD-CT than by enhanced T1- and T2-weighted MR.

Three patients with five or fewer lesions on DDD-CT had lesions too numerous to count on contrast MR. Two patients had lesions in the basal ganglia, which on DDD-CT mimicked calcification rather than metastasis (Fig. 1). Although the possibility of an enhancing lacunar infarction could not be entirely excluded, patient age, coexisting metastases, and absence of clinical findings to support infarction suggested that these were metastases.

Lesions in the posterior fossa were generally much better localized and characterized on MR than on CT (Fig. 3), and MR was particularly advantageous in differentiating intraparenchymal from dural/meningeal lesions. One patient with melanoma had a solitary expansile clival mass that was surgically proved to be chordoma rather than metastasis. In one case, metastasis could not be confidently diagnosed on MR or on CT, and follow-up studies with clinical correlation suggested that the lesions represented subacute infarction rather than metastasis.

T2-weighted images were more sensitive than DDD-CT for detecting infratentorial lesions, but less sensitive than DDD-CT for detecting supratentorial metastases. In part, this stemmed from the difficulty in accurately characterizing lesions on T2-weighted images, since raters noted many more equivocal lesions on T2-weighted images (19 lesions) than on

either contrast MR (10 lesions) or DDD-CT studies (11 lesions). Slightly more definite metastases were noted on T2-weighted images than on DDD-CT (40 vs 37), and only the one patient with multiple tiny posterior fossa metastases had definite metastases on T2-weighted images that were not initially recognized as metastases on contrast-enhanced MR and/or DDD-CT.

Because tissue confirmation was not available for all lesions, a gold standard for comparing sensitivity and specificity of DDD-CT with MR on a lesion by lesion basis was not possible. Follow-up studies demonstrating disease progression in a majority of our patients in spite of radiation and/or chemotherapy, however, suggest that the additional lesions detected on MR probably represented metastases. Follow-up evaluations as of July 1990 indicated persistent or progressive brain metastases in one, systemic metastases in four, clinical and/or radiologic evidence of multisystem metastases in four, and death attributed to progressive metastatic disease in 10. One patient was lost to follow-up after surgical resection of a solitary metastasis. One patient with definite metastases on MR and DDD-CT and CT-guided biopsy suggestive of multiple sclerosis, and one patient with lung carcinoma and equivocal lesions on both DDD-CT and MR examinations was presumed to have infarction rather than metastasis. One patient with definite metastasis from melanoma on all studies had a secondary primary tumor (chordoma) rather than metastasis.

Discussion

Primary malignancies implicated in cerebral metastases in descending order of frequency are lung, breast, melanoma, renal, stomach, prostate, and thyroid [1], with sarcoma, lymphoma, and leukemia found increasingly in patients with immune disorders. Leptomeningeal metastases tend to occur in primary hematologic malignancies, such as lymphoma or leukemia; in children with a variety of CNS primary tumors; or in common adult malignancies, such as breast or lung carcinoma. Multiplicity of lesions is helpful for suggesting metastatic disease, although other diseases must be considered, particularly in patients with immune compromise. Multiple cerebral metastases generally are treated with radiation therapy, perhaps with chemotherapy, while solitary lesions diagnosed on the basis of contrast-enhanced CT studies may be surgically resected [14]. A recent study by Patchell et al. [15] found an increased time of survival and an improved quality of life in patients with surgically resected solitary metastasis as compared with those receiving radiation therapy after biopsy alone. Eleven percent of patients presumed preoperatively to have a solitary metastasis on the basis of CT, low-field-strength MR, and clinical findings had other neoplastic or inflammatory/infectious disease at surgery [15].

The ideal imaging study for suspected metastases requires sensitivity to lesion detection; anatomic resolution for surgical planning; ability to differentiate metastasis from other diseases; sensitivity to coexisting diseases; minimal invasiveness; and acceptable safety/toxicity, availability, examination time, and cost. Prior to the development of MR contrast agents, contrast-enhanced CT or DDD-CT were the proce-

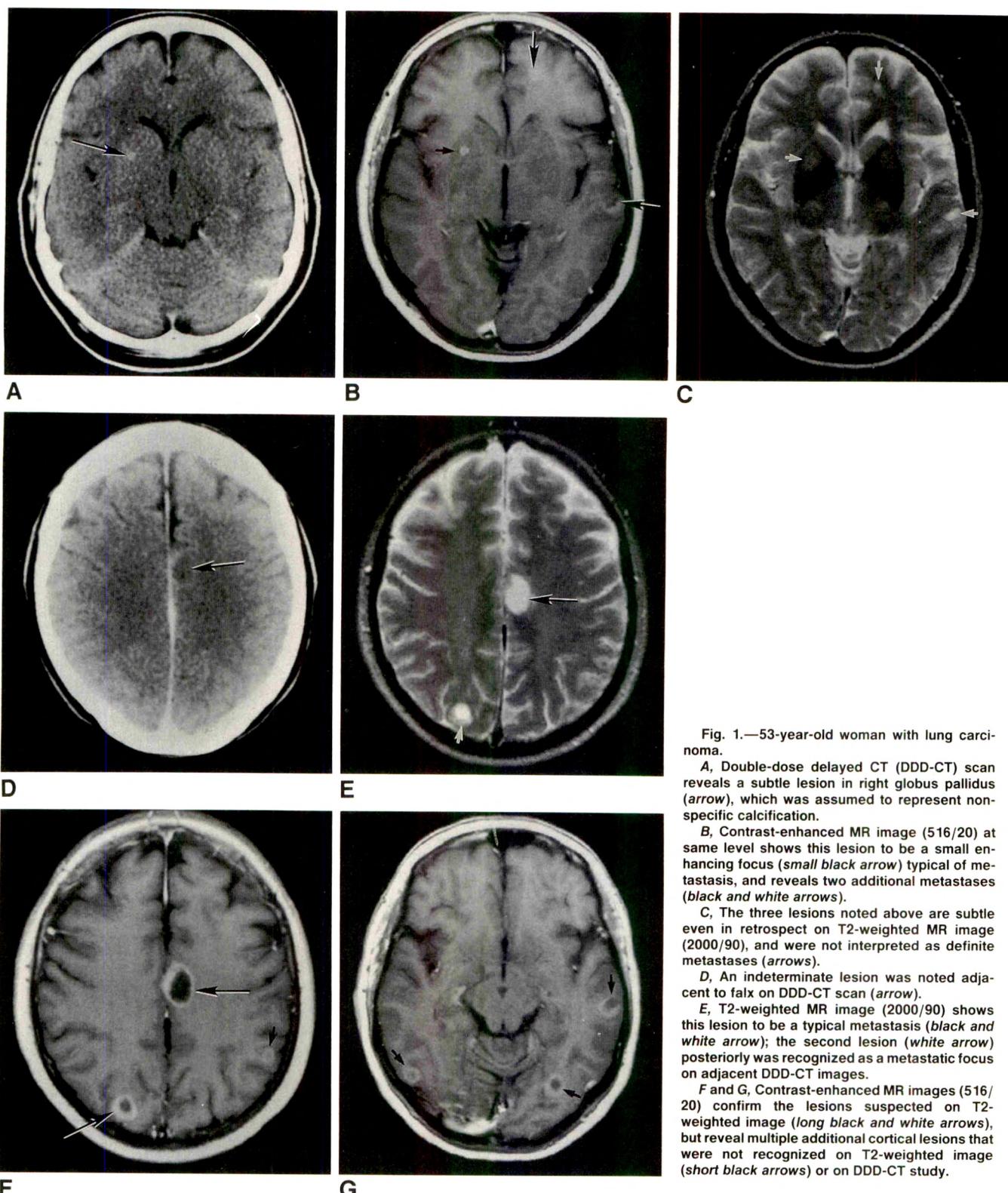


Fig. 1.—53-year-old woman with lung carcinoma.

A, Double-dose delayed CT (DDD-CT) scan reveals a subtle lesion in right globus pallidus (arrow), which was assumed to represent non-specific calcification.

B, Contrast-enhanced MR image (516/20) at same level shows this lesion to be a small enhancing focus (small black arrow) typical of metastasis, and reveals two additional metastases (black and white arrows).

C, The three lesions noted above are subtle even in retrospect on T2-weighted MR image (2000/90), and were not interpreted as definite metastases (arrows).

D, An indeterminate lesion was noted adjacent to falx on DDD-CT scan (arrow).

E, T2-weighted MR image (2000/90) shows this lesion to be a typical metastasis (black and white arrow); the second lesion (white arrow) posteriorly was recognized as a metastatic focus on adjacent DDD-CT images.

F and **G**, Contrast-enhanced MR images (516/20) confirm the lesions suspected on T2-weighted image (long black and white arrows), but reveal multiple additional cortical lesions that were not recognized on T2-weighted image (short black arrows) or on DDD-CT study.

dures of choice for demonstration and localization of cerebral metastases. CT is widely available, often less expensive than MR, more sensitive to acute hemorrhage and bone abnormalities, and can be performed in obtunded, unstable, or uncooperative patients [16].

Shalen et al. [11] found that a high-dose infusion of contrast followed by delayed CT imaging increased sensitivity for detecting metastases by as much as 67% as compared with immediate CT scanning [11]. If diagnosis had been based solely on the findings of CT performed immediately after

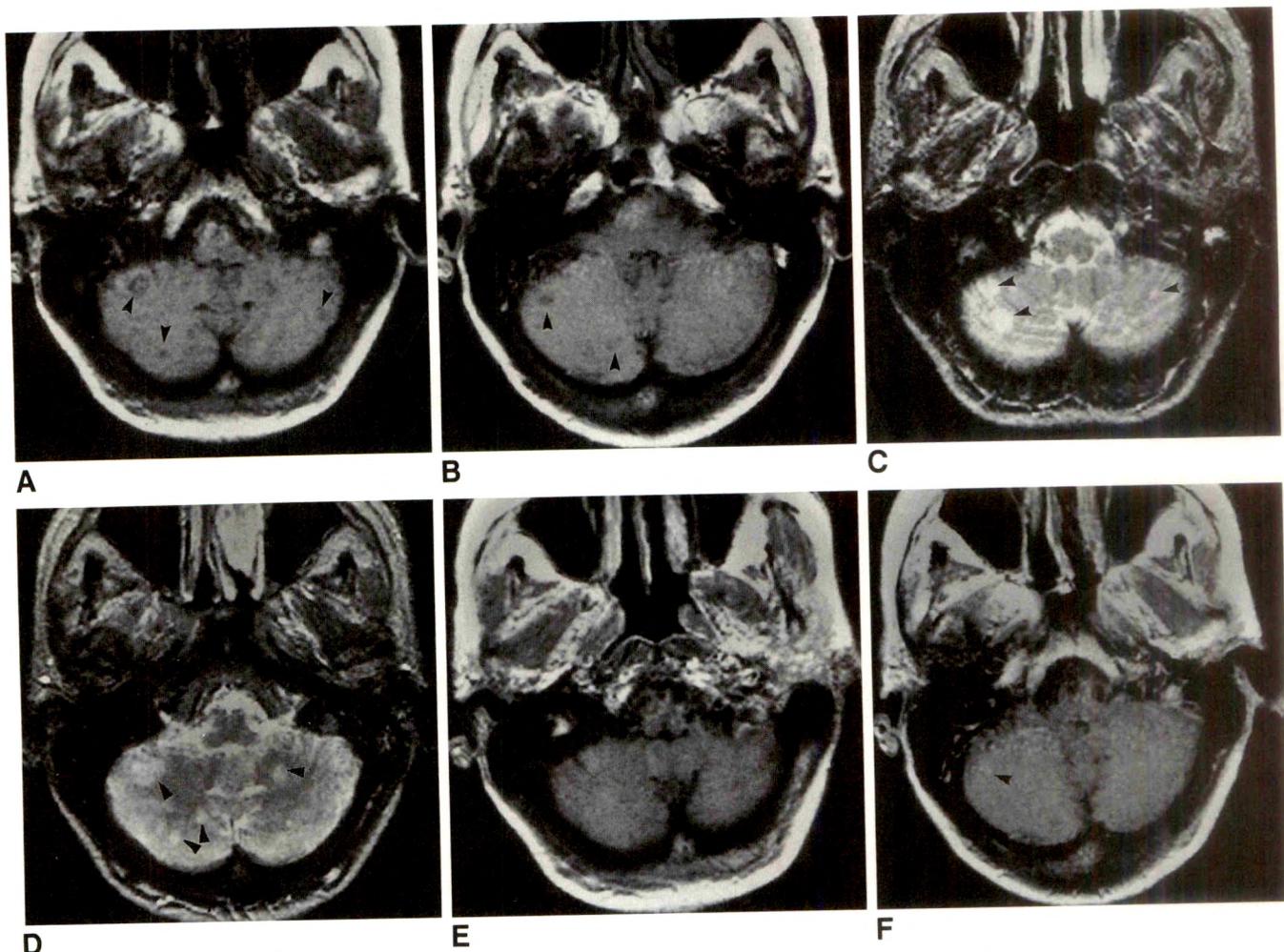


Fig. 2.—63-year-old woman with multiple infratentorial metastases, best seen on T2-weighted MR images. Double-dose delayed CT (DDD-CT) scan was interpreted as showing one definite posterior fossa mass.

A and B, Precontrast axial T1-weighted MR image (500/20) at 0.5 T faintly reveals multiple subtle hypointense foci in both cerebellar hemispheres (arrowheads).

C and D, Multiple hyperintense foci (arrowheads) are recognizable on T2-weighted MR images (2300/90).

E and F, After contrast administration, multifocal lesions enhance to approximate isointensity with normal parenchyma. Only one definite lesion (arrow in *F*) was recognized on these postcontrast T1-weighted MR images (500/20).

contrast administration, 11.5% of the studies would have shown false-negative results [11]. At our institution, DDD-CT has been the routine CT technique for patients thought to have cerebral metastases, particularly since many of our patients receive a relatively high dose of contrast anyway in conjunction with staging or follow-up studies of the chest, abdomen, and/or pelvis. Delayed contrast-enhanced CT can be completed after other metastatic survey examinations without additional appointments or additional contrast injections, although drawbacks include the high dose of iodinated contrast required, the toxicity and anaphylaxis associated with iodinated contrast, ionizing radiation, interference from Hounsfield artifact, and insensitivity for leptomeningeal metastases [17]. Prior studies have suggested that both a high contrast dose (74–80 g I) [11–13] and delayed scanning are important for disease detection. Although substitution of nonionic for ionic contrast agents might result in reduced renal toxicity or allergic reactions, use of nonionic contrast agents

produces a substantial increase in the cost of DDD-CT examinations.

Studies of contrast-enhanced MR for diagnosing cerebral metastases to date have largely been in comparison with routine contrast-enhanced CT [5, 7, 8, 10]. Comparative data on DDD-CT vs contrast-enhanced MR are needed in order to choose the optimum imaging method. Compared with CT, MR is often more expensive, not as widely available, relatively slow, less sensitive for detecting acute hemorrhage, particularly at lower field strengths, and less easily scheduled or combined with other staging imaging studies. Although early noncontrast MR studies were promising for hemorrhagic or melanin-containing lesions [18, 19], noncontrast MR was insensitive for detection of leptomeningeal disease, lesions adjacent to CSF interfaces, small lesions without associated hemorrhage or edema, or acute hemorrhage; they also lacked specificity, with many entities having similar MR intensities on T2-weighted images [8, 9, 20–22].

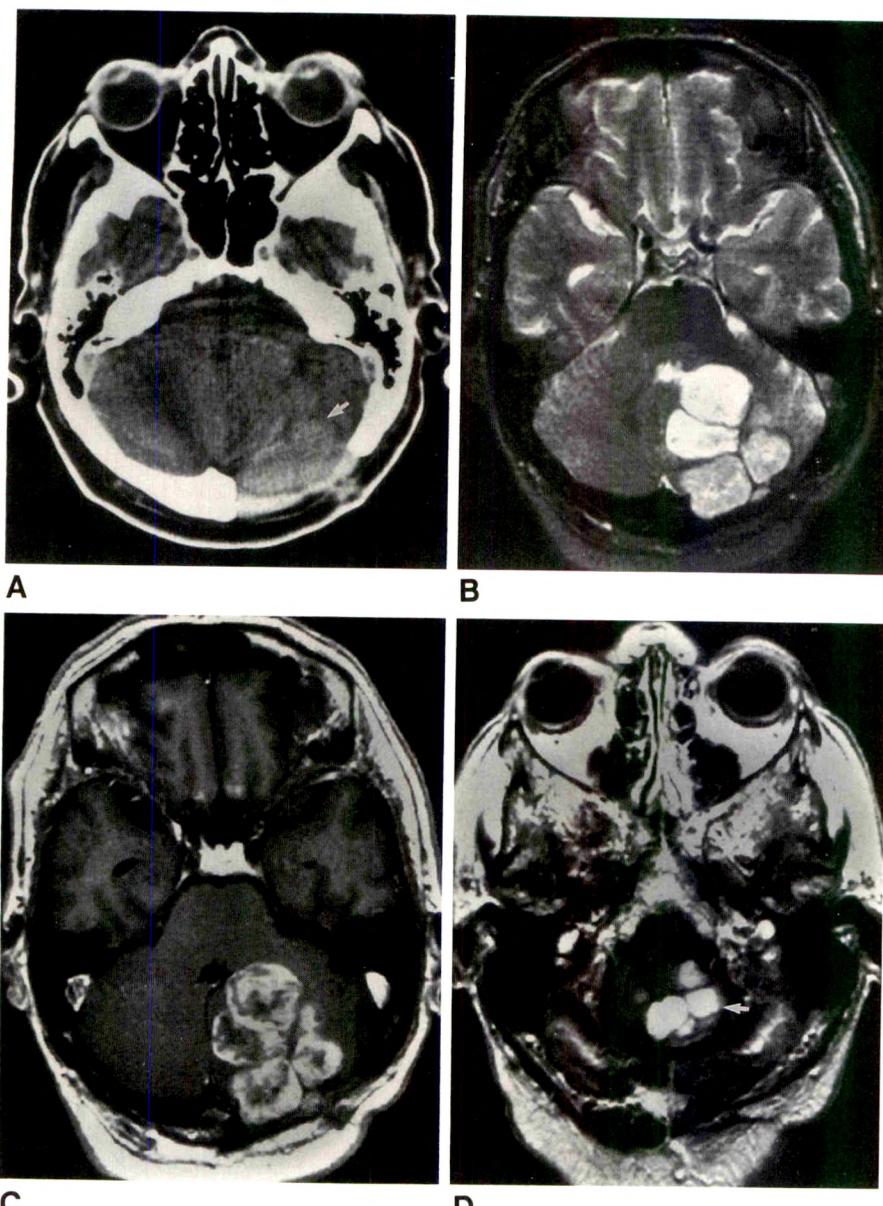


Fig. 3.—A recurrence of metastasis from an unknown primary tumor in the posterior fossa in a patient with prior surgical resection is best seen by MR imaging.

A, Double-dose delayed CT (DDD-CT) scan shows poorly enhancing mass at surgical site (arrow).

B, This extensive lesion is much better demarcated from normal parenchyma on T2-weighted MR image (2180/90).
C and **D**, This multifocal and/or multilobular mass enhances markedly (**C**) and extends to foramen magnum (**D**) (arrow) on T1-weighted MR studies (566/20).

Paramagnetic contrast agents have resulted in improved MR sensitivity in detecting metastases [4, 5, 7, 8]. The results of the present study of patients with equivocal or solitary lesions on DDD-CT indicate that contrast-enhanced MR is substantially more sensitive than DDD-CT for lesion detection and localization of cerebral metastatic disease. On the other hand, 21 patients had at least one definite lesion on both DDD-CT and contrast-enhanced MR, suggesting similar sensitivity for overall disease detection. The high percentage of patients with definite metastasis on DDD-CT by retrospective interpretation suggests a study bias in favor of this technique, since the DDD-CT interpretations were in doubt at the time of the actual examination and prompted the referral for MR. Alternatively, use of contrast-enhanced MR to clarify equivocal DDD-CT findings may introduce a bias in favor of that technique.

The improved lesion detection by contrast MR held true in this series not only for studies performed with high-field-strength magnets and short echo times but also for lower-field-strength magnets (0.5 T) with relatively long echo times (TE = 30) and resultant reduced sensitivity to T1 shortening from paramagnetic contrast enhancement and greater flow-related artifacts [5, 23]. Contrast MR permitted superior detection of lesions near dense bone either cortically or in the posterior fossa, and provided confident identification of metastatic lesions in unusual locations (basal ganglia). In patients under consideration for neurosurgical resection, the superior anatomic definition and multiplanar demonstration of lesions was useful for surgical planning.

Studies performed in accordance with our scanning protocol (Table 1) were more sensitive than the DDD-CT studies and could be completed efficiently within an acceptable scan

time. Only one scan was sufficiently degraded by motion as to be unacceptable in spite of a study population with varying degrees of neurologic impairment, although this high percentage of acceptable MR studies may be skewed by the possibility that obviously uncooperative or impaired patients were screened out. Several approaches can be taken to increase the likelihood of obtaining a successful MR study in this population. A complete noncontrast T1-weighted axial scan can often be omitted unless a specific question of hemorrhage vs metastasis is clinically important. The occasional problem in differentiating hemorrhage from enhancement can generally be resolved on the T2-weighted image [10]. Other options include a repeat noncontrast T1-weighted scan at a later date, a noncontrast CT to exclude acute hemorrhage, or a very delayed T1-weighted scan (i.e., several hours after contrast administration), assuming that T1 shortening from enhancement may in some cases diminish while hemorrhage would be stable over a period of several hours [6, 8]. Higher field strength magnets, flow compensation, and improved technology in general result in improved images in less time per MR sequence. Thus MR degradation by motion of uncooperative or unstable patients is reduced. On one hand, studies to date have suggested that a brief delay after contrast enhancement is important for optimal lesion detection [6, 8, 10]; thus, the primary effect of faster MR sequences might be reduced motion rather than a shortened MR examination time. On the other hand, the increased signal-to-noise ratio and shorter echo times with technological improvements in scanning might lessen the advantages of delayed postcontrast images described with earlier-generation MR technology [6, 8].

An efficient MR scanning protocol is important for patient tolerance, motion reduction, and scan time, with potential reductions in examination cost. T2-weighted imaging after contrast administration and elimination of a routine precontrast T1-weighted axial sequence permit a total scan time of about 20–30 min without significant loss of information or degradation of T2-weighted images. Higher doses of gadopentetate dimeglumine may prove advantageous for detection of subtle lesions, although this requires further evaluation of cost-effectiveness and toxicity ([24] and Haustein et al., paper presented at the annual meeting of the Society of Magnetic Resonance in Medicine, New York, August 1990). We agree with previous investigators that the T2-weighted sequence should routinely be a part of the MR examination for suspected metastases [7–10]. It serves as an important complementary sequence for recognition of other lesions (infarct, sequelae of therapy, and vasogenic edema), and rarely demonstrates subtle lesions that might be overlooked otherwise. Earlier investigators have not identified clinically significant degradation of T2-weighted images attributable to gadopentetate dimeglumine given in pharmacological doses [2, 4, 6]. If noticeable T2 shortening due to marked paramagnetic contrast enhancement did occur, this might result in improved definition of the metastatic focus apart from high signal intensity of adjacent vasogenic edema. In the uncommon event that a lesion is rendered isointense with normal parenchyma by T2 shortening, the surrounding abnormal signal from edema on proton-density or T2-weighted images and/or en-

hancement on T1-weighted images should be sufficient to avoid overlooking the lesion [8].

Although our study includes only patients with equivocal findings on DDD-CT, the implications of our results require careful consideration. Our study does not address the role of contrast MR in the patient with an unequivocally normal DDD-CT; in this population the diagnostic yield of contrast MR might be lower, particularly in centers performing extensive routine screening or frequent follow-up studies. Those patients with no lesions on either examination, those with multiple lesions on both examinations, and those with one lesion on DDD-CT who are not candidates for surgical resection could be adequately assessed with either technique. Although contrast MR in this study proved helpful for confirming the number and location of lesions, this additional information may prove essential for only a limited patient population; that is, candidates for surgical resection. The advantage of detecting additional lesions in the neurosurgical candidate is controversial, since the data supporting surgical resection is based on contrast CT and low-field-strength MR findings of a solitary lesion [15]. Whether detection of additional lesions on MR that are undetected on contrast-enhanced CT predicts reduced survival or results in better patient selection for surgical resection requires further study.

Clinical settings in which DDD-CT may be preferable to contrast-enhanced MR include the patient with acutely altered mental status in order to optimize sensitivity to acute hemorrhage (noncontrast) and minimize motion and scanning time; patients having follow-up studies for known multiple metastases; patients with contraindications to MR or to paramagnetic contrast; and patients who primarily have bone metastases. Although few leptomeningeal/dural and/or bone lesions occurred in this study, other reports suggest advantages of contrast MR for leptomeningeal disease, and limitations of contrast MR compared with noncontrast MR for detecting bone lesions [25]. CT or radionuclide bone scan are the preferable imaging techniques to establish the presence and location of bone metastases, although MR with and without contrast with fat suppression may prove equivalent or superior for anatomic detail (Dillon et al., paper presented at the annual meeting of the American Society of Neuroradiology, Los Angeles, March 1990).

We conclude that contrast-enhanced MR is substantially more sensitive than DDD-CT for detection of cerebral metastases in patients with equivocal DDD-CT examinations. Post-contrast T2-weighted images followed by delayed T1-weighted images are a reasonable compromise to achieve more efficient and shorter MR scan times. Contrast MR demonstrated additional lesions in 37% of patients who had solitary or equivocal lesions on DDD-CT; thus, contrast MR may prove important in the selection of patients for surgical resection. This technique also provided superior anatomic localization and demonstrated both supra- and infratentorial lesions that were not shown on DDD-CT images. In patients with equivocal DDD-CT findings for cerebral metastases, contrast-enhanced MR is superior to DDD-CT for lesion detection; however, the ultimate significance of this improved sensitivity requires further study to elucidate its impact on the choice of treatment method, the patient's quality of life and

rate of survival, and the economic ramifications of greater use of MR imaging.

ACKNOWLEDGMENTS

The authors acknowledge the assistance of Francine Hollowell, Sandy Sullivan, and photographers Roz Vecchio and Jack Kearse in the preparation of this manuscript.

REFERENCES

- Russell DJ, Rubinstein LJ. Secondary tumors of the nervous system. In: *Pathology of tumors of the nervous system*, 5th ed., Baltimore: Williams & Wilkins, 1989:825-841
- Carr DH, Brown J, Bydder GM, et al. Gadolinium-DTPA as a contrast agent in MRI: initial clinical experience in 20 patients. *AJR* 1984;143:215-224
- Runge VM, Schorner W, Niendorf HP, et al. Initial clinical evaluation of gadolinium DTPA for contrast-enhanced magnetic resonance imaging. *Magn Reson Imaging* 1985;3:27-35
- Niendorf HP, Laniado M, Semmler W, Schorner W, Felix R. Dose administration of gadolinium-DTPA in MR imaging of intracranial tumors. *AJNR* 1987;8:803-815
- Claussen C, Laniado M, Schorner W, et al. Gadolinium-DTPA in MR imaging of glioblastomas and intracranial metastases. *AJNR* 1985;6:669-674
- Schorner W, Laniado M, Niendorf HP, Schubert C, Felix R. Time-dependent changes in image contrast in brain tumors after gadolinium-DTPA. *AJNR* 1986;7:1013-1020
- Healey ME, Hesselink JR, Press GA, Middleton MS. Increased detection of intracranial metastases with intravenous Gd-DTPA. *Radiology* 1987;165:619-624
- Russell EJ, Geremia GK, Johnson CE, et al. Multiple cerebral metastases: detectability with Gd-DTPA-enhanced MR imaging. *Radiology* 1987;165:609-617
- Sze G, Shin J, Drol G, Johnson C, Liu D, Deck MDF. Intraparenchymal brain metastases: MR imaging versus contrast-enhanced CT. *Radiology* 1988;168:187-194
- Sze G, Milano E, Johnson C, Heier L. Detection of brain metastases: comparison of contrast-enhanced MR with unenhanced MR and enhanced CT. *AJNR* 1990;11:785-791
- Shalen PR, Hayman LA, Wallace S, Handel SF. Protocol for delayed contrast enhancement in computed tomography of cerebral neoplasia. *Radiology* 1981;139:397-401
- Hayman LA, Evans RA, Hinck VC. Delayed high iodine dose contrast computed tomography. *Radiology* 1980;136:677-684
- Davis JM, Davis KR, Newhouse J, Pfister RC. Expanded high iodine dose in computed cranial tomography: a preliminary report. *Radiology* 1979;131:373-380
- Posner JB. Surgery for metastases to the brain. *N Engl J Med* 1990;322:544-545
- Patchell RA, Tibbs PA, Walsh JW, et al. A randomized trial of surgery in the treatment of single metastases to the brain. *N Engl J Med* 1990;322:494-500
- Zimmerman RD, Heier LA, Snow RB, Liu DPC, Kelly AB, Deck MDF. Acute intracranial hemorrhage: intensity changes on sequential MR scans at 0.5 T. *AJNR* 1988;9:47-57
- Lee YY, Glass JP, Geoffray A, Wallace S. Cranial computed tomographic abnormalities in leptomeningeal metastasis. *AJNR* 1984;5:559-563
- Woodruff WW, Djang WT, McLendon RE, Heinz ER, Voorhees DR. Intracerebral malignant melanoma: high-field-strength MR imaging. *Radiology* 1987;165:209-213
- Atlas SW, Grossman RI, Gomori JM, et al. Imaging of intracranial metastatic melanoma. *J Comput Assist Tomogr* 1987;11:577-582
- Davis PC, Friedman NC, Fry SM, Malko JA, Hoffman JC, Braun IF. Leptomeningeal metastasis: MR imaging. *Radiology* 1987;163:449-454
- Gomori JM, Grossman RI, Goldberg HI, Zimmerman RA, Bilaniuk LT. Intracranial hematomas: imaging by high field MR. *Radiology* 1985;157:87-93
- Kondziolka D, Bernstein M, Resch L, et al. Significance of hemorrhage into brain tumors: clinicopathological study. *J Neurosurg* 1987;67:852-857
- Richardson DN, Elster AD, Williams DW III. Gd-DTPA-enhanced MR images: accentuation of vascular pulsation artifacts and correction by using gradient-moment nulling (MAST). *AJNR* 1990;11:209-210
- Goldstein H, Kashanian FK, Blumetti RF, Holyoak WL, Hugo FP, Blumenfeld DM. Safety assessment of gadopentetate dimeglumine in U.S. clinical trials. *Radiology* 1990;174:17-24
- West MS, Russell EJ, Breit R, Sze G, Kim KS. Calvarial and skull base metastases: comparison of nonenhanced and Gd-DTPA-enhanced MR images. *Radiology* 1990;174:85-91

Pictorial Essay

Tubes in the Alimentary and Respiratory Tracts: Appearances on CT Scans of the Head and Neck

Donald B. Price¹

The purpose of this essay is to illustrate the appearances of various tubes in the nose, mouth, esophagus, and trachea on CT scans of the head and neck.

A large variety of tubes are present in the upper aerodigestive passages in many patients undergoing CT scanning of the head and neck. Intubation of the trachea via a tracheostomy or oral or nasal routes is used for ventilation and to protect the airway from aspiration. Esophageal intubation, usually via the nose, is done for feeding or suctioning.

Familiarity with the various appearances of these tubes on CT scans is important to avoid confusion and to identify potential clinical problems. Appreciation of the normal course and appearance of aerodigestive tubes is necessary in order to identify an aberrant course, such as accidental esophageal placement of a tracheal tube or tracheal placement of a feeding tube. Abnormal air collections must also be recognized to detect injuries resulting from traumatic tube placement. The CT scans must be viewed at both narrow and wide window settings, and digital scout radiographs should be scrutinized.

The CT density of the walls of most nasogastric and tracheal tubes is around -200 H, and thus they are less dense than soft tissues. The radiopaque stripes in many of the tubes measure +2000 to +3000 H.

Nasal Intubation

Nasotracheal and nasogastric tubes passing through the nostril and nasopharynx may be visible on CT scans (Fig. 1A),

where they are seen as a bright density along the nasopharyngeal wall (Fig. 1B). Tubes may lie in the piriform sinus (Fig. 1C) or remain in the midline, medial to the aryepiglottic folds (Fig. 1D). In the laryngopharynx the tube lies posterior to the cricoid lamina (Fig. 1E).

Nasogastric tubes commonly used in adults range from 8 to 20 French (approximately 2.7–6.7 mm). Endotracheal tubes range from 5.5 to 9.0 mm. Therefore, it is not possible to unambiguously distinguish nasogastric from endotracheal tubes on the basis of diameter.

A Foley or other balloon catheter may be inserted into the nasopharynx for treatment of epistaxis. The balloon, which is usually filled with water, may produce a confusing appearance on CT scans, particularly if the balloon is only partly in the plane of section (Fig. 2) [1]. The use of appropriate window settings serves to avoid this confusion.

Oral Intubation

Two devices are commonly seen in the mouth on CT. One is the orotracheal tube used for mechanical respiratory ventilation. The other is the oral airway (Fig. 3) used to keep the patient from biting the orotracheal tube and tongue and to serve as an alternative air passage. Oral airways may be H-shaped (Fig. 4) or oval when seen in cross section (Fig. 3). They are made of plastic or rubber and have variable CT densities (Fig. 5).

Received September 13, 1990; accepted after revision October 31, 1990.

¹ Department of Radiology, Winthrop-University Hospital, Mineola, NY 11501.

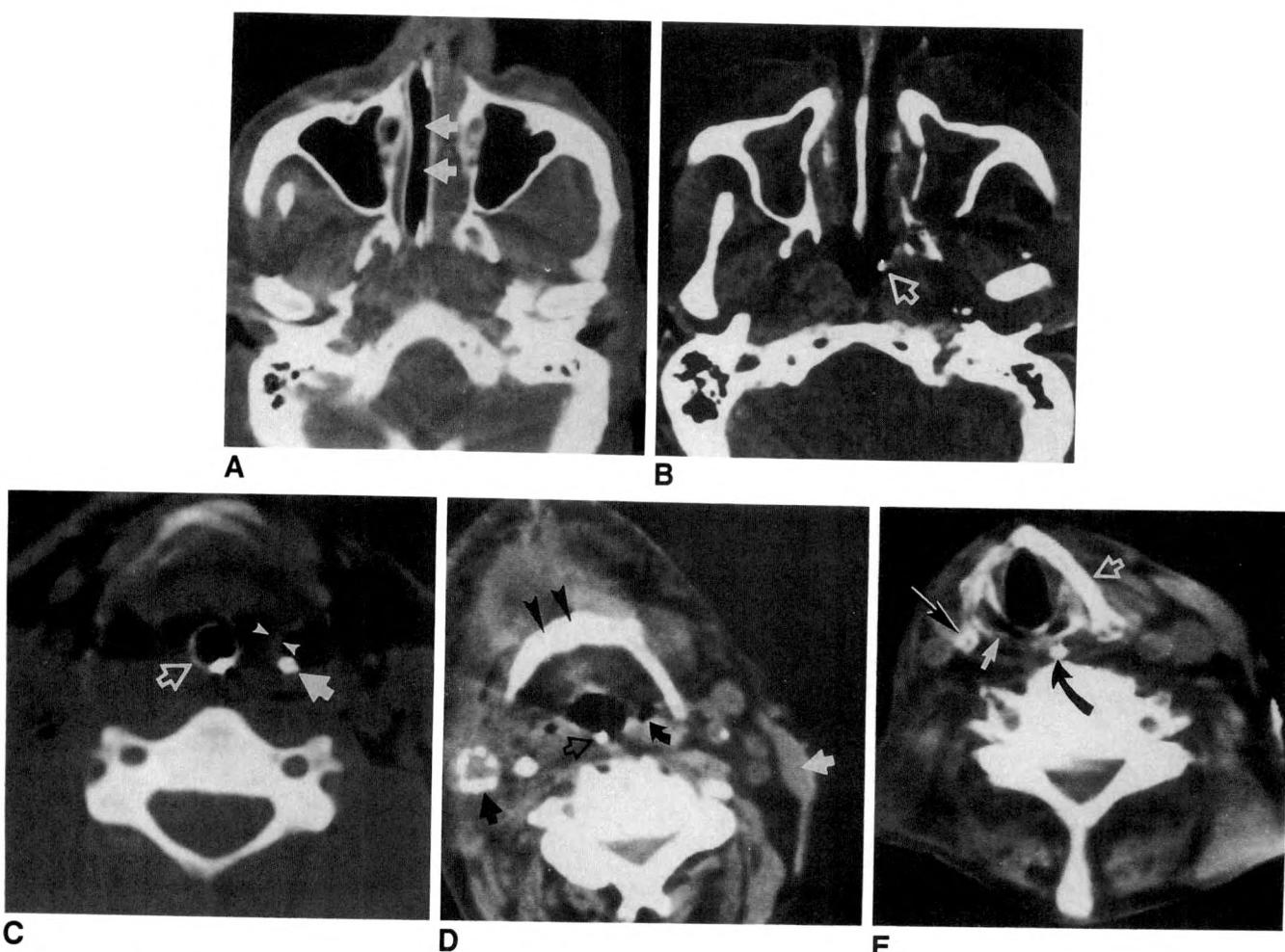


Fig. 1.—CT scans show nasal tubes at several levels.

A, Nasotracheal tube (arrows) in nostril.

B, Nasogastric tube (arrow) on left side at nasopharyngeal level. Note fractures of left maxillary sinus and pterygoid plates.

C, Hypopharyngeal level. Nasogastric tube (solid arrow) passes through left piriform sinus, lateral to aryepiglottic fold (arrowheads). Endotracheal tube (open arrow) is in midline. This patient suffered blunt chest trauma in a motor vehicle accident. Emphysema of deep tissue may have resulted from initial trauma or from traumatic intubation.

D, Hypopharyngeal level. In this patient, nasogastric tube (open arrow) passes in midline. Sternocleidomastoid muscle (straight white arrow) is absent on right side owing to radical neck dissection. Piriform sinus (curved arrow); hyoid bone (arrowheads); calcification in wall of carotid artery (solid black arrow).

E, Laryngeal level. Nasogastric tube (curved arrow) passes posterior to cricoid lamina (solid white arrow) in same patient as in D. Thyroid cartilage (open arrow); inferior cornu of thyroid cartilage (long straight black arrow).

Tracheal Intubation

Mechanical ventilation is often used in cases of respiratory failure, for relief of upper airway obstruction, or during surgery. The route of access to the airway is determined by the urgency of the need for the tube, the anticipated duration that it will be in place, and the patient's anatomy.

If intubation is required for only a short time, orotracheal intubation is usually preferred because of its relative ease of performance and safety [2]. Nasotracheal intubation is used if intubation is required for more than a day or so [3], for intraoral operations, and when upper airway abnormalities make orotracheal intubation difficult. Nasotracheal intubation is more comfortable for patients who are awake.

Both nasotracheal and orotracheal tubes pass through the larynx. Endotracheal tubes are in direct contact with the free

margins of the vocal cords and posterior commissure (Fig. 6), which explains the postintubation development of glottic and subglottic granulomas, scarring, and strictures.

Prolonged inflation of the endotracheal tube cuff at a pressure exceeding capillary arteriolar pressure causes tracheal ischemic necrosis, which ultimately leads to tracheomalacia [2]. Overdistension of the balloon cuff, an important sign of tracheomalacia [4], may be seen on CT (Fig. 7). The diameter of the balloon cuff should be compared with the tracheal caliber above and below the cuff; a ratio of cuff diameter to tracheal diameter greater than 150% has been found to be a predictor of tracheal damage [4].

Tracheostomy

Long-term intubation is uncomfortable and associated with significant complications. Tracheostomy is generally per-

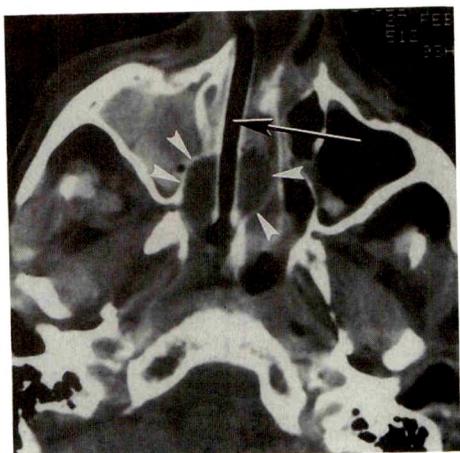


Fig. 2.—CT scan of Foley catheter (arrow) with water-filled balloon (arrowheads) in posterior choana. High-density contents of right maxillary sinus due to hemorrhage.

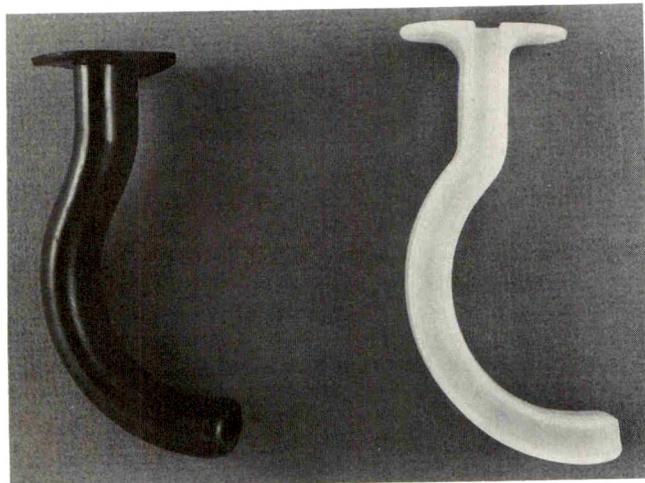


Fig. 3.—Two common oral airways.
Left, Guedel type (Rusch, Inc., Duluth, GA). Device is oval in cross section.
Right, Berman airway (Portex, Wilmington, MA). Airway is H-shaped in cross section.

formed on an elective basis in patients who require prolonged intubation [3].

The tracheostomy usually involves incision of the second and third and sometimes part of the fourth tracheal cartilages and division of the thyroid isthmus. The first cartilage is spared in order to avoid damage to the larynx.

CT scans may show superficial or deep soft-tissue emphysema after tracheostomy (Fig. 8). Secretions in the trachea above the tracheostomy can be identified also (Fig. 9).

Cricothyroidotomy

Cricothyroidotomy (incision of the cricothyroid membrane) is technically simpler than standard tracheostomy. Although

the vocal cords are 1.5–2.0 cm above the cricothyroid membrane, there is a significant rate of vocal cord damage [5]. Therefore, cricothyroidotomy generally is reserved for emergent situations, terminally ill patients, and patients with unusual anatomic situations that prohibit standard tracheostomy. CT reveals that the tube enters the airway above the cricoid ring (Fig. 10). Inferiorly the tube is indistinguishable from other types of tracheal tubes.

In high tracheostomies, the first tracheal cartilage is divided and the tube is inserted just below the cricoid ring. This may be done to avoid a recent sternotomy (Fig. 11). It may be difficult to distinguish between tubes placed by cricothyroidotomy and high tracheostomy on CT because of volume averaging. The digital scout radiograph may not be helpful in this regard as it does not provide consistent visualization of the laryngeal cartilages. Furthermore, many examinations of the neck in intubated patients are performed as part of a chest CT study for which an anteroposterior scout view was generated. Usually, the details of the surgical procedure are available and need not be deduced from the CT scan. However, when the medical history is inadequate or unavailable, understanding the relationships illustrated in this article may be useful.

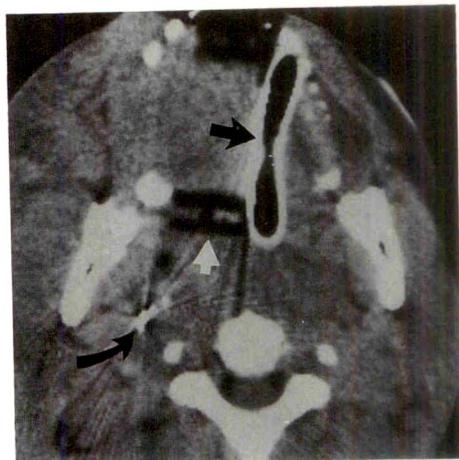
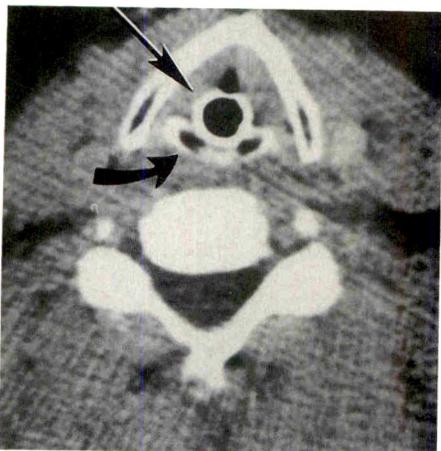


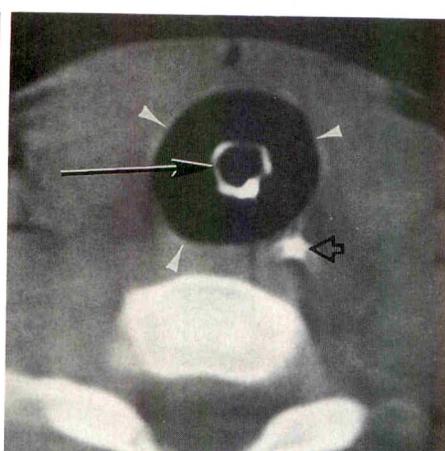
Fig. 4.—Cross section of H-shaped oral airway (white arrow) on CT scan. Ootracheal tube (straight black arrow); bullet fragment (curved arrow).



Fig. 5.—CT scan of airways shown in Fig. 3.
Left, Guedel airway. Density = +1024 H.
Right, Berman airway. Density = -142 H.

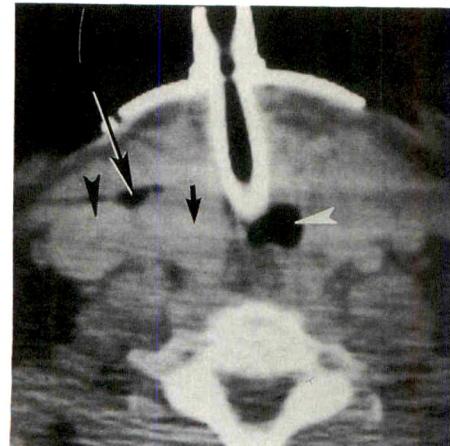


6

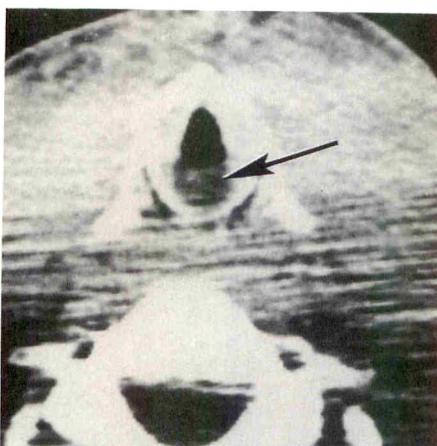


7

Fig. 6.—CT scan of endotracheal tube passing through glottis. Tube is in direct contact with free margins of vocal cords and mucosal surface of posterior commissure. Vocal cord (straight arrow); cricoid lamina (curved arrow).



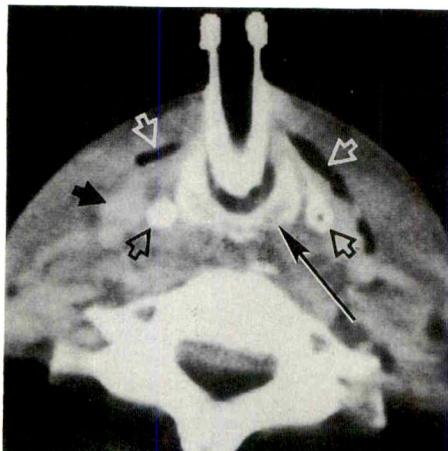
8



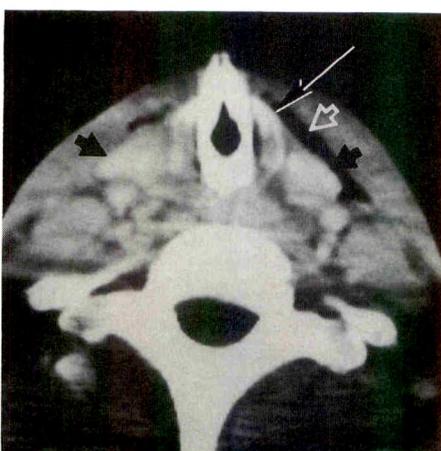
9

Fig. 8.—CT scan of standard tracheostomy tube and location. Note small amount of emphysema in deep tissue plane (long arrow). Trachea (white arrowhead); internal jugular vein (black arrowhead); right lobe of thyroid (short arrow).

Fig. 9.—CT scan of accumulated airway secretions (arrow) above tracheostomy.



A



B

Fig. 10.—CT scans of cricothyroidotomy. **A.** Tube enters above cricoid ring. Cricoid cartilage, while ring-shaped, has a greater vertical dimension posteriorly. Posterior part of cricoid cartilage (long solid arrow); inferior cornua of thyroid cartilage (open black arrows).

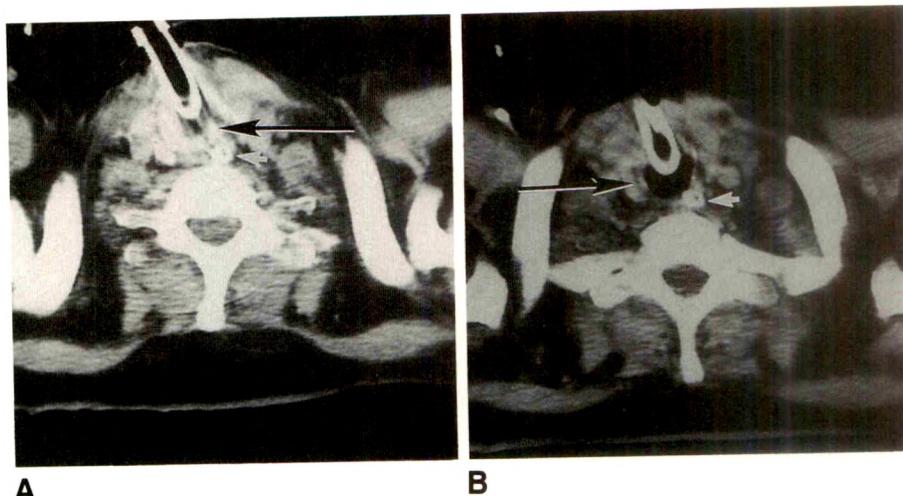
B. Next inferior slice. Anterior part of cricoid cartilage (long solid arrow) is now in view.

Thyroid gland (short solid arrows); emphysema of deep tissue plane (open white arrows).

Fig. 11.—CT scans of high tracheostomy.
A, If viewed out of context of adjacent slices, this image cannot be distinguished from Fig. 10A. Cricoid cartilage (long arrow).

B, Next inferior slice. It can be seen that tube enters airway below cricoid cartilage. Volume-averaged undersurface of cricoid cartilage (long arrow).

Nasogastric tube (short arrows).



REFERENCES

- Houston LW. Neuroradiology case of the day. Foley catheter simulating nasopharyngeal mass. *AJR* 1986;146:1095-1096
- Stoelting RK. Endotracheal intubation. In: Miller RD, ed. *Anesthesia*, 2nd ed. New York: Churchill-Livingstone, 1986:527-536
- Grillo HC. Tracheostomy and its complications. In: Sabiston DC, ed. *Textbook of surgery*, 13th ed. Philadelphia: Saunders, 1986:2000-2006
- Ravin CE, Handel DB, Kariman K. Persistent endotracheal tube cuff overdistension: a sign of tracheomalacia. *AJR* 1981;137:408-409
- Esses BA, Jafek BW. Cricothyroidotomy: a decade of experience in Denver. *Ann Otol Rhinol Laryngol* 1987;96:519-524

Videotape Review



MRI of the Brain Stem. By Murray A. Solomon. (Tape 2 in series 2 of Murray Solomon's Magnetic Resonance Video Review.) Burlingame, CA: Murray Solomon's MRVR, (408) 374-8897, 1990. Single tape, \$125, series of 6 tapes, \$545

Imaging of the brainstem with CT and some other techniques can be difficult. When CT is used, interpetrous beam-hardening artifacts and streak artifacts from the internal occipital protuberance make evaluation of the brainstem suboptimal or impossible in many cases. These problems do not exist with MR imaging, which is superior to other imaging techniques in delineating normal and abnormal brainstem anatomy and disease.

This 90-min videotape, *MRI of the Brain Stem*, is tape 2 in series 2 in a subscription series entitled Murray Solomon's Magnetic Resonance Video Review. The stated objective of the videotape is to provide a complete discourse that systematically covers the topic. Dr. Solomon has succeeded in this objective.

The tape begins with a review of normal anatomy of the brainstem; aqueduct of Sylvius; and the cranial nuclei, including lesions that affect the nuclei. Common pitfalls and mistakes are discussed. This section is followed by a discussion of pathologic states that affect the brainstem. The conditions reviewed are pontine ischemic changes, pontine infarcts, pontine hemorrhage, pontine arteriovenous malformations, brainstem gliomas, metastatic disease to the brainstem, and infection of the brainstem. Degenerative diseases, including olivopontocerebellar degeneration, spinocerebellar degeneration, and supranuclear palsy, conclude the videotape. The discussions on central pontine myelinolysis and degenerative diseases of the brainstem are the highlights of the tape. In addition to discussing the MR

features of these conditions, Dr. Solomon discusses the clinical features and correlation of these conditions. This is helpful and excellent.

The overall quality of the speaker's delivery, tone, style, and presentation is quite good. The videotape is well organized, and Dr. Solomon's presentation flows easily from one subject to another. The quality of the MR images is excellent. The anatomic diagrams used in this presentation are adequate but could have been improved for greater clarity and understanding of this complex area of the brain. The references are current and useful. However, the format of videotape presentations does not allow the use of references in the same manner as conventional written presentations do, and videotapes certainly do not replace the radiologic literature.

Videotape presentations are an alternative, efficient, and, at times, entertaining method of teaching. I highly recommend for purchase *MRI of the Brain Stem*. It is geared for private radiologists and residents in diagnostic radiology programs and also should be valuable for group learning and discussions. It is a worthwhile acquisition for departmental video libraries.

Solomon Batnitzky
University of Kansas Medical Center
Kansas City, KS 66103

Hamartomas of the Tuber Cinereum: CT, MR, and Pathologic Findings

Orest B. Boyko¹
 John T. Curnes²
 W. Jerry Oakes³
 Peter C. Burger⁴

The neuroimaging studies, clinical evaluations, and surgical and pathologic findings in five children with biopsy-proved hamartomas of the tuber cinereum were reviewed. Surgical and/or MR findings showed that patients with precocious puberty had pedunculated lesions while those with seizures had tumors that were sessile with respect to the hypothalamus. The radiologic studies included six MR examinations in four patients and CT studies in all five patients. Three children presented with precocious puberty and two with seizures, one of which was a gelastic (spasmodic or hysterical laughter) type of epilepsy. MR studies were obtained both before and after surgery in two patients, only preoperatively in a third patient, and only postoperatively in the fourth child. MR was superior to CT in displaying the exact size and anatomic location of the hamartomas in all cases. The mass was isointense with gray matter on sagittal and coronal T1-weighted images, which best displayed the relationship of the hamartoma to the third ventricle, infundibulum, and mammillary bodies. Intermediate- or T2-weighted images showed signal characteristics of the hamartoma to be isointense (one case) or hyperintense (two cases) relative to gray matter. The difference in T2 signal intensity did not correlate with any obvious differences in histopathology. CT showed attenuation isodense with gray matter, and no calcium. There was no enhancement on CT. There was no enhancement on MR in the one case in which contrast medium was administered. Preservation of the posterior pituitary bright spot was noted on all pre- and postoperative T1-weighted MR scans.

In children presenting with precocious puberty or seizure, MR assessment of the region of the third ventricle is necessary to exclude hypothalamic hamartoma, which appears as a pedunculated or sessile mass that is isointense with gray matter.

AJNR 12:309–314, March/April 1991; AJR 156:1053–1058, May 1991

Received October 6, 1988; revision requested November 30, 1988; revision received October 12, 1990; accepted October 17, 1990.

¹ Department of Radiology, Duke University Medical Center, Durham, NC 27710. Address reprint requests to O. B. Boyko.

² Greensboro Radiology Associates, Greensboro, NC 27415.

³ Department of Surgery and Pediatrics, Duke University Medical Center, Durham, NC 27710.

⁴ Department of Pathology, Duke University Medical Center, Durham, NC 27710.

0361-803X/91/1565-1053\$00.75 © American Roentgen Ray Society

Hamartoma of the tuber cinereum is a rare malformation usually discovered during a workup for precocious puberty or, more rarely, seizures. The CT features of this lesion have been described and are useful in the differential diagnosis [1–5], but MR might be expected to provide better detail of these generally small lesions [6]. To date, MR findings in 31 cases of tuber cinereum hamartoma have been published [7–17], but only 10 of these were biopsy-proved. We report the use of CT and MR (1.5 T) in the workup and management of five children with biopsy-proved hamartomas.

Materials and Methods

We retrospectively reviewed five cases of hypothalamic hamartoma from our neuropathologic files. Four patients had MR studies performed on a GE Signa (Milwaukee, WI) MR system operating at 1.5 T. A multislice, multiecho spin-echo sequence of axial, sagittal, and coronal T1-weighted images, 500/20 (TR/TE), as well as intermediate-weighted (first echo) and T2-weighted (second echo) images, 2500/40, 80, were obtained. Two signal averages were obtained on 3- and 5-mm-thick slices, with a 256 × 128 matrix. In a follow-up MR examination, one patient received IV contrast medium. Patients included three girls and two

TABLE 1: Hamartoma of Tuber Cinereum: Clinical, CT, MR, Surgical, Histopathologic, and Follow-up Findings

Case No.	Age (Years)	Sex	Clinical History/ Diagnosis	CT Findings	Macroscopic MR and Surgical Findings	MR Signal Intensity ^a			Pituitary Bright Spot	Pathology ^b	Clinical and Imaging Follow-up
						T1	1st Echo	T2			
1	5	F	Precocious puberty, menstruation at 6 mo., axillary/pubic hair at 4½ yr, bone age = 13 yr, increased go- nadotropin, in- creased estro- gen, normal neu- rologic exam	Suprasellar nonenhanc- ing mass	Pedunculated	Isointense	Hyper- intense	Hyperintense	Present	Harmartoma, pial vascular sur- face	Resolved precocious puberty, postoperative MR showed no residual tumor and mild dilatation of third ventricle
2	5	M	Seizures, 3-mo his- tory of absence of seizures with urination, hyper- activity, normal neurologic exam, normal endocrin- ologic exam	Suprasellar nonenhanc- ing mass	Sessile	Isointense	Isointense	Hyperintense	Present	Harmartoma, no pial vascular surface	Controlled seizures at 3 mo on medication, postopera- tive MR showed residual tumor, no change in signal intensity, no enhancement with contrast on MR
3	2	F	Precocious puberty, 3-mo history of menses, in- creased estro- gen, normal neu- rologic exam	Nonenhancing parasellar mass subjacent to basilar artery	Pedunculated	Not per- formed preop- eratively	Not per- formed preop- eratively	Not per- formed preop- eratively	Not performed preoperatively	Harmartoma	Normal endocrinologic exam at 3 yr, postoperative MR showed no evidence of tu- mor, pituitary bright spot was present
4	6	F	Seizures, infantile laughing/gelastic seizures, normal endocrinologic exam	Suprasellar nonenhanc- ing mass	Sessile, tem- poral lobectomy	Isointense	Hyper- intense	Hyperintense	Present	Harmartoma	Persistent but decreased fre- quency of seizures at 1 yr
5	6	M	Precocious puberty, onset over 1 yr; increased gonad- otropin; normal neurologic exam	Suprasellar nonenhanc- ing mass	Pedunculated	Not per- formed preop- eratively	Not per- formed preop- eratively	Not per- formed preop- eratively	Not performed preoperatively	Harmartoma, pial vas- cular sur- face	Stable for 6 yr postopera- tively

^a Relative to gray matter.

^b Histologically, all cases had nodular and short lamina of well-formed ganglion cells; mild to moderate gliosis, with widely separated axons, some of which were myelinated.

boys, ranging in age from 2 to 6 years old. Five patients had CT scans, which were acquired on a GE 8800 or 9800 scanner (Milwaukee, WI) both before and after contrast infusion. Three-millimeter-thick slices were obtained through the sella and suprasellar region.

The histologic sections of all five cases were reviewed.

Results

The clinical, CT, MR, surgical, histopathologic, and follow-up clinical and imaging findings in all five patients are summarized in Table 1. The three patients with pedunculated hamartomas presented with precocious puberty and the two with sessile lesions had seizures. All three preoperative MR studies demonstrated lesions isointense with gray matter on T1-weighted images (Figs. 1A, 2A, 2B) and hyperintense relative to gray matter on the second echo of the T2-weighted images (Figs. 1C, 2D, 3C). The presence of myelinated axons on Luxol fast blue stain did not correlate with any T2 shortening in the lesions. The intermediate (first echo) T2-weighted images showed either isointensity (Fig. 2C) or hyperintensity (Figs. 1B and 3B) relative to gray matter (Table 1). There was no contrast enhancement in the one case in which it was administered (Fig. 2E). There was no contrast enhancement on CT scanning (Fig. 3A), and no calcium was seen in any of the five cases. The posterior pituitary bright spot was present on all pre- and postoperative MR studies.

Discussion

Tuber cinereum is descriptively named for the region including the small bilateral protuberances of gray matter, the middle hypothalamic nuclei located between the infundibular stalk and the large, prominent mammillary bodies. An important efferent pathway from these nuclei is the tuberoinfundibular tract. Evidence suggests that these axons carry secretory granules, containing releasing hormones, allowing modulation of gonadotropins [18].

Hamartomas of the tuber cinereum are congenital, nonneoplastic heterotopias. Grossly, they may be pedunculated (Fig. 3) or broader-based, involving more of the hypothalamus (Figs. 1, 2, 4A). The first case was described in 1934 [19]. Histologically, the hamartoma closely resembles normal gray matter (Fig. 4B), and some neurons are reminiscent of those found in the adjacent hypothalamus. Some of the axons are myelinated. A variable amount of fibrillary gliosis may be found [20]. The pathologic changes seen in these masses are less striking than the gliotic nodules of tuberous sclerosis or the ganglion cell neoplasms. The latter are noted for abnormal neurons, a frequently prominent glial component, desmoplasia, and calcification.

The hamartoma in each of our cases most closely resembled gray matter in its signal characteristics on T1-weighted images. Similar MR findings have been reported by Hahn et al. [8] in two biopsy-proved cases imaged at 1.5 T. In eight other reports of biopsy-proved hamartomas [10, 12-15, 21] imaged at other or undisclosed field strengths, the tumors were isointense with gray matter in six cases [10, 12-15] and had areas of hyperintensity in two cases [21] on T1-weighted images. It has been suggested [10] that optic and hypothalamic gliomas tend to have prolonged T1 relaxation (hypointensity). Solid craniopharyngiomas also tend to be hypointense on T1-weighted scans, while cystic craniopharyngiomas often have prolonged T1, a possible characteristic differentiating these from noncystic hypothalamic hamartomas [10]. In the postoperative evaluation of these patients, T1-weighted images are the most helpful in outlining the anatomy of the floor of the third ventricle and the suprasellar cistern.

We found that the hamartoma may be isointense, slightly hyperintense, or markedly hyperintense relative to gray matter on the intermediate echo, but it was always hyperintense in relation to gray matter on the second echo of T2-weighted images. Although a variance in myelinated axons and the effect of myelin on T2 shortening [22] and the presence of gliosis could affect the variability of the T2 signal, it was not

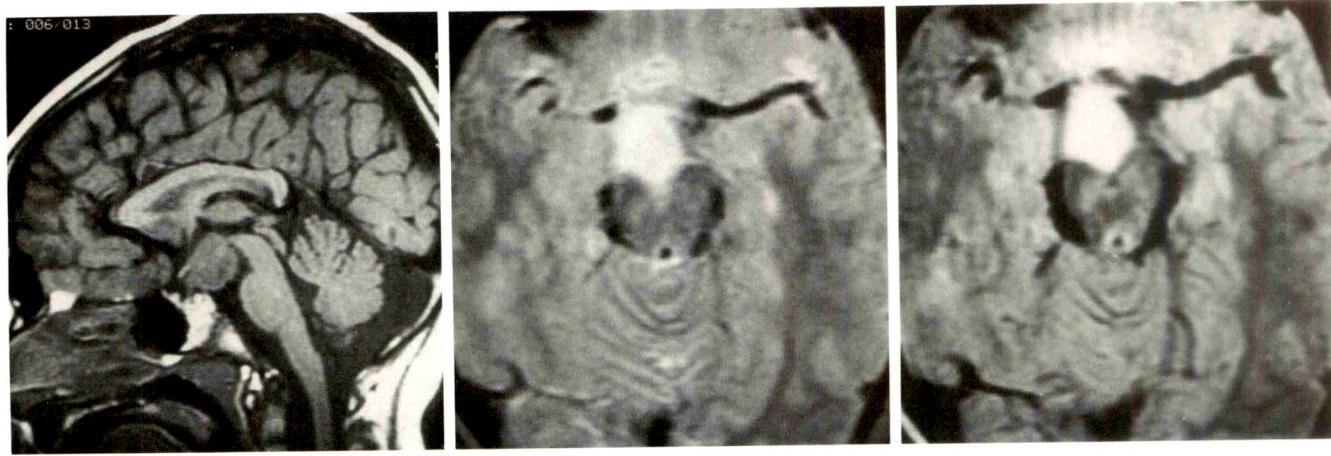


Fig. 1.—Case 4.

A, Sagittal T1-weighted MR image shows sessile hamartoma in typical third ventricular location, isointense with gray matter, infiltrating the floor of the hypothalamus. Posterior pituitary bright spot is present.

B and C, Axial T2-weighted MR images, first echo (B) and second echo (C), show that signal intensity has increased markedly with respect to gray matter.

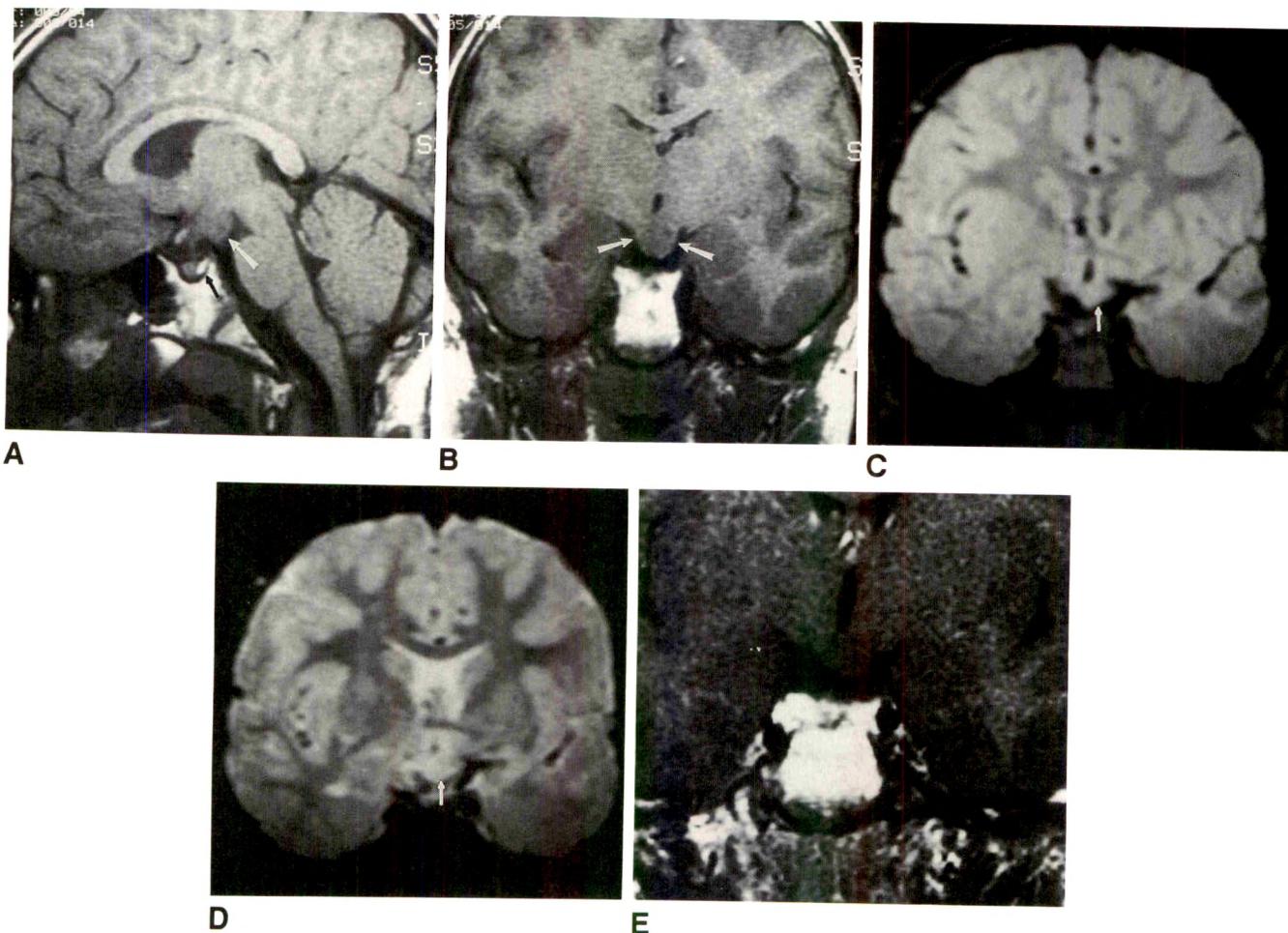


Fig. 2.—Case 2.

A, Sagittal T1-weighted MR image (500/20) shows 1.5-cm sessile mass with signal intensity isointense with gray matter. Mass is diffusely attached to and originating from the tuber cinereum (white arrow). Infundibular and optic recesses of third ventricle are obliterated, but posterior pituitary bright spot is preserved (black arrow).

B and **C**, Coronal T1-weighted (**B**) and first-echo T2-weighted (**C**) MR images reveal that the tumor has signal characteristics isointense with gray matter, has a broad base of attachment, and projects from left side of hypothalamus into suprasellar cistern (white arrows).

D, Coronal second-echo T2-weighted MR image shows the tumor to be hyperintense relative to gray matter (arrow).

E, Contrast-enhanced MR image (500/20) shows no tumor enhancement.

obvious from the comparison of histopathology and MR images in the present series why the lesion in case 2 (Fig. 2C) was isointense and the lesions in cases 1 (Fig. 3B) and 4 (Fig. 1B) were hyperintense relative to gray matter on the T2-weighted first-echo image.

Although hamartomas are benign and represent heterotopic rests of cells, all biopsied cases in the literature [10, 12–15, 21], including ours, had increased T2 signal on the second-echo image (Figs. 1C, 2D, 3C), which may make distinguishing hamartoma from glioma difficult. In fact, in a series of 59 suprasellar masses, MR signal characteristics were nonspecific in 70% of cases [15]. Thus, distinguishing hamartoma from glioma by T2 MR signal intensity may be somewhat limited, but isointensity relative to gray matter on the intermediate- or first-echo T2-weighted images may be more indicative of hamartomas.

On enhanced CT, the hamartoma appears as an isodense mass without definite enhancement, reflecting an intact blood-brain barrier. In our only MR case in which contrast material was administered, no enhancement was present (Fig. 2E). Histologically, tumor neovascularity was not present.

While CT suggested the preoperative diagnosis in all five patients, two of the five underwent water-soluble contrast CT cisternography to confirm the findings. MR as a noninvasive technique was unequivocally positive in the three instances in which it was obtained preoperatively (cases 1, 2, 4). In addition, MR with its direct multiplanar capabilities has the advantage of allowing for the evaluation of any associated intracranial congenital abnormalities [23]. Diebler and Ponsot [1] and Naidich and Zimmerman [2] have reported associated congenital anomalies with midline hamartomas; including callosal agenesis, optic malformation, and hemispheric dysgen-

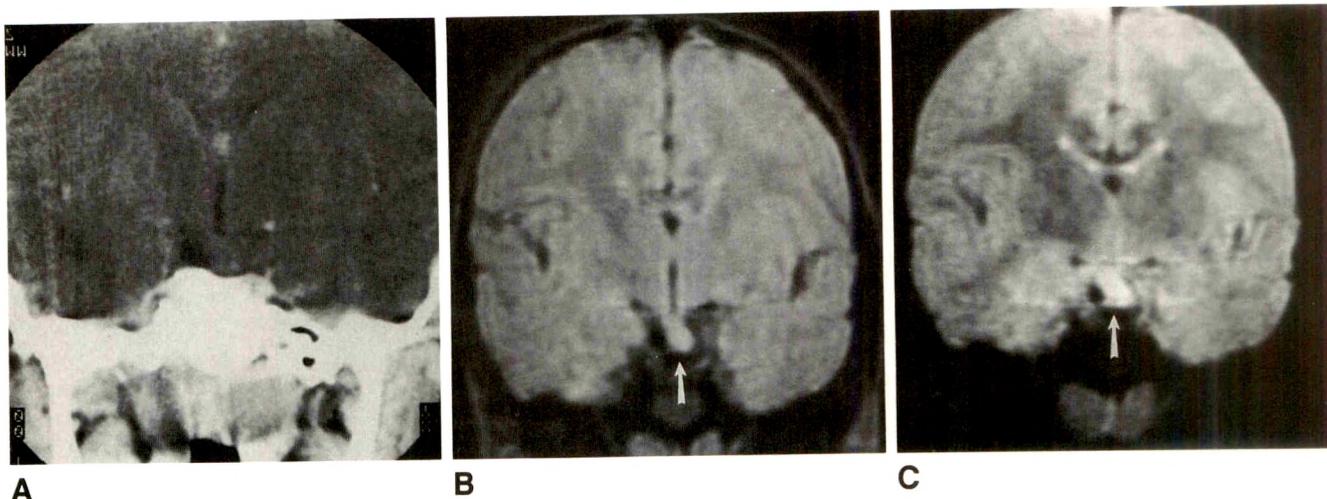
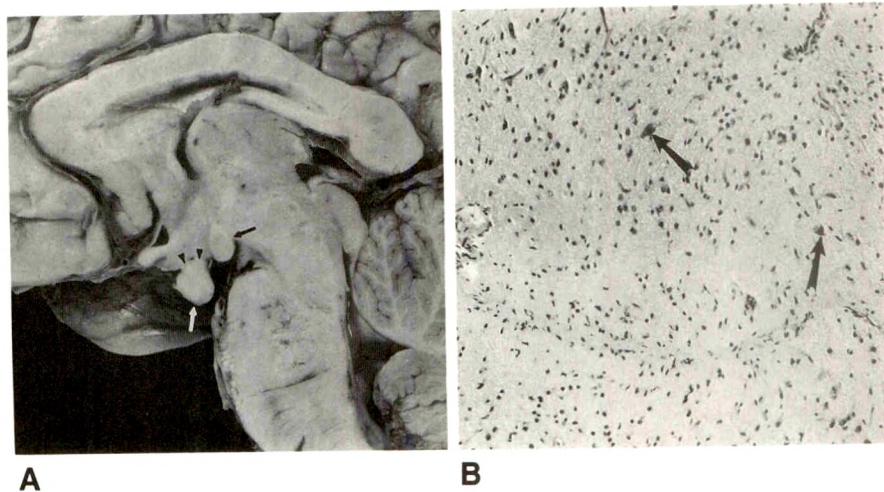
**A****B****C**

Fig. 3.—Case 1.
A, Coronal CT scan with contrast infusion reveals the relationship of the mass to the hypothalamus and floor of the third ventricle.
B and **C**, Coronal T2-weighted MR images, first echo (2500/40) (**B**) and second echo (2500/80) (**C**), show pedunculated mass that is slightly hyperintense relative to gray matter (arrows).

**A****B**

esis (heterotopias and microgyria), suggesting an insult occurring around the first month of gestation [1]. They refer to the hamartomas and congenital anomalies as a dysraphic syndrome. None of the five cases in our series displayed any associated intracranial congenital anomalies.

Clinical presentations in our five patients reflect the experience previously reported in the literature: precocious puberty and/or seizures. The mechanism whereby a hamartoma causes precocious puberty has not been clarified. One hypothesis suggests that the inhibitory pathways from the hypothalamus to the posterior pituitary and infundibulum are interrupted by mechanical compression [20, 24]. The fact that precocious puberty occurs with other lesions around the hypothalamus, such as glioma, supports this theory. Other cases seem to point to a direct neurosecretory role by the hamartoma itself [25-27]. Absence of the posterior pituitary bright spot on MR images has been reported to be associated with interruption of the stalk with resultant diabetes insipidus

[28, 29]. In all of our cases, the bright MR signal of the posterior pituitary on T1-weighted images was preserved, even when the infundibular recess was obliterated, the stalk was compressed, and hormonal evidence of precocious puberty existed (Figs. 1A and 2A). This observation could be interpreted as indicating that (1) gonadotropin-releasing-factor neurons are more resistant to compression than are vasopressin neurons, (2) only complete transection of the stalk results in loss of the posterior pituitary signal, (3) the tumor does affect the pituitary stalk but the mechanism for precocious puberty is neurosecretion from the hamartoma itself, and (4) the posterior pituitary bright spot signal has no relationship with the hypothalamic gonadotropin-releasing-factor neurons.

Some reports have found that seizures are associated with larger lesions [1]. Two of our patients (cases 2 and 4), both with large lesions, presented with seizures. The size of these hamartomas was approximately the same as that in the

patient in case 1, who had precocious puberty. Hypotheses for the seizures include (1) interconnection of the hamartomatous neurons with those of the limbic system or (2) association of the seizures with midline abnormalities or hemispheric malformations. One of our patients' seizures consisted of absence states, while the other patient with seizures had the rarer, but virtually pathognomonic, gelastic epilepsy, resulting in spasmodic laughter, which has been reported with hamartomas [1]. The onset of this type of laughter in infancy, its frequency, and its character, distinguish it from the epileptic laughter associated with temporal lobe seizures [11]. The mechanism for this ictal laughter is unclear, representing either mechanical stimulation of the floor of the third ventricle by the tumor, causing epileptic discharge from the hypothalamus, or some kind of automatism or release phenomenon [11]. Temporal lobe epilepsy can also be associated with laughter.

Postoperative MR imaging showed no tumor in two cases in which pedunculated lesions were resected (cases 1 and 3), suggesting that a careful microsurgical approach to these lesions can result in total resection and excellent clinical outcome. This series, as well as other sporadic reports [3, 24, 30], refutes the position that no case has been published in which this mass has been completely or partially removed [1]. Exophytic lesions, associated with precocious puberty, lying anterior to the basilar artery can be resected, resulting in the amelioration of symptoms. Pedunculated, prepontine masses may be diagnosed preoperatively with more confidence, but intrinsic lesions may need biopsy to differentiate hamartomas from gliomas.

In summary, in children presenting with precocious puberty or seizures, masses of the third ventricle with MR signal characteristics suggestive of gray matter should lead to a confident preoperative diagnosis of tuber cinereum hamartoma.

REFERENCES

- Diebler C, Ponsot G. Hamartomas of the tuber cinereum. *Neuroradiology* 1983;25:93-101
- Naidich TP, Zimmerman RA. Primary brain tumors in children. *Semin Roentgenol* 1984;19:100-114
- Kyuma Y, Kato E, Sekido K, et al. Hypothalamic hamartoma successfully treated by operation. *J Neurosurg* 1985;62:288-290
- Lin SR, Bryson MM, Gobien R, et al. Radiologic findings in hamartomas of the tuber cinereum and hypothalamus. *Radiology* 1978;127:697-703
- Frank G, Cacciari E, Cristi G, et al. Hamartomas of the tuber cinereum and precocious puberty. *Childs Brain* 1982;9:222-231
- Sartor K, Karnaze MG, Winthrop JD, Gado M, Hodges FJ. MR imaging in infra-, and para-, and retrosellar mass lesions. *Neuroradiology* 1987;29:19-29
- Brant-Zawadzki M, Kelly W. In: *Magnetic resonance imaging of the central nervous system*. New York: Raven, 1987:162
- Hahn FJ, Leibrock LG, Juseman CA, Makos MN. The MR appearance of hypothalamic hamartomas. *Neuroradiology* 1988;30:65-68
- Hubbard AM, Egelhoff JC. MR imaging of large hypothalamic hamartomas in two infants. *AJNR* 1989;10:1277
- Burton EM, Ball WS, Crone K, Dolan LM. Hamartoma of the tuber cinereum: a comparison of MR and CT findings in four cases. *AJNR* 1989;10:497-501
- Berkovic SF, Andermann F, Melanson D, et al. Hypothalamic hamartomas and ictal laughter: evolution of a characteristic epileptic syndrome and diagnostic value of magnetic resonance imaging. *Ann Neurol* 1988;23:429-439
- Kanazawa J, Uozumi T, Sakoda K, et al. Magnetic resonance imaging of hypothalamic hamartoma. *Neurosurgery* 1988;16:585-588
- Markin RS, Leibrock LG, Huseman CA, McComb RD. Hypothalamic hamartoma: a report of 2 cases. *Pediatr Neurosci* 1987;13:19-26
- Barral V, Brunelle F, Brauner R, et al. MRI of hypothalamic hamartomas in children. *Pediatr Radiol* 1988;18:449-452
- Karnaze MG, Sartor K, Winthrop JD, et al. Suprasellar lesions: evaluation with MR imaging. *Radiology* 1986;161:77-82
- Beningfield SJ, Bonnici F, Cremin BJ. Magnetic resonance imaging of hypothalamic hamartomas. *Br J Radiol* 1988;61:1177-1180
- Kalifa G, Demange P, Sellier N, et al. Magnetic resonance imaging of the sella and juxtasellar area in children. *Ann Radiol* 1986;29:669-673
- Carpenter MB. *Core text of neuroanatomy*, 3rd ed. Baltimore: Williams & Wilkins, 1985:265-288
- Le Marquand HS, Russell DS. A case of pubertas praecox (macrogenitosmia praecox) in a boy associated with a tumor in the floor of the third ventricle. *Berks Hosp Rep* 1934;3:31-61
- Russell DS, Rubinstein LJ. *Pathology of tumors of the nervous system*, 5th ed. Baltimore: Williams & Wilkins, 1989
- Nishio S, Fujiwara S, Aiko Y, et al. Hypothalamic hamartoma. Report of two cases. *J Neurosurg* 1989;70:640-645
- Curnes JT, Burger PC, Djang WT, Boyko OB. MR imaging of compact white matter pathways. *AJNR* 1988;9:1061-1068
- Curnes JT, Laster DW, Koubek TD, et al. MRI of corpus callosal syndrome. *AJNR* 1986;7:617-622
- Alvarez-Garijo JA, Albiach VJ, Vila MM, et al. Precocious puberty and hypothalamic hamartoma with total recovery after surgical treatment. Case report. *J Neurosurg* 1983;58:583-585
- Judge DM, Kulik HE, Page R, et al. Hypothalamic hamartoma. A source of luteinizing-hormone-releasing factor in precocious puberty. *N Engl J Med* 1977;297:7-10
- Takeuchi J, Handa H, Miki Y, et al. Precocious puberty due to a hypothalamic hamartoma. *Surg Neurol* 1979;11:456-460
- Culler FL, James HE, Simon ML, et al. Identification of gonadotropin-releasing hormone in neurons of a hypothalamic hamartoma in a boy with precocious puberty. *Neurosurgery* 1985;17:408-412
- Fujisawa I, Nishimura K, Asato R, et al. Posterior lobe of the pituitary in diabetes insipidus: MR findings. *J Comput Assist Tomogr* 1987;11:221-225
- Colombo N, Berry I, Kucharczyk J, et al. Posterior pituitary gland: appearance on MR images in normal and pathologic states. *Radiology* 1987;165:481-485
- Kammer KS, Perlman K, Humphreys RP, et al. Clinical and surgical aspects of hypothalamic hamartoma associated with precocious puberty in a 15-month-old boy. *Childs Brain* 1980;6:150-157

Intra- and Paraorbital Lesions: Value of Fat-Suppression MR Imaging with Paramagnetic Contrast Enhancement

Robert D. Tien¹
 Pauline K. Chu¹
 John R. Hesselink¹
 Jerzy S zumowski²

The orbital area of 18 individuals was examined by using a combination of fat-suppression contrast-enhanced MR imaging to determine whether contrast between fat and surrounding tissues could be improved over that obtained with conventional fat-suppression techniques alone. We used a hybrid technique combining two independent methods of fat suppression. Subjects consisted of 16 patients and two normal volunteers. Fifteen individuals received gadopentetate dimeglumine, and conventional T1-weighted, T2-weighted, and fat-suppression T1-weighted images were obtained. The fat-suppressed T1-weighted images obtained after contrast administration provided more information than did the conventional MR images. Intraorbital and paraorbital lesions could be distinguished easily from intraorbital fat that had been suppressed. Cases of chorioretinitis and optic neuritis could be confidently diagnosed only by this technique. Cases of optic nerve meningioma and mixed conal lesions also were better appreciated. Because of sharp contrast between tissue planes, this technique was helpful for detecting any intraorbital invasion from paraorbital lesions.

Fat-suppression MR imaging with paramagnetic contrast enhancement can significantly improve the delineation of both normal and abnormal structures and better define lesional margins in the orbit, where large amounts of fat are present. Our results support earlier findings, and we suggest that postcontrast fat-suppressed T1-weighted imaging be used instead of conventional T1-weighted postcontrast imaging in evaluating orbital and paraorbital lesions.

AJNR 12:245-253, March/April 1991; AJR 156:1059-1067, May 1991

In regions of high fat content, such as the orbit, anatomic details are not optimally appreciated on conventional MR images. Although contrast enhancement can improve the ability to distinguish between a lesion and surrounding structures, distinction between enhanced structures and fatty tissue remains difficult in areas with significant amounts of fat. Various fat-suppression techniques have been devised that significantly improve the depiction of anatomic details [1]. In addition, in a preliminary study, the administration of a paramagnetic contrast agent, gadopentetate dimeglumine, in combination with a modified chopper fat-suppression technique was found to be the best way to depict lesions located in areas with large amounts of fat [2]. We applied this technique, focusing on orbital lesions, to determine if these structures would similarly reveal significantly improved anatomic detail.

Materials and Methods

MR imaging of the orbit was performed in 16 consecutive patients and two volunteers (12 males, six females), ranging in age from 5 months to 72 years (average, 32 years). Fifteen subjects received gadopentetate dimeglumine (Magnevist; Berlex, Cedar Knolls, NJ). The pathologic diagnoses are given in Table 1.

All MR studies were performed on a 1.5-T unit (Signa; General Electric, Milwaukee, WI) with a quadrature head coil. The studies included a conventional unenhanced T1-weighted

Received May 8, 1990; revision requested July 2, 1990; revision received October 4, 1990; accepted October 10, 1990.

¹ Department of Radiology and the Magnetic Resonance Institute, UCSD Medical Center, 225 Dickinson St., San Diego, CA 92103. Address reprint requests to R. D. Tien.

² Department of Radiology, Oregon Health Sciences University, Portland, OR 97201.

0361-803X/91/1565-1059\$00.75 © American Roentgen Ray Society

TABLE 1: Composition of the Study Group (*n* = 18)

Diagnosis	No.
Normal	3
Global lesions	
Cytomegalovirus chorioretinitis	1
Chorioretinitis	1
Choroidal melanoma	1
Intraconal lesions	
Optic neuritis	1
Optic meningioma	1
Muscle cone lesion	
Graves disease	1
Extraconal lesions	
Plexiform neurofibroma	1
Epibulbar dermoid	1
Dacryocystocele	1
Mixed intra- and extraconal lesions	
Plexiform neurofibroma	2
Adenoid cystic carcinoma	1
Lesions adjacent to the orbit	
Sphenoid meningioma	1
Adenoid cystic carcinoma of the maxillary sinus	1
Polypsis of the ethmoid sinus	1

spin-echo series, 600/20 (TR/TE), in 15 patients; proton-density and T2-weighted imaging, 3000/30,80, in 14 patients; and a T1-weighted fat-suppression image in all patients. In addition, contrast-enhanced T1-weighted images were obtained in eight patients.

We used a hybrid technique of fat suppression in the spin-echo mode of data acquisition. The technique incorporates two independent physical mechanisms for lipid signal elimination. The advantages of the frequency-selective excitation method and chopper [3-6] phase-sensitive variant of the Dixon method [7] were combined into a single two-excitation sequence.

A diagram of the hybrid sequence is presented in Figure 1, in which our implementation, a so-called 1331 frequency-selective pulse [8] was incorporated with an in- and out-of-phase data collection. The effect of pulse sequence on the fat and water magnetization vectors is represented in detail in Figure 2. The resulting water-only image is characterized by a more uniform fat signal suppression and a better suppression factor than if either method was used independently. The performance of the hybrid sequence has been tested on phantoms and volunteers, and the results have been presented in a separate study [3]. This technique achieves high-level lipid suppression without increasing imaging time or image postprocessing. The technique requires B_0 field homogeneity over the field of view exceeding the chemical shift difference between lipid and water. With this condition, the hybrid method has been applied with a high-field-strength magnet; however, it might be used with a mid-field-strength magnet if the field homogeneity permits.

Images were obtained in the coronal or axial plane, or both. Other imaging parameters included a 16-cm field of view, 3-mm slice thickness with 1-mm interslice gap, a 256 × 192 matrix, and 1-4 excitations. The resultant conventional images and paired fat-suppression images were carefully compared for demonstration of normal anatomic detail, increased conspicuity of enhancing lesions, delineation of lesional margins, and existence of an interface between lesions and normal structures.

Results

The pathologic diagnoses are listed in Table 1.

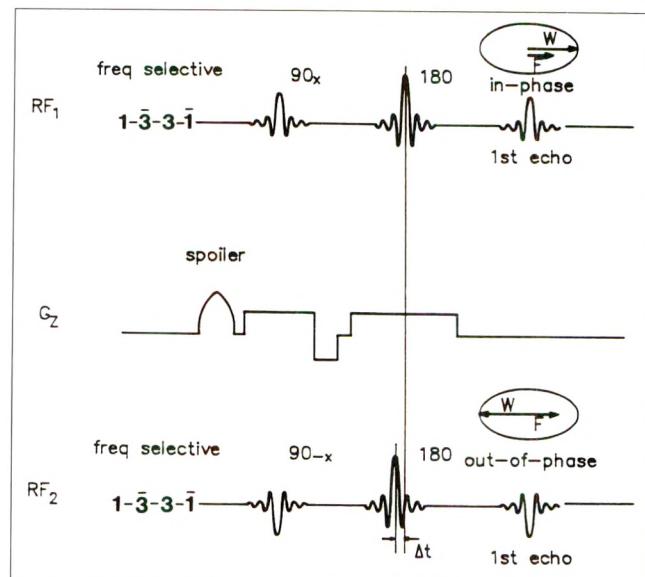


Fig. 1.—Diagram of hybrid pulse sequence used in this study. A frequency-selective pulse centered on fat resonance (in this case the 1331 pulse described by Hore [8]) is followed by chopper fat signal elimination. Two independent mechanisms of fat suppression applied together in one sequence substantially improve the effectiveness of fat/water signal separation.

Normal Subjects

The precontrast T1-weighted hybrid images showed the reversal of normal T1 contrast, with ratios of the signal intensity strongly positive between the optic nerve and fat, lacrimal gland and fat, and extraocular muscle and fat. The thicknesses of the optic nerve, muscle contour, and lacrimal gland were clearly represented (Fig. 3). Intracanalicular optic nerves were clearly seen when surrounding intracanalicular fat and fatty marrow signal were eliminated (Fig. 4). After contrast administration, the muscles and lacrimal gland enhanced intensely. However, the optic nerve did not enhance (Fig. 3H). The conventional long TR/long TE images did not suppress the intraorbital fat signal satisfactorily in all patients in our study. Compared with conventional spin-echo images (either T1- or T2-weighted), the postcontrast hybrid T1-weighted images gave the best normal anatomic definition between intraorbital structures. There was a magnetic susceptibility artifact on hybrid images between the sinuses and frontal lobes along the frequency-encoding axis due to air and soft-tissue interface (Figs. 3F and 3I). In our limited experience (to date, about 30 patients), the artifact was usually small, was found mainly in the frontal lobes, and did not interfere with the clear visualization of the orbit.

Global Lesions

Strong and distinct, irregular enhancement of the posterior chorioretina was clearly noted on axial postcontrast hybrid T1-weighted images in two patients with acute blindness (Fig. 5). One patient had conventional postcontrast T1-weighted imaging in the coronal plane but this was unremarkable (Fig.

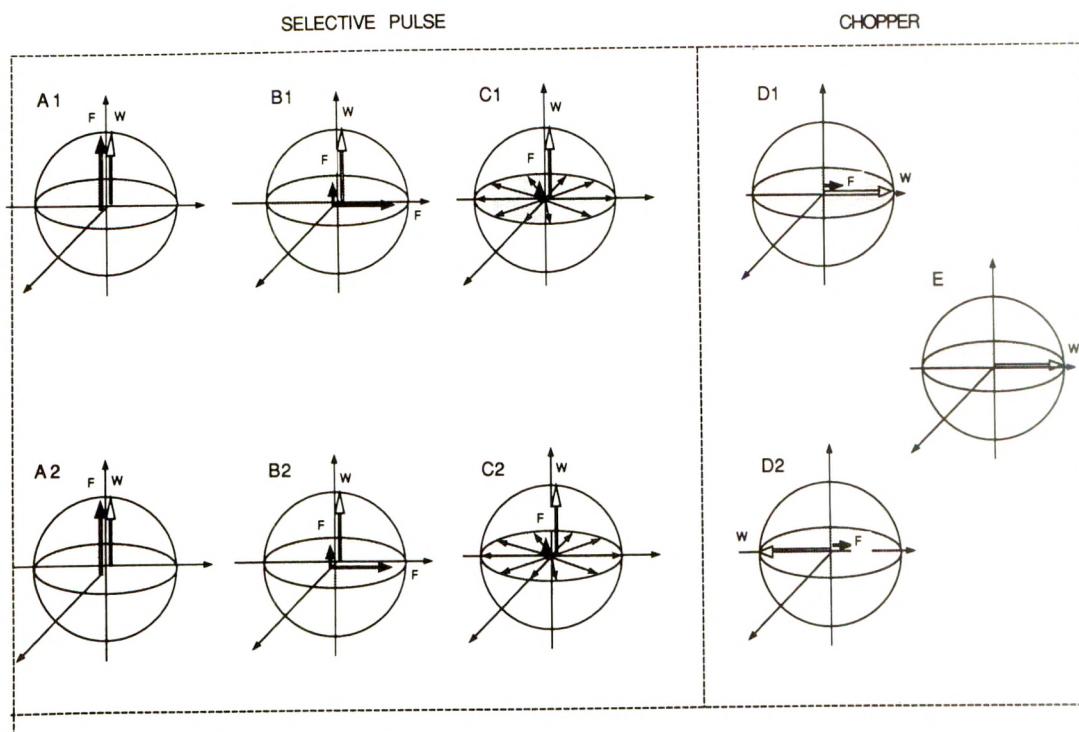


Fig. 2.—Graphic representation of magnetic behavior in the hybrid pulse sequence as applied to lipid signal suppression with the frequency of the MR scanner tuned to water resonance and the frequency-selective pulse centered on fat resonance.

During the first excitation (A1) the lipid magnetization is rotated into the transverse plane (B1) and dephased by the spoiler gradient (C1). This frequency-selective pulse provides partial elimination of the lipid signal subject to the limitations of magnetic field B_0 and RF inhomogeneities. The rest of the sequence operates on the remaining lipid and water magnetizations to produce the in-phase echo (D1).

During the second excitation, the frequency-selective pulse and dephasing gradients are repeated (A2, B2, C2); however, the phase of the slice-selective pulse is reversed and the timing of the refocusing pulse is adjusted to produce the out-of-phase echo (D2). Averaging by subtraction during the data acquisition, as in the original chopper fat-suppression sequence, results in elimination of the remnant lipid component in the final image (E).

5C). Chorioretinitis was diagnosed (one patient had cytomegalovirus infection, one had retinal biopsy, which revealed herpesvirus infection). These findings were unidentifiable on conventional proton-density and T2-weighted images (Figs. 5D and 5E).

One patient had presumed choroidal melanoma diagnosed by sonography. Despite being told that the chances of success with iodine-125 plaque implantation were minimal because his tumor was so large, the patient chose the plaque implant instead of enucleation. Although we did not obtain tissue in this case, the diagnostic accuracy was believed to be very high. The postcontrast hybrid T1-weighted image clearly showed the inhomogeneously enhancing posterior global mass. The tumor could be seen on conventional proton-density images but not as well, and it could not be identified at all on conventional T2-weighted images (Fig. 6).

Intraconal Lesions

In the patient with right optic neuritis resulting from CNS sarcoidosis, conventional T1- (Fig. 7A) and T2-weighted images failed to show any size or signal abnormalities of the optic nerves. The postcontrast T1-weighted image (Fig. 7B) showed mild enhancement of the upper portion of the posterior right optic nerve. However, the postcontrast hybrid T1-

weighted image (Fig. 7C) clearly demonstrated the strong enhancement (to the same degree as muscle) of the right optic nerve over its entire cross section from the retrobulbar portion to the intracanalicular portion, suggesting the inflammatory nature of the disease.

In another patient with suspected left optic nerve meningioma (Fig. 8), the bumpy mass was demonstrated by conventional T1-weighted imaging (before and after contrast administration) and by precontrast hybrid T1-weighted imaging. However, the linear low signal interface between the tumor and optic nerve (so-called tram-track sign, characteristic of the optic nerve meningioma) could be easily identified on the postcontrast hybrid T1-weighted image.

Muscle Cone Lesion

In one woman with clinical hyperthyroidism and mild right exophthalmos, MR was requested to rule out Graves disease. On conventional T1-weighted images, slightly thickened right inferior and perhaps medial rectus muscles were noted (Fig. 9A). On postcontrast T1-weighted fat-suppression images, the thickened right inferior and medial rectus muscles, as well as surrounding inflammatory infiltrate, were imaged clearly (Fig. 9B).

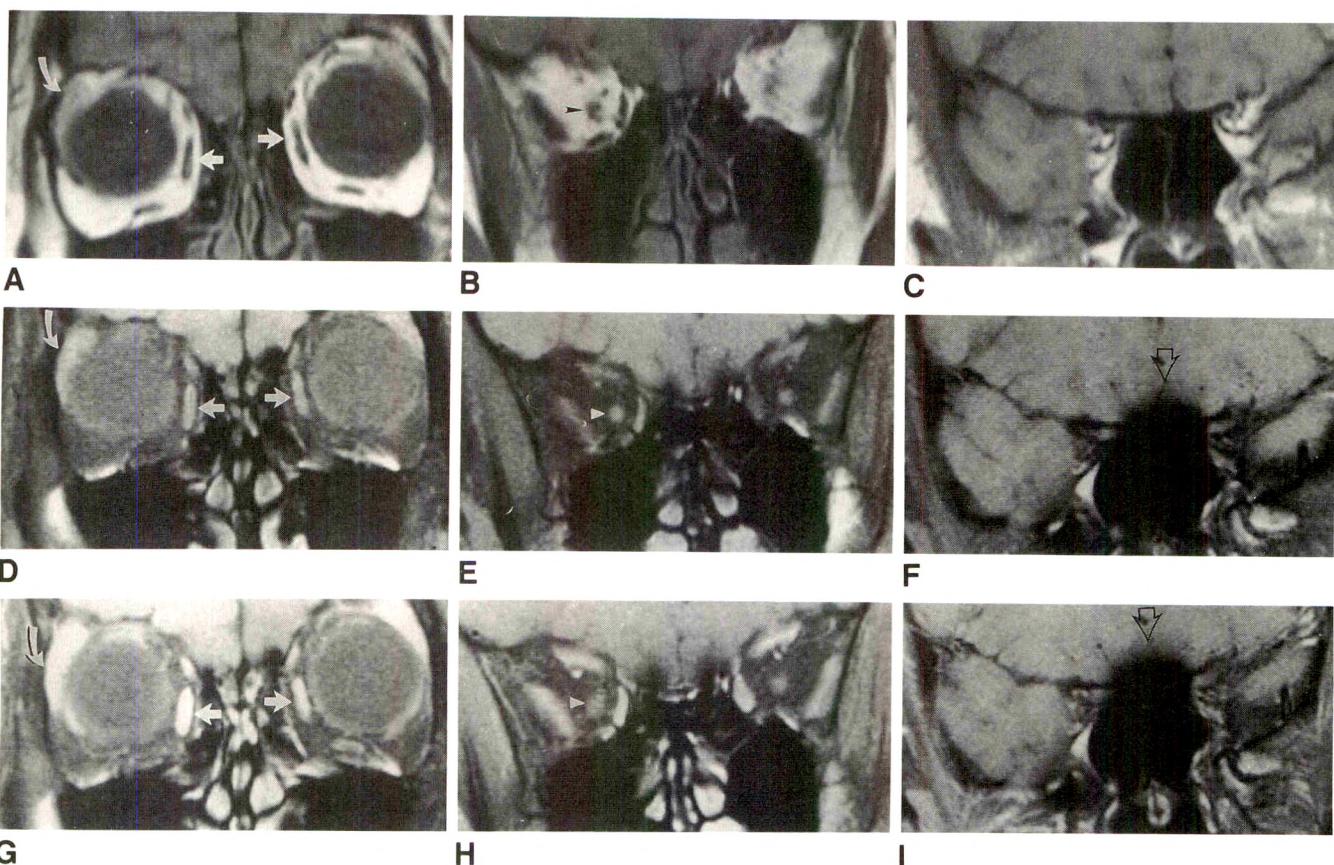


Fig. 3.—Normal volunteer. Coronal T1-weighted images (600/20/2) (A–C), coronal T1-weighted images with fat suppression (D–F), and postcontrast coronal T1-weighted images with fat suppression (G–I). Margins and outlines of extraocular muscles (straight white arrows), optic nerves (arrowheads), and lacrimal glands (curved arrows) are much better defined on fat-suppression images. Extraocular muscles enhance intensely and they appear slightly larger than on conventional T1-weighted images. Also, there is increased magnetic susceptibility artifact at ethmoid air cells and subfrontal regions on the fat-suppression images (open black arrows); however, the orbits are not affected significantly.

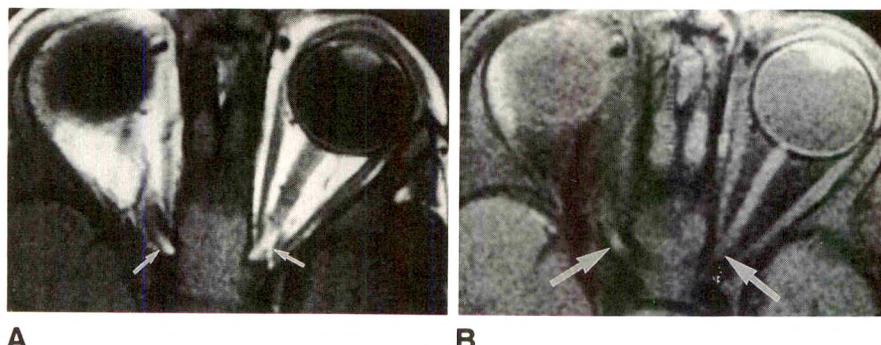


Fig. 4.—Normal volunteer.
A, Axial T1-weighted image (600/20/2). Intracanalicular portion of optic nerves was obscured by high-signal fat (arrows).

B, Axial T1-weighted image with fat suppression. Intracanalicular portion of optic nerves (arrows) is seen much better on fat-suppression image.

Extraconal Lesions

One young patient with neurofibromatosis and an orbital mass identified on CT scan was studied. The postcontrast hybrid T1-weighted image clearly showed the enhancing wormlike mass and its extraconal location, but its entire extent could not be clearly identified on conventional MR images.

An infant with clinically diagnosed Goldenhar syndrome was studied to rule out any brain abnormality. A small left epibulbar mass of high signal intensity was noted on T1-weighted

images (Figs. 10A and 10B). Hybrid T1-weighted imaging successfully suppressed the high signal portion of the mass, proving it to be a fatty mass (Fig. 10C) and confirming the diagnosis of epibulbar dermoid, which is one of the associated congenital abnormalities in Goldenhar syndrome.

One infant with a left-sided lower eyelid mass was studied. Conventional MR images showed a well-defined oval mass in the left medial canthus that was of low signal intensity on T1-weighted images and of high intensity on T2-weighted images. The hybrid T1-weighted images showed the mass to

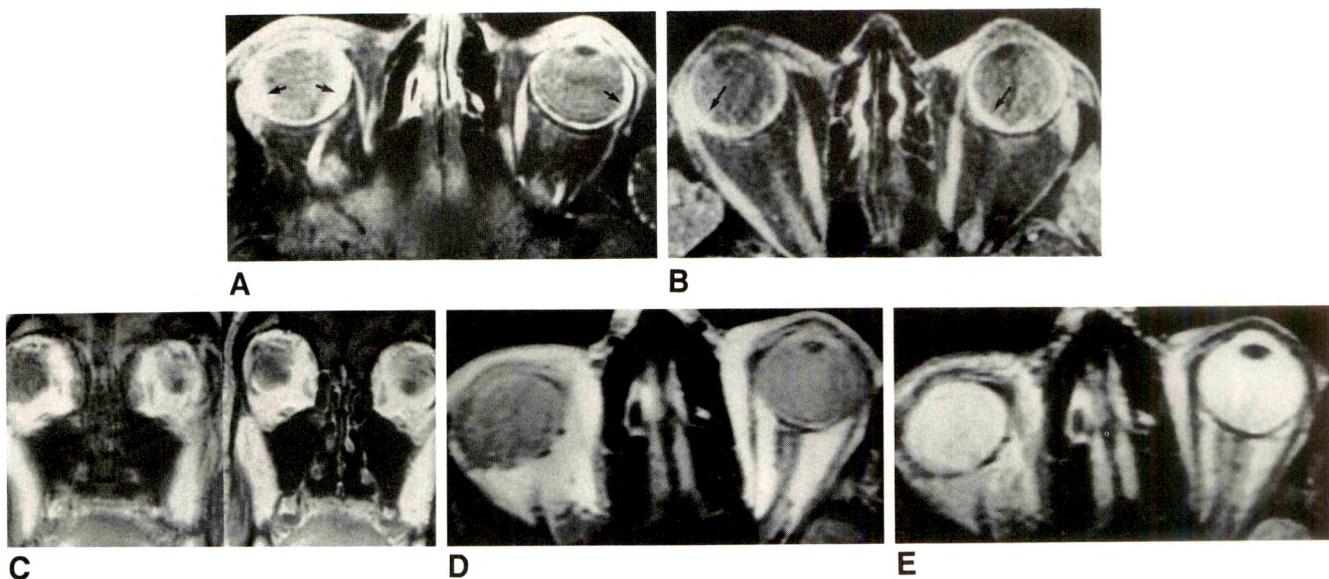


Fig. 5.—Two patients with acute vision loss.

A and *B*, Postcontrast axial T1-weighted images (600/20/2) with fat suppression in patients 1 (*A*) and 2 (*B*) show bilateral abnormal, irregularly thickened and enhanced chorioretina (arrows).

C-E, Conventional spin-echo images of patient 1 are unremarkable: postcontrast T1-weighted image (600/20/2) (*C*), proton-density image (*D*), and T2-weighted image (2000/20,80/2) (*E*). The diagnosis of chorioretinitis was established clinically.

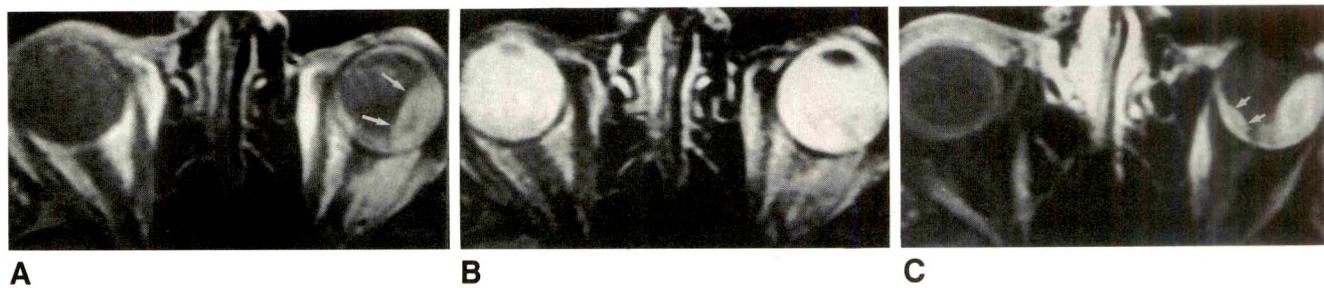


Fig. 6.—60-year-old man with choroidal melanoma diagnosed by sonography.

A, Proton-density image (2000/30/2) shows a lenticular-shaped mass in left lateral globe (arrows).

B, T2-weighted image (2000/80/2) is unremarkable.

C, Postcontrast fat-suppression image (600/20/2) clearly shows the mass. The right extension of mass (arrows) is seen better here than on proton-density image.

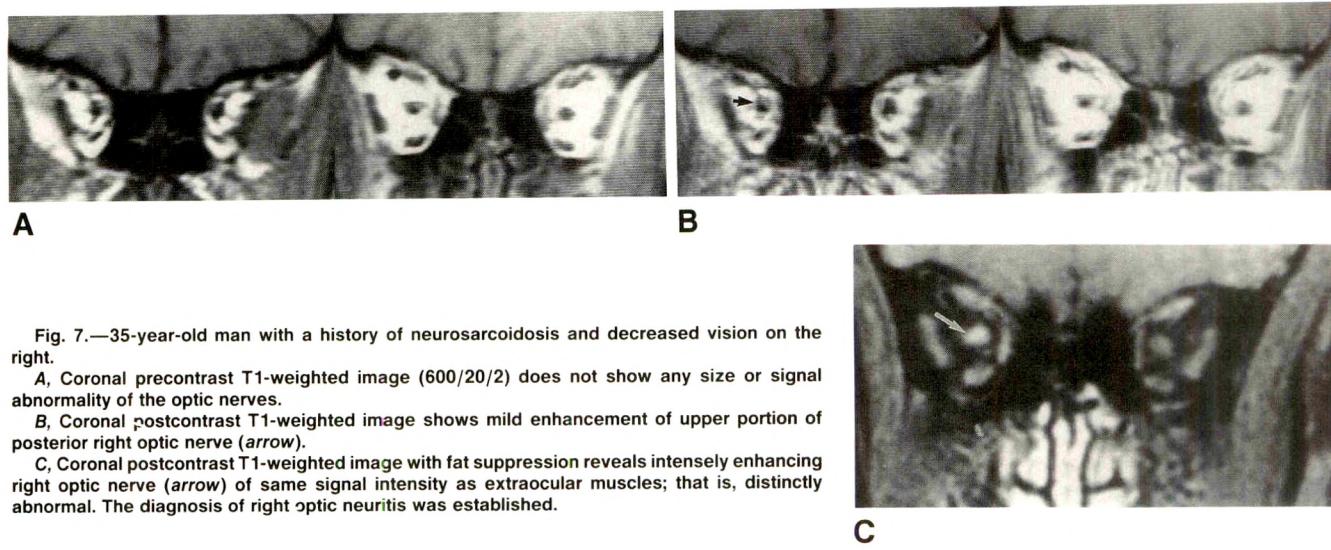
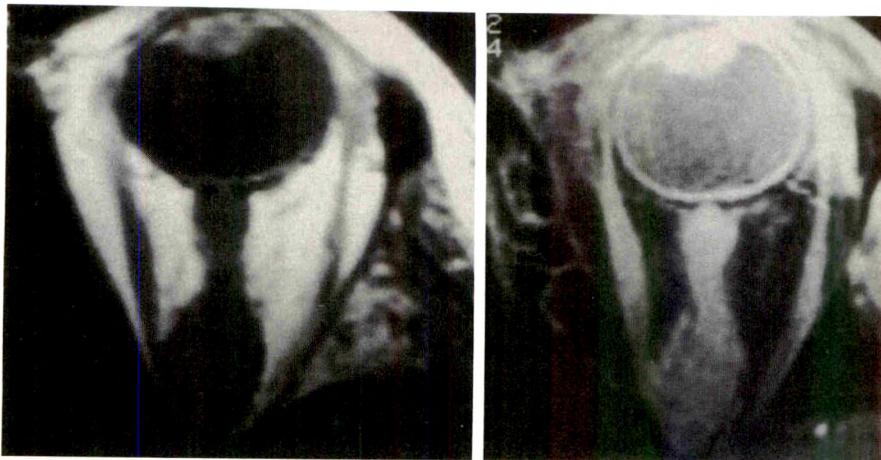


Fig. 7.—35-year-old man with a history of neurosarcoidosis and decreased vision on the right.

A, Coronal precontrast T1-weighted image (600/20/2) does not show any size or signal abnormality of the optic nerves.

B, Coronal postcontrast T1-weighted image shows mild enhancement of upper portion of posterior right optic nerve (arrow).

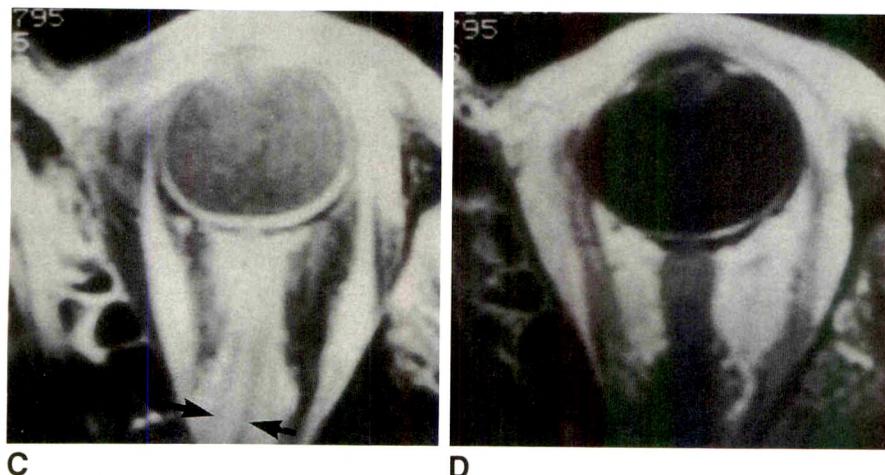
C, Coronal postcontrast T1-weighted image with fat suppression reveals intensely enhancing right optic nerve (arrow) of same signal intensity as extraocular muscles; that is, distinctly abnormal. The diagnosis of right optic neuritis was established.



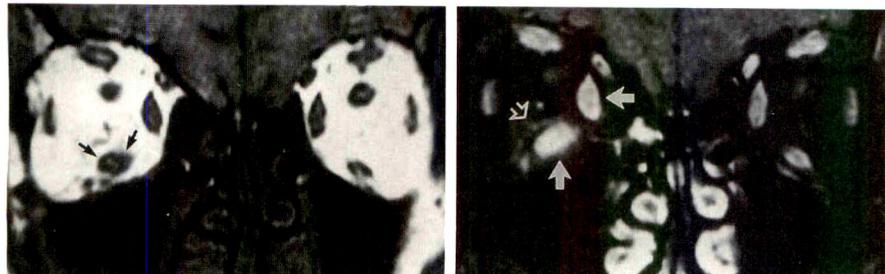
A **B**

Fig. 8.—60-year-old woman with left visual loss.

A–D, Axial T1-weighted image (600/20/2) (*A*), T1-weighted image with fat suppression (*B*), postcontrast T1-weighted image with fat suppression (*C*), and postcontrast T1-weighted image without fat suppression (*D*) all show bumpy perineural tumor. In *C*, the tram-track sign (arrows) is clearly visible, which is typical of optic nerve meningioma.



C **D**

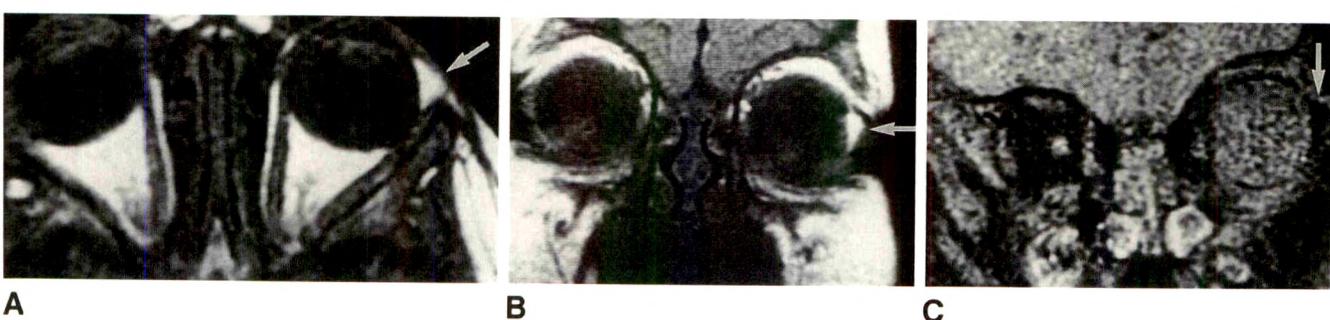


A **B**

Fig. 9.—33-year-old woman with hyperthyroidism and mild right exophthalmos.

A, Coronal T1-weighted image (600/20) shows mild thickening of right inferior rectus muscle (arrows) and perhaps of right medial rectus muscle.

B, Postcontrast coronal T1-weighted image (600/20) clearly shows the thickened and intensely enhancing right inferior and medial rectus muscles (solid arrows) as compared with left eye. Inflammatory infiltrate around right inferior rectus muscle is also noted (open arrow).



A **B** **C**

Fig. 10.—5-month-old boy with clinical probability of Goldenhar syndrome.

A and *B*, Axial (*A*) and coronal (*B*) T1-weighted images (600/20/2) reveal high-signal tissue in left epibulbar space (arrows) just inferior to lacrimal gland.

C, Coronal T1-weighted image (600/20/1) with fat suppression completely suppresses the signal from this tissue (arrow), thus indicating its fatty nature. This tissue is consistent with an epibulbar dermoid, which is frequently seen in patients with Goldenhar syndrome. Because the baby was waking up from sedation, we performed the sequence by using 1 excitation and a 256 × 128 matrix to shorten the study time. Thus, these images have a low signal-to-noise ratio.

Fig. 11.—20-year-old man with neurofibromatosis.

A, Coronal T1-weighted image (600/20/2) reveals a dysplastic right bony orbit. High-signal intraorbital fat appears to herniate into upper maxillary sinus (straight white arrow). Also, abnormal soft tissue in right face (curved white arrows) and large optic nerve (black arrow) are noted. Some metallic susceptibility artifacts were seen in right temporal region (arrowheads), induced by clips from a prior biopsy.

B, Coronal postcontrast T1-weighted image (600/20/2) with fat suppression shows the enhancing plexiform neurofibromas involving the optic nerve (curved black arrow), muscle cone (open white arrows), and right facial muscles (curved white arrow). Margins of tumors can be seen much better.

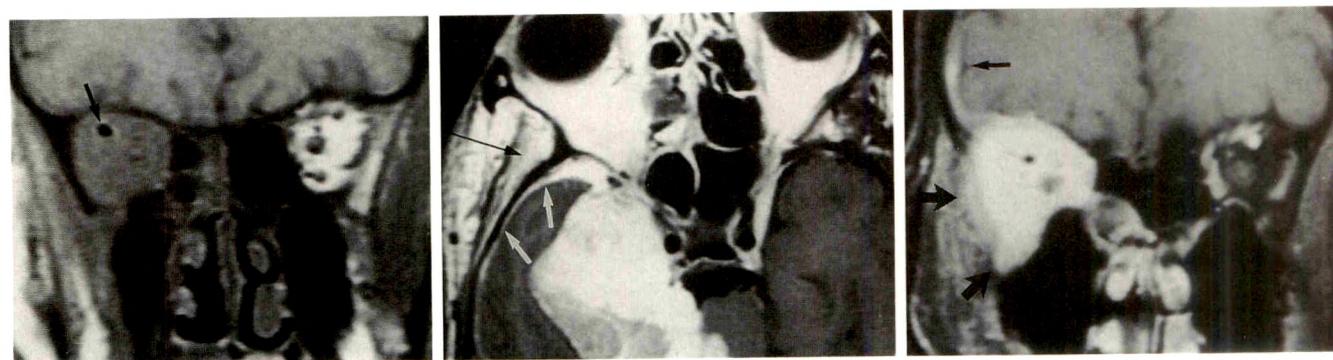
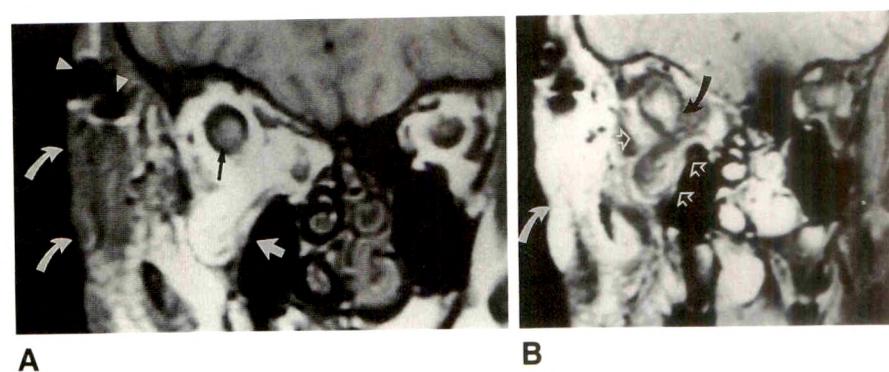
**A****B****C**

Fig. 12.—35-year-old man with a history of adenoid cystic carcinoma of the right submandibular gland.

A, Coronal T1-weighted image (600/20/2) shows right orbit filled with tumor. A small hypointense artifact from radioactive material implant is noted (arrow).

B, Axial postcontrast T1-weighted image shows enhancing tumor in right orbit and its large intracranial component. Leptomeningeal spread (white arrows) and sphenoid infiltration (black arrow) are evident.

C, Postcontrast T1-weighted image with fat suppression clearly shows both the inferior and lateral margins of tumor (large black arrows) and leptomeningeal tumoral extension (small black arrow).

be hyperintense relative to surrounding suppressed fatty tissue, and the margins of the mass were depicted better than on conventional MR images. This was proved to be a dacryocystocele.

Mixed Intra- and Extraconal Lesions

The postcontrast hybrid T1-weighted images were superior for detecting the enhancing tumors and for depicting the lesion margins in three patients with intraorbital masses—two plexiform neurofibromas (Fig. 11) and one adenoid cystic carcinoma (Fig. 12).

Lesions Adjacent to the Orbit

One patient with left sphenoid ridge meningioma was studied to evaluate the possibility of invasion of the lesion into the optic canal. The postcontrast hybrid T1-weighted images clearly demonstrated the enhancing sphenoid meningioma and showed the intracanalicular optic nerve to be intact.

Two other patients had soft-tissue masses in the sinuses with possible intraorbital invasion. One had adenoid cystic carcinoma of the left maxillary sinus, with the tumor attached to the floor of the orbit, and another patient had ethmoidal

masses that proved to be polyposis (Fig. 13). In each case, the postcontrast hybrid coronal T1-weighted images demonstrated sharper tissue margin contrast between the enhanced mass and the intraorbital contents than did the conventional MR images.

Discussion

Large amounts of fat in the orbit outline the optic nerve sheath and extraocular muscle sheaths, globe, and orbital vessels. High contrast/noise ratios are obtained on T1-weighted images for most anatomic structures except the lacrimal gland. However, the high-intensity bands perpendicular to the frequency-encoding axis at the fat-water interface from chemical-shift misregistration can be seen parallel to the long axis of the optic nerve sheath and muscles on the axial images, and above and below the nerve and muscles on the coronal images, in accordance with the direction of the frequency-encoding gradient, which obscures the details of the optic nerve and extraocular muscles ([1] and Quencer et al., paper presented at the annual meeting of the Radiological Society of North America, Chicago, December 1988). Also, the intracanalicular segment of the optic nerve is often obscured by marrow signal from the adjacent bony canal, and

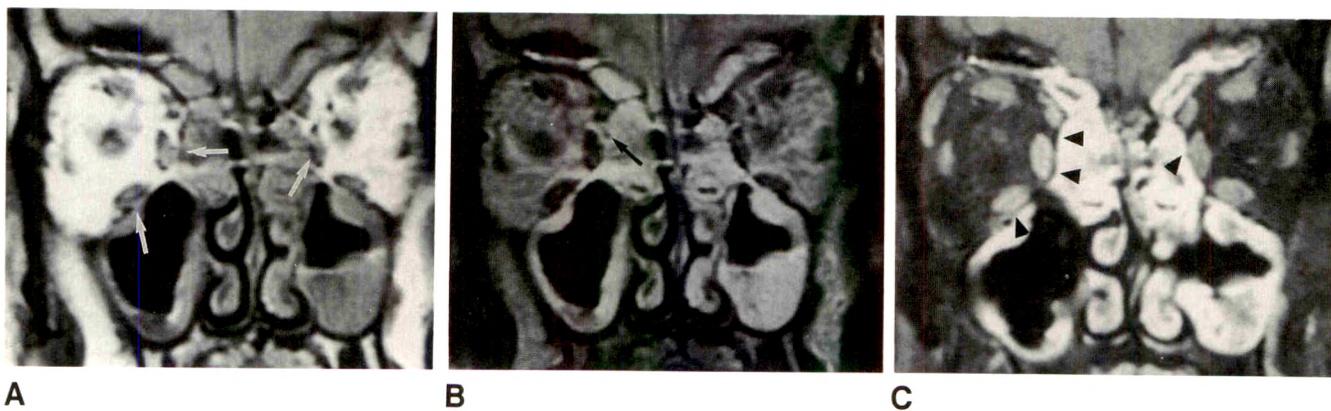


Fig. 13.—17-year-old boy with biopsy-proved ethmoidal polyposis.

A and **B**, Conventional coronal T1-weighted image (600/20/2) (**A**) and conventional coronal T2-weighted image (2000/70/2) (**B**) show diffuse soft tissue in ethmoidal and frontal sinuses. However, the orbital and polypoid tissue interface is not entirely distinct (white arrows in **A**, black arrow in **B**). **C**, Postcontrast T1-weighted image (600/20/2) with fat suppression sharply delineates entire tissue interface (arrowheads). There is no evidence of intraorbital invasion by this soft tissue.

the high-signal orbital fat interfaces with the separation of the optic nerve, CSF, and dural sheath. The posterior wall of the globe contrasts poorly with adjacent vitreous humor.

With current fat-suppression techniques, the signal intensity relationships between the optic nerve and fat, lacrimal gland and fat, and muscle and fat reversal to strongly positive ratios, resulting in a more accurate representation of the thickness of the optic nerve, muscles, and contour of the lacrimal gland [4] (Fig. 3). The elimination of chemical-shift artifact results in truer anatomic borders. The intracanalicular optic nerve is more clearly identified owing to removal of the surrounding fatty marrow signal (Fig. 4). After contrast administration, the extraocular muscles and lacrimal glands enhance intensely but the optic nerves do not enhance (Fig. 3H). As a result, the margins of these structures are seen even better than with noncontrast fat-suppression T1-weighted imaging. The posterior wall of the globe also enhances as a thin, smooth line of high signal intensity, probably from the combined enhancement of vasculature structures in the chorioretina, the uveal-scleral coat, and the posterior fascial sheath of the eye (Tenon capsule). Although we used a combination of the frequency-selective excitation method and the chopper variant of Dixon's method, other methods of fat suppression can be used provided that fat is suppressed uniformly [8, 9]. For example, it has been demonstrated that the gradient reversal technique has been applied successfully to eliminate lipid signal in the orbits [8]. However, the use of STIR (short T1 inversion recovery) sequences might be suboptimal in conjunction with the paramagnetic contrast agent because while the STIR sequence eliminates the fat signal, it also decreases the signal of the lesion—a phenomenon known as negative enhancement [10].

The two cases of chorioretinitis (Fig. 5) were only detected on postcontrast fat-suppressed T1-weighted images as irregularly thickened enhancing bands that were distinctly different from normal enhancing tissue. In the case of choroidal melanoma, the postcontrast fat-suppressed T1-weighted image gave the best definition of the tumor. It was also seen well

on noncontrast proton-density images, but was totally isointense with vitreous on T2-weighted images. Because of the sharp contrast between the vitreous posterior wall of the globe and suppressed adjacent intraorbital fat, we believe postcontrast fat-suppressed T1-weighted imaging will give the best definition of the margins of an enhancing global tumor. In the case of optic neuritis, the involved optic nerve enhanced to a similar degree as the extraocular muscles, and was distinctly abnormal on postcontrast fat-suppressed T1-weighted images (Fig. 7C). The diagnosis could not be made confidently on any other MR sequences. In a general article reviewing fat-suppression imaging with contrast-enhanced imaging [5], the authors stated that while they had limited experience with this technique in acute optic neuritis, enhancement might be expected in the acute demyelinating-inflammatory stage. Our preliminary, limited experience concurs with that postulate.

The tram-track sign, typical of optic meningioma, was only seen with certainty on postcontrast fat-suppression T1-weighted imaging because of better tissue contrast between the tumor and perineurial subarachnoid space (Fig. 8). Owing to large amounts of intraorbital fat, tumor invasion into the orbit is always a problem for conventional MR. The high-signal orbital fat frequently obscures the margins of tumor, and volume-averaging artifact from fat always causes difficulty in noncontrast T1-weighted imaging. After contrast administration, the enhancing tumor blends with the orbital fat and further degrades the images. We found that postcontrast fat-suppression T1-weighted imaging gave superior contrast for detecting enhancing tumor and its margins in any intraorbital compartment. Inflammatory infiltration of the paramuscular fat in Graves disease could only be seen on postcontrast T1-weighted fat-suppression images (Fig. 9). Dermoid is also a common lesion in the area of the lacrimal fossa. A single fat-suppression T1-weighted image can easily provide the diagnosis (Fig. 10). The conventional long TR/long TE images did not suppress intraorbital fat signal satisfactorily, and chemical-shift artifact was still noticed in our patients. We found these

sequences were not very useful in diagnosing orbital lesions. Owing to the insensitivity of conventional MR imaging for detecting bony cortex and the possibility of a lesion being obscured by interference from the high-signal intraorbital fat, CT is still frequently requested to assess the possibility of intraorbital invasion by tumor or infection from adjacent compartments, such as maxillary sinuses, ethmoidal sinuses, and sphenoid ridge. However, the sharp contrast between enhancing masses relative to the suppressed intraorbital fat on postcontrast fat-suppressed T1-weighted images may be useful in evaluating intraorbital extension of a lesion, although the integrity of the bone itself is still difficult to assess (Fig. 13). The specific reason that the lesion margins were displayed better on the hybrid, contrast-enhanced image in the patient with ethmoidal polyposis is not entirely clear; however, the most likely explanation is that the inflammatory process in the ethmoidal sinuses induced secondary edema in the adjacent orbital fat. With contrast administration plus fat suppression, the enhancing polyps and inflammatory membranes within the sinuses are contrasted against the nonenhancing edema.

In conclusion, although we found the hybrid technique promising, we need to emphasize that these preliminary results are based on a limited number of patients. We believe this fat-suppression technique has benefits and that it can be performed without increasing imaging time and image postprocessing. Uneven fat suppression can happen with a large field of view as a result of field inhomogeneity [5], although, to date, we have not noticed any uneven fat suppression in the orbits. We did, however, note a small increased magnetic susceptibility artifact between the ethmoid sinuses and frontal lobe due to air–soft tissue interface (Figs. 3F and 3I), but this artifact did not reduce our diagnostic accuracy. Conventional T1- and T2-weighted imaging might still be useful in certain cases of intraocular tumor, such as uveal melanotic melanoma, if enough melanin exists, since melanin can appear hyperintense on T1 images and hypointense on T2 images [11, 12]. The signal intensities on MR of our patient with choroidal melanoma did not help the diagnosis, probably owing to the low melanin content of the tumor [11].

Our preliminary data suggest that fat-suppression T1-weighted imaging is a useful adjunct in evaluating orbital and paraorbital lesions. Moreover, postcontrast fat-suppressed T1-weighted imaging is most beneficial and should replace conventional postcontrast T1-weighted imaging, as it provides the best anatomic details, improves the detection of the enhancing lesions, and defines tissue interfaces better without increasing imaging or postprocessing time.

ACKNOWLEDGMENT

We appreciate the editorial effort by Cathy Fix.

REFERENCES

1. Simon J, Szumowski J, Totterman S, et al. Fat-suppression MR imaging of the orbit. *AJNR* **1988**;9:961–968
2. Simon J, Szumowski J. Chemical shift imaging with paramagnetic contrast material enhancement for improved lesion depiction. *Radiology* **1989**;171:539–543
3. Szumowski J, Eisen JK, Vinitski S, et al. Hybrid methods of chemical-shift imaging. *Magn Reson Med* **1989**;9:379–388
4. Poon CS, Szumowski J, Plewes DB, et al. Fat/water quantitation and differential relaxation time measurement using chemical shift imaging technique. *Magn Reson Imaging* **1989**;7:369–382
5. Szumowski J, Plewes DB. Separation of lipid and water MR imaging signals by chopper averaging in the time domain. *Radiology* **1987**;165:247–250
6. Haase A, Frahm J, Hanicke W, et al. 1H NMR chemical shift selective (CHESS) imaging. *Phys Med Biol* **1985**;30:341–344
7. Dixon WT. Simple proton spectroscopic imaging. *Radiology* **1984**;189:193–194
8. Hore PJ. Solvent suppression in Fourier transform NMR. *J Magn Reson* **1983**;55:283–291
9. Atlas SW, Grossman RI, Hackney DB, et al. STIR MR imaging of the orbit. *AJNR* **1988**;9:969–974
10. Bydder GM, Steiner RE, Blumgart LH, et al. MR imaging of the liver using short T1 inversion recovery sequences. *J Comput Assist Tomogr* **1985**;9:1084
11. Peyster RG, Augsburger JJ, Shields JA, et al. Intraocular tumors: evaluation with MR imaging. *Radiology* **1988**;168:773–779
12. Mafee MF, Peyman GA, Grisolano JE, et al. Malignant uveal melanoma and simulating lesions: MR imaging evaluation. *Radiology* **1986**;160:773–780

Book Review



Maxillofacial Imaging. By Angelo M. Delbalso. Philadelphia: Saunders, 815 pp., 1990. \$125

This book has several contributing authors and covers virtually all regions of the head and neck. As with all books with more than one author, the quality of the illustrations and the text varies, but in general the book achieves a high quality. The authors are both clinicians and radiologists, with representatives from dentistry as well as medicine. The selection of authors of the various chapters was an attempt by Delbalso to integrate the clinical and imaging aspects. This is extremely difficult to accomplish when such a wide field is covered.

The book has many good points. Chapters 1-3, which include the first 136 pages, deal to a large extent with trauma. The first chapter, on panoramic zonography, is an advocacy type of discussion, and many of the illustrations are not particularly convincing. The fractures that are shown could be seen better with high-quality plain films and CT scans. The authors suggest that the equipment should be expanded beyond classic dental imaging to include trauma of the midface and mandible, a point that is not proved. Chapter 4, on sinus disease, is a marked improvement and starts out with a detailed well-labeled section on anatomy that should be quite helpful to beginners in head and neck radiology. The discussions on pathology are concise and adequately cover the field. Minor mistakes are apparent but not alarmingly so. For instance, on page 143, Figure 4-3B reputedly shows air cells in the crista galli. To me, it has the appearance of an air cell in the frontal sinus septum, which is frequently a clinical problem because of poor drainage. On the same page, the discussion of agger nasi cells is vague rather than giving the specific location, which is anterior to the middle meatus.

Chapter 9, on radiology of the jaw, is good and has an excellent discussion of mandibular tumors. All of the illustrations are quite clear. The classification of tumors provides readers a ready reference. An interesting technique is used for references in this chapter. Suggestions for further reading are listed under disease entities so that an

interested student readily can select authoritative sources for detailed knowledge on the subject.

Many of the chapters must be considered from a neutral point of view. They provide good introductions to the numerous topics covered; however, because of the volume of material covered, the discussions have little depth. The reader would need a book like those by Mancuso or Som and Burgeron for a complete discussion of malignancies of the head and neck. As with any text, some of the techniques illustrated clearly are outmoded, such as air cisternography for acoustic neuroma and some of the early illustrations from CT and MR. Many of the tomograms of the temporal mandibular joint leave much to be desired. On a positive note, the chapters on tumors of the mouth and oral cavity are outstanding. High-quality CT scans are provided throughout the chapter. The labeling of normal anatomy is excellent. The techniques used for examination are all clearly written. The authors of the chapter even include excellent MR images of the tongue and oral cavity. The chapter on the paranasal sinuses is well worth reading and is illustrated clearly. Many of the images of fascial fractures are quite helpful.

In summary, this book can be recommended to radiologists and members of the dental profession as a handy reference for more common problems of maxillofacial imaging. The more unusual or exotic problems still will require searches of the literature or more detailed texts for elucidation. Medical students and paramedical personnel could make good use of this book as an introduction to many of the facets of maxillofacial imaging. The authors and the publishers are to be congratulated on assembling such a large volume of material at such a reasonable price in a quality publication.

William Hanafee
University of California, Los Angeles
Los Angeles, CA 90024-1721

Effects of Magnetic Susceptibility Artifacts and Motion in Evaluating the Cervical Neural Foramina on 3DFT Gradient-Echo MR Imaging

Jay S. Tsuruda¹
Kent Remley

The purpose of this study was to evaluate in vitro the effects of magnetic susceptibility and motion on the estimation of neural foraminal diameter with three-dimensional Fourier transformation (3DFT) gradient-recalled MR imaging as compared with CT. A cervical spine phantom was constructed from desiccated human cervical vertebral bodies embedded in a water-based proteinaceous gel. The phantom was imaged with thin-section 1.5-mm axial CT and 1.5-mm axial 3DFT gradient-recalled MR using a constant TR (35 msec) and flip angle (5°), while the TE was varied from 11 to 22 msec. During imaging, the phantom either was kept stationary or underwent subtle, intermittent motion. Compared with CT, MR consistently underestimated the diameters of the neural foramina, leading to overestimation of neural foraminal stenosis. The degree of overestimation varied directly with increasing TE values, from 8% (TE = 11 msec) to 27% (TE = 22 msec). Motion artifacts also increased foraminal overestimation and mimicked osseous hypertrophy.

The effect of image degradation due to motion was noted to increase with longer TE values. Image degradation caused by magnetic susceptibility and motion artifacts can be minimized by using the shortest TE possible. We do not recommend the use of 3DFT gradient-recalled MR imaging for the evaluation of cervical radiculopathy if patient motion is anticipated.

AJNR 12:237–241, March/April 1991; AJR 156:1069–1073, May 1991

MR imaging of the cervical spine is currently the preferred method at our institution in the initial evaluation of patients with cervical radiculopathy. With the recent implementation of three-dimensional Fourier transformation (3DFT) gradient-recalled-echo (GRE) imaging for the evaluation of cervical radiculopathy [1], thin-section (1.5–2.0 mm) images that demonstrate adequate image contrast and signal-to-noise can be obtained. At our institution we have anecdotally found that in most instances 3DFT GRE images provide excellent detail of the neural foramina, comparable to that of CT images. However, in some of our patients there has been an overestimation of the degree of neural foraminal stenosis on 3DFT GRE MR when compared with CT and surgical findings. Since partial-volume effects theoretically should be reduced with thin-section 3DFT GRE imaging, a reason for this discrepancy was sought.

Magnetic susceptibility effects inherent with GRE imaging have been suggested as one possible reason for this discrepancy [2–4]. In addition, 3DFT GRE studies are also sensitive to patient motion, presumably owing to the addition of a second phase-encoded gradient, which is required for resolving the individual slices [1]. Therefore, we designed a study with a phantom model to evaluate the effects of magnetic susceptibility and/or motion on the estimation of neural foraminal diameter when using 3DFT GRE MR imaging.

Received July 17, 1990; revision requested September 24, 1990; revision received October 22, 1990; accepted October 24, 1990.

Presented at the annual meeting of the American Society of Neuroradiology, Los Angeles, March 1990.

¹ Both authors: Department of Radiology, Box 0628, University of California, San Francisco, 505 Parnassus Ave., San Francisco, CA 94143-0628. Address reprint requests to J. S. Tsuruda.

0361-803X/91/1565-1069\$00.75
© American Roentgen Ray Society

Materials and Methods

A phantom model was constructed with desiccated cadaveric vertebrae from the C5 through the T1 levels. The spinous processes were immobilized in clay, and a "vertebral column" was formed and embedded in a water-based proteinaceous gel. The composition of this gel [5] was specifically designed to give T1 and T2 relaxation properties that mimic soft tissue. The overall cross-sectional diameter of the entire phantom was similar to that of an adult human neck.

Thin-section CT (GE 9800 unit, General Electric, Milwaukee, WI) was performed with axial 1.5-mm-thick contiguous sections (140 kV, 120 mA, 3 sec, and 14-cm field of view [FOV]). The images were magnified two times and viewed at bone-review settings (length × width = 550 × 1500). The neural foramen was identified as the obliquely oriented soft-tissue space, immediately cephalad to the disk space, bordered by the vertebral body and uncinate process anteriorly and medially and the corresponding superior facet of the articular pillar posteriorly. A single cross-sectional diameter, representing the largest oblique cross section, was taken at each of the three levels bilaterally. All measurements were obtained by using electronic calipers while the image was visualized on the CT monitor. Since three levels were included in the phantom, a total of six foraminal measurements (two at each level) were obtained.

The identical phantom was scanned at 1.5 T (General Electric Signa unit) by using a 5-in. (12.7-cm) posterior planar surface coil. Multiple 3DFT GRE acquisitions were obtained with these parameters: 35/11, 15, 20, 22/2 (TR/TEs/excitations), 256 × 128 × 64 matrix, 20-cm FOV, and 1.5-mm-thick partitions. The slice-select phase-encoding gradient was oriented in the z axis, thus yielding 64 axial partitions. The imaging time for this protocol was 9 min 32 sec.

The TE was varied from 11 to 22 msec for each acquisition, keeping the TR constant, and the neural foramina were electronically measured at levels identical to the locations on the CT images while viewing the images on the MR monitor with twofold magnification. Three measurements were obtained from each neural foramen and averaged. A percent difference from the CT measurement was calculated by using the formula:

$$\frac{\text{CT measurement} - \text{MR measurement}}{\text{CT measurement}} \times 100 = \% \text{ difference.}$$

For each acquisition, the average percent difference was obtained by calculating the mean of the percent differences at all three levels.

The MR studies were then repeated using the same acquisition parameters with TE values of 11, 15, 20, or 22 msec. During the image acquisition, motion was induced by gently rocking the phantom back and forth by 2–3 mm for approximately 5 sec separated by 30 sec of nonmotion in which the phantom was returned to the same starting position. All motion was induced by hand from the same person, positioned within the bore of the magnet, for all four studies. The neural foraminal measurements were then made as before at the same levels.

Results

The average neural foraminal diameter on CT measured 5.3 mm (range, 4.8–5.8) (Fig. 1A). In all cases, the dimensions measured with MR were less; thus, overestimation of neural foraminal stenosis was a consistent finding. In the nonmotion MR studies, the sequence that correlated best with CT measurements had the shortest TE (11 msec) (Fig. 1B). In this case, the average percent difference was the smallest (8%). As the TE was increased from 11 to 22 msec, the measured foraminal diameter progressively decreased and the percent difference between the CT and MR measurements correspondingly increased up to a maximum of 27%. The results are depicted in Figure 2.

After motion was introduced during the MR acquisition, the neural foraminal measurements during motion were compared with the nonmotion sequences (Fig. 3). On the motion images, the degree of underestimation of the neural foraminal diameter (overestimation of foraminal stenosis) was uniformly greater for each selected TE (Fig. 2). The smallest amount of artifact was encountered at TE = 11 msec (17%); it increased markedly as the TE was increased. In addition, qualitative assessment from motion degradation revealed exaggerated osseous contours that mimicked osseous hypertrophy and

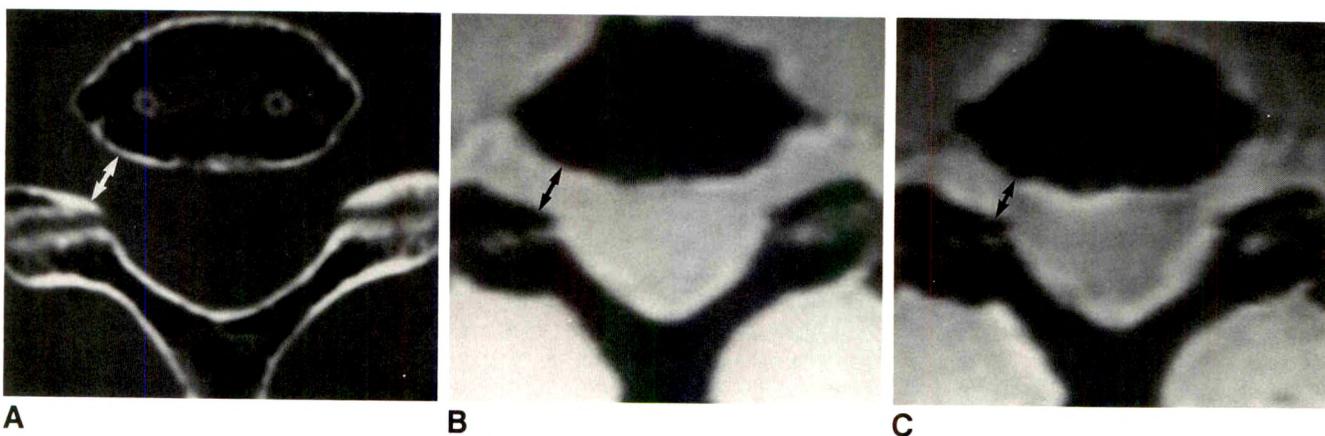


Fig. 1.—Axial sections through C7-T1 level.

A and B, CT section (A) and corresponding GRE 35/11 image (B) show similar osseous morphology of neural foramina.

C, Slight irregularity and narrowing of neural foramina on GRE 35/15 image is attributed to magnetic susceptibility artifact. Arrows indicate typical placement of measurement cursors (see text). In this example, dimensions of right C7-T1 neural foramen were 5.3 mm (CT), 4.9 mm (GRE 35/11), and 4.4 mm (GRE 35/15).

spur formation (Fig. 3B). In some instances, the background intensity of the soft tissue within the neural foramen and the spinal canal was quite heterogeneous, with signal loss not conforming to any anatomic structure (Fig. 3B) and approaching the intensity of bone. Accurate measurements of the neural foraminal diameter were difficult to obtain. In these cases, a gross estimate was obtained. The degree of apparent "motion" artifact was greatest with a TE of 22 msec. As a result, the data obtained at this TE were thought to be unreliable and were not included in the final results. A summary of all neural foraminal measurements is presented in Table 1.

Discussion

MR imaging of the cervical spine has proved to be a valuable tool in the evaluation of cervical radiculopathy. Previous reports have discussed the utility of spin-echo and GRE two-dimensional Fourier transformation (2DFT) imaging [2, 6] with favorable results. More recently, 3DFT GRE imaging has

been reported to offer an advantage over 2DFT techniques due to the reduction of partial-volume averaging, thus improving diagnostic confidence [1].

Our clinical experience with 3DFT GRE in the routine initial evaluation of cervical radiculopathy has usually provided very good correlation with CT findings. However, on occasion, neural foraminal stenosis appears significantly greater with 3DFT GRE, producing false-positive results. Because of the variable manifestations of this apparent artifact among different patients, it was thought that magnetic susceptibility alone could not account for these findings and other factors such as patient motion may be contributory. Our phantom model was developed to investigate a possible reason for these observations.

Magnetic susceptibility artifact involving the cervical spine on 2DFT GRE imaging has been reported [3]. This artifact occurs when magnetic induction from an applied magnetic field varies between different tissues, resulting in local field inhomogeneity. Spins subjected to these intrinsic magnetic field gradients lose phase coherence, with a resulting decrease in the signal intensity of the imaging voxel. There is also spatial misregistration in areas of greatly differing magnetic susceptibility, resulting in geometric distortion with variable effect on pixel intensity [7].

TABLE 1: Foraminal Diameters at Three Different Vertebral Levels as Measured on CT and MR Images

Images Measured	Right Side/Left Side (mm)			% Difference from CT ^a
	C5-C6	C6-C7	C7-T1	
CT	5.8/5.4	5.3/5.1	5.3/4.8	
GRE 35/11				
Without motion	5.5/5.4	4.5/4.4	4.9/4.6	8
With motion	5.0/4.4	4.4/3.8	4.3/4.4	17
GRE 35/15				
Without motion	5.4/4.8	4.4/4.3	4.4/4.6	12
With motion	5.4/4.7	4.1/3.5	3.7/3.4	22
GRE 35/20				
Without motion	5.0/4.1	4.2/3.3	4.4/3.7	23
With motion	4.9/4.0	4.5/3.1	4.3/2.9	26
GRE 35/22				
Without motion ^b	5.0/4.3	3.9/3.7	3.7/2.8	27

^a % Difference was calculated according to the formula: [(CT measurement - MR measurement)/CT measurement] × 100.

^b Dimensions on GRE 35/22 images obtained "with motion" were difficult to measure accurately and were not included in the final results.

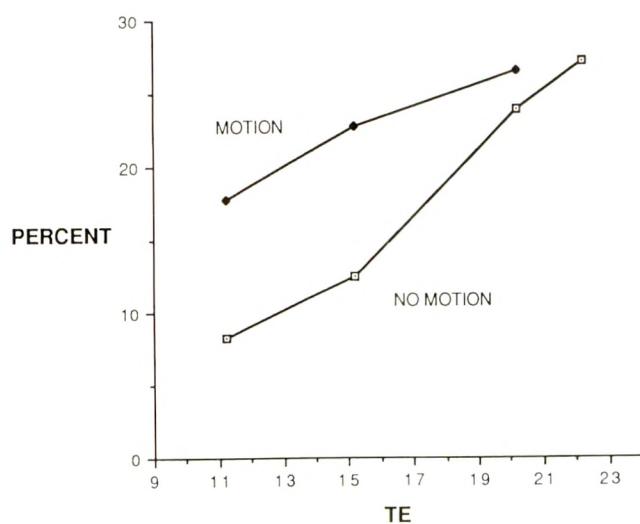
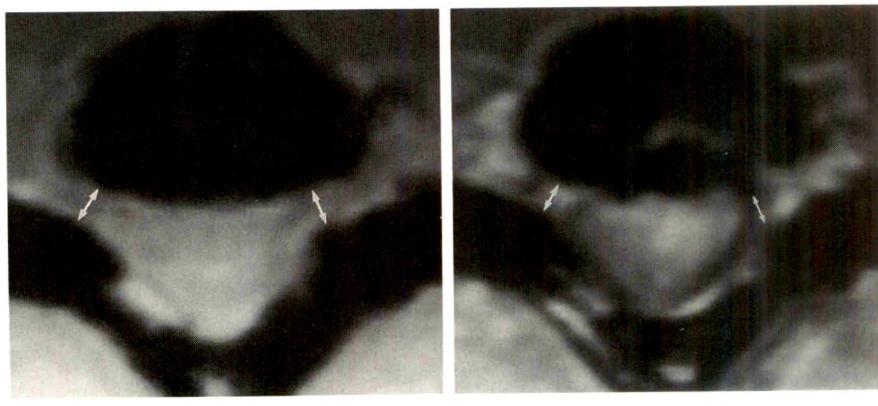


Fig. 2.—Graphic representation of percent overestimation of neural foraminal stenosis as a function of TE. Data from stationary as well as moving phantoms are shown.

Fig. 3.—Effect of phantom motion.

A and **B**, GRE 35/15 images at C6-C7 level without (**A**) and with (**B**) motion. Motion-induced pseudoosseous hypertrophy resulting in overestimation of neural foraminal stenosis is evident with increased heterogeneity within soft-tissue matrix causing reduction of sharp interfaces between bone and soft tissue. In this example, left neural foramen demonstrates the greatest motion degradation and corresponding reduction in measurement accuracy (see text). Left neural foraminal dimensions are 4.3 mm without motion and approximately 3.5 mm with motion. Dimensions on right are 4.4 and 4.1 mm, respectively.



A

B

Significant magnetic susceptibility differences have been shown to occur at bone-soft tissue interfaces such as the neural foramina, at air-soft tissue interfaces such as the skull base, or in regions of high paramagnetism such as hemorrhage [2, 4, 8]. GRE imaging is more vulnerable to this artifact than spin-echo imaging is owing to the lack of a 180° pulse; therefore, the loss of spin refocusing is sensitive to gradient inhomogeneities and the artifacts will become progressively greater as the TE or main magnetic field is increased. With increasing severity of artifacts, distortion of the bone-soft tissue interfaces on GRE images of the cervical spine results in apparent enlargement of osteophyte size and progressive narrowing of the spinal canal and neural foramina. As a result, GRE scanning should be performed with a TE of 20 msec or less [2].

In our experimental findings, the initial phantom study showed the effect of magnetic susceptibility on image quality. With a TE of 11 msec, there was reasonable correlation between MR and CT in the estimation of neural foraminal diameter (8% overestimation). However, even with a slight increase in the TE to 15 msec, there was a detectable increase in the overestimation to 12%. This degree of overestimation is important since a TE of 15 msec is the minimum possible with our current software due to the requirements of gradient-moment nulling used to reduce pulsatile CSF artifacts. As a result, the interpretation of any given clinical study needs to consider this factor. With TEs in the range of 20–22 msec, corresponding to overestimations of 23–27%, this artifact was determined to be unacceptable.

The degree of magnetic susceptibility is also directly proportional to voxel size and inversely proportional to increasing spatial resolution [9]. Larger voxels allow stronger intrinsic magnetic field gradients to build up across the imaging volume, thus causing greater geometric distortion and phase dispersion and resulting in signal loss. A constant voxel size of 1.8 mm³ was used in this study. Although the impact of changes in voxel size was not addressed, decreasing voxel dimensions would be expected to reduce magnetic susceptibility effects in a fashion similar to TE reduction.

An attempt was made to measure the impact of hypothetical patient motion by minimally rocking the phantom in a random fashion. This motion significantly affected the accuracy of the measurements of neural foraminal diameter, with the greatest percent difference noted at the highest TE range. This was especially true when the motion-degraded study was performed with TE = 22 msec, which leads to uninterpretable images. Also, even at the shortest TE tested (TE = 11 msec), motion can still contribute to image distortion (17% vs 8% overestimation). The relative contribution of motion to image degradation was less apparent at longer TEs, that is, the two curves from Figure 2 converge. This probably occurred because the baseline (nonmotion) images at longer TEs already were degraded from magnetic susceptibility, and further motion degradation, although real, may have been somewhat obscured.

Qualitatively, phantom motion distorts the bone-soft tissue interface (Fig. 3), causing small areas of osseous hypertrophy to be enlarged and creating new regions of irregular bone

contours. These findings are quite disconcerting since the amount of motion to create this artifact was quite minimal and could easily be duplicated in any given clinical setting. Also, distinguishing an abnormal finding from a motion-induced artifact is not straightforward since both may have similar morphology. Therefore, critical evaluation of fine detail is not possible if any motion degradation is being considered. The greater inhomogeneity of the background soft tissue with motion (Fig. 3A) may provide a clue to the presence of motion artifacts. However, in an actual patient study, this inhomogeneity may be less obvious owing to the greater range of soft-tissue intensities.

The genesis of the motion artifact is thought to be the additional phase-encoding gradient required to resolve individual slices or partitions in a 3DFT acquisition [1]. Therefore, motion can cause both in-plane phase-encoding artifacts as well as out-of-plane artifacts owing to movement of neighboring voxels outside the partition of interest. It should be remembered that further motion degradation *in vivo* may be caused by physiologic phenomena such as CSF pulsations and flow within the epidural venous plexus. Determining the exact role of these additional factors would require construction of more complex physiologic phantoms.

An additional reason for overestimation may have been the truncation artifact that is associated with the use of 128 phase-encoding steps. This type of artifact may reduce image sharpness at bone-soft tissue interfaces and can be reduced if a matrix with 256 phase-encoding steps is used. In our experimental model, a matrix with 128 phase-encoding steps was selected since this is used for our clinical patients. This smaller matrix size was selected in an attempt to reduce the total imaging time with a 3DFT acquisition [1]. The consequences of increasing the matrix size were not tested; however, it is expected that a reduction in the degree of overestimation would occur for all TE values. Nonetheless, the positive effect of reducing the truncation artifact by doubling the phase-encoding matrix (with an associated twofold increase in the imaging time to over 18 min) might be offset by the greater chance of patient motion during this longer study.

Because of our results with a phantom, we have adopted a policy of using 3DFT GRE imaging only when there is total patient cooperation. This technique is never used if even the slightest image degradation is seen on the scout sagittal localizing images. In these instances, the 3DFT acquisition should be substituted with a multislice 2DFT GRE axial sequence. Other methods of reducing motion artifacts such as improved physical restraints, psychological preparation to reduce apprehension [10], or modifying data acquisition in order to encode and compensate for motion [11, 12] need further investigation.

In summary, when imaging with short TE 3DFT GRE MR, a degree of magnetic susceptibility artifact exists that may be within acceptable limits. However, the magnetic susceptibility artifact will increase significantly when longer TEs are used. Motion artifacts cause consistent image degradation and result in both quantitative overestimation of neural foraminal stenosis and a qualitative distortion of the bone-soft tissue interface that mimics degenerative osseous hypertrophy, pos-

sibly leading to a misdiagnosis. Motion artifact also increases with longer TEs. Imaging at the shortest possible TE will reduce but not totally eliminate both magnetic susceptibility and motion artifacts. The use of 3DFT GRE MR is not recommended if patient motion is anticipated.

ACKNOWLEDGMENTS

We thank Klaus Aicher and the Contrast Media Laboratory, University of California, San Francisco, for assistance in preparation of the phantom.

REFERENCES

1. Tsuruda J, Norman D, Dillon W, Newton T, Mills D. Three-dimensional gradient-recalled MR imaging as a screening tool for the diagnosis of cervical radiculopathy. *AJNR* **1989**;10:1263-1271
2. Czervionke L, Daniels D. Cervical spine anatomy and pathologic processes. In: Lee S, Zimmerman R, eds. *The radiologic clinics of North America. Imaging in neuroradiology*, part II. Philadelphia: Saunders, **1988**:931-936
3. Czervionke L, Daniels D, Wehrli F, et al. Magnetic susceptibility artifacts in gradient-recalled echo MR imaging. *AJNR* **1988**;9:1149-1155
4. Schick R, Wismer G, Davis K. Magnetic susceptibility effects secondary to out-of-plane air in fast MR scanning. *AJNR* **1988**;9:439-442
5. Madsen E, Fullerton G. Prospective tissue-mimicking materials for use in NMR imaging phantoms. *Magn Reson Imaging* **1982**;1:135-141
6. Kulkarni M, Narayana P, McCardle C, Yeakley J, Campagna N, Wehrli F. Cervical spine MR imaging using multislice gradient echo imaging: comparison with cardiac gated spin echo. *Magn Reson Imaging* **1988**;6:517-525
7. Ludeke K, Roschmann P, Tischler R. Susceptibility artefacts in NMR imaging. *Magn Reson Imaging* **1985**;3:329-343
8. Young I, Khenia S, Thomas D, et al. Clinical magnetic susceptibility mapping of the brain. *J Comput Assist Tomogr* **1987**;11(1):2-6
9. Young I, Cox I, Bryant D, Bydder G. The benefits of increasing spatial resolution as a means of reducing artifacts due to field inhomogeneities. *Magn Reson Imaging* **1988**;6:585-590
10. Quirk M, Letendre A, Ciottone R, Lingley J. Evaluation of three psychological interventions to reduce anxiety during MR imaging. *Radiology* **1989**;173:759-762
11. Blackband S. Spatial localization for motion-rejected NMR imaging: SLO-MOTION. *Magn Reson Med* **1990**;13:263-270
12. Ehman R, Felmlee J. Adaptive technique for high-definition MR imaging of moving structures. *Radiology* **1989**;173:255-263

Videotape Review



MRI of MS and White Matter Disease. By Murray A. Solomon. (Tape 1 in series 2 of Murray Solomon's Magnetic Resonance Video Review.) Burlingame, CA: Murray Solomon's MRVR, (408) 374-8897, 1990. Single tape, \$125; series of 6 tapes, \$545

This 110-min videotape on MR imaging of white matter disease begins with a review of the clinical and pathophysiologic background of multiple sclerosis (MS); this is followed by MR images of patients who have MS. For the other diseases discussed, the presentation of the clinical and pathologic background is intermixed with imaging findings. The intended audience is persons who have little or no background or experience in MR imaging or neuroradiology.

Despite its length, this tape is of scant value to its intended audience. The presentation is remarkably poorly organized. The first 40 min are devoted to a review of MS that is so repetitious that it contains relatively little information. The many tables used throughout the tape appear to have been photographed directly from textbooks and review articles. Consequently, the type is far too small to be read comfortably on a video monitor. The sources of these tables are never stated, and no indication is given that this material has been used with permission of the copyright owners. The discussion of the appearance of MS lesions does not mention the role of gadopentetate dimeglumine in characterizing acute inflammation or in distinguishing old from new lesions. The tape has no review of the appearance of the normal brain; therefore, some of the statements about MS could be misleading for a person whose background in MR is minimal. Dr. Solomon indicates that gradient-echo images should not be used for diagnosing MS. The adequacy of such images naturally depends on the imaging sequence and pulse parameters used and on the quality of the imaging unit. Because of the range of techniques available, sweeping recommendations about the usefulness of gradient-echo imaging should be made cautiously.

Reproduction of the MR images is poor, and frequent readjustments of brightness and contrast controls are necessary to try to optimize image quality. The presentation of imaging information is quite disorganized. The section on MS imaging patterns begins with a listing of a series of patterns of MR findings in MS. The first of these patterns is illustrated. Then the discussion digresses into a consideration of "blind spots," then to descriptions of other lesions that appear similar to MS, and then to discussions of progressive multifocal leukoencephalopathy. Dr. Solomon never returns to the rest of the MS patterns that he had begun to illustrate.

Many of the cases are presented in a misleading manner. For example, one illustration is unenhanced short TR short TE spin-echo images of a cavitated MS plaque with peripheral hyperintensity. Dr. Solomon indicates that this is typical of an acute plaque but does not clarify whether the hyperintensity on the short TR images or the

cavitation is the typical feature. Obviously cavitations often are found in older plaques and cannot be taken as evidence that a lesion is acute. A case of central pontine myelinolysis (CPM) is presented. It is suggested that hypointensity in the pons on short TR short TE lesions is characteristic of CPM, with no indication that any lesion that lengthens T1 can result in hypointensity on such images. A case of transverse myelitis is illustrated. The point is made that the absence of swelling of the cord indicates that the lesion is subacute or chronic. Contrast-enhanced images are not presented. As patients may have clinically acute transverse myelitis without cord swelling, it is quite misleading to suggest that all acute demyelinating lesions in the cord are accompanied by swelling. Long TR long TE images of the spinal cord of a patient with Guillain-Barré syndrome are presented. These show a focal hyperintensity in the cord, and this is presented as if this finding were characteristic of the disease. In fact, the presence of a hyperintense lesion in the cord in a patient with Guillain-Barré syndrome would require at least an explanation and might indicate a need to reconsider the diagnosis.

In summary, this tape has a number of serious problems: (1) The image quality is quite poor. (2) Extended portions of the tape have no MR images presented at all. (3) Only a single reference is offered, and no references are given to support many of the generalizations that I contend are inaccurate. (4) The presentation is extremely repetitive and poorly organized. The tape appears to have been created by splicing together a series of shorter lectures, with no attempt at editing to alleviate repetition. (5) No acknowledgment is given of the sources of a large amount of copyright-protected material.

Radiologists who desire a comprehensive discussion of MS and other white matter diseases would be far better served by consulting standard neurology textbooks such as those by Adams and Victor or by Asbury, McKhann, and McDonald. Any standard textbook of MR imaging or neuroradiology will include a discussion of white matter diseases. Although buying both a clinical neurology text and an MR imaging text would be more expensive than this videotape, 110 min spent reading these sources would yield far more reliable information than would an equal investment of time spent viewing this tape.

David B. Hackney
Hospital of the University of Pennsylvania
Philadelphia, PA 19104

Pictorial Essay

Conventional MR Neuroangiography

Taher El Gammal¹ and Betty Sue Brooks

MR angiography of the brain plays an important role in the diagnosis of vessel thrombosis and dissection, giant aneurysms, and occult vascular malformations. This essay highlights some of the features of the intra- and extracranial circulation that make conventional MR neuroangiography valuable in the demonstration of vascular anatomy and vascular disease.

MR angiography is expected to become a widely used diagnostic tool in the near future with continued refinement of specialized techniques that use, for example, time-of-flight or phase-contrast methods [1–4]. At the present time, however, there are a number of important limitations in the use of these specialized techniques, and MR angiography is usually performed as an adjunct to the routine spin-echo or gradient-echo MR study of the brain. For the purposes of this pictorial essay, *conventional MR neuroangiography* will be used to designate the anatomic depiction of the intracranial and extracranial vessels that is available from routine spin-echo and gradient-echo MR examinations of the brain. Conventional MR neuroangiography continues to have an important role, especially in the diagnosis of vessel thrombosis and dissection, giant aneurysms, and occult vascular malformations.

Careful scrutiny of the visualized portions of the intracranial and extracranial circulation is an essential part of the routine interpretation of every MR brain examination. This presentation will highlight some of the features that continue to make the conventional MR neuroangiogram extremely valuable in the demonstration of vascular anatomy and vascular disease.

Normal Vascular Anatomy and Developmental Variants

The major intracranial vessels are well depicted on routine MR studies. The circle of Willis is clearly identified, especially on spin-density and T2-weighted transaxial images (Fig. 1A). The coronal projection is optimal for visualization of the basilar artery and its branches (Fig. 1B). Developmental anomalies of the circle of Willis also may be well shown (Fig. 2).

MR has contributed to our understanding of the anatomy of the periventricular zone of white matter in immediate relation to the anterolateral aspects of the angles of the frontal horns. Histologic study of the rounded, hyperintense foci seen on T2-weighted images in this location has confirmed that this is a normal finding [4]. We have also noted that on gadopentetate dimeglumine-enhanced sections, lenticulostriate vessels and terminal subependymal veins can be seen coursing toward and within the same region (Fig. 3), suggesting that there is a contribution to these hyperintense foci from the perivascular Virchow-Robin spaces that accompany these vessels.

Enhanced MR sections obtained with flow-compensation technique may provide additional information, including more extensive visualization of the venous sinuses and, in particular, intense enhancement of the cavernous sinuses. The cavernous internal carotid artery is then exceptionally well depicted in relation to the cavernous sinus (Fig. 3C). Another advantage of flow compensation is the improved contrast between the brightly enhancing cavernous sinuses and the pituitary gland (Figs. 3D–3F).

Received September 20, 1990; accepted after revision November 20, 1990.

Presented in part at the annual meeting of the American Roentgen Ray Society, Washington, DC, May 1990.

¹ Both authors: Department of Radiology, Division of Neuroradiology, University of Alabama at Birmingham, 619 S. 19th St., Birmingham, AL 35233. Address reprint requests to T. El Gammal.

AJR 156:1075–1080, May 1991 0361–803X/91/1565–1075 © American Roentgen Ray Society

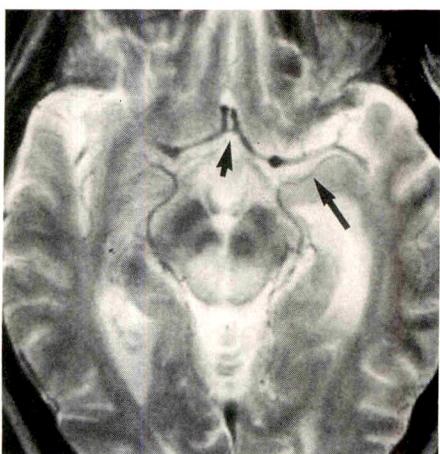
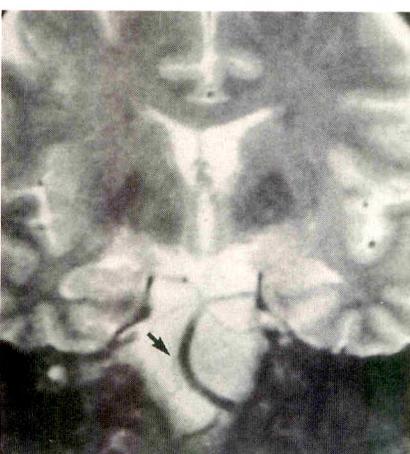
**A****B**

Fig. 1.—Intracranial vessels on T2-weighted spin-echo MR images (2500/90).

A, Transaxial section shows normal vessels at base of brain. Note anterior communicating artery (short arrow) and bilateral uncal vessels (long arrow).

B, Vertebrabasilar circulation on coronal projection. Coronal sections provide excellent delineation of basilar artery and its branches. Note anterior inferior cerebellar artery on right (arrow) and superior cerebellar and posterior cerebral arteries.

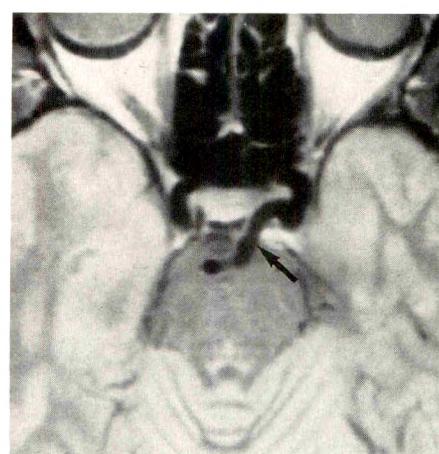


Fig. 2.—Spin-density transaxial MR image (2000/20) shows persistent embryologic carotico-basilar communication of a trigeminal artery (arrow).

Arteriosclerosis, Vascular Occlusive Disease, and Vascular Dissection

Conventional MR angiography performed with flow-compensation technique may produce high signal intensity from rephasing in portions of the cerebral arteries. In cases of suspected occlusive disease, a repeat series without flow compensation should be performed.

Occlusion of the intracranial carotid arteries will usually be depicted easily, particularly on T2-weighted images without flow compensation. Lumen narrowing and focal stenosis also can be seen, but are better outlined by MR angiography. Conventional MR angiography alone shows the changes in the vessel wall produced by irregular thickening due to arteriosclerosis (Fig. 4). Carotid and basilar thrombosis with occlusion also can be identified (Figs. 5 and 6). Conventional MR angiography remains the method of choice for the evaluation of arterial dissection (Fig. 7). Conventional MR angiography also is superior to MR angiography in showing collateral circulation in patients with moyamoya disease.

Tumor Vascularity and Tumoral Vascular Displacement and Encasement

Conventional MR angiography provides important preoperative information when multiple serpiginous void signals within a mass reveal its marked vascularity (Fig. 8). Contrast enhancement also can be used to show tumor hypervascularity. In patients with sellar and parasellar masses, conventional MR angiography may be used to outline the parasellar vascular anatomy, obviating preoperative catheter angiography in many cases (Fig. 9). Direct tumor invasion of the cavernous sinus by pituitary tumors may be diagnosed by loss of the normal intense enhancement of the cavernous sinus (Fig. 9). In other cases, conventional MR angiography

may provide indirect detection of invasion when lateral deviation of the lateral dural cavernous sinus wall is seen.

Vascular Malformations

Advantages of conventional MR angiography in the evaluation of vascular malformations include depiction of the lesion nidus and lesion extent in multiplanar projections. Conventional MR angiography also shows to advantage deep extension of the malformation and involvement of the ventricular system, as well as associated ischemic changes in the adjacent parenchyma that may result from parasitic effect of the malformation (Fig. 10).

Venous angiomas are seen most easily on conventional MR angiography with the use of gadopentetate dimeglumine. Cavernous angiomas have a distinctive MR appearance comprising a central, primarily high signal intensity; a mulberrylike appearance with some signal heterogeneity; and surrounding low signal caused by hemosiderin deposition. The same MR appearance is rarely mimicked by well-margined vascular tumors and thrombosed arteriovenous malformations. More often, a chronic intraparenchymal cerebral hematoma may have a very similar appearance for up to 2 years after hemorrhage. The presence of enhancement after injection of gadopentetate dimeglumine favors the diagnosis of cavernous angioma over chronic intracerebral hematoma (Fig. 11).

Intracerebral Hemorrhage

Conventional MR angiography may elucidate or provide clues to the underlying cause of an intraparenchymal hematoma (Fig. 12). With conventional MR angiography, the void signal of a small peripheral mycotic aneurysm even can be shown in association with a large intracerebral hematoma.

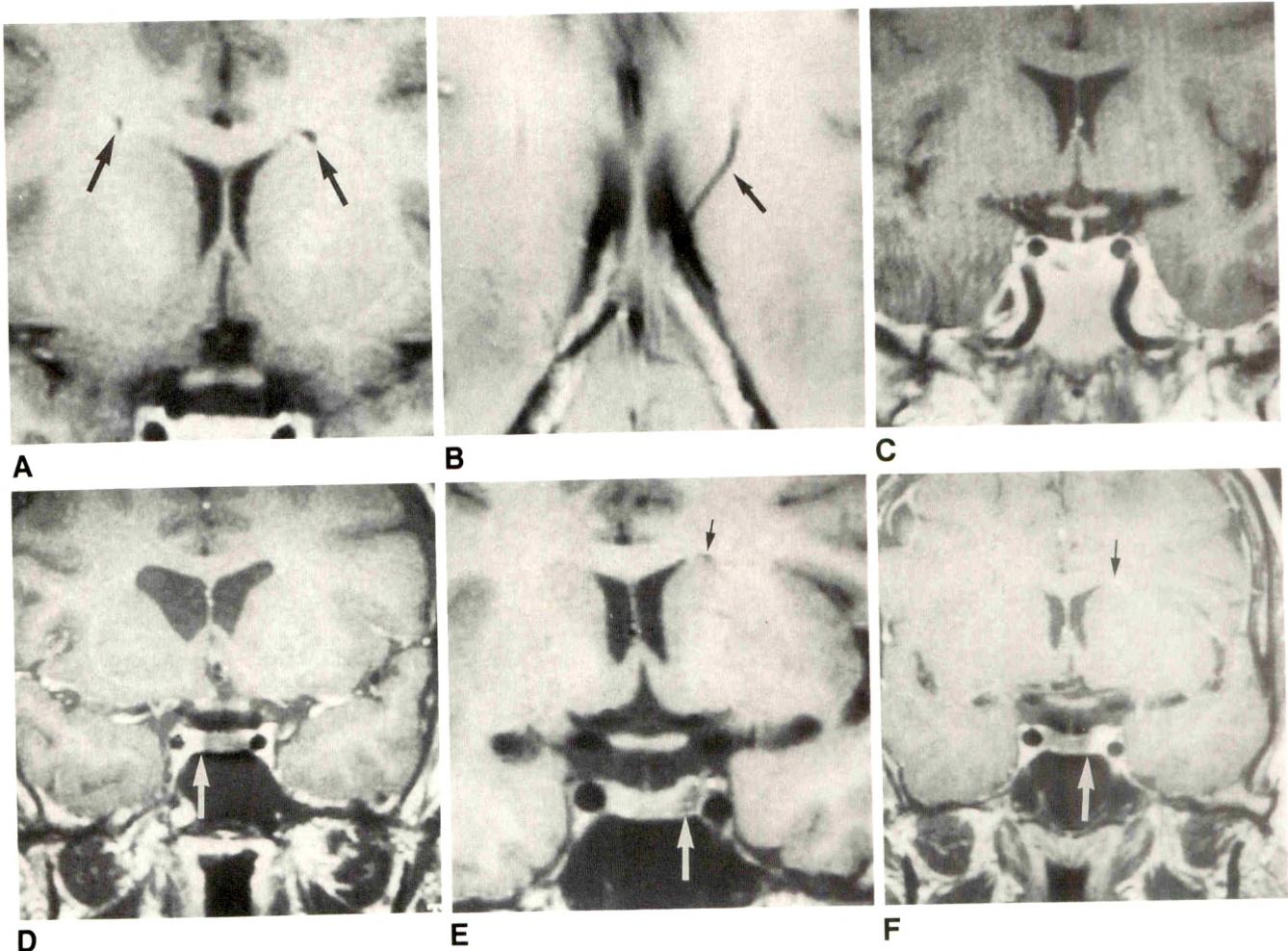


Fig. 3.—Conventional MR neuroangiography with contrast enhancement.
A and B, Coronal (A) and transaxial (B) T1-weighted enhanced MR images without flow compensation (500/15) show signal void close to angles of frontal horns (A, arrows). Transaxial image (B) shows corresponding subependymal vein coursing toward frontal horn (arrow).
C, Coronal T1-weighted image (500/15) accurately shows signal void in course of intracranial carotid arteries in relation to contrast-enhanced cavernous sinuses.

D–F, T1-weighted enhanced coronal studies obtained with flow compensation in two patients. In D, normal asymmetry (arrow) is seen in size of right and left enhanced cavernous sinuses. Images in another patient obtained without (E) and then with (F) contrast injection with flow compensation illustrate that low signal on unenhanced image (E, white arrow) could be misinterpreted as a pituitary microadenoma but is clearly shown to be part of left cavernous sinus after contrast administration (F, white arrow). Black arrows indicate vessel enhancement near angle of left frontal horn, as was shown in patient in A and B.

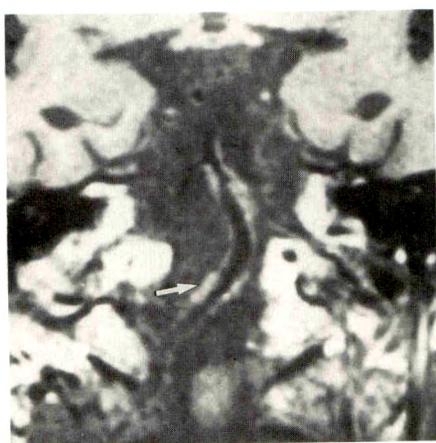


Fig. 4.—Basilar artery arteriosclerosis. Coronal T1-weighted MR image (800/20) shows ectatic basilar artery with irregular thickening of vessel wall (arrow).

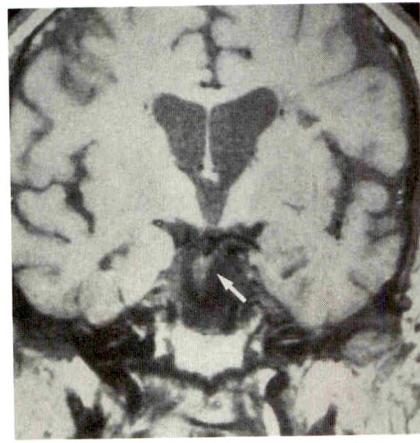


Fig. 5.—MR image of basilar artery thrombosis with pontine infarct. High signal in distal basilar artery is due to thrombus (arrow). Terminal basilar artery tip shows signal void of normal flow coming from carotid circulations. Flow-compensation techniques were not used.

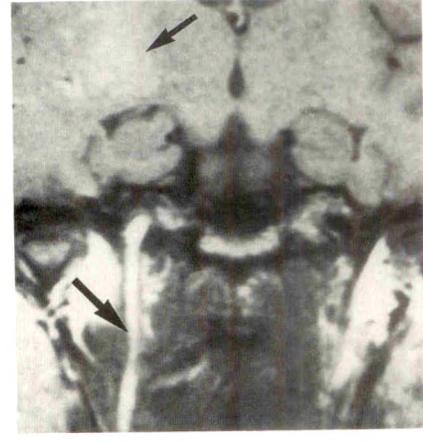


Fig. 6.—Recent right internal carotid artery thrombosis. Coronal T1-weighted MR image (800/20) shows long, linear, high signal of thrombus (large arrow) in upper cervical internal carotid artery. Hemorrhagic infarct (small arrow).

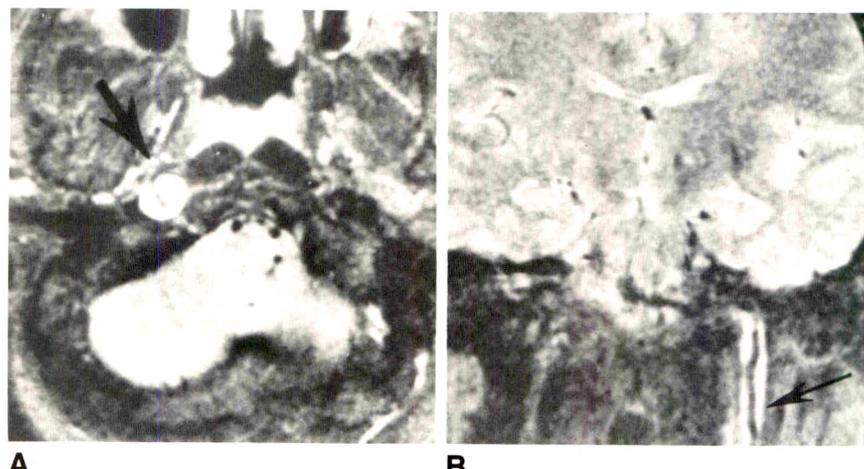


Fig. 7.—Internal carotid artery dissection in two patients.

A, Dissection of right internal carotid artery produces high signal of extraluminal clot surrounding a small signal void of normal flow in compromised lumen on transaxial T2-weighted MR image (2000/70) (arrow).

B, Coronal T2-weighted MR image (2000/70) in another patient shows dissection of cervical left internal carotid artery (arrow).

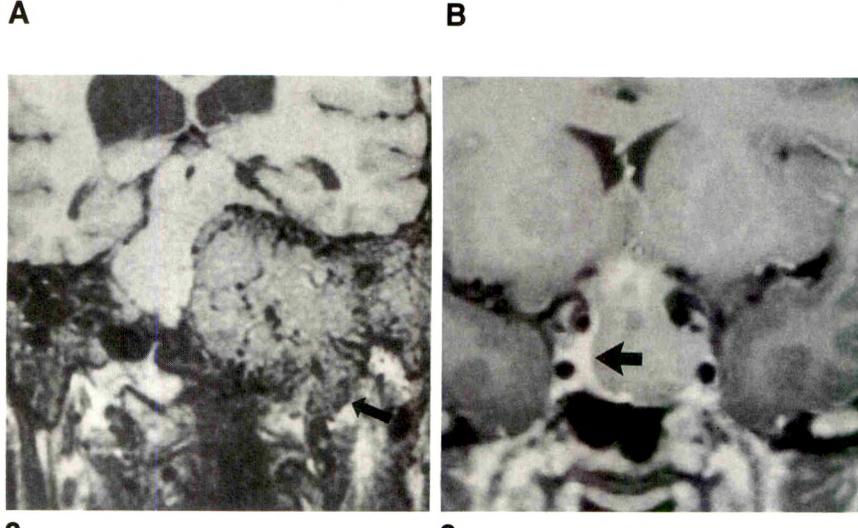


Fig. 8.—Large vascular glomus jugulare tumor. T1-weighted coronal MR image (800/20) shows numerous serpiginous signal voids of extremely hypervascular tumor. Note tonguelike extension into occluded left internal jugular vein (arrow).

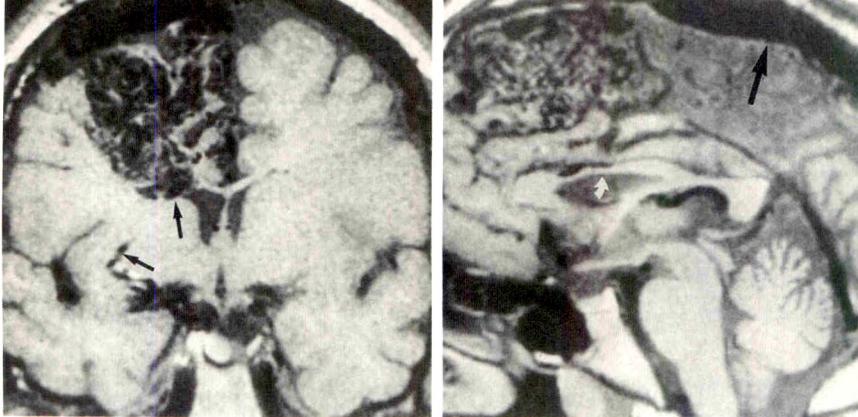


Fig. 9.—Coronal T1-weighted MR image (500/15) shows chromophobe adenoma with cavernous sinus invasion. Tumoral invasion of left cavernous sinus is evident without arterial encasement. This is contrasted with normal appearance of cavernous sinus on right side (arrow).

Fig. 10.—Coronal and midsagittal T1-weighted MR images (800/20) show extension of large right frontal arteriovenous malformation to angle of frontal horn.

A, Hypertrophy of lenticulostriate arteries (arrows).

B, Marked enlargement of superior sagittal sinus is caused by high flow of venous drainage of arteriovenous malformation (straight arrow). Note significant reduction in volume of corpus callosum (curved arrow) consequent to atrophy from parasitic effect of arteriovenous malformation.

Intracranial Aneurysms

Conventional MR angiography has proved extremely useful in the delineation of large and intermediate-sized intracranial aneurysms with proper definition of the aneurysm sac and of mural thrombus when present. MR angiography may miss or incompletely outline large aneurysms because of signal loss

from turbulence and slow flow [2]. However, conventional MR angiography also has significant limitations. The void signal of the anterior clinoid processes can simulate an internal carotid artery aneurysm. A basilar artery pseudoaneurysm may be produced by CSF pulsations in relation to the basilar artery tip. This is more commonly seen in children. Conventional MR angiography may not provide adequate demonstra-

Fig. 11.—*A* and *B*, Unenhanced transaxial T2-weighted MR image (2500/90) (*A*) and enhanced midsagittal MR image (500/15) (*B*) of pontine cavernous angioma. Enhancement of cavernous angioma seen in *B* is helpful in distinguishing old cerebral hemorrhage without an underlying angioma from a vascular malformation. In a chronic hemorrhage, there is no enhancement after contrast injection.

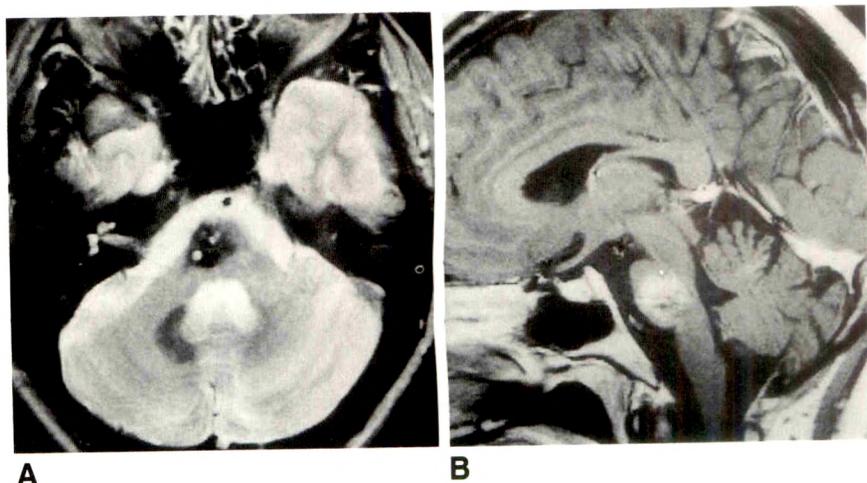


Fig. 12.—Pontine hemorrhage resulting from venous angioma.

A and *B*, T1-weighted midsagittal (*A*) and coronal (*B*) MR images before (*A*) and after (*B*) contrast enhancement. Cause of large hematoma in pons seen in *A* is revealed by contrast-enhanced image (*B*) to be a venous angioma. Linear enhancement of malformation is well demonstrated in *B* (arrow). Enhanced scans are the most accurate means of MR depiction of venous angioma.

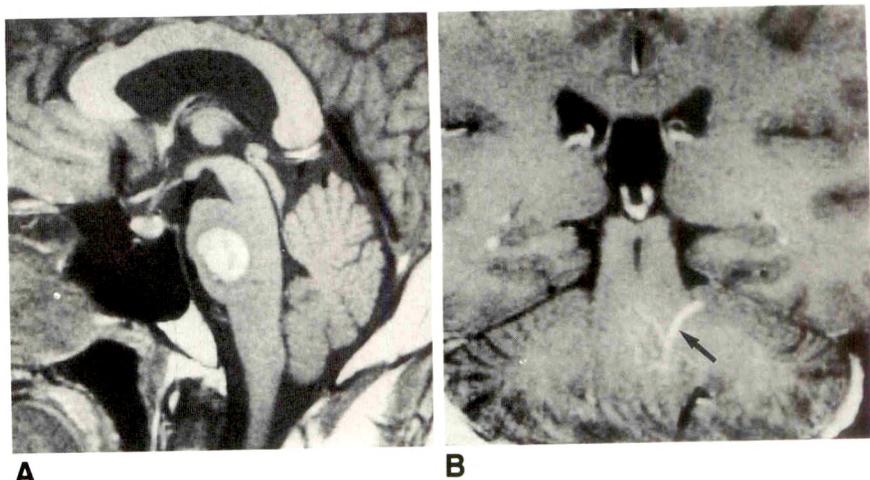
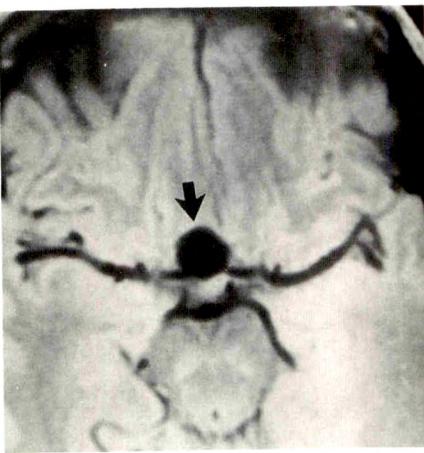
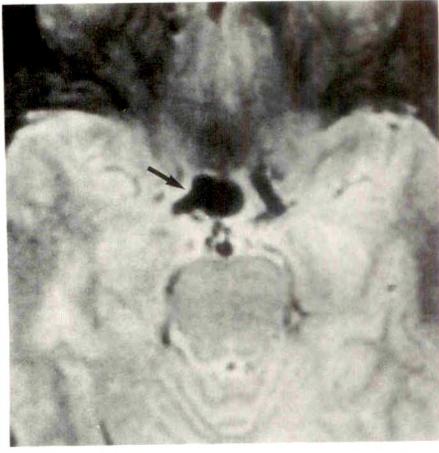
**A****B****C**

Fig. 13.—Patient with giant supraclinoid internal carotid artery aneurysm.

A and *B*, Midsagittal T1-weighted MR image (800/20) (*A*) and high transaxial intermediate-density MR image (2000/20) (*B*) suggest possibility of anterior communicating artery aneurysm (arrows).

C, Lower T2-weighted MR image (2000/70) shows probable origin of aneurysm at level of terminal internal carotid artery (arrow).

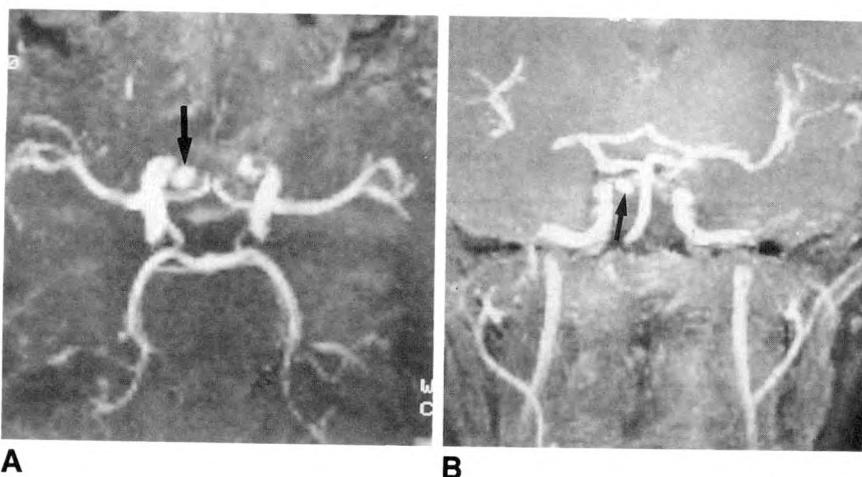
**A****B**

Fig. 14.—MR angiography of right intracavernous carotid artery aneurysm. Conventional MR angiography suggested an aneurysm vs a loop of intracavernous carotid artery.

A and **B**, MR angiograms show a medium-sized intracavernous aneurysm (arrows) definitely and with precision. Aneurysm arises at level of anterior cavernous sinus as seen on both transaxial (**A**) and coronal (**B**) views.

tion of the aneurysm origin or neck in some cases (Fig. 13). MR angiography has distinct and definite advantages in the delineation of the origin and neck of intracranial aneurysms in most patients (Fig. 14).

REFERENCES

- Dumoulin CL, Hart HH. Magnetic resonance angiography. *Radiology* 1986;161:717-720
- Masaryk TH, Modic MT, Ross JS, et al. Intracranial circulation: preliminary clinical results with three-dimensional (volume) MR angiography. *Radiology* 1989;171:793-799
- Pernicone JR, Siebert JE, Potchen EJ, Pera A, Dumoulin CL, Souza SP. Three-dimensional phase-contrast MR angiography in the head and neck: preliminary report. *AJR* 1990;11:457-466, *AJR* 1990;155:167-176
- Sze G, De Armond SJ, Brant-Zawadzki M, Davis RL, Norman D, Newton TH. Foci of MRI signal (pseudo lesions) anterior to the frontal horns: histologic correlations of a normal finding. *AJR* 1986;7:381-387, *AJR* 1986;147:331-337

Pictorial Essay



Imaging Characteristics of Tuberous Sclerosis

Douglas G. Bell,¹ Bernard F. King, Robert R. Hattery, J. William Charboneau, Alan D. Hoffman, and O. Wayne Houser

Tuberous sclerosis is a neurocutaneous syndrome with a wide variety of clinical, pathologic, and radiologic manifestations. First described in 1880 by Bourneville [1], a French physician, the disease is named for the firm, whitish, tuberlike nodules arising from the cerebral convolutions of its victims (Fig. 1). Historically recognized by Vogt's clinical triad (1908) of adenoma sebaceum, seizures, and mental retardation, tuberous sclerosis is characterized by a unique array of multiorgan hamartomatous involvement. Interestingly, only 29% of patients with tuberous sclerosis develop all the features of the classic triad, and approximately 6% of patients with tuberous sclerosis never develop any of the features of the triad. The most frequently involved organs are the skin, brain, retina, lungs, heart, skeleton, and kidneys. Examples of the classic radiologic features are provided herein. Inheritance is autosomal dominant with a high penetrance and variable expressivity. The prevalence of tuberous sclerosis is at least one in 9500 persons.

Skin

Cutaneous lesions are present in 96% of patients. These include facial angiofibroma (adenoma sebaceum, Fig. 2), forehead/scalp fibrous plaques, peri/subungual fibromas, hypomelanotic macules, and shagreen patches. The first three are considered pathognomonic of tuberous sclerosis. Incidentally, the term adenoma sebaceum is a misnomer, and the preferred term is facial angiofibroma. These facial lesions are not adenomas of the sebaceous glands, but rather fibrous hamartomas of the dermis.

CNS

Classic CNS involvement includes subependymal glial nodules, cortical tubers, and subependymal giant-cell astrocytomas. Subependymal glial nodules are benign nodules composed primarily of astrocytes. Present in 80% of patients with tuberous sclerosis, they are usually located within the walls of the lateral ventricles and have a tendency to calcify (Fig. 3). Tuberous sclerosis is characterized by a unique array of multiorgan hamartomatous involvement. Interestingly, only 29% of patients with tuberous sclerosis develop all the features of the classic triad, and approximately 6% of patients with tuberous sclerosis never develop any of the features of the triad. The most frequently involved organs are the skin, brain, retina, lungs, heart, skeleton, and kidneys. Examples of the classic radiologic features are provided herein. Inheritance is autosomal dominant with a high penetrance and variable expressivity. The prevalence of tuberous sclerosis is at least one in 9500 persons.

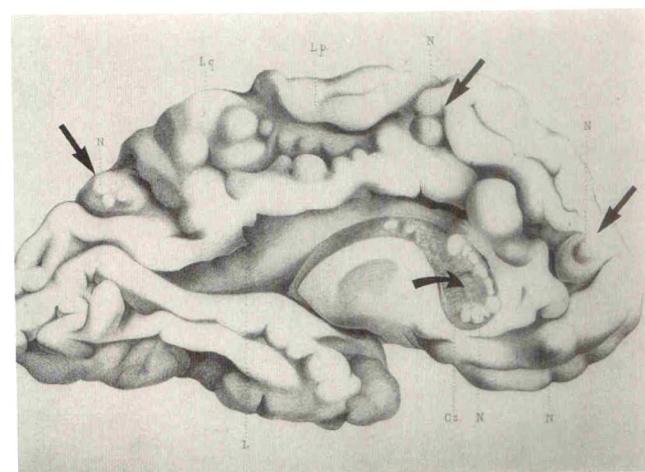


Fig. 1.—Drawing from 1880 depicts medial surface of left hemisphere with cortical tubers (straight arrows) and ventricular nodules (curved arrows). (Reprinted with permission from Bourneville [1].)

Received October 12, 1990; accepted after revision November 29, 1990.

¹ All authors: Mayo Clinic Foundation, 200 First St., S.W., Rochester, MN 55905. Address reprint requests to D. G. Bell.

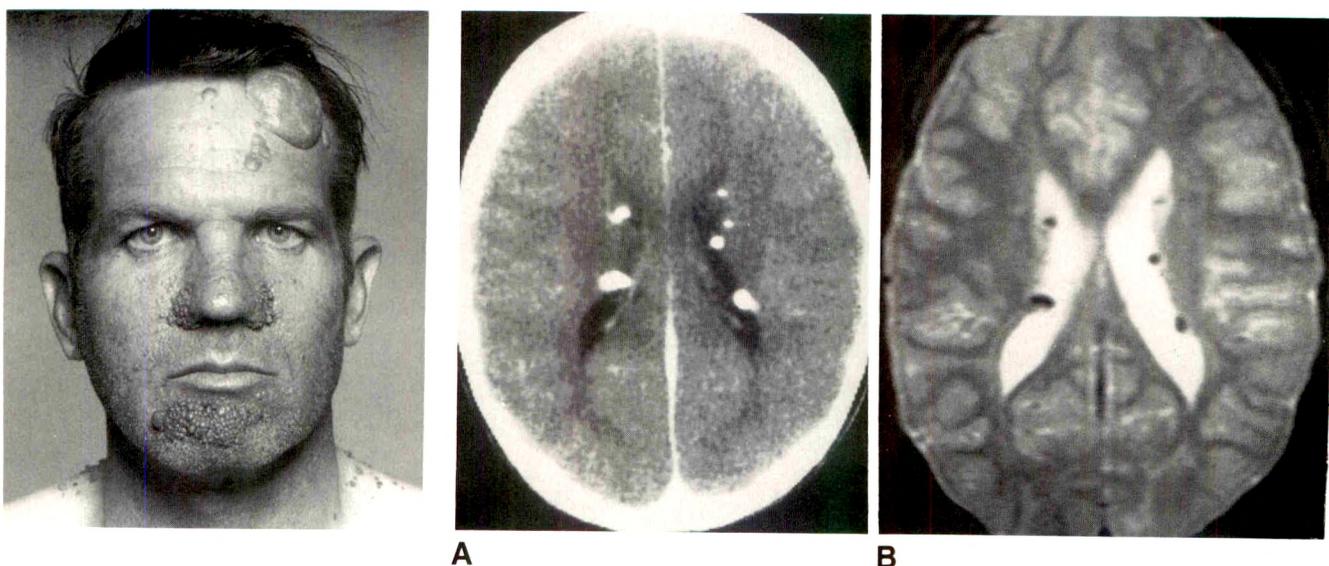


Fig. 2.—Large fibrous plaque on forehead and facial angiofibroma (adenoma sebaceum). Facial angiofibromas are bilaterally symmetrical, involving the cheeks, nasolabial folds, and chin. (Reprinted with permission from Gomez [2].)

Fig. 3.—*A*, CT scan of multiple calcified subependymal nodules along lateral ventricles. Degeneration manifest by calcification occurs in vast majority of nodules and may exist at birth or evolve during infancy and childhood.

B, Axial MR image (2500/80) at similar level shows low signal intensity in multiple subependymal nodules due to dense calcification. In general, nodules are better seen on T1-weighted images, whereas tubers are more readily detected on T2-weighted images.

(Fig. 4). Although they may contain calcifications (Fig. 5), their usual gross appearance is that of firm, pale, widened gyri. Cerebral involvement is more common than cerebellar. Subependymal giant-cell astrocytomas are histologically benign tumors typically arising from, or within, the head of the caudate nucleus. Expansion of tumor into the lateral ventricle with resultant obstruction of the foramina of Monro may cause

hydrocephalus (Figs. 6 and 7). Subependymal giant-cell astrocytomas probably arise from subependymal glial nodules.

Eye

Retinal hamartomas are present in almost 50% of patients with tuberous sclerosis. These benign tumors are histologi-

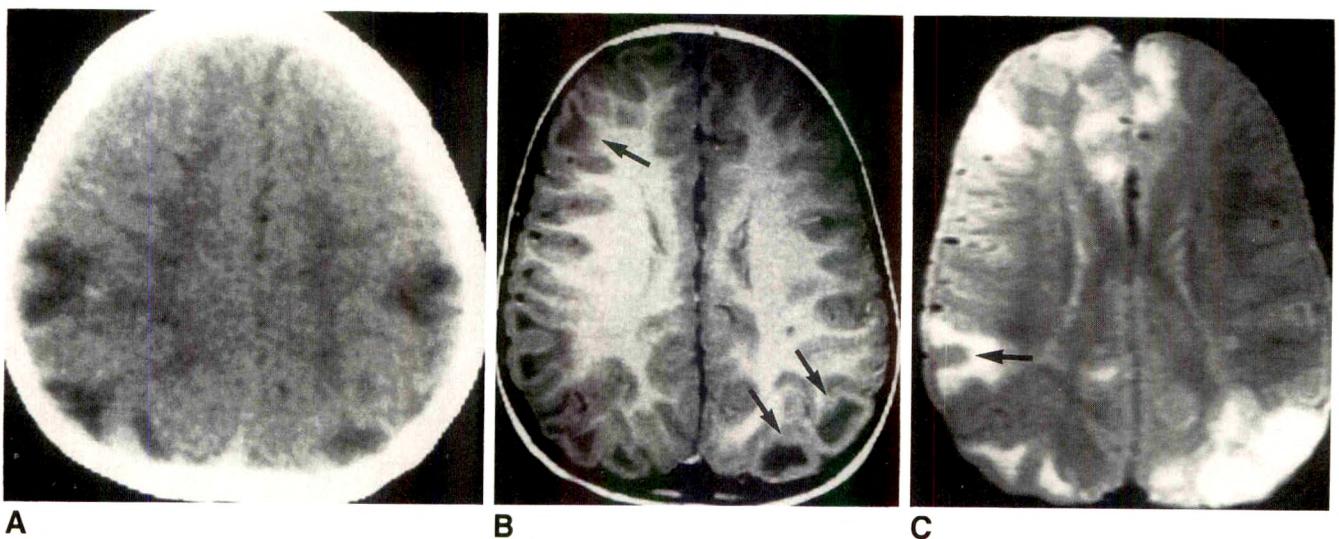


Fig. 4.—*A*, CT scan of multiple hypodense cortical and subcortical lesions consistent with tubers. Some of these lesions may become isodense with age and actually "disappear" on CT.

B, Axial MR image (500/20) at a similar level shows multiple hypointense cortical/subcortical tubers. Note classic "gyral core" lesions in right frontal and left parietal lobes (arrows). In gyral core lesions on T1-weighted images an isointense normal-appearing cortex seems to surround an otherwise "empty" gyrus.

C, Axial MR image (2000/20) at same level shows multiple hyperintense cortical/subcortical tubers with a characteristic "sulcal island" in right parietal lobe (arrow). Sulcal islands consist of a ringlike hyperintense T2 signal enclosing an island of isointense cerebral cortex. (Reprinted with permission from Nixon et al. [3].)

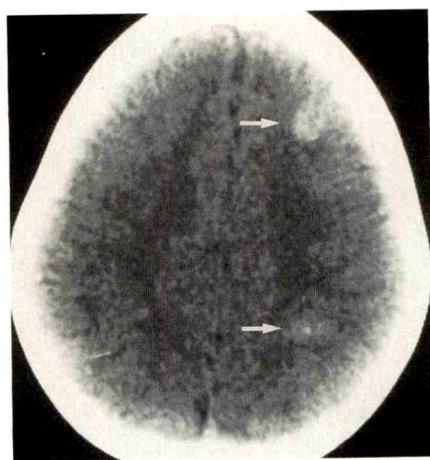


Fig. 5.—Cortical/subcortical tubers (arrows) may calcify, as evidenced by this unenhanced CT scan. Progressive calcification of tubers is not unusual.

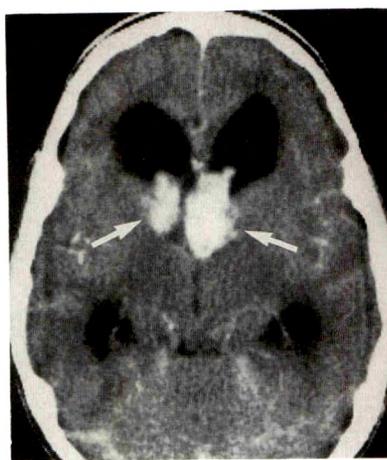


Fig. 6.—CT scan of subependymal giant-cell astrocytoma (arrows) near foramina of Monro shows marked contrast enhancement. Note secondary lateral ventricular dilatation. (Reprinted with permission from Gomez [2].)

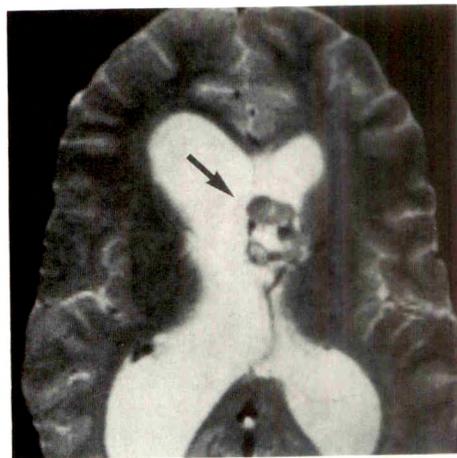
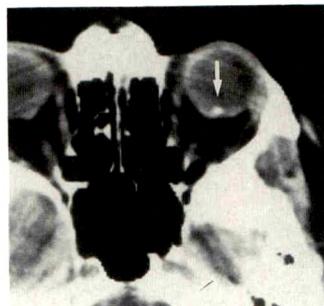


Fig. 7.—Axial MR image (2500/80) shows a partially calcified subependymal giant-cell astrocytoma (arrow) near foramen of Monro, causing hydrocephalus. Typically, these tumors arise from a subependymal nodule located in inferior head of caudate nucleus.

Fig. 8.—Unenhanced CT scan shows a calcified retinal hamartoma (arrow) in left eye of a patient with tuberous sclerosis.



cally similar to subependymal glial nodules with the same tendency to become calcified (Fig. 8). They are usually asymptomatic and best detected with ophthalmoscopy. Although not pathognomonic of tuberous sclerosis, their presence is helpful in confirming the diagnosis.

Lung

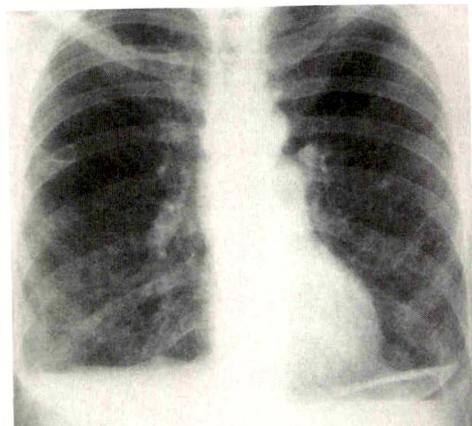
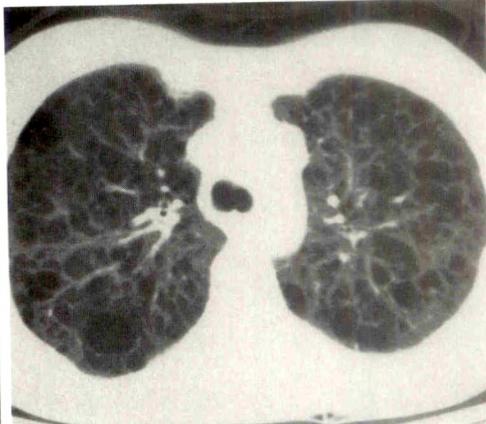
Significant pulmonary findings occur in less than 1% of patients with tuberous sclerosis (Figs. 9 and 10). The clinical, pathologic, and radiologic features are very similar to those of pulmonary lymphangiomyomatosis. Presenting symptoms include exertional dyspnea, spontaneous pneumothorax, and hemoptysis. Eighty-four percent of patients with tuberous sclerosis and pulmonary findings are female, with an average age at presentation of 34 years. Eighty-six percent of these patients will die of a respiratory cause.

Heart

Cardiac rhabdomyomas are true hamartomas found in approximately 30% of patients with tuberous sclerosis. Occurring almost exclusively in children, they are usually diagnosed by echocardiography and may be intracavitary or embedded within the ventricular wall (Figs. 11 and 12). Symptomatic

Fig. 9.—*A*, Chest radiograph of 46-year-old woman with tuberous sclerosis (TS) shows hyperinflation with diffuse, linear opacities throughout both lungs. Onset of pulmonary changes in TS occurs later in life than involvement of other organ systems.

B, CT scan of chest for evaluation of persistent pneumothorax after open lung biopsy shows innumerable cystic air spaces throughout both lungs. CT frequently depicts cystic changes not apparent on chest radiographs.

**A****B**

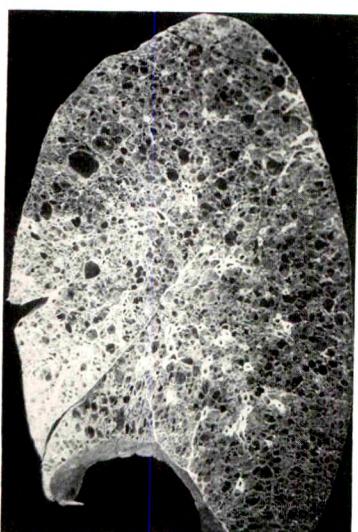


Fig. 10.—Gross specimen of right lung from a patient with tuberous sclerosis shows diffuse pulmonary cystic changes that are morphologically indistinguishable from pulmonary lymphangiomatosis.

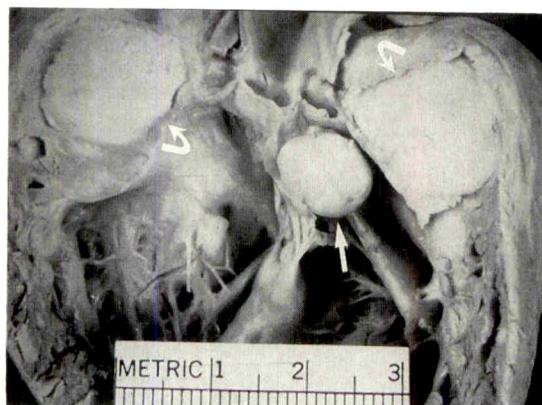
lesions may cause obstruction to blood flow, arrhythmias, or impaired ventricular function.

Bone

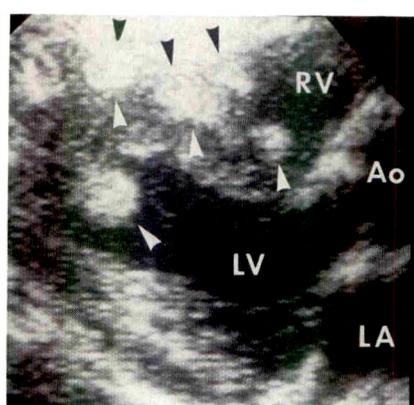
Skeletal involvement is typically asymptomatic and present in approximately 50% of patients with tuberous sclerosis. The most common finding includes sclerotic patches in the pelvis, lumbar spine (Fig. 13), or cranium. Undulating periosteal new bone and cysts of the metatarsals, metacarpals, and phalanges also may be seen (Fig. 14).

Kidney

Renal lesions in tuberous sclerosis consist of angiomyolipomas and benign, simple cysts. The tumors are benign, nonencapsulated, and composed of various proportions of



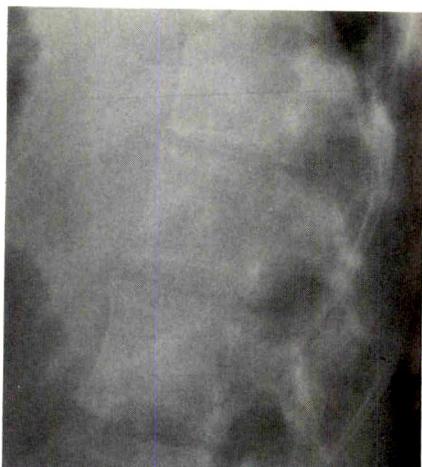
11



12

Fig. 11.—Opened left ventricle shows a large, bisected intramural rhabdomyoma (curved arrows) and smaller intracavitary rhabdomyoma (straight arrow) near aortic valve. This patient also had a large intracavitary, pedunculated rhabdomyoma obstructing mitral orifice and producing mitral stenosis. (Reprinted with permission from Gomez [2].)

Fig. 12.—Long-axis echocardiogram shows multiple intracavitary rhabdomyomas in left and right ventricular apices (arrowheads). RV = right ventricle, Ao = aorta, LV = left ventricle, LA = left atrium. (Figure provided courtesy of William K. Freeman, Mayo Clinic.)



13



14

Fig. 13.—Radiograph of sclerotic patches in lumbar spine that can mimic blastic metastases. Similar lesions may occur in pelvis and skull. (Reprinted with permission from Gomez [2].)

Fig. 14.—Radiograph of periosteal new bone along metatarsal shafts. (Reprinted with permission from Gomez [2].)

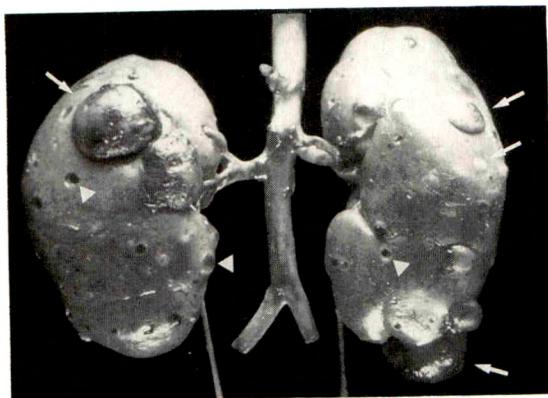
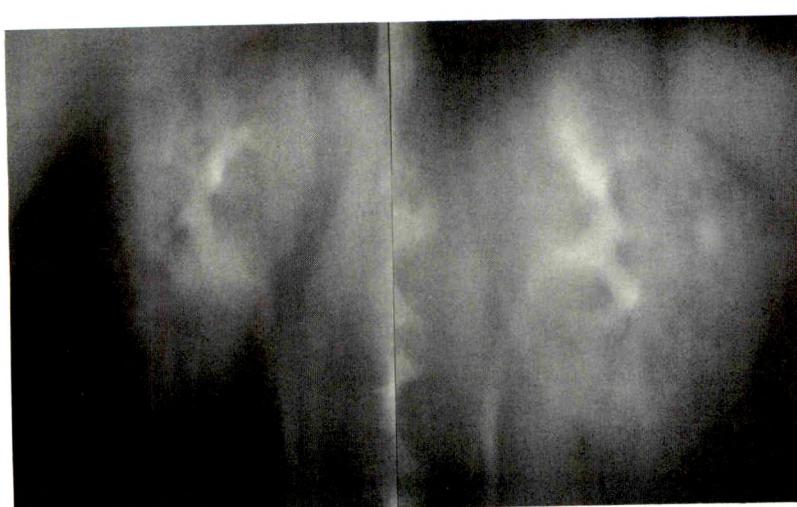


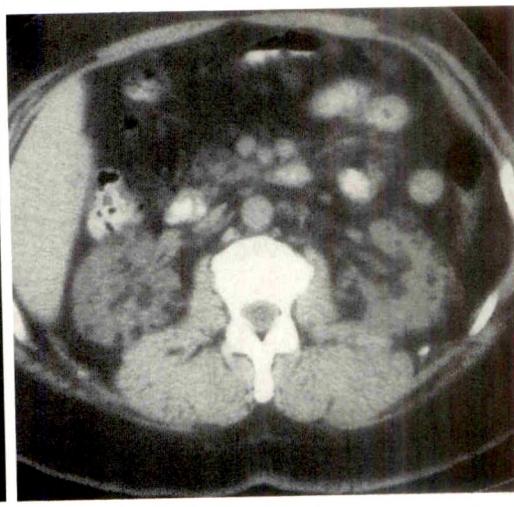
Fig. 15.—Gross specimen shows classic appearance of renal tuberous sclerosis with enlarged kidneys due to multiple, bilateral angiomyolipomas (arrows) and cysts (arrowheads). (Reprinted with permission from Gomez [2].)

blood vessels, smooth muscle, and fat. An individual tumor may be composed predominantly of fat with very little smooth muscle or composed mostly of smooth muscle with very little fat. Arising in the renal cortex or medulla, they are usually multiple and bilateral (Figs. 15–20) and present in 50–80% of patients with tuberous sclerosis [4]. Their prevalence appears to increase with age. Potential complications include spontaneous hemorrhage (Fig. 21), flank pain, and, rarely, progressive renal failure.

We recently reviewed the CT and sonographic findings in 36 patients (age range, 7 months to 67 years) at our institution who had tuberous sclerosis and a diagnosis of renal angiomyolipoma. Bilateral angiomyolipomas were seen in 89% and multiple lesions (≥ 3), in one or both kidneys, were diagnosed in 86%. The largest tumor identified was approximately 10 cm in diameter. However, in the majority (2/3) of cases, the visualized tumors were all less than 1 cm in diameter.



A



B

Fig. 16.—*A*, Tomogram from an excretory urogram shows a diffusely abnormal nephrogram due to multiple, bilateral, small renal masses consistent with angiomyolipomas and cysts in a patient with tuberous sclerosis.

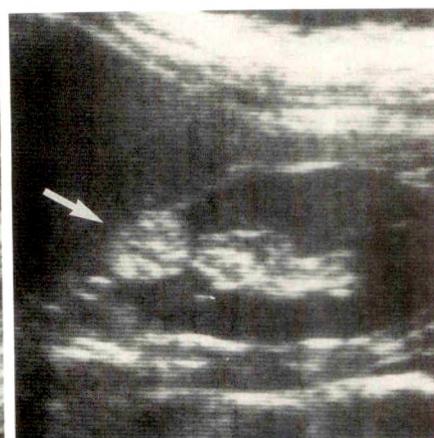
B, Unenhanced CT scan shows multiple masses are fat-density renal angiomyolipomas. Demonstration of fat within a renal mass on CT is virtually diagnostic of angiomyolipoma. Use of 5-mm-thin sections and unenhanced scans improves accuracy of detecting fat in small lesions in which partial-volume effect may be significant.

Fig. 17.—Longitudinal sonogram of right kidney shows multiple small hyperechoic angiomyolipomas. Larger lesions (arrows) are 0.5–1.0 cm in diameter. Additional scattered, tiny, echogenic foci (arrowhead) are consistent with angiomyolipomas less than 5 mm in diameter.

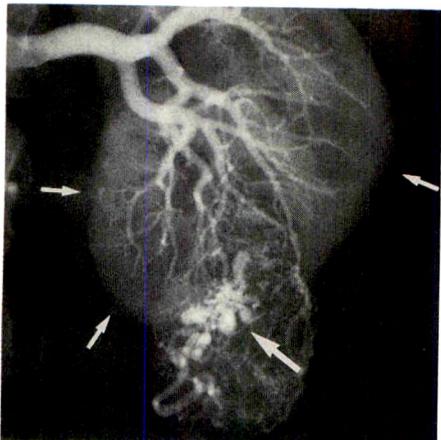


Fig. 18.—Longitudinal sonogram of right kidney in a patient without tuberous sclerosis shows a single, hyperechoic angiomyolipoma in upper pole (arrow). Echogenicity of angiomyolipomas is typically greater than or equal to (as in this case) that of renal sinus fat. Because other renal lesions (including 5% of renal cell carcinomas) may also be similar to renal sinus fat in echogenicity, CT may be necessary for further evaluation in some cases. (Reprinted with permission from Gomez [2].)

17



18

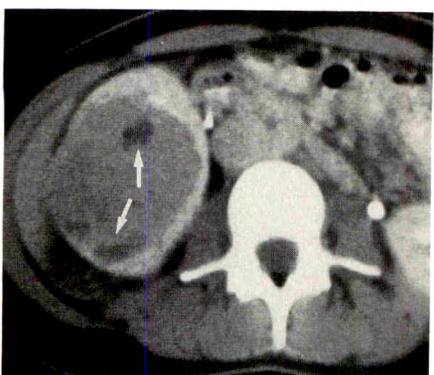


19

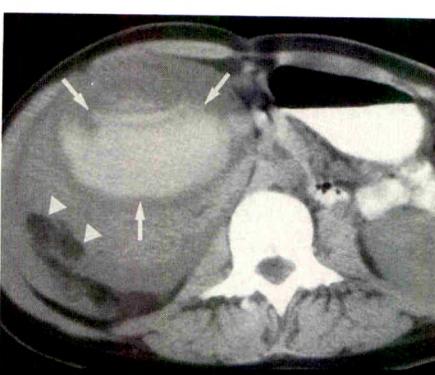


20

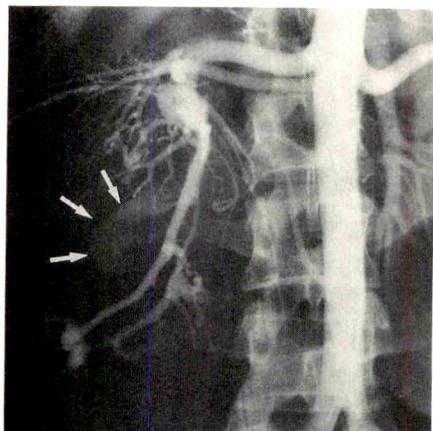
Fig. 19.—Renal arteriogram shows characteristic serpentine vessels and grape-like arterial aneurysms (large arrow) in a lower-pole angiomyolipoma. Some additional tiny angiomyolipomas are also identified (small arrows).



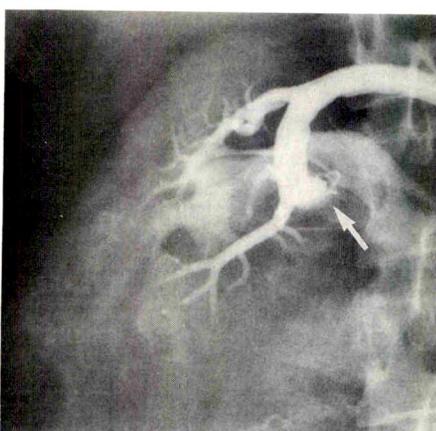
A



B



C



D

Fig. 20.—Coronal MR image (500/20) through kidneys of a patient with pulmonary lymphangiomyomatosis shows multiple, fat-intensity renal angiomyolipomas in right upper pole (arrows).



Fig. 22.—Imatron (fast CT) shows multiple, large, bilateral renal cysts in a 5-year-old boy with tuberous sclerosis and no family history of polycystic renal disease. No angiomyolipomas were identified.

Fig. 21.—A, CT scan of large angiomyolipoma in right kidney of patient with tuberous sclerosis contains only small amounts of fat (arrows).

B, After mild, blunt abdominal trauma, note high-density collection of acute hemorrhage (arrows) arising from angiomyolipoma. Fat within angiomyolipoma has been displaced posterolaterally (arrowheads).

C, Midstream abdominal aortogram shows displaced vessels and arterial aneurysms with active bleeding (arrows) in midportion of large angiomyolipoma in right lower pole.

D, Particle embolization and coil placement (arrow) successfully controlled bleeding. Residual tumor stain is seen throughout angiomyolipoma. Surgery was not needed in this case.

Renal cysts in tuberous sclerosis are benign with a characteristic microscopic lining of hyperplastic eosinophilic epithelium. They may be few and asymptomatic or macroscopically resemble autosomal dominant polycystic kidney disease (Fig. 22). Occurring in the renal cortex or medulla, their prevalence is uncertain but is less than that of angiomyolipomas.

REFERENCES

1. Bourneville D-M. Sclérose tubéreuse des circonvolutions cérébrales: idiotie et épilepsie hémiplégiique. *Arch Neurol (Paris)* 1880;1:81-91
2. Gomez MR, ed. *Tuberous sclerosis*, 2nd ed. New York: Raven Press, 1988
3. Nixon JR, Houser OW, Gomez MR, Okazaki H. Cerebral tuberous sclerosis: MR imaging. *Radiology* 1989;170:869-873
4. Stillwell TJ, Gomez MR, Kelalis PP. Renal lesions in tuberous sclerosis. *J Urol* 1987;138:477-481

**1990 ARRS
Executive Council
Award**

Intravascular Sonography in the Detection of Arteriosclerosis and Evaluation of Vascular Interventional Procedures

Christopher E. Engeler¹
 Joseph W. Yedlicka
 Janis Gissel Letourneau
 Wilfrido R. Castañeda-Zúñiga
 David W. Hunter
 Kurt Amplatz

The purpose of this study was to evaluate the use of intravascular sonography for the detection of arteriosclerosis and to determine the effects of vascular interventional procedures on the arterial wall. A catheter-based 20-MHz transducer was used. Forty patients were studied. Twelve had clinical evidence of peripheral vascular disease, 13 were healthy renal donors, and 15 underwent vascular interventional procedures. The aorta and the ipsilateral iliac artery were examined in real time under fluoroscopic guidance and the results were compared with angiography. Sonography in eight of the 13 renal donors showed arterial wall abnormalities in the absence of angiographic evidence of disease. Sonography of the 15 patients after angioplasty or atherectomy demonstrated plaque fractures, intramural dissections, or atherectomy grooves.

Our experience suggests that intravascular sonography is of value in reducing the use of angiography to monitor progress or complications of vascular interventional procedures.

AJR 156:1087-1090, May 1991

Miniaturization of sonographic transducers has recently been achieved with transducer crystal thicknesses under 0.1 mm. Accordingly, feasible transducer frequencies are in the range of 15–30 MHz. Axial resolution is on the order of 0.1 mm, as we have determined with a wire model *in vitro*. Such high-frequency sonographic transducers have been mounted on catheters for cross-sectional intraluminal imaging. Either radial-array or mechanical scanning is possible [1]. The radial-array transducer has no moving parts; however, the volume of the transducer increases with the number of crystals mounted at the catheter tip. With mechanical scanning, the crystal is rotated 360° to accumulate B-mode data for axial display. Both types of transducers are now available commercially. Current catheter designs allow introduction through 7- to 8-French sheaths and have over-the-wire guidance capabilities.

This study focuses on the demonstration of arteriosclerotic disease with this technology, including the ability of sonography to detect early arteriosclerosis, to characterize advanced disease, and to depict the effects of revascularization procedures on the arterial wall. The vessels examined include the iliac arteries, superficial femoral arteries, saphenous vein *in situ* bypass graft, and popliteal arteries.

Materials and Methods

Forty patients were examined with both conventional angiography and intravascular sonography. These included 13 renal donors 20–72 years old (mean age, 38 years), 12 patients with symptoms of peripheral vascular disease, and 15 patients who had had 23 interventional vascular procedures. The interventional procedures included angioplasty (13 lesions), atherectomy (seven lesions), stent placement (three lesions), or a combination of these techniques (seven lesions). Seven patients underwent iliac artery angioplasty. Three

Received March 21, 1990; accepted after revision November 20, 1990.

Presented at the annual meeting of the American Roentgen Ray Society, Washington, DC, May 1990.

¹ All authors: Department of Diagnostic Radiology, Box 292 UMHC, The University of Minnesota Hospital and Clinic, 420 Delaware St. S.E., Minneapolis, MN 55455. Address reprint requests to C. E. Engeler.

0361-803X/91/1565-1087
 © American Roentgen Ray Society

patients had common iliac artery stenting after angioplasty had failed. Angioplasty and/or atherectomy were used in five superficial femoral arteries, two popliteal arteries, and one saphenous vein in situ bypass graft.

A member of the angiography team ran the sonographic equipment, making measurements of stenoses with the built-in software and recording still images on film. The real-time images were interpreted by at least two radiologists present during the procedure.

The presence of a three-layered arterial wall representing the tunica intima, media, and adventitia was documented and abnormal echogenicity or thickening evaluated. The arterial walls were characterized by established sonographic criteria [2-5]. Increased echogenicity corresponded to a higher lipid content of an atheroma, and acoustical shadowing represented focal or plaquelike calcifications in advanced lesions. The hypoechoic media served as a baseline to assess the

thickness of advanced intimal deposits. The spectrum of arteriosclerosis is summarized in Figure 1.

A catheter-based miniature sonographic device was used in all patients (Boston Scientific Corp., Watertown, MA). With this system, the transducer crystal with a resonant frequency of 20 MHz is mounted at the end of a flexible shaft. It is rotated at 900 rpm within a 6.6-French sheath of 100-cm length. Sterile water provides acoustic coupling between the transducer crystal and the sheath. B-mode scans are obtained by 360° rotation of the transducer. Real-time images are displayed at 15 frames per second by the supporting, dedicated sonographic instrumentation (Diasomics, Inc., Milpitas, CA). After diagnostic conventional angiography, the sonographic catheter assembly was introduced percutaneously through a 7-French sheath and guided fluoroscopically to the area of interest.

No complications related to the sonographic catheter were encountered. We usually limited the sonographic examination to less than 10 min. Access to the vessels of interest was direct and did not require the use of the available over-the-wire guidance capability.

Results

In eight of the 13 renal donors, several abnormalities of the arterial wall were shown by sonography but were not detected by angiography: fatty streaks, diffuse or asymmetric intimal thickening (Fig. 2), and focal calcified lesions. A three-layered appearance of the vessel wall, an appearance thought by some investigators to be a normal sonographic finding [3], was not appreciated in the aorta or iliac arteries in five of the renal donors and was most apparent in patients with advanced arteriosclerosis in whom diffuse intimal thickening was seen.

In the 12 patients with known peripheral vascular disease, sonograms of the aorta and iliac arteries revealed more extensive arteriosclerotic changes than were evident angiographically. The character and transmural extent of disease as well as the cross-sectional analysis of the vascular lumen

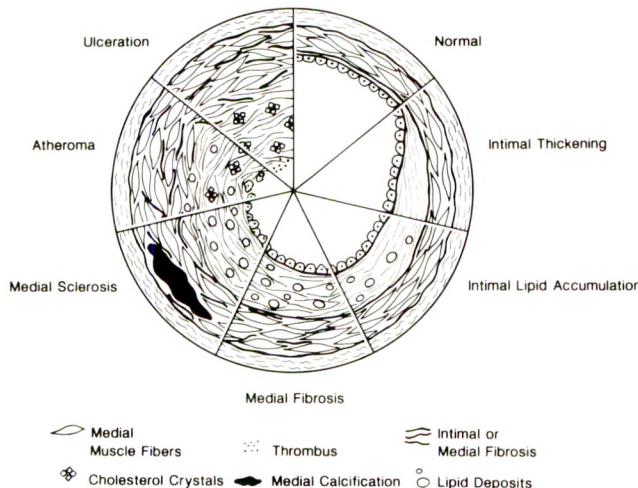
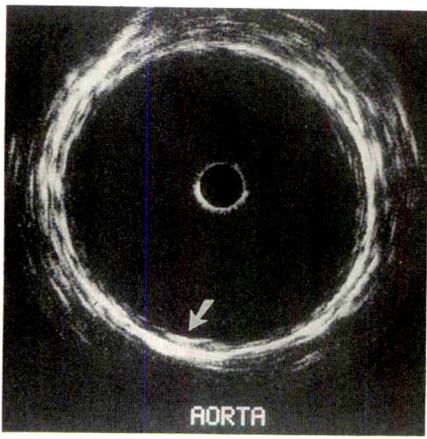
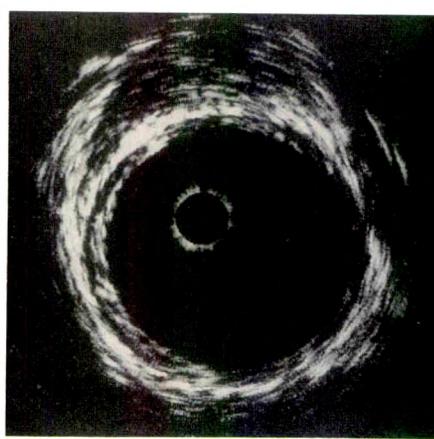


Fig. 1.—Schematic representation of pathologic spectrum of arteriosclerosis.



A



B

Fig. 2.—45-year-old renal donor with normal aortogram.

A, Sonogram of fatty streak, seen as bright intimal echoes at 6 o'clock position in upper abdominal aorta (arrow).

B, Distal abdominal aorta. Asymmetric echogenic thickening of intima on sonogram is characteristic of early atherosclerotic disease.

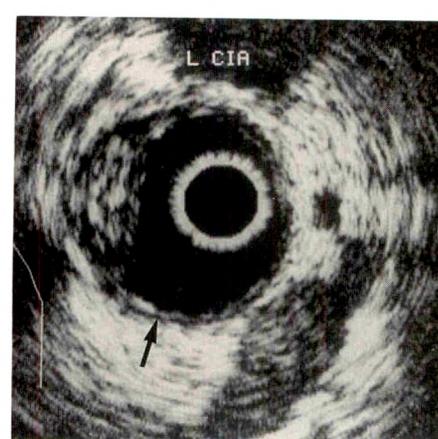


Fig. 3.—64-year-old man with claudication.

Sonogram of large, soft atheroma in common iliac artery. Hypoechoic tunica media (arrow) delineates original lumen.

was possible on the sonograms (Fig. 3). The information gained by sonography was most striking in two areas: (1) for the analysis of the composition of the arteriosclerotic abnormality, for example, the presence of lipids or calcium in atheromata, which could not be displayed by conventional angiography; and (2) in the determination of the degree of underlying diffuse arteriosclerotic disease, which was not apparent angiographically because of its circumferential distribution. In the absence of focal lesions, such a vessel may appear normal on angiograms.

In the 15 patients who underwent interventional revascularization procedures (Figs. 4-6), sonography provided the following information: diagnosis of complications such as local perforation of the arterial wall after atherectomy (one case); presence of intimal dissections after angioplasty (10 cases); fractured plaques (six cases); and evidence of an incomplete result of the initial revascularization procedures, indicating the need for additional intervention (seven cases). This decision was based on the sonographic findings alone.

Discussion

It is possible with high-resolution sonography to differentiate the layers of the arterial wall [3-5]. We were able to identify all three layers in 35 of the 40 patients studied. The inability to visualize the three layers of the arterial wall in five renal donors may be due to the thinness of the intima in these healthy individuals.

Intimal hyperplasia is particularly evident in vascular grafts when veins have been used as arterial conduits for long periods of time. Progressive luminal narrowing leads to recurrent arterial insufficiency. Intimal hyperplasia in a 15-year-old saphenous vein graft is demonstrated sonographically in Figure 4. Atherectomy was an effective method for removing hyperplastic intimal deposits in this case.

We observed great variations in the size and echogenicity of pathologic arterial deposits, as has been noted by other investigators [2-5]. Simple atherosomas are echogenic owing to the deposition of lipids in the tunica intima. Even small,

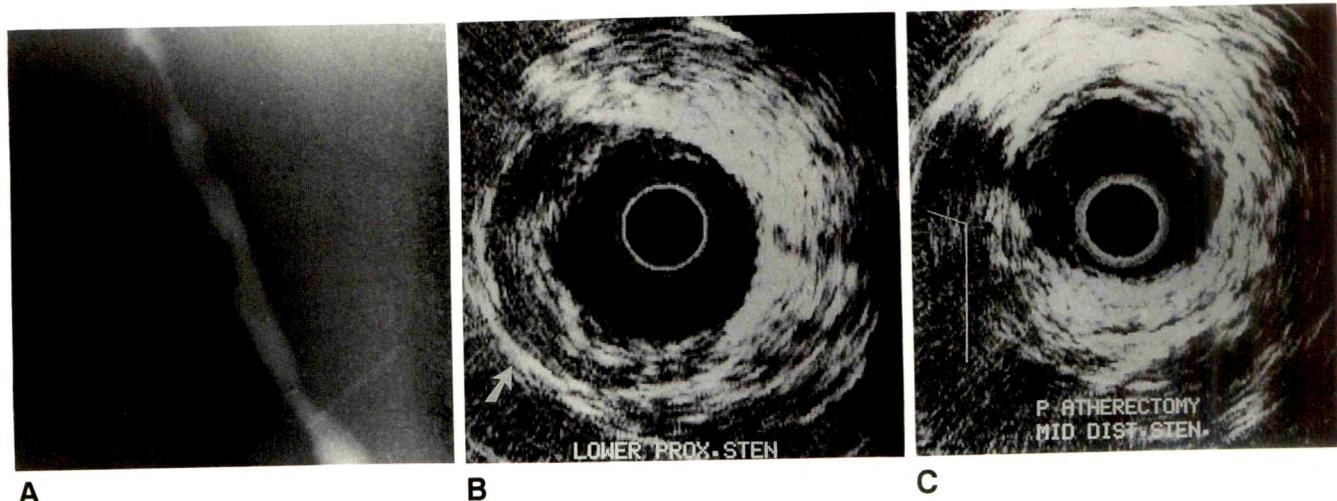


Fig. 4.—15-year-old saphenous vein *in situ* bypass graft.

A, Angiogram shows irregular contours.

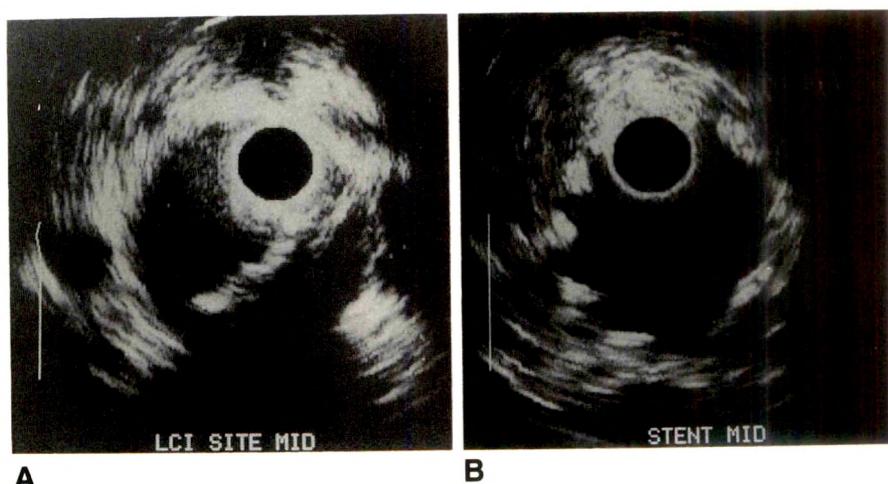
B, Sonogram shows severe, asymmetric intimal hyperplasia. Echogenic adventitia (arrow) is at perimeter of pathologic proliferation.

C, Sonogram shows incomplete, eccentric removal of intimal hyperplasia after atherectomy.

Fig. 5.—46-year-old diabetic man.

A, Sonogram shows large, calcified flap with acoustical shadowing inferiorly in common iliac artery after angioplasty. Pressure gradient is 20 mm Hg across lesion.

B, Good sonographic result after stent placement. No pressure gradient.



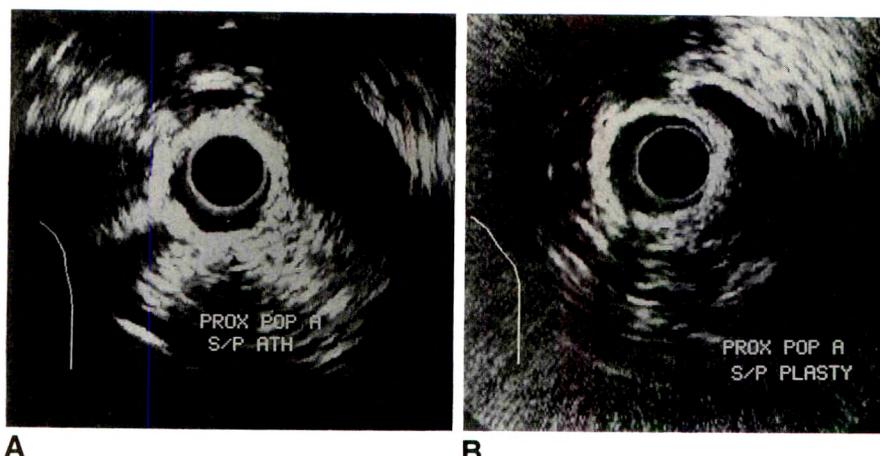


Fig. 6.—48-year-old diabetic patient with popliteal artery medial sclerosis.

A, Sonogram shows irregularities of calcified vessel wall, due to atherectomy.

B, Bursting of calcified media at 7 o'clock position after angioplasty.

focal echogenic deposits could be detected in eight of the 13 renal donors without corresponding angiographic abnormalities. An increased fibrous component is expected to decrease echogenicity. Calcification of an atheroma is obvious when there is total reflection of the ultrasound beam. Early investigators have correlated images from a prototype high-resolution intravascular sonographic unit in vitro with histologic findings [3, 6]. Figures 2 and 3 show variations of atherosclerotic disease.

Circumferential vascular calcification is shown well with intravascular sonography in patients with medial sclerosis, a vascular disease typically encountered in association with long-standing diabetes mellitus. Ultrasound waves are unable to pass beyond the highly reflective tunica media. The calcifications of medial sclerosis and more focal arteriosclerotic disease can be differentiated sonographically. Figure 6 shows a case of severe medial sclerosis in a popliteal artery.

Intravascular sonography can both characterize the diseased vessel as well as confirm the effect of angioplasty. The cross-sectional image furnished by intravascular sonography can be used to calculate the area and flow through a vessel. This information is similar to that given by measured pressure gradients and is most likely more accurate in situations with impaired run-off or distal occlusions. The technology for catheter-based Doppler measurement of blood velocity is available and may be combined with imaging to determine blood flow [7]. Breaks in the vessel wall, either in the intima or media, may be visualized, particularly if this occurs in a calcified lesion. Intimal flaps are commonly encountered after angioplasty but may not be evident in single, or even multiple, angiographic projections. Such flaps greatly increase the risk of restenosis at the site of angioplasty. In our experience, intravascular sonography has aided in recognizing these complications and has led to additional angioplasty, atherectomy, or stenting procedures in about half of the cases (Figs. 5A and 6B).

Intravascular sonography characterizes arterial disease by demonstrating the thickness and composition of the wall. While further experience is necessary, it is notable that the larger the pathologic deposits, the greater the relative merits

of atherectomy over angioplasty. This situation is found in severe intimal hyperplasia and large intimal flaps. In the case of severe calcific medial sclerosis, atherectomy weakened the wall sufficiently for angioplasty to be performed after initial attempts with angioplasty had failed to permanently increase the lumen diameter (Fig. 6). In other situations, atherectomy may be used as a secondary procedure to remove intimal flaps caused by angioplasty.

Intravascular stents are designed to overcome the inherent capacity of vessels to collapse. The true lumen of a stent cannot be established without the use of several radiographic projections. We have confirmed the proper expansion of three iliac artery stents with intravascular sonography and were able to measure the cross-sectional area of a stented vessel directly and establish the relationship of the stent to adjacent structures such as other vessels or masses. In the long-term follow-up of stents, intravascular sonography may be used to evaluate endothelialization. Figure 5 shows a case of iliac artery stent placement.

REFERENCES

1. Bom N, ten Hoff H, Lancee CT, Gussenboven WJ, Bosch JG. Early and recent intraluminal ultrasound devices. *Int J Card Imaging* 1989;4:79-88
2. Isner JM, Rosenfeld K, Losardo DW, et al. Percutaneous intravascular US as adjunct to catheter-based interventions: preliminary experience in patients with peripheral vascular disease. *Radiology* 1990;175:61-70
3. Gussenboven WJ, Essed CE, Frijman P, et al. Intravascular echographic assessment of vessel wall characteristics: a correlation with histology. *Int J Card Imaging* 1989;4:105-116
4. Picano E, Landini L, Distante A, Benassi A, Sarnelli R, L'Abbate A. Fibrosis, lipids, and calcium in human atherosclerotic plaque: in vitro differentiation from normal aortic walls by ultrasonic attenuation. *Circ Res* 1985;56:556-562
5. Eckmann A, Kuhn FP, Störkel S, Grönninger J, Kaiser L. Sonomorphologische Charakterisierung arterio-sklerotischer Plaques—Möglichkeiten und Grenzen der hochauflösenden B-Scan-Sonographie. *ROFO* 1988;149(1):15-21
6. Meyer CR, Chiang EH, Fechner KP, Fitting DW, Williams DM, Buda AJ. Feasibility of high-resolution, intravascular ultrasonic imaging catheters. *Radiology* 1988;168:113-116
7. White NW Jr, Yock PG. Intravascular ultrasound: catheter-based Doppler and two-dimensional imaging. *Cardiol Clin* 1989;7(3):525-535

Percutaneous Transluminal Angioplasty of the Subclavian Arteries: Long-term Results in 52 Patients

Andrija Hebrang¹
Josip Maskovic²
Berislav Tomac³

We studied the long-term results of percutaneous transluminal angioplasty of the subclavian artery in treating stenosis (43 patients) or occlusion (nine patients). In all 52 patients, the blood pressure before treatment in the arm on the involved side was at least 30 mm Hg lower than that in the opposite arm. Thirty-nine patients (75%) had symptoms of vertebrobasilar insufficiency (dizziness, blurred vision, ataxia). Angioplasty was successful in 40 (93%) of 43 patients with stenosis and in five (56%) of nine patients with occlusion. In the successfully treated patients, follow-up angiograms showed absence of narrowing greater than 30% stenosis, and the blood pressure in the treated arm equaled that in the opposite arm. The patients were followed up for 6–48 months (mean, 29 months). During this time, the blood pressure in the treated arm remained normal in 41 (91%) of 45 patients. The symptoms of vertebrobasilar insufficiency subsided in 28 (72%) of 39 patients.

These results suggest that percutaneous transluminal angioplasty is useful for treating subclavian artery stenosis or occlusion.

AJR 156:1091–1094, May 1991

Percutaneous transluminal angioplasty (PTA) is used to treat obstruction or stenosis of the subclavian arteries more often than of any other supraortic vessels. The technique and results of dilatation [1–5] have been described. Studies of small series of patients have been reported [6], but more reports on technical success, complications, and long-term results are needed. In this article, we report the technical success, complications, and long-term follow-up of PTA of the subclavian arteries in 52 patients who underwent this procedure.

Subjects and Methods

PTA was performed in the subclavian arteries of 52 patients 38–66 years old (mean age, 57 years). The indications for the procedure and the technique used were the same in all cases. All patients had symptoms of brachial ischemia during exercise (47 patients) or at rest (five patients). Symptoms of vertebrobasilar insufficiency were present in 39 patients (75%). These symptoms included dizziness ($n = 19$), blurred vision ($n = 5$), ataxia ($n = 2$), or a combination of these symptoms ($n = 13$). The initial clinical examinations included blood pressure measurements in both arms and Doppler sonography of the cervicobrachial arteries during exercise and at rest. Systolic blood pressure was lower on the affected side in all patients (30–50 mm Hg in 38 patients and more than 50 mm Hg in the remaining 14 patients).

Transfemoral aortic arch angiography and selective subclavian angiography were performed in 49 patients. In three patients with occluded iliac arteries, selective transcutaneous intraarterial digital subtraction angiography via the unaffected arm was performed [7, 8]. A high-grade stenosis (more than 50%) was found in 43 patients. Twenty-five had stenosis of the subclavian artery proximal to the vertebral artery (length, 10–21 mm) with retrograde blood flow in the vertebral artery. Eighteen had stenosis distal to the vertebral artery (length, 8–18 mm), and nine had stenosis at the origin of the vertebral artery (length, 11–24 mm).

Technical success was determined by angiography, which was performed immediately

Received September 29, 1989; accepted after revision October 30, 1990.

¹ Department of Radiology, Clinical Hospital "Dr. O. Novosel," Faculty of Medicine, University of Zagreb, Zajceva 19, 41000 Zagreb, Yugoslavia. Address reprint requests to A. Hebrang.

² Department of Radiology, Clinical Hospital "Firule," Spinciceva 1, 58000 Split, Yugoslavia.

³ Department of Neuroradiology, St. Johannes Hospital, Hospitalstrasse 6–8, 58 Hagen, Germany.

0361-803X/91/1565-1091
© American Roentgen Ray Society

after angioplasty. An absence of stenosis or residual stenosis less than 30% of the arterial diameter was considered a technical success. Clinical success was defined as a reduction in the difference in blood pressure between the treated and the untreated arms to less than 10 mm Hg. Long-term follow-up was available in all patients for periods of 6–48 months (mean, 29 months) and included measurement of blood pressure in both arms and Doppler sonography every 6 months. Follow-up angiography was performed in patients with a difference in blood pressure that was between the treated and untreated arms greater than 20 mm Hg.

Angioplasty Procedure

PTA was performed via the transfemoral approach in 49 patients and via a transaxillary approach in three patients with impassable iliac arteries. The subclavian artery was catheterized via a femoral approach with an H1 head-hunter catheter (William Cook Europe, Bjaeverskov, Denmark). After the catheter was placed proximal to the stenosis and a 160-cm-long J guidewire with a 3-mm radius (William Cook Europe) was carefully advanced through the stenosis, the tip of the guidewire remained deep in the axillary artery during the dilatation to prevent dislocation of the balloon catheter. If the stenosis was very narrow, or the subclavian artery was occluded, a straight guidewire was used to pass the affected part of the artery [6]. The angiographic catheter was then exchanged for a balloon catheter. Polyethylene balloon catheters (William Cook Europe) with maximal pressures up to 12 atm (1.2×10^6 Pa) were used. The balloon length was 2 or 4 cm, and its diameter was 8, 9, or 10 mm. For each case, the balloon used was 1 cm longer than the stenosis and had the same diameter as that of the unaffected part of the artery measured on the angiogram (taking into account the magnification, 10% with our equipment [Triplex Angiomatic, Siemens, Erlangen, Germany]). The part of the artery distal to the stenosis was considered normal if poststenotic dilatation was not present. If it existed, the arterial diameter just proximal to the stenosis was measured.

In three patients treated via the axillary approach, a straight catheter (William Cook Europe) was positioned just distal to the stenosis or occlusion. After the insertion of a straight guidewire, followed by an angiographic catheter, a guidewire was inserted into the aorta. The angiographic catheter was replaced with the balloon catheter, following the same procedure used in the transfemoral approach. During angioplasty in nine patients, the balloon was inflated across the origin of the vertebral artery. The middle part of the balloon was placed at the previously marked site of stenosis or occlusion. Dilatation was performed by using 5 atm (5×10^5 Pa) pressure. Immediate follow-up angioplasty was performed via an angioplasty catheter after the withdrawal of the catheter over the guidewire.

All patients were given acetylsalicylic acid, 250 mg/day for 3 days before and 3 months after the procedure. The first 30 patients did not receive heparin. The other patients were given 5000 units of heparin intraarterially.

Results

Technical success was achieved in 40 (93%) of 43 patients with stenosis and in five (56%) of nine patients with occluded subclavian arteries. Incompletely dilated stenoses were found in patients in whom the initial subclavian arterial diameter was wider than 8 mm because balloon catheters 9 or 10 mm in diameter were not available at the beginning of the study. In these cases, subsequent angiograms showed a stenosis but

blood pressure was normal (Fig. 1). In three patients with proximal stenoses, the guidewire could not pass through the narrowed lumen. As the axillary artery pulse was not palpable, this approach was not used. All 45 patients in whom angioplasty was technically successful had blood pressure differences between the treated and the untreated arms of less than 10 mm Hg. In one patient with two stenoses at the proximal part of the right subclavian artery, only the proximal stenosis was successfully dilated. Because blood pressure was normal, the distal stenosis was not treated (Fig. 2). Long-term clinical results of all patients were analyzed by the life table method (Table 1) [9]. In all 45 patients in whom angioplasty was technically successful, blood pressure in the treated arm remained normal during the first year. The difference in blood pressures between the two arms was less than 10 mm Hg. In the second year, blood pressure in one patient became abnormal (35 mm Hg lower than in the untreated arm), giving an 84.6% cumulative success rate for PTA. Blood pressure decreased in three additional patients during the third year. Blood pressures on the treated side were between 30 and 45 mm Hg lower than those on the untreated side. The accumulated clinical success at the third year was 78.8%. Follow-up Doppler sonograms of the cervicobrachial arteries were normal in all but four patients during the second and third years. In three of them, the initial subclavian stenoses were proximal to the vertebral origin, and flow in the vertebral artery was reversed. The follow-up Doppler study performed 30 months later showed reversible flow in the vertebral artery in all three patients. The fourth patient had an occluded subclavian artery before angioplasty. All four patients in whom PTA failed had symptoms of brachial artery ischemia during exercise. The symptoms of vertebrobasilar insufficiency disappeared in 28 (72%) of 39 patients, including dizziness in 14 of 19, blurred vision in two of five, ataxia in one of two, and combined symptoms in 11 of 13 patients. The symptoms subsided during the first year of follow-up.

Discussion

Technical success after angioplasty in this series of patients was achieved in 93% of patients with narrowed subclavian arteries. Previous reports have shown technical success rates between 62% [4] and 100% [10, 11]. In a larger series, Mathias et al. [12] had good initial results in 28 (88%) of 32 patients. The three patients in our study in whom dilatation was unsuccessful had stenoses of the proximal part of the subclavian artery. Other authors [4] also reported difficulty in introducing a guidewire into proximal stenoses.

The technical success of PTA in occluded subclavian arteries (56%) was quite different from that in stenoses (93%) because of the difficulty in passing through the occluded area. Because of the good technical success rate, we believe that PTA is the treatment of choice for patients with stenosis or obstruction of the subclavian artery.

The results of clinical follow-up in our patients were similar to those reported by other authors. After 25 months, Wilms et al. [13] reported successful results, including relief of symptoms, in 18 (86%) of 21 patients. Brückman et al. [14]

Fig. 1.—64-year-old patient with stenosis of left subclavian artery.

A, Initial angiogram shows stenosis of prevertebral part of left subclavian artery.

B, Follow-up angiogram after angioplasty shows residual stenosis of less than 30% of arterial diameter. Blood pressure in treated arm returned to normal.

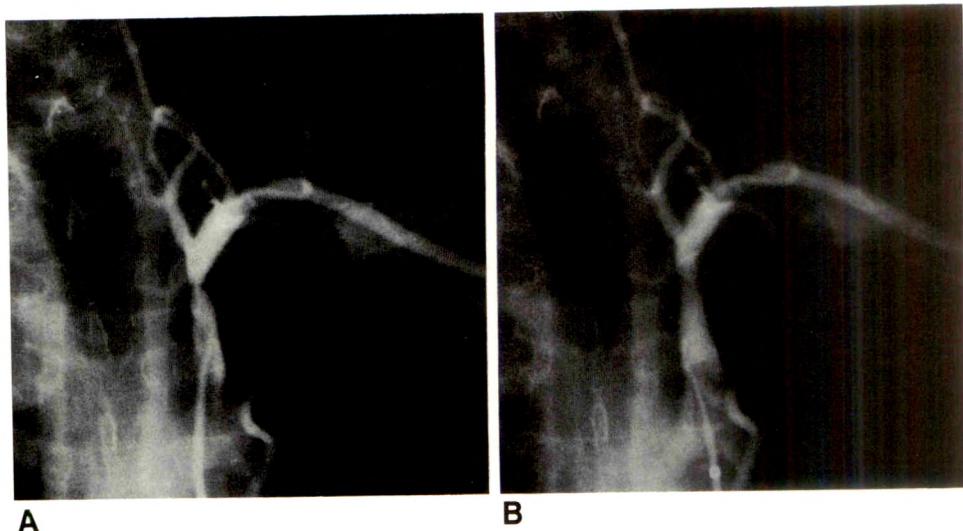


Fig. 2.—52-year-old patient with two stenoses of right subclavian artery.

A, Initial angiogram shows stenoses distal to vertebral artery.

B, Angiogram after percutaneous transluminal angioplasty shows a successfully dilated proximal stenosis; distal stenosis was not treated because blood pressure returned to normal after dilatation of proximal stenosis.

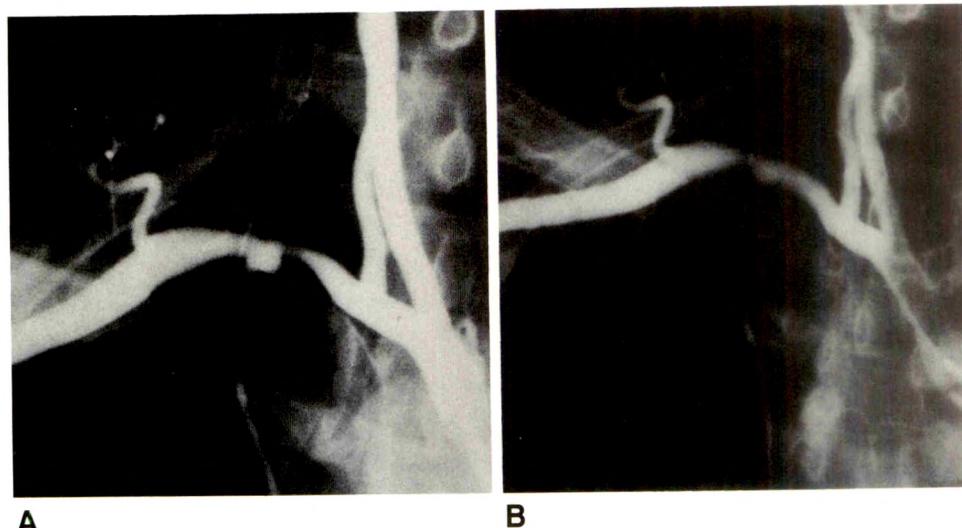


TABLE 1: Life Table Analysis of the Clinical Results After Percutaneous Transcubital Angioplasty of the Stenosed or Occluded Subclavian Arteries

Postangioplasty Interval	No. of Cases		Clinical Success (%) ^a	
	Total	Unsuccessful	Interval	Cumulative
0-1 year	52	7	86.5	86.5
1-2 years	45	1	97.8	84.6
2-3 years	44	3	93.1	78.8
3-4 years	41	0	100.0	78.8

^a Clinical success in the first through third postangioplasty years was assessed by examinations including blood pressure measurements and Doppler sonograms of the brachiocephalic arteries.

reported alleviation of symptoms in 70% (mean follow-up, 28 months) of 52 treated patients with the subclavian steal syndrome. When a subclavian stenosis is located near the origin of the vertebral artery, the angioplasty balloon must be inflated across the origin of the vertebral artery. Vitek [15] reported good technical results without complications in 12

patients with that diagnosis. The results were similar in our nine patients. In all nine patients, the stenosis was located less than 10 mm proximal or distal to the vertebral origin. During angioplasty, the vertebral artery was temporarily occluded. In four patients with proximal stenoses, the vertebral flow before angioplasty was retrograde. In the remaining five patients, the subclavian stenoses were distal to the vertebral arteries. In all cases, blood pressure was normal in the treated arm and neurologic symptoms were absent during the follow-up period.

The use of heparin during PTA of the subclavian arteries has not been universally accepted. Vitek et al. [10] did not use heparin and believed it was necessary only for PTA of small arteries. Like Motarjame et al. [3], who performed their first 15 procedures without heparin, we also avoided it in our first 30 patients. No differences in complication rates were observed between the patients treated with heparin and those not treated with it. Because of the comparable complication rates in these two groups, we do not recommend the use of heparin in PTA of subclavian arteries.

REFERENCES

1. Bachman DM, Kim RM. Transluminal dilatation for subclavian steal syndrome. *AJR* 1980;135:995-996
2. Novelline RA. Percutaneous transluminal angioplasty: newer applications. *AJR* 1980;135:983-988
3. Motarjeme A, Keifer JW, Zuska AJ. Percutaneous transluminal angioplasty of the brachiocephalic arteries. *AJR* 1982;138:457-462
4. Gordon RL, Haskell J, Hirsch M, Shifrin E, Weinman E, Romanoff H. Transluminal dilatation of the subclavian artery. *Cardiovasc Intervent Radiol* 1985;8:14-19
5. Mathias K, Schlosser V, Reinke M. Katheterrekanalisation eines Subklaviaverschlusses. *ROFO* 1980;132:346-347
6. Motarjeme A, Keifer JW, Zuska AJ, Nabawi P. Percutaneous transluminal angioplasty for the treatment of subclavian steal. *Radiology* 1985;155:611-613
7. Tomac B, Hebrang A. New catheter technique for transcutaneous intraarterial DSA of the aortic arch and supraaortic vessels. *Neuroradiology* 1989;31:80-84
8. Tomac B, Hebrang A. Selektive ambulante transbrachiale intraarterielle DSA der supraaortalen Arterien. *ROFO* 1990;152:191-195
9. Cutler SJ, Ederer F. Maximum utilization of the life table method in analyzing survival. *J Chron Dis* 1958;8:699-712
10. Vitek JJ, Keller FS, Duvall ER, Gupta KL, Chandra-Sekar B. Brachiocephalic artery dilatation by percutaneous transluminal dilatation. *Radiology* 1986;158:779-785
11. Arlart IP. Ballonkatheterdilatation in der Behandlung des Subclavian-Steal-Syndroms. *ROFO* 1988;149:263-266
12. Mathias K, Bockenheimer S, Von Reuther G, Heiss HW, Ostheim-Dzervycz W. Katheterdilatation Hirnversorgender Arterien. *Radiologie* 1983;23:208-214
13. Wilms G, Baert A, Dewaele D, Vermylen J, Nevelsteen A, Suy R. Percutaneous transluminal angioplasty of the subclavian artery: early and late results. *Cardiovasc Intervent Radiol* 1987;10:123-128
14. Brückmann H, Hutschenreuter M, Ringelstein EB, Zeumer H. Die Bedeutung der Vertebralangiographie für die Diagnostik und Therapie der vertebrobasilären Durchblutungsstörungen unter besonderer Berücksichtigung gefäßrekanalisierender Verfahren. *Radiologie* 1987;27:495-501
15. Vitek JJ. Subclavian artery angioplasty and origin of the vertebral artery. *Radiology* 1989;170:407-409

Conventional Screen/Film vs Reduced Exposure Photostimulable Phosphor Plate Imaging in Lower Extremity Venography: An ROC Analysis



Edward L. Siegel¹
Larry T. Cook
Michael B. Parsa

Half-exposure phosphor plates used in venography substantially reduce the total X-ray exposure to a patient while increasing the chance that all images will be of excellent diagnostic quality. Simultaneous half-exposure phosphor plate and full-exposure conventional screen/film venograms were obtained of 35 patients and compared by using receiver operating characteristic (ROC) analysis. The area under the ROC curve ranged from 0.67 to 0.78 for conventional films and 0.68 to 0.91 for phosphor plates. Group performances on conventional films vs phosphor plates were not statistically different. No statistically significant difference in individual performance with the two techniques was seen in seven of the eight interpreters at the 95% confidence level. The eighth interpreter performed significantly better with phosphor plates than with conventional films. Interpreters with and without specific experience in phosphor plate venography were grouped separately, and performance of the two groups was compared in each technique. No difference in performance was found between the groups when interpreting conventional venograms, but, when interpreting phosphor plate venograms, the group with specific experience performed significantly better than they had with conventional venograms, and significantly better than the other group did at interpreting either conventional or phosphor plate venograms.

We conclude that phosphor plate venograms made at a 50% reduction in X-ray exposure are equal to, and may surpass, conventional screen/film venograms for diagnosing acute venous thrombosis of the calf and thigh. We recommend expanding the indications for phosphor plate radiography to include contrast venography of the lower extremities.

AJR 156:1095-1099, May 1991

Photostimulable phosphor plate (PP) imaging is a recent technological innovation that uses a reusable phosphor storage plate in place of the conventional film and intensifier screen combination. After X-ray exposure, the latent image on the PP is read by a laser scanning device, digitized, and stored in a $2K \times 2K$ data array. The PP is then erased and recycled [1]. The digital image is sent to a laser printer where it is printed on a 25.7×36.4 cm film (Fuji CR 780, Fuji Tokyo, Japan) in either a one-on-one format, which is two-thirds size, or a two-on-one format, which is one-half size. The optical densities of a typical PP film range from 0.20 to 2.87.

The digital format of the data acquired in PP imaging has several advantages over conventional film [2]. Image manipulations, including windowing, gray-scale reversal, magnification, filtration, and enhancement, are all easily and quickly accomplished through the interactive image-processing workstation. PP digital images are perfectly suited for image archival on high-density optical or magnetic storage media, and for transmission via local or wide area networks. Although most radiology departments are not equipped to realize these latter benefits, many authors think that these capabilities will become increasingly important in the coming years [3].

In addition to the inherent advantages of digitally formatted data, PP imaging offers the further benefit of extremely wide latitude in radiographic exposure.

Received October 11, 1990; accepted after revision November 21, 1990.

¹ All authors: Department of Diagnostic Radiology, University of Kansas Medical Center, 39th St. & Rainbow Blvd., Kansas City, KS 66103. Address reprint requests to E. L. Siegel at 2155 Bell Memorial Hospital.

0361-803X/91/1565-1095
© American Roentgen Ray Society

Typically, PP sensitivity is linear over a range of 5 μ R to 50 mR (1.29×10^{-9} C/kg to 12.9×10^{-6} C/kg) [4]. This corresponds to screen/film system speeds of 20 to 2000. Consequently, patients' exposure can be decreased significantly, and retakes due to errors in radiographic technique are virtually eliminated.

PP systems have been extensively investigated and are now in routine use for chest, skeletal, pediatric, and gastrointestinal studies at several centers [5-16]. We report here on our early clinical experience in applying PP technology with the Digiscan system (Siemens Medical Systems, Iselin, NJ) to contrast venography of the lower extremities. To our knowledge, a systematic comparison between PP imaging and conventional films (CF) in lower extremity venography has not been previously reported.

Materials and Methods

Previous investigations from this laboratory had indicated that satisfactory images of a lower extremity venography phantom could be obtained with PP exposed at 50% of the exposure required for a conventional 400 speed screen/film system [17]. The intent of this study was to compare venograms made with a conventional screen/film system (Kodak TMG, Lanex regular screens) with venograms made at half the screen/film exposure with PP. We restricted our study to patients with lower extremity venograms who were referred to our department between August 1, 1989, and March 31, 1990. All patients enrolled in the study gave written informed consent before the procedure.

All venograms were obtained with a total dose of 150 ml iohexol (Omnipaque 240, Winthrop, New York, NY), by using the technique of Rabinov and Paulin [18]. Phosphor plates (35×43 cm) were loaded into spot film cassettes and alternated with standard film cassettes. An average of three PP images were exposed per patient. Tube kilovoltage was held constant throughout each patient's procedure. CF exposures were phototimed and the exposure factors noted. After each CF exposure the milliampere-second setting was manually set at half the corresponding CF dose, and the exposure was repeated with a PP. This resulted in matching CF and half-exposure PP images for comparison, and obviated any additional injection of contrast medium.

The exposed PP were read by the automated laser scanning device and processed with an operator-selected processing mode and printing format. The processing mode selected was the manufacturer's proprietary algorithm for lower extremities with contrast. The algorithm produced two renditions of each image. The first was a "standard" image derived from the original data with minimal filtration or enhancement. The second image was processed with an unsharp masking algorithm to enhance higher spatial frequencies, resulting in sharper edge detail. When the two-on-one printing format was selected by the operator, both the standard and enhanced images were printed. Selection of the one-on-one format resulted in printing only the standard image. The technologist selected only the mode and print format. This resulted in both one-on-one and two-on-one print format films being used in the study. No additional enhancement was used deliberately to highlight lesions.

During the study period, a total of 60 patients were referred for lower extremity venograms. Images from 35 examinations were included in this study. Twenty-five patients were excluded for a variety of reasons. In 16 cases, no PP images were obtained. These were generally patients who arrived after hours, when the additional technical staff required to make the exposure modifications was not

available. In three of these cases, no PP images were obtained because the equipment was down for routine maintenance. Two cases were excluded because the CF images could not be located. Seven cases were eliminated because the CF and PP images were not comparable views.

The 35 image pairs were submitted to a jury consisting of four board-certified radiologists experienced in interpreting vascular studies. The films were evaluated for the presence of acute venous thrombosis. Each juror considered the films alone and was asked to respond with "yes," "no," or "equivocal." The votes of the jurors were compiled and their consensus was used, together with a final review, to identify 12 cases of acute venous thrombosis [19]. The 35 patients included in the study consisted of 10 men and 25 women. Ages ranged from 22 to 86 years (mean, 52.8 years; SD, 16.8 years). Twelve cases of acute venous thrombosis included seven deep venous thromboses, one isolated superficial venous thrombosis, and four isolated muscular branch thromboses. Venous insufficiency of various degrees either in isolation or superimposed on other findings, was present in 21 patients. Chronic venous occlusion or evidence of previous venous thrombosis was seen in five cases, three of which had superimposed acute deep venous thrombosis. One patient had mild venous insufficiency and extrinsic popliteal vein compression due to a Baker cyst.

Eight study participants were selected from our department. Four were board-certified radiologists who do not routinely interpret venograms. The remaining four were fourth-year residents with recent training in venography with both CF and PP. None of the interpreters served on the jury. The films were randomized for presentation to the participants, and the interpreters were divided into two groups. Group 1, composed of three staff radiologists and one resident, interpreted the CF images first, followed by the PP images 1 month later. The second group, composed of three residents and one staff radiologist, interpreted the PP images first, followed by the CF images 1 month later. In no case was the interval between interpretation sessions less than 4 weeks. The conventional and PP films were interpreted on the alternator in the usual reading room. No time limit was imposed.

In order to perform an ROC analysis, it was necessary to obtain graded responses from the study participants. In previous studies we had used a simple grading scale of one to five. However, because of the confusion attendant to this qualitative rating procedure, we tried to make the rating scale more concrete through our instructions to the participants. The instructions included the accepted angiographic criteria for diagnosing venous thrombosis [20]. If these criteria were met, a positive response was indicated, and the respondent was asked for the descriptors that best matched the search time (i.e., first glance, quick search, or longer search) and visibility of the lesion (i.e., conspicuous, intermediate, or inconspicuous). If the criteria for acute venous thrombosis were not met, a negative response was indicated and a certainty descriptor (i.e., definitely or probably) was given.

The descriptive ratings were converted to a numerical score of one to five for definitely negative, probably negative, positive-inconspicuous (longer search), positive-intermediate (quick search), and positive-conspicuous (first glance), respectively. The rating of probably negative was for those cases in which there were questionable findings that might have been clarified on other views not available to the interpreters. With this rating scheme, no film received a rating of one or five from all of the observers.

The observers' response data were analyzed with an ROC technique [21]. These data were not pooled, so that an ROC area, A_z , was calculated for each reader and for each film type, CF and PP. Data were analyzed by using the program CORROC2 [22], which uses a maximum likelihood estimation technique to calculate binomial ROC parameters, accounting for the correlations between pairs of

responses for each case. We used the parameter A_z for comparison purposes.

Comparisons were performed for each interpreter, CF vs PP. Comparisons also were made between pairs of interpreters within each category, CF or PP. The paired t test [23] was used to compare collective performance in CF vs PP. Group performance of staff vs resident radiologists was compared with the unpaired t test. There were 280 responses in each category and 560 total responses. Values of p less than or equal to .05 indicate that performances are different at the 95% confidence level.

Results

Individual interpretation times varied from 11 to 40 min. No significant difference was found between interpretation times for CF vs PP for individual participants, and no correlation was found between interpretation time and performance as measured by the A_z parameter (Pearson's $r = .25$, $p = .34$). The areas under the ROC curves for each interpreter and each film type are shown in Table 1, together with the calculated standard deviation for each value. The performance (A_z) of the interpreters on CF ranged from 0.67 to 0.78, and on PP ranged from 0.68 to 0.91. Comparison of these results using the paired t test yielded $t = 1.20$ with an associated $p = .27$. Consequently, no statistical difference exists between the interpreters' performance as a group on CF and PP.

The two-tailed t test in the program, CORROC2, was used to look for differences in performance (A_z) for each interpreter on CF and PP. Only interpreter 8 showed a statistically significant difference in performance for these two tasks ($p = .02$). Group performance of residents on CF vs PP, and staff radiologists on CF vs PP, was compared by using the paired t test. Group performance of residents vs staff for each task was compared by using the unpaired t test. No significant difference was found between groups on CF ($p = .34$) nor was any difference found in staff radiologists' performance on CF vs PP ($p = .31$). However, group performance of the residents was improved on PP vs CF ($p = .05$) and was superior to the group performance of staff radiologists on both PP ($p = .04$) and CF ($p = .05$).

Pairwise comparisons of all interpreters in CF were calculated with CORROC2. None of the A_z values in each pair are close to being significantly different. Analogous comparisons

of interpreters in PP were calculated and showed that the performances of interpreters 2 and 3 (staff radiologists) were significantly lower than those of interpreters 4, 7, and 8 (senior residents) at the 95% confidence level. Consequently, as a group, the eight interpreters showed more variability in performance on PP than on CF.

Discussion

Digital radiography with PP technology has been evaluated at our institution since early 1989. We, and others, have found this technology to be very useful in a variety of clinical applications [5-16]. Lower extremity venography with PP offers several advantages over CF venography. First, we have shown that a significant reduction in X-ray exposure is possible without any sacrifice in the diagnostic quality of the images. In this study, all PP images were exposed at 50% of the dose required for an identical CF exposure. Second, retakes due to errors in radiographic technique are eliminated because of the extremely wide latitude of the PP imaging system (Fig. 1). This benefits the patient not only by minimizing the radiation exposure, but also by minimizing the need for additional injections of contrast medium. Elimination of retakes also improves productivity because venography is a labor-intensive task for the radiologist. A third advantage derives from the ability to manipulate the imaging data digitally. In many patients, body part thickness varies markedly through the calf and leg. This results in portions of the film being over- or underexposed. With CF, overexposed regions

TABLE 1: Diagnostic Performance (A_z) for Each Reader

Reader	CF		PP	
	A_z	SD	A_z	SD
1	.78	.08	.74	.12
2	.78	.10	.68	.10
3	.70	.10	.65	.12
4	.76	.09	.90	.06
5	.70	.09	.76	.10
6	.78	.09	.83	.09
7	.78	.05	.86	.05
8	.67	.10	.91	.05
Mean	.74	.09	.79	.10

Note.—CF = conventional film, PP = photostimulable phosphor plate, SD = standard deviation. Paired t test: $t = 1.20$, $p = .27$.

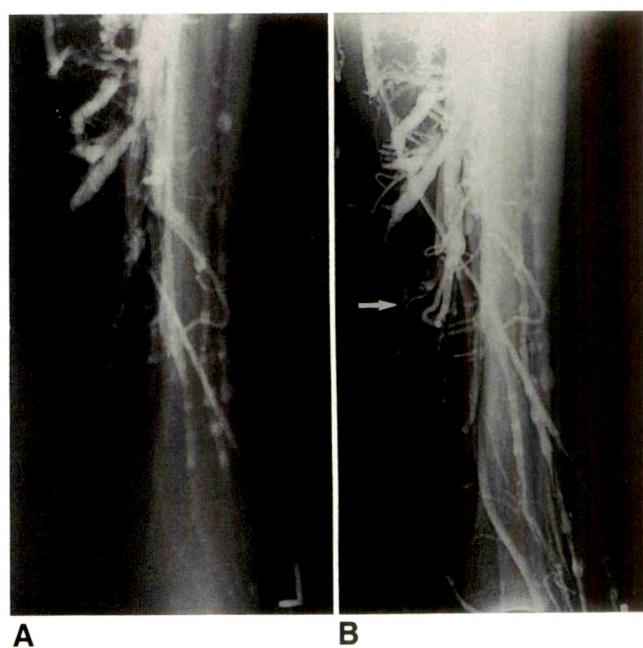


Fig. 1.—Extensive thrombosis of deep, muscular (arrow) and superficial veins.

A, Conventional film is overexposed because of improper setting of phototimer density control. Thrombus could be seen only with the aid of a hot light.

B, Phosphor plate is unaffected by overexposure due to extremely wide latitude.

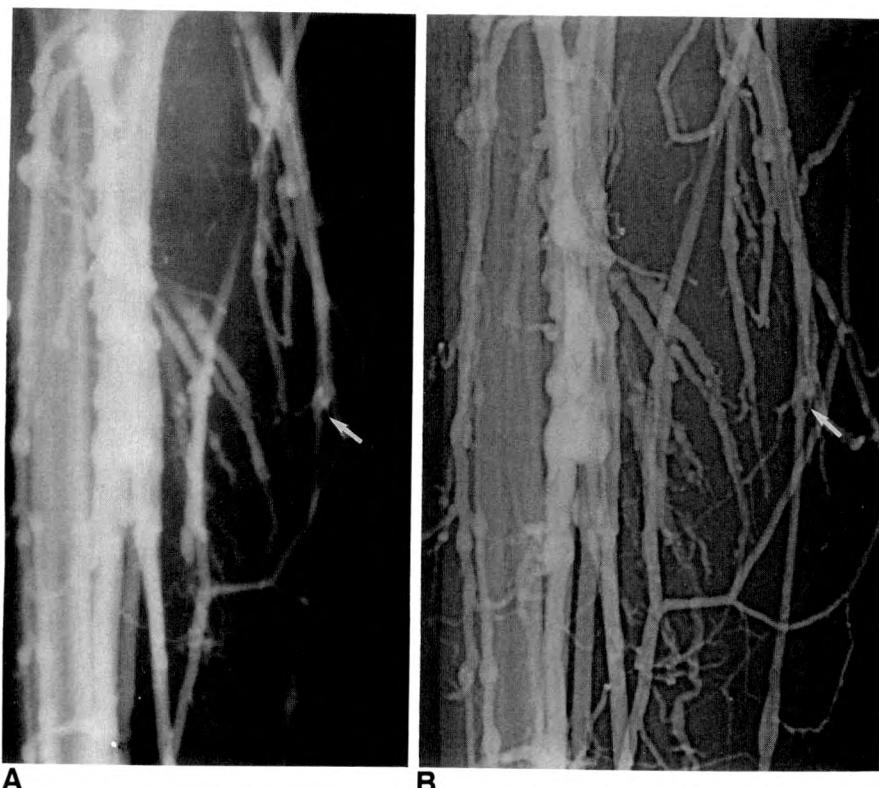


Fig. 2.—Small isolated thrombus (arrow) in a superficial vein.

A, Conventional film.

B, Phosphor plate with edge enhancement improves conspicuity of subtle abnormality.

on the film can usually be evaluated with the aid of a hot light, but underexposed regions are often uninterpretable. The digitized data from PP images can be displayed at an interactive workstation by using various window and level settings to visualize all regions of the image optimally. Furthermore, the visibility of subtle abnormalities can often be improved by digital filtration and enhancement of the imaging data (Fig. 2).

In our study, the time required for the individual interpretation tasks did not vary significantly between the first and second sessions. Seven of the eight interpreters showed no statistically significant difference in diagnostic performance between CF and PP images. Interpreter number 8 performed significantly better with PP ($A_z = .91$ for PP, $A_z = .67$ for CF) despite the fact that the PP images were analyzed first. Interestingly, A_z decreased for three of the four interpreters in Group 1 and all four interpreters in Group 2 during the second reading sessions. This phenomenon is believed to be an artifact due to the composition of the two groups and the order in which each group analyzed the films. Compared with the value of A_z for CF, the value of A_z for PP decreased for three of the four staff radiologists but increased for all four of the residents. Although with the exception of interpreter number 8 the differences in A_z for individual interpreters were not statistically significant, grouped data for residents vs staff radiologists did point out some interesting trends. Although our data indicate a very high degree of consistency among the interpreters when analyzing CF venograms, pairwise comparisons of individual A_z for PP show interpreters 2 and 3 (both staff radiologists) to be significantly lower than interpreters 4, 7, and 8 (all senior residents). As a group, residents interpreting PP venograms did significantly better than with

CF venograms and also outperformed staff radiologists on both PP and CF venograms. We believe that this reflects differences in experience and training. The participating staff radiologists all have broad general experience, including CF venography, but have had little if any previous contact with PP venography. In contrast, the residents, although relatively less seasoned, all have recent training and experience with this technique.

We have shown that, with PP venography, an X-ray exposure reduction of 50% can be achieved without any sacrifice in the diagnostic accuracy of the study. Our data indicate that some training and experience with the technique is necessary to achieve optimal interpreter performance. Furthermore, our data suggest that, as the radiologist gains the requisite experience, PP technology may actually yield improvement in the diagnostic accuracy of the procedure. On the basis of this study, we conclude that the indications for PP imaging should be expanded to include lower extremity venography.

REFERENCES

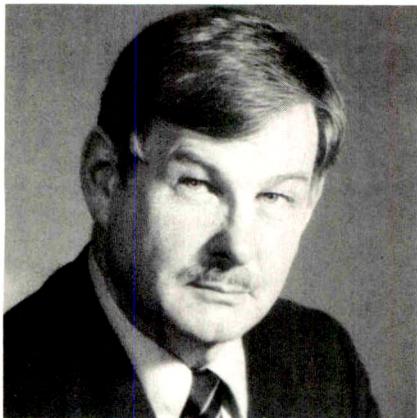
- Sonoda M, Tahano M, Miyahara J, Kato H. Computed radiography utilizing scanning laser stimulated luminescence. *Radiology* **1983**;148:833-838
- Murphy MD, Bramble JM, Cox GG, McMillan JH, Dwyer SJ III, Harvey PC. Experience in the use of an image-processing workstation for a photostimulable phosphor radiographic system. *J Dig Imag* **1990**;3:60-65
- Hillman BJ, Fajardo LL. Clinical assessment of phosphor-plate computed radiography: equipment, strategy, and methods. *J Dig Imag* **1989**;2:220-227
- Blume H. Stimulable phosphor systems: technical aspects. In: Peppler WW, Alter AA, eds. *Proceedings of the Chest Imaging Conference*. Madison: University of Wisconsin Press, **1987**:194-207
- Fajardo LL, Hillman BJ, Pond GD, Carmody RF, Johnson JE, Ferrell WR.

- Detection of pneumothorax: comparison of digital and conventional chest imaging. *AJR* **1989**;152:475-480
6. Fuhrman C, Feist JH, Cooperstein L, et al. High-resolution storage phosphor chest imaging. In: Peppler WW, Alter AA, eds. *Proceedings of the Chest Imaging Conference*. Madison: University of Wisconsin Press, **1987**:194-207
 7. Fuhrman CR, Gur D, Good B, Rockette H, Cooperstein LA, Feist JH. Storage phosphor radiographs vs conventional films: interpreters' perceptions of diagnostic quality. *AJR* **1988**;150:1011-1014
 8. Hillman BJ, Fajardo LL. Scientific assessment of the clinical utility of phosphor plate computed radiography. *Proc SPIE* **1989**;1091:245-249
 9. Kehler M, Albrechtsson V, Andersson B, Larusdottir H, Lundin A, Pettersson H. Assessment of digital chest radiography using stimulable phosphor. *Acta Radiol* **1989**;30:581-586
 10. Kehler M, Albrechtsson V, Andresdottir A, Larusdottir H, Lundin A. Accuracy of digital radiography using stimulable phosphor for diagnosis of pneumothorax. *Acta Radiol* **1990**;31:47-52
 11. Kogutt MS, Jones JP, Perkins DD. Low-dose digital computed radiography in pediatric chest imaging. *AJR* **1988**;151:775-779
 12. Marioka C, Brown K, Hayrapetian A, Kangarloo H, Balter S, Huang HK. ROC analysis of chest radiographs using computed radiography and conventional analog films. *Proc SPIE* **1989**;1091:168-171
 13. Merritt CRB, Matthews CC, Tutton RH, et al. Clinical application of digital radiography: computed radiographic imaging. *RadioGraphics* **1985**;5:397-414
 14. Nakano Y, Togashi K, Nishimura K, et al. Stomach and duodenum: radiographic magnification using computed radiography. *Radiology* **1986**;160:383-387
 15. Sakuma H, Takeda K, Hirano T, et al. Plain chest radiograph with computed radiography. *AJR* **1988**;151:27-30
 16. Schaefer CM, Greene R, Oestmann JW, et al. Digital storage phosphor imaging versus conventional film radiography in CT-documented chest disease. *Radiology* **1990**;174:207-210
 17. Siegel EL, Lee KR, Templeton AW, Dwyer SJ III, Cox GG, Bialek J. Phosphor plate computed venography: comparison with conventional and digital image intensifier radiographic systems. *Radiology* **1989**;173(P):477
 18. Rabinov K, Paulin S. Roentgen diagnosis of venous thrombosis in the leg. *Arch Surg* **1972**;104:134-144
 19. Ker M, Seely GW, Stempski MO, Patton D. A protocol for verifying truth of diagnosis: preliminary report. *Invest Radiol* **1988**;23:485-487
 20. Rabinov K, Paulin S. Venography of the lower extremities. In: Abrams HL, ed. *Abrams angiography*. Boston: Little, Brown, **1983**:1877-1921
 21. Metz CE. ROC methodology in radiology imaging. *Invest Radiol* **1986**;21:720-733
 22. Metz CE, Wang PL, Kronman HB. A new approach for testing the significance of differences between ROC curves measured from correlated data. In: Deconinck F, ed. *Information processing in medical imaging*. The Hague: Martinus Nijhoff, **1984**:431-445
 23. Metz CE. Some practical issues of experimental design and data analysis in radiological ROC studies. *Invest Radiol* **1989**;24:234-245

Memorial



John Wickwire Loop, 1924–1990



We lost one of our most intelligent, creative, and congenial colleagues with the passing of John Loop. Early in his career John became an accomplished neuroradiologist. Later he focused on issues in medical efficacy, and lastly he became expert in image transmission and management. He made important contributions to our specialty and to the University of Washington, where for 31 years he served its missions, trainees, and patients with grace and distinction.

John was born in Belvidere, IL, in 1924 and was educated at Depauw University, The University of Wyoming, and Harvard Medical School. He trained in radiology at the University of Chicago in the company of such luminaries as Paul Hodges, Russell Morgan, and Robert Moseley in the era when radiology was just beginning its leap into high

With his characteristic keen perception of new trends and opportunities, John foresaw specialization in diagnostic radiology and was among the early Americans to opt for post-residency training in what was to become our first subspecialty, neuroradiology. At the time, Sweden was breaking all the barriers in interventional radiology, and John sought a fellowship at the University of Lund for what proved to be a most influential year, 1956–1957. There he mastered the principles of cerebral angiography and pneumoencephalography and found Maj Teorell, a medical student who later became a pediatrician, his first wife, and mother of his five children. He also became acquainted with the fledgling Department of Radiology at the University of Washington, where in 1959 he began his teaching and research career.

In the new department, John introduced radiologist-performed angiography, air studies, and myelography at a time when neurosurgery conventionally dominated such procedures. With gas myelography, he showed thoracic myelopathy in neurofibromatosis, and with colleagues in neurosurgery he explored intraoperative intracranial angiography. A large regional population of persons with hydrocephalus allowed him to describe the development of diploic lamination after successful ventricular shunting.

His neuroradiologic orientation also led to his second interest in radiology, the evaluation of medical efficacy in diagnostic radiology. His paper in 1971 with Russell Bell, "The Utility and Futility of Radiologic Examination of the Skull for Injury," was a landmark notice of the overuse of medical resources and an early statement of a much larger problem that hitherto had received little organized attention. This interest dominated his efforts for a decade. With industrial engineering techniques, he studied technicians' and physicians' efficiency in radiography, and with the advent of CT, he evaluated the contribution of this technique to the management of cerebrovascular disease and trauma.

His expertise led to his recruitment, together with Lee Lusted, to direct the first organized effort by the American College of Radiology (ACR) to develop guidelines for the more efficacious use of specific radiologic examinations. The principles, now translated into "algorithms," persist despite constantly revised details as our technology evolves. This work led to his appointment to the Medical Radiation Advisory Committee of the United States Public Health Service, to his participation in several national conferences on quality assurance, and to his membership on several special study sections of the National Institutes of Health. Many of his contributions are to be found in publications of agencies, committees, and conferences.

The third decade of John's productive life was dominated by his interest in electronic imaging and communications. Early on, he recognized potential applications of computers in radiology and, subsequently, those possibilities in image transmission, archiving, and distribution. Together with Alan Rowberg (whom he lured from General Electric), the MITRE Corporation, and a team of engineers, he directed a large multiyear program for a digital imaging network and picture archiving system for the U. S. Army. Although this consuming undertaking reached its goals, John probably enjoyed even more the satellite image transmission system he developed

so that he could interpret in Seattle radiographs made in Sitka and Mt. Edgecumbe, AK, where he regularly consulted and fished for salmon.

Nationally, John served his colleagues in radiology through the ACR from 1971 to 1990 in a succession of committee and commission appointments on efficacy studies, quality assurance, electronic imaging, and ACR planning. In Seattle, he served as attending physician at several hospitals and as chief of radiology at Harborview Hospital from 1971 to 1987. In this capacity, he transformed the department from a clinical service unit to a productive academic component of the University of Washington School of Medicine. He served on the University's faculty from 1959, as Professor from 1976 to 1990 and as acting chairman of the Department of Radiology from 1978 to 1984. His interests in public health led to professorship in the School of Public Health and Community Medicine, and his collegial temperament led to the chairmanship of the tenure committee of the University Senate. For his many local and national accomplishments, John was named Distinguished Citizen of the State of Washington in 1986.

John was much more than a professional person. He had charm and a certain charisma. He was a large man with a light heart, quick to respond and to find humor in the moment. He had a towering intelligence to match his figure, wit to entertain, and an engaging manner to delight his friends and admirers. He was noted for incisive commentary and was seldom without information, whatever the subject. Evenings with him were notably enhanced by the gourmet meals he planned and prepared. Yet, he had a private side: a privacy borne of accomplishment, self-confidence, and personal pride. John faced serious adversity more than once, each time surmounting it with his own resources and the strength that comes from loving and devoted children. Each challenge enhanced his nobility, including the last, his duel with colon cancer. In that duel, John was supported lovingly by his second wife, Joan.

John was a true academician, a devoted father, and a loyal friend. He had myriad admirers, both inside and outside medicine. Together with his family, they mourn the passing of a noble individual who enriched their lives and helped guide the evolution of diagnostic radiology.

Melvin M. Figley
Bainbridge Island, WA 98110-5369

Ligamentous Compression of the Celiac Axis: CT Findings in Five Patients

Randall M. Patten¹
 Douglas M. Coldwell
 Yoram Ben-Menachem

Compression of the celiac trunk by the median arcuate ligament of the diaphragm is an uncommon angiographic and surgical finding that rarely may be symptomatic. We retrospectively reviewed contrast-enhanced abdominal CT scans in five patients with severe ligamentous compression of the celiac axis, confirmed by surgery and/or angiography, and compared the findings with those of enhanced scans of 100 consecutive patients without known ligamentous compression. In all five patients with ligamentous celiac artery compression, CT showed effacement or narrowing of the celiac trunk by an anterior soft-tissue band. Dilated peripancreatic collateral vessels were seen in four cases, and poststenotic dilatation of the distal celiac trunk was seen in two cases. The normal appearance of the vasculature was seen in the majority (76%) of the 100 control subjects, but in eight patients the celiac origin was obscured on CT scans, and in 16 patients the celiac trunk appeared narrow or effaced.

Our experience suggests that severe ligamentous celiac artery compression can be identified on CT. However, the isolated CT finding of effacement or obscuration of the celiac axis occurs sufficiently often in normal patients that it is not adequate evidence to establish the diagnosis of celiac artery compression.

AJR 156:1101-1103, May 1991

Compression and stenosis of the celiac trunk by the median arcuate ligament of the diaphragm is a well-recognized angiographic and surgical finding, characterized by the following: moderate to severe stenosis of the proximal celiac trunk caused by compression by fibrous diaphragmatic bands, poststenotic dilatation of the distal portion of the celiac axis, and the formation of collateral vessels. Median arcuate ligament syndrome occurs in a select group of patients with celiac compression who have abdominal anginalike symptoms and who may benefit from surgical division of the ligamentous band. Although the syndrome was first reported in 1963 [1] and angiographic findings were described in 1965 [2], the CT finding of celiac compression by the median arcuate ligament has not been previously reported. We describe the CT appearance of severe ligamentous compression of the celiac trunk in five cases with angiographic and surgical correlation.

Materials and Methods

We retrospectively reviewed the abdominal CT findings in five cases of severe celiac axis stenosis encountered in a 4-year period. The diagnosis of celiac artery compression by the median arcuate ligament of the diaphragm was established by characteristic appearance on aortography and selective splanchnic arteriography in all cases and was confirmed surgically in three cases. Angiographic criteria for the diagnosis included eccentric stenosis of the proximal celiac trunk, delayed filling of the celiac branches by collateral flow, and lack of atherosclerosis in other vessels (Figs. 1 and 2A). In the three surgically proved cases, the proximal celiac axis was bound tightly to the aorta by fibrous and ligamentous bands arising from the diaphragmatic crura. In the two remaining cases, surgery was not performed.

CT studies were performed for evaluation of metastatic disease (three patients), abdominal

Received October 12, 1990; accepted after revision November 12, 1990.

¹ All authors: Department of Radiology, (SB-05), University of Washington School of Medicine, 1959 N.E. Pacific St., Seattle, WA 98195. Address reprint requests to R.M. Patten at Rainier Medical Imaging Center, 11811 N.E. 128th St., Kirkland, WA 98034.

0361-803X/91/1565-1101\$00.75 © American Roentgen Ray Society

trauma (one patient), and abdominal pain (one patient). The median arcuate ligament syndrome was not clinically suspected in any of the patients. There were four men and one woman in the series, ranging in age from 19 to 67 years (average age, 52 years). CT findings about the celiac axis were tabulated and correlated with angiographic (all five cases) and surgical findings (three cases).

To determine whether CT findings about the celiac axis in these patients were specific for the diagnosis of significant median arcuate ligament compression, we compared the CT appearance of the celiac axis in patients with ligamentous celiac compression with the appearance of the celiac trunk in 100 consecutive patients undergoing IV contrast-enhanced abdominal CT studies for unrelated reasons. CT studies were performed for evaluation of suspected or known metastatic disease (52 cases), abdominal pain (27 cases), trauma (13 cases), and miscellaneous indications (eight cases). There were 54 men and 46 women ranging in age from 8 to 87 years (average age, 56 years). All CT examinations (study and control groups) were

performed during bolus administration of IV contrast material by using a GE 8800 or 9800 scanner (Milwaukee, WI) and 10-mm collimated axial slices at 10-mm intervals.

Results

In all five cases, effacement of the celiac axis was apparent on the CT scans. A thin, discrete, soft-tissue band extending across the anterior aspect of the celiac trunk was seen in three patients (Fig. 2B), whereas in the other two patients a more poorly defined linear soft-tissue density obscured the origin of the celiac trunk. In two patients, CT showed post-stenotic dilatation of the celiac trunk anterior to the soft-tissue band (Fig. 3), a finding confirmed angiographically in both cases.

At angiography, occlusion or severe stenosis of the celiac trunk was seen in all five patients. Branches of the celiac artery were filled by retrograde collateral flow from the gastroduodenal artery, pancreaticoduodenal arteries, and pancreatic arcade. Large collateral vessels about the pancreatic head and dilatation of the gastroduodenal artery were seen on contrast-enhanced CT images in four cases (Fig. 2C).

In one patient, examined because of abdominal trauma, CT showed acute occlusion of the left renal artery and complex splenic lacerations in addition to effacement of the celiac artery. CT findings about the celiac axis, initially interpreted to be due to acute vascular trauma, were correctly diagnosed as median arcuate ligament compression at angiography and confirmed at laparotomy. Surgical exploration in this patient was complicated by bleeding from multiple collaterals within the pancreatic arcade.

In one patient, examined for chronic poorly defined abdominal pain, celiac artery compression was the only positive radiologic finding. Further diagnostic workup was negative. However, the patient refused surgical intervention.

Review of CT findings about the celiac axis in the control patients showed normal appearances of the vessels in the majority (76%) of subjects. The celiac trunk was well opaci-

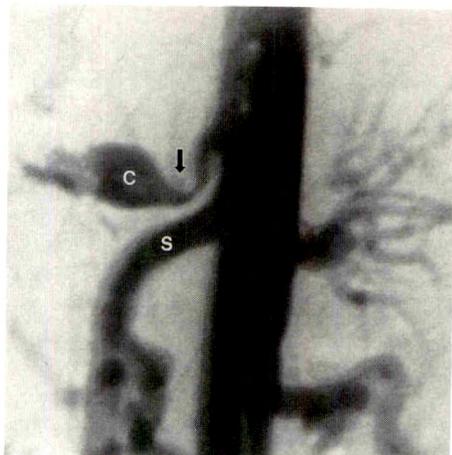


Fig. 1.—61-year-old man with colonic carcinoma and solitary resectable metastasis to left lobe of liver. Lateral aortogram shows marked narrowing of celiac trunk from extrinsic superior impression (arrow). Note post-stenotic dilatation of distal celiac artery (C). Compression by median arcuate ligament was found at surgery. S = superior mesenteric artery.

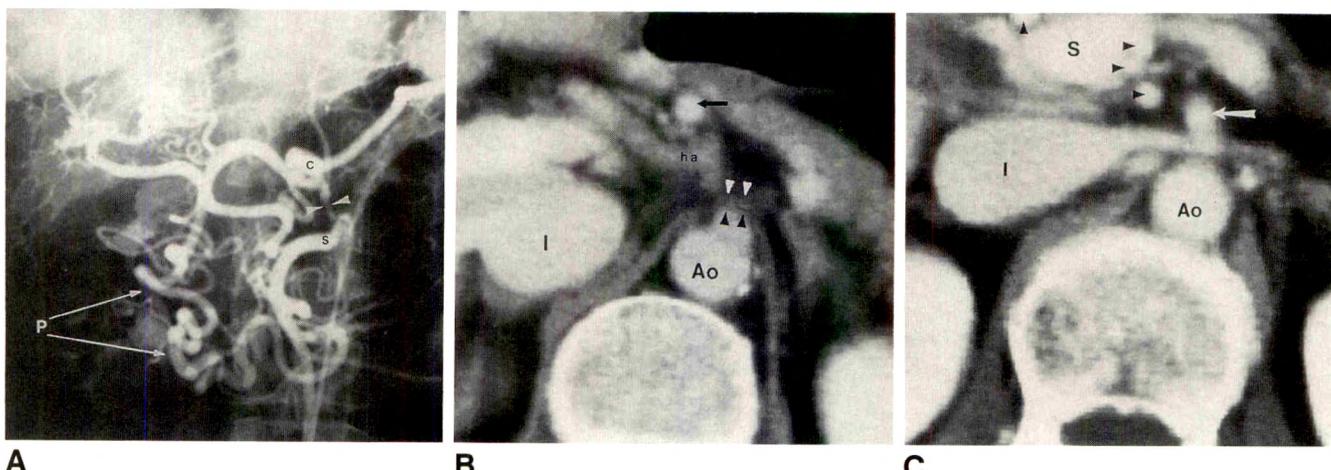


Fig. 2.—67-year-old woman with significant ligamentous compression of celiac trunk.

A, Selective superior mesenteric arteriogram shows nearly complete occlusion of celiac trunk (arrowheads) and slow retrograde filling of celiac distribution through enlarged and tortuous pancreaticoduodenal arcade (P). C = distal celiac trunk, S = superior mesenteric artery.

B, CT scan at level of origin of celiac axis shows thin soft-tissue band (arrowheads) and apparent discontinuity of celiac trunk and common hepatic artery (ha). This apparent vascular interruption could be result of partial volume artifact, although this explanation would not account for difference in densities between aorta (Ao), hepatic artery, and large collateral branch of pancreaticoduodenal arcade (arrow). I = inferior vena cava.

C, CT scan at level slightly inferior to B shows multiple collateral vessels (arrowheads) in pancreaticoduodenal arcade. Ao = aorta, I = inferior vena cava, S = superior mesenteric vein, arrow = superior mesenteric artery.

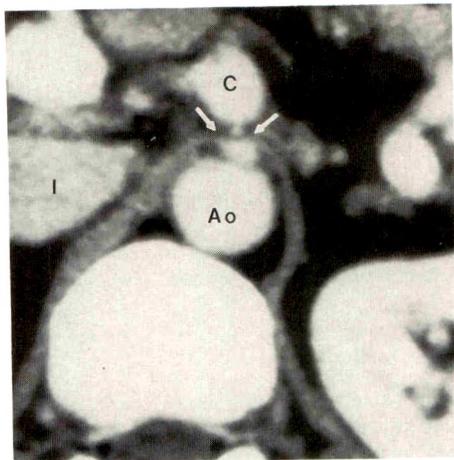


Fig. 3.—56-year-old man with celiac compression. CT scan at level of celiac axis shows compression of celiac trunk by a thin ligamentous band (arrows). Note poststenotic dilatation of distal celiac trunk (C). Ao = aorta; I = inferior vena cava.

fied, and its origin from the abdominal aorta was clearly seen. In eight patients, the origin of the celiac trunk could not be clearly defined; in 16 patients, the celiac trunk appeared to be effaced or narrowed. Collateral vessels about the head of the pancreas and poststenotic dilatation of the celiac trunk were not seen in any of these patients.

Discussion

The crura on either side of the aortic hiatus are united by a fibrous arch, the median arcuate ligament. Usually, this ligament passes posteriorly and inferiorly to the origin of the celiac axis. In 1965, Dunbar and colleagues [2] described a clinical syndrome of postprandial abdominal pain and malabsorption attributed to compression of the celiac trunk by the unyielding median arcuate ligament passing anterior to the artery and tightly compressing it against the aorta. Surgical ligation of the constricting ligamentous band has been performed with variable success [3-7], and many surgeons no longer accept the "median arcuate ligament syndrome" as a clinical entity [8].

Although controversy regarding the clinical syndrome continues, compression of the celiac axis by the median arcuate ligament is a well-documented anatomic variant, seen to variable degree in from 10% to 24% of patients [9]. The origin of the celiac trunk undergoes variable caudal migration during embryogenesis, and may vary in location from the level of the 11th thoracic to the first lumbar vertebra; either a high celiac origin or an inferior extension of the median arcuate ligament may therefore contribute to ligamentous compression of the celiac artery. Variable degrees of compression of the celiac trunk have been demonstrated by angiography in 13% to 50% of patients [8, 10, 11], and severe stenosis of the celiac axis may be found in 1% of abdominal arteriograms [12]. Severe stenosis of the celiac trunk is commonly associated with enlargement of the arteries of the pancreaticoduodenal arcade, which supply the distribution of the celiac axis via retrograde flow from the superior mesenteric artery.

The five cases presented demonstrate that severe compression of the celiac axis can be recognized by CT also. Although optimal CT technique would include bolus adminis-

tration of IV contrast material and thinly collimated axial slices through the region of the celiac trunk, these cases were identified only in retrospect and therefore CT evaluation of the celiac axis was not optimized for each case. Nevertheless, characteristic findings of a soft-tissue band anterior to the celiac artery and the presence of peripancreatic collateral vessels were noted. Occasionally, poststenotic dilatation of the celiac trunk also may be seen distal to the constricting band. The sensitivity and specificity of these findings are unknown. Effacement or poor definition of the origin of the celiac trunk on thick axial CT scans is encountered frequently as a normal variant or as a consequence of partial-volume artifact. If collateral vessels are not recognized, the solitary finding of effacement of the celiac axis does not appear to be reliable CT evidence for the diagnosis of significant celiac artery compression.

Although median arcuate ligament syndrome remains a controversial clinical syndrome, the ability to recognize significant celiac artery compression by CT is nevertheless important. In the acutely traumatized patient, effacement of the celiac trunk from a constricting band may erroneously suggest arterial injury. Moreover, the presence of multiple collateral vessels associated with severe stenosis of the celiac trunk poses a significant surgical risk and should be recognized on preoperative CT. Additionally, for the unwary angiographer, there is increased risk of arterial dissection due to repeated attempts at catheterization of the celiac artery when the trunk is significantly compressed. This is particularly true in the case of embolization of hepatic tumors in which superselective catheterization is necessary. As most of these patients are examined with abdominal CT, attention to the celiac axis may alert the angiographer to potential difficulties. Finally, in some patients with severe celiac artery compression, chronic abdominal pain, and malabsorption, surgical resection of the constricting median arcuate ligament may provide a definitive cure. In these cases, recognition of the characteristic CT findings may suggest proper diagnosis and therapy.

REFERENCES

1. Harjola PT. A rare obstruction of the coeliac artery. *Ann Chir Gynaecol* 1963;52:547
2. Dunbar JD, Molnar W, Berman FF, Marable SA. Compression of the celiac trunk and abdominal angina. *AJR* 1965;95:731-743
3. Stoney RJ, Wylie EJ. Recognition and surgical management of visceral ischemic syndromes. *Ann Surg* 1966;164:714-721
4. Marable SA, Kaplan MF, Berman FF, et al. Celiac compression syndrome. *Am J Surg* 1968;115:97-102
5. Carey JP, Stemmer EA, Connolly JE. Median arcuate ligament syndrome: experimental and clinical observations. *Arch Surg* 1969;99:441-446
6. Kernohan RM, Barros AAB, Cranley B, Johnston HML. Further evidence supporting the existence of the celiac artery compression syndrome. *Arch Surg* 1985;120:1072-1076
7. Plate G, Eklof B, Vang J. The celiac compression syndrome: myth or reality? *Acta Chir Scand* 1981;147:201-203
8. Szilagyi DE, Ryan RL, Elliott JP, Smith JP. The celiac artery compression syndrome: does it exist? *Surgery* 1972;72:849-863
9. Lindner HH, Kemprud E. A clinicopathologic study of the arcuate ligament of the diaphragm. *Arch Surg* 1971;103:600-605
10. Bron KM, Redman HC. Splanchnic artery stenosis and occlusion: incidence, arteriographic and clinical manifestations. *Radiology* 1969;92:323-328
11. Reuter S. Accentuation of celiac compression by the median arcuate ligament of the diaphragm during deep expiration. *Radiology* 1971;98:561
12. Cornell S. Severe stenosis of celiac axis: analysis of patients with and without symptoms. *Radiology* 1971;99:311

Forthcoming Articles

REVIEW ARTICLE

Recent advances in MR imaging/spectroscopy of cerebral ischemia. Baker LL, Kucharczyk J, Sevick R, Mintorovitch J, Moseley ME

CARDIOVASCULAR RADIOLOGY

Perivalvular pseudoaneurysm complicating bacterial endocarditis: MR detection in five cases. Akins EW, Slone RM, Wiechmann BN, Browning M, Martin TD, Mayfield WR

BREAST RADIOLOGY

Pictorial essay. Mammographic and CT findings after breast reconstruction using a rectus abdominis musculocutaneous flap. Loyer EM, Kroll SS, David CL, DuBrow RA, Libshitz HI

GASTROINTESTINAL RADIOLOGY

Treatment of critically ill patients with sepsis of unknown cause: value of percutaneous cholecystostomy. Lee MJ, Saini S, Brink JA, et al.

Abdominal CT findings after liver transplantation in 66 patients. Dupuy D, Costello P, Lewis D, Jenkins R

Diagnosis of pancreatic transplant dysfunction: value of gadopentetate dimeglumine-enhanced MR imaging. Fernandez MDP, Bernardino ME, Neylan JF, Olson RA

Recurrent hepatocellular carcinoma after partial hepatectomy: the value of treatment with transcatheter arterial chemoembolization. Nakao N, Kamino K, Miura K, et al.

Altered swallowing function in elderly patients without dysphagia: radiologic findings in 56 cases. Ekberg O, Feinberg MJ

Pictorial essay. Peritoneal carcinomatosis with ascites. Goerg C, Schwerk W-B

Case report. Diffuse intraabdominal lymphoma complicating idiopathic myelofibrosis: CT demonstration. Goodman P, Kumar R, Alperin JB

Case report. Spontaneous resolution of bile plug syndrome. Lang EV, Pinckney LE

GENITOURINARY RADIOLOGY

Clinical stage I carcinoma of the cervix: value of MR imaging in determining degree of invasiveness. Lien HH, Blomlie V, Kjørstad K, Abeler V, Kaalhus O

Diverticula of the female urethra: diagnosis by endovaginal and transperineal sonography. Keefe B, Warshauer DM, Tucker MS, Mittelstaedt CA

SKELETAL RADIOLOGY

Sarcoma in Paget disease of bone: clinical, radiologic, and pathologic features in 22 cases. Moore TE, King AR, Kathol MH, El-Khoury GY, Palmer R, Downey PR

FETAL AND PEDIATRIC RADIOLOGY

Pictorial essay. MR imaging in fetal anomalies. Benson RC, Colletti PM, Platt LD, Ralls PW

Determination of functional residual capacity from digital radiographs of the normal neonatal chest: studies in a rabbit model. White KS, Muelenaer AA Jr, Beam CA, Effmann EL

The deformed petrous bone: a new plain film sign of premature lambdoid synostosis. Fernbach SK, Feinstein KA

Pictorial essay. Abnormalities of the orbit and its content in children: CT and MR imaging findings. Hopper KD, Sherman JL, Boal DKB

Case report. Disseminated hepatic and splenic lesions in cat scratch disease: imaging features. Rappaport DC, Cumming WA, Ros PR

NEURORADIOLOGY

Degenerative narrowing of the cervical spine neural foramen: evaluation with high-resolution 3DFT gradient-echo MR imaging. Yousem DM, Atlas SW, Goldberg HI, Grossman RI

Gadopentetate dimeglumine-enhanced MR imaging in children following surgery for brain tumor: spectrum of meningeal findings. Hudgins PA, Davis PC, Hoffman JC Jr

Intracranial cryptococcosis in immunocompromised patients: CT and MR findings in 29 cases. Tien RD, Chu PK, Hesselink JR, Duberg A, Wiley C

Benign lymphoepithelial parotid tumors in AIDS patients: CT and MR findings in nine cases. Kirshenbaum KJ, Nadimpalli SR, Friedman M, Kirshenbaum GL, Cavallino RP

VASCULAR RADIOLOGY

Obstruction of the infrarenal portion of the abdominal aorta: results of treatment with balloon angioplasty. Ravimandalam K, Rao VRK, Kumar S, et al.

Case report. The use of a balloon catheter to control hemorrhage from the subclavian artery after removal of an inadvertently placed catheter. Millward SF, Lamb MN, Barron PT

Case report. Control of hemobilia by embolization of a hepatic artery false aneurysm and arteriointobilary fistula via a T-tube track. Beningfield SJ, Bornman PC, Krige JE, Terblanche J

SONOGRAPHY

Pictorial essay. Sonographic artifacts and their origin. Scanlan KA

PERSPECTIVES

Radiology Summit 1990. Specialization in radiology: trends, implications, and recommendations. Thrall JH, Wittenberg J

Commentary. Generalists vs specialists: time to decide. Forrest JV

Teleradiology: costs of hardware and communications. Dwyer SJ III, Templeton AW, Batnitzky S

Information overload and management in radiology. Hendee WR

ARRS 1991 MEETING CASE OF THE DAY ANSWERS

Introduction. O'Connor JF

General diagnosis case of the day. Eschelman DJ, Panageas E, Rosen MP, Romo LV, O'Connor JF

Chest case of the day. Eschelman DJ, Gibbens DT, Fielding JR, et al.

Abdominal case of the day. Eschelman DJ, Duva-Frissora AD, Martin LC, et al.

Neuroradiology case of the day. Parker DR, Eschelman DJ, Gibbens DT, Rabinov JD, O'Connor JF

Pediatric case of the day. O'Connor JF, Martin LC, Chen HH, et al.

Technical Note



Retrieval of a 4-French Diagnostic Catheter Fragment from the Common Carotid Artery by Using a Stone Basket

Renato Travelli¹ and Thomas H. Cogbill²

As a result of the increased use of smaller catheters and of central venous catheter placement, embolization of a catheter fragment occurs more frequently than before. This can result in severe complications and death. The retrieval of a 4-cm, 4-French catheter fragment from the right common carotid artery is described. This technique can be used in most vessels.

Case Report

A 70-year-old man with diabetes mellitus, bilateral carotid bruits, and temporary ischemic attacks was admitted for study of the aortic arch and bilateral carotid arteriography.

After examining the aortic arch with digital subtraction angiography, we advanced a 4-French Simmons 2 catheter through a 5-French sheath into the ascending aorta. The proper curve had been formed by twisting the catheter to allow passage into the right common carotid artery. A test injection showed flow of contrast material, not from the distal end of the catheter but more proximally to it. The catheter was then removed through the sheath, but the distal end, about 4 cm long, remained in the common carotid artery. The sheath was replaced by an 8-French sheath, and through this an 8-French, JR4 catheter with a Judkins right coronary artery configuration (Fig. 1) was advanced into the common carotid artery, and a 3-French, Bard (C. R. Bard, Covington, GA) basket was advanced through the catheter (Fig. 2). The open basket was closed on the proximal part of the catheter fragment, and this was retracted into the catheter and removed through the sheath.

Right and left carotid arteriograms were then obtained with a 7-French Simmons 2 catheter, and the procedure was completed. The study showed a very tight stenosis of the origin of the right internal carotid artery and mild stenosis of the left internal carotid artery. A small filling defect, probably atherosclerotic in nature, was noted in the siphon of the right internal carotid artery. Out of concern that a small catheter fragment could have migrated there, we obtained a CT scan of the base of the head after taping a portion of the catheter to the skin for comparison. This showed no evidence of a foreign body. The patient underwent a right carotid endarterectomy 2 days after arteriography and was discharged in good condition 3 days later.

Discussion

Four-French catheters offer definite advantages, particularly for use in small vessels, such as in children, or in catheterizations that use the axillary or brachial arteries as entry points. However, the thin catheter wall is more brittle and subject to potential rupture.

Several devices for removal of fragments from the vascular system have been described. These include the helical urologic basket (Dormia) [1-7], loop snare [2, 3, 5, 7], hook catheter [3, 5, 6], hook guidewire [3], grasping forceps [7], bronchoscopic forceps (in large veins) [3, 5, 7], and Fogarty balloon catheter [3].

When one end of the foreign body is free, the loop snare

Received October 1, 1990; accepted after revision November 20, 1990.

This work was supported in part by the Gundersen Medical Foundation.

¹ Department of Radiology, Gundersen Clinic, Ltd., 1836 South Ave., La Crosse, WI 54601. Address reprint requests to R. Travelli.

² Department of General and Vascular Surgery, Gundersen Clinic, Ltd., 1836 South Ave., La Crosse, WI 54601.

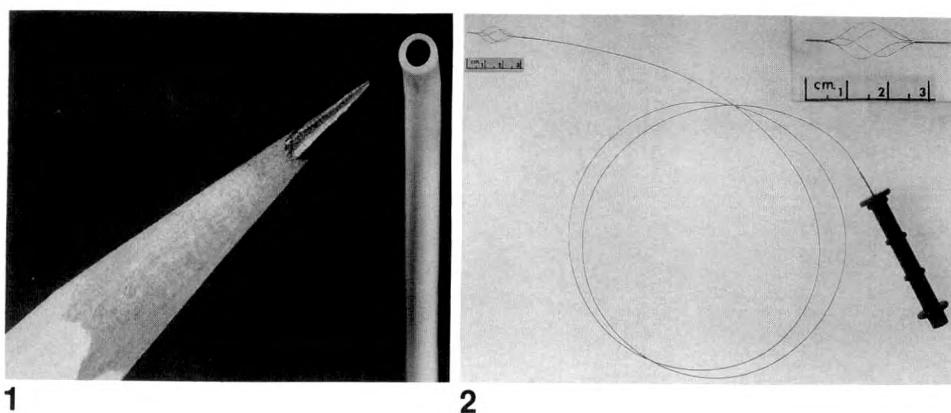


Fig. 1.—Distal end of JR4, 8-French catheter. Catheter shown is in right coronary artery configuration, but its shape can be easily modified. (Pencil for comparison.)

2

1

has been the most widely used, because it was the first described. The urology helical stone basket also has been used frequently. Both instruments can be purchased as sets from Cook (Cook Co., Bloomington, IN). The 3-French ureteroscopic stone basket (Bard), which has 115 cm of working length, is meant for use in urology and is not heparinized.

The intact basket system advanced through a coaxial catheter can allow the advancement of the basket to almost any distal location. Although smaller catheters can be used, the use of a large catheter such as the JR4 (8-French; Fig. 1) allows considerably more motion of the ureteroscopic stone basket and the possibility to capture part or the entire foreign body inside the large opening of the nontapering distal end. The JR4 catheter manufactured by Bard has a soft tip, which might prevent the fragment from being snapped when it is withdrawn into the guiding catheter. We used this catheter in a right coronary Judkins configuration. The shape, however, can be modified with warm water or with a heat gun. This we achieved on another occasion after inserting a 5-French catheter through the 8-French JR4 to preserve the lumen.

The advantages of the stone basket are that it can be opened to the full diameter of a small vessel, can be rotated with torsion of the coaxial catheter or of the basket wire, can be opened or closed with relative ease, and is more likely to

engage the end of a catheter fragment. Any small foreign body could conceivably be retrieved also.

The 3-French basket described is one of the smallest available when compared with other retrieval instruments described in the literature. It can be used coaxially in preformed catheters, and in our case it allowed expeditious retrieval of a catheter fragment from a relatively small vessel.

REFERENCES

- Chuang VP. Nonoperative retrieval of Gianturco coils from abdominal aorta. *AJR* 1979;132:996-997
- Dotter CT, Rosch J, Bilbao MC. Transluminal extraction of catheter and guide fragments from the heart and great vessels: 29 collected cases. *AJR* 1971;111:467-472
- Fisher RG, Ferreyro R. Evaluation of current techniques for nonsurgical removal of intravascular iatrogenic foreign bodies. *AJR* 1978;130:541-548
- Fjalling M, List AR. Transvascular retrieval of an accidentally ejected tip occluder and wire. *Cardiovasc Intervent Radiol* 1982;5:34-36
- Gerlock AJ Jr, Mirfakhraee M. Retrieval of intravascular foreign bodies. *J Thorac Imag* 1987;2(2):52-60
- Grabenoeger F, Dock W, Pinterits F, Appel W. Fixed intravascular foreign bodies: a new method for removal. *Radiology* 1988;167:555-556
- Kadir S, Athanasoulis CA. Percutaneous retrieval of intravascular foreign bodies. In: Athanasoulis CA, Green RE, Pfister RC, Roberson GH, eds. *Interventional radiology*. Philadelphia: Saunders, 1982:379-390

Commentary

Visual Acuity Testing of Radiologists—Is It Time?

William H. Straub,¹ David Gur, and Barbara C. Good

The radiologic process consists of a chain of events that could loosely be referred to as acquiring, processing, displaying, detecting (observing), interpreting, and reporting (communicating). The detection phase alone is made up of a number of physical and psychological phenomena that are likely to be important parts of the process. One of them, visual acuity, has been subject to very little scrutiny in radiology.

However, the perception of image quality by radiologists/observers and their ability to diagnose correctly may depend not only on the quality of the image presented but on the radiologists' visual acuity [1]. Although other variables, such as the observer's training, experience, search patterns [2], viewing time, and distance from the image [3], are also important, visual acuity is the most easily measured and the most readily corrected variable related to observers. Nevertheless, to our knowledge, only one recent report even mentions a preliminary evaluation of the status of corrected visual acuity at a given time for a small group of practicing radiologists [4]. No information at all has been published concerning how radiologists feel about the importance of visual acuity to their profession or what their attitudes are toward requirements for periodic vision testing.

We recently performed a spot check of the visual acuity of 28 staff radiologists (six women, 22 men; ages 30–70 years) at our institution under a protocol approved by the institutional review board. During this check, an optometrist examined the 28 radiologists with Snellen and Jaeger eye charts. From a self-selected group (the study was carried out on a voluntary basis and less than half of our faculty participated), which we realize may have biased this preliminary observation, 82%

(23/28) of those tested had the equivalent of 20/20 near vision with or without corrective lenses, and 18% (5/28) had lower acuity. The latter group could benefit from corrective lenses or changes in their existing prescriptions.

At about the same time that the check for acuity was administered, we sent a survey to members of our radiology staff. Forty-three of the 70 who received it responded. Results of this survey revealed that although the majority (67%) of radiologists in our department had had their visual acuity tested within the 2 years before the study, 19% had *not* had their vision checked within 3 years of the time of the study, and 9% had not had it checked within 5 years. To one of the questions in our survey, 56% of the respondents indicated that visual testing *should* be required of practicing radiologists; 37% thought it should be optional. Only 7% felt it should *not* be required.

The deterioration of visual acuity usually occurs with aging and is generally inescapable. It is typically a slow, subtle process and can go undetected for significant periods. Our own small study showed that five of our 28 radiologists could improve their visual acuity marginally by using corrective lenses for the first time or by changing existing prescriptions. The cost of this improvement would be relatively small—the gains potentially significant, although yet undocumented.

We were unable to include a contrast sensitivity test in the spot check of our radiologists, but we believe that this test should be an integral part of a vision examination for radiologists. However, for the detection of high-frequency information (≥ 2 line pairs/mm) on images that are viewed at distances of 30 cm or more, a direct relationship has been shown between resolution and the contrast required for detection of

Received October 9, 1990; accepted after revision November 29, 1990.

¹ All authors: Department of Diagnostic Radiology, University of Pittsburgh School of Medicine, Pittsburgh, PA 15261. Address reprint requests to W. H. Straub.

the feature. Decreased visual acuity (as measured by the Snellen and Jaeger tests) could significantly increase the threshold contrast required to detect and identify high-frequency information [5]. Although there are many detection tasks in which high-frequency information may not be a significant factor (e.g., nuclear medicine procedures), for a number of critical detection tasks (e.g., microcalcifications on mammograms) this is an important issue.

Increasing emphasis on quality assurance and mounting liability claims after missed lesions dictate that we make every reasonable attempt to optimize the performance of diagnostic systems. This should include making the observer a focus of our efforts as well as images that are observed. Perhaps it is time that the profession of radiology—an occupation in which vision is most important— institute mandatory periodic visual acuity and contrast sensitivity testing. It would not be unreasonable for such tests to be used as periodic checks on the visual acuity of those currently practicing and/or even as a condition for licensure. Similar requirements exist for nonmedical occupations that rely heavily on visual performance.

That only 7% of our surveyed staff opposed required periodic examinations of visual acuity suggests that attitudes among radiologists may not be a significant barrier to imple-

mentation of periodic testing. If there are concerns about the test's becoming a formal requirement carried out by an optometrist or an ophthalmologist, visual acuity could be self-checked periodically by radiologists themselves.

In recent years, a great deal of research effort and funding have been spent on investigations into questions of image resolution and its possible effect on observer performance. If we have expended so much to improve the resolution of the acquired and displayed image, how can we neglect to examine the visual acuity of the person who is looking at that image?

REFERENCES

1. Brogdon BD, Kelsey CA, Moseley RD. Factors affecting perception of pulmonary lesions. *Radiol Clin North Am* 1983;21:633-654
2. Kundel HL, LaFollette PS Jr. Visual search patterns and experience with radiological images. *Radiology* 1972;103:523-528
3. Kelsey CA, Moseley RD, Mettler FA Jr, et al. Observer performance as a function of viewing distance. *Invest Radiol* 1981;16:435-445
4. Bass JC, Chiles C. Visual skill: correlation with detection of solitary pulmonary nodules. *Invest Radiol* 1990;25:994-998
5. Ginsburg AP. Proposed new vision standards for the 1980's and beyond: contrast sensitivity. Dayton, OH: Air Force Publication No. AFAMRL-TR-80-121, September 1981

Letters

Throw It Away, Sam

As a general internist, I am not normally a reader of the *AJR*. However, a colleague of mine was so surprised and amused by the article by Rennie and Bero [1] on controlled circulation journals that he passed along his copy. Needless to say, I, too, was surprised and amused. The article displays a lack of understanding of the continuing education habits of the American physician. It is also an example of what happens when academics begin doing research on topics for which they have little understanding of the underlying issues.

First, let us agree that "legitimate" journals are not the same as what Rennie and Bero call the "throwaways." This is the same as agreeing that diamonds are not the same as pearls or that a Lincoln is not the same as a Chevy. This agreement, however, does not then allow us to claim that the legitimate journals are good and the throwaways are bad—unless, of course, the object is to be an academic snob.

Before we can claim that one is "better" than the other, we must look at the objectives to be met. If the objective is to acquire new scientific information, then we should read legitimate journals. However, if we are looking for easy-to-read review articles, information on primary patient care, or practical tips on improving practice, then we should look to the throwaways.

It is clear from their recommendations that Rennie and Bero think that the average practitioner is a dumb boob who believes everything that is in a throwaway and blindly accepts the advertising. It is also clear that they think the average practitioner should take the time—away from either a busy practice or family—to read and critically study articles that have no immediate impact on his or her ability to provide direct patient care.

I wish Rennie and Bero would spend as much research time and effort on finding ways to get patients to comply with such important things as losing weight, eating a sensible diet, exercising regularly, and stopping smoking. Then we would have less disease and could spend the time critically reading.

Alan S. Kaplan
Potomac, MD 20854

REFERENCE

1. Rennie D, Bero LA. Throw it away, Sam: the controlled circulation journals. *AJR* 1990;155:889-892

Reply

We, too, were "surprised and amused," but only because Dr. Kaplan makes our case for us so well.

He is right: He cannot claim throwaways to be good or bad—but we can. If Dr. Kaplan cools down a little, he will find that we actually bothered to come up with data on the quality of the throwaways. Those data do in fact allow us to claim that most of the throwaways we studied were terrible. Now Dr. Kaplan clearly did not like this conclusion. The problem with his ad hominem attacks is that they are based on no data at all.

There would have been little point in writing our article if we believed that physicians were fools. Having spent 30 years as a physician, dealing with thousands of physicians, one of us (DR) is gratified at the rich variety of his colleagues and their extraordinary intelligence. The other of us (LB), who designs and evaluates educational systems for physicians, has plenty of proof that physicians have a great capacity for learning.

The basic point of our article [1] was a simple one: Physicians cannot retain any reasonable autonomy if they do not undertake the hard task of keeping up with the literature of their specialty, and to do that, they have to learn how to analyze and critique scientific papers. If they do not, they cede all responsibility to others who may have far less experience and far less wisdom. The fact that an article is an "easy-to-read review" may be nice, but we warn against its uncritical acceptance. Certainly, enough good original work is published weekly in the legitimate journals—work that has a direct impact on any physician's ability to provide direct patient care—for no one to have to waste time on irrelevant articles. It may not be quite so easy to read, but it is the real stuff.

It's hard to know what to make of Dr. Kaplan's last paragraph. The programs that he mentions are all ones we support strongly. We both spend an important part of our time in a large and very time-consuming research effort for the prevention of smoking. One of us has done research into, has published on, and regularly lectures to the lay public on aspects of exercise, including getting patients to take more of it. The other of us spends time researching methods to improve the use of medications by patients and physicians and in educating teens about substance abuse and sexually transmitted diseases. We do not presume to tell Dr. Kaplan what to do, though he might consider shooting from somewhere other than the hip.

Drummond Rennie
Lisa Bero
*Institute for Health Policy Studies
University of California, San Francisco
San Francisco, CA 94109*

REFERENCE

- Rennie D, Bero LA. Throw it away, Sam: the controlled circulation journals. *AJR* 1990;155:889-892

Throwaway Journals

My compliments to Rennie and Bero for their excellent assessment of throwaway magazines: "Throw It Away, Sam: The Controlled Circulation Journals" [1]. Further applause is due you, for obtaining permission to publish this in the *AJR*. I only wish you had placed it up front with your "Special Articles," where it would be seen by more readers.

It seems that academic or publishing radiologists do not understand that these magazines detract advertising revenues from the legitimate journals on which we depend for the dissemination of peer-reviewed, scientifically valid information. Advances in our specialty would crumble with the loss of these legitimate journals, and we would be left with nothing but vendor advertising and hype.

I have, for many years, brought this fact to the attention of colleagues who serve on editorial boards and who engage in productive scholarship. Some are so enamored by someone wanting them or their material, or by the honorarium involved, that they care little that their support of these commercial magazines hurts radiologic science and education. Others indicate that they had not realized the harm that these publications were doing and would no longer aid the publications' endeavours. I agree completely with the solutions proposed by Rennie and Bero and would urge the *AJR* to send reprints of this article to all the members of its editorial board and all academic department chairmen.

Irvin I. Kricheff
*NYU Medical Center
New York, NY 10016*

REFERENCE

- Rennie D, Bero LA. Throw it away, Sam: the controlled circulation journals. *AJR* 1990;155:889-892

Transbronchial Aspiration of an Intrathoracic Cyst

A 37-year-old man had dysphagia for 3 months and had lost 20 lb (9.1 kg) in body weight. Radiographs of the chest showed a well-circumscribed, 40-cm, right-sided paratracheal mass (Fig. 1A). An esophagogram showed posterior displacement of the esophagus. CT showed a mass with a density of 5.6 H. No parenchymal lesions were noted, and no adenopathy was seen. Bronchoscopy showed bulging of the right tracheal wall 4 cm above the carina. An 18-gauge Mill-Rose needle was used via the transtracheal route to aspirate 3 ml of cloudy, acellular fluid. Radiographs obtained after the aspiration showed a right-sided pleural effusion and absence of the paratracheal lesion (Fig. 1B). Thoracentesis showed an exudative effusion with no malignant cells or bacterial growth. The patient no longer complained of dysphagia, and he eventually regained the lost weight. Follow-up chest radiographs showed no recurrence of the cyst and complete resolution of the effusion.

To date, diagnosis and treatment of intrathoracic cysts have been surgical. Whyte [1] and associates have shown that transthoracic aspiration of a bronchogenic cyst is safe and effective. Others [2]

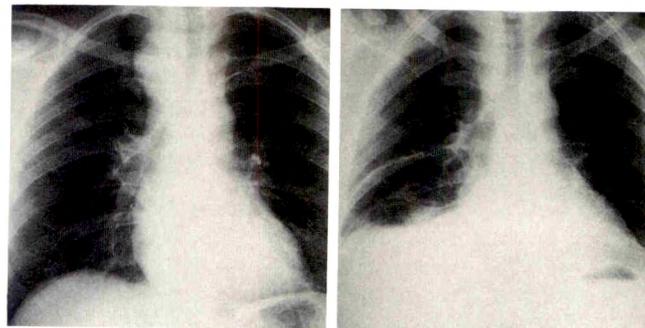
**A****B**

Fig. 1.—Transbronchial aspiration of intrathoracic cyst.
A, Initial chest radiograph shows right-sided paratracheal mass.
B, Chest radiograph obtained after transbronchial aspiration shows resolution of mass and a right-sided pleural effusion.

have reported that transbronchial aspiration of a bronchogenic cyst causes an immediate decrease in the size of the cyst, a decrease in related symptoms, and complete resolution of the cyst. Although histologic examination of a pathologic specimen is required for accurate diagnosis, the presence of a nonbloody, acellular fluid suggests the diagnosis of cyst [3]. We performed a transtracheal aspiration of the mass seen on chest radiograph for therapeutic as well as diagnostic reasons. A pleural effusion complicated the procedure, but the effusion resolved completely.

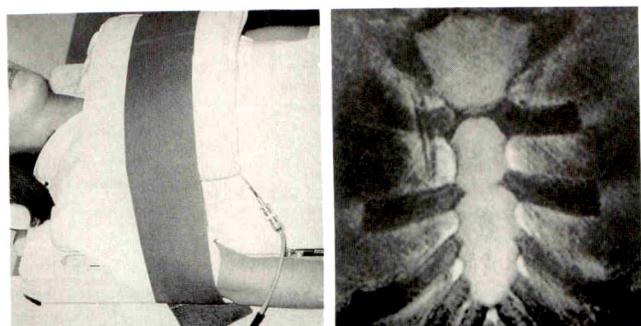
Louis J. Arno
Richard A. Miller
Alan Klukowicz
Benjamin H. Safirstein
*Saint Michael's Medical Center
Newark, NJ 07109*

REFERENCES

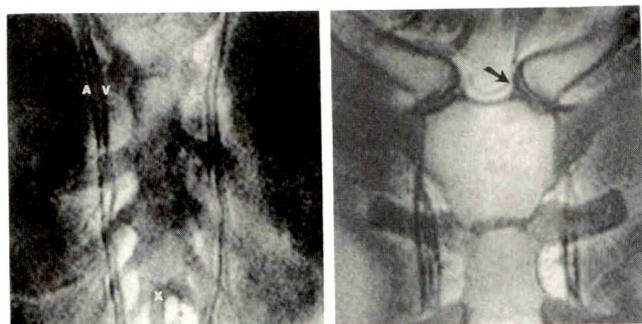
- Whyte MKB. Central bronchogenic cyst: treatment by extrapleural percutaneous aspiration. *Br Med J* 1989;299:1457-1458
- Schwartz AR, Fishman EK, Wang KP. Diagnosis and treatment of a bronchogenic cyst using transbronchial needle aspiration. *Thorax* 1986; 41:326-327
- Schwartz DB, Beals TF, Wimbush KJ, Hammersley J. Transbronchial fine needle aspiration of bronchogenic cysts. *Chest* 1988;85:573-575

MR Imaging of the Anterior Chest Wall by Using a Flat Coil

To assess the usefulness and limitation of MR of the anterior chest wall, we used a flat coil originally designed for imaging of the spine to image the anterior chest wall. We studied 20 healthy volunteers 20-85 years old. Nine were men, and 11 were women. A 0.2-T permanent magnet unit (Hitachi MRP 20-1, Hitachi Corp., Tokyo) and a 250 × 40 mm flat coil were used (Fig. 1). Coronal T1-weighted images were obtained first. If visualization of the sternum and parasternal region was limited, axial T2-weighted and balanced images were added. Scan sequences were spin-echo (SE) 500/38 (TR/TE) with a scan time of 4 min 34 sec (coronal) and SE 2000/38, 110 with a scan time of 9 min 8 sec (axial). A slice thickness of 5 mm, a 256 × 256 matrix, and four (SE 500/38) and two (SE 2000/38, 110) excitations were used. We also examined four patients who had abnormalities: fracture (two), metastatic carcinoma (one), and multiple myeloma (one).



1 2A



2B 2C

Fig. 1.—Positioning of flat coil and patient for MR imaging of anterior chest wall.

Fig. 2.—Coronal MR images of anterior chest wall of normal subject.

A, Image at center of sternal body.

B, Image taken 5 mm posterior to A. A = internal mammary artery, V = internal mammary vein, X = xyphoid process.

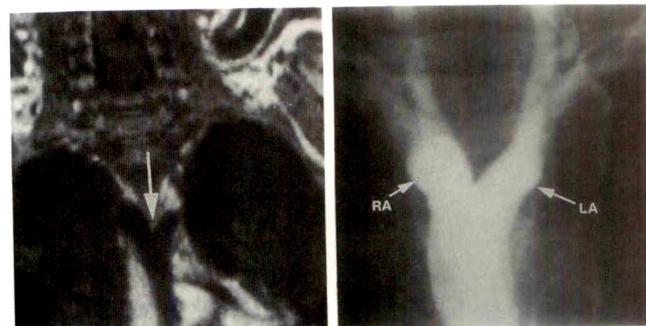
C, Image centered at sternoclavicular joint. Arrow = articular disk of sternoclavicular joint.

The sternum, costal cartilages, sternoclavicular joints, and internal mammary vessels were well depicted on coronal T1-weighted images (Fig. 2). Axial T2-weighted and balanced images did not add further information. The sternum had homogeneous signal intensity similar to that of fat. Costal cartilages were seen as homogeneous low-signal-intensity structures. In older subjects, foci of ossification with fatty marrow were identified in the cartilage. Osseous fusion of the manubriosternal joint was seen in two of the 20 subjects. Internal mammary arteries and veins were visualized in the parasternal region. Structures in the retrosternal region were not well seen because of cardiac motion. Fractures and neoplastic involvement were well depicted on the coronal images.

Shigeru Ehara
Miyoshi Sugisawa
Masako Matsuda
and colleagues
Ohshuku-Onsen Hospital
Center for Radiological Science
Iwate Medical University
Morioka 020, Japan

Vascular Ring: Diagnosis with MR

A 10-month-old infant was examined because of recurrent bronchopneumonia, inspiratory and expiratory stridor, and dysphagia. Chest radiographs showed widening of the superior me-



A B

Fig. 1.—Vascular ring.
A, T1-weighted MR image shows bifurcation of single-outlet aorta (arrow).
B, Aortogram shows right (RA) and left (LA) arches.

diastinum to the right of the trachea and localized tracheal narrowing. Laryngoscopy showed anterior, extrinsic tracheal compression. A barium swallow showed a posterior esophageal constriction that persisted throughout the various phases of swallowing.

ECG-gated MR performed at 0.5 T showed a double aortic arch with the right and left carotid and subclavian arteries arising independently from each arch and retroesophageal reconstitution of a single aorta (Fig. 1). Axial images correlated well with both the barium swallow and the laryngoscopic findings. Aortography provided good correlation with the MR findings, indicating preferential flow of contrast material toward the right arch and separate common carotid and subclavian arteries.

The most common vascular ring is a double aortic arch (65% in the series of Vallette et al. [1]). A double aorta is the result of failure of involution of the right fourth dorsal aortic segment, which normally involutes to form the proximal portion of the right fourth arch and becomes incorporated into the subclavian artery. The left arch in a double system characteristically is anterior and the smaller of the pair; the right arch is often larger [2, 3]. In our case, the infant had a single ascending arch that bifurcated, providing separate left and right carotid and subclavian vessels.

Raymond K. Tu
June M. Unger
University of Wisconsin, Clinical Sciences Center
Madison, WI 53792

REFERENCES

1. Vallette RC, Arensman RM, Falterman KW, Oshsner JL. Tracheoesophageal compression syndromes related to vascular ring. *South Med J* 1989;82:338-340
2. Hastreiter AR, D'Cruz IA, Cantez T. Right-sided aorta. *Br Heart J* 1966;28:722-725
3. Neuhauser EBD. The roentgen diagnosis of double aortic arch and other anomalies of the great vessels. *AJR* 1946;56:1-12

Inverted Meckel Diverticulum Shown by Enteroclysis

We report a case of inverted Meckel diverticulum without intussusception that was detected by enteroclysis.

A 32-year-old man had had chronic recurrent bleeding in the lower

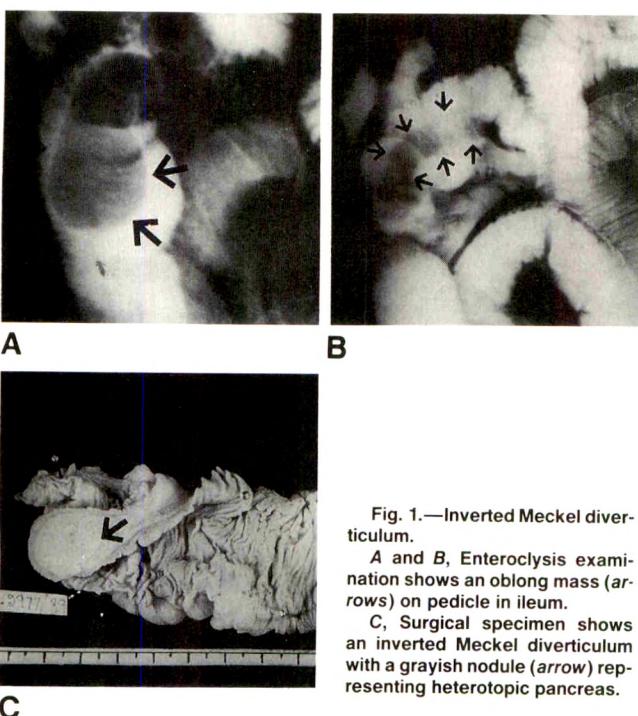


Fig. 1.—Inverted Meckel diverticulum.

A and B, Enteroclysis examination shows an oblong mass (arrows) on pedicle in ileum.

C, Surgical specimen shows an inverted Meckel diverticulum with a grayish nodule (arrow) representing heterotopic pancreas.

gastrointestinal tract for 8 years. Findings on upper gastrointestinal endoscopy and colonoscopy were normal. Enteroclysis examination showed a well-defined, oblong filling defect with a pedicle in the distal ileum (Figs. 1A and 1B). At surgery, a polypoid mass 2×1 cm with a long pedicle was found in the ileum and was resected. The surgical specimen showed a pedunculated polyp 3.5 cm long originating along the antimesenteric border of the intestine. The cut surface of the polyp revealed fatty tissue with a central grayish-white area (Fig. 1C). Microscopic examination showed invaginated mesenteric fat, normal muscularis propria, patchy submucosal fibrosis interspersed with foci of Brunner glands, and heterotopic pancreatic tissue. The diagnosis was inverted Meckel diverticulum with heterotopic duodenal mucosa and pancreas. No evidence of ulceration, diverticulitis, or ischemia was seen.

Some researchers think that enteroclysis is more accurate than routine barium studies for examination of the small bowel, and the value of enteroclysis in the detection of Meckel diverticulum has been shown [1]. To our knowledge, only one case report of inverted Meckel diverticulum without intussusception seen on barium examination has been published [2].

B. Nagi

R. Kochhar

A. K. Malik

and colleagues

*Postgraduate Institute of Medical Education & Research
Chandigarh-160 012, India*

REFERENCES

- Maglinte DDT, Elmore MF, Isenberg M, Dolan PA. Meckel diverticulum: radiologic demonstration by enteroclysis. *AJR* 1980;134:925-932
- Freeny PC, Walker JH. Inverted diverticula of the gastrointestinal tract. *Gastrointest Radiol* 1979;4:57-59

Percutaneous Management of Duodenal and Retroperitoneal Hematoma

A 25-year-old woman with diabetes had an endoscopic duodenal biopsy as part of a workup for malabsorption. Twelve hours after the biopsy, she had severe epigastric pain, which required narcotic analgesics for relief. Thirty-six hours after the procedure, she started having bilious vomiting. On examination, an ill-defined, tender lump was detected in the right lumbar region. A diagnosis of duodenal perforation with leak was considered. A Gastrograffin (meeglumine diatrizoate) study, sonography, and CT showed complete obstruction at the level of the third part of the duodenum with typical features of an intramural hematoma, associated with a large retroperitoneal hematoma and possible duodenal perforation (Fig. 1).

The patient was treated conservatively for 5 days with no improvement in her status. Because of her rapidly deteriorating condition and uncontrolled diabetes, it was decided to drain the hematoma percutaneously rather than surgically. Real-time sonographic guidance and a single-step technique [1] were used to introduce an 8.3-French pigtail catheter (Cook Inc., Bloomington, IN) percutaneously into the hematoma. Altered blood (250 ml of thin brownish-black fluid) was drained through the catheter, and the size of the cavity diminished markedly. The cavity was flushed intermittently (through the indwelling catheter) with antibiotic saline solution for the next 2 days, until the return fluid was clear. After aspiration of the hematoma, the volume of material aspirated via the nasogastric tube diminished markedly, and the patient was able to accept food orally the next day. Four days after the drainage, the catheter was removed, and the patient was discharged from the hospital. Follow-up barium study 2 weeks later showed a normal duodenal loop.

Intramural duodenal hematomas usually are associated with blunt abdominal trauma [2], clotting disorders, and child abuse. Though bowel perforation is a well-known complication of gastrointestinal endoscopy and biopsy [3], duodenal intramural and retroperitoneal hematomas have not been reported after endoscopic biopsy. The accepted management of duodenal hematomas in children is conservative; most hematomas resolve spontaneously with this approach [2]. In adults, management is more controversial (conservative vs

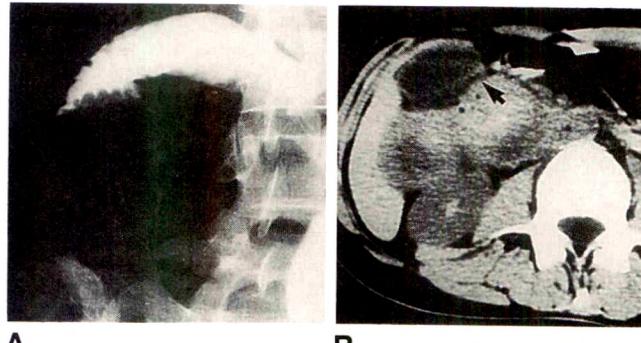


Fig. 1.—Duodenal and retroperitoneal hematoma.

A, Gastrograffin (meeglumine diatrizoate) study shows complete obstruction of third part of duodenum by a sharply marginated filling defect, which is causing widening of duodenal lumen. Duodenal segment proximal to obstruction is displaced superiorly and laterally with thickened and crowded mucosal folds. No extraluminal leak of contrast material is seen.

B, Unenhanced CT scan at level of duodenum shows a large, well-defined, dumbbell-shaped mass between right kidney and gallbladder fundus. Mass has internal areas of high attenuation (62 H) suggestive of a hematoma. Specks of air seen within mass anteriorly are indicative of a bowel perforation. Duodenum is displaced anteriorly (arrow).

surgical). However, if complete duodenal obstruction and/or perforation is present, surgery is preferred [4].

In our patient, percutaneous drainage of the hematoma was entirely satisfactory. The patient recovered completely without any complications. The tamponade effect of the hematoma probably prevented any leak of duodenal contents and allowed time for the perforation to seal spontaneously.

Percutaneous drainage of duodenal hematomas has not been reported previously. Our experience illustrates the simplicity of the procedure and its success, which obviates surgical intervention. Though a simple needle aspiration of the hematoma should suffice, in a patient with a suspected or evident duodenal perforation, it may be prudent to leave a drainage catheter in place to drain any duodenal secretions that may leak into the hematoma cavity.

Rajeev Jain
Sukhpal Sawhney
Rita Ghose
Manorama Berry
*All India Institute of Medical Sciences
New Delhi, 110029 India*

REFERENCES

1. Raz S. A simple method of pyonephrosis drainage. *Lancet* 1971;2: 529-530
2. Touloukian RJ. Protocol for the non-operative treatment of obstructing intraluminal duodenal hematoma during childhood. *Am J Surg* 1983;145:330-334
3. Bilbao MK, Dotter CT, Lee TG, Katon RM. Complications of endoscopic retrograde cholangiopancreatography (ERCP): a study of 10,000 cases. *Gastroenterology* 1976;70:314-320
4. Jordan GL Jr. Injury to the pancreas and duodenum. In: Mattox KL, Moore EE, Feliciano DV, eds. *Trauma*. East Norwalk, CT: Appleton & Lange. 1988:473-494

Biliary Cystadenoma and Cystadenocarcinoma

We would like to reply to the article by Korobkin et al. [1], "Biliary Cystadenoma and Cystadenocarcinoma: CT and Sonographic Findings," that appeared in the September 1989 issue of the *AJR*. Korobkin et al. state that biliary cystadenomas can be distinguished from hydatid cysts of the liver with the help of serologic tests. However, accurate serologic tests are difficult to obtain, as false-positive and false-negative results can be in the range of 15-20% [2].

Some sonographic clues can be used to distinguish hydatid cyst from cystadenoma. The main problem is the multilocular type of cystadenoma. We think that hydatid cysts can be differentiated from cystadenomas on the basis of oval or round daughter cysts and the thick wall of the hydatid cyst. The wall of a cystadenoma is thinner and never gives the appearance of oval or round cysts of the secondary vesicles. That is, loculations in cystadenomas are not oval or round as daughter cysts are; they have many compartments and fine septations.

Gharbi et al. [3] have classified hydatid disease of the liver into five types. Types II and III are characteristic of hydatid cysts, whereas types I and V are suggestive of hydatid cyst in countries in which such cysts are endemic. In this classification, type IV cysts may be difficult to distinguish from hepatic tumors. However, in this group, hyper- and hypoechoic areas coexist, which helps to differentiate hydatid disease from cystadenoma. The main problem is type IV cysts, in which the fluid collection retains its borders but is divided by septa of various thicknesses and completeness. On sonograms, daughter cysts or secondary vesicles create the appearance of a

honeycomb. Niron and Ozer [4] characterized the multilocular type as "cyst within a cyst," collapsed germinal layer indicated by "the ultrasonographic water lily sign," and evidence of "hydatid sand" within the cyst.

We think that the most important points in the differentiation of cystadenomas from hydatid disease are the daughter cysts and the resulting honeycomb appearance. The thickness of the walls is another point for differentiation. In the classification of Gharbi et al., types I, IV, and V do not create any difficulty. On the other hand, type II, which has a split wall, is pathognomonic for hydatid cyst.

Hydatid cyst is endemic in our country, and we think that many patients have characteristic and pathognomonic sonographic features. Cystadenomas, which are multilocular cystic tumors, can be distinguished sonographically from hydatid disease on the basis of daughter cysts, thickness of the cyst wall, and split walls.

A. M. Agildere
M. Haliloglu
O. Akhan

*Hacettepe University, Medical School
06100 Sıhhiye-Ankara, Turkey*

REFERENCES

1. Korobkin MT, Stephens DH, Lee JKT, et al. Biliary cystadenoma and cystadenocarcinoma: CT and sonographic findings. *AJR* 1989;153: 507-511
2. Beggs I. The radiology of hydatid disease. *AJR* 1985;145:639-648
3. Gharbi AJ, Hassine W, Brauner WB, Dupuch K. Ultrasound examination of the hydatid liver. *Radiology* 1981;139:459-463
4. Niron EA, Ozer H. Ultrasound appearances of liver hydatid disease. *Br J Radiol* 1981;54:335-338

Reply

We agree that the diagnosis of hydatid cyst of the liver often is made readily, especially if the characteristic round or oval daughter cysts are present or the "split-wall" feature is recognized. In a small percentage of cases, the type IV lesion described by Gharbi et al. [1] may be difficult to differentiate from biliary cystadenoma or cystadenocarcinoma. We thank Drs. Agildere, Haliloglu, and Akhan for their interest in our paper [2] and for their reminder of the imaging features that often permit a confident diagnosis of hydatid cysts.

Melvyn Korobkin
Isaac R. Francis
Michael B. Alpern
and colleagues
*University of Michigan Medical Center
Ann Arbor, MI 48109*

REFERENCES

1. Gharbi AJ, Hassine W, Brauner WB, Dupuch K. Ultrasound examination of the hydatid liver. *Radiology* 1981;139:459-463
2. Korobkin MT, Stephens DH, Lee JKT, et al. Biliary cystadenoma and cystadenocarcinoma: CT and sonographic findings. *AJR* 1989;153: 507-511

Multinodular Splenic Sarcoidosis: Discordant CT and Sonographic Findings

Sarcoidosis is a systemic granulomatous disease of unknown etiology. It frequently affects the mediastinal and hilar lymph nodes

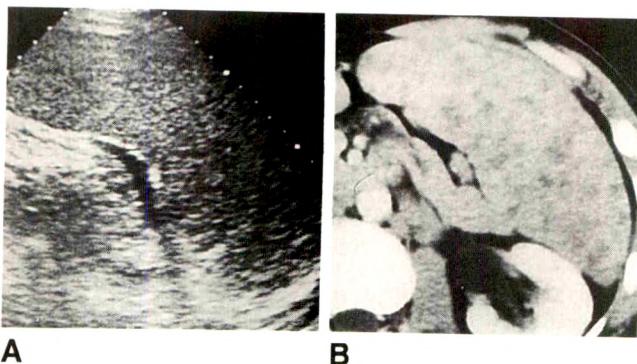


Fig. 1.—Splenic sarcoidosis.
A, Longitudinal sonogram of spleen shows homogeneous splenomegaly without evidence of nodules.
B, Contrast-enhanced CT scan shows multiple nodular hypodense areas scattered within normal splenic parenchyma.

but can involve any organ or tissue. We describe an unusual case of multinodular splenic sarcoidosis in which the abdominal CT and sonographic findings were in disagreement. To our knowledge, this discordance has not been reported previously.

A 30-year-old man with sarcoidosis was admitted for evaluation of acute pain in the left flank. Plain abdominal radiographs showed a left-sided ureteral calculus at the left uretero-ovesical junction. Chest radiographs showed a diffuse reticulonodular pattern without hilar lymphadenopathy. An abdominal sonogram showed homogeneous hepatosplenomegaly and retroperitoneal lymphadenopathy. Unenhanced CT also showed hepatosplenomegaly and mesenteric and retroperitoneal lymphadenopathy; however, contrast-enhanced CT revealed multiple hypodense splenic lesions several centimeters in diameter. Even with the knowledge that nodules were visible on CT, no parenchymal abnormality was recognized on the sonogram (Fig. 1).

The finding of multiple splenic lesions in sarcoidosis is extremely rare, and only sporadic cases have been reported [1–3]. In our case, unenhanced CT showed multiple isodense lesions; on contrast-enhanced CT scans, the nodules became hypodense relative to normal splenic tissue. Our CT findings are similar to those previously reported [1–3]. However, the value of sonography in such cases has not been discussed.

In our patient, CT showed multinodular splenic involvement, whereas sonography showed homogeneous splenomegaly. We are not certain why the sonographic and CT findings were discordant, but it seems likely that the superiority of CT was due to the lack of contrast enhancement by the nodules. Failure to identify them on sonograms indicates that the acoustic impedance of the nodules is similar to that of normal splenic tissue.

Although CT findings do not confirm a diagnosis of splenic sarcoidosis, we think that the hypodense splenic nodules on contrast-enhanced CT scans, seen in our patient, represent giant granulomatous sarcoid nodules. Follow-up CT showed that the splenic abnormalities had resolved after appropriate treatment.

T. Franquet
J. A. Oteo
R. Cozcolluela
J. M. Casas
Hospital "Virgen del Camino"
Pamplona 31008, Spain

REFERENCES

- Mathieu D, Vanderstigel M, Schaffer A, Vasile N. Computed tomography of the splenic sarcoidosis. *J Comput Assist Tomogr* 1986;10:676–680
- Meranze S, Coleman B, Arger P, Mintz M, Markowitz L. Retroperitoneal manifestations of sarcoidosis on computed tomography. *J Comput Assist Tomogr* 1985;9:50–52
- Alvarez FJ, Escalada J, Comet R, Garcia F, Biosca M. CT diagnosis of splenic multifocal lesions and abdominal lymphadenopathy secondary to sarcoidosis. *Comput Med Imaging Graph* 1988;12:255–257

Fatal Bleeding After Fine-Needle Aspiration Biopsy of a Small Hepatocarcinoma

A 60-year-old man with advanced cirrhosis confirmed by biopsy was admitted because of arthritis of the sternoclavicular joint and sepsis. Sonograms showed a 2.7-cm hypoechoic lesion in the right hepatic lobe, near the gallbladder, heterogeneous bright echogenicity of the liver indicative of cirrhosis, and ascites (Fig. 1). A transhepatic fine-needle biopsy was performed with a 22-gauge needle. The final diagnosis was well-differentiated hepatocellular carcinoma. Coagulation factors were within the normal range. The day after the biopsy, hypotension developed, and the hematocrit decreased. The patient received a transfusion of 1500 ml of blood, and a laparotomy was performed. A point of bleeding was found, a small artery in a tumor nodule in the right lobe of the liver. Hemoperitoneum was noted, but the amount of blood was not specified. Surgical treatment consisted of local hemostasis only. One day after laparotomy, the patient died, probably because of persistent bleeding. The critical condition of the patient after laparotomy did not permit another operation. No autopsy was performed.

Of 2000 abdominal fine-needle biopsies performed in the last 9 years, we have had major complications (hemoperitoneum) in only three patients. Two had cirrhosis and coagulation factors below normal values. The other patient is described here. In a review of 63,108 cases, Smith [1] found a total of 101 major complications (0.16%). Four patients died, a mortality rate of 0.006%. In their series of 3500 fine-needle biopsies, Nelsoe et al. [2] had one patient who had fatal bleeding after fine-needle aspiration of a liver metastasis.

A. Martinez-Noguera
L. Donoso
P. Coscojuela
Hospital de Sant Pau
08025-Barcelona, Spain

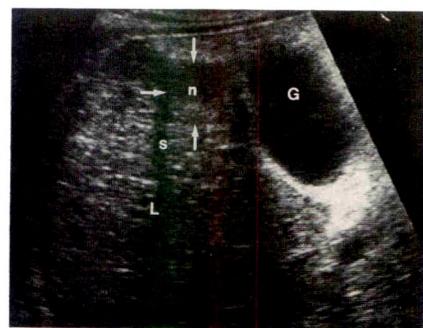


Fig. 1.—Sonogram shows small nodule (n) in right hepatic lobe (L), near gallbladder (G), and acoustic shadow (S).

REFERENCES

- Smith EH. The hazards of fine needle aspiration biopsy. *Ultrasound Med Biol* 1984;10:629

2. Nelsoe CH, Nielsen L, Torp-Pedersen S, Holm HH. Major complications and deaths due to interventional ultrasonography: a review of 8000 cases. *JCU* 1990;18:179-184

Sonography of Umbilical Cord Hematoma

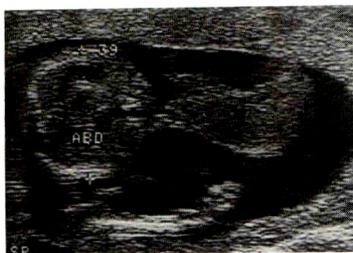
Few cases of umbilical cord hematomas diagnosed on the basis of sonographic findings have been reported [1-4]. In those cases, the hematomas were spontaneous or due to amniocentesis or to in utero blood transfusion. All were diagnosed after 25 weeks gestation. I report a case of sonographic detection of a cord hematoma at 17 weeks gestation.

Because of her age, a 42-year-old woman, para 4, gravida 8, had amniocentesis for genetic reasons 17 weeks after her last menstrual period. A sonogram performed 9 days before the amniocentesis was normal. A sonogram performed 24 hr after the amniocentesis showed a 2 × 5 cm echogenic mass in the umbilical cord. The mass was adjacent to the fetal abdomen, contiguous with the umbilical cord, and mobile in the amniotic fluid. Fluid, interpreted as sections of the umbilical vein, could be seen inside the mass (Fig. 1). Fetal heart rate and fetal activity were normal. Within a few days, sonography showed resorption of the mass. The pregnancy was otherwise uncomplicated. A normal neonate was born vaginally at term.

The sonographic features of hematoma of the umbilical cord are the hematoma's location, usually adjacent to the fetal abdomen or to the placenta; its continuity with the umbilical cord; and its mobility in the amniotic fluid, if fetal death has not occurred. A fresh hematoma in the cord appears as an echogenic mass [1, 3]. This is consistent with the sonographic appearance of a hematoma before lysis of the clot has occurred. A longstanding hematoma is usually hypoechoic and may be septated [2, 4]. The differential diagnosis includes (1) defects of the abdominal wall, such as umbilical hernia, omphalocele, and laparoschisis, and (2) cord masses, such as allantoic cyst, omphalomesenteric cyst, mucoid cyst, hemangioma, and teratoma.

Luc R. M. Morin
Valognes Hospital
F50700 Valognes, France

Fig. 1.—Umbilical cord hematoma. Sonogram shows 2 × 5 cm echogenic mass adjacent to fetal abdomen (ABD). Umbilical vein can be seen on both sides of abdominal wall: inside abdomen and at one end of mass close to fetal abdomen. (Reprinted with permission from [5].)



REFERENCES

- Keckstein G, Tschürtz S, Schneider V, Hütter W, Terinde R, Jonatha WD. Umbilical cord hematoma as a complication of intrauterine intravascular blood transfusion. *Prenat Diagn* 1990;10:59-65
- Ruvinski ED, Wiley TL, Morrisson JC, Blake PG. In utero diagnosis of umbilical cord hematoma by ultrasonography. *Am J Obstet Gynecol* 1981;140:833-834
- Sutro WH, Tuck SM, Moesevitz A, Novotny PL, Archbold F, Irwin GA. Prenatal observation of umbilical cord hematoma. *AJR* 1984;142:801-802
- Virot G, Macé J, Virot JG, Blanc JM. L'hématome du cordon, apport de l'échographie. *Rev Fr Gynecol Obstet* 1982;77:131-133
- Morin LRM, Bonan J, Vendrolini G, Bourgeois C. Sonography of umbilical cord hematoma following genetic amniocentesis. *Acta Obstet Gynecol Scand* 1987;66:669-670

Antenatal Diagnosis of Sacrococcygeal Teratoma Facilitated by Combined Use of Doppler Sonography and MR Imaging

We report a case of benign sacrococcygeal teratoma diagnosed antenatally on the basis of findings on Doppler sonography and MR imaging.

A 23-year-old pregnant woman was referred for evaluation of a possible fetal sacral tumor. Gestational age was 39 weeks. Sonography showed a cystic mass with a solid part involving the fetal sacrum (Figs. 1A and 1B). On color Doppler imaging, blood flow could be visualized within the solid part of the tumor, and blood-flow velocity waveforms with small diastolic components were recorded (Fig. 1B). T1-weighted MR images showed a large cystic tumor (Fig. 1C) contiguous with the fetal presacral area (Fig. 1D). The wall of the tumor had the same high-signal intensity as the fetal subcutaneous tissue, and a mild high-intensity component reflecting fat was noted within the tumor (Fig. 1E). The spine appeared to be intact, and no evidence of a hydrocephalus was seen.

On the same day that the sonogram was performed, the patient was delivered of a female infant weighing 4004 g who had a large sacral tumor. No neurologic abnormality was identified. On the 10th postnatal day, the mass and entire coccyx were excised. Histologic examination confirmed the diagnosis of benign cystic teratoma. At this writing, the infant is 11 months old and doing well, with intact bowel, bladder, and lower-extremity functions.

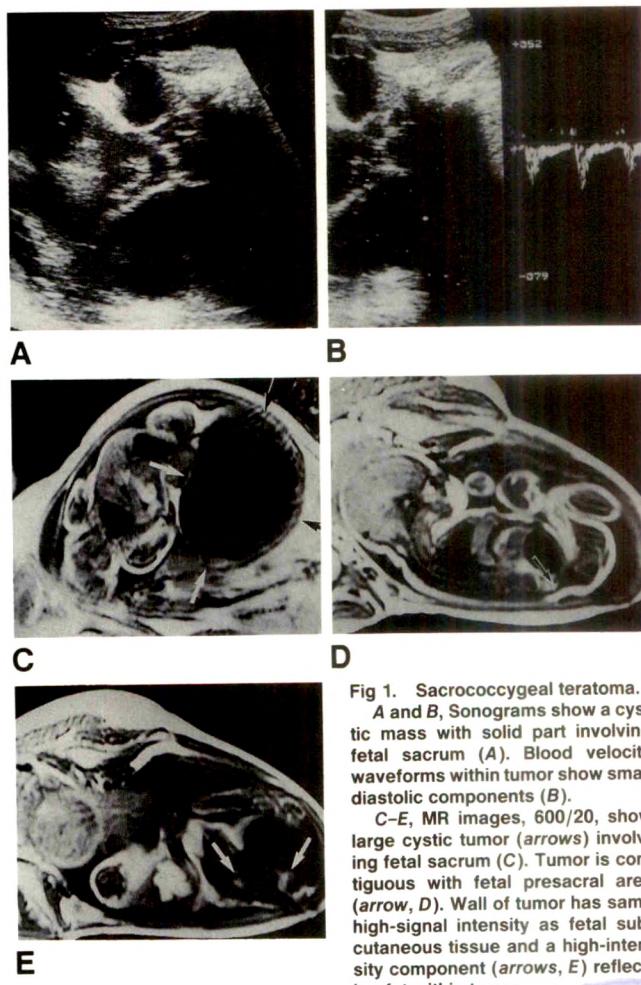


Fig 1. Sacrococcygeal teratoma. A and B, Sonograms show a cystic mass with solid part involving fetal sacrum (A). Blood velocity waveforms within tumor show small diastolic components (B).

C-E, MR images, 600/20, show large cystic tumor (arrows) involving fetal sacrum (C). Tumor is contiguous with fetal presacral area (arrow, D). Wall of tumor has same high-signal intensity as fetal subcutaneous tissue and a high-intensity component (arrows, E) reflecting fat within tumor.



A malignant teratoma is rapidly fatal; the average survival time after diagnosis is 9 months [1]. Therefore, differentiation between benign and malignant sacrococcygeal teratoma must be made early. In our patient, MR imaging provided definitive information for an antenatal diagnosis of fetal sacrococcygeal teratoma. In the presence of a malignancy, the Doppler signals generally have high velocity with markedly large diastolic components [2]. The resistance index ([systolic velocity - end-diastolic velocity]/systolic velocity) of blood-flow velocity waveforms of malignant tumors is less than 0.7 [2]. The blood-flow velocity waveforms obtained in our case, a benign fetal sacrococcygeal teratoma, had only small diastolic components with high pulsatility, and the resistance index was 0.89. Therefore, a benign lesion was diagnosed antenatally, and the histologic examination confirmed the diagnosis.

Kohkichi Hata
Toshiyuki Hata
Manabu Kitao
and colleagues

*Shimane Medical University
Izumo 693, Japan*

REFERENCES

1. Valdiserri RO, Yunis EJ. Sacrococcygeal teratomas: review of 68 cases. *Cancer* 1981;48:217-221
2. Hata T, Hata K, Senoh D, et al. Doppler ultrasound assessment of tumor vascularity in gynecologic disorders. *J Ultrasound Med* 1989;8:309-314

Anterior Spinal Artery Syndrome Caused by Infarction of the Conus Medullaris

We report a case in which MR showed a lesion of the ventral aspect of the conus medullaris that suggested the diagnosis of an anterior spinal artery syndrome. The postulated cause was infarction of the conus as a result of occlusion of the artery of Adamkowitz.

A 41-year-old man had sudden pain in the lower back and buttocks radiating down both lower extremities. Lower-extremity paraparesis, bilateral paresthesias, and urinary and fecal incontinence followed within the next 48 hr. Deep tendon reflexes were absent below the knees. The patient had dissociated sensory loss with diminished pain and temperature sensation, with sparing of proprioception of the lower extremities and perirectal region. The findings were considered typical for a lesion causing anterior myelopathy at or below the L4 level. MR of the lumbar and thoracic spine 5 days after the onset of pain showed a linear area of increased signal intensity involving the conus medullaris on T2-weighted sequences (Fig. 1A). T1-weighted sequences obtained before and after IV administration of contrast material were normal. Follow-up studies on day 13 showed contrast enhancement of the lesion (Fig. 1B).

The anterior median spinal artery supplies most of the anterior gray columns, the peripheral rim of white matter anteriorly, and the ventral portions of the dorsal gray columns, roughly the ventral two thirds of the spinal cord. Occlusion of the artery usually produces

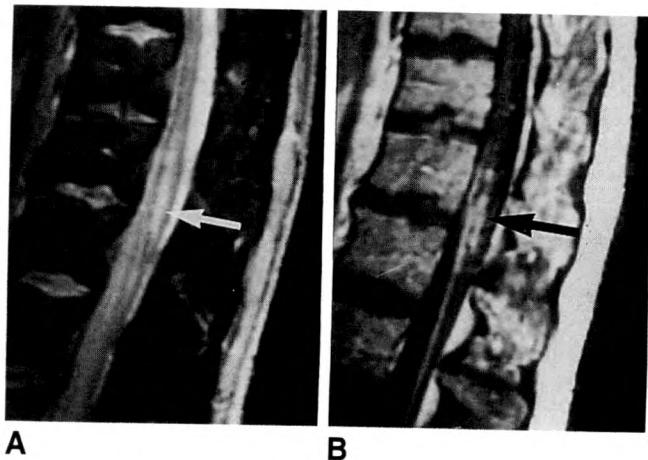


Fig. 1.—Anterior spinal artery syndrome caused by infarction of conus medullaris.

A, Sagittal T2-weighted MR image (SE 2000/80) obtained 5 days after onset of pain shows increased signal at conus medullaris (arrow). No contrast enhancement was seen on T1-weighted sequences.

B, Contrast-enhanced sagittal T1-weighted MR image (SE 600/20) obtained 13 days after onset of pain shows conus medullaris with enhancement of its ventral aspect (arrow).

abrupt onset of radicular or diffuse pain, flaccid weakness, sphincter dysfunction, and decreased or absent pain and temperature sensation below the level of the lesion. Because the dorsal column is spared, vibration and position senses are preserved [1, 2].

In our case, failure of the lesion to enhance during the early stages of the acute process, with enhancement occurring during the second week, was compatible with the diagnosis of cord infarction. Other demyelinating conditions that were considered, such as multiple sclerosis, typically show enhancement early in the acute phase. Infarction of the cord frequently results from arteriovenous malformations, occlusive lesions of the aorta, such as advanced atherosclerosis or dissecting aneurysm, or surgical lesions requiring aortic cross-clamping [1-4]. No underlying cause was identified in this case.

Risa S. Dunn
Stephen N. Wiener
*The Mt. Sinai Medical Center
Cleveland, OH 44106*

REFERENCES

1. Sandson TA, Friedman JH. Spinal cord infarction: report of 8 cases and review of the literature. *Medicine* 1989;68:282-292
2. Adams RD, Victor M. *Principles of neurology*, 4th ed. New York: McGraw-Hill, 1989:131, 732-735
3. Dillon WP, Norman D, Newton TH, Bolla K, Mark A. Intradural spinal cord lesions: Gd-DTPA-enhanced MR imaging. *Radiology* 1989;170:229-237
4. Anderson NE, Willoughby EW. Infarction of the conus medullaris. *Ann Neurol* 1987;21:470-474

Letters are published at the discretion of the Editor and are subject to editing.
Letters to the Editor must not be more than two double-spaced, typewritten pages. One or two figures may be included. Abbreviations should not be used. See Author Guidelines, page A5.
Material being submitted or published elsewhere should not be duplicated in letters, and authors of letters must disclose financial associations or other possible conflicts of interest.
Letters concerning a paper published in the AJR will be sent to the authors of the paper for a reply to be published in the same issue. Opinions expressed in the Letters to the Editor do not necessarily reflect the opinions of the Editor.

Review of Current Literature



Initials and addresses of corresponding authors are provided in parentheses for each article so that the reader can obtain reprints directly. Abstracts are printed verbatim from each journal.

The New England Journal of Medicine

A comparison between heparin and low-dose aspirin as adjunctive therapy with tissue plasminogen activator for acute myocardial infarction. Hsia J, Hamilton WP, Kleiman N, et al. (JH, George Washington University, 2150 Pennsylvania Ave., N.W., Washington, DC 20037). *N Engl J Med* 323(22):1433-1437, Nov. 1990

Background. We report the results of the Heparin-Aspirin Reperfusion Trial, a collaborative study comparing early intravenous heparin with oral aspirin as adjunctive treatment when recombinant tissue plasminogen activator (rt-PA) is used for coronary thrombolysis during acute myocardial infarction.

Methods. Two hundred five patients were randomly assigned to receive either immediate and then continuous intravenous heparin (starting with a 5000-unit bolus; n = 106) or immediate and then daily oral aspirin (80 mg; n = 99) together with rt-PA (100 mg intravenously over a six-hour period) initiated within six hours of the onset of symptoms. We evaluated the patency of the infarct-related artery by angiography 7 to 24 hours after beginning rt-PA infusion, the frequency of reocclusion of the artery by repeat angiography on day 7, and ischemic or hemorrhagic complications during the hospital stay.

Results. At the time of the first angiogram, 82 percent of the infarct-related arteries in the patients assigned to heparin were patent, as compared with only 52 percent in the aspirin group ($P < 0.0001$). Of the initially patent vessels, 88 percent remained patent after seven days in the heparin group, as compared with 95 percent in the aspirin group (P not significant). The numbers of hemorrhagic events (18 in the heparin and 15 in the aspirin group) and recurrent ischemic events (8 in the heparin and 2 in the aspirin group) were similar in the two groups.

Conclusions. Coronary patency rates associated with rt-PA are higher with early concomitant systemic heparin treatment than with concomitant low-dose oral aspirin. This observation has important implications for clinical practice and should be considered in the design and interpretation of clinical trials involving coronary thrombolytic therapy.

Late pulmonary sequelae of bronchopulmonary dysplasia. Northway WH Jr, Moss RB, Carlisle KB, et al. (WHN Jr., Dept. of Diagnostic Radiology and Nuclear Medicine, Stanford University Medical Center, Stanford, CA 94305). *N Engl J Med* 323(26):1793-1799, Dec. 1990

Background. Bronchopulmonary dysplasia is a chronic lung disease that often develops after mechanical ventilation in prematurely born infants with respiratory failure. It has become the most common

form of chronic lung disease in infants in the United States. The long-term outcome for infants with bronchopulmonary dysplasia has not been determined.

Methods. We studied the pulmonary function of 26 adolescents and young adults, born between 1964 and 1973, who had bronchopulmonary dysplasia in infancy. We compared the results with those in two control groups: 26 age-matched adolescents and young adults of similar birth weight and gestational age who had not undergone mechanical ventilation, and 53 age-matched normal subjects.

Results. Sixty-eight percent of the subjects with bronchopulmonary dysplasia in infancy (17 of the 25 tested) had airway obstruction, including decreases in forced expiratory volume in one second, forced expiratory flow between 25 and 75 percent of vital capacity, and maximal expiratory flow velocity at 50 percent of vital capacity, as compared with both control groups ($P < 0.0001$ for all comparisons). Twenty-four percent of the subjects with bronchopulmonary dysplasia in infancy had fixed airway obstruction, and 52 percent had reactive airway disease, as indicated by their responses to the administration of methacholine or a bronchodilator. Hyperinflation (an increased ratio of residual volume to total lung capacity) was more frequent in the subjects with a history of bronchopulmonary dysplasia than in either the matched cohort ($P < 0.0006$) or the normal controls ($P < 0.0004$). Six of the subjects who had bronchopulmonary dysplasia in infancy had severe pulmonary dysfunction or current symptoms of respiratory difficulty.

Conclusions. Most adolescents and young adults who had bronchopulmonary dysplasia in infancy have some degree of pulmonary dysfunction, consisting of airway obstruction, airway hyperreactivity, and hyperinflation. The clinical consequences of this dysfunction are not known.

Tumor angiogenesis and metastasis: correlation in invasive breast carcinoma. Weidner N, Semple JP, Welch WR, Folkman J (NW, Dept. of Pathology, Brigham and Women's Hospital and Harvard Medical School, 75 Francis St., Boston, MA 02115). *N Engl J Med* 324(1):1-8, Jan. 1991

Background. Experimental evidence suggests that the growth of a tumor beyond a certain size requires angiogenesis, which may also permit metastasis. To investigate how tumor angiogenesis correlates with metastases in breast carcinoma, we counted microvessels (capillaries and venules) and graded the density of microvessels within the initial invasive carcinomas of 49 patients (30 with metastases and 19 without).

Methods. Using light microscopy, we highlighted the vessels by staining their endothelial cells immunocytochemically for factor VIII. The microvessels were carefully counted (per 200 \times field), and their density was graded (1 to 4+), in the most active areas of neovascularization, without knowledge of the outcome in the patient, the presence or absence of metastases, or any other pertinent variable.

Results. Both microvessel counts and density grades correlated with metastatic disease. The mean (\pm SD) count and grade in the patients with metastases were 101 ± 49.3 and 2.95 ± 1.00 vessels, respectively. The corresponding values in the patients without metastases were significantly lower— 45 ± 21.1 and 1.38 ± 0.82 ($P = 0.003$ and $P \leq 0.001$, respectively). For each 10-microvessel increase in the count per $200\times$ field, there was a 1.59-fold increase in the risk of metastasis (95 percent confidence interval, 1.19 to 2.12; $P = 0.003$). The microvessel count and density grade also correlated with distant metastases. For each 10-microvessel increase in the vessel count per $200\times$ field, there was a 1.17-fold increase in the risk of distant metastasis (95 percent confidence interval, 1.02 to 1.34; $P = 0.029$).

Conclusions. The number of microvessels per $200\times$ field in the areas of most intensive neovascularization in an invasive breast carcinoma may be an independent predictor of metastatic disease either in axillary lymph nodes or at distant sites (or both). Assessment of tumor angiogenesis may therefore prove valuable in selecting patients with early breast carcinoma for aggressive therapy.

Long-term outcome after surgical repair of isolated atrial septal defect: follow-up at 27 to 32 years. Murphy JG, Gersh BJ, McGoon MD, et al. (BJG, Division of Cardiovascular Diseases and Internal Medicine, Mayo Clinic, 200 First St. S.W., Rochester, MN 55905). *N Engl J Med* 323(24):1645–1650, Dec. 1990

Background. Atrial septal defects have been surgically correctable for more than 30 years. The long-term survival rates among patients treated in the early era of cardiac surgery are poorly documented, but such data are of critical importance to the future medical care, employability, and insurability of these patients.

Methods. To determine the natural history of surgically corrected atrial septal defects, we studied all 123 patients who underwent repair of an isolated defect (ostium secundum or sinus venosus) at the Mayo Clinic between 1956 and 1960, 27 to 32 years after the procedure. The follow-up status of all patients was determined by written questionnaires and telephone interviews. Hospital records and death certificates were obtained if interim hospitalization or death had occurred.

Results. The overall 30-year actuarial survival rate among survivors of the perioperative period was 74 percent, as compared with 85 percent among controls matched for age and sex. The perioperative mortality was 3.3 percent (four deaths). Actuarial 27-year survival rates among patients in the younger two quartiles according to age at operation (≤ 11 years and 12 to 24 years) were no different from rates among controls—97 percent and 93 percent, respectively. In the two older quartiles (25 to 41 years and > 41 years), 27-year survival rates were significantly less ($P < 0.001$)—84 percent and 40 percent, respectively—than in controls (91 and 59 percent). Independent predictors of long-term survival according to multivariate analysis were age at operation ($P < 0.0001$) and systolic pressure in the main pulmonary artery before operation ($P < 0.0027$). When repair was performed in older patients, late cardiac failure, stroke, and atrial fibrillation were significantly more frequent.

Conclusions. Among patients with surgically repaired atrial septal defects, those operated on before the age of 25 have an excellent prognosis, but older patients require careful, regular supervision.

Chest

The chest roentgenogram in pulmonary tuberculosis patients seropositive for human immunodeficiency virus type 1. Long R, Maycher B, Scalcini M, Manfreda J (RL, C5116, Dept. of Medicine, University of Manitoba, Winnipeg, Manitoba, Canada R2H 2A6). *Chest* 99(1):123–127, Jan. 1991

To determine the impact that co-infection with HIV has on the radiographic presentation of pulmonary tuberculosis, we examined the chest roentgenograms obtained before treatment in 225 HIV-tested adult Haitians with bacillary (smear or culture or both) positive

pulmonary tuberculosis. There were 67 HIV-seropositive and 158 HIV-seronegative patients. Intrathoracic adenopathy alone was more common and parenchymal infiltrates less common in HIV-seropositive patients ($p < 0.05$). Although a parenchymal infiltrate was less likely to be cavitating in the HIV-seropositive group ($p < 0.05$) when cavitary parenchymal disease was present, HIV seropositivity did not affect the number of cavities (single or multiple) or the size of the largest cavity. Patients with AIDS were significantly more likely to have a chest radiographic pattern consistent with primary tuberculosis (80 percent) than HIV-seropositive patients without AIDS (30 percent), and the latter were significantly more likely to have such a pattern than HIV-seronegative patients (11 percent) ($p < 0.05$). The HIV-seropositive patients were equally infectious, regardless of the pattern of disease (primary vs postprimary). Even though pulmonary tuberculosis in an HIV-seropositive adult probably results from reactivation of dormant foci or reinfection, the pattern on the chest roentgenogram often suggests primary disease, especially if the patient has AIDS.

Gastroenterology

The epidemiology of inflammatory bowel disease: a large, population-based study in Sweden. Ekbom A, Helmick C, Zack M, Adami H-O (AE, Dept. of Surgery, University Hospital, Uppsala, Sweden). *Gastroenterology* 100:350–358, 1991

Previous population-based incidence studies of inflammatory bowel disease are limited by small numbers, short duration, or inadequate case-finding. To address these problems, we identified all persons with confirmed ulcerative colitis ($n = 2509$) or Crohn's disease ($n = 1469$) in the Uppsala Health Care Region from 1965 to 1983. Age-specific incidence rates by sex were slightly greater for males with ulcerative colitis and females with Crohn's disease. Incidence rates for ulcerative colitis and females with Crohn's disease. Incidence rates for ulcerative colitis and Crohn's disease were higher in urban than rural areas. The annual incidence rate of ulcerative colitis increased from less than 7 per 100,000 to more than 12 per 100,000 during the study period, while the rate for Crohn's disease remained between 5 and 7 per 100,000. The increase in the incidence of ulcerative colitis was the result of a marked increase in the number of patients with ulcerative proctitis. Analyses by 5-year birth cohorts suggest that those born from 1945 through 1954 were at higher risk for ulcerative colitis and Crohn's disease, and that this effect was accounted for by those born in the first half of the year. The seasonality in the cohort effect, combined with the urban preponderance of disease, suggests that environmental causes may be involved in ulcerative colitis and Crohn's disease.

Reprinted with permission by the American Gastroenterological Association.

Digestive Diseases and Sciences

Peptic ulcer perforation as the presentation of Zollinger-Ellison syndrome. Waxman I, Gardner JD, Jensen RT, Maton PN (PNM, Bldg. 10, Rm. 9C-103, National Institutes of Health, Bethesda, MD 20892). *Dig Dis Sci* 36(1):19–24, Jan. 1991

We examined the characteristics of patients with Zollinger-Ellison syndrome who developed a perforation prior to diagnosis to determine whether any clinical features were useful markers of the syndrome. Of 160 patients with Zollinger-Ellison syndrome, perforation occurred prior to the diagnosis being made in 11 (7%). At surgery, perforations were found in the duodenum in six cases and in the jejunum in five. In no case was tumor identified at emergency surgery, and the diagnosis of Zollinger-Ellison syndrome was made only in the postoperative period when excessive gastric secretions were noted. Neither acid output nor serum gastrin concentration were useful predictors for perforation. The patients, six men and five women, were 27–61 years old (median 48) and one had MEN-1. Three patients had no symptoms prior to the perforation. The other eight had

symptoms for 1–15 years, with diarrhea occurring in 45% of the cases. Following the diagnosis of Zollinger-Ellison syndrome, patients were given medication to control gastric acid hypersecretion. Eight patients remained well, but the three patients who had had a partial gastrectomy had a complicated course despite medical therapy. Although features of perforation in Zollinger-Ellison syndrome are not specific, jejunal perforation or perforation associated with a history of diarrhea is suggestive of the diagnosis. Serum gastrin should be measured in every case and a partial gastrectomy avoided.

Diagnosis of *Campylobacter pylori* gastritis. Mertz H, Lafrance N, Kafonek D, Yardley J, Hendrix T (HM, Division of Gastroenterology, Dept. of Medicine, UCLA School of Medicine, 44–138 Center Health Sciences, Los Angeles, CA 90024-1684). *Dig Dis Sci* 36(1):1–4, Jan. 1991

Campylobacter pylori is a bacterium that inhabits gastric mucosa. It causes chronic active gastritis and is highly associated with duodenal ulcer. *Campylobacter pylori* has a urease enzyme (not present in man), which allows diagnosis by a [¹⁴C]urea breath test. We compared two noninvasive tests, the breath test and serum ELISA, compared to biopsy and histologic diagnosis. Twenty-two patients who underwent gastroduodenoscopy for evaluation of possible peptic ulcer disease entered the study. The breath test detected the organism in eight of eight patients biopsy-positive for the organism (sensitivity 100%). The breath test was negative in 12 of the 14 patients who were biopsy-negative (specificity 86%). The ELISA was performed in 14 patients. It was positive in 5 of 5 patients biopsy-positive for the organism (sensitivity 100%) and negative in 7 of 9 patients who were biopsy-negative (specificity 78%). We conclude that both the ELISA and the [¹⁴C]urea breath test are excellent noninvasive methods to detect *Campylobacter pylori*. However, only the breath test is suitable for following the response to treatment, as it detects the presence of the organism rather than an immune response to it.

Scintigraphic assessment of leukocyte infiltration in acute pancreatitis using technetium-99m-hexamethyl propylene amine oxide as leukocyte label. Schölerich J, Schümichen C, Lausen M, et al. (JS, Medizinische Universitätsklinik Hugstetter Str. 55, D-7800 Freiberg, Germany). *Dig Dis Sci* 36(1):65–70, Jan. 1991

The infiltration of leukocytes has been linked to the pathophysiology of complicated or severe pancreatitis. We have tested the ability of leukocyte scintigraphy using technetium-99m-hexamethyl propylene amine oxide (HM-PAO) as label to demonstrate the localization of leukocytes in the pancreas during acute pancreatitis. Twenty-eight patients with acute pancreatitis (eight with biliary, 13 with alcoholic, and seven with unknown origin) were studied with leukocyte scintigraphy using planar imaging and single photon emission computed tomography (SPECT). Fourteen patients had a mild (group I), 11 a severe (group II), and three a lethal outcome (group III) of pancreatitis. All patients of group III, six of group II, and two of group I had a positive leukocyte scan. Thus, the sensitivity of leukocyte scintigraphy for the detection of a lethal course of acute pancreatitis was 100%, of a severe course 54%, and of a severe or lethal course 64%. The specificity of a negative scan for a mild pancreatitis was 86%. Comparison of the results of leukocyte scintigraphy with those of contrast enhanced CT showed that six of eight patients with pancreatic necrosis in CT had a positive leukocyte scan, but only five of 20 patients without detectable pancreatic necrosis in CT. In summary, leukocyte infiltration into the pancreas during pancreatitis can be demonstrated by noninvasive leukocyte scintigraphy using technetium-99m-HM-PAO as label. A correlation between the severity of the disease and leukocyte infiltration exists.

Clinical Orthopaedics and Related Research

Bone fragility of the peripheral skeleton during fluoride therapy for osteoporosis. Schnitzler CM, Wing JR, Gear KA, Robson HJ (CMS, Medical School, York Rd., Parktown, Johannesburg 2193, South Africa). *Clin Orthop* 261:268–275, Dec. 1990

Bone fragility during fluoride therapy for osteoporosis was observed in 24 (37.5%) of 64 patients treated with sodium fluoride, calcium, and vitamin D for 2.5 years who developed episodes of lower-limb pain during treatment. Eighteen (28%) of these patients had clinical and roentgenographic features of 41 stress fractures and 12 new spinal fractures. There were 26 periarticular, six femoral neck, three pubic rami, three tibia and fibula, one greater trochanter, and two subtrochanteric fractures. Vertebral fractures appeared first, then periarticular, then femoral neck, and lastly long-bone shaft fractures. All fractures were spontaneous in onset. The peripheral fracture rate during treatment was three times that in untreated osteoporosis. Roentgenograms must be repeated at intervals of three to four weeks before the pathognomonic callus becomes visible, and the diagnosis can be made. Trabecular stress fractures tend to occur in the first 18 months of treatment, and cortical stress fractures occur after 30 months of therapy.

The Journal of Urology

Prospective comparison of plain abdominal radiography with conventional and digital renal tomography in assessing renal extracorporeal shock wave lithotripsy patients. Sacks EM, Fajardo LL, Hillman BJ, et al. (EMS, Dept. of Radiology, University of Arizona College of Medicine, Tucson, AZ). *J Urol* 144:1341–1346, Dec. 1990

Most publications citing the effectiveness of renal extracorporeal shock wave lithotripsy have used plain abdominal radiography to assess residual calculi after treatment. We compared radiologist sensitivity and specificity in the detection of calculi on plain abdominal radiographs versus conventional film-screen and digital renal tomograms in extracorporeal shock wave lithotripsy patients. Of the patients 50 were imaged before and within 24 hours after lithotripsy. Six radiologists evaluated the resultant 300 studies for the presence and location of calculi. The mean sensitivity for digital tomograms was 83% for pre-lithotripsy and post-lithotripsy studies, which was significantly higher than for plain abdominal radiography and conventional tomography after lithotripsy. However, there were significantly more false positive stone diagnoses associated with digital tomogram interpretation. Signal detection analysis verified the over-all superiority of digital tomography for post-extracorporeal shock wave lithotripsy imaging. Calculus detection by conventional and digital tomography is superior to detection by plain abdominal radiography. However, because we did not perform delayed imaging, it is not possible to say what impact digital tomography might have on the management of extracorporeal shock wave lithotripsy patients.

Surgical management and prognosis of renal cell carcinoma invading the vena cava. Hatcher PA, Anderson EE, Paulson DF, Carson CC, Robertson JE (EEA, Box 3124, Duke University Medical Center, Durham, NC 27710). *J Urol* 145:20–24, Jan. 1991

A total of 44 patients with renal cell carcinoma and vena caval tumor thrombus underwent surgical resection. Of these patients 27 had primary tumor confined within Gerota's fascia, negative lymph nodes and no distant metastases (stage T3cNOM0). Patients who underwent extraction of a mobile tumor thrombus from the vena cava had a 69% 5-year survival rate (median 9.9 years) but patients with tumor thrombus directly invading the vena cava had a 26% 5-year survival rate (median 1.2 years), which improved to 57% (median 5.3 years) if the involved vena caval side wall was resected successfully. Of these patients 17 had renal cell carcinoma with vena caval thrombus as well as extrafascial extension, regional lymphadenopathy or distant metastases, and the 5-year survival rate was less than 18% in all groups (median survival less than 0.9 years). Prognosis was determined by the pathological stage of the renal cell carcinoma and by the presence or absence of vena caval side wall invasion but not by the level of tumor thrombus extension. Patients with incomplete resection of localized renal cell carcinoma with tumor thrombus do not survive any longer than those with extensive cancer, positive lymph nodes or distant metastases. However, when partial venacaval

vectomy establishes negative surgical margins then survival markedly improves.

Pediatrics

A new system for location of endotracheal tube in preterm and term neonates. Blayney M, Costello S, Perlman M, Lui K, Frank J (MP, Division of Neonatology, The Hospital for Sick Children, 555 University Ave., Toronto, Ontario, Canada M5G 1X8). *Pediatrics* 87(1):44-47, Jan. 1991

A randomized, controlled trial was conducted to evaluate a new noninvasive system for placement of the endotracheal tube, based on a magnetic field interference-sensing technique. Seventy-two neonates treated by the standard technique were compared with 70 treated by the new system (TRACH MATE), with radiographic localization as the standard. As judged by the author(s) on the morning after the intubation, correct initial placement was achieved in 69 (78%) of 88 intubations using the new system, compared with 71 (66%) of 107 using the standard technique (Fisher's Test, one-tailed, $P = .044$). Repositioning was actually done in 23 (26%) of 88 TRACH MATE intubations, compared with 42 (39%) of 107 standard intubations, but in none of the TRACH MATE intubations (Fisher's test, one-tailed; $P = .014$). Endotracheal tube position (high, low, or appropriate) was correctly determined by TRACH MATE in 77 (90%) of 85 intubations; the position was not recorded on three occasions. No differences in the number of complications (eg, unplanned extubations, distal displacement, subglottic stenosis) were found between the two groups. It is concluded that the TRACH MATE technique is superior to the standard clinical method in initial placement of the endotracheal tube.

Reprinted by permission of PEDIATRICS © 1991.

The Journal of Nuclear Medicine

Recognition of distinctive patterns of gallium-67 distribution in sarcoidosis. Sulavik SB, Spencer RP, Weed DA, Shapiro HR, Shiu ST, Castriotta RJ (SBS, Pulmonary Division, Dept. of Medicine, Rm. L-2080, University of Connecticut Health Center, Farmington, CT 06032). *J Nucl Med* 31:1909-1914, 1990

Assessment of gallium-67 (^{67}Ga) uptake in the salivary and lacrimal glands and intrathoracic lymph nodes was made in 605 consecutive patients including 65 with sarcoidosis. A distinctive intrathoracic lymph node ^{67}Ga uptake pattern, resembling the Greek letter lambda, was observed only in sarcoidosis (72%). Symmetrical lacrimal gland and parotid gland ^{67}Ga uptake (panda appearance) was noted in 79% of sarcoidosis patients. A simultaneous lambda and panda pattern (62%) or a panda appearance with radiographic bilateral, symmetrical, hilar lymphadenopathy (6%) was present only in sarcoidosis patients. The presence of either of these patterns was particularly prevalent in roentgen Stages I (80%) or II (74%). We conclude that simultaneous (a) lambda and panda images, or (b) a panda image with bilateral symmetrical hilar lymphadenopathy on chest X-ray represent distinctive patterns which are highly specific for sarcoidosis, and may obviate the need for invasive diagnostic procedures.

Gallbladder perforation: correlation of cholescintigraphic and sonographic findings with the Niemeier classification. Swayne LC, Filippone A (LCS, Dept. of Diagnostic Radiology, Morristown Memorial Hospital, 100 Madison Ave., Morristown, NJ 07960). *J Nucl Med* 31:1915-1920, 1990

We respectively analyzed the cholescintigrams and sonograms of 36 consecutive patients with gallbladder perforation to (a) determine the sensitivity of each for the preoperative detection of gallbladder perforation and (b) correlate the findings with the modified Niemeier classification. Cholescintigraphic criteria of perforation (free spill, pericholecystic hepatic activity, and scintigraphic gallstone ileus sign) were detected in 14 of 28 (50%) cases, while sonographic criteria of perforation (pericholecystic fluid or pneumobilia with gallstones) were present in 18% (4 of 22) of patients ($p < 0.05$). Cholescintigraphic patterns of perforation associated with the Niemeier classification were: Type I (acute free perforation), 3 of 7 scans demonstrated free spill; Type II (subacute pericholecystic abscess), 9 of 19 scans showed pericholecystic activity; and Type III (chronic cholecystoenteric fistula), 1 of 3 scans showed a scintigraphic gallstone ileus. Thus, although cholescintigraphy appears superior to sonography, both modalities are relatively insensitive for the detection of gallbladder perforation.

Journal of Thoracic Imaging

Lung disorders due to drug abuse. McCarroll KA, Roszler MH (KAM, Dept. of Radiology, 3L-8, Detroit Receiving Hospital, 4201 St. Antoine, Detroit, MI 48201). *J Thorac Imaging* 6(1):30-35, Jan. 1991

Drug-related diseases of the lungs have been noted with increasing frequency in urban patients. These entities are also being seen in smaller urban and suburban settings, however. The spectrum of pathology is also changing coincident with the marked increase in crack cocaine use. The incidence of abnormal chest radiographs in cocaine users admitted with pulmonary complaints has ranged from 12% to 55%. Findings have included focal air space disease, atelectasis, pneumothorax, pneumomediastinum, and pulmonary edema. Pulmonary complications related to injections of illicit drugs have included pulmonary infection, pulmonary edema, particulate embolism, and talcosis. The "pocket shot" places the patient at risk for a unique set of complications. Radiologists should be aware of this wide spectrum of pulmonary disease that may be related to this increasingly frequent social problem.

Journal of Ultrasound in Medicine

Seminal vesicles: imaging and intervention using transrectal ultrasound. Asch MR, Toi A (AT, Dept. of Radiology, Toronto General Hospital, 200 Elizabeth St., Toronto, Ontario, Canada M5G 2C4). *J Ultrasound Med* 10:19-23, Jan. 1991

The seminal vesicles are difficult to evaluate clinically. Transrectal ultrasound (TRUS) has only recently allowed adequate assessment of these structures and their disorders. As the use of TRUS increases, radiologists must familiarize themselves with diseases of the seminal vesicles and the normal and abnormal appearance at ultrasound. This paper presents four cases illustrating the uncommon disorders that TRUS can demonstrate in the seminal vesicles: ectopic ureter entering the seminal vesicle, symmetrically enlarged seminal vesicles with male infertility, a pelvic arteriovenous malformation mimicking a seminal vesicle cyst, and tuberculosis. In two patients, TRUS was used to guide needle aspiration of seminal vesicle contents safely and to inject contrast for radiography.

Reprinted with permission by the American Institute of Ultrasound in Medicine.

News

Basic Concepts and Practical Issues in Dysphagia

The Johns Hopkins Swallowing Center is sponsoring Basic Concepts and Practical Issues in Dysphagia, May 2-3, at the Johns Hopkins Medical Institutions, Baltimore. The conference, which is designed for newcomers to the field of dysphagia, will explain airway-foodway interrelationships, the importance of nutrition, and neurophysiologic aspects. Category 1 credits will be awarded. Fee: physicians, \$225; other health professionals, \$165. Information: Program Coordinator, The Johns Hopkins Medical Institutions, Office of Continuing Education, Turner Bldg., 720 Rutland Ave., Baltimore, MD 21205; (301) 955-2959.

Blood Vessel Imaging Using Ultrasound Techniques

Blood Vessel Imaging Using Ultrasound Techniques will be held May 8-10 at the Overmead Hotel, Torquay, United Kingdom. This intensive residential course/workshop will discuss the application of echo and Doppler ultrasound techniques in the investigation of the cardiovascular system. A combination of lectures, demonstrations, and workshops will cover the basic principles of these techniques and review the current state of ultrasound arteriography and venography. Specialist sessions will deal with applications of these techniques in the assessment of the cerebral, peripheral, abdominal, obstetric, and neonatal vasculature. Information: Mr. K. N. Humphries, Blood Vessel Imaging Course, 10 Swale Dr., Chandlers Ford, Hampshire SO5 3QY, United Kingdom.

Mackinac Island Imaging Conference

The Dept. of Diagnostic Radiology, William Beaumont Hospital, Royal Oak, MI, will offer Mackinac Island Imaging Conference, July 8-11, at the Grand Hotel, Mackinac Island, MI. The conference is intended to be both a refresher course and an update on the practical aspects of modern radiologic imaging and interventional techniques. Afternoon workshops will discuss diagnostic problems and will focus on major anatomic and pathologic entities. Guest faculty: M. P. Federle, J. B. Kneeland, C. R. B. Merritt, and W. R. Webb. Category 1 credit: 21 hr. Fee: physicians (non-Beaumont alumni), \$400; residents and Beaumont alumni, \$200. Information: Program Coordinator, Miss Mary Anne Smith, William Beaumont Hospital, 3601 W. Thirteen Mile Rd., Royal Oak, MI 48072-2793; (313) 551-6199.

Evaluation & Treatment of the Injured Athlete

Boston University, School of Medicine, is sponsoring Evaluation & Treatment of the Injured Athlete: Sports Medicine Update 1991, July 22-26, at the Chatham Bars Inn, Chatham (Cape Cod), MA. Course director: Anthony Schepsis. Fee: physicians, \$435; others, \$295. Information: Dept. of Continuing Medical Education, Boston University, School of Medicine, 80 E. Concord St., Boston, MA 02118-2394; (617) 638-4605.

Pittsburgh Breast Imaging Seminar

The 11th annual Pittsburgh Breast Imaging Seminar will be held Aug. 1-4 at the Westin William Penn Hotel, Pittsburgh. The seminar will include a review course for technologists for the ARRT Mammography Certification examination. Course codirectors: Kathleen M. Harris, Ellen B. Mendelson, Ingrid E. Naugle, and William R. Poller. Guest faculty: G. W. Eklund, R. McLelland, M. Moskowitz, D. L. Page, and E. A. Sickles. Category 1 credit: 20 hr. Information: Pittsburgh Breast Imaging Seminar, c/o Pittsburgh Radiology Associates, 3471 5th Ave., Ste. 301, Pittsburgh, PA 15213; (412) 648-6043.

Radiation, Physics, and Biology

The NYU Medical Center, Post-Graduate Medical School, will present Radiation, Physics, and Biology, Aug. 26-30, at the NYU Medical Center, New York City. This refresher course is designed specifically for residents in diagnostic radiology and nuclear medicine. The format is didactic; the physics of diagnostic and nuclear radiology and radiobiology are presented in a concentrated form. The emphasis is on concepts. Questions are distributed as a specific aid to study. Category 1 credit: 32 hr. Fee: \$575. Information: NYU Medical Center, Post-Graduate Medical School, 550 First Ave., New York, NY 10016; telephone: (212) 340-5295; fax: (212) 340-5293.

Sonography Update Conference and Exhibit

The Dept. of Radiology, University of California, San Diego, School of Medicine, is sponsoring the 7th annual Sonography Update Conference and Exhibit, Sept. 11-13, at the Hotel Del Coronado, Coronado.

ado (San Diego), CA. The course is designed to provide practicing sonographers and physicians with an update on diagnostic ultrasound. Invasive techniques such as endovaginal sonography, biliary lithotripsy, and percutaneous biopsy (intravascular ultrasound), and interventional techniques will be discussed in dedicated workshops. "Break Out" sessions will give participants an opportunity to meet with specialists (physicians and sonographers) in more informal settings. Program directors: Sandra Hagen-Ansert and John R. Forsythe. Category 1 credit: pending. Fee: physicians, \$420; residents, fellows, and technologists, \$300. Information: Dawne Ryals, Ryals and Associates, P. O. Box 1925, Roswell, GA 30077-1925; telephone: (404) 641-9773; fax: (404) 552-9859.

Mallinckrodt Institute's 60th Anniversary Celebration

The Mallinckrodt Institute of Radiology, Washington University School of Medicine, St. Louis, is sponsoring a radiology program, Sept. 12-14, at the Hyatt Regency Hotel at Union Station, St. Louis, to commemorate the Institute's 60th anniversary and the School's 100th anniversary. The scientific sessions on diagnostic and radiation oncology are designed to review practical aspects of the application of recent research and technologic advances to the solution of clinical problems. The major clinical service, educational, research, commercial, governmental, and ethical issues expected to affect the specialty of radiology will be examined during a special session. Director: William A. Murphy, Jr. Guest faculty: P. Alderson, J. Armstrong, J. Bedwinek, C. Bogardus, G. Glasgow, L. Holman, J. Kinzie, M. Loberg, G. Lundberg, H. MacMahon, H. Madoc-Jones, A. Margulis, J. Marks, V. Marx, B. Mittal, J. Potchen, M. Solomon, R. Stanley, J. Taveras, F. Valeriote, and P. Weyman. Category 1 credit: 16 hr. Fee: \$350. Information: Barbara Getz, 12th Fl., Mallinckrodt Institute of Radiology, 510 S. Kingshighway, St. Louis, MO 63110; (314) 362-7470.

Transrectal Ultrasound in the Diagnosis and Management of Prostate Cancer

Huron Valley Radiology, Catherine McAuley Health Systems, Ann Arbor, MI, will present the 6th International Symposium on Transrectal Ultrasound in the Diagnosis and Management of Prostate Cancer, Sept. 13-14, at the Fairmont Hotel, Chicago. Category 1 credit: 15 hr. Information: Diversified Conference Management, Inc., P. O. Box 2508, Ann Arbor, MI 48103; (313) 665-2535 or (800) 458-2535.

Sonography Registry Review

The Dept. of Radiology, University of California, San Diego, School of Medicine, will present Sonography Registry Review, Sept. 14-15, at the Hotel Del Coronado, Coronado (San Diego), CA. The course is designed primarily for senior students in sonography and practicing sonographers who desire a comprehensive review of the entire field of sonography in preparation for the national registry boards in diagnostic ultrasound. The course will cover ultrasound physics and instrumentation, abdominal applications, gynecologic and obstetric applications, and echocardiology. Accreditation and fees will be announced. Information: Dawne Ryals, Ryals and Associates, P. O. Box 1925, Roswell, GA 30077-1925; telephone (404) 641-9773; fax: (404) 552-9859.

Applied Ultrasound: Accent on Doppler

The Dept. of Radiology, University of Alabama at Birmingham, will present Applied Ultrasound: Accent on Doppler, Sept. 23-26, at the Ritz-Carlton Resort Hotel, Laguna Niguel, CA. The course will provide a state-of-the-art review of selected topics in ultrasound. The theme will be the integration of spectral and color duplex Doppler imaging into ultrasound practice. The course will include lectures, live demonstrations, hands-on experience, and opportunities for interactions with faculty members. Program directors: Lincoln L. Berland and Mitzi Fields. Category 1 credit will be awarded. Fee: physicians, \$425; residents, fellows, and technologists, \$300. Information: Dawne Ryals, Ryals and Associates, P. O. Box 1925, Roswell, GA 30077-1925; telephone: (404) 641-9773; fax: (404) 552-9859.

Diagnosis of Musculoskeletal Disorders

The International Skeletal Society will present Diagnosis of Musculoskeletal Disorders: State-of-the-Art, Sept. 25-28, at the Hotel Del Coronado, Coronado (San Diego), CA. The program will review current knowledge and trends in the diagnosis of musculoskeletal disorders. Emphasis will be on MR, CT, sonography, scintigraphy, arthrography, clinical concepts, and therapy. Participants will become familiar with the advantages and disadvantages of all the important diagnostic methods used in the analysis of diseases of bone, joints, and soft tissue; the selection of an optimal diagnostic protocol; and the importance of cooperation among various specialists in the proper evaluation of such diseases. Program director: Donald L. Resnick. Information: Dawne Ryals, Ryals and Associates, P. O. Box 1925, Roswell, GA 30077-1925; telephone: (404) 641-9773; fax: (404) 552-9859.

Diagnosis and Treatment of Bone and Soft-Tissue Tumors

The Depts. of Orthopaedic Surgery, Radiology, and Surgery, the Division of Oncology, and the Office of Continuing Medical Education, University of California, Davis, Medical Center, are sponsoring the 3rd annual symposium, Diagnosis and Treatment of Bone and Soft-Tissue Tumors, Nov. 21-23, at the Hyatt Regency, Sacramento, CA. The program will emphasize the multidisciplinary nature of the subject, provide information from recent clinical trials, and discuss up-to-date diagnostic and surgical techniques. Workshops at the new University of California, Davis, Medical Center, Cancer Center will be included. Category 1 credit will be awarded. Information: Karen Buckman, Office of Continuing Medical Education, University of California, Davis, School of Medicine, 2701 Stockton Blvd., Sacramento, CA 95817; telephone: (916) 734-5390; fax: (916) 736-0188.

Sterling Winthrop Visiting Professorship and Guest Lectureships at the Armed Forces Institute of Pathology

Sterling Drug, Inc., through its diagnostic imaging divisions of Winthrop Pharmaceuticals, Sterling-Winthrop, and Sterling Research Group, has awarded the Armed Forces Institute of Pathology a grant to support a new program, the Sterling Winthrop Visiting Professorship in Diagnostic Imaging, and financial backing for a well-established program, the National Visiting Guest Lectureships, which now will be

named the Sterling Winthrop National Guest Lectureships. The 1990–1991 Sterling Winthrop Visiting Professor in Diagnostic Imaging is Anne G. Osborn, University of Utah. The 1990–1991 Sterling Winthrop National Guest Lecturers are Michael J. Pitt, University of Arizona; John B. Campbell, University of Florida; Donald W. Chakeres, Ohio State University; Bruce J. Hillman, University of Arizona; Donald L. Resnick, University of California, San Diego; Gordon Gamsu, University of California, San Francisco; Pablo R. Ros, University of Florida; and Joel E. Lichtenstein, University of Cincinnati.

The American Board of Radiology Examinations

Written examinations for the American Board of Radiology (ABR) are scheduled for Oct. 3–4, 1991; Oct. 1–2, 1992; and Oct. 14–15, 1993. Oral examinations will be held at the Executive West Hotel in Louisville, KY, June 3–7, 1991; June 1–5, 1992; and May 31–June 4, 1993. The ABR will accept applications for admission to the examinations after July 1, but not later than Sept. 30 in the year preceding the year in which the examination is to be taken. For application forms and further information: Office of the Secretary, The American Board of Radiology, 300 Park, Ste. 440, Birmingham, MI 48009.

Meeting and Course Review

For the reader's convenience, a summary of upcoming meetings and courses is provided. Detailed listings are given in the *AJR* issue given in parentheses.

Cyanoacrylate Embolization Course, times arranged, Baltimore (July 1990)
Visiting Fellowships in Ultrasound, times arranged, Baltimore (Aug 1990)
Visiting Fellowships in Interventional Radiology, times arranged, Baltimore (Oct 1990)
Swallowing Center Preceptorship, times arranged, Baltimore (Jan)
Imaging Fellowship, times arranged, Miami Beach, FL (Jan)
Radiology Review Course, April 28–May 3, Miami Beach, FL (Feb)
Abdominal Ultrasound, April 29–May 2, Philadelphia (March)
Prostate Ultrasound, May 3, Philadelphia (March)
MR Imaging Fellowships at LAC/USC Imaging Science Center, May 6–10, June 3–7, Aug. 5–9, Sept. 16–20, Oct. 7–11, and Nov. 4–8, Los Angeles (Feb)
International Radiopharmaceutical Dosimetry Symposium, May 7–10, Oak Ridge, TN (Jan)
Oncologic Imaging of Endocrine Gland Tumors, May 9–10, Rome (April)
Thoracic Imaging 1991, May 13–17, Toronto (Jan)
Leading Edge in Diagnostic Ultrasound, May 16–17, Atlantic City, NJ (March)
Yale Clinical MRI, May 20–22, New Haven, CT (April)
Mammographic Interpretation: A Practical Approach, May 20–23, Sept. 23–26, and Oct. 28–31, Boston (March)
Yale Symposium on Duplex and Color Doppler Ultrasound, May 23–24, New Haven, CT (April)
Sonography Symposium, May 24–25, Nashville, TN (Feb)

International Pediatric Radiology '91, May 27–31, Stockholm (March)
American College of Cryosurgery Annual Meeting, June 6–10, La Jolla, CA (March)
MRI Fellowships at Johns Hopkins, June 17–21, Baltimore (Oct 1990)
Contemporary Medical Imaging VIII, June 19–23, Destin, FL (Feb)
Advanced Techniques in MRI, June 22–28, Kiawah Island, SC (March)
Leeds Gastroenterology Course for Radiologists, July 1–5, Leeds, England (Dec 1990)
International Congress of Radiation Research, July 7–12, Toronto (May 1990)
Neuroradiology in the Rockies, July 7–12, Snowmass at Aspen, CO (Feb)
Mammography and the Search for Breast Cancer, July 12–13, Rochester, NY (April)
Alaska 91—Cruise the Inland Passage—Magnetic Resonance Imaging at Sea, July 14–21 (April)
Advances in Gastroenterology, July 15–19, Coronado (San Diego), CA (March)
Radiology for the Non-Radiologist, July 18–21, Coronado (San Diego), CA (March)
Issues in Musculoskeletal Imaging and Magnetic Resonance Imaging, July 22–27, Laguna Niguel, CA (March)
Contemporary Diagnostic Imaging, July 29–Aug. 2, Aspen, CO (April)
Body Imaging, Aug. 5–9, Santa Fe, NM (April)
Imaging of the Head, Spine, and Musculoskeletal System, Aug. 12–16, Whistler, B.C. (April)
Radiology for Clinicians, Aug. 12–16, Coronado (San Diego), CA (April)
Society of Computed Body Tomography Summer Practicum, Aug. 18–22, Keystone, CO (April)
Diagnostic Imaging Update, Aug. 26–30, Vancouver, B. C. (April)
World Congress in Ultrasound, Sept. 1–6, Copenhagen (Sept 1990)
International Workshop on Hypertrophic Osteoarthropathy, Sept. 8–11, Dubrovnik, Yugoslavia (Jan)
European Society of Gastrointestinal Radiologists Annual Meeting, Sept. 8–11, Oxford, England (March)
European Congress of Radiology 1991, Sept. 15–20, Vienna, Austria (Oct 1990)

AJR carries announcements of courses, symposia, and meetings of interest to its readers if received a minimum of 5 months before the event. There is no charge; receipt of items by the *AJR* Editorial Office is not acknowledged. Submit items for publication typed double-spaced. Provide title, date, location, brief description, sponsor, course directors, fees, category I credit, and address and telephone number for additional information. Faculty from the host institution will not be listed. Guest faculty names will appear **only** if initials are provided. Mail news items to *AJR* Editorial Office, 2223 Avenida de la Playa, Suite 103, La Jolla, CA 92037-3218.



American Roentgen Ray Society: Officers, Committees, and Membership Information

Officers

President: M. Paul Capp

President-elect: John A. Kirkpatrick, Jr.

1st Vice-president: A. Everette James, Jr.

2nd Vice-president: Andrew K. Poznanski

Secretary: Joseph T. Ferrucci, Jr.

Treasurer: Beverly P. Wood

Executive Council: R. J. Alfidi, R. N. Berk, M. P. Capp, W. J. Casarella, N. R. Dunnick, R. G. Evens, J. T. Ferrucci, Jr., A. E. James, Jr., J. A. Kirkpatrick, Jr., A. M. Landry, Jr., J. E. Madewell, A. A. Moss, A. K. Poznanski, L. F. Rogers, R. J. Stanley, J. H. Thrall, K. H. Vydareny, N. O. Whitley, B. P. Wood, G. R. Leopold, chairman

Committees

Editorial Policy: R. N. Berk, E. Buonocore, Melvin M. Figley, S. v. W. Hilton, M. S. Huckman, C. A. Rohrmann, Jr., R. J. Stanley, R. I. White, W. J. Casarella, chairman

Education and Research: C. B. Higgins, B. J. Hillman, R. A. McLeod, R. J. Stanley, W. M. Thompson, N. O. Whitley, chairman

Finance and Budget: R. J. Alfidi, R. K. Gedgaudas-McClees, J. R. Thornbury, K. H. Vydareny, J. H. Thrall, chairman

Nominating: G. A. W. Gooding, L. F. Rogers, K. H. Vydareny, chairman

Publications: E. Buonocore, C. A. Rohrmann, Jr., R. J. Stanley, R. I. White, W. J. Casarella, chairman

Membership: J. E. Madewell, A. A. Moss, K. H. Vydareny, R. J. Alfidi, chairman

Representatives to Other Organizations

American Board of Radiology: J. A. Kirkpatrick, Jr., E. C. Klatte, L. F. Rogers

American College of Radiology: J. M. Dennis, R. A. Gagliardi, J. E. Madewell, B. L. McClellan, R. J. Stanley

American Medical Association: S. F. Ochsner, delegate; K. L. Krabbenhoft, alternate; K. L. Kidd, CPT Advisory Committee

American National Standards Institute: M. E. Haskin

National Council on Radiation Protection and Measurements: F. Miraldi, E. L. Saenger

Armed Forces Institute of Pathology: J. E. Madewell

Meeting Arrangements

Annual Meetings: May 5-10, 1991, Sheraton Boston, Boston; May 10-15, 1992, Marriott's World Center, Orlando, FL

Annual Meeting Committee: H. C. Carlson, J. K. Crowe, N. R. Dunnick, R. R. Lukin, R. J. Stanley, R. D. Steele, Jr., A. M. Landry, Jr., chairman

Instructional Courses: Bruce L. McClellan, associate chairman; R. J. Stanley, chairman

Scientific Program: P. Arger, E. Buonocore, D. O. Davis, K. B. Hunter, D. Kushner, T. C. McLoud, W. A. Murphy, Jr., L. B. Talner, J. H. Thrall, J. A. Kirkpatrick, chairman

Scientific Exhibits: J. R. Haaga, R. G. Ramsey, N. R. Dunnick, chairman

ARRS Membership

An application form is printed in the February issue of the Journal. For consideration at the 1992 ARRS meeting, send completed forms before February 1, 1992, to American Roentgen Ray Society, 1891 Preston White Dr., Reston, VA 22091. Active members are graduates of an approved medical or osteopathic school or hold an advanced degree in an allied science. They must practice radiology or work in an associated science in the United States or Canada and be certified by the American Board of Radiology, American Osteopathic Board of Radiology, or Royal College of Physicians of Canada or otherwise adequately document training and credentials. Corresponding members are foreign radiologists or scientists who are active in radiology or an allied science. Members-in-training are residents or fellows in radiology or postgraduate students in an allied science. Additional application forms can be obtained from the ARRS offices in Reston, VA.

Business Office

Paul Fullagar, Executive Director, American Roentgen Ray Society, 1891 Preston White Dr., Reston, VA 22091; (703) 648-8992.

Classified Advertisements

Positions Available

DIAGNOSTIC RADIOLOGIST, HOUSTON—Immediate opening for 2 BC/BE radiologists, 1 with special interest in nuclear medicine, to join 7 BC radiologists associated with large internal medicine clinic near the Texas Medical Center. Primarily outpatient practice with regular hours, also cover adjacent 150-bed hospital. On-site ultrasound, CT, MRI, and nuclear medicine. Experience in angio and interventional is desired. Please send CV to Robert B. Hall, Administrator, Diagnostic Clinic of Houston, 6448 Fannin, Houston, TX 77030; (713) 797-9191. 5a

CHEST RADIOLOGIST, CLEVELAND CLINIC FOUNDATION—The Cleveland Clinic Foundation has an opening for a staff position in the Section of Thoracic Imaging. The foundation is a 1000-bed hospital with a large outpatient population and an international referral base. Successful applicants will be involved in all diagnostic modalities, including CT, MRI, and interventional procedures. A strong interest in teaching, research, and patient care is required. Applicants should be board-certified, fellowship-trained, or have equivalent experience. Excellent salary and benefit package. Send CV to Moulay A. Meziane, M.D., Head, Section of Thoracic Imaging, Cleveland Clinic Foundation, One Clinic Center Dr., Cleveland, OH 44195-5021. The Cleveland Clinic Foundation is an equal opportunity employer. 5-10ap

FACULTY POSITION IN THORACIC RADIOLOGY—The Dept. of Radiology at the Massachusetts General Hospital is seeking a diagnostic radiologist to fill a full-time position in thoracic radiology. The candidate should have additional training in thoracic radiology and be willing to participate in standard film interpretation, CT, MRI, and interventional procedures in the thorax, as well as graduate and undergraduate teaching and research activities. Academic rank commensurate with training and experience. Send inquiries with CV and 3 letters of reference to Theresa C. McLoud, M.D., Dept. of Diagnostic Radiology, Massachusetts General Hospital, Boston, MA 02114. Massachusetts General Hospital is an equal opportunity/affirmative action employer and encourages women and minority candidates to apply. 5ap

DIAGNOSTIC RADIOLOGIST, EL PASO, TX—BE/BC radiologist with special competence in body imaging sought to join busy hospital radiology practice at a community medical center with a total of 330 beds. Modern imaging dept. with 1.5-T GE MR, CT, nuclear medicine with SPECT, ultrasound, angiography with DSA, mammography, and diagnostic radiography. Excellent salary, vacation, and benefits leading to early partnership. Send inquiries with CV to Roy K. Poth, M.D., 1625 Medical Center Dr., El Paso, TX 79902. 5-8ap

CHIEF, RADIOLOGY SERVICE—The VA Medical Center, Long Beach, CA, is seeking an academically oriented, board-certified radiologist for the position of Chief, Radiology Service. The medical center is a tertiary-care medical center affiliated with the College of Medicine, University of California, Irvine. Candidates should have a strong background in clinical radiology, a significant record of research accomplishments, and should possess demonstrated teaching and management skills. The successful candidate will qualify for academic appointment at the University of California, Irvine College of Medicine. The VA is an equal opportunity employer. U.S. citizenship is required. All interested candidates should submit a CV and the names of 3 references to David Webb, M.D., Acting Chief of Staff, VA Medical Center, 5901 E. 7th St., Long Beach, CA 90822. 5-6a

SUPERB PARTNERSHIP POSITION IN LAS VEGAS, NV—Rapidly expanding, 7-member group practice covering 2 full-service imaging centers and a small hospital has an immediate opening. We are looking for an additional board-certified radiologist with an uncommon dedication to excellence in patient care. Our outpatient facilities include 2 MR, 2 CT, angio with a 4-bed recovery area, 5 ultrasound, 5 mammography, 2 SPECT, plus R & F. This is an excellent opportunity for a partnership position with a well-respected group in a growing community. Please send CV to Dr. Mark Winkler, SDMI, 2950 S. Maryland Pkwy., Las Vegas, NV 89109. 5-10a

NEURORADIOLOGIST—Join the current staff of 2 neuroradiologists at William Beaumont Hospital, a modern, tertiary-care medical center in southeastern Michigan with residency and fellowship programs in diagnostic radiology. The dept. is expanding its state-of-the-art facilities to accommodate increasing demands on patient care. Area offers 1 of the best educational and recreational facilities. Excellent compensation. Write to Jalil Farah, M.D., Chairman, Diagnostic Radiology, William Beaumont Hospital, 3601 W. 13 Mile Rd., Royal Oak, MI 48073. 5-7a

CHEST RADIOLOGIST—The Massachusetts General Hospital is recruiting a senior staff radiologist with special competence in pulmonary and cardiac imaging. The candidate should be board-certified in radiology and have at least 5 yr of specialty experience. The applicant must be qualified to conduct CT, MRI, fluoroscopy, and plain film interpretation. Send a current CV and letter of inquiry to Reginald Greene, M.D., Associate Radiologist-in-Chief, Dept. of Radiology, Massachusetts General Hospital, Boston, MA 02114. The Massachusetts General Hospital is an equal opportunity employer. 5ap

RADIOLOGIST/INTERVENTIONAL NEURO-RADIOLOGY—The Dept. of Radiology at the University of Minnesota has a full-time position available in the interventional neuroradiology section at the rank of tenured associate professor or tenured professor beginning as soon as possible. At the associate professor level, minimum requirements are 4 yr postresidency experience, a professional distinction in research and writing, and demonstrated effectiveness in teaching and advising. Appointment at the rank of professor requires a minimum of 6 yr postresidency experience, a national reputation in research, and evidence of leadership in candidate's professional field. Responsibilities will include all facets of interventional neuroradiology as well as graduate and undergraduate medical instruction. Research performance will be strongly encouraged and evaluated. Salary is negotiable and competitive, and is dependent on past scholarly productivity and post-M.D. experience. Applicants must be licensed or able to obtain a license to practice medicine in the state of Minnesota before appointment date. Applications will be accepted through June 15, 1991. Send letters to Wilfrido Castaneda, M.D., Professor, Dept. of Radiology, Box 292 UMHC, University of Minnesota, 420 Delaware St., S.E., Minneapolis, MN 55455. The University of Minnesota is an equal opportunity educator and employer. 5a

DIRECTOR OF NEURORADIOLOGY—Position available for Director of Neuroradiology in 700-bed, university-affiliated teaching hospital with fully approved residency program. Modern equipment includes digital subtraction angiography, 2 CT, and 1 MRI. Staff of 12 full-time radiologists. Excellent salary and fringe package. Send CV to David Bryk, M.D., Maimonides Radiology Associates, P.C., 4802 Tenth Ave., Brooklyn, NY 11219. 5-7ap

DIAGNOSTIC RADIOLOGIST with skills in CT, MR, interventional, ultrasound, and nuclear medicine needed to join group of 8 board-certified radiologists. Growing practice in eastern Washington at a 228-bed hospital, a new multimodality imaging center, and 2 private offices. Potential for long-term practice is excellent. Top-notch school system, including 3 first-rate universities. Excellent hunting, fishing, boating, and skiing. Contact L. E. Creelius, M.D., N. 5901 Lidgerwood, Ste. 18B, Spokane, WA 99207; (509) 482-2385. 5-10ap

STAFF RADIOLOGIST—St. Paul-Ramsey Medical Center, a major affiliate hospital of the University of Minnesota, is seeking a well-qualified assistant professor radiologist. This acute-care, 275-bed hospital is 1 of the primary teaching institutions of the University of Minnesota and is a designated regional center for trauma and burns. This 8-member section is fully equipped with state-of-the-art facilities for ultrasonography, CT, and MRI. A general radiologist with well-rounded skills in all modalities is sought. Research will be encouraged but not required. There will be an affiliate faculty appointment with the University of Minnesota. Rank and salary will depend on past scholarly activity and post-M.D. experience. Applicants must be able to obtain a license to practice medicine in the state of Minnesota before the appointment date, which is negotiable. Applications will be accepted through June 15, 1991. Send letters to David L. Swanson, M.D., Interim Chair, Dept. of Medical Imaging, St. Paul-Ramsey Medical Center, 640 Jackson St., St. Paul, MN 55101-2595. The University of Minnesota and St. Paul-Ramsey Medical Center are equal opportunity educators and employers. 5a

CHIEF OF RADIOLOGY—This is a non-tenure track position available at the rank of assistant, associate, or full professor. St. Paul-Ramsey Medical Center, a major affiliate hospital of the University of Minnesota, is seeking a well-qualified individual to head the Section of Radiology. This acute-care, 275-bed hospital is 1 of the primary teaching institutions of the University of Minnesota and is a designated regional center for trauma and burns. This 9-member section is fully equipped with state-of-the-art facilities for ultrasonography, CT, and MRI. The successful candidate for this position will have well-developed administrative and managerial skills and an unequivocal commitment to patient care, education, and collaborative interaction with other hospital depts. Development of a radiology residency program in conjunction with the University of Minnesota is seen as a highly desirable near-term goal. Research will be encouraged. Faculty rank and salary depend on past scholarly productivity and post-M.D. experience. Applicants must be able to obtain a license to practice medicine in the state of Minnesota before the appointment date, which is negotiable. Applications will be accepted through July 1, 1991. Send letters to John J. Marini, M.D., Chair, Radiology Search Committee, St. Paul-Ramsey Medical Center, Division of Pulmonary Medicine, 640 Jackson St., St. Paul, MN 55101-2595. The University of Minnesota is an equal opportunity educator and employer. 5a

BC/BE RADIOLOGIST, SOUTHEASTERN MICHIGAN—Seven radiologists covering a 350-bed community hospital with a new women's center seek a radiologist with a fellowship in ultrasound and special interest in OB ultrasound. Practice involves all aspects of imaging modalities including MRI. Competitive compensation package leading to partnership. Send inquiries and a CV with references to Bhaskar U. Shenai, M.D., Professional X-Ray Center, 67 Cass Ave., Mt. Clemens, MI 48043. 5-7ap

RADIOLOGIST/PULMONARY RADIOLOGY

The Dept. of Radiology at the University of Minnesota has a full-time position available in the pulmonary radiology section at the rank of tenure-track assistant professor as soon as possible. Minimum requirements are board certification in radiology, 1 yr postresidency specialty training or experience in pulmonary radiology, and a demonstrated involvement in quality research accepted or published in peer-reviewed journals. Responsibilities will include all facets of pulmonary radiology as well as graduate and undergraduate medical instruction. Research performance will be strongly encouraged and evaluated. Salary is negotiable and competitive, and is dependent on past scholarly productivity and post-M.D. experience. Applicants must be licensed or able to obtain a license to practice medicine in the state of Minnesota before appointment date. Applications will be accepted through June 15, 1991. Send letters to Marvin Goldberg, M.D., Associate Professor, Dept. of Radiology, Box 292 UMHC, University of Minnesota, 420 Delaware St., S.E., Minneapolis, MN 55455. The University of Minnesota is an equal opportunity educator and employer. 5a

INTERVENTIONAL RADIOLOGIST—The Hospital of the University of Pennsylvania is seeking an interventional radiologist to serve as assistant professor of radiology in the School of Medicine of the University of Pennsylvania. The angiography/interventional radiology section includes 3 other staff angiographers, 4 fellows, and 1 or 2 rotating residents. This is an extremely busy clinical practice involving the entire spectrum of angiographic and interventional procedures. Strong academic and research interests are a major requirement for this position. Send inquiries to Constantin Cope, M.D., Dept. of Radiology, Hospital of the University of Pennsylvania, 3400 Spruce St., Philadelphia, PA 19104. The University of Pennsylvania is an equal opportunity employer. 5a

DIAGNOSTIC RADIOLOGIST/PARTNERSHIP POTENTIAL—Well-established, multioffice practice offers an outstanding opportunity for growth to a BC/BE radiologist. Procedures include standard radiography and fluoroscopy, mammography, nuclear medicine, and ultrasound. IVF-associated procedures are a key specialty. Large referral base. Physician has 25+ yr experience and needs to share the burden of a still-expanding practice. Collateral earnings potential by reading for other medical groups with imaging capability. We are located in the Boston area near major roadways; you can live in any of Boston's beautiful suburbs. First-class equipment and excellent technologists will support your efforts. Please send your current CV and a cover letter to Box L21, AJR (see address this section). 5-7a

FLORIDA, STAFF RADIOLOGIST—Opportunity for board-certified/eligible diagnostic radiologist, with experience in reading plain films, fluoroscopy, ultrasound, CT, nuclear medicine, and some angiography, in the radiology service at this Dept. of Veterans Affairs (VA) Medical Center. Affiliation in surgery with the University of Florida. Excellent employment benefits including 30 days paid vacation and 15 days paid sick leave per yr; liberal life and health insurance benefits; malpractice insurance; and retirement program. Moving expenses paid. Lake City, FL, is located in northern Florida with a mild climate yr round. Extensive outdoor recreational activities, reasonable cost of living, no state income tax, fine schools, local community college, and nearby universities provide opportunities for continuing education and cultural diversion. Licensure in any state acceptable. Contact or send CV to Richard Parker, M.D., Chief of Radiology, VA Medical Center, Lake City, FL 32055-5898; (904) 755-3016, ext. 2543. An equal opportunity employer. 5a

THE MEDICAL COLLEGE OF PENNSYLVANIA

is seeking a faculty member in vascular/interventional radiology at the associate/assistant professor level. The hospital is a 400-bed teaching facility. There are 3 interventional rooms including a new Toshiba biplane, C-arm, and biplane digital unit; a GE biplane unit with digital capabilities; and a new GE R-F room with digital fluoroscopy. Individual should have a fellowship and/or extensive clinical experience in the field. Salary is commensurate with experience and is very competitive. Responsibilities include clinical duties, supervision of residents, teaching of medical students, and research activities. Applications should be sent to George L. Popky, M.D., Professor and Chairman, Dept. of Radiologic Sciences, The Medical College of Pennsylvania, 3300 Henry Ave., Philadelphia, PA 19129. The Medical College of Pennsylvania is an equal opportunity employer. 5a

NUCLEAR MEDICINE—The UCLA Dept. of Radiological Sciences is seeking a board-certified radiologist in nuclear medicine and/or radiology at the assistant professor level with extensive experience in positron emission tomography and related imaging methods. Added experience in imaging processing and mathematical modeling is desirable. Send application, CV, and names and addresses of 3 references or inquiries to Hooshang Kangarloo, M.D., Chairman, Dept. of Radiological Sciences, UCLA Medical Center, Los Angeles, CA 90024-1721. An EO/AE employer. 5-7a

IMMEDIATE OPENING—BC diagnostic radiologist, imaging fellowship preferred, with experience in general radiology and expertise in interventional procedures and angiography, sought to join a group of 4 active, university-trained radiologists. Modern, 220-bed hospital in south suburb of Chicago with active ER and outpatient services. State-of-the-art equipment includes MRI, CT, ultrasound, nuclear medicine, and mammography. Attractive and competitive benefits package leading to early partnership. Contact John M. Nayden, M.D., South Suburban Hospital, 17800 S. Kedzie Ave., Hazel Crest, IL 60429; (708) 799-8010, ext. 3276. 5-7a

VETERANS AFFAIRS MEDICAL CENTER, AUGUSTA, GA, is seeking a physician, board-eligible/certified in radiology. Subspecialty interest in chest, skeletal, GI, or interventional radiology is desirable, but not essential. This 1142-bed, tertiary-care medical center is affiliated with the Medical College of Georgia. Faculty appointment commensurate with qualifications and experience. Augusta enjoys a moderate climate, reasonable cost of living, numerous recreational facilities, and institutions of higher learning. An equal opportunity employer. For additional information, contact George T. Jamarik, M.D., Chief, Radiology Service at (404) 823-2236. 5a

DENVER, CO—The University of Colorado Health Sciences Center, Dept. of Radiology, Denver, CO, is continuing its expansion and is recruiting for full-time academic faculty positions in skeletal radiology, chest radiology, mammography, and general radiology. The level of faculty appointment will depend on the applicant's previous relevant experience. Applicants should demonstrate devotion to patient care, dedication to teaching, and interest in independent or collaborative research. Candidates interested in working in a stimulating academic and exciting clinical environment are encouraged to send their CV to Michael L. Manco-Johnson, M.D., Professor and Chairman, Dept. of Radiology, Box C277, University of Colorado Health Sciences Center, 4200 E. 9th Ave., Denver, CO 80262; (303) 270-7719. The University of Colorado Health Sciences Center is committed to equal opportunity and affirmative action. 5-6a

MAMMOGRAPHY, UNIVERSITY OF PENNSYLVANIA, HALF- OR FULL-TIME POSITION

Exceptional opportunity in academic mammography within a high-volume, rapidly expanding, breast imaging section. Ongoing screening and problem-solving mammography, breast ultrasound, and collaborative projects. Academic rank and salary commensurate with credentials. Resident and student teaching responsibilities along with negotiable participation in bone and chest outpatient radiology. Position available immediately. Applicant must be ABR-certified and able to obtain license in Pennsylvania. U of P is an affirmative action, equal opportunity employer, and specifically encourages applications from women and minorities. Send letter and CV to Rosalind H. Troupin, M.D., Dept. of Radiology, H.U.P., 3400 Spruce St., Philadelphia, PA 19104. 5-7a

DIAGNOSTIC RADIOLOGIST—BC/BE with expertise in general radiology including CT and ultrasound sought for 85-physician, multispecialty group practice in southern California community. Close to the ocean, with easy access to city and recreational areas, and excellent schools. Contact David B. Luce, M.D., Medical Director, Bay Shores Medical Group, Inc., 3625 Del Amo Blvd., Ste. #270, Torrance, CA 90503; (213) 371-6551. 5-6a

LOCUMS NATIONWIDE—BC or BE diagnostic radiologists needed for nationwide locums. Opportunities range from 1 wk to several mo. Exceptional compensation and all travel expenses. Call Professional Temporary Services, Inc., 790 Cardinal Rd., P.O. Box 2702, New Bern, NC 28561; (800) 872-4534. 5-8a

NEURORADIOLOGIST—The University of Louisville, Dept. of Diagnostic Radiology, is seeking a BC/BE diagnostic radiologist to fill a full-time faculty position as chief of neuroradiology. The candidate must have had additional training in neuroradiology and be willing to participate in undergraduate and graduate teaching and in research activities. This is a fine opportunity in a growing and busy dept. with excellent equipment. Tenure- and non-tenure-track appointments available; academic rank commensurate with training and experience; and compensation negotiable and competitive. Send inquiries with CV and 3 references to Hollis A. Thomas, M.D., Professor and Chairman, Dept. of Diagnostic Radiology, Humana Hospital-University of Louisville, 530 S. Jackson St., Louisville, KY 40202. The University of Louisville is an equal opportunity/affirmative action employer and encourages women and minority candidates to apply. 5-6a

THE UNIVERSITY OF MASSACHUSETTS MEDICAL CENTER, a tertiary-care hospital situated 40 mi. from Boston, is seeking a third pediatric radiologist. The pediatric dept. services central and eastern Massachusetts as well as southern New Hampshire and northern Connecticut. All medical and surgical pediatric subspecialties are represented and a broad range of pediatric pathology is encountered. Pediatric radiologists have the primary responsibility in ultrasound, CT, MRI, and interventional procedures in general radiologic exams. Competitive salaries and generous benefits are provided. For further information, contact Paul K. Kleinman, M.D., Dept. of Radiology, University of Massachusetts Medical Center, 55 Lake Ave., N., Worcester, MA 01655; (508) 856-3124, fax (508) 856-4669. 5xa

DIAGNOSTIC RADIOLOGIST—Immediate opening leading to partnership in expanding, 4-member, hospital-based practice near Boston. Seeking recently trained BC/BE radiologist with skills and experience in general radiology, ultrasound, mammography, CT, and angio/interventional. Interested persons should contact Steven Sitzman, M.D., The Malden Hospital, One Hospital Rd., Malden, MA 02148; (617) 322-7560. 5-7ap

BC RADIOLOGIST sought for growing Washington, DC/Baltimore, MD, area. Established, 4-person radiology group is extending an excellent opportunity for a full-time radiologist with a fellowship or expertise in MRI. Experience in CT, ultrasound, and mammography necessary. Busy, 150-bed, growing hospital; private-office practice; and new free-standing MRI facility. Salary leading to partnership. Reply with CV to Paul S. Zimmons, M.D., Greater Laurel Beltsville Hospital, 7100 Contee Rd., Laurel, MD 20707; (301) 953-2655. 5ap

PRACTICE OPPORTUNITY IN FAST-GROWING LAS VEGAS, NV—Expanding, 6-member radiology group is seeking 2 additional BE/BC radiologists for July 1991 and Jan. 1992. We currently serve 2 hospitals with an outpatient imaging center to open in Jan. 1992. Outstanding salary and benefits package leading to full partnership in 2 yr. Send CV or contact Marc Pomerantz, M.D., Head of Search Committee, 1925 Spode Ave., Henderson, NV 89014; (702) 388-4640. 5-9ap

POSITION AVAILABLE IN MIDATLANTIC SMALL TOWN WITH COUNTRY LIVING, progressive medical community, easy access to major metropolitan regions, and a university hospital. Unique, diverse, academically oriented MR, CT, and conventional radiology practice that leaves time for family, reflection, or other interests. Direct an independent CT facility, read MR images at same site, and read conventional radiographs nearby if desired. Night call minimal. Compensation flexible and negotiable. Share duties with 2 other physicians. Write Box L25, AJR (see address this section). 5-6ap

BC/BE RADIOLOGIST—Full-time staff radiologist sought for active, tertiary-care medical center. Duties include interpreting general diagnostic films (excluding mammography), performing radiologic procedures and fluoroscopy, and supervising and training residents with affiliated medical center. Additional subspecialty skills or training in ultrasound/CT, and/or angiography and interventional procedures are beneficial. Candidate should be qualified to hold a faculty position with Yale University School of Medicine, and must be a U.S. citizen or qualify as a permanent resident of the United States. CV and letters of reference should be sent to Caroline Taylor, M.D., Chief, Radiology, Dept. of Veterans Affairs Medical Center, West Haven, CT 06516. The DVA Medical Center and Yale University are equal opportunity/affirmative action employers. Applications from women and minority group members are encouraged. Application deadline is Aug. 1, 1991. 5-7a

GENERAL DIAGNOSTIC RADIOLOGIST for northern New Jersey hospital and practice. Position to include general radiology with basic angiography and interventional procedures with competence in MRI. Must be board-eligible/certified. Excellent salary and benefits leading to partnership. Board certification required for partnership. Inquiries and CVs may be sent to Arthur Siegel, M.D., Passaic Radiology Associates, P.A., 1031 McBride Ave., Ste. D-210, West Paterson, NJ 07424. 5ap

IMAGING RADIOLOGIST—Join the current staff of 5 imaging radiologists (MR/CT/ultrasound) at William Beaumont Hospital, a modern, tertiary-care medical center in southeastern Michigan with residency and fellowship programs in diagnostic radiology. The dept. is expanding its state-of-the-art facilities to accommodate increasing demands on patient care. Area offers 1 of the best educational and recreational facilities. Excellent compensation. Write to Jalil Farah, M.D., Chairman, Diagnostic Radiology, William Beaumont Hospital, 3601 W. 13 Mile Rd., Royal Oak, MI 48073. 5-7a

DIAGNOSTIC RADIOLOGISTS—The Graduate Hospital has 2 openings for BC/BE radiologists with subspecialty training or substantial experience in neuroradiology and body imaging, respectively. The successful applicants will join a group of 13 radiologists, all with subspecialty expertise. The group is based in a modern, very well equipped, 320-bed teaching hospital in center city Philadelphia that is affiliated with the University of Pennsylvania School of Medicine. Send inquiries to Jerome G. Jacobstein, M.D., Dept of Radiology, The Graduate Hospital, Philadelphia, PA 19146; (215) 893-2050. 5ap

DIAGNOSTIC RADIOLOGIST needed before July 1991 to share slot in five-person radiology group. New associate works half-time in 1 to 4-wk blocks, 4-8 mo/yr. Desirable North Carolina location. Send reimbursement requirements and CV to Box L23, AJR (see address this section). 5ap

PROFESSOR AND CHAIR, DEPT. OF DIAGNOSTIC RADIOLOGY, University of Kentucky, College of Medicine, A. B. Chandler Medical Center, Lexington, KY. Nominations and applications are invited for the position of professor and chairman of the Dept. of Diagnostic Radiology at the University of Kentucky College of Medicine. The dept. is composed of the divisions of general diagnosis, special procedures, and nuclear medicine. A new world-class MRI and spectroscopy center (MRISC) will open the summer of 1991. The dept. serves a 465-bed, university, tertiary-care hospital. The dept. currently occupies 24,000 sq. ft. of space (not including the new MRISC and nuclear medicine). There are 19 full-time faculty with 16 diagnostic radiology residents plus 4 5-yr. combined nuclear medicine and diagnostic radiology residents. We are seeking a candidate with an outstanding record of achievement in academic radiology with administrative experience and a proven record of scientific excellence. Candidates should submit a CV and the names of references to Frank C. Miller, M.D., Chairman, Search Committee for Chairmanship of Diagnostic Radiology, University of Kentucky, Chandler Medical Center, 800 Rose St., MN 318, Lexington, KY 40536-0084. The University of Kentucky is located in Lexington, KY, in the heart of the beautiful bluegrass region. The University of Kentucky is an affirmative action, equal opportunity employer, and actively seeks the candidacy of minorities and women. 5a

STAFF RADIOLOGIST—Miami Veterans Affairs Medical Center is seeking 1 full-time and 1 part-time staff radiologist for its teaching hospital affiliated with the University of Miami Medical School. Candidates must be board-eligible or certified. Interested physicians should send CV and list of references to Personnel Service (05C3/Jean Little), Veterans Affairs Medical Center, 1201 N.W. 16 St., Miami, FL 33125; (305) 324-4455, ext. 3617. Equal opportunity employer. 5-6a

TEN-PERSON RADIOLOGY GROUP located in Corpus Christi is seeking a new associate to start July 1990 or as late as July 1991. Must be board-certified or eligible. Will perform all diagnostic studies, including interventional, CT, MRI, nuclear medicine, and ultrasound. Please send CV to Search Committee, P.O. Box 5608, Corpus Christi, TX 78465-5608. 5xa

BROAD SPECTRUM RADIOLOGIST/UPSTATE NEW YORK—Radiologist wanted for hospital-based practice 90 mi. northwest of New York City. Excellent recreational activities and easy access to metropolis. All modalities available. Excellent salary and benefits leading to early partnership. Immediate availability, but can wait for right applicant. Call G. Bilick; (914) 794-3300, ext. 2216 or send CV to P.O. Box 144, Harris, NY 12742. 3-6ap

THE DEPT. OF RADIOLOGY AT TRIPLEX ARMY MEDICAL CENTER, HONOLULU, HI, is recruiting academic radiologists for several divisions of the dept. including ultrasound, chest, skeletal, neuro, and general diagnostic radiology. Our dept. offers a fully accredited residency program with 20 residents and 16 attending full-time staff. Numerous consultants from across the country lecture on a continuing and regular basis. The hospital is a modern, tertiary-care center serving Hawaii and the entire Pacific Basin. A strong residency program, diverse and interesting patient population, excellent equipment, and a tropical lifestyle are positive aspects of the practice. Academic credentials and/or experience are necessary. Recently graduated fellows are encouraged to apply. Board certification is mandatory. Candidates should be particularly interested in patient care, teaching, and research. Salary and benefits are competitive and generous. Triplex is an EO/EEO employer. Please contact Mark F. Hansen, M.D., Col., MC, Chief, Dept. of Radiology, TAMC, HI 96859-5000; (808) 433-6393. 8-7a

FULL/PART-TIME BC/BE RADIOLOGIST wanted for 187-bed GM&S VA Medical Center. Excellent GE equipment, duplex Doppler ultrasound, diagnostic, and fluoroscopic. CT interpretation desirable. 18,000 procedures/yr. State university city amid hills and lakes in northwest Arkansas with cultural and recreational attractions. Competitive salary and excellent benefits/retirement. Call chief of staff; (501) 444-5050. 5xa

GOOD LIFE, GOOD MONEY—Radiologist needed for growing practice that covers 2 hospitals as well as 2 free-standing clinics. Modalities include R&F, general, mammography, CT, MRI, nuclear medicine, SPECT, and special procedures. Denton, population 60,000, located 30 mi. north of Dallas/Fort Worth, has 2 recreational lakes within 15 mi. and 2 major universities. Attractive financial and benefit packages with early partnership are offered. Contact Family Radiology with CV at 1614 Scripture, Ste. 2, Denton, TX 76201; (817) 387-6159. 5-6a

DIAGNOSTIC RADIOLOGIST—Due to the recent merger of residency programs with St. Luke's Hospital and Truman Medical Center, UMKC, School of Medicine, we are expanding the number of staff positions at the academic rank of assistant or associate professor level. The dept. currently performs 87,000 exams/yr. Strong teaching background required. Compensation commensurate with qualifications and experience. Send letter of interest and CV to Fong Tsai, M.D., Professor and Chairman, University of Missouri-Kansas City, Radiology Dept., 2301 Holmes, Kansas City, MO 64108. 4-6ap

DIAGNOSTIC RADIOLOGIST, IMMEDIATE OPENING—Ten-person radiology group seeks a diagnostic radiologist with fellowship training, including body MRI/body imaging, to join a busy, hospital-based practice located in rapidly growing north Dallas. GE 1.5-T magnet, Toshiba midfield magnet, 2 GE 9800 scanners, Acuson 128 with color flow Doppler, and new special procedures suite with DSA. Please send CV to Box K54, AJR (see address this section). 5xa

UTMB, GALVESTON, TX—The Dept. of Radiology of the University of Texas Medical Branch in Galveston has openings for persons trained and experienced in ultrasonography and mammography. The opportunity for academic advancement is great and benefits are generous. Salaries are competitive and living conditions are desirable. Interested persons should contact Melvyn H. Schreiber, M.D., Chairman, Dept. of Radiology, UTMB, Galveston, TX 77550; (409) 761-1823. UTMB is an equal opportunity M/F/H/V affirmative action employer. UTMB hires only individuals authorized to work in the United States. 4-9a

IMMEDIATE OPENINGS, CHARLOTTE, NC— Service-oriented, 7-member group seeks 2 new associates in CT/ultrasound/MR and nuclear medicine. Fellowship training and/or staff level experience required. Must be willing to participate in all phases of general diagnostic radiology practice. Interventional experience helpful but not required. We serve 2 hospitals with a total of 260 beds. Equipment includes 3 GE 9800 CT, GE Signa 1.5-T MRI, Acuson and Toshiba ultrasound with color Doppler, 3 Toshiba SPECT, and Siemens 750 ZLC. Competitive salary leading to partnership after 2 yr. Send CV to Carl J. Eisenberg, M.D., Mercy Hospital, 2001 Vail Ave., Charlotte, NC 28105; (704) 379-5860. 3-5ap

RADIOLOGIST—Large, private-practice group in upstate New York seeks board-certified radiologist with general interests and preferably with fellowship training. Practice includes mix of private and teaching hospitals, offices, urban and rural settings. All modalities including 3 MRI units. This is an extremely high-quality practice offering excellent benefits and an opportunity for long-term security through shareholder status. Send CV to Box K50, AJR (see address this section). 4-6a

RADIOLOGIST—The Elko Regional Medical Center seeks a board-certified/eligible diagnostic radiologist to work at the medical center as well as the local community hospital. CT, mammography, ultrasound, nuclear medicine, and some interventional training or experience required. Guaranteed salary for 6 mo leading to full partnership. Excellent benefit package including malpractice insurance. Elko is a thriving community surrounded by mountains and wilderness areas. Recreation yr round. Please send CV to Cherie Atwood, Administrator, Elko Regional Medical Center, 762 14th St., Elko, NV 89801; (702) 738-3111. 4-6ap

SENIOR FACULTY POSITION IN GI/GU RADIOLOGY—Dartmouth-Hitchcock Medical Center is seeking a senior faculty member at the associate or full professor level with experience and interest in GI/GU radiology. Clinical responsibility will be in an entirely new, 400-bed, clinical facility opening Sept. 1991, with state-of-the-art instrumentation. Position will involve responsibility for residency training in GI/GU area. Proven record of academic performance including research and teaching with an interest in providing academic guidance for energetic staff of younger radiologists necessary. Interested candidates write with CV to P. K. Spiegel, M.D., Chairman, Dept. of Diagnostic Radiology, Dartmouth-Hitchcock Medical Center, Hanover, NH 03756. AA/EOE. 5xa

CHEST RADIOLOGIST, THOMAS JEFFERSON UNIVERSITY HOSPITAL—The Dept. of Radiology at Jefferson has an opening for a thoracic radiologist at either the junior or senior level. The position encompasses plain film radiography, CT, and percutaneous thoracic interventions. Involvement in mammography, other general diagnostic areas, and ultrasound can also be incorporated, depending on the interests of the candidate. Dedicated, nonclinical research time is provided, and the dept. has excellent research facilities and support. Our chest radiology practice is expanding rapidly and close working relationships are maintained with pulmonary medicine and thoracic surgery. Teaching is also emphasized, with a large residency program and a thoracic radiology fellowship. Excellent faculty income and benefits. This is a fine opportunity for a radiologist with academic interests to join a dynamic and rapidly growing dept. Interested candidates should contact David C. Levin, M.D., Chairman, Dept. of Radiology, Thomas Jefferson University Hospital, Philadelphia, PA 19107; (215) 955-7264. Jefferson is an equal opportunity/affirmative action employer. 4-6a

CHIEF OF DIAGNOSTIC RADIOLOGY—The Louis A. Weiss Memorial Hospital is a 275-bed, expanding affiliate of The University of Chicago that performs approximately 65,000 radiologic exams/yr. Applicants should have broad experience in general diagnostic radiology and administrative skills. An interest in teaching or research would be advantageous. The successful applicant will be appointed to the faculty at The University of Chicago. Academic rank and compensation commensurate with experience. Candidate should be board-certified and licensed to practice in Illinois. Interested parties should send their CVs to Heber MacMahon, M.D., Chairman, Weiss Search Committee, Dept. of Radiology, The University of Chicago, 5841 S. Maryland, Box 429, Chicago, IL 60637; (312) 702-1604, fax (312) 702-1161. Affirmative action/equal opportunity employer. 4-6ap

RADIOLOGIST—Faculty position for ABR- or FRCP-qualified radiologist at assistant- or associate-member level in the Diagnostic Imaging Dept., St. Jude Children's Hospital, Memphis, TN. Growing, well-equipped dept. includes ultrasound, CT, nuclear radiology, MR imaging, and spectroscopy. Position provides excellent opportunities for clinical research in oncologic imaging. Candidate may also receive faculty appointment at University of Tennessee. Interested parties should contact Barry D. Fletcher, M.D., Chairman, Dept. of Diagnostic Imaging, St. Jude Children's Research Hospital, Memphis, TN 38101. Affirmative action/equal opportunity employer. 4-5ap

ANGIOGRAPHER/INTERVENTIONAL RADIOLOGIST, TOLEDO, OH—Quality-oriented, 22-radiologist group is seeking a board-certified, university-trained radiologist with angiography/interventional fellowship experience. Group covers 850-bed tertiary hospital, 350-bed suburban hospital, 3 outpatient offices, and performs 240,000 exams/yr. Position leads to equal partnership and combines excellent salary with very generous vacation time. All practice locations within 15 min of each other and are situated in an area of superb, family-oriented living with excellent schools. Send CV to Drs. David Parker or Keith Wilson, Roemer Bldg., 3912 Sunforest Ct., Toledo, OH 43623; (419) 471-4438 days. 4-6ap

DALLAS, TX—A 12-member, subspecialty group seeks a board-certified, general radiologist for an immediate opening. Fellowship training preferred, but will consider qualified individual with special expertise. CT/ultrasound, MRI, nuclear medicine, or angiography background particularly helpful. All imaging modalities available (state-of-the-art CT, angi, ultrasound, R & F, SPECT nuclear medicine, and MRI center). Salary and bonuses are excellent. Health and malpractice paid. No buy-in to partnership. Send CV to H. Stuart Peake, M.D., P.O. Box 814129, Dallas, TX 75381; (214) 888-7055. 4-9ap

IMMEDIATE OPENING FOR BC/BE GENERAL RADIOLOGIST with experience in interventional and vascular radiology. Join a group of 4 radiologists in a 160-bed hospital located in Allentown, PA, about 60 mi. northwest of Philadelphia. The daily practice includes all aspects of general radiology, CT, ultrasound, and nuclear medicine. Please call or send CV to Asad Shohadai, M.D., Allentown Osteopathic Medical Center, 1736 Hamilton St., Allentown, PA 18104; (215) 770-8700. 5xa

COLORADO MOUNTAINS—Opportunity for BC/BE radiologist in part-time, solo practice available July 1991. Gunnison has abundant outdoor activities including water sports and excellent downhill skiing. Four yr college in town. Hospital-based or private practice available. Contact Robert Austin, Gunnison Valley Hospital, 214 E. Denver, Gunnison, CO 81230; (303) 641-1456. 4-5a

RADIOLOGISTS—A 4-member, rapidly growing practice in McAllen, TX needs 2 general, BC/BE radiologists. Hospital-based practice plus imaging center with 1.5-T GE MRI, 9800 GE CT, Sophy SPECT camera, color Doppler ultrasound, mammography, and fluoroscopy. Early partnership, excellent salary/opportunity. Contact William Martin, M.D.; (512) 682-0888. 4-6ap

VASCULAR/INTERVENTIONAL RADIOLOGIST The University of Miami, School of Medicine, is currently recruiting a full-time vascular and interventional radiologist. The Interventional Section provides radiologic services at Jackson Memorial Medical Center and Veterans Administration Medical Center. About 3000 exams per yr are performed by this section, including all diagnostic and interventional vascular procedures except for cardiac and neuroradiologic studies. We also have an active nonvascular interventional service involving thoracic and abdominal intervention. The section currently consists of 5 staff members and 3 fellows. Residents rotate through the service on a monthly basis. Candidates must be board-certified or eligible, with fellowship training or equivalent experience. Rank and salary commensurate with qualifications. Please send CV to Jose M. Yrizarry, M.D., Chief, Vascular/Interventional Radiology Section, University of Miami School of Medicine, Dept. of Radiology (R-109), P.O. Box 016960, Miami, FL 33101; (305) 549-6894. The University is an affirmative action/equal opportunity employer. 4-5ap

MUSCULOSKELETAL RADIOLOGIST, MALLINCKRODT INSTITUTE OF RADIOLOGY/WASHINGTON UNIVERSITY—The musculoskeletal section is enlarging and has need for an additional person at the instructor, assistant professor, or associate professor level. The section performs all aspects of musculoskeletal imaging including CT, MRI, bone biopsy, and arthrography of all joints. The section also performs all diagnostic and screening mammography and breast procedures and directs emergency dept. radiology. The volume of clinical material is large. Teaching, academic, and working conditions are well-supported. Send CV to Louis A. Gilula, M.D., or William A. Murphy, M.D., Mallinckrodt Institute of Radiology, Barnes Hospital, 510 S. Kingshighway Blvd., St. Louis, MO 63110. 3-6a

RADIOLOGIST, CAPITOL DISTRICT, NEW YORK STATE—Well-established, hospital-based group practice in upstate New York seeks a board-certified, general diagnostic radiologist with special competence and interest in nuclear medicine and MRI. Angiography and interventional experience will be helpful. This will be an additional opening to a 5-person group currently performing all aspects of radiology. Salary first yr leading to full partnership. Please send CV to John J. Gorman, M.D., Dept. of Medical Imaging, St. Clare's Hospital, 600 McClellan St., Schenectady, NY 12304; (518) 382-2310. 4-7ap

HEAD, CROSS-SECTIONAL IMAGING SECTION The Dept. of Radiology, University of Rochester Medical Center, Strong Memorial Hospital, Rochester, NY, is seeking a board-certified radiologist with subspecialty experience in body imaging for a faculty position as Head of Cross-Sectional Imaging Section, including ultrasound, CT, MRI, and body interventional. Strong Memorial Hospital is a 750-bed, tertiary-care hospital. State-of-the-art MRI, CT, and ultrasound equipment is available. Teaching of medical students, radiology residents, and fellows and the opportunity for developing research projects are afforded. Rank and salary are commensurate with experience. Interested candidates should forward CV to Robert E. O'Mara, M.D., Chair, Dept. of Radiology, Box 648, University of Rochester Medical Center, Rochester, NY 14642; (716) 275-2733. EO/AA/M-F employer. 3-6ap

DIAGNOSTIC RADIOLOGIST needed in Conway Hospital, a community hospital located 10 mi. west of the resort/seaside community of Myrtle Beach, SC. The dept. performs 44,000 exams/yr including CT, MRI, nuclear medicine, ultrasound, mammography, and special procedures. All exams are done on state-of-the-art equipment. Our 3-person group offers a very strong financial package with all benefits including 17-wk vacation. Lovely, rapidly growing resort area includes 60 mi. of sandy beaches, 70 golf courses, and beautiful seaside homes. Contact Gary Rike, M.D., P.O. Box 917, Conway, SC 29526; (803) 347-7277. 12-5ap

DIAGNOSTIC RADIOLOGIST, PART-TIME, TUCSON, AZ—Radiologist to join 24-person group on approximately 1/2-time basis with 1-yr renewable contract. No night or weekend call, work every other Saturday a.m. Includes health, life, disability, and malpractice insurance. General diagnosis, mammography, CT, and ultrasound. Contact R. O. Broome, M.D., Radiology, Ltd., 6516 E. Carondelet Dr., Bldg. C, Tucson, AZ 85710. 3-5ap

NO-CALL RADIOLOGIST FOR SOUTHERN CALIFORNIA BEACHES—Position is now available with premier, 21-member group to help staff a growing number of outpatient facilities. Fellowship training in mammography/ultrasound is required. The group operates 5 Acuson imagers and 8 dedicated mammography units. Please send CV to Robert Hurwitz, M.D., 355 Placentia Ave., Ste. 207, Newport Beach, CA 92663. For faster reply, please call our dept. secretary, Denise, at (714) 645-9500. 4-6ap

FACULTY OPENING IN THORACIC IMAGING The Johns Hopkins University Hospital has an opening at the junior faculty level in the Division of Thoracic Imaging. The division is fully integrated across all modalities including MRI, CT, and interventional procedures. Research opportunities are exceptional with protected research time available to rapidly establish an academic career. Academic rank and salaries will be determined by previous experience. The candidate must be board-certified. Contact Elias A. Zerhouni, M.D., Director, Thoracic Imaging & MRI Divisions, Dept. of Radiology, Johns Hopkins Hospital, Baltimore, MD 21205; (301) 955-4062. 1-6a

CROSS-SECTIONAL IMAGING/MRI, CT, ULTRASOUND—The Dept. of Radiology, Strong Memorial Hospital, University of Rochester, Rochester, NY, is seeking a board-eligible/certified radiologist for its body imaging section. An appointment as assistant professor or higher is available at a level appropriate to experience. One yr fellowship training or equivalent experience is required. Research and teaching opportunities are afforded in a strong academic dept. with state-of-the-art radiologic equipment. Send letter of inquiry to Robert E. O'Mara, M.D., Chair, Dept. of Radiology, Box 648, University of Rochester Medical Center, Rochester, NY 14642; (716) 275-2733. EO/A/A-M/F employer. 3-6ap

OREGON—Group of 13 radiologists in Salem, OR, seeks BC/BE radiologist with general radiology skills. Practice includes 454-bed community hospital, large out-patient office, and multispecialty clinic. Near ideal family community and recreational amenities. Send CV to John Eyre, M.D., Salem Radiology, 919 Oak St., S.E., Salem, OR 97301. 2-5ap

NEURORADIOLOGIST, BIG SKY COUNTRY—Group of 5 radiologists seek a BC, fellowship-trained colleague. Hospital and busy clinical practice. Must be a capable, general diagnostic radiologist. One yr to partnership. Send letter/CV to Bruce Pinkerton, M.D., Dept. of Diagnostic Radiology, Deaconess Medical Center, P.O. Box 2547, Billings, MT 59103. 2-7ap

DUKE UNIVERSITY MEDICAL CENTER/STAFF RADIOLOGISTS

Duke University Medical Center is seeking qualified candidates for staff positions in the Dept. of Diagnostic Radiology. A limited number of staff positions currently are available in the following sections: general diagnostic, pediatric, chest, vascular/interventional, and musculoskeletal radiology. We offer an excellent salary and benefits package. The radiology dept. is state-of-the-art in diagnostic imaging with diverse resources available for clinical, teaching, and academic pursuits. Staff members have guaranteed academic time and research support. Interested board-certified radiologists with appropriate experience should phone Robert Vandemark, M.D. at (919) 681-2711 ext. 5233, for additional information. Letters of inquiry should be sent to Carl E. Ravin, M.D., Dept. of Radiology, Box 3808, Duke University Medical Center, Erwin Rd., Durham, NC 27710. AA/EOE. 2-7a

MAMMOGRAPHY FACULTY POSITION—The Dept. of Radiology at Johns Hopkins University Hospital has a faculty position available in mammography. The mammography section is part of the thoracic imaging division. The section offers a strong potential for academic growth with emphasis on original research and teaching. Protected academic time is available for candidates interested in developing a strong academic career. Support, resources, and opportunities are available for creative research. The candidate can also participate in all other aspects of diagnostic imaging as desired. Academic rank and salary will be determined by previous experience. Candidate must be board-certified. Contact Elias A. Zerhouni, M.D., Director, Thoracic Imaging and MRI Divisions, Dept. of Radiology, Johns Hopkins Hospital, Baltimore, MD 21205; (301) 955-4062. 1-6a

DIRECTOR, DIAGNOSTIC RADIOLOGY—Applications accepted for Director, Diagnostic Radiology, OHSU, Portland, OR. Faculty position opens on or about July 1, 1991. Associate or full professor based on experience. Musculoskeletal radiology fellowship, minimum of 5 yr as Vice-Chairman or Director of Diagnostic Radiology required. Send CV to William Weidner, M.D., Diagnostic Radiology, UHN-72, Oregon Health Sciences University, Portland, OR 97201-3098; (503) 494-4498. Equal opportunity, affirmative action employer. 3-6a

PEDIATRIC RADIOLOGIST—Division of Pediatric Radiology, OHSU, Portland, OR, invites applications for a faculty position available on or about July 1, 1991. Completion of approved fellowship in pediatric radiology and ABR certification required. Send CV to William Weidner, M.D., Diagnostic Radiology, UHN-72, Oregon Health Sciences University, Portland, OR 97201-3098; (503) 494-4498. Equal opportunity, affirmative action employer. 3-6a

RADIOLOGIST NEEDED with experience in CT, ultrasound, nuclear medicine, mammography, and general radiology to provide vacation coverage for 2 practices in rural western Montana. One practice requires some traveling. Position would be excellent for person who wishes to semiretire in a pleasant scenic area. Great opportunity for recreational activities. Send inquiries to Tyler H. Gill, M.D., 1200 Westwood Dr., Hamilton, MT 59840; (406) 363-2211. 2-6a

DIAGNOSTIC RADIOLOGIST, TEXAS—Progressive, well-diversified group (15 radiologists) has immediate opening for a BC/BE diagnostic radiologist with competence in a broad range of modalities. Additional consideration for fellowship. Excellent opportunity with excellent salary and benefits. Send CV with letter of inquiry to Will Gray, M.D., 1101 N. 19th St., Abilene, TX 79601. 3-5ap

COME TO CALIFORNIA WITH A LICENSE FROM ANY STATE

Loma Linda VA Hospital has a vacancy for a board-certified radiologist. A current license from any state is acceptable. Loma Linda is located 70 mi. east of Los Angeles near beaches, mountain ski resorts, and southland theme parks. This is a 500-bed, full-service hospital with a comprehensive diagnostic facility including ultrasound, CT, and MRI integrated with the Loma Linda University Medical Center residency training program. Opportunities exist to pursue clinical or academic interests. For additional information, contact Peter Dure-Smith, M.D., Chief, Radiology (114), Jerry L. Pettis Memorial Veterans Hospital, 11201 Benton St., Loma Linda, CA 92357; (714) 422-3069, fax (714) 422-4106. Equal opportunity employer. 3-8ap

SAN ANTONIO, TX—Group covering multiple hospitals and clinics seeks radiologists with imaging and angiography skills. Send CV to Search Committee, M & S X-Ray Associates, P.O. Box 15920, San Antonio, TX 78212-9510. 3-8ap

UCLA SCHOOL OF MEDICINE, CARDIOVASCULAR RADIOLOGIST—The UCLA Dept. of Radiological Sciences is recruiting for a full-time position in academic cardiovascular radiology. Title will be determined by level of training and experience. American Board of Radiology certification and eligibility for California licensure is required. Send detailed resume, including references, to Hooshang Kangarloo, M.D., Chair, Dept. of Radiological Sciences, UCLA School of Medicine, Los Angeles, CA 90024-1721. An equal opportunity/AA employer. 3-5a

Positions Desired

JULY 1991 RADIOLOGY RESIDENCY POSITION SOUGHT—Radiology resident currently in second yr of training seeks to transfer into the third yr of academic university program. Planning a career in academic radiology. Have training in all modalities and research experience in medical imaging. Excellent references. Send replies to Box L27, AJR (see address this section). 5bp

ASSISTANT PROFESSOR, DIRECTOR MRI CENTER—Significant experience in musculoskeletal and neuro MR (MR fellowship), interventional bone, and MR and bone teaching. Responsible for MR fellowship. Looking for academic position with clinical research, musculoskeletal MR and/or neuro MR, and/or interventional. Please reply to Box K52, AJR (see address this section). 4-5bp

Fellowships and Residencies

FELLOWSHIP IN BODY CT/MRI AND ULTRASOUND—The Dept. of Radiology of New York Medical College has 2 openings for a 1-yr imaging fellowship starting in July 1992. Westchester County Medical Center is a 650-bed, tertiary-care facility offering advanced training with state-of-the-art equipment. Equipment includes 2 Siemens Hi-Q CT scanners, GE Signa 1.5-T MR, ISG 3D reconstruction console, and 6 ultrasound imagers (Acuson and Diasonics). Applicants must have completed an approved residency in diagnostic radiology and must be board-eligible or certified. Please contact Andrew Schechter, M.D., Director, MRI, Dept. of Radiology, New York Medical College, Valhalla, NY 10595; (914) 285-8550. 5-6cp

FELLOWSHIPS IN PEDIATRIC RADIOLOGY AND PEDIATRIC NEURORADIOLOGY—The Dept. of Radiology, Children's Hospital Medical Center, Cincinnati, OH, offers 1- or 2-yr fellowships in pediatric radiology beginning July 1, 1993. A 1-yr pediatric neuroradiology fellowship program is also offered and may be taken separately or combined with 1 yr of adult neuroradiology fellowship at the University of Cincinnati Medical Center. Children's Hospital Medical Center (CHMC) is a 355-bed institution. The dept. performs over 105,000 radiologic exams annually in the largest children's hospital and ambulatory practice in the U.S. The dept. has 14 full-time faculty pediatric radiologists, 6 fellows, and many resident trainees. Five pediatric radiology and 1 pediatric neuroradiology fellowship positions are available annually. Training includes all aspects of pediatric imaging: neonatal radiology, neuroimaging, musculoskeletal radiology, cardiovascular and thoracic imaging, abdominal imaging, oncologic imaging, ultrasonography, nuclear medicine, CT, MRI, and vascular/interventional procedures. The dept. has an active clinical service with state-of-the-art equipment as follows: digital fluoroscopy; Acuson, Al, and ATL ultrasound units with Doppler and color flow Doppler capabilities; planar SPECT gamma cameras; GE 9800 Quick CT scanner; 1.5-T GE MRI with spectroscopy; and cardiac catheterization/angiographic suite with digital vascular imaging. The fellowship provides a broad clinical experience in pediatric radiology as well as numerous opportunities to participate in both clinical and basic research. Candidates must be board-certified or board-qualified in diagnostic radiology and must be able to obtain an Ohio medical license. Salary and fringe benefits are highly competitive. Applications are due before Jan. 1992, with interviews scheduled during the fall and winter of 1991–1992. There are numerous career opportunities in pediatric radiology in academic and private practice settings. To receive more information about the fellowships at CHMC or careers in pediatric radiology, please contact Donald R. Kirks, M.D., Director, Dept. of Radiology, Children's Hospital Medical Center, Cincinnati, OH 45229-2899; (513) 559-8058. Children's Hospital Medical Center and the University of Cincinnati College of Medicine are affirmative action/equal opportunity employers. 5–4cp

IMAGING FELLOWSHIP—A 1-yr fellowship in ultrasound, MRI, and body CT is available July 1, 1992–June 30, 1993, at a 576-bed teaching hospital. The Dept. of Radiology performs more than 140,000 exams with state-of-the-art equipment. The ultrasound section is responsible for all aspects of sonography including OB-GYN, pediatric, abdominal, and small parts. Extensive training in color flow imaging, duplex Doppler, transvaginal, transrectal techniques, and sonographically guided procedures. Two GE MRI scanners and 2 GE 9800 Quick CT units provide high-volume caseloads in these areas. Opportunities are available for participation in imaging research. For further information, please contact Marcela Bohm-Velez, M.D., Imaging Fellowship Director, West Penn Hospital, 4800 Friendship Ave., Pittsburgh, PA 15224. 5–10c

FELLOWSHIP IN ULTRASOUND/CT/ANGIO/INTERVENTIONAL—There is an unexpected opening for a 1-yr fellowship program available beginning July 1991 at Lehigh Valley Hospital Center (LVHC) in Allentown, PA. The fellowship program offers training in CT (head and body), ultrasound, angiography (neuro and visceral), and interventional radiography. MRI experience is also available. LVHC is a 492-bed, acute-care, university-affiliated hospital. For further information, contact Robert Kricun, M.D., Dept. of Radiology, Lehigh Valley Hospital Center, P.O. Box 689, Allentown, PA 18105. 5cp

FELLOWSHIP IN BODY CT/MRI AND ULTRASOUND—The Dept. of Radiology of New York Medical College has an unexpected opening for 1-yr imaging fellowship starting in July 1991. Westchester County Medical Center is a 650-bed, tertiary-care facility offering advanced training with state-of-the-art equipment including 2 Siemens Hi-Q CT scanners, GE Signa 1.5-T MR, ISG 3D reconstruction console, and 6 ultrasound imagers (Acuson and Diasonics). Applicants must have completed an approved residency in diagnostic radiology and must be board-eligible or certified. Please contact Andrew Schechter, M.D., Director, MRI, Dept. of Radiology, New York Medical College, Valhalla, NY 10595; (914) 285-8550. 5–6cp

RADIOLOGY RESIDENCY—Unexpected position available for second and third yr resident beginning July 1, 1991. Fully approved diagnostic radiology residency program. For further information, contact William L. Crawford, M.D., St. Elizabeth Hospital Medical Center, 1044 Belmont Ave., Youngstown, OH 44501-1790; (216) 746-7211. 5cp

CARDIOVASCULAR-INTERVENTIONAL RADIOLOGY FELLOWSHIP—Unexpected opening available July 1, 1991, for a 1-yr fellowship program at a 750-bed teaching hospital. Extensive clinical experience involving all aspects of cardiovascular imaging, interventional vascular and nonvascular procedures, and availability for clinical or animal research. Send CV and inquiries to Oscar H. Gutierrez, M.D., Dept. of Radiology, Box 648, University of Rochester, Rochester, NY 14642-8648. An equal opportunity employer (M/F). 5–8c

IMMEDIATE OPENING, FELLOWSHIP IN PEDIATRIC RADIOLOGY—Position available for fellowship in pediatric radiology, 1- or 2-yr, beginning July 1, 1992, or July 1, 1993. Full training with abundant hands-on experience with all imaging modalities. Supported by strong Dept. of Pediatrics with a good mixture of patient material. Excellent teaching on a 1-to-1 basis and ample opportunity for pursuing academic interests. Apply to Leonard E. Swischuk, M.D., Dept. of Radiology, The University of Texas Medical Branch, Child Health Center, C-65, Galveston, TX 77550; (409) 761-2096. UTMB is an equal opportunity M/F/H/V affirmative action employer. UTMB hires only persons authorized to work in the United States. 5–7c

ANGIOGRAPHY/INTERVENTIONAL RADIOLOGY FELLOWSHIP—Because of an unexpected vacancy, New York Medical College offers a 1-yr fellowship to begin July 1, 1991. The program includes training in all phases of diagnostic angiography and interventional radiologic techniques. Training is based at Westchester County Medical Center, a 650-bed, tertiary-care center located on the medical college campus in a prestigious suburban setting only about ½ hr from New York City. Active participation in clinical management of patients is emphasized. Approximately 900 procedures were performed in 1990. Current research interests include transmesenteric sclerosis of portal varices and hepatic arterial chemoembolization. A new digital interventional suite was opened in 1990. A digital biplane imaging suite is anticipated in 1991. Applications are also being accepted for a 1-yr fellowship to begin July 1, 1992. For additional information and application, contact Stuart Katz, M.D., Dept. of Radiology, New York Medical College, Valhalla, NY 10595; (914) 285-8388. 5cp

FELLOWSHIP IN CALIFORNIA, JULY 1991—Interventional, cross-sectional imaging (MRI, CT, ultrasound) at a large trauma center. Send CV to Dr. Levan, Dept. of Radiology, St. Mary Medical Center, 1050 Linden Ave., Long Beach, CA 90813 or call (213) 491-9900 for information. 5–7cp

FELLOWSHIP IN CROSS-SECTIONAL IMAGING

The Dept. of Radiology, Dartmouth-Hitchcock Medical Center, has an opening for July 1992 for a 1-yr fellowship in MRI/CT/ultrasound. Training includes experience in all aspects of MRI, including neuro and body, CT, and ultrasound, including obstetric and vascular imaging. Imaging-guided biopsies and drainage procedures will be an integral part of the program. The Medical Center has a completely new 420-bed, tertiary-care hospital with state-of-the-art imaging equipment opening in the fall of 1991. Protected research time will be available for the fellow. There is ample opportunity for clinical radiologic research as well as technology assessment and outcome analysis in collaboration with Dartmouth Medical School Center for Evaluative Sciences. For further information, contact Robert D. Harris, M.D., Dept. of Radiology, Dartmouth-Hitchcock Medical Center, Hanover, NH 03756; (603) 646-5686. 5c

FELLOWSHIPS AT MEMORIAL SLOAN-KETTERING CANCER CENTER

The Dept. of Medical Imaging at the Memorial-Sloan Kettering Cancer Center (MSKCC), a Cornell University Medical College affiliate, in New York City, has fellowships available beginning July 1, 1991. This is an excellent opportunity for intensive clinical training and research with a competitive salary and benefits. Send inquiries regarding cross-sectional imaging to J. Caravelli, M.D., or R. Castellino, M.D.; breast imaging to D. Dershaw, M.D.; and nuclear medicine to S. Larson, M.D., Memorial Sloan-Kettering Cancer Center, 1275 York Ave., New York, NY 10021. Integrated fellowships also are available, based at both New York Hospital (NYH) and MSKCC, during which the fellows rotate between the 2 institutions. Applicants are selected conjointly. Inquiries to New York Hospital should be addressed to Dept. of Radiology, 525 E. 68th St., New York, NY 10021. Send inquiries regarding neuroradiology to G. Krol, M.D., at MSKCC or R. Zimmerman, M.D., at NYH; and vascular/interventional to J. Botet, M.D., at MSKCC or T. Sos, M.D., at NYH. 5–6cp

MUSCULOSKELETAL RADIOLOGY FELLOWSHIP

Applications are now being accepted for a musculoskeletal fellow position for 1992 at the Cleveland Clinic Foundation (CCF). CCF is a 1000-bed, tertiary-care, teaching medical center with a large radiology residency program. Local, national, and international patients provide an interesting and varied mix of bone pathology. Training includes all aspects of musculoskeletal radiology including MR, CT, arthrography, biopsy, bone densitometry, and a large plain film experience. Fellowship includes patient care, teaching, and research. There is a close working relationship with the orthopedic, rheumatology, and endocrinology depts. There are presently 4 musculoskeletal staff in the section. For further information, please contact Bradford J. Richmond, M.D., Head, Section of Musculoskeletal Radiology, Desk A-21, 9500 Euclid Ave., Cleveland, OH 44195; (216) 444-3931. 5–10c

INTEGRATED CHEST RADIOLOGY FELLOWSHIP AT JOHNS HOPKINS UNIVERSITY HOSPITAL

The Dept. of Radiology, Division of Thoracic Imaging, Johns Hopkins University is offering a 1- to 2-yr academically oriented fellowship in chest radiology. The fellowship offers an integrated experience in cross-sectional imaging, including over 4000 chest CT and 1000 thoracic MRI exams/yr. Strong research interests in high-resolution CT, MRI, digital imaging methods, and interventional thoracic radiology offer the candidate an exciting environment to work in. The fellowship is available starting July 1, 1991. Contact Elias A. Zerhouni, M.D., Director of Thoracic Imaging and MRI, Dept. of Radiology, Johns Hopkins Hospital, Baltimore, MD 21205; (301) 955-4062. 1–6c

FELLOWSHIPS AT THOMAS JEFFERSON UNIVERSITY HOSPITAL—The Dept. of Radiology at Thomas Jefferson University Hospital in Philadelphia offers the following fellowship programs each yr. Ultrasound/CT/MRI — Jefferson's ultrasound division is 1 of the largest in the world and performs all currently available exams including obstetric, vascular, lithotripsy, invasive, and endoluminal. We also operate 4 GE 1.5-T MRI units and 3 CT scanners. Contact Barry Goldberg, M.D., regarding this program. Cardiovascular/interventional — this division is housed in a new suite containing Philips angio units with DSA and performs the full range of vascular and non-vascular interventional procedures. Contact Geoffrey Gardiner, Jr., M.D. Neuro/ENT radiology — very active clinical services supply a wealth of material to this division, which is housed in a neurosciences imaging center containing all imaging modalities. Contact Carlos Gonzalez, M.D. Breast Imaging — Jefferson's new breast imaging center performs approximately 85 studies/day including ultrasound and needle localizations. Contact Stephen Feig, M.D. Chest — includes biopsies and CT. Contact Robert Steiner, M.D. MRI — a dedicated body MRI program including excellent research opportunities in addition to a large clinical case load. Contact Matthew Rifkin, M.D. Ultrasound — a dedicated ultrasound program. Contact Barry Goldberg, M.D. Musculoskeletal — includes MRI of the musculoskeletal system. Contact David Karasick, M.D. All program directors listed above can be contacted at the Dept. of Radiology, Thomas Jefferson University Hospital, Philadelphia, PA 19107. Jefferson is an equal opportunity/affirmative action employer. 5xcp

WOMEN'S IMAGING FELLOWSHIP—A 1-yr fellowship is available at Oregon Health Sciences University, Portland, OR. Training includes hysterosalpingography, fallopian tube recanalization, mammography and breast procedures, obstetrical ultrasound, pelvic ultrasound including vaginal ultrasound, and pelvic and breast MRI. Please contact Amy Thurmond, M.D., Director of Women's Imaging, Oregon Health Sciences University, L340, 3181 S.W. Sam Jackson Park Rd., Portland, OR 97201; (503) 494-7576. 4-6c

IMAGING FELLOWSHIP (CT, ULTRASOUND, MRI)—William Beaumont Hospital, a 970-bed, modern, tertiary-care teaching and academic institution in southeast Michigan, offers a 1-yr fellowship in sectional body imaging. The fellowship will provide extensive clinical experience in body CT, ultrasound, and MRI including CT and ultrasound-guided procedures, conventional and color-flow Doppler exams, prostatic and endovaginal sonography. Ample elective time is also provided for other rotations of individual interest. Candidates must be board-certified or eligible in diagnostic radiology and have a valid Michigan medical license. Four positions are available for July 1992. Salary and fringe benefits are highly competitive. For further information, write to Ali Shirkhoda, M.D., Chief, Imaging Division, William Beaumont Hospital, 3601 W. 13 Mile Rd., Royal Oak, MI 48073; (313) 551-1001. 4-6c

FELLOWSHIP IN ULTRASOUND/CT/ANGIO/INTERVENTIONAL—A 1-yr fellowship program available beginning July 1992 at Lehigh Valley Hospital Center in Allentown, PA. LVHC is a 492-bed, acute-care, university-affiliated hospital. The fellowship program offers training in CT (head and body), ultrasound, angiography (neuro and visceral), and interventional radiography. MRI experience is also available. For further information, contact Robert Kricun, M.D., Dept. of Radiology, Lehigh Valley Hospital Center, P.O. Box 689, Allentown, PA 18105. 2-7c

FELLOWSHIP IN CARDIOVASCULAR/INTERVENTIONAL RADIOLOGY—A 1-yr fellowship in cardiovascular/interventional radiology is available at the Dartmouth-Hitchcock Medical Center in Hanover, NH, beginning July 1992. DHMC is the major teaching component of Dartmouth Medical School and is situated in a classic northern New England town. Training includes all aspects of diagnostic angiography (including neuro and pulmonary), vascular and nonvascular interventional techniques. This includes IVC filter placement, atherectomy, thrombolysis, biliary and urologic interventions, as well as biopsy and drainage procedures using multiple imaging modalities. We have a close working relationship with the depts. of vascular and general surgery. Approximately 2000 diagnostic and interventional procedures are performed/yr. The dept. will be moving to a new, tertiary-care, 429-bed hospital, in fall 1991, equipped with 2 new, state-of-the-art digital interventional suites and a 4-bed recovery room. Candidates must have completed an accredited diagnostic radiology residency program, must be certified or eligible by the ABR, and must be eligible for medical licensure in the state of New Hampshire. For further information, please contact Louis I. Juravsky, M.D., FRCPC, Dept. of Diagnostic Radiology, Dartmouth-Hitchcock Medical Center, 2 Maynard St., Hanover, NH 03756. Dartmouth College is an equal opportunity/affirmative action educator and employer. 5xcp

CARDIOVASCULAR AND INTERVENTIONAL RADIOLOGY—The Harvard Medical School and Brigham and Women's Hospital, Dept. of Radiology, is offering a 2-yr fellowship starting July 1, 1992, in cardiovascular and interventional radiology including peripheral and coronary angiography, cardiac catheterization, digital vascular imaging, all types of interventional procedures, noninvasive vascular techniques, and cardiovascular MRI. Research time available for participation in original or ongoing clinical and/or laboratory projects. Please send CV to B. Leonard Holman, M.D., Chairman, Dept. of Radiology, Brigham and Women's Hospital, 75 Francis St., Boston, MA 02115. Brigham and Women's Hospital/Harvard Medical School is an affirmative action/equal opportunity educator and employer. 3-8c

FELLOWSHIP IN CARDIOVASCULAR/INTERVENTIONAL RADIOLOGY—A 1-yr fellowship in cardiovascular/interventional radiology is available at the Dartmouth-Hitchcock Medical Center in Hanover, NH, beginning July 1991. DHMC is the major teaching component of Dartmouth Medical School and is situated in a classic northern New England town. Training includes all aspects of diagnostic angiography (including neuro and pulmonary), vascular and nonvascular interventional techniques. This includes IVC filter placement, atherectomy, thrombolysis, biliary and urologic interventions, as well as biopsy and drainage procedures using multiple imaging modalities. We have a close working relationship with the depts. of vascular and general surgery. Approximately 2000 diagnostic and interventional procedures are performed/yr. The dept. will be moving to a new, tertiary-care, 429-bed hospital, in fall 1991, equipped with 2 new, state-of-the-art digital interventional suites and a 4-bed recovery room. Candidates must have completed an accredited diagnostic radiology residency program, must be certified or eligible by the ABR, and must be eligible for medical licensure in the state of New Hampshire. For further information, please contact Louis I. Juravsky, M.D., FRCPC, Dept. of Diagnostic Radiology, Dartmouth-Hitchcock Medical Center, 2 Maynard St., Hanover, NH 03756. Dartmouth College is an equal opportunity/affirmative action educator and employer. 5xcp

ABDOMINAL IMAGING FELLOWSHIP—The Dept. of Radiology at the University of Florida is offering 1-yr fellowships in abdominal imaging beginning July 1, 1991, and July 1, 1992. Minimum requirements include successful completion of an accredited radiology residency. The fellowship includes training in all aspects of abdominal imaging (gastrointestinal and genitourinary radiology, CT, ultrasound, and MRI) by a 3-person subspecialty faculty. The program offers full clinical experience and research opportunities. Applicants must be eligible to obtain a license in the state of Florida. For additional information, contact Pablo R. Ros, M.D., Professor, Dept. of Radiology, Box J-374, Gainesville, FL 32610-0374; (904) 395-0288. The University of Florida is an equal opportunity/affirmative action employer and encourages applications from women and minorities. 10-6c

FELLOWSHIPS AT ALBANY MEDICAL CENTER—The Dept. of Radiology at the Albany Medical Center offers the following fellowship programs each yr with openings available July 1992: ultrasound and body CT/MR — Wide variety of exams with state-of-the-art equipment including Acuson ultrasound, 3 GE CT scanners, and GE Signa 1.5-T MR. Contact James Peters, M.D.; neuro-radiology — regional referral center for neurosciences with extensive exposure to MR, CT, and angiography. Abundant research opportunities. Contact William Wagle, M.D.; angiography/interventional — busy, clinical service with in-depth experience in arteriography, lymphangiography, angioplasty, and interventional procedures. Contact Mohammad Sarrafzadeh, M.D. All program directors can be reached at the Dept. of Radiology, A-113, Albany Medical Center, 43 New Scotland Ave., Albany, NY 12208; (518) 445-3277. AMC is an equal opportunity, affirmative action employer. 4-6cp

UNIVERSITY OF WASHINGTON FELLOWSHIP IN DIAGNOSTIC IMAGING SCIENCES—The Diagnostic Imaging Sciences Center of the Dept. of Radiology at the University of Washington in Seattle is recruiting for 2 fellowship positions in radiology science research. The research fellowship program is funded by NCI Training Grant T32 CA 096552 and combines a 2-yr, fully funded, laboratory-based, educational and research program with a guaranteed clinical fellowship after successful completion of the radiology science program. Candidates should have successfully completed 2 or 3 yr of a diagnostic radiology residency and must have a strong interest and commitment to a career in academic radiology. The research fellowship program will combine academic courses and a thesis project that will lead to a masters degree in biomedical imaging at the University of Washington. A portion of each fellow's time will be spent in clinical subspecialty radiology training to keep the fellows clinically astute and to provide additional clinical experience. The Radiology Imaging Research Laboratory at the University of Washington consists of over 20,000 sq. ft. of dedicated research space and includes more than 25 full-time scientists, state-of-the-art equipment in MRI, NMR spectroscopy, PET, SPECT, DIN/PACS, angiography, ultrasound, and image processing. Four MRI instruments, including a GE Signa system, are dedicated to research use. Candidates interested in the Radiology Research Sciences Program should contact James A. Nelson, M.D., Dept. of Radiology, SB-05, University of Washington, Seattle, WA 98195; (206) 543-3757. The University of Washington is an equal opportunity employer. 5-6c

DUKE UNIVERSITY MEDICAL CENTER FELLOWSHIP POSITIONS — Duke University Medical Center is seeking qualified candidates for fellowship positions in the Dept. of Diagnostic Radiology. Currently there are positions available in the following areas: chest, musculoskeletal, and vascular/interventional radiology, ultrasound, advanced diagnostic imaging, MRI, neuroradiology, abdominal imaging, mammography, and research fellowships. The radiology dept. is state-of-the-art in diagnostic imaging with diverse resources available for clinical, teaching, and academic pursuits. Fellowship training is generally organized by organ systems, although experience can be individualized to accommodate special interests. Salary and benefits are competitive and academic time is guaranteed. For additional information, please phone Richard Leder, M.D. at (919) 681-2711 ext. 5310. Applications are due Feb. 1 of the preceding yr and can be obtained by writing to N. Reed Dunnick, M.D., Dept. of Radiology, Duke University Medical Center, Erwin Rd., Box 3808, Durham, NC 27710. AA/EOE. 2-7c

NEURORADIOLOGY FELLOWSHIP—The Dept. of Radiology, Strong Memorial Hospital, University of Rochester School of Medicine and Dentistry offers a 1- or 2-yr neuroradiology fellowship to begin July 1, 1991. Training is offered in MRI, CT, and special procedures, with the opportunity to perform both pediatric and carotid ultrasound. Assistance in teaching of medical students and residents is expected. Additional training in maxillofacial, dental, and ENT radiology also is available, as is the opportunity to perform both clinical and laboratory research. A very strong neuroscience community exists. The dept. consists of 25 radiologist faculty, 16 residents, and 3-5 fellows. State-of-the-art equipment is available in all modalities including new single and biplane angiographic systems, 3 third-generation CT, a 1.5-T MRI, and a midfield MR. Strong Memorial Hospital is a 750-bed, tertiary-care hospital with 100 beds dedicated to pediatric diseases. Candidates must have completed an accredited diagnostic radiology residency program, be board-certified or eligible, and have a New York state medical license by July 1, 1991. Send inquiries to Robert E. O'Mara, M.D., Box 648, University of Rochester Medical Center, Rochester, NY 14642; (716) 275-2733. EO/AA/M-F employer. 1-6c

FELLOWSHIP IN MRI at Central Massachusetts Magnetic Imaging Center, July 1992 through June 1993. CMMIC is a consortium of 3 area teaching hospitals (The Medical Center of Central Massachusetts, St. Vincent Hospital, and the University of Massachusetts Medical Center) with clinical, research, and teaching responsibilities. CMMIC currently uses 2 clinical 1.5-T GE Signa systems and a 2.0-T GE Fremont CSI research system. The fellowship will include thorough training in MRI physics, imaging principles, clinical applications, and image interpretation. Duties will include image interpretation of neuro, musculoskeletal, abdominal, pediatric, and cardiac studies; daily supervision of scanning; teaching file maintenance; and participation in CMMIC's teaching and research activities. Requirements include satisfactory completion of a 4-yr, accredited radiology training program and board-eligibility/certification. Please send inquiries to James Lingley, M.D., Medical Director, CMMIC, Inc., 387 Plantation St., Worcester, MA 01605. 4-5cp

UNEXPECTED OPENING FOR VASCULAR AND INTERVENTIONAL FELLOWSHIP BEGINNING JULY 1991

July 1991 is offered at the University of Maryland. The fellow will participate in all aspects of diagnostic vascular radiology, as well as nonvascular interventional procedures, including percutaneous and laser angioplasty, embolization, biliary and GU intervention, and insertion of IVC filters. Contact Gerald S. Johnston, M.D., 22 S. Greene St., Baltimore, MD 21201; (301) 328-3477. The University of Maryland is an affirmative action/equal opportunity employer and encourages applications from members of minority groups. 3-5cp

Other

VISITING PROFESSORSHIPS, THOMAS JEFFERSON UNIVERSITY HOSPITAL—The Dept. of Radiology at Thomas Jefferson University Hospital in Philadelphia is offering visiting professorships over the next several yr, while some of our faculty members are on sabbatical leave. These positions can have either a 6-mo or 1-yr term. In particular, we are seeking candidates with expertise in either ultrasound or general diagnostic radiology, but emphasis in other areas may be acceptable as well. Funding for these positions is appropriate for a senior faculty member from another institution on sabbatical with partial funding of his/her own, or for a junior faculty member. These positions are also open to highly qualified foreign radiologists with current academic appointments at prestigious foreign medical schools. Visiting faculty members will do some clinical work in our dept. and also have access, for research or educational purposes, to state-of-the-art imaging modalities of all types, as well as well-equipped physics and physiology research laboratories. Interested persons should contact David C. Levin, M.D., Chairman, Dept. of Radiology, Thomas Jefferson University Hospital, Philadelphia, PA 19107. Jefferson is an equal opportunity/affirmative action employer. 5xe

Tutorials/Courses

ALASKA 1991-CRUISE THE INLAND PASSAGE, BREAST IMAGING AT SEA, JULY 7-14, 1991, AND MRI AT SEA, JULY 14-21, 1991—Medical Seminars International, Inc., 18981 Ventura Blvd., Ste. 303, Tarzana, CA 91356; (818) 774-9077, fax (818) 774-0244. 3-6d

AJR Classified Advertisements Information

Box Responses and Address for Ad Placement

Write Box _____, AJR, 2223 Avenida de la Playa, Suite 103, La Jolla, CA 92037-3218; Telephone: (619) 459-2229; FAX: (619) 459-8814.

How to Place an Ad

AJR accepts classified advertising for Positions Available, Positions Desired, Fellowships and Residencies, and Tutorials/Courses. Ads are accepted by mail or FAX.

Rates: \$6.00/line with a \$30 minimum charge. Box service is \$10 additional for each month the ad appears. There are discounts for multiple insertions: 10% for 2-3 insertions; 20% for 4 or more. To estimate lines, count all words and divide by 7.

Billing: Ads *must* be prepaid, or advertisers will be billed after the ad appears providing a purchase order number is submitted with the advertising copy. Terms are net 30 days.

Deadlines: 6 weeks prior to issue date. For specific deadlines, telephone the AJR editorial office.

Estimating Ad Charges

Line charge: divide total words by 7 and multiply by \$6.00 \$ _____

Multiple insertions? If so, multiply by number X _____

Subtotal \$ _____

Discount applies to two or more insertions. Subtract 10% if ad appears 2-3 months; 20% if 4 months or more - _____

Subtotal \$ _____

Box response requested? If so, multiply number of months by \$10.00 + _____

Approximate advertising charge \$ _____

An informed approach to the great threats
of our time from *Physicians for Social Responsibility*...



THE **PSR** QUARTERLY



A Journal of Medicine and Global Survival

"After years of talking and writing about the role of medicine and public health in responding to the great threats of our time, the PSR physicians now intend to create a forum where such discussions can be captured in a single publication."

—Jennifer Leaning, M.D.
Editor-in-Chief

Jennifer Leaning, M.D.

EDITOR-IN-CHIEF

Christine K. Cassel, M.D.

H. Jack Geiger, M.D.

ASSOCIATE EDITORS

Drawing on the best traditions in medical science, *The PSR Quarterly* will publish peer-reviewed articles examining health-related aspects of nuclear, biological, and chemical warfare; environmental change; natural and technological disasters; and relevant social policies.

The PSR Quarterly welcomes articles, reports, and letters from authors with divergent views. Contributors who would like to submit manuscripts or propose articles should write to the Editor: Jennifer Leaning, M.D., 10 Brookline Place West, Brookline Massachusetts 02146.

CHARTER SAVINGS!

SUBSCRIBE NOW, while charter rates are in effect! To order, call TOLL FREE:

1-800-638-6423

Or complete and mail this coupon.

PUBLISHED BY
WILLIAMS & WILKINS



THE PSR QUARTERLY

A Journal of Medicine and Global Survival
Quarterly • Beginning March 1991

- | | |
|-------------------------------------------------|---------------------------------|
| <input type="checkbox"/> Individual \$48/yr. | <input type="checkbox"/> 3 yrs. |
| <input type="checkbox"/> Institutional \$85/yr. | <input type="checkbox"/> 2 yrs. |
| <input type="checkbox"/> In-training* \$25/yr. | <input type="checkbox"/> 1 yr. |

Add \$15/yr for postage outside the U.S. Rates valid until October 31, 1991. Orders outside the U.S. must be prepaid in U.S. dollars. Maryland subscribers add 5% sales tax. Canadian subscribers add 7% GST.

Payment options: Bill me
 Check enclosed (payable to Williams & Wilkins)
 AmEX MasterCard VISA

Acct. # _____ Exp. date _____

Signature _____

Name _____

Address _____

City/State/Zip _____

*Specify institution
and training status _____

Note: PSR members will receive the journal as a benefit of their membership.

Return to: Williams & Wilkins, P.O. Box 23291,
Baltimore, MD 21203-9990.

FORM 52541

J0079S01

SPECIAL ARTICLE

- 903 Anaphylaxis associated with latex allergy during barium enema examinations. Ownby DR, Tomlanovich M, Sammons N, McCullough J

REVIEW ARTICLE

- 909 Review. Colorectal cancer: cross-sectional imaging for staging of primary tumor and detection of local recurrence. Thoeni RF

PULMONARY RADIOLOGY

- 917 Factors affecting the development of pneumothorax associated with thoracentesis. Raptopoulos V, Davis LM, Lee G, Umal C, Lew R, Irwin RS
921 Prevalence of air bronchograms in small peripheral carcinomas of the lung on thin-section CT: comparison with benign tumors. Kuriyama K, Tateishi R, Doi O, et al.
925 CT evaluation of solitary pulmonary nodules: value of 185-H reference phantom. Swensen SJ, Harms GF, Morin RL, Myers JL
931 Pictorial essay. Imaging of the azygos lobe: normal anatomy and variations. Mata J, Cáceres J, Alegret X, Coscojuela P, De Marcos JA

GASTROINTESTINAL RADIOLOGY

- 939 Perspective. The economic implications of radiologic screening for colonic cancer. Gelfand DW, Ott DJ
945 Sonography of the gallbladder: significance of striated (layered) thickening of the gallbladder wall. Teeffey SA, Baron RL, Bigler SA
949 Pictorial essay. Sonography of focal lesions of the spleen. Goerg C, Schwerk WB, Goerg K
955 Case report. Giant esophageal ulcer due to Clinoril. Levine MS, Rothstein RD, Laufer I
957 Case report. CT appearance of retrograde jejunoduodenogastric intussusception: a rare complication of gastrostomy tubes. Weber A, Nadel S
961 Inverted colonic diverticulum: air contrast barium enema findings in six cases. Glick SN
965 Yersinia terminal ileitis: sonographic findings in eight patients. Matsumoto T, Iida M, Sakai T, Kimura Y, Fujishima M
969 Pictorial essay. CT of AIDS-related lymphoma. Townsend RR
975 Pictorial essay. Anatomic variants and artifacts in ERCP interpretation. Guilliver DJ, Cotton PB, Baillie J
981 Subcapsular hepatic necrosis in liver transplantation: CT appearance. Abécassis J-P, Parienté D, Hazebrucq V, Houssin D, Chapuis Y, Bonnin A

GENITOURINARY RADIOLOGY

- 985 Lacunae: a urographic finding in chronic obstructive uropathy. Talner LB, Webb JAW, Dail DH
989 Pictorial essay. MR imaging of the seminal vesicles. Scaf E, Nuruddin RN, Hricak H, McClure RD, Demas B
995 Stones and infection in renal caliceal diverticula: treatment with percutaneous procedures. Ellis JH, Patterson SK, Sonda LP, Platt JF, Sheffner SE, Woolsey EJ
1001 Vaginal reconstruction with rectus abdominis myocutaneous flap: CT findings. Willing SJ, Pursell SH, Koch SR, Tobin GR
1005 Case report. Pancreatitis causing focal caliectasis. Fishman M, Talner LB
1007 Technical note. Retrograde replacement of internal double-J ureteral stents. Yedlicka JW Jr, Aizpuru R, Hunter DW, Castañeda-Zúñiga WR, Amplatz K

SKELETAL RADIOLOGY

- 1011 Review. Condensing osteitis of the clavicle: a rare but frequently misdiagnosed condition. Greenspan A, Gerscovich E, Szabo RM, Matthews JG II
1017 Fibrous dysplasia vs adamantinoma of the tibia: differentiation based on discriminant analysis of clinical and plain film findings. Bloem JL, van der Heul RO, Schuttevaer HM, Kuipers D

- 1025 Pictorial essay. MR appearance of the distended ilio-psoas bursa. Varma DGK, Richli WR, Charnsangavej C, Samuels BI, Kim EE, Wallace S

PEDIATRIC RADIOLOGY

- 1029 Interobserver and intraobserver variations in sonographic renal length measurements in children. Schlesinger AE, Hernandez RJ, Zerin JM, Marks TI, Kelsch RC
1033 Case report. Anomaly of the descending aorta: a case of persistent double dorsal aorta. Formanek AG, Weisner KM, Lantz PE
1037 Case report. Primary lymphoma of the CNS in an infant with AIDS: imaging findings. Douek P, Bertrand Y, Tran-Minh VA, Patet JD, Souillet G, Philippe N

NEURORADIOLOGY

- 1039 Diagnosis of cerebral metastases: double-dose delayed CT vs contrast-enhanced MR imaging. Davis PC, Hudgins PA, Peterman SB, Hoffman JC Jr
1047 Pictorial essay. Tubes in the alimentary and respiratory tracts: appearances on CT scans of the head and neck. Price DB
1053 Hamartomas of the tuber cinereum: CT, MR, and pathologic findings. Boyko OB, Curnes JT, Oakes WJ, Burger PC
1059 Intra- and paraorbital lesions: value of fat-suppression MR imaging with paramagnetic contrast enhancement. Tien RD, Chu PK, Hesselink JR, Szumowski J
1069 Effects of magnetic susceptibility artifacts and motion in evaluating the cervical neural foramina on 3DFT gradient-echo MR imaging. Tsuruda JS, Remley K
1075 Pictorial essay. Conventional MR neuroangiography. El Gammal T, Brooks BS
1081 Pictorial essay. Imaging characteristics of tuberous sclerosis. Bell DG, King BF, Hattery RR, Charboneau JW, Hoffman AD, Houser OW

VASCULAR RADIOLOGY

- 1087 Intravascular sonography in the detection of arteriosclerosis and evaluation of vascular interventional procedures. Engeler CE, Yedlicka JW, Letourneau JG, Castañeda-Zúñiga WR, Hunter DW, Amplatz K
1091 Percutaneous transluminal angioplasty of the subclavian arteries: long-term results in 52 patients. Hebrang A, Maskovic J, Tomac B
1095 Conventional screen/film vs reduced exposure photostimulable phosphor plate imaging in lower extremity venography: an ROC analysis. Siegel EL, Cook LT, Parsa MB
1101 Ligamentous compression of the celiac axis: CT findings in five patients. Patten RM, Coldwell DM, Ben-Menachem Y
1105 Technical note. Retrieval of a 4-French diagnostic catheter fragment from the common carotid artery by using a stone basket. Travelli R, Cogbill TH

COMMENTARY

- 1107 Visual acuity testing of radiologists—is it time? Straub WH, Gur D, Good BC

OTHER CONTENT

- Book and videotape reviews 916, 930, 948, 954, 960, 968, 984, 1010, 1036, 1052, 1068, 1074
938 Radiology Centennial Celebration announcement
944 History page
1016 Radiologic-Pathologic Conference
1024 Medicine in American Art
1100 Memorial, John Wickwire Loop
1104 Forthcoming articles
1109 Letters
1117 Review of current literature
1121 News
1124 American Roentgen Ray Society information
1125 Classified advertisements
A15 Guidelines for authors
A20 AJR business and subscriber information

Dec 16/93



American
Journal of
Roentgenology



June 1991



EG 3350, Sodium Chloride, Sodium Bicarbonate and Potassium Chloride for Oral Solution

New...the taste patients prefer.

results of a double-blinded multicenter study¹ comparing NuLYTELY and GoLYTELY:

Preference. Patients prefer the taste of NuLYTELY 3 to 1¹

Efficacy & Safety. NuLYTELY is as safe and effective as GoLYTELY^{1,2}

Another clinical success from the makers of GoLYTELY

PRESCRIBING SUMMARY: Before prescribing, see complete prescribing information.

INDICATIONS AND USAGE: NuLYTELY is indicated for bowel cleansing prior to colonoscopy.

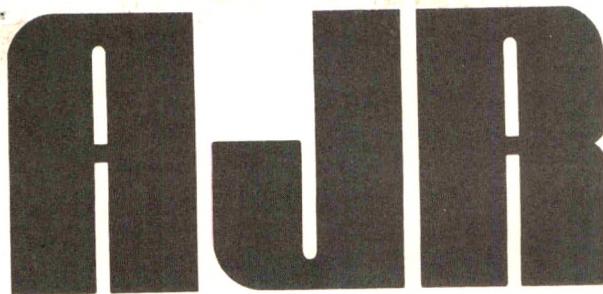
CONTRAINdications: NuLYTELY is contraindicated in patients with gastrointestinal obstruction, gastric retention, bowel perforation, toxic colitis or toxic megacolon.

WARNINGS: No additional ingredients, e.g. flavorings, should be added to the solution. NuLYTELY should be used with caution in patients with severe ulcerative colitis.

ADVERSE REACTIONS: Nausea, abdominal fullness and bloating are the most common adverse reactions (occurring in up to 50% of patients) to administration of NuLYTELY. Abdominal cramps, vomiting, and anal irritation occur less frequently. These adverse reactions are transient and subside rapidly. Isolated cases of urticaria, rhinorrhea and dermatitis have been reported with a related drug (GoLYTELY[®]) which may represent allergic reactions.

CAUTION: Federal law prohibits dispensing without prescription.

STORAGE: Store in sealed container at 25°C. When reconstituted, keep solution refrigerated. Use within 48 hours. Discard unused portion. NDC 52268-0300-01



American Journal of Roentgenology
Diagnostic Imaging and Related Sciences

Editor-In-Chief Robert N. Berk, *La Jolla, California*
University of California, San Diego
School of Medicine and Medical Center

Editor Emeritus Melvin M. Figley, *Seattle, Washington*

Associate Editor Saskia von Waldenburg Hilton, *San Diego, California*

Consulting Editor Michael S. Huckman, *Chicago, Illinois*

Statistician Charles C. Berry, *San Diego, California*

Editorial Board

John R. Amberg
Ithamar Aviad
Mark E. Baker
Lawrence W. Bassett
Michael A. Bettman
Felix S. Chew
N. Reed Dunnick
David K. Edwards
Ronald G. Evens
David S. Feigin
Sandra K. Fernbach
Richard H. Gold
William R. Hendee

John R. Hesselink
Charles B. Higgins
Melvyn T. Korobkin
Faye C. Laing
Thomas L. Lawson
Robert G. Levitt
Bruce L. McClellan
Richard P. Moser
Albert A. Moss
Jeffrey H. Newhouse
Donald L. Resnick
Stewart R. Reuter
Charles A. Rohrmann, Jr.

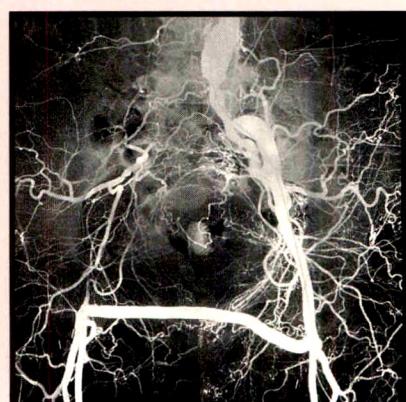
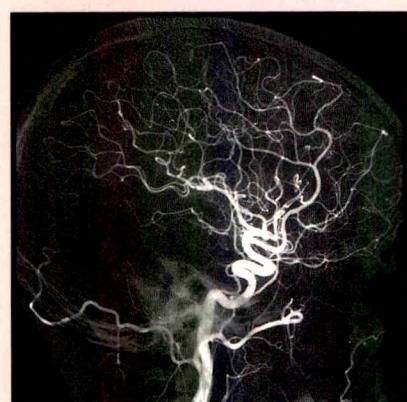
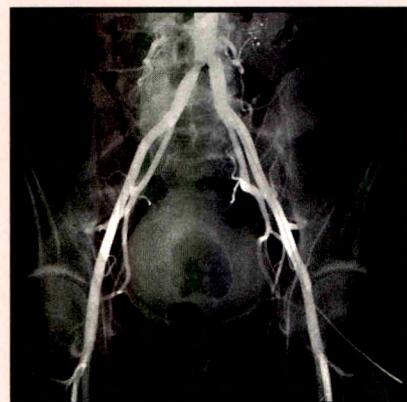
Peter M. Ronai
Sjef H. J. Ruijs
Stuart S. Sagel
David J. Sartoris
Stefan C. Schatzki
William P. Shuman
Edward A. Sickles
Barry A. Siegel
David D. Stark
Edward T. Stewart
Murali Sundaram
Eric vanSonnenberg
Robert K. Zeman

Editorial Staff: Margaret Levene, *managing editor*; Katie L. Spiller, Barbara Rose, Barbara L. Halliburton, and Janine Anderson, *manuscript editors*; Nancy Rydbeck, *office manager*; Sheri Smith, *administrative assistant*; Linda J. Waggoner, *administrative secretary*

AJR, AMERICAN JOURNAL OF ROENTGENOLOGY (ISSN 0361 803X) is the official journal of the American Roentgen Ray Society and is published monthly by Williams & Wilkins, 428 E. Preston St., Baltimore, MD 21202. Annual dues include \$50 for journal subscription. Second-class postage paid at Baltimore, MD, and at additional mailing offices. Postmaster, send address changes (Form 3579) to AJR, 428 E. Preston St., Baltimore, MD 21202. Subscription rates \$125 (\$180 foreign); institutions \$135 (\$190 foreign); in training \$25 (\$80 foreign); single copy \$18 (\$22 foreign). The GST number for Canadian subscribers is 123394371. Airmail rates furnished on request. Indexed by *Current Contents* and *Index Medicus*. Copyright © 1991 by American Roentgen Ray Society.



The Comfortable Choice
for Angiography



AJR Guidelines for Authors

Address new and revised manuscripts, correspondence, and classified ads to the Editor:

AJR Editorial Office
2223 Avenida de la Playa, Suite 103
La Jolla, CA 92037-3218

Telephone: (619) 459-2229; FAX: (619) 459-8814

Inquiries regarding subscriptions, display advertising, reprints, or permission to republish AJR material should be addressed to the publisher:

The Williams & Wilkins Co.
428 E. Preston St.
Baltimore, MD 21202 Telephone: 1-800-638-6423

The AJR publishes original contributions to the advancement of medical diagnosis and treatment. Submitted manuscripts should not contain previously published material and should not be under consideration for publication elsewhere. Papers dealing with neuroradiology should be addressed to: American Journal of Neuroradiology, Dept. of Diagnostic Radiology, 1653 W. Congress Pkwy., Chicago, IL 60612. At the discretion of the AJR Editor, AJNR articles that are of interest to the general reader may be republished in the AJR. Neuroradiologic papers sent to the AJR will be forwarded to the Editorial Office of the AJNR.

Manuscript decisions are based on peer review. Reviewers receive manuscripts without title pages to ensure an unbiased review. Statements made in the article, including changes made by the Editor or manuscript editor, are the responsibility of the author and not of the AJR or its publisher. Authors will be sent the edited manuscript, galley proof, and proofs of illustrations. If the corresponding author will be unavailable to review galleys, arrangements should be made for a coauthor or colleague to read and return the proof.

The following guidelines are based on instructions set forth in the **Uniform Requirements for Manuscripts Submitted to Biomedical Journals** (*Ann Intern Med* 1988;108:258-265). Articles will be edited, however, to conform to the individual style of AJR.

General Guidelines for Major Papers

Abstract. Clearly state (in 200 words or less) the purpose, methods, results, and conclusions of the study. Include actual data.

Introduction. Briefly describe the purpose of the investigation and explain why it is important.

Methods. Describe the research plan, the materials (or subjects), and the methods used, in that order. Explain in detail how disease was confirmed and how subjectivity in observations was controlled.

Results. Present results in a clear, logical sequence. If tables are used, do not duplicate tabular data in text, but do describe important trends and points.

Discussion. Describe the limitations of the research plan, materials (or subjects), and methods, considering both the

purpose and the outcome of the study. When results differ from those of previous investigators, explain the discrepancy.

AUTHOR'S CHECKLIST

For priority handling, complete the following checklist, sign the copyright form on the reverse side of this page, and include both with the manuscript.

Two copies of the manuscript (the original and a photocopy) and two complete sets of figures are submitted. One copy has been retained by the author.

If appropriate, AJR Guidelines for case reports, technical notes, pictorial essays, or letters to the Editor have been followed. (See page A15.)

The manuscript, including references, figure legends, and tables, is typed double-spaced on 8½ × 11 in. (21.6 × 27.9 cm) nonerasable paper. Right-hand margins are not justified.

All manuscript pages are numbered consecutively beginning with the abstract. Authors' names do not appear on the manuscript pages.

The manuscript is organized as follows: title page, blind title page (title only), abstract, introduction, methods, results, discussion, acknowledgments, references, tables, figure legends, and figures.

Informed consent has been obtained from patients who participated in clinical investigations. If experiments were performed on animals, authors complied with NIH guidelines for use of laboratory animals.

Use of unfamiliar acronyms and abbreviations is kept to a minimum. When abbreviations are used they are defined at first mention, followed by the abbreviation in parentheses.

Metric measurements are used throughout, or the metric equivalent is given in parentheses.

Names and locations (city and state only) of manufacturers are given for equipment and nongeneric drugs.

Title Page

The following information is given: title of article; names and complete addresses (including zip code) of all authors; current addresses of authors who have moved since study; acknowledgment of grant or other assistance. The corresponding author is clearly identified, and a current address, phone number, and FAX number are given.

A blind title page is included in each copy of the manuscript, giving only the title (without the authors' names) for use in the review process.

Abstract

An abstract of approximately 200 words concisely states the purpose, methods, and results of the study in one paragraph. Actual data are included. Conclusions are stated in a second, summary paragraph.

No abbreviations or reference citations are used.

References

- _____ References (not to exceed 35) are typed double-spaced starting on a separate page and are **numbered consecutively in the order in which they appear in the text.**
- _____ All references are cited in the text and are enclosed in brackets and typed on line with the text (not superscript).
- _____ Unpublished data are not cited in the reference list, but are cited parenthetically in the text, for example, (Smith DJ, personal communication), (Smith DJ, unpublished data). This includes papers submitted, but not yet accepted, for publication.
- _____ Papers presented at a meeting are not cited in the reference list, but are cited parenthetically in the text (e.g., Smith DJ et al., presented at the annual meeting of the American Roentgen Ray Society, May 1990). After first mention, use (Smith DJ et al., ARRS meeting, May 1990).
- _____ Inclusive page numbers (e.g., 333–335) are given for all references.
- _____ Journal names are abbreviated according to *Index Medicus*.
- _____ Style and punctuation of references follow the format illustrated in the following examples (all authors are listed when six or fewer; when seven or more authors, the first three are listed, followed by "et al."):

Journal article

1. Long RS, Roe EW, Wu EU, et al. Membrane oxygenation: radiographic appearance. *AJR* 1986;146:1257–1260

Book

2. Smith LW, Cohen AR. *Pathology of tumors*, 6th ed. Baltimore: Williams & Wilkins, 1977:100–109

Chapter in a book

3. Breon AJ. Serum monitors of bone metastasis. In: Clark SA, ed. *Bone metastases*. Baltimore: Williams & Wilkins, 1983:165–180

Tables

- _____ Each table is typed double-spaced on a separate page without vertical or horizontal rules; each has a short, descriptive title. Tables do not exceed two pages in length and contain at least four lines of data.

_____ Tables are numbered in the order in which they are cited in the text.

_____ Abbreviations are defined in an explanatory note below each table.

_____ Tables are self-explanatory and do not duplicate data given in the text or figures.

_____ All arithmetic (percentages, totals, differences) has been double checked for accuracy, and tabular data agree with data given in the text.

Figures and Legends

_____ Two complete sets of original figures are submitted unmounted in labeled envelopes.

_____ Figures are clean, unscratched, 5 × 7 in. (13 × 18 cm) glossy prints with **white borders**. A separate print is submitted for each figure part.

_____ All figure parts relating to one patient have the same figure number.

_____ Each figure is labeled on the back with the figure number and an arrow indicating "top." For black-and-white figures, labeling is done on a gummed label, which is then affixed to the back of the print. **Never** use labels on **color** figures, but write figure number on the back lightly in pencil. **Never** use ink on front or back of any figures.

_____ Author's names are *not* written on the backs of figures.

_____ Only removable (rub-on) arrows and letters are used on the figures. Symbols are uniform in size and style and are not broken or cracked.

_____ Images are uniform in size and magnification.

_____ Line drawings are done in black ink on a white background. They are professional in quality, and all use the same size type. (Only glossy prints are acceptable.)

_____ Written permission has been obtained for use of all previously published illustrations (and copies of permission letters are included), and an appropriate credit line is given in the legends.

_____ Legends are typed double-spaced, and figure numbers correspond with the order in which the figures are cited in the text.

Transfer of Copyright Agreement, Conflict of Interest Acknowledgment, Certification of Coauthors, and Exclusive Publication Statement

Complete copyright to the article entitled:

is hereby transferred to the American Roentgen Ray Society (for United States government employees to the extent transferable), effective if and when the article is accepted for publication in the *American Journal of Roentgenology*. In the case of the authors who are officers or employees of the United States government, the American Roentgen Ray Society recognizes that works prepared by officers or employees of the United States government as part of their official government duties are in the public domain.

Authors reserve all proprietary rights other than copyright, such as patent rights and the right to use all or part of this article in future works of their own. The authors retain the right of replication, subject only to crediting the original source of publication and receiving written permission from the publisher.

Authors guarantee that this manuscript contains no matter that is libelous or otherwise unlawful, invades individual privacy, or infringes any proprietary rights.

Authors understand that they will receive no royalty or other compensation from the American Roentgen Ray Society or the publisher.

Authors guarantee that the editor has been or will be informed of any proprietary or commercial interest or conflicts of interest the authors may have that relate directly or indirectly to the subject of this article.

All authors certify that they have made substantive and specific intellectual contributions to the article and assume public responsibility for its content.

Finally, the authors certify that none of the material in this manuscript has been published previously or is currently under consideration for publication elsewhere.

First author/date

Second author

Third author

Fourth author

Fifth author

Sixth author

This agreement must be signed by all authors in order for the manuscript to be published.

Case Reports

A case report is a brief description of a special case that provides a message that transcends the individual patient.

Format. There is no abstract. The introduction should be a short paragraph giving the general background and the specific interest of the case. No more than one case should be described in detail (similar ones can be mentioned briefly in the discussion). Emphasis should be on the radiologic aspects; clinical information must be limited to that necessary to provide a background for the radiology. The discussion should be succinct and should focus on the specific message and relevance of radiologic methods. A review of the literature is not appropriate.

Length. Maximum of five double-spaced, typewritten pages, including the references but not the title page or figure legends.

References. Maximum of eight.

Figures. Maximum of four, unless the text is shortened accordingly. Legends must not repeat the text.

Tables and Acknowledgments. Not appropriate in case reports.

Technical Notes

A technical note is a brief description of a specific technique or procedure, modification of a technique, or equipment of interest to radiologists.

Format. No abstract, headings, or subheadings are required. If headings are used, they should be a combination of "Case Report," "Materials and Methods," "Results," and "Discussion." A brief one-paragraph introduction should be included to give the general background. Discussion should be limited to the specific message, including the uses of the technique or equipment. Literature reviews and lengthy case reports are not appropriate.

Length. Maximum of five double-spaced, typewritten pages, including the references but not the title page or figure legends.

References. Maximum of eight.

Figures. Maximum of two, unless the text is shortened accordingly.

Tables and Acknowledgments. Not appropriate in technical notes.

Pictorial Essays

A pictorial essay is an article that conveys its message through illustrations and their legends. Unlike other AJR articles, which are based on original research, pictorial essays serve primarily as teaching tools, like exhibits at a scientific meeting. They are not encyclopedic book chapters. The abstract should be a short, introductory paragraph.

Length. Maximum of four double-spaced, typewritten pages, including the references but not the title page or figure legends.

References. Maximum of four.

Figures. Maximum of 30 figure parts. Number should be as few as necessary to convey the message of the paper.

Tables and Acknowledgments. Not appropriate in pictorial essays.

Letters to the Editor and Replies

Letters to the Editor and Replies should offer objective and constructive criticism of published articles. Letters may also discuss matters of general interest to radiologists. Do not end a letter with a hand-written signature.

Format. All letters should be typed double-spaced on nonletterhead paper, with no greeting or salutation. Name and affiliation should appear at the end of the letter. Titles for letters should be short and pertinent. The title for a reply is simply "Reply."

Length. Maximum of two double-spaced, typewritten pages, including references.

References. Maximum of four.

Figures. Maximum of two.

Tables and Acknowledgments. Not appropriate in Letters to the Editor and Replies.

Opinions, Commentaries, and Perspectives

Opinions, commentaries, and perspectives are special articles dealing with controversial topics or issues of special concern to radiologists.

Format. Include a title page but no abstract. Headings may be used to break up the text.

Length. Maximum of five double-spaced, typewritten pages.

References. Maximum of five.

Tables and Figures. Maximum of four.

Computer Page Articles

Articles published on the computer page deal with practical computer applications to radiology.

Format. Include a title page and an abstract.

Length. Maximum of eight double-spaced, typewritten pages.

References. Maximum of five.

Figures and Tables. Maximum of five. Computer printouts are not acceptable. Figures must be submitted as 5 x 7 in. glossy prints.

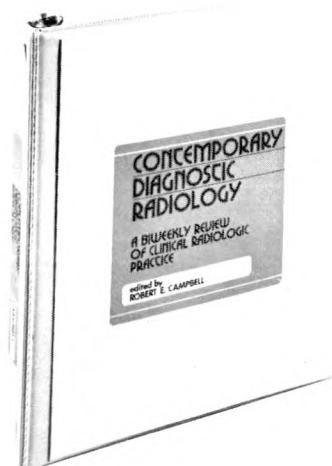
You learn from your experience with **CONTEMPORARY DIAGNOSTIC RADIOLOGY**

Editor: Robert E. Campbell, M.D.

A Biweekly Review of Clinical Radiologic Practice—26 issues a year!

One of your toughest jobs is keeping up with the many new developments that affect radiology. That's why you want **Contemporary Diagnostic Radiology**...an effective and convenient way to perfect your skills and maintain your professional status.

Contemporary Diagnostic Radiology is designed as a continuing education program that lets you work at your own pace. Every two weeks you'll receive an issue that covers a single topic or procedure in detail. Read the information and study the clearly reproduced radiographs—and then, if you choose, respond to a comprehensive examination in the strictest confidence. You set the pace. Each biweekly lesson brings you pertinent review of the basics in bone radiology...gastrointestinal radiology...pediatric radiology...genitourinary radiology...MR imaging...and all of the topics you want to know more about.



Contemporary Diagnostic Radiology works two ways. You may choose to subscribe to the non-scoring version, receiving every issue as an important element of your professional reading. The scoring version, however, supplements your reading and computer-coded examinations with confidential result responses, making you eligible for Continuing Medical Education credits co-sponsored by the University of Pennsylvania School of Medicine.

"As an organization for continuing medical education, the University of Pennsylvania School of Medicine designates this continuing medical education activity as meeting the criteria for 1 credit hour per bi-weekly issue in Category I for Educational Materials for the Physician's Recognition Award of the American Medical Association provided it has been completed according to instructions."

You can begin this ongoing program **today**. **Contemporary Diagnostic Radiology** is a year-round program, so you can join at any time. To begin your lessons, just fill out the enclosed card and return it to us. Or call **FREE** 1-800-638-6423 from anywhere in the U.S. or Canada. You'll find that **Contemporary Diagnostic Radiology** is the most efficient and inexpensive way to keep up with your dynamic field.

Williams & Wilkins

P.O. Box 23291
Baltimore, Maryland 21203-9990



Broadway House
2-6 Fulham Broadway
London SW6 1AA England

clip & mail

CONTEMPORARY DIAGNOSTIC RADIOLOGY

- Yes! I want to keep pace in my field! Begin my 26-issue subscription:
 Send me the scoring version (\$240)
 Send me the non-scoring version (\$197)
 Send me the resident non-scoring version* (\$120) (add \$57 for optional airmail delivery outside the U.S.; in Canada, also add 7% GST.)
 new subscription renewal

name _____

address _____

city/state/zip _____

payment options

- payment enclosed
 American Express

- bill me
 MasterCard
 VISA

printed in USA

card # _____ expiration date _____

signature/P.O. # _____

Maryland residents add 5% sales tax. Subscriptions outside the U.S. must be prepaid in U.S. dollars only. Rates valid through October 31, 1991. Please allow 8 weeks for delivery of your first issue, up to 16 weeks for surface delivery outside the U.S. Optional airmail rates add \$57 per subscription.

*Residents are eligible for the special in-training rate for up to three years. When requesting this rate, please include training status and institution. _____



Don't forget: you can order with a **TOLL-FREE** call to 1-800-638-6423 from anywhere in the U.S. or Canada.

Williams & Wilkins

P.O. Box 23291
Baltimore, Maryland 21203-9990

CDR 52740

Broadway House
2-6 Fulham Broadway
London SW6 1AA England

J1091S01

AJR Business and Subscriber Information

The American Roentgen Ray Society

AJR, American Journal of Roentgenology, is published monthly to disseminate research on current developments in the radiologic sciences and commentary on topics related to radiology. It is published by the American Roentgen Ray Society, 1891 Preston White Dr., Reston, VA 22091; (703) 648-8992. Inquiries regarding society business, the annual ARRS meeting, and membership should be addressed to the Society at the above address.

Correspondence Concerning the AJR

Correspondence regarding display (not classified) advertising, subscriptions, address changes, reprints, and permission requests should be addressed to Williams & Wilkins, 428 E. Preston St., Baltimore, MD 21202; (301) 528-4000.

Correspondence regarding editorial matters and classified advertising should be addressed to Editorial Office, AJR, 2223 Avenida de la Playa, Ste. 103, La Jolla, CA 92037-3218; telephone (619) 459-2229; FAX (619) 459-8814. For information on manuscript submission, see Guidelines for Authors, pages A13-A15.

Subscriber Information

Subscription requests and inquiries should be sent to Williams & Wilkins, 428 E. Preston St., Baltimore, MD 21202. ARRS annual dues include \$50 for journal subscription. Subscription rates are as follows: nonmembers, \$125/year (\$180 foreign); institutions, \$135 (\$190 foreign); nonmember in-training, \$25 (\$80 foreign). Single copies of the Journal may

be purchased for \$18 (\$22 foreign). Airmail rates will be furnished on request. The GST number for Canadian subscribers is 123394371.

Call toll-free, 1-800-638-6423 (in Maryland call 1-800-638-4007), with subscription questions or problems. Please have the mailing label from your latest issue available when you call.

If a subscriber receives a damaged copy of the *AJR* or fails to receive an issue, the subscriber should notify Williams & Wilkins (428 E. Preston St., Baltimore, MD 21202) within 60 days of publication (90 days for foreign subscribers) and that issue will be replaced.

Change of address information should be sent to Williams & Wilkins, 428 E. Preston St., Baltimore, MD 21202. Allow 90 days for address changes.

Copyrights, Permissions, and Reprints

The American Roentgen Ray Society holds the copyright for all material published in the *AJR*. No part of this publication may be reproduced without permission from the ARRS. Requests for such permission should be addressed to Williams & Wilkins, 428 E. Preston St., Baltimore, MD 21202.

For reprints of a particular article, please contact the author designated in the footnotes for that article.

Indexes

The *AJR* provides volume and yearly indexes (subject and author) in the June and December issues each year. *AJR* articles are also indexed in *Current Contents*, *Index Medicus*, and the cumulative index published by *Radiology*.



The new Rapid Access imaging system features unique technology to give you four processing options—for example, emergency room images in less than 40 seconds!

It's not just fast—we've redesigned every step of the imaging chain for the highest quality and consistency. Innovative new T-Mat films, new X-Omat processors, film handling equipment, and chemicals mean maximum productivity for you and your staff.

Plus, the Kodak team provides another key to productivity—superlative service, with support ranging from architectural advice to operator training.

For more about how the speed, versatility, and consistency of the KODAK Rapid Access System can benefit you, your staff, and your patients, contact your Kodak account manager.

Kodak. Quality you can see in your bottom line.

MORE THAN FAST. INTRODUCING RAPID ACCESS. **KODAK**

The first choice in quality imaging...worldwide



Review Article

Recent Advances in MR Imaging/Spectroscopy of Cerebral Ischemia

Lori L. Baker,¹ John Kucharczyk, Robert J. Sevick, Jan Mintorovitch, and Michael E. Moseley

Recent advances in high-resolution MR imaging and multinuclear spectroscopy have stimulated studies of the functional relationships between tissue hypoperfusion, cellular energy depletion, and brain edema associated with cerebral ischemia. The very slow ($\mu\text{m/sec}$) random translational motion of water protons in various brain tissues and intracranial fluid compartments can now be assessed with MR diffusion imaging. More slowly diffusing protons in ischemic tissues can be differentiated from normal parenchyma, CSF, and flowing blood, enabling the detection and localization of ischemic regions within minutes of the onset of stroke. Perfusion imaging "snapshots," obtained in as little as 25 msec with echoplanar MR methods, permit the evaluation of tissue washin/washout kinetics of contrast agents in the microvasculature, and thus the quantification of brain perfusion on a regional basis. Also, delineation of major intra- and extracranial arterial and venous structures with MR angiography, acquired with two- or three-dimensional Fourier transformation techniques, has enabled accurate noninvasive assessments of vascular occlusive disease. Finally, improvements in MR spectroscopic techniques have facilitated investigations of metabolic regulation and bioenergetics in experimental animal models of cerebral ischemia, as well as in stroke patients. Combined MR imaging and spectroscopy will likely play an important role in differentiating reversibly from irreversibly ischemic brain tissues and in the investigation of various neuroprotective pharmaceuticals.

The development of MR imaging has greatly improved clinical diagnostic capabilities in the early detection and characterization of cerebral ischemia [1–7]. The strength of MR imaging in depicting ischemic changes is based principally on

its exquisite sensitivity to the presence of increased tissue water content (cerebral edema). Clinically, hyperintensity may be seen on T2-weighted spin-echo images at approximately 6–12 hr after the ischemic event and as early as 2–3 hr after experimentally induced ischemia in animals [8, 9]. Recently, with the development of diffusion-weighted MR imaging [10–13] and contrast-enhanced echoplanar imaging [14, 15], changes in signal intensity in animal studies have been reported to occur within minutes of arterial occlusion. At the same time, *in vivo* MR spectroscopy has gained importance as a noninvasive method for evaluating ischemia-induced changes in cerebral metabolism [10, 16–23]. The combination of MR imaging and spectroscopy [10, 16, 18], now possible on both experimental and clinical MR units, offers a novel approach to elucidating the metabolic and structural alterations associated with early ischemia. This "integrated examination" may also eventually play a key diagnostic role in the evaluation of the reversibility of ischemic tissue injury [20, 21, 23] and the pharmacotherapeutic response to investigational neuroprotective agents [13, 16, 18].

MR imaging and spectroscopy of cerebral ischemia was last reviewed in the *AJR* in 1987 [2]. Since then there have been major advances in MR imaging techniques. In particular, the development and use of diffusion-weighted imaging and contrast-enhanced echoplanar imaging have stimulated numerous research studies. The purpose of this article is to describe the current capabilities of MR imaging/spectroscopy of acute cerebral ischemia. Attention is focused on the results

Received September 24, 1990; accepted after revision December 4, 1990.

¹ All authors: Department of Radiology, Neuroradiology Section, Box 0628, Room L358, University of California, San Francisco, 505 Parnassus Ave., San Francisco, CA 94143. Address reprint requests to J. Kucharczyk.

AJR 156:1133–1143, June 1991 0361–803X/91/1566–1133 © American Roentgen Ray Society

of recent experimental studies that indicate that diffusion-weighted and echoplanar MR techniques may improve the temporal sensitivity and spatial accuracy of MR in the detection and characterization of stroke.

Pathophysiology of Ischemic Injury

Hypoperfusion is the common initiating stimulus for ischemic injury. However, a number of other factors such as oxygen tension, carbon dioxide and hydrogen ion concentrations, and serum glucose levels contribute to the final outcome [24–26]. Global ischemia typically causes selective necrosis in the cerebral neocortex, hippocampus, and striatum [27]. With focal or regional ischemia, on the other hand, the specific vascular territory that is occluded has the largest impact on the anatomic extent and pattern of neural damage [28, 29].

Atherosclerosis, arterial dissection, and subarachnoid hemorrhage-induced vasospasm can all produce major cerebral infarcts [2]. Venous occlusion, seen principally in hypercoagulable states such as pregnancy, in inflammatory disease of the paranasal sinuses, in systemic sepsis, and with tumor invasion of the dural venous sinuses, can cause cerebral venous hypertension leading to reduced perfusion pressure; regional cerebral edema; and, subsequently, breakdown of the blood-brain barrier [30]. Infarction resulting from hypoxia and hypoperfusion of a systemic origin often is associated with cardiac failure, arrhythmias, or cardiac bypass surgery. Infarcts often occur in "watershed zones" between the major arterial territories or in terminal vascular regions, such as the basal ganglia [2, 30].

The adult human brain receives about 750 ml of blood per minute, or 15% of the total resting cardiac output. Normal cerebral blood flow (CBF) averages $50\text{--}55 \text{ ml} \cdot 100 \text{ g}^{-1} \cdot \text{min}^{-1}$, with a range of approximately $40\text{--}67 \text{ ml} \cdot 100 \text{ g}^{-1} \cdot \text{min}^{-1}$ [31]. The CBF of gray matter is three- to fourfold higher than that of white matter. CBF is efficiently autoregulated at perfusion pressures between 60 and 180 mm Hg. Below approximately 60 mm Hg the autoregulatory mechanisms become progressively ineffective and eventually fail [27, 32].

Reductions in CBF below the threshold for autoregulation result in diminished oxygen delivery to neuronal cell membranes; disrupted oxidative phosphorylation; and, in turn, reduced biosynthesis of adenosine triphosphate (ATP) from glucose. Neurons and glia then resort to an obligatory but also much less efficient form of energy production, anaerobic glycolysis. The decreased availability of ATP impairs normal transmembrane sodium-potassium pump function; as a result, extracellular sodium accumulates within brain cells and intracellular potassium is lost to the extracellular space. Other high-energy phosphates, such as phosphocreatine, are also depleted, and inorganic phosphate and lactate accumulate, causing tissue acidosis. The osmotic gradient created within brain cells by the relatively high concentrations of sodium and lactic acid facilitates the rapid influx of water into neurons and glia.

Cytotoxic edema is initiated within minutes of onset of ischemia and can produce an increase in brain tissue water

of 3–5% [33, 34]. Subsequent endothelial cell injury [35, 36] results in a loss of integrity of the blood-brain barrier, thereby facilitating extravasation of proteins from the intravascular space as well as an accumulation of extravascular water (vasogenic edema) hours later [33, 34]. The severity of vasogenic edema is influenced by many factors, including the degree of reperfusion and the extent of collateral flow to the ischemic area [37–42]. Reperfusion of the occluded vascular bed can exacerbate brain edema by increasing fluid exudation into the tissues [40–42]. Cerebral edema associated with ischemia is typically most prominent within the first week and subsequently decreases in extent [2]. Further evolution results in atrophy and encephalomalacia of ischemic regions [2, 30].

MR Imaging of Cerebral Ischemia

The signal intensity on proton MR images is a function of T1 and T2 relaxation times, proton density, and molecular microscopic and macroscopic motion. In stroke patients, signal hyperintensity can be observed on T2-weighted spin-echo images (e.g., 2000/25/1 [TR/TE/excitations]) from 6 to 12 hr after the ischemic event [1–7]. Adjacent sulci are often effaced because of mass effect (Fig. 1). One recent investigation found that acute infarction may also produce subtle arterial enhancement on T1-weighted images following IV administration of gadopentetate dimeglumine [43]. In the subacute stage, mass effect and edema gradually diminish. At this stage, enhancement of ischemic zones with gadopentetate dimeglumine is an indication of blood-brain barrier breakdown. This follows a time course similar to that for enhanced CT, with enhancement occurring most commonly between 2 and 6 weeks after the ischemic event [2, 30].

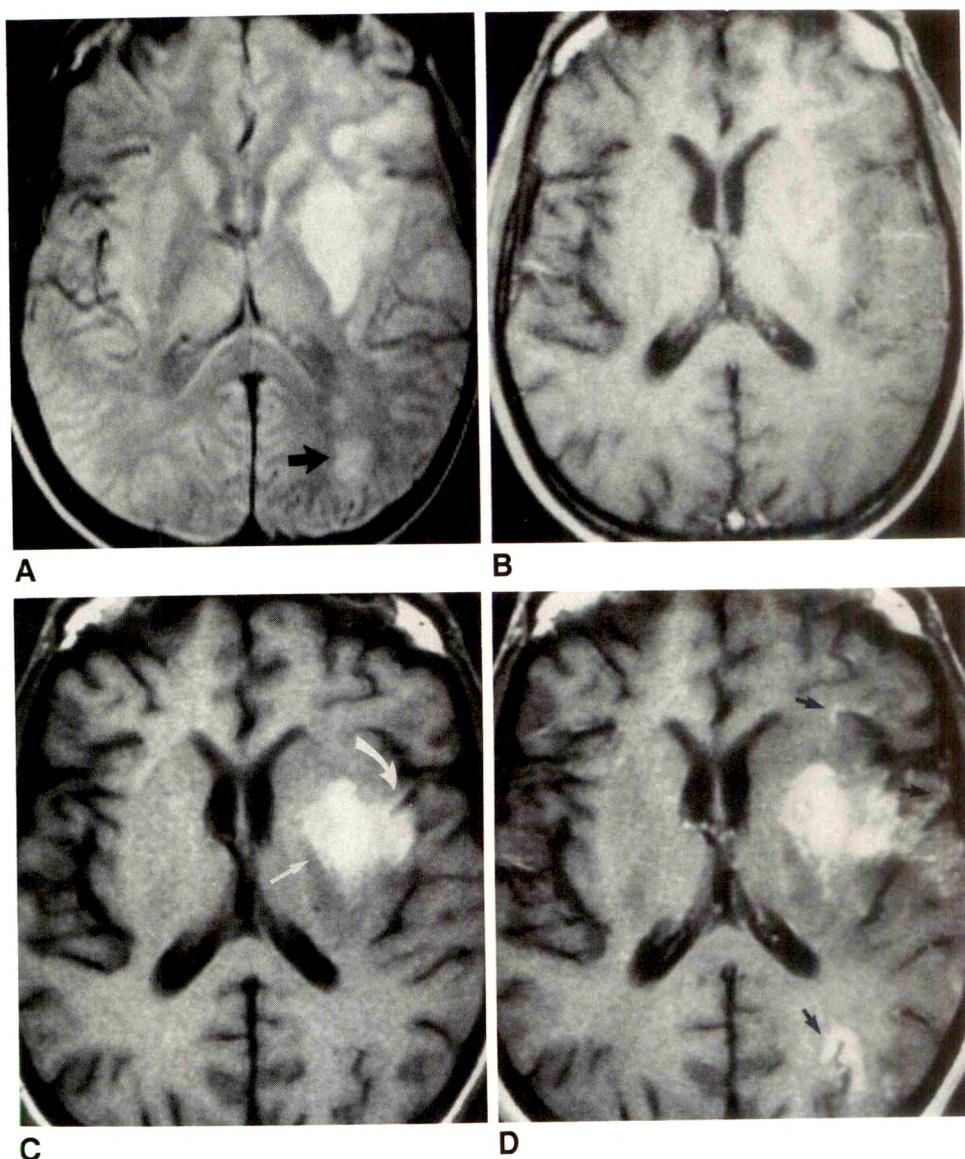
Detection of hemorrhage complicating cerebral infarction can be of considerable clinical importance, as it may alter case management [44]. Secondary hemorrhage occurs in up to 40% of patients with cerebral infarction [2] and may be manifested either as petechial cortical hemorrhage or parenchymal hematoma (Fig. 1). Areas of petechial hemorrhage, which are in general clinically inconsequential, tend to develop in patients with nonembolic infarcts [30, 45]. Hemorrhage is more common in patients with embolic strokes. In this setting, there is lysis of the intravascular embolus with reconstitution of normal perfusion pressure to an ischemically damaged blood-brain barrier and resultant extravasation of blood into the extravascular space [2, 30, 45]. Larger areas of parenchymal hemorrhage tend to develop in these patients than in those with nonembolic infarcts. The signal intensity in the hematoma is based on complex interactions between numerous factors, including the oxidation state of hemoglobin; paramagnetic properties of the degradation products; and physiologic parameters, such as oxygen tension, brain edema, and hematocrit [46].

With progressive atrophy and gliosis, the infarcted territory will gradually assume signal characteristics similar to those of CSF, with surrounding brain demonstrating abnormal signal owing to cellular loss and increased tissue water content. Often there is accompanying ventricular and sulcal enlarge-

Fig. 1.—**A**, First echo of axial T2-weighted MR image (2000/25/1) shows signal hyperintensity involving left basal ganglia and insular cortex. Small focus of hyperintensity is also present in left occipital region (arrow).

B, Corresponding T1-weighted image (600/17/1) shows mass effect with effacement of sylvian cistern and arterial enhancement. Findings are compatible with acute middle cerebral artery territory stroke.

C and **D**, Axial T1-weighted MR images (600/20/2) obtained 1 week later. On unenhanced image (**C**), subacute hematoma in basal ganglia (straight arrow) and petechial cortical hemorrhage (curved arrow) are both seen as regions of T1 shortening (hyperintensity). After IV administration of gadopentetate dimeglumine (**D**), gyral enhancement pattern is evident (arrows).



ment, and chronic residua of hemorrhage may be present (Fig. 2).

CBF decreases with increasing age [47, 48]. The reasons for this include chronic hypoperfusion, hypoxia, and arteriolar disease. Because the deep white matter and basal ganglia are supplied by long, slender perforating arterioles without significant collateralization, these areas are especially vulnerable to chronic ischemic injury. A number of studies have suggested that hypertension may play a role in the development of chronic ischemic injury leading to increased subcortical signal intensity [49, 50]. However, other studies found that subcortical hyperintensities were seen in healthy elderly persons with no history of hypertension [51, 52].

MR imaging in elderly persons without neurologic impairment has revealed the relatively common presence (30–80%) of small, patchy, focal regions of hyperintensity located within the periventricular white matter, centrum semiovale, and basal ganglia on first- and second-echo T2-weighted images [52,

53]. Various theories have been proposed in the neuropathology literature to explain the MR findings of normal aging and have been summarized in a recent review article on the subject [52]. However, many postmortem studies are limited by incomplete clinical data regarding vascular risk factors, neurologic status, and systemic disease. It appears likely that the signal alterations observed in the deep white matter and basal ganglia are related at least in part to chronic ischemia [54, 55].

MR imaging also allows direct noninvasive assessment of cerebral hemodynamics on a regional basis. Patent blood vessels with rapid flow typically demonstrate intraluminal signal loss or *flow void* on routine spin-echo T1- and T2-weighted images due to *time-of-flight* (TOF) effects and turbulence [56, 57]. The absence of intravascular flow void is suggestive of slow flow states or occlusion. One recent study noted that intraluminal signal, which was generally isointense on T1- and T2-weighted images, was seen in patients with

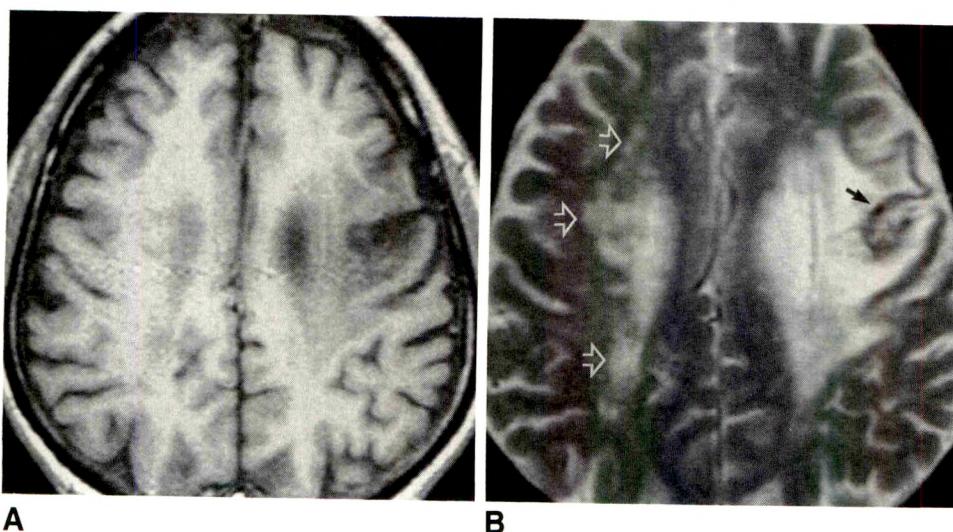


Fig. 2.—A, Axial T1-weighted MR image (500/11/2) shows parenchymal loss surrounded by area of low signal intensity in left frontoparietal region.

B, Corresponding axial T2-weighted image (2300/85/1) shows high signal intensity in infarcted territory and T2 shortening (hypointensity) due to hemosiderin deposition (solid arrow). Small-vessel ischemic infarcts are present in periventricular white matter (open arrows).

intracranial internal carotid occlusion [58]. Absence of intravascular flow void or replacement by isointense or hyperintense signal has also been observed in dural sinus thrombosis [59, 60]. However, accurate assessment of dural sinus patency may be hampered by intraluminal artifacts, in particular flow-related enhancement, that simulate intraluminal clot. The use of gradient-recalled echo (GRE) sequences may help in the diagnosis, since the patent sinus normally demonstrates high signal intensity owing to flow-related enhancement on GRE images. In the presence of sinus thrombosis, there is loss of flow-related enhancement and replacement by clot, which generally is of low signal [61]. However, the signal characteristics of intraluminal clot are dependent on the stage of evolution. One recent study described subacute sinus thrombus that was hyperintense on GRE images owing to the T1 shortening effect of methemoglobin [62]. Preliminary studies suggest that phase-contrast MR angiography (MRA) may be useful in the detection of sinus thrombosis [63].

MR Angiography

Recent developments in MRA techniques have added significantly to the usefulness of MR imaging as a clinically important noninvasive method for the evaluation of vascular structures [64–67]. A comprehensive analysis of the wide variety of MRA techniques currently implemented clinically as well as those under investigation is beyond the scope of this article, and the reader is referred to recent reviews on the subject [64–68]. However, a brief overview of the more fundamental MRA techniques as applied to the evaluation of cerebrovascular disease is presented here.

Vessel delineation is possible with MRA because of the excellent image contrast resolution between stationary tissue and flowing blood. GRE pulse sequences are used to acquire MRA studies with either the two-dimensional (2-D) or three-dimensional (3-D) Fourier transformation technique. Flow contrast is obtained with either TOF techniques based on the longitudinal magnetization differences of inflowing unsatu-

rated spins and stationary saturated spins or phase-contrast techniques that use gradient pulses to produce different phase shifts for flowing and stationary spins.

3-D TOF imaging techniques involve a volume data acquisition from which thin slices or partitions are then obtained. Image postprocessing is performed by using a maximum-intensity projection that may be performed from any angle, resulting in images that are tailored to the anatomy of the individual patient, allowing optimal depiction of vascular disease. Because the source of intraluminal signal results from unsaturated flowing protons, veins and arteries with slower flow may become saturated, resulting in signal loss. 3-D TOF techniques are especially sensitive to saturation effects owing to the use of volume data acquisitions and are most useful for evaluating arteries with rapid flow, such as the circle of Willis [64, 69].

In contrast to 3-D TOF, images in 2-D MRA are produced by acquiring sequential thin slices that minimize saturation effects. 2-D techniques, therefore, are preferable when evaluating venous or arterial structures with slower velocities such as the extracranial carotid arteries. Presaturation bands located superiorly or inferiorly to the current imaging slice allow selective visualization of vascular structures as they saturate venous or arterial flow, respectively. One recent study demonstrated the advantage of using contiguous 1.5-mm axial 2-D slices, vs 3-D techniques, for delineating extra-cranial carotid arteries [70].

MRA also shows potential for determining the direction and velocity of blood flow. Velocity information derived from TOF techniques, such as presaturation bolus tracking, results from changes in the longitudinal magnetization of flowing protons. This method used a presaturation pulse, which serves to "label" a bolus of blood that is then imaged with cine low-flip-angle GRE sequences [71]. Velocity is then determined by dividing the distance the bolus has traveled by the time between bolus labeling and the "read" cycle. Phase-sensitive techniques enable velocity determinations by detecting phase shift as flowing protons course along a magnetic field gradient [72].

Early Detection of Ischemic Injury with Diffusion-Weighted MR Imaging

MR imaging methods capable of detecting pathophysiologic changes within minutes of onset of cerebral ischemia are currently under intensive scrutiny. In vivo diffusion imaging, first described by LeBihan et al. [73, 74], is a new MR technique that is sensitive to the microscopic motion of water protons. By comparison, the signal intensity on T2-weighted spin-echo MR appears to be influenced primarily by tissue water content or concentration.

A diffusion-weighted image is obtained by modifying a spin-echo pulse sequence with the addition of strong diffusion-sensitizing gradients (Fig. 3). Depending on the durations of

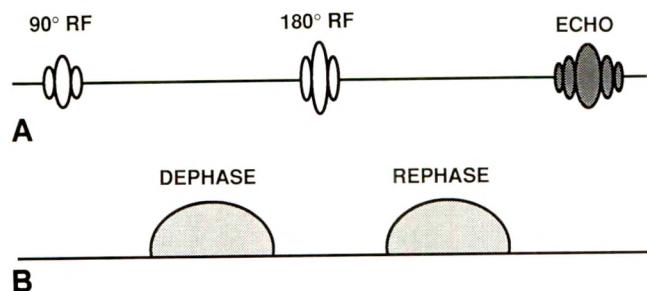


Fig. 3.—Diagrams illustrating spin-echo and diffusion-weighted pulse sequences.

A, Conventional spin-echo pulse sequence consists of 90° and 180° RF pulses followed by echo sampling at time TE after 90° RF pulse.

B, Diffusion-weighted pulse sequence involves addition of strong diffusion-sensitizing gradients to spin-echo pulse sequence, placed symmetrically between 90° and 180° RF pulses and 180° RF pulse and echo readout. After 90° RF pulse, magnetization components precess at different frequencies and lose synchrony (dephasing). The first diffusion-sensitizing gradient pulse causes even greater dephasing. Subsequent 180° RF pulse and second diffusion-sensitizing gradient pulse rephase (and thereby form an echo from) only stationary protons. Diffusing spins do not dephase/rephase completely, leading to significant echo attenuation.

TR and TE, the resulting signal-intensity changes in the image can reflect water proton diffusion behavior as well as T1 and T2 relaxation effects. Increasing the duration and amplitude of the gradients (the b value) increases the sensitivity of the image to molecular diffusion of water. Acquiring two or more images with two or more different b values enables a calculation of the apparent diffusion image. Recently, measured apparent diffusion coefficients of about 1×10^{-5} cm²/sec were obtained for human brain, with values for gray matter 10–20% higher than those for white matter [10].

Recent work using an animal model of middle cerebral artery (MCA) occlusion has demonstrated the increased sensitivity of diffusion-weighted images over T2-weighted images in the early detection of stroke [10–13]. Hyperintensity was observed on diffusion-weighted images as early as 45 min after MCA occlusion (Fig. 4A), whereas T2-weighted images failed to show clear evidence of injury for 1.5–3.0 hr (Fig. 4B). The measured apparent diffusion coefficient in the hyperintense ischemic brain regions was approximately half that in the contralateral MCA territory [10], indicating slower microscopic proton motion or diffusion in the injured tissues. Reversal of the diffusion-weighted hyperintensity was found with reflow after 30 min of MCA occlusion [12]. Close correlations were found also between increases in diffusion-weighted MR signal intensity and disrupted phosphorus-31 and proton metabolite levels evaluated with surface-coil MR spectroscopy [10]; with intravascular T2*-shortening contrast agents, which reveal perfusion deficits [11, 13]; and with postmortem histopathology [10–13].

Although the results of these experiments indicate that diffusion-weighted MR imaging can significantly advance the time of detection of cerebral ischemic insults, the precise nature and pathophysiologic significance of diffusion-weighted MR hyperintensity has not been firmly established.

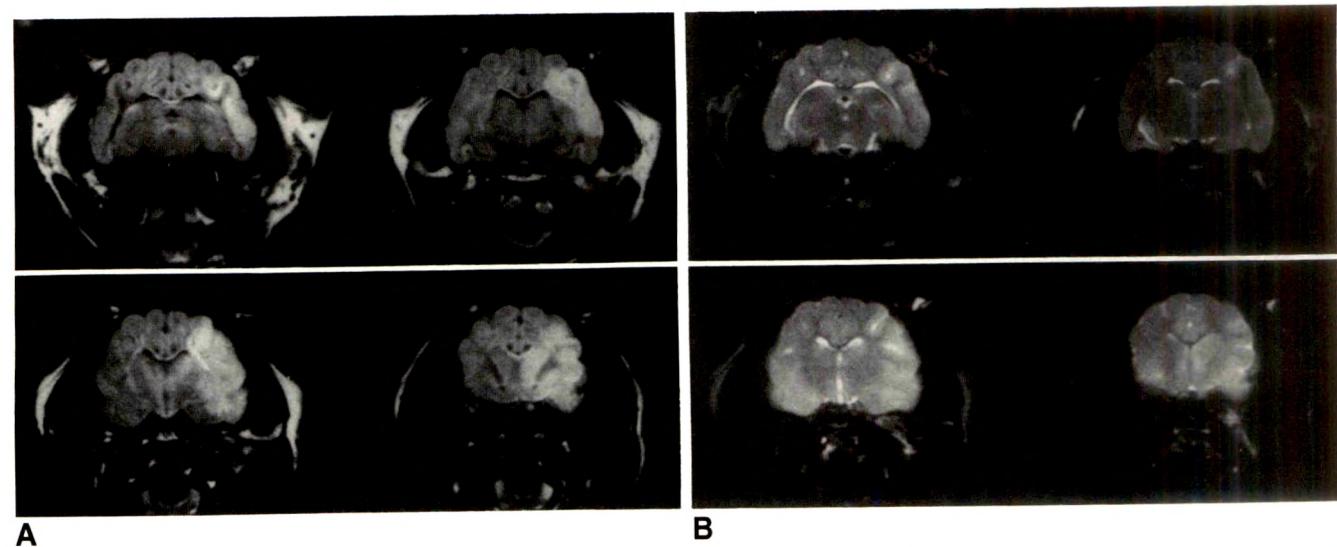


Fig. 4.—A, Diffusion-weighted 1000/80/4 MR images (3-mm slice, 1-mm slice gap, 80-mm field of view, b = 1413 sec/mm²) of cat brain at four coronal levels obtained 45 min after occlusion of right middle cerebral artery (MCA). Increased signal intensity is seen throughout MCA vascular territory in ipsilateral hemisphere.

B, Corresponding T2-weighted spin-echo 2800/160/2 images (3-mm slice, 1-mm slice gap, 80-mm field of view) obtained approximately 1.5 hr after MCA occlusion. Ischemic tissue injury (hyperintensity) in MCA vascular territory is not seen as clearly as on diffusion-weighted MR images.

A reduction in brain tissue temperature in hypoperfused or ischemic regions theoretically could account for the hyperintensity observed on diffusion-weighted MR images. LeBihan et al. [74] used a phantom heated inside a 0.5-T whole-body imaging system to demonstrate that a 1% change in temperature corresponds to a 2.4% change in diffusion coefficient. Busto et al. [75] found that brain temperature in ischemic regions may fall by up to 7°C after bilateral carotid/vertebral artery occlusion in an animal model. Clearly, further experiments are needed to establish unequivocally the role of tissue hypothermia as a source of the observed hyperintensity on the diffusion-weighted images.

Changes in tissue osmolality associated with ischemia also may exert some influence on the hyperintensity observed on diffusion images. A significant increase in osmolality of ischemic brain occurs within 2–6 min of arterial occlusion [76]. This increase in brain osmolality correlates with water content [77] and therefore could be responsible for the early accumulation of edema and reduced apparent diffusion coefficient after ischemic injury.

Another possible explanation is that ischemia may precipitate a loss of cellular volume control resulting from a drop in brain pH [78]. Sodium ions taken up as a result of activated Na^+/H^+ transmembrane exchange would then cause water to flow into cells to maintain osmotic balance, resulting in cytotoxic edema [79]; slower microscopic proton diffusion; and, consequently, hyperintensity on diffusion-weighted images.

A final plausible theory is that physiologic motion within the cranium might contribute to the differences in apparent proton diffusion in normally perfused vs ischemic regions. A reduction in CBF would attenuate brain pulsatile motion, thereby leading to a decrease in apparent proton diffusion and diffusion-weighted hyperintensity in the ischemic regions [73, 74]. Further studies are necessary to assess the relative importance of postischemic hypothermia, increased tissue osmolality, cytotoxic edema, and reduction in brain pulsatile motion to diffusion-weighted hyperintensity.

Current problems limiting the widespread clinical use of diffusion-weighted imaging include the inherent sensitivity to both physiologic and gross patient motion. Many acute stroke patients are very ill and disoriented, and may not be able to remain still for the 60- to 90-min period required to complete an MR diffusion imaging study. Additionally, coils capable of producing the required gradient strengths (5 G/cm compared with 1 G/cm in routine clinical applications) are not yet widely available for clinical systems.

Whatever the exact cause of diffusion-weighted hyperintensity, it would appear to represent an imaging marker of very early ischemic tissue damage. As therapeutic intervention in early stroke comes closer to becoming a reality, diffusion-weighted MR imaging may be expected to assume an increasingly important diagnostic role.

Perfusion Imaging of Acute Cerebral Ischemia

Paramagnetic contrast agents, such as gadopentetate dimeglumine, have had limited value in the MR assessment of acute cerebral ischemia because enhancement is dependent

on blood-brain barrier breakdown [80], which is a relatively delayed postischemic event [33, 34]. Recent studies have shown that magnetic-susceptibility contrast agents, such as dysprosium-DTPA-bis(methylamide) (Dy-DTPA-BMA), may offer a sensitive method of assessing changes in blood volume or tissue perfusion associated with ischemia [11, 15]. Magnetic susceptibility imaging is designed to have a high degree of T2* weighting [81, 82]. In normal brain, lanthanide chelates like Dy-DTPA-BMA are confined to the intravascular space by the intact blood-brain barrier [81, 82]. A field gradient is induced between the capillary space and the surrounding perfused tissue, resulting in significant but transient signal loss in regions with normal blood flow [82]. This magnetic susceptibility effect is much larger than that caused by T1 relaxivity changes [81, 82]. This agent also has the additional advantage of providing contrast enhancement without actually crossing the blood-brain barrier.

Studies using IV administration of Dy-DTPA-BMA in an animal model of unilateral MCA occlusion [11, 15] have demonstrated that the agent causes a 50–60% reduction in the signal intensity of normally perfused brain tissue on T2-weighted images. Nonperfused or ischemic zones appear by default to be relatively hyperintense. Dy-DTPA-BMA-enhanced MR imaging significantly advanced the time of detecting regional acute ischemia compared with unenhanced T2-weighted images [11, 15]. Small infarcts that were inconspicuous or missed altogether on unenhanced T2-weighted images could be seen clearly after administration of Dy-DTPA-BMA (Fig. 5).

Preliminary clinical data using magnetic-susceptibility MR imaging with gadopentetate dimeglumine have demonstrated that stroke, vascular stenosis, arteriovenous malformation, and neoplasm show patterns of enhancement different from those of peritumoral edema and normal brain tissue [83]. In 11 of 15 patients with stroke, no significant change in signal intensity was observed in the core of the infarct during the first pass of contrast material, suggesting a marked reduction in blood volume or flow to the region. The same study also indicated that dynamic information regarding cerebral circulation time can be obtained by evaluating the temporal characteristics of contrast-induced enhancement of the MCA territory and cerebellum/brainstem in patients with carotid stenosis and vertebrobasilar insufficiency, respectively.

A final notable advantage of magnetic susceptibility imaging is that it can be combined with new "ultrafast" MR techniques, like echoplanar imaging, to resolve the passage of intravascular contrast material through the capillary bed, thereby permitting kinetic modeling of regional blood flow and volume. The preliminary use of this technique is described below.

Ultrafast-Scan MR Imaging

Cerebral transit times are on the order of seconds [14, 83, 84], necessitating the use of high-speed imaging to remove spatial-temporal limitations and produce "real-time" images of the brain microcirculation. Echoplanar imaging is a subsecond MR technique that largely eliminates the motion artifact problems associated with diffusion-weighted imaging as well as

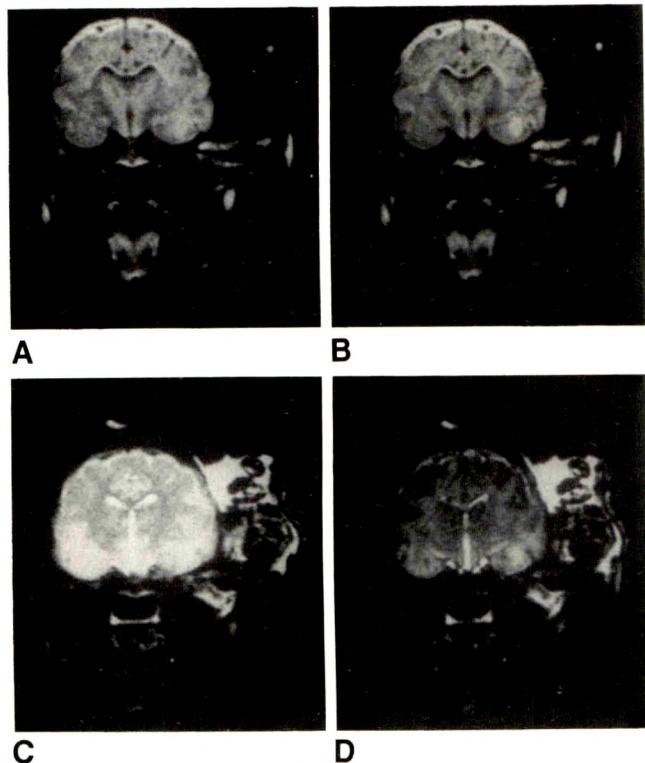


Fig. 5.—Coronal MR images of brain of cat pretreated with a calcium channel blocker 15 min before unilateral occlusion of middle cerebral artery (MCA).

A and B, Diffusion-weighted image (100/80/4) obtained 1 hr after MCA occlusion (**A**) shows a focal hyperintensity in ipsilateral temporal lobe that is better defined in a diffusion-weighted image obtained 5 hr after arterial occlusion (**B**).

C and D, Corresponding T2-weighted images (2800/160/2) obtained 55 min after occlusion. On image obtained after administration of Dy-DTPA-BMA (0.5 mmol/kg IV) (**D**), a small area of perfusion deficiency (hyperintensity) is visible in same region of temporal lobe. Unenhanced T2-weighted image (**C**) fails to show any corresponding area of edema. Signal intensities in all images have been scaled to background noise levels. Close spatial correlation between regions of hyperintensity on diffusion-weighted MR image and areas of high signal intensity on T2-weighted images after Dy-DTPA-BMA administration suggests that this magnetic-susceptibility contrast agent can be very useful for early detection of cerebral ischemic insults.

standard spin-echo MR methods. Combined with specific MR contrast agents, like Dy-DTPA-BMA and gadopentetate dimeglumine-BMA, the perfusion characteristics of normal and ischemic brain can be assessed quantitatively, thus enabling calculations of blood flow. Images are acquired by rapidly switching a phase gradient during echo formation while the readout gradient either is left on constantly or is pulsed.

In recent studies with contrast-enhanced GRE planar MR imaging in experimental animals (Kucharczyk J et al., presented at the annual meeting of the Western Neuroradiological Society, October 1990), Dy-DTPA-BMA administration significantly decreased the time for detection of ischemic tissue injury and clearly defined brain regions with perfusion deficits (Fig. 6). In another study [77], global hypercapnia was induced in dogs to evaluate the relationship between contrast-induced signal change and brain blood volume. For dynamic contrast studies, 2-D GRE images, 1000/14 (128 × 64 ma-

trix), were acquired in 25 msec. By integrating the concentration-time data on a voxel-by-voxel basis, functional images were generated depicting regional variations in CBF before, during, and after hypercapnia.

A major stimulus for further development of echoplanar imaging is the widely held view that this technique can provide dynamic information about CBF that is not available from MRA or conventional MR imaging. Although echoplanar MR imaging requires very-high-strength, rapidly switching gradient coils, these are now becoming available on many MR systems. However, limitations for immediate clinical use include image distortion due to field inhomogeneities, sampling methodologies, resolution, and low signal-to-noise ratio [14]. Thus, it is unclear how soon echoplanar MR imaging will become a routine MR procedure in the assessment of ischemia in patients.

Combined MR Imaging/Spectroscopy: The Integrated Examination

As a result of improvements in magnetic field homogeneity and increases in magnetic field strength, the combination of high-resolution MR imaging and spectroscopy is now becoming feasible for investigating the metabolic and structural abnormalities associated with cerebral ischemia. In effect, MR imaging represents a refinement of the application of MR spectroscopic principles with one significant difference [2, 85]. In MR imaging, the signal is obtained by systematically altering the homogeneity of the external magnetic field, which results in a change in the resonant frequency of a specific population of nuclei, allowing spatial localization within tissue. In MR spectroscopy, by comparison, an external magnetic field with a very homogeneous background is applied to the region of interest. Any deviation in the expected relaxation characteristics of a nucleus reflects its specific chemistry and thereby serves to identify the compound or metabolite. Instead of the image display obtained with MR imaging, MR spectroscopy yields plots of spectral peaks that reflect concentrations of various cell metabolites in a region of interest.

MR spectroscopy is the only noninvasive technique capable of measuring millimolar concentrations of phosphorus metabolites; amino and fatty acids; lactate; and other metabolically relevant compounds, including neurotransmitters. ^{31}P MR spectroscopy has played a major role in the noninvasive assessment of ischemia-induced alterations in cell metabolism [2, 10, 16–20]. Subtle frequency differences (chemical shifts) between various phosphate nuclei are measured by an MR spectrometer and plotted as peaks relative to an internal reference (phosphocreatine). The intensity of these peaks directly reflects the number of nuclei giving rise to the signal. On this basis, ATP resonances can be delineated from other phosphate-containing molecules, including sugar phosphates, inorganic phosphates, phosphodiesters, and phosphocreatine. Brain intracellular pH can be calculated from the ^{31}P spectrum by comparing the difference in chemical shift between the inorganic phosphate peak and the phosphocreatine peak.

Acute stroke is associated with several significant meta-

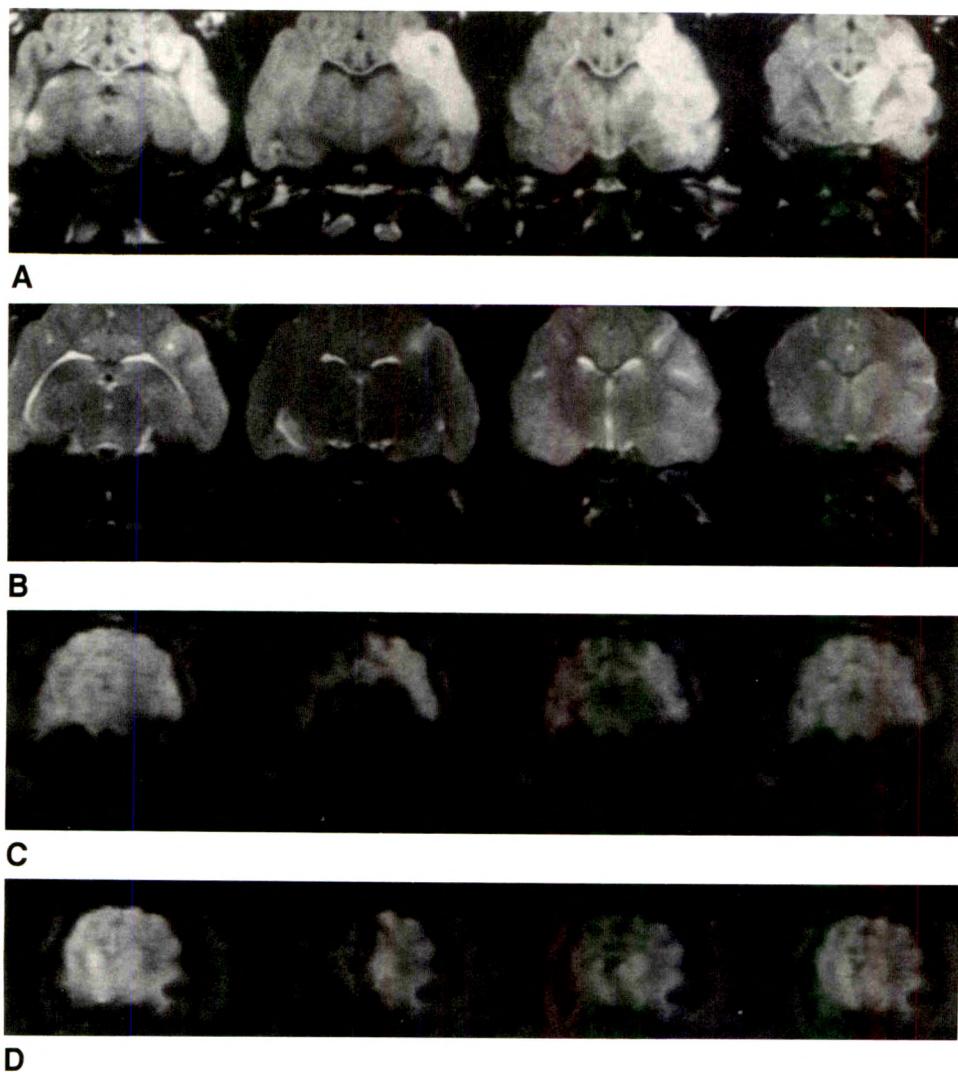


Fig. 6.—*A*, Diffusion-weighted MR image (100/80/4). Hyperintensity is visible at four coronal levels of middle-cerebral-artery (MCA) vascular territory 30 min after occlusion of artery.

B, Corresponding T2-weighted images (2800/160/2) of the same cat obtained approximately 90 min after MCA occlusion do not show evidence of ischemic damage as clearly as diffusion-weighted images did.

C and *D*, Sequential echoplanar images enhanced with Dy-DTPA-BMA (0.25 mmol/kg), corresponding to most posterior (*C*) and anterior (*D*) coronal levels. Contrast washin causes signal hypointensity in perfused tissues, leaving poorly perfused regions of brain supplied by MCA hyperintense.

bolic alterations [17, 18, 23], in contrast to subacute and chronic cerebral infarction, in which MR spectroscopy demonstrates only small changes in phosphorus spectra [19]. Studies of experimental regional ischemia in a cat model of unilateral MCA occlusion have implicated both energy depletion and lactic acidosis. Acute cerebral ischemia is associated with an early onset of reciprocal changes in phosphocreatine and inorganic phosphate (decreased phosphocreatine/inorganic phosphate [PCr/Pi] ratio) and a decrease in intracellular pH [13, 18, 30]. Detection of metabolic disruption by MR spectroscopy is especially important at this early stage of ischemia because the increase in mobile protons in the region of tissue injury is not reliably visualized on spin-echo T1- and T2-weighted MR images (Fig. 7). Recent experimental studies [10, 18] have shown that signal hyperintensity was not observed on T2-weighted images for 1.5–3.0 hr after arterial occlusion, whereas clear evidence of metabolic disruption could be seen in ^{31}P spectra obtained by surface-coil MR spectroscopy within minutes after the onset of ischemia.

High-resolution ^1H MR spectroscopy is also expected to improve our understanding of the metabolic alterations that accompany cerebral ischemia, particularly those related to acid-base balance [16, 17, 21, 22, 86–88]. Acquisition of well-defined ^1H spectra initially was hampered by the dominant water and lipid signal in living tissues. However, with the development of improved spectral editing and localization techniques, separation of metabolites with low proton concentrations is now more feasible [86–88]. High-resolution ^1H MR spectra of mammalian brain have been obtained from small volumes of tissue localized in various cortical and subcortical regions by using a 1.5-T MR system [89]. Resonances were demonstrated from lipids, lactate, acetate, *N*-acetylaspartate, gamma-aminobutyrate glutamine, aspartate, creatine, phosphocreatine, and choline compounds, and spectra were found to be highly reproducible.

To date, few studies have directly addressed the applicability of proton MR spectroscopy in the clinical setting of stroke [21, 22]. The available data indicate, however, that

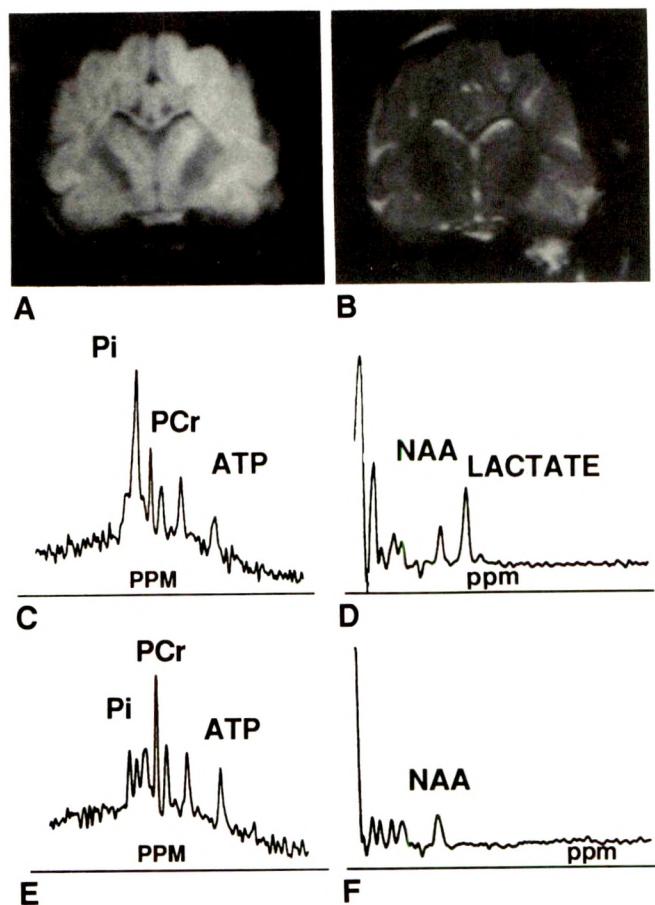


Fig. 7.—Integration of ^{31}P and ^1H MR spectroscopy with diffusion-weighted and T2-weighted spin-echo MR images.

A, Diffusion-weighted coronal MR image (1000/80/4) of cat brain obtained 30 min after unilateral occlusion of middle cerebral artery (MCA) shows high signal intensity in ipsilateral hemisphere.

B, T2-weighted image (2800/160/2), by comparison, does not clearly indicate presence of ischemic injury.

C and D, ^{31}P (C) and ^1H (D) MR spectra from ischemic cat brain. Increase in inorganic phosphate (Pi)/phosphocreatine (PCr) and lactate/ N -acetylaspartate (NAA) ratios correlates with high signal intensity on diffusion-weighted image.

E and F, ^{31}P (E) and ^1H (F) MR spectra from normal cat brain.

ATP = adenosine triphosphate.

ischemia causes a detectable decrease in intracellular pH concomitantly with an increase in lactate concentration; ATP and phosphocreatine are depleted, while inorganic phosphate is markedly increased. Once reliable spatial localization is achieved, MR spectroscopy should become more useful clinically in evaluating dynamic changes in brain tissue responses to anesthesia, drugs, and ischemic insults.

Combined MR imaging/spectroscopy may be particularly important in assessing the potential for reversibility of ischemic brain damage. Several recent experimental studies have demonstrated a close temporal and functional relationship between ischemia-induced metabolic dysfunction, lactic acidosis, and changes in the cortical electroencephalogram (EEG). Typically, the PCr/Pi ratio declines precipitously in parallel with changes in EEG amplitude during severe stroke [20]. Mild stroke, established by EEG criteria, produced a

much smaller decrement in PCr/Pi. In another animal study [23], the changes in cerebral phosphorus metabolites, intracellular pH, and lactate during 30 min of complete global ischemia and 2 hr of reperfusion were monitored by time-shared ^1H and ^{31}P in vivo MR spectroscopy. Ischemia caused a significant decrease in intracellular pH and a concomitant elevation in lactate; ATP and phosphocreatine were totally depleted, while inorganic phosphate was markedly increased. Within 1 hr of restoration of blood flow, high-energy phosphate and lactate levels had been restored to close to their baseline levels. These results indicate that MR spectroscopy can accurately establish the quantitative changes in cerebral metabolite dynamics during temporary ischemia. This is of particular importance in the evaluation of reversible ischemic injury, since it is during this period that therapeutic interventions may have their greatest impact.

Initial studies have also shown that combined MR imaging/spectroscopy can be used for the in vivo evaluation of cerebral tissue responses to various neuroprotective agents. Several recent experimental studies have focused on the putative cytoprotective role of calcium or sodium/calcium channel blockers in the treatment of acute ischemia [13, 18]. In one study that used a cat model of permanent unilateral occlusion of the MCA, the evolution of cerebral injury was assessed with a combination of proton MR imaging and $^{31}\text{P}/^1\text{H}$ MR spectroscopy [13]. Compared with untreated controls, a significant reduction in the extent of brain edema was seen in cats that received the channel blocker. Substantial quantitative differences in ^{31}P and ^1H spectra were found between drug-treated and control animals, suggesting that the cerebroprotective action was related to cellular metabolic processes that preserve ATP and attenuate lactic acidosis during the ischemic period. Improvements in the sensitivity of investigational MR imaging techniques, and the development of other intravascular contrast agents that do not rely on disruption of the blood-brain barrier for demonstration of ischemic injury, may be of further value in assessing the efficacy of various pharmacotherapeutic regimens.

Unresolved Issues

The overall goal of MR research on cerebral ischemia is the early differentiation of normal from acutely ischemic tissue. The new developments in imaging and spectroscopy suggest that MR capabilities have progressed beyond the stage of visualization of static neuroanatomy and are now increasingly targeted on characterizing dynamic pathophysiologic processes associated with ischemia.

It seems likely, for example, that studies in the near future will be focused on the MR identification of the ischemic "penumbra" as a region of reversibly injured brain tissue. Magnetic-susceptibility contrast-enhanced echoplanar MR imaging will be used to generate mean transit time data to produce functional perfusion maps of at-risk brain parenchyma. Perfusion imaging also will enable evaluations of the topography of cerebral hypoperfusion in end-arterial compared with well-collateralized brain tissues. Regions of arterial

stasis will be identified and compared with changes observed subsequently on diffusion- and T2-weighted MR images.

Significant research effort will be devoted also to evaluating the temporal profile of ischemia-induced cerebral edema, and especially the differentiation of cytotoxic from vasogenic edema. The current hypothesis that diffusion-weighted image hyperintensity may reflect early-onset cytotoxic edema, whereas T2-weighted hyperintensity represents vasogenic edema [11, 12], is already under active investigation in several laboratories in the United States, Europe, and Japan.

Image-guided localized ^{31}P and ^1H MR spectroscopy may be used to differentiate reversibly from irreversibly injured brain tissue in terms of metabolic criteria. This may help determine whether there are threshold PCr/Pi or lactate/ N -acetylaspartate ratios above which injury is irreversible, but below which the tissue potentially can be resuscitated. Similarly, future MR spectroscopic studies may reveal whether an irreversible threshold exists for ischemia-induced tissue acidosis, the measurement of which can be closely estimated from the chemical-shift position of inorganic phosphate in the ^{31}P spectrum. Finally, combined MR imaging and spectroscopy will likely become an important technique for screening drugs with putative cerebroprotective benefits in ischemia. In particular, magnetic-susceptibility contrast-enhanced MR imaging may help to establish whether vasodilatation is an important component of a drug's mechanism of action.

REFERENCES

- Levy LM, Killian JM, Mawad M, Presiozi T, Bryan RN. Acute cerebral infarction: early diagnosis with MR (abstr). *AJNR* **1989**;10:872
- Brant-Zawadzki M, Weinstein PR, Bartkowski H, Moseley M. MR imaging and spectroscopy in clinical and experimental cerebral ischemia: a review. *AJNR* **1987**;8:39-48; *AJR* **1987**;148:579-588
- Brant-Zawadzki M, Solomon M, Newton TH, Weinstein P, Schmidley J, Norman D. Basic principles of magnetic resonance imaging in cerebral ischemia and initial clinical experience. *Neuroradiology* **1985**;27(6):517-520
- Kistler JP, Buonanno FS, DeWitt LD, David KR, Brady TJ, Fisher CM. Vertebral-basilar posterior cerebral territory stroke-delineation by proton nuclear magnetic resonance imaging. *Stroke* **1984**;15(3):417-426
- Bryan RN, Willcott MR, Scheider NJ, Ford JJ, Derman HS. Nuclear magnetic resonance evaluation of stroke. A preliminary report. *Radiology* **1983**;149:189-192
- Sipponen JT. Uses of techniques. Visualization of brain infarction with nuclear magnetic resonance imaging. *Neuroradiology* **1984**;26:387-391
- DeWitt LD, Kistler JP, Miller DC, Richardson EP Jr, Buonanno FS. NMR-Neuropathologic correlation in stroke. *Stroke* **1987**;18(2):342-351
- Bose B, Jones SC, Lorig R, Friel HT, Weinstein M, Little JR. Evolving focal cerebral ischemia in cats: spatial correlation of nuclear magnetic resonance imaging, cerebral blood flow, tetrazolium staining, and histopathology. *Stroke* **1988**;19:28-37
- Brant-Zawadzki M, Pereira B, Weinstein P, et al. MR imaging of acute experimental ischemia in cats. *AJNR* **1986**;7:7-11
- Moseley M, Cohen Y, Mintorovitch J, et al. Early detection of regional cerebral ischemia in cats: comparison of diffusion- and T2-weighted MRI and spectroscopy. *Magn Reson Med* **1990**;14:330-346
- Moseley ME, Kucharczyk J, Mintorovitch J, et al. Diffusion-weighted MR imaging of acute stroke: correlation with T2-weighted and magnetic susceptibility-enhanced MR imaging in cats. *AJNR* **1990**;11:423-429
- Mintorovitch J, Moseley ME, Chileutt L, Shimizu H, Cohen Y, Weinstein PR. Comparison of diffusion- and T2-weighted MRI for the early detection of cerebral ischemia and reperfusion in rats. *Magn Reson Med* (in press)
- Kucharczyk J, Mintorovitch J, Asgari H, Derugin N, Sevick R, Moseley M. Ischemic brain damage is reduced by a novel sodium/calcium ion channel modulator RS-87476. *Radiology* (in press)
- Rosen BR, Belliveau JW, Veree JM, Brady TJ. Perfusion imaging with NMR contrast agents. *Magn Reson Med* **1990**;14:249-265
- Moseley ME, Kucharczyk J, Kurhanewicz J, et al. Early detection of perfusion deficits induced by regional cerebral ischemia in cats: T2-weighted magnetic susceptibility MRI using a nonionic dysprosium contrast agent. In: *Book of abstracts. Society of Magnetic Resonance in Medicine. Eighth annual meeting*. Berkeley, CA: Society of Magnetic Resonance in Medicine, **1989**:43
- Kucharczyk J, Moseley M, Kurhanewicz J, Norman D. MRS of ischemic/hypoxic brain disease. *Invest Radiol* **1989**;24:951-954
- Gulyai L, Schnall M, McLaughlin AC, Leigh JS Jr, Chance B. Simultaneous P-31 and H-1 nuclear magnetic resonance studies of hypoxia and ischemia in the cat brain. *J Cereb Blood Flow Metab* **1987**;7:543-551
- Kucharczyk J, Chew W, Derugin N, et al. Nicardipine reduces ischemic brain injury. Magnetic resonance imaging/spectroscopy study in cats. *Stroke* **1989**;20:268-274
- Bottomey PA, Drayer BP, Smith LS. Chronic adult cerebral infarction studied by phosphorus NMR spectroscopy. *Radiology* **1986**;160:763-766
- Komatsu S, Nioka S, Greenberg JH, et al. Cerebral energy metabolism measured in vivo by P-31-NMR in middle cerebral artery occlusion in the cat: relation to severity of stroke. *J Cereb Blood Flow Metab* **1987**;7:557-562
- Bruhn H, Frahm J, Gyngell ML, Merboldt ML, Hanicke W, Sauter R. Cerebral metabolism in man after acute stroke: new observations using localized H-1 NMR spectroscopy. *Magn Reson Med* **1989**;9:126-131
- Berkelbach van der Sprekkel JW, Luyten PR, van Rijen PC, Tulleken CAF, den Hollander JA. Cerebral lactate detected by regional H-1 magnetic resonance spectroscopy in a patient with cerebral infarction. *Stroke* **1988**;19:1556-1560
- Chang LH, Shirane R, Weinstein PR, James TL. Cerebral metabolite dynamics during temporary complete ischemia in rats monitored by time-shared H-1 and P-31 NMR spectroscopy. *Magn Reson Med* **1990**;13:6-13
- Berne RM, Winn HR, Rubio R. The local regulation of cerebral blood flow. *Prog Cardiovasc Dis* **1981**;24:243-260
- Ginsberg MD. Local metabolic responses to cerebral ischemia. *Cerebrovasc Brain Metab Rev* **1990**;2:58-93
- Branston NM, Strong AJ, Symon L. Extracellular potassium activity, evoked potentials, and tissue blood flow. *J Neurol Sci* **1977**;32:305-321
- Brierley JB, Graham DI. Hypoxia and vascular disorders of the central nervous system. In: Adams JH, Corsellis JAN, Duchen LW, eds. *Greenfield's neuropathology*, 4th ed. New York: Wiley, **1984**:125-207
- Brint S, Jacewicz M, Kiessling M, Tanabe J, Pulsinelli W. Focal brain ischemia in the rat: methods for reproducible neocortical infarction using tandem occlusion of the distal middle cerebral and ipsilateral common carotid arteries. *J Cereb Blood Flow Metab* **1988**;8:474-485
- Bozzao L, Fantozzi LM, Bastianello S, Bozzao A, Fieschi C. Early collateral blood supply and late parenchymal brain damage in patients with middle cerebral artery occlusion. *Stroke* **1989**;20:735-740
- Brant-Zawadzki M, Kucharczyk W. Vascular disease: ischemia. In: Brant-Zawadzki M, Norman D, eds. *Magnetic resonance imaging of the central nervous system*. New York: Raven, **1987**:221-234
- Betz E. Cerebral blood flow: its measurement and regulation. *Physiol Rev* **1972**; 52:595
- Astrup J, Siesjo BK, Symon L. Thresholds in cerebral ischemia—the ischemic penumbra. *Stroke* **1981**;12:723-725
- Gotoh O, Asano T, Koide T, Takakura K. Ischemic brain edema following occlusion of the middle cerebral artery in the rat. I. The time courses of the brain water, sodium and potassium contents and blood-brain barrier permeability to I-125 albumin. *Stroke* **1985**;16:101-109
- Hossmann RA, Shrier FJ. Experimental brain infarcts in cats. I. Pathophysiological observations. *Stroke* **1980**;11(6):583-592
- Chiang J, Kowada A, Ames A III, Majno G. Cerebral ischemia. III. Vascular changes. *Am J Pathol* **1968**;52:455-476
- Tamura A, Asano T, Sano K. Correlation between rCBF and histological changes following temporary middle cerebral artery occlusion. *Stroke* **1980**;11:487-493
- Ames A III, Wright RL, Kowada M, Thruston JM, Majno G. Cerebral ischemia. II. The no-reflow phenomenon. *Am J Pathol* **1968**;52:437-453
- Fisher EG, Ames A III, Hedley-Whyte ET, O'Gorman S. Reassessment of

- cerebral capillary changes in acute global ischemia and their relationship to the "no-reflow phenomenon." *Stroke* **1977**;8:36-39
39. Levy DE, Van Ultert RL, Pike CL. Delayed postischemic hypoperfusion: a potentially damaging consequence of stroke. *Neurology* **1979**;29:1245-1252
 40. Ginsberg MD, Budd WW, Welsh FA. Diffuse cerebral ischemia in the cat. I. Local blood flow during severe ischemia and recirculation. *Ann Neurol* **1978**;3:482-492
 41. Miller CL, Lampard DG, Alexander K, Brown WA. Local cerebral blood flow following transient cerebral ischemia. I. Onset of impaired reperfusion within the first hour following global ischemia. *Stroke* **1980**;11:534-541
 42. Kagstrom E, Smith M-L, Siesjo BK. Recirculation in the rat brain following incomplete ischemia. *J Cereb Blood Flow Metab* **1983**;3:183-192
 43. Crain MR, Yuh WTC, Greene GM, Sato Y, Ryals TJ, Loes DJ. MR imaging of acute early stroke. In: *Book of abstracts. Society of Magnetic Resonance in Medicine. Ninth annual meeting*. Berkeley, CA: Society of Magnetic Resonance in Medicine, **1990**:5
 44. Hart RG, Lockwood KL, Hakim AM, et al. Immediate anticoagulation of embolic stroke: brain hemorrhage and management options. *Stroke* **1984**;15:779-789
 45. Horning CR, Dorndorf W, Agnoli AL. Hemorrhagic cerebral infarction: a progressive study. *Stroke* **1986**;17:179-184
 46. Gomori JM, Grossman RI. Mechanisms responsible for the MR appearance and evolution of intracranial hemorrhage. *RadioGraphics* **1988**;8:427-440
 47. Melamad E, Lavy S, Bentin S, Cooper YR, Rinot Y. Reduction in regional cerebral blood flow during normal aging in man. *Stroke* **1980**;11:31-36
 48. Shaw TG, Mortel KF, Meyer JS, Rogers RL, Hardenberg J, Cataia MM. Cerebral blood flow changes in benign aging and cerebrovascular disease. *Neurology* **1984**;34:855-862
 49. Kirkpatrick JB, Hayman LA. White-matter lesions in MR imaging of clinically healthy brains of elderly subjects: possible pathologic basis. *Radiology* **1987**;162:509-511
 50. Awad IA, Johnson PC, Spetzler RF, et al. Incidental subcortical lesions identified on magnetic resonance imaging in the elderly. II. Postmortem pathological correlations. *Stroke* **1986**;17:1090-1097
 51. Fazekas F, Chawluk JB, Alavi A, et al. MR signal abnormalities at 1.5 T in Alzheimer's disease and normal aging. *AJNR* **1987**;8:421-426
 52. Drayer BP. Imaging of the aging brain. Part 1. Normal findings. *Radiology* **1988**;166:785-796
 53. Brant-Zawadzki M, Fein G, Van Dyke C, Kiernan R, Davenport L, de Groot J. MR imaging of the aging brain: patchy white-matter lesions and dementia. *AJNR* **1985**;6:675-682
 54. DeReuck J, Crevits L, DeCoster W, et al. Pathogenesis of Binswanger chronic progressive subcortical encephalopathy. *Neurology* **1980**;30:920-928
 55. Burger PC, Burch JG, Kunze U. Subcortical arteriosclerotic encephalopathy (Binswanger's disease): a vascular etiology of dementia. *Stroke* **1976**;7:626-631
 56. Mills CM, Brant-Zawadzki M, Crooks LE, et al. Nuclear magnetic resonance: principles of blood flow imaging. *AJR* **1984**;142:165-170
 57. Bradley WG, Waluch V. Blood flow: magnetic resonance imaging. *Radiology* **1985**;154:443-450
 58. Katz BH, Quencer RM, Kaplan JO, Hinks RS, Post MJD. MR imaging of intracranial carotid occlusion. *AJNR* **1989**;10:345-350
 59. Sze G, Simmons B, Krol G, Walker R, Zimmerman RD, Deck MDF. Dural sinus thrombosis: verification with spin-echo techniques. *AJNR* **1988**;9:679-686
 60. McMurdo SK, Brant-Zawadzki M, Bradley WG, et al. Dural venous thrombosis: study using intermediate field strength MR imaging. *Radiology* **1986**;161:83-86
 61. Daniels DL, Czervionke LF, Hendrix LE, et al. Gradient recalled echo MR imaging of superior sagittal sinus occlusion. *Neuroradiology* **1989**;31:134-136
 62. Yousem DM, Balakrishnan J, Debrun GM, Bryan RN. Hyperintense thrombus on GRASS MR images: potential pitfall in flow evaluation. *AJNR* **1990**;11:51-58
 63. Rippe DJ, Boyko OB, Spritzer CE, et al. Demonstration of dural sinus occlusion by the use of MR angiography. *AJNR* **1990**;11:199-201
 64. Edelman RR, Matle HP, Atkinson DJ, Hoogewoud HM. MR angiography. *AJR* **1990**;154:937-946
 65. Masaryk TJ, Laub GA, Modic MT, Ross JS, Haacke EM. Carotid CNS flow imaging. *Magn Reson Med* **1990**;14:308-314
 66. Heinz E, Yeates A, Djang W. Significant extracranial carotid stenosis: detection on routine cerebral MR images. *Radiology* **1989**;170:843-848
 67. Schmalbrock P, Yuan C, Chakeres DW, Kohli J, Pelc NJ. Volume MR angiography: method to achieve very short echo times. *Radiology* **1990**;175:861-865
 68. Masaryk TJ. MR angiography. In: Kressel HY, Modic MT, Murphy WA, eds. *RSA syllabus. Special course MR 1990*. Oakbrook, IL: Radiologic Society of North America, **1990**:57-62
 69. Ruggieri PM, Laub G, Masaryk TJ, Modic MT. Intracranial circulation: pulse sequence consideration in three dimensional (volume) MR angiography. *Radiology* **1989**;171:785-791
 70. Keller PJ, Drayer BP, Fram EK, Williams KD, Dumoulin CL, Souza SP. MR angiography with two-dimensional acquisition and three-dimensional display: work in progress. *Radiology* **1989**;173:527-532
 71. Edelman RR, Matle HP, Kleefield J, Silver MS. Quantification of blood flow with dynamic MR imaging and presaturation bolus tracking. *Radiology* **1989**;171:551-556
 72. Weeden VJ, Rosen BR, Chesler D, Brady TJ. MR velocity imaging by phase display. *J Comput Assist Tomogr* **1985**;9:530-536
 73. LeBihan D, Breton E, Lallemand, Grenier P, Cabanis E, Laval-Jeantet M. MR imaging of intravoxel incoherent motions: application to diffusion and perfusion in neurologic disorders. *Radiology* **1986**;161:401-407
 74. LeBihan D, Breton E, Lallemand D, Aubin M, Vignaud J, Laval-Jeantet M. Separation of diffusion and perfusion in intravoxel incoherent motion MR imaging. *Radiology* **1988**;168:497-505
 75. Busti R, Dietrich WD, Globus MT. Small differences in intraischemic brain temperature critically determine the extent of cerebral ischemic injury. *J Cereb Blood Flow Metab* **1987**;7:729-738
 76. Bandaranayake MN, Nemoto ME, Stezoski W. Rat brain osmolality during barbiturate anesthesia and global brain ischemia. *Stroke* **1978**;9:249-284
 77. Hatashita S, Hoff JT. Biomechanics of brain edema in acute cerebral ischemia. *Stroke* **1988**;19:91-97
 78. Goldman SA, Pulsinelli WA, Clarke WY. The effects of extracellular acidosis on neurons and glia in vitro. *J Cereb Blood Flow Metab* **1989**;9:471-477
 79. Seijo BK. Membrane events leading to glial swelling and brain edema. In: Inaba J, Klatzo I, Spatz M, eds. *Brain edema*. Berlin: Springer-Verlag, **1985**:200-209
 80. McNamara MT, Brant-Zawadzki M, Berry I, et al. Acute experimental cerebral ischemia: MR enhancement using Gd-DTPA. *Radiology* **1986**;158:701-704
 81. Belliveau JW, Rosen BR, Kandor HL, et al. Functional cerebral imaging by susceptibility contrast NMR. *Magn Reson Med* **1990**;14:538-546
 82. Villringer A, Rosen BR, Belliveau JW, et al. Dynamic imaging with lanthanide chelates in normal brain: contrast due to magnetic susceptibility effects. *Magn Reson Med* **1988**;6:164-175
 83. Edelman RR, Matle HP, Atkinson DJ. Cerebral blood flow: assessment with dynamic contrast-enhanced T2*-weighted MR imaging at 1.5 T. *Radiology* **1990**;176:211-220
 84. Morawetz RB, De Girdam U, Ojemann RB, Marcoux FW, Crowell RM. Cerebral blood flow determined by hydrogen clearance during middle cerebral artery occlusion in unanesthetized monkeys. *Stroke* **1978**;9:143-149
 85. Moseley ME, Berry I, Chew WM, Brant-Zawadzki M, James TL. Magnetic resonance spectroscopy principles and potential applications. In: Brant-Zawadzki M, Norman D, eds. *Magnetic resonance imaging of the central nervous system*. New York: Raven, **1987**:107-113
 86. Hanstock CC, Boisvert DP, Bendall MR, Allen PS. In vivo assessment of focal brain lactate alterations with NMR proton spectroscopy. *J Cereb Blood Flow Metab* **1988**;8:208-214
 87. Barany M, Langer BG, Glick RP, Venkatasubramanian PN, Wilbur AC, Spigos DG. In vivo H-1 spectroscopy in humans at 1.5 T. *Radiology* **1988**;167:839-844
 88. Sauter R, Loeffler W, Bruhn H, Frahm J. The human brain: localized H-1 spectroscopy at 1.0 T. *Radiology* **1990**;176:221-224
 89. Frahm J, Bruhn H, Gyngell ML, et al. Localized proton NMR spectroscopy in different regions of the human brain in vivo. Relaxation times and concentrations of cerebral metabolites. *Magn Reson Med* **1989**;11:47-63

Renal Oncocytoma

William E. Palmer¹ and Felix S. Chew

A 53-year-old man had microscopic hematuria. An excretory urogram showed a large mass with an enhancing rim in the upper pole of the left kidney (Fig. 1). A sonogram showed a complex cystic lesion that on CT had a nonenhancing, low-attenuation center; an enhancing, thick, irregular wall with a few flecks of calcification; and a sharply circumscribed peripheral margin. On MR, the center and the surrounding wall of the lesion were heterogeneous; the left renal vein and the inferior vena cava were patent. Because the differential diagnosis included renal cell carcinoma, a radical left nephrectomy was performed. The renal capsule was intact around a 15-cm cystic tumor containing clear red fluid and clotted blood. The final pathologic diagnosis was renal oncocytoma.

Renal oncocytoma is an uncommon, benign tumor that originates in the epithelium of the proximal tubules. Although renal oncocytoma is often detected as an incidental renal mass in an asymptomatic adult, it must be differentiated from other renal tumors, particularly renal cell carcinoma. Radiologic features typical of oncocytoma, including a solid mass with homogeneous enhancement, sharp margination, central stellate scar (detectable by sonography, CT, or MR), and an angiographic spoked-wheel pattern, may occur in renal cell

carcinomas [1-3]. Cystic necrosis and calcification are rare in oncocyotma and more common in renal cell carcinoma. On MR, these lesions can be distinguished only if tumor thrombus is shown in the renal vein or inferior vena cava [4].

Treatment is surgical enucleation or heminephrectomy. If preoperative differentiation from renal cell carcinoma is uncertain, radical nephrectomy may be necessary.

REFERENCES

1. Quinn MJ, Hartman DS, Friedman AC, et al. Renal oncocytoma: new observations. *Radiology* 1984;153:49-53
2. Neisius D, Braedel HU, Schindler E, Hoene E, Alloussi S. Computed tomographic and angiographic findings in renal oncocytoma. *Br J Radiol* 1988;61:1019-1025
3. Levine E, Huntrakoon M. Computed tomography of renal oncocytoma. *AJR* 1983;141:741-746
4. Ball DS, Friedman AC, Hartman DS, Radecki PD, Caroline DF. Scar sign of renal oncocytoma: magnetic resonance imaging appearance and lack of specificity. *Urol Radiol* 1986;8:46-48

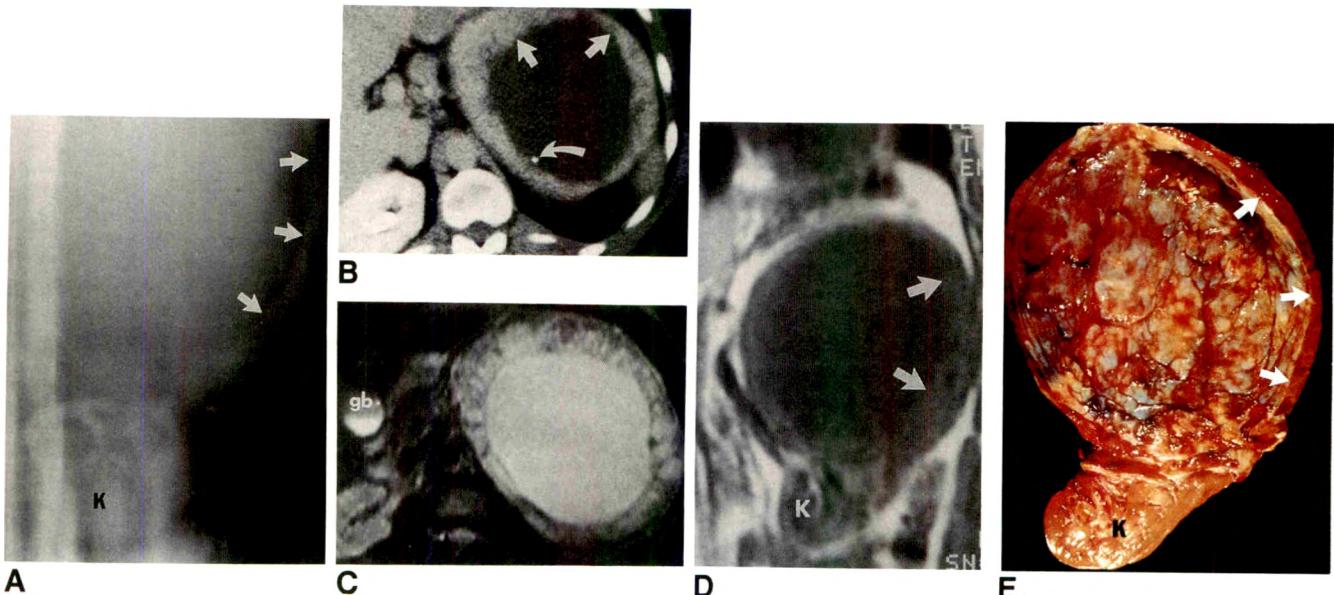


Fig. 1.—Renal oncocytoma.

A, Excretory urogram shows a large mass with enhancing rim (arrows) in upper pole of kidney.

B, Contrast-enhanced CT scan shows mass has well-circumscribed margin, nonenhancing low-attenuation center, irregular wall (straight arrows), and calcification (curved arrow).

C, T2-weighted axial MR image shows fluid center of mass.

D, T1-weighted coronal MR image shows 15-cm, well-circumscribed, cystic mass with irregular rim of variable thickness (arrows).

E, Cut gross specimen of evacuated cavity of mass. Clotted blood adheres to whitish lining; wall has variable thickness (arrows).

K = lower pole of kidney; gb = gallbladder.

From the weekly radiologic-pathologic correlation conferences conducted by Jack Wittenberg. Pathology editor: Andrew E. Rosenberg. Radiology editors: Felix S. Chew, Daniel P. Barboriak, William E. Palmer, Daniel I. Rosenthal.

¹ All authors: Department of Radiology, Massachusetts General Hospital and Harvard Medical School, 32 Fruit St., Boston, MA 02114. Address reprint requests to F. S. Chew.

Review Article

Imaging the Pleura: Sonography, CT, and MR Imaging

Theresa C. McLoud¹ and Christopher D. R. Flower²

A variety of imaging techniques can be used to evaluate the pleura and the pleural space. Standard radiographs are the most common. In this article, however, we review the use of three other imaging techniques: sonography, CT, and MR imaging. Sonography allows easy identification of pleural fluid and loculation and differentiation from pleural masses; CT is best for characterizing location and composition of pleural masses; MR is somewhat limited, but is best for imaging superior sulcus carcinoma.

Sonography

The pleura is a relatively superficial structure and therefore is accessible to sonography [1, 2]. Pathologic processes involving the pleura and the pleural space, either directly or indirectly, may be characterized with sonography according to their acoustic properties. Sonography and CT should be considered complementary. CT is more sensitive for the detection of pleural fluid and thickening and the identification of focal masses involving the pleura and chest wall. Sonography is readily available and is less expensive than CT. Mobile compact sonographic machines with variable frequency transducers permit bedside imaging. Sonography may be performed with the patient recumbent or sitting, and the procedure can be combined with fluoroscopy, if necessary, for interventional procedures. Images can be made in the sagittal and coronal planes, and pleural fluid can be characterized.

Technique

The chest radiograph acts as a guide to sonography. Most scanning is done through the intercostal space by using either

3.5- or 5.0-MHz sector transducers or variable frequency array transducers. Comparison with the normal hemithorax is helpful in establishing correct calibration of the equipment. The ribs and the interface of lung and pleura are readily identified, with the latter reflecting most of the acoustic energy and appearing as a bright white line often associated with distal reverberation echoes.

Pleural Fluid

Although small quantities of fluid may be detected on sonograms made with the patient in the lateral decubitus position, this is time consuming and may be impossible in severely ill patients. Fluid may be difficult to detect on chest radiographs in the presence of extensive pulmonary consolidation or collapse. Loculated fluid has no plain film features that allow its differentiation from a solid pleural mass. Sonography is valuable not only in establishing the presence of fluid, but also as a guide to aspiration [3-5].

Pleural aspiration performed without imaging guidance is likely to be difficult when the quantity of fluid is small, when the fluid is loculated rather than free flowing, when there is associated pulmonary consolidation or collapse, and when the hemidiaphragm is high. Inadvertent puncture of the diaphragm, and therefore of the liver and spleen, probably occurs frequently when thoracentesis is performed by inexperienced physicians. Lung, compressed by adjacent fluid, is identified by fluid-filled (hypoechoic) tubular structures and air-filled (highly reflective) linear structures (Figs. 1 and 2).

Most pleural fluid collections, whether free flowing or loculated, are hypoechoic with a sharp, highly echogenic line delineating the visceral pleura and lung (Fig. 3). As the under-

Received August 31, 1990; accepted after revision November 21, 1990.

¹Department of Radiology, Harvard Medical School, Massachusetts General Hospital, Boston, MA 02114. Address reprint requests to T. C. McLoud.

²Department of Diagnostic Radiology, Addenbrooke's Hospital, Cambridge, England CB2 2QQ.

AJR 156:1145-1153, June 1991 0361-803X/91/1566-1145 © American Roentgen Ray Society

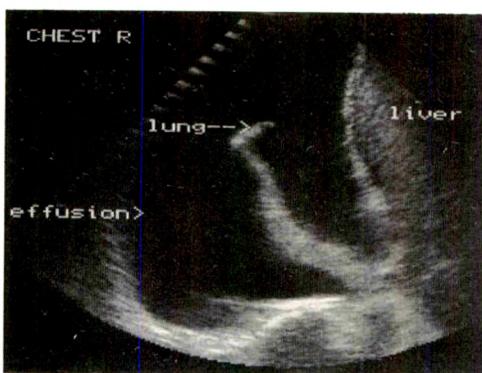


Fig. 1.—Sonogram of collapsed right lower lobe surrounded by a large pleural effusion.



Fig. 2.—Sonogram of highly reflective bronchi (straight arrow) in consolidated lung. Note associated effusion containing thin, mobile strands (curved arrows).

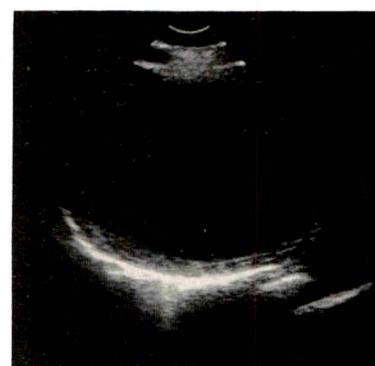


Fig. 3.—Empyema shown as a transonic space on sonogram. Thin echogenic layer at posterior aspect represents debris and bright line of high reflectivity, interface with lung.



Fig. 4.—Empyema appears on sonogram as a transonic space divided into multiple secondary loculations by curvilinear septa. This is the result of unsuccessful catheter drainage followed by decortication.

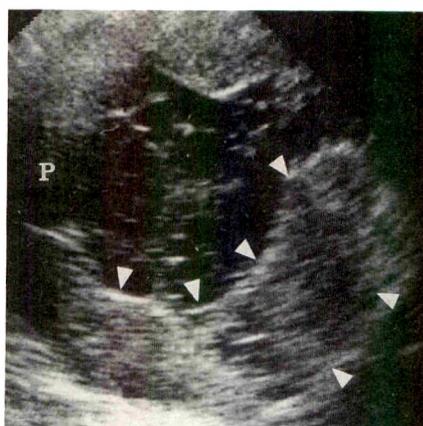


Fig. 5.—Mesothelioma. Sonogram shows a thick rind of tumor (arrowheads) encasing pleural fluid (P).

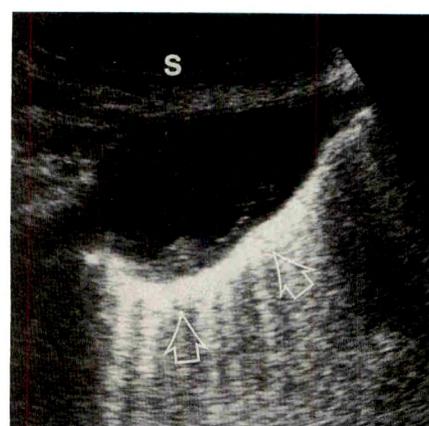


Fig. 6.—Pleural deposit of metastatic adenocarcinoma localized by sonography before percutaneous biopsy. Skin surface (S). Interface with lung (arrows).

lying lung usually contains air, posterior echo enhancement, which one would expect to see with fluid collections elsewhere in the body, is not present. Because some pleural and chest wall tumors, notably lymphomas and neurogenic neoplasms, transmit ultrasound with the production of few or no echoes, they can be mistaken for pleural fluid [6]. For these reasons, sonography is not 100% specific, and needle aspiration should be performed as part of the sonographic examination.

When thin, mobile, linear structures are seen in an otherwise hypoechoic space, they invariably serve to distinguish pleural fluid from a solid pleural mass [7]. These structures probably represent strands of fibrin, are usually of barely measurable thickness, and move in a gently undulating fashion with respiration (Fig. 2). They tend to occur in exudates that are rich in protein. In certain circumstances (e.g., some empyemas, patients who have had a series of bloody taps,

and those with metastatic pleural disease) the septa are so profuse that they have a honeycomb appearance. These changes, which cannot be shown by CT, predict significant difficulties with tube drainage (Fig. 4). Rarely, fluid collections are represented by a uniform mass of tiny echogenic structures that move in a swirling fashion with respiration. This uncommon picture is seen in isolated cases of empyema, hemothorax, or exudates caused by pleural malignancy.

Pleural Masses

Both focal and diffuse pleural thickening, whether due to tumor or inflammation, is exquisitely demonstrated by CT [8], but difficult to detect with sonography unless the thickening is a centimeter or more. Thickening is better detected by sonography when it is accompanied by fluid (Fig. 5).

Pleural Biopsy

Pleural biopsy may be required whether or not a pleural fluid reaction is present. In the presence of pleural fluid, thoracoscopy is a valuable procedure outside the realm of the radiologist, as is thoracotomy, a procedure of final resort. Just as radiologists have found a role in identifying pleural fluid for aspiration, they now perform pleural biopsy under sonographic control [9]. Not only is the best and safest site readily identified, the depth of the parietal pleura from the skin is accurately established.

The combination of biopsy with a Cope or Abrams needle and pleural fluid cytology and culture gives a high yield of positive results for effusions that result from malignancy or tuberculosis. Pleural biopsy in the absence of accompanying fluid is very difficult without either CT or sonographic guidance [10, 11] (Fig. 6). Because the differentiation of benign from malignant pleural disease and indeed the distinction of one malignant pleural neoplasm from another is notoriously difficult, histologic samples should always be obtained when possible; the development of high-speed, 18- and 20-gauge cutting needles (Biopsy, Radiplast AB, Stockholm, Sweden) appears to be a major advance in this regard [10].

Pleural Drainage

Until recently it has been standard clinical practice to drain pleural fluid collections by repeated needle aspiration or by closed tube drainage, whether the fluid is a transudate, inflammatory exudate, empyema, or a result of metastatic malignancy or hemorrhage. Furthermore, it has been customary to perform these procedures without imaging guidance. Repeated needle aspiration is disagreeable for the patient and may be unsuccessful because it can provoke the formation of fibrinous septa within the fluid and thereby cause loculation. Conventional tube drainage is performed with large-gauge tubes (24–28 French), which are introduced blindly; this is often a very uncomfortable procedure and is associated with a small but significant number of complications (including laceration of the lung, diaphragm, liver, spleen, and stomach) and a remarkably high failure rate [12]. This is attributable to blockage or kinking of the tube in some cases, but the most important cause of failure is malposition of the tube, particularly if the fluid collection is loculated. Image guidance (with CT or sonography) provides a clear and precise demonstration of the collection and its relation to the underlying lung and adjacent diaphragm. Multiple separate loculi will be particularly well shown on CT scans and indicate the need for a proportionate number of drains or surgery. Several studies attest to the value of imaging guidance in achieving successful drainage [13–17]. Furthermore, this is achieved with relatively small-bore (12–14 French) catheters. The procedure is much less painful for the patient than large-tube insertion, and the catheters are pliable enough to be reasonably comfortable when in situ. As long as the catheter is kept irrigated with normal saline and constant suction is applied (usually 25 cm water) it is very unusual for the catheter to become blocked. With this technique, successful drainage of empyemas is achieved in about 80% of patients. Two factors make suc-

cessful aspiration of pus and some other inflammatory and malignant effusions difficult: a thick rind of pleura (pleural peel) and secondary loculation. The degree of pleural thickening tends to relate to the age of the collection, although this is not always the case; nevertheless, it emphasizes the importance of performing drainage as early as possible. A recent study suggests that a thickened pleura does not necessarily preclude successful catheter drainage and that pleural peels may resolve after drainage, making decortication unnecessary [18]. Secondary loculations, which are particularly likely to occur with hemothoraces, empyemas, and some malignant pleural lesions, are difficult to detect with CT but are clearly shown on sonograms and predict the likely failure of tube drainage. Because loculations are usually due to fibrinous strands, it seems logical to try to break them down mechanically with a guidewire at the time of catheter placement or to dissolve them with a fibrolytic agent. Neither method has been particularly successful, although a recent study with urokinase was encouraging [19].

CT

CT may show abnormalities of the pleura at an earlier stage than do other imaging techniques. It is also useful in the distinction of pleural from parenchymal disease, in determining the precise location and extent of pleural disease, and in certain instances it permits characterization of tissue density within a lesion by means of analysis of attenuation coefficients.

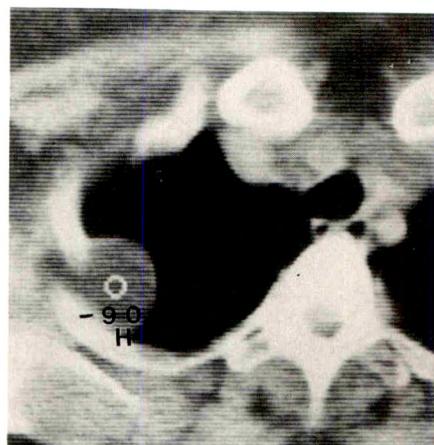
Technique

Standard posteroanterior and lateral radiographs should always be obtained before any CT study. CT scans should be performed in suspended respiration at total lung capacity. Standard techniques for examination of the thorax include 10-mm collimation with slices obtained at 10-mm intervals from the thoracic inlet through the posterior lung recesses, and viewing at both soft-tissue and lung windows.

In our experience, the routine use of IV contrast material is not necessary. However, contrast enhancement may be useful in differentiating cystic from solid lesions, in identifying areas of necrosis, and in differentiating lung abscesses from empyemas. Ideally the contrast material should be administered in a bolus with rapid injection, preferably by using a mechanical injector.

General Characteristics of Pleural Lesions

Plain films often fail to distinguish a peripheral parenchymal lesion from a pleural process. Typically pleural and extra-pleural lesions have obtuse angles with the chest wall, in contradistinction to subpleural processes in the pulmonary parenchyma, in which the angle is more likely to be acute. CT has been shown to be superior to plain films in the differentiation of pleural from parenchymal disease [20]. However, there is considerable overlap in the appearance of extrapleural, pleural, and parenchymal lesions even with the use of cross-

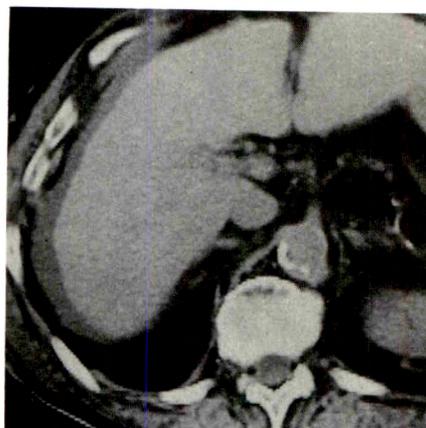


7

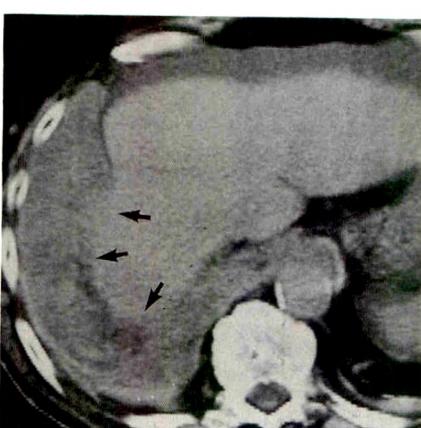


8

Fig. 7.—CT scan of intrapleural lipoma. Although lesion is pleural, angles of interface with chest wall are acute. Attenuation value of -90 H and homogeneous density establish diagnosis as lipoma. (Reprinted with permission from Epler et al. [22].)



A



B

Fig. 9.—CT scans of interface sign.
A, Ascites. A distinct interface is between ascitic fluid and liver.
B, Pleural effusion. A hazy indistinct interface is between pleural effusion and liver laterally (arrows). Ascites is present anteriorly.

Fig. 8.—CT scan of displaced-crus sign. Diaphragmatic crus (arrow) is displaced laterally by a right-sided pleural effusion.

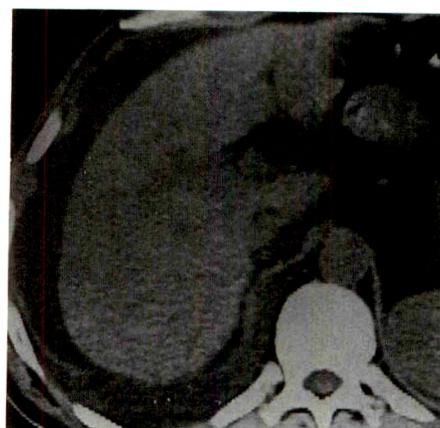


Fig. 10.—CT scan of diaphragm sign. Patient with both ascites and pleural fluid. Pleural effusion (E) lies outside diaphragm. Ascites (A) can be identified medial to or inside diaphragmatic contour (arrows).

sectional axial imaging displays [21] (Fig. 7). For example, if a lung lesion infiltrates the pleura, the result is obtuse angulation with the chest wall [21].

Pleural Fluid

Free-flowing pleural fluid produces a sickle-shaped opacity in the most dependent part of the thorax posteriorly. Located fluid collections are seen as lenticular opacities of fixed position. When free fluid lies in the posterior costophrenic recess adjacent to the diaphragm, it may be difficult to differentiate from ascites. Several CT features have been described that aid in the differentiation of pleural fluid from ascites. These include the displaced-crus sign [23], the interface sign [24], the diaphragm sign [25], and the bare-area sign [26]. If the diaphragmatic crus is displaced away from the spine by an abnormal fluid collection, the fluid is located in the pleural

space. Ascites, on the other hand, lies lateral and anterior to the crus (Fig. 8). The interface sign describes a sharp interface that can be identified between fluid and the liver or spleen when ascites is present [24] (Fig. 9). If the diaphragm is identifiable adjacent to an abnormal fluid collection in the right upper quadrant, then the diaphragm sign is probably the most reliable means of differentiating fluid from ascites. The location of the diaphragm is readily visible in patients with ascites, but may not be identified in patients with pleural effusions [27]. Pleural effusion is visualized outside the hemidiaphragm, whereas ascites is seen within the hemidiaphragmatic contour (Fig. 10). Finally, in the right hemithorax, restriction of peritoneal fluid by the coronary ligaments from the bare area of the liver is another useful distinguishing sign.

In regard to tissue-density characteristics, CT is rarely helpful in differentiating transudates from exudates or in the diagnosis of chylous pleural effusions [21, 28]. Pleural hemorrhage however, if acute, can be identified either by the

presence of a fluid/fluid level or because of increased density of the pleural fluid collection.

It is often difficult to differentiate empyemas, particularly those associated with bronchopleural fistula, from lung abscesses. Both may contain air/fluid levels. Several criteria for differentiating lung abscesses from empyemas have been proposed. Abscesses tend to have a spherical shape and a relatively thick wall. Empyemas, on the other hand, conform to the shape of the chest wall and are more likely to be lenticular with thinner walls [29]. One particularly helpful sign is lung compression by the empyema space, that is, the bronchi and vessels of the adjacent pulmonary parenchyma are displaced and compressed around the pleural fluid collection (Fig. 11). In contrast, in lung abscesses the bronchi and vessels of the adjacent lung appear to end abruptly at the margins of the abscess [30]. The most specific sign of empyema can be identified after the administration of contrast material. The split pleura sign consists of identification of the separation of visceral and parietal pleura, both of which enhance after administration of contrast material [30] (Fig. 12).

Pneumothorax

The majority of pneumothoraces are accurately demonstrated on standard chest radiographs. However subtle pneumothoraces may not be visible, particularly in patients who are radiographed while supine. These include acutely traumatized patients as well as patients maintained on ventilator therapy. Such occult pneumothoraces are well shown by CT [31].

Pleural Disease Induced by Asbestos Exposure

Pleural plaques are the most common manifestation of asbestos exposure. Although the majority of plaques can be identified by routine radiographs, CT has been shown to be more sensitive in this regard [32, 33]. Both the demand for

and cost of CT make it an unrealistic choice as a screening examination in persons who have been exposed to asbestos. However, it can be extremely helpful in differentiating pleural plaques from lung nodules and in resolving equivocal findings on standard radiographs. Diffuse pleural thickening is also a manifestation of asbestos exposure. Subcostal fat may mimic pleural thickening in obese persons. Typically it appears as a symmetric, smooth, soft-tissue density that parallels the chest wall and is of greatest thickness over the apices. In problem cases, CT may distinguish fat from either diffuse thickening or localized plaques [34]. Subcostal fat can be identified on CT scans as low-density tissue internal to the ribs and external to the parietal pleura (Fig. 13).

Rounded atelectasis is a form of collapse that develops in patients with pleural disease [36, 37], particularly in patients exposed to asbestos. On the standard chest radiograph, rounded atelectasis appears as a spherical, sharply marginated mass abutting the pleura. Pleural thickening is always present and frequently is of greatest dimension near the mass. The comet tail sign is produced by the crowding together of bronchi and blood vessels that extend from the lower border of the mass to the hilum [38]. Although these features may be appreciated on standard radiographs, CT shows the characteristic features, including the associated pleural thickening and peripheral location of the mass, to better advantage (Fig. 14).

Benign Pleural Tumors

Benign pleural tumors are relatively uncommon. They usually fall into one of two types, benign fibrous mesotheliomas (fibromas) and lipomas.

Lipomas may occur in either the pleural space or mediastinum. These lesions are asymptomatic and are usually discovered incidentally on chest radiographs. A definitive diagnosis is usually not possible on standard films. However, CT clearly delineates the pleural origin of these lesions in the majority of cases and their fatty composition (-50 to -150

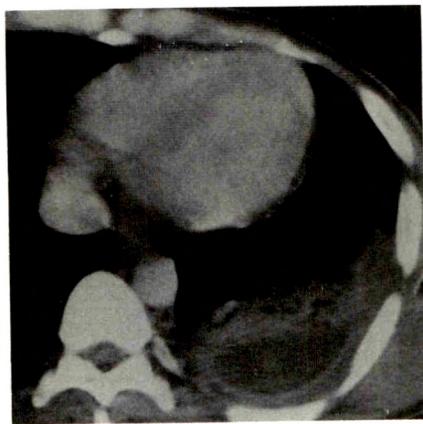


Fig. 11.—CT scan of empyema. Note lenticular fluid collection posteriorly. Adjacent lung is compressed and displaced by empyema space.

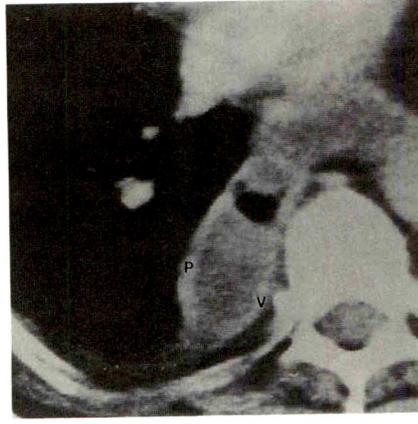


Fig. 12.—CT scan of split-pleura sign. Enhancement and separation of visceral (V) and parietal (P) pleura in a loculated posterior empyema.



Fig. 13.—Subcostal fat in patient exposed to asbestos. Note low-density tissue internal to rib and external to parietal pleura (arrows). (Reprinted with permission from McLoud [35].)

Hounsfield units) [39] (Fig. 7). Benign lipomas have a completely uniform fatty density, although linear soft-tissue strands due to fibrous stroma may be present. On the other hand, thymolipomas, angioliopomas, and teratomas are characterized by islands of soft-tissue density interspersed with fat [40, 41]. Liposarcomas can be differentiated from lipomas easily by their higher and heterogeneous density [42].

Benign fibrous mesotheliomas or fibromas are the most common benign tumors occurring in the pleura. Unlike their malignant counterpart, fibrous mesotheliomas have been associated with prolonged survival after surgical resection. Usually, they appear as solitary, often lobulated, well circumscribed and noncalcified soft-tissue masses either in the periphery of the hemithorax or related to the interlobar fissure. CT findings include well delineated, often lobulated soft-tissue masses in close relation to a pleural surface [43]. Although an obtuse angle of the mass with respect to the pleural surface may not be identified in every case, a smoothly tapering margin is characteristic and may indicate a pleural location [43]. Displacement of adjacent lung parenchyma with compressive atelectasis and bowing of the bronchi and pulmonary vessels around the masses is often noted. However, accurate diagnosis of benign mesotheliomas is not possible unless a pedicle is demonstrated. In such cases these tumors may be pedunculated and can exhibit changes in location and shape on CT when the patient is supine or prone [44]. When fibrous mesotheliomas attain a very large size, they may become locally invasive into the chest wall with associated rib destruction. CT can readily demonstrate such invasion.

Malignant Pleural Disease

Pleural malignancy may result from direct spread of a primary malignant tumor of the lung, such as bronchogenic carcinoma, to the pleural surface, metastases originating from extrathoracic primary tumors, direct seeding of tumor implants from primary thoracic neoplasms (thymoma), and primary malignant tumors of the pleura (malignant mesothelioma). CT is now used extensively in the evaluation of patients with suspected pleural malignancy. Malignant pleural disease is a common clinical problem. Twenty-five percent of

all pleural effusions in older patients in a general hospital setting are malignant in origin [45]. In patients with proved malignant pleural effusions or malignant pleural thickening, CT may provide useful diagnostic information about the presence of an underlying primary lung cancer or diffuse parenchymal metastases from a tumor of extrathoracic origin. CT should be performed after complete drainage of the effusion in order to permit optimal visualization of the underlying lung parenchyma.

Bronchogenic carcinoma.—The most frequent cause of pleural malignancy is bronchogenic carcinoma; it constitutes 35–50% of cases in most series [21, 46, 47]. When bronchogenic carcinoma involves the pleura diffusely with a resultant pleural effusion, the tumor is considered unresectable. However, peripheral tumors may directly invade the adjacent pleura locally with further spread to the chest wall. This is frequently demonstrated only by CT [48]. However, it is often difficult to distinguish true invasion of the parietal pleura from tumor contiguity. In such cases, accurate staging by CT is difficult. Invasion of the pleura by adjacent lung tumors usually results in obtuse angulation between the lesion and the adjacent chest wall [49].

Malignant mesothelioma.—Malignant mesotheliomas are rare tumors. In 70% of cases, a history of asbestos exposure can be obtained [50].

The CT appearance usually consists of a pleural effusion in association with a markedly thickened, irregular, and often nodular pleura (Fig. 15). The tumor may encase the underlying lung and extend into the pleural fissures. Occasionally only a pleural effusion is identified [51, 52].

CT can be particularly helpful in evaluating the degree of tumor extent, particularly its invasion into the mediastinum, contralateral pleura, chest wall, or extension through the diaphragm into the peritoneum [52]. Treatment includes either pleurectomy or extrapleural pneumonectomy. The postoperative hemithorax can be evaluated with CT, and residual or recurrent disease can be shown [53]. CT may detect unsuspected pleural plaques on the opposite side also, helping to confirm the diagnosis.

Metastatic disease.—Pleural metastases from extrathoracic primary tumors occur most frequently from neoplasms of the breast and gastrointestinal tract including the pancreas,

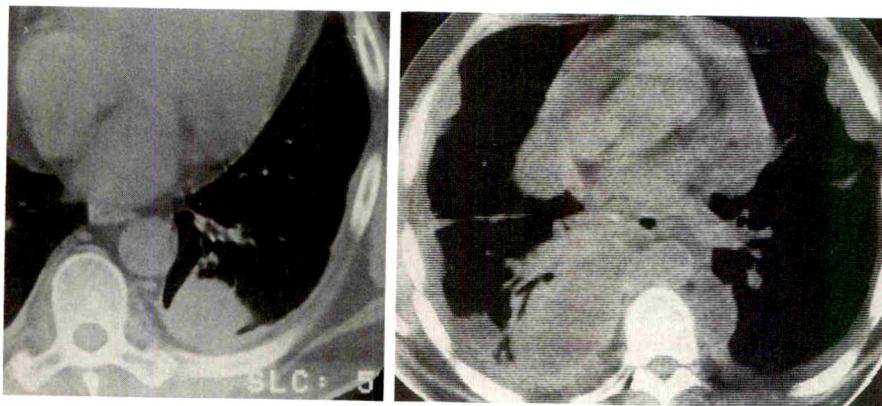


Fig. 14.—CT scan of rounded atelectasis. Well-defined mass abuts pleura with associated pleural thickening. Vessels are crowded together and converge toward lesion, creating a whorled appearance.

Fig. 15.—CT scan of malignant mesothelioma. Nodular pleural thickening encases right lung and extends along mediastinal pleural surface. Pericardium and opposite pleura are also involved.

kidneys, and ovaries [54]. The most common manifestation is malignant pleural effusion. The underlying focus of malignancy is often difficult to identify. However, in such instances, CT may be useful in showing small hematogenous metastases to the lung parenchyma.

However, pleural metastases may appear identical to malignant mesothelioma, characterized by diffuse pleural thickening and encasement of the underlying lung. Differentiation of metastatic disease from a benign pleuritis or fibrothorax may be difficult in some instances. However, in most cases, the pleural thickening is nodular and frequently encases the entire lung, including the mediastinal pleural surface [55].

Pleural lymphoma.—Pleural effusions in lymphoma may be caused by lymphatic obstruction due to enlarged hilar or mediastinal nodes or by direct involvement of the pleural space [56]. The characteristic CT appearance of direct pleural involvement consists of localized, broad-based lymphomatous pleural plaques, which often are difficult to see on standard radiographs [57]. These plaques may originate in the subpleural chain of lymphatics and are likely to occur with non-Hodgkin lymphomas [21]. Lymphoma may also involve the pleura and chest wall by direct extension from the anterior mediastinum.

Pleural seeding.—Direct pleural seeding from intrathoracic neoplasms not only occurs with bronchogenic carcinoma but with a primary mediastinal tumor (malignant thymoma). Malignant thymoma may also involve the pleura by direct contiguous spread. Pleural seeding often occurs as recurrent disease after surgery, and therefore CT is recommended in the follow-up of patients with a history of surgery or radiation therapy. Areas of pleural seeding appear as localized, well-defined pleural masses with or without pleural effusion [58] (Fig. 16).

MR Imaging

The role of MR imaging in the evaluation of the pleura is somewhat limited. MR does provide certain advantages because of its ability to image the thorax directly in the axial, coronal, and sagittal planes. The normal pleural space cannot be visualized with current MR imaging techniques. In regard to pulse sequence selection, T1-weighted images offer the greatest signal-to-noise ratio, have excellent contrast between abnormalities in the pleural space and extrapleural fat,

and are preferred for anatomic resolution [59]. T2-weighted images may offer tissue-specific information concerning pleural lesions and allow better evaluation of pleural processes that have invaded the chest wall because of the increased tumor-to-muscle contrast.

Pleural Fluid

Fluid collections in the pleural cavity show a low signal intensity on T1-weighted images and a high relative signal intensity on T2-weighted images because of their water content. However, as with most other body fluid collections, signal-intensity measurements and relaxation-time calculations are not sufficiently reliable to be helpful in the differential diagnosis [62]. Differentiation of transudates from exudates is not possible *in vivo* [60, 61]. However, subacute or chronic hemorrhage can be recognized by very high signal intensity on both T1- and T2-weighted images [61]. We have also found it possible to differentiate subacute and chronic hematomas in the pleural space as well as chylous pleural effusions from other types of pleural fluid collections (Figs. 17 and 18). In subacute or chronic hematomas, a concentric-ring sign may be observed; this consists of an outer dark rim composed of hemosiderin and bright signal intensity in the center because of the T1 shortening effects of methemoglobin [62, 63].

Pleural Tumors

Benign pleural tumors.—CT is the imaging method of choice in the assessment of benign pleural tumors. MR provides little incremental information in the assessment of such lesions. Pleural lipomas can be readily identified by signal characteristics; such lesions are of bright signal intensity on T1-weighted images and also moderately bright on T2-weighted images.

Bronchogenic carcinoma.—MR imaging can detect chest wall invasion in patients with carcinoma of the lung when CT findings are equivocal [64]. However, isolated invasion of the parietal pleura is more difficult to determine. MR findings indicative of chest wall invasion include a high-signal focus within the chest wall or chest wall thickening with increased signal on T2-weighted spin-echo images. MR is particularly helpful in staging superior sulcus carcinomas. Sagittal and

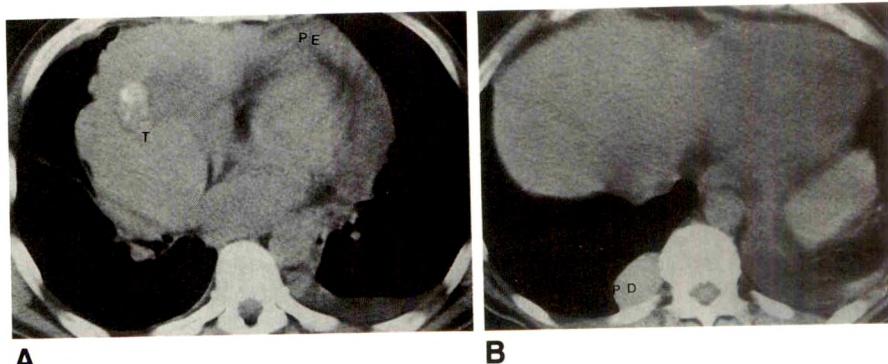


Fig. 16.—CT scans of malignant thymoma.
A, Large, right-sided calcified mediastinal mass (T) associated with a pericardial effusion (PE).

B, Localized pleural deposit (PD) in right paravertebral area.

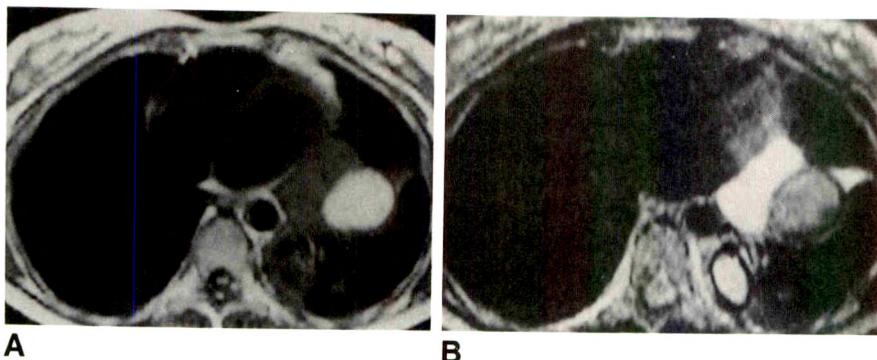


Fig. 17.—MR of chylous effusion.

A, T1-weighted MR image shows fluid collection in major fissure, which is of low signal intensity medially (water content) and high signal intensity laterally (fat).

B, T2-weighted MR image. Fluid medially has a long T2 value, and fatty component shows T2 shortening with signal intensity similar to that of subcutaneous fat.

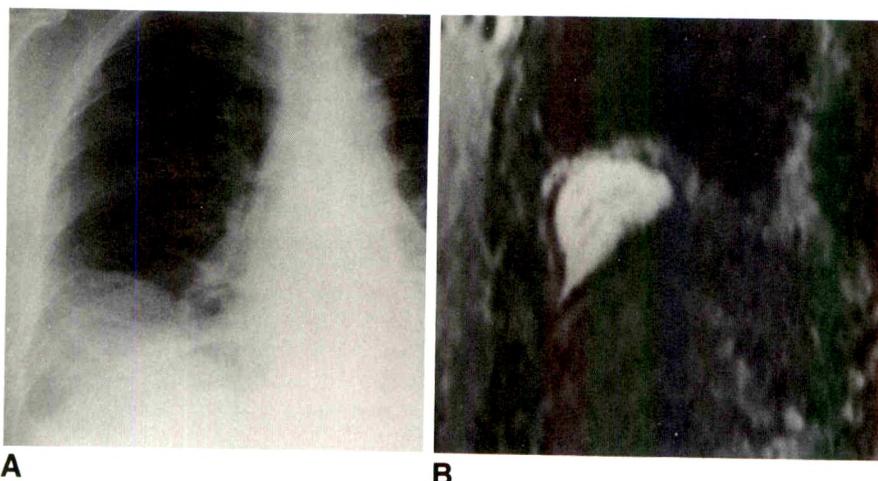


Fig. 18.—**A**, Middle-aged alcoholic man incidentally found to have a right-sided effusion and a mass at right base on chest radiograph. Patient did not remember any recent trauma, although he presumably sustained falls because of his alcoholism.

B, T2-weighted MR image shows classic features of a hematoma. Note low-signal-intensity rim (hemosiderin) and bright signal intensity of methemoglobin.

coronal images allow assessment of invasion of the spinal canal, extension of tumor into the base of the neck, and involvement of the brachial plexus and subclavian artery [65].

Malignant pleural mesothelioma.—Although CT has been shown to be quite effective in defining the extent of disease in malignant pleural mesothelioma, MR may have certain advantages in that regard because of its ability to image in multiple planes. The tumors have intermediate signal intensity on T1-weighted images. The T2-weighted images show a slight increase in signal intensity, with focal areas of very high signal intensity due to pleural fluid [66]. The extent of tumor and its effects on adjacent structures can be well appreciated on coronal MR images. We have observed that MR may be extremely useful in determining mediastinal invasion and extension into the chest wall or below the diaphragm.

Conclusions

The roles of sonography, CT, and MR imaging in the evaluation of pleural diseases are complementary. Sonography is indicated whenever bedside mobile examinations are required. The main role of sonography is in the evaluation of patients who have undergone an unsuccessful thoracentesis. It allows easy identification of pleural fluid and the presence of loculation. It provides a guide to aspiration, and it permits the ready distinction of pleural fluid from pleural masses. Sonography also provides an easy and safe method for guiding closed pleural biopsy of either pleural masses or

processes that cause diffuse pleural thickening. Although CT offers an alternative method for such biopsies, it is usually only mandatory for areas of thickening or tumors that are small and poorly identified. Furthermore, sonography is usually the first method of choice in providing imaging guidance for pleural drainage procedures, particularly when pleural fluid is loculated.

On the other hand, CT is the preferable imaging technique for the characterization of pleural masses in regard to their location (i.e., pleural or parenchymal) and their composition. The extent and degree of pleural thickening are also better ascertained by CT scanning, and CT is more likely to determine either the characteristics or presence of an associated underlying malignant tumor. CT is also the method of choice in the assessment of pleural changes due to asbestos exposure. Finally, in the evaluation of malignant processes of the pleura, CT provides unique information about the extent of disease and invasion of the chest wall and other surrounding structures. The role of MR imaging in the evaluation of the pleura is somewhat limited. However, MR is the imaging method of choice in the evaluation of superior sulcus carcinomas.

REFERENCES

1. Gryminski J, Krakowka P, Lypacewicz G. The diagnosis of pleural effusion by ultrasonic and radiological techniques. *Chest* 1976;70:33-37
2. Joyner CR Jr, Herman RJ, Reid JM. Reflected ultrasound in the detection and localization of pleural effusion. *JAMA* 1967;200:129-132
3. Lipscomb DJ, Flower CDR, Hadfield JW. Ultrasound of the pleura: an assessment of its clinical value. *Clin Radiol* 1981;32:289-290

4. Hirsch JH, Rogers JV, Mack LA. Real-time sonography of the pleural opacities. *AJR* **1981**;136:297–301
5. O'Moore PV, Mueller PR, Simeone JF, et al. Sonographic guidance in diagnostic and therapeutic interventions in the pleural space. *AJR* **1987**;149:1–5
6. Rosenberg ER. Ultrasound in the assessment of pleural densities. *Chest* **1983**;84:283–285
7. Marks WM, Filly RA, Callen PW. Real-time evaluation of pleural lesions: new observations regarding the probability of obtaining free fluid. *Radiology* **1982**;142:163–164
8. Leung AN, Muller NL, Miller RR. CT in the differential diagnosis of pleural disease. *AJR* **1990**;154:487–492
9. Muller PR, Saini S, Simeone JF, et al. Image guided pleural biopsies: indications, technique, and results in 23 patients. *Radiology* **1988**;169:1–4
10. Gleeson F, Lomas DJ, Flower CDR, Stewart S. Powered cutting needle biopsy of the pleura and chest wall. *Clin Radiol* **1990**;41:199–200
11. Ikezoe J, Sone S, Higashihara T, Morimoto S, Arisawa J, Kuriyama K. Sonographically guided needle biopsy for diagnosis of thoracic lesions. *AJR* **1984**;143:220–234
12. Davis WC, Johnson LF. Adult thoracic empyema revisited. *Am Surg* **1978**;44:362–368
13. Westcott JL. Percutaneous catheter drainage of pleural effusion and empyema. *AJR* **1985**;144:1189–1193
14. vanSonnenberg E, Nakamoto SK, Mueller PR, et al. CT and ultrasound guided catheter drainage of empyemas after chest tube failure. *Radiology* **1984**;151:349–353
15. Hunnam GR, Flower CDR. Radiologically guided percutaneous catheter drainage of empyemas. *Clin Radiol* **1988**;39:121–126
16. Silverman SG, Mueller PR, Saini S, et al. Thoracic empyema: management with image guided catheter drainage. *Radiology* **1988**;169:5–9
17. Merriam MC, Cronan JJ, Dorfman GS, Lambiase RE, Haas RA. Radiographically guided percutaneous catheter drainage of pleural fluid collections. *AJR* **1988**;151:1113–1116
18. Neff CC, vanSonnenberg E, Lawson DW, Patton AS. CT follow-up of empyemas: pleural peels resolve after percutaneous catheter drainage. *Radiology* **1990**;176:195–197
19. Moulton JS, Moore PT, Mencini RA. Treatment of loculated pleural effusions with transcatheter intracavity urokinase. *AJR* **1989**;153:941–945
20. Pugatch RD, Faling LJ, Robbins AH, Snider GL. Differentiation of pleural and pulmonary lesions using computed tomography. *J Comput Assist Tomogr* **1978**;2:601–606
21. Naidich DP, Zerhouni EA, Siegelman SS. The pleura and chest wall. In: *Computed tomography of the thorax*. New York: Raven Press, **1984**:243–268
22. Epler GR, McLoud TC, Munn CS, Colby TV. Pleural lipoma: diagnosis by computed tomography. *Chest* **1986**;90:265–268
23. Dwyer RA. The displaced crus: a sign for distinguishing between pleural fluid and ascites on computed tomography. *J Comput Assist Tomogr* **1978**;2:598–599
24. Teplick JG, Teplick SK, Goodman L, Haskin ME. The interface sign: a computed tomographic sign for distinguishing pleural and intra-abdominal fluid. *Radiology* **1982**;144:359–362
25. Alexander S, Proto AV, Clark RA. CT differentiation of subphrenic abscess and pleural effusion. *AJR* **1983**;140:47–51
26. Naidich DP, Megibow AJ, Hilton S, Hulnick DH, Siegelman SS. Computed tomography of the diaphragm: periaphragmatic fluid localization. *J Comput Assist Tomogr* **1983**;7:641–649
27. Halvorsen RA, Fedyshin PJ, Korobkin M, Foster WL, Thompson WM. Ascites or pleural effusion? CT differentiation: four useful criteria. *RadioGraphics* **1986**;6:135–149
28. Rawkin RN, Raval B, Finley R. Primary chylopericardium: combined lymphangiographic and CT diagnosis (case report). *J Comput Assist Tomogr* **1980**;4:869–870
29. Barber CE, Hedlund LW, Oddson TA, Putman CE. Differentiating empyemas and peripheral pulmonary abscesses: the value of computed tomography. *Radiology* **1980**;135:755–758
30. Stark DD, Federle MP, Goodman PC, Podrasky AE, Webb WR. Differentiating lung abscess and empyema: radiography and computed tomography. *AJR* **1983**;141:163–167
31. Tocino I, Miller MH, Frederick PR, Bahr AL, Thomas F. CT detection of acute pneumothorax in head trauma. *AJR* **1984**;143:989–990
32. Kreel L. Computed tomography in the evaluation of pulmonary asbestos. *Acta Radiol* **1976**;17:405–412
33. Kreel L. Computed tomography of the lung and pleura. *Semin Roentgenol* **1978**;13:213–225
34. Sargent EN, Boswell WD, Ralls PW, Markowitz A. Subpleural fat pads in patients exposed to asbestos: distinction from non-calcified pleural plaques. *AJR* **1984**;152:273–277
35. McLoud TC. Asbestos-related diseases: the role of imaging techniques. *Postgrad Radiol* **1989**;9:65–74
36. Blesovsky A. The folded lung. *Br J Dis Chest* **1966**;60:19–22
37. Mintzer RA, Gore RM, Vogelzang RL, Holz S. Rounded atelectasis and its association with asbestos induced pleural disease. *Radiology* **1981**;139:567–570
38. Schneider HJ, Felson B, Gonzales LL. Rounded atelectasis. *AJR* **1980**;134:225–232
39. Chalaoui J, Sylvestre J, Dussault RG, Pinsky M, Palayew MJ. Thoracic fatty lesions, some usual and unusual appearances. *J Can Assoc Radiol* **1980**;32:197–201
40. Yeh HC, Gordon A, Kirschner PA, Cohen BA. Computed tomography and sonography of thymolipoma. *AJR* **1983**;140:1131–1133
41. Biondetti PR, Fiore D, Perrin B, Ravasini R. Infiltrative angiolioma of the thoracoabdominal wall. *J Comput Assist Tomogr* **1982**;6:847
42. Mendez G, Isilkoff MB, Isilkoff SK, Sinner WN. Fatty tumors of the thorax demonstrated by lung CT. *AJR* **1979**;133:207–212
43. Dedrick CG, McLoud TC, Shepard JO, Shipley RT. Computed tomography of localized pleural mesothelioma. *AJR* **1985**;144:275–280
44. Weisbrod GL, Yee AC. Computed tomographic diagnosis of a pedunculated fibrous mesothelioma. *J Can Assoc Radiol* **1983**;34:147–148
45. Leff A, Hopewell PC, Costello J. Pleural effusion from malignancy. *Ann Intern Med* **1978**;88:532–537
46. Scerbo J, Keltz H, Stone DJ. A prospective study of closed pleural biopsies. *JAMA* **1971**;218:377–380
47. Ryan CJ, Rodgers RF, Unni KK, Hepper NGG. The outcome of patients with pleural effusion of indeterminate cause at thoracotomy. *Mayo Clin Proc* **1981**;56:145–149
48. Webb WR, Jeffrey RB, Godwin JD. Thoracic computed tomography in superior sulcus tumors. *J Comput Assist Tomogr* **1981**;5:361–365
49. Williford ME, Hidalgo H, Putman CE, Korobkin M, Ram PC. Computed tomography of pleural disease. *AJR* **1983**;140:909–914
50. Elmes PC. The epidemiology and clinical features of asbestosis and related diseases. *Postgrad Med J* **1966**;42:623–635
51. Kreel L. Computed tomography in mesotheliomas. *Semin Oncol* **1981**;8:302–312
52. Alexander E, Clark RA, Colley DP, Mitchell SE. CT of malignant pleural mesothelioma. *AJR* **1981**;137:287–291
53. Libshitz HI. Malignant pleural mesothelioma: the role of computed tomography. *CT* **1984**;8:15–20
54. Meyer PC. Metastatic carcinoma of the pleura. *Thorax* **1966**;21:437–443
55. Leung AN, Muller NL, Miller RR. Differential diagnosis of diffuse pleural disease with CT. *Radiology* **1989**;173(P):139
56. Black LF. Subject review: the pleural space and pleural fluid. *Mayo Clin Proc* **1982**;47:493–506
57. Burginer FA, Hamlin DJ. Intrathoracic histiocytic lymphoma. *AJR* **1981**;146:499–504
58. Zerhouni EA, Scott WW, Baker RR, Wareham MD, Siegelman SS. Invasive thymomas: diagnosis and evaluation by computed tomography. *J Comput Assist Tomogr* **1982**;6:92–100
59. Hahn D. Mediastinum and lung. In: Stark DD, Bradley WG, eds. *Magnetic resonance imaging*. St. Louis, MO: Mosby, **1988**:804–860
60. Davis SD, Henscke CI, Yankelevitz DF, Cahill PT, Yi Y. MR imaging of pleural effusions. *J Comput Assist Tomogr* **1990**;14:192–198
61. Tshcholakoff D, Sechtem U, de Geer G, Schmidt H, Higgins CB. Evaluation of pleural and pericardial effusions by magnetic resonance imaging. *Eur J Radiol* **1978**;7:169–174
62. Hahn PF, Stark DD, Vici LG, Ferruci JT Jr. Duodenal hematoma: the ring sign in MR imaging. *Radiology* **1986**;159:379–382
63. Bradley WG. MRI of hemorrhage and iron in the brain. In: Stark DD, Bradley WG, eds. *Magnetic resonance imaging*. St. Louis, MO: Mosby, **1988**:359–374
64. Haggard AM, Pearlberg JL, Froelich JW, et al. Chest-wall invasion by carcinoma of the lung: detection by MR imaging. *AJR* **1987**;148:1075–1078
65. McLoud TC, Filion RB, Edelman RR, Shepard JO. MR imaging of superior sulcus carcinoma. *J Comput Assist Tomogr* **1989**;13:233–239
66. Lorigan JG, Libshitz HI. MR imaging of malignant pleural mesothelioma. *J Comput Assist Tomogr* **1989**;13:617–620

Book Review



Congenital Heart Disease. Echocardiography and Magnetic Resonance Imaging. By Charles B. Higgins, Norman H. Silverman, Barbara A. Kersting-Sommerhoff, and Klaus Schmidt. New York: Raven, 405 pp., 1990. \$135

The revolution in body imaging brought about by the widespread distribution of MR imagers continues to outpace our ability to keep up with new technical developments, diagnostic inferences, and diagnostic indications. A rapid proliferation of textbooks on MR has reflected the growing need for radiologists to maintain proficiency in this area.

Few texts have been devoted to cardiac MR imaging, undoubtedly reflecting the limited clinical practice of cardiac MR. However, the experience at many university medical centers around the world clearly has shown the usefulness of MR for the precise diagnosis of congenital heart disease and for the diagnosis and quantification of morphologic and hemodynamic changes in patients with acquired heart disease.

Higgins, Silverman, Kersting-Sommerhoff, and Schmidt and their contributors have written a textbook of cardiac morphology and function derived from MR and echocardiographic techniques. Emphasizing the complementarity of MR and echocardiography, the authors describe the current state of the art for precise anatomic diagnosis of congenital heart disease, as well as preoperative planning and postoperative follow-up of these patients. The illustrations are top quality and are adequately and clearly labeled. The experience of the authors is apparent in their detailed discussions.

This is an important book. It is well organized, complete, and actually quite readable. Of course, this is not a text to be read cover to cover and subsequently lost on a library shelf. Rather, it is an excellent clinical reference that belongs near the consoles of MR imagers. The first chapters on tomographic anatomy, tomographic cardiac imaging, and cardiac situs and connections provide a solid basis for later chapters dealing with specific malformations and clinical problems. These subsequent chapters describe the pathologic and anatomic changes, emphasizing the complementary roles of echocardiography and MR. The authors do not get caught up in the excitement of MR imaging; the limitations of this evolving technology are stated at the outset. However, its obvious value is immediately apparent, as is its incredible potential for use in clinical problem solving.

The importance of this book is more than the breadth and depth

of the clinical information provided. The authors have shown that cardiac anatomy, physiology, and pathology are within the grasp of diagnostic radiologists who perform MR examinations. The drift of cardiac diagnosis away from diagnostic radiologists into the realm of pediatric and adult cardiologists was reinforced by the rise of diagnostic cineangiography, an equipment-intensive technique with little use other than for cardiac diagnosis. Thus, cardiac imaging became cineangiographic imaging, and the role of the diagnostic radiologist was superseded by that of adult and pediatric cardiologists who performed cardiac catheterizations.

As the authors show, commercially available MR imagers can provide excellent images of the heart in health and disease. Thus, the substrate for cardiac diagnosis is no longer largely unavailable to diagnostic radiologists. As the authors indicate in their preface, the text is a practical guide for specialists in cardiac diagnosis. However, the authors underestimate their case; cardiac imaging can be performed in radiology departments, and cardiac diagnosis can and should be made by radiologists. This text should encourage directors of academic radiology departments to train their residents in radiologic cardiac diagnosis and to emphasize the role of MR in the workup and examination of patients with heart disease. Furthermore, it should encourage diagnostic radiologists who perform MR to exert their expertise in imaging science and to play a role in cardiac diagnosis.

Radiology residents and practicing radiologists somehow have gotten the notion that cardiac diagnosis is mysterious and more difficult than diagnosis of disorders in other body areas, thus taking it out of the realm of diagnostic radiology. This is not true, and the authors of this text have shown the significant diagnostic support that radiologists can provide in the management of patients who have cardiac disease. The authors should be congratulated on their excellent textbook. Diagnostic radiologists should recognize the opportunity that MR provides for increasing their role in the diagnosis and management of patients with heart disease.

Lawrence M. Boxt
College of Physicians and Surgeons of Columbia University
New York, NY 10032

Perivalvular Pseudoaneurysm Complicating Bacterial Endocarditis: MR Detection in Five Cases

E. William Akins¹
 Richard M. Slone¹
 Bret N. Wiechmann¹
 Michael Browning²
 Tomas D. Martin^{2,3}
 William R. Mayfield²

Bacterial endocarditis usually affects the valve leaflets, but erosion into the valve anulus and adjacent myocardium may form a myocardial abscess. Perivalvular abscesses can drain into the ventricles or aorta, forming a life-threatening pseudoaneurysm. We reviewed our experience with cardiac MR imaging of this disorder. Fourteen patients with complicated bacterial endocarditis underwent ECG-gated spin-echo cardiac MR imaging in addition to conventional duplex two-dimensional echocardiography (2-D echo). Angiography was performed in seven patients, six of whom underwent surgery for valve replacement. MR imaging detected the pseudoaneurysms in all five of the surgically proved cases, while 2-D echo detected only three. Clinical follow-up suggested there were no false-negative examinations, but no autopsy data were available for confirmation. Postoperative MR imaging studies were conducted in three patients, revealing two recurrent pseudoaneurysms and one thrombosed aneurysm.

Cardiac MR imaging provides useful pre- and postoperative information in patients with perivalvular pseudoaneurysms due to endocarditis.

AJR 156:1155–1158, June 1991

Perivalvular pseudoaneurysm is a serious complication of bacterial endocarditis. The perivalvular inflammatory process may erode the wall or form an abscess draining into the vascular system, resulting in a pseudoaneurysm. Identification of the presence and location of a perivalvular pseudoaneurysm is important in planning medical or surgical therapy. Although two-dimensional echocardiography (2-D echo) has shown promise as a noninvasive means of evaluating this process, limitations of 2-D echo for recognition and localization of pseudoaneurysms have been described [1–3].

Perivalvular pseudoaneurysm has received little attention in the radiologic literature [4, 5]. We report our experience with cardiac MR imaging in conjunction with 2-D echo for the detection of aortic perivalvular pseudoaneurysms in patients with endocarditis.

Subjects and Methods

Received September 26, 1990; accepted after revision December 11, 1990.

¹ Department of Radiology, University of Florida College of Medicine, Box J-374, JHMHC, Gainesville, FL 32610-0374. Address reprint requests to E. W. Akins.

² Department of Surgery, University of Florida College of Medicine, Gainesville, FL 32610-0374.

³ Present address: Cardiothoracic Surgery, Emory Clinics, Atlanta, GA 30322.

0361-803X/91/1566-1155
 © American Roentgen Ray Society

Fourteen patients with clinical symptoms of bacterial endocarditis and symptoms suggesting the presence of perivalvular pseudoaneurysms had 2-D echo and ECG-gated cardiac MR imaging. MR was performed with four different instruments: a 1.5-T Signa unit (General Electric, Milwaukee, WI), a 1.5-T Magnetom unit (Siemens, Iselin, NJ), a 1.0-T Magnetom unit, and a 0.15-T Technicare (Solon, OH) unit. The low-field images were obtained with dedicated cardiac coils and were of good quality. T1-weighted ECG-gated spin-echo images were obtained by using a TR equal to the R-R interval and a single TE of 15–30 msec. Axial, coronal, long-axis oblique, and other oblique imaging planes were used as needed based on the pertinent anatomy. Gradient-echo cine cardiac MR was used to supplement conventional images in the most recent case. All MR studies were interpreted by the principal author.

Duplex 2-D echo was performed and interpreted by experienced cardiologists who used a transcutaneous technique and high-resolution real-time equipment with multiple viewing

windows and planes of section. In one patient, intraoperative transesophageal 2-D echo was performed also.

Cardiac catheterization and angiography were performed in seven of the patients. Six patients underwent cardiac surgery for valve replacement; a pseudoaneurysm was repaired in five of these.

The studies were performed and interpreted prospectively. A chart review was conducted to gather details of the clinical histories and review the MR, 2-D echo, and angiographic reports. In all cases the 2-D echo examination was performed first, and the study was not blinded.

The 14 patients (seven men and seven women) included in the study had a mean age of 57 years (range, 23–81). Three had prosthetic aortic valves and two had prosthetic mitral valves. Bacterial endocarditis was diagnosed in all patients, and specific organisms were cultured in 10 (*Staphylococcus aureus* in five, *Streptococcus faecalis* in one, *Staphylococcus epidermidis* in one, *Streptococcus viridans* in one, and *Enterococcus* in one).

Results

The MR depictions of perivalvular pseudoaneurysms were of low-intensity perivalvular outpouchings or cystic cavities representing flowing blood within the lumen of the pseudoaneurysm (Figs. 1A, 1B, and 2A). The aneurysms varied in size from approximately 2 × 2 cm in greatest dimensions to 8 × 10 × 4 cm. All five perivalvular pseudoaneurysms were

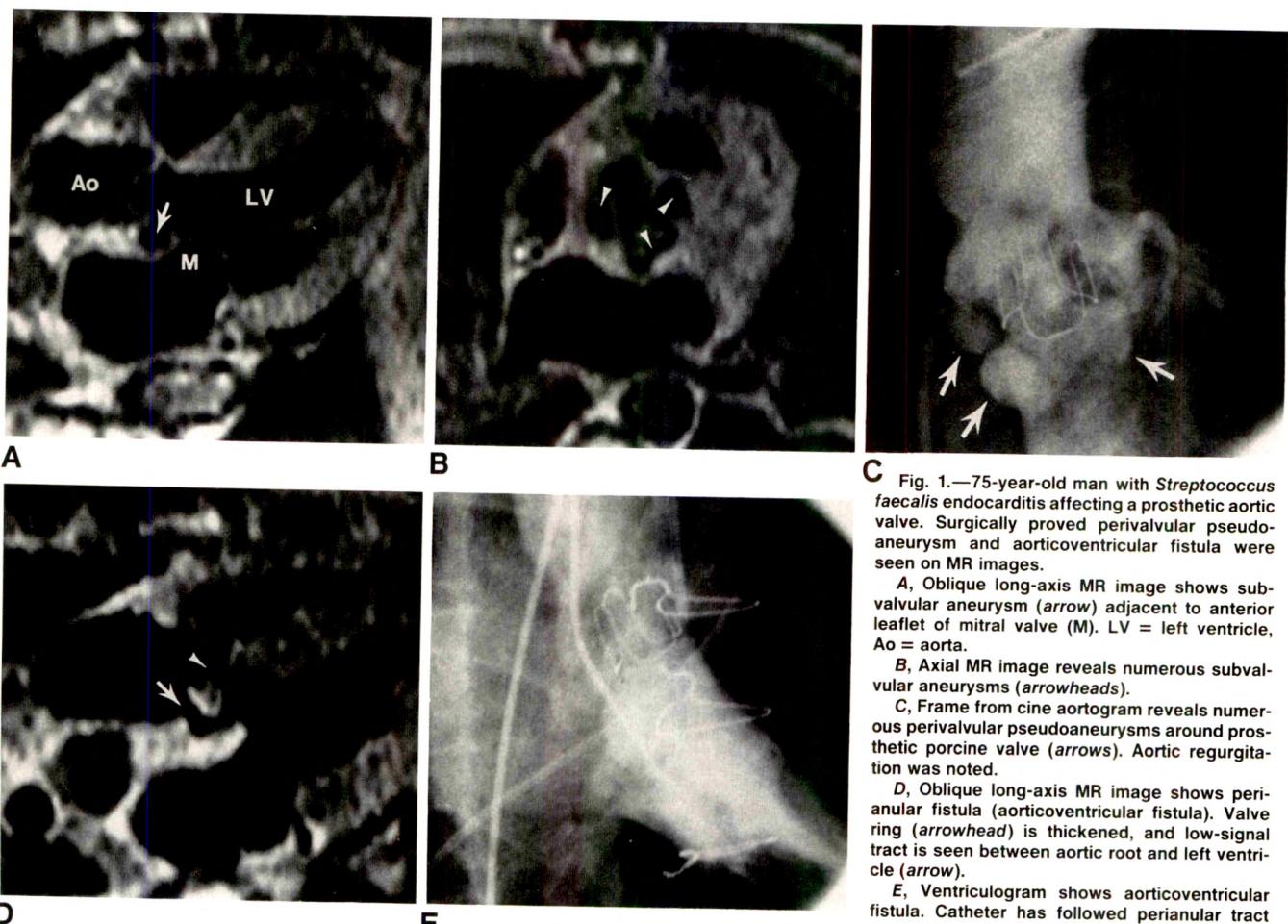
related to aortic valve endocarditis; three of these involved prosthetic valves.

The frequency of perivalvular pseudoaneurysms in our series of 14 patients was 36% (5/14). MR detected all five surgically proved pseudoaneurysms (100%), whereas 2-D echo detected only three (60%). The size and location of the pseudoaneurysms were confirmed surgically in all five cases during attempted aneurysm closure, valve annular debridement, and valve replacement. No pseudoaneurysms were seen on images that were not found surgically. Clinical follow-up in the nine other patients without recognizable pseudoaneurysms revealed no late sequelae indicative of pseudoaneurysm development. However, no postmortem data were available for confirmation.

Two patients with pseudoaneurysms died within the postoperative period. Follow-up MR studies were performed in the remaining three cases, revealing two cases of recurrent pseudoaneurysm and one thrombosed aneurysm. The thrombosed aneurysm was evidenced by high signal intensity in the area of the previous aneurysm cavity (Fig. 2C).

Discussion

Endocarditis is usually isolated to the valve leaflets, but aggressive bacteria such as *Staphylococcus aureus* have a



C Fig. 1.—75-year-old man with *Streptococcus faecalis* endocarditis affecting a prosthetic aortic valve. Surgically proved perivalvular pseudoaneurysm and aorticoventricular fistula were seen on MR images.

A, Oblique long-axis MR image shows subvalvular aneurysm (arrow) adjacent to anterior leaflet of mitral valve (M). LV = left ventricle, Ao = aorta.

B, Axial MR image reveals numerous subvalvular aneurysms (arrowheads).

C, Frame from cine aortogram reveals numerous perivalvular pseudoaneurysms around prosthetic porcine valve (arrows). Aortic regurgitation was noted.

D, Oblique long-axis MR image shows perianular fistula (aorticoventricular fistula). Valve ring (arrowhead) is thickened, and low-signal tract is seen between aortic root and left ventricle (arrow).

E, Ventriculogram shows aorticoventricular fistula. Catheter has followed perianular tract caused by endocarditis.

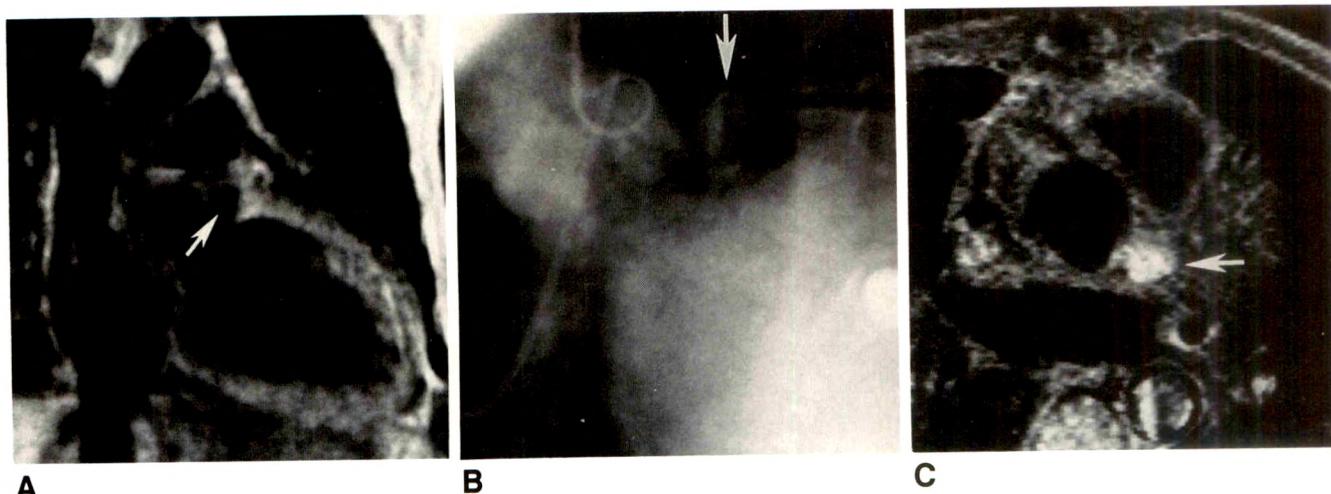
**A****B****C**

Fig. 2.—54-year-old man with enterococcal endocarditis affecting prosthetic aortic valve.

A, Preoperative coronal MR image shows periaortic pseudoaneurysm arising from left coronary cusp (arrow) near left coronary artery.

B, Aortogram confirms pseudoaneurysm (arrow) and reveals aortic regurgitation.

C, Postoperative axial MR image after valve replacement and patch repair shows high signal intensity from thrombosis in aneurysm (arrow).

tendency to invade the valve anulus, forming a perivalvular abscess. The abscess usually drains into the lumen of the ventricle or aorta, forming a pseudoaneurysm of the valve ring. Valve ring abscesses occur in approximately 30% of patients with native valve infectious endocarditis [6] and are not always diagnosed clinically or radiologically, but are found at surgery or autopsy. Valve ring abscesses involve the aortic anulus much more often (95%) than the mitral valve [6]. Valve ring abscesses are much more common and more extensive in the presence of prosthetic valve endocarditis [7].

Clinical signs suggestive of valve ring abscess include a high-degree atrial ventricular block, recent onset of aortic insufficiency, pericarditis, and persistent sepsis despite the use of antibiotics [6]. Valvular regurgitation is always present in patients with a valve ring abscess [6, 8]. The presence of a valve ring abscess is a very poor prognostic factor, carrying a high surgical mortality rate and a poor long-term survival rate [9, 10]. Most authorities believe that surgical intervention is essential in patients with bacterial endocarditis complicated by valve ring abscess [11, 12].

Preoperative recognition of perivalvular pseudoaneurysm is desired by cardiac surgeons for the proper selection of patients for early valve replacement and to prepare for pseudoaneurysm repair, aortic anulus debridement, and valve replacement. The presence of an abscess complicates valve replacement and increases the risk of reinfection and valve dehiscence [13]. Surgical management involves debridement of infected tissue, repair of the aneurysm by patch or homograft insertion, and then replacement of the valve [9].

In a combination of four series totaling 96 cases, cardiac catheterization detected 18 (69%) of 26 abscesses preoperatively [13–16]. Thus, improvements in the diagnostic imaging of this condition are clearly needed, and noninvasive assessment, if adequate to plan surgery, seems warranted.

2-D echo can detect vegetations and assess valvular insufficiency, which greatly influences treatment. 2-D echo has

also been able to detect perivalvular pseudoaneurysms [17–19]. An echo-free cavity is the classic diagnostic sign, but is seldom observed [17]. 2-D echo is often limited by artifacts induced by valve prostheses, and superficial windows are not always sufficient to provide excellent valvular visualization. However, the advent of transesophageal echocardiography may greatly influence the role of 2-D echo in the assessment of this condition [20].

Our study shows the ability of gated cardiac MR to detect perivalvular pseudoaneurysms in patients with infectious endocarditis. The usefulness of MR in the detection and characterization of aortic root abscesses in isolated cases has been reported by us and by others [4, 5, 21, 22]. In this study, MR detected more aneurysms than transcutaneous duplex 2-D echo did. For complete assessment of the aortic anulus and related structures, oblique imaging planes are used to supplement the standard axial and coronal planes. We noted that recurrent perivalvular pseudoaneurysms after attempted surgical repair can be recognized by MR. The poor clinical success rate of surgery in this study is comparable to the high mortality rates and high recurrence rates published [10]. This is the largest study reported thus far on the use of MR in assessing perivalvular pseudoaneurysms. We would expect the role of MR imaging in patients with endocarditis to expand with the use of gradient-echo techniques, which improve the assessment of valve function. A study comparing cardiac MR using cine flow-sensitive sequences with transesophageal echocardiography for the recognition of perivalvular pseudoaneurysms would be useful as these technologies develop.

MR provides useful preoperative information about patients with perivalvular pseudoaneurysms due to endocarditis. MR may also be used postoperatively to assess recurrence of the aneurysm. Cardiac MR, 2-D echo, and Doppler flow assessment are complementary, noninvasive tests for examining patients with acute endocarditis.

REFERENCES

1. Neumann JL, Danchin N, Godenier JP, Villemot JP, Faivre G. Two-dimensional echocardiographic recognition of aortic valve ring abscess. *Eur Heart J* **1984**;5(suppl C):59-65
2. Tanaka M, Takeuchi E, Abe T. Detection of aortic valve ring abscess by intraoperative epicardial two-dimensional echocardiography (brief communication). *Am Heart J* **1989**;117(3):692-695
3. Hui P, Ports T. Left ventricular pseudoaneurysm presenting as unstable angina (brief communication). *Am Heart J* **1989**;118(2):400-402
4. Akins EW, Limacher M, Sloane RM, Hill JA. Evaluation of an aortic annular pseudoaneurysm by MRI: comparison with echocardiography, angiography and surgery. *Cardiovasc Intervent Radiol* **1987**;10:188-193
5. Winkler ML, Higgins CB. MRI of perivalvular infectious pseudoaneurysms. *AJR* **1986**;147:253-256
6. Arnett EN, Roberts WC. Valve ring abscess in active infective endocarditis. Frequency, location and clues to clinical diagnosis from the study of 95 necropsy patients. *Circulation* **1976**;54(1):140-145
7. Arnett EN, Roberts WC. Prosthetic valve endocarditis. Clinicopathologic analysis of 22 necropsy patients with comparison of observations in 74 necropsy patients with active infective endocarditis involving natural left-sided cardiac valves. *Am J Cardiol* **1976**;38(3):281-292
8. Miller SW, Dinesmore RE. Aortic root abscess resulting from endocarditis: spectrum of angiographic findings. *Radiology* **1984**;153(2):357-361
9. Mills SA. Surgical management of infective endocarditis. *Ann Surg* **1982**;195(4):367-383
10. Richardson JV, Karp RB, Kirklin JW, Dismukes WE. Treatment of infective endocarditis: a 10-year comparative analysis. *Circulation* **1978**;58(4):590-597
11. D'Agostino RS, Miller DC, Stinson EB, et al. Valve replacement in patients with native valve endocarditis: what really determines operative outcome? *Ann Thorac Surg* **1985**;40(5):429-438
12. David TE, Komeda M, Brofman PR. Surgical treatment of aortic root abscess. *Circulation* **1989**;80(3):1269-274
13. Croft CH, Woodward W, Elliott A, et al. Analysis of surgical versus medical therapy in active complicated native valve infective endocarditis. *Am J Cardiol* **1983**;51:1650-1655
14. Welton DE, Young JB, Raizner AE, et al. Value and safety of cardiac catheterization during active infective endocarditis. *Am J Cardiol* **1979**;44(7):1306-1310
15. Mills J, Abbott J, Utley JR, Ryan C. Role of cardiac catheterization in infective endocarditis. *Chest* **1977**;72(5):576-582
16. Hosenpud JD, Greenberg BH. The preoperative evaluation in patients with endocarditis: is cardiac catheterization necessary? *Chest* **1983**;84(6):690-694
17. Ellis SG, Goldstein J, Popp RL. Detection of endocarditis associated perivalvular abscess by two-dimensional echocardiography. *J Am Coll Cardiol* **1985**;5(3):647-653
18. Saner HE, Asinger RW, Homans DC, Helseth HK, Elsperger KJ. Two-dimensional echocardiographic identification of complicated aortic root endocarditis: implications for surgery. *J Am Coll Cardiol* **1987**;10(4):859-868
19. Scanlan JG, Seward JB, Tajik AJ. Valve ring abscess in infective endocarditis: visualization with wide angle two-dimensional echocardiography. *Am J Cardiol* **1982**;49(7):1794-1800
20. Taams MA, Gussenhover EJ, Bos E, et al. Enhanced morphological diagnosis in infective endocarditis by transesophageal echocardiography. *Br Heart J* **1990**;63:109-113
21. Miller SW, Palmer EL, Dinesmore RE, Brady TJ. Gallium-67 and magnetic resonance imaging in aortic root abscess. *J Nucl Med* **1987**;28(10):1616-1619
22. Jeang MK, Fuentes F, Gately A, Byrnes J, Lewis M. Aortic root abscess: initial experience using magnetic resonance imaging. *Chest* **1986**;89(4):613-615

Pictorial Essay



Mammographic and CT Findings After Breast Reconstruction with a Rectus Abdominis Musculocutaneous Flap

Evelyne M. Loyer,¹ Stephen S. Kroll,² Cynthia L. David,¹ Ronelle A. DuBrow,¹ and Herman I. Libshitz¹

This essay illustrates the radiologic appearance of the reconstructed breast and the abdominal wall after breast reconstruction with a transverse rectus abdominis musculocutaneous (TRAM) flap. The findings are based on a retrospective study of 42 mammograms, 17 abdominal CT scans, and two CT scans each of the chest and pelvis of patients who underwent this procedure.

Breast reconstruction is an important part of the treatment of mastectomy patients and is performed with increasing frequency. Various methods of reconstruction are available, all of which are intended to create a natural-appearing breast. Some require the use of implants; others are based on the use of musculocutaneous flaps.

The transverse rectus abdominis musculocutaneous (TRAM) flap technique is a modified abdominoplasty in which abdominal skin and fat are transferred to the chest and used to reconstruct the absent breast. It is currently the most frequent method of reconstruction at many institutions [1, 2].

Mammography of the reconstructed breast is performed to detect local tumor recurrence in the chest wall. CT of the abdomen is also frequently performed in these patients as part of their follow-up for metastatic disease.

Surgical Procedure

The TRAM flap method of breast reconstruction (Fig. 1) uses an ellipse of lower abdominal fat and skin and one or both rectus abdominis muscles. One or both muscle pedicles may be used. The blood supply depends on perforating vessels from the underlying rectus abdominis muscles. The vascular supply is preserved by leaving intact the superior epigastric vessels. The umbilicus is left behind in the abdomen, usually creating a small round defect in the skin of the flap.

The flap is rotated around its attachment just below the junction of the xiphoid process and the costal margin. If a single muscle pedicle is used, it most often is taken from the side opposite that of the reconstructed breast. A subcutaneous tunnel is dissected between the abdomen and the site of the reconstructed breast, and the flap, along with its muscular pedicle, is passed through the tunnel. Although the flap itself becomes located entirely at the new breast site, part of the muscle pedicle (or pedicles) remains permanently in the tunnel.

At the site of the previous mastectomy, an incision is made in the skin and subcutaneous fat in such a way that it is

Received August 30, 1990; accepted after revision December 10, 1990.

¹ Department of Diagnostic Radiology, The University of Texas M.D. Anderson Cancer Center, 1515 Holcombe Blvd., Houston, TX 77030. Address reprint requests to H.I. Libshitz.

² Department of General Surgery, Section of Plastic and Reconstructive Surgery, The University of Texas M.D. Anderson Cancer Center, 1515 Holcombe Blvd., Houston, TX 77030.

AJR 156:1159-1162, June 1991 0361-803X/91/1566-1159 © American Roentgen Ray Society

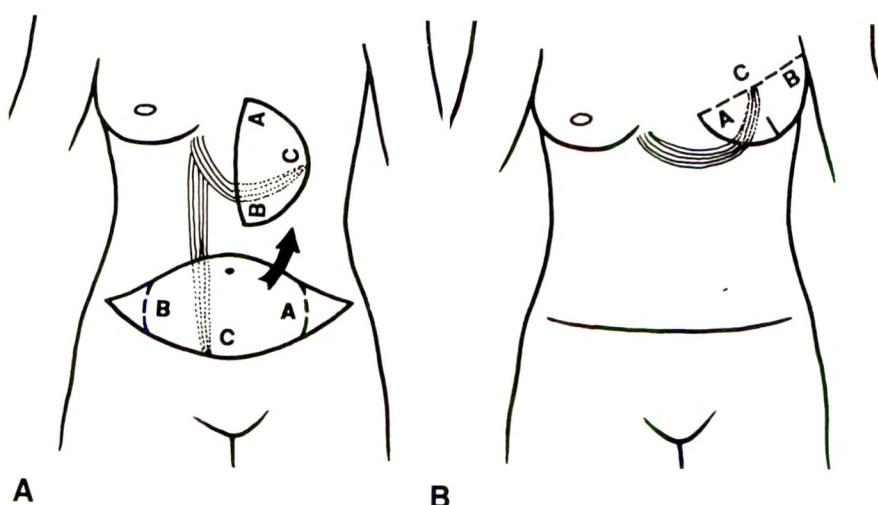


Fig. 1.—Surgical procedure: single muscle pedicle.

A, Diagram shows location of donor site and intermediate position of flap.

B, Diagram shows location of musculocutaneous flap to form new breast.

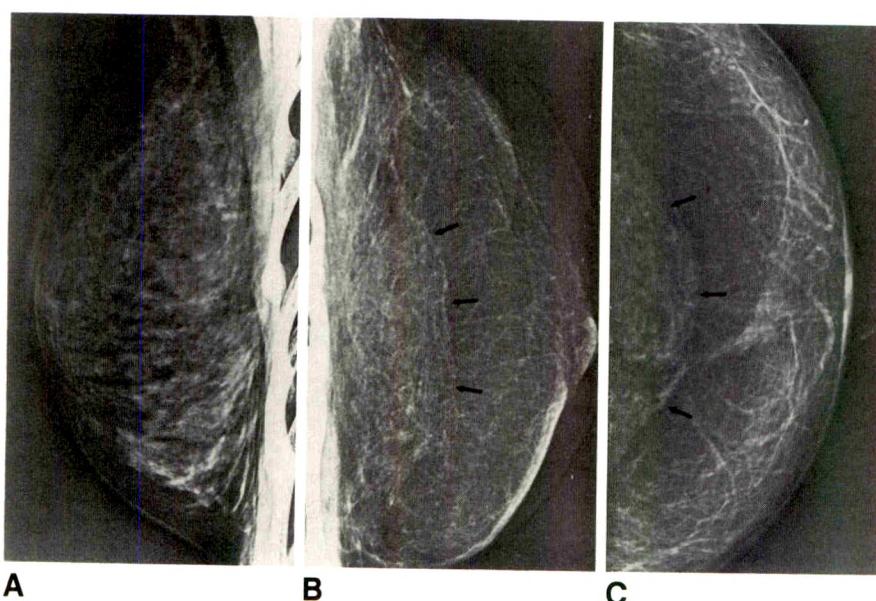


Fig. 2.—A, Normal left breast, mediolateral mammogram.

B and C, Reconstructed right breast, mediolateral (B) and craniocaudal (C) mammograms. Absence of ductal pattern is seen when compared with normal side. Elevated rectus muscle is seen along chest wall (arrows).

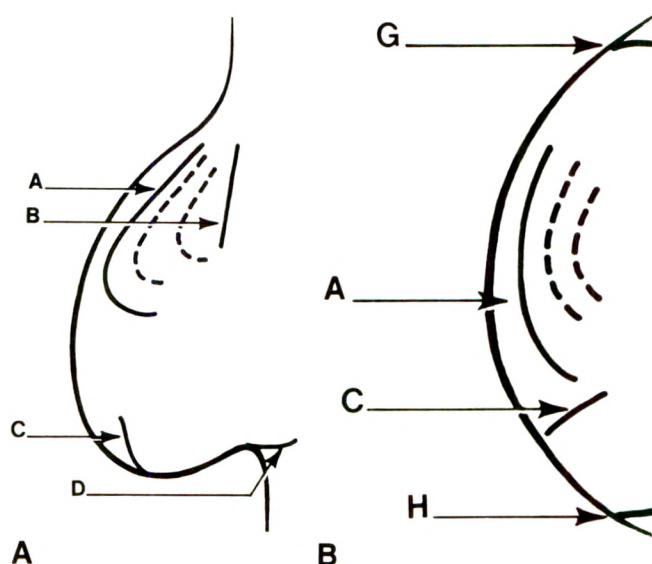


Fig. 3.—A and B, Diagrams show scars as seen on medial and contact lateral views (A) and on craniocaudal view (B). Line A corresponds to superior edge of flap. (Dotted line shows variable position of scar.) Lines G and H were rarely seen and correspond to lateral and medial edges of flap. Line B was inconsistently related to lateral edge of flap. Line C results from closure of defect created in flap by dissection of umbilicus.

symmetric with the contralateral inframammary fold. The flap is then inserted in the defect created by this incision and sculpted into a facsimile of the absent breast. The abdominal wall defects are closed primarily.

Imaging Findings

On mammography, the reconstructed breast has a relatively homogeneous, predominantly fatty appearance (Fig. 2),

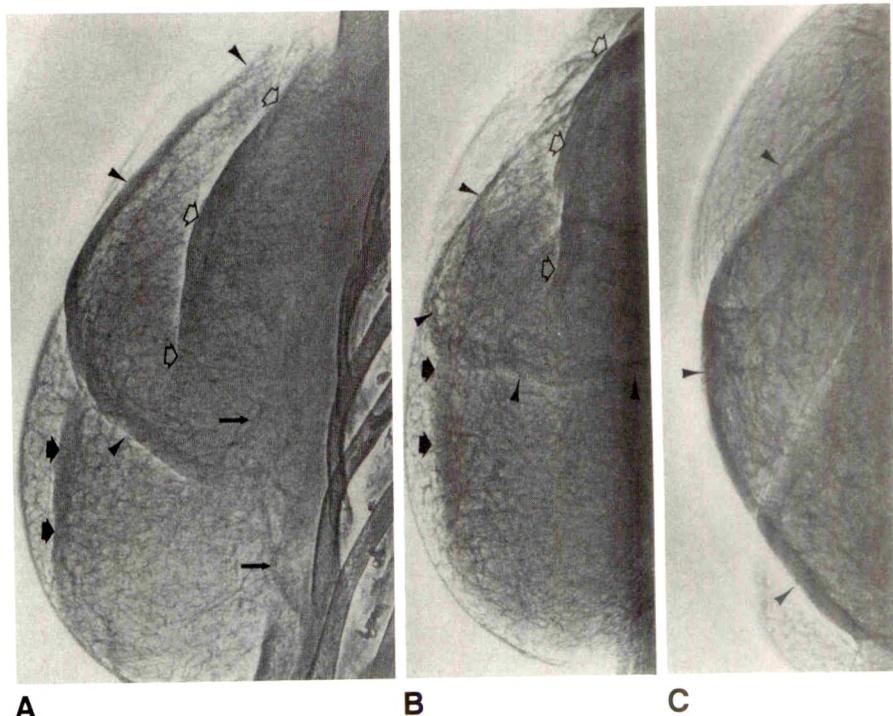


Fig. 4.—A–C, Mediolateral (A), contact lateral (B), and craniocaudal (C) mammograms of reconstructed left breast show superior edge of flap scar A (arrowheads), lateral edge of flap scar B (open arrows), and closure of umbilical defect scar C (short solid arrows). Elevated rectus muscle is evident (thin solid arrows).

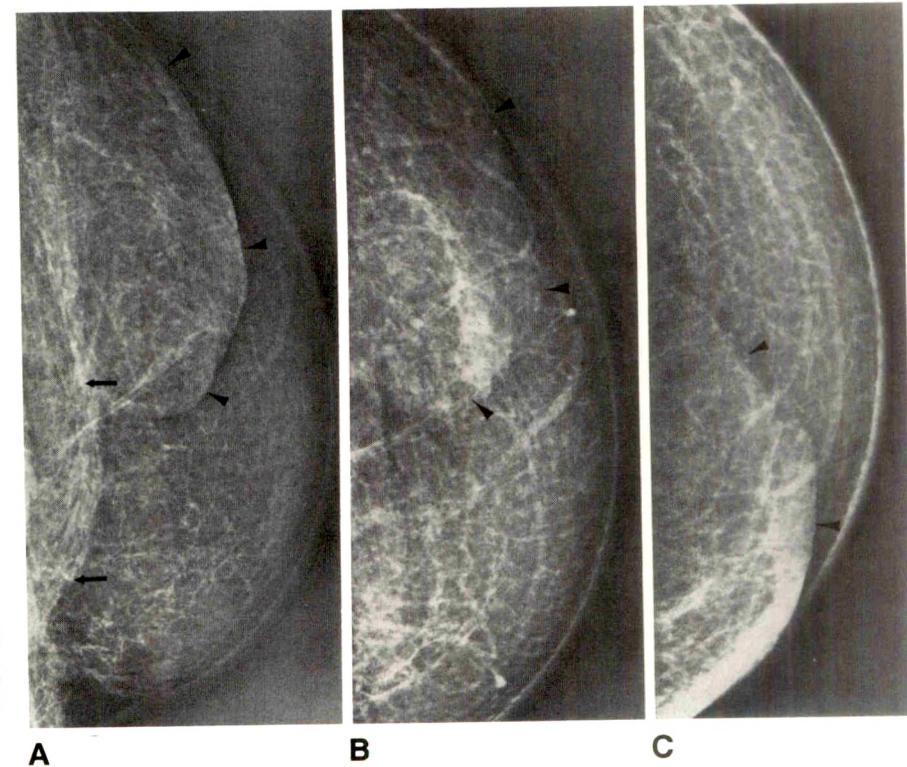
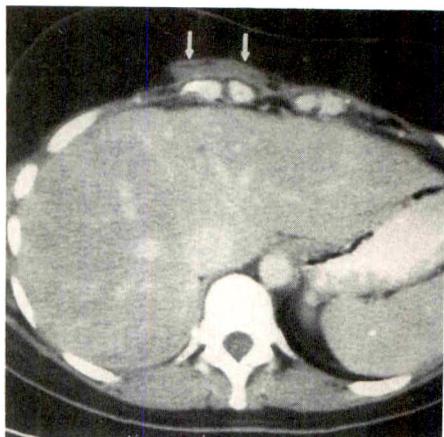
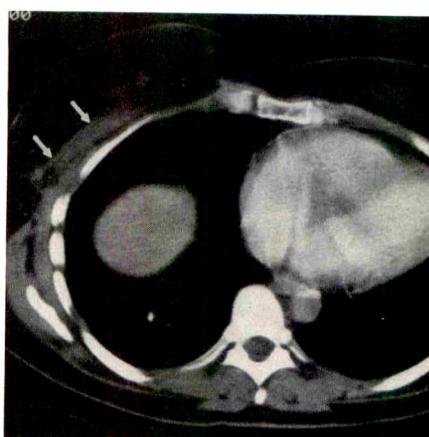


Fig. 5.—A–C, Mediolateral (A), contact lateral (B), and craniocaudal (C) mammograms of reconstructed right breast show superior edge of flap only (scar A, arrowheads) and elevated rectus muscle (arrows).



A

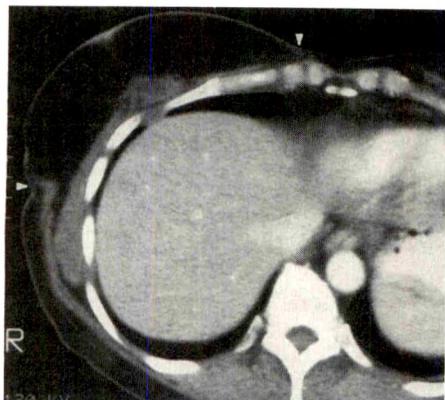


B

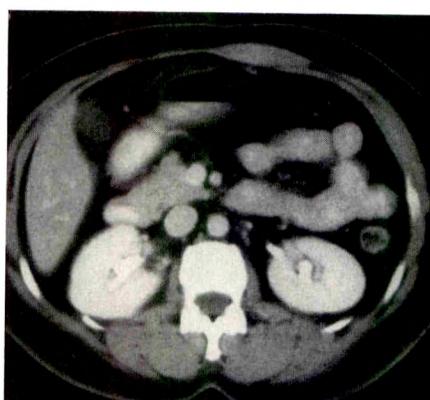
Fig. 6.—Reconstruction of right breast by using a single muscle pedicle from left side.

A, CT scan shows left rectus muscle (arrows) in upper abdominal wall.

B, CT scan shows left rectus abdominus muscle (arrows) along chest wall deep in reconstructed breast. Note absence of periglandular connective tissue in reconstructed breast.



7



8

Fig. 7.—CT scan of reconstructed right breast shows triangular opacity in mid and upper breast, most likely related to rectus abdominis muscle. Medial and lateral scars (arrowheads) are noted also.

Fig. 8.—CT scan of abdomen obtained after reconstruction of breast by using single right muscle pedicle. Right rectus abdominis muscle is no longer seen. Fascia transversalis constitutes anterior abdominal wall.

which can be similar to the pattern seen in postmenopausal women. This pattern however, is less organized and more amorphous, with fewer vascular and connective tissue opacities and without ductal structures or supporting ligaments.

On the mediolateral and contact lateral views, the elevated rectus muscle(s) is seen as a vertically oriented opacity anterior to the pectoralis major muscle (Figs. 2B and 2C). Because of its deep position in the breast, it is less frequently seen on the craniocaudal view. The volume of the muscle varies from an obvious, well-defined bulky mass to faint, almost imperceptible strands of tissue.

Scars are visible in all reconstructed breasts. They are either related to the reconstruction technique itself (closure of the flap, suture of the umbilical defect) or were present before the reconstruction (mastectomy scar, abdominal scar included in the flap). Although variation in the appearance of the scars is considerable, some common patterns can be defined (Figs. 3–5).

The scar that unites the flap to the skin of the chest wall has a somewhat ovoid pattern. Line A (Figs. 3–5) corresponds to the superior edge of the flap, which is usually seen on the contact and mediolateral views. It is seen on the craniocaudal view only if located low enough on the breast. Line D (Fig. 3) represents the inferior edge of the flap, which can be seen on contact and mediolateral views. Line C (Figs. 3 and 4) corresponds to the scar created in the skin portion of the flap by the dissection around the umbilicus. Line B (Figs. 3 and 4) is inconsistently seen and correlates either with the lateral edge

of the flap, the original mastectomy scar, or a prominent skin fold. Lines G and H on the craniocaudal view were rarely seen and also correspond to the lateral edges of the flap.

On CT, the reconstructed breasts have a homogeneous fatty density. The elevated rectus abdominis muscle(s) can be followed from approximately the level of the epigastrium up into the mound of the new breast. It is seen against the chest wall with a horizontal to oblique orientation (Fig. 6). Scars are observed medially and laterally extending from the skin posteriorly to the chest wall (Fig. 7). The findings due to the reconstruction are superimposed on the postmastectomy changes. The anatomy of the residual pectoralis muscle is highly variable and sometimes suggests local recurrence [3, 4].

On abdominal CT, an abdominal wall defect is seen clearly in all patients, involving one or both rectus muscles. The level of rotation of the pedicle is in the epigastrium, where muscle tissue can be seen crossing the midline (Fig. 8).

REFERENCES

1. Kroll SS. Cancer concepts in breast reconstruction after mastectomy. *Tex Med* 1989;85:40–46
2. Hartrampf CR, Scheflan M, Black PW. Breast reconstruction with a transverse abdominal island flap. *Plast Reconstr Surg* 1982;69(2):216–225
3. Shea WJ, deGeer G, Webb WR. Chest wall after mastectomy: 1. CT appearance of normal postoperative anatomy, postirradiation changes, and optimal scanning techniques. *Radiology* 1987;162:157–161
4. Shea WJ, deGeer G, Webb WR. Chest wall after mastectomy: 2. CT appearance of tumor recurrence. *Radiology* 1987;162:162–164

Treatment of Critically Ill Patients with Sepsis of Unknown Cause: Value of Percutaneous Cholecystostomy



Michael J. Lee¹
 Sanjay Saini¹
 James A. Brink^{1,2}
 Peter F. Hahn¹
 Joseph F. Simeone¹
 Mary C. Morrison^{1,3}
 David Rattner⁴
 Peter R. Mueller¹

Because of the difficulty in diagnosing acute cholecystitis in critically ill patients with severe intercurrent illness by clinical and imaging methods or percutaneous aspiration of the gallbladder, a trial of percutaneous cholecystostomy was performed in 24 patients in the intensive-care unit with persistent, unexplained sepsis after a complete clinical, laboratory, and radiologic search showed no alternative source of infection. Persistent high fevers, despite antibiotic therapy, were present in all patients, with elevated WBC count in 18 patients, vague abdominal tenderness in 11, and septic shock requiring vasopressors in 15. Sonographically, all patients had distended, spherical gallbladders, six had gallstones, eight had wall thickening, three had pericholecystic fluid, and four had Murphy's sign. All patients were seen by a senior abdominal surgeon, who agreed to a trial of percutaneous cholecystostomy. Fourteen patients (58%) responded to percutaneous cholecystostomy, as evidenced by a decrease in WBC count, defervescence, and the ability to be weaned off vasopressors. Bile cultures were positive in four patients. Ten patients (42%) did not respond to percutaneous cholecystostomy; five eventually died of unrelated causes. A respiratory source of infection was eventually found in three of these 10 patients, with no proved source of infection in the remainder. No complications related to catheter insertion occurred in this group of patients. Bile leaks occurred in two patients when the percutaneous cholecystostomy catheter was removed, but without serious consequence.

Our experience suggests that a lower threshold for performing percutaneous cholecystostomy in this difficult clinical subset of patients is worthwhile.

AJR 156:1163–1166, June 1991

Since its introduction, percutaneous cholecystostomy has become widely established as a safe and effective method of decompressing the gallbladder in patients with acute cholecystitis who are at high risk for surgery [1–3]. Our early experience with 80 percutaneous cholecystostomies confirmed the safety, ease of execution, and low complication rate of this technique. Previous authors [1, 2] have performed cholecystostomy in these high-risk patients, only when clinical, laboratory, or imaging studies or diagnostic gallbladder aspiration have suggested acute cholecystitis. However, as our experience with percutaneous cholecystostomy grew, a subset of patients emerged in whom the diagnosis of acute cholecystitis was difficult and the indications for percutaneous cholecystostomy were unclear. These were usually patients in the intensive care unit (ICU) who had multiorgan disease, persisting unexplained sepsis, and who were referred for abdominal CT or sonography to exclude cholecystitis (acalculous or calculous) or other intraabdominal source of sepsis.

Our experience with this subset of patients, in accord with the literature, suggested that sonography, clinical examination, and biliary scintigraphy were not completely reliable in excluding acute cholecystitis in this clinical situation [4–8]. Similarly, percutaneous aspiration of the gallbladder with Gram staining and culture of bile, although initially promising [9], recently has been proved inadequate, with a diagnostic sensitivity of less than 50% [10].

Received October 29, 1990; accepted after revision December 27, 1990.

¹ Department of Radiology, Massachusetts General Hospital, 32 Fruit St., Boston, MA 02114. Address reprint requests to P.R. Mueller.

² Present address: Mallinckrodt Institute of Radiology, Washington University Medical School, 510 S. Kingshighway Blvd., St. Louis, MO 63110.

³ Present address: Radiology Department, North Broward Medical Center, 201 Sample Rd., Pompano Beach, FL 33064.

⁴ Department of Surgery, Massachusetts General Hospital, 32 Fruit St., Boston, MA 02114.

0361-803X/91/1566-1163

© American Roentgen Ray Society

For these reasons, and because these patients are at increased risk for acute acalculous cholecystitis, we decided to lower our threshold for performing percutaneous cholecystostomy in this group of patients. Percutaneous cholecystostomy was performed in 24 patients in the ICU who had persisting, unexplained sepsis to exclude acute cholecystitis as a possible source of infection. Findings on mobile sonographic examinations done to exclude cholecystitis were abnormal in some patients, but frequently sonography revealed only a distended gallbladder containing sludge. That finding is indicative of bile stasis, which frequently occurs in patients who have prolonged critical illness, and which carries an increased risk of bile inspissation, obstruction of the cystic duct, and acute cholecystitis [11]. The results, selection criteria integrating clinical data and sonographic findings, and potential complications of this approach in this group of patients are discussed.

Subjects and Methods

Twenty-four patients undergoing percutaneous cholecystostomy to treat sepsis of unknown origin were studied prospectively. Selection criteria included persistent sepsis of unknown cause and a distended, tense gallbladder at sonography. All patients had complex medical and surgical problems, including respiratory failure or acute respiratory distress syndrome (21 patients), recent major abdominal or thoracic surgery (12), congestive cardiac failure (seven), renal failure (six), pancreatitis (five), and multiple trauma (one). All patients were on respiratory ventilators in the ICU and receiving total parenteral nutrition. All 24 patients had high fever (body temperature $>101^{\circ}\text{F}$ [38.3°C]), 15 were receiving vasopressors for septic shock, 18 had elevated WBC counts, and 11 had vague abdominal pain or tenderness. Abdominal pain was difficult to assess or localize because all of the patients were unconscious, but a grimace or tensing of the abdominal musculature was elicited on clinical palpation. All patients were receiving antibiotics at the time of percutaneous cholecystostomy; these were not changed in the 24 hr before or after the procedure. Percutaneous cholecystostomy was performed only after complete clinical, imaging, and laboratory tests had ruled out other septic sources. Tests performed in all patients to exclude other sources of sepsis included multiple blood, urine, and sputum cultures; cultures of tips of central line catheters; abdominal CT scans; and serial chest radiographs. All cultures were negative, and radiologic studies were either normal or showed stable disease. Biliary scintigraphy was not performed. Mild, nonspecific elevation of liver enzyme levels occurred in 20 patients; the remaining four had normal results on liver function tests. In all cases, we consulted with an experienced abdominal surgeon, who agreed to a trial of percutaneous cholecystostomy to evaluate the response of each patient.

Mobile sonography was performed on all patients to exclude acute cholecystitis. The main sonographic criterion used to select patients to undergo percutaneous cholecystostomy was a distended, tense gallbladder containing sludge (seen in 20 of 24 patients). An abnormally distended gallbladder was not defined by measurements of volume or size, but rather by the appearance of a spherical shape as opposed to the usual pear shape. Other sonographic criteria suggesting acute cholecystitis, such as gallstones, wall thickening, pericholecystic fluid, and the presence of Murphy's sign, were evaluated also. Although sonography was performed on other patients with a similar clinical status in this period, acute cholecystitis was not considered if the gallbladder appeared normal on sonography.

For the purposes of this study, a positive response to percutaneous cholecystostomy was defined as defervescence, disappearance of abdominal tenderness on palpation, an overall improvement in clinical well-being occurring within 24 hr after percutaneous cholecystostomy, a decrease in WBC count to normal, and the ability to be weaned from vasopressors within 3 days. A negative response occurred when the patient's clinical course was unaltered by percutaneous cholecystostomy, with persisting fevers, high WBC counts, and a continuing need for vasopressor therapy.

Cholecystostomy catheters were placed transhepatically into the gallbladder under sonographic guidance, using previously described techniques [1, 3]. An attempt was made to enter the gallbladder in its bare area to decrease the possibility of bile leakage into the abdominal cavity. Catheters used ranged from 7- to 12-French in size and had locking features. Early in our experience, seven percutaneous cholecystostomies were performed in the radiology department by using a combination of sonography and fluoroscopy and the Seldinger technique. For these patients, first the gallbladder was punctured with an 18-gauge sheath needle under sonographic guidance. A 0.038-in. (0.097 mm) guidewire was inserted through the sheath, the tract was dilated, and the cholecystostomy catheter was placed into the gallbladder under fluoroscopic control. We now prefer to perform percutaneous cholecystostomies at the bedside by using a single-stick trocar system with sonographic guidance [12]. This technique is more compatible with critically ill patients in the ICU and was performed in the remaining 17 patients. In all cases, specimens were sent for Gram stains and culture.

Results

A dramatic improvement in the clinical condition of 14 patients was observed within 24 hr. Signs of improvement included defervescence of fever (14 patients) and disappearance of abdominal pain and tenderness (nine). In addition, WBC counts returned to normal in 11 patients, and vasopressors were discontinued in nine. Sonographic features, before cholecystostomy, in those patients who responded included distended gallbladders (14 patients), pericholecystic fluid (two), gallstones (three), wall thickening (five), and presence of Murphy's sign (four; Table 1). Six of the responders had only a distended gallbladder with or without sludge, and one other patient had wall thickening in addition. The remaining patients had a combination of sonographic signs. One of the patients in the group who responded to treatment died 3 weeks after percutaneous cholecystostomy of severe congestive cardiac failure. Cholecystectomy was performed in one patient in this group and methyl *tert*-butyl ether (MTBE) dissolution therapy was performed in another when their clinical conditions stabilized (both had gallstones). Cholecystostomy was, therefore, the definitive therapy in 13 of these 14 patients.

No clinical response was observed in the other 10 patients. Sonographically, before cholecystostomy, gallbladder distension and sludge were the sole imaging features in five patients, gallstones were present in three, wall thickening in three, and pericholecystic fluid in one (Table 1). Five of these patients eventually died of a combination of sepsis and multiorgan failure. A respiratory source of infection was eventually found in three of the 10 nonresponders, but no definitive source of infection was ever determined in the remaining seven patients.

TABLE 1: Sonographic Findings Before Percutaneous Cholecystostomy

Finding	Number of Responders (%)	Number of Nonresponders (%)	Total Number (%)
Gallstones	3 (21)	3 (30)	6 (25)
Sludge	11 (79)	9 (90)	20 (85)
Wall thickening	5 (36)	3 (30)	8 (33)
Pericholic fluid	2 (14)	1 (10)	3 (12)
Murphy's sign	4 (29)	0 (0)	4 (17)
Total	14 (100)	10 (100)	24 (100)

One patient had a laparotomy for suspected ischemic bowel disease, at which the gallbladder appeared normal.

No grossly purulent material was aspirated from the gallbladder in any patient in this series. Bile cultures were positive in four patients and blood cultures in one. The duration of percutaneous catheter drainage varied between 10 days to 3 months (mean, 1.3 months). No complications related to catheter insertion occurred in this series. Bile leaks, related to catheter withdrawal, occurred in two patients. Abdominal pain subsided in one patient after 24 hr of observation. The catheter was immediately reinserted into the gallbladder in the second patient, when contrast material was seen leaking into the abdominal cavity during catheter removal under fluoroscopic control.

Discussion

Detection of sepsis originating from the gallbladder (calculous or acalculous cholecystitis) is particularly difficult in patients who are unresponsive and have multiorgan failure [4–8]. Clinical and biochemical markers are often nonspecific in the presentation of acute acalculous or calculous cholecystitis in this situation and contribute to the delay in diagnosis and treatment [11]. Pain and tenderness in the right upper quadrant can be absent. Moreover, it is often difficult to elicit clinical signs and symptoms in patients who are on respirators and have decreased mental awareness.

Similarly, the accuracy of sonography in the diagnosis of acute acalculous cholecystitis has been reported to be as low as 58% [13]. Sonographic signs such as wall thickening and pericholecystic fluid, which were seen in some patients in this series, are often nonspecific indicators of acute cholecystitis and may be seen with various entities such as ascites, hypoalbuminemia, and hepatitis, among others [14]. Cholescintigraphy with 99m Tc-iminodiacetic acid, although highly accurate in the diagnosis of acute cholecystitis (95%) under normal circumstances [15], has a high false-positive rate in patients who have fasted for longer than 14 hr (false-positive in all four patients studied) [6], have severe intercurrent illness (50% false-positive rate) [7], or are receiving total parenteral nutrition, as were all the patients in this series (92% false-positive rate) [8].

Initial reports suggested that percutaneous gallbladder aspiration and analysis of bile would be helpful in confirming the

gallbladder as the source of sepsis [9]. However, recent reports have questioned the efficacy of percutaneous bile aspiration in these critically ill patients, who often are already receiving antibiotics. McGahan and Lindfors [10], in a recent study, estimated the sensitivity of Gram stains or cultures on percutaneous bile aspirate as less than 50%. The presence of WBCs signifies infection; however, their absence is not reliable for excluding infection in patients receiving antibiotics. In addition, cultures are definitive when positive, but are not available immediately. Therefore, negative Gram stains or cultures are meaningless in this population of patients.

Because of this lack of sensitivity in the diagnosis of acute cholecystitis in these critically ill patients, and the need for early diagnosis and treatment, we elected to perform a therapeutic trial of direct percutaneous cholecystostomy in this subset of patients. Selection criteria included persistent sepsis of unknown origin after other sources of sepsis were excluded and gallbladder distension, often with retained sludge, as defined by sonography. Acalculous cholecystitis is known to occur more frequently in these patients with prolonged critical illness, who have an increased risk of bile inspissation, obstruction of the cystic duct, and acute cholecystitis [10].

Our results emphasize the poor sensitivity of sonography in diagnosing cholecystitis in these patients. Gallstones were present equally in both responders and nonresponders, and one patient who did not respond had a distended gallbladder, sludge, gallstones, wall thickening, and pericholecystic fluid (Table 1). Murphy's sign was the most specific sonographic sign in that all four patients in whom the sign was elicited responded to percutaneous cholecystostomy. However, the absence of Murphy's sign on sonography did not preclude a positive response to percutaneous cholecystostomy. Clinically, the presence of abdominal tenderness (11 of 24 patients) was strongly suggestive of cholecystitis in this study, with nine of 11 patients responding to percutaneous cholecystostomy. However, abdominal pain or tenderness may be hard to elicit in ventilated ICU patients, as in five of our responders who did not have any clinical signs or symptoms of cholecystitis.

One would expect a high failure-of-response rate using this approach, and indeed, 10 (42%) of 24 patients in this series did not respond to percutaneous cholecystostomy. Our concern about this approach is that the nonspecificity of selection criteria (both imaging and clinical) used might lead to unnecessary procedures performed on the gallbladder in this subset of patients. However, percutaneous cholecystostomy was performed only after both the clinical and the radiologic data were reviewed with an experienced abdominal surgeon and after a careful search had excluded other sources of sepsis. Thus, percutaneous cholecystostomy was not performed randomly on all patients in the ICU who might have only one abnormality, such as a distended gallbladder. Still, because of the nonspecific selection criteria, placement of catheters in patients with normal gallbladders was unavoidable. An equivalent dilemma in general surgery is the removal of a certain percentage of normal appendices in patients with abdominal pain to avoid the grave error of misdiagnosing patients with

acute appendicitis. However, in this series, percutaneous cholecystostomy did have a significant positive effect for these patients in that surgical cholecystostomy or cholecystectomy was avoided and the gallbladder was eliminated as the source of sepsis. Importantly, no serious cholecystostomy-related complications occurred in these patients.

Bile leaks, without serious clinical consequence, did occur in two patients in this series when the catheters were removed after 10 days. To minimize this risk, we now leave catheters in situ for a minimum of 2–3 weeks and perform cholecystocholangiography to ensure patency of the cystic duct and common bile duct before removing the catheter. Injection of contrast media through the catheter during removal also helps to outline the percutaneous tract and ensure its maturity.

In summary, we believe that a trial of percutaneous cholecystostomy in critically ill ICU patients with persisting, unexplained fever and a distended, tense gallbladder on sonography is worthwhile, because of the often nonspecific clinical and sonographic findings of acute cholecystitis in these patients. One must first exclude all other potential sources of sepsis before contemplating percutaneous cholecystostomy. Sonographically, a distended, tense gallbladder with Murphy's sign in the presence of abdominal pain suggests the presence of acute cholecystitis and strongly predicts a positive response to percutaneous cholecystostomy. A positive response to percutaneous cholecystostomy may also occur in patients with no localizing signs, because of the difficulty in eliciting clinical data in these patients. If no response occurs, surgery has been avoided and the gallbladder has been eliminated as the cause of sepsis. The low complication rate found in this and other series [1–3, 16], coupled with the fact that percutaneous cholecystostomy can be performed quickly and safely at the bedside, makes it an ideal technique for critically ill patients in the ICU.

REFERENCES

1. McGahan JP, Lindfors KK. Percutaneous cholecystostomy: an alternative to surgical cholecystostomy for acute cholecystitis. *Radiology* 1989; 173:481–485
2. Vogelzang RL, Nemcek AA. Percutaneous cholecystostomy: diagnostic and therapeutic efficacy. *Radiology* 1988;168:29–34
3. Lindemann SR, Tung G, Silverman SG, Mueller PR. Percutaneous cholecystostomy: a review. *Semin Intervent Radiol* 1988;5:179–185
4. Laing FC, Federle MP, Jeffrey RB, Brown TW. Ultrasonic evaluation of patients with acute right upper quadrant pain. *Radiology* 1981;140: 449–455
5. Samuels BL, Freitas JE, Bree RL, Schwab RE, Heller JT. A comparison of radionuclide hepatobiliary imaging and real-time ultrasound for the detection of acute cholecystitis. *Radiology* 1983;147:207–210
6. Larsen MJ, Klingensmith WC III, Kuni CC. Radionuclide hepatobiliary imaging: nonvisualization of the gallbladder secondary to prolonged fasting. *J Nucl Med* 1982;23:1003–1005
7. Kalff V, Froelich JW, Lloyd R, Thrall JH. Predictive value of an abnormal hepatobiliary scan in patients with severe intercurrent illness. *Radiology* 1983;146:191–194
8. Shuman WP, Gibbs R, Rudd TG, Mack LA. PIPIDA scintigraphy for cholecystitis: false positives in alcoholism and total parenteral nutrition. *AJR* 1982;138:1–5
9. McGahan JP, Walter JP. Diagnostic percutaneous aspiration of the gallbladder. *Radiology* 1985;155:619–622
10. McGahan JP, Lindfors KK. Acute cholecystitis: diagnostic accuracy of percutaneous aspiration of the gallbladder. *Radiology* 1988;167:669–671
11. Long TN, Heimbach DM, Carrico CJ. Acalculous cholecystitis in critically ill patients. *Am J Surg* 1987;136:31–36
12. McGahan JP. A new catheter design for percutaneous cholecystostomy. *Radiology* 1988;166:49–52
13. Mirvis SE, Vainright JR, Nelson AW, et al. The diagnosis of acute acalculous cholecystitis: a comparison of sonography, scintigraphy, and CT. *AJR* 1986;147:1171–1175
14. Cooperberg PL, Gibney RG. Imaging of the gallbladder 1987. *Radiology* 1987;163:605–613
15. Weissman HS, Frank MS, Bernstein LH, Freeman LM. Rapid and accurate diagnosis of acute cholecystitis with 99m-Tc-HIDA cholescintigraphy. *AJR* 1979;132:523–528
16. vanSonnenberg E, Wittich GR, Casola G, et al. Diagnostic and therapeutic percutaneous gallbladder procedures. *Radiology* 1986;160:23–26

Abdominal CT Findings After Liver Transplantation in 66 Patients

Damian Dupuy¹
 Philip Costello¹
 David Lewis²
 Roger Jenkins²

CT scanning is used frequently to assess the condition of patients after liver transplantation. The CT records of 174 adult patients who underwent liver transplantation were studied retrospectively to determine the number and timing of CT studies as well as the frequency and significance of the findings. One-hundred seventy CT scans were obtained in 66 (38%) of the 174 patients, with a mean of 2.6 scans/patient. The interval between transplantation and scanning was 1 day to 24 months; in 59 (89%) of 66 patients, the first CT scan was obtained within 30 days. The acute indications for CT scanning were fever or leukocytosis in 54 (92%) of 59 patients and abnormal liver function tests in five (8%) of 59 patients. CT scans obtained more than 30 days after transplantation were repeat scans in all but seven patients. Indications in this latter group were the same as for the acute group, plus evaluation of hepatic neoplasia in three patients. CT findings included periportal low attenuation in 41 (62%) of 66 patients; ascites in 25 (38%); splenomegaly in 19 (29%); loculated intraperitoneal noninfected fluid collections in 13 (20%); intrahepatic, splenic, pancreatic, or perihepatic abscesses in seven (11%); hepatic infarction in six (9%); splenic infarction in three (4%); and hepatic calcification in two (3%). Other major abnormalities included inferior vena caval thrombosis (one patient), pseudoaneurysm of the hepatic artery with rupture (one patient), and recurrent hepatocellular carcinoma (one patient).

CT scanning after liver transplantation is used predominantly in the acute setting to evaluate for liver infarction or intraabdominal abscess. In this setting, CT showed these abnormalities, in addition to tumor recurrence or vascular abnormalities, in 15 (23%) of 66 patients.

AJR 156:1167-1170, June 1991

Orthotopic liver transplantation has become the therapeutic option of choice for the treatment of end-stage liver disease. Improved survival has been noted, particularly since the beginning of the era of cyclosporine therapy [1]. CT and sonography are used widely for the complex postsurgical management of this condition and its complications [2-5]. Letourneau et al. [3] described the CT findings in a primarily pediatric population after liver transplantation. Major abnormalities included localized extrahepatic fluid collections, biliary obstruction, hepatic parenchymal abnormalities, and vascular thrombosis. We report the timing and indications for CT scanning as well as the various findings and their frequency in an adult population after liver transplantation.

Received October 4, 1990; accepted after revision December 7, 1990.

¹ Department of Diagnostic Radiology, New England Deaconess Hospital and Harvard Medical School, 185 Pilgrim Rd., Boston, MA 02215. Address reprint requests to P. Costello.

² Department of Surgery, New England Deaconess Hospital and Harvard Medical School, Boston, MA 02215.

0361-803X/91/1566-1167
 © American Roentgen Ray Society

Materials and Methods

From July 1983 to October 1989, liver transplants were performed in 174 adults at our institution. In 100 of these patients, records were available for review, or the patient survived beyond the first postoperative day. CT scans were obtained in 66 (66%) of these patients; the total number of scans was 170. Indications for liver transplantation in decreasing order of frequency included chronic active or acute hepatitis B, primary biliary cirrhosis, sclerosing cholangitis, Laennec cirrhosis, cryptogenic cirrhosis, drug- or toxin-induced hepatitis, cholangiocarcinoma, alpha₁-antitrypsin deficiency, hemochromatosis, hepatoma, and lupoid hepatitis.

Orthotopic liver transplantation was performed with end-to-end hepatic artery, portal vein, infra- and suprahepatic inferior vena cava, and choledochocholeodochostomy anastomoses except in patients with sclerosing cholangitis, who underwent hepaticojejunostomies.

The indications for CT were fever or leukocytosis in 59 (89%) patients, abnormal increase or persistent elevation in liver function tests (e.g., serum alanine aminotransferase/serum aspartate aminotransferase ratio and bilirubin) in seven patients (11%), and repeat scans for evaluation of hepatic neoplasia in three patients or hypotension in one patient. In the acute postoperative setting, there was often a combination of fever or leukocytosis and abnormal liver function tests, and the indication for scanning was classified into one category or the other according to whether the clinicians were ruling out infectious collections or intrinsic problems with the donor liver, such as infarction. If the CT scan was ordered within the first 30 days, then the CT study was considered to be in the acute postoperative setting. CT was performed with IV contrast material unless the patient was allergic to contrast material or had an elevated creatinine level (>3.0 mg/dl). Contrast material was infused as 200 ml of iothalamate meglumine 43% or infused as 120 ml of diatrizoate meglumine 60% at 3.0 ml/sec for 15 sec and then 1 ml/sec for the rest of the study. Dilute oral diatrizoate meglumine was given when tolerated by the patient. CT slices of 8 mm were obtained at 8-mm intervals through the liver and then at 16-mm intervals to the symphysis pubis. Studies were done on a General Electric 8800, Siemens CRH, or Siemens Somatom Plus unit.

CT-guided aspiration procedures were performed with 18- or 21-gauge spinal needles when a fluid collection appeared loculated or in an abnormal location (e.g., isolated to the lesser sac).

All charts were reviewed retrospectively in order to assess the impact of the CT findings. CT scans were correlated with available clinical and pathologic information.

Results

During the 6-year period covered by this study, 170 CT scans were obtained after liver transplantation in 66 patients; a mean of 2.6 scans were obtained per patient. Scanning was performed between 1 and 24 months after transplantation. CT scans were obtained within the first 30 days in 59 (89%) of 66 patients, within the first 6 months in six (9%) of 66 patients, and after 6 months in one patient (2%).

Hepatic parenchymal abnormalities were seen in 14 patients. They were rounded or wedge-shaped peripheral areas of decreased attenuation and showed no evidence of contrast enhancement. In 10 of 14 patients the area of low attenuation was smaller than the area of the lobe in which it occurred. Seven cases were classified as infarction on the basis of their peripheral location, wedge shape, and lack of enhancement, which in four cases corresponded to the vascular supply of an entire lobe. In one patient, thrombosis of the left portal vein was confirmed at surgery for a biliary tract leak. Three patients died suddenly of this complication. In the fourth, a large abscess developed in the infarcted lobe, and the patient eventually died from infectious complications after retransplantation. In the setting of presumed infection, percutaneous aspiration procedures were performed in five of 10 patients with small areas of low attenuation; *Pseudomonas* grew from aspirated fluid in one patient (Fig. 1). One hepatic fluid collection developed in a patient with infarction of the right lobe. The collection involved the entire right upper quadrant and contained extensive amounts of air. Because of the extensive size of the collection, surgery was performed, and a large hepatic abscess was found in the completely infarcted right lobe (Fig. 2).

Other parenchymal abnormalities included a simple cyst in

a donor liver and recurrent hepatocellular carcinoma metastasizing to the donor liver, which required a left lateral hepatic segmentectomy 19 months after liver transplantation (Fig. 3).

Hepatic calcification was seen in two patients (Fig. 4). The appearance of calcification occurred within 2 weeks of presumed liver infarction in one patient and within 4 weeks in the other. The calcification was located peripherally in the area of infarction and the distribution was patchy. Pathologic evidence of infarction was found in both of these patients, and both died within 75 days of surgery: one from a disseminated fungal infection including endocarditis and the other from massive liver necrosis, pseudomonal sepsis, and acute meningitis. Histology of the liver in the first patient showed areas of infarction, presumably from septic emboli, and mild cellular rejection. The liver in the second patient had ischemic changes, most with frank coagulative necrosis and extracellular calcium.

Even though CT scans were obtained emergently because of abnormal liver function tests in five of 59 patients, there were no documented cases of biliary obstruction.

Intraperitoneal, noninfected fluid collections or abscesses were present in 18 patients. More than one area of fluid was seen in three of these patients (Fig. 5). Fluid was seen in various locations: subhepatic (10 patients), lesser sac (four), ligamentum teres (two), subdiaphragmatic (two), and porta hepatitis (one). Of the 18 patients with these collections, CT-guided aspiration procedures were performed in 12; positive bacteriologic cultures were positive in three (25%) of the 12 patients.

Periportal low attenuation was present in 41 patients. This finding did not correlate with an adverse clinical outcome, and 31 of 41 patients were alive and doing well up to 6 months after surgery.

Vascular complications were seen in only two patients despite the extensive vascular surgery required. In one patient, thrombosis of the inferior vena cava developed that extended from the hepatic veins to the right external iliac vein (Fig. 6). A previous side-to-side portacaval shunt resulted in subsequent massive dilatation of the inferior vena cava. Thrombosis developed, presumably because of turbulent blood flow at the level of the infrahepatic caval anastomosis. In another patient, a pseudoaneurysm of the hepatic artery anastomosis (caused by a perianastomotic infection) ruptured, causing massive hemoperitoneum and death.

Splenic abnormalities resulted mainly from enlargement (19 patients) and infarction (e.g., wedge-shaped areas of low attenuation that resolved with time and without intervention) (three patients). The only clinically significant splenic abnormality was a large abscess, which was drained percutaneously. This abscess grew *Staphylococcus aureus* and was thought to be caused by seeding from concomitant staphylococcal bacteremia. Extraabdominal findings that were seen on all the acute postoperative CT scans in these patients were pleural effusions and basilar atelectasis.

Discussion

Liver transplantation is the primary treatment for end-stage liver disease. As the survival rate increases, the complexities of caring for patients increase. CT scanning has been used to diagnose the various complications related to prolonged immunosuppression, vascular surgery, biliary construction, and altered coagulability.

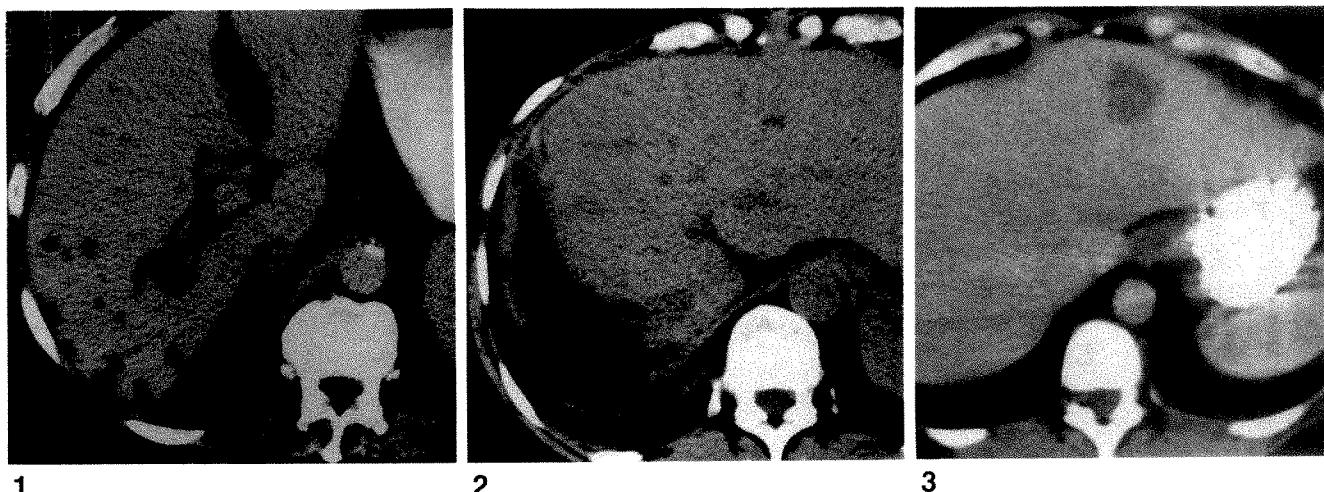


Fig. 1.—Liver abscess in a 59-year-old febrile man 2 months after liver transplantation. CT scan shows multiple low-attenuation lesions in right lobe of liver. Cultures of aspirated fluid were positive for *Pseudomonas*.

Fig. 2.—Hepatic abscess in a 50-year-old woman 15 days after liver transplantation. CT scan shows large area of peripheral attenuation involving entire right lobe of liver. Surgical removal of right lobe showed large abscess in infarcted lobe.

Fig. 3.—Liver metastases in a 36-year-old woman 17 months after liver transplantation for hepatocellular carcinoma. CT scan shows hypodense area in medial segment of left lobe. Pathologic examination after segmentectomy revealed metastatic hepatocellular carcinoma.

Fig. 4.—Calcification in hepatic infarction.

A, Earlier CT scans of patient in Fig. 3 showed infarction of entire right lobe. CT scan obtained 4 weeks after infarction shows patchy, peripheral calcification in area of infarction.

B, 45-year-old man with liver transplant. CT scan shows peripheral hepatic parenchymal calcification 2 weeks after liver infarction.

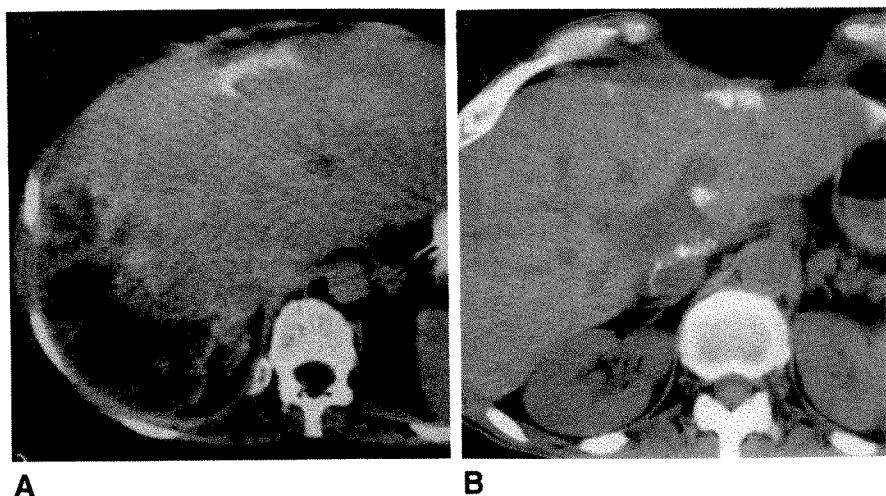


Fig. 5.—Multiple intraperitoneal fluid collections in a 60-year-old man with fever 6 weeks after liver transplantation. CT scan shows loculated fluid in lesser sac, which has a needle in it, and loculated fluid surrounded by ligamentum teres, which contains air caused by needle aspiration. Both collections were sterile seromas.

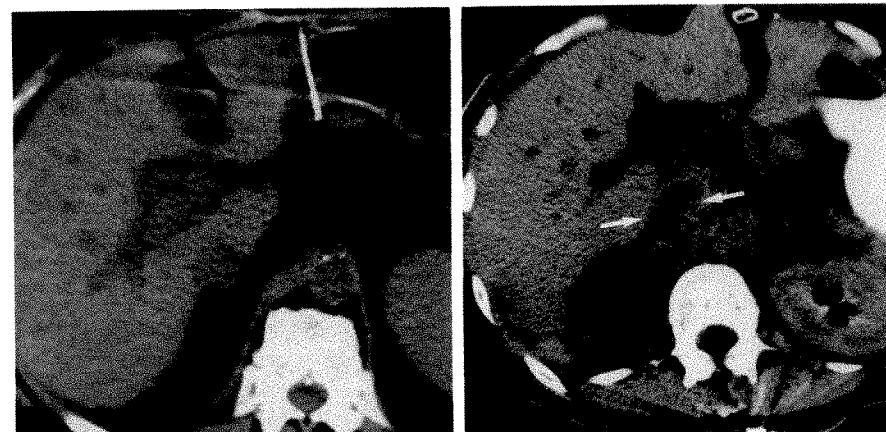


Fig. 6.—Inferior vena cava thrombosis in a 47-year-old man 16 days after liver transplantation. CT scan shows thrombus (arrows) extending inferiorly into right common and external iliac veins.

5

6

Atelectasis and pleural fluid were the most frequent CT findings in this population of patients, as has been described previously [6]. The most frequent CT finding directly related to the transplantation operation in our series of patients was periportal low attenuation. Although Wechsler et al. [7] found periportal edema a useful CT sign for liver transplant rejection, we and others [8, 9] have found that this CT finding is nonspecific, with no convincing relationship to liver rejection or clinical outcome. This common finding in our series may have been a result of impaired lymphatic drainage in the transplanted liver, as was described in a pig model of liver transplantation [10]. Several investigators have attempted to correlate liver rejection with certain radiologic features. Their results have indicated that most findings are nonspecific [11, 12]. Liver rejection is still primarily diagnosed histologically.

Fever and leukocytosis were common indications for CT scanning, and exclusion of infected intraabdominal fluid collections was the primary goal. In our series, 27% of these patients had loculated fluid collections (e.g., hematoma, seroma, biloma) in various abdominal compartments; the collections were infected in 25% of the patients. Because of the complex surgical and medical problems related to these patients, clinicians find it difficult to predict which patients have infected fluid collections and, therefore, are likely to order a CT scan to rule out abscess. This may explain the low percentage of infected fluid collections. The CT appearance of intraperitoneal fluid collections is nonspecific, and we were unable to predict which fluid collections were infected based on their CT scan appearance. Therefore, we recommend CT-guided aspiration of any suspicious collection in the setting of possible infection.

The numerous possible vascular complications of liver transplantation are related to the many different anastomoses, bleeding diastheses, and numerous liver biopsies of these patients. Hepatic parenchymal hemorrhage was seldom seen after liver biopsy. This is surprising because altered coagulability from graft dysfunction and lack of vascular innervation preventing regulatory vasoconstriction would seem to make hepatic hemorrhage more likely. One case of pseudoaneurysm rupture of the hepatic artery was seen that led to massive hemoperitoneum and death. Tobben et al. [13] described 11 cases of pseudoaneurysm formation in liver transplant patients that were related to either biopsy, infection, or anastomosis. They also reported that 67% of the diagnoses were made by studying CT findings. In our case the diagnosis was suspected on CT, but angiography was used for confirmation. Portal vein thrombosis was seen in only four children in a study by Zajko et al. [14]. We encountered one case of left portal vein thrombosis that was suggested on CT by the distribution of the associated infarction. In general, CT can suggest vascular compromise when areas of parenchymal abnormalities exist, but in our experience, further evaluation by other methods is needed.

In addition, one case of inferior vena caval thrombosis occurred, presumably owing to a discrepancy in the graft-host caval size that existed because of dilatation of the native inferior vena cava from prior portacaval shunt surgery. CT with contrast enhancement should be able to show thrombosis if large vessels such as the inferior vena cava or portal vein are involved. However, as stated before, thrombosis of smaller vessels may be only suggested by parenchymal abnormalities.

Hepatic parenchymal infarction is a common complication in liver transplant patients. Some authors [14, 15] state that in the presence of infarction, the prevalence of hepatic arterial thrombosis is 85%. They also state that these patients should undergo retransplantation to prevent hepatic failure. Our experience in adults who have liver transplants is that small areas of hepatic infarction are insignificant, and retransplantation is not performed. In fact, we do not routinely perform angiography in such patients. In patients with large areas of infarction corresponding to an entire lobe, the prognosis is poor. This suggests that these patients should undergo retransplantation before infection or liver failure develops.

Hepatic calcification in liver transplantation has not been reported before in the radiologic literature. The two cases that we saw exhibited large areas of infarction with necrosis and calcification. Hypercalcemia has been seen previously [16] in failed liver transplantation and may explain the calcium deposition in one of our cases. The mechanism, as has been hypothesized with pulmonary calcifications in liver transplant patients [6], may relate to metabolic alkalosis, multiple infusions of calcium chloride to counteract the citrate anticoagulant of transfused blood, or infection.

Biliary complications were encountered infrequently. In fact, only two bilomas were identified, and biliary obstruction was not seen. This may be explained by the fact that T-tube cholangiograms were obtained initially in all these patients to search for extravasation or obstruction. Thus, these complications were found and corrected without the need for further diagnostic imaging.

REFERENCES

- Starzl TE, Demetris AJ, Van Thiel D. Liver transplantation. *N Engl J Med* 1989;321:1092-1099
- Davis PL, Van Thiel DH, Zajko AB, et al. Imaging in hepatic transplantation. *Semin Liver Dis* 1989;9:90-101
- Letourneau JG, Day DL, Maille CW, et al. Liver allograft transplantation: postoperative CT findings. *AJR* 1987;148:1099-1103
- Letourneau JG, Day DL, Ascher NL, et al. Abdominal sonography after hepatic transplantation: results in 36 patients. *AJR* 1987;149:299-303
- Longley DG, Skolnick ML, Zajko AB, Bron KM. Duplex Doppler sonography in the evaluation of adult patients before and after liver transplantation. *AJR* 1988;151:687-696
- Costello P, Williams CR, Jenkins RW, et al. The incidence and implications of chest radiographic abnormalities following orthotopic liver transplantation. *Can Assoc Radiol J* 1987;38:90-95
- Wechsler RJ, Munoz SJ, Needlman L, et al. The periportal collar: a CT sign of liver transplant rejection. *Radiology* 1987;165:57-60
- Kaplan SB, Sumkin JH, Campbell WL, et al. Periportal low-attenuation areas on CT: value as evidence of liver transplant rejection. *AJR* 1989;152:285-287
- Stevens SD, Heiken JP, Hanto DW, et al. Periportal collar on CT scan after liver transplantation: reliability as a sign of allograft rejection. *Radiology* 1990;177(P):116
- Marincek B, Barbier PA, Becker CD, et al. CT appearance of impaired lymphatic drainage in liver transplants. *AJR* 1986;147:519-523
- Bauman J, Campbell WL, Demetris AJ, Zajko AB. Intrahepatic cholangiographic abnormalities in liver transplants: correlation with biopsy evidence of rejection and other disorders. *AJR* 1989;152:275-279
- Dominguez R, Cuervas-Mons V, Van Thiel DH, et al. Radiographic features of liver allograft rejection. *Gastrointest Radiol* 1986;11:326-329
- Tobben PJ, Zajko AB, Sumkin JH, et al. Pseudoaneurysms complicating organ transplantation: roles of CT, duplex sonography, and angiography. *Radiology* 1988;169:65-70
- Zajko AB, Bron KM, Starzl TE, et al. Angiography of liver transplant patients. *Radiology* 1985;157:305-311
- Segel MC, Zajko AB, Bowen A, et al. Hepatic artery thrombosis after liver transplantation: radiologic evaluation. *AJR* 1986;146:137-141
- Gerhardt A, Greenberg A, Reilly JJ Jr, et al. Hypercalcemia: a complication of advanced chronic liver disease. *Arch Intern Med* 1987;147:274-277

Diagnosis of Pancreatic Transplant Dysfunction: Value of Gadopentetate Dimeglumine-Enhanced MR Imaging

Maria del Pilar Fernandez¹
 Michael E. Bernardino¹
 John F. Neylan²
 Richard A. Olson³

Sixteen MR studies performed in four patients who had undergone combined pancreatic and renal transplantation were reviewed retrospectively to determine if dynamic gadopentetate dimeglumine-enhanced gradient-echo imaging is useful in the early diagnosis of pancreatic transplant rejection. The MR studies were performed between 3 days and 6 months after transplantation and consisted of T1- and T2-weighted spin-echo images as well as a gradient-echo image prior to administration of an IV bolus of gadopentetate dimeglumine (0.1 mmol/kg). After injection of gadopentetate dimeglumine, a static dynamic gradient-echo scan was obtained. Signal-intensity measurements were determined for each of the gradient-echo images and used to generate an enhancement curve. Because T2 values have previously been used as an objective indicator of rejection, the mean T2 of each pancreatic transplant was calculated also. The MR results were compared with clinical and laboratory data and/or percutaneous biopsy results. In six studies of normally functioning pancreatic allografts, the percent enhancement during the first minute of the enhancement curve was $98 \pm 23\%$ (1 SD). In six episodes of acute dysfunction (rejection or infarction), the first-minute enhancement was $42 \pm 20\%$. In four cases of dysfunction, the finding of an abnormal enhancement curve preceded a significant drop in urinary amylase by 1–4 days. The calculated T2 value was prolonged in only two cases in which biopsy-proved pancreatic infarction had occurred. No prolongation of T2 was evident in four cases of rejection alone.

These results suggest that mean T2 calculation at 1.5 T may not be a reliable indicator of pancreatic transplant rejection, but that gadopentetate dimeglumine-enhanced gradient-echo MR imaging of the pancreatic transplant may be a reliable early indicator of pancreatic transplant dysfunction.

AJR 156:1171–1176, June 1991

Pancreatic transplants are being performed more frequently in the treatment of type I diabetes mellitus. Although the success rate of pancreatic transplantation has increased with improvements in the operative and perioperative management of these patients [1], postoperative pancreatic transplant dysfunction is commonly seen and may result from one or more causes including rejection, ischemia, pancreatitis, and sepsis.

Postoperative pancreatic transplant function is routinely monitored with several laboratory tests such as those for oral glucose tolerance and serum glucose, serum amylase, and urinary amylase levels. However, because no single, reliable, noninvasive indicator of early rejection is available, transplant rejection remains the most common cause for loss of endocrine graft function [2–4].

Several reports [5–11] describe the imaging of pancreatic transplants with perfusion scintigraphy, CT, sonography, cystography, and MR. Previously described MR imaging of pancreatic transplants included conventional spin-echo imaging and calculation of the mean T2 of the pancreatic transplant (on a 0.35-T unit). To our knowledge, the use of gadopentetate dimeglumine-enhanced MR in the evaluation of pancreatic transplants has not been reported [11]. The purpose of this article was to determine whether dynamic gadopentetate dimeglumine-

Received September 24, 1990; accepted after revision December 6, 1990.

¹ Department of Radiology, Emory University School of Medicine, 1364 Clifton Rd., N.E., Atlanta, GA 30322. Address reprint requests to M. d. P. Fernandez.

² Department of Medicine, Emory University School of Medicine, Atlanta, GA 30322.

³ Department of Surgery, Emory University School of Medicine, Atlanta, GA 30322.

0361-803X/91/1566-1171

© American Roentgen Ray Society

enhanced gradient-echo imaging of the pancreatic transplant is useful in the early diagnosis of pancreatic rejection. Additionally, in order to determine if the mean T2 at high field strength is a predictor of transplant rejection, the mean T2 of each pancreatic transplant was calculated and correlated with clinical and laboratory data.

Materials and Methods

From August 1989 through April 1990, 16 MR studies were performed in four of the first six patients who had undergone combined cadaveric renal and pancreatic transplantation at our institution. The other two patients were markedly claustrophobic and could not tolerate MR examination. Our study group consisted of two men and two women 22–47 years old (mean, 33 years). In each case, pancreaticoduodenal cystostomy was the method of transplantation. The number of studies performed in each of the four patients was four in case 1, six in case 2, five in case 3, and one in case 4. A second study performed in case 4 was nondiagnostic owing to motion artifact, and therefore was not included in our series. The MR examinations were performed randomly during a variable interval of 3 days to 6 months after pancreatic transplantation. The clinical impression at the time of each MR examination was as follows: normal function in eight cases; acute dysfunction in four cases; and stable or stable impaired function in four cases, each of which had previously been treated for one or more episodes of acute dysfunction.

A 1.5-T Philips (Eindhoven, the Netherlands) magnet was used for all examinations. Axial spin-echo 1-cm images with T1, 316/15 (TR/TE), and T2, 2000–2016/30,60 or 50,100, weighting were obtained before IV administration of gadopentetate dimeglumine. Gradient-echo imaging, 30–50/13–14/80° (TR/TE/pulse angle), was performed before and after an IV bolus of gadopentetate dimeglumine (0.1 mmol/kg) was administered in less than 30 sec. The first two of the 16 gradient-echo examinations were performed with axial imaging. Subsequently, a sagittal T1-weighted image through the pancreas was used to select the optimal imaging plane for the dynamic scan (Fig. 1). An off-axis coronal image angled through the pancreatic transplant was determined to be the most successful in showing the maximal length of the pancreatic transplant. An unenhanced 10- or

12-mm-thick off-axis coronal gradient-echo image was obtained. This same coronal slice (single breath-hold with scan duration of 12 sec) was imaged several times after injection of gadopentetate dimeglumine. In the majority of cases, the coronal slice was repeated 16 times during a 5-min period (scan-to-scan interval of 8 sec). On each slice of the dynamic scan, measurements of signal intensity were determined at five different regions of interest symmetrically spaced within the pancreatic transplant. The average signal intensity (SI) was calculated for each image of the dynamic scan. Each signal intensity value was divided by the mean signal intensity of the background. The percent enhancement was determined for each image by using the formula,

$$\begin{aligned} \% \text{ Enhancement} = & \frac{[(\text{enhanced SI}/\text{enhanced background SI})]}{} \\ & - (\text{unenhanced SI}/\text{unenhanced background SI}) \\ & \div (\text{unenhanced SI}/\text{unenhanced background SI}) \\ & \times 100\%. \end{aligned}$$

These values were plotted to generate an enhancement curve. These curves were analyzed for degree of signal enhancement, with particular attention to the maximal percent enhancement obtained during the 1-min period at the onset of gadopentetate dimeglumine bolus injection. The 1-min time frame was chosen because gadopentetate dimeglumine is known to be rapidly distributed in the extravascular space [12].

Additionally, three separate regions of interest (one in the head, one in the body, one in the tail) were used to calculate the mean T2 of each pancreatic transplant. In the patient who had undergone surgical debridement of the pancreatic tail and a portion of the pancreatic body, only two regions of interest were obtained (one in the head, one in the proximal body). The following formula was used for calculation of the mean T2:

$$T2 = (TE_2 - TE_1)/[\ln(SI_1/SI_2)],$$

where SI_1 = signal intensity on first echo and SI_2 = signal intensity on second echo.

The MR results were correlated with clinical and laboratory data and/or results of percutaneous biopsy to determine if the enhancement curve and/or mean T2 are indicators of pancreatic function. The clinical progress notes and laboratory data of each patient were

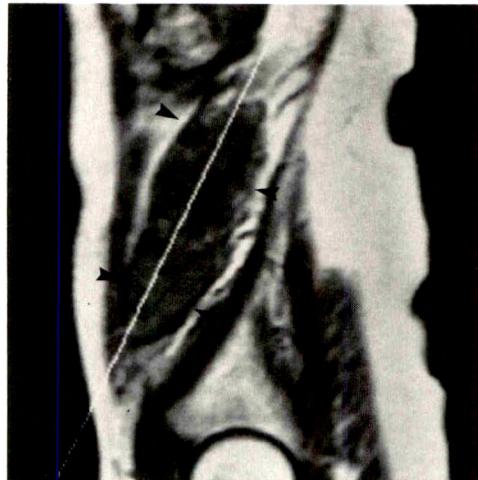


Fig. 1.—Sagittal T1-weighted MR image, 235/20, used to select off-axis coronal slice as imaging plane for gradient-echo dynamic scan of pancreatic transplant (arrowheads).

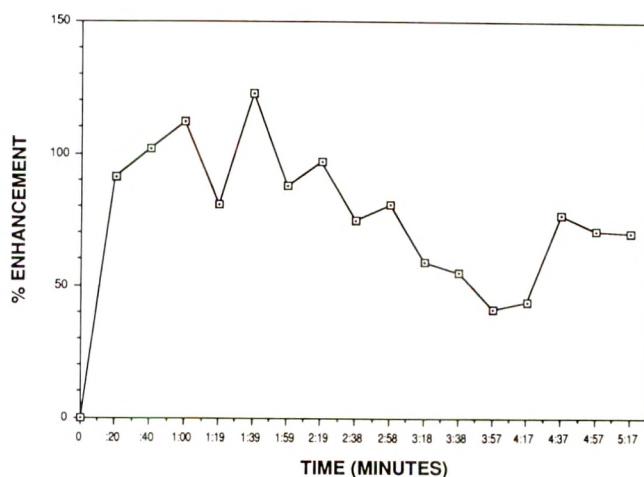
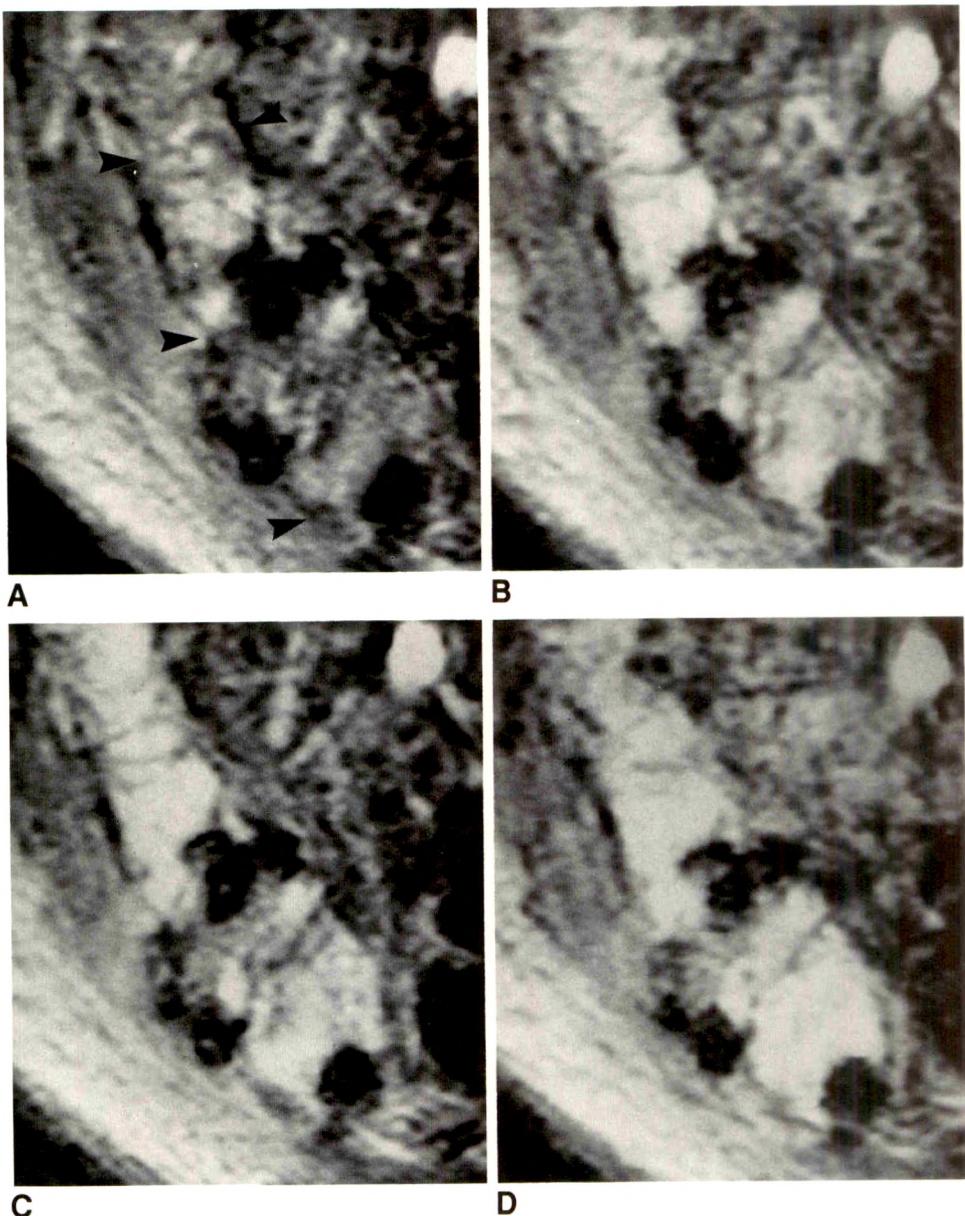


Fig. 2.—Graph shows enhancement obtained for normally functioning pancreatic transplant. Enhancement during first minute after IV bolus of gadopentetate dimeglumine was 112%.

Fig. 3.—A–D, Dynamic gradient-echo MR images, 31/14/80°, of a normally functioning pancreatic transplant (arrowheads) show progressive enhancement of transplant 20 sec (A), 1 min (B), 1:41 min (C), and 2:21 min (D) after IV bolus of gadopentetate dimeglumine. Enhancement at 1 min (B) was 121%.



reviewed independently by one radiologist and one transplant physician. Parameters that suggested pancreatic rejection included fever; graft tenderness; significant drop in the urinary amylase level; hyperglycemia; and in some cases, concomitant renal transplant dysfunction. Pathologic correlation with percutaneous biopsy of the pancreatic transplant (performed with an 18-gauge automated-needle device) was possible for five of the MR studies. Four of these five biopsies were obtained within 24 hr of the MR examination. The results of the biopsies were as follows: rejection in two cases; infarction of both the pancreatic head and tail in the third case; and infarction of the pancreatic tail, but normal histologic appearance of the head in the fourth case. In the fifth case, percutaneous biopsy of a normally functioning transplant was performed to evaluate moderately severe graft tenderness. The biopsy confirmed the absence of rejection or pancreatitis, and graft tenderness was attributed to

traumatic hematoma overlying the pancreatic allograft. Pathologic correlation was not available for the remaining 11 MR examinations.

On the basis of the clinical course of each patient and/or pancreatic transplant biopsy results, each of the 16 MR studies was placed in one of three categories: (1) normally functioning transplant (six studies), (2) acute transplant dysfunction (six studies), and (3) treated rejection (four studies). The category of treated rejection included any transplant in which there was no suggestion of acute dysfunction at the time of MR examination, but which had been previously treated for rejection. The discrepancy between this final categorization of the 16 MR examinations and the original clinical impressions of pancreatic transplant function as described previously in this section can be explained: In two cases of presumably normally functioning transplant, review of the laboratory data demonstrated a significant decrease in the urinary amylase level 4 days after the MR examination.

In both of these cases, the MR enhancement curves showed diminished early enhancement. Therefore, it was believed that in these two cases, the MR study was actually performed very early in the development of acute dysfunction. Thus, these two cases are more appropriately grouped in the acute dysfunction category.

Duplex sonography, scintigraphy, and limited CT (for the purpose of CT-directed transplant biopsy) were also performed in all of these patients. However, most of these studies were not performed within 24 hr of the MR examination. Therefore, a comparison of the MR findings with the findings of these other techniques was not performed.

Results

In six studies of normally functioning pancreatic transplants, the percent enhancement during the first minute varied from 63% to 126%. The average maximal first-minute enhancement was $98 \pm 23\%$ (1 SD) (Figs. 2 and 3).

Six studies were performed during acute pancreatic transplant dysfunction (Figs. 4 and 5). This group included four episodes of rejection, one episode of nearly complete pancreatic graft infarction, and one episode of partial graft infarction. The first-minute maximal enhancement varied from 15% to 70% (mean, $42 \pm 20\%$). In four of these six cases of acute dysfunction, the finding of an abnormal enhancement curve preceded a significant drop in urinary amylase by 1–4 days. In five of these six studies, the first-minute enhancement was diminished by at least 40% from the maximal first-minute enhancement obtained on a prior normal baseline study. In the sixth case (28% first-minute enhancement), the MR study 7 days after pancreatic transplantation was the first posttransplantation study. The clinical course of this patient during the following days confirmed the presence of pancreatic rejection. In two of the four cases of rejection, a delayed maximal percent enhancement (135% and 169%, respectively) was seen more than 4 minutes after injection of gadopentetate dimegumine. The configuration of the enhancement curve for the transplant with partial graft infarction was very similar to

that seen in several cases of rejection. Therefore, on the basis of the mean enhancement curve alone, partial infarction could not be distinguished from rejection. The one case of nearly complete infarction showed minimal variability (i.e., relatively flat curve) in the small amount of enhancement present over the 5-min period after injection of gadopentetate dimegumine.

The four studies placed in the treated rejection group showed variable enhancement during the first minute after injection of a bolus of gadopentetate dimegumine (range, 8–130%; mean, $67 \pm 45\%$). Two of these studies (8% and 47% first-minute enhancement) were performed on a single pancreatic transplant that had stable but impaired function after one episode of rejection and one episode of partial infarction that led to surgical debridement of the necrotic allograft tissue. Each of these two studies showed delayed maximal enhancement (98% and 145%, respectively), which occurred more than 2½ min after administration of the gadopentetate dimegumine bolus. No further percutaneous biopsies have been done of this transplant. Therefore, it is uncertain whether the persistently abnormal enhancement curves reflect incomplete normalization of perfusion after acute rejection/partial infarction, or whether an element of chronic rejection accounts for the abnormal enhancement. The remaining two studies were performed on two transplants, each of which, on the basis of clinical parameters, was functioning normally after an episode of rejection. Both MR studies showed improved enhancement when compared with MR studies performed during the episode of rejection. However, in one of these two cases, the percent enhancement was 38 percentage points less than that obtained on the original normal baseline study.

The mean T₂ of normally functioning pancreatic allografts varied from 64 to 93 msec, with an average of 76 ± 9 msec (1 SD). The mean T₂ of the allografts undergoing rejection varied from 70 to 83 msec, with an average of 78 ± 5 msec. The mean T₂ of the allograft that had an infarcted tail but a normal head was 129 msec. In this case, the T₂ of the pancreatic head was 79 msec, but the T₂ of the body and tail were 152 and 157 msec, respectively. The mean T₂ of the allograft with biopsy-proved infarction of both pancreatic head and tail was 137 msec. Therefore, the average T₂ value for the infarcted tissue in these two cases was 146 ± 9 msec. In cases of treated rejection, the mean T₂ varied from 67 to 83 msec, with an average of 74 ± 6 msec.

Discussion

The success rate of pancreatic transplantation has improved in recent years because of advancements in the management of pancreatic allograft recipients [1, 13]. However, pancreatic rejection continues to be the cause of graft loss or nonfunction in a significant percentage of cases. This number could be reduced if a sensitive and specific method were devised for detecting pancreatic rejection early in the clinical course when antirejection therapy is most effective.

Pancreatic allograft function is monitored routinely with multiple laboratory tests, including those for oral glucose tolerance and serum glucose, serum amylase, and urinary

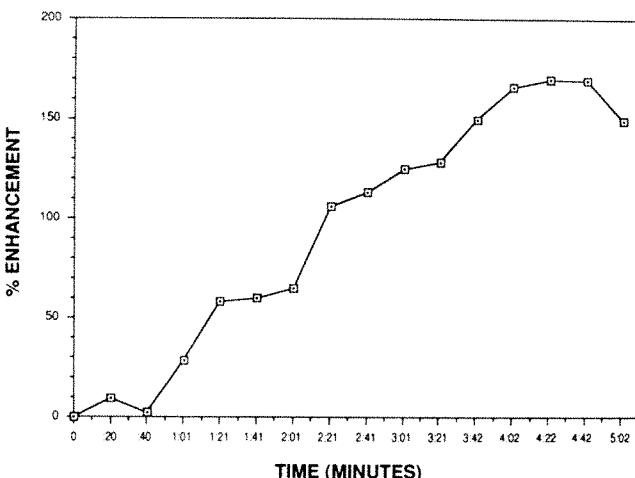
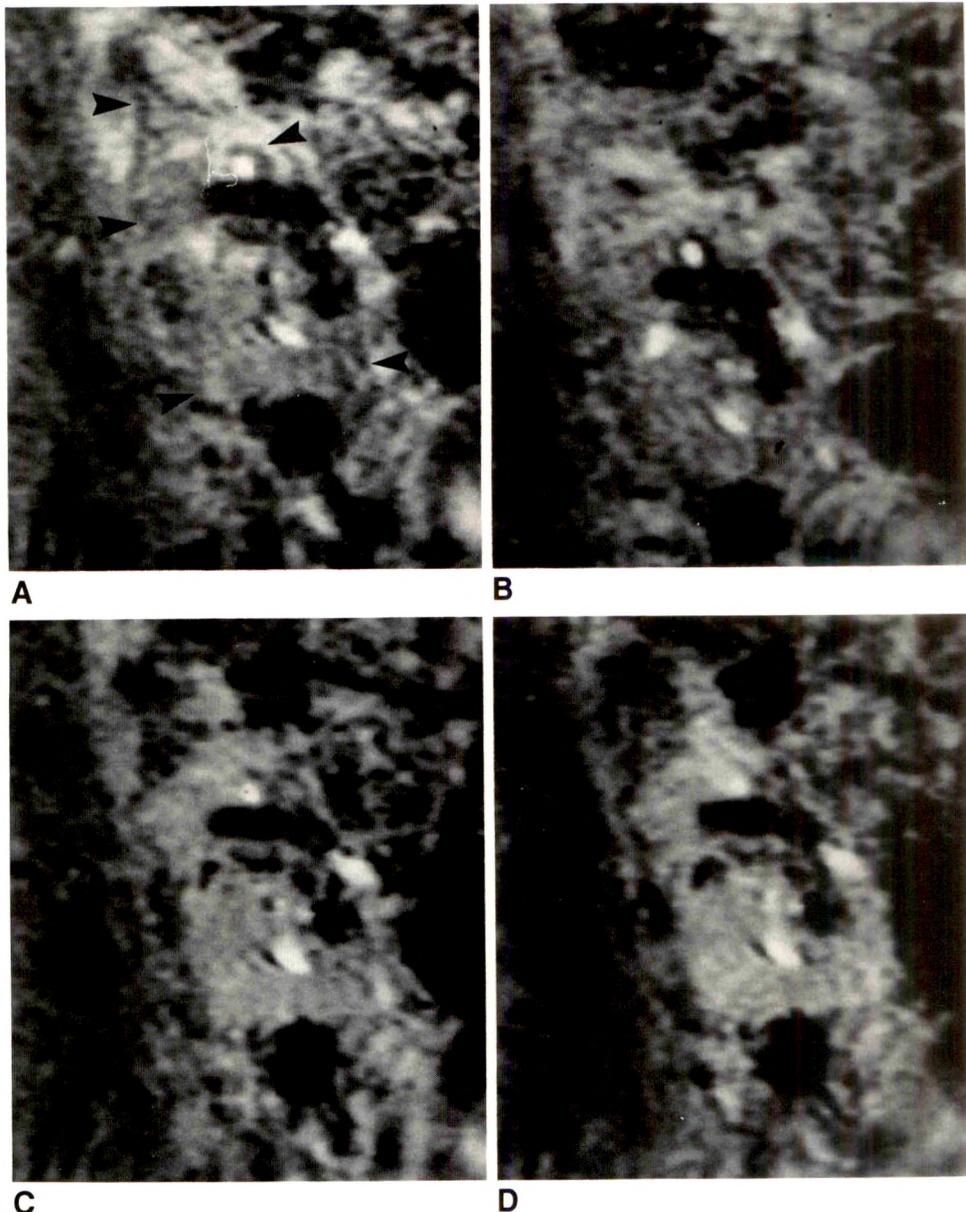


Fig. 4.—Graph shows enhancement curve obtained for a pancreatic transplant undergoing early acute rejection. Maximal enhancement during first minute after IV bolus of gadopentetate dimegumine was 28%.

Fig. 5.—A-D. Dynamic gradient-echo MR images, 31/14/80°, of a pancreatic transplant (arrowheads) during rejection, before (A) and 16 sec (B), 1:05 min (C), and 1:54 min (D) after IV bolus of gadopentetate dimeglumine show delayed enhancement and poor definition of pancreatic transplant. Maximal enhancement during first minute was 70%.



amylase levels. However, no single test has been shown to be a reliable indicator of early pancreatic rejection. Hyperglycemia is seen when irreversible damage to the pancreas has occurred, thereby precluding the effectiveness of antirejection therapy begun at the onset of hyperglycemia [4]. Although a drop in urinary amylase typically precedes hyperglycemia by several days [4, 14], a low value is not a specific marker for rejection [15, 16].

Several reports [11] have been published on the role of imaging in the evaluation of pancreatic transplants. Cystography is used routinely to exclude duodenal cystostomy anastomotic leaks [17]. CT has been successful in the detection of peripancreatic fluid collections, but because of a lack of specificity, it is not useful in the early diagnosis of rejection [5, 10]. Scintigraphy has been used to evaluate transplant

perfusion and graft size [10, 18, 19]. Doppler sonography has been used to determine patency of transplant vessels and to calculate the resistive indexes of arteries within the pancreatic transplant [6]. Previously described MR of the pancreatic transplant included conventional spin-echo imaging and calculation of the mean T2 of the pancreatic transplant [7-9]. To our knowledge, no previous reports on gadopentetate dimeglumine-enhanced MR in the evaluation of pancreatic allografts have been published.

In our study, gradient-echo images before and after administration of an IV bolus of gadopentetate dimeglumine were obtained in addition to conventional spin-echo images of the pancreatic transplant. Analysis of the generated enhancement curves indicates that impairment of enhancement occurs in cases of rejection or infarction. In four cases of acute pan-

creatic transplant dysfunction, impaired enhancement was noted 1–4 days before there was a significant drop in the urinary amylase level.

Although we did not perform a detailed qualitative visual analysis of the spin-echo images as described by Yuh et al. [7, 9], the mean T2 of each pancreatic transplant was calculated and correlated with the clinical impression of transplant function. The similarity of the mean T2 for normally functioning transplants (76 msec) and acutely rejecting transplants (78 msec) suggests that the signal intensity on the T2-weighted image may not be a reliable indicator of transplant rejection. In the cases of rejection, the diagnosis of acute transplant dysfunction could be made on the basis of abnormal enhancement curves but not on the signal intensity of the transplant on T2-weighted spin-echo images. However, in cases of infarction, there was markedly increased signal intensity of the infarcted tissue on the T2 spin-echo images and prolongation of the mean T2 (146 msec). Therefore, in cases of infarction, enhanced studies may not provide any additional information about the infarcted tissue, but should indicate which portions of the transplant, if any, have normal function.

A limitation of our study is that all cases of acute pancreatic dysfunction were caused by rejection or infarction. Therefore, we did not determine the configuration of the enhancement curve in other types of pancreatic dysfunction (e.g., pancreatitis). Additionally, although a distinct configuration of the enhancement curve was noted in the one case of essentially complete pancreatic infarction, analysis of the mean enhancement curves alone did not permit differentiation among four cases of acute rejection, one case of partial infarction, and two cases of treated rejection. Thus, enhanced MR may be a sensitive but nonspecific indicator of pancreatic transplant dysfunction.

Given the small number of patients in our study and the limited causes of pancreatic transplant dysfunction, it is inappropriate to make definitive conclusions regarding the role of gadopentetate dimeglumine-enhanced MR of pancreatic transplants. Clearly, it is necessary to repeat this study with a larger group of patients with various types of transplant dysfunction and to compare the MR results with those of other imaging techniques. If it is confirmed in a larger series that abnormal MR enhancement precedes the clinical suggestion of transplant dysfunction, the role of enhanced MR as a screening examination for the early detection of transplant dysfunction may be justified, even if enhanced MR is found to be a nonspecific indicator of early dysfunction. Those patients with abnormal enhancement then could be selected for percutaneous automated-needle core biopsy of the allograft, allowing early and objective diagnosis [20, 21] of pancreatic rejection before immunosuppressive therapy is started. Additionally, the combination of enhanced MR and conventional spin-echo imaging should provide the same information (graft size, detection of peri- or intrapancreatic fluid collections/hemorrhage, and graft perfusion) currently obtained by an expensive combination of imaging (CT, sonography, nuclear medicine). By obviating these other techniques, the cost of an MR examination should be more acceptable.

In summary, mean T2 calculation with the use of a 1.5-T magnet may not be a reliable indicator of pancreatic transplant rejection. However, gadopentetate dimeglumine-enhanced gradient-echo imaging of the pancreatic transplant appears to be a sensitive technique for the early detection of pancreatic transplant dysfunction. Because our series is small, further studies are necessary to determine the statistical significance and practical clinical applications of our data.

REFERENCES

- Perkins JD, Fromme GA, Narr BJ, et al. Pancreas transplantation at Mayo. II. Operative and perioperative management. *Mayo Clin Proc* **1990**; 65:483–495
- Ekberg H, Allen RDM, Greenberg ML, et al. Percutaneous fine needle aspiration biopsy of canine pancreas allograft provides diagnosis of treatable rejection. *J Surg Res* **1989**;47:348–353
- Tyden G, Reinhold F, Brattstrom C, et al. Diagnosis of rejection in recipients of pancreatic grafts with enteric exocrine diversion by monitoring pancreatic juice cytology and amylase excretion. *Transplant Proc* **1987**;19(5):3892–3894
- Schulak JA, Dreyvano TF. Experimental pancreas allograft rejection: correlation between histologic and functional rejection and the efficacy of antirejection therapy. *Surgery* **1985**;98(2):330–337
- Moulton JS, Munda R, Weiss MA, Lubbers DJ. Pancreatic transplants: CT with clinical and pathologic correlation. *Radiology* **1989**;172:21–26
- Patel B, Wolverson MK, Mahanta B. Pancreatic transplant rejection: assessment with duplex US. *Radiology* **1989**;173:131–135
- Yuh WTC, Wiese JA, Abu-Yousef MM, et al. Pancreatic transplant imaging. *Radiology* **1988**;167:679–683
- Vahey TN, Glazer GM, Francis IR, et al. MR diagnosis of pancreatic transplant rejection. *AJR* **1988**;150:557–560
- Yuh WTC, Hunsicker LG, Nghiem DD, et al. Pancreatic transplants: evaluation with MR imaging. *Radiology* **1989**;170:171–177
- Patel B, Markivee CR, Manhanta B, Vas W, George E, Garvin P. Pancreatic transplantation: scintigraphy, US, and CT. *Radiology* **1988**;167:685–687
- Low RA, Kuni CC, Letourneau JG. Pancreas transplant imaging: an overview. *AJR* **1990**;155:13–21
- Saini S, Stark DD, Brady TJ, Wittenberg J, Ferrucci JT Jr. Dynamic spin echo MRI of liver cancer using gadolinium-DTPA: animal investigation. *AJR* **1986**;147:357–362
- Sutherland DER. Pancreas transplantation. *Diabetes Metab Rev* **1987**;3(4):1061–1090
- Prieto M, Sutherland DER, Fernandez-Cruz L, Heil JB, Najarian JS. Rejection in pancreas transplantation. *Transplant Proc* **1987**;19(1):2348–2349
- Munn SR, Engen DE, Barr D, Carpenter HA, Perkins JD. Differential diagnosis of hypoamylasuria in pancreas allograft recipients with urinary exocrine drainage. *Transplantation* **1990**;49(2):359–362
- Perkins JD, Munn SR, Marsh CL, Barr D, Engen DE, Carpenter HA. Safety and efficacy of cystoscopically directed biopsy in pancreas transplantation. *Transplant Proc* **1990**;22(2):665–666
- Woolsey EJ, Tauscher JR, Dafoe CD. Pancreas transplantation with pancreatico-duodenocystostomy for exocrine drainage: cystographic findings. *AJR* **1987**;149:507–509
- Kuni CC, du Cret R, Boudreau RJ. Pancreas transplants: evaluation using perfusion scintigraphy. *AJR* **1989**;153:57–61
- George EA, Salimi Z, Carney K, Castaneda M, Garvin PJ. Radionuclide surveillance of the allografted pancreas. *AJR* **1988**;150:811–816
- Allen RDM, Wilson TG, Grierson JM, et al. Percutaneous pancreas transplant fine needle aspiration and needle core biopsies are useful and safe. *Transplant Proc* **1990**;22(2):663–664
- Bernardino ME, Fernandez M, Neylan J, Hertzler G, Whelchel J, Olson R. Pancreatic transplants: CT-guided biopsy. *Radiology* **1990**;177:709–711

Recurrent Hepatocellular Carcinoma After Partial Hepatectomy: Value of Treatment with Transcatheter Arterial Chemoembolization

Norio Nakao¹
Keiji Kamino¹
Kohi Miura¹
Takayuki Hayashi¹
Mitsunori Ohnishi¹
Yukio Takayasu¹
Takashi Miura¹
Eizo Okamoto²

The usefulness of transcatheter arterial chemoembolization (TACE) of the hepatic artery was retrospectively evaluated in 66 patients who underwent the procedure for treatment of hepatocellular carcinoma that recurred after partial hepatectomy. The materials infused were Gelfoam sponge or Gelfoam sponge plus Lipiodol and an anticancer agent. A control group of 15 patients with recurrent tumor received oral anticancer agents alone. The cumulative survival rate for the TACE group was 88% for the first year, 57% for 2 years, 42% for 3 years, and 27% for 5 years, whereas that of the control group was 80% for the first year, 27% for 2 years, and 18% for 3 years. Thus, the prognosis of the TACE group was significantly better ($p \leq .01$, log-rank test) than that of the control group. The survival rate was inversely correlated with the ratio of the volume of the recurrent tumor to the volume of the whole residual liver.

These results suggest that TACE is more effective than oral chemotherapy for treatment of hepatocellular carcinoma that recurs after partial hepatectomy.

AJR 156:1177-1179, June 1991

In patients who have undergone partial hepatectomy for hepatocellular carcinoma (HCC), the tumor often recurs postoperatively in the remaining liver parenchyma. Recurrent HCC of this type is difficult to treat with further resection of the liver and usually is treated with chemotherapy given orally or by arterial infusion. The results of such therapy have so far been unsatisfactory [1-5].

Treatment of unresectable HCC by transcatheter arterial chemoembolization (TACE) of the hepatic artery has been reported to have satisfactory results [6-9]. We performed TACE with the use of Gelfoam, Lipiodol, and/or an anticancer agent in 66 patients in whom HCC recurred after partial hepatectomy and found the results to be better than those for patients who were treated with oral chemotherapy.

Materials and Methods

Eighty-one patients with recurrent tumor after partial hepatectomy for primary HCC who were treated at the Hyogo College of Medicine from September 1977 to December 1986 were included in the study. Sixty-six were treated with TACE and 15 received oral chemotherapy. TACE was used in 54 men and 12 women with a mean age of 57 years; oral chemotherapy was used in 14 men and one woman with a mean age of 60 years.

No significant difference was seen between the two groups in the morphologic features of the tumor and the results of liver function studies at the time of hepatectomy and recurrence. The mean tumor sizes for the TACE and oral chemotherapy groups, respectively, were 3.7 ± 2.7 cm and 5.1 ± 3.2 cm at the time of hepatectomy and 2.8 ± 3.0 cm and 3.2 ± 2.6 cm at the time of recurrence. At initial surgery, liver cirrhosis was present in 53 (80%) of the 66 patients in the TACE group and in 11 (73%) of the 15 patients in the oral chemotherapy group. At the time of recurrence, the bilirubin levels of the TACE and oral chemotherapy groups, respectively, were 0.61 ± 0.24 mg/dl and 0.84 ± 3.2 mg/dl; the respective 15-min indocyanine green retention ratios were $13 \pm 11\%$ and $16 \pm 13\%$. The proportion of

Received September 10, 1990; accepted after revision January 3, 1991.

¹ Department of Radiology, Hyogo College of Medicine, 1-1 Mukogawa-cho, Nishinomiya 663, Japan. Address reprint requests to N. Nakao.

² Department of Surgery, Hyogo College of Medicine, Nishinomiya 663, Japan.

0361-803X/91/1566-1177
© American Roentgen Ray Society

multinodular tumors (multiple tumors of approximately the same size) to nodular (solitary) tumors at the time of recurrence was 45:21 for the TACE group and 11:4 for the oral chemotherapy group.

Transarterial embolization was performed as follows. The tip of a catheter was introduced into the hepatic artery via the femoral artery, and embolization of the hepatic artery was done with 0.5- to 1.0-mm cubes of Gelfoam sponge (Upjohn, Kalamazoo, MI). The celiac and hepatic arteries are tortuous in many postoperative cases, and in some cases the hepatic artery is occluded and the tumor is fed only by very fine collateral arteries, making superselective catheterization difficult. The Tracker catheter (Target Therapeutics, San Jose, CA) and the Radifocus guidewire (Terumo Co., Tokyo, Japan) greatly facilitate superselective catheterization in such cases.

In 50 of the 66 cases, an emulsion consisting of 3.0–8.0 ml (mean, 4.5 ml) of Lipiodol (iodized oil, Laboratoire Guerbert, Aulnay-sous-Bois, France) plus an anticancer agent (20 mg of Adriamycin or 10 mg of mitomycin C or both) was infused immediately before embolization. In 16 cases, the anticancer agent was infused together with the Gelfoam sponge. The oral chemotherapy regimen used in this retrospective study was not standardized.

After TACE, the serum alpha-fetoprotein (AFP) level was measured every month and a CT scan was obtained every 3 months. When tumor recurrence after TACE was noted on the CT images or through elevation of the serum AFP level, TACE treatment was repeated by using the same procedure that was done with the first TACE. In most cases, TACE was repeated once or twice a year during the course of the disease.

The patients in the oral chemotherapy group, consisting of those who refused to undergo TACE (usually because they did not want to be hospitalized or thought the procedure might be painful), received an anticancer agent orally. The anticancer agent used for this group was 5-fluorouracil at a dose of 100–150 mg/day or tegafur at a dose of 200–300 mg/day. The treatment was continued as long as the condition of the patient permitted. The prognoses for the TACE and oral chemotherapy groups were then compared to determine the usefulness of TACE in the treatment of postoperative recurrence of HCC.

For more accurate assessment of the TACE group, it was further divided into three subgroups according to the ratio of the volume of the recurrent tumor to the whole liver volume (relative tumor ratio, E) at the time of the first TACE treatment: $E = 100\% \times (\text{tumor volume} / \text{volume of liver parenchyma})$. Group E1 was defined as those for whom $E \leq 20\%$; for group E2, $20\% < E < 40\%$; for group E3, $E \geq 40\%$. In addition, TACE patients were also classified into two groups according to whether the tumor was nodular or multinodular at the time of the first TACE treatment.

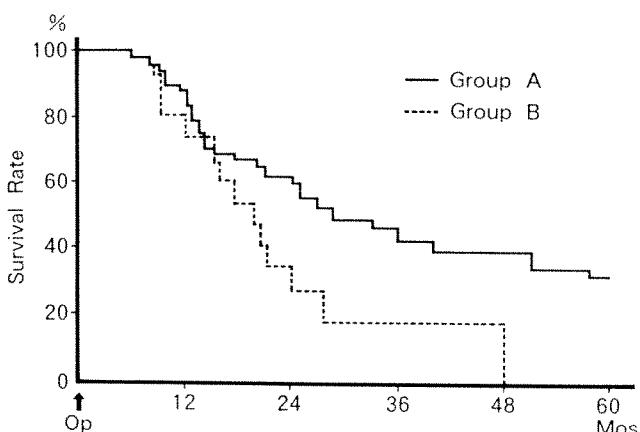


Fig. 1.—Cumulative survival rates in months (Mos.) after hepatectomy (Op) in groups treated for recurrent hepatocellular carcinoma with transarterial embolization of the hepatic artery or oral chemotherapy (calculated by Kaplan-Meier method). Group A = Transarterial chemoembolization performed for recurrent tumor. Group B = Oral chemotherapy group.

Results

Cumulative Survival Rates

The cumulative survival rates for the patients who underwent TACE for recurrent HCC after hepatectomy and the oral chemotherapy group were calculated with the Kaplan-Meier method (Fig. 1). The survival rate for the TACE group was 88% the first year, 57% for 2 years, 42% for 3 years, 38% for 4 years, and 27% for 5 years. The rate for the oral chemotherapy group was 80% the first year, 27% for 2 years, and 18% for 3 years. The prognosis for the TACE group was significantly better ($p < .01$) than that for the oral chemotherapy group (using the log-rank test). The median survival time was 34.2 months for the TACE group and 18.2 months for the oral chemotherapy group.

Relationship Between Survival Rate and Relative Tumor Ratio

Of the 66 patients in the TACE group, 23 were in group E1, 30 in group E2, and 13 in group E3. The oral chemotherapy group was not large enough for such a grouping to provide useful data. The cumulative survival rates for each E subgroup in the TACE group are shown in Figure 2. The survival rate for group E1 was 100% the first year, 90% for 2 years, and 80% for 3 years. This group had the best prognosis. The rate for E2 was 65% for 6 months, 28% for 1 year, and 8.5% for 2 years. A significant difference ($p < .01$, log-rank test) was seen in the survival rate between the three groups.

Survival Rate and Tumor Type

For the TACE group, the cumulative survival rates for both the nodular group and the multinodular group are shown in Figure 3. For the 21 cases with nodular tumors, the cumulative survival rate was 69% for the first year, 42% for 2 years, 40% for 3 years, and 20% for 4 and 5 years. For the 45 cases with multinodular tumors, the rate was 51% for the first year, 42%

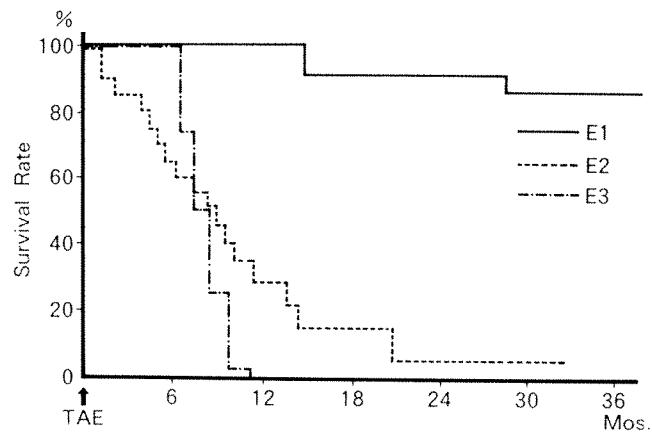


Fig. 2.—Cumulative survival rates in months (Mos.) after transarterial embolization (TAE), classified according to relative tumor ratio (E) in recurrent hepatocellular carcinoma. $E = 100\% \times (\text{tumor volume} / \text{volume of liver parenchyma})$. For group E1, $E \leq 20\%$; for group E2, $20\% < E < 40\%$; for group E3, $E \geq 40\%$.

for 2 years, 20% for 3 years, and 15% for 4 years. No significant difference in prognosis was seen between the two groups (log-rank test).

Discussion

It has been shown histologically that transcatheter hepatic arterial embolization in HCC causes necrosis of tumor cells [10, 11]. However, it is difficult to judge how much embolization actually contributes to improvement of the prognosis of HCC patients, as 80–90% of such patients have the additional complication of liver cirrhosis and liver function varies at the time of treatment [1]. There have been few reports in which the effectiveness of embolization was accurately evaluated by comparing it with other therapy.

In our study, no significant difference was seen in the rates of cirrhosis (approximately 80%) between the TACE and oral chemotherapy groups, and there was no significant difference in liver function between the two groups at the time of tumor recurrence. Moreover, the type of tumor at the time of recurrence did not differ significantly between the two groups. As all other conditions were virtually the same, the difference in prognosis between the two groups seen in Figure 1 suggests that TACE had a favorable effect on prognosis.

Although the patients in this study all underwent TACE rather than embolization alone, the favorable prognosis of the TACE group may have been due more to the effects of arterial embolization than to the chemotherapeutic agent. In another study we conducted on the value of TACE and embolization alone in treating cases of unresectable HCC, no significant difference was found between the group that received anticancer drugs and the group that did not. This was probably because the antitumor effect of the anticancer agents was obscured by the large necrotic effect of embolization on the tumor. However, because the amount of anticancer drugs we used was relatively small, the value of TACE in comparison with embolization needs to be assessed further by prospective studies.

The survival rate of 109 patients who underwent partial hepatectomy at our institution in the same period as the TACE and oral chemotherapy groups, but who had no tumor recurrence during the next 5 years, was 90% for the first

year, 75% for 2 years, 53% for 3 years, 47% for 4 years, and 41% for 5 years. The causes of death in the group without recurrence were primarily hepatic failure and the rupture of varices related to liver cirrhosis. These survival rates do not differ greatly from those for the TACE group and suggest the usefulness of TACE for recurrent tumors after partial hepatectomy for HCC.

The prognosis for the TACE group was better than that for 785 cases of unresectable HCC complicated by liver cirrhosis that were treated with TACE in our department. The survival rate in these cases was 72% the first year, 58% for 2 years, 38% for 3 years, 24% for 4 years, and 8% for 5 years. If TACE is assumed to be as effective as hepatectomy for HCC tumors, these figures suggest that liver function greatly affects patient prognosis, because liver function is usually better in resectable cases than in unresectable ones [12]. Thus, it is understandable that the prognosis differed according to the relative tumor ratio, as shown in Figure 2, where the difference in the volume of liver parenchyma around the tumor was considered. These results also agree with those found when embolization alone is performed in unresectable HCC.

Considering that recurrent tumors are apt to multiply even if they are initially of the solitary type and that complete tumor necrosis is rarely obtained with a single TACE treatment, it is reasonable that the prognosis did not depend on whether the tumors were solitary or multiple at the time of the first TACE treatment (Fig. 3).

The results of this study show that TACE offers a better prognosis than oral chemotherapy does when HCC recurs after partial hepatectomy.

REFERENCES

1. Liver Cancer Study Group of Japan. Survey and follow-up study of primary liver cancer in Japan. *Acta Hepatol Jpn* 1986;27:1161–1169
2. Sciarri E, Simonetti RG, LeMoli S, Pagliaro L. Adriamycin treatment for hepatocellular carcinoma: experience with 109 patients. *Cancer* 1985;56:2751–2755
3. Olweny CLM, Toya T, Katongole-M'Bidde E, Mugerwa J, Kyawazi SK, Cohen H. Treatment of hepatocellular carcinoma with Adriamycin: preliminary communication. *Cancer* 1975;36:1250–1257
4. Falkson G, Moertel CG, Lavin P, Pretorius FJ, Carbone PP. Chemotherapy studies in primary liver cancer: a prospective randomized clinical trial. *Cancer* 1978;42:2149–2156
5. Okuda K, Ohtsuki T, Obata H, et al. Natural history of hepatocellular carcinoma and prognosis in relation to treatment study of 850 patients. *Cancer* 1985;56:918–928
6. Clouse ME, Lee RGL, Duszak EJ, et al. Peripheral hepatic artery embolization for primary and secondary hepatic neoplasms. *Radiology* 1983;147:407–411
7. Chuang VP, Wallace S. Hepatic artery embolization in the treatment of hepatic neoplasms. *Radiology* 1981;140:51–58
8. Yamada R, Sato M, Kawabata M, Nakatsuka H, Nakamura K, Takashima S. Hepatic artery embolization in 120 patients with unresectable hepatoma. *Radiology* 1983;148:397–401
9. Beers BV, Roche A, Cauquil P, Jamart J, Pariente D, Ajavon Y. Transcatheter arterial chemotherapy using doxorubicin, iodized oil and Gelfoam embolization in hepatocellular carcinoma. *Acta Radiol* 1989;30:415–418
10. Tanaka N, Okamoto E, Toyosaka A, Nakao N. Pathohistological evaluation of hepatic artery ligation (HAL) or transcatheter arterial embolization (TAE) on primary carcinoma of the liver. *Jpn J Surg* 1983;6:518–528
11. Nakamura H, Tanaka T, Hori S, et al. Transcatheter embolization of hepatocellular carcinoma: assessment of efficacy in cases of resection following embolization. *Radiology* 1983;147:401–405
12. Okamoto E, Tanaka N, Yamanaka N, Toyosaka A. Results of surgical treatments of primary hepatocellular carcinoma: some aspects to improve long-term survival. *World J Surg* 1984;8:360–366

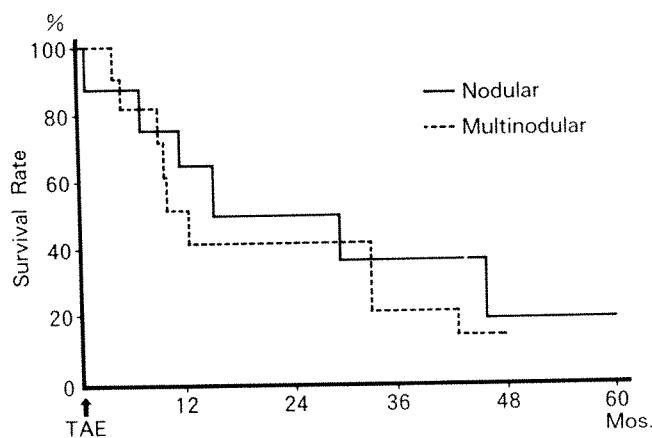


Fig. 3.—Cumulative survival rates in months (Mos.) after transarterial embolization (TAE) for recurrent hepatocellular carcinoma classified by tumor type: nodular (solitary, n = 21) or multinodular (multiple tumors of approximately the same size, n = 45).

Medicine in American Art

An American Leonardo

Stefan C. Schatzki¹

An American Leonardo, Samuel F. B. Morse was better known throughout much of his life as an important painter rather than as the inventor of the telegraph. Morse was born in Charlestown, MA, in 1791 and graduated from Yale in 1810. The following year he went to London and studied at the Royal Academy, primarily with the American painters Washington Allston and Benjamin West. Having achieved a modicum of fame in England, he returned to the United States in 1815 to find an American public that had no interest in the historical paintings that were in vogue at the time in England. In order to support himself, he began to paint portraits of important and influential Americans, and during the next 10 years became one of America's most prestigious portrait painters. In 1826, a small group of prominent artists founded the National Academy of Design and selected Morse as its first president. The academy remains today not only an honor society of artists selected by their peers but also a major source of art instruction. Despite being involved primarily with the development of the telegraph during the last 10 years of his tenure, Morse remained president of this prestigious body until 1845.

Morse's good friend, the surgeon Dr. Frederick Gore King, was the first professor of anatomy at the National Academy of Design until 1829, when he died at the age of 27. After his appointment at the National Academy, King also began to teach anatomy at The College of Physicians and Surgeons in New York. As was frequently true in the 19th century, anatomy instruction to medical and art students was similar.

Morse did not totally neglect historical paintings, and in 1822 painted perhaps the best known depiction of the House of Representatives (Corcoran Gallery, Washington, DC), and in 1833, produced a large work entitled *The Exhibition Gallery of the Louvre* (Terra Museum, Chicago). This painting was widely exhibited with a text by Morse's friend James Fenimore Cooper, with the hope that it would stimulate Americans to have a greater interest in fine art.

In 1829, Morse returned to Europe to restudy classical paintings in preparation for being chosen to paint one of the four large panels in the Rotunda of the new Capitol in Washington, DC. He first became interested in the telegraph during discussions about electromagnetism with a group of passengers on the ship *Sully* during his return trip from Europe in 1832. Despite the strong support of his fellow artists, he was not chosen to participate in the Capitol project. Disillusioned and shaken, despite being appointed New York University's first professor of fine arts in 1834 and continuing to serve as president of the National Academy, Morse painted relatively little after 1835 and worked feverishly on the development of the telegraph.

Morse had a basic knowledge of electromagnetism from his exposure to scientists at Yale. By the time Morse left the *Sully* in 1832, he had already recorded in his notebook some basic ideas on the development of the telegraph, including the first rudiments of the Morse code. By 1837 he had developed a working model, but he struggled to get support for the following 6 years. In 1843, a Congressional appropriation allowed him to string a telegraph line from Baltimore, MD, to the Supreme Court in Washington, DC, where on May 24, 1844, Morse tapped out his famous message: "What hath God wrought."

The telegraph earned Morse the prosperity that he had never achieved as a painter. Despite this security, this American Leonardo never returned to painting, which had given him his early fame, and died a world-renowned figure in 1872.



Samuel F. B. Morse (1791–1872). *Dr. Frederick Gore King*. Oil on canvas, 34.5 × 27.5 in. National Academy of Design, New York.

¹ Department of Radiology, Mount Auburn Hospital, 330 Mount Auburn St., Cambridge, MA 02238.
AJR 156:1180, June 1991 0361-803X/91/1566-1180 © American Roentgen Ray Society

Altered Swallowing Function in Elderly Patients Without Dysphagia: Radiologic Findings in 56 Cases

Olle Ekberg^{1,2}
Michael J. Feinberg³

Swallowing disorder is an increasing problem in our aging population. A majority of these patients have a functional abnormality of the oral, pharyngeal, and/or esophageal stage of swallowing. However, what constitutes normalcy is not well understood, and baseline swallowing in elderly persons without dysphagia has not been adequately described. We therefore evaluated 56 persons with a mean age of 83 years who had no symptoms of dysphagia or eating difficulty. Videofluoroscopy and radiographs with the subject erect and recumbent were obtained. Normal deglutition, as defined in young persons, was present in only 16%. Oral abnormalities (difficulty ingesting, controlling, and delivering bolus relative to swallowing initiation) were seen in 63%. Pharyngeal dysfunction (bolus retention and lingual propulsion or pharyngeal constrictor paresis) was seen in 25%. Pharyngoesophageal segment abnormalities were observed in 39% (mostly cricopharyngeal muscle dysfunction). Esophageal abnormalities (mostly motor in nature) were observed in 36%.

What has been described as swallowing dysfunction in young persons may not be abnormal in very elderly persons. It is difficult to distinguish the effect of normal aging from the effects of specific diseases or gradual degenerative changes.

AJR 156:1181-1184, June 1991

Swallowing impairment increases in prevalence with advancing age and is a major health care problem in the aged [1-5]. Dynamic imaging has become an important part of the diagnostic workup of elderly patients with signs or symptoms of deglutition problems. The oral, pharyngeal, and esophageal stages are not as efficient or synchronous in these persons. However, it is not always clear when the observed alterations represent pathologic changes or are caused by the aging process itself. Developing criteria of normalcy for such a complex function is difficult even in younger populations. Previous studies [6, 7] of pharyngeal function in asymptomatic persons have demonstrated considerable variation in morphodynamics. Recently, small cross-sectional investigations of normal oropharyngeal function have documented changes in the duration of bolus movement and various other events that are related to aging [8-10]. To our knowledge no studies examining the prevalence of functional alterations that are commonly considered abnormal in the very aged have been done. The purpose of our work was to examine deglutition in an asymptomatic elderly population.

Received October 15, 1990; accepted after revision December 31, 1990.

¹ Department of Radiology, Hospital of the University of Pennsylvania, 3400 Spruce St., Philadelphia, PA 19104.

² Present address: Department of Radiology, Malmö General Hospital, S-21401 Malmö, Sweden. Address reprint requests to O. Ekberg.

³ Department of Radiology, Albert Einstein Medical Center, York and Tabor Rds., Philadelphia, PA 19141.

0361-803X/91/1566-1181

© American Roentgen Ray Society

Materials and Methods

Patients who were referred for examination of the upper gastrointestinal tract were asked to participate. During the routine upright ingestion of liquid barium for double-contrast examination, the ingestion, oral cavity, pharynx, and esophagus were examined during fluoroscopy and video (VHS), in lateral and frontal projection, as well as oblique projection of the esophagus with the patient prone or supine.

The patients were asked to take a mouthful of barium from a cup and then hold it in the

mouth to test for adequacy of containment. The volume taken was not controlled or registered but was that of the patient's own discretion. They were then asked to swallow on command. At least two swallows in lateral projection centered over the oral cavity and two centered over the pharynx were imaged. An additional two swallows centered over the mouth and pharynx in frontal projection were imaged. In an erect position, the patient also was given one teaspoon of barium paste, which was monitored in lateral projection, following the paste from ingestion until it reached the stomach. Oral and pharyngeal function was assessed only in an erect position and not recumbent. The esophagus was then examined with the patient erect. The barium used was EZ-HD, with a barium content of 250% w/v. When deemed necessary, the esophagus was examined with the patient recumbent also, with a 50% w/v barium suspension. This triphasic examination was attempted in all nonaspirators.

A total of 56 patients were included. They denied any prior or present difficulties with swallowing. Caregivers accompanying some patients confirmed the presence of a normal swallowing behavior.

There were 22 men and 34 women ranging in age from 72 to 93 years (mean, 83 years). Of the patients, 31 had no history of neurologic disease known to impair swallowing. The rest of the patients (25 persons) had such a history, namely dementia in 15 patients, Parkinson disease in seven patients, and cerebrovascular disease in three patients.

Results

The results are summarized in Table 1. A synchronous and symmetric swallowing function without morphodynamic abnormalities was seen in only nine patients (16%). Few struc-

TABLE 1: Swallowing Function in 56 Elderly Persons Without Dysphagia

Function	No. (%)
Normal function	
Oral, pharyngeal, pharyngoesophageal segment, and esophageal function	9 (16)
Misdirected swallowing	
In subepiglottic segment of laryngeal vestibule	11 (20)
Minor into supraglottic segment of laryngeal vestibule or trachea	25 (45)
Oral dysfunction	
Sensorimotor incoordination	9 (16)
Too large or rapid ingestion	8 (14)
Leak	7 (13)
Dissociation	20 (36)
Pharyngeal dysfunction	
Defective closure of laryngeal vestibule	3 (5)
Retention	11 (20)
Defective oropharyngeal propulsion	6 (11)
Defective down tilt of epiglottis	4 (7)
Constrictor paresis	5 (9)
Pharyngoesophageal segment dysfunction	
Defective opening	13 (23)
Early closure (only)	4 (7)
Web	3 (5)
Killian-Jamieson diverticulum ^a	2 (4)
Zenker diverticulum	1 (2)
Esophageal	
Dysfunction	20 (36)
Esophagitis	3 (5)

^a This diverticulum protrudes inferior to the cricopharyngeal muscle and laterally [11].

tural or morphodynamic abnormalities were seen; these included webs, rings, diverticula, esophagitis, and hiatal hernia.

The most common dysfunction was found in the oral stage of swallowing. The oral stage is voluntarily controlled, although it is largely automatic. Incoordination of sensorimotor behavior refers to the bolus being held in an abnormal position or processed for a considerable time before swallowing. Ingestion of too big a bolus or ingestion that was too rapid was common. The structure and function of the oral cavity in these elderly persons are not sufficient for what they put in their mouths. This may also explain why a high frequency of dissociation between the oral and pharyngeal stages was found. Muscular weakness or impaired afferent information caused leakage of barium from the oral cavity over the back of the tongue in seven patients.

Altered function in the pharyngoesophageal segment was most frequently seen as defective opening at the level of the cricopharyngeal muscle. Other abnormalities in the pharyngoesophageal segment were morphodynamic, such as webs and diverticula. Webs were moderate in depth and seen only during maximal distension of the pharyngoesophageal segment. They caused no retention of barium craniad to them. Interestingly, diverticula of Killian-Jamieson type were more common than those of Zenker type.

Patients with a history of neurologic disease known to impair swallowing had a higher frequency of dysfunctions than did patients with no such history. This was particularly true for oral sensorimotor incoordination (32% vs 3%), dissociation between the oral and pharyngeal stages (48% vs 26%, Fig 1), and constrictor paresis (20% vs 0%).

Of 36 patients (64%) who had misdirected swallowing, 16 (44%) had oral dysfunction only, four (11%) had pharyngeal dysfunction only, and eight (22%) had both oral and pharyngeal dysfunction.

Esophageal dysfunction was present in 20 patients (36%). Twelve patients had hiatal hernia, and three of these had esophagitis due to gastroesophageal reflux as well.

Discussion

Swallowing in younger persons without dysphagia has been shown to be symmetric and synchronous [6, 7]. Compared with an earlier study [6] that addressed swallowing in asymptomatic younger persons (mean age, 52 years), we found that elderly persons had a much higher frequency of abnormalities. The frequency of normal function in that series of younger persons was about 20% and is of the same magnitude as that observed in a prior study of dysphagic patients that included patients over the age of 75 years. This circumstance may indicate that there is a subpopulation of patients who have a more stable swallowing function than the rest have. In the nondysphagic population, they may represent those with a true normalcy, whereas in the dysphagic population, they may have dysphagia for other reasons, and the reason is not revealed during the radiologic study. Selection of patients may be biased in that they already were scheduled for a barium examination of the upper gastrointestinal tract. Our

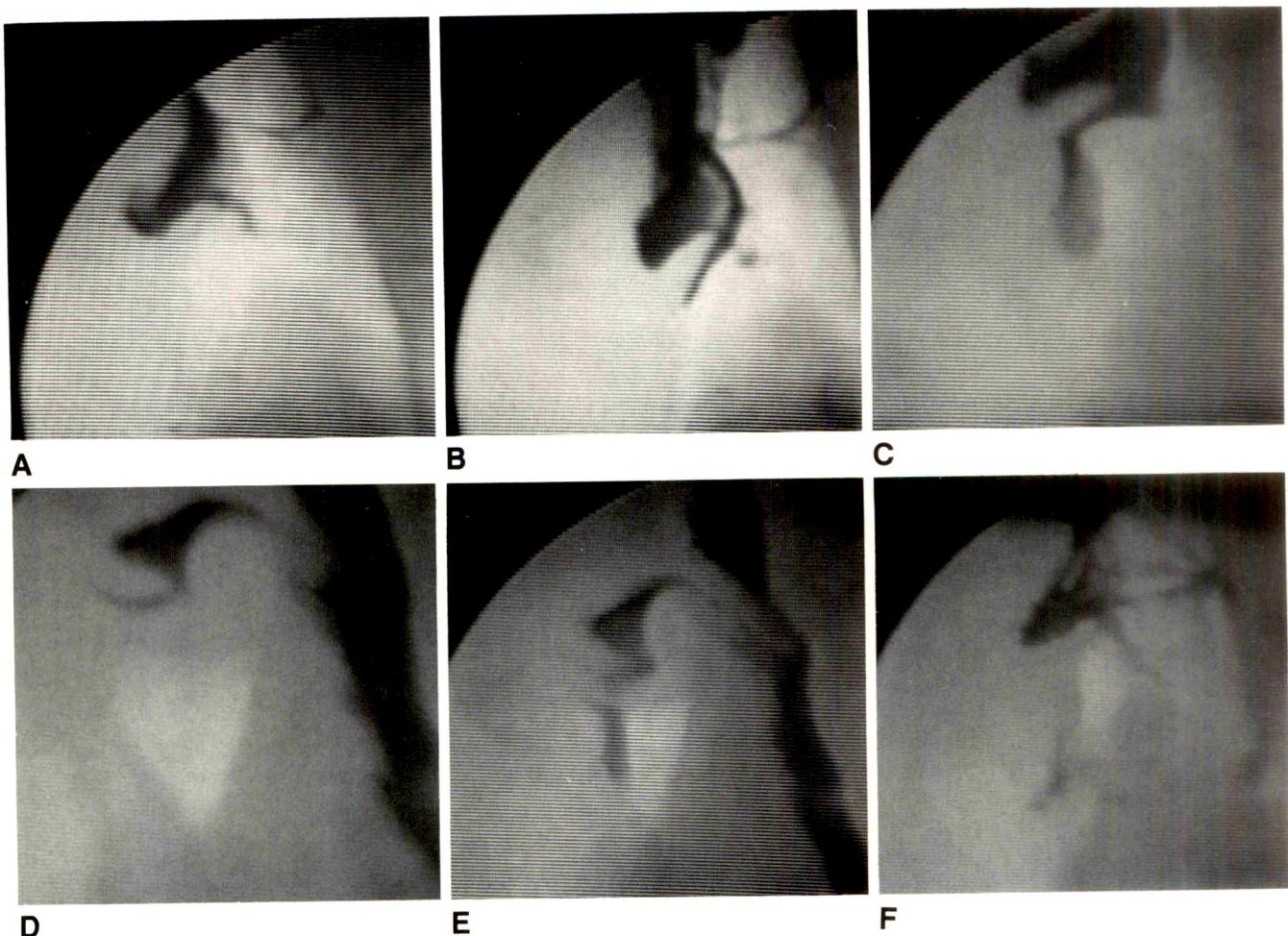


Fig. 1.—*A–F*, Sequence from a videoradiographic examination of barium swallow in an elderly patient without dysphagia. Barium flows over back of tongue into valleculae (*A*). Barium also reaches into subepiglottic segment of laryngeal vestibule (*B*) and further down into supraglottic segment (*C*). A 3-sec delay occurs before pharyngeal swallow is elicited (*D*). Barium is squirted inferiorly beyond vocal cords into trachea (*E*). After swallowing, no barium is retained in pharynx (*F*). Misdirection of barium was solely due to dissociation of oral and pharyngeal stages of swallowing. It is not clear whether this is due to afferent or efferent deficit or a central-processing impairment.

inclusion criteria were the same as we used before [6], but were not as rigorous as those of Curtis et al. [7].

The effect of aging on response programming has been shown to imply an increase in reaction time, especially with increasing complexity of the movements; that is, older people require progressively more time to react after interpretation of afferent information [12]. Any afferent stimulus needs to be coded and identified and the appropriate response determined. Older persons require more time for processing the signal. However, older persons are not different in the processing of complex movement, but simply slower [13].

It has been shown that muscle strength declines with age [14]. This is primarily related to a decline in muscle mass but also to a change in morphology and biochemistry, that is, alteration of muscle fiber composition with decrease in size of fast-twitch fibers (type 2) [15]. However, the number of functioning muscle motor units declines with age [16]. The remaining motor units are enlarged and tend to have fewer fast-twitch fibers. These enlarged motor units partially main-

tain muscle mass, even when strength deteriorates. The pressure created between the tongue and the palate also has been shown to decrease with age [9]. Oral transit time also decreases with age [10]. To such neuromotor impairment is added the decrease in chemosensory perception with age that diminishes the senses of taste and smell [17].

Altered function in the pharyngoesophageal segment was six times as common in older persons as in younger asymptomatic subjects [6]. A prior study also has shown a decrease in time of opening of the pharyngoesophageal segment with age [8]. Moreover, compliance of the pharyngoesophageal segment diminishes with age and is seen as decreased maximal opening [10]. In two prior studies of patients with dysphagia, the close correlation between age and cricopharyngeal dysfunction was pointed out [1, 18]. A close relationship also exists between such incoordination and other swallowing dysfunctions [19]. The underlying pathophysiology is not well understood. However, a high frequency of fibrosis was found in a histopathologic study [20]. In patients with a visible

cricopharyngeus during the whole span of swallowing, fibrosis is likely, whereas a neuromotor dysfunction is seen as a transient indentation. Such dysfunction also is likely to account for defective closure between swallows.

Only two prior studies seem to have approached the changing function of the esophagus in very old persons. In one of these studies, dysfunction (i.e., absent or weak peristalsis and tertiary peristalsis) was prevalent [21]. In another study, however, disordered motility was regularly associated with disease [22]. The prevalence of motor dysfunction in our study may indicate that these persons in fact have subclinical disease.

The observed aberrations may be explained merely by the test situation. Many patients complain about the taste and consistency of the barium suspension. Also, the unfamiliar environment in the radiography suite may add to a stressful situation. A highly standardized technique must be used to position the patient. Alignment and slight extension of the neck may induce decompensation. However, every effort was made to keep the patient as comfortable as possible during the test.

The altered function observed may be due to normal aging (primary aging). However, we do not know if our study population suffered from subclinical disease, or disease in an early stage, such as neuromuscular disease (secondary aging). Such disease might affect afferent or efferent control and include central dissociation. This is a likely explanation in the patients with different types of neurologic disease. The degenerative changes may already have involved areas of importance for swallowing, even though the patients were asymptomatic. However, some of the patients did not have any disease known to potentially involve swallowing. Such neurologic disease might involve the CNS as, for example, gray and white matter disease does. Neuropathy, such as that seen in diabetes and alcoholism, also may be subclinical but still have importance for oral and pharyngeal function.

Our conclusion is, therefore, that nondysphagic elderly persons have altered function without impairment. The most common problem is oral sensorimotor incoordination. However, the gaps in our knowledge of the true cause of dysphagia and swallowing dysfunction do not invalidate the observations made during radiologic evaluation of barium swallowing. These facts also make assessment of dysphagic elderly persons difficult, because the distinction between altered function due to normal aging and altered function due to disease is not clear. However, misdirection of barium into

the airways was always minor in asymptomatic elderly persons. Therefore, major aspiration is likely to be due to disease and not to be a result of normal aging.

REFERENCES

- Ekberg O, Wahlgren L. Dysfunction of pharyngeal swallowing: a cineradiographic study in 854 dysphagial patients. *Acta Radiol* 1985;26:389-395
- Borgström PS, Ekberg O. Pharyngeal dysfunction in the elderly. *J Diagn Imaging* 1988;2:74-81
- Sheth N, Diner WC. Swallowing problems in the elderly. *Dysphagia* 1988;2:209-215
- Groher ME, Bukatman R. The prevalence of swallowing disorders in two teaching hospitals. *Dysphagia* 1986;1:3-6
- Donner MW, Jones B. Editorial. *Gastrointest Radiol* 1985;10:194-195
- Ekberg O, Nylander G. Cineradiography of the pharyngeal stage of deglutition in 150 individuals without dysphagia. *Br J Radiol* 1982;55:255-257
- Curtis DJ, Cruess DF, Dachman AH. Normal erect swallowing: normal function and incidence of variations. *Invest Radiol* 1985;20:717-726
- Tracy JF, Logemann JA, Kahrilas PJ, Jacob P, Kobara M, Krugler C. Preliminary observations on the effects of age on oropharyngeal deglutition. *Dysphagia* 1989;4:90-94
- Shaker R, Dodds WJ, Hogan WJ, Stember AK. Effect of aging on swallow-induced lingual palatal closure pressure. *Gastroenterology* 1990;98:1478-1484
- Shaw DW, Cook IJ, Dent J, et al. Age influences oropharyngeal and upper esophageal sphincter function during swallowing. *Gastroenterology* 1990;98:A390
- Ekberg O, Nylander G. Lateral diverticula from the pharyngo-esophageal junction area. *Radiology* 1983;146:117-122
- Light KE, Spirduso WW. Effects of adult aging on the movement complexity factor of response programming. *J Gerontol* 1990;45P:107-109
- Larish DD, Stelmach GE. Preprogramming, programming, and reprogramming of aimed hand movements as a function of age. *J Motor Behavior* 1982;14:322-340
- Kullman DA, Plato CC, Tobin JD. The role of muscle loss in the age-related decline of grip strength: cross-sectional and longitudinal perspectives. *J Gerontol* 1990;45M:82-88
- Clarkson PM, Kroll W, Melchionda AM. Age, isometric strength, rate of tension development of fibre type composition. *J Gerontol* 1981;36:648-753
- Campbell MJ, McComas AJ, Petito F. Physiological changes in aging muscles. *J Neurol Neurosurg Psychiatry* 1973;36:174-182
- Moeller T. Sensory changes in the elderly. *Dent Clin North Am* 1989;33:25-31
- Curtis DJ, Cruess DF, Berg T. The cricopharyngeal muscle: a video-recording review. *AJR* 1984;142:497-500
- Ekberg O, Wahlgren L. Pharyngeal dysfunctions and their interrelationship in patients with dysphagia. *Acta Radiol* 1985;26:659-664
- Torres WE, Clements JL, Austin GE, Knight K. Cricopharyngeal muscle hypertrophy: radiologic-anatomic correlation. *AJR* 1984;141:927-930
- Soergel KH, Zboralske FF, Amberg JR. Presbyesophagus: esophageal motility in nonagenarians. *J Clin Invest* 1964;48:1472-1478
- Hollis JB, Castell DO. Esophageal function in elderly men: a new look at "presbyoesophagus." *Ann Intern Med* 1974;80:371-374

Pictorial Essay

Peritoneal Carcinomatosis with Ascites

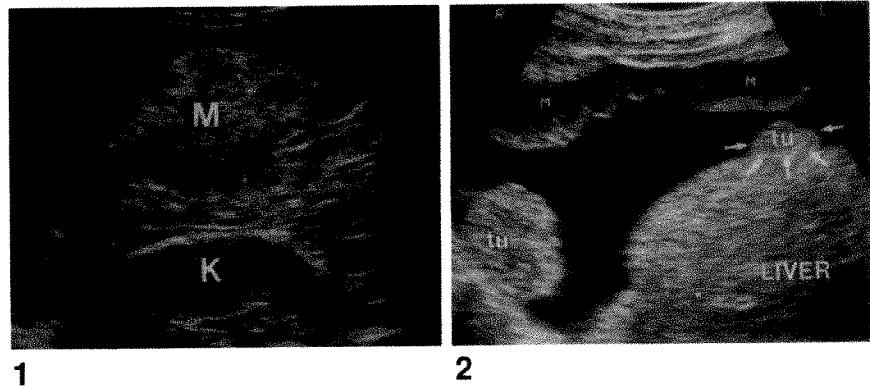
Christian Goerg¹ and Wolf-B. Schwerk²

This essay illustrates the sonographic features of peritoneal carcinomatosis by reviewing our experience with 65 patients in whom malignant ascites was proved pathologically.

The diagnosis of malignant ascites was one of the earliest uses of abdominal sonography [1–4]. The purpose of this essay is to illustrate the sonographic features of peritoneal carcinomatosis on the basis of our experience with 65 patients with pathologically proved malignant ascites. The distribution of the fluid and the presence of peritoneal metastases, intestinal adhesions, omental matting, intraabdominal masses, lymphadenopathy, and hepatic metastases were evaluated in each case. Patients were studied with an electronic real-time scanner with curved-array transducers (LSC, Picker International, Highland Heights, OH). Scans were obtained with 3.5- and 5.0-MHz transducers.

Fig. 1.—Direct visualization of peritoneal metastases. Sonogram in a patient with malignant melanoma and malignant ascites shows nodular tumor (M) in visceral peritoneum. K = kidney.

Fig. 2.—Direct visualization of peritoneal metastases. Sonogram in a patient with hypernephroma shows predominantly sheetlike metastases (M) in parietal peritoneum and nodular tumor (tu) in visceral peritoneum (arrows).



Received June 14, 1990; accepted after revision December 4, 1990.

¹ Department of Internal Medicine, Division of Hematology/Oncology, Philipps-University, Baldingerstrasse, D-3550 Marburg, Germany. Address reprint requests to C. Goerg.

² Department of Internal Medicine, Division of Gastroenterology, Philipps-University, D-3550 Marburg, Germany.

AJR 156:1185–1187, June 1991 0361-803X/91/1566-1185 © American Roentgen Ray Society

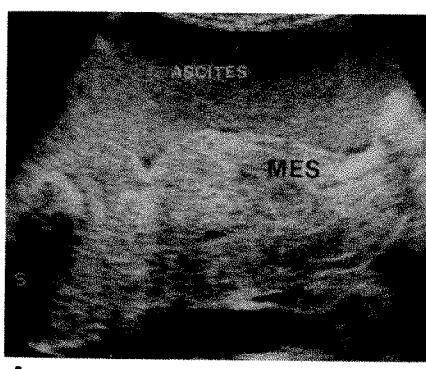
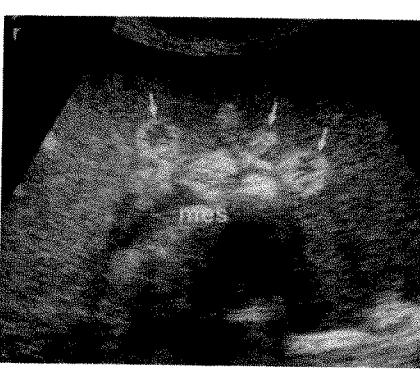
**A****B**

Fig. 3.—Nonspecific signs of malignant ascites.
A, Longitudinal sonogram in a patient with malignant lymphoma shows multiple echoes in ascites and echogenic bowel mesentery (MES). Paracentesis revealed chylous ascites. S = shadow of bowel loop.

B, Transverse sonogram shows adhesions of bowel loops (arrows) to mesenteric root. Laparotomy revealed lymphomatous involvement of mesenteric structures.

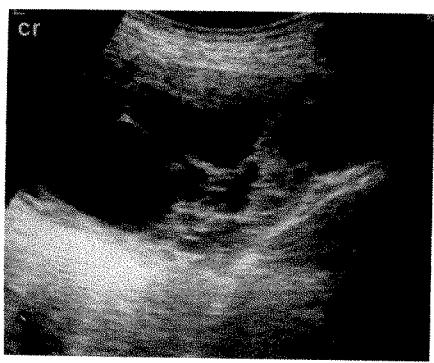
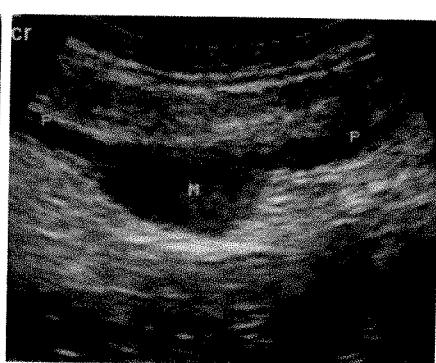
**A****B**

Fig. 4.—Indirect and direct signs of peritoneal carcinomatosis.

A, Sonogram in a patient with hypernephroma shows multiseptate ascites.

B, Sonogram shows direct visualization of nodular metastasis (M) in parietal peritoneum (P).

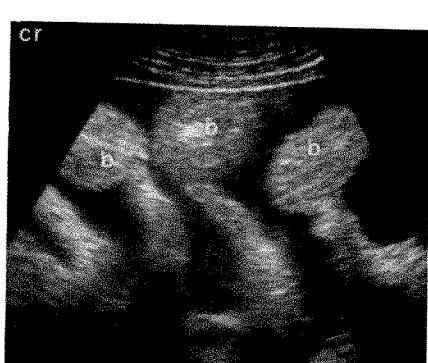


Fig. 5.—Transudative ascites. Sonogram in a patient with right ventricular failure shows fluid dispersed throughout abdomen; bowel loops (b) were seen to float freely within ascites and assume a vertical position.

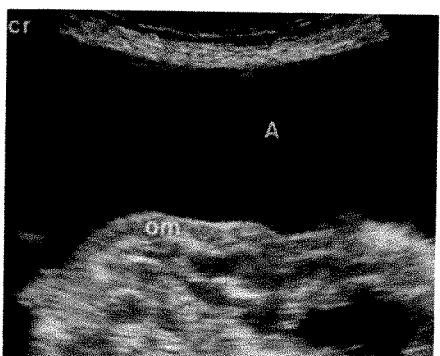
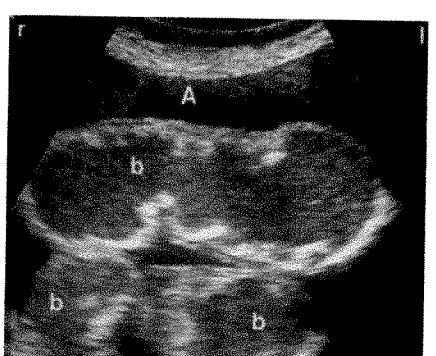
**A****B**

Fig. 6.—Nonspecific signs of malignant ascites.

A, Longitudinal sonogram in a patient with gastric carcinoma and a large amount of ascites (A) shows compressed omentum (om) adherent to adjacent structures during real-time examination.

B, Transverse sonogram shows echogenic bowel walls (b) matted together during real-time examination.

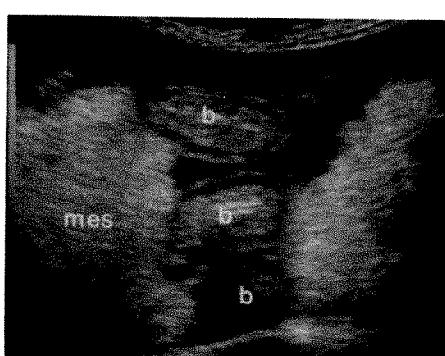
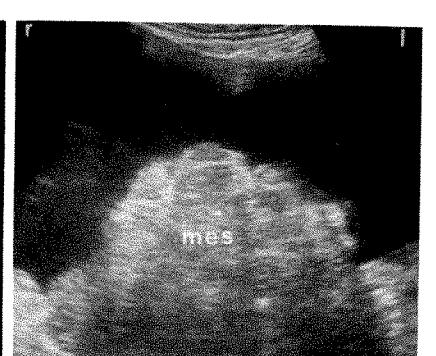
**7****8**

Fig. 7.—Nonspecific signs of malignant ascites. Sonogram in a patient with histologically proved carcinoid of mesenteric root (mes). Bowel loops (b) were adherent to mesentery during real-time examination.

Fig. 8.—Nonspecific signs of malignant ascites. Sonogram in a patient with adenocarcinoma of occult primary tumor and malignant ascites shows shrinkage of bowel mesentery (mes). Bowel loops were adherent to mesentery during real-time examination.

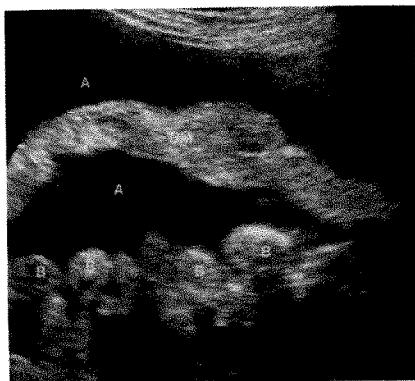


Fig. 9.—Nonspecific signs of malignant ascites. Sonogram in a patient with rhabdomyosarcoma of pelvic cavity and ascites (A) shows diffuse enlargement of greater omentum (OM). Compression and displacement of small-bowel loops (B) were appreciated during real-time examination.

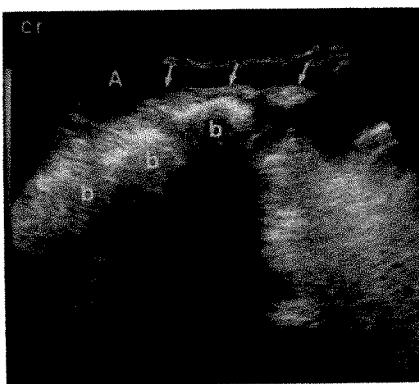


Fig. 10.—Nonspecific signs of malignant ascites. Sonogram in a patient with uterine cancer and a small amount of ascites (A) shows matted bowel loops (b) attached to greater omentum (arrows) during real-time examination. Laparotomy revealed peritoneal carcinomatosis.

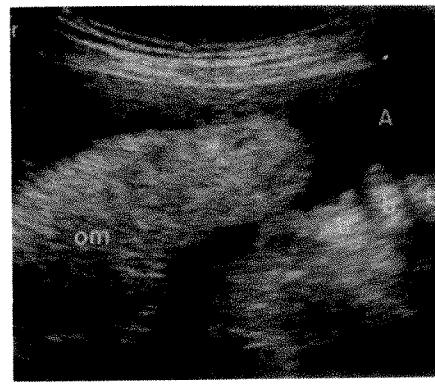


Fig. 11.—Nonspecific signs of malignant ascites. Sonogram in a patient with malignant ascites (A) of unknown origin shows diffuse enlargement of greater omentum (om). Bowel loops (b) appeared attached during real-time examination. Fine-needle aspiration revealed metastatic tumor of greater omentum.

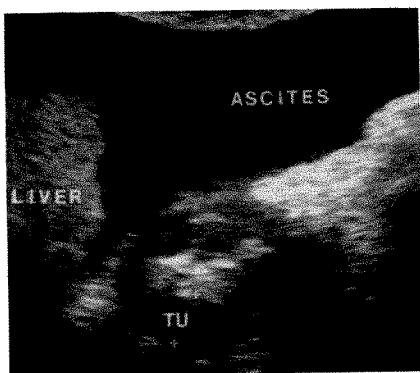


Fig. 12.—Nonspecific signs of malignant ascites. Sonogram in a patient with marked ascites shows thickening (TU) of gastric antrum resulting from histologically proved gastric carcinoma.



Fig. 13.—Nonspecific signs of malignant ascites. Sonogram shows marked ascites (A) and a large echogenic intraabdominal mass (TU). Small-bowel loops (B) appeared compressed and displaced. Fine-needle biopsy revealed ovarian cancer.

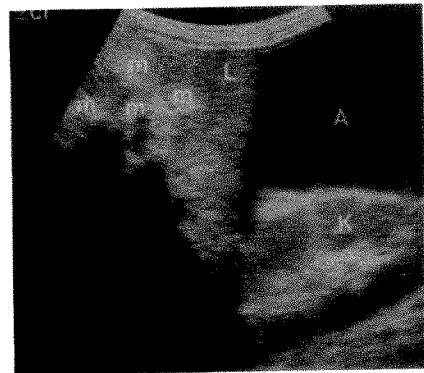


Fig. 14.—Nonspecific signs of malignant ascites. Sonogram in a patient with colonic cancer and large amount of ascites (A) shows calcification of liver metastases (m). L = liver, K = kidney.

due to fat globules in a proteinaceous fluid, chylous ascites, or hemoperitoneum (Fig. 3). Septa with interlacing linear bands of echoes within the intraperitoneal fluid occurs (Fig. 4). In patients with ascites due to portal hypertension, loops of small bowel are often draped around the mesentery and assume a vertical position (Fig. 5).

Bowel loops should be considered matted only if they are not consistently separated by fluid on real-time examination despite changes in position (Figs. 6–8). The greater omentum, which can be identified in the presence of ascites (Fig. 9), may be bound to the bowel (Fig. 10) or infiltrated with tumor (Fig. 11). Ancillary findings such as lymphadenopathy, intraabdominal masses (Figs. 12 and 13), or hepatic metastases

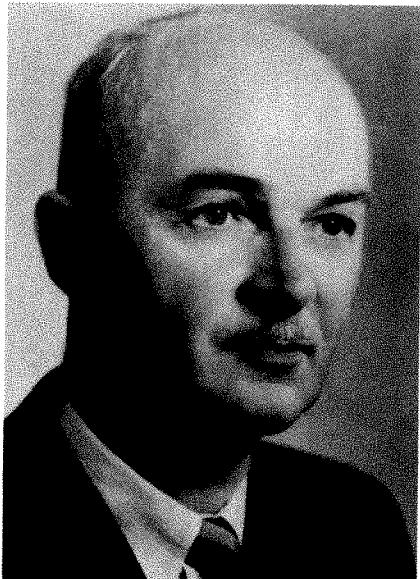
(Fig. 14) are often helpful in distinguishing benign from malignant ascites.

REFERENCES

1. Goldberg BB. Ultrasonic evaluation of intraperitoneal fluid. *JAMA* 1976;235:2427–2430
2. Yeh HC, Wolf BS. Ultrasonography in ascites. *Radiology* 1977;124:783–790
3. Edell SL, Geffer WB. Ultrasonic differentiation of types of ascites fluid. *AJR* 1979;133:111–114
4. Tsujimoto F, Miyamoto Y, Tada S. Differentiation of benign from malignant ascites by sonographic evaluation of gallbladder wall. *Radiology* 1985;157:503–504

Memorial

Robert Alexander MacPherson, 1903–1990



Robert A. MacPherson graduated with a degree in medicine from Queen's University in Kingston, Ontario, in 1929 and subsequently trained there in radiology. After practice in Ontario, he moved to Winnipeg in 1939 and became head of radiology in 1948 at the University of Manitoba and the Winnipeg General Hospital. He had a profound influence on local radiology and medical practice.

The times were difficult during his career. His training and early practice took place

during the depression. When he came to Winnipeg, the depression still lingered, and Canada entered World War II. Postwar reconstruction took time, but the foundations for a larger and stronger department were set. He recruited Arthur E. Childe, who was a world leader in neuroradiology and pediatric radiology and the author of the section on neuroradiology in *Golden's Looseleaf Textbook of Radiology*, which was widely used by most residents in Canada and the United States. Drs. MacPherson and Childe had their private practice in the Medical Arts Building, where most of the heads of the clinical departments of the University of Manitoba had their offices. The partnership provided radiology services to the two largest medical clinics in Canada. Most of the members of the clinics attended at the Winnipeg General Hospital and taught at the University. Dr. Childe was the director of the radiology department of the Winnipeg Children's Hospital. The secretary of MacPherson and Childe's private office managed the University radiology department.

It was a time of volunteer teaching and research. The residents were few, but well trained. The teaching hospitals cared for a large number of indigent patients. The members of the attending staff worked in hospitals in the morning and consulted with their private patients in the afternoon. The formal teaching rounds in radiology occurred in the private office between 5 p.m. and 6 p.m. on Monday afternoons, and the attending staff discussed the cases while the residents observed. Personal instruction was the order of

the day, rather than the organized departments of the present.

At the time, the American Roentgen Ray Society chose its members after the presentation of a thesis. "Bob" MacPherson's thesis was on gastrointestinal radiology, of which he was a master. His hands were dry from excessive radiation from abdominal palpation in the era of dark adaptation and red goggles.

He served as director of the Medical Arts Building in 1961–1962, a recognition by his fellow physicians, who had great confidence in his leadership. He was president of the Canadian Association of Radiologists in 1953, a Royal College examiner for certification in diagnostic radiology, and a member of the executive committee that organized the International Congress of Radiology in Montreal.

After Bob's retirement, his successor relied heavily on him for guidance, and the department underwent considerable expansion of its space, with the introduction of a modern large residency program. Unfortunately, Dr. MacPherson was denied a planned decade of golf in Florida, visits to grandchildren, and service to his original alma mater. He had undergone a gastrectomy many years before, and failure to detect peripheral neuropathy led to an invalid state, which he bore with dignity and with great support from his wife, Maxine. He is survived by three children and 11 grandchildren. He is remembered as an important leader in the evolution of Canadian radiology.

Douglas W. MacEwan
Winnipeg, Manitoba, Canada R3A 1R9

Case Report

Diffuse Intraabdominal Lymphoma Complicating Idiopathic Myelofibrosis: CT Demonstration

Philip Goodman,¹ Rajendra Kumar,¹ and Jack B. Alperin²

Idiopathic myelofibrosis with myeloid metaplasia is an uncommon condition in which primary fibrosis of the bone marrow is associated with extramedullary hematopoiesis. Intraabdominal involvement in this disease is usually confined to the spleen, liver, and lymph nodes but may include a wide variety of other sites [1, 2].

Several recent reports have noted the development of non-Hodgkin lymphoma in patients with idiopathic myelofibrosis [3–5]. We present CT findings in a patient with myelofibrosis and concomitant intraabdominal extramedullary hematopoiesis and lymphoma. To our knowledge, the CT appearance of intraabdominal lymphoma with extramedullary hematopoiesis complicating myelofibrosis has not been previously reported.

Case Report

A 70-year-old woman had weakness, dizziness, and dyspnea on exertion. Her history was significant only for treatment of chronic anemia, and physical examination was normal except for a pulse rate of 88 beats per minute, marked pallor, and splenomegaly. Complete blood count showed pancytopenia with severe normocytic anemia. Bone marrow could not be aspirated. A bone marrow biopsy showed myelofibrosis. A radionuclide bone marrow scan revealed severely diminished bone marrow activity.

The patient required multiple transfusions of packed RBCs, and 4 months after the initial presentation a splenectomy was performed to decrease erythrocyte sequestration. Except for hepatosplenomegaly, no obvious abnormalities were noted in the abdomen at the time of

surgery. Pathologic examination of the spleen showed myeloid metaplasia. She remained transfusion-dependent despite treatment with interferon, immunoglobulin G, and steroids.

Five months later, the patient complained of increasing lower abdominal pain, distention, and constipation. On physical examination, firm mobile masses were palpated in the lower abdomen, and rectal examination revealed guaiac-positive stool. Abdominal CT scan showed multiple low-density masses in the subcapsular portion of the liver, with focal extension into the hepatic parenchyma. Bulky masses were noted in the omentum, mesentery, and peripancreatic region also (Fig. 1). Percutaneous biopsy of one of these masses revealed myeloid metaplasia with numerous atypical cell forms.

In order to relieve the patient's obstructive bowel symptoms, low-dose radiation therapy was administered to the entire abdomen, including the pelvis, during the next 3 weeks, for a total dose of 1000 cGy. After treatment, the patient's symptoms resolved, and on physical examination, the palpable abdominal masses were found to have decreased in size.

Shortly after discharge from the hospital, the patient was readmitted with severe gastrointestinal bleeding and hypotension. Upper gastrointestinal tract endoscopy revealed a bleeding ulcer in the gastric antrum. Despite heater probe applications, the ulcer continued to bleed and required surgical treatment consisting of vagotomy, pyloroplasty, and oversewing of the ulcer. Extensive masses were noted in the abdomen, and biopsies of the greater omentum and the peritoneal wall were performed. Pathologic examination of the biopsy specimens revealed large-cell lymphoma, which was of B-cell type on immunohistochemical staining.

A coagulopathy then developed that led to bleeding into the abdomen. Two liters of blood were evacuated from the peritoneal cavity during a second exploratory laparotomy. Postoperatively, the patient continued to bleed because of disseminated intravascular

Received December 17, 1990; accepted January 10, 1991.

¹ Department of Radiology, The University of Texas Medical Branch, Galveston, TX 77550. Address reprint requests to P. Goodman.

² Department of Internal Medicine, Division of Hematology-Oncology, The University of Texas Medical Branch, Galveston, TX 77550.

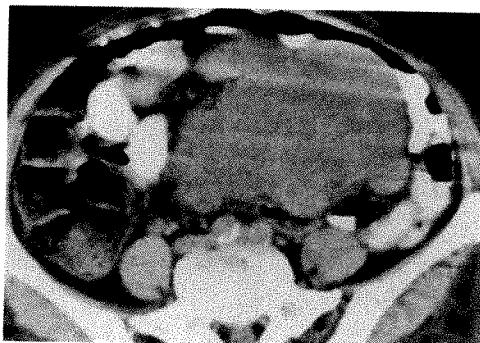


Fig. 1.—CT scan at level of iliac crests shows a large homogeneous intraabdominal mass displacing loops of bowel.

coagulation. Despite massive transfusions of blood components, she died approximately 1 year after her initial presentation.

Discussion

Idiopathic myelofibrosis with myeloid metaplasia is a chronic disease characterized by fibrosis of the bone marrow and development of extramedullary hematopoiesis. Hepatosplenomegaly, anemia, and a leukoerythroblastic blood count are hallmarks of this condition. Death usually results from complications, including hemorrhage, infection, and cardiovascular disease [1, 2].

The most common sites of extramedullary hematopoiesis are the spleen, liver, and lymph nodes. Diverse areas of involvement, due to the presence of multipotential stem cells in mesenchymal tissues, have also been reported in the thorax, CNS, and abdomen. Although these foci of extramedullary hematopoiesis are often asymptomatic, occasionally they may be large enough to produce significant complications such as spinal cord compression, pleural or pericardial effusion, ascites, and bowel obstruction [1, 2].

Involvement of intraabdominal and retroperitoneal structures by extramedullary hematopoiesis may also mimic lymphoma or other intraabdominal neoplasms on CT and sonography, thereby resulting in delayed or incorrect diagnosis and treatment [6, 7]. Moreover, several case reports have described patients with intraabdominal extramedullary hematopoiesis associated with idiopathic myelofibrosis in whom non-Hodgkin lymphoma developed without prior treatment with radiation or cytotoxic drugs [3–5]. Both radiation and cytotoxic drugs had been implicated in the previously reported cases of malignant transformation in idiopathic myelofibrosis [1, 8].

In our patient, the diffuse intraabdominal masses seen on CT were not present at the time of splenectomy 5 months earlier, and she had not received radiation therapy or cytotoxic chemotherapy before their appearance. This case thus represents spontaneous development of diffuse intraabdominal lymphoma in a patient whose initial bone marrow biopsies were consistent with idiopathic myelofibrosis. Although a coincidental association is considered unlikely, the pathogenesis of lymphoma complicating idiopathic myelofibrosis is uncertain. Immune mechanisms may play a role, because immunologic abnormalities have been documented in both lymphoma and idiopathic myelofibrosis [4, 5]. Another theory suggests that both diseases may develop from an abnormality affecting a common pluripotential stem cell [4, 5].

Diffuse intraabdominal lymphoma can mimic extramedullary hematopoiesis on CT scans [6, 7]. For this reason, radiologists must be careful to include both conditions in the differential diagnosis of intraabdominal masses in patients with idiopathic myelofibrosis. Although CT provides information regarding the presence of intraabdominal masses and their extent, a percutaneous thin-needle aspiration biopsy is essential for differentiating these two complications in patients with myelofibrosis [7].

ACKNOWLEDGMENT

We are grateful to Ray A. Verm of Houston, TX, for providing additional clinical information about the patient presented in this manuscript.

REFERENCES

1. Glew RH, Haese WH, McIntyre PA. Myeloid metaplasia with myelofibrosis: the clinical spectrum of extramedullary hematopoiesis and tumor formation. *Johns Hopkins Med J* 1973;132:253–265
2. Shaver RW, Clore FC. Extramedullary hematopoiesis in myeloid metaplasia. *AJR* 1981;137:874–876
3. Jennings WH, Li C-Y, Kiely JM. Concomitant myelofibrosis with agnogenic myeloid metaplasia and malignant lymphoma. *Mayo Clin Proc* 1983;58:617–619
4. Epstein RJ, Joshua DE, Kronenberg H. Idiopathic myelofibrosis complicated by lymphoma: report of two cases. *Acta Haematol* 1985;73:40–44
5. Bogliolo GV, Lerza RA, Ruggieri C, Pannacciulli IM. Occurrence of spontaneous malignant lymphoma in the course of idiopathic myelofibrosis. *Am J Hematol* 1988;27:230–232
6. Koehler PR, Mancuso AA. Pitfalls in the diagnosis of retroperitoneal adenopathy. *J Can Assoc Radiol* 1982;33:197–201
7. Shawker TH, Hill M, Hill S, Garra B. Ultrasound appearance of extramedullary hematopoiesis. *J Ultrasound Med* 1987;6:283–290
8. Clausen KP. Reticulosarcomatosis in primary myelofibrosis. *Cancer* 1968;22:136–141

Clinical Stage I Carcinoma of the Cervix: Value of MR Imaging in Determining Degree of Invasiveness

Hans H. Lien¹
 Viggo Blomlie¹
 Kjell Kjørstad²
 Vera Abeler³
 Olav Kaalhus⁴

The depth of tumor invasion measured at histologic examination is the most important prognostic factor in early-stage carcinoma of the uterine cervix. The ability of MR to estimate the depth of tumor invasion was studied in 47 patients who subsequently underwent radical hysterectomy. In two patients, MR failed to detect tumors with infiltration depths of 2 and 4 mm. The maximum sagittal tumor length along the axis of the cervix (D) and the maximum tumor area on sagittal (S) and axial (A) images were measured with MR. The depth of tumor infiltration determined histologically (I) correlated with the degree of infiltration noted on MR images. The univariate correlation coefficients for log I vs log D, log S, and log A were .87, .84, and .77, respectively. By stepwise inclusion of the variables in a multivariate analysis, the contributions to the coefficient of determination from including log S and log A after log D were less than 1%. The regression analysis showed that the best estimate for the depth of invasion was close to half of the sagittal tumor length measured on MR, $I = D/2$.

Our experience shows that MR is valuable in determining the degree of invasiveness in clinical stage I tumors.

AJR 156:1191-1194, June 1991

Early-stage cancer of the uterine cervix has an excellent prognosis and can be cured by surgery or radiotherapy. The most important prognostic factor is the size of the tumor, measured as depth of infiltration into the cervical stroma [1-6]. Accurate assessment of tumor size is important because it has therapeutic implications. Tumors with infiltration depths of less than 5 mm have a very limited metastatic potential, and patients with such tumors have a long-term survival rate of almost 100% [7]. Radical treatment procedures may not be needed in these patients. To date, the only reliable method to determine invasion depth has been histologic examination of the removed organ.

Several studies have shown that MR imaging is useful for detecting and staging carcinoma of the cervix [8-11]. In the present prospective study, we compared the results of MR imaging in 47 patients treated for stage I cancer with the findings in the operative specimen. In particular, the correlation between the size of the tumor on MR and the depth of invasion noted on histologic examination was investigated.

Received September 27, 1990; accepted after revision December 27, 1990.

¹ Department of Diagnostic Radiology, The Norwegian Radium Hospital, Montebello N-0310 Oslo 3, Norway. Address reprint requests to H. H. Lien.

² Department of Gynecologic Oncology, The Norwegian Radium Hospital, Oslo 3, Norway.

³ Department of Pathology, The Norwegian Radium Hospital, Oslo 3, Norway.

⁴ Department of Biophysics, Cancer Research Institute, The Norwegian Radium Hospital, Oslo 3, Norway.

0361-803X/91/1566-1191

© American Roentgen Ray Society

Subjects and Methods

Fifty-nine patients with cervical cancer of clinical stage I entered this prospective study in a consecutive and unselected manner. Each patient had a complete clinical workup consisting of a clinical staging examination under anesthesia, dilatation and curettage, multiple tumor biopsies, cystoscopy, chest radiography, and excretory urography. All patients underwent radical hysterectomy and lymphadenectomy. In eight patients, histologic examination of the surgical specimen showed no residual tumor, indicating that it had been completely removed by preoperative conization, large biopsies, or curettage. MR images were of inferior quality

in four patients. The remaining 47 patients form the basis for the present report. The patients were 22–67 years old (mean, 42).

Examinations were performed with a 1.5-T Signa System (General Electric, Milwaukee, WI). Spin-echo (SE) pulse sequences were used and included a coronal localizer series followed by sagittal and axial T2-weighted series (2000/20–80 [TR/TE]) and an axial T1-weighted series (600/20). Except for the localizer series, all sequences were performed with a 256 × 256 matrix and two excitations. Slice thickness was 5 mm with 2.5-mm gaps. The field of view was 36 cm. The patients did not fast before the examinations. Patients were given two glasses of water 30–45 min before the study to fill the bladder.

MR images were evaluated by two radiologists who knew the clinical stage of the disease. The findings were assigned by consensus after the images were interpreted in conference. The criterion for tumor was a lesion of high or relatively high signal intensity replacing the low-signal-intensity fibrous cervical stroma on T2-weighted images.

The following measurements were made (Fig. 1): the maximum length of the tumor in the sagittal plane along the long axis of the cervix (D), the angle at the intersection of the main axis of the cervix and the axial direction in the sagittal plane (u), the maximum tumor area on sagittal images (S), and the maximum tumor area on axial images (A). Distance and angle measurements were performed with the cross-hair cursor on the monitor. Areas were defined by tracing the tumor region with the cursor.

All patients were subjected to radical abdominal hysterectomy according to the Wertheim/Meigs technique, which includes removal

of the parametrium and upper part of the vagina as well as total pelvic lymphadenectomy. The cervix/isthmus was cut off and sliced in clockwise radial-length sections 2–3 mm thick. In each section the maximum depth of tumor invasion into the cervical wall was measured by means of a calibrated microscope.

Statistical Methods

The data were subjected to both univariate and multivariate correlation analysis, with the depth of infiltration as the dependent variable and the MR parameters as mutually independent variables.

In a special model, the volume of the tumor as calculated from the MR parameters was taken as the sole independent variable. In this model, the tumor was thought of as an ellipsoid with the distance D as a principal axis. The calculated tumor volume (V) was then

$$V = \frac{8 \times S \times A}{3 \times \pi \times D} \sqrt{1 + [(\pi \times D^2/4S)^2 - 1] \sin^2 u}$$

As an average semiaxis length (L) of the ellipsoid, the variable

$$L = (V/\pi)^{1/3}$$

was used.

Logarithmic transforms of the variables were used to obtain approximately normally distributed values when the original data were not normally distributed, as assessed by normal score tests.

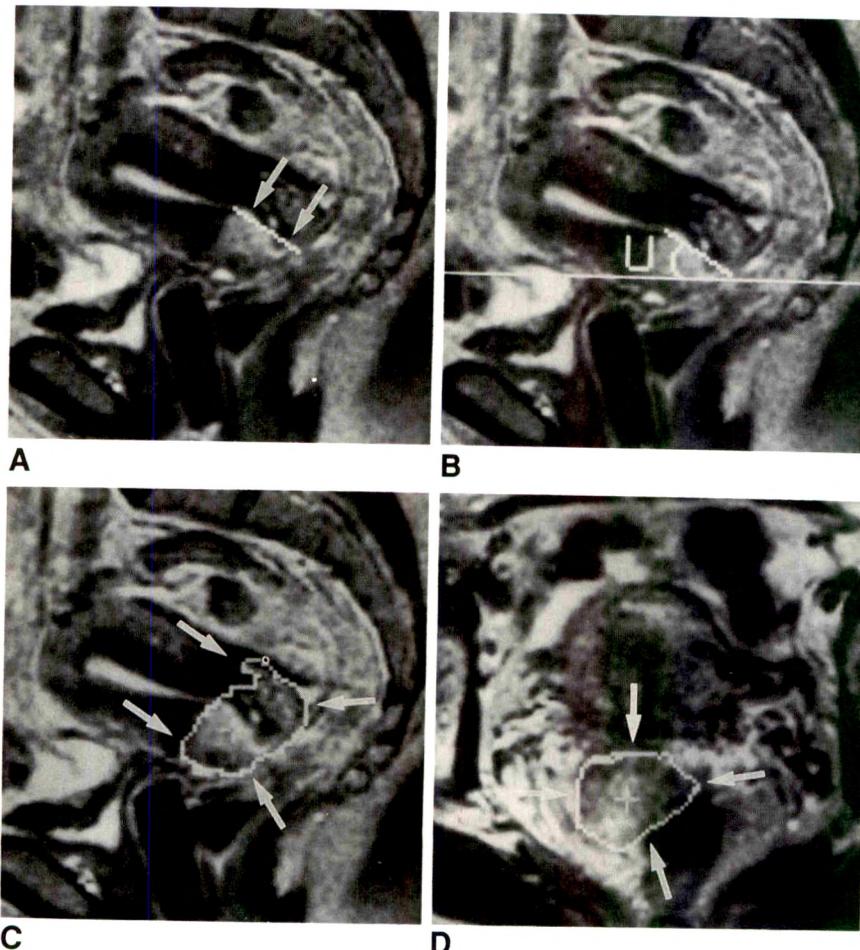


Fig. 1.—T2-weighted MR images (SE 2000/80) show high-signal tumor replacing low-signal fibrous stroma. Invasion depth was 15 mm at histologic examination.

A, Maximal tumor length along axis of cervix (arrows).

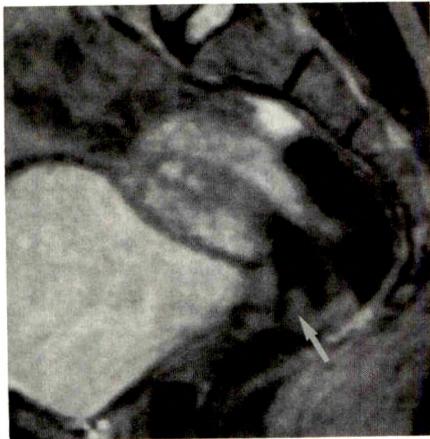
B, Angle (u) at intersection of main axis of cervix and axial plane.

C, Maximal sagittal tumor area (arrows).

D, Maximal axial tumor area (arrows).



A



B

Fig. 2.—T2-weighted sagittal MR images (SE 2000/80) in patient with tumor invasion measuring 2 mm at histologic examination of left anterior cervical lip.

A, Section through cervical canal shows normal low-signal fibrous stroma.
B, Section 7.5 mm to left of A. Small high-signal lesion erodes fibrous stroma anteriorly (arrow).

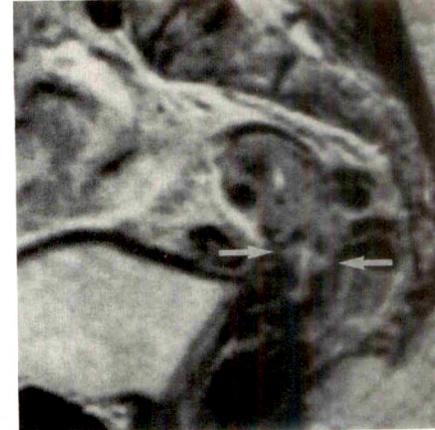


Fig. 3.—T2-weighted sagittal MR image (SE 2000/80) in patient with endocervical tumor and 5-mm invasion depth at histologic examination. High-signal tumor extends into fibrous stroma (arrows).

Results

MR demonstrated the lesion in 45 patients, five of whom had tumors with invasion depths of 5 mm or less at histologic examination (Figs. 2 and 3). MR failed to show two tumors with invasion depths of 2 and 4 mm.

The logarithmic transforms of the values of D, S, and A in the 45 tumors found at both histologic and MR examinations were interrelated. The pairwise mutual correlation factors of log D, log S, and log A ranged from .89 to .94. The results of the linear regression analysis of log I vs each of these three MR parameters are shown in Table 1. The univariate correlation coefficients were .87, .84, and .77, respectively. As expected, the regression coefficients were close to 1.0, 0.5, and 0.5, respectively, since D is a linear measure (mm) and S and A are areas (mm^2). No significant dependence of the invasion depth on the angle u alone was found.

The results of the multivariate analysis are shown in Table 2. By stepwise inclusion of the variables, the contributions to the coefficient of determination from including log S and log A after log D were less than 1%. The correlation coefficient of log I vs the logarithm of the calculated MR volume (V) was .82, which was lower than for the variables used above. Finally, the simple dependence $I = D/2$ was examined and found to yield a correlation coefficient that was not significantly lower than that for the previous regression dependence. This line is shown in Figure 4, which contains the scatterplot of the individual D and I observations. A linear regression of $(I - D/2)^2$ vs D^2 yielded a standard deviation of approximately 2.5 mm for the smallest tumors, 10% of D for

a large tumor, and $I = 12.5 \pm 3.5$ mm for a medium-sized tumor of $D = 25$ mm.

Discussion

In previous MR studies of cervical carcinoma, much attention has been paid to the stage of the disease [8, 10–12]. Within each stage, tumor volume is of importance for the prognosis; small tumors have a better prognosis than large ones. The depth of invasion as measured at histologic examination has been found to be of particular importance [1–7]. Therefore, we focused on the value of MR in predicting the invasion depth of the tumor. Invasion depth was not measured directly, because conventional transverse MR images are usually not perpendicular to the long axis of the cervix. A true cross section through the cervix can be obtained by using an oblique imaging plane [13]. This may permit measurement of the invasion depth into the cervical wall, but this off-axis scanning sequence was not used in the present series. The fact that the tumor itself often distorts the cervical canal and thereby precludes its identification still poses a problem.

The present results show that MR can give reliable information about depth of tumor invasion at histologic examination. The latter has a high linear correlation with the main diameter D and the square root of the sagittal and axial tumor areas determined from the MR images. Because the best estimate for the depth of invasion was close to half of the sagittal tumor length measured on MR, $I = D/2$, the more

TABLE 1: Univariate Linear Regression Analysis of Depth of Infiltration vs MR Parameters of 45 Tumors: Logarithmic Transforms

Variable	Intercept \pm SE	Antilog Intercept	Regression Coefficient \pm SE	Correlation Coefficient (r)	Relative SD (%)	Significance Level (p)
Log I vs log D	-0.37 ± 0.13	0.43	1.02 ± 0.05	.87	35	<.001
Log I vs log S	-0.22 ± 0.13	0.60	0.48 ± 0.05	.84	40	<.001
Log I vs log A	-0.20 ± 0.16	0.63	0.46 ± 0.06	.77	45	<.001

Note.—I = maximum depth of tumor invasion measured histologically; D = maximum sagittal length of tumor on MR; S = maximum tumor area on sagittal images; A = maximum tumor area on axial images.

TABLE 2: Stepwise Multivariate Analysis of Depth of Infiltration vs MR Parameters of 45 Tumors: Logarithmic Transforms

Variable	Intercept/Regression Coefficient \pm SE	Significance Level (p)
Intercept	-0.34 \pm 0.13	
Log D	0.85 \pm 0.27	.003
Log S	0.15 \pm 0.15	.320 ^a
Log A	-0.06 \pm 0.11	.590 ^a

Note.—D = maximum length of tumor measured on MR; S = maximum tumor area on sagittal images; A = maximum tumor area on axial images. Correlation coefficient = .87; relative SD = 35%.

^a Not significant.

cumbersome measurement of the sagittal and axial areas can be eliminated. In addition, D can be determined with a higher precision than the other MR parameters, leaving it as the best choice for predicting the depth of invasion. One difficulty, however, may be locating the external os in the case of an exophytic tumor.

In light of the ability of MR to show small lesions, we speculate whether concomitant inflammation and edema have made lesion demonstration easier by contributing to the high signal within the cervix. This could lead to overestimation of tumor size with MR. However, appreciable inflammatory reaction was found only in one patient in whom a 2-mm zone of reaction added to the 2-mm invasion depth of the tumor. Also, statistical analysis showed significant correlation between MR findings and invasion depth at histologic examination, even for small tumors.

The images were interpreted in conference, and no study was made of interobserver reproducibility of tumor size determinations. With regard to intraobserver variations, we reevaluated nine cases. It is difficult to perform an independent reevaluation, because the previous data are remembered by the radiologist. However, the variance of the results obtained

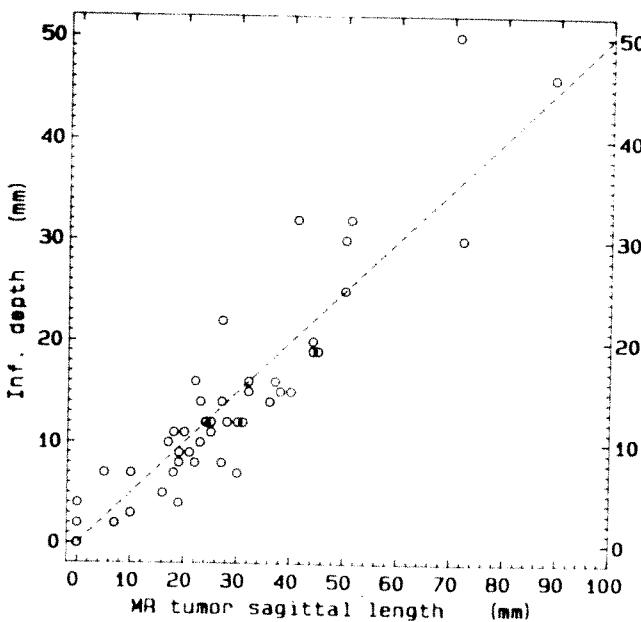


Fig. 4.—Scatterplot of individual observations of sagittal tumor length on MR and infiltration (Inf.) depth at histologic examination.

by the new evaluation was not larger than the variance in the regression analysis.

One weakness of the present study is the fact that four patients had been excluded because of images of inferior quality. The reasons were artifacts from small-bowel motion (two patients) and a retroverted uterus that did not lie still because of variable gas filling the rectum (two patients). We tried to eliminate the former problem with elevation of bowel by means of urine in the bladder. Therefore, all patients were given two glasses of water to drink 30–45 min before the examination. However, the bladder filling still was insufficient in some cases. Our routines have been changed since the present study. A spasmolytic drug is now administered whenever the sagittal images (the first of the two long TR sequences) show disturbing artifacts from bowel motion. In patients with a distended gas-filled rectum, a rectal tube is used also. After these changes in procedures, satisfactory results have been obtained in all cases.

The crucial point in the treatment of small tumors is the choice of method. Radical hysterectomy with pelvic lymphadenectomy is a major surgical procedure and should be performed only if less radical methods are inadequate. The same is true for radical radiotherapy. Treatment centers have different policies with regard to indications for radical procedures. Clinical and histopathologic criteria are to a certain degree subjective, and regardless of the indications, accurate assessment of tumor size is necessary as part of the pretreatment workup. MR seems to be of value in this respect.

REFERENCES

- Baltzer J, Koepcke W. Tumor size and lymph node metastases in squamous cell carcinoma of the uterine cervix. *Arch Gynecol Obstet* 1979;227:271–278
- Burghardt E, Pickel H. Local spread and lymph node involvement in cervical cancer. *Obstet Gynecol* 1978;52:138–145
- FIGO news. Staging of gynecological tumors. *Int J Gynecol Obstet* 1989;28:189–193
- Chung CK, Nahhas WA, Stryker JA, Curry SL, Abt AB, Mortel R. Analysis of factors contributing to treatment failures in stages IB and IIA carcinoma of the cervix. *Am J Obstet Gynecol* 1980;138:550–556
- Van Nagell JR, Donaldson ES, Parker JC, van Dyke AH, Wood EG. The prognostic significance of cell type and lesion size in patients with cervical cancer treated by radical surgery. *Gynecol Oncol* 1977;5:142–151
- Piver MS, Chung WS. Prognostic significance of cervical lesion size and pelvic node metastases in cervical carcinoma. *Obstet Gynecol* 1975;46:507–510
- Iversen T, Abeler V, Kjørstad KE. Factors influencing the treatment of patients with stage IA carcinoma of the cervix. *Br J Obstet Gynaecol* 1979;86:593–597
- Hricak H, Lacey CG, Sandles LG, Chang YCF, Winkler ML, Stern JL. Invasive cervical carcinoma: comparison of MR imaging and surgical findings. *Radiology* 1988;166:623–631
- Rubens D, Thornbury JR, Angel C, et al. Stage IB cervical carcinoma: comparison of clinical, MR, and pathologic staging. *AJR* 1988;150:135–138
- Togashi K, Nishimura K, Sagoh T, et al. Carcinoma of the cervix: staging with MR imaging. *Radiology* 1989;171:245–251
- Kim SH, Choi BI, Lee HP, et al. Uterine cervical carcinoma: comparison of CT and MR findings. *Radiology* 1990;175:45–51
- Waggenspack GA, Amparo EG, Hannigan EV. MR imaging of uterine cervical carcinoma. *J Comput Assist Tomogr* 1988;12:409–414
- Baumgartner BR, Bernardino ME. MR imaging of the cervix: off-axis scan to improve visualization of zonal anatomy. *AJR* 1989;153:1001–1002

Diverticula of the Female Urethra: Diagnosis by Endovaginal and Transperineal Sonography

Bernadette Keefe¹
 David M. Warshauer¹
 M. Susan Tucker²
 Carol A. Mittelstaedt¹

Diverticula of the female urethra can be difficult to diagnose. Invasive contrast studies (voiding cystourethrography or double-balloon urethrography) or urethroscopy are frequently required for definitive diagnosis. Although transabdominal sonography has been able to visualize large diverticula, this technique has not proved useful in routine screening. In this study, we examined the use of higher frequency (5 MHz) near-focus endovaginal or transperineal sonography for the diagnosis of urethral diverticula. Five patients with radiographically proved (three with double-balloon urethrography and two with voiding cystourethrography) urethral diverticula were examined with endovaginal (two cases) or transperineal (four cases) sonography. In all five cases, sonography showed the diverticula previously demonstrated on the contrast study. The spatial relationship of the diverticula to the urethra, an important consideration at surgery, was shown more clearly by sonography than by contrast radiography.

These findings suggest that sonography may be useful as a noninvasive screening technique for urethral diverticula.

AJR 156:1195-1197, June 1991

The diagnosis of diverticula involving the female urethra has traditionally been based on either contrast radiography (excretory urography, voiding cystourethrography, or double-balloon urethrography) or urethroscopy [1-3]. Since its introduction in 1959 by Lang and Davis [4], the double-balloon or positive-pressure urethrogram has been the radiologic method of choice [1, 5, 6]. Although this method has an accuracy of approximately 90% [5], it is somewhat difficult to perform, uncomfortable for patients, and invasive. Because of these drawbacks, we performed endovaginal and/or transperineal sonography in cases of urethral diverticula to determine if sonography could achieve visualization equal to that of contrast radiography. We report here our technique and results in five cases.

Subjects and Methods

Five women with a radiographic diagnosis of urethral diverticula were studied with sonography. In three cases, the diagnosis had been made by double-balloon urethrography; in two cases, voiding cystourethrography was used. Surgical confirmation was available in four cases. Urethroscopy confirmed the diagnosis in two patients, one of whom also underwent surgery.

Sonography was done with either a 5-MHz linear transducer (GE Medical Systems, Milwaukee, WI) placed within the vagina (two cases) or a 5-MHz sector transducer (Acuson Corp, Mountainview, CA) placed on the perineum at the level of the urethra (four cases). One patient was scanned by using both the endovaginal and transperineal approach.

The patients were scanned in the dorsal lithotomy position after voiding. Stirrups were used for improved exposure. Both sagittal and coronal images of the urethra were obtained when scanning transperineally. Because of the design of the transducer, only sagittal images could be obtained when the endovaginal approach was used.

Received November 1, 1990; accepted after revision December 5, 1990.

¹ Department of Radiology (CB #7510), Third Floor, Old Infirmary Bldg., University of North Carolina, Chapel Hill, NC 27599-7510. Address reprint requests to B. Keefe.

² Division of Urology, Department of Surgery (CB #7235), Burnett Womack Bldg., University of North Carolina, Chapel Hill, NC 27599-7235.

0361-803X/91/1566-1195

© American Roentgen Ray Society

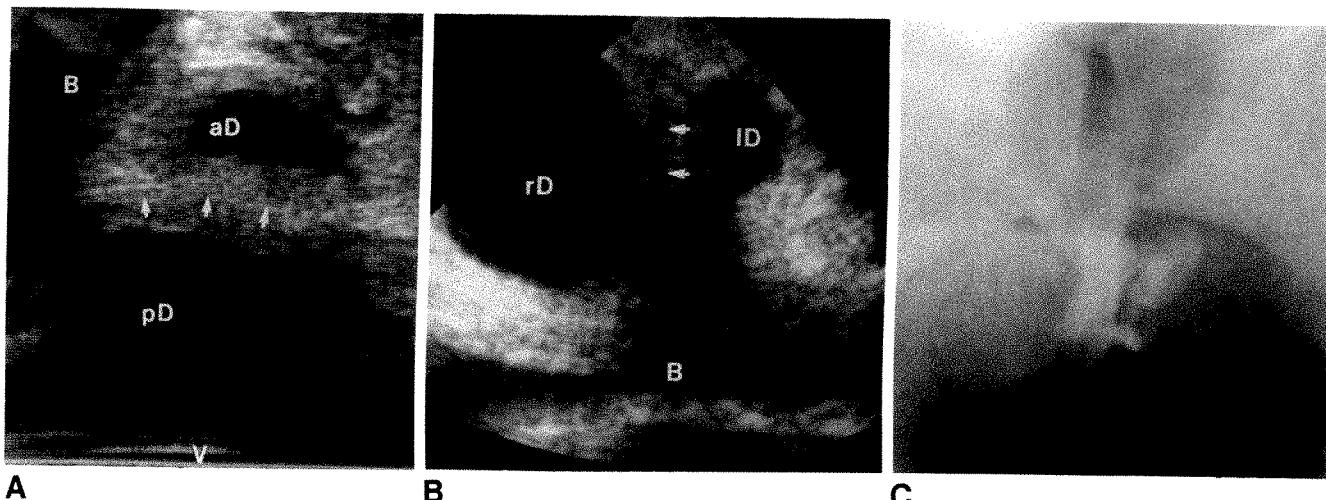


Fig. 1.—29-year-old woman with a palpable vaginal mass.

A, Sagittal endovaginal sonogram shows a large (4 cm) diverticulum with anterior (aD) and larger posterior (pD) component. Arrows = urethra, B = bladder, V = vagina.

B, Coronal transperineal sonogram shows diverticulum with larger right-sided (rD) and smaller left-sided (ID) component. Arrows = urethra, B = bladder.

C, Double-balloon urethrograph shows only smaller left-sided component of diverticulum.

Results

In all five of these cases, sonography showed the urethral diverticula that were subsequently proved to be present. In one case, the diverticulum noted at sonography and confirmed at surgery was significantly larger than the diverticulum visible on radiographs (Figs. 1A–1C). In another case in which surgery and radiography showed a single multiseptated diverticulum, sonography showed two smaller diverticula (Figs. 2A and 2B).

In each case, the spatial relationship of the diverticulum to the urethra was shown more clearly with sonography than with contrast radiography. This was particularly true for transperineal sonography, with its ability to obtain both sagittal and coronal images. In one case, anterior extension not appreciated on contrast radiography was clearly shown by sonography (Fig. 3). The precise opening of the diverticulum, however, could not be confidently identified with either technique.

Although we initially performed sonography from an endovaginal approach, the transperineal route was thought to afford both improved visualization and ease of operation, and this method alone was used in later cases. The sonographic examination was well tolerated, and no complaints from patients were noted. Most studies were completed in 5–10 min. On the other hand, both the voiding cystourethrogram and particularly the double-balloon urethrograph were often considered uncomfortable or painful by these patients. In the one pregnant patient, sonography was able to replace radiography in the initial workup.

Discussion

The female urethra is surrounded by an intricate net of paraurethral ducts and glands. Most diverticula are thought to result from infection and obstruction of these glands. When

rupture of the resultant retention cyst or abscess occurs into the urethra, a diverticulum is formed. Other factors that may play a role in fewer cases include a congenital origin and direct trauma from instrumentation, insertion of foreign bodies, or childbirth [1, 5, 7]. The majority of diverticula open into the middle third of the urethra, and approximately one third of all patients have multiple or compound diverticula [4, 5].

Diverticula occur in from 1% to 6% of the general population [1]. Although approximately 20% of patients with diverticula are asymptomatic, these lesions are frequently associated with chronic lower urinary tract symptoms including dysuria, hematuria, dyspareunia, and incontinence [5, 7]. The classic presentation of dribbling after voiding, presence of a mass, and expression of pus from the urethra on physical examination, however, is uncommon. The diagnosis is frequently delayed; it is established by contrast radiography only after years of symptoms [3]. Voiding cystourethrography has been used for screening, but has an overall accuracy of only 65% [5]. Positive-pressure or double-balloon urethrography with the Tratner or Davis catheter has been the radiographic method of choice, with an accuracy of 90% [5]. CO₂ urethroscopy also has been used for diagnosis with similar reported accuracy [5].

Urethral diverticula also have been shown on transabdominal sonography. Lee and Keller [8] first described the sonographic appearance in 1977. Subsequent reports by Wexler and McGovern [9] and Pliskow and Silver [10] in 1980 have confirmed this appearance as a cystic structure at or below the bladder base and with or without septa and internal debris. In each of these studies, the described diverticula were between 2.0 and 4.5 cm in diameter. Because of its suspected relative insensitivity for smaller lesions, transabdominal sonography has not gained wide acceptance as a screening technique.

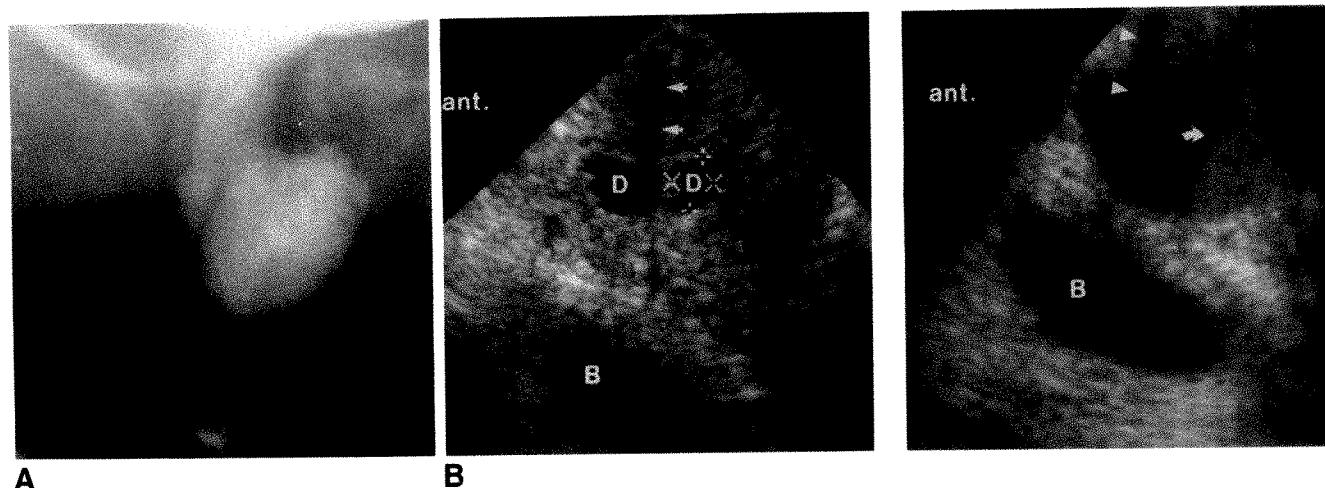


Fig. 2.—21-year-old woman with 6-year history of recurrent urinary tract infections and urethral burning.

A, Voiding cystourethrogram shows a single left-sided diverticulum.
B, Sagittal transperineal sonogram to left of urethra shows two small (6 mm), apparently separate diverticula (D), which at surgery proved to be part of a single larger multiseptate diverticulum. Arrows = left edge of urethra, B = bladder.

Fig. 3.—64-year-old woman with a 5-year history of recurrent urinary tract infections and dribbling after voiding. Sagittal transperineal sonogram angled slightly to left of midline shows a large (3 cm) predominantly posterior diverticulum with a small anterior (ant.) extension. Note fluid-debris level (arrow) in posterior component of diverticulum. Arrowheads = urethra, B = bladder.

The introduction of higher frequency, near-focus endovaginal probes led us to reexamine the use of sonography as a screening technique for urethral diverticula. In this initial study, all diverticula seen by contrast radiography were identified on endovaginal or transperineal sonography. In one case, a diverticulum that appeared to be small on double-balloon urethrogram was shown to be significantly larger on transperineal sonography. The presence of contained debris within the diverticula or partial occlusion of its orifice may have been responsible for this difference. In an additional case in which surgery and radiography showed a single multiseptated diverticulum, sonography showed two smaller diverticula. This discrepancy may have been due to partial collapse of the diverticulum. Although the sonograms were done after voiding, in this case we speculate that sufficient time had elapsed between voiding and the examination for the diverticulum to empty partially.

Other advantages of transperineal sonography include improved three-dimensional visualization of the diverticula in relation to the urethra. The anteroposterior relationship particularly is important in surgical planning and is shown well on sagittal sonograms. Whether the information from sonography will be sufficient to supplant contrast radiography in surgical planning is uncertain.

The major advantage of transperineal sonography, however, is the noninvasive nature of the study. This should not only reduce the risk of infection in these patients, who often have chronic bacterial infection of the urethra, but should also improve patients' comfort significantly. The absence of ionizing radiation is also a consideration because the majority of patients are in their childbearing years [11].

The sonographic appearance of urethral diverticula is characteristic but not pathognomonic of this entity. The differential diagnosis includes, less commonly, Gardner duct cysts, vaginal inclusion cysts, ectopic ureteroceles, endometrioma, and Skene gland abscesses [10].

Our results suggest that transperineal sonography may be useful as a screening technique for the detection of urethral diverticula.

REFERENCES

1. Boyd SD, Raz S. Female urethral diverticula. In: Raz S, ed. *Female urology*. Philadelphia: Saunders, 1983:378-393
2. Peters WA, Vaughan ED. Urethral diverticulum in the female: etiologic factors and postoperative results. *Obstet Gynecol* 1976;47:549-552
3. Stewart M, Bredland PM, Stidolph NE. Urethral diverticula in the adult female. *Br J Urol* 1981;53:353-359
4. Lang EK, Davis HJ. Positive pressure urethrography: a roentgenographic diagnostic method for urethral diverticula in the female. *Radiology* 1959;72:401-405
5. Drutz HP. Urethral diverticula. *Obstet Gynecol Clin North Am* 1989;16:923-929
6. Greenberg M, Stone D, Cochran ST, et al. Female urethral diverticula: double-balloon catheter study. *AJR* 1981;136:259-264
7. Lee RA. Diverticulum of the urethra: clinical presentation, diagnosis, and management. *Clin Obstet Gynecol* 1984;27:490-498
8. Lee TG, Keller FS. Urethral diverticulum: diagnosis by ultrasound. *AJR* 1977;128:690-691
9. Wexler JS, McGovern TP. Ultrasonography of female urethral diverticula. *AJR* 1980;134:737-740
10. Pliskow N, Silver TM. Ultrasonic diagnosis of urethral diverticulum. *Urology* 1980;15:625-626
11. Davis HJ, Telinde RW. Urethral diverticula: an assay of 121 cases. *J Urol* 1958;80:34-39

Book Review

Computed Tomography, Anatomy, and Morphometry of the Lower Extremity. By H.-M. Hoogewoud, G. Rager, and H.-B. Burch. New York: Springer-Verlag, 124 pp. and floppy disk, 1990. \$163.50

The authors state that the aims of this book are to provide an atlas for physicians, radiologists, and orthopedists that can serve as a quick reference for the interpretation of CT scans, to describe the normal structure as a basis for recognition of pathologic processes, and to provide a teaching tool of cross-sectional anatomy for students. In addition, they want to show how CT can be used to acquire measurements of the lower extremity. Most of the book is dedicated to the first three of these aims. The final section is concerned with CT measurements of the lower limb. This includes rather specific measurements of the center-column diaphysis angle, the anteversion angle, and the center-edge angle. Finally, a method of determining coverage of the femoral head and weight-bearing surface of the hips is described, both in a brief section and more fully in the computer software, which is included in the back cover of the book.

The book is extremely well produced, with fine illustrations and high-quality prints. The floppy disk is IBM compatible and provides a comprehensive program on three-dimensional reconstruction, particularly of the femoral head and acetabulum. I have several criticisms, however. As the authors admit, many texts dealing with cross-sectional anatomy are available. Admittedly, the methods that the authors have used provide extremely good correlation between the anatomic sections and the CT scans, and the authors have gone to considerable trouble with their technique. Nevertheless, I am not certain that another text on this subject is needed. Furthermore, I find the method of labeling the illustrations somewhat irritating: Num-

bered lines point to the anatomic features, and the legends are listed numerically below the illustrations. It is always difficult to provide clear labeling of structures as complex as the lower extremity; however, I find this particular method time-consuming and difficult to use.

The inclusion of the section on measurements is also a little confusing. The three-dimensional graphics software provided is certainly an interesting program, but I think it has a limited application in orthopedics. Only a few orthopedic surgeons and radiologists have sufficient interest in this area to warrant the somewhat time-consuming reformatting. In addition, many of the modern rapid scanners have high-quality three-dimensional reformatting capability and could provide similar types of information. The program itself is obviously the result of a great deal of effort on behalf of the authors and may have value in the small setting with a dedicated radiologist who has the time to perform this type of detailed study. Furthermore, for the price of the book, this certainly is an inexpensive method of obtaining this technology.

Overall, however, I am not certain that this book will have a large market. Many cross-sectional atlases are available, and I am not certain that the addition of the three-dimensional graphics software will be of sufficient interest to the average radiologist or orthopedist.

Jeremy W. R. Young
University of Maryland Hospital
Baltimore, MD 21201

Sarcoma in Paget Disease of Bone: Clinical, Radiologic, and Pathologic Features in 22 Cases

Timothy E. Moore¹
 Alan R. King²
 Mary H. Kathol¹
 Georges Y. El-Khoury¹
 Renzi Palmer²
 Peter R. Downey^{3,4}

The clinical, radiologic, and histologic features of 22 cases of Paget sarcoma were reviewed to determine in which patients with Paget disease these tumors are most likely to develop and what radiologic findings suggest the diagnosis. Clinical findings at presentation included pain and/or a mass (11 patients), pathologic fracture (seven), and neurologic symptoms (four). Survival time in 20 patients ranged from 5 days to 2.5 years. Two patients were lost to follow-up: one at 2 years and one at 8 years. There were 16 high-grade osteosarcomas, three chondrosarcomas, two fibrosarcomas, and one malignant fibrous histiocytoma. The most common site was the femur. Tumors also were observed in unusual sites. In one case of multifocal osteosarcoma, the tumor involved only pagetic bone. In 15 patients, Paget disease was polyostotic, clinically significant, and had been documented previously. In four patients, a sarcoma developed near the site of a fracture that had occurred between 2 months and 15 years previously. All cases showed radiologic evidence of a destructive lesion; other findings included a mass and evidence of tumor mineralization. Periosteal reaction was not observed. All but one tumor developed in a site of osteoblastic or mixed osteoblastic and lytic Paget disease.

Our results suggest that sarcomas can develop in any part of any bone affected by Paget disease but are more likely to occur with advanced disease and to present with a destructive lesion without periosteal reaction.

AJR 156:1199–1203, June 1991

Although sarcomatous degeneration is a rare complication of Paget disease (reportedly less than 0.1% [1]), uncomplicated Paget disease is a common disorder among elderly persons of European origin, and therefore, the total number of these tumors is significant. The prevalence of sarcomas in Paget disease increases with age [2], and in view of the increasing numbers of elderly persons in our population, we can probably expect to see more of this disorder in the future. The aims of this study were (1) to correlate the histologic features with the radiologic findings; (2) to determine the relationship between the severity of Paget disease and the development of sarcomas; and (3) to study the age and sex distribution, presenting clinical features, and prognosis. All cases of sarcoma in Paget disease recorded in the Middlemore Hospital Bone Tumour Registry in Auckland, New Zealand, were reviewed in addition to three cases from the Auckland Hospital Paget's Clinic. The patients presented between January 1961 and April 1989.

Materials and Methods

Twelve men and 10 women with Paget disease and sarcoma, 48–87 years old (mean and median age, 71 years), were included in this study (Fig. 1). (Inclusion in the study was based on histologic evidence of Paget disease and sarcoma in the same specimen or in specimens immediately adjacent to each other or histologic evidence of a sarcoma that could be identified radiologically as a region of cortical destruction or as a mass within or arising from pagetic bone.) All 22 patients had histologic sections from biopsies available for review. The radio-

Received October 9, 1990; accepted after revision December 26, 1990.

¹ Department of Radiology, The University of Iowa College of Medicine, Iowa City, IA 52242. Address reprint requests to T. E. Moore, Department of Radiology, The University of Iowa Hospitals and Clinics, Iowa City, IA 52242.

² Department of Pathology, Middlemore Hospital, Auckland Area Health Board, Auckland, New Zealand.

³ Department of Radiology, Middlemore Hospital, Auckland Area Health Board, Auckland, New Zealand.

⁴ Present address: Department of Radiology, Flinders Medical Centre, Bedford Park, South Australia 5042, Australia.

0361-803X/91/1566-1199
 © American Roentgen Ray Society

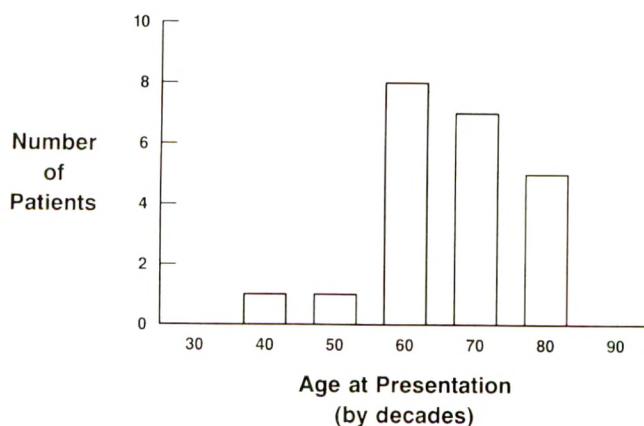


Fig. 1.—Graph shows age of patient at presentation in 22 cases of Paget sarcoma.

graphs could not be found in two of the older cases. However, these two did have radiology reports diagnosing Paget disease, in addition to histologic evidence of Paget disease in bone adjacent to the tumors. Radiographs of the remaining 20 cases were reviewed independently by three radiologists.

Results

Clinical Presentation

Presenting features included pain without palpable mass (five patients), painful mass (five), painless mass (one), pathologic fracture (seven), neurologic symptoms (cranial nerve palsies, lower limb weakness, incontinence [three]), and vomiting and dehydration (one).

Histologic Findings

Of the 22 cases, 16 showed histologic features of osteosarcoma, three of chondrosarcoma, two of fibrosarcoma, and one of malignant fibrous histiocytoma. Histologically, all osteosarcomas showed malignant cells producing osteoid, but cartilage with malignant features also was frequently present. Some showed occasional collections of multinucleated giant cells. All osteosarcomas were considered on the basis of nuclear atypia to be high grade. The single case of multifocal osteosarcoma showed dense malignant osteoid and bone at all tumor sites. Two of the three chondrosarcomas were of intermediate grade; the third showed spindle cells but no osteoid synthesis. Two tumors showed moderately pleomorphic spindle cells arranged in a herringbone growth pattern characteristic of fibrosarcoma. One tumor exhibited a storiform arrangement of malignant cells among which were scattered cells with multiple, bizarre, or multilobulated nuclei. This tumor had no evidence of osteoid, and it was classified as a malignant fibrous histiocytoma.

Distribution

Of 21 solitary tumor sites, the femur was the most commonly affected (eight cases). There were three in the humerus;

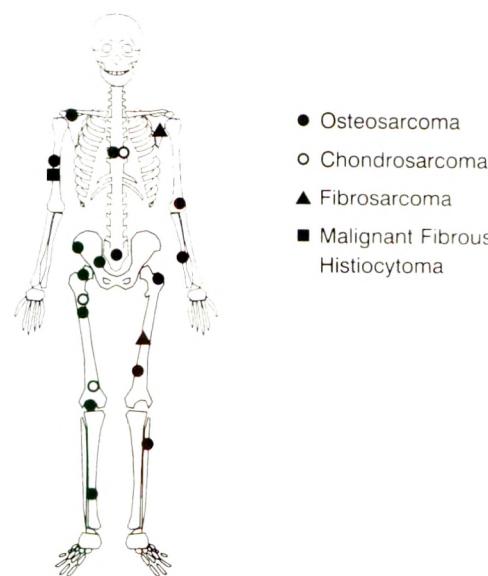


Fig. 2.—Drawing shows skeletal distribution of 21 solitary Paget sarcomas.

two each in the innominate bone, thoracic spine, and scapula; and one each in the tibia, fibula, ulna, and sacrum (Fig. 2). One multifocal osteosarcoma had numerous lesion sites. These lesions were found at autopsy to affect only pagetic bone, and this patient also had lung metastases. Radiographs taken before and after malignant degeneration supported the histologic findings of involvement only of pagetic bone.

Location Within Long Bones

Ten osteosarcomas occurred in long bones, of which only three were in the typical metaphyseal location for de novo osteosarcomas. Five developed in the diaphysis and two in the epiphysis.

Severity of Paget Disease

Seventeen patients had polyostotic Paget disease confirmed by bone scans or radiographs. In the remaining five patients, the extent of involvement could not be determined because they did not have bone scans or skeletal surveys, and additional asymptomatic regions of Paget disease could not be excluded totally.

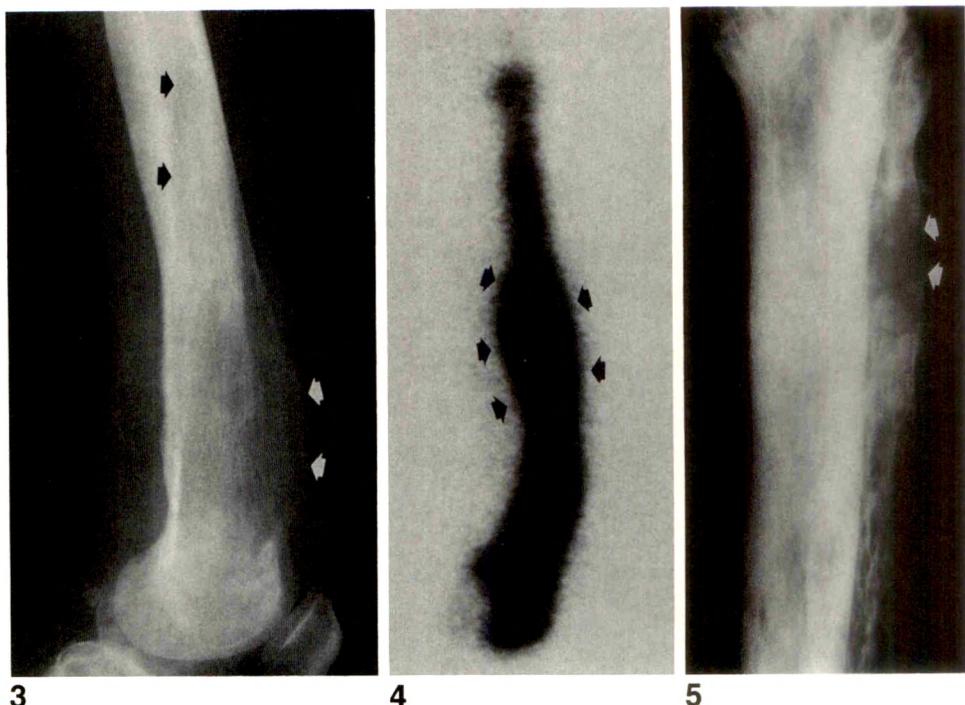
There was documented evidence of symptomatic Paget disease existing before the development of a tumor in 17 patients, 15 of whom had polyostotic Paget disease.

In 21 patients, the radiologic changes of Paget disease were observed to be sclerotic, representing a late stage of disease or, when films were not available, advanced Paget disease was described in radiology reports. In only one patient did a sarcoma (osteosarcoma) develop while the affected bone was still in the early lytic phase of Paget disease (Fig. 3).

Fig. 3.—Paget osteosarcoma of femur. Radiograph shows osteosarcoma developing within a region of early Paget disease of distal femur. Note oblique line (black arrows) that marks junction of lytic-phase Paget disease and normal bone. Also note destructive expansive lesion (white arrows) in anterior femoral cortex.

Fig. 4.—Paget osteosarcoma of ulna. 99m Tc-methylene diphosphonate (MDP) bone scan of forearm shows increased activity from both tumor (arrows) and pagetic bone of ulna. Remainder of forearm and hand are barely visualized because of preferential uptake of radionuclide by ulna.

Fig. 5.—Paget osteosarcoma of fibula. Tibia and fibula show changes of advanced Paget disease. A lytic lesion (arrows) of proximal fibular shaft is shown on radiograph. This bears a resemblance to aggressive osteolytic changes sometimes seen in benign Paget disease, but focal nature and degree of cortical destruction are more typical of a neoplastic process.



Previous Fractures

In three patients, a sarcoma developed at or near the site of a healed femoral fracture that had occurred 3, 6, and 15 years previously. Another patient had a biopsy at the time of a femoral neck fracture and a second biopsy 1 month later. The biopsy specimens showed pagetic bone without evidence of tumor. One month later, considerable destruction was present, and the femoral head was excised and found to consist largely of tumor, with neoplastic material also at the previous biopsy site.

Radiologic Findings

The radiologic features of malignant change, bone destruction or a soft-tissue mass, were fairly obvious in 19 of the 20 cases available for review. In one patient, who had a painful mass over the thoracic spine, the sarcoma was not recognized radiographically before biopsy and, even in retrospect, it was difficult to identify the destructive lesion in the T9 spinous process.

Of the 20 cases in which radiographs were available for review, four showed mostly osteoblastic changes that were more osteoblastic than the adjacent pagetic bone and typical of tumorous bone, seven showed mixed osteoblastic and lytic changes, eight showed mainly lytic changes, and one showed a large mass with calcification characteristic of cartilage tumor extending into the adjacent soft tissues. All of the blastic lesions were found to be osteosarcomas. Two of the mixed lesions were chondrosarcomas, and five were osteosarco-

mas. The lytic destructive lesions consisted of five osteosarcomas, two fibrosarcomas, and one malignant fibrous histiocytoma. The mass containing cartilage-type calcification was a chondrosarcoma. All cases showed destruction of the cortex but no periosteal reaction. In nine cases, extension into the soft tissues of a partially calcified or ossified tumor mass was visible on conventional radiographs.

Three cases had technetium-99m methylene diphosphonate (99m Tc-MDP) bone scans available for review. These showed evenly increased radionuclide uptake within both the tumor and pagetic bone (Fig. 4), and thus did not contribute to the diagnosis.

Prognosis

One patient was lost to follow-up after 2 years. At that time, he had no evidence of recurrence or metastases. Of the remaining 21, only one was a 5-year survivor, and he was known to be in good health 8 years after a left hip disarticulation for a femoral shaft osteosarcoma. He was then 75 years old, but he subsequently has been lost to follow-up. He had agreed to amputation only and had refused chemotherapy. He did not have symptomatic Paget disease before presentation, and, to the best of our knowledge, he had monostotic Paget disease. He was also the only patient in the series whose radiologic changes of Paget disease, at the time the sarcoma was detected, had not progressed beyond the lytic stage (Fig. 3). Of the 20 patients who are known to have died, survival ranged from 5 days to 2.5 years after their initial biopsies.

Discussion

Although the average age of 71 years in this series is a little older than that of any other study with more than 20 patients (most studies report mean ages of 60–65 years), this may not represent a significant difference between this population and the populations in other studies. Price and Goldie [2] found a mean age of 68 years, which is similar to that in our series. The male predominance is a well-recognized finding in other studies [3–6], with many reporting ratios of 1.5:1.0 to 2:1. Brackenridge [7], in a statistical study of the literature, found a 76% age-adjusted male preponderance of Paget sarcomas but only 56% in uncomplicated Paget disease.

The three cases with ^{99m}Tc -MDP bone scans showed increased or equal uptake of radionuclide at the tumor site when compared with the adjacent pagetic bone (Fig. 4), in contrast to the findings of Smith et al. [5], who reported a relative decrease in uptake. We suggest that ^{99m}Tc -MDP bone scans are often of little value in the diagnosis of Paget sarcomas but may aid in the diagnosis of multifocal Paget sarcomas and the identification of other areas of Paget disease. Yeh et al. [8] found gallium scans to be more helpful than bone scans in the diagnosis of Paget sarcoma.

The skeletal distribution of sarcomas seems to reflect the distribution of uncomplicated Paget disease, as has been suggested by other studies [2, 6, 9], although the humerus appears to be affected relatively more frequently [2, 4, 5, 10]. Several studies have drawn attention to the rarity of these lesions in the bones of the forearm [6, 11], but our case in the ulna is by no means unique. The first known patient with a Paget sarcoma, reported by Sir James Paget, died of a lesion that involved the radius [12]. One of our cases involved the fibula, known to be a very rare site even for uncomplicated Paget disease (Fig. 5) [4, 13, 14]. As far as we are aware, no reports of a solitary Paget sarcoma developing in this site have been published, although Haibach et al. [3] reported a case of a multifocal Paget sarcoma that involved both the tibia and fibula. Vertebral Paget sarcomas are reported to be exceedingly rare [2, 15], yet we had three solitary cases in our series, and the multicentric tumor showed many vertebral lesions. It appears that any bone affected by Paget disease may have the potential to undergo sarcomatous change.

The case of multifocal osteosarcoma raises some interesting points. Both radiologically and at autopsy, it appeared that the tumors involved only pagetic bone. Tumor deposits were found in the right petrous temporal bone, thoracic and lumbar vertebral bodies, and the medial end of the left clavicle. They were also seen radiologically to involve much of the pelvis. Because the tumor deposits appeared to involve only pagetic bone, the possibility of a multicentric origin must be considered. The controversy over whether multifocal Paget sarcomas are metastases or multiple primary tumors has been reviewed by several investigators [4, 11, 16]. The apparent involvement of only pagetic bone certainly favors multiple primary tumors in our case, and other investigators have found similar cases in their series [11]. Smith et al. [5] state that metastases to pagetic bone are rare, and they therefore consider these lesions multicentric. However, others [4, 16, 17] have reported pulmonary metastases in Paget sarcoma

patients in whom nonpagetic bone showed foci of sarcoma. This suggests that at least some of these cases are the result of metastatic disease.

Although less than 10% of all patients with Paget disease have polyostotic symptomatic disease [18], most patients in our study had a history of polyostotic symptomatic Paget disease, often of many years' duration before development of the neoplasm. Other Paget sarcoma studies have shown high prevalences of polyostotic disease, ranging from 57% to 100% [5, 6, 9]. Only one patient in our series showed lytic Paget disease that had not progressed to the more advanced osteoblastic or mixed lytic and osteoblastic stage. This patient also was the only long-term survivor (Fig. 3).

The poor prognosis in this disorder is confirmed by all previous studies. Smith et al. [5] found no significant change in survival rate from 1927 to 1982, despite enormous advances in diagnostic, anesthetic, and therapeutic techniques. They think that, although the older age of these patients may be a factor, the main reason is the almost invariably high grade of these tumors. Our histologic sections also showed high grade of the osteosarcomas; chondrosarcomas, fibrosarcomas, and the malignant fibrous histiocytoma were not universally high grade, yet survival of these patients also was poor, ranging from 21 days to 9 months from the date of biopsy.

Development of a sarcoma at or near the site of an old healed femoral fracture has been reported before [2, 10]. Porretta et al. [10] suggested that the superimposition of the fracture-healing process on the underlying fibroblastic and osteoblastic activity of Paget disease could lead to neoplasia. Price and Goldie [2] suggested that an occult neoplasm is the cause of the pathologic fracture rather than Paget disease. In our study, one patient had a sarcoma at the site of a healing fracture, where two previous biopsies had shown no tumor and only Paget disease. Despite the lack of any detectable tumor in the earlier biopsies, we still think this was a case of a pathologic fracture through a tumor and that the previous biopsies had sampled the wrong region. However, in three other patients, sarcomas developed near healed fractures 3–15 years after the fractures had occurred. With one possible exception, the sarcomas did not develop at the exact sites of the previous fractures but were simply in the vicinity. Our study and others [5, 6, 9] suggest that Paget sarcomas are more likely to occur in sites of advanced and clinically significant Paget disease, and these are also the sites in which complete pathologic fractures are more likely to occur [19]. We think that advanced Paget disease is susceptible to both pathologic fractures and sarcomatous change, but we consider it unlikely that a healing fracture predisposes pagetic bone to neoplasia.

Our finding of cortical destruction in all cases is similar to that of the study of Smith et al. [5]. We think that the possibility of neoplastic change must be considered whenever this finding is observed in pagetic bone. However, destructive lesions in pagetic bone may also be caused by coincidental metastases or myeloma [5] or by giant-cell tumors of pagetic bone [4, 20]. The development of giant-cell tumors in pagetic bone, although rare, is unlikely to be coincidental. These lesions

probably represent another form of neoplastic change due to Paget disease, although some authors believe they actually represent giant-cell reparative granulomas [20]. The benign process of negative focal bone balance after immobilization may lead to appearances suggestive of bone destruction [21]. Very aggressive Paget disease may show regions of apparent cortical destruction (Fig. 5) or associated soft-tissue mass, which may require a biopsy to exclude the diagnosis of sarcomatous change [22].

Although the most important role of the radiologist in the diagnosis of Paget sarcomas is the identification of a region of probable neoplastic change, in many cases it is also possible to be more specific as to tumor type. In our series, the tumor with a calcified matrix was a chondrosarcoma, whereas the four osteoblastic lesions showed the typical tumorous bone appearance of osteosarcomas. The lytic and mixed lytic and osteoblastic lesions were, however, less specific. Although all the sarcomas of fibrous tissue origin (two fibrosarcomas and one malignant fibrous histiocytoma) were lytic, there were also five lytic osteosarcomas (Figs. 3 and 5). Among the mixed osteoblastic and lytic lesions, it was sometimes difficult to distinguish tumorous bone from calcified chondral matrix, and this group contained both chondrosarcomas and osteosarcomas.

The lack of any periosteal reaction indicating malignancy may be a reflection of either the nature of the pagetic bone or the age of these patients. It is our experience that fractures and neoplastic lesions in older patients appear to cause less periosteal reaction than is seen in younger persons. Other series also have found periosteal reaction to be uncommon in Paget sarcoma [5, 6].

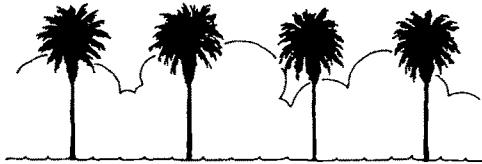
In conclusion, it appears that any part of any bone affected by Paget disease may have the potential for malignant change, and this is more likely to occur when the disease is long standing and radiologically advanced. Fractures that precede the development of Paget sarcomas may represent either a pathologic fracture through an unrecognized tumor or a fracture with later development of a tumor. It seems likely that multifocal Paget osteosarcomas are true multicentric lesions. A destructive process in pagetic bone, especially involving the cortex, should alert the radiologist to the possibility of malignant change. In some cases, specific findings such as a dense osteoblastic appearance or a chondroid matrix may suggest the tumor type. Finally, despite recent advances in the diagnosis and management of these lesions, Paget sarcomas continue to have a very poor prognosis.

ACKNOWLEDGMENTS

We thank Aileen Isaac and Vivienne Prince for their help in collecting data and for coordinating the research efforts from two countries.

REFERENCES

- Merkow RL, Lane JM. Paget's disease of bone. *Orthop Clin North Am* **1990**;21:171-189
- Price CHG, Goldie W. Paget's sarcoma of bone: a study of eighty cases from the Bristol and the Leeds Bone Tumour Registries. *J Bone Joint Surg [Br]* **1969**;51-B:205-224
- Haibach H, Farrell C, Dittrich FJ. Neoplasms arising in Paget's disease of bone: a study of 82 cases. *Am J Clin Pathol* **1985**;83:594-600
- McKenna RJ, Schwinn CP, Soong KY, Higinbotham NL. Osteogenic sarcoma arising in Paget's disease. *Cancer* **1964**;17:42-66
- Smith J, Botet JF, Yeh SDJ. Bone sarcomas in Paget disease: a study of 85 patients. *Radiology* **1984**;152:583-590
- Wick MR, Siegal GP, Unni KK, McLeod RA, Greditzer HG III. Sarcomas of bone complicating osteitis deformans (Paget's disease): fifty years' experience. *Am J Surg Pathol* **1981**;5:47-59
- Brackenridge CJ. A statistical study of sarcoma complicating Paget's disease of bone in three countries. *Br J Cancer* **1979**;40:194-200
- Yeh SDJ, Rosen G, Benua RS. Gallium scans in Paget's sarcoma. *Clin Nucl Med* **1982**;7:546-552
- Huvos AG, Butler A, Bretsky SS. Osteogenic sarcoma associated with Paget's disease of bone: a clinicopathologic study of 65 patients. *Cancer* **1983**;52:1489-1495
- Porretta CA, Dahlin DC, Janes JM. Sarcoma in Paget's disease of bone. *J Bone Joint Surg [Am]* **1957**;39-A:1314-1329
- Schajowicz F, Araujo ES, Berenstein M. Sarcoma complicating Paget's disease of bone: a clinicopathological study of 62 cases. *J Bone Joint Surg* **1983**;65-B:299-307
- Paget J. On a form of chronic inflammation of bones (osteitis deformans). *Trans R Med Chir Soc* **1877**;60:37-63
- Guyer PB. Paget's disease of bone: the anatomical distribution. *Metab Bone Dis Rel Res* **1981**;45:239-241
- Merrick MV, Merrick JM. Observations on the natural history of Paget's disease. *Clin Radiol* **1985**;36:169-174
- Yochum TR. Paget's sarcoma of bone. *Radiolge* **1984**;24:428-433
- Syame J. Multifocal Paget's sarcoma of bone with sclerosis. *Aust Radiol* **1969**;13:219-223
- Sear HR. Osteogenic sarcoma as a complication of osteitis deformans: some personal experiences and reflections. *Br J Radiol* **1949**;22:580-587
- Wallach S. When should Paget's disease be treated? In: Wallach S, ed. *Paget's disease of bone*. Chicago: Professional Communications Associates, **1979**:67-68
- Barry HC. *Paget's disease of bone*. London: Livingstone, **1969**
- Case records of the Massachusetts General Hospital (Case 1-1986). *N Engl J Med* **1986**;314:105-113
- Maldaque B, Malghem J. Dynamic radiologic patterns of Paget's disease of bone. *Clin Orthop* **1987**;217:126-151
- Monson DK, Finn HA, Dawson PJ, Simon MA. Pseudosarcoma in Paget disease of bone: a case report. *J Bone Joint Surg [Am]* **1989**;71-A:453-455



Come to the
American Roentgen Ray Society
92nd
ANNUAL MEETING
Orlando, FL

Marriott's Orlando World Center
May 10-15, 1992

Scientific Program (200 papers)
Instructional Courses (60 hours)
Categorical Course on Neuroradiology
The Caldwell Lecture
Award Papers
Scientific Exhibits
Social, Golf, and Tennis Programs
Guest Programs

Pictorial Essay



MR Imaging of Fetal Anomalies

Robert C. Benson,^{1,2} Patrick M. Colletti,¹ Lawrence D. Platt,^{3,4} and Philip W. Ralls¹

MR imaging can be used to confirm the presence of most gross fetal anomalies detected by sonography in the second and third trimesters. The MR imaging findings in 25 cases of fetal anomalies first identified on sonography are illustrated.

Previous studies have described the potential use of MR imaging in obstetric diagnosis [1, 2]. Small case series of MR of fetal anomalies have been reported [3, 4]. We describe our experience with using MR imaging to evaluate fetal anomalies in 25 cases.

Materials and Methods

Institutional approval to use MR to evaluate pregnancies with suspected congenital anomalies was obtained. Twenty-five patients with fetal anomalies as shown by sonography were examined by MR. Gestational ages were between 12 and 40 weeks, with six second-trimester and 19 third-trimester pregnancies.

Imaging was done with a 0.5-T superconducting system. Axial, coronal, and sagittal 10-mm-thick 300–500/20 (TR/TE) images were acquired. Occasional 2000/80 or field-echo images were obtained. Oblique views were used on two cases with oblique lie. No maternal sedation was used.

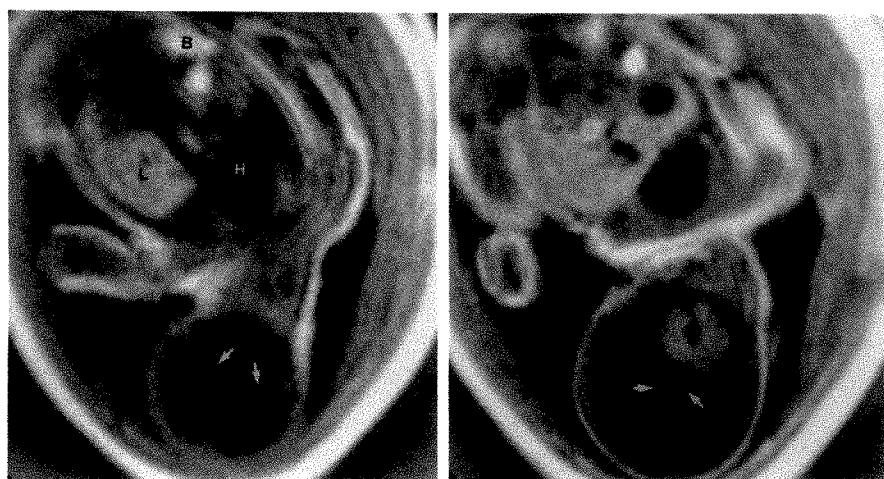


Fig. 1.—Fetal hydrocephalus, 40 weeks' gestation.

A and **B**, Coronal MR images show severe hydrocephalus. Tentorium (arrows), fetal heart (H), fetal liver (L), and meconium-filled bowel (B) are seen, as is placenta (P).

Received October 15, 1990; accepted after revision December 3, 1990.

¹ Department of Radiology, University of Southern California School of Medicine, LAC/USC Medical Center, 1200 N. State St., Los Angeles, CA 90033. Address reprint requests to P.M. Colletti.

² Present address: Department of Radiology, Anaheim General Hospital, 3350 W. Ball Rd., Anaheim, CA 92804.

³ Department of Obstetrics/Gynecology, University of Southern California School of Medicine, LAC/USC Medical Center, 1200 N. State St., Los Angeles, CA 90033.

⁴ Present address: Department of Obstetrics and Gynecology, Cedars-Sinai Medical Center, 8700 Beverly Blvd., Los Angeles, CA 90048.

Images were correlated retrospectively with real-time sonography and postdelivery fetal configurations.

Results

Twenty-two (88%) of 25 fetal anomalies were identified with MR. This includes 18 (95%) of 19 third-trimester studies (95%) and four (67%) of six second-trimester studies. All seven patients with polyhydramnios and the one patient with oligohydramnios were accurately identified.

Fetal anatomy was best visualized by short TR, short TE imaging. Fetal motion produced artifacts that compromised imaging in the three patients with anomalies that were not identified.

Anomalies of the fetal head and neck were clearly shown by MR. Fetal hydrocephalus was well shown in four cases (Fig. 1), because the dilated low-signal ventricles contrasted well with the intermediate-signal brain. Cranial defect in anencephaly was shown as absence of brain and skull rostral to the face (Fig. 2) in two cases.

Anomalies of the fetal body were usually shown well with MR. Two cases of thoracoomphalopagus displayed the thoracoabdominal union and a conjoined liver and common peri-

cardium (Fig. 3). The relatively high signal of meconium in extraabdominal fetal bowel was noted in two omphaloceles and two cases of gastroschisis. In addition, the omphaloceles exhibited a rounded "contained" shape (Fig. 4), whereas the gastroschisis appeared more serpiginous (Fig. 5). Decreased signal was seen in the dilated renal pelvis of fetal hydronephrosis (Fig. 6). Fetal ascites was also well shown in this case of prune belly; however, less severe fetal hydronephrosis was not seen in two other cases. A large congenital ovarian cyst showed a signal intensity slightly greater than that of the fetal bladder (Fig. 7).

The fetal spine was identifiable but difficult to evaluate completely. A large meningocele with associated hydrocephalus and a large sacral teratoma were easily seen.

Discussion

MR images obtained under current protocols can display most gross fetal anomalies previously detected by sonography in the second and third trimesters. MR imaging will most likely be useful as a secondary technique to confirm fetal abnormalities such as hydrocephalus. Advantages of MR

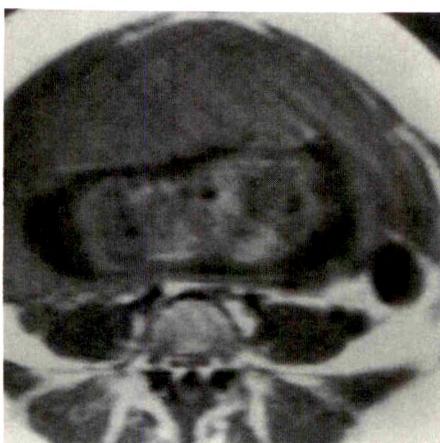


A



B

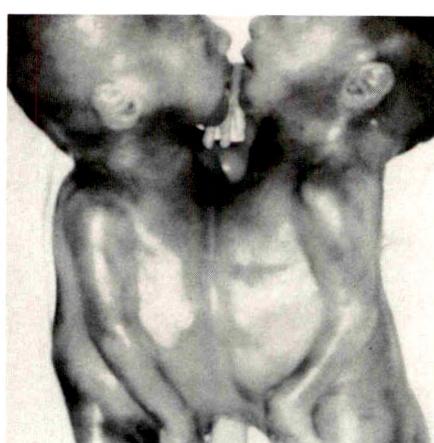
Fig. 2.—Acrania, 34 weeks' gestation.
A, Sagittal MR image shows cranial defect (arrows).
B, Photograph of fetus shows a large cranial defect.



A

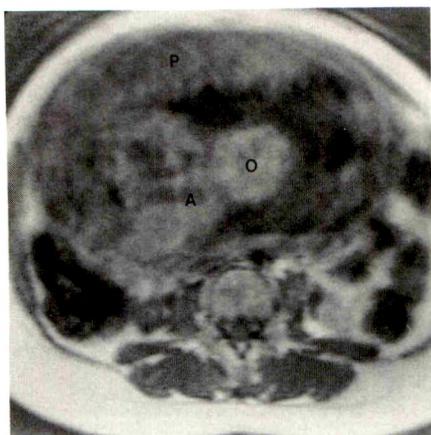


B

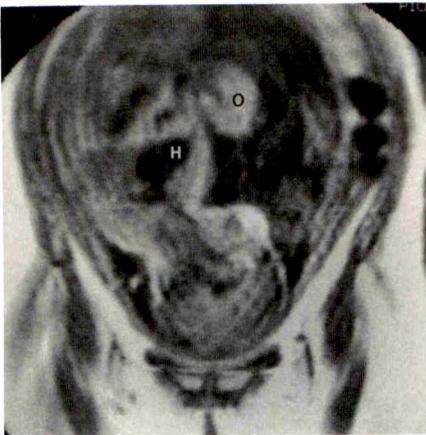


C

Fig. 3.—Thoracoomphalopagus, 23 weeks' gestation.
A-C, Transverse (A) and coronal (B) MR images and photograph (C) of conjoined fetuses. Fetal abdomens, hearts (H), and conjoined livers (L) are seen.



A

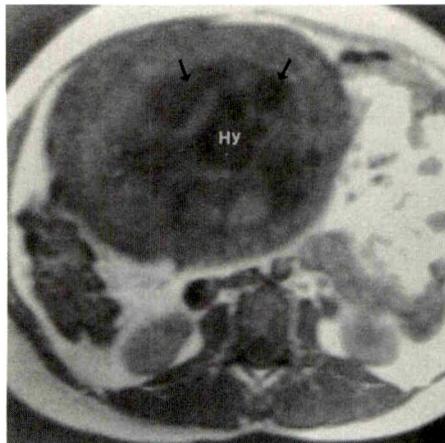


B

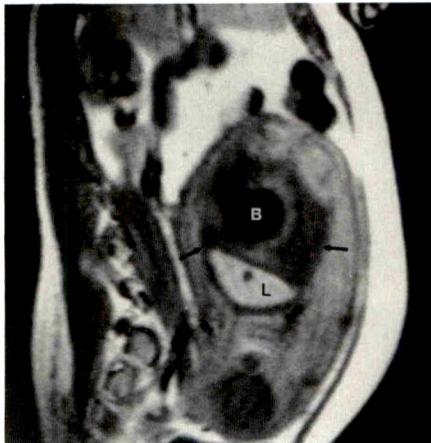


Fig. 4.—Omphalocele, 40 weeks' gestation.
A and B, Axial (A) and coronal (B) MR images show a relatively homogeneous bowel containing omphalocele (O) projecting from fetal abdomen (A). P = placenta, H = fetal heart.

Fig. 5.—Gastroschisis, 37 weeks' gestation.
Coronal MR image shows high-signal meconium in discrete extraabdominal loops of bowel (arrows). P = placenta, H = fetal heart.



A



B



C

Fig. 6.—Prune belly and posterior urethral valves, with hydronephrosis and fetal hydrops, 35 weeks' gestation.
A-C, Axial (A) and sagittal (B and C) MR images show hydronephrosis (Hy), fetal ascites (arrows), and hydropic skin thickening (arrowheads). B = fetal bladder, L = fetal liver.

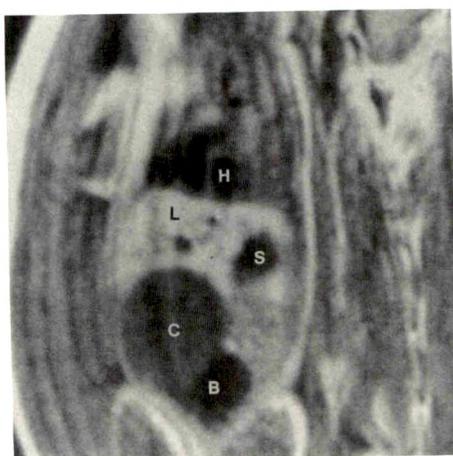


Fig. 7.—Ovarian cyst, 39 weeks' gestation. Sagittal MR image shows fetal cyst (C), fetal liver (L), stomach (S), bladder (B), and heart (H).

include multiparameter tissue contrast and a large field of view. Disadvantages include expense and relatively long imaging times. Although fetal motion may result in image degradation, the problem is encountered less often in later pregnancy, particularly if the fetus is markedly abnormal. Fetal sedation with maternal diazepam [4] may be used if necessary. As more rapid MR imaging becomes available, it is likely that fetal anomalies will be better delineated.

REFERENCES

- McCarthy SM, Filly RA, Stark DD, et al. Obstetrical magnetic resonance imaging: fetal anatomy. *Radiology* 1985;154:427-432
- Weinreb JC, Low T, Cohen JM, Kutler M. Human fetal anatomy: MR imaging. *Radiology* 1985;157:715-720
- McCarthy SM, Filly RA, Stark DD, Callen PW, Golbus MS, Hricak H. Magnetic resonance imaging of fetal anomalies in utero: early experience. *AJR* 1985;145:677-682
- Williamson RA, Weiner CP, Yuh WTC, Abu-Yousef MM. Magnetic resonance imaging of anomalous fetuses. *Obstet Gynecol* 1989;73:952-956

Book Review

Angiocardiography in Congenital Heart Malformations. By Benigno Soto and Albert D. Pacifico. Mt. Kisco, NY: Futura, 669 pp., 1990, \$175

Angiocardiography in Congenital Heart Malformations, published in 1990, is the summation of almost two decades of work in the field of cardiac radiologic diagnosis in children. The authors, Soto and Pacifico, together with Barcia and Bargeron, to whom they give respectful credit, revolutionized angiocardiography by introducing new techniques for better visualization of cardiac anatomy. Their aim was "to transfer anatomic information into black and white motion pictures." The means of achieving this ambitious aim were a variety of new projections, collectively referred to as "axial views." These were anatomically far more correct than the anteroposterior, lateral, and ordinary oblique views customarily used until then. An integral part of the authors' quest was an insistence on rigorous comparison between anatomic specimens and cineangiograms. From these efforts came a better overall understanding of congenital malformations of the heart.

The book begins with a brief, concise chapter on angiographic techniques. In addition to describing the axial projections in detail, catheters, contrast agents, and radiographic techniques are discussed also. This introduction alone could be useful for someone setting up a new angiographic laboratory. Appropriately for an anatomically oriented book, chapter 2 deals with cardiac morphology from the point of view of angiocardiography, and with what the authors call sequential analysis of angiograms. Excellent correlations with anatomic specimens are included throughout the book, and the correlations are particularly detailed in this section. Thereafter, the authors present the spectrum of congenital malformations in the framework of sequential analysis. Their approach is based on the embryologic development of the heart (e.g., pulmonary venous abnormalities are in the chapter on atrial lesions.) The authors adhere to their own logic throughout; the pulmonary atresias are included with the anomalies of the ventriculoarterial connections, whereas valvular pulmonary stenosis is found with the anomalies of the

pulmonary arteries. The last section is devoted to the myocardium. The coronary arteries are in this section, of course, rather than in the one on the aorta. The approach is consistent, and the text is lucid. The illustrations are excellent, including the chest films, and are labeled extensively. The references, at the end of each chapter, are entirely sufficient rather than exhaustive.

This impressive work is rather monolithic. Therefore, it is difficult to criticize minor details, such as the choice of this or that catheter, a particular combination of projections, anesthesia vs sedation, and so forth. My concerns are on a more fundamental level. When *Diagnosis of Congenital Heart Disease* by Kjellberg et al. was first published in the mid-1950s, it opened a wide new vista for cardiac radiology because it represented the cutting edge in the field, far ahead of practically everyone else. In contrast, Soto and Pacifico's book is a superb summary of great past achievements. And, in all fairness, it does not fill a void. *Angiocardiography of Congenital Heart Disease* by Freedom et al., published in 1984, covers the same ground at almost the same length, even if the approach and organization are different.

The diagnosis of congenital heart disease has changed drastically since the mid-1970s. Soto and Pacifico mention echocardiography in the text but only occasionally correlate their material with sonograms. And, no reference is made to MR imaging of the heart. I recommend this beautiful book to all those who wish to learn angiocardiography or who use this technique regularly. To learn about a modern, integrative approach to cardiac imaging, we will have to resort to other texts.

M. T. Gyepes
Miller Children's Hospital
Long Beach, CA 90801

John Caffey Award

Determination of Functional Residual Capacity from Digital Radiographs of the Normal Neonatal Chest: Studies in a Rabbit Model



Keith S. White^{1,2}
Andre A. Muelenaer, Jr.³
Craig A. Beam⁴
Eric L. Effmann^{1,5}

Spirometric measurement of lung volume in an infant or uncooperative child is often a difficult and time-consuming procedure. Previous investigators have successfully estimated total lung capacity in adults and older children by using chest radiography. The purpose of this study was to assess the accuracy of functional residual capacity (FRC) determination from chest radiographs in an animal model of the normal neonatal chest. FRC was determined with the helium dilution (HeD) method in 13 anesthetized, intubated, and paralyzed rabbits (weight range, 1.5–3.9 kg). FRC was then estimated from digital frontal and lateral chest radiographs. The radiographic estimate was made by applying measurements taken from the radiographic film pair to a geometric model of the chest. The best-fit model assumed an elliptical cross section for the intrathoracic cavity, heart, paraspinal structures, and diaphragm in the axial plane. Linear regression on independently determined HeD and radiographically determined FRC yielded a slope of 1.02 ($p < .001$), an intercept of -3.02 cm^3 ($p = .565$), and a correlation coefficient of 0.96 ($p < .001$).

We conclude that radiographic FRC estimates closely approximate HeD estimates in a rabbit model of the normal neonatal chest.

AJR 156:1209–1214, June 1991

Measurements of total lung capacity and maximum flow volumes are unreliable in the uncooperative infant because these volumes depend on effort. Functional residual capacity (FRC) is one measurable volume that the child will generally maintain during multiple respiratory cycles regardless of inspiratory effort or respiratory rate.

Functional residual capacity is defined as the volume of gas in the chest at end tidal volume. Helium dilution (HeD) and nitrogen washout are the two most widely applied methods of FRC determination. In infants with gas trapping, FRC measurements with gas dilution underestimate the total end-expiration thoracic gas volume (TGV), and thus HeD measurements are of limited value in infants with respiratory disease. Although body plethysmography is the method that has been used to measure TGV, the accuracy of this method in the neonate has been questioned [1].

Hurtado and Fray [2] first introduced the idea of lung volume estimation by using chest radiographs. Barnard and coworkers [3] later described a model of the thoracic cavity as a series of stacked elliptical cylindroids. Subsequently, Loyd and coworkers [4], and Pierce et al. [5] described variations of this technique. These methods all estimate lung volume by applying measurements taken directly from radiographs to a geometric model of the chest. Radiographic estimates of lung volume have also been obtained with planimetry [6, 7].

Reports of radiographic estimates of lung volume in children are few. Hiller et al. [8] evaluated a geometric method in children 12 to 19 years old and found correlation coefficients ranging from 0.927 to 0.930 when comparison was made with helium dilution estimates of lung volume. Salam and Warwick [9], Shepard

Received August 16, 1990; accepted after revision December 5, 1990.

Recipient of the John Caffey gold award at the annual meeting of the Society of Pediatric Radiologists, Cincinnati, OH, April 1990.

¹ Department of Radiology, Duke University Medical Center, Durham, NC 27710.

² Present address: Department of Radiology, Children's Hospital Medical Center, Eiland and Bethesda Aves., Cincinnati, OH 45229-2899.

³ Department of Pediatrics, Division of Pulmonary Disease, Duke University Medical Center, Durham, NC 27710.

⁴ Departments of Radiology and Family and Community Medicine, Division of Biometry, Duke University Medical Center, Durham, NC 27710.

⁵ Present address: Department of Radiology, Children's Hospital and Medical Center, 4800 Sand Point Way, N.E., Seattle, WA 98105. Address reprint requests to E.L. Effmann.

0361-803X/91/1566-1209

© American Roentgen Ray Society

and Seliger [10], and Campbell [11] have achieved similar results in children. To our knowledge, radiographic lung-volume determinations have never been rigorously tested in neonates or infants.

We developed a computer program that applies a geometric model of the neonatal chest to a pair (frontal/lateral) of digital radiographs to estimate lung volume. This paper details the model used and compares computer-generated lung-volume estimates of FRC with directly measured volumes in a phantom set and volumes determined with helium dilution in a rabbit model of the normal neonatal chest.

Methods

Radiographic Volume Estimation

Conventional film images were digitized with a Dupont FD 2000 (Dupont, Wilmington, DE) digitizer into 512×512 element arrays (pixel size, 0.0211 mm^2). Digital image arrays were then made available to a SUN 3/280 computer system (SUN Microsystems, Mountain View, CA) for display and processing. The computer program was designed to display the images and allow user definition of anatomic boundaries on the images with a mouse. A user-defined anatomic landmark (usually the dome of the diaphragm) designating equivalent vertical (axial plane) position was marked on each image. The calculated vertical offset was subsequently used to pair equivalent axial planes from the two orthogonal images. Boundaries for the intrathoracic cavity, heart, diaphragm, and paraspinal structures were then traced on each image (Fig. 1). Strict criteria for boundary definition were established by comparing a frontal/lateral film pair to an axial CT scan in a sample rabbit. Trace interfaces were selected so as to minimize interpolation at ambiguous borders. The boundary of the intrathoracic cavity was defined as the interface of the lung with the ribs on the frontal projection and the interface with the sternum and the posterior margin of vertebral bodies on the lateral projection. The heart's boundary was defined by the interface of heart with lung on the frontal view. The posterior margin of the heart on the lateral projection was defined by the posterior wall of the trachea. The paraspinal boundary was defined by the lung/paraspinal soft-tissue interface or lateral margins of the vertebral bodies on the frontal view and anterior/posterior margins of the spine on the lateral view. The

diaphragm margins were defined by their interface with the lung. In cases in which the lateral projection showed two diaphragm shadows, the boundary was defined halfway between the shadows.

Axial slices (of 1 pixel thickness) in each image were defined by elements in the two-dimensional image array with the same y coordinate. Equivalent frontal/lateral axial slices were selected by applying the vertical offset defined previously. Frontal and lateral dimensions of the intrathoracic cavity, heart, diaphragm, and paraspinal structures were then determined from the traced anatomic boundaries for each axial slice by the computer program (Fig. 2). The lateral dimension of the paraspinal structures was doubled to compensate for the aorta and inferior vena cava, which had no reliably definable boundaries on the images. These anatomic dimensions were then applied to a geometric model to give an estimate of volume of each structure in that axial slice. Two geometric models were tested. In both models, the volume (V) of a structure for an axial slice was estimated by multiplying a constant (c) by the product of the frontal dimension (F_d), lateral dimension (L_d), and slice thickness (S_t):

$$V = c \times F_d \times L_d \times S_t.$$

Model I used the formula for an ellipse in which the constant $c = \pi/4$ ($c = 0.785$). This same elliptical formula was used for all structures. In model II, a different constant c was determined for each structure from axial CT scans. These scans were acquired through the chest of an anesthetized, intubated rabbit at continuous 5-mm intervals with a GE 9800 scanner. For each slice, the frontal and lateral dimensions and the area (A) of each structure were measured. A constant c was calculated for each structure in each axial plane of the chest such that

$$c = A/(F_d \times L_d).$$

A mean value of c was calculated for each structure and used in model II.

Volumes of the intrathoracic cavity, heart, diaphragm, and spine were estimated by adding calculated volumes from each axial slice. Conversion from volume units of cubic pixels to cubic centimeters included a correction factor for magnification. The magnification correction factor was determined from each radiograph by measuring a coin of known diameter that was placed at the midpoint of the chest during the radiographic exposure. The diameter of the coin in pixels

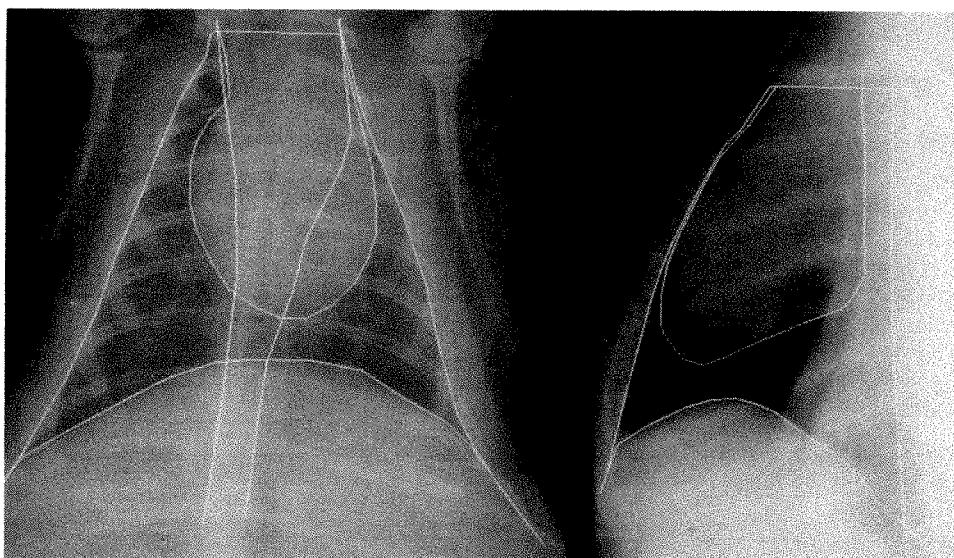


Fig. 1.—Digital frontal and lateral chest radiographs of a rabbit with traced margins of intrathoracic cavity, paraspinal structures, heart, and diaphragm.

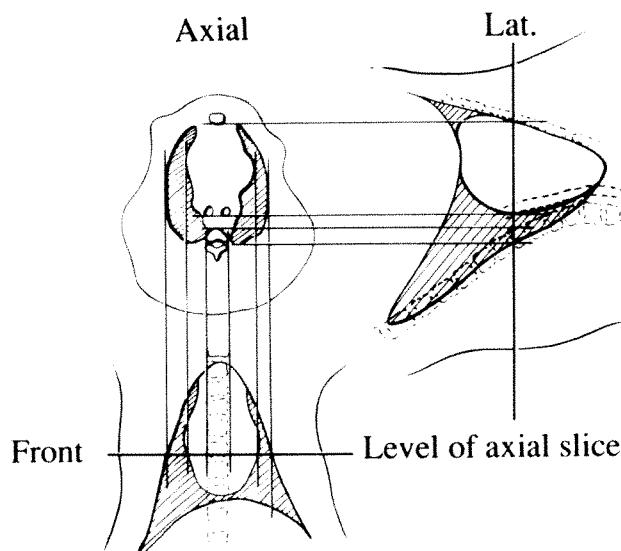


Fig. 2.—Graphic depiction of a representative axial slice through mid-chest. Frontal and lateral dimensions of anatomic structures in axial plane are defined by traced boundary points of frontal/lateral film pair at corresponding axial position.

was determined by the user's defining the edges of the coin with the mouse. The true centimeter pixel conversion factor could then be determined. Lung volume was then calculated by subtracting the volumes of the heart, paraspinal structures, and diaphragm from the intrathoracic volume.

FRC estimation further required correction for volume occupied by lung tissue and blood. Because no estimation of this correction could be found in the literature, seven white rabbits (wt., 1.93–3.40 kg) were anesthetized and endotracheally intubated. In each case, the intrathoracic cavity was opened, both pulmonary hilae were simultaneously clamped, and the lungs were removed. The lung tissue and pulmonary blood were then weighed and the pulmonary tissue and blood volume per kilogram of body weight was estimated by dividing the weight of tissue and blood by the product of the body weight of the rabbit and density of compact lung tissue (1.06 g/cm^3). The mean value of the seven estimates was used as the correction factor.

Volume Estimation by HeD

To determine FRC by HeD, a helium analyzer (Model D-67 Helium Analyzer, Warren E. Collins, Braintree, MA) was calibrated with a known concentration of helium. Fifty milliliters of helium (9.58%) in air balance was drawn into a syringe, and 25 ml was injected into the analyzer and the concentration was recorded. The remaining 25 ml of helium was attached directly to the endotracheal tube via a stopcock, and 10 25-ml breaths were cycled in and out. The end-expiratory sample was analyzed, and FRC was calculated by using standard equations [12]. FRC was corrected for dead-space volume of the stopcock, endotracheal tube, and large conducting airways. The length and diameter of the trachea and main bronchi were measured from the chest radiographs. Correction for dead space in large conducting airways was achieved by assuming a cylindrical geometry for each airway segment. Correction from atmospheric temperature (22°C) and pressure to body temperature and pressure was performed by using the factor 1.10 [13].

Validation

The computer method of lung volume determination was first validated on a phantom set. The chest was simulated by a 60-ml plastic syringe in which the plunger simulated the diaphragm. Three wooden cylinders of various lengths were used to approximate the spine, and a small sphere simulated the heart (Fig. 3). A coin of known diameter was positioned beside the midpoint of the syringe as a magnification correction template. Frontal and lateral radiographs were obtained at five different syringe-plunger positions and with variably sized simulated spines in a double-blind fashion. One investigator measured the volume from each film pair by the computer method. Computer-estimated lung volume was determined three times for each film pair in order to determine variability in the computer method. The second investigator measured the simulated spines and heart with a micrometer and subtracted those volumes from the preset syringe volume to obtain simulated lung volume directly for each experiment.

Thirteen New Zealand white rabbits weighing between 1.5 and 3.9 kg were then studied with HeD and radiographic methods. Rabbits were fasted before the studies. On the day of the study, each rabbit was anesthetized and sedated with intramuscular xylazine (7 mg/kg), ketamine hydrochloride (50 mg/kg), and acepromazine maleate (0.5 mg/kg). After intubation with a 3.0-mm cuffed endotracheal tube, the rabbits were ventilated at a tidal volume of 10 ml/kg and a respiratory rate equal to their resting rate. After administration of a pancuronium bromide 1.7 mg/kg intraperitoneally, the rabbits were hyperventilated. Three sets of correlated HeD and radiographic FRC determinations were made for each rabbit. Five minutes separated each measurement set, which consisted of two HeD estimates and a single film pair. For each set, the respirator was suspended and the rabbits were allowed to exhale passively to FRC. Two determinations of FRC were then performed by using standard HeD techniques with concomitant acquisition of a frontal/lateral film pair.

Three determinations of radiographic FRC were made for each film pair. The FRC determinations by HeD and by radiographs were performed by different investigators, each of whom was unaware of the others' findings.

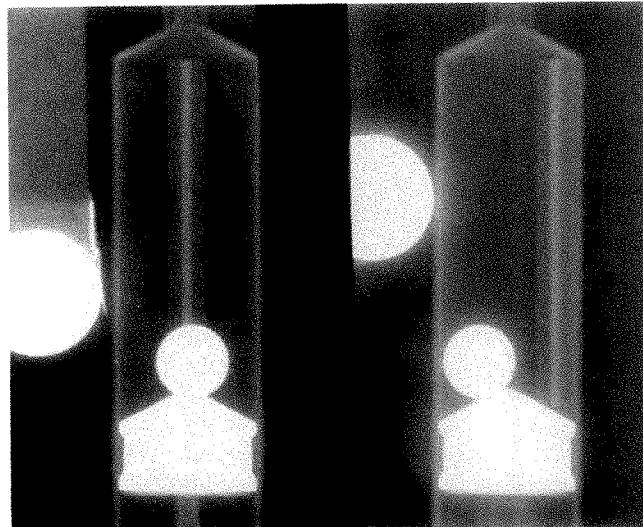


Fig. 3.—Frontal and lateral radiographs of lung-volume phantom.

Statistical Methods

Standard simple linear-regression methods [14] were used for the analysis of the phantom data. Exploratory analysis and residual plots provided no evidence to reject the required assumptions for the usual normal-theory simple linear-regression model. This analysis was supplemented by the analysis of paired differences in FRC determinations by the two methods. This analysis used a *t* test on the differences after exploratory confirmation of approximate normality in the distribution of the paired differences.

Rabbits were selected to represent as wide a range of weights, and hence lung volumes, as possible. Sample size was dictated by practical considerations.

For each measurement set, the two HeD measurements were averaged and the three radiographic estimates averaged so that the data from each rabbit then consisted of the three FRC determinations from HeD and the three radiographic FRC determinations. These determinations were made alternatively across time, yielding six sequential determinations.

A repeated measures analysis of variance model was first used to investigate the presence of a systematic relationship of the determinations with type of determination (HeD or radiographic) and time. Time was not found to be a significant (at the 5% level) main or interaction effect. As such, the HeD FRC determinations and the radiographic FRC determinations were averaged across time for each animal, and this pair of averages was used in the primary analysis. A similar, but secondary, analysis of the so-called "model II" radiographic FRC determinations also was made.

Before modeling, agreement between the various methods of FRC estimation was explored by using *t* tests on the three sets of paired differences (model I-HeD, model II-HeD, and model I-model II) after exploratory confirmation of approximate normality. This analysis was then followed by exploratory analysis of the relationship between mean FRC by model I and mean FRC by HeD determination.

Results

Comparison of computer-estimated lung volume and directly measured volume in the phantom set yielded a very strong linear relationship, with a Pearson correlation coefficient of .999 ($p < .001$; Fig. 4). The computer method underestimated true volume by between 0.831 and 0.455 cm³ on average (95% confidence interval on the average paired difference). Therefore, with 95% confidence, we estimate the computer method to underestimate true volume by a maximum of 6.9% and a minimum of 1.3% over the volume range tested (12–36 cm³).

Geometric shape constants *c* determined for method II were *c*(intrathoracic) 0.84, *c*(heart) 0.83, *c*(paraspinal) 0.97, and *c*(diaphragm) 0.85. The experimentally determined mean correction factor for lung tissue and pulmonary blood volume per kilogram body weight was 4.3 ml/kg.

Comparison between mean radiographic and mean HeD estimates in the rabbit series showed high linear correlation (Fig. 5). The radiographic model I-HeD and model II-HeD correlation coefficients were .96 ($p < .001$) and .96 ($p < .001$), respectively. A linear regression analysis of radiographic volume estimates on HeD FRC determinations showed that in both cases the null hypothesis of unity slope would not be rejected (Table 1). In addition, a paired-difference analysis showed no significant differences between HeD, model I, and model II (Table 2). A post-hoc analysis of power indicates this study had an 80% chance of detecting an

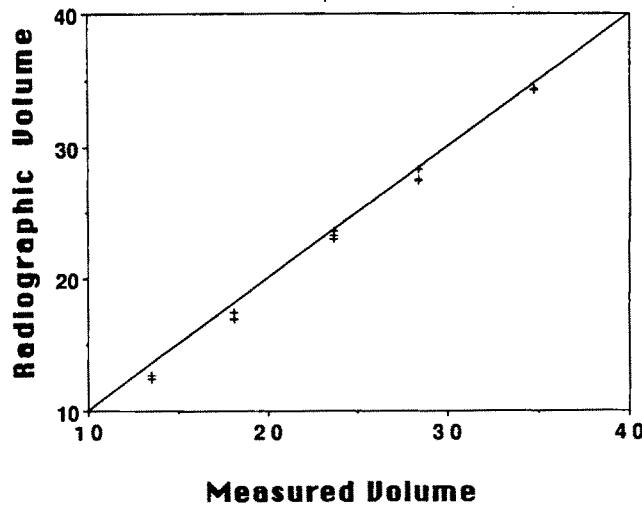


Fig. 4.—Scatter plot comparing radiographic and directly measured "lung volume" in phantom set.

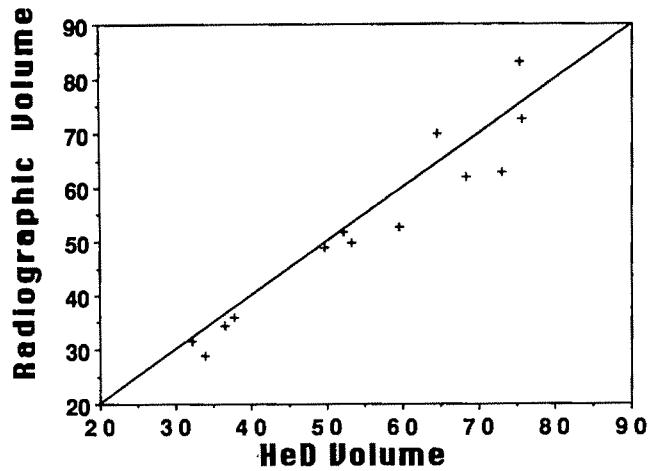


Fig. 5.—Scatter plot comparing radiographic model I and helium dilution (HeD) estimates of functional residual capacity in rabbits.

average difference between HeD and radiographic mean determinations as small as 4 cm³.

As mentioned, statistical analysis did not show any systematic relationship between the measurements and the order they were taken in. Hence, variability in these estimates is regarded as random "error." By using repeated measures analysis of variance, the standard deviation of HeD measurements from the same measurement set is estimated to be 2.18 cm³, and the standard deviation of the radiographic measurements from the same set is estimated to be 1.06 cm³.

Discussion

The results of the phantom experiment validate the film digitization, image tracing, and computer algorithm. The minimal underestimation of true volume could be due to systematic error in the computer method or in the method of direct volume measurement. Because the geometry of the phantom

TABLE 1: Parameter Estimates from Simple Linear Regression on Helium Dilution Determinations of Functional Residual Capacity

Model	n	Parameter	Estimate	Standard Error	p Value
Rabbit model I	13	Intercept	-3.02	5.096	.565
		Slope	1.02	0.090	<.001
Rabbit model II	13	Intercept	-4.00	5.069	.4471
		Slope	1.03	0.089	<.001

TABLE 2: Analysis of Paired Differences in Determinations of Functional Residual Capacity

Model	n	Mean	Standard Error	95% Confidence Interval
Model I, helium dilution	13	-2.09	1.323	(-4.98, 0.788)
Model II, helium dilution	13	-2.13	1.322	(-5.01, 0.754)
Model I, model II	13	0.03	0.138	(-0.27, 0.330)

was compatible with the elliptical model, errors in volume determination were probably unrelated to the computer algorithm itself. Rather, the most likely systemic errors in the computer method are error in magnification correction and error in manual tracing. Tracing error would most likely relate to boundary unsharpness and interpolation by the user in areas of border ambiguity. Strict adherence to tracing rules and optimization of radiographic technique should minimize these effects.

A small error in the linear magnification correction results in a larger error in the volume estimate (because the factor is cubed in volume calculation). For example, a 1% underestimate of true pixel to centimeter conversion results in a 3% underestimate of true volume. Magnification correction can be determined from a reference template for each radiographic image or by maintenance of strict tube/subject/film geometry for all radiographic exposures. Because of variability of body geometry, we favor the reference template method. The wider the separation between reference points, the less the error induced by inaccurate boundary determination.

Comparison between HeD and radiographic estimates of functional residual capacity in the rabbit series showed excellent linear correlation. Interpretation of the estimates of the linear relationship of radiographic FRC on HeD FRC must be done with care owing to the fact that the "independent" variable in this case is measured with error. As discussed by Snedecor and Cochran [14], the impact of measurement error in simple linear regression by the method of least squares is to underestimate the true slope of the relationship. However, as our regression analysis was on the means of replicate determinations, which were relatively widely spread across the interval of measurement, the attenuation effect should be negligible. As with the phantom set, the radiographic method tended to underestimate FRC slightly, although this trend was not statistically significant. In addition to systematic errors in magnification and tracing discussed earlier, two additional

sources of error must be considered: possible error in HeD determination of FRC and error in the geometric model itself.

There are three methods for determination of FRC: gas dilution, whole-body plethysmography, and radiography. The plethysmographic and radiographic methods reflect the total intrathoracic gas volume. Gas-dilution methods measure only the volume of the lungs that is in direct communication with the conducting airways. Discrepancy between the helium dilution and radiographic FRC determinations would tend to err in the direction of the HeD underestimating FRC. In disease-free rabbits, this discrepancy should be negligible. Further studies in animals with lung disease are needed to determine if this relationship will be maintained.

FRC determination by dilution of an inert gas (neon) has been validated in rabbits [13]. By using a similar 10-breath technique for HeD, we measured FRC-HeD as 20.6 cm³/kg. Our radiographic and FRC determinations are comparable with plethysmographic and neon-dilution determinations in rabbits of similar weights by other investigators [13, 15].

The application of a geometric model to the chest is by necessity an approximation. Although model II is intuitively more accurate than model I is, our results do not validate this impression. In model I, the intrathoracic volume and the volumes of the heart, paraspinal structures, and diaphragm are all underestimated. However, subtracting low-volume estimates of the intrathoracic structures from a low estimate of intrathoracic volume to give the FRC estimate tends to compensate for the inaccuracy of the model. Because model II was determined from a single rabbit, the rabbit model may not accurately represent the anatomy of the population as a whole, resulting in bias. The elliptical model is appealing because of widespread applicability over a wide range of subject size.

The rabbit was chosen to model the neonatal chest because of the similar size of the adult rabbit to the neonatal human, with expected similarity of lung volumes. Chest wall compliance is probably similar in rabbits and infants [16]. Consequently, it is expected that functional residual capacities will be similar for equivalently sized lungs. The HeD FRC estimates average 20.6 cm³/kg, which closely approximates published gas dilution measurements (FRC/kg) in rabbits [13] and human infants [17]. This study indicates that FRC can be accurately estimated from digitized radiographs in an animal model of the normal neonate. Extension of this work to evaluation of diseased subjects can be expected to have some increased error because of the inability to accurately predict the volume of tissue and blood in diseased lung. Nonetheless, this error is probably smaller than the error seen in HeD FRC determinations in patients with air trapping, as evidenced by superior correlation between radiographic and plethysmographic FRC estimates as compared with HeD plethysmographic FRC correlation [18]. Additional studies are needed to test and to validate this method in the evaluation of lung volume in the healthy and diseased infant.

ACKNOWLEDGMENTS

The authors thank Charles T. Wheeler for his excellent technical assistance, Laurence Hedlund for invaluable advice in data acquisi-

tion, Jacqueline Wright for preparation of the manuscript, and Estelle H. Cline for her help in data acquisition.

REFERENCES

- Beardsmore CS, Stocks J, Silverman M. Problems in measurements of thoracic gas volume in infancy. *J Appl Physiol* 1982;52:995-999
- Hurtado A, Fray WW. Studies of total pulmonary capacity and its subdivisions. II. Correlation with physical and radiologic measurements. *J Clin Invest* 1933;12:807
- Barnhard HJ, Pierce JA, Joyce JW, Bates JH. Roentgenographic determination of total lung capacity. A new method evaluated in health, emphysema and congestive heart failure. *Am J Med* 1960;28:51-60
- Loyd HM, String ST, DuBois AB. Radiographic and plethysmographic determination of total lung capacity. *Radiology* 1966;86:7-14
- Pierce RJ, Brown DJ, Holmes M, Cumming G, Denison DM. Estimation of lung volumes from chest radiographs using shape determination. *Thorax* 1979;34:726-734
- Pratt PC, Klugh GA. A method for the determination of total lung capacity from posteroanterior and lateral chest roentgenograms. *Am Rev Respir Dis* 1967;96:548
- Harris TR, Pratt PC, Kilburn KH. Total lung capacity measured by roentgenograms. *Am J Med* 1971;50:756-763
- Hiller EJ, Kirkpatrick JA, Huang NN. Radiographic determination of total lung capacity in patients with cystic fibrosis. *J Pediatr* 1971;78:435
- Salam H, Warwick WJ. Measurement of total lung capacity by a roentgenography-planimetry method in children 4-16 years of age. *Respiration* 1978;36:177-182
- Shephard RJ, Seliger V. On the estimation of total lung capacity from chest x-rays: radiographic and helium dilution estimates on children aged 10-12 years. *Respiration* 1969;26:327-336
- Campbell SC. Estimation of total lung capacity by planimetry of chest radiographs in children 5 to 10 years of age. *Am Rev Respir Dis* 1983;127:106
- Zarins LP. Closed circuit helium dilution method of lung volume measurement. In: Clausen JL, ed. *Pulmonary function testing: guidelines and controversies*. New York: Academic Press, Inc., 1982:129-140
- Takezawa J, Miller FJ, O'Neill JJ. Single breath diffusing capacity and lung volumes in small laboratory mammals. *J Appl Physiol* 1980;48:1052-1059
- Snedecor GW, Cochran WG. *Statistical methods*, 7th ed. Ames: The Iowa State University Press, 1980:171-172
- Caldwell EJ, Fry DL. Pulmonary mechanics in the rabbit. *J Appl Physiol* 1969;27:280-285
- Gillespie JR. Mechanisms that determine functional residual capacity in different mammalian species. *Am Rev Respir Dis* 1983;128:574-577
- Ronchette R, Stocks J, Keith I, Godfrey S. An analysis of a rebreathing method for measuring lung volume in the premature infant. *Pediatr Res* 1975;9:797-802
- Ries AL, Clausen JL. Lung volumes. In: Wilson AF, ed. *Pulmonary function testing: indications and interpretations*. Orlando, FL: Grune and Stratton, 1985:69-85

American Roentgen Ray Society Residents' Award Papers, 1992

The ARRS announces competition for the 1992 President's Award and two Executive Council Awards for the best papers concerning the clinical application of the radiologic sciences.

Awards

The winner of the President's Award will receive a certificate and a \$2000 prize. The winners of the two Executive Council Awards will each be given a certificate and a prize of \$1000. The winners will be announced on March 16, 1992. Winning papers will be presented at the ARRS annual meeting at Marriott's Orlando World Center, Orlando, FL, May 10-15, 1992. Winning papers will be submitted for early publication in the *American Journal of Roentgenology*. All other papers will be returned to the authors.

Regulations

Eligibility is limited to residents or fellows in radiology who have not yet completed 4 years of approved training in a radiologic discipline. A letter from the resident's department chairman attesting to this status must accompany the manuscript. The resident must be the sole or senior author and be responsible for all or most of the project.

Submitted manuscripts must not exceed 5000 words and have no more than 10 illustrations. Four copies of the manuscript and illustrations are required. Submitted manuscripts should not contain previously presented or published material and should not be under consideration for publication elsewhere.

Deadline for submissions is February 14, 1992. Send papers to

Nancy O. Whitley, M.D.
Chairman, Committee on Education & Research
American Roentgen Ray Society
Department of Radiology
University of Maryland Medical Systems Hospital
22 S. Greene St.
Baltimore, MD 21201

The Deformed Petrous Bone: A New Plain Film Sign of Premature Lambdoid Synostosis

Sandra K. Fernbach¹
Kate A. Feinstein

Towne-view skull radiographs of 38 infants with unilateral lambdoid synostosis were reviewed. The diagnosis of lambdoid synostosis was based on other plain film findings, CT findings, or clinical examination. All patients had deformity of the ipsilateral petrous bone, presumably because of pressure caused by redirected brain growth. Specific changes included flattening of the petrous ridge and depression of the roof of the mastoid portion of the petrous bone and adjacent structures such as the semicircular canals.

Flattening of the petrous ridge and depression of the roof of the mastoid portion of the petrous bone are useful signs of lambdoid synostosis when sutural closure has produced sutural indistinctness rather than sclerosis.

AJR 156:1215-1217, June 1991

Plain film diagnosis of craniosynostosis is remarkably accurate [1]. This is especially true in children with sagittal, coronal, and metopic synostosis, because the plain film findings are multiple and well described in the literature [2-4]. CT has been a useful adjunct to standard skull radiography, as it both shows the deformity and excludes alternative intracranial disease [5].

Unilateral lambdoid synostosis reportedly accounted for approximately 1% of cases of craniosynostosis in a large surgical series [6]. In a smaller series of 204 children, it was not even mentioned as an isolated finding [7]. Because it is relatively uncommon and does not deform facial structures, unilateral lambdoid synostosis may be difficult to diagnose clinically and radiologically. It may be underdiagnosed for the same reasons.

We recently observed a specific change in the ipsilateral petrous bone in children with unilateral lambdoid synostosis. This report describes our experience in 38 affected infants.

Materials and Methods

Thirty-eight infants (27 boys, 11 girls) with unilateral lambdoid synostosis were identified when the skull radiographs of approximately 600 children were reviewed as part of a government-funded project based in Colorado. The study was begun to determine whether the reported rise in cases of craniosynostosis in Colorado was accurate and, if so, if there were any environmental agents that might be implicated in this rise. One author was a nonfunded coinvestigator in this project. Of these 38 infants, CT scans had been obtained in 30. The children were 2-16 months old (mean, 6.9 months) at the time of the radiologic studies. Clinical findings in all 38 children revealed skull deformity consistent with the diagnosis of unilateral lambdoid synostosis.

Diagnosis of suture closure was based on seeing both primary and secondary changes on plain films and CT scans. Primary changes are those that occur at the suture itself: sclerosis, indistinctness, or beaking (Figs. 1 and 2). Secondary changes are few and consist of plagiocephaly due to smallness and flattening of the ipsilateral occiput (Figs. 1 and 2). CT

Received October 22, 1990; accepted after revision December 11, 1990.

¹ Both authors: Department of Radiology, Northwestern University Medical School and The Children's Memorial Hospital, 2300 Children's Plaza, Chicago, IL 60614. Address reprint requests to S. K. Fernbach.

0361-803X/91/1566-1215
© American Roentgen Ray Society

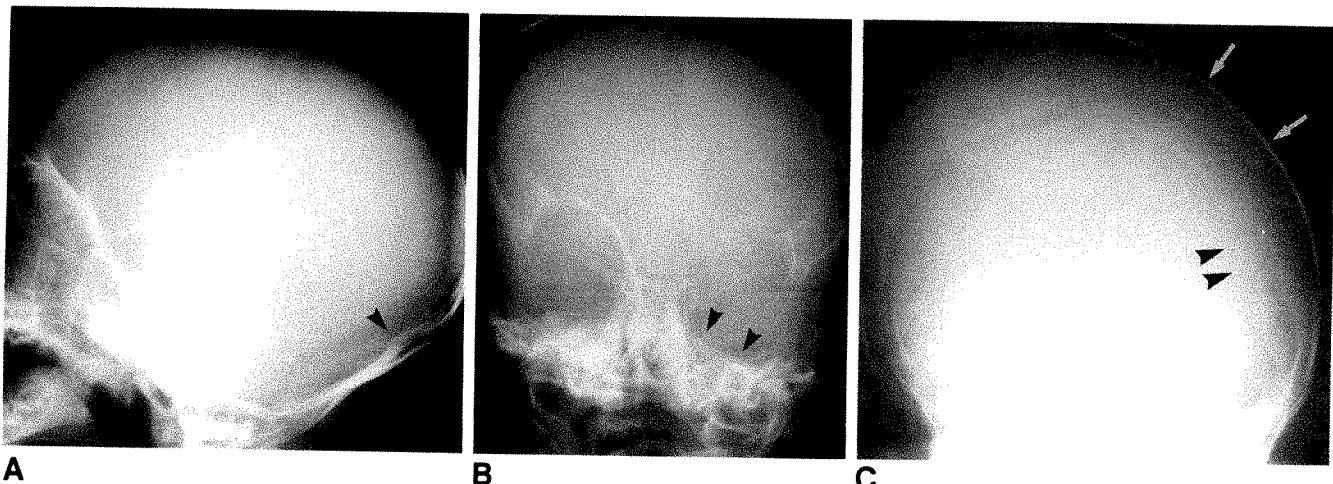


Fig. 1.—Skull radiographs of left lambdoid synostosis.

A, Lateral view. Flattening and indentation of occiput on affected side is associated with sclerosis along suture (arrowhead). **B**, Anteroposterior view. Orbita are symmetric, but middle cranial vault is expanded (arrowheads). On this view it is difficult to determine whether depression of petrous bone is real or from positioning. **C**, Towne view. Occiput on left (arrows) is less rounded than on unaffected side. Abnormal suture is less well defined than normal, especially in its midsection (arrowheads).

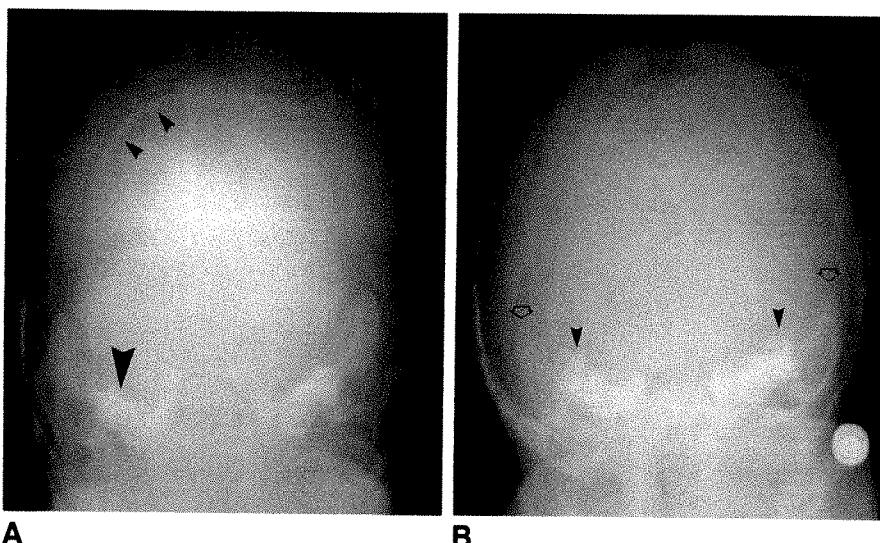


Fig. 2.—Towne view radiographs of two patients with right lambdoid synostosis.

A, Sclerosis along superior aspect of right lambdoid suture (small arrowheads) is a primary sign of synostosis. Ipsilateral petrous bone is depressed (large arrowhead).

B, Affected suture is less distinct than lucent normal suture. Mastoid tip (arrows) and semicircular canals (arrowheads) are lower on side with indistinct suture.

and three-dimensional reconstructions allowed visualization of the deformity in multiple planes and, when bone window settings were used, of the primary sutural changes as well (Figs. 3 and 4).

In no child were there underlying intracranial pathologic changes to cause the plagiocephaly or abnormality of another suture. That is, aside from the cosmetic deformity of the skull, no abnormality was detected on CT or clinical examination.

We attempted to categorize the changes as mild, moderate, or severe and to correlate the degree of deformity with the age of the patient, assuming that older infants would have more deformity.

Results

Unilateral lambdoid synostosis was on the right in 27 infants (71%) and on the left in 11 (29%).

Primary sutural changes were visible on the Towne projection in all children, although in many the changes were subtle and consisted only of indistinctness (Figs. 1 and 2B). On lateral skull radiographs, primary sutural changes were seen inconsistently. Detection of morphologic changes of the skull

was dependent on the degree of deformity present and the angle at which the Towne projection was done. For the abnormality to be seen best, the X-ray beam should be tangential to the deformed region.

Secondary changes were seen in the petrous bone in all children (Figs. 1, 2, and 4). Specifically, the ipsilateral petrous ridge was depressed. Adjacent portions of the petrous bone such as the semicircular canals were depressed also. When the mastoid air cells were developed, these, too, were lower on the affected side. Similar changes were present on direct CT scans.

The degree of deformity did not appear to increase with age.

Discussion

When suture closure occurs prematurely, the growing brain exerts pressure on adjacent bony structures. Closure in the first 2 years of life, the period of most rapid brain growth, can

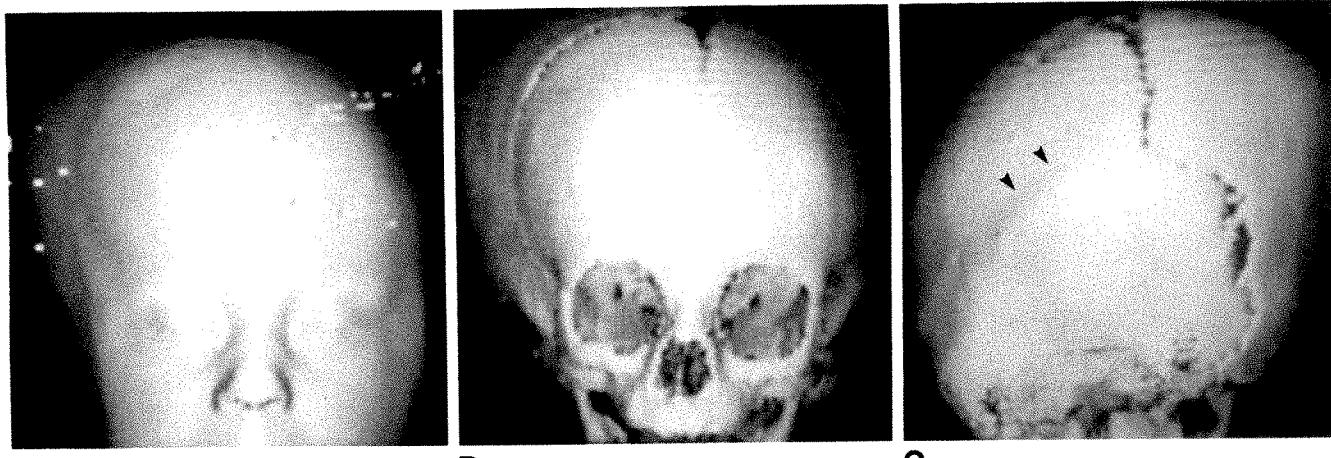


Fig. 3.—Three-dimensional CT scan of left lambdoid synostosis (same patient as in Fig. 1).
A and B, Anteroposterior views. Left side of cranial vault is small, and there is compensatory enlargement of contralateral parietal region. Soft-tissue reconstruction shows little facial deformity.
C, Posterior view. Closed suture appears as a slight heaping up of bone (arrowheads). This contrasts to blackness of patent sagittal and contralateral lambdoid sutures. On this view, posterior aspect of head is skewed, much like facial skewing seen in children with unilateral coronal synostosis.

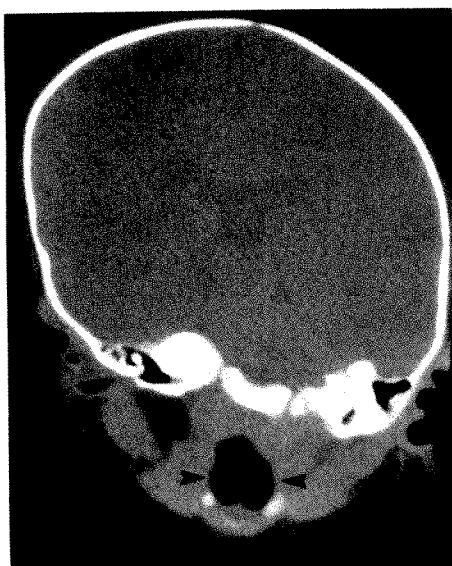


Fig. 4.—Direct coronal CT scan of left lambdoid synostosis. There is relative symmetry of airway and hyoid bone (arrowheads). Changes in cranial vault have caused sagittal suture to deviate to affected side. Petrous bone and mastoid air cells are deformed and depressed, as on plain radiographs.

result in profound calvarial remodeling and deformity. The scaphocephaly produced by sagittal suture synostosis is easily recognized clinically. The calvarial asymmetry seen in children with unilateral coronal synostosis develops because of the ipsilateral constrictive and contralateral expansive forces. Corresponding bony changes are present in the facial bones and, at a greater distance from the closed suture, in the middle fossa. The sphenoid bone becomes more vertical and petrous bones are displaced downward.

Few such secondary changes have been described in children with lambdoid synostosis. However, the presence of such secondary changes should not be surprising. The unusual opportunity to study a large number of affected children

within a short interval allowed us to detect the bony deformity. The small number of children with unilateral lambdoid synostosis in previous series may represent the truly low prevalence of this form of craniostenosis or a selection bias, as the deformity in the posterior calvaria has incited less clinical and surgical interest than facial deformities have.

Recognition of the deformity of the petrous bone should enhance the ability of the radiologist to diagnose unilateral lambdoid synostosis. These secondary signs may be especially useful when the Towne view is positioned or exposed suboptimally by obviating additional films. Familiarity with the petrous changes also will allow a more confident diagnosis when radiographs inadequately show primary changes at the lambdoid suture.

Lambdoid synostosis appears to be more common than previously thought. Awareness of the newly described sign of mastoid and petrous depression will make diagnosis of lambdoid synostosis easier and more accurate.

ACKNOWLEDGMENT

We thank Sally Gartman for help in manuscript preparation.

REFERENCES

- Gellad FE, Haney PJ, Sun JCC, Robinson WL, Raok CVG, Johnson GS. Imaging modalities of craniostenosis with surgical and pathological correlation. *Pediatr Radiol* 1985;15:285-290
- Nathan MH, Collins VP, Collins LC. Premature unilateral synostosis of the coronal suture. *AJR* 1961;86:433-446
- Tod PA, Yelland JDN. Craniostenosis. *Clin Radiol* 1971;22:472-486
- Fernbach SK, Naidich TP. Radiological evaluation of craniostenosis. In: Cohen MM Jr, ed. *Craniostenosis: diagnosis, evaluation and management*. New York: Raven, 1986:191-214
- Adam RU, Lee SH, Truex RC. Computed tomography in primary craniostenosis. *J Comput Tomogr* 1980;4:125-130
- Shillito J, Matson DD. Craniostenosis: a review of 519 surgical patients. *Pediatrics* 1968;41:829-853
- Anderson FM, Geiger L. Craniostenosis: a survey of 204 cases. *J Neurosurg* 1965;22:229-240

Book Review

Radiology of the Eye and Orbit. Edited by Thomas H. Newton and Larissa T. Bilaniuk. (Vol. 4 in the series Modern Neuroradiology.) New York: Raven, 320 pp., 1990. \$115

This is a good book. If we consider what the authors have done, it probably should be called a great book. Neuroradiologists and radiology libraries should buy this book. Radiology residents and fellows and practicing radiologists who do even a little orbital imaging should skim the work at least. It is a remarkably up-to-date review of orbital imaging at a bargain price.

The book highlights three commonly used orbital imaging techniques: MR, sonography, and CT. MR is covered in chapters 1-5, orbital sonography in chapters 6 and 7, and CT in chapters 8 and 9. Chapters 8 and 9 were published previously in volume 3 of the Modern Neuroradiology series. I think that they were included in *Radiology of the Eye and Orbit* so that persons who wish to buy only this volume of the series would still have a complete work.

Each imaging technique is covered in an orderly fashion. The chapters on MR start with technical aspects and move on to ocular anatomy, ocular pathology, orbital anatomy, and orbital pathology. Highlighting the oculus is appropriate and nicely done. Sonography is covered, first by relating principles and techniques and then by considering ocular and orbital pathology. CT receives similar treatment, with chapter 8 on orbital anatomy and chapter 9 on ocular and orbital pathology. The book has significant ophthalmologic contributions; three of the 11 contributors are ophthalmologists. This avoids a frequent shortcoming of books of this type. Clinically managed imaging, orbital sonography, is covered thoroughly.

A small price is paid for freshness, however. A broad range of MR abnormalities are illustrated, but relatively few are gadolinium-enhanced or fat-suppression images. However, these techniques are discussed thoroughly and are illustrated adequately, unlike in any other MR text to date. Generally, anatomic-pathologic correlation is slightly weak. Information on histology and anatomic dissection adds interest to a text of this type. However, if I were to choose, I would underplay these also in order to illustrate more clinical imaging. After all, imaging examples and brief text are what the reader will seek out this book for. Along the same line, classic anatomy is not covered. For example, the book does not have elegant descriptions of orbital angles and their variations. Again, I agree with the authors in excluding this material in order to streamline the text. The apparently rapid production of this book seems to have resulted in poor proofreading. This may be embarrassing to the publisher, but it means nothing to the clinical practitioner.

Chapter 1, "Magnetic Resonance Imaging: Technical Aspects," has a strong prejudice for General Electric terminology. It would have been nice to include techniques and terminology on a broad range of equipment, stating the brand names. Chapters 2 and 3 cover MR

ocular anatomy and ocular pathology. These are illustrated profusely and are generally well written. Minor contradictions occur in the text. For example, page 3.11 seems to have two introductory paragraphs on retinoblastoma. The first one states that the tumor is derived from either photoreceptor or neuronal retinal cells. The next states that it arises from retinal photoreceptors. This is a minor complaint in a text of this quality.

Chapter 4 discusses MR orbital anatomy, and chapter 5 covers MR orbital pathology. The introductory paragraph on orbital anatomy is refreshingly honest. It simply states that detailed material on orbital anatomy should be sought in other texts. The chapter then goes on to provide a brief but useful review of the anatomic structures visible on MR imaging. The chapter on pathologic changes is so complete that it even covers secondary orbital involvement by paranasal sinus fungal disease. Unfortunately, the description of signal aberrations associated with the fungus is incomplete. Many fungi actively store metals, especially iron. The legend for figure 5.67D is, therefore, misleading when it says, "The low intensity in the ethmoidal and nasal lesion is related to high viscosity and lack of free water. The moderately low intensity in the right maxillary sinus is the result of thick inflammatory exudate." When taken in perspective with the entire chapter, this is a minor complaint.

Chapters 6 and 7 review orbital sonography. The quality of these chapters is unsurpassed by any other radiology text. It is easy for a radiologist to ignore orbital sonography, as it generally is performed by ophthalmologists. Such ignorance is unacceptable to the authors of this text. Chapters 8 and 9 cover CT anatomy and pathology. These are well-illustrated contributions with a frank text. For example, page 9.3 states, "Retinoblastoma is virtually the only cause of intraocular calcification below the age of 3 years." Such practical statements are seldom included in texts, leaving radiology residents with a bewildering list of differential diagnostic possibilities and no really practical idea of which diseases in the list are most likely or how to exclude unreasonable possibilities quickly.

Each chapter has an extensive bibliography. The index appears to be a professional job. I could not find an entry that was not cross-referenced.

I would purchase a copy of this book myself. In fact, I may need two copies, as my copy already has been loaned out to residents and fellows and is a popular circulating book. I have recommended that we purchase a copy of this book for our departmental library.

Stephen S. Gebarski
University of Michigan Hospital
Ann Arbor, MI 48109-0030

Pictorial Essay

Abnormalities of the Orbit and Its Contents in Children: CT and MR Imaging Findings

Kenneth D. Hopper,¹ John L. Sherman,² and Danielle K. B. Boal¹

This essay illustrates the CT and MR features of congenital anomalies of the orbit, diseases of the globe, inflammatory and infectious disorders of the orbit, orbital trauma, and primary and secondary tumors of the orbit in children.

The increasing application of CT and MR imaging to diseases of the orbit and its contents has had a dramatic impact in pediatric ophthalmology [1–4]. This essay illustrates the CT and MR findings in congenital anomalies of the orbit,



A

B

Fig. 1.—Anophthalmia in a male neonate.

A and *B*, Axial CT scan (*A*) and sagittal left orbital T1-weighted MR image (*B*) show absence of both eyes. (Reprinted with permission from Hopper et al. [1].)



Fig. 2.—Duplication cyst in a 1-year-old infant.
CT scan shows a duplication cyst (arrow) behind left globe. (Reprinted with permission from Hopper et al. [1].)

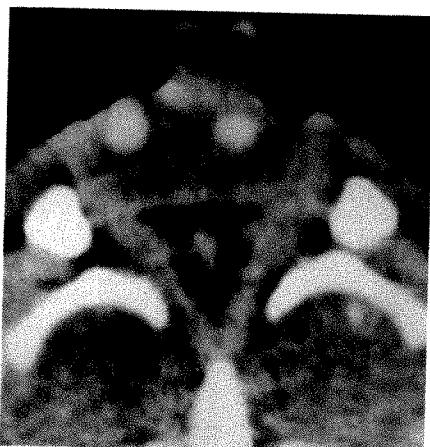
Received October 1, 1990; accepted after revision December 6, 1990.

Presented at the annual meeting of the American Roentgen Ray Society, Washington, DC, May 1990.

¹ Department of Radiology, The Pennsylvania State University, The Milton S. Hershey Medical Center, P.O. Box 850, Hershey, PA 17033. Address reprint requests to K. D. Hopper.

² Washington Imaging Center, 2801 University Blvd., Wheaton, MD 20902.

AJR 156:1219–1224, June 1991 0361-803X/91/1566-1219 © American Roentgen Ray Society



3



4

Fig. 3.—Cyclops in a neonate. CT scan shows a common enlarged midline orbit and globe with two lenses.



5



6

Fig. 4.—Coloboma in a 2-year-old girl. MR image shows microphthalmia, persistent hyperplastic primary vitreous, and a coloboma (arrow). A coloboma is an incomplete closure of primitive choroidal fissure of optic stalk. A small cyst is seen along posterior globe at optic nerve-globe junction. (Reprinted with permission from Hopper et al. [1].)

Fig. 5.—Septooptic dysplasia in a 4-year-old girl with blindness in the left eye and decreased visual acuity in the right eye. Prominent anterior recess of third ventricle and small optic canal are typical. Absence or defects in septum pellucidum and pituitary insufficiency are also common. Coronal MR image shows marked atrophy/hypoplasia of both optic nerves.

Fig. 6.—Fibrous dysplasia in a 3-year-old boy. CT scan shows fibrous dysplasia of sphenoid bone and posterior orbital wall.

diseases of the globe, inflammatory and infectious disorders of the orbit, orbital trauma, and primary and secondary tumors of the orbit in children.

Congenital Anomalies

Anophthalmia (absence of the globe, Fig. 1) is a rare, sporadically occurring abnormality that can be difficult to differentiate from severe microphthalmos, or small globe. A retrobulbar duplication cyst (Fig. 2) results from defective closure of the embryonic fissure. Cyclopia (Fig. 3) and synophthalmia are caused by a total or partial fusion of the optic vesicles, respectively, preventing normal orbital separation. A coloboma is an incomplete closure of the primitive choroidal fissure of the optic stalk (Fig. 4). Septooptic dysplasia is a rare anomaly associated with decreased vision and hypoplasia of the optic nerves (Fig. 5). Fibrous dysplasia can cause orbital deformity and optic nerve compression (Fig. 6). Neurofibromatosis commonly involves the eye, manifested by

orbital, optic nerve (Fig. 7), and eyelid ("bag-of-worms") tumors (Fig. 8).

Diseases of the Globe

It is frequently difficult clinically to differentiate retinoblastoma from benign diseases, or pseudogliomas, as children with these diseases all present with leukokoria. Retinoblastoma is the primary intraocular malignant tumor of childhood. Although it usually presents as a calcified nodular mass (Fig. 9), occasionally, a tumor is uncalcified. Ten percent are familial and up to 25% are either multifocal within the same eye or are bilateral. Bilateral retinoblastomas occasionally may be associated with a pineal neuroectodermal tumor, a so-called "trilateral" retinoblastoma.

Coats disease (retinal telangiectasia) is a primary retinal vascular anomaly characterized by telangiectasia and accumulation of lipoproteinaceous exudate in the retina and sub-retinal space. Patients present with a dense vitreous without

Fig. 7.—Neurofibromatosis in a 17-year-old boy.
A, CT scan shows optic nerve meningioma.
B, CT scan shows bilateral intraventricular meningiomas.

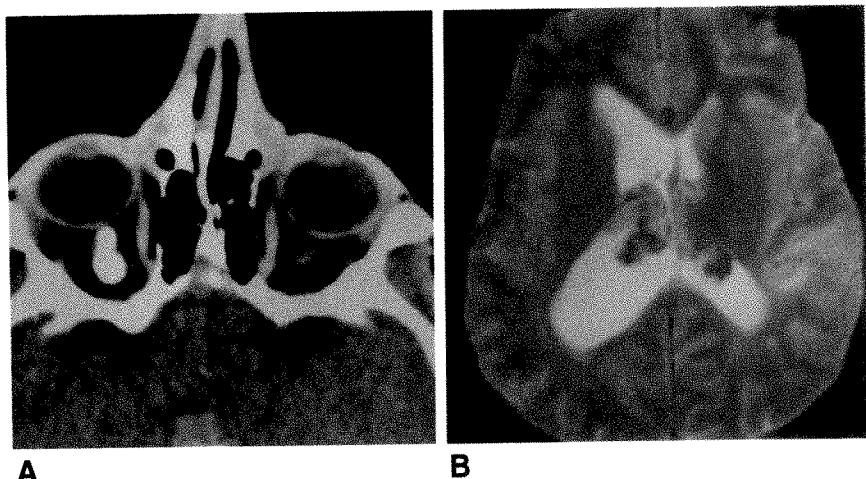


Fig. 8.—Plexiform neurofibroma in a 1-year-old girl with neurofibromatosis.

A and **B**, Axial (**A**) and coronal (**B**) MR images show left eyelid plexiform neurofibroma that extends extraconally into orbit (**A**) and left cavernous sinus (**B**).

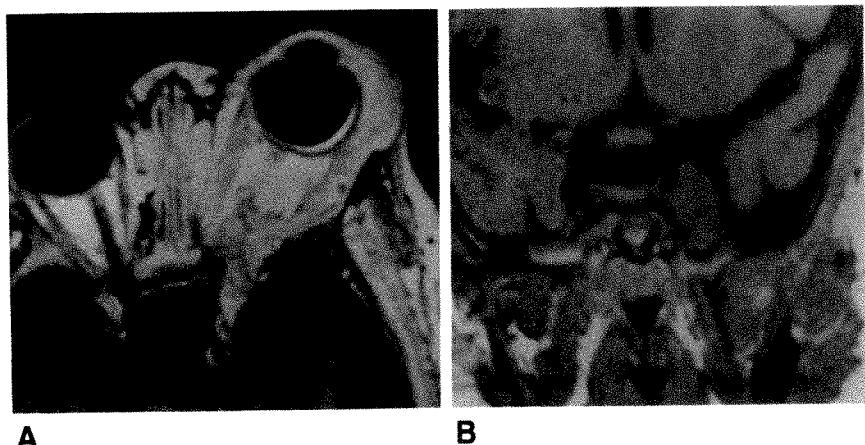


Fig. 9.—Retinoblastoma in a 1-year-old girl. CT scan shows a calcified right bulbar mass proved at surgery to be a retinoblastoma.

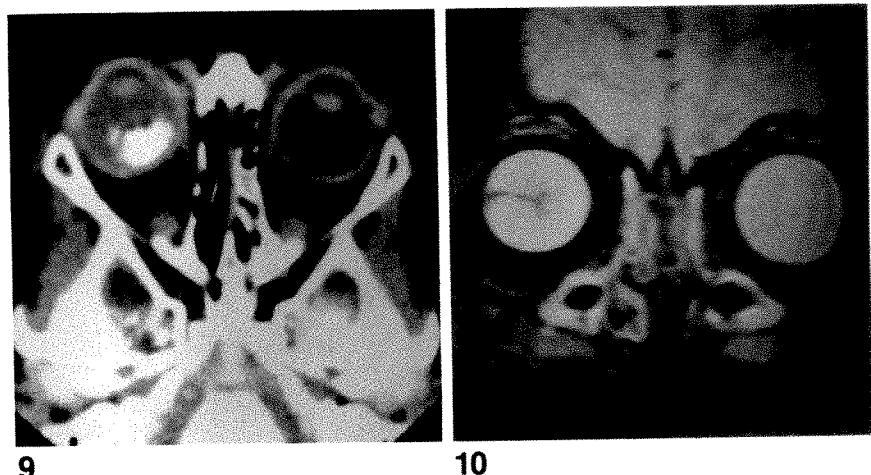


Fig. 10.—Persistent hyperplastic primary vitreous in a 3-year-old child. Coronal T2-weighted MR image shows a cone-shaped, noncalcified central retrobulbar density (also see Fig. 4). Usually this is caused by persistent primary hyaloid, but occasionally represents detached dysplastic retina. Increased intensity of right eye is due to hemorrhage. (Reproduced with permission from Magill et al. [5].)

a focal mass, and calcification is seen occasionally. Persistent hyperplastic primary vitreous is a persisting hyperplasia of the embryonic hyaloid vascular system (Figs. 4 and 10). The friability of these vessels may lead to intravitreous hemor-

rhage. Retrobulbar fibroplasia or retinopathy of prematurity is seen in premature infants who develop traction retinal detachments from prolonged oxygen therapy. Sclerosing endophthalmitis is a granulomatous uveitis caused by *Toxocara canis*

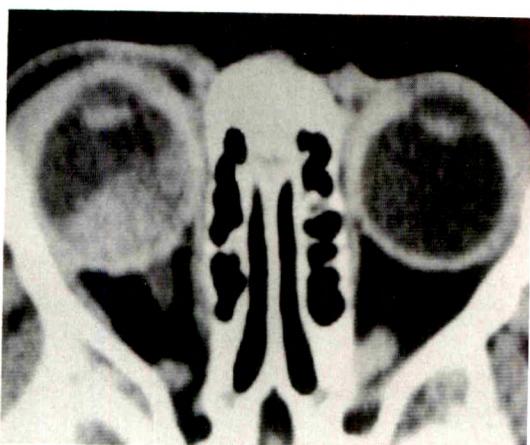


Fig. 11.—Medulloepithelioma in a young child with leukokoria. CT scan shows a noncalcified mass in right globe. Medulloepitheliomas are usually well-defined, enhance markedly, and may erode or induce hyperostosis in orbital wall.

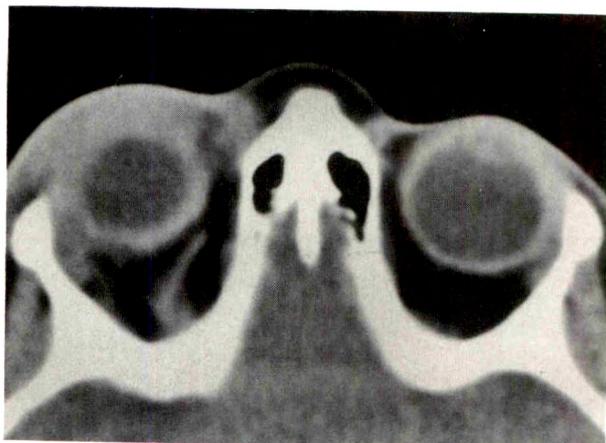


Fig. 12.—Preseptal cellulitis in a 7-year-old girl. CT scan shows superficial right orbital edema and inflammatory infiltration.

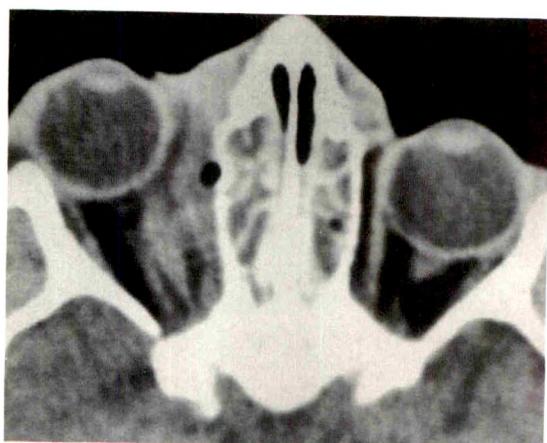


Fig. 13.—Subperiosteal abscess in a 9-year-old girl with medial right orbital cellulitis. CT scan shows a subperiosteal abscess resulting in ethmoidal sinus disease.

infestation of the eye. Chorioretinitis is present in 80%, and dense vitreous without a discrete mass is usually seen. Medulloepitheliomas (Fig. 11) are rare intraocular tumors that occur from the primitive medullary epithelium.

Inflammatory and Infectious Diseases

Infections and inflammations in and around the eye are the most common orbital disorders of childhood. Although most are preseptal (Fig. 12), more serious orbital infections are frequently associated with paranasal sinus disease, penetrating trauma, or dental or middle ear disease, or they can be an extension of preseptal disease. A subperiosteal abscess between the periorbital and lamina papyracea usually follows ethmoidal sinusitis (Fig. 13). CT and MR are useful to differentiate preseptal, lacrimal, and eyelid infectious processes from true orbital cellulitis.

Graves disease is occasionally seen in children. As with adults, exophthalmos, a generalized increase in the orbital fat, and diffuse symmetric enlargement of the extraocular muscles are common. Orbital pseudotumor may present like Graves disease with exophthalmos and extraocular muscle enlargement. However, the muscle involvement is more asymmetric and the proptosis is painful.

Optic neuritis can occur in children. As with adults, the sudden onset of a central vision deficit and orbital pain are common. Although many older patients with optic neuritis will develop multiple sclerosis, the cause in children is frequently unknown. Occasionally, optic neuritis may accompany other infectious, inflammatory, and granulomatous processes.

Orbital Trauma

Penetrating eye injuries are more common in children, with orbital foreign bodies and infection serious sequelae. Blunt trauma can cause orbital fractures, optic nerve avulsion, orbital hematomas, retinal tears, and even rupture of the globe itself (Fig. 14).

Primary Tumors

Rhabdomyosarcoma is the most common malignant tumor of the orbit in children. Most affected children are 8–10 years old and present with rapidly progressing exophthalmos and ptosis of the upper lid caused by these highly malignant and invasive tumors. Dermoids and epidermoids are the most common benign orbital tumors of childhood and are found in the upper temporal or upper nasal quadrants. Dermoids (Fig. 15) grow slowly, cause adjacent bony erosion, and usually do not cause visual symptoms. The fat content of these tumors aids in their diagnosis.

Several orbital vascular abnormalities affect children, including orbital varices, arteriovenous malformations, carotid-cavernous fistulas, capillary and cavernous hemangiomas, blood cysts, glomus tumors, and hemangiopericytomas. Arteriovenous malformations involving the orbit are rare, usually originate intracranially, and communicate with the orbit via the cavernous sinus. Capillary hemangiomas (Fig. 16) are

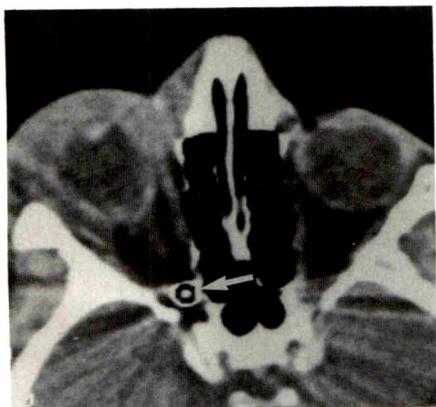


Fig. 14.—Orbital trauma in a 15-year-old boy. CT scan shows rupture of a globe and prominent preseptal edema/hemorrhage from a BB (arrow). In orbital trauma, CT is generally superior in evaluating bony integrity of orbit and face and in detecting metallic foreign bodies. MR, on the other hand, detects ocular and optic nerve injuries better than CT does.



Fig. 15.—Dermoid in a 3-year-old girl. CT scan shows a well-defined low-intensity mass in left preseptal region.

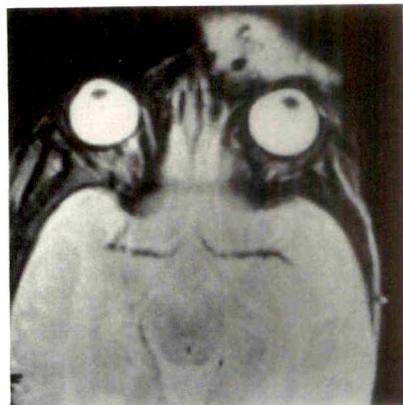


Fig. 16.—Capillary hemangioma in a 5-month-old infant. T2-weighted MR image shows a superficial capillary hemangioma around left eye. Capillary hemangiomas are isolated, usually superficial tumors that are found in neonates and often regress with age.

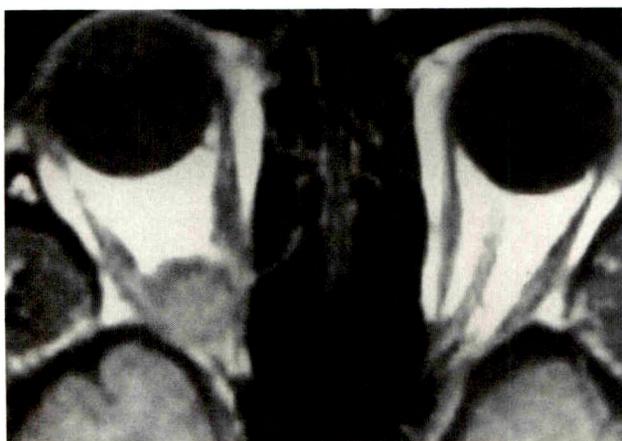


Fig. 17.—Cavernous hemangioma in a 16-year-old child. T1-weighted MR image shows a well-defined intraconal cavernous hemangioma.



Fig. 18.—Lymphangioma in a 4-year-old boy. CT scan shows a right multilocular, predominantly intraconal lymphangioma. Lymphangiomas are congenital tumors consisting of dilated lymphatic channels surrounded by lymphoid tissue. They are benign, slow-growing, encapsulated tumors that cause increased exophthalmos and orbital expansion. (Reprinted with permission from Hopper et al. [1].)

isolated, usually superficial tumors found in the neonate. Cavernous hemangiomas present as homogeneously enhancing intraconal masses that will displace but not involve the optic nerve (Fig. 17). Lymphangiomas are benign, slow-growing, encapsulated tumors that cause increased exophthalmos and orbital expansion (Fig. 18). Sudden intratumoral hemorrhage is common, resulting in sudden increased proptosis. Lymphoma of the orbit presents with either diffuse infiltration or a focal mass. Acute leukemia can infiltrate the retinal and optic nerves.

Other less common tumors may primarily involve the orbit, including lacrimal gland tumors, melanoma, and neural sheath tumors (schwannoma and neurofibroma). Osteomas arising within the frontal and ethmoid sinuses may involve the orbit secondarily. Teratomas usually present at or shortly after

birth with gross enlargement of the orbit and distortion of the orbital structures and the face. Optic nerve gliomas (Fig. 19) occur primarily in the 2- to 6-year-old child and may be localized or extend intracranially to involve the chiasm.

Secondary Tumors

In children, metastasis involvement of the orbit is less common than primary tumor. Intraocular metastases are extremely rare in children, whereas malignant tumors in adults commonly metastasize to the ocular choroid. Neuroblastoma (Fig. 20) generally occurs in the child younger than 2 years

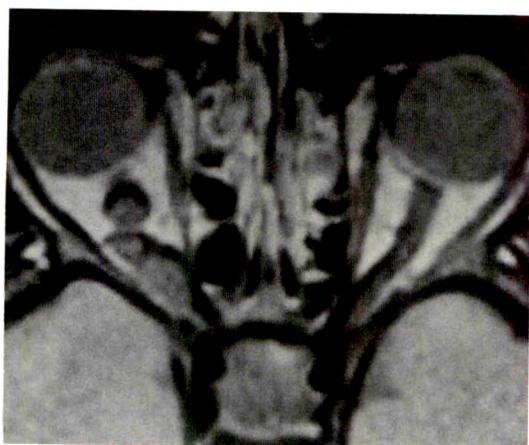


Fig. 19.—Optic nerve glioma in an 18-year-old girl. Axial MR image shows a serpiginous right optic nerve glioma. Optic nerve gliomas occur primarily in 2- to 6-year-old children and may remain localized or involve chiasm.



Fig. 21.—Midline granuloma in a 14-year-old child. CT scan shows central destruction and deformity of nasal cavity and left orbit.

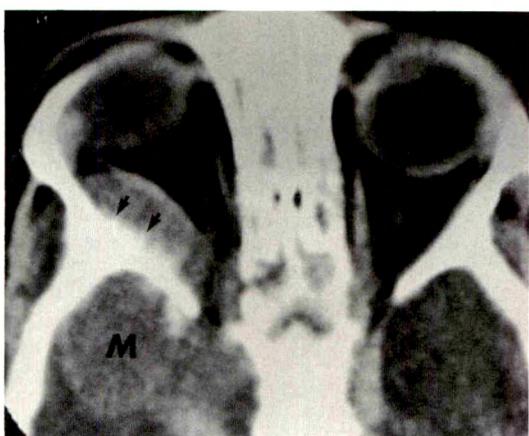


Fig. 20.—Metastatic neuroblastoma in a 1-year-old infant. CT scan shows spiculated thickening of orbital roof, wall, and floor (arrows). M = mass. (Reprinted with permission from Hopper et al. [1].)

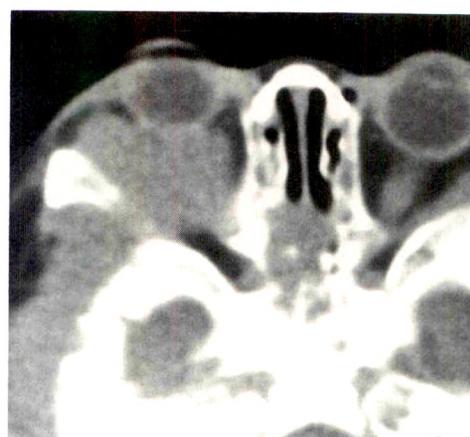


Fig. 22.—Sarcoma in a 6-month-old boy. CT scan shows extensive undifferentiated sarcoma of scalp, right temporoparietal bones, and invasion into right eye.

old and may be either metastatic or primary in the orbit. Histiocytosis involves the orbit in 10% of patients. Ewing sarcoma peaks in occurrence in the second decade and occasionally metastasizes to the orbit. A midline granuloma is a destructive inflammatory process that can affect not only the nasal cavity, but adjacent structures as well (Fig. 21). Invasion of the orbit from adjacent tumors is seen with extraorbital rhabdomyosarcoma; undifferentiated sarcomas (Fig. 22); and other anaplastic, small round cell tumors. Mucoceles of the frontal and ethmoidal sinuses may encroach on the orbit.

REFERENCES

1. Hopper KD, Haas DK, Sherman JL. The radiologic evaluation of congenital and pediatric lesions of the orbit. *Semin Ultrasound CT MR* 1988;9:413-427
2. Crawford JS, Morin JD, eds. *The eye in childhood*. Philadelphia: Grune & Stratton, 1983
3. Mafee MF, ed. Imaging in ophthalmology, part I. *Radiol Clin North Am* 1987;25:381-666
4. Mafee MF, ed. Imaging in ophthalmology, part II. *Radiol Clin North Am* 1987;25:667-895
5. Magill HL, Hanna SL, Brooks MT, et al. Pediatric case of the day. *RadioGraphics* 1990;10:515-518

Case Report

Spontaneous Resolution of Bile-Plug Syndrome

Elvira V. Lang¹ and Lee E. Pinckney²

Conjugated hyperbilirubinemia in infants can be a diagnostic challenge: clinical findings of primary biliary obstruction and of hepatocellular disease with associated cholestasis can be identical. The task of the radiologist is to identify the patients who may benefit from surgery. These patients include infants with extrahepatic biliary atresia, choledochal cysts, tumors of the common bile duct, or bile duct scarring after spontaneous perforation. The existing literature includes the bile-plug syndrome in the surgically correctable category [1, 2]. We report a case of spontaneous resolution of bile-plug syndrome.

Case Report

The patient is a boy with X-linked lamellar ichthyosis who was born full-term. For replacement of cutaneous fluid losses, a Broviac catheter was placed under general anesthesia 8 days after birth. Blood lost during surgery was replaced by transfusion. Postoperative stridor necessitated parenteral alimentation until day 18. At that time, nasojejunal feedings were well tolerated, and at 3 weeks of age the child was fed perorally.

At birth, the bilirubin level was 4 mg/dl (direct, 0.3 mg/dl); at 2 weeks, it was 5.5 mg/dl (direct, 2.0 mg/dl). During the third week after birth, the bilirubin level increased to 20.4 mg/dl (direct, 9.8 mg/dl) and liver enzyme levels, which had been normal, rose to SGOT 181, SGPT 146, GGT 129 mg/dl. Abdominal sonography during this third week showed progressive dilatation of the biliary tree on two separate occasions. Sludge was found in the right hepatic duct and common bile duct. The common bile duct was 8 mm wide and was obstructed distally (Fig. 1A). Twelve hours later, immediately before surgery, sonography revealed a normal biliary tree (Fig. 1B). The infant's bilirubin level dropped to 15.3 mg/dl (direct, 7.3 mg/dl) within

48 hr and to 1.7 mg/dl (direct, 0.8 mg/dl) within the next 5 days. Within 4 weeks, bilirubin and liver enzyme levels had returned to normal.

During a 3-year follow-up, the infant developed normally without recurrent signs of biliary obstruction. The skin condition was well controlled with ointments and maternal care.

Discussion

Bile-plug syndrome is defined as extrahepatic obstruction of the bile ducts by bile sludge in term infants without anatomic abnormalities, congenital chemical defects of bile, or hepatocellular lesions [1, 2]. Cholestasis and precipitations of bile also can develop in association with abnormal composition of bile in cystic fibrosis [3], hepatocellular damage, prolonged erythroblastic jaundice [4], or total parenteral nutrition [5]. In those cases, the term *inspissated bile syndrome* commonly is used.

Bile-plug syndrome is treated surgically. Techniques include retraction of the bile plug via a duodenostomy and papillotomy [2], manual propulsion of the plug into the duodenum [1], and intraoperative irrigation of the biliary system with saline [6] or mucolytic agent [7]. Our case illustrates that obstructing bile plugs can pass spontaneously and that an immediate preoperative sonogram may prevent unnecessary surgery. We chose to perform immediate preoperative sonography because of our experience with another case of bile-plug syndrome in which resolution of the bile plug was proved surgically. Our second infant had developed normally until the age of 3 weeks, when his stool became acholic. Asympto-

Received September 27, 1990; accepted after revision January 14, 1991.

¹ Division of Diagnostic Radiology, Stanford University, Stanford, CA 94305. Address reprint requests to E. V. Lang, VA Medical Center (V-114), 3801 Miranda Ave., Palo Alto, CA 94304.

² Department of Radiology, Children's Hospital San Diego, 8001 Frost St., San Diego, CA 92123.

AJR 156:1225-1226, June 1991 0361-803X/91/1566-1225 © American Roentgen Ray Society

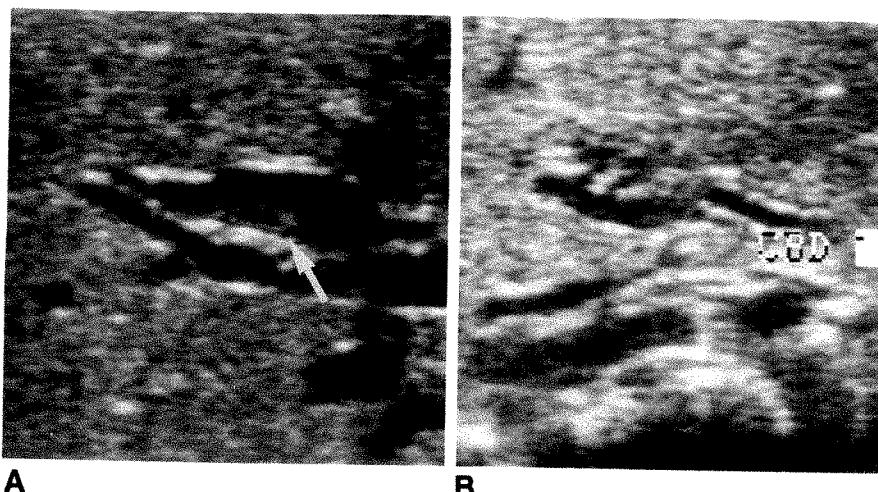


Fig. 1.—A. Abdominal sonogram shows sludge (arrow) and marked dilatation of common bile duct.

B. Abdominal sonogram shows resolution of biliary obstruction. Common bile duct (CBD) has normal diameter.

matic jaundice followed, and sonography showed dilatation of the intra- and extrahepatic biliary tree with sludge in the right hepatic duct. A percutaneous transhepatic cholangiogram confirmed the dilatation of the biliary tree and revealed complete obstruction of the distal common bile duct. Fifteen hours later, during laparotomy, the biliary tree was found to be entirely decompressed and patent.

The documentation of spontaneous resolution of bile-plug syndrome in two infants has significant implications in the selection of treatment options. Further studies are needed to define the factors that make spontaneous resolution more likely. Until such factors are established, abdominal sonography in surgical candidates may prevent unnecessary operative intervention.

REFERENCES

1. Bernstein J, Braylan R, Brough AJ. Bile-plug syndrome: a correctable cause of obstructing jaundice in infants. *Pediatrics* 1969;43:273-276
2. Levy JM, Kuss JJ, Karli A, et al. Le syndrome du bouchon bilaire. *Arch Franc Pediatr* 1979;36:801-806
3. Davies C, Daneman A, Stringer DA. Inspissated bile in a neonate with cystic fibrosis. *J Ultrasound Med* 1986;5:335-337
4. Breunung VM, Mitschke I. Das inspissated bile syndrome. *Kinderärztl Praxis* 1968;11:491-503
5. Touloukian RJ, Seashore JH. Hepatic secretory obstruction with total parenteral nutrition in the infant. *J Pediatr Surg* 1976;10:353-360
6. Mahr MA, Hugosson C, Nazar HM, et al. Bile-plug syndrome. *Pediatr Radiol* 1988;19:61-64
7. Brown DM. Bile plug syndrome: successful management with a mucolytic agent. *J Pediatr Surg* 1990;25:351-352

Case Report

Disseminated Hepatic and Splenic Lesions in Cat-Scratch Disease: Imaging Features

Daniel C. Rappaport,¹ William A. Cumming, and Pablo R. Ros

Cat-scratch disease is a bacterial infection that usually affects children and adolescents after being scratched by a domestic cat [1]. The disease manifests itself most commonly as a unilateral regional lymphadenitis. Hepatic and splenic involvement are unusual manifestations [2]. We report the CT features of cat-scratch disease of the liver and spleen in one patient. In addition, we report the CT features in three patients and the sonographic features in two other patients with cat-scratch disease.

Case Report

A 5.5-year-old girl had a 4-week history of vague abdominal pain and body temperature elevated to 40°C. Physical examination was unremarkable, in particular no evidence was seen of regional adenopathy. On further questioning, the patient apparently had close contact with cats, but did not give a definite history of being scratched. Results of liver function tests were normal; the patient had a skin test positive for cat-scratch disease.

CT examination was performed both before and after IV contrast administration (Figs. 1A and 1B). The images were viewed at both a wide window setting (level of 50 H and window of 240 H) and a narrow window setting (level of 100 H and window of 80 H). Multiple, well-defined, low-attenuation lesions, ranging in diameter from 3 mm to 2 cm, were scattered throughout both lobes of the liver and the spleen.

The lesions became more apparent and more numerous after injection of IV contrast material, and in addition, peripheral enhancement of a large hepatic lesion was seen. The lesions were better

seen on the narrow window settings. Follow-up study 1 month later showed almost complete resolution of the hepatic and splenic lesions.

Subsequently, we have reviewed four other patients with visceral lesions and cat-scratch disease; two had sonographic examinations and three had CT examinations. The sonographic studies in both showed multiple hypoechoic lesions, ranging in diameter from 3 mm to 3 cm, throughout the liver (Fig. 2) and in the spleen of one patient.

The three patients who had CT examinations showed remarkable similarities to our first patient in the distribution, appearance, and size of the visceral lesions. An open liver biopsy performed on one patient showed well-demarcated nodules, ranging from 3 to 7 mm in diameter with slightly hyperemic margins. The diagnosis made on the basis of the frozen section was necrotizing granuloma. The four other patients had a positive clinical diagnosis and skin test for cat-scratch disease, but biopsy was not performed.

Discussion

Cat-scratch disease is characterized pathologically by a granulomatous or suppurative response to a Gram-negative organism that has been inoculated into a patient by a domestic cat. Clinically, the patients have fever and unilateral and possibly suppurative lymphadenitis. The diagnosis is made in the appropriate clinical setting when a patient has had intimate exposure to a cat, has an inoculation site, and has a skin test positive for cat-scratch disease [3].

The patients may have malaise, headache, sore throat, rash, parotid swelling, encephalopathy, an oculoglandular syndrome of Parinaud, osteolytic lesions, mesenteric adenitis,

Received October 29, 1990; accepted after revision January 23, 1991.

¹ All authors: Department of Radiology, Box J-374, JHMHC, University of Florida College of Medicine, Gainesville, FL 32610-0374. Address reprint requests to D. C. Rappaport.

AJR 156:1227–1228, June 1991 0361-803X/91/1566-1227 © American Roentgen Ray Society

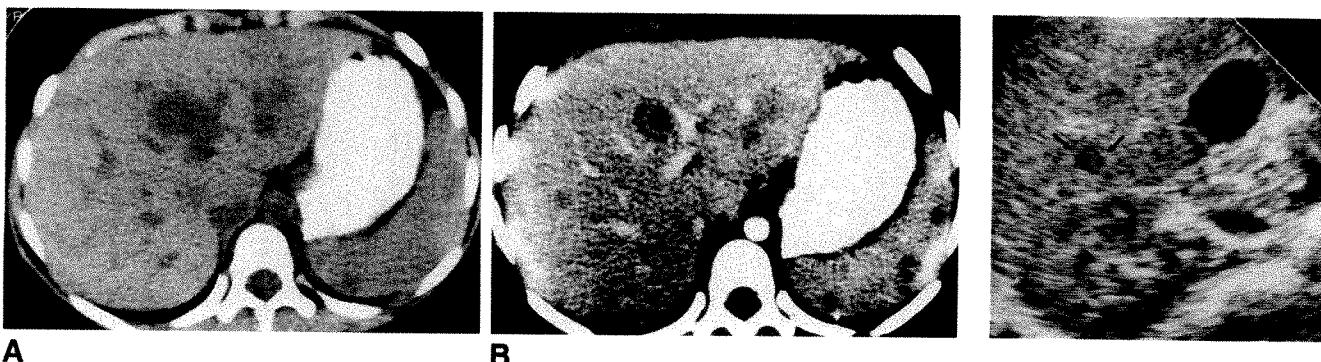


Fig. 1.—5.5-year-old girl with a 2-week history of fever. No peripheral adenopathy was present. Results of liver function tests showed slightly elevated levels.

A, Unenhanced CT scan shows 2-cm, low-attenuation lesion just anterior to left portal vein. A 5-mm, low-attenuation lesion is in posterior aspect of spleen.

B, CT scan obtained after administration of IV contrast material shows enhancement in large liver lesion, a second lesion in right lobe of liver, and multiple lesions within spleen.

anicteric hepatitis, and splenomegaly [3]. The disease gradually resolves in 2–4 months.

Hepatic and splenic involvement in cat-scratch disease has been considered unusual. It was first reported in an autopsy series by Inglis and Tonge [4], who presented three cases with "visceral granulomatous lesions." Subsequently, a few cases of visceral involvement with cat-scratch disease have been reported [5–8]. Three patients reported by Lenoir et al. [2] had granulomatous hepatitis on open biopsy; two of these had multiple, low-attenuation lesions in the liver on CT scans. Delbeke et al. [5] described disseminated hepatic and splenic lesions in a patient who had no peripheral lymphadenopathy. Four patients with cat-scratch disease with hepatic and splenic abscesses also were described by Riskallah et al. [6]; three had necrotizing granulomas on biopsy. A patient with isolated splenic lesions and a normal liver biopsy was described recently [3].

Overall, the true prevalence of hepatic and splenic involvement in cat-scratch disease is difficult to ascertain. Moriarity and Margileth [3] found splenomegaly in 12%. Clinical splenomegaly does not imply granulomatous splenic involvement, and its absence does not exclude disseminated granulomas, as was the case in all five of our patients.

All five of our patients had scattered, multiple, low-attenuation or hypoechoic lesions, 3 mm to 2 cm in diameter. None had radiologic evidence of hepatosplenomegaly. We think that although hepatic and splenic involvement have been considered unusual manifestations of cat-scratch disease, it most likely is more common than is clinically recognized.

The differential diagnosis should include other granulomatous disease, such as tuberculosis and sarcoidosis; infectious

diseases, such as ascariasis and other pyogenic abscesses, including *Candida* infections; and neoplastic diseases, such as lymphoma and metastatic disease. The distribution of the disease and the clinical setting may make it possible to narrow the diagnostic possibilities. In the appropriate clinical setting, when the typical radiologic findings occur as we have described them, patients should be questioned about exposure and possible inoculation by a cat. The findings on enhanced CT or sonography are apparently quite typical, so that a biopsy probably is not necessary. If a patient has a clinical diagnosis of cat-scratch disease, follow-up examination at a 3-month interval may preclude biopsy.

REFERENCES

- Carithers HA. Cat scratch disease: an overview based on a study of 1,200 patients. *Am J Dis Child* 1985;139:1124–1133
- Lenoir AA, Storch GA, DeSchryver-Kecskemeti K, Shackelford GD. Granulomatous hepatitis associated with cat scratch disease. *Lancet* 1988;1:1132–1136
- Moriarity RA, Margileth AM. Cat scratch disease. *Infect Dis Clin North Am* 1987;1:575–590
- Inglis JA, Tonge JL. A disease with visceral granulomatous lesions of unknown etiology. *Med J Aust* 1950;1:433–436
- Delbeke D, Sandler MP, Shaff MI, Miller SF. Cat scratch disease: report of a case with liver lesions and no lymphadenopathy. *J Nucl Med* 1988;29:1454–1456
- Riskallah MF, Meyer L, Ayoub EM. Hepatic and splenic abscesses in cat scratch disease. *Pediatr Infect Dis J* 1988;7:191–195
- Cox F, Perlman S, Sathyaranayana J. Splenic abscesses in cat scratch disease: sonographic diagnoses and follow-up. *JCU* 1989;17:511–514
- Rocco VK, Roman RJ, Eigenbrodt EH. Cat scratch disease: report of a case with hepatic lesions and a brief review of the literature. *Gastroenterology* 1985;89:1400–1406

Degenerative Narrowing of the Cervical Spine Neural Foramina: Evaluation with High-Resolution 3DFT Gradient-Echo MR Imaging

David M. Yousem¹
 Scott W. Atlas
 Herbert I. Goldberg
 Robert I. Grossman

Conventional two-dimensional Fourier transform (2DFT) MR evaluation of osteophytic disease of the cervical neural foramina is limited by section thickness, signal-to-noise problems, and CSF flow artifacts. We evaluated the role of thin-section, high-resolution, gradient-refocused three-dimensional Fourier transform (3DFT) MR imaging in assessing degenerative foraminal narrowing in the cervical spine. Contiguous 1.5-mm axial 3DFT gradient-recalled acquisition in the steady state MR images of 120 neural foramina at 60 disk levels were evaluated blindly and independently by three neuroradiologists. High-resolution axial CT was used as the gold standard in all patients. 3DFT MR was found to agree with CT in the detection of neural foraminal narrowing and in the determination of the cause of the narrowing in approximately 76% of neural foramina. The accuracy for the assessment of neural foraminal narrowing on 3DFT MR ranged from 73% to 82% when a 5°-flip-angle, high-intensity CSF technique was used. When using the 30°-flip-angle, low-intensity CSF technique, the accuracy ranged from 66% to 86%. When the cause of narrowing was evaluated, the 5° and 30° studies agreed with CT in 70–92% and 48–88% of the levels, respectively. When lesions were missed on MR, it was usually because of osteophytic disease. The interobserver concordance of MR and CT interpretations was higher for detecting the presence of narrowing than its cause.

This MR technique is a useful method in the evaluation of foraminal stenosis since contrast between disk, cord, osteophyte, and CSF is high without the need for intrathecal injections. The wide range of interpreter accuracy and interobserver correlation is attributed to a steep learning curve for evaluating the MR images.

AJNR 12:229–236, March/April 1991; AJR 156:1229–1236, June 1991

While MR imaging has become a well-accepted method for evaluating spinal cord disease, its use in the cervical spine has been limited by its decreased effectiveness in evaluating bony degenerative disease. In patients with cervical radiculopathy, neural foraminal narrowing may be caused by degenerative osteophytes or laterally herniated disks. Bony osteophytic disease has not been depicted clearly by conventional two-dimensional Fourier transform (2DFT) MR techniques. The 2DFT images have been limited by section thickness, signal-to-noise (S/N) problems with thin sections, as well as artifacts emanating from CSF flow [1–4].

We evaluated the ability of thin (1.5 mm)-section, high-resolution three-dimensional Fourier transform (3DFT) MR imaging with gradient refocusing to assess foraminal disease of the cervical spine. Techniques resulting in high-intensity CSF (i.e., low flip angle) and low-intensity CSF (i.e., high flip angle) were compared by using high-resolution CT as the gold standard.

The object of this investigation was to evaluate the accuracy and interobserver reliability of 3DFT volumetric imaging of the neural foramina of the cervical spine relative to the imaging gold standard, high-resolution CT. We hoped to ascertain whether the perceived insensitivity of MR in bony disease persisted when a thin-section, high-resolution technique was used.

Received June 6, 1990; revision requested August 15, 1990; revision received September 6, 1990; accepted September 7, 1990.

¹ All authors: Department of Radiology, Neurology Section, Hospital of the University of Pennsylvania, 3400 Spruce St., Philadelphia, PA 19104. Address reprint requests to D. M. Yousem.

0361-803X/91/1566-1229

© American Roentgen Ray Society

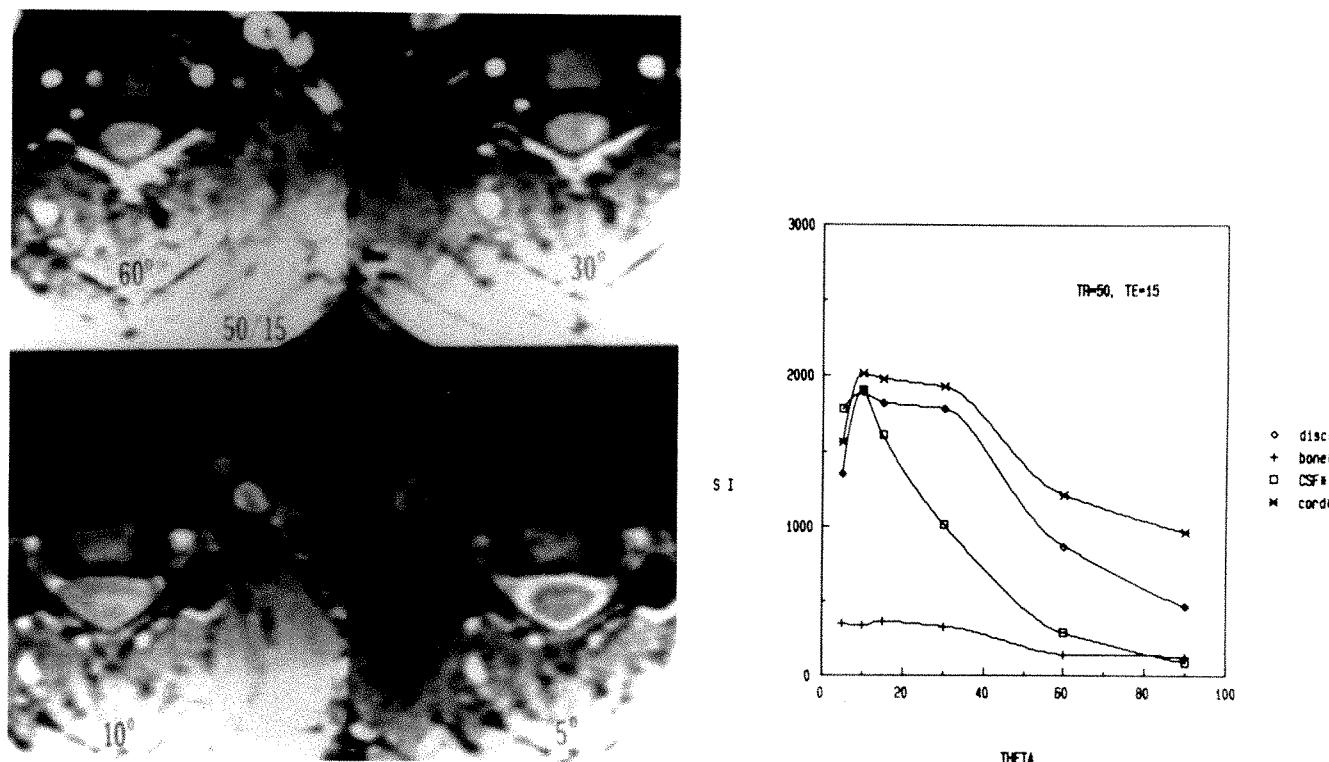


Fig. 1.—Evaluation of signal and contrast with a 3DFT volume gradient-echo series, 50/15, with varying flip angles at the same anatomic level. Window width and level are kept constant to demonstrate effect of variations in flip angle.

A, CSF-bone contrast is very high and CSF-cord contrast is high with 5° and 10° flip angles (bottom right and left, respectively); CSF is bright, but cord-CSF contrast at 10° is low. At 30° and 60° (top right and left, respectively), there is high CSF-cord contrast owing to dark-intensity CSF. Bone-CSF distinction decreases at 30° and 60°. Disk is high in intensity at all flip angles.

B, Graph of signal intensity (SI) vs 5°, 10°, 15°, 30°, 60°, and 90° flip angles shows maximum bone-CSF, bone-disk, and bone-cord contrast at 10°; however, disk, cord, and CSF are of similar intensity at this flip angle. The 5° sequence, which distinguishes between cord, CSF, and disk while maintaining high bone contrast, is preferable. The 30° sequence shows the highest CSF-cord and CSF-disk contrast, while maintaining high signal to noise, which drops off for all flip angles after 30° owing to saturation effects. CSF-bone contrast decreases with high flip angles.

Subjects and Methods

In order to determine the flip angle that would optimize contrast in the cervical spine, scans were obtained in a normal volunteer, varying the angle of nutation from 5° to 90° (Fig. 1A). The TR and TE were held constant at 50 and 15 msec, respectively (as were the receive and transmit attenuations), with gradient-moment nulling applied. Signal intensities of a region of interest in the CSF, spinal cord, disk, and vertebral body were determined for each flip angle (Fig. 1B). From this preliminary study, it was determined that a 5° flip angle produced high-intensity CSF, optimized CSF-bone contrast, and maintained CSF-cord differentiation. The 30° sequence generated low-intensity CSF and produced the greatest CSF-cord and CSF-disk contrast while maintaining high signal intensity in the cord and disk. These flip angles were selected for routine use on a 1.5-T General Electric Sigma scanner. The minimum TE was selected, 11 msec for the 30° series and 15 msec for a flow-compensated 5° series; the TR was maintained at 50 msec. The TE of the 30° series was reduced to its minimum value to obtain the highest S/N and low-intensity CSF, and to minimize susceptibility artifacts. The TE of 15 msec for the 5° sequence was necessarily higher because gradient-moment nulling was added to obtain high-intensity CSF and to reduce CSF flow artifacts.

As part of the routine study of the cervical spine, we routinely obtain a sagittal 800/20–25/2 (TR/TE/excitations) scan with 3-mm contiguous slices. These images often, but not always, include the

neural foramina if the patient is not very scoliotic and localization is not a problem. For the purposes of this study, which was to evaluate the foramina on axial MR images comparable to axial CT scans, we did not use these images as part of the assessment. The sagittal 800/25 and the two axial 3DFT sequences described above make up the entire routine cervical spine protocol for degenerative disease at our institution.

Twenty-one patients referred to the neuroradiology section for evaluation of disk disease of the cervical spine underwent CT examination as well as 3DFT gradient-echo thin-section MR imaging using protocols determined from the normal volunteer study. One hundred twenty neural foramina were included in the cervical spine studies. The MR and CT scans were reviewed independently and blindly by three senior members of the American Society of Neuroradiology with extensive CT and MR experience. The evaluators were not provided with the patients' clinical symptoms. CT and MR scans were interpreted separately and randomly.

The evaluators were provided with high-resolution axial CT images of the neural foramina, which included 41 postmyelography 1.5-mm thin section levels, two postmyelography 3.0-mm section levels, and 17 unenhanced 3-mm section levels with two neural foramina at each level (120 neural foramina). The MR evaluations consisted of two separate series that used the 3DFT technique with gradient-recalled acquisition in the steady state, 1.5-mm contiguous sections, a 256 × 128 matrix, and one excitation. In one series the flip angle was 5° with a TR of 50 msec and TE of 15 msec (50/15/5°) and first-order

gradient moment nulling, which generated high-intensity CSF. The second series used parameters of 50/11/30° without gradient-moment nulling, which generated low-intensity CSF. Although 64 slices were obtained in the data set, only 60 1.5-mm contiguous sections were displayed because of aliasing artifacts.

All spinal levels that were evaluated by both CT and MR were included in this study. While MR scans routinely covered from C2–C3 to C7–T1 in a 60-slice series, the CT scans were selected on the basis of findings at myelography or by the request of the referring clinician. Thus, the CT levels determined which MR images were obtained for comparison. In this study, the reviewers evaluated four levels at C2–C3, seven levels at C3–C4, 12 levels at C4–C5, 16 levels at C5–C6, 17 levels at C6–C7, and four levels at C7–T1 (and two neural foramina at each level).

The evaluation of each neural foramen consisted of a numeric score of 0 (within normal limits or minimally narrowed) or 1 (moderately to severely narrowed). When the images were uninterpretable, they were called indeterminate. The indeterminate label was used when scans were technically suboptimal for foraminal visualization (either owing to aliasing, motion degradation, or metallic artifact) or when the evaluators believed there was insufficient contrast between CSF and bone and disk to determine confidently whether the neural foramen was narrowed or not. MR and CT standards were provided for the two grades (0 and 1) in order to obtain a uniform grading scale and to avoid individual biases (Fig. 2). Each individual interpreter's CT scans were evaluated in the same fashion. The CT interpretations were used as the gold standard with which to compare that evaluator's MR interpretations. Despite the fact that 1.5- and 3.0-

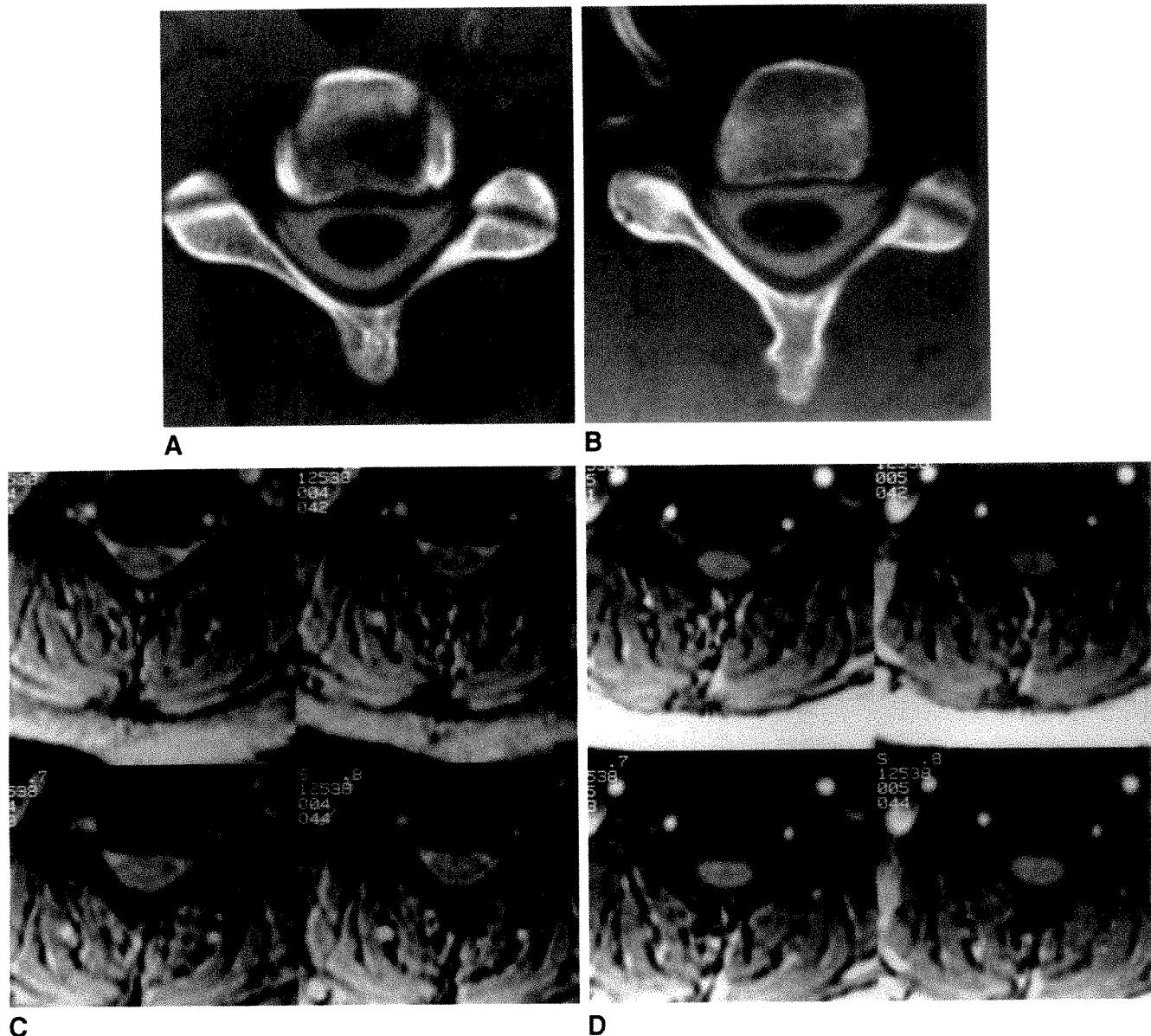


Fig. 2.—Example of grade 0 neural foramina in a 36-year-old woman.

A and B, Postmyelography CT images through the C4–C5 disk and foraminal level show normal neural foramina bilaterally.

C, Bright CSF 50/15/5° MR technique shows intermediate-intensity disk and nerve root sleeves, with lower-intensity cord and exiting nerve roots at the same level. Neural foramina are not narrowed.

D, At same level. Dark CSF 50/11/30° MR series shows intermediate-intensity disk and cord with lower-intensity CSF nerve root sleeves. Note lower degree of contrast in foramina between bone and CSF.

mm-thick sections and postmyelography and unenhanced CT studies were used as the gold standard, the results of the MR correlation did not vary for each subtype of CT technique (see Results), so using this "nonuniform" gold standard was justifiable.

Thin-section CT was used as the gold standard for several reasons: (1) patients without significant foraminal narrowing do not undergo surgery; (2) patients often are treated conservatively for radiculopathy; (3) from an anterior approach (the preferred operative technique at this institution for disk disease), the neural foramen cannot be

visualized directly, and histopathology cannot assess for the size of the neural foramen; (4) a surgical selection bias exists in favor of surgery in patients with disk herniation; and (5) determination of neural foraminal narrowing should be done preoperatively.

Each neural foramen, when scored as moderately or severely narrowed, was also assessed as to the cause of the narrowing on both CT and MR. The options for this part of the evaluation included bony narrowing, diskogenic narrowing, both bony and disk narrowing, or indeterminate or uninterpretable. The CT interpretations for the

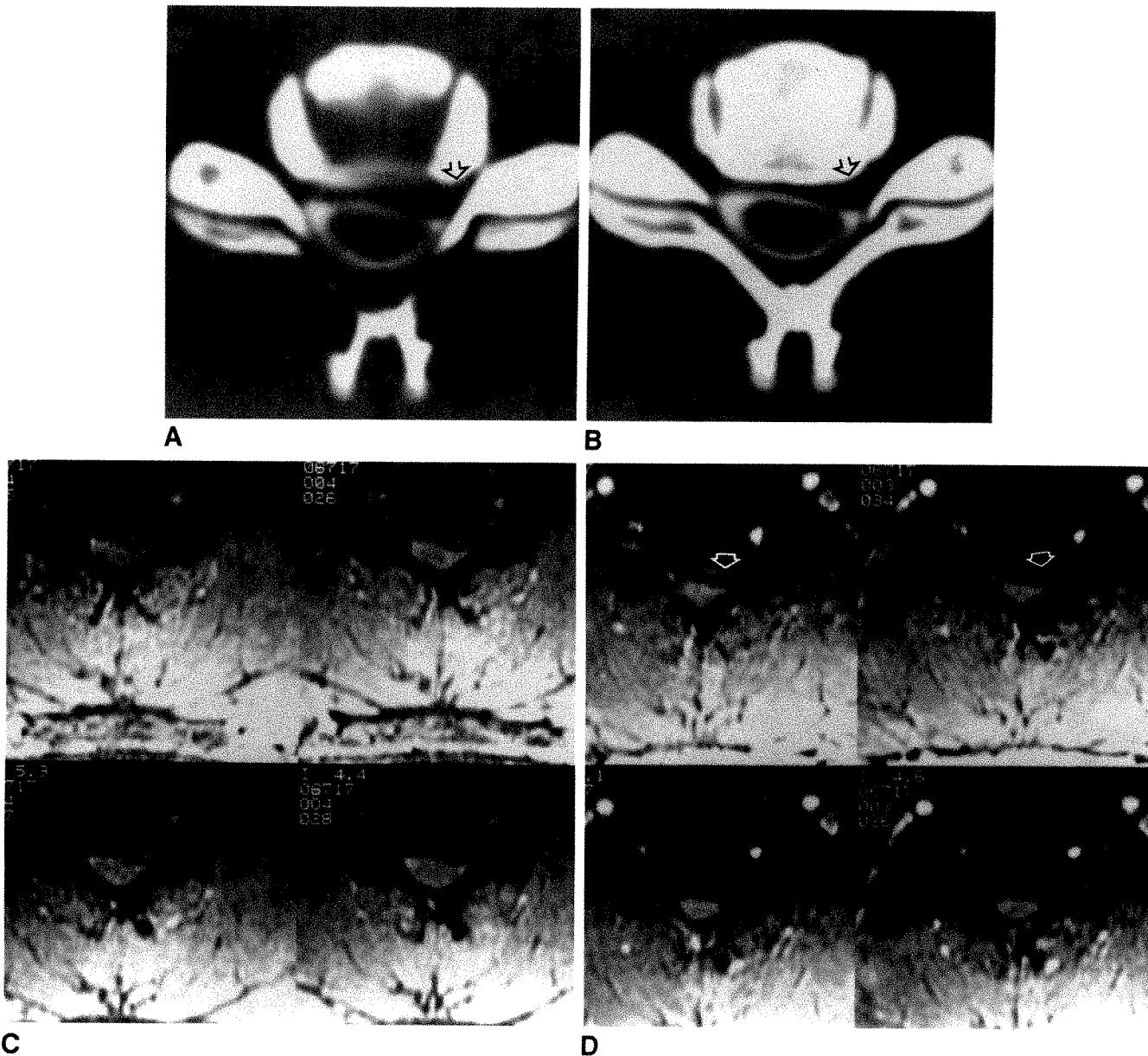


Fig. 3.—27-year-old man with left C5-C6 radiculopathy.

A and **B**, Postmyelogram CT scans through disk level (**A**) and at foramina (**B**) show left-sided, focally herniated disk (arrows) entering foramen. Two of three evaluators diagnosed herniated disk only and one diagnosed herniated disk and bony osteophyte as the cause of foraminal narrowing (on the basis of "hypertrophied" left Luschka joint seen better on a higher section). All examiners believed the foramen was narrowed.

C, High-intensity CSF MR technique shows intermediate-intensity disk material with low-intensity rim extending to left neural foramen. Bony neural canal in lower left image is narrowed laterally. Interpretation by two evaluators was bony osteophyte and herniated disk causing foraminal narrowing, while one evaluator diagnosed herniated disk alone.

D, Low-intensity CSF images show disk herniation (arrows) to left side. Hypointensity posterior to disk was believed to represent CSF and therefore was considered herniated disk by one examiner (not the same who considered it herniated disk on the high-intensity CSF series), but was considered bony osteophyte and herniated disk by the other two.

cause of the neural foraminal narrowing were used as the proof of diagnosis for each independent observer's MR interpretation.

In order to evaluate interobserver concordance, the CT and MR grades of the neural foramina were compared for each level. If any one evaluator graded the narrowing as indeterminate on either CT or MR, the level was not included in the concordance figures for that observer. A similar analysis for interobserver concordance regarding the cause of narrowing was made. Again, levels labeled indeterminate were removed from the analysis of the evaluator who labeled the neural foramen as indeterminate.

One evaluator graded the CT scans twice (in two separate sessions) to determine intraobserver variation with a "proved" method.

Results

On the basis of each evaluator's own interpretation of the CT scans, the accuracy for the assessment of neural foraminal narrowing in 3DFT MR ranged from 73% to 82% with the low-flip-angle, high-intensity CSF technique. When using the 30°-flip-angle, low-intensity CSF technique, the accuracy ranged from 66% to 86% (Table 1). No significant differences were noted in the CT-MR correlation values when 1.5- or 3-mm-thick CT images were interpreted. The average accuracy rate of the three evaluators when grading the MR images (combining 5° and 30° data) vs the 3-mm-thick CT sections was 74.2% and vs the 1.5-mm-thick CT slices was 77%.

The 5° MR series did not detect narrowing that was evident on CT in 27 studies, while the 30° series did not detect CT-documented narrowing in 41 neural foramina. Of 17 cases in which narrowing was seen on CT to be caused by disk herniation, MR was interpreted as normal in one instance (5.9%) on both the 5° and 30° series. In the 141 levels of CT-documented bony narrowing, the 5° MR series was interpreted as normal in 26 (18.4%) instances, while the 30° MR series was interpreted as normal in 40 (28.4%) instances (Table 2). No case of CT-documented bone and disk narrowing (15 instances) was interpreted as normal on MR.

When the interpretations on 5° MR and CT disagreed, the evaluators were twice as likely to consider foraminal narrowing on the 5° series when there was none by CT than they were to interpret the 5° MR as normal when CT showed foraminal narrowing. Thus, the average false-positive (i.e., CT negative, MR positive) rate for the three interpreters was 16.1% (15.3%, 11.7%, and 20.8% for evaluators 1, 2, and 3, respectively) for the 5° series. The average false-negative (i.e., CT positive, MR negative) rate was 8.0% (11.1%, 6.3%, and 6.7% for evaluators 1, 2, and 3, respectively) for the 5°

TABLE 1: Identification on MR of the Presence and Cause of CT-Verified Narrowing of Neural Foramina

Evaluator No.	Presence of Narrowing (%)		Cause of Narrowing (%)	
	5° Series	30° Series	5° Series	30° Series
1	74	66	70	48
2	82	86	73	76
3	73	78	92	88
Average	76	77	78	75

Note.—Although the variation in the evaluators' accuracy in interpreting the 30° series was wider than that of the 5° series, the two series had similar average accuracies with CT as the proof of diagnosis.

TABLE 2: Analysis of Discrepancies Between MR and CT Interpretations of the Cause of Neural Foraminal Narrowing

MR Series/Interpretation	CT Diagnosis		
	Bony Osteophyte (n = 141)	Disk Herniation (n = 17)	Combination (n = 15)
5°			
Bony osteophyte	0	2	4
Disk herniation	5	0	1
Combination	14	6	0
Normal	26	1	0
30°			
Bony osteophyte	0	3	10
Disk herniation	2	0	2
Combination	11	0	0
Normal	40	1	0

Note.—Interpretations of all three evaluators were combined; indeterminate interpretations were excluded. The "combination" diagnosis was used when both bony osteophytes and disk herniations were found.

TABLE 3: Number of Neural Foraminal Levels Uninterpretable on MR

Evaluator No.	MR Series	
	5°	30°
1	3	11
2	7	29
3	0	5
Total	10	45

Note.—All levels were interpretable on CT. The high number of indeterminate levels seen with the 30° technique was due to the lower contrast between CSF and bone, which caused decreased confidence in determining if bony protrusion existed in the neural foramen. Technical artifacts accounted for far fewer uninterpretable levels.

series. When the individual interpretations of the 30° series and CT disagreed, the evaluators overcalled foraminal narrowing with an average false-positive rate of 10.2% (9.1%, 7.5%, and 13.3% for evaluators 1, 2, and 3, respectively). The false-negative rate for the 30° series was 13.3% (24.5%, 6.5%, and 8.3% for evaluators 1, 2, and 3, respectively).

A marked difference was noted in the number of total indeterminate/uninterpretable examinations. For the three evaluators, no levels were deemed indeterminate on CT, 10 on the 5° series, and 45 on the 30° series (Table 3). This led to false elevation of the accuracy of the 30° values since the denominator for the ratios was lower with the 30° series (i.e., accuracy figures were calculated after omitting any case where an indeterminate score was given).

When the cause of the narrowing was evaluated, the 5° and 30° studies agreed with CT in 70–92% and 48–88% of the levels, respectively (Table 1 and Figs. 3 and 4). The most frequent disagreement occurred when narrowing on CT was reported to be due to osteophyte, but MR was reported as showing both bony and disk disease (Table 2). Of 141 instances when an evaluator interpreted the CT scan as showing osteophytic narrowing, the MR image was interpreted as showing both bony and diskogenic narrowing in 14 instances (9.9%) on the 5° series and in 11 instances (7.8%) with the 30° technique. The next most frequent error was when the CT scan was interpreted as showing bone and disk narrowing, but the MR image was interpreted as showing just bony encroachment.

Interobserver concordance in evaluating the foramina on the 5° series ranged from 77% to 90% for the presence of narrowing and 49% to 69% for its cause (Table 4). With the 30° series, interobserver concordance ranged from 66% to 81% for the presence of narrowing and from 70% to 78% for its cause. The range of interobserver concordance on CT was 81–87% for the presence of foraminal narrowing and 80–94% for the cause of narrowing.

In order to assess the highest expected level of accuracy obtainable with any neuroimaging study for cervical foraminal narrowing, we tested intraobserver concordance on CT, a method widely regarded as a proven tool for this entity. The

intraobserver concordance for evaluating the CT scans was 85.5% for the presence of and 94% for the cause of narrowing (interpreter 2).

Discussion

Initial MR studies evaluating the neural foramina were hindered by section thickness (≥ 4 mm) and interslice gap limitations [1–4]. This led to unfavorable comparisons with postmyelography CT in studies with surgical confirmation, particularly with regard to the evaluation of osteophytic neural foraminal stenosis [2–4]. MR interpretations with thick sec-

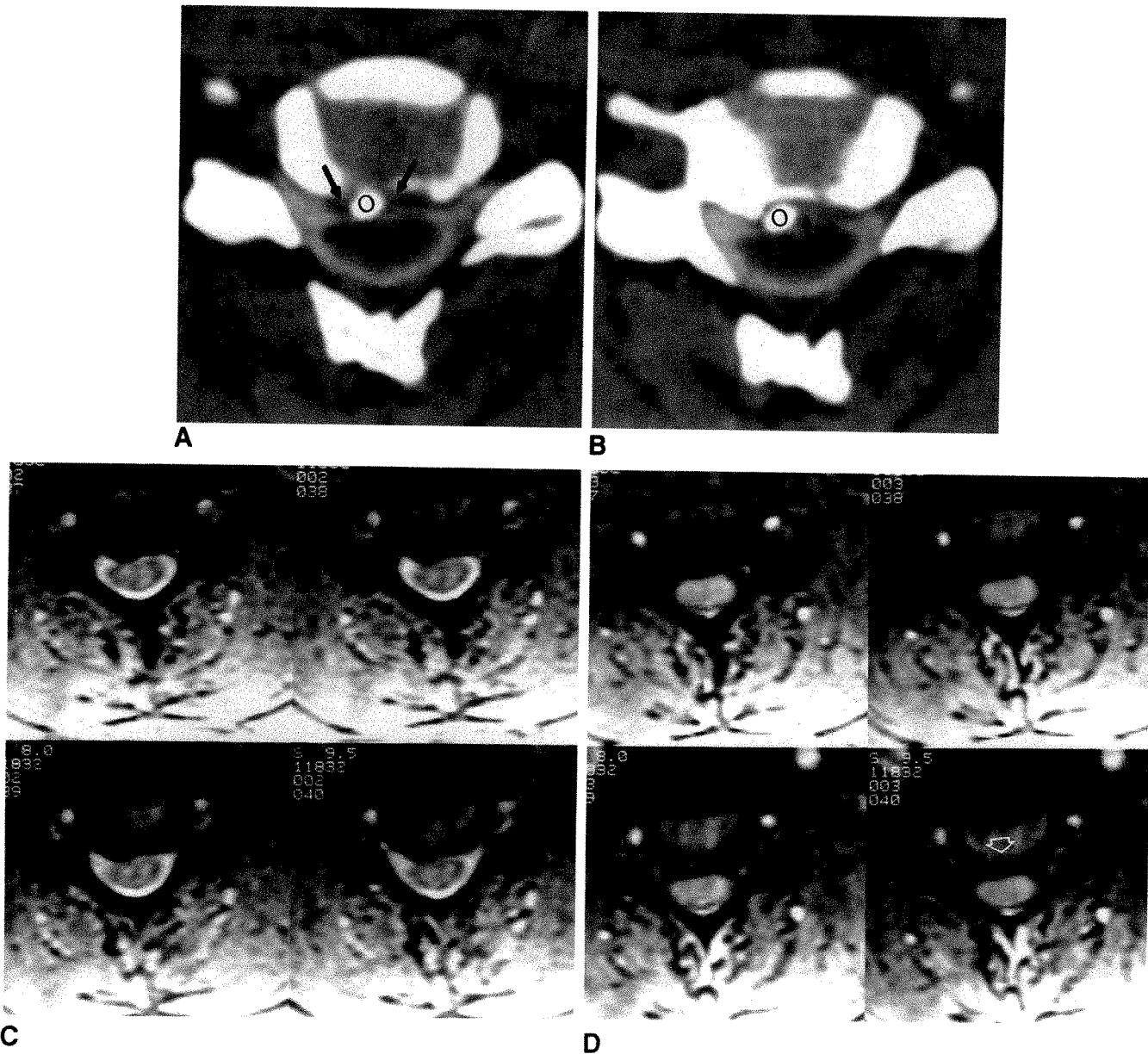


Fig. 4.—Postmyelogram CT and 3DFT MR in a patient with herniated disk and bony degenerative change.
A and B, Postmyelogram CT images show minimal disk material (arrows) and dense osteophyte (o) projecting posteriorly and approaching cord surface. Neural foramen is not narrowed.
C, 3DFT low-flip-angle images suggest mild right foraminal narrowing, predominantly due to osteophytic disease.
D, Disk contribution to foraminal narrowing (arrow) is seen somewhat better on dark CSF higher-flip-angle series.

TABLE 4: Interobserver Concordance as to the Presence and Cause of Neural Foraminal Narrowing on MR and CT Images

Finding/ Evaluator Nos.	MR (%)		CT (%)
	5° Series	30° Series	
Presence of narrowing			
1 and 2	77	71	87
1 and 3	82	66	81
2 and 3	90	81	84
Average	83	73	84
Cause of narrowing			
1 and 2	49	70	82
1 and 3	63	74	80
2 and 3	69	78	94
Average	61	75	86

Note—Interobserver concordance was better on CT interpretations than on MR interpretations. This difference was most striking in examinations of the cause of neural foraminal narrowing.

tions typically underreported foraminal stenosis. Accuracy as to the cause of foraminal narrowing also has been reported to be less with MR than CT. The explanations for the relative inaccuracy of MR imaging included the variable presence of bone marrow within the osteophyte resulting in obscuration of spurs (being similar in intensity to disk material), osteophytes masking disk herniations, and volume averaging [2–4]. Because of these findings it is widely held that conventional spin-echo MR lacks specificity and sensitivity in evaluating bony foraminal disease. We sought to further explore this belief with the 3DFT pulse sequence.

With 3DFT gradient-echo imaging, an entire volume of tissue is excited and data are collected from the entire slab. Scan times are reduced by limiting TR, thus limiting patient motion artifacts, yet high S/N is maintained by obtaining data from an entire imaging slab [5–7]. In order to spatially encode the information, a phase-encoding gradient is applied both along slice-selection (z) axis as well as the in-plane phase-encoding (y) axis [5, 6]. By using a relatively short TR, many thin section slices can be obtained contiguously while maintaining a reasonable scan time. The benefits of 3DFT imaging derive from the ability to obtain thin, contiguous sections (which do not suffer significantly from cross-talk and partial-volume effects). Thinner sections reduce problems with volume averaging and reduce magnetic susceptibility artifacts. A distinguishing feature when compared with the two-dimensional sequential mode relates to the improvement in S/N when exciting a slab of tissue. Whereas in the 2DFT mode, the S/N is independent of the number of locations scanned, S/N in 3DFT increases as the square root of the number of slice encodings. Thus, the S/N is proportional to both the square root of the number of slices and the square root of the number of excitations. Therefore, for instance, by halving the number of excitations and doubling the number of slice encodings, the S/N remains unchanged. This permits increased coverage of pertinent anatomy without the penalty of lengthened acquisition times. Unlike in two-dimensional imaging, where slice thickness is essentially limited by the available gradient power, slab partitioning into slices in three-dimensional imaging is achieved by phase encoding. Current imaging techniques allow slice thicknesses as thin as 0.7 mm,

but, in general, section thickness is limited solely by S/N in 3DFT scanning. Section thickness on conventional 2DFT MR is limited by gradient strength. As with 2DFT imaging, S/N in three-dimensional imaging scales proportional to voxel size, so one sacrifices S/N to achieve very thin sections.

The advantage of reducing the TE to as short as possible derives from the resulting reduction in susceptibility artifacts. This is particularly important at bony interfaces in the cervical spine. To a lesser degree, shorter TEs will contribute to maintaining high S/N as relaxation occurs in this interval.

Applied to the cervical spine, 3DFT gradient-echo techniques allow acquisition of 60 1.5-mm contiguous sections from C2–C3 to C7–T1 in 6.5 min. The high bone–CSF–nerve-root sleeve contrast when low-flip-angle (<10°) techniques are used allows excellent visualization of foraminal anatomy and disease (Fig. 1) [6, 7]. Typically, four to five 1.5-mm-thick slices through the foramina are obtained to evaluate narrowing or lateral disk herniations. Although surgical intervention for bony neural foraminal disease often is not indicated, its detection is important to explain the patient's symptoms since other more peripheral lesions can mimic nerve root compression. Additionally, when significant neural foraminal narrowing is coupled with disk herniations, the surgical management may be altered.

Because of the infrequency of surgical intervention for bony narrowing of cervical neural foramina, this study relied on CT as the gold standard for evaluating the foramina. When there is no significant narrowing, it is impossible to get surgical proof, a point we acknowledged when determining the methodology for this study. Conservative, nonsurgical management, possibly even with the use of steroids, is an alternative to surgery in many cases. Even when surgery is performed, an anterior approach may be preferred for disk disease, which limits the surgeon's ability to detect how narrowed the foramen is and occasionally by what process. For these reasons, we used thin-section CT as our gold standard. In doing so, however, we realized that no true comparison could be made of the accuracy of MR and CT. We thus set CT's accuracy at 100%, so MR could never be proved to be better than CT in this study. Our intention was to see how well the two techniques correlated with each other. We intentionally studied the neural foramina because evaluation of bony disease is one of MR's weakest areas.

Our study demonstrates that interpretation of 3DFT gradient-echo MR agrees with CT in the determination of neural foraminal narrowing in over 75% of the cases with both the 5° and 30° flip angle series, when adequate studies are available. Of the cases in which the evaluators failed to detect abnormalities on MR that were seen by CT, 66 (97%) of 68 were because of bony encroachments. Therefore, the relative insensitivity of MR to bony disease found with spin-echo and 2DFT sequences appears to persist even with thin-section 3DFT gradient-echo imaging. Part of the difficulty in detecting bony encroachments on foramina is the fact that the dura and anulus, both of low signal intensity on gradient-echo images, may be mistaken for bone. Nonetheless, the overall accuracy (84%) of the 3DFT MR technique for the best evaluator approached that of intraobserver concordance in interpreting postmyelography CT images (85.5%). Also in this study, 3DFT

MR was more likely to be interpreted as showing foraminal stenosis when none was present on CT than not to demonstrate stenosis when CT was interpreted as having shown it.

MR image interpretation concurred with that of CT as to the cause of the narrowing in 78% (5°) and 71% (30°) of the levels when both studies agreed they were narrowed. Most of the cases in which the interpretations of the causes of the narrowing differed between CT and MR consisted of instances where bone and disk were confused with bone alone (65%). In fact, one might wonder whether MR, with its superior soft-tissue resolution, may be more accurate than CT in these cases. It is likely that remnants of hard disk herniations seen on MR may be present in some of the cases reported as bony osteophytes only on CT.

The interobserver concordance with MR was greater with the bright CSF technique (overall 83.0%) than the dark CSF series (73%) for the grading of narrowing. We believe that this is because of the lower contrast between the bony margins of the foramen and the CSF with the dark CSF 30° technique. The uncertainties of our interpreters regarding the foraminal margins in the presence of dark CSF is reflected in the very large number of indeterminate images with this technique (45 instances). One interpreter had a particularly difficult time distinguishing between bone and CSF in the lateral foramina and believed he could not confidently determine if the foramen was narrowed or not. The mean CT interobserver concordance (84% for grading) was in the same range of values as the 5° bright CSF results (83%) and compares favorably with the intraobserver concordance of the CT reading (85.5%). Because the evaluator's accuracy for grading the narrowing on MR scans (84%) was nearly the same as his accuracy in interpreting the CT scans on different days (85.5%), the study suggests that the maximum accuracy that one could expect to obtain in grading narrowing is approximately 85%, regardless of the technique.

The average CT inter- and intraobserver concordance were 85% and 94%, respectively, for the cause of narrowing. The comparative MR values of 75% for the 30° technique and 61% for the 5° technique suggest that CT is more reproducible in identifying the cause of narrowing. A steep learning curve may still exist in the MR technique, however, as evidenced by the wide range of values among evaluators.

Hedberg et al. [8] studied the efficacy of gradient-echo MR in the evaluation of cervical radiculopathy in 1988. They used low flip angles and 5-mm contiguous sections. In 29 of 30 locations, surgery confirmed the MR findings: in only one case of a ventrolateral osteophyte did the patient's clinical symptoms and surgical findings disagree with the MR impression. The MR-CT myelography correlation was 100% in 25 patients. These results led the authors to conclude that "MR imaging is the initial procedure of choice for the evaluation of suspected cervical radiculopathy" [8]. The use of thin-section 1.5-mm contiguous 3DFT imaging should only enhance the enthusiasm for MR in this area. Our results suggest that the enthusiasm should be tempered by the understanding that MR interpretation will disagree with CT in up to 25% of cases, even in the hands of experienced neuroradiologists.

A recent nonblinded, nonrandomized study compared 3DFT thin-section MR with 2DFT techniques in the evaluation of neural foramina [9]. Because this study used contiguous 1.5- to 2.0-mm 3DFT slices and compared them with 4-mm 2DFT scans with 1-mm interslice gaps, the results were not

surprising. The thinner slice technique provided greater detail of narrowing, and the apparent image contrast subjectively was greater with the high-intensity CSF 3DFT technique than with low-intensity CSF technique [9].

Many artifacts can degrade the 3DFT images. Motion in this 6.5-min series, including swallowing and respiratory motion, may prevent adequate evaluation of the foramina [5, 6]. Aliasing, in which the upper and lower slices are "wrapped around" each other, degrades slices at the extremes of the slab, typically the upper and lower first four slices. Therefore, one may have to sacrifice visualization of the C2-C3 level if clinical suspicion of disease is at the C7-T1 level in order to ensure high-quality images at the lower level. Ferromagnetic artifact in the postoperative cervical spine also will degrade gradient-echo images.

In our routine evaluation of the cervical spine, we use a contiguous 3-mm-thick sagittal 800/20/2 spin-echo sequence, followed by the 5° 50/15/1 3DFT sequence with gradient-moment nulling, a 256 × 128 matrix, and 60 1.5-mm contiguous sections. We also include the 30° 50/11/1 sequence without gradient-moment nulling. Our results suggest that 3DFT gradient-echo, thin, contiguous-section MR imaging is useful in assessing the neural foramina, since its accuracy in the best of interpreters approaches that of the intraobserver concordance when double reading CT scans, approximately 85%. The wide range of variability in our evaluators' grading of foramina suggests that the learning curve for MR interpretation probably has not peaked as it has with CT, and therefore its accuracy is strongly interpreter dependent.

Presumably, as neuroradiologists gain more experience with the technique, the reliability and reproducibility of MR interpretation will increase. It is still more difficult for MR to depict small bony encroachments on the foramina than to detect herniated disk material. The large number of indeterminate or uninterpretable images on the 30° technique, coupled with the superior bone-CSF contrast on the 5° technique, suggests that the latter is the more useful examination in the evaluation of the foramina.

REFERENCES

1. Czervionke LF, Daniels DL, Ho PSP, et al. Cervical neural foramina: correlative anatomic and MR imaging study. *Radiology* 1988;169:753-759.
2. Modic MT, Masaryk TJ, Mulopulos GP, Bundschuh CV, Han JS, Bohlman H. Cervical radiculopathy: prospective evaluation with surface coil MR imaging, CT with metrizamide, and metrizamide myelography. *Radiology* 1986;161:753-759.
3. Brown BM, Schwartz RH, Frank E, Blank NK. Preoperative evaluation of cervical radiculopathy and myelopathy by surface-coil MR imaging. *AJNR* 1988;9:859-866.
4. Modic MT, Masaryk TJ, Ross JS, Mulopulos GP, Bundschuh CV, Bohlman H. Cervical radiculopathy: value of oblique MR imaging. *Radiology* 1987;163:227-231.
5. Wehrli FW, Atlas SW. Fast imaging: principles, techniques, and clinical applications. In: Atlas SW, ed. *Magnetic resonance imaging of the brain and spine*. New York: Raven Press, 1990:1013-1078.
6. Carlson J, Crooks L, Ortendahl D, Kramer DM, Kaufman L. Signal-to-noise ratio and section thickness in two-dimensional versus three-dimensional Fourier transform imaging. *Radiology* 1988;166:266-270.
7. Enzmann DR, Rubin JB, Wright A. Cervical spine MR imaging: generating high signal CSF in sagittal and axial images. *Radiology* 1987;163:233-238.
8. Hedberg MC, Drayer BP, Flom RA, Hodak JA, Bird CR. Gradient echo (GRASS) MR imaging in cervical radiculopathy. *AJNR* 1988;9:145-151.
9. Tsuruda JS, Norman D, Dillon W, Newton TH, Mills DG. Three-dimensional gradient-recalled MR imaging as a screening tool for the diagnosis of cervical radiculopathy. *AJNR* 1989;10:1263-1271.

Gadopentetate Dimeglumine-Enhanced MR Imaging in Children Following Surgery for Brain Tumor: Spectrum of Meningeal Findings

Patricia A. Hudgins¹
Patricia C. Davis
James C. Hoffman, Jr.

Gadopentetate dimeglumine-enhanced MR imaging was performed in 51 consecutive postoperative pediatric neurosurgical patients with a diagnosis of brain tumor. These studies were examined retrospectively to determine the spectrum of meningeal findings in this patient population. Patterns of enhancement were correlated with type of surgery, interval since surgery, clinical and CSF findings, and the use of radiation and steroid therapies. Normal postoperative meningeal findings include no meningeal enhancement or mild focal or diffuse dural enhancement. More moderate dural or subdural enhancement may be seen in clinically well children who have postsurgical subdural collections, or who have a remote history of serious meningeal disease (meningitis or subarachnoid hemorrhage). In all six cases in which nodular dural, leptomeningeal, or ependymal enhancement was seen, recurrent local tumor, leptomeningeal metastases, or infection were present. Leptomeningeal tumor or infection should be suspected if such patterns of enhancement are noted. Parameters that did not appear to affect the pattern of meningeal enhancement included type of surgery, interval since surgery, or therapeutic radiation.

AJNR 12:301-307, March/April; AJR 156:1237-1243, June 1991

MR is essential for initial and follow-up imaging of pediatric patients with intracranial lesions. Advantages of MR include superior soft-tissue contrast, multiplanar capability, and absence of beam-hardening artifacts in the posterior fossa [1-4]. Gadopentetate dimeglumine has proved to be a useful adjunct for demonstration of lesions that disrupt the blood-brain barrier, for extraaxial lesions, and for leptomeningeal diseases [5-12].

Recent reports describe meningeal enhancement with gadopentetate dimeglumine following a wide variety of CNS surgical procedures, primarily in adults [10, 13-15]. In children, the expected postoperative enhancement patterns, the time course of this enhancement, and the relationship of this enhancement to radiation therapy have not been reported. Children with brain tumors are a unique population and are different from adults: they more commonly have lesions located in the posterior fossa, neurosurgical intervention frequently involves both tumor biopsy or resection and placement of ventricular shunts, and leptomeningeal spread of tumor is a common complication.

In this series, patterns of meningeal enhancement on MR in 31 children with known brain tumors and prior cranial surgical procedures were correlated with the interval and type of surgery, clinical and CSF evaluations, and other therapeutic treatments used (radiation and steroid therapy). From these data we attempted to identify the spectrum of findings associated with normal patterns of postoperative meningeal enhancement. Analysis of nine cases of documented meningeal disease revealed pattern differences that suggest tumor or infection in the postoperative child.

Received May 3, 1990; revision requested July 6, 1990; revision received August 27, 1990; accepted September 10, 1990.

¹ All authors: Department of Radiology, Section of Neuroradiology, Emory University School of Medicine, 1364 Clifton Rd., N. E., Atlanta, GA 30322. Address reprint requests to P. A. Hudgins.

0361-803X/91/1566-1237
© American Roentgen Ray Society

Materials and Methods

Over a 10-month period, from September 1988 to July 1989, 58 consecutive contrast-enhanced brain MR examinations were performed in a total of 38 pediatric patients with CNS neoplasia. Seven patients were excluded from the study owing to absence of recognizable enhancement of normal structures on immediate postenhancement sequences, indicating that these patients did not receive contrast medium. The study group then consisted of 31 patients who underwent 51 postoperative enhanced MR examinations. The population comprised 18 boys and 13 girls aged 11 months to 18 years (mean, 9 years 5 months). Nineteen patients had one postoperative enhanced MR study and 12 had two or more follow-up enhanced MR studies. Twenty scans were obtained after ventricular shunt placement and craniotomy, 12 after CT-guided biopsy and shunt placement, 10 after craniotomy only, six after ventricular shunt placement, and three after CT-guided biopsy. Enhanced MR was performed to define a known lesion or to evaluate the efficacy of surgical intervention. Clinical findings (neurologic status; interval since surgery, radiation, and chemotherapy; and other significant CNS illnesses including meningitis, hemorrhage, and shunt malfunctions) and CSF analyses (29/31) were studied by chart review.

Thirty of the 31 patients had histologic or cytologic confirmation of a CNS neoplasm. One child without histologic proof had a presumed germ cell tumor of the pineal region on the basis of MR intensities suggesting fat. Neoplasms are listed in Table 1.

MR was performed with a 1.5-T superconducting magnet (Philips Medical Systems, Shelton, CT) operating at 0.5 T (17 scans) or 1.5 T (34 scans). All studies were performed with a head coil and a spin-

echo technique. All patients had an initial localizing sagittal sequence, 400-800/20, 30/1 (TR/TE/excitations), at 5-mm slice thickness, followed by axial T2-weighted images, 1900-2200/50-100. Additional unenhanced short TR sequences (400-800/20, 30/1) in either the coronal or axial plane were completed in 28 of 31 patients. After obtaining written informed consent, gadopentetate dimeglumine (Magnevist, Berlex Laboratories, Wayne, NJ) was given in a dose of 0.1 mmol/kg IV. At least one immediate (beginning within 5 min of contrast administration) short TR sequence was completed in all patients, with additional enhanced sequences in 20 of 31 patients. Imaging planes were chosen for optimal demonstration of the primary lesion.

The unenhanced and enhanced short TR sequences were compared retrospectively by two experienced neuroradiologists. Five meningeal characteristics were evaluated: (1) degree of enhancement (mild, moderate, or marked); (2) distribution of the enhancement (diffuse or focal); (3) if focal, the proximity of the enhancement to the surgical site; (4) location of enhancement (dural, pia-arachnoidal, or ependymal); and (5) nodularity of enhancement.

Results

The distribution and location of meningeal enhancement patterns, mean interval since surgery, child's clinical status, existence of significant leptomeningeal disease, and history of radiation therapy are noted in Table 2. Thirty-eight of 51 scans revealed either no meningeal enhancement or only mild dural enhancement, either diffuse or focal at the surgical site (Fig. 1). Detailed findings on the 13 of 51 scans with more extensive enhancement are given in Table 3. Four of the 13 scans (cases 1, 2 [scan 1], 3, and 4) showed bilateral postoperative collections in the subdural space (Fig. 2). These children were clinically well. Two of the 13 with more extensive enhancement (case 2 [scans 2 and 3]) were seen in a patient with chemical meningitis based on clinical and CSF analysis (Fig. 3). This child had a cystic craniopharyngioma and the meningitis was attributed to subarachnoid contamination by intracystic contents. This patient was scanned during acute illness and again 3 months later when the illness had resolved. Both scans showed moderate, smooth, diffuse dural enhancement. One patient (case 5) who had a craniotomy and radia-

TABLE 1: Neoplasms Identified in Children Studied with Enhanced MR

Tumor Type	No. of Patients
Astrocytoma	9
Craniopharyngioma	6
Neuroblastoma	3
Ependymoma	3
Chiasmal-hypothalamic astrocytoma	3
Other (one each: ependymoblastoma, medulloblastoma, gliosarcoma, meningioma, choroid plexus papilloma, pineoblastoma, pineal region tumor [probably teratoma])	7

TABLE 2: Patterns of Meningeal Enhancement on MR Imaging

Meningeal Enhancement on MR	No. of Scans (n = 51)	Interval Since Surgery (Mean)	Clinical Status	Significant LM Disease	No. with RT	Interval Since RT (Mean)
None	9	1 wk-10 yr (3½ yr)	Healthy	None	7	6 wk-6½ yr (8 mo)
Dural or subdural						
Mild						
Diffuse	20	1 d-5 yr (3½ yr)	Healthy	None	12	1 mo-8 yr (2 yr)
Focal (surgical site)	9	5 d-9½ yr (2½ yr)	Healthy	None	5	1 yr-10 yr (8 yr)
Moderate	7	2 wk-8 yr (16½ mo)	Healthy, 5	PO SDH, 4; S/P remote SAH, 1; chemical meningitis, 2	2	3 mo-8 yr (5½ mo)
Nodular	4	3 mo-9 mo (6 mo)	Healthy, 3; febrile after HF Tx, 1	Normal CSF	4	1 mo-4 mo (2½ mo)
Pia-arachnoid	1	1 mo	III	Meningeal abnormalities on PE; CSF cytology; LM pineoblastoma	NP	-
Ependymal	1	2 mo	III	CSF + Aspergillus	NP	-

Note.—LM = leptomeningeal; RT = radiation therapy; wk = week(s); mo = month(s); yr = year(s); d = day(s); PO = postoperative; SDH = subdural hematoma; S/P = status post (after); SAH = subarachnoid hemorrhage; HF Tx = hyperfractionation treatment; NP = not performed; PE = physical examination.

Fig. 1.—14-year-old child 4 years after craniotomy and shunt placement for craniopharyngioma, now clinically well.

A. Coronal unenhanced short-TR MR image (600/30) shows ferromagnetic artifacts at craniotomy site (arrows).

B. Enhanced short-TR MR image (600/30) reveals thin, symmetric dural enhancement over both convexities and along interhemispheric fissure (white arrows). If unenhanced study had not been performed, ferromagnetic artifacts at craniotomy site (black arrows) might have been mistaken for meningeal enhancement.

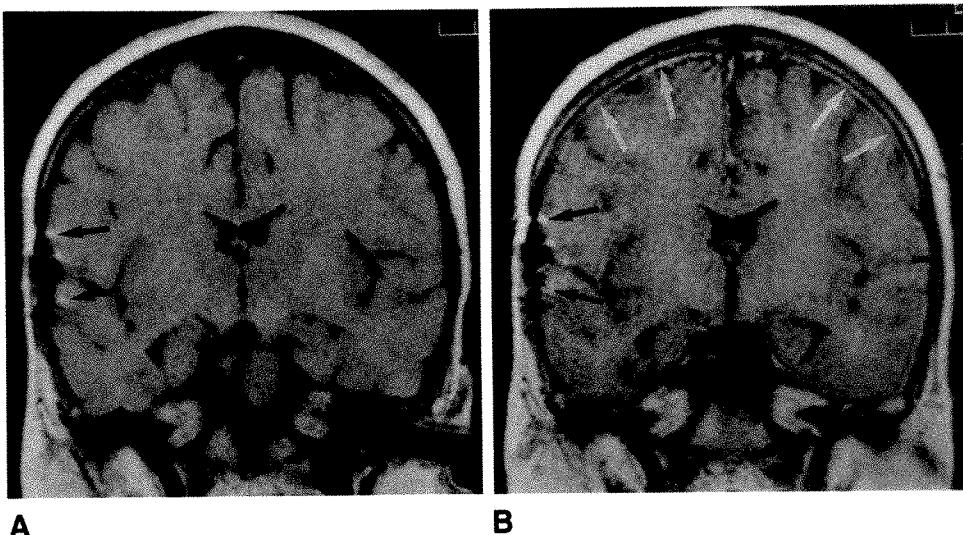


TABLE 3: Abnormal Patterns of Meningeal Enhancement

Case No.	Tumor Detected	Scan No. (Interval Since Previous Study)	Pattern of Enhancement	Reason for Enhancement Pattern
1	Craniopharyngioma	1	Moderate: dural, biconvexity	Postcraniotomy SDH; clinically well
2	Craniopharyngioma	1	Moderate: dural, biconvexity	Postcraniotomy SDH; clinically well
		2 (3 mo)	Moderate: dural; bifrontal & biparietal enhancement more prominent & diffuse	Chemical meningitis based on CSF/clinical findings
		3 (3 mo)	Moderate: dural; no change	Acute illness clinically improved
3	Hypothalamic astrocytoma	1	Moderate: dural, biconvexity	Postshunt SDH; clinically well
4	Pineal region	1	Moderate: dural, tentorial	Postshunt SDH; clinically well
5	Ependymoma	1	Moderate: dural, prepontine	3 yr S/P SAH; multiple shunt revisions; clinically well
6	Brainstem astrocytoma	1	Nodular: dural, CP angle	Known subtotal resection (presumed residual tumor); clinically well
		2 (2 mo)	Moderate: dural/subdural enhancement in prepontine cistern (CP angle nodule unchanged)	S/P hyperfractionation therapy; CSF normal
7	Medulloblastoma (CP angle)	1	Nodular: dural, CP angle	Subtotal resection (presumed residual tumor)
8	Pineoblastoma	2 (2 mo)	No change	Clinically well
		1	Marked: leptomeningeal; nodular: suprasellar, prepontine, pineal region	Leptomeningeal metastases; CSF cytology
9	Cerebellar astrocytoma	1	Intraventricular	<i>Aspergillus</i> ventriculitis & mycotic aneurysm

Note.—mo = month(s); yr = year(s); SDH = subdural hematoma; S/P = status post (after); SAH = subarachnoid hemorrhage; CP = cerebellopontine.

tion therapy for an ependymoma and had undergone multiple shunt revisions experienced a subarachnoid hemorrhage of uncertain origin. The MR examination showed moderate dural enhancement, although the patient was clinically well at that time. One patient (case 6 [scan 1]) had undergone subtotal resection of a brainstem glioma; enhanced MR showed a residual tumor nodule in the cerebellopontine angle, although the patient was clinically well. The patient then underwent hyperfractionation therapy, and a sequential enhanced MR study 2 months later (scan 2) revealed progression of enhancement. This focal enhancement was in the prepontine

cistern, and precise localization to a specific meningeal layer was not possible. The patient's only symptom was recurrent fever; he was otherwise clinically well and CSF was negative. In case 7, two scans showed focal nodular enhancement in the cerebellopontine angle; this represented residual tumor (Fig. 4). The patient had undergone subtotal resection of a medulloblastoma and was otherwise clinically well. One patient (case 8) had marked nodular leptomeningeal enhancement remote from the primary tumor site consistent with leptomeningeal metastases; CSF cytology at that time revealed metastatic pineoblastoma (Fig. 5). One patient (case

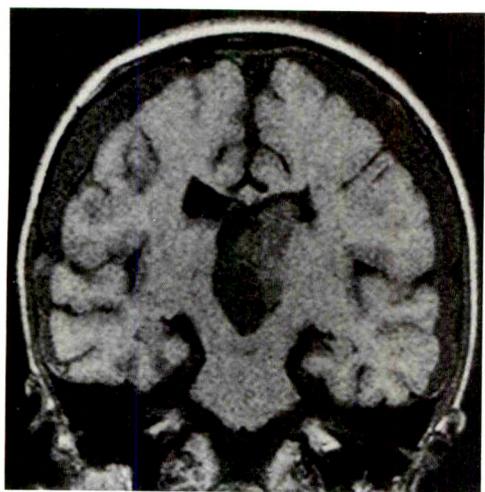
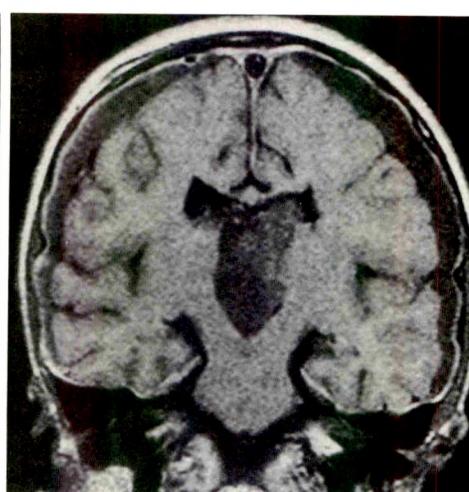
**A****B**

Fig. 2.—6-year-old child 2 weeks after biventricular shunt placement for hydrocephalus resulting from hypothalamic astrocytoma.

A, Coronal unenhanced short-TR MR image (600/30) shows large bilateral low-intensity subdural collections that developed after shunt placement.

B, Enhanced short-TR MR image (600/30) shows symmetric thin rim of dural enhancement along periphery of subdural effusions. The child is well, without meningeal symptoms.

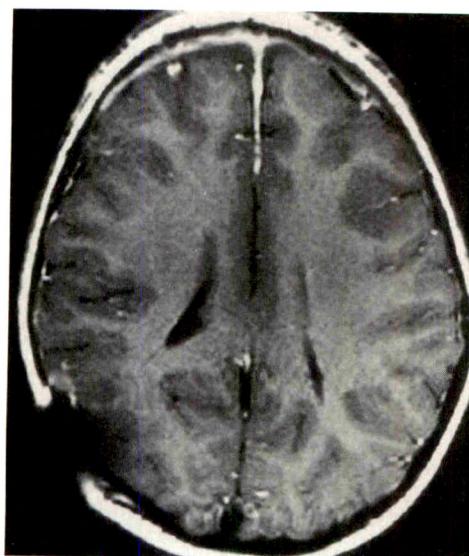
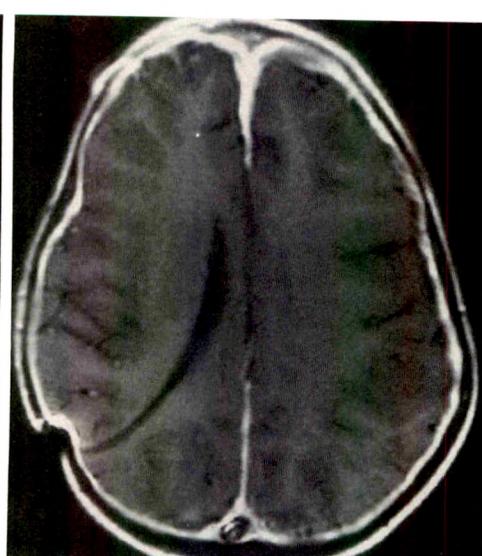
**A****B**

Fig. 3.—3-year-old girl with cystic craniopharyngioma.

A, Enhanced short-TR MR image (600/30) 1 month after biventricular shunt placement and frontal craniotomy reveals moderate bifrontal and interhemispheric dural enhancement. CT scan confirmed small bilateral subdural effusions. The child was clinically well.

B, Enhanced short-TR MR image (800/20) 4 months later reveals more extensive and prominent dural enhancement. CSF and clinical findings confirm chemical meningitis, probably resulting from spill of cystic tumor contents.

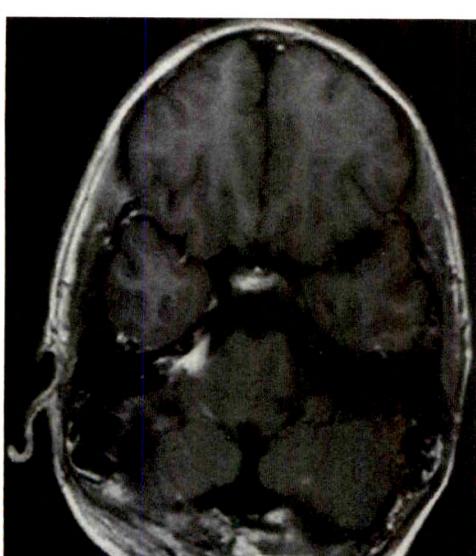
**4****5**

Fig. 4.—14-year-old boy 3 months after craniectomy for subtotal resection of medulloblastoma. Enhanced short-TR MR image (800/20). Nodular enhancement in right cerebellopontine angle represents known residual tumor.

Fig. 5.—4-year-old girl after ventricular shunt placement and CT-guided biopsy of pineal region tumor (pineoblastoma). Sagittal enhanced short-TR MR image (500/20) shows abnormal enhancement along ventral medulla. At this time, CSF was positive for tumor cells.

9) had undergone total resection of a cerebellar astrocytoma. Four months after surgery, the patient was acutely ill and an enhanced scan revealed ependymal enhancement of the right lateral ventricle (Fig. 6). CSF was positive at this time for *Aspergillus*, and the patient subsequently died from a mycotic aneurysm.

The pattern of enhancement associated with each neurosurgical procedure is shown in Table 4. No enhancement pattern was specific or isolated to a particular surgical procedure. The prevalence of enhancement was approximately equal after craniotomy and shunt placement.

Twenty-nine of the 51 scans were obtained after high-dose (5000 R [1290 mC/kg] or greater) radiation; the interval since radiation ranged from 1 month to 10 years (Table 2). All children receiving postoperative radiation were treated with high-dose steroids during part or all of the duration of radiation therapy. By the end of the radiation treatment, most had been tapered from steroids. The exact course and time of steroid taper were not available. Children in whom scans were obtained years after radiation therapy were not on steroid therapy at the time of the MR scan.

Sequential scans were obtained in 12 patients; in only four was there any change in meningeal enhancement. In one patient progression of enhancement on the second scan was temporally related to chemical meningitis. In a second patient, nodular dural enhancement due to residual cerebellopontine angle tumor progressed to moderate dural enhancement in the prepontine cistern following hyperfractionation therapy. This child was febrile with repeated normal CSF analyses following radiation therapy. Following neurosurgical procedures, postsurgical subdural hygromas developed in two patients. Progression of dural enhancement from mild to moderate was seen in both; these children were clinically well. In eight of 12 patients, there was no change in the pattern or degree of enhancement.

The unenhanced T1-weighted image was helpful for accurate interpretation of the enhanced scan (Fig. 1). In a number of cases, ferromagnetic artifacts localized to the craniotomy

site, presumably resulting from minute metallic fragments, resulted in an area of high signal along the meningeal surface; this appearance simulated postoperative dural enhancement. One patient who had undergone gross total resection 10 years before for an ependymoma had an acute, severe headache; a focal extraaxial hematoma was seen on MR at the suboccipital craniectomy site. This hematoma was manifested by high signal intensity on T1-weighted sequences and did not change in appearance following enhancement. Without the unenhanced sequence, the hemorrhagic collection might have been misinterpreted as enhancing recurrent tumor.

Discussion

Enhanced MR imaging with gadopentetate dimeglumine has emerged as the technique of choice for evaluating the postoperative pediatric neurosurgical patient. Except in the most uncomplicated clinical settings, such as shunt malfunction or sequential evaluation of uncomplicated extraaxial collections, MR imaging has supplanted CT in this area. In addition to its well-known advantages over CT, such as multiplanar capability, improved soft-tissue contrast, and lack

TABLE 4: Correlation of Surgical Procedures and Pattern of Enhancement

Enhancement on MR	No. of Scans (n = 51)			
	Shunt and Craniotomy	Shunt and Biopsy	Craniotomy	Shunt Biopsy
None	3	2	1	1
Dural or subdural				2
Mild				
Focal	5	2	1	0
Diffuse	5	7	5	3
Moderate	5	0	0	2
Other ^a	2	1	3	0
Total	20	12	10	6
				3

^a Comprises nodular/dural, ependymal, leptomeningeal.

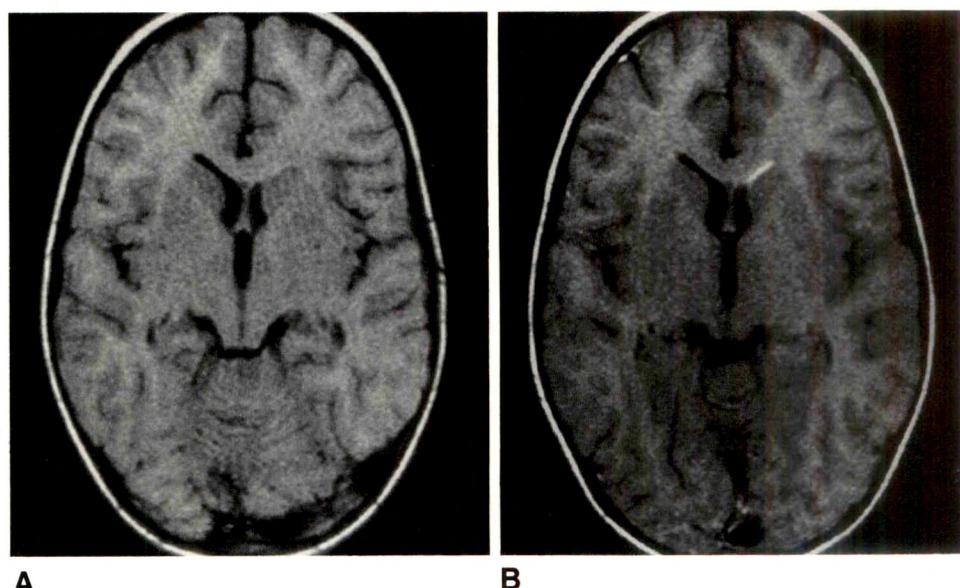


Fig. 6.—4-year-old boy 2 months after suboccipital craniectomy for gross total resection of cerebellar astrocytoma.

A, Axial unenhanced short-TR MR image (550/30) shows mild asymmetry of frontal horns; it is otherwise normal.

B, Enhanced short-TR MR image (550/30) reveals ependymal enhancement in frontal horn of left lateral ventricle. CSF culture revealed *Aspergillus*; the patient subsequently died of complications of a mycotic aneurysm.

of ionizing radiation, recent reports suggest that contrast-enhanced MR is more sensitive than contrast-enhanced CT in revealing and characterizing meningeal lesions [10]. Particularly because of beam-hardening artifacts, CT is poor in evaluating meningeal abnormalities at the base of the skull and inner table of the calvaria, regions visualized discretely on MR. Furthermore, while breakdown of the blood-brain barrier is a requirement for abnormal enhancement on both CT and MR, it has been suggested that enhanced MR may be more sensitive than enhanced CT and may reveal the breakdown at an earlier stage [8].

The blood-brain barrier is a physiologically complex structure. Simplistically, it comprises cerebral capillaries with tight junctions, the function of which is to prevent the free passage of molecules into the brain tissue [16]. The meninges, comprising the dura, the arachnoid, and the pia, are a significant site of blood-brain barrier. The dura itself is devoid of blood-brain barrier; capillary junctions within the dura are not tight and, therefore, form no barrier to prevent the free passage of molecules. One would anticipate that since it is devoid of a blood-brain barrier, the dura would enhance intensely and predictably following the administration of IV contrast material. However, it is relatively avascular, and the second requirement for contrast enhancement, an adequate delivery of contrast material via arteries and capillaries, is not met. This is the explanation for the variable enhancement pattern of the dura on both CT and MR. Both layers of the arachnoid and the pia have tight junctions within the capillaries, and, therefore, have a functional blood-brain barrier. For this reason, and despite the relative vascularity of the arachnoid and pia, enhancement within the arachnoid and the pia is not seen normally following contrast administration for either MR or CT. If arachnoidal or pial enhancement is seen, leptomeningeal disease should be suspected.

A wide variation in gadopentetate dimeglumine enhancement patterns of the dura in postoperative patients has been described [10, 13, 14]. As the enhancement pattern in the intact dura is variable [17], it is not surprising that the traumatized dura might show a variety of enhancement patterns. If this spectrum of normal postoperative enhancement patterns is familiar, recognition of pathologic meningeal enhancement is facilitated.

The ability to detect dural and leptomeningeal lesions is of particular importance in children with intracranial neoplasms, as a number of the common pediatric tumors (medulloblastoma, ependymoma, pineal region tumors, and anaplastic astrocytomas) may metastasize to the leptomeninges via the CSF. While enhanced MR is more sensitive than enhanced CT in detecting leptomeningeal enhancement, it is no more specific. Criteria for differentiation between insignificant (i.e., postoperative) and significant (i.e., neoplastic, inflammatory) meningeal enhancement have not been established for the pediatric population. The goal of this article is to describe the normal appearances of the dura and leptomeninges in the postoperative neurosurgical pediatric patient with an intracranial neoplasm.

Common postoperative findings in clinically well patients varied from no dural enhancement to smooth, thin dural enhancement, either immediately at the operative site or more

diffusely over the convexities. These findings may persist for prolonged periods (e.g., 10 years) postoperatively. A history of prior therapeutic radiation appeared to have no recognizable relationship to the presence or degree of enhancement. Similarly, the specific type of neurosurgical procedure performed had no relationship to the presence or degree of enhancement. In all cases in this study, therefore, the presence of mild, smooth dural enhancement, either focal or diffuse, implied benign postoperative meningeal changes.

A common cause of moderate dural or subdural enhancement is a subdural postoperative collection, usually nonhemorrhagic. Our experience was similar to that of other investigators in that the enhancement occurred in the peripheral portion of the collection [10]. During the organization phase of a subdural collection, numerous capillaries permeate the outer aspect of the hematoma or hygroma, forming a membrane that is relatively vascular, especially when compared with the inner avascular membrane on the arachnoidal side of the clot [18]. This explains the different degree of enhancement within a subdural collection.

Other causes of moderate dural enhancement in our series included remote subarachnoid hemorrhage and acute or remote chemical meningitis. Interestingly, enhancement in one patient persisted long after resolution of acute illness. Additional experience with enhanced MR is required to determine whether or not these findings eventually resolve. It is significant that this moderate enhancement does not always predict the presence of serious acute or active disease, but instead may be a manifestation of prior meningeal disease.

In each of the four cases (a total of six scans) in this series of enhancement of the pia-arachnoid or ependyma, or of nodular dural enhancement, a pathologic process other than simple benign postoperative enhancement was demonstrated. Although we noted only two patients with patterns of ependymal or leptomeningeal enhancement, both had significant disease. Even after intraventricular shunt placement, no ependymal enhancement was seen on 38 scans obtained after the procedure. On the basis of this limited experience, we believe that leptomeningeal or ependymal enhancement should suggest recurrent tumor or infection.

Nodular dural or subdural enhancement was not a pattern seen on scans of clinically well children. Four scans in our series showed nodular dural enhancement; in all cases this represented recurrent or residual exophytic tumor.

Radiation therapy may result in blood-brain barrier breakdown, but at clinical doses this effect may be delayed [19]. This may explain why no increase in meningeal enhancement was apparent in the subset of patients scanned soon after receiving radiation therapy. Additionally, steroid therapy stabilizes the blood-brain barrier [16, 20-23] and is often administered during part or all of the radiation course. This may be a second explanation for the lack of an increased prevalence of enhancement following radiation. Although in theory radiation may result in delayed blood-brain barrier breakdown, 14 of 29 patients scanned 1 year or more after radiation therapy had no evidence of blood-brain barrier breakdown. Thus, radiation-induced disruption of the blood-brain barrier in the relatively avascular meninges is probably subclinical and below the threshold of detection with enhanced MR. Abnormal

meningeal enhancement should not be ascribed to radiation therapy until other causes have been excluded.

No patient in this series with normal dura, pia, arachnoid, or ependyma on enhanced MR had evidence of leptomeningeal or ependymal disease based on clinical or laboratory data. However, we do not propose that a normal enhanced MR examination absolutely excludes meningeal disease. Other investigators have described normal enhanced MR scans of the brain and spine in patients with cytologically proved leptomeningeal disease; presumably this could also occur intracranially with either neoplasia or infection [10] (Yousem DM, Grossman RI, presented at the annual meeting of the Radiological Society of North America, November 1989). Rather, the appearance of the dura, leptomeninges, and ependyma on enhanced MR scans complements the clinical examination and CSF findings.

Our current technique in this patient population includes a T2-weighted axial sequence and an unenhanced T1-weighted sequence through the surgical site and prior tumor bed. We then repeat the T1-weighted sequence immediately after the administration of contrast material. Most patients undergo at least one additional T1-weighted sequence in another plane. If a patient has a tumor with a known propensity for metastasis to the leptomeninges, the entire brain is scanned after enhancement.

Conclusions

Mild focal or diffuse dural enhancement is a normal finding on enhanced MR in the pediatric patient who has undergone biopsy, craniotomy, or intraventricular shunt placement for an intracranial neoplasm or associated hydrocephalus. Benign-appearing meningeal enhancement was noted on some scans obtained 8 or more years after surgery. Prior radiation therapy did not appear to increase the prevalence or degree of meningeal enhancement. Moderate dural enhancement may occur in clinically well patients with postsurgical subdural collections or when there is a history of remote serious meningeal disease such as a subarachnoid hemorrhage or meningitis. Nodular dural enhancement, leptomeningeal enhancement, or ependymal enhancement were patterns not seen in our clinically well postsurgical group of patients. On the basis of our small population of patients who exhibited such enhancement, these patterns of enhancement may suggest serious disease, such as leptomeningeal tumor, residual tumor, or meningitis. Finally, enhanced T1-weighted sequences and careful contrast administration techniques are essential for optimal use of enhanced MR in the postoperative pediatric patient.

REFERENCES

- Kucharczyk W, Brant-Zawadzki M, Sobel D, et al. Central nervous system tumors in children: detection by magnetic resonance imaging. *Radiology* 1985;155:131-136
- Lee BCP, Kneeland JB, Deck MDF, Cahill PT. Posterior fossa lesions: magnetic resonance imaging. *Radiology* 1984;153:137-143
- Smith AS, Weinstein MA, Modic MT, et al. Magnetic resonance with marked T2-weighted images: improved demonstration of brain lesions, tumor, and edema. *AJNR* 1985;6:691-697
- Hasso AN, Fahmy JL, Hinshaw DB. Tumors of the posterior fossa. In: Stark DD, Bradley WG, eds. *Magnetic resonance imaging*. St. Louis: Mosby, 1988:425-427
- Elster AD, Rieser GD. Gd-DTPA-enhanced cranial MR imaging in children: initial clinical experience and recommendations for its use. *AJNR* 1989;10:1027-1030
- Brant-Zawadzki M, Berry I, Osaki L, Brasch R, Murovic J, Norman D. Gd-DTPA in clinical MR of the brain: 1. Intraaxial lesions. *AJNR* 1986;7:781-788
- Berry I, Brant-Zawadzki M, Osaki L, Brasch R, Murovic J, Newton TH. Gd-DTPA in clinical MR of the brain: 2. Extraaxial lesions and normal structures. *AJNR* 1986;7:789-793
- Mathews VP, Kuharik MA, Edwards MK, D'Amour PG, Azzarelli B, Dreesen RG. Gd-DTPA-enhanced MR imaging of experimental bacterial meningitis: evaluation and comparison with CT. *AJNR* 1988;9:1045-1050
- Sze G, Abramson A, Krol G, et al. Gadolinium-DTPA in the evaluation of intradural extramedullary spinal disease. *AJNR* 1988;9:153-163
- Sze G, Soletsky S, Bronen R, Krol G. MR imaging of the cranial meninges with emphasis on contrast enhancement and meningeal carcinomatosis. *AJNR* 1989;10:965-975
- Frank JA, Girton M, Dwyer AJ, Wright DC, Cohen PJ, Doppman JL. Meningeal carcinomatosis in the VX2 rabbit tumor model: detection with Gd-DTPA-enhanced MR imaging. *Radiology* 1988;167(3):825-829
- Berns DH, Blaser S, Ross JS, Masaryk TJ, Modic MT. MR imaging with Gd-DTPA in leptomeningeal spread of lymphoma. *J Comput Assist Tomogr* 1988;12(3):499-500
- Elster AD, DiPersio DA. Cranial postoperative site: assessment with contrast-enhanced MR imaging. *Radiology* 1990;174:93-98
- Burke JW, Podrasky AE, Bradley WG. Meninges: benign postoperative enhancement on MR images. *Radiology* 1990;174:99-102
- Destian S, Heier LA, Zimmerman RD, Morgello S, Deck MDF. Differentiation between meningeal fibrosis and chronic subdural hematoma after ventricular shunting: value of enhanced CT and MR scans. *AJNR* 1989;10:1021-1026
- Sage MR. Blood-brain barrier: phenomenon of increasing importance to the imaging clinician. *AJNR* 1982;3(2):127-138
- Kilgore DP, Breger RK, Daniels DL, Pojunas KW, Williams AL, Haughton VM. Cranial tissues: normal MR appearance after intravenous injection of Gd-DTPA. *Radiology* 1986;160:757-761
- Burger PC, Vogel FS. *Surgical pathology of the nervous system and its coverings*, 2nd ed. New York: Wiley, 1982:153-156
- Kun LE. The brain and spinal cord. In: Moss WT, Cox JD, eds. *Radiation oncology. Rationale, technique, results*. St. Louis: Mosby, 1989:597
- Marty R, Cain ML. Effects of corticosteroid (dexamethasone) administration on the brain scan. *Radiology* 1973;107:117-121
- Laster DW, Moody DM, Ball MR. Resolving intracerebral hematoma: alteration of the "ring sign" with steroids. *AJR* 1978;130:935-939
- Eisenberg HM, Barlow CF, Lorenzo AV. Effect of dexamethasone on altered brain vascular permeability. *Arch Neurol* 1970;23:18-22
- Sears ES, Tindall RSA, Zarnow H. Active multiple sclerosis. Enhanced computerized tomographic imaging of lesions and the effect of corticosteroids. *Arch Neurol* 1978;35:426-434

Book Review

Pocket Atlas of Normal CT Anatomy of the Head and Brain. By Anton N. Hasso and Miyuki Shakudo. New York: Raven, 85 pp., 1990. \$14.95, softcover

Pocket Atlas of Normal CT Anatomy of the Head and Brain, a brief 5 × 7 in. (12.7 × 17.8 cm) softcover book in a series being released by Raven Press, has been compiled by Anton Hasso of Loma Linda University School of Medicine and Miyuki Shakudo of Osaka, Japan. The purpose of this small book is to help the reader recognize and identify important anatomic features of the brain, the orbit, and the skull base. The authors have accomplished this goal as succinctly as possible; the book has no narrative or explanatory text and no references or other embellishments.

The atlas contains 83 CT scans with numbered arrows. The various landmarks and structures indicated by the arrows are listed and named beneath each picture, without comments. The atlas begins with a series of CT scans of the brain of an adult; these are followed by images of the brains of a 1-year-old and a 2-year-old. Coronal scans of the brain complete this part. The second half of the book, about 40 illustrations, deals with the orbit, the skull base, and the temporal bone. The soft tissues of the face, the nasopharynx, the oropharynx, and the oral cavity are not illustrated.

The quality of the illustrations is good to excellent despite the fact that some images are from 1984. Occasionally, the arrows point at

features that are not really visible in the illustrations (this concerns mainly the middle ear ossicles); in all probability, the features were visible on the original images. I note, with gratitude, that the authors abstained from the commonplace abuse of letting the numbered arrows refer to an endless list of anatomic terms at the front or back of the book; the explanations are offered on each page. The authors selected and highlighted important features and areas with care, and irrelevant minutiae were left out. The anatomic structures named are those that every serious interpreter must be familiar with. The atlas does not claim to be intended for trained neuroradiologists but rather for persons who spend much less time with images of this kind: fledgling neurologists, neurosurgeons, ophthalmologists, and otolaryngologists, and all others who make their first trip into the minefield of digital imaging. The book accomplishes its limited purpose quite well and should be a most useful companion for the neophyte during the initial reading sessions at the viewing board.

Folke J. Brahma
Veterans Affairs Medical Center
San Diego, CA 92161

Intracranial Cryptococcosis in Immunocompromised Patients: CT and MR Findings in 29 Cases

Robert D. Tien¹
 Pauline K. Chu¹
 John R. Hesselink¹
 Arthur Duberg¹
 Clayton Wiley²

CT and MR scans of 29 immunocompromised patients (28 with AIDS or ARC, one with diabetes mellitus) who had documented intracranial cryptococcal infection were reviewed retrospectively. All patients had CT studies; 26 received iodinated contrast agent. CT findings included normal results in nine of 29, atrophy only in 13 of 29, nonenhancing lesions in three of 29, enhancing lesions in two of 20, and foci of leptomeningeal calcification in two of 29. Ten patients had both CT and MR studies, and four received gadopentetate dimeglumine. Among these 10 patients, five had normal CT studies and one showed moderate central atrophy. All 10, however, had abnormal MR findings. We observed four patterns: (1) parenchymal cryptococcoma (3/10); (2) numerous clustered tiny foci that were hyperintense on T2-weighted images and non-enhancing on postcontrast T1-weighted images, located relatively symmetrically in the basal ganglia bilaterally and in midbrain, representing dilated Virchow-Robin spaces (4/10); (3) multiple miliary enhancing parenchymal and leptomeningeal nodules (1/10); and (4) a mixed pattern, consisting of dilated Virchow-Robin spaces with mixed lesions such as cryptococcoma and miliary nodules (2/10). In the group of six patients with dilated Virchow-Robin spaces (patterns 2 and 4), two received gadopentetate dimeglumine, but the Virchow-Robin space lesions did not enhance; among the remaining four patients, two received gadopentetate dimeglumine (one with pattern 1 and one with pattern 3) and the lesions did enhance. Three patients in our study subsequently died and autopsies were performed. The postmortem results revealed dilated Virchow-Robin spaces filled with fungi in the basal ganglia, which correlated well with MR findings.

The high frequency of invasion of the perivascular Virchow-Robin spaces by *Cryptococcus* detectable by MR is noteworthy, and we recommend this imaging technique when CNS cryptococcosis is suspected.

ANJR 12:283-289, March/April 1991; AJR 156:1245-1251, June 1991

Cryptococcus neoformans is one of the most common infectious agents causing CNS infections in immunocompromised patients [1]. However, previous reports on the ability of CT to detect abnormalities have been disappointing [2, 3]. MR has proved to have higher sensitivity than CT for detecting many CNS abnormalities. This article describes the CT and MR imaging features of intracranial cryptococcosis with emphasis on MR imaging.

Materials and Methods

We studied 29 cases of CNS cryptococcal infection retrospectively from the records of our institution. In 19 patients only CT was performed; in 10 patients both CT and MR studies were obtained. Patients ranged in age from 19 to 57 years; all were men. Twenty-eight patients (97%) had AIDS or AIDS-related complex (ARC) and one had diabetes mellitus. Of the 28 patients with AIDS or ARC, 26 were homosexual and two were hemophiliacs who had contracted the disease through blood transfusions. In all cases, the CNS cryptococcosis was diagnosed by positive CSF antigen titer and culture.

Cranial CT studies had been done with a GE 9800 scanner for each patient at the time of

Received May 11, 1990; revision requested August 13, 1990; revision received September 12, 1990; accepted September 13, 1990.

¹ Department of Radiology, UCSD Medical Center, 225 Dickinson St., San Diego, CA 92103. Address reprint requests to R. D. Tien.

² Department of Pathology, UCSD Medical Center, San Diego, CA 92103.

0361/803X/91/1566-1245

© American Roentgen Ray Society

initial presentation with CSF findings during admission. Twenty-six patients also had iodinated contrast studies. Five-millimeter-thick transaxial images were obtained through the brain. Ten patients also had MR studies on a 1.5-T GE Signa unit, and four patients received IV gadopentetate dimeglumine. In one patient (patient 29), a follow-up MR study was performed after antifungal treatment. MR studies generally were performed between 1 and 3 days after the CT scans were obtained. The CT and MR studies were reviewed and compared to look for distinctive features of cryptococcosis. Autopsies were conducted (between 4 and 7 days after imaging studies were performed) on the three patients who died, and postmortem results were correlated with the CT and MR studies.

Results

The CT and MR results are summarized in Table 1 and the CT findings are detailed in Table 2. Normal findings were seen in about one third of the patients (9/29) and various degrees of central or cortical atrophy only in about one half of the patients (13/29). Cerebral atrophy is a well-known feature of human immunodeficiency virus (HIV) infections involving the CNS [4] and was to be expected in view of our patient population (97% had AIDS or ARC). Three patients had nonenhancing small lesions in the brain (patients 18, 19, 24) and two patients had an enhancing lesion in the right frontal lobe (patients 20 and 25). Small foci of calcification in the leptomeningeal spaces and parenchyma were seen in two patients without an associated enhancing lesion (patients 17 and 22). These might represent the sequelae from a long-

standing cryptococcal infection before admission to our hospital.

Among the 10 patients who also had MR studies, four received IV gadopentetate dimeglumine (Table 3). We observed four patterns of abnormal MR findings: (1) a parenchymal mass (cryptococcoma) in three patients (patients 20, 25, 28) (Fig. 1); (2) numerous tiny foci, which are hyperintense on T2-weighted images and nonenhancing on postcontrast T1-weighted images located relatively symmetrically in the basal ganglia bilaterally and also in the midbrain (which represent dilated Virchow-Robin spaces) in four patients (patients 21, 24, 26, 27) (Fig. 2); (3) multiple miliary enhancing parenchymal and leptomeningeal-cisternal nodules in one patient (patient 22) (Fig. 3); and (4) a mixed pattern, consisting of dilated Virchow-Robin spaces with mixed lesions such as cryptococcoma and miliary nodules in two patients (patients 23 and 29) (Figs. 4 and 5). In the group of six patients with dilated Virchow-Robin spaces (patterns 2 and 4), two patients received gadopentetate dimeglumine (patients 26 and 23). While the Virchow-Robin space lesions did not enhance, the other parenchymal and leptomeningeal lesions did show enhancement (patient 23). Two other patients received gadopentetate dimeglumine (patients 20 and 22), and their lesions enhanced. We found that among pattern 1 MR lesions (cryptococcoma) CT was able to demonstrate the two frontal lobe cases (patients 20 and 25), but missed a small lesion in midbrain owing to beam-hardening artifact (patient 28). In four cases of pattern 2 MR abnormalities (dilated Virchow-Robin space), CT studies missed three of them except the most severe instance (patient 24), which showed nonenhancing lucencies without mass effect in the basal ganglia bilaterally. In the patient with pattern 3 MR lesions (miliary enhancing nodules), CT scans showed foci of punctate calcification in the parenchyma and leptomeninges without enhancing lesions. The last two patients, who had pattern 4 MR lesions (mixed pattern), had CT scans that were unremarkable. One of these showed complete resolution of the lesions on a follow-up MR scan obtained after antifungal treatment (patient 29) (Fig. 5). Three patients in our study (patients 16, 24, 26) subsequently died, and autopsies were performed. The postmortem results in all three cases revealed dilated Virchow-Robin spaces filled with fungi in basal ganglia and small numbers of surrounding perivascular chronic inflammatory cells that consisted primarily of macrophages (Figs. 6 and 7). The pathologic findings correlated well with the presumptive dilated Virchow-Robin space lesions previously noted on MR (patients 24 and 26).

Discussion

Cryptococcus neoformans, the only *Cryptococcus* species known to be pathogenic in humans, can be isolated from soil contaminated by bird excreta. Most human infections are thought to be acquired through inhalation. Cryptococcosis is commonly associated with debilitating diseases, such as lymphoma, leukemia, multiple myeloma, sarcoidosis, tuberculosis, diabetes mellitus, and lupus erythematosus; it is also seen after glucocorticoid therapy. In the pre-AIDS era, up to 50% of patients in some reports had no form of immunodeficiency, but some impairment of lymphocyte response to cryptococci had been found in most cases [4]. By the time the diagnosis

TABLE 1: CT and MR Findings in 29 Immunocompromised Patients with CNS Cryptococcosis

Patients	CT Findings	MR Findings
1-12	Atrophy	Not performed
13-16	Normal	Not performed
17	Punctate small foci of calcification	Not performed
18	Atrophy; nonenhancing lucency	Not performed
19	Atrophy; nonenhancing lucency	Not performed
20	Small enhancing nodule	Pattern 1
21	Atrophy	Pattern 2
22	Atrophy with punctate calcifications	Pattern 3
23	Normal	Pattern 4
24	Nonenhancing lucent foci	Pattern 2
25	Enhancing mass	Pattern 1
26	Normal	Pattern 2
27	Normal	Pattern 2
28	Normal	Pattern 1
29	Normal	First MR image = pattern 4; posttreatment image = normal

TABLE 2: CT Findings in 29 Immunocompromised Patients with CNS Cryptococcosis

CT Findings	No. of Patients
Normal	9
Atrophy	13
Nonenhancing lesions	3
Enhancing lesions	2
Foci of calcification	2

of systemic cryptococcosis is established, 70% of patients have neurologic abnormalities [5].

Today, with the increase in AIDS cases, *Cryptococcus* ranks third after HIV and *Toxoplasma gondii* on the list of infectious agents causing CNS disease in AIDS [1]. Approximately 5% of AIDS patients develop CNS cryptococcosis [6]. The most common CNS infection caused by cryptococci is meningitis. The pathology ranges from mild congestion to meningeal thickening and distention of the subarachnoid space by abundant mucoid exudate. The characteristic absence of marked inflammatory reaction with only mild infiltration by lymphocytes and histiocytes is noteworthy.

The choroid plexus of the trigone is involved frequently, and spinal cord and spinal nerve roots may also be affected [7, 8]. Fungi may enter the Virchow-Robin space and give rise to small cysts (so-called "soap bubbles") or gelatinous pseudocysts in the parenchyma [9]. Deep gray matter structures, such as the basal ganglia, thalamus, and substantia

nigra, may also contain multiple small cystic spaces; however, cerebral edema seldom occurs. In the immunologically intact host, these fungi usually induce a chronic granulomatous reaction.

In one review of the CT scans of 35 patients (among them 28 patients with AIDS) who had intracranial cryptococcal infection [2], the studies were found to be normal in 43%. Positive findings included diffuse atrophy in 34%, mass lesions (cryptococcoma) in 11%, hydrocephalus in 9%, and diffuse cerebral edema in 3%. One case of gelatinous pseudocysts of the basal ganglion and one case of intraventricular cryptococcal cyst were encountered. The diffuse atrophy pattern is most likely related to HIV infection rather than to fungal infection. The gelatinous pseudocysts were reported as nonenhancing cystic lesions of low density on contrast-enhanced CT [9] and of low signal intensity on T1-weighted MR images but high signal intensity—similar to CSF—on T2-weighted MR images [2].

TABLE 3: The Patterns of MR Findings in 10 Immunocompromised Patients with CNS Cryptococcosis

Pattern	No. of Patients	No. of Patients Who Received Gadopentetate Dimeglumine	MR Findings
1: Cryptococcoma: parenchymal mass	3	1	Mass enhanced with contrast
2: Dilated Virchow-Robin spaces	4	1	No evidence of enhancement
3: Miliary nodular lesions	1	1	Multiple enhancing nodules in the parenchyma and leptomeningeal spaces
4: Mixed pattern (pattern with mixed lesions such as patterns 1 and 3)	2	1	Dilated Virchow-Robin spaces did not enhance; other lesions enhanced

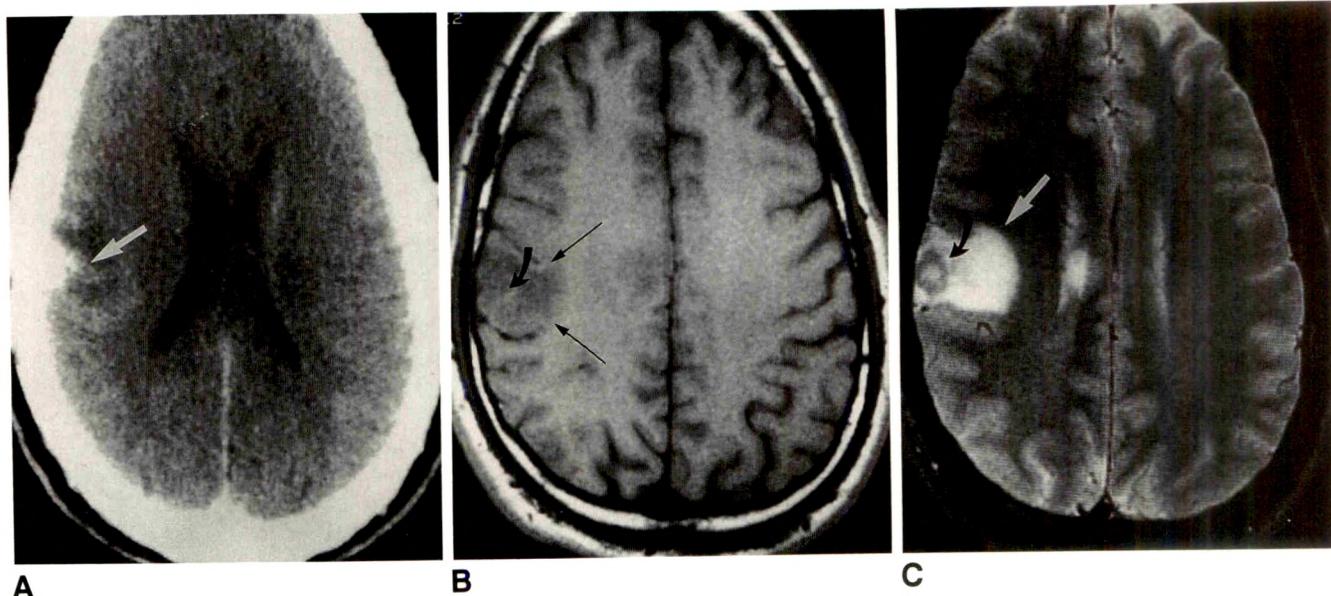


Fig. 1.—Pattern 1 (patient 25).

A, Contrast-enhanced CT scan shows small enhancing mass in right posterior frontal region abutting on skull with adjacent edema (arrow).

B, Axial T1-weighted (600/20/2) MR image shows mass to be iso- to slightly hypointense relative to gray matter (curved arrow) with peripheral hypointensity representing edema (straight arrows).

C, Axial T2-weighted (2500/80/2) MR image shows mass to be isointense with gray matter (black arrow), with a hyperintense center, perhaps representing central cystic-necrotic change. Peripheral edema is noted (white arrow).

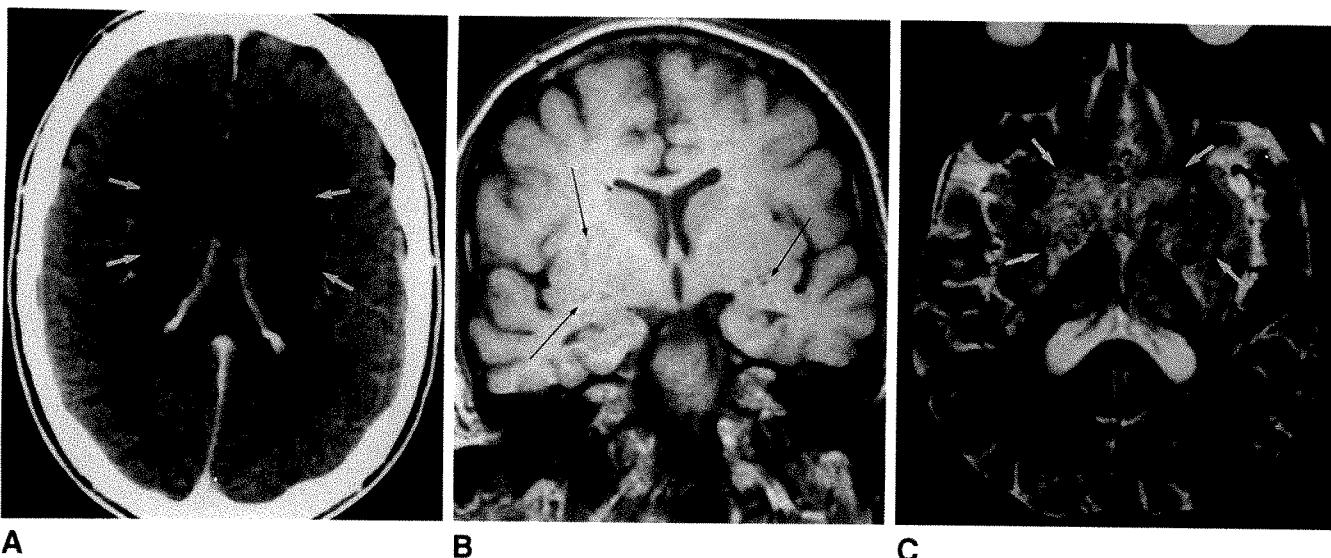


Fig. 2.—Pattern 2 (patient 24).
A, Contrast-enhanced CT scan shows nonenhancing lucencies in basal ganglia bilaterally without mass effect (arrows).
B, Coronal T1-weighted (600/20) MR image shows multiple tiny hypointense foci in basal ganglia bilaterally (arrows). These represent dilated Virchow-Robin spaces.
C, Axial T2-weighted (2500/80) MR image shows multiple clustered tiny hyperintense foci in basal ganglia bilaterally (arrows), which represent dilated Virchow-Robin spaces.

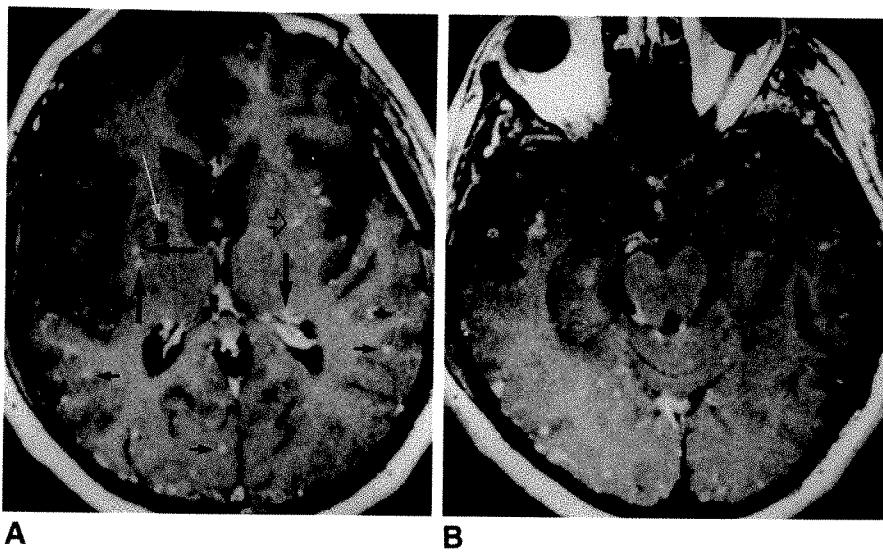


Fig. 3.—Pattern 3 (patient 22).
A, Postcontrast axial T1-weighted (600/20) MR image shows hypointense focus in right basal ganglia (large Virchow-Robin space, long white arrow). Hyperintense left putamen lesion noted on T2-weighted MR image (not shown) has enhanced (open arrowhead). Two enhancing nodules are noted in right external capsule, subependymal regions (large black arrows), and leptomeningeal-cisternal spaces (small black arrows), which cannot be seen on T2-weighted images.
B, Postcontrast axial T1-weighted (600/20) MR image at a lower level shows multiple enhancing nodules in leptomeningeal-cisternal space.

In another report of CT findings in 20 patients with CNS cryptococcal infection [3], only one patient was immunocompromised, secondary to systemic lupus erythematosus, and was treated with steroids and Cytoxan. Of these patients, 50% had normal CT scans, 25% had hydrocephalus, 15% had gyral enhancement, 15% had focal nodules, 10% had decreased white matter attenuation, and 5% had patchy uptake of contrast agent. The gyral enhancement, decreased white matter attenuation, and patchy uptake of contrast material are thought to represent various combinations of inflammation and pseudocyst formation in the meninges, perivascular Virchow-Robin space, and adjacent cerebral tissue [3]. The difference in the findings in these two reports is due to differences in the patient populations. The group with 28

AIDS patients revealed a high percentage of atrophy owing to HIV infection and a lower percentage of hydrocephalus [2]. Recently, Wehn and coworkers [10] reported two patients with AIDS complicated by cryptococcal meningitis who had focal hypodense, nonenhancing lesions on CT in the basal ganglia, with corresponding areas of increased T2 and decreased T1 signal on nonenhanced MR imaging. These lesions corresponded precisely to the distribution of the perforating arteries. The pathologic specimen showed these lesions to be small cystic collections of cryptococcal organisms in the dilated Virchow-Robin spaces with minimal inflammatory reaction. Balakrishnan et al. [11] also recently reported that the CNS cryptococciosis involvement of the basal ganglia in AIDS patients has a unique appearance on MR images,

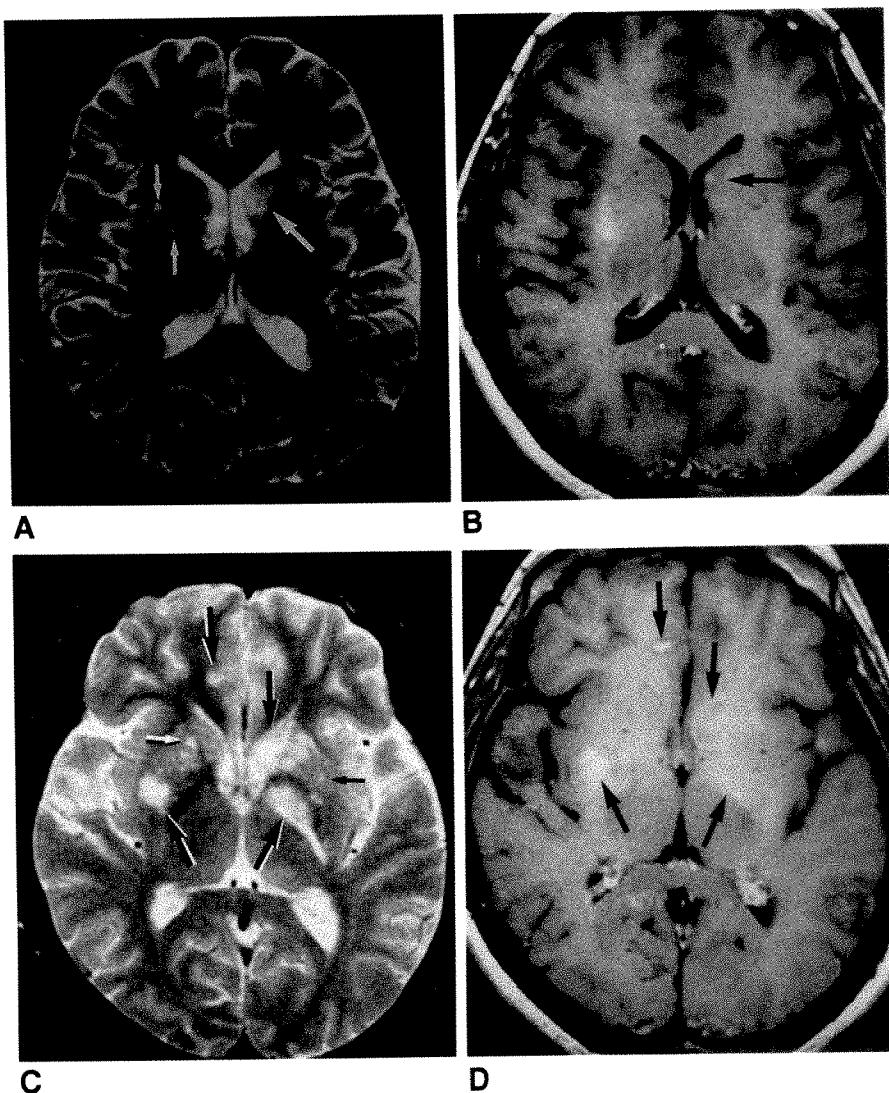
Fig. 4.—Pattern 4 (patient 23).

A, Axial T2-weighted (2500/80) MR image shows hyperintense lesion occupying left caudate nucleus (large arrow) and some smaller, clustered hyperintense lesions in right putamen (small arrows).

B, Postcontrast axial T1-weighted (600/20) MR image at same level as in **A** shows irregular enhancement in left caudate nucleus (cryptococcoma) (arrow). However, the clustered right putamen lesions (dilated Virchow-Robin spaces) did not enhance.

C, Axial T2-weighted (2500/80) MR image at a lower level shows varying irregularly sized hyperintense lesions in right putamen, left globus pallidus, left internal capsule posterior limb, left caudate nucleus, and right frontal lobe (large arrows). Small clustered hyperintense foci are present in anterior putamen regions bilaterally, representing dilated Virchow-Robin spaces (small arrows).

D, Postcontrast T1-weighted (600/20) MR image at same level as in **A** shows enhancing lesions (arrows), which correlate well with irregular lesions seen on T2-weighted images. However, the clustered lesions seen on T2-weighted images (Virchow-Robin spaces) did not enhance.



seen as bilateral, small, well-defined foci of high signal on T2-weighted images clustered in the basal ganglia. This appearance was not found with any of the other diseases, including toxoplasmosis, seen in their study.

The MR patterns of intracranial cryptococcosis in AIDS patients from our study (Table 3) included (1) cryptococcoma, (2) dilated Virchow-Robin spaces, (3) miliary enhancing nodules in the parenchyma and leptomeningeal-cisternal spaces, and (4) a mixed pattern. Pattern 1 (cryptococcoma) and pattern 3 (miliary nodules) are different presentations of hematogenous spread of the fungi. A breakdown occurs in the blood-brain barrier of the parenchymal lesions, and neovascular growth takes place around the leptomeningeal granulomas; hence, the lesions enhance with contrast agent. Although the leptomeningeal nodules are unremarkable on T2-weighted images, the postcontrast T1-weighted images can clearly demonstrate the lesions and are essential. As the vessels approach the CNS, they first course through the subarachnoid space and enter the cortex as thin-walled vessels. Between the vessel wall and the limiting glial membrane is the Virchow-Robin (perivascular) space. Normally this space

gradually dwindles in size and ends as a fusion of perivascular and pial basement membranes. The space can be followed deep into the basal ganglia, white matter of the cerebellar peduncles, brainstem, and spinal cord. Near the termination of the space, the vessels become capillaries [12-15].

Heier et al. [16] found that slightly dilated Virchow-Robin spaces could be found in all age groups, probably as a normal condition. However, these researchers also noted that larger perivascular spaces are significantly associated with aging. In our patients, the dilated Virchow-Robin spaces were found in young patients who would not be expected to manifest this degree of dilatation under normal circumstances.

Jungreis et al. [17] pointed out that the greater sensitivity of MR imaging has allowed dilated perivascular spaces to be seen with greater frequency, and sometimes normal Virchow-Robin spaces have been mistaken for infarcts. Both these authors and others [16, 18] found that lesions in the lower one third of the putamen had the signal characteristics of CSF and were located in sites that corresponded to the distribution of the perforating arteries; these were thought to be dilated Virchow-Robin spaces. In contrast, lesions in the upper two

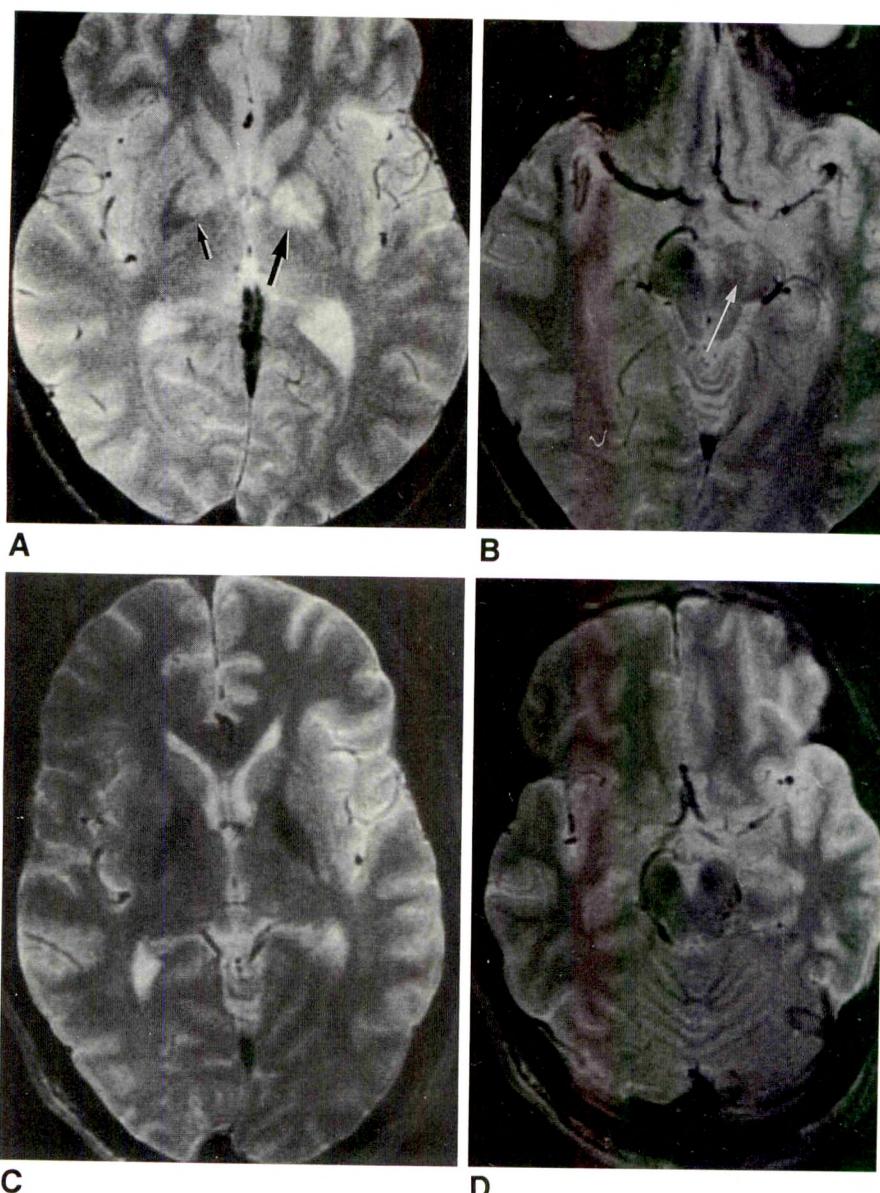


Fig. 5.—Pattern 4, pre- and posttreatment (patient 29).

A, Axial T2-weighted (2500/80) MR image shows clustered lesions in right basal ganglia (small arrow), which may represent dilated Virchow-Robin spaces. The left basal ganglia lesion (large arrow) is more confluent in shape and larger in size; this probably represents a cryptococcoma.

B, Axial T2-weighted (2500/80) MR image at midbrain level shows an enlarged left cerebral peduncular inhomogeneous hyperintense lesion (arrow) representing a cryptococcoma.

C and **D**, Axial T2-weighted (2500/80) MR images at same levels as in **A** and **B** after anti-fungal treatment show total resolution of lesions.

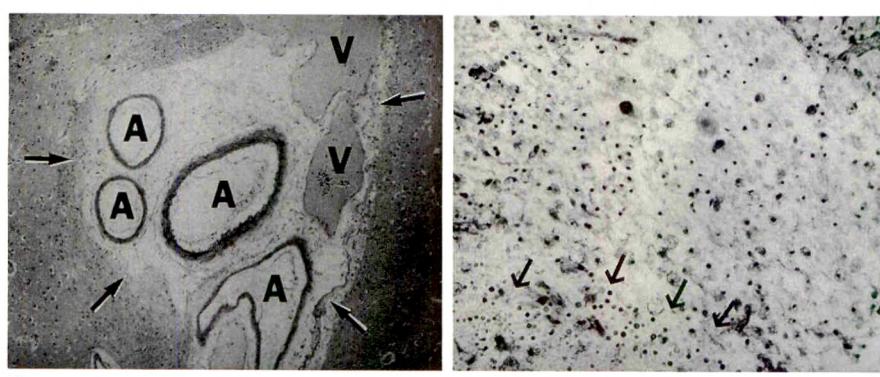


Fig. 6.—Paraffin section from the brain of patient 26. Several arteries (A) and veins (V) are noted within a dilated Virchow-Robin space (arrows) in the basal ganglia. (H and E $\times 40$)

Fig. 7.—Within this dilated Virchow-Robin space of the basal ganglia, numerous lipid-filled macrophages surround a pocket (outlined by arrows) of darkly stained circular organism (*Cryptococcus neoformans*). (PAS $\times 160$)

thirds of the putamen differed in signal characteristics and were presumed to represent lacunar infarction. However, in our patients, the lesions were all of identical intensity throughout the upper and lower basal ganglia regions, having the same signal intensity as CSF. In addition, the areas of high signal intensity appeared to be more numerous, with some even showing confluence, which correlated well with the histologic findings.

Fungal invasion of the perivascular spaces has been described in the literature [19, 20]. Dilated Virchow-Robin spaces filled with fungi are relatively isointense to slightly hypointense relative to gray matter on T1-weighted images, slightly hyperintense on proton-density-weighted images, and hyperintense on T2-weighted images (i.e., with the same signal intensity as CSF). They usually occur symmetrically in both upper and lower basal ganglia and are round or oval. Because the blood-brain barrier remains intact, no contrast enhancement is seen on either CT or MR studies (pattern 2). As the fungi invade the brain parenchyma and are not confined in the Virchow-Robin spaces, they can become confluent and patchy in appearance on T2-weighted images and enhance after contrast administration (pattern 4). In addition, some edematous changes may involve the internal capsule and track along the corticospinal tracts into the midbrain and pons. Nevertheless, the pattern 2 MR appearance (bilateral, numerous, small, well-defined foci of high signal on T2-weighted images and nonenhancing with contrast agent) is suggestive of CNS cryptococcosis but not pathognomonic, as we have seen one AIDS patient with CNS coccidioidomycosis documented by CSF culture and another patient with leukemia and systemic candidiasis whose MR study was very similar in appearance. Patterns 1 and 3 can be seen in various neoplastic and granulomatous diseases, and pattern 4 is the mixed pattern, which is nonspecific. In AIDS or ARC patients with lesions in the basal ganglia, toxoplasmosis and lymphoma should always be considered; however, these lesions usually show contrast enhancement and edema. The classic finding of hydrocephalus was not commonly seen in immunocompromised patients in a previous report [2], which is in keeping with our findings. Also, no evidence of diffuse confluent basal cisternal-leptomeningeal enhancement, which is often present in bacterial and tuberculous meningitis, was seen in any of our cases. This most likely is attributable to the lack of inflammatory leptomeningeal reaction and adhesions within the cisternal spaces in the immunocompromised patients that normally cause hydrocephalus. In a series of 24 patients with HIV encephalitis confirmed at autopsy, 18 had radiologic evidence of atrophy [21]. Atrophy was identified in more than half the cases in our patient population (16/29), which most likely was the result of CNS HIV infection.

CT can diagnose intraparenchymal masses and can detect foci of calcification, indicating the chronicity of these fungal infections. However, routine CT usually does not reveal dilated Virchow-Robin spaces [16-18] in the basal ganglia, which were evident on CT in only one of the six patients (patient 24) with positive MR findings in our series. In addition, these spaces could not be identified in the lower midbrain and pons by CT owing to beam-hardening artifacts.

In conclusion, MR imaging provides valuable information about CNS abnormalities in cryptococcal infections in immunocompromised patients. Of note are the dilated, fungi-filled Virchow-Robin spaces in the basal ganglia and midbrain seen by MR in a high percentage of patients. Although these lesions are not pathognomonic, rapid recognition can be helpful in determining proper treatment.

ACKNOWLEDGMENT

The authors are grateful to Catherine Fix for excellent editorial suggestions.

REFERENCES

1. Gabuzda DH, Hirsch MS. Neurologic manifestations of infection with human immunodeficiency virus. Clinical features and pathogenesis. *Ann Intern Med* 1987;107:383-391
2. Popovich MJ, Arthur RH, Helmer E. CT of intracranial cryptococcosis. *AJNR* 1990;11:139-142
3. Tan CT, Kuan BB. Cryptococcus meningitis, clinical-CT scan considerations. *Neuroradiology* 1987;29:43-46
4. Perfect JR, Durack DT, Gallis HA. Cryptococcemia. *Medicine* 1983;62:98-109
5. Rowland LP. *Merritt's textbook of neurology*, 8th ed. Philadelphia: Lea & Febiger, 1988:146-148
6. Eng RHK, Bishburg E, Smith SM, Kapilo, R. Cryptococcal infections in patients with acquired immune deficiency syndrome. *Am J Med* 1986;81:19-23
7. Weenink HR, Bruyn GW. Cryptococcus in the nervous system. In: Vincken PJ, Bruyn GW, eds. *Handbook of clinical neurology*, vol. 35. Amsterdam: North Holland, 1978:459-502
8. Penar PL, Kim J, Chiyatte D, et al. Intraventricular cryptococcal granuloma. Report of two cases. *J Neurosurg* 1988;68:145-148
9. Garcia CA, Weisberg LA, Lacorte WSJ. Cryptococcal intracerebral mass lesion: CT-pathologic considerations. *Neurology* 1985;35:731-734
10. Wehn SM, Heinz R, Burger PC, et al. Dilated Virchow-Robin spaces in cryptococcal meningitis associated with AIDS: CT and MR findings. *J Comput Assist Tomogr* 1989;13:756-762
11. Balakrishnan J, Becker PS, Kumar AJ, Zinreich SJ, McArthur JC, Bryan RN. Acquired immunodeficiency syndrome: correlation of radiologic and pathologic findings in the brain. *RadioGraphics* 1990;10:201-215
12. Mirfakhraee M, Crofford MJ, Guinto FC, et al. Virchow-Robin space: path of spread in neurosarcoïdosis. *Radiology* 1986;158:714-720
13. Patek PR. Perivascular spaces in mammalian brain. *Anat Rec* 1944;88:1-24
14. Nelson E, Blinzingher K, Hager H. Electron microscopic observations on the subarachnoid and perivascular spaces of the Syrian hamster brain. *Neurology* 1961;11:285-295
15. Jones EG. On the mode of entry of blood vessels into the cerebral cortex. *J Anat* 1970;106:507-520
16. Heier LA, Bauer CJ, Schwartz L, et al. Large Virchow-Robin spaces: MR-clinical correlation. *AJNR* 1989;10:929-936
17. Jungreis CA, Kanal E, Hirsch WL, et al. Normal perivascular spaces mimicking lacunar infarction: MR imaging. *Radiology* 1988;169:101-104
18. Braffman BH, Zimmerman RA, Trojanowski JQ, et al. Brain MR: pathologic correlation with gross and histopathology. 1. Lacunar infarction and Virchow-Robin spaces. *AJNR* 1988;9:621-628, *AJR* 1988;151:551-558
19. Fetter BF, Klinton GK, Hendry WS. *Mycoses of the central nervous system*. Baltimore: Williams & Wilkins, 1967:89-123
20. Minckler J. *Pathology of the nervous system*. New York: McGraw-Hill, 1968:494-497
21. Chrysikopoulos HS, Press GA, Grafe MR, Hesselink JR, Wiley CA. Encephalitis caused by human immunodeficiency virus: CT and MR imaging manifestations with clinical and pathologic correlation. *Radiology* 1990;175:185-191

Memorial



John Joonjae Lee, 1940–1990



Dr. John Joonjae Lee died on July 11, 1990, after 2 years of battle against cancer. Born on December 8, 1940, in Seoul, South

Korea, he received his M.D. degree from the Korea University College of Medicine in 1965. After a 3-year service in the Korean army ending in 1968, he came to the United States for a rotating internship at St. Mary's Hospital in Brooklyn, NY. He served his residency in pathology at Maimonides Medical Center in Brooklyn. In 1970, he went to Thomas Jefferson University Hospital in Philadelphia for his residency in diagnostic radiology for 3 years. He continued at Thomas Jefferson for his fellowship in neuroradiology until 1974, when he became staff radiologist at Providence Hospital in Southfield, MI. In 1976, he transferred to St. Joseph Hospital in Mt. Clemens, MI, where he stayed for the rest of his career. There he served as a partner in the Professional X-Ray Center, P.C.

Dr. Lee was a diplomate of the American Board of Radiology (1975), a member of the American College of Radiology (1977), and a senior member of the American Society of

Neuroradiology (1979). He served as president of the Korea University Medical College Alumni Association in Michigan from 1987 to 1989.

Dr. Lee was a dedicated physician who always maintained high standards of quality and full integrity and had boundless enthusiasm for his work. He never ceased to refine and expand his medical education, continually and diligently striving to be the best radiologist. Though his interests ranged from antiques to golf, his first love and pride was his beloved family.

Dr. Lee is survived by his beloved wife, Sun Hee; sons, Stephen, Kenneth, and Christopher; and daughter, Alexandra. As his colleague, Dr. Victor Curatolo, noted, "The best final tribute to Dr. Lee is to live as he did and to carry on with his principles in our personal affairs and our work."

K. Francis Lee
Miami, FL

Benign Lymphoepithelial Parotid Tumors in AIDS Patients: CT and MR Findings in Nine Cases

Kevin J. Kirshenbaum¹
 S. R. Nadimpalli¹
 Michael Friedman²
 Gary L. Kirshenbaum³
 Robert P. Cavallino¹

Benign lymphoepithelial parotid neoplasm with associated cervical adenopathy is a newly described head and neck manifestation of HIV infection, characterized previously as purely cystic masses on both CT and MR evaluations. The CT and MR findings in nine cases of surgically proved benign lymphoepithelial parotid lesions are presented. Five (56%) of the nine cases demonstrated masses that appeared other than cystic, reflecting a greater variety of radiologic appearances than previously reported. The majority of these cystic masses contained solid components and therefore could not be labeled as cysts; instead, they were considered to be benign lymphoepithelial parotid lesions. For patients with parotid gland enlargement, the lack of a characteristic CT/MR appearance of these lesions necessitates an evaluation of clinical history and a determination of whether cervical adenopathy is present in order to determine their underlying origin.

AJNR 12:271-274, March/April 1991; AJR 156:1253-1256, June 1991

Lymphadenopathy in AIDS and AIDS-related conditions is a universal finding, with nodes being especially prominent in the cervical region. It has been estimated that 41% of patients with AIDS present with, or have on initial evaluation, head and neck manifestations. Of this group, 8% have enlarging neck masses [1].

Benign lymphoepithelial parotid cysts and hyperplastic cervical adenopathy have recently been described as new head and neck manifestations of HIV infection seen in AIDS patients. Their radiologic appearance has been described as purely cystic masses with low attenuation values (10-18 H) on CT [2]. Reportedly, the MR characteristics of these parotid lesions, dictated by high water content, include low signal intensity on T1-weighted studies, intermediate signal intensities on proton-density-weighted studies, and bright signal intensities on T2-weighted scans. These typical findings were consistently demonstrated in all previously reported cases.

This article reports the findings in nine patients, all HIV positive, who were found to have benign lymphoepithelial parotid neoplasms and hyperplastic cervical adenopathy. Unlike previous investigators, we found varying CT and MR appearances of the parotid lesions, including purely cystic and mixed cystic-solid tumors. We therefore concluded that in patients with parotid gland enlargement, benign lymphoepithelial parotid tumors are not always purely cystic in appearance and that the presence or absence of cervical adenopathy and clinical history is crucial in guiding the clinician to their underlying origin.

Materials and Methods

The CT or MR scans of nine patients who had undergone superficial parotidectomy between October 1985 and July 1989 were reviewed retrospectively. Three of the nine patients were evaluated with CT. From these, two unenhanced scans (Toshiba 650) and one enhanced scan (50-ml bolus of Omnipaque 300) (Toshiba 600S) were obtained. The remaining

Received May 8, 1990; revision requested July 7, 1990; revision received September 29, 1990; accepted September 30, 1990.

¹ Department of Radiology, Illinois Masonic Medical Center, 836 W. Wellington Ave., Chicago, IL 60657. Address reprint requests to K. J. Kirshenbaum.

² Department of Head and Neck Surgery, Illinois Masonic Medical Center, Chicago, IL 60657.

³ Department of Pathology, Illinois Masonic Medical Center, Chicago, IL 60657.

0361-803X/91/1566-1253
 © American Roentgen Ray Society

TABLE 1: Clinical Data and Imaging Results

Patient No.	No. of Lesions	Age (years)	Sex	CT	Signal Intensity			Unilateral/Bilateral	Cervical Nodes
					T1	Mixed	T2		
1	1	41	M	Cystic mass*				Unilateral	NA
2	2	41	F	Thick septated mass, peripherally enhancing				Unilateral	NA
3	1	53	F	Uniformly enhancing				Unilateral	Bilateral
4	4	47	M		↑↓	↑	↑↑	Bilateral	Bilateral
5	2	40	M		↑↓	↑	↑↑	Unilateral	Bilateral
6	5	49	M		↑↓	↑	↑↑	Bilateral	Bilateral
7	1	28	M		↑↓	↑	↑↑	Bilateral	Bilateral
8	4	29	M		↑	↑↑	↑↑↑	Unilateral	Bilateral
9	1	28	M		NA	↑	↑↑	Unilateral	Bilateral

* Unenhanced CT examination.

Note.—NA = not available, ↓ = low signal intensity, ↑↓ = mixed signal intensity, ↑ = high signal intensity.

six patients were evaluated with MR imaging; four on a 0.35-T (Dionics) scanner and two on a 1.5-T (GE) scanner. The CT and MR images were analyzed with respect to number of lesions, solid vs cystic characteristics, unilateral vs bilateral parotid lesions, and presence of cervical adenopathy.

Results

Table 1 presents a summary of clinical and imaging results for all nine patients included in this study. All were proved HIV positive.

Of the three patients evaluated with CT, one (patient 1) had an unenhanced examination, which showed a homogeneous cystic unilateral parotid mass with a CT attenuation value of 18. CT sections through the neck were not obtained in this case and therefore the presence of cervical adenopathy was unknown.

The two patients (patients 2 and 3) evaluated with contrast-enhanced CT demonstrated a peripherally enhancing septated mass (Fig. 1) and a unilateral, single, uniformly enhancing mass, respectively, clearly revealing soft-tissue characteristics.

The remaining six patients were evaluated with MR imaging. All signal intensities were compared with respect to adjoining sternocleidomastoid muscle. Three patients (patients 4, 5, and 6) demonstrated mixed signal intensity on T1-weighted images, intermediate signal intensity on proton-density-weighted images, and high signal intensity on T2-weighted images. These findings are consistent with complex, partially cystic masses with soft-tissue components (Figs. 2 and 3). Microscopic examination revealed atrophy of gland parenchyma, marked lymphocytic infiltration with atypical follicular hyperplasia, and replacement of ducts by solid islands of epithelial and myoepithelial cells, consistent with benign lymphoepithelial lesions (Fig. 2D). This histologic appearance has been seen in association with HIV-induced lymphadenopathy as well as with autoimmune and other forms of sialadenitis [3].

Two other patients (patients 7 and 8) evaluated with MR imaging showed progressively increasing signal intensity masses on T1-, proton-density-, and T2-weighted studies, respectively, consistent with cystic mass lesions with proteinaceous fluid content (Fig. 4). In one patient (patient 9) eval-

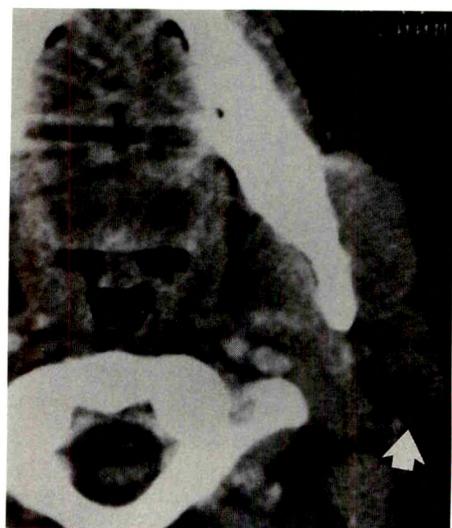


Fig. 1.—Patient 2: Postcontrast axial CT scan shows enhancing, complex, partially cystic mass (arrow); with portions demonstrating soft-tissue characteristics.

uated by MR, no T1-weighted images were obtained; however, proton-density- and T2-weighted images revealed increasing signal intensities, respectively.

After parotidectomy, pathologic evaluation was done on all specimens. Grossly, there was nodular or diffuse salivary gland enlargement, with pink-tan fleshy nodules as large as 4.5 cm in maximal diameter. In some instances, recognizable salivary gland parenchyma was seen attached to these nodules. Four of the specimens had grossly visible cysts, which ranged in size from 1.5–3.5 cm in maximal diameter. Specimen findings correlated well with their respective CT/MR appearance, in that four of nine lesions demonstrated primarily homogeneous cystic change.

Discussion

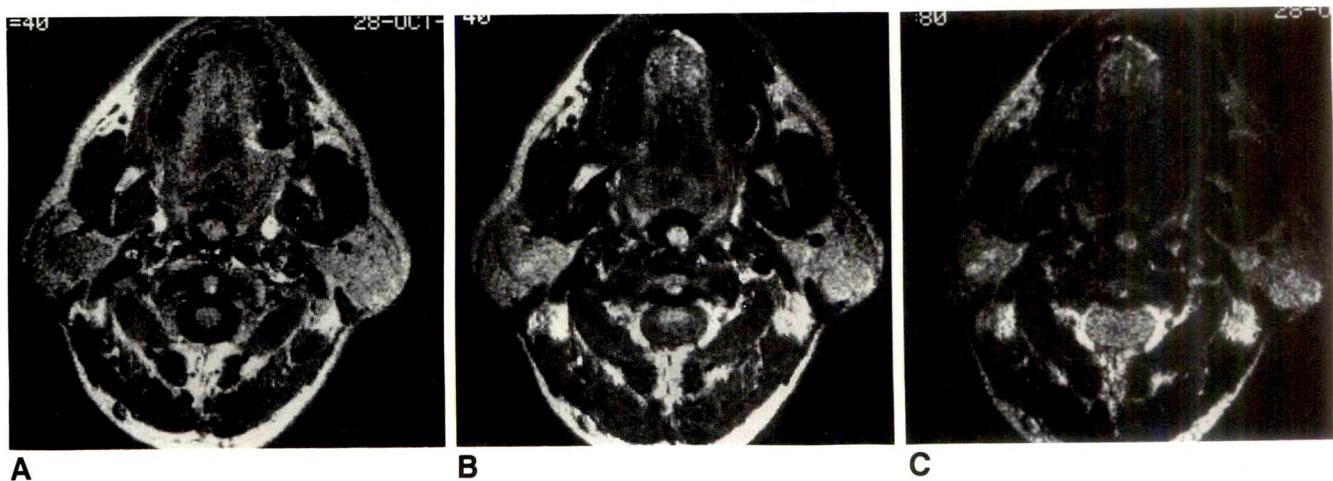
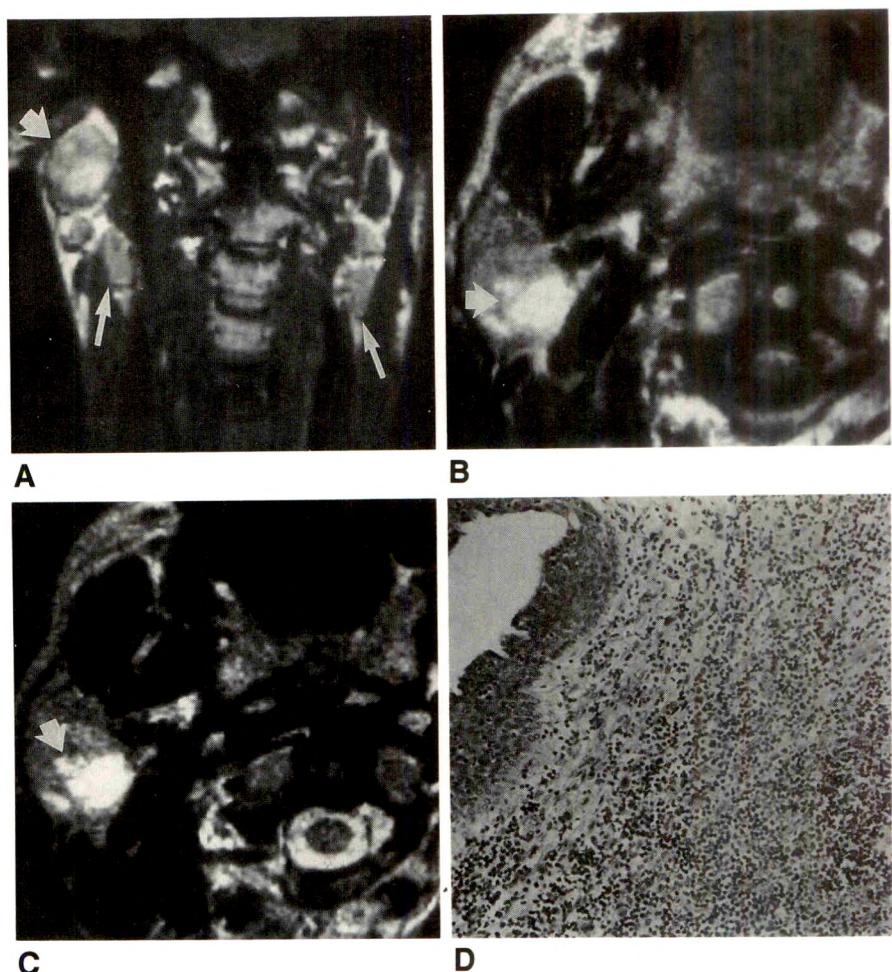
Benign lymphoepithelial parotid lesions with associated hyperplastic cervical adenopathy in AIDS patients is a relatively new entity reported in the radiologic literature. The pathogen-

Fig. 2.—Patient 5.

A, Coronal T1-weighted (500/40/1) MR image shows large right parotid mass (wide arrow) with mixed intensity. Bilateral cervical adenopathy is also shown (thin arrows).

B and C, Axial mixed (1500/40/1) (B) and T2-weighted (3000/80/2) (C) images show right parotid mass (arrow) with high signal intensity characteristics.

D, Histologic section of parotid mass reveals cystic dilatation of salivary gland duct with extensive lymphocytic infiltration and replacement of ducts by solid islands of epithelial and myoepithelial cells, consistent with benign lymphoepithelial lesion.

**Fig. 3.—Patient 6.**

A-C, Axial MR images show bilateral mass lesions demonstrating mixed, intermediate, and moderately high signal intensity characteristics on T1-weighted (500/40/1) (A), mixed (2000/40/1) (B), and T2-weighted (2000/80/2) (C) images, respectively.

esis of benign lymphoepithelial lesions has not been determined with absolute certainty. This lesion does not appear to be a true neoplasm and is most likely a reactive phenomenon. It may represent a form of sialadenitis or reactive changes in

intraluminal lymph nodes. When seen in association with HIV infection, the latter situation appears most likely. The HIV agent is targeted against lymphoid cells, resulting in generalized lymphadenopathy throughout the body, including intra-



Fig. 4.—Patient 7.
A-C, Axial MR images show right parotid mass (arrow in A) demonstrating progressively increasing signal intensity characteristics on T1-weighted (600/30/1) (A), mixed (2000/40/1) (B), and T2-weighted (2000/80/2) (C) images, respectively.

parotid lymph nodes that manifest as benign lymphoepithelial lesions.

A total of 18 cases have previously been reported [2, 4], with parotid lesions characterized on CT and MR as purely cystic masses with low attenuation values on CT and low, intermediate, and high signal intensities on T1-, proton-density-, and T2-weighted MR scans, respectively. Holliday et al. [2] have proposed that this appearance is sufficiently characteristic for the diagnosis of benign lymphoepithelial parotid disease.

In our retrospective review of nine patients, we found varying CT and MR appearances to the parotid lesions. Five (56%) of the nine patients demonstrated complex cystic masses with definite soft-tissue components, while the other four demonstrated primarily homogeneous cystic characteristics. These findings reflect a greater variety of radiologic appearances than has previously been reported, with pathologic correlation confirming the variable presence of both cystic and solid components in these lesions.

In addition, there has been a reported predominance of bilateral parotid involvement, with 15 of the 18 previously reported cases showing bilaterality. Our study reveals a unilateral predominance with only three of nine patients demonstrating bilateral parotid lesions. All 18 of the published cases

were men, while our study includes two women, in whom this disease has not previously been described, probably reflecting the increasing frequency of HIV infection in women.

In conclusion, we have demonstrated a variable radiologic appearance of parotid masses, among which the majority contained solid components. We therefore suggest that they be labeled benign lymphoepithelial parotid lesions rather than cysts. Thus, since one cannot rely on a characteristic cystic CT/MR appearance of benign lymphoepithelial parotid lesions, the diagnosis must be assisted by the presence or absence of cervical adenopathy and clinical history.

REFERENCES

1. Marausen DC, Sooy CD. Otolaryngologic and head and neck manifestations of acquired immunodeficiency syndrome (AIDS). *Laryngoscope* 1985; 95:401-404
2. Holliday RA, Cohen WA, Schinella RA, et al. Benign lymphoepithelial parotid cysts and hyperplastic cervical adenopathy in AIDS-risk patients: a new CT appearance. *Radiology* 1988;168:439-441
3. Smith F, Rajedo H, Panebar N, et al. Benign lymphoepithelial lesion of the parotid gland in intravenous drug users. *Arch Pathol Lab Med* 1988;112:742-745
4. Shugar JMA, Som PM, Jacobson AK, et al. Multicentric parotid cysts and cervical adenopathy in AIDS patients. A newly recognized entity: CT and MR manifestations. *Laryngoscope* 1988;98:772-775

Obstruction of the Infrarenal Portion of the Abdominal Aorta: Results of Treatment with Balloon Angioplasty

K. Ravimandalam¹
 V. R. K. Rao
 Sunil Kumar
 A. K. Gupta
 Santhosh Joseph
 M. Unni
 A. S. Rao

Our experience in the treatment of stenoses of the infrarenal portion of the abdominal aorta with balloon angioplasty in 27 patients is reported. Clinical findings were lower limb claudication (all patients), impotence (eight patients), and blue-toe syndrome (two patients). The underlying disease was atherosclerosis in 24 patients and nonspecific aortoarteritis in three patients. Dilatation was successful in all patients. Embolic occlusions of the left common iliac artery (one patient) and left superficial femoral artery (one patient) were the only major complications. Claudication in the affected limb continued in the first patient; the second died when diagnostic angiography, performed 3 months after angioplasty, caused a severe atheroembolus. Of the other 25 patients, nine of the 10 followed up for 13–48 months and all seven followed up for 3–8 months were free of symptoms. Six of eight patients with sexual dysfunction had normal function after angioplasty. Seven patients still awaited follow-up and one was lost to follow-up.

Our experience suggests that balloon angioplasty is an effective treatment of stenoses of the infrarenal portion of the abdominal aorta.

AJR 156:1257–1260, June 1991

Stenoses of the lower abdominal aorta and its bifurcation occur in a small but distinct subset of patients with vascular disease. Surgery has been the traditional treatment for these lesions—endarterectomy for focal stenoses and bypass operations for more extensive disease [1, 2]. In recent years, balloon angioplasty has gained increasing acceptance as an alternative to surgery for these lesions [3–9]. In addition to its well-known advantages over surgery, namely, lower cost, shorter procedure time and hospital stay, and lower morbidity and mortality rates, angioplasty has the virtue of preserving and improving sexual function, which is frequently compromised after surgery.

We report our experience with balloon angioplasty of the lower abdominal aorta in 27 patients (24 patients with atherosclerosis and three with nonspecific aortoarteritis).

Materials and Methods

Twenty-seven patients (25 men and two women 22–70 years old; mean, 44 years) underwent balloon angioplasty of the infrarenal portion of the abdominal aorta. All patients had disabling claudication of the lower limbs; eight had impotence; and two had painful, bluish discoloration of one or more toes (blue-toe syndrome). All but one of the men were smokers, and three were diabetic. On the basis of clinical and angiographic criteria, the cause was considered to be atherosclerosis in 24 patients and nonspecific aortoarteritis in three patients.

Angiography was performed via the transaxillary/brachial artery route in 12 patients and via the transfemoral route in 11 patients; IV digital subtraction angiography was performed in four patients. Doppler ankle-brachial pressure indexes were measured in 23 patients (six before angioplasty and 17 after angioplasty). The assessment of sexual dysfunction in eight patients was subjective and was based on the response of the patients to queries regarding the nature and severity of impotence.

Received August 20, 1990; accepted after revision December 3, 1990.

¹ All authors: Department of Radiology, Sree Chitra Tirunal Institute for Medical Sciences & Technology, Trivandrum 695 011, Kerala, India. Address reprint requests to K. Ravimandalam.

0361-803X/91/1566-1257
 © American Roentgen Ray Society

Angiography performed before treatment showed focal lower abdominal aortic stenoses in 24 patients. In five patients the stenoses were well above the aortic bifurcation. In 19, the stenoses were at the aortic bifurcation with or without involvement of one or both iliac arteries. In three patients, extensive lesions involved multiple sites in the lower abdominal aorta.

All balloon dilatations were done via the transfemoral route; the two-balloon technique (kissing balloons) was used in 22 patients (balloon sizes were 7–10 mm), and the single-balloon technique was used in five patients (balloon sizes were 9–12 mm; USCI-Bard, Billerica, MA). The lesions were crossed with 0.035-in. (0.9-mm) floppy-tipped, straight guidewires (William Cook Europe A/S, Bjaeverskov, Denmark). If resistance was encountered while crossing the lesion, the wire was changed for a Wholey Hi-Torque Floppy wire (Peripheral Systems Group, Mountain View, CA). A 7-French dilator was initially threaded over the wire. Heparin was given intraarterially (5000 IU) immediately after the lesion was crossed. Thereafter, the dilator was exchanged for a balloon catheter of appropriate size, with care being exercised that the balloon diameter (or the sum of the diameters in the case of two balloons) did not exceed that of the prestenotic segment. The balloons were inflated four or five times for 30–40 sec each time. Inflation without resistance and disappearance of balloon indentation were taken as the endpoints of dilatation. Follow-up angiograms were obtained to confirm the adequacy of the lumen. Postprocedure medication consisted of IV heparin (40,000 IU for 48 hr), low-molecular-weight dextran (500-ml infusion for 24 hr), and long-term oral antiplatelet therapy consisting of 325 mg aspirin and 200 mg dipyridamole daily.

Results

During angioplasty, guidewires and balloon catheters successfully crossed the lesions from both femoral arteries in 22 patients and from one femoral artery in five patients. In the latter group, the procedure was done electively with a single balloon in one patient with a focal stenosis at the level of the ostium of the inferior mesenteric artery. In the other four patients, the reasons for using the single-balloon technique were failure to puncture the opposite femoral artery (three patients) and failure to cross an eccentric stenosis (one patient). In the last patient, the left common iliac ostium was protected with a balloon catheter kept across the bifurcation.

All lesions yielded to balloon dilatation without much resistance, requiring no more than normal hand pressure. Postdilatation angiograms revealed luminal widening in all patients. Although the lumen diameter equaled the immediate prestenotic segment in 24 patients, residual stenosis of less than 25% (of the prestenotic segment) was seen in three patients.

Nine of the 10 patients who were followed up for 13–48 months (mean, 22 months) were free of symptoms at the last follow-up. In one patient who continued to smoke, the aorta occluded again after 2 years. All seven patients who were followed up for 3–8 months (mean, 4.4 months) were asymptomatic. Immediate and follow-up ankle-brachial indexes measured after angioplasty in 17 patients were 0.90–1.33 (mean, 1.07). Follow-up had not yet been performed in seven recently treated patients; one patient was lost to follow-up. Representative cases are illustrated in Figures 1–4.

Six of eight men who had had sexual dysfunction reported significant improvement in erectile function after angioplasty.

Emboli caused occlusion of the left common iliac artery in one patient and of the left superficial femoral artery in another. The first patient continued to have symptoms in the left leg but refused any further intervention. In the second patient, who presented initially with blue-toe syndrome, severe and rapidly progressive ischemia of both lower limbs developed after undergoing angiography 3 months later, necessitating above-knee amputations. The patient ultimately died of renal failure and bowel ischemia. Bleeding at the puncture site sufficient to require transfusion occurred in two patients, and infection at the puncture site occurred in one patient.

Discussion

The first reports of successful balloon angioplasty for abdominal aortic stenosis were from Velasquez et al. [3] and Grollman et al. [4]. More recently, larger studies of 14 or more patients [5–9] have reported excellent initial and long-term results. The longest postangioplasty follow-up of a patient was 9 years [10]. Of the 25 complication-free, successful dilatations in our series, 16 of the first 17 patients who have

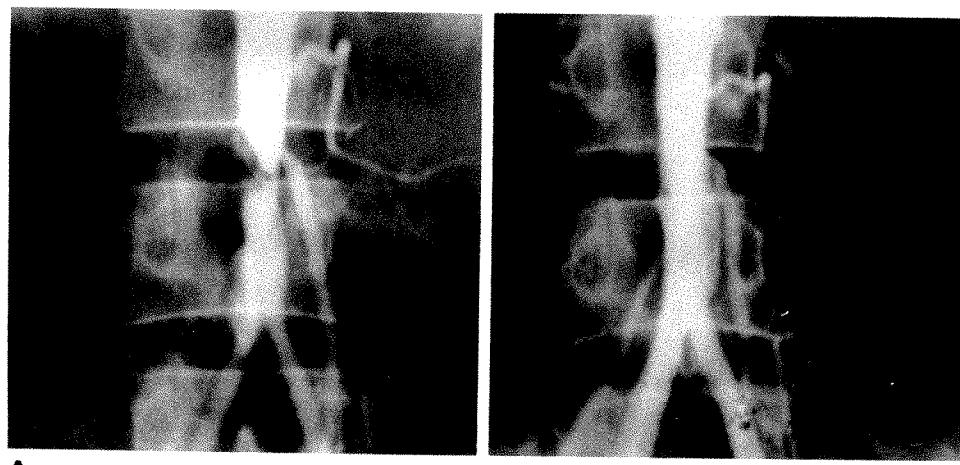


Fig. 1.—40-year-old man with a 1½-year history of claudication and impotence.

A, Transaxillary aortogram shows stenosis of abdominal aorta at level of inferior mesenteric artery.

B, Angiogram obtained after dilatation with a single 12-mm balloon. Lumen of inferior mesenteric artery is preserved. The patient was still asymptomatic with normal sexual function 27 months later.

Fig. 2.—51-year-old man with 1-year history of claudication and impotence.

A, Transaxillary aortogram shows eccentric stenosis of aortic bifurcation.

B, Aortogram after angioplasty with two 7-mm balloons shows fully patent lumen with regression of collaterals. At 13 months, the patient had normal sexual function and was free of claudication.

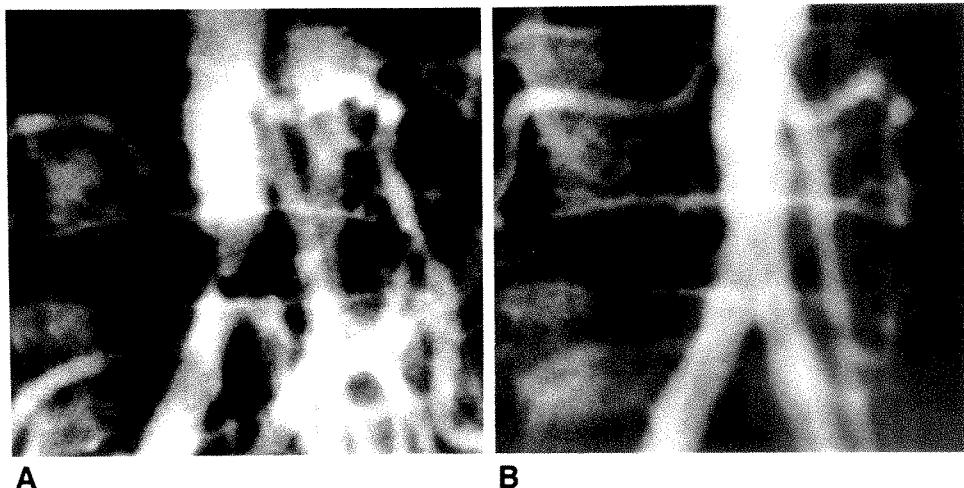


Fig. 3.—48-year-old man with an 8-year history of buttock and lower limb claudication.

A, IV digital subtraction angiogram shows occlusion of aortic bifurcation and collateral circulation through large inferior mesenteric artery. Run-off in common iliac arteries is seen faintly (arrowheads).

B, After angioplasty with two 7-mm balloons, lumen is restored with mild residual narrowing.

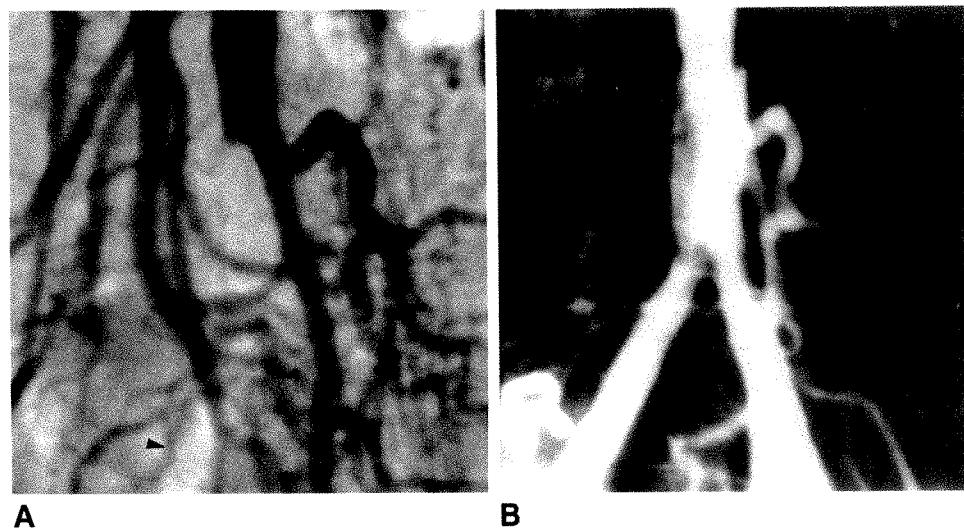
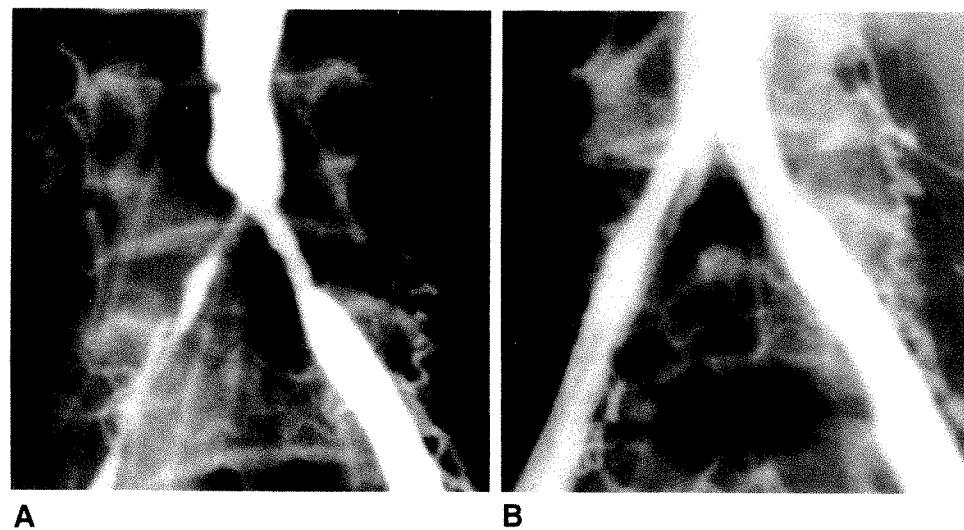


Fig. 4.—22-year-old woman with a 6-month history of hypertension and severe lower limb claudication.

A, Aortogram shows severe aortic and iliac stenoses due to nonspecific aortoarteritis.

B, Aortogram after dilatation shows extensive intimal tears. Patient was asymptomatic at 6 months.



been followed up are asymptomatic. These results compare well with those of previously published series. The focal nature of the lesions in most of the patients, the large caliber of the artery, and the volume of blood flow through the dilated segment are all factors contributing to the good results.

The general advantages of angioplasty over surgery, namely, shorter procedure time and hospital stay, less morbidity and mortality, and less expense, are well known. On the other hand, the specific advantage in aortoiliac angioplasty relates to the preservation and improvement of sexual function in men. Sexual dysfunction after aortoiliac surgery may be attributable either to the rerouting of blood from the abdominal aorta to the lower limb vessels in aortobifemoral procedures or to neurologic damage, particularly of the hypogastric plexus [11]. Restoration of sexual function is one of the advantages of angioplasty, and six of eight patients in our series with impotence reported normal sexual function after angioplasty.

Lesions in the aortic bifurcation are dilated with two balloons, whereas more proximal lesions can be treated with a single balloon. The two incidents of embolic occlusion in our series occurred in patients in whom single balloons were used for lesions located well above the bifurcation. It can be conjectured that fragments from the compressed plaque take the easiest path into the opposite iliac artery when single balloons are used, whereas two balloons (one from each side of the groin) tend to protect the iliac ostia. Also, the two-balloon technique provides access to both iliac arteries in case any further intervention is necessary. At the present time, we use only the two-balloon technique for all lesions of the infrarenal aorta irrespective of location. The balloon size should be carefully chosen to avoid overstretching and risk of rupture.

Caution needs to be exercised during both diagnostic angiography and interventional procedures in patients with blue-toe syndrome. In this manifestation of atheroembolism, the embolic fragments may consist of fibrin-platelet particles detaching from mural thrombi aggregating on stenotic plaques or cholesterol crystals discharged from ulcerated plaques [12]. Catheter-induced atheroembolism, quite surprisingly, is not reported often. Palmer and Warren [13] documented three cases and reviewed 16 others. We encountered one such complication. This patient underwent three arterial catheterizations, and episodes of limb ischemia occurred after each; the first two episodes were transient but the third was irre-

versible with fatal consequences. Although histologic evidence of cholesterol embolism was not obtained, the initial blue-toe presentation, the angiographic appearance of the bulky irregular plaque, the initial preservation of the femoral and peripheral pulses after catheter withdrawal, the subsequent rapid progress of the ischemia, the failure of the embolectomy to arrest the progress, and the massive nature of the tissue necrosis lend credence to our belief that cholesterol embolism was responsible for the death.

ACKNOWLEDGMENTS

We thank the Director of the Institute for permission to publish this article and P. J. George and Joy Abraham for illustrations.

REFERENCES

- DeLaurentis DA, Friedmann P, Wolferth CC, Wilson A, Naide D. Atherosclerosis and the hypoplastic aortoiliac system. *Surgery* 1978;83:27-37
- Constantino MJ, Smith RB, Perdue GD. Segmental aortic occlusion. An unusual lesion found in menopausal women. *Arch Surg* 1979;114:317-318
- Velasquez G, Castañeda-Zúñiga W, Formanek A, et al. Nonsurgical aortoplasty in Leriche syndrome. *Radiology* 1980;134:359-360
- Grollman JH, Del Vicario M, Mittal AK. Percutaneous transluminal abdominal aortic angioplasty. *AJR* 1980;134:1053-1054
- Tegtmeier CJ, Kellum CD, Kron IL, Mentzer RM. Percutaneous transluminal angioplasty in the region of the aortic bifurcation. *Radiology* 1985;157:661-665
- Charlebois N, Saint-Georges G, Hudon G. Percutaneous transluminal angioplasty of the lower abdominal aorta. *AJR* 1986;146:369-371
- Morag B, Rubinstein Z, Kassler A, Schneiderman J, Levinkopf M, Bass A. Percutaneous transluminal angioplasty of the distal abdominal aorta and its bifurcation. *Cardiovasc Interv Radiol* 1987;10:129-133
- Odurny A, Colapinto RF, Sniderman KW, Johnston KW. Percutaneous transluminal angioplasty of abdominal aortic stenoses. *Cardiovasc Interv Radiol* 1989;12:1-6
- Yakes WF, Kumpe DA, Brown SB, et al. Percutaneous transluminal aortic angioplasty: techniques and results. *Radiology* 1989;172:965-970
- Tadavarthy AK, Sullivan WA, Nicloff D, Castañeda-Zúñiga WR, Hunter DW, Amplatz K. Aorta balloon angioplasty: 9-year follow-up. *Radiology* 1989;170:1039-1040
- Cooley DA, Wukasch DC. *Techniques in vascular surgery*. Philadelphia: Saunders, 1979:143-145
- Kaufmann JL, Karmody AM, Leather RP. Atheroembolism and microthromboembolic syndromes (the blue toe syndrome and disseminated atheroembolism). In: Rutherford RB, ed. *Vascular surgery*, 3rd ed. Philadelphia: Saunders, 1989:565-572
- Palmer FJ, Warren BA. Multiple cholesterol emboli syndrome complicating angiographic techniques. *Clin Radiol* 1988;39:519-522

Case Report

Use of a Balloon Catheter to Control Hemorrhage from the Subclavian Artery After Removal of an Inadvertently Placed Catheter

Steven F. Millward,¹ M. Nicholas Lamb,¹ and Philip T. Barron²

The use of a percutaneous transluminal angioplasty (PTA) balloon catheter to control hemorrhage after arterial rupture during PTA is well established [1–4]. We report a patient in whom a PTA catheter was used for temporary occlusion of the subclavian artery to control hemorrhage during removal of an inadvertently placed catheter.

Case Report

A 73-year-old woman had a long history of non-insulin-dependent diabetes mellitus, hypertension, coronary artery disease, and chronic renal failure requiring dialysis. She had a polytetrafluoroethylene arteriovenous graft in her left arm that was infected with *Staphylococcus aureus*. The graft was debrided under local anesthesia, and the wound was left open.

The next day, she became dyspneic, hypotensive, and mildly confused. A 12-French double-lumen catheter (Vas-Cath, Mississauga, Ontario) was inserted for hemodialysis via a left subclavian route. The procedure was complicated by her dyspnea and hypotension and some difficulty was encountered with entering the subclavian vein. Eventually, venous-appearing blood was withdrawn from the puncture needle, and the catheter was introduced into what was thought to be the subclavian vein. The patient was dialyzed with the catheter four times in 5 days. During this time, her condition improved, but it became evident that the catheter was in the subclavian artery. It was decided to remove the catheter 5 days after its insertion.

The right common femoral artery was punctured, and a selective left subclavian arteriogram was obtained (Fig. 1A). This showed that the dialysis catheter entered the artery 3 cm distal to the origin of the vertebral artery and that the subclavian artery measured 10 mm in

diameter. A 7-French PTA catheter with a 10-mm-diameter balloon 4 cm in length was then introduced (Medi-tech, Watertown, MA). It was positioned under fluoroscopic guidance so that the balloon was distal to the vertebral origin and overlapped the catheter's entry site. The dialysis catheter was removed and brisk hemorrhage occurred. The angioplasty balloon was inflated, and direct manual pressure was applied to the external wound. After 2 min, the balloon was deflated, and the direct pressure was removed to assess hemostasis. Immediate brisk hemorrhage occurred and manual pressure was reapplied, but this failed to control the bleeding. Therefore the PTA balloon was reinflated across the bleeding site (Fig. 1B). Manual pressure was removed to determine the efficacy of the balloon tamponade, and no hemorrhage occurred. After another 2 min, the balloon was deflated and no bleeding occurred. The balloon was then reinflated for a further 5 min and then deflated once again without recurrence of bleeding. Direct manual pressure on the subclavian artery was maintained for 15 min with the balloon still in position but not inflated. Hemorrhage did not recur. The PTA catheter was then pulled back into the proximal subclavian artery, and a selective digital subtraction angiogram of the left subclavian artery was obtained. No contrast extravasation was seen, and the catheter was then removed. No subsequent hemorrhage or complication has been noted after 6 months of follow-up. No evidence of limb ischemia was found during follow-up.

Discussion

Manual pressure would probably have been adequate to obtain hemostasis if the 12-French catheter were being removed from a superficial artery such as the common femoral

Received December 4, 1990; accepted after revision January 22, 1991.

¹Division of Diagnostic Radiology, Ottawa Civic Hospital, 1053 Carling Ave., Ottawa, Ontario, Canada K1Y 4E9. Address reprint requests to S. F. Millward.

²Division of General Surgery, Ottawa Civic Hospital, 1053 Carling Ave., Ottawa, Ontario, Canada K1Y 4E9.

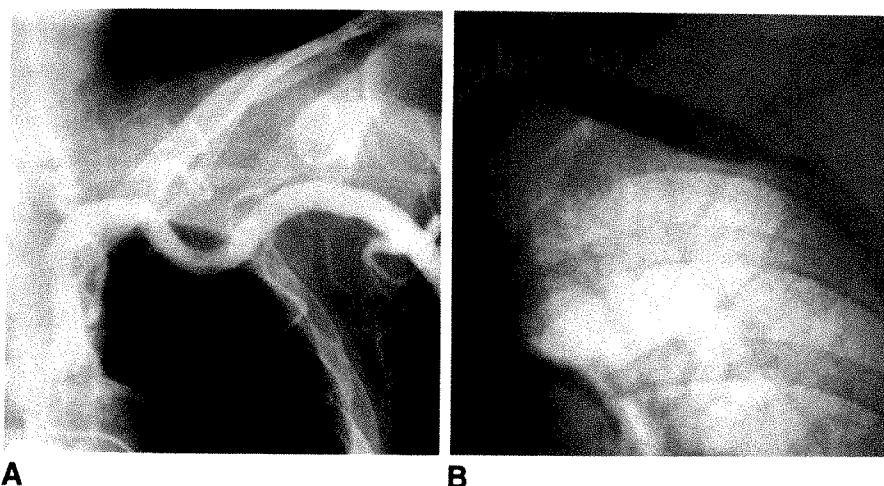


Fig. 1.—A, Selective left subclavian arteriogram shows catheter used for dialysis entering artery 3 cm distal to vertebral origin.

B, Angiogram shows angioplasty balloon inflated across puncture site.

artery, even after it had been in place 5 days. However, the site of entry in the subclavian artery made manual pressure ineffective. Therefore, simple removal of the subclavian catheter could have caused severe arterial hemorrhage requiring surgical intervention for control. This would have involved general anesthesia, and difficult, time-consuming surgical access with possible resection of the clavicle to obtain control of the vessel [5]. The patient's age, coronary artery disease, congestive heart failure, diabetes, and renal failure also made her a poor risk for surgery. It was for this reason that possible alternatives were explored and the decision to attempt intraluminal tamponade was made. The procedure had two advantages. First, it achieved control of the hemorrhage with minimal blood loss, but only temporarily disrupted distal blood flow. Second, if it had been unsuccessful, and surgical intervention had been required, the balloon would have provided proximal control of the artery before surgical exposure.

Treatment of arterial rupture during PTA by temporary balloon occlusion followed by surgical repair is well established [1–3]. Only one case report describes the use of balloon occlusion to control bleeding from the iliac artery after rupture during PTA without subsequent surgery [4]. Balloon catheters and detachable balloons have been used for occlusion of traumatic and spontaneous arterial bleeding, both before surgery and as definitive treatment [6, 7]. However, we are not aware of a previous report describing the use of a balloon

catheter to control bleeding from an arterial injury caused by an inadvertently placed catheter without the need for subsequent surgical repair. An angioplasty balloon catheter was used in this patient because an occlusion balloon catheter was not available. However, an appropriately sized occlusion balloon catheter would probably also have been appropriate. In a patient with a large catheter in an artery inaccessible to direct manual pressure, balloon tamponade can be used to achieve hemostasis.

REFERENCES

1. Simonetti G, Rossi P, Passariello R, et al. Iliac artery rupture: a complication of transluminal angioplasty. *AJR* 1983;140:989–990
2. Villarica J, Gross RC. Treatment of angioplasty-related iliac artery rupture without bypass surgery (case report). *AJR* 1986;147:389–390
3. Chong WK, Cross FW, Raphael MJ. Iliac artery rupture during percutaneous angioplasty. *Clin Radiol* 1990;41:358–359
4. Joseph N, Levy E, Lipman S. Angioplasty-related iliac artery rupture: treatment by temporary balloon occlusion. *Cardiovasc Intervent Radiol* 1987;10:276–279
5. Haimovici H, Callow A, De Palma R, Ernst C, Hollier L. *Vascular surgery: principles and techniques*, 3rd ed. Norwalk, CT: Appleton and Lange, 1989:207–209
6. Belkin M, Dunton R, Crombie H, Lowe R. Preoperative percutaneous intraluminal balloon catheter control of major arterial hemorrhage. *J Trauma* 1988;28:548–550
7. Wholey MH. The technology of balloon catheters in interventional angiography. *Radiology* 1977;125:671–676

Case Report

Control of Hemobilia by Embolization of a False Aneurysm and Arterioportobiliary Fistula of the Hepatic Artery

S. J. Beningfield,¹ P. C. Bornman,² J. E. J. Krige,² and J. Terblanche²

Hemobilia is a potentially lethal condition, frequently caused by iatrogenic trauma [1, 2]. Percutaneous transarterial methods are being used increasingly as the preferred form of therapy [1–4]. We report a case of hemobilia due to a false aneurysm and arterioportobiliary fistula in the hepatic artery that was successfully treated by transcatheter embolization via a T-tube track, an approach not previously described.

Case Report

A 40-year-old woman had cholangitis and obstructive jaundice. Sonography showed intrahepatic and extrahepatic biliary dilatation and a 10-mm calculus in the lower main bile duct, confirmed by ERCP. After successful endoscopic sphincterotomy, the Dormia basket became entrapped around the stone during attempted endoscopic extraction because of a hitherto undiagnosed stricture in the distal bile duct. A right-sided percutaneous external biliary drain was placed to prevent cholangitis. An unsuccessful attempt to free the endoscopically placed basket with a second Dormia basket passed via the external drain track was made 4 days later. At laparotomy the next day, the calculus and entwined basket were removed by cholecystectomy, and a cholecystectomy was performed. Intraoperative removal of the external biliary drain, however, was followed by major hemorrhage from the intrahepatic bile ducts. Hemorrhage was controlled by temporary digital compression of the porta hepatis. The common bile duct was then closed over a T tube.

On the seventh postoperative day, another major episode of hemobilia occurred through the T tube. A selective hepatic angiogram showed a 2-cm false aneurysm and arterioportal shunt from one of the two major branches of the right hepatic artery, which arose from the superior mesenteric artery (Fig. 1A). The portal vein was patent with normal flow. Superselective catheterization was not possible because of the adverse anatomy and proximal atheroma; therefore, embolization of the proximal right branch of the hepatic artery was done with Gianturco coils (Cook Co., Bloomington, IN). The postembolization angiogram showed no filling of the false aneurysm or the arterioportal fistula. Six days later the patient had yet another major hemorrhage from the T tube and was referred for reembolization. Collateral flow via the second branch of the right hepatic artery to the false aneurysm and arterioportal shunt was blocked with Gianturco coils as distally as possible, just proximal to the gastroduodenal artery. No further bleeding occurred.

An angiogram obtained 7 days later showed extensive fine collaterals reconstituting the false aneurysm and arterioportal shunt (Fig. 1B). Consequently, a 5-French 0.038-in. (0.96 mm) lumen cobra catheter was passed over a guidewire via the T-tube track into the involved right bile ducts. A small intraluminal filling defect at the site of the bleeding false aneurysm seen on cholangiography was gently probed with the catheter tip. This caused a sudden dilution of the contrast material in the biliary tree, with blood refluxing up the T-tube track alongside the cobra catheter. This was easily controlled by inflating an occlusion balloon catheter at the site of the aneurysm.

After a few minutes the cobra catheter was again passed into the area of the fistula with entry of its tip into the portal vein (confirmed

Received December 4, 1990; accepted January 7, 1991.

¹ Department of Radiology, University of Cape Town and Groote Schuur Hospital, Observatory 7925, Cape Town, South Africa. Address reprint requests to S. J. Beningfield.

² Department of Surgery, University of Cape Town and Groote Schuur Hospital, Observatory 7925, Cape Town, South Africa.

AJR 156:1263–1265, June 1991 0361-803X/91/1566-1263 © American Roentgen Ray Society

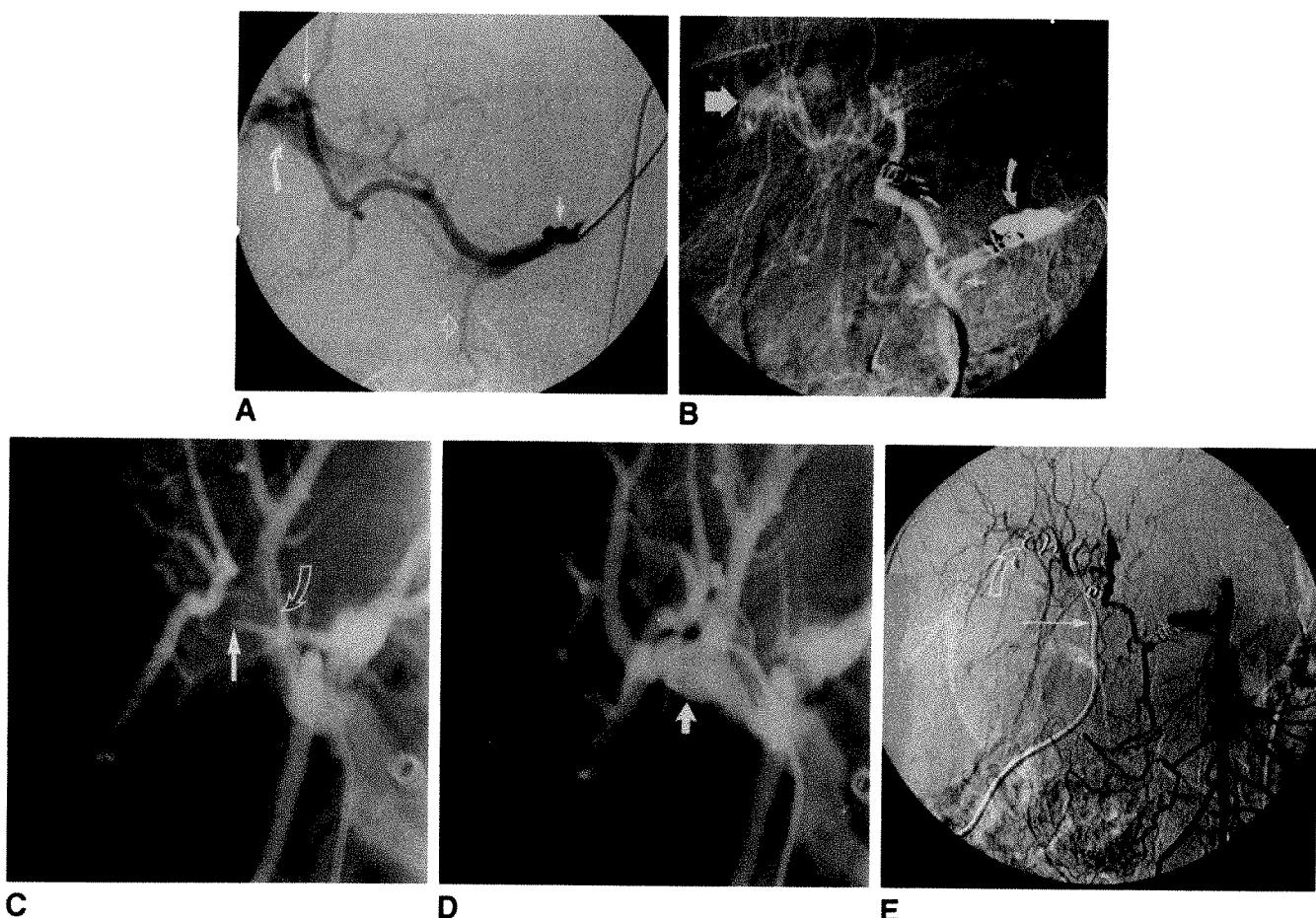


Fig. 1.—A, Angiogram shows tip of sidewinder catheter in right hepatic artery, atheroma (short solid arrow), and site of false aneurysm and fistula (long arrow) with filling of portal vein (curved arrow). Gastroduodenal artery (open arrow) arises from other right segmental branch.

B, After staged embolization of both segmental branches of right hepatic artery, angiogram obtained after injection of contrast medium into origin of right hepatic artery (curved arrow) shows persistent filling of false aneurysm (wide arrow) by collaterals, including gastroduodenal artery (small arrow).

C, Angiogram obtained after cobra catheter was passed via T-tube track and tip (straight arrow) entered portal vein shows filling defect in bile ducts due to hematoma (curved arrow).

D, Angiogram obtained after injection of contrast medium at same position as in C fills portal vein (arrow).

E, After final embolization, angiogram shows occlusion of false aneurysm and fistula by 8-mm Gianturco coil (curved arrow) placed via T-tube track. Note external biliary drain passed via T-tube track (straight arrow).

by contrast injection. Figs. 1C and 1D). An 8-mm coil was then deposited in the fistula, with the distal end in the portal vein branch and the proximal end in the bile duct. A hepatic angiogram obtained 3 days later showed no aneurysm or fistula (Fig. 1E). A month later the stenosis of the distal common bile duct was dilated to 6 mm with a Gruntzig balloon catheter on two occasions. The patient has been well in the following 14 months.

Discussion

Although vascular injury after percutaneous transhepatic biliary drainage (PTBD) has been reported in up to 32% of cases, only one in six injuries caused significant bleeding [2]. Probable causes for early hemorrhage are direct trauma and infection and for late hemorrhage are pressure erosion, cath-

eter exchanges, progressive liver disease, coagulopathy, or tumor involvement [1, 2, 5, 6]. Although cure may be spontaneous [2], hepatic artery embolization is the method of choice for treating this serious complication of PTBD [1, 2]. Ideally, embolization of the artery should be done close to the injury, but this may be impossible despite the use of a variety of guidewires and catheters. Apart from Gianturco coils, embolic agents include gelatin sponge [2-4], tissue adhesives [4], or detachable balloons [1] and, more recently, platinum microcoils passed through Tracker catheters [7] (Target Therapeutics, San Jose, CA). Nonselective particle embolization can be dangerous and has been associated with at least two deaths [2], and was not considered further because of the arterioportal fistula.

One of the first reports of the use of the nonarterial route in performing embolization of a false aneurysm in the hepatic

artery was by Rosen et al. [5], who used the existing transhepatic drainage catheter tract. A similar approach used a balloon catheter for tamponade [6]. This route was not available in our patient because the drain had been withdrawn.

This report demonstrates the feasibility of using a T-tube track as an alternative biliary route for the embolization of a false aneurysm and arterioportal fistula in the hepatic artery when the conventional angiographic approach fails. In view of the potential difficulty of localization and the risk of provoking hemorrhage, occlusion balloon catheters, immediate surgical backup, and availability of cross-matched blood are advised. Endoscopic retrograde cholangiographic guidance may also be feasible by using a technique similar to that described for embolization of external biliary fistulas [8]. Intraoperative cholangiographically guided embolization is another alternative, depending on availability of adequate fluoroscopy. The importance of considering repeated angiography to confirm sustained occlusion of arterial lesions despite initially satisfactory angiographic findings is also emphasized.

REFERENCES

- Mitchell SE, Shuman LS, Kaufman SL, et al. Biliary catheter drainage complicated by hemobilia: treatment by balloon embolotherapy. *Radiology* 1985;157:645-652
- Hoevels J, Nilsson U. Intrahepatic vascular lesions following nonsurgical percutaneous transhepatic bile duct intubation. *Gastrointest Radiol* 1980;5:127-135
- Goldblatt M, Goldin AR, Schaff MI. Percutaneous embolization for the management of hepatic artery aneurysms. *Gastroenterology* 1977;73:1142-1146
- Kadir S, Athanasoulis CA, Ring EJ, Greenfield A. Transcatheter embolization of intrahepatic arterial aneurysms. *Radiology* 1980;134:335-339
- Rosen RJ, Rothberg M. Transhepatic embolization of hepatic artery pseudoaneurysm following biliary drainage. *Radiology* 1982;145:532-533
- Sniderman KW, Morse SS, Rapoport S, Ross GR. Hemobilia following transhepatic biliary drainage: occlusion of an hepatoportal fistula by balloon tamponade. *Radiology* 1985;154:827
- Morse SS, Clark RA, Puffenbarger A. Platinum microcoils for therapeutic embolization: Nonneuroradiologic applications. *AJR* 1990;155:401-403
- Krige JEJ, Bornman PC, Beningfield SJ, Nieuwoudt JHM, Terblanche J. Endoscopic embolization of external biliary fistulae. *Br J Surg* 1990;77:581-583



The Radiology Outreach Foundation (ROF) is a nonprofit corporation whose goal is to help disadvantaged countries improve their health care by providing radiology equipment, books, consultation, education, and training to their practitioners. This assistance is on an application basis that is independent of political, ethnic, or religious orientation of the grantee. It depends on the need of the people and the ability of the ROF to meet that need. The ROF is approved by the U.S. Internal Revenue Service as a tax-exempt organization. It is endorsed by the following radiologic societies: American Association of Women Radiologists, American College of Radiology, American Roentgen Ray Society, Association of University Radiologists, Radiological Society of North America, Society of Chairmen of Academic Radiology Departments, Society for Pediatric Radiology, European Society of Pediatric Radiology.

All donations to the ROF are tax deductible. Persons who would like to contribute financially to the ROF, would be interested in being a visiting professor, would like to send books or journals to any of the institutions supported by the ROF, or would like further information about the ROF should write to Charles A. Gooding, M.D., President, Radiology Outreach Foundation, 3415 Sacramento St., San Francisco, CA 94118 USA.

ARRS 91st Annual Meeting, May 5–10, 1991, Boston, MA

Introduction to Research Seminar

Robert J. Stanley¹

In the spring of 1990, leaders from the American Roentgen Ray Society (ARRS), the Association of University Radiologists (AUR), and the Radiological Society of North America (RSNA) decided to sponsor Introduction to Research Seminar for 80 second-year residents from separate programs. The plan was to have the first 40 residents attend the seminar at the November 1990 meeting of the RSNA and have the second group of 40 attend a similar seminar at the May 1991 ARRS meeting.

The results of an exit questionnaire and the impressions of the faculty members who took part indicated that the RSNA seminar was a success. The organizers of the ARRS meeting had the advantage of knowing the results of the questionnaire and thus were able to modify the program accordingly for the second group of residents.

Seminar Format

The basic format of the seminar remained the same. The timing of the eight separate sessions (Table 1) did not conflict with any of the instructional courses, thus allowing the residents to attend the resident-masters tutorials, many of the other instructional courses, and the categorical course on body and spinal MR imaging.

Many of the faculty members from the RSNA seminar participated in the ARRS seminar. Slightly less time was spent on issues dealing with the National Institutes of Health and more on critiquing the scientific literature and on the rationale for prospective clinical research studies. Two Figley Fellows, Felix Chew of Harvard and Judith Chezmar of Emory, were members of the panel who discussed the selection of an academic career. Dr. Chew also discussed peer review of manuscripts. The analysis of a successful grant proposal, an exercise of considerable value and one that has been used in the Conjoint Committee's "Grantsmanship" program, was included in the Boston seminar.

Social events on Saturday and Tuesday evening and a Role Model Luncheon on Wednesday completed the program. Finally, thanks to the smaller size of the ARRS meeting, all of the residents were able to stay in the hotel that served as the meeting site.

TABLE 1: Introduction to Research Seminar, 1991 ARRS Meeting

Session	Topic	Speaker
1	Welcome	Officers of ARRS, AUR, and RSNA
	Introduction	C. Douglas Maynard
	Principles of Clinical Research	Barbara J. McNeil
2	Conducting a Peer Review of a Manuscript	Felix Chew
3	Industry's Role in Research	James H. Thrall
	Imaging Research	William R. Brody
	Introduction to Technology Assessment	Bruce J. Hillman
4	Preparation and Delivery of an Oral Presentation	Ruth G. Ramsey
	The Rationale for Technology Assessment Studies	Ronald G. Evens
5	How to Write a Grant Proposal	Harold L. Kundel
	Prospective Clinical Research Studies	Richard L. Baron
6	Radiology Journalism: The Final Step in Research	Robert N. Berk, Margaret Levene
	Animal Models and Experimental Design	Andrew Taylor
	The Excitement of an Academic Career (Role Model Luncheon)	C. Douglas Maynard
7	How the NIH Works	David G. Bragg
	Grant Critique Panel	Naomi P. Alazraki, moderator; Constantine A. Gastonis, Barbara J. McNeil, Clare M. Tempary
8	Selection of an Academic Career Panel	Panel: Harry Z. Mellins, moderator; Susan A. Mulligan, Felix Chew, Paul Molina, and Judith Chezmar

¹ Department of Radiology, The University of Alabama at Birmingham, 619 S. 19th St., Birmingham, AL 35233.

Pictorial Essay

Sonographic Artifacts and Their Origins

Kathleen A. Scanlan¹

Artifacts are encountered daily in clinical sonography. They may be observed in B-mode gray-scale imaging, spectral pulsed Doppler imaging, and color Doppler imaging. Most of these distortions can be understood at a basic level by an appreciation of the form of the focused sound beam, the interaction of sound with tissue, and assumptions made about the spatial assignment of reflected echoes. Sonographic systems assign depth based on the time interval of round-trip echo travel and assume a straight line and singular path from transducer to reflector and

reflector to transducer. The same speed of sound is assumed in all tissues for the purposes of spatial assignment. Some inherent acoustic artifacts are used reflexively to characterize tissue. Strong acoustic enhancement behind an anechoic structure confirms the diagnosis of a cyst. Clean acoustic shadowing distal to an echogenic focus in the gallbladder leads us to the diagnosis of gallstones. If unrecognized, acoustic artifacts can cause serious misdiagnoses. Several commonly encountered artifacts are illustrated, with a basic physical explanation of their occurrence.

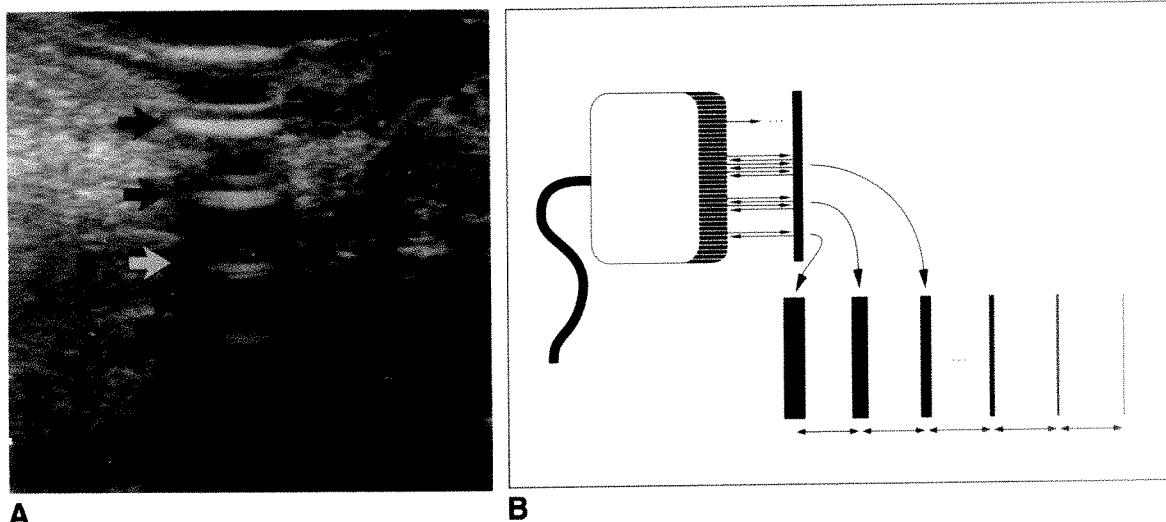


Fig. 1.—Reverberation bands.

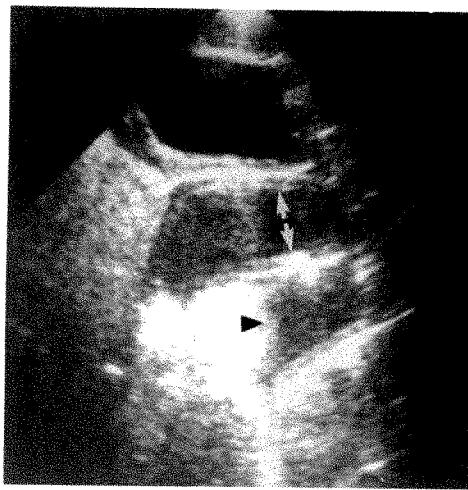
A, Endorectal sagittal sonogram of prostate. Air bubble trapped within fluid-filled condom causes repeated reverberation bands (arrows) as sound beam travels multiple round-trips between transducer face and highly reflective air bubble. Artifact completely obscures image. If air bubble cannot be eliminated, image can be improved by tipping bubble to end of condom.

B, Drawing shows that bright parallel bands at uniform intervals are created by sound beam traveling multiple round-trips between transducer face and a highly reflective interface. Additional bright band is registered at each multiple of round-trip distance.

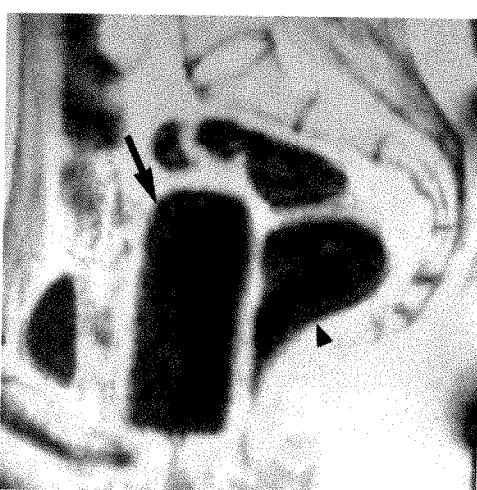
Received October 1, 1990; accepted after revision December 13, 1990.

¹ Department of Radiology, University of Wisconsin, Clinical Science Center, 600 Highland Ave., Madison, WI 53792. Address reprint requests to K. A. Scanlan.

AJR 156:1267–1272, June 1991 0361-803X/91/1566-1267 © American Roentgen Ray Society



A

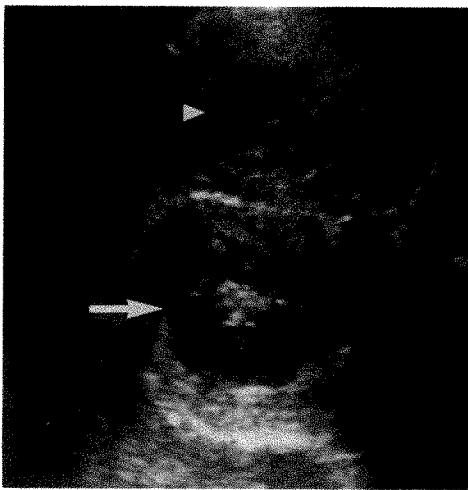


B

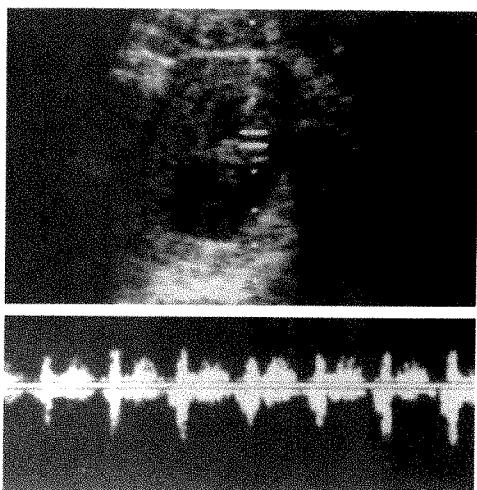
Fig. 2.—Reverberation pseudomass.

A. Sagittal midline sonogram of pelvis in patient with possible pelvic abscess after vaginoplasty. Vaginal mold is identified posterior to bladder (arrows). Hypoechoic structure (arrowhead) posterior to vaginal mold suggested abscess.

B. MR image obtained 4 days later shows no fluid interposed between vaginal mold (arrow) and rectum (arrowhead). Appearance of abscess was created by reverberation.



A



B

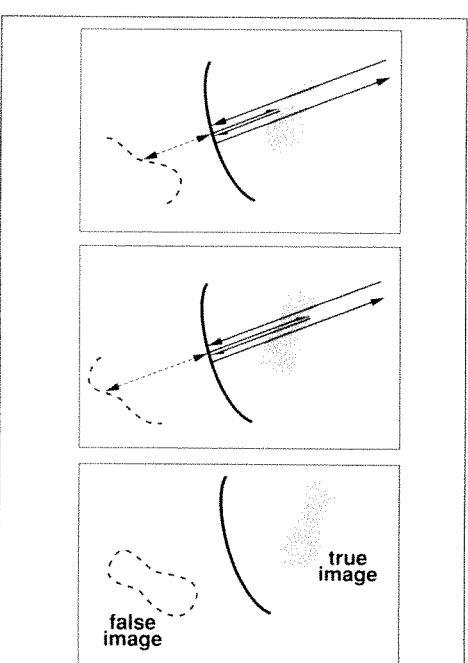
Fig. 3.—Mirror-image pseudomass.

A. Transabdominal sonogram of pelvis shows intrauterine gestation (arrowhead). Simulation of duplicate gestational sac (arrow) complete with fetal pole in extrauterine location was caused by mirroring from highly reflective portion of sigmoid colon. Artifact disappeared on repeat study. Water enema can be used in this situation if colon is suspected as the "mirror."

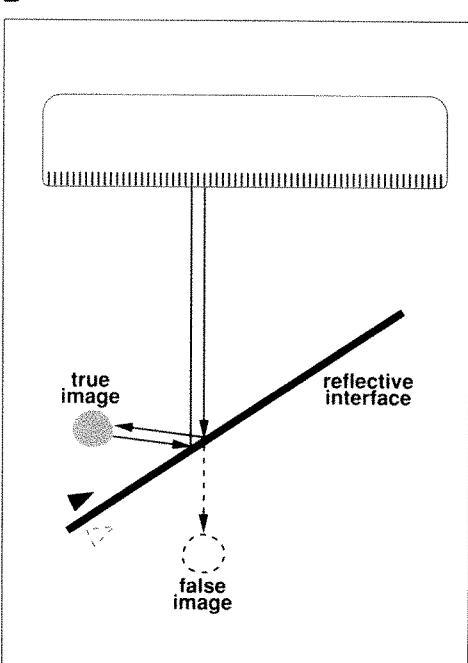
B. Doppler examination shows heartbeat originating in extrauterine duplicate gestational sac.

C. Drawing shows mechanism of mirror-image simulation of a mass. True mass is duplicated by additional round-trip reverberations that develop between points within mass and reflective interface. Additional distance traveled by reverberated sound registers spatially as a mirror image of mass appearing equidistant on opposite side of reflector.

D. Drawing shows mechanism of mirror-image localization of a Doppler signal. If interrogating pulse first strikes a reflective interface such as pleura or gas-filled rectum and then interrogates a small moving reflector, returned frequency information will be spatially displaced (dashed arrow) by a distance of additional round-trip (short arrows) between specular reflector and small moving reflector. Arrowheads indicate direction of flow.



C



D

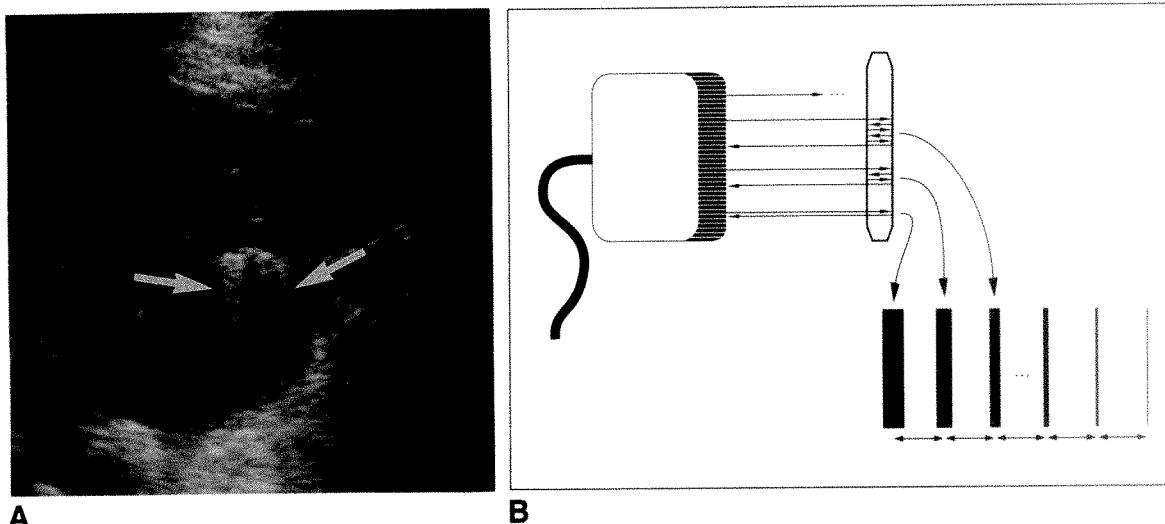


Fig. 4.—Comet-tail artifact.

A, Longitudinal sonogram of gallbladder. Comet-tail artifacts (arrows) arising from anterior gallbladder wall were initially mistaken for gas. Cholecystectomy specimen revealed cholesterosis. In this case, short-path reverberations presumably arose within a cholesterol crystal or globule. Similar short-path reverberations can occur within clusters of microbubbles.

B, Drawing shows mechanism of comet-tail artifact. Sound beam interacts with tissue that causes it to undergo multiple short-path reverberations. Short path may be generated within cholesterol, metallic substances, or a cluster of microbubbles. Each multiple of the short path is registered spatially as a bright line, resulting in a trail of closely spaced bright lines behind the source of artifact.

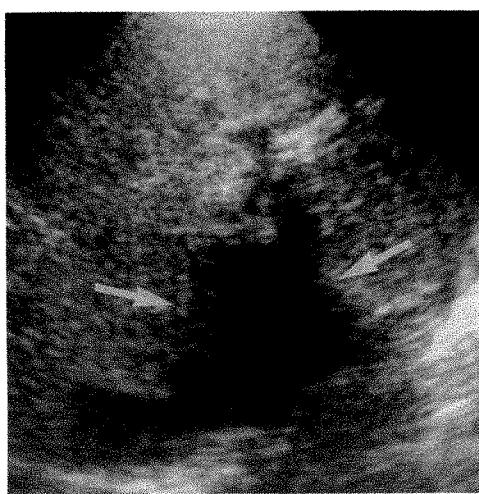


Fig. 5.—Attenuation artifact on transverse sonogram of liver. Partial attenuation of sound beam by fibrofatty portal structures causes a hypoechoic area simulating neoplasm (arrows). Scanning from an alternative window that does not traverse attenuating area will demonstrate normal echogenicity in questionable area.

Real-Time Gray-Scale Imaging

Reverberation

When a sound beam is perpendicular to an interface, the amount of reflected sound depends on the amplitude of the incident beam and the acoustic impedance difference between the two media. With large differences, the reflection of sound is maximized. This phenomenon tends to occur at soft-tissue/gas and fluid/gas interfaces. Sound reflected from such an interface will strike the transducer and reenter the patient a second time. When this echo returns again to the trans-

ducer, it will receive a spatial assignment twice as deep as the original reflector. This "round-trip" of the sound may be repeated several times [1].

A *reverberation artifact* is usually seen as bright parallel lines occurring at regular intervals (Fig. 1). Echoes that have taken more time to return to the transducer are electronically boosted by the equipment. This is done to compensate for the tissue attenuation of returning deep echoes in the normal imaging situation and serves to enhance the reverberation artifact.

A *reverberation pseudomass* may be created by returned echoes from a gas- or fluid-filled structure located deep to the transducer, usually in the pelvis (Fig. 2). The near "wall" of the pseudomass results from the primary reflection from the tissue/gas-fluid interface and the reverberated echo creates the far wall. Only one or two reverberated echoes may be seen because of a relatively large time-distance interval, making this type of reverberation artifact much more difficult to recognize.

A *mirror-image pseudomass* may occur adjacent to highly reflective acoustic interfaces such as the diaphragm, pleura, and bowel. Reverberations develop between the real mass and the reflective surface. This phenomenon doubles the round-trip time for each point within the mass and thus registers the echoes created by the mass equidistant on the opposite side of the reflector surface (Fig. 3C) [2]. When a mirror-image mass is registered above the diaphragm, it is easily recognizable as artifact. The same situation may be created in abdomen or pelvis adjacent to a highly reflective interface, usually bowel wall. Here the artifact is more difficult to recognize as it can mimic an actual abnormality (Fig. 3A). Doppler signals in both pulsed and color Doppler also may be "mirrored" from a very reflective interface (Fig. 3B) [3]. The interrogating frequency may strike the reflective surface first,

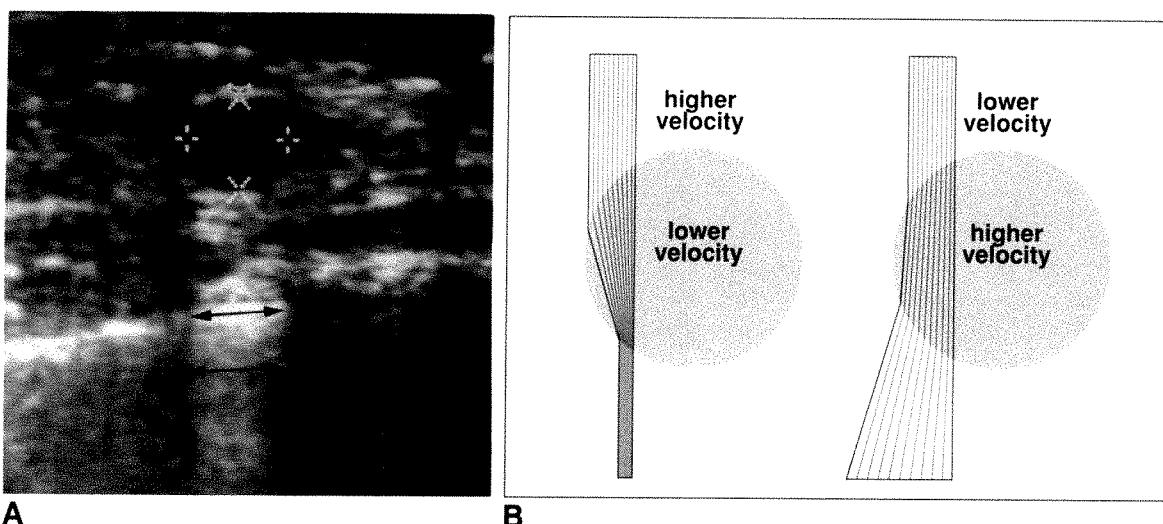


Fig. 6.—Refraction.

A, Longitudinal sonogram of breast. Narrow refractive bands (arrows) are seen at margins of a simple cyst. Bands occur because sound beam is refracted at curved interface between a higher (breast)- and lower (cyst)-velocity tissue.

B, Simplified illustration shows how a relatively higher- to lower-velocity path will refract and narrow sound beam, creating thin refractive artifacts at margin of lower-velocity cyst. A lower- to higher-velocity path in the same situation will cause spreading of sound beam.

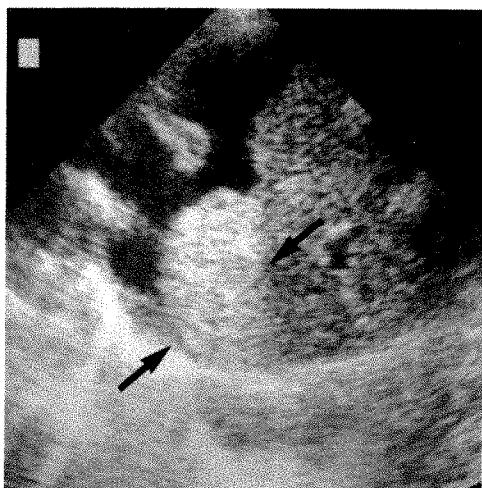


Fig. 7.—Through-transmission artifacts. Nodular projection at dome of cirrhotic liver appears on sonogram to have a higher echogenicity than remaining liver, simulating an echogenic mass (arrows). This appearance is created because portion of beam traveling through ascites is attenuated much less than portion traveling through liver. If nodular projection is scanned through a soft-tissue window it will have the same echogenicity as main body of liver.

the moving reflector second, then travel back to the reflective surface, and finally be registered at the transducer face. The added round trip between the strong reflective interface and the moving reflector causes a spatial displacement deep to the interface resulting in a mirror-image Doppler signal (Fig. 3D).

The *comet-tail* or *ring-down* artifact appears as a line of intense, nearly continuous echoes trailing behind a small reflector (Fig. 4). This artifact probably arises from multiple short-path reverberations. The short path could arise within a cluster of microbubbles or within a focus of cholesterol deposition. The comet tail can also be identified behind sub-

stances that have a very large acoustic impedance mismatch with soft tissues, such as metal.

Attenuation

Partial attenuation of the sound beam by absorption, reflection, and refraction will cause a distal area of decreased echogenicity. When a fibrofatty area in a solid organ causes partial attenuation of the sound beam, an area of low echogenicity can occur in otherwise uniform parenchyma. This finding may suggest an area of neoplastic involvement if the source of the artifact is not recognized (Fig. 5). When this type of abnormality is suspected, scanning from an alternate window can resolve the issue.

Refraction

Refractive shadows occur when the sound beam is at an oblique angle of incidence to the boundary between two media (Fig. 6A). The amount of reflection and refraction occurring depends on the angle at which the beam strikes the interface. Whether the beam converges or diverges depends on whether the sound path is from a higher-velocity medium (soft tissue) to a lower-velocity medium (such as a cyst) or from a lower-velocity medium to a higher-velocity medium (Fig. 6B). Refractive artifacts can mimic shadowing from calcified structures or simply can obscure evaluation of the tissue in the area of artifact.

Through-Transmission Artifacts

Tissue that lies deep to fluid-filled structures appears more echogenic than normal because the attenuation of sound is less in fluid than in soft tissue. This artifact may be encountered when scanning through ascites, cysts, or fluid collections such as hydroceles. Kidneys scanned through ascites

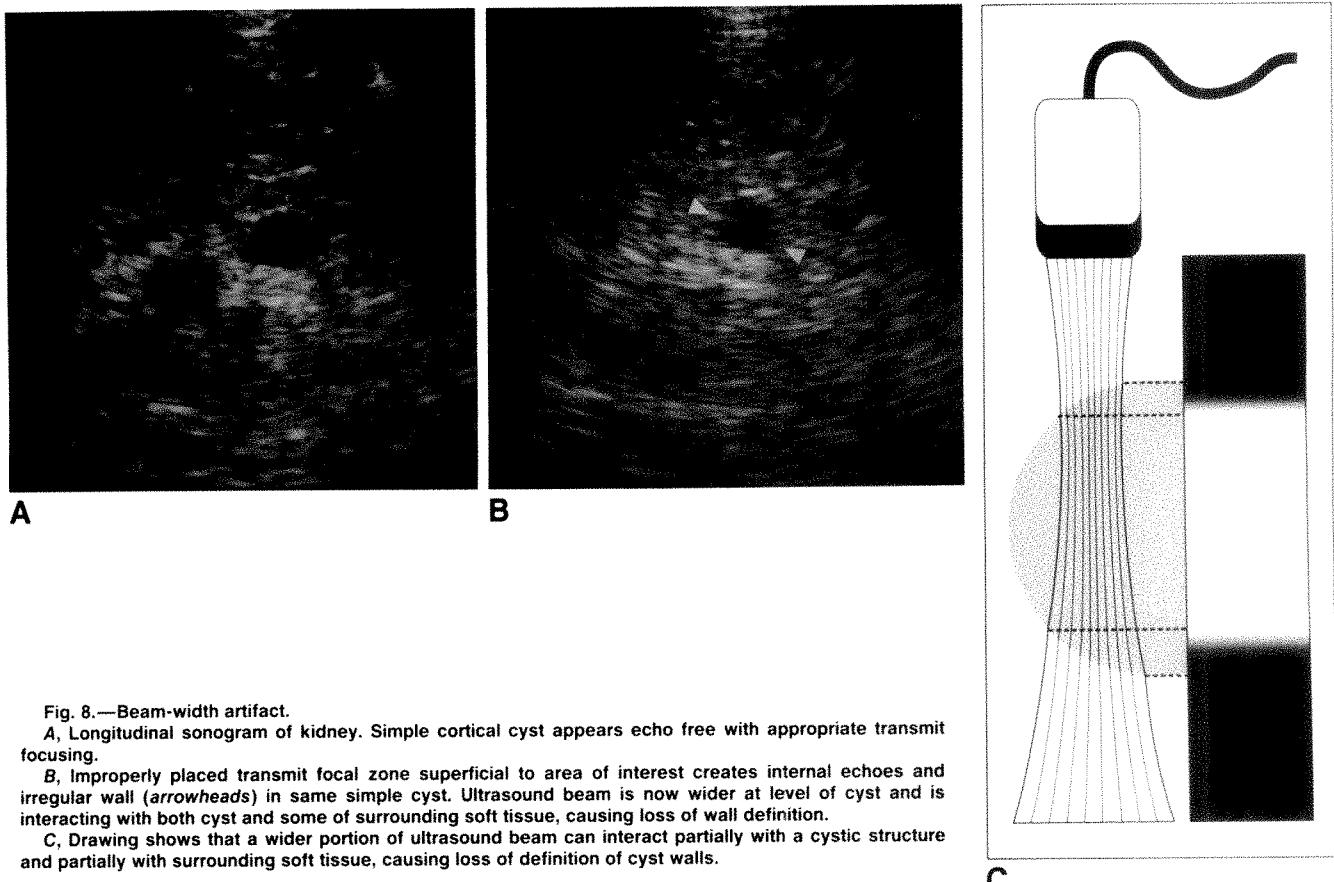


Fig. 8.—Beam-width artifact.

A, Longitudinal sonogram of kidney. Simple cortical cyst appears echo free with appropriate transmit focusing.

B, Improperly placed transmit focal zone superficial to area of interest creates internal echoes and irregular wall (arrowheads) in same simple cyst. Ultrasound beam is now wider at level of cyst and is interacting with both cyst and some of surrounding soft tissue, causing loss of wall definition.

C, Drawing shows that a wider portion of ultrasound beam can interact partially with a cystic structure and partially with surrounding soft tissue, causing loss of definition of cyst walls.

may appear more echogenic than normal, leading to an erroneous diagnosis of medical-renal disease. The artifact can be particularly confusing when a nodular liver is scanned through ascites (Fig. 7).

Beam-Width Artifact

The ultrasound beam has a definite width that varies along its course depending on the focusing characteristics of the

transducer. If the beam is too wide, one portion of the ultrasound beam may be interacting with a fluid-filled structure while another portion of the beam interacts with adjacent soft tissue (Fig. 8C). This can create spurious echoes registered within the cystic structure (Figs. 8A and 8B). The effect can be minimized by using the narrowest sound beam available, focusing the beam at the site of interest, and scanning through the central portion of the cyst. This phenomenon will also

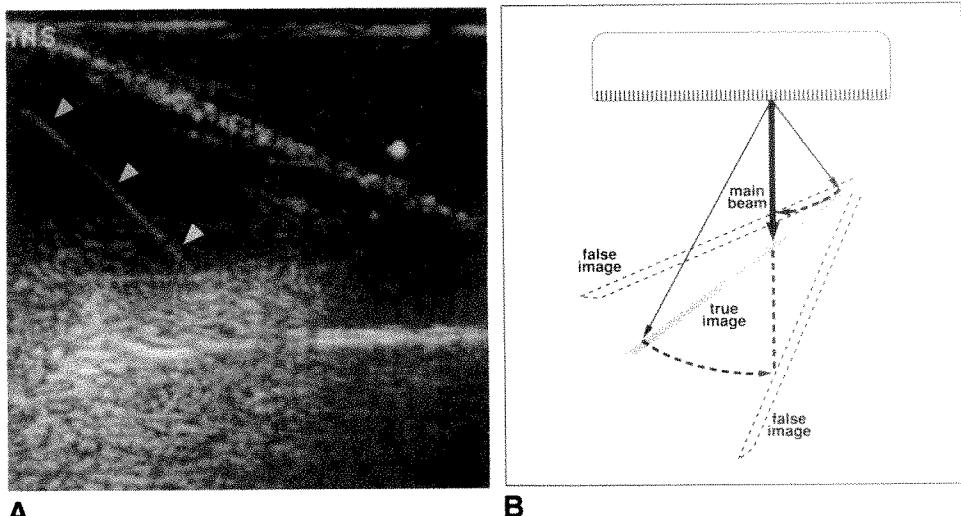


Fig. 9.—Side-lobe/grating-lobe artifacts.

A, Sonogram of biopsy needle imaged with linear transducer shows a linear artifact (arrowheads) created by off-axis grating lobes.

B, Drawing shows method by which lower-intensity off-axis grating lobes generated by a linear array create faint linear images at angles to a metallic needle path.

cause masses of low contrast to be less apparent or missed entirely because of reduced contrast at the borders.

Side-Lobe/Grating-Lobe Artifacts

Several low-intensity sound beams are often located peripheral to the main axis of the ultrasound beam (Fig. 9B). These are of a much lower intensity than the main beam but create significant artifacts when they interact with highly reflective acoustic surfaces. Side lobes may cause specular

or diffuse echoes within the image [4]. Specular artifacts occur adjacent to curved, highly reflective surfaces such as diaphragm, bladder, and gallbladder, while diffuse echoes tend to occur adjacent to bowel gas. The same phenomenon may cause the appearance of multiple needle paths during guided biopsy (Fig. 9A).

Focal-Zone Banding

The ultrasound beam is of varying intensities along its course, and further electronic transmit focusing of the beam can create bands of increased intensity. This phenomenon can create bands of increased echogenicity in an organ that should be homogeneous (Fig. 10).

Speed-of-Sound Artifacts

These artifacts usually involve abnormal spatial assignment as well as an element of refraction when media with two different speeds of sound are traversed by the sound beam (Fig. 11C). Sonographic equipment assigns spatial location on the basis of round-trip time, assuming an average tissue velocity of 1540 cm/sec. Scanning through media with differing speeds of sound such as cartilage, fluid, and fat will cause inaccurate depth assignment (Figs. 11A and 11B).

REFERENCES

1. Hykes D, Hedrick WR, Starchman DE. *Ultrasound physics and instrumentation*. New York: Churchill Livingstone, 1985
2. Laing FC. Commonly encountered artifacts in clinical ultrasound. *Semin Ultrasound* 1983;4(1):27-43
3. Reading CC, Charboneau JW, Allison JW, et al. Color and spectral Doppler mirror-image artifact of the subclavian artery. *Radiology* 1990;174:41-42
4. Laing FC, Kurtz AB. The importance of ultrasonic side-lobe artifacts. *Radiology* 1982;145:763-768

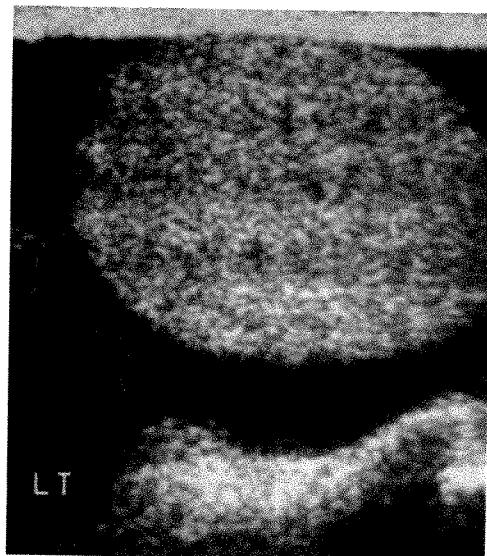


Fig. 10.—Focal-zone banding. Electronic transmit multilevel focusing creates bands of increased echogenicity owing to areas of increased intensity in sound beam. Artifact can be recognized by altering level of focus within area scanned.

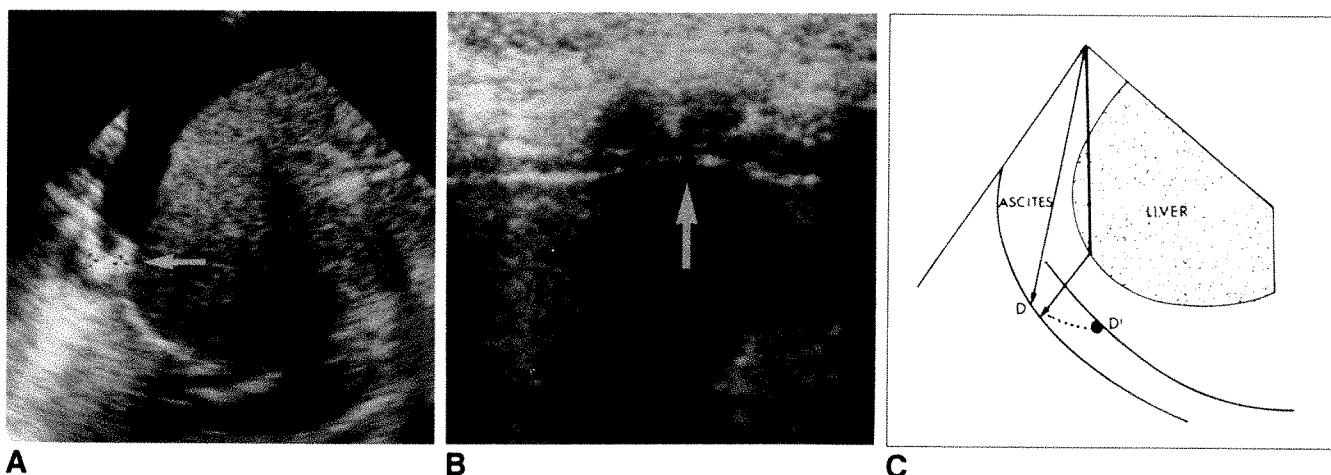


Fig. 11.—Speed-of-sound artifacts.

A, Longitudinal sonogram of liver. Portion of diaphragm scanned through ascites (lower speed of sound) is displaced 9 mm deeper than portion scanned through liver (arrow). Refraction creates a short segment of double diaphragm.

B, Longitudinal sonogram of liver. Because speed of sound through cartilage is higher than 1540 cm/sec, subadjacent liver capsule is artificially placed closer to transducer, creating a small pseudomass (arrow).

C, Simplified illustration of origin of displaced and duplicated diaphragm. Sound beam is refracted by traveling through media that conduct sound at different speeds. D and D' indicate two different spatial placements of a point on diaphragm caused by this phenomenon.

Perspective

Radiology Summit 1990: Specialization in Radiology—Trends, Implications, and Recommendations

James H. Thrall¹ and Jack Wittenberg

Increasing specialization among radiologists is a well-established trend and—most broadly—is a consequence of the increasing sophistication and complexity of medical practice finding expression in the practice of radiology. The strength of the trend toward more specialization is great enough that the debate and controversy of the past decade about whether specialization and the accreditation of specialties is good for radiology has given way, without “official” resolution or even consensus, to a discussion of how best to go forward: to define areas of specialization; to protect and enhance the practice of radiology in an era of specialization; and to protect and enhance the legitimate career aspirations of individual radiologists, whether their primary interests are oriented toward general or specialty practice. The following observations are based on a panel discussion with approximately 25 participants from a wide variety of private and academic practice backgrounds that took place as part of the 1990 Radiology Summit in Asheville, NC.

Background and Assessment

The panel chose not to attempt a rigid definition of either specialist or generalist. Rather, it held the view that a generalist was someone whose work concerned multiple organ systems and/or multiple technologies, but not necessarily in all organ system areas, and that a specialist was someone

with additional experience or training in an area but who might not work exclusively in that area. On the basis of this viewpoint, there was consensus that specialization had become a pervasive part of the practice of radiology. In large private groups and most academic practices, specialization is already highly developed. However, even in small private practice groups, there is a strong trend toward individuals taking on responsibilities in specialties, especially in nuclear medicine, neuroradiology, mammography, and angiography/interventional procedures. Perhaps ironically, representatives of large groups and especially large academic practices expressed a problem in finding radiologists to do general work, whereas small groups felt increasing pressure to find radiologists to meet emerging needs for more specialized practice. The two most important factors driving the degree of specialization in current practice appeared to be department or group size and practice venue. A recurrent theme was that specialty-trained radiologists in private practice frequently do a significant amount of general radiology (at least until the group or practice size is large enough to sustain a full-time specialist); this was far less common in many academic practices.

Drivers of Change

The panel considered the trends inside and outside of radiology that had been most important in driving the change

Received November 26, 1990; accepted after revision December 27, 1990.

Participants in the 1990 Radiology Summit panel were James H. Thrall (moderator), R. Nick Bryan, William J. Casarella, Donald W. Chakeres, Carl J. D'Orsi, Raymond A. Gagliardi, Milton Gallant, Jeffrey T. Goodwin, Thomas S. Harle, Anton N. Hasso, Ray Kilcoyne, Donald R. Kirks, Kenneth L. Krabbenhoft, Theresa C. McLoud, Thomas F. Meaney, Michael T. Modic, Henry P. Pendergrass, Lee F. Rogers, Alfred R. Smith, Robert J. Stanley, Lynne Steinbach, Michael S. Tenner, Ina L. Tonkin, Arina van Breda, Jack Westcott, Jack Wittenberg, and James E. Youker.

¹ Both authors: Department of Radiology, Massachusetts General Hospital Boston, MA 02114. Address reprint requests to J. H. Thrall.

AJR 156:1273–1276, June 1991 0361-803X/91/1566-1273 © American Roentgen Ray Society

toward more specialization. Three factors stand out. First, and probably by far the most important, has been the unprecedented creation of new radiologic knowledge in the past two decades. This explosive growth has profoundly increased the level of sophistication in diagnosis and treatment that our specialty can now offer to patients. The increases in knowledge and breadth of practice have made it impossible for any one person to practice at the "state of the art" in all areas of radiology.

Second, turf battles over who provides services have created a need for radiologists to achieve the highest possible levels of expertise to defend the boundaries of their practices. Such levels of expertise require specialized focus, which includes both clinical and research dedication.

Third, and parallel in time with the foregoing factors, have been changes in privileging criteria fostered by the Joint Commission on Accreditation of Hospitals Organization (JCAHO) to require more specificity and a stronger link between performance assessment and the granting of privileges. Specialization provides a natural mechanism for addressing both issues.

Several other factors were considered significant, although less important, than the three just enumerated. Increasing subspecialization in other fields has raised the expectations of referring physicians about the level of expertise held by radiologists. Likewise, there has been an increasing level of sophistication and expectation among patients. Third-party payers are also beginning to look at levels of expertise and are linking specialization to their willingness to reimburse for complex procedures. Lastly, the growth and development of strong specialty organizations within radiology has fostered the development of specialization. As professional and scientific organizations have gained strength, stature, and membership, they have become focal points for their respective specialties. In fact, it is from the specialty organizations that requests have been generated for official accreditation of training programs in their respective specialties.

What Are the Radiology "Specialties"?

Radiology embraces multiple imaging technologies, which are in turn applied to all of the organ systems in the body. This has raised the question of whether it is more logical to segment practice on the basis of an organ system orientation or a technological orientation. The clear consensus was that the organ system approach is ultimately the most logical and strongest one because it allows the specialist in radiology to learn the clinical and surgical aspects of the respective organ systems, thereby having parity in knowledge with the clinicians with whom he or she interacts.

New technologies are often introduced by people who are dedicated to the technology; but as the technology matures, it becomes progressively incorporated into the organ system matrix. The consensus was to accept and encourage this evolutionary paradigm. This approach has been successfully applied in both CT and MR imaging. There has been less integration of nuclear medicine and sonography into organ system specialty practices, but this too appears to be evolv-

ing, albeit slowly. Another important area of activity not completely defined by the organ system approach is interventional radiology. However, the majority of academic departments and private practices include vascular/interventional procedures as a separate area of specialization. The view expressed by a number of people on the panel was that vascular/interventional radiology may actually evolve as a separate area of practice akin to the separation between diagnostic and therapeutic radiology.

Accreditation and Certification

In discussing specialization, it is important to define and understand the difference between *accreditation* and *certification*. Accreditation applies to training programs, not individuals. It is the province of the Residency Review Committee (RRC) working under the aegis of the Accreditation Council on Graduate Medical Education (ACGME). The ACGME in turn is jointly sanctioned by the American Board of Medical Specialties (ABMS), American Medical Association (AMA), American Hospital Association (AHA), American Association of Medical Colleges, and Council of Medical Specialty Societies. The specific charge to the RRCs is the accreditation of hospital-based graduate medical education programs. The process of achieving accreditation for a new specialty is complex, but begins with a specialty group or society or other organization forwarding a request to the radiology RRC. The RRC develops special training requirements and works with the RRCs of the other specialties, as well as the other interested organizations including the ABMS, AMA, and AHA, to obtain final approval.

Certification is the province of the various specialty boards. For radiology, it is the American Board of Radiology (ABR), and the term applies to persons who seek certification after residency (or fellowship) training. One of the concerns in the process of accreditation and certification is that accreditation might be granted to training programs without the opportunity for individuals for certification. The ABR has agreed to consider certification paths for people completing newly accredited programs in neuroradiology and pediatric radiology.

Potential Benefits of Specialization

The consensus of the panel was that specialization results in important benefits to radiology and to patients having radiologic procedures. Most importantly, patients benefit from higher-quality clinical care as a result of the higher levels of expertise brought to bear by specialty-trained radiologists. Specialty programs, particularly in academic centers, are focal points for research and innovation in the development of new procedures and technology.

The presence of specialty-trained radiologists has a positive impact on residency training programs, although caution was expressed that the experience of the resident must be protected when fellowship training is offered in a particular specialty area. The special requirements for RRC accreditation of specialty fellowship training programs take such considerations into account.

Greater expertise has unquestionably helped the competitive position of radiology in turf wars with other branches of medicine. The greater the level of expertise, the more likely that a given area of practice is retained within radiology.

The panel also believed that opportunities for specialization within radiology were a positive factor in recruiting high-quality medical students into radiology. A corollary point is the high level of career satisfaction expressed by specialists.

Potential Problems Associated with Specialization

Specialization results in longer training and therefore higher costs to both the trainee and the institution providing the training. It is not clear how the higher cost to institutions will be subsidized in an era of shrinking reimbursement. It is also a concern that the total training time encompassing medical school, residency, and specialty training has become very long. The ABR and RRC must take this into account by developing options that minimize the requirements for specialty qualification.

One of the most important problems associated with specialization is its impact on staffing requirements. The consensus of the panel was that specialization requires more people and that it results in more complex departmental and practice organization. A recurrent theme was that the force driving increased staffing needs is that new, highly specialized procedures are very physician-time intensive, particularly because many of them require direct hands-on involvement by physicians. New procedures such as intraoperative sonography have actually been given up by some radiology departments owing to the extreme demands on physicians' time.

Another theme permeating the discussions was the issue of flexibility. This was regarded as more of a problem in the academic than in the private practice environment but an issue for both. In private practice there is frequently not enough work for a full-time specialist, and many groups, as a matter of policy, require specialists to provide general radiology cross coverage to retain flexibility and parity of effort within the group. In academic practices, such cross coverage is more difficult to achieve because of the career interests and orientation of the specialists. The loss of the flexibility of cross coverage directly increases staffing requirements. The higher staffing costs in this setting are not offset in any way by reimbursement, which remains the same regardless of the level of expertise brought to bear.

It was noted that the American College of Radiology Committee on Manpower has determined that there is a current shortage of radiologists, with the possibility of a much greater shortage of radiologists by the year 2000. The net increase from recent initiatives to increase the number of positions in some training programs is expected to fall far short of fulfilling projected needs. The manpower shortage was thought to be greater in nonmetropolitan areas and is particularly acute in some specialties. For example, the Society for Pediatric Radiology maintains a directory of positions that currently lists approximately 70 unfilled positions. The panel believed that one of the major risks to the field of radiology from a manpower shortage could be loss of turf if there are not enough

radiologists to perform requested procedures, particularly highly specialized and/or interventional procedures.

There was some belief within the panel that increasing specialization has also created problems of access for patients and delay in service to both patients and referring physicians in some practice settings. This occurs when only a few specialists can perform or review a particular study. It was noted that clinicians are under pressures of their own that are different from those in the past and have developed heightened expectations for timeliness of service.

Discussions on the merits of specialization and specialty certification must take into account the potential threat of diminishing the value of the basic certification in radiology. Despite the degree of specialization that is occurring, "general radiology" continues to constitute the bulk of the work in both private and academic practice. Caution must be taken to ensure that in the rush for specialization, the importance of maintaining high-quality general radiology credentials is not lost to trainees, referring physicians, and reimbursers.

On a positive note, it was thought that the creation of specialists within radiology and the granting of specialty accreditation and certification would not create undue medicolegal exposure to generalists or lead to the obsolescence of generalists. Historically, specialization has not resulted in medicolegal problems, as exemplified in the internal medicine experience. Also, on the basis of the experience in internal medicine, as long as the demand for general services is sufficient, obsolescence should not be a problem.

The panel spent considerable time discussing the issue of credentialing and privileging in light of new JCAHO guidelines and standards. A consensus was not attained on how best to approach the problem. In one view, specialists who restricted their practices were considered at risk for losing privileges in areas not actively pursued. A countervailing viewpoint was that credentialing and privileging documents can be structured to accommodate a broad definition of "core" or "general" radiology and protect specialists from broad loss of privileges. A recurrent theme in the discussion was the desirability of maintaining a hybrid or blended practice so that specialists could maintain skills outside of the specific areas of interest.

Another issue not leading to consensus was the potential for competition within the field of radiology, between groups with and without a particular specialist. One point of view held that groups with expertise in a specialty might invade the turf or even the institutions of other groups not having that expertise. At the other end of the spectrum was the view that cross coverage between groups and the development of innovative affiliation arrangements could actually represent a solution to the need by small groups to provide increased specialization and expertise.

Implications: What Will Increased Specialization Require?

From the foregoing discussion, it is clear that the sanctioning of specialties through the RRC accreditation process and the subsequent development of certification testing by the

ABR are fundamental to the orderly evolution of specialization in radiology. This process is underway, and is guided by a superstructure of oversight organizations outside of radiology.

A major issue within the purview of radiology and its constituent organizations is the definition of residency and fellowship curricula. The panel entered into a spirited discussion of the 4-year radiology residency curriculum and its relationship to specialty training. Any future specialty certification will require 4 years of basic residency training in radiology, followed by 1 or more years of additional training in that specialty, before eligibility for specialty certification. With the exception of the 6-month requirement in nuclear medicine, the board does not currently have specific time requirements linked to individual specialties. On the other hand, the ABR is clearly concerned that some training programs are offering de facto 1-year fellowships or periods of focused training within the 4-year time frame. The consensus of the panel was that individual programs should be allowed to retain the greatest flexibility possible to fit the needs of individual departments, trainees, and regions of the country. Moreover, because radiology is in a dynamic era of change, it is not realistic to overlegislate the time required for training in each component. The panel believed that there is a significant need and even an obligation for the radiology RRC and the ABR to make clear statements regarding the degree of flexibility of training programs in establishing their curricula.

Conclusions and Recommendations

Specialization has become an important and pervasive part of radiology practice. Specialization has strengthened radiol-

ogy and should be regarded as a positive force and direction in the natural evolution of the field.

Specialization has aggravated the manpower shortage in radiology through the development of time-intensive highly specialized procedures and techniques. The American College of Radiology should continue to review manpower projections and consider what steps can be taken to increase radiology manpower. The alternative is the potential loss of areas of practice and shrinkage of the boundaries of radiology.

Retaining flexibility is a key factor in sustaining specialization in both academic and private practices. Radiology groups and individual radiologists should strongly consider how to retain general cross-coverage capability to guarantee timeliness of service and access and to address staffing shortages.

Credentialing and privileging strategies need to be refined to accommodate both specialists and generalists. Some areas, such as interventional radiology, may require new standards linked to experience, whether or not those standards include specification of actual numbers of cases for privileging and reprivileging.

Specialization promotes better care of patients. Innovative practice models should be developed and encouraged to provide access to the highest level of specialization possible. This may require collaboration between heretofore competing groups.

Training curricula must be developed for specialties and the relationship between residency training and fellowship training better defined. The ABR and the radiology RRC are encouraged to make policy statements to guide residency program directors in the structuring of the 4-year radiology residency curriculum. The most flexibility possible is highly desirable to allow programs to tailor their curricula to their own special circumstances and opportunities.

The reader's attention is directed to the commentary on this article, which appears on the following pages.

Commentary

Generalists vs Specialists: Time to Decide

John V. Forrest¹

In this issue, Thrall and Wittenberg [1] summarize the Radiology Summit discussions on subspecialization in diagnostic radiology. Changes in radiology in the past two decades have overwhelmed many radiologists and practices. Styles of radiologic practice, systems for accrediting programs, and training and certification of radiologists are still changing rapidly, and we will need to adapt further in the near future. Forums such as the Radiology Summit are an excellent way to identify the needs of our speciality, because all national radiology organizations must be involved in this process. It is particularly appropriate for the Association of University Radiologists and the American Board of Radiology (ABR) to help guide this evolution.

Two related problems are addressed in the report by Thrall and Wittenberg; these are already upon us and need to be addressed now.

The Difficulty in Achieving Competence in All of Diagnostic Radiology

The volume of new information is large, and the complexity of new technologies and procedures is increasing rapidly. I know of no radiologist who has not eliminated some aspect of imaging practice from his or her repertoire. Systems of training and certification now leave this to individual preference and specific practice needs after the board examination. Most board examiners would agree that passing a segment of the boards does not indicate an ability to practice at a high level of competency in that subspecialty. Thrall and Witten-

berg report that some of the summit participants foresee vascular/interventional radiology breaking off from the rest of the field as radiation oncology has done. Some groups and individuals have decided that this is a practical way to divide work responsibilities and to meet the obligation to keep current. It is now appropriate for training programs and the ABR to also consider a split into imaging- and procedure-oriented tracks, each of which would require greater depth of experience and knowledge in certain areas. Smaller practices may find it impossible to cover daily service and on-call needs with this division of responsibilities. However, individual radiologists will be much better able to develop and keep up the skills and information necessary to practice at a high level if they eliminate either interventional or advanced imaging.

The Need for Organ-Based Subspecialization in Radiology

More and more diagnostic radiologists are completing fellowships because of personal interest and increased need for expertise in certain areas. However, with the notable exception of neuroradiology, the large majority of fellowships offered and chosen are in technique-oriented fields: nuclear medicine, MR imaging, sonography, and interventional radiology. Another major subspecialty field, pediatric radiology, is not technique oriented but it is certainly not organ system oriented either.

At the summit, "the clear consensus was that the organ system approach is ultimately the most logical and strongest

This article is a commentary on the preceding article by Thrall and Wittenberg.

¹ Department of Radiology, Veterans Administration Medical Center (114) and University of California, School of Medicine, 3350 La Jolla Village Dr., San Diego, CA 92161. Address reprint requests to J. V. Forrest.

one." One reason for this approach was particularly well stated by a recent fellowship applicant (Tigges S, personal communication, January 1991):

On my first day of bone radiology as a resident, the chief of the service asked me what aspects of radiology I found stimulating. Among other things, I expressed an interest in a possible imaging fellowship. The chief smiled, took a sip from his ever present coffee mug and said: "I'm the best pneumoencephalographer in the department." His message was clear: methods of imaging change, but anatomy and pathology remain constant. Mastery of the anatomy and disease processes affecting a particular organ system facilitate image interpretation. Gaining expertise in a single method of imaging puts the imager into a tenuous position; the modality may become obsolete or be lost to another specialty. A thorough understanding of an organ system makes it much simpler to apply established and future imaging techniques to a clinical problem.

If we look at the distribution of fellowship positions, the programs offering fellowships and the radiology residents choosing them are obviously not in agreement with this position. This may reduce our ability to keep up with the needs of organ-oriented clinicians for clinical imaging and research.

Because the interests of residents, the needs of academic medical centers, and the marketplace have produced mainly technique-oriented fellowship programs, we seem to be at an impasse for developing organ system subspecialty radiologists. Changing the nature of most of our fellowship programs

or adding more training time will not be palatable or practical. I suggest as an alternative that we require each resident and each fellow to add an organ-based "major" area as part of residency and fellowship training that would be similar to a major area in undergraduate studies. This would not entail additional years of training for existing residencies or fellowships but, it is hoped, would produce radiologists who were interested and expert in various now neglected organ systems.

Requirements of this major could include extra time on appropriate services, regular attendance at subspecialty clinical conferences, a research or clinical paper, and extra board examinations in the subspecialty field for certification.

Major benefits could accrue from such a system: the ability of radiology to handle the needs of organ-based subspecialty colleagues would be enhanced, more residents might be attracted to academic careers as a way of participating most fully in the advances in their organ-based field, and the required research or clinical paper would also add to the body of knowledge in radiology.

Recognition of this training with appropriate certification by the ABR would be necessary in the long run. Initially, larger academic centers could start such programs to encourage research and academic careers. If this proved successful in developing radiologists who better meet the sophisticated needs of clinical colleagues, the ABR could add it as a requirement for certification.

REFERENCE

1. Thrall JH, Wittenberg J. Radiology summit 1990: specialization in radiology—trends, implications, and recommendations. *AJR* 1991;156: 1273-1276

Perspective

Teleradiology: Costs of Hardware and Communications

Samuel J. Dwyer III,¹ Arch W. Templeton, and Solomon Batnitzky

Teleradiology systems [1, 2] are a unique combination of digital data networks and computer systems. Their function is the electronic transmission of radiographs or radiologic images from one site to another. Teleradiology systems use wide area networks (WANs) to provide prompt interpretation of radiologic images for patients in underserved areas and in medical facilities having no full-time radiologists. These systems can improve emergency service coverage and integrate multihospital/clinic health care provider consortiums (i.e., health maintenance organizations).

Available teleradiology systems use a variety of hardware and communication systems. The hardware chosen for a teleradiology system is dependent on the type of images to be transmitted. The purpose of this article is to illustrate the hardware and wide area communication costs of a diagnostic teleradiology system.

Site Characteristics

The elements of a diagnostic teleradiology system are illustrated in Figure 1. Images to be transmitted may be radiographs or image data acquired from digitally formatted imaging techniques (CT, MR, nuclear medicine, sonography, digital subtraction angiography, and computed radiography). A laser film digitizer [3, 4] is used to convert the analog film into digital image data. The laser film digitizer (FD-2000, Du Pont, Wilmington, DE) digitizes a 14- by 17-in. (36- by 43-cm) film to 1682 × 2084 pixels by using a 210- μm pixel size. The pixel bit depth is 12 bits and the dynamic range is 0.01–3.50 optical film density. Transmission of the digital image data is accomplished by the WAN. A network access controller is

required for interfacing to the WAN. The network uses digital telephony technology for the transmission of digital data. These networks are a mixture of communication links consisting of circuit switching, packet/message switching, fiber-optics cables, or satellite links. The computer system at each site accomplishes the following: acquires and archives the digital image, displays and manipulates digital images [5], and controls the laser film digitizers/printers and the network access controller. The received digital image data are printed on a laser film printer and displayed on an interactive gray-scale work station [5].

We describe the following example: A teleradiology system is to be implemented by using a WAN connecting three hospital sites and an academic radiology department. The characteristics of each site are presented in Table 1. Two of the sites are military hospitals that use civilian contract radiology services. The third site is a private hospital located in a small community in an urban area and has one full-time staff radiologist. The radiology department of the state university medical center has 13 senior staff radiologists.

The sites on the network have decided to transmit 25% of their examinations to the radiology department of the state university medical center. Radiographs from special procedures will not be transmitted. Each site on the WAN will pay for its hardware, maintenance, and communication costs.

Hardware Costs

Sites on the teleradiology system use the DuPont laser film digitizer for digitizing 14- by 17-in. radiographic films (for purposes of calculations, this digital array size is assumed to

Received August 31, 1990; accepted after revision December 26, 1990.

¹ All authors: Department of Diagnostic Radiology, University of Kansas Medical Center, 39th and Rainbow Blvd., Kansas City, KS 66103. Address reprint requests to S. J. Dwyer III.

AJR 156:1279–1282, June 1991 0361-803X/91/1566-1279 © American Roentgen Ray Society

be 2 kilobytes \times 2 kilobytes \times 12 bits). These digital data are transmitted to the radiology department at the University of Kansas Medical Center, where they are recorded on 14- by 17-in. laser-sensitive film by a laser film printer (Digicam, Siemens Medical Systems, Iselin, NJ). Image data from CT, nuclear medicine, and sonography may be acquired for transmission by one of two methods. Multiformat film recordings may be digitized, transmitted, and printed by the laser film printer. Alternatively, the teleradiology system could be interfaced to each imaging method for acquisition and transmission of the digitally formatted image data. The transmitted digital image data are received and archived by the receiving computer system. The received digital image data are first

displayed on the interactive gray-scale display work station. The work station is used to establish optimum window/level settings for the laser film printer. The laser film-printed images are interpreted, and a typed consultation report is returned to the transmitting site. The work station is also used to enhance an image and transmit it to the original sending site. The work stations also may be used for two-way consultation on specific images. The hardware equipment required at each site and its costs are shown in Table 2.

The $N \times 56$ -kilobit/sec multiplexer (Digital Access, San Jose, CA) used at each site executes a dial-up of " N 56-kilobit/sec" switched lines. The user selects the desired value of N . The value of N may be selected as any integer from 1 to 24. If N equal to 1 is selected, then one 56-kilobit/sec switched line (digital service [DS] 1 0) will be established between the transmitting and receiving sites. If N equal to 24 is selected, then 24 56-kilobit/sec switched lines are established. The image data are then transmitted in parallel. The transmitting $N \times 56$ -kilobit/sec multiplexer encodes the image data into numbered Ethernet (Cross Com, Boston, MA) packets. These numbered packets are reassembled at the receiving site. This protocol solves the problem of switched path differences due to varying circuit switching route lengths.

Each site will purchase its required equipment on a prorated 3-year period (or 5-year period) and pay for equipment maintenance. This will cost the hospital/clinic sites \$84,933 per year for a 3-year period. After 3 years, only the maintenance cost of \$19,600 per year will be incurred. The radiology department at the state university medical center will pay for its required equipment at a cost of \$146,633 each year for 3 years. After 3 years, only the maintenance costs of \$34,300 per year will be incurred.

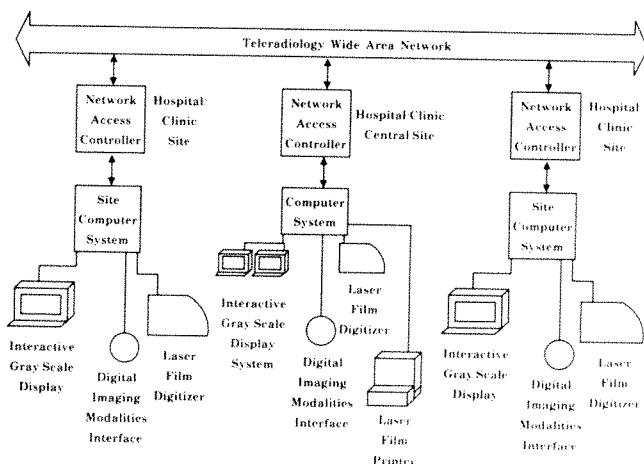


Fig. 1.—Elements of a diagnostic teleradiology system.

TABLE 1: Characteristics of Sites on Teleradiology Network

Sites on Teleradiology System	Active Hospital Beds at Each Site	Radiology Coverage at Site	No. of Radiologic Examinations per Day					
			Conventional Radiographs ^a	CT ^b	MR Imaging ^c	Nuclear Medicine ^d	Sonography ^e	Special Procedures ^f
State university medical center radiology department	475	13 Senior staff	500	34	17	62	24	10
Military hospital (48 miles from medical center)	50	Contract radiology (5 half days/week)	27	None	None	None	None	3
Military hospital (150 miles from medical center)	100	Contract radiology (1 radiologist 5 days/week)	66	8	None	7	12	7
Private hospital (168 miles from medical center)	84	1 Senior staff	82	4	None	2	10	2

^a An average of four film images/conventional radiographic examination; 2048 \times 2048 \times 12 bits/film image; 8.0 megabytes/image; 256 megabits/examination.

^b An average of 30 digital images per CT examination; 512 \times 512 \times 12 bits/image; 0.5 megabytes per CT image; 120 megabits/CT examination; three multiformat films/CT study.

^c An average of 50 digital images per MR examination; 256 \times 256 \times 12 bits; 0.13 megabytes per MR image; 52 megabits/MR examination; five multiformat films/MR study.

^d An average of 26 digital images per nuclear medicine examination; 128 \times 128 \times 8 bits; 0.016 megabytes per image; 3.3 megabits/nuclear medicine examination; three multiformat films/nuclear medicine study.

^e An average of 36 digital images per sonographic examination; 512 \times 512 \times 6 bits; 0.25 megabytes per image; 54 megabits/sonographic examination; four multiformat films/sonographic study.

^f An average of 12 archived images per special procedure; 1024 \times 1024 \times 8 bits; 1 megabyte per image; 96 megabits/special procedure examination; three multiformat films/special procedure.

TABLE 2: Hardware and Hardware Costs for Sites on Teleradiology Network

Sites	Estimated Hardware and Maintenance Costs
Hospitals/clinics	
Laser film digitizer	\$ 72,000
Interactive gray-scale display	38,000
Optical disk archiving	23,000
Site computer system	45,000
Network access controller	10,000
Maintenance costs (10% per year of hardware costs)	19,600
Total	\$207,600
State university medical center radiology department	
Laser film printer	\$ 78,000
Laser film digitizer	72,000
Optical disk archiving	50,000
Center computer system	55,000
Network access controller	10,000
Interactive gray-scale workstation	70,000
Maintenance costs (10% per year of hardware costs)	34,300
Total	\$369,300

Communication Costs

The teleradiology WAN is illustrated in Figure 2. To achieve a reasonable image throughput on the WAN, a DS-1 service (1.544-megabit signaling speed) was chosen. A mixture of local carrier service and long-haul carrier service (fiber-optics network) is required because of variability of available public service communications' equipment. Interfacing to the long-haul carrier's fiber-optics network (US Sprint, Atlanta, GA) is accomplished at points of presence. The remaining distances to each site are implemented by the local carrier providing access to DS-1 services. Communication costs consist of access charges and user charges. The access charges at each site for DS-1 service vary depending on the available digital equipment at the local carrier's central office exchange.

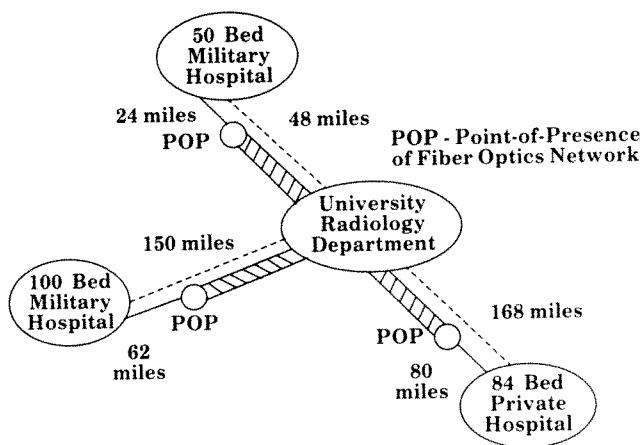


Fig. 2.—Teleradiology wide area network.

In Table 3, the communication costs are shown. Two types of WAN costs are presented. The dedicated point-to-point T1 carrier service (1.544-megabit signaling speed) is a fixed monthly cost no matter how much each link is used on the WAN. The $N \times 56$ kilobits is a dial-up, switched-line communication protocol. The access charges are the same as for T1 carrier service, but the usage charge is based only on the number of minutes used and not on the distance. Hence, if an N of 24 is selected, then DS-1 service is provided at \$0.06 per minute of use.

Discussion

The diagnostic teleradiology system is a film-to-film system. Each radiologic film is digitized at the transmitting site, transmitted on the WAN, and printed on a laser film recorder at the receiving site. The laser-printed film is placed on a standard light box for viewing and interpretation. The laser film digitizer generates a standard 2-kilobyte \times 2-kilobyte \times 12-bit digital array, but digital array sizes up to 4 kilobytes \times 5 kilobytes \times 12 bits are possible. The laser printer records a 4-kilobyte \times 5-kilobyte \times 12-bit digital array on laser-sensitive film. It uses interpolation methods to print a 2-kilobyte \times 2-kilobyte \times 12-bit digital image into a full-sized film.

The gray-scale work stations at each teleradiology site are used to review images that have been digitized or received. The digital images are archived by each site computer system for consultation and queuing if needed during transmission or reception.

The communication costs shown in Table 3 compare two distinct types of WANs. The T1 carrier service is a point-to-point link. The tariffs of this point-to-point service provide the 24-hr user with some cost benefits. The cost benefits of this point-to-point tariff are not realized unless it is fully utilized. The $N \times 56$ -kilobit WANs offer the casual user a dial-up configuration and user costs for actual transmission only. The $N \times 56$ -kilobit transmission controller establishes $N \times 56$ -kilobit switched circuits, routes the labeled packets of image data, and reassembles them at the receiving site. This parallel method of transmission makes the usage charges independent of the number of N switched circuits. User charges are based on cost per minute rather than cost per mile. It should be noted that the charges for T1 point-to-point and that of $N \times 56$ -kilobit/sec dial-up services are similar. However, the dial-up feature is preferable. Access charges are fixed at each site by the local exchange carrier's available digital telephony equipment.

The signaling speeds of DS-1 service (1.544 megabits) often differ by a factor of four or five from the actual throughput rates. A throughput rate is the actual time required to send and receive a digital image. Factors affecting throughput rates are the time used for the communications' protocols, computer image transfer times, and disk/memory transfer times. The use of higher digital signaling speed services would be desirable. However, such services as DS-3 (44.736 megabits) are unavailable outside of urban areas.

The availability of fiber-optic WANs will reduce the communications' costs of a teleradiology system. The bandwidths

TABLE 3: Communication Costs for Digital Service-1

Sites on Teleradiology System	No. of Examinations Transmitted per Day	No. of Images Transmitted per Day	Megabits Transmitted per Month ^a	Access Charges per Month ^b	T1 Carrier Costs/Month (Point to Point) ^c	N × 56-kilobit/sec Costs/Month (Dial-up) ^d
50-Bed military hospital 48 miles from UMC	7 (Conventional)	28	41,216	\$1700	\$3832	\$2583
100-Bed military hospital 150 miles from UMC	24 (2 CT, 2 NM, 3 sonography, 17 conventional)	288	109,480 (135,424)	354	3169	2700 (3253)
84-Bed private hospital 168 miles from UMC	25 (1 CT, 1 NM, 3 sonography, 20 conventional)	244	124,322 (144,256)	3500	6436	6164 (6591)

Note.—CT, nuclear medicine, and sonographic image data will be transmitted and recorded on a laser film printer. No special procedure images will be transmitted. All conventional screen-film radiographs will be digitized to 2 kilobytes × 2 kilobytes × 12 bits and transmitted on a laser film printer. UMC = university medical center; NM = nuclear medicine.

^a At 23 days/month × bits/image × images/day. Numbers in parentheses reflect digitizing multiformat films for CT, nuclear medicine, and sonography.

^b Vary depending on digital equipment provided by local carrier service.

^c At \$1810/month + \$6.70/mile + access charges/month.

^d Equals access charges/month + (tariff/min × 1 min/60 sec × 1 sec/56 kilobits × bits/month × 1.2), where tariff is \$0.06/min and 1.2 is protocol overhead. Costs in parentheses reflect those for digitizing multiformat films for CT, nuclear medicine, and sonography.

available with fiber-optic WANs enable widespread use of teleradiology systems.

REFERENCES

1. Gitlin JN. Teleradiology. *Radiol Clin North Am* 1986;24:55-68
2. Batnitzky S, Rosenthal SJ, Siegel EL, et al. Teleradiology: an assessment. *Radiology* 1990;177:11-17
3. Giger ML. Film digitization technical requirements. In: Peppler WW, Alter A, eds. *Proceedings of the chest imaging conference '87*. Madison, WI: Medical Physics, 1987:92-100
4. Seeley GW, Fajardo LL, Ker M, et al. Evaluation of the DuPont teleradiology system. *Proc SPIE* 1989;1093:106-108
5. Arenson RL, Chakraborty DP, Seshadri SB, Kundel HL. The digital imaging workstation. *Radiology* 1990;176:303-315

Perspective

Information Overload and Management in Radiology

William R. Hendee¹

The Problem

In the past two decades, medical imaging has experienced an unprecedented explosion in its capacity to generate information concerning patients. It is hard to imagine that only 20 years ago medical imaging was confined to radiography, fluoroscopy, static imaging with radiopharmaceuticals, and bistable sonographic systems. At that time the following imaging technologies were not present in the clinical arena: CT, gray-scale and real-time sonography, Doppler sonography, single-photon and positron-emission tomography, interventional angiography, digital subtraction angiography and digital radiography, and MR imaging. Rather primitive equipment was used routinely for mammography and angiography, and computers were viewed as a novelty for researchers rather than as integral components of imaging systems. In many ways the evolution of medical imaging from a craft into a science in the past two decades is the result of the integration of computers into the technology of imaging. Today, radiology is leading medicine into the modern era of information generation by computer-dominated electronic systems.

The ability of modern radiologists to generate information about patients is nothing short of spectacular, and the pivotal role of imaging services in patient care is a reflection of this ability.

Although growth in the production of radiologic information has been astounding, little has changed in the way that the information is managed and used in the clinical arena. Most physicians still request imaging studies on printed forms, and most radiologists still interpret the studies from hard-copy

images, usually on film. Studies are still stored in and retrieved from a hard-copy file room full of film folders and typed records. This approach to information management in radiology was seriously deficient 20 years ago; today it is a disaster. Twenty years ago, interpretive and consultative services in radiology were compromised by lost films and inefficient processes for retrieving and displaying radiologic information. Today, with many more studies of various types often performed in each patient and reduced tolerance of referring physicians and administrators for inefficiency and dalliance, traditional mechanisms for managing information in radiology are outmoded and unresponsive to the needs of patients and physicians [1].

The Solution

The challenge facing medical imaging today has been characterized well by Pattee [2] in his analysis of general systems theory: "As systems grow in size and complexity, they reach a limit where a new level of hierarchical control is necessary if they are to function reliably." This challenge can be met only by establishing a new approach to information management in medical imaging. This approach must increase the efficiency with which radiologists can store, retrieve, and interpret imaging data, and must improve their ability to provide consultative services to referring physicians in a timely fashion. The approach must be integrated within information networks that acquire imaging data in digital form and use computers to manage the transmission, display, and storage of the infor-

Received October 31, 1990; accepted after revision December 27, 1990.

Presented as the Charles C. and Mary Elizabeth Lovely Distinguished Visiting Professor Lecture for 1990 at the Health Science Center of the University of Tennessee, Memphis, October 1990.

¹ American Medical Association, 515 N. State St., Chicago, IL 60610. Address reprint requests to W. R. Hendee.

AJR 156:1283-1285, June 1991 0361-803X/91/1566-1283 © American Roentgen Ray Society

mation. Information networks for digital imaging data are called picture archiving and communications systems (PACS) or digital imaging networks. To achieve maximum usefulness, these networks should be interfaced with radiology information systems and hospital information systems to provide totally integrated, computer-based information networks for the display and analysis of information about patients. An integrated information network of this configuration is referred to as an information management, archiving, and communications system (IMACS).

Challenges of IMACS

The challenge of information overload and management in medical imaging today is addressable only by implementation of some type of IMACS in radiology services. These systems, however, present their own set of problems, including some that can be solved only by fundamental changes in the way radiologists work. Any institution contemplating an IMACS should carefully think through these problems and develop a well-structured strategy for their solution before embarking on an installation.

Cost

An IMACS is a major capital investment that is not directly reimbursable through additional fees levied for services rendered. Reimbursements for imaging studies are not increased simply because the studies are acquired and managed by an IMACS. An IMACS must be considered an up-front, nonreimbursable commitment made by the institution to improve patients' care, and not a technology that will yield a direct return on investment. This feature of an IMACS presents a major challenge to institutions already struggling with financial solvency. Most institutions should probably address this challenge by implementing an IMACS in stages, even though a staged approach may be somewhat more expensive in the long run.

Operation and Archival Storage

The operations of acquiring, storing, retrieving, selecting, viewing, interpreting, reporting, and transmitting images present major challenges for designers of IMACS work stations. Often, multiple images from each of several imaging technologies must be reviewed for analysis of a patient's condition, and the radiologist must be able to navigate conveniently among them for the purpose of selecting and studying those most useful in arriving at a diagnosis. The number and physical arrangement of video monitors needed in a work station, and the processes of storing and rapidly retrieving images for display on the monitors, are unresolved issues that currently are being examined in a number of institutions. Radiology departments and hospitals produce massive amounts of information about patients, and handling and presenting these data in an efficient and rapid manner challenge the capacity of information technologies currently available. Techniques to compress these data without loss of essential information are

being examined by several investigators in an effort to overcome some of the limitations of current technologies. These examinations include efforts to separate the essential from the esthetic properties of images, with the recognition that at least some images can be degraded in appearance without loss of information critical to the diagnosis of the patient's condition.

Interface Standards

Trying to connect different imaging devices and display modules into a PACS or an IMACS presents challenges that sometimes are almost insurmountable. These units often have unusual connection requirements for maintenance of signal fidelity, and their interface with a PACS network, and integration of the PACS with radiology and hospital information systems, can be a technical enigma. Several professional organizations and equipment vendors are working to develop standard input and output characteristics for IMACS components, but universal standards are not expected before the late 1990s. In the meantime, institutions usually must provide either in-house or consultant technical expertise to achieve a working system for information management.

Previous Records

A radiology facility is not simply a place where imaging studies are performed and interpreted. It also is a massive repository of films and records of previous studies that serve as a radiologic history of patients who have received health care at the institution. Transition of the facility to an IMACS must include consideration of the conversion of the existing repository to digital format. This conversion is both costly and disruptive. On the other hand, retention of the existing film file in analog form requires that the facility operate in both digital and analog mode for several years. The complexity of a parallel operation should not be underestimated. Most institutions planning an IMACS network extend the transition over a phase-in period of several years. Dual operation is a clumsy and costly process, but in most cases is preferable to a more rapid transition that requires substantial up-front expenditures and hasty conversion of the existing film file into digital form.

Soft-Copy Viewing

Radiologists are accustomed to interpreting images from hard-copy (film) images. Referring physicians are also comfortable viewing images on film. Adjusting to soft-copy (video) images for analysis and interpretation is not easy, as demonstrated by the continued reliance on film images for interpreting digital studies such as CT and MR imaging. This reliance is often justified by criticism of the spatial resolution and other characteristics of video monitors, with the implication that film images are required to ensure that essential information is not overlooked in the interpretation. New video monitors with 2000- by 2000-pixel spatial resolution and 12-bit intensity resolution provide improved spatial and contrast

fidelity. These monitors promise to overcome many of the limitations of earlier video display units and to remove their shortcomings as an excuse for continued dependence on film images. Nevertheless, work habits and existing prejudices will continue to impede the adoption of video images for critical interpretation, and the transition to complete soft-copy viewing and analysis probably will require several years in even the most progressive radiology facilities.

Turf Disputes

Imaging procedures increasingly are being viewed by non-radiology specialties as potentially lucrative services to be exploited for revenue generation. Installation of an IMACS is likely to enhance this interest, because an IMACS facilitates transmission of images directly to clinical specialists for interpretation. An IMACS has the potential, in fact, to convert a radiology operation from a consultative medical discipline to a laboratory service that conducts patient studies and produces medical images for transmission to nonradiologists for interpretation. The threat of malpractice suits arising from missed diagnoses and the cost of liability insurance to protect against such suits are deterrents to nonradiologists' interpreting IMACS-supplied images. However, the superior interpretive skills of radiologists are their major protection against loss of professional stature. These skills should be reinforced by frequent demonstration of the diagnostic acumen of radiologists in conferences and papers directed to nonradiologists.

Real-Time Radiology

Most radiology departments strive to provide reports to clinicians within a prescribed time (usually 24–72 hr) after an imaging study has been performed. In some cases, an immediate consultation can be obtained, but such requests are disruptive to departmental routine and usually are discouraged except for emergencies. Often film images are available to the referring physician well before the radiologist's report. Not infrequently, the referring physician acts on his or her own review of the images without waiting for the report. With a PACS or IMACS, images will be available to referring physicians even more quickly and conveniently, and nonradiologists will be even more tempted to interpret them without input from radiologists. To counter this temptation, radiologists will need to provide their interpretations in a more rapid and responsive manner. In fact, radiologists may be required to function in an on-line, real-time fashion with respect to decisions affecting patient care, rather than in their present manner as an off-line, batch-mode processing operation. Whether or not radiology will be able (or willing) to function as a real-time operation remains to be seen. One incentive for conceding to these new demands could be the growing reluctance of third-party carriers to reimburse for image interpretations delivered too late to affect decisions concerning patient care.

Redirection of Radiologic Focus

Radiologists have long been torn between a fascination with the technologies of imaging and a dedication to the use of the technologies to enhance the care of patients. This struggle for the energy and intellect of radiologists has been particularly intense over the past two decades as exceedingly complex technologies have entered the arena of medical imaging. The consequence has been a focus on the inward-directed interests of radiologists toward the technology of imaging and a resulting decline in the attention of radiologists to outward-directed interests encompassing their interaction with referring physicians and patients [3]. One major advantage of an IMACS is its potential for providing greater automation and control over the technology of acquiring and handling radiologic information. Realization of this potential should permit radiologists to focus more directly on the needs of referring physicians for attentive and timely radiologic consultations and on the needs of patients for radiologic procedures administered as compassionately and pleasantly as possible.

Conclusions

Shannon [4] has emphasized that

If complexity is not conquered by the discovery of organizing principles that restore simplicity, [and] if the power to integrate the multitude of professional and administrative fragments into a cohesive service entity is not developed, medicine will reorganize in some unexpected way that will likely dramatically alter and degrade its character.

This statement is particularly relevant to the discipline of medical imaging, where the complexity is profound and the fragments are multitudinous and diffuse. An IMACS offers opportunities to apply organizing principles to the discipline that reduce the complexity and integrate the fragments into a cohesive entity. These systems present their own challenges, however, including technical and economic hurdles as well as substantial changes in the way radiologists go about their work. If these challenges can be surmounted, an IMACS offers tremendous opportunities to restore medical imaging to a predominantly consultative and patient-oriented medical service.

REFERENCES

1. Hendee WR. You can't drink and whistle at the same time. *J Digital Imaging* 1990;3:5-9
2. Pattee H. *Hierarchy theory: the challenge of complex systems*. New York: George Braziller, 1973
3. Greenes R. The radiologist as clinical activist: a time to focus outward. In: Mun S, Greberman M, Hendee W, Shannon R, eds. *Information management and communication in patient care*. Los Alamitos, CA: IEEE Computer Society Press, 1990:136-140
4. Shannon R. IMACS and radiology: defining the problems. In: Mun S, Greberman M, Hendee W, Shannon R, eds. *Information management and communication in patient care*. Los Alamitos, CA: IEEE Computer Society Press, 1990:45-53

Forthcoming Articles

REVIEW ARTICLE

Review article. Oriental cholangiohepatitis: pathologic, clinical, and radiologic features. *Lim JH*

CARDIOPULMONARY RADIOLOGY

Right and left ventricular stroke volume measurements with velocity-encoded cine MR imaging: *in vitro* and *in vivo* validation. *Kondo C, Caputo GR, Semelka R, Foster E, Shimakawa A, Higgins CB*

Case report. Traumatic rupture of the diaphragm without visceral herniation: CT diagnosis. *Holland DG, Quint LE*

Case report. Delayed appearance of localized pericardial effusion after cardiac surgery. *Miyake H, Iwanaga S, Suzuki K, et al.*

BREAST RADIOLOGY

The prevalence of carcinoma in palpable vs nonpalpable mammographically detected breast lesions. *Bassett LW, Liu T-H, Giuliano AE, Gold RH*

Lobular carcinoma *in situ* of the breast: clinical, pathologic, and mammographic features. *Beute BJ, Kalisher L, Hutter RVP*

Radiographic density of nonfatty, noncalcified breast masses on mammography: value in differential diagnosis. *Jackson VP, Dines KA, Bassett LW, Gold RH, Reynolds HE*

GASTROINTESTINAL RADIOLOGY

Obstructive extrahepatic recipient and donor bile duct dilatation complicating orthotopic liver transplantation: imaging and laboratory findings. *Miller WJ, Campbell WL, Zajko AB, et al.*

Thin layer chromatography used to monitor cholesterol gallstone dissolution by methyl tert-butyl ether. *D'Agostino HB, van Sonnenberg E, Schteingart CD, Hofmann AF, Casola G, Mathieson JR*

Intraperitoneal contrast material improves the CT detection of peritoneal metastases. *Halvorsen RA Jr, Panushka C, Oakley GJ, Letourneau JG, Adcock LL*

Afferent loop syndrome: sonographic findings in seven cases. *Lee DH, Lim JH, Ko YT*

Case report. Intramural and intraperitoneal hemorrhage due to duodenal ulcer. *Radin DR*

Case report. Aortoenteric fistula manifested as an intramural duodenal hematoma. *Zeppa MA, Forrest JV*

GENITOURINARY RADIOLOGY

Radiocontrast-associated renal dysfunction: incidence and risk factors. *Lautin EM, Freeman NJ, Schoenfeld AH, et al.*

Radiocontrast-associated renal dysfunction: a comparison of low-osmolality and conventional high-osmolality contrast media. *Lautin EM, Freeman NJ, Schoenfeld AH, et al.*

Commentary. The evaluation of contrast-related renal failure. *Bettmann MA*

Urinary tract calculi that form on surgical staples: a characteristic radiologic appearance. *Dangman BC, Lebowitz RL*

Ureteral pseudodiverticula: frequent association with uroepithelial malignancy. *Wasserman NF, Zhang G, Posalaky IP, Reddy PK*

Sonographic imaging of the cervix during the third trimester of pregnancy: value of the transperineal approach. *Hertzberg BS, Bowie JD, Weber TM, Carroll BA, Kliewer MA, Jordan SG*

Organic vs functional obstruction of the fallopian tubes: differentiation with prostaglandin antagonist and beta 2 agonist-mediated hysterosalpingography and selective ostial salpingography. *Lang EK*

MUSCULOSKELETAL RADIOLOGY

MR examination of the knee: interpretation with multiscreen digital workstation vs hardcopy format. *Brown JJ, Malchow S, Totty WG, et al.*

Effect of radiation therapy on thoracic and lumbar bone marrow: evaluation with MR imaging. *Yankelevitz DF, Henschke CI, Knapp PH, Nisce L, Yi Y, Cahill P*

Pictorial essay. Normal and degenerated intervertebral disk: *in vivo* and *in vitro* MR imaging with histopathologic correlation. *Schiebler ML, Grenier N, Fallon M, Camerino V, Zlatkin M, Kressel HY*

Overall body fat and regional fat distribution in young women: quantification by using MR imaging. *Gerard EL, Snow RC, Kennedy DN, et al.*

Unidirectional joint communications in wrist arthrography: an evaluation of 250 cases. *Wilson AJ, Gilula LA, Mann FA*

PEDIATRIC RADIOLOGY

Safety belt injuries in children with lap-belt ecchymosis: CT findings in 61 patients. *Savit CJ, Taylor GA, Newman KD, et al.*

A simplified sonographic approach for measuring spleen size in infants and children. *Rosenberg HK, Markowitz RI, Kolberg H, Park C, Hubbard A, Bellah RD*

NEURORADIOLOGY

MR imaging of the brain in patients with diabetes insipidus. *Tien R, Kucharczyk J, Kucharczyk W*

MR imaging of intracerebral blood: diversity in temporal pattern at 0.5 and 1.0 T. *Zyed A, Hayman LA, Bryan RN*

Dural sinus occlusion: evaluation with phase-sensitive gradient-echo MR imaging. *Tsuruda JS, Shimakawa A, Pelc NJ, Saloner D*

Pictorial essay. Differential diagnosis of head and neck lesions based on their site of origin. Part I: The suprathyroid part of the neck. *Harnsberger HR, Osborn AG*

Pictorial essay. Differential diagnosis of head and neck lesions based on their space of origin. Part II. The infrathyroid portion of the neck. *Smoker WRK, Harnsberger HR*

The radiologic evaluation of the normal and diseased posterior cervical space. *Parker GD, Harnsberger HR*

VASCULAR AND INTERVENTIONAL RADIOLOGY

Stenoses of vascular anastomoses after hepatic transplantation: treatment with balloon angioplasty. *Raby N, Karani J, Thomas S, O'Grady J, Williams R*

Randomized double-blind trial of midazolam/placebo and midazolam/fentanyl for sedation and analgesia in lower extremity angiography. *Cragg AH, Smith TP, Berbaum KS, Nakagawa N*

Case report. Spontaneous fracture of a vena tech inferior vena caval filter. *Awh MH, Taylor FC, Lu C-T*

Technical note: Preoperative CT-guided percutaneous localization of small masses with a Kopans needle. *Finch IJ*

DIGITAL IMAGING

Pictorial essay. Artifacts in computed radiography. *Solomon SL, Jost RG, Glazer HS, Sagel SS, Anderson DJ, Molina PL*

MEETING NEWS

Meeting news. The Society of Gastrointestinal Radiologists: 20th annual meeting, February 1991. *Whalen E*

ARRS Case of the Day

The correct diagnoses or "answers" for the Case of the Day series presented at the recent ARRS meeting in Boston and previewed in the April issue of the *AJR* are given on the following pages. For each case, the images are repeated, and occasionally a few additional images are presented along with a description of the radiologic findings and a brief discussion of the abnormality or disease. The cases are current from the daily teaching conferences of the Boston University Medical Center, Department of Radiology, and they were prepared by members of the resident staff. Several of the cases prepared had been slated for submission for publication as case reports but the residents and staff graciously agreed instead to permit their use as ARRS Cases of the Day. The most credit, however, should go to our chief resident, David Eschelman, who organized, edited, and facilitated the entire task with minimal advice and mainly encouragement from me. The cases represent a wide range of abnormalities, and I hope that they have been of interest to those attending the meeting and to the readership of the *AJR*. Congratulations are in order for those who succeeded in making correct diagnoses.

I thank Robert N. Berk and the editorial staff of the *AJR* for their cooperation, help, and encouragement in preparing these cases for publication. Jerome T. Glickman, director of the Department of Educational Media of Boston University School of Medicine, provided extensive consultation in the preparation of the exhibit format and panels for the meeting. I appreciate the images provided by Elsie Levin and Norman Sadowsky, Sagoff Breast Center of the Faulkner Hospital, Boston, MA, in addition to other complementary studies from Philip Arena, Brockton Hospital, Brockton, MA, and Roy Strand, Children's Hospital, Boston, MA.

Last, but not least, I thank John A. Kirkpatrick, Jr., president, for the invitation to participate in this most important function.

John F. O'Connor
Department of Radiology
Boston University Medical Center
Boston, MA



General Diagnosis Case of the Day

David J. Eschelman,¹ Ellen Panageas, Max P. Rosen, Laura Vitale Romo, and John F. O'Connor

Case 1: Aneurysm of the Ductus Arteriosus

A large mediastinal mass was discovered on the chest radiograph (Figs. 1A and 1B) of a 73-year-old man with well-controlled hypertension. Several faint, curvilinear calcifications were noted in the lateral margin of the mass. The superior border of the mass appeared to abut the aorta. Chest CT (Figs. 1C and 1D) showed that the enhancing mass originated from the inferior aspect of the aortic arch and extended inferiorly, adjacent to the ascending aorta, to the level of the main pulmonary artery. Aortography (Figs. 1E and 1F) was performed 6 months later after chest radiographs (not shown) revealed enlargement of the mass. Aortography showed the 1-cm neck of the aneurysm arising from the inferior surface of this tortuous atherosclerotic aorta, just distal to the left subclavian artery. The remainder of the aneurysm did not opacify because of thrombosis that had occurred since the CT scan was obtained. The patient underwent resection of the 8 × 6 × 6 cm aneurysm of the ductus arteriosus, and the aorta was repaired with a Dacron patch graft.

Aneurysm of the ductus arteriosus is a rare entity in adults, with fewer than 25 cases reported in the literature. The ductus arteriosus is a short tubular connection between the left pulmonary artery and aorta. A remnant of the left sixth aortic arch, it normally undergoes physiologic closure soon after birth, but complete anatomic obliteration requires up to 12 weeks. Aneurysms within the ductus arteriosus usually result from incomplete closure. In the few reports of aneurysms involving a patent ductus arteriosus in adults, it is uncertain whether the ductus arteriosus recanalized or original patency persisted [1].

Normal closure of the ductus arteriosus begins before birth and proceeds from the pulmonary artery to the aortic end. Through a complex process of intimal thickening, endothelial invagination, smooth-muscle cell migration, and hyaluronic acid production, closure of this muscular artery is achieved [2]. When closure is incomplete, the pulmonary side closes and the aortic side remains patent. This may result from increased amounts of elastic tissue within the ductus arteriosus. Therefore, the ductus arteriosus resembles an elastic artery such as the aorta rather than a muscular artery [3]. In addition, low levels of hyaluronic acid have been associated with faulty closure [2]. Patency of the aortic side of the ductus

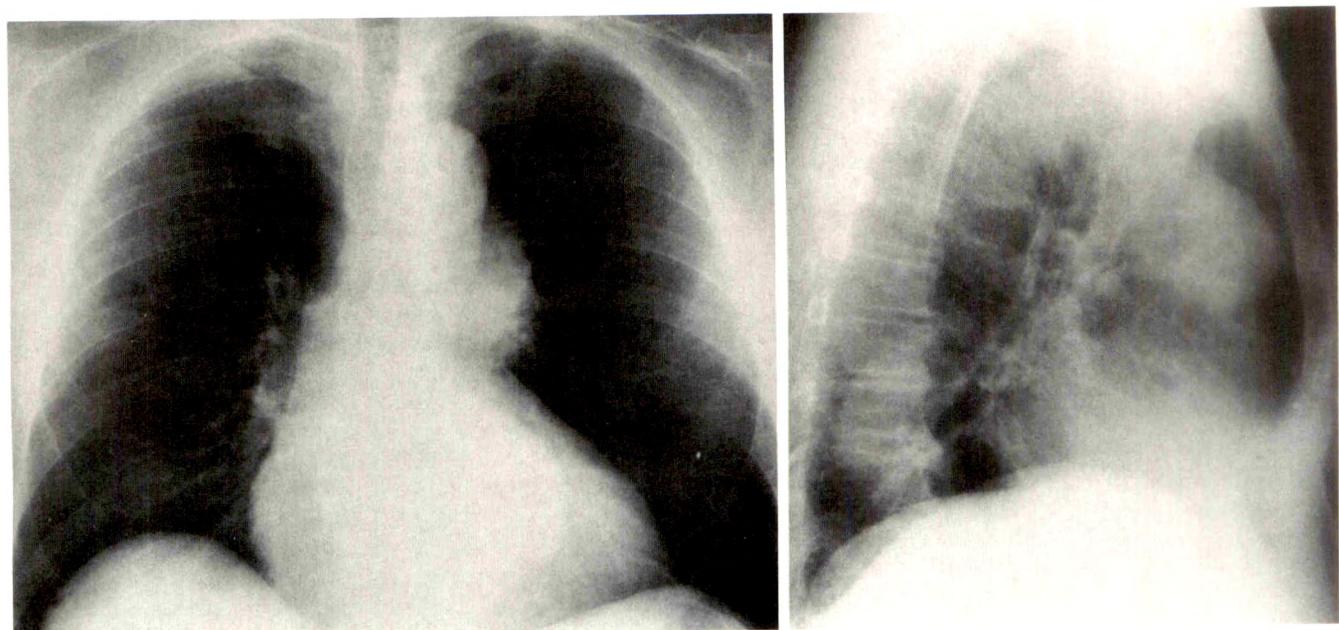
arteriosus allows exposure to the high systemic pressure within the aorta with subsequent dilatation and aneurysm formation [3, 4]. Some note that many adults with ductus arteriosus aneurysms are hypertensive [5, 6].

Clinically, most signs are related to mass effects. Dyspnea, cough, and transient or persistent dysphonia due to compression of the left recurrent laryngeal nerve are the most common [1, 7]. However, in a review of 21 cases, an abnormal chest radiograph was the most common reason for further investigation [5]. Complications such as rupture, dissection, distal embolization, and hemorrhage from fistulous connection to the esophagus or bronchus have been described [1, 7]. The average diameter is 5 cm, with one aneurysm as large as 8 × 11 cm reported [5].

On chest radiographs, the ductus arteriosus aneurysm may be perceived as a change in the contour of the aortic arch or aortopulmonary window. Although adenopathy, neoplasms, or aneurysms related to the aorta itself are certainly more common masses at this site, Danza et al. [7] suggest two radiographic features indicative of a ductus arteriosus aneurysm. These signs are parietal calcification at the periphery of the lesion and/or mottled calcification at the aortic side of the mass in addition to a small pedicle linking the lesion to the pulmonary artery. This pedicle may be obscured with large aneurysms. CT will show the relationship of the aneurysm to the aortic arch and pulmonary artery, while possibly revealing calcifications not detected by plain radiographs. The diameter of the lesion and presence of mural thrombus also will be identified. Angiography is highly specific, showing the neck of the aneurysm just distal to the origin of the left subclavian artery [1, 4, 7]. Unlike true aneurysms of the aortic arch or false aneurysms resulting from trauma or prior aortic dissection, ductus arteriosus aneurysms are saccular, have a narrowed neck at the aortic orifice, and lack severe atheromatous change [5].

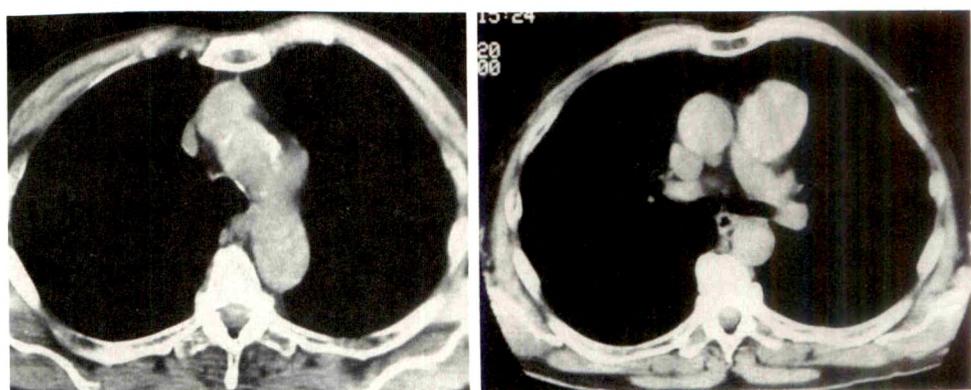
Although rare, ductus arteriosus aneurysms require consideration in the differential diagnosis of mediastinal masses because they have a 60% fatality rate due to complications. Criteria for resection include lesions greater than 3 cm in diameter, symptomatic aneurysms, and any that show progressive enlargement. It has been suggested that enlargement is not a finite process; therefore, any ductus arteriosus

¹ All authors: Department of Radiology, Boston University Medical Center, 88 E. Newton St., Boston, MA 02118. Address reprint requests to J. F. O'Connor.
AJR 156:1288–1294, June 1991 0361-803X/91/1566-1288 © American Roentgen Ray Society



A

B



C

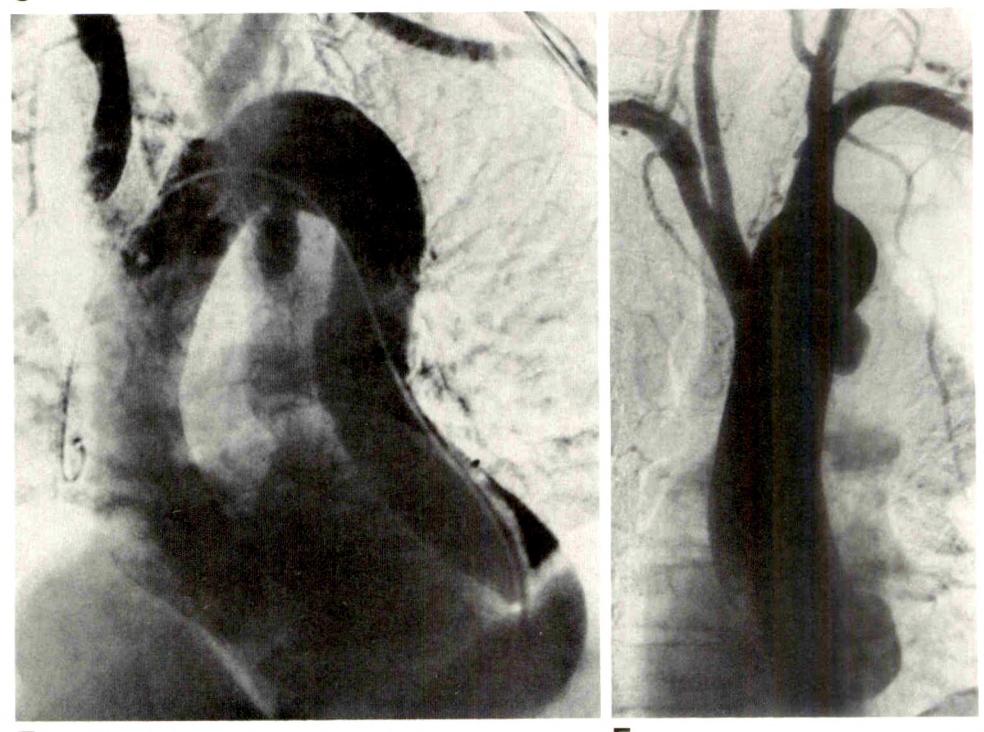
D

Fig. 1.—Case 1: Aneurysm of ductus arteriosus.

A and **B**, Posteroanterior (**A**) and lateral (**B**) chest radiographs show a mediastinal mass in aortopulmonary window, which appears to abut aorta on lateral radiograph. Several thin, curvilinear calcifications are seen in lateral border of this mass.

C and **D**, Axial CT scans at level of aortic arch (**C**, unenhanced) and carina (**D**, enhanced). Neck of aneurysm arises from inferior aspect of aortic arch. Enhancing $8 \times 6 \times 6$ cm aneurysm extends inferiorly, adjacent to ascending aorta, to level of main pulmonary artery.

E and **F**, Subtracted left anterior oblique (**E**) and anteroposterior (**F**) projections from aortogram show 1-cm neck of aneurysm arising from inferior aspect of aortic arch, just distal to origin of left subclavian artery. This examination was performed 6 months after CT scanning, during which time thrombus formed within aneurysm. A large soft-tissue mass corresponding to aneurysm is seen on anteroposterior projection lateral to neck of aneurysm in aortopulmonary window. Remainder of aorta is tortuous and atherosclerotic with ulcerating plaque.



E

F

aneurysms, regardless of size or symptoms, should be removed [1, 5].

Laura Vitale Romo
David J. Eschelman

REFERENCES

- Traughber PD, Wojtowycz MM, Karwande SV, et al. Roentgenologic CPC: enlarging mediastinal mass. *Invest Radiol* 1987;22:240-243
- DeReeder EG, Girard N, Poelmann RE, Van Munsteren JC, Patterson DF, Gittenberger-De Groot AC. Hyaluronic acid accumulation and endothelial cell detachment in intimal thickening of the vessel wall: the normal and genetically defective ductus arteriosus. *Am J Pathol* 1988;132:574-585
- Gittenberger-De Groot AC. Persistent ductus arteriosus: most probably a primary congenital malformation. *Br Heart J* 1977;39:610-618
- Cohen BA, Efremidis SC, Dan SJ, Robinson B, Rabinowitz JG. Aneurysm of the ducts arteriosus in an adult. *J Comput Assist Tomogr* 1981;5: 421-423
- Mitchell RS, Seifert FC, Miller DC, Jamieson SW, Shumway NE. Aneurysm of the diverticulum of the ductus arteriosus in the adult: successful surgical treatment in five patients and review of the literature. *J Thorac Cardiovasc Surg* 1983;86:400-408
- Borow KM, Hessel SJ, Sloss LJ. Fistulous aneurysm of ductus arteriosus. *Br Heart J* 1981;45:467-470
- Danza FM, Fusco A, Breda M, Bock E, Lemmo G, Colavita N. Ductus arteriosus aneurysm in an adult. *AJR* 1984;143:131-133

Case 2: Intranodal Gold Deposits in Woman with Rheumatoid Arthritis

A 45-year-old woman with a long history of chrysotherapy for rheumatoid arthritis had screening mammography. Routine mediolateral oblique views (Figs. 2A and 2B) revealed innumerable punctate densities in several axillary lymph nodes on both sides. A magnification view (Fig. 2C) showed the fine, intranodal, linear and punctate densities.

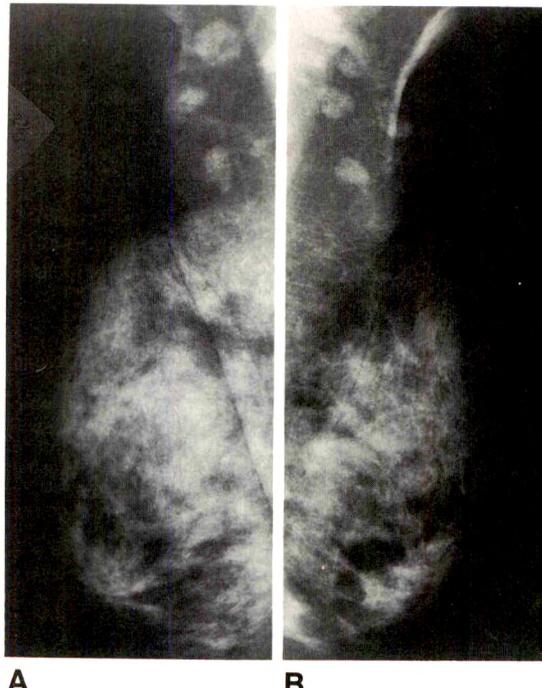


Fig. 2.—Case 2: Intranodal gold deposits in woman with rheumatoid arthritis.
A and B, Bilateral mediolateral oblique mammograms reveal fine, punctate densities in several axillary lymph nodes.

C, Intranodal gold deposits from prolonged chrysotherapy are revealed as multiple, irregular, linear and punctate metallic densities on this magnification compression view.



The initial appearance of breast carcinoma as dense intranodal microcalcifications is exceptionally rare. However, Bruwer et al. [1] have described this appearance of punctate intranodal densities in patients receiving intramuscular gold injections for rheumatoid arthritis. Gold therapy may be very effective for active rheumatoid arthritis, possibly delaying or preventing the progression of erosions in some patients [2]. Although approximately half of the injected gold is eliminated via urine and stool, the rest remains in the body, often for years after therapy is stopped. Organs retaining the highest concentrations of injected gold are lymph nodes, adrenal glands, liver, kidneys, bone marrow, and spleen [1].

David J. Eschelman

REFERENCES

- Bruwer A, Nelson GW, Spark RP. Punctate intranodal gold deposits simulating microcalcifications on mammograms. *Radiology* 1987;163: 87-88
- Abramowicz M, ed. Drugs for rheumatoid arthritis. *Med Lett Drugs Ther* 1989;31:61-64

Case 3: Giant-Cell Tumor of the Temporal Bone

A 25-year-old man came to the emergency department with swelling on the right side of his head that had progressed for several months. He denied any history of trauma.

A lateral skull radiograph (Fig. 3A) showed an expansile, lytic lesion involving the temporal bone. An unenhanced CT scan of the head at soft-tissue window settings showed that the central portion of the lesion contained heterogeneous soft tissue and calcifications (Fig. 3B). Images filmed at bone

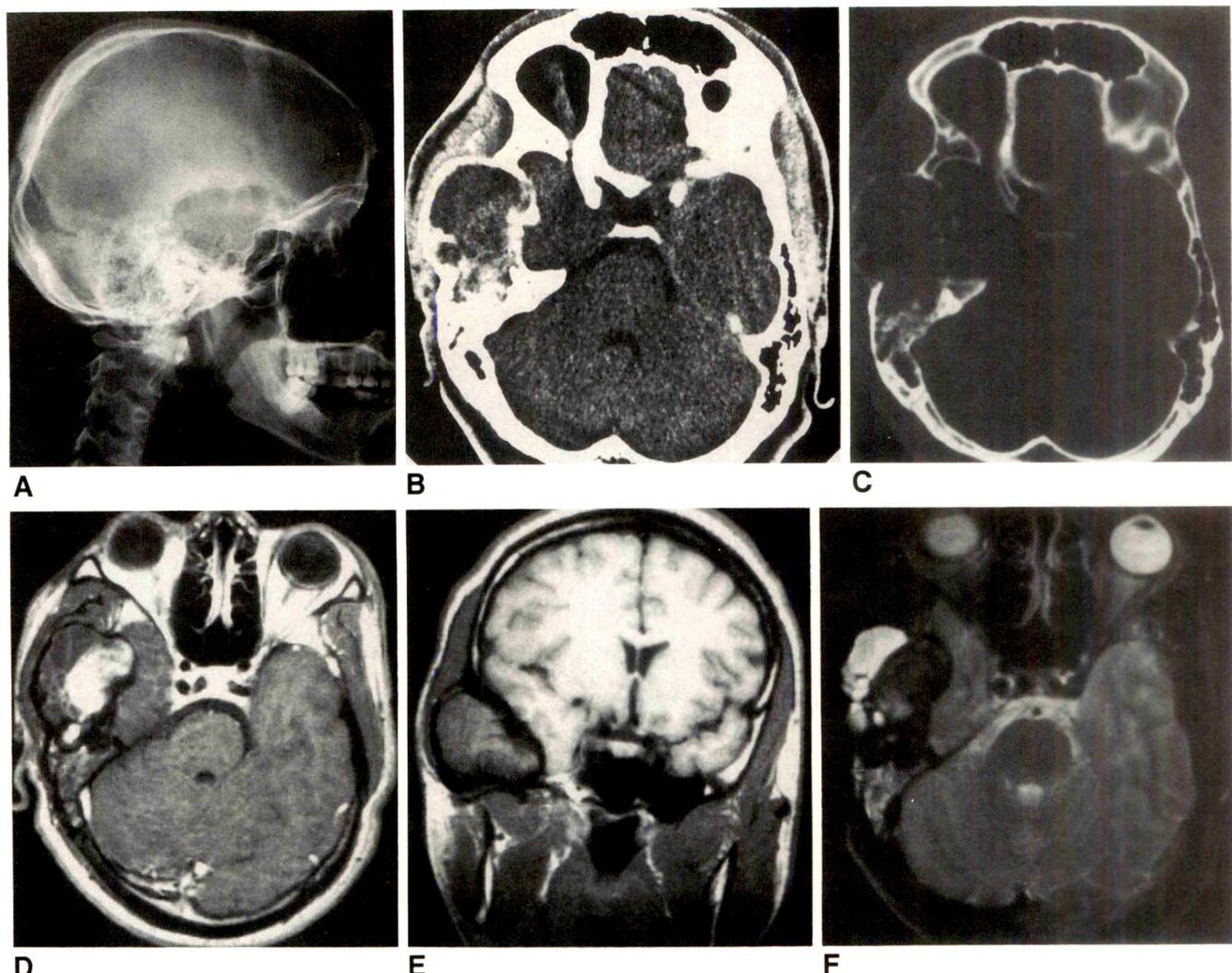


Fig. 3.—Case 3: Giant-cell tumor of the temporal bone.

A, Lateral skull radiograph shows an expansile, lytic lesion involving temporal bone.

B, Axial unenhanced CT scan of head obtained with soft-tissue window settings shows that center of lesion contains heterogeneous soft tissue and calcifications.

C, Axial unenhanced CT scan of head obtained with bone windows shows that lesion has greatly expanded diploic space. Lesion extends into anterior portion of petrous bone.

D, Axial T1-weighted (500/15) MR image of head after IV administration of gadopentetate dimeglumine shows lesion is composed of two distinct tissues. When compared with unenhanced T1-weighted image (E), medial portion enhances, consistent with a solid component. Outer portion, which contains septa but does not enhance, is suggestive of a cystic component.

E, Coronal T1-weighted (560/15) unenhanced MR image of head shows encroachment of diploic space at base of skull, compression of temporal lobe, and distortion of middle cranial fossa.

F, Axial T2-weighted (3000/90) MR image of head shows bright signal from outer aspect of lesion, which confirms presence of a lateral cystic component. Signal from inner portion of lesion is dark, consistent with a solid component.

windows showed that the lesion had greatly expanded the diploic space and that the lesion extended into the anterior portion of the petrous bone (Fig. 3C). MR images of the head were then obtained. After IV administration of gadopentetate dimeglumine, T1-weighted (500/15) axial MR images showed that the lesion was composed of two distinct tissues (Fig. 3D). When compared with unenhanced T1-weighted images (Fig. 3E), the medial portion enhanced, which was consistent with a solid component. The lateral portion, which contained septa but did not enhance, was suggestive of a cystic component. Axial T2-weighted (3000/90) MR images (Fig. 3F)

showed bright signal from the outer aspect of the lesion, which confirmed the presence of a lateral cystic component. The signal from the inner portion of the lesion was dark, consistent with a solid component.

Giant-cell tumors classically involve long tubular bones, occur in the third to fourth decades, and have a high (40–60%) recurrence rate after resection. Malignant degeneration may occur, especially after radiation therapy [1].

The giant-cell reparative granuloma, a separate clinicopathologic entity, has been described and may have an identical radiologic appearance. This entity is a reactive granulomatous

process in response to intraosseous hemorrhage or inflammation. Often a history of trauma can be elicited. This lesion most commonly involves the mandible and maxilla and occurs in the first and second decades. The course is always benign. Curettage is usually the only treatment needed. Recurrence is extremely rare [1, 2].

Both giant-cell tumors and giant-cell reparative granulomas have been reported in the temporal bone. Pathologic differentiation between these two entities is often very difficult and depends on the local distribution and shape of the giant cells, the presence or absence of hemosiderin and osteoid, and the shape of the stromal fibroblasts [2].

By 1974 there had been 23 reported cases of giant-cell tumor of the temporal bone. In 1974 all cases were reviewed, and 18 of the 23 cases were reclassified as giant-cell reparative granulomas [2]. Between 1980 and 1990, several published cases of similar lesions [3-9] have been reported as giant-cell tumors.

Max P. Rosen

REFERENCES

- Resnick D, Kyriakos M, Gleenway GD. In: Resnick D, Naiwayama G, eds. *Diagnosis of bone and joint disorders*, 2nd ed. Philadelphia: Saunders, 1988:3757-3776
- Hirschi S, Katz A. Giant cell reparative granuloma outside the jaw bone. *Hum Pathol* 1975;5:171-181
- Cook HF, Miller R, Yamada R. Giant cell tumor of the infratemporal fossa: report of case. *J Oral Maxillofac Surg* 1986;44:651-656
- Wilbur AC, Choi KH, Tan WS, Jafar JJ, Spigos DG. Giant cell tumor of the sphenoid bone mimicking a pituitary tumor. *AJNR* 1986;7:361-362
- Kiwit JCW, Schober R, Nicola N, Schirmer M, Wechsler W. Osteoclastomas of the petrous bone. *Surg Neurol* 1986;26:59-62
- Carmody RF, Rickles DJ, Johnson SF. Giant cell tumor of the sphenoid bone. *J Comput Assist Tomogr* 1983;7:370-373
- Tandon DA, Deka RC, Chaudhary C, Misra NK. Giant cell tumor of the temporosphenoidal region. *J Laryngol Otol* 1988;102:449-451
- Findlay JM, Chiasson D, Hudson AR, Chuli M. Giant cell tumor of the middle cranial fossa. *J Neurosurg* 1987;66:924-928
- Henderson BTH, Whitwell H. Giant cell tumor of the skull: case report. *Neurosurgery* 1988;23:120-122

Case 4: Primary Retroperitoneal Teratoma

This previously healthy 25-year-old woman had persistent lower back pain for 2 months after a motor vehicle accident. MR images (Figs. 4A and 4B) showed a right-sided retroperitoneal mass with signal intensities corresponding to fat, calcium, and soft-tissue components. The sonographic study (Figs. 4C and 4D) showed a solid suprarenal tumor containing a hyperechoic region consistent with fat and a heterogeneous region with focal calcifications. To better evaluate these tissue elements, CT was performed (Fig. 4E), verifying the large adipose component as well as the calcified and soft-tissue areas in this well-encapsulated tumor. At surgery, the right adrenal gland was found to be normal and the retroperitoneal mass was completely resected. Pathologic examination of the specimen revealed a mature retroperitoneal teratoma (Fig. 4F).

Primary retroperitoneal teratomas are rare, representing 5-10% of primary retroperitoneal tumors [1]. The mean age of

patients ranges between 13 and 16 years, with cases reported in a fetus and in patients up to 82 years old [2-4]. Fewer than 10-20% occur after the age of 30 years, with 43-55% diagnosed in the first decade of life [4]. Most authors have reported a higher prevalence among females.

Teratomas derive from germ cells that failed to migrate to normal gonadal locations. Germ cells are totipotential, undergoing variable differentiation into tissue components that represent derivatives of ectoderm, mesoderm, and endoderm [1, 2]. Macroscopically, the cystic teratomas are generally benign, containing sebaceous material and mature tissue. The solid teratomas are frequently malignant, composed of immature embryonic tissue in addition to fatty, cartilaginous, fibrous, and bony elements [3-5]. Teratomas occur in many locations, including the ovaries, testes, anterior mediastinum, retroperitoneal space, presacral and coccygeal areas, intracranial sites, neck, and abdomen [1, 2]. The size of retroperitoneal teratomas varies, with the largest reported tumor weighing 36 kg [4, 6].

Of the retroperitoneal tumors reported in adults, 26% were malignant. This frequency is higher than the reported frequency of malignancy of teratomas in children, which ranges from 7% to 10% [2, 3, 6]. Calcifications, which are visible in 60-83% of retroperitoneal teratomas on CT scans, cannot predict benignity. Even though 74% of benign teratomas contain calcifications, they also occur in 25% of malignant ones [5, 6]. Evaluation of the size, cystic or solid components, or presence of calcifications cannot consistently indicate malignancy or potential for recurrence [7].

Retroperitoneal teratomas are usually asymptomatic. The clinical features in infancy include a palpable mass or increase in abdominal girth [4, 7]. In adults, benign teratomas are generally symptomatic, characterized by nausea, vomiting, abdominal distension and pain, back pain, edema of the lower extremities, or urinary obstruction in rare instances [1, 2, 4]. Malignant teratomas in children and adults tend to progress rapidly and are associated with acute symptoms usually including pain. Metastases to the inguinal region, liver, and pancreas have been reported [4].

Retroperitoneal teratomas can be imaged by plain radiography, excretory urography, sonography, CT, and MR imaging. Plain radiographs usually show a soft-tissue mass that displaces the bowel. In 61% of cases, calcification within the tumor or a calcific rim in a cyst wall implies the diagnosis. The characteristic demonstration of bone or teeth is a rare finding in retroperitoneal teratomas [1, 4, 6]. Fat may be identified as a radiolucency on radiographs with a detection rate of 60% compared with CT [5].

Sonography can be used to evaluate the cystic, solid, or complex components of the tumor. Specular echoes, acoustic shadowing produced by calcium in the teratoma, and occasionally a fat-fluid level are seen [5, 8]. Sonography, however, may fail to show calcium when compared with CT scans [5]. In addition, the echogenicity of fat varies from echogenic to echolucent, precluding differentiation from other types of soft tissue [5]. As echogenicity depends not on fat alone but also on tissue interfaces with different acoustic impedance, most feel CT is better than sonography for diagnosing fatty tumors [5, 8].

Fig. 4.—Case 4: Primary retroperitoneal teratoma.

A, Sagittal T1-weighted (500/20) MR images show a large right-sided retroperitoneal mass. Bulk of tumor consists of fat, which appears as regions of high signal intensity. Calcifications appear as foci of very low intensity. Soft-tissue components of tumor appear as regions of intermediate intensity.

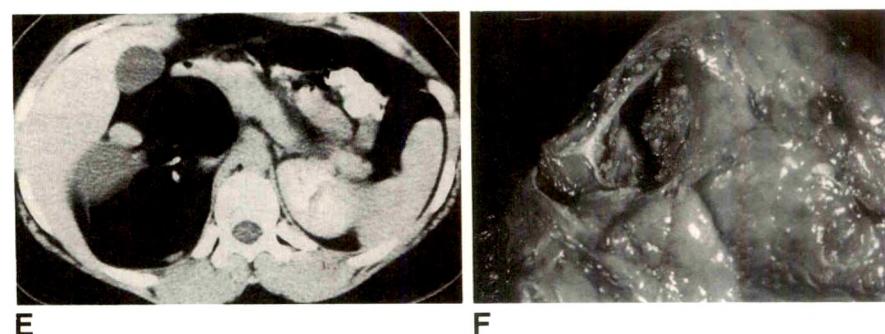
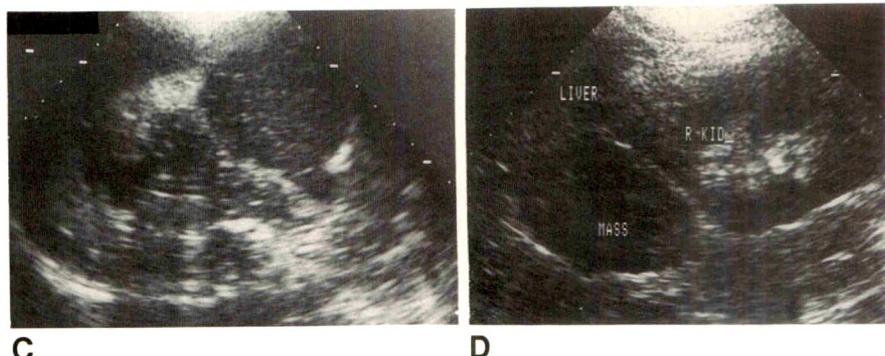
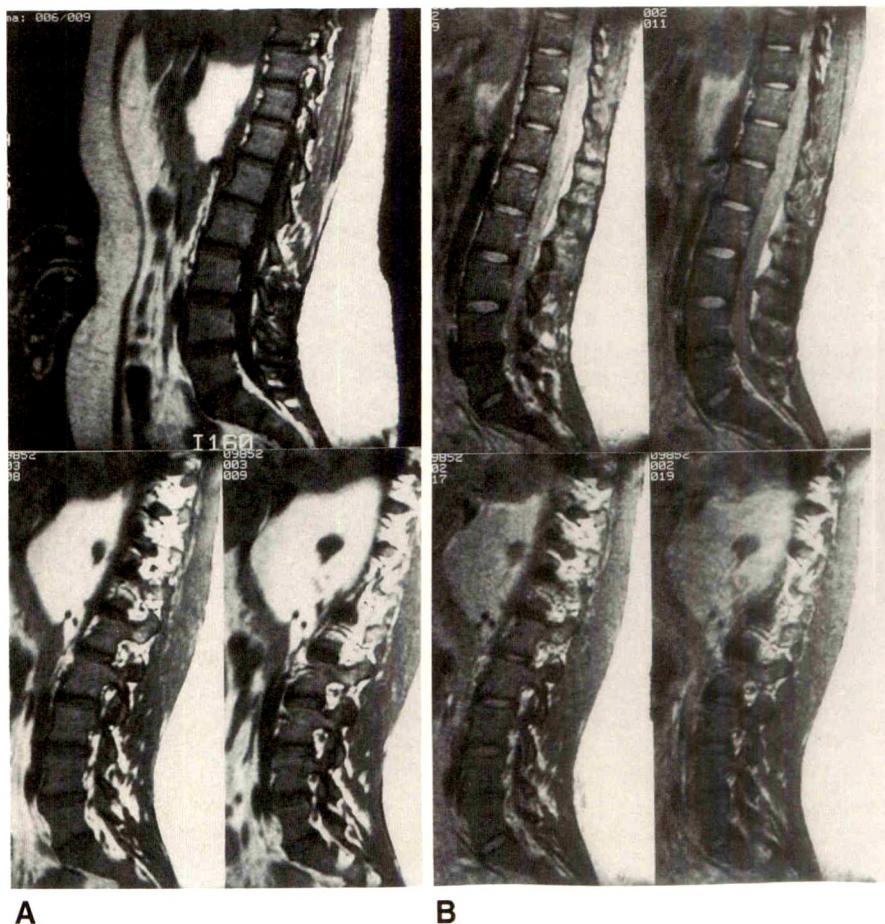
B, Sagittal T2-weighted (2000/40) MR images show fat, calcium, and soft-tissue components of retroperitoneal teratoma.

C, Longitudinal sonogram shows a 12 × 9 cm right-sided suprarenal teratoma containing a solid hyperechoic fatty component, a heterogeneous component with echogenic foci, and acoustic shadowing produced by calcium in tumor.

D, Longitudinal sonogram shows that right kidney is separated from mass and is displaced inferiorly and anteriorly. There is no evidence of hydronephrosis.

E, Transaxial contrast-enhanced CT scan shows a well-encapsulated retroperitoneal teratoma that contains multiple tissue elements, including soft tissue, fat, and areas of calcification.

F, Gross specimen of predominantly fatty retroperitoneal teratoma.



CT shows the typical attenuation numbers of fat, proteinaceous fluid, and subtle calcifications. An almost pathognomonic CT finding is a fatty portion of the tumor and a horizontal interface with dependent fluid, which probably represents sebum [5, 8]. CT is superior to sonography not only in characterizing retroperitoneal teratomas but also in defining the tumor extent to surrounding organs and in evaluating the cyst wall [5, 8]. CT, however, cannot reliably demonstrate adherence to adjacent structures but can predict invasion [8].

The value of MR imaging in detecting retroperitoneal tumors has not been fully established. Available information indicates that MR imaging is unable to show calcifications in most of the patients studied with retroperitoneal teratomas [9]. MR imaging, however, can distinguish the fluid, fat, calcium, and soft-tissue elements [9]. Possible uses include determining local spread of tumor, predicting resectability, and evaluating for recurrence. Currently, cross-sectional imaging techniques provide information about the location and morphology of retroperitoneal teratomas.

The radiologic findings in this case are characteristic of a retroperitoneal teratoma. Detection of this tumor is essential because if left untreated, the mortality rate is essentially 100% [1, 4]. Surgery may be difficult when tissue adherence, which occurs in malignant and benign teratomas, hinders complete

removal of the tumor [6]. Patients have an excellent prognosis after resection of benign retroperitoneal teratomas [1, 4, 6].

Ellen Panageas

REFERENCES

1. Gschwend J, Burke TW, Woodward JE, Heller PB. Retroperitoneal teratoma presenting as an abdominal-pelvic mass. *Obstet Gynecol* **1987**;70:500-502
2. Engel RM, Elkins RC, Fletcher BD. Retroperitoneal teratoma: review of the literature and presentation of an unusual case. *Cancer* **1968**;22:1068-1073
3. Lambrianides AL, Walker MM, Rosin RD. Primary retroperitoneal teratoma in adults. *Urology* **1987**;29:310-312
4. Pantoja E, Llobet R, Gonzalez-Flores B. Retroperitoneal teratoma: historical review. *J Urol* **1976**;115:520-523
5. Davidson AJ, Hartman DS, Goldman SM. Mature teratoma of the retroperitoneum: radiologic, pathologic and clinical correlation. *Radiology* **1989**;172:421-425
6. Bruneton JN, Diard F, Drouillard JP, Sabatier JC, Tavernier JF. Primary retroperitoneal teratoma in adults. *Radiology* **1980**;134:613-616
7. Billmire DF, Grosfeld JL. Teratomas in childhood: analysis of 142 cases. *J Pediatr Surg* **1986**;21:548-551
8. Friedman AC, Pyatt RS, Hartman DS, Downey EF Jr, Olson WB. CT of benign cystic teratomas. *AJR* **1982**;138:659-665
9. Cohen MC, Weetman RM, Provisor AJ, et al. Efficacy of magnetic resonance imaging in 139 children with tumors. *Arch Surg* **1986**;121:522-529



Chest Case of the Day

David J. Eschelman,¹ Douglas T. Gibbons, Julia R. Fielding, Laura Vitale Romo, Daryl R. Parker, Nicolas Argy, and John F. O'Connor

Case 1: Tuberculous Empyema Necessitatis

A 24-year-old man had an enlarging, painless mass in the right lateral chest wall. He had also noted a recent weight loss. Physical examination revealed a soft, nontender, sub-

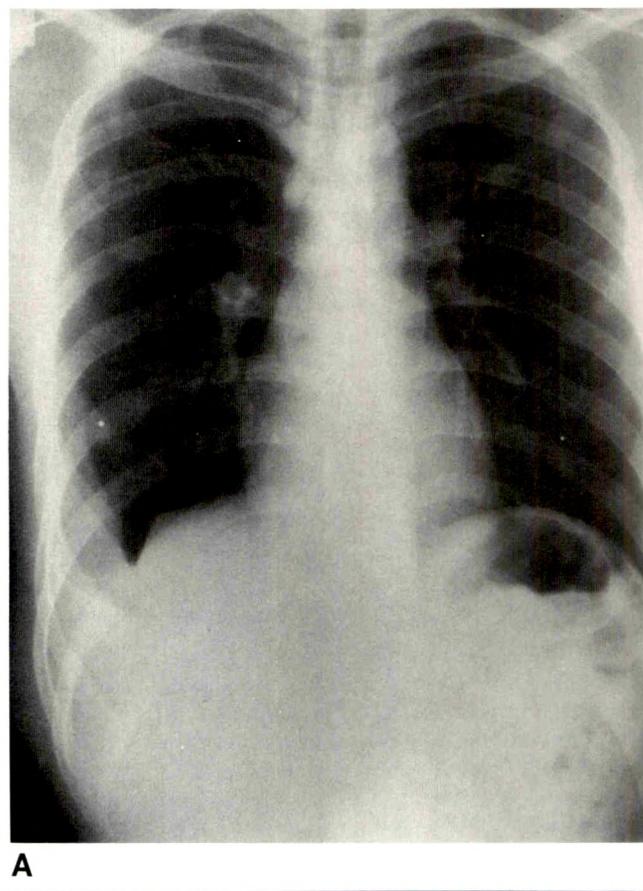
cutaneous mass in the right lateral chest wall between the ninth and 12th ribs. The right side of the lower thorax was dull to percussion, and breath sounds were diminished at the lung base.

Fig. 1.—Case 1: Tuberculous empyema necessitatis.

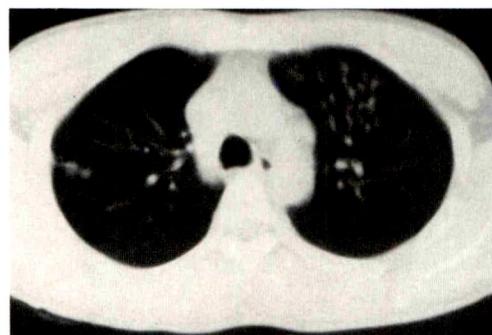
A, Chest radiograph shows an area of fibronodular scarring in left upper lobe with retraction of left hilum. Pleural collection is present in right costophrenic angle with an adjacent chest wall mass. Periosteal reaction is noted in anterior aspect of 10th and 11th ribs on right side.

B, Chest CT scan at lung window setting shows fibronodular scarring in left upper lobe.

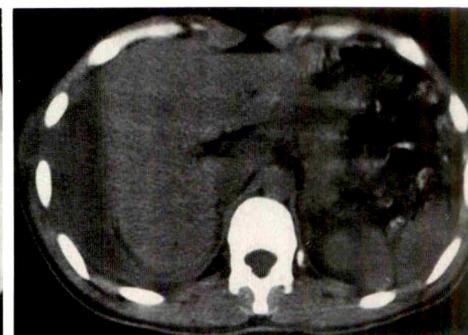
C, CT scan of upper abdomen shows right-sided pleural fluid collection extending into overlying soft tissues.



A



B



C

A posteroanterior chest radiograph (Fig. 1A) showed a right-sided, homogeneous, mass lesion obscuring the costophrenic angle and involving the adjacent extrathoracic soft tissues. Periosteal reaction was seen in the anterior aspects of the right 10th and 11th ribs. Fibronodular scarring, especially in the left upper lobe, was noted in addition to retraction of the left hilum. CT of the chest (Fig. 1B) revealed fibronodular scarring, mainly in the upper lobe of the left lung. CT of the upper abdomen (Fig. 1C) showed a large, right-sided, well-encapsulated, pleural, low-attenuation collection with extension through the parietal pleura into the adjacent soft tissues of the inferolateral chest wall. A needle biopsy yielded acid-fast bacilli. Subsequent culture was positive for *Mycobacterium tuberculosis*.

Empyema necessitatis (a cold abscess necessitating drainage) is a collection of inflammatory tissue that usually extends directly from the pleural cavity into the thoracic wall, forming a mass in the extrapleural soft tissues [1, 2]. It is a rare complication of a chronic pleural empyema, usually becoming clinically apparent many years after the acute infection. Although accounting for only 10% of pleural empyemas, *M. tuberculosis* is responsible for 73% of empyema necessitatis [3]. Rarer causes of empyema necessitatis include malignancy, other pyogenic lung abscesses, blastomycosis, and actinomycosis [1, 4].

Tuberculous empyema is usually the result of a subpleural caseous focus rupturing into the pleural space [5]. Rarely, it is due to hematogenous spread, extension from thoracic lymph nodes, or extension from a subdiaphragmatic focus [3, 6]. If tuberculous empyema is inadequately treated, it may spontaneously decompress or require operative drainage. After spontaneous pleural perforation, extension usually follows fascial planes. Other sites of empyema extension include the vertebral column, paravertebral soft tissues, retroperitoneum, and more rarely the esophagus, flank, groin, and pericardium [1-3, 7, 8].

Clinically, patients with isolated pleural empyema are frequently asymptomatic. In empyema necessitatis, patients can have pleuritic chest pain worsening with deep inspiration and rarely a nonproductive cough. Most commonly they have an enlarging, painful mass in the chest wall.

Radiologically, CT findings of a thick-walled, well-encapsulated, pleural mass associated with an extrapleural mass in the chest wall are highly suggestive of tuberculous empyema necessitatis. Although direct communication between the pleural and chest wall collections is rarely demonstrated, CT is helpful in the detection and characterization of this complication of pleural tuberculosis [1, 9].

Douglas T. Gibbens
Nicolas Argy

REFERENCES

- Bhatt GM, Austin HM. CT demonstration of empyema necessitatis. *J Comput Assist Tomogr* 1985;9:1108-1109
- Peterson MW, Austin JHM, Yip CK, McManus RP, Jaretzki A. CT findings in transdiaphragmatic empyema necessitatis due to tuberculosis. *J Comput Assist Tomogr* 1987;11:704-706
- Sindel EA. Empyema necessitatis. *Q Bull Sea View Hosp* 1940;6:1-49
- Felson B. The extrapleural space. *Semin Roentgenol* 1977;12:327-333
- Berger HW, Mejia E. Tuberculous pleurisy. *Chest* 1973;63:88-92
- Sibley JC. A study of 200 cases of tuberculous pleurisy with effusion. *Am Rev Tuberculosis* 1950;62:314-323
- Tees FJ. Empyema necessitatis. *Arch Surg* 1923;7:321-331
- Marks MI, Eickhoff TC. Empyema necessitatis. *Am Rev Respir Dis* 1970;101:759-761
- Glicklich M, Mendelson DS, Gendal ES, Teirstein AS. Tuberculous empyema necessitatis: computed tomographic findings. *Clin Imaging* 1990;14:23-25

Case 2: Cutaneous T-Cell Lymphoma Involving Both Breasts

This 61-year-old woman had a 10-year history of progressive skin ulcerations diagnosed by skin biopsy in 1982 as cutaneous T-cell lymphoma (CTCL), previously known as mycosis fungoides. She complained to her dermatologist at this time of dysphagia and groin swelling. Physical examination revealed diffuse lymphadenopathy and ulcerating, nodular skin lesions of the trunk and extremities. Multiple, bilateral breast masses also were palpated. Results of a barium swallow were normal. A CT study was performed to delineate the extent of the lymphadenopathy (Figs. 2A and 2B). CT scans through the chest showed extensive axillary adenopathy, left internal mammary adenopathy, and multiple soft-tissue masses in both breasts. The breast masses were further evaluated by mammography (Figs. 2C and 2D), which revealed several well-defined, round lesions in both breasts without associated microcalcifications or skin changes. Biopsy of each breast was performed, and the masses were found to be T-cell lymphoma.

CTCL encompasses mycosis fungoides, Sézary syndrome, reticulum cell sarcoma, lymphoma cutis, and most T-cell leukemias [1]. First described in 1806 by Jean Louis Alibert, CTCL is a malignant lymphoma that begins in the skin. The annual incidence in the United States is increasing and now surpasses that of Hodgkin disease [2]. Prevalence is estimated at 40,000 to 50,000 cases [3]. CTCL occurs twice as often in males as in females and is the only lymphoma more common in blacks than whites. It is usually diagnosed in the fifth decade of life. The causative agent is unknown; however, there is an association with human T-cell lymphoma virus (HTLV) [1, 3]. There is no cure for the disease, but many palliative therapies are in use. Cutaneous lesions are treated with topical steroids, nitrogen mustard, ultraviolet light, and electron beam therapy. Extracutaneous disease requires systemic chemotherapy, radiation therapy, or photophoresis, sometimes in combination. The mean survival time after diagnosis is 3 to 10 years.

CTCL progresses through three clinical stages, termed patch or premycotic, plaque, and tumor [1, 3]. The macular lesions in the patch stage resemble several benign dermatoses and are localized to the trunk and extremities. Plaques may develop from patch lesions or arise de novo in any area of the body. They are raised, scaly, and pruritic. Painless tumors or nodules generally originate in plaques and often ulcerate. Extracutaneous disease eventually occurs in 50% of all patients. Spread occurs hematogenously and via the lymphatics, although not in an organized fashion. The liver is the organ most often affected. Gastrointestinal, cardiac, pulmonary, renal, and central and peripheral nervous system

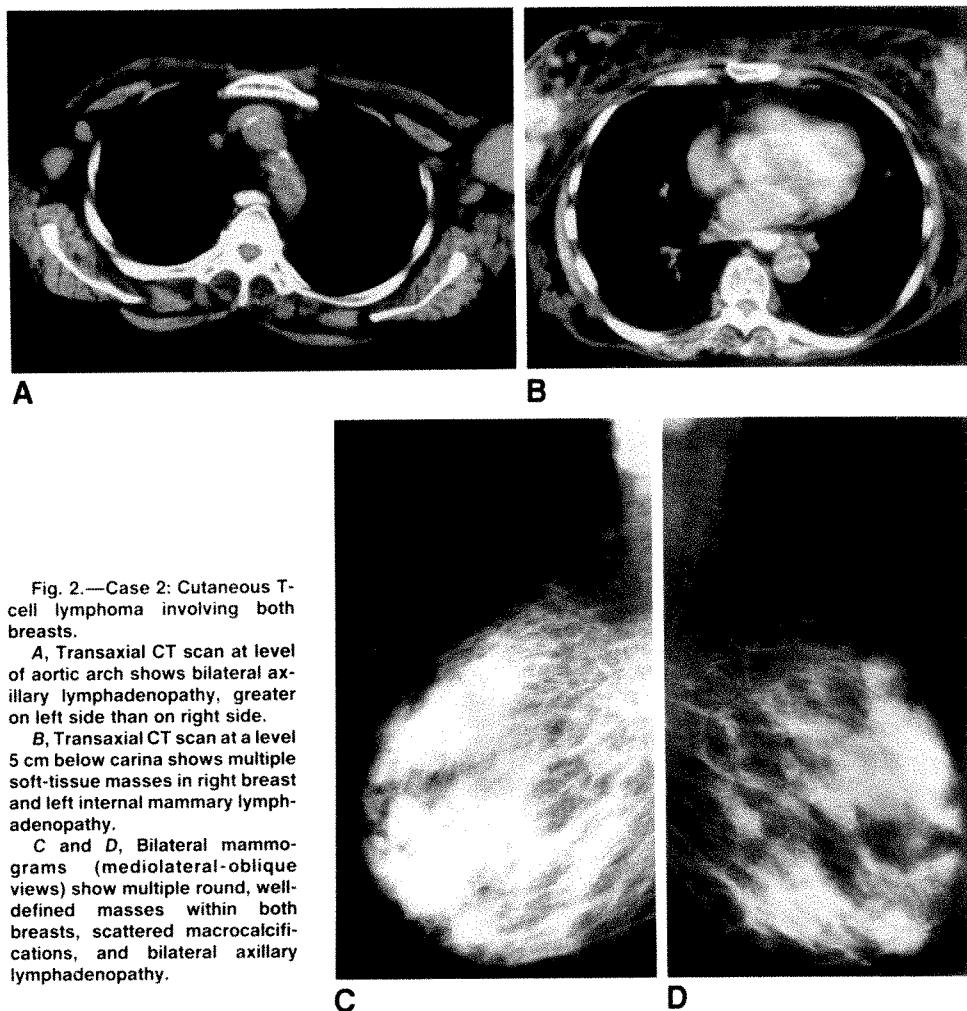


Fig. 2.—Case 2: Cutaneous T-cell lymphoma involving both breasts.

A, Transaxial CT scan at level of aortic arch shows bilateral axillary lymphadenopathy, greater on left side than on right side.

B, Transaxial CT scan at a level 5 cm below carina shows multiple soft-tissue masses in right breast and left internal mammary lymphadenopathy.

C and D, Bilateral mammograms (mediolateral-oblique views) show multiple round, well-defined masses within both breasts, scattered macrocalcifications, and bilateral axillary lymphadenopathy.

involvement have been observed [1]. To our knowledge, no prior reports have described involvement of the breast. The bones are usually spared. When present, lesions are generally osteolytic. The presence of extracutaneous disease mandates the use of systemic therapy and has a poorer prognosis.

The diagnosis of CTCL is generally made by punch biopsy of a skin lesion in the patch or plaque stage. Imaging defines the extent of extracutaneous disease and can be used to monitor the response to therapy. CT is useful in identifying lymphadenopathy and visceral involvement. Chest radiographs may reveal pulmonary nodules, patchy infiltrates, and hilar lymphadenopathy in the late stages of the disease [1]. Lymphoma manifests itself in the breast parenchyma in many ways. Mammography may show a single nodule, multiple masses, an increased interstitial pattern, or diffuse increase in density [4, 5]. Massive axillary lymphadenopathy is rarely seen with breast carcinoma and should raise the suspicion of lymphoma [6]. In identifying the presence of extracutaneous disease, the radiologist assists in defining appropriate therapy for CTCL for prolonging patients' survival.

Julia R. Fielding

REFERENCES

- Knoble RM, Edelson RL. Cutaneous T cell lymphoma. *Med Clin North Am* 1986;70:109-138
- Weinstock MA, Horn JW. Mycosis fungoides in the United States. *JAMA* 1988;260:42-46
- Worobec-Victor S. Cutaneous T cell lymphoma. *N J Med* 1989;86:395-400
- Meyer JE, Kopans DB, Long JC. Mammographic appearance of malignant lymphoma of the breast. *Radiology* 1980;135:623-626
- Aubanel D, Bruneton JN. Gynecologic lymphomas. In: Bruneton JN, Schneider M, eds. *Radiology of lymphomas*. New York: Springer-Verlag, 1986:99-102
- Kopans DB. *Breast imaging*. Philadelphia: Lippincott, 1989:305-307

Case 3: Endodermal Sinus Tumor of the Mediastinum

This 28-year-old man had a 3-month history of pain in the right shoulder and a 1-month history of hemoptysis, dysphagia, and night sweats. He had an elevated serum level of the beta subunit of human chorionic gonadotropin and alpha-fetoprotein (AFP). Chest radiographs (Figs. 3A and 3B) showed a vaguely defined anterior mediastinal mass with

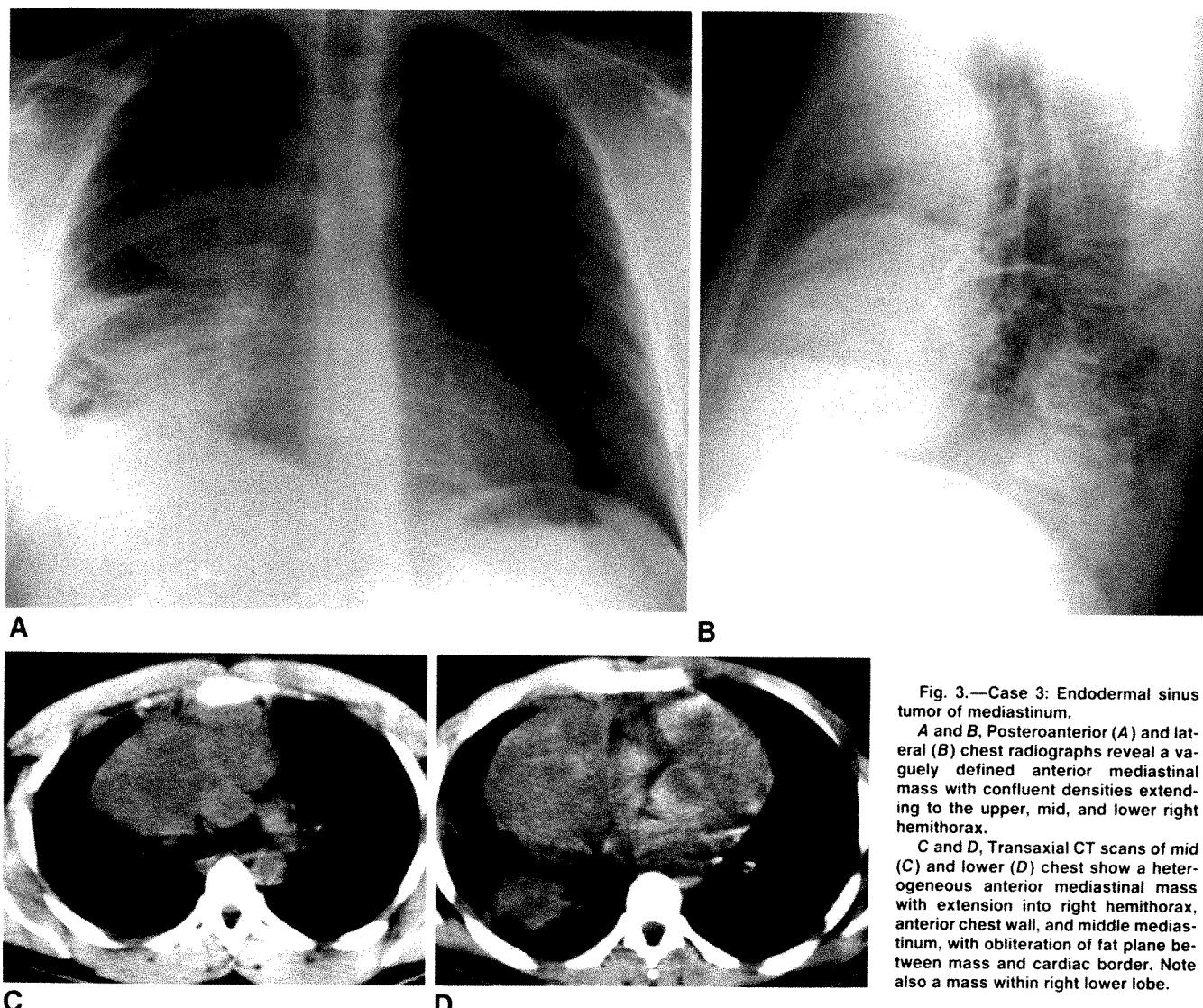


Fig. 3.—Case 3: Endodermal sinus tumor of mediastinum.

A and B, Posteroanterior (**A**) and lateral (**B**) chest radiographs reveal a vaguely defined anterior mediastinal mass with confluent densities extending to the upper, mid, and lower right hemithorax.

C and D, Transaxial CT scans of mid (**C**) and lower (**D**) chest show a heterogeneous anterior mediastinal mass with extension into right hemithorax, anterior chest wall, and middle mediastinum, with obliteration of fat plane between mass and cardiac border. Note also a mass within right lower lobe.

confluent densities in the upper, mid, and lower right hemithorax. Chest CT (Figs. 3C and 3D) revealed a large, heterogeneous anterior mediastinal mass with irregular borders. The tumor extended into the right hemithorax, displacing the right middle lobe bronchus, with growth continuing to the anterior chest wall through the upper sternum and into the middle mediastinum with obliteration of the fat planes between the mass and the right cardiac border, suggesting invasion. A second necrotic-appearing mass was present next to the major fissure on the right side within the right lower lobe. Findings on scrotal sonography (not shown) were normal. Abdominal CT, MR imaging of the thoracic and lumbar spine, and bone scanning (not shown) revealed hepatic, vertebral, sternal, and calvarial metastases. A pathologic specimen obtained by open biopsy was diagnostic of an endodermal sinus tumor of the mediastinum.

Endodermal sinus tumors are the rarest of the germ cell tumors. Germ cell tumors are divided into the seminomas and the nonseminomas, namely the endodermal sinus tumors, teratomas, choriocarcinomas, and embryonal carcinomas. Although this group of tumors is classically associated with the

gonads, extragonadal sites such as the mediastinum are primary sites of occurrence. On the whole, germ cell tumors account for approximately 20% of all mediastinal tumors and cysts. Like their gonadal counterparts, mediastinal germ cell tumors also are derived from primitive germ cell elements [1].

The presence of germ cell elements in the mediastinum has been a topic of great debate. Originally, it was proposed that these mediastinal tumors were metastatic from gonadal tissue. In the absence of definable gonadal tumor, it was theorized that there must be an undefinable regressed focus. Today, however, the most favored explanation is failure of germ cells to migrate along the urogenital ridge to the gonads [2].

Whereas seminomas affect males only, the nonseminomatous tumors also affect females, although a male predilection is maintained. Germ cell tumors affect persons in the 20–30 year age range. Mediastinal endodermal sinus tumors, embryonal carcinomas, and choriocarcinomas are not only more aggressive lesions than their seminomatous counterparts, but they are also more aggressive when compared with their

identical histologic testicular counterparts. The single most favorable prognostic factor for mediastinal endodermal sinus tumors is complete resectability. Endodermal sinus tumors secrete AFP, and tumor activity is strongly correlated with the serum level. Human chorionic gonadotropin is detectable in some cases of endodermal sinus tumor; however, it is generally accepted that this endocrinopathy is due to small foci of choriocarcinoma or embryonal carcinoma within the endodermal sinus tumor [3, 4].

As do all germ cell tumors, endodermal sinus tumors arise within the anterior mediastinum. Extension into the middle or posterior mediastinum and the lung may occur. Bony invasion by direct extension, particularly of the sternum, is not uncommon. Chest radiographs are used in making initial observations. In the last decade, CT has been found to better define the tissue characteristics and extent of tumor invasion of endodermal sinus tumors and germ cell tumors as a whole.

CT has been very useful in differentiating between the nonseminomatous and seminomatous germ cell tumors. Seminomas have been described as large, sharply demarcated masses that are usually of homogeneous attenuation. Chest wall invasion is rare, as is the development of pleuropericardial effusions. In contrast, the nonseminomatous tumors have spiculated borders and are of heterogeneous attenuation. The areas of lower attenuation within the tumors are due to necrosis and hemorrhage. A strong tendency for bony invasion and fat plane obliteration exists. Calcification and thick capsules that enhance after IV administration of contrast material have been described. Pleural effusions are more common [5-8].

Although CT may be helpful in differentiating between the two subtypes of germ cell tumors, its use in differentiating germ cell tumors from other tumors of the anterior mediastinum is more questionable. Thymomas, carcinoid tumors, lymphoma, and mediastinal metastases must also be considered in the differential diagnosis of heterogeneous anterior mediastinal masses by CT. Although benign thymomas are usually round or oval masses of homogeneous attenuation, thymomas that undergo cystic degeneration gain irregular borders along with the tendency to invade fat planes. Some may also calcify. CT features do not differentiate these thymomas from the nonseminomatous germ cell tumors [5, 7, 8]. In addition, cystic forms of Hodgkin disease or mediastinal lymph nodes involved by metastatic disease may also resemble the nonseminomatous germ cell tumors [5, 6]. Carcinoid, although usually a well-circumscribed mass, may show fat plane obliteration and calcification [5].

In conclusion, some advances have been made to better characterize germ cell tumors of the anterior mediastinum. Difficulty still exists, however, in differentiating germ cell tumors from other anterior mediastinal tumors. Germ cell tumors should always be considered in the differential diagnosis of an anterior mediastinal mass in a young patient.

Laura Vitale Romo
Daryl R. Parker

REFERENCES

- Rosai J. Ackerman's surgical pathology. St. Louis: Mosby, 1989:367
- Luna MA, Valenzuela-Tamariz J. Germ-cell tumors of the mediastinum:

- postmortem findings. *Am J Clin Pathol* 1976;65:450-454
- 3. Knapp RH, Hurt RD, Payne S, et al. Malignant germ cell tumors of the mediastinum. *J Thorac Cardiovasc Surg* 1985;89:82-89
- 4. Truong LD, Harris L, Mattioli C, et al. Endodermal sinus tumor of the mediastinum. *Cancer* 1986;58:730-739
- 5. Lee KS, Im JG, Han CH, Han MC, Kim CW, Kim WS. Malignant primary germ cell tumors of the mediastinum: CT features. *AJR* 1989;153:947-951
- 6. Blomie V, Lien H, Fossa SD, Jacobsen AB, Stenwig AE. Computed tomography in primary non-seminomatous germ cell tumors of the mediastinum. *Acta Radiol* 1988;29:289-292
- 7. Levitt RG, Husband JE, Glazer HS. CT of primary germ-cell tumors of the mediastinum. *AJR* 1984;142:73-78
- 8. Mori K, Eguchi K, Moriyama H, Miyazawa N, Kodama T. Computed tomography of anterior mediastinal tumors: differentiation between thymoma and germ cell tumor. *Acta Radiol* 1987;28:395-398

Case 4: Lateral Thoracic Meningocele in a Patient with Neurofibromatosis

A 52-year-old man came to the emergency department with shortness of breath and wheezing. A posteroanterior chest radiograph (Fig. 4A) revealed a round, well-circumscribed, left paravertebral, soft-tissue mass measuring 6 cm next to the T5-T6 vertebral bodies. A short focal scoliosis convex toward the lesion, cutaneous neurofibromas in the extrathoracic soft tissues on the right side, and rib notching also were seen. A lateral chest radiograph (Fig. 4B) showed a posterior mediastinal mass in the upper thoracic region with enlarged neural foramina and scalloping of the dorsal surfaces of the T5-T8 vertebral bodies. Lateral view of myelogram (Fig. 4C) showed a rounded meningocele corresponding to the posterior mediastinal soft-tissue mass on chest radiographs, as well as widening of the subarachnoid space with extension of contrast material into scalloped vertebral bodies.

Lateral paravertebral meningoceles are an uncommon anomaly of the meninges manifested by lateral extrusion of the dura and arachnoid through an enlarged intervertebral foramen into the extrapleural thoracic gutter [1]. Males and females are equally affected, most commonly between 30 and 50 years of age [2]. Eight-five percent of paravertebral meningoceles are seen in patients with neurofibromatosis [3]. Moreover, thoracic paraspinal masses are more likely to be meningoceles than neurofibromas in these patients [1, 4-6]. The majority (70%) of lateral thoracic meningoceles are right sided [1]. They frequently occupy a single neural foramen in the upper thoracic region (T3-T7), usually T5-T6 [7]. Their size varies from almost undetectable to nearly the size of the hemithorax itself. In neonates, large meningoceles may cause significant respiratory compromise [2].

Clinically, patients with lateral thoracic meningoceles may have a cough or dyspnea, but more commonly they are asymptomatic. Some patients have pain (23%); minor neurologic symptoms including sensory deficits, weakness, and hyperreflexia (10%); or severe paresis (9%) [8]. The acute symptoms in this patient were unrelated to his known diagnosis of neurofibromatosis.

Chest films of patients with lateral thoracic meningoceles usually exhibit a short focal scoliosis of the upper thoracic spine, convex toward the lesion. However, kyphosis may be more prominent than is scoliosis [9]. The neural foramina are enlarged, with thinning of adjacent pedicles, focal increase in

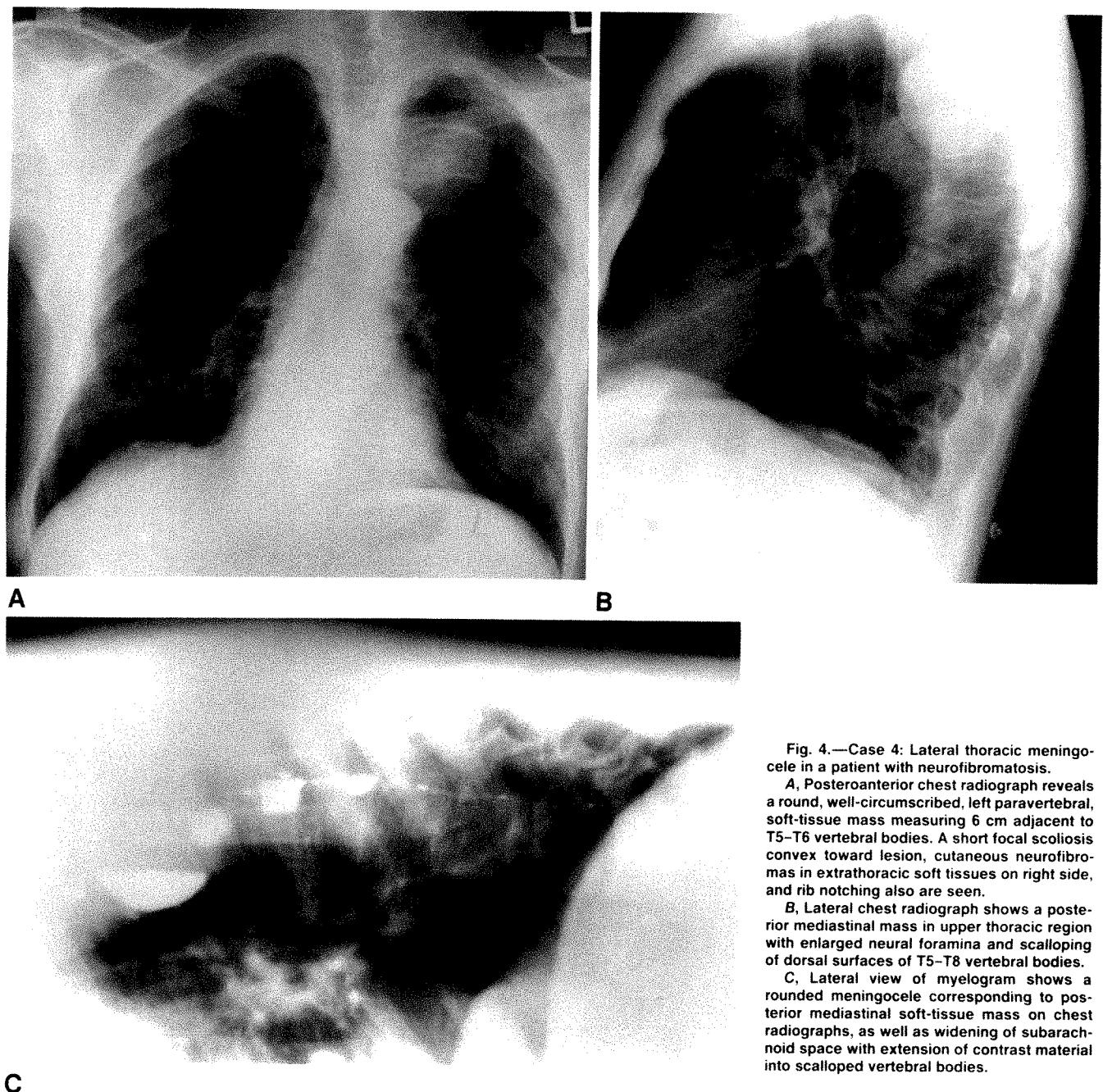


Fig. 4.—Case 4: Lateral thoracic meningocele in a patient with neurofibromatosis.

A, Posteroanterior chest radiograph reveals a round, well-circumscribed, left paravertebral, soft-tissue mass measuring 6 cm adjacent to T5-T6 vertebral bodies. A short focal scoliosis convex toward lesion, cutaneous neurofibromas in extrathoracic soft tissues on right side, and rib notching also are seen.

B, Lateral chest radiograph shows a posterior mediastinal mass in upper thoracic region with enlarged neural foramina and scalloping of dorsal surfaces of T5-T8 vertebral bodies.

C, Lateral view of myelogram shows a rounded meningocele corresponding to posterior mediastinal soft-tissue mass on chest radiographs, as well as widening of subarachnoid space with extension of contrast material into scalloped vertebral bodies.

interpediculate distance, thinned lamina, and scalloping of the dorsal surfaces of adjacent vertebral bodies [7]. The adjacent intercostal space may be widened, with erosion of contiguous rib margins [10]. Fused or hypoplastic ribs and vertebrae may coexist [2, 3, 10]. Adjacent ventral roots may be hypoplastic or absent on the ipsilateral or contralateral side of the meningocele [2]. MR signal intensity of CSF within the meningocele may appear brighter than that within the spinal canal because of damped CSF pulsations [11].

Douglas T. Gibbens
Nicolas Argy

REFERENCES

1. Bunner R. Lateral intrathoracic meningocele. *Acta Radiol* 1959;51:1-9
2. Chandler A, Herzberger EE. Lateral intrathoracic meningocele: case report with preoperative diagnosis. *AJR* 1963;90:1216-1219
3. Erkuivrawat S, El Gammal T, Hawkins J, et al. Intrathoracic meningoceles and neurofibromatosis. *Arch Neurol* 1979;36:557-559
4. Kent EM, Blades B, Valle AR, Graham EA. Intrathoracic neurogenic tumors. *J Thorac Surg* 1944;13:116-161
5. Blades B. Mediastinal tumors: report of cases treated at Army thoracic centers in the United States. *Ann Surg* 1946;123:749-765
6. Hagelstam L. On the deformities of spine and multiple neurofibromatosis (von Recklinghausen). *Acta Chir Scand* 1946;93:169-193
7. Naidich TP, McLone DG, Harwood-Nash DC. Arachnoid cysts, paravertebral meningoceles, and perineurial cysts. In: Newton TH, Potts DG, eds. *Computed tomography of the spine and spinal cord*. San Anselmo, CA: Clavadel Press, 1983:388-390
8. Miles J, Pennybacker J, Sheldon P. Intrathoracic meningocele: its development and association with neurofibromatosis. *J Neurol Neurosurg Psychiatr* 1969;32:99-110
9. Healy JF, Wells MV, Carlstrom T, Rosenkrantz H. Lateral thoracic meningocele demonstrated by computerized tomography. *Comput Tomogr* 1980;4:159-163
10. Shealy CN, Le May M. Intrathoracic meningocele: two additional cases of this rare entity. *J Neurosurg* 1964;21:880-883
11. Flannigan-Sprague BD, Modic MT. The pediatric spine: normal anatomy and spinal dysraphism. In: Modic MT, Masaryk TJ, Ross JS, eds. *Magnetic resonance imaging of the spine*. Chicago: Year Book Medical, 1989:244

Abdominal Case of the Day

David J. Eschelman,¹ Audrey D. Duva-Frissora, Lisa C. Martin, Daryl R. Parker, Margo M. Moskos, Douglas T. Gibbens, and J. F. O'Connor

Case 1: Metastatic Carcinoid Presenting as a Duodenal Mass

A 48-year-old man had anorexia, a 20-lb weight loss in 6 months, abdominal pain, and episodic shortness of breath. A several-month history of diarrhea and cutaneous flushing also were elicited. Physical examination revealed upper abdominal tenderness and a 2 × 3 cm perumbilical mass.

Upper gastrointestinal study (Fig. 1A) showed a 2.5-cm, smooth, intraluminal polypoid mass in the duodenal bulb. Contrast-enhanced CT of the abdomen (Fig. 1B) revealed multiple low-attenuation lesions with necrotic centers in the liver that were consistent with metastases, along with peritoneal studding, right hydronephrosis, right hydroureter, and mesenteric adenopathy. Contrast-enhanced pelvic CT (Fig. 1C) showed adenopathy next to the right ureter; mesenteric adenopathy and thickening, representing desmoplastic reaction; and dilated small bowel. Subsequent hepatic biopsy was diagnostic for metastatic carcinoid.

The most common primary small-bowel tumor is carcinoid, comprising one third of all small intestinal neoplasms, followed by adenocarcinoma, lymphoma, and sarcoma. Carcinoids arise from primitive neuroectodermal tissue and are capable of producing various vasoactive hormones. Of all gastrointestinal carcinoids, approximately 25–35% originate in the small bowel. The appendix is the most common site [1]. Seventy-five percent of malignant carcinoids originate in the ileum. Involvement of the duodenum is rare relative to the rest of the gastrointestinal tract [2]. When carcinoid tumors involve the duodenum, they occupy the bulb and periampullary region up to 80% of the time [3]. Approximately one third of small-bowel carcinoids are multiple, one third present with metastasis, one third are malignant, and one third are associated with a second separate malignant tumor [4].

Tumor growth is slow but continuous, leading to regional lymph node involvement or distant metastasis. They tend to grow out of the lumen into the submucosa, then muscularis mucosa, and eventually serosa. Small carcinoids rarely exhibit malignant features, whereas tumors larger than 2 cm are frequently metastatic. As frequent mitosis and cellular atypia are unusual features of carcinoid behavior, malignancy is determined by invasion and metastasis. The majority of pa-

tients with carcinoids are asymptomatic [3, 5]. Symptomatic lesions worsen prognosis, as regional lymph node metastasis is seen in 90% of symptomatic carcinoids. Symptoms, including skin flushing, diarrhea, tachycardia, abdominal pain, intestinal obstruction, asthma, and right-sided valvular heart disease, constitute the carcinoid syndrome [4]. This syndrome is thought to be mediated by serotonin and results from small-bowel primary tumors only after extensive metastatic liver disease is present. Carcinoid limited to the small intestine and mesentery does not usually produce the clinical syndrome because amines released into the portal venous system are inactivated as they pass through the liver.

The radiologic spectrum of carcinoids is more diverse than that of most gastrointestinal neoplasms because of the different growth patterns and tissue reactions incited by this disease [6]. Barium studies usually reveal single or multiple submucosal nodules. Multiple, diffuse intramural nodules can resemble lymphoma, other diffuse metastatic disease, Peutz-Jeghers syndrome, and neurofibromatosis [6]. Intestinal bowel loops show diffuse narrowing, separation, and focal compression because of intraluminal nodules. Serotonin release can cause segmental hyperperistalsis, hypertrophy of the muscularis mucosa, and regional mesenteric scarring [4]. Commonly, the bowel and/or mesentery show the effects of a dense desmoplastic reaction. This desmoplastic reaction, the most common radiologic finding, causes abrupt bowel angulation and straightening of the normal mucosal pattern [6]. Pleating of folds, narrowing, and fixation also are common, giving the appearance of metastatic disease, postoperative adhesions, inflammatory masses, retroperitoneal fibrosis, Crohn disease, and endometriosis involving the small bowel [7].

Carcinoids are usually small and are rarely seen on CT. CT findings include radiating mesenteric densities, indicating a desmoplastic reaction. This finding, combined with rounded mesenteric masses or liver metastasis, is highly suggestive of carcinoid [8]. Local invasion or lymphatic spread to mesenteric lymph nodes produces a peculiar thickening and retraction of involved mesenteric fat, which may secondarily produce venous or lymphatic obstruction. Lymphadenopathy in the paraaortic and paracaval area is often bulky and may mimic lymphoma. Similar findings can be seen in patients with retractile mesenteritis, a disease of unknown cause charac-



Fig. 1.—Case 1: Metastatic carcinoid presenting as a duodenal mass.
A, Spot radiograph of duodenum from an upper gastrointestinal series shows a 2.5-cm, smooth, intraluminal, polypliod mass in duodenal bulb.
B, Contrast-enhanced transaxial CT scan of upper abdomen shows multiple low-attenuation lesions with necrotic centers in liver that are consistent with metastases, along with peritoneal studding, right hydronephrosis, right hydrourere, and mesenteric adenopathy.
C, Contrast-enhanced transaxial CT scan of mid pelvis shows adenopathy next to right ureter; mesenteric adenopathy and thickening, representing desmoplastic reaction; and dilated small bowel.

terized by fibrofatty thickening of the mesentery, and in patients with peritoneal mesothelioma [9].

The angiographic triad of carcinoid includes faint to moderate staining at the primary site; vascular changes that include narrowing, obstruction of the distal mesenteric cascade, clustering of irregular kinked vessels, and encasement of the central mesentery; and hypervascular liver metastases. This triad is a highly specific aid to preoperative diagnosis, as well as localization and staging of small intestinal carcinoids [10]. Moreover, the injection of epinephrine can accentuate the tumor stain of primary carcinoids and hepatic metastases [11].

Scintigraphy with ^{131}I -metaiodobenzylguanidine (MIBG) can allow specific localization of intestinal carcinoids and metastasis. MIBG, an analogue of norepinephrine, is concentrated in tumors of neuroectodermal origin, such as pheochromocytomas, neuroblastomas, medullary thyroid carcinomas, and carcinoids. These other tumors are rare and easily differentiated from carcinoid on the basis of their location, clinical features, and laboratory patterns of hormonal secretion [12].

Douglas T. Gibbons
Daryl R. Parker

REFERENCES

- Godwin JD. Carcinoid tumors: an analysis of 2837 cases. *Cancer* 1975;36:560-569
- Warren KW, McDonald WM, Humelogan CJ. Periampullary and duodenal carcinoid tumors. *Gut* 1964;5:448-453
- Wengrower D, Fisch A. Primary duodenal carcinoid. *Am J Gastroenterol* 1987;82:1069-1070
- Lappas JC, Maglinte DDT. The small bowel. In: Putman CE, Ravin CE, eds. *Textbook of diagnostic imaging*. Philadelphia: Saunders, 1988: 868-869
- Balthazar EJ. Carcinoid tumors of the alimentary tract. I. Radiologic diagnosis. *Gastrointest Radiol* 1978;3:47-56
- Bank S, Goldstein HM, Dodd GD. The roentgenologic spectrum of small intestinal carcinoid tumors. *AJR* 1975;123:274-280
- Maglinte DDT. The small bowel: neoplasms. In: Taveras JM, Ferrucci JT, eds. *Radiology*, 3rd ed. Philadelphia: Lippincott, 1988;4:1-2
- Cockayne BM, Fishman EK, Jones B, Siegelman SS. Computed tomography of abdominal carcinoid tumor. *J Comput Assist Tomogr* 1985;9:38-42
- Seigel RS, Kuhns LR, Borlaza GS, McCormick TL, Simmons JL. Computed tomography and angiography in ileal carcinoid tumor and retractive mesenteritis. *Radiology* 1980;134:437-440
- Kirkhwala M, Balthazar EJ. Carcinoid tumors of the alimentary tract. II. Angiographic diagnosis of small intestinal and colonic lesions. *Gastrointest Radiol* 1978;3:57-61
- Goldstein HM, Miller M. Angiographic evaluation of small intestinal carcinoid tumors: value of epinephrine. *Radiology* 1975;115:23-28
- Adolph JMG, Kimmig BN, Georgi P, zum Winkel K. Carcinoid tumors: CT and $\text{I}-131$ meta-iodo-benzylguanidine scintigraphy. *Radiology* 1987;164:199-203

Case 2: Cytomegalovirus Pseudotumor of the Cecum

A 36-year-old man with AIDS had a 1-month history of watery diarrhea and episodic fevers. A small-bowel series showed spasticity and marked bowel wall thickening of the terminal ileum and cecum (Fig. 2A). Abdominal CT confirmed a mass in the right lower quadrant that was surrounding the cecum (Figs. 2C and 2D) and showed extensive retroperitoneal adenopathy (Fig. 2B). A right-sided ileocolectomy was performed. Pathologic examination revealed a cytomegalovirus-mediated inflammatory pseudotumor within the muscularis and submucosa with complete mucosal sparing.

Cytomegalovirus is ubiquitous, infecting the majority of Americans at some point. In the immunocompetent patient, the primary infection usually results in a subacute illness similar to infectious mononucleosis [1]. However, in the immunocompromised patient, cytomegalovirus infection transforms into an aggressive opportunistic infection that can cause significant morbidity and mortality. Virtually any organ system can be infected [1].

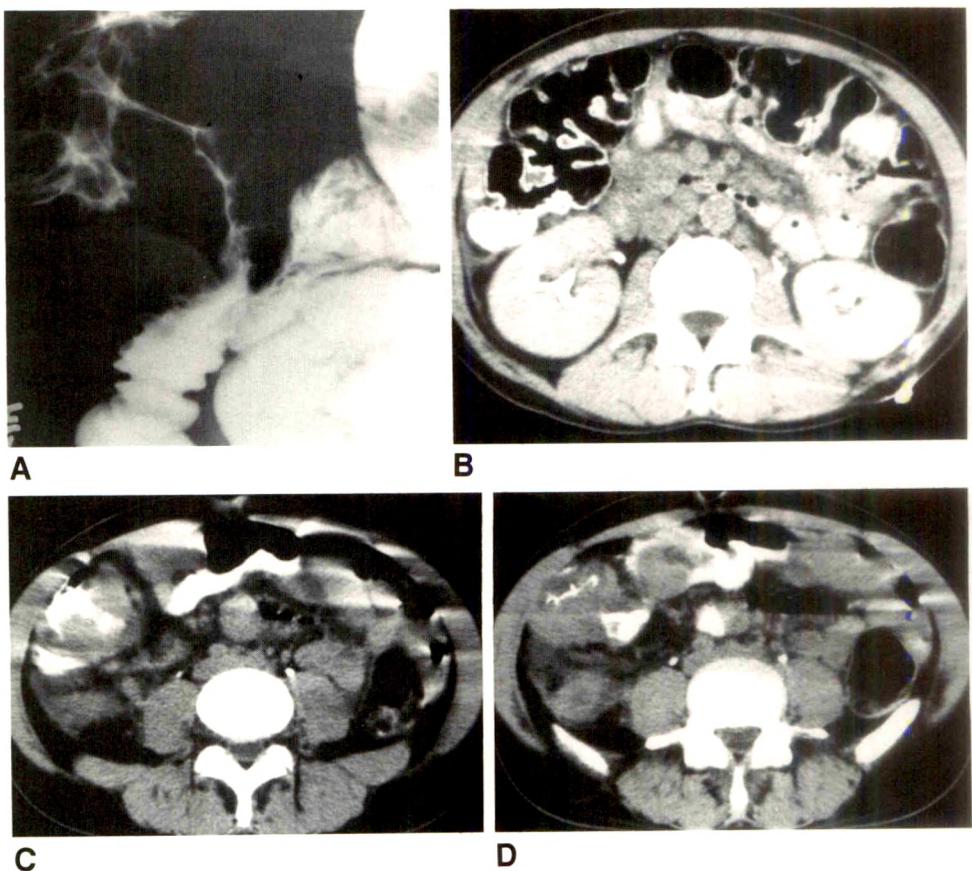
Cytomegalovirus is a common gastrointestinal pathogen in patients with AIDS. In an autopsy series of 97 patients with AIDS, Dannenberg [2] reported systemic cytomegalovirus infection in 68% and gastrointestinal involvement in 43% of

Fig. 2.—Case 2: Cytomegalovirus pseudotumor of cecum.

A, Radiograph of cecum and terminal ileum from a small-bowel series. Spasticity of terminal ileum and cecum with bowel-wall thickening is shown.

B, Transaxial CT scan of mid abdomen shows extensive retroperitoneal adenopathy.

C and D, Transaxial CT scans of abdomen show an apparent mass surrounding cecum caused by bowel-wall thickening.



patients. Any segment of the gastrointestinal tract from the mouth to the anus, including the pancreas, liver, and biliary tree, can be infected with the virus [3]. The infectious insult usually manifests as a nonspecific ulcerative disease, most commonly cytomegalovirus colitis. Cytomegalovirus can cause a localized vasculitis within the bowel wall, progressing to ischemic necrosis, hemorrhage, toxic megacolon, and perforation [2, 4, 5].

Because the gastrointestinal response to infection is limited regardless of the pathogen, radiologic abnormalities are generally nonspecific. The more common radiologic findings associated with cytomegalovirus include focal or diffuse mucosal ulceration and granularity, bowel wall thickening, loss of haustrations, and thickened mucosal folds [5–7]. Our case is unusual in that the virus induced an inflammatory pseudotumor involving the muscular wall and submucosa of the cecum while sparing the mucosa. A similar cytomegalovirus pseudotumor of the stomach was reported in an immunocompetent patient [8].

The gastrointestinal tract is a major target in patients with AIDS. Most patients experience weight loss related to gastrointestinal dysfunction resulting from infections, neoplasms, or nonspecific causes [4]. Other entities in the differential diagnosis in this patient include tuberculosis, *Mycobacterium avium-intracellulare*, amebiasis (although rarely involving the terminal ileum), *Yersinia*, periappendiceal abscess, inflamma-

tory bowel disease, lymphoid hyperplasia, lymphoma, and Kaposi sarcoma.

The radiologist should be aware of the diverse radiologic manifestations of cytomegalovirus and its high prevalence in the immunocompromised population. Newer antiviral agents such as ganciclovir and trisodium phosphonoformate are proving to be effective [1]. An aggressive diagnostic approach to identify a treatable abnormality may decrease the high morbidity and mortality rates associated with cytomegalovirus and many other opportunistic infections of the gastrointestinal tract.

Audrey D. Duva-Frissona

REFERENCES

1. Sissons JG, Bonysiewicz LK. Human cytomegalovirus infection. *Thorax* 1989;44:241–246
2. Dannenberg AJ. Cytomegalovirus infection of the gastrointestinal tract. *Gastroenterology* 1987;92:1362
3. Santangelo WC, Krejs GJ. Southwestern Internal Medicine Conference: GI manifestations of the acquired immunodeficiency syndrome. *Am J Med Sci* 1986;292:328–334
4. Kotler DP. Intestinal and hepatic manifestations of AIDS. *Adv Intern Med* 1989;34:43–72
5. Megibow AJ, Balthazar EJ, Hulnick DH. Radiology of nonneoplastic gastrointestinal disorders in acquired immune deficiency syndrome. *Semin Roentgenol* 1987;22:31–41
6. Teixidor HS, Honig CL, Norsoph E. Cytomegalovirus infection of the

- alimentary canal: radiologic findings with pathologic correlation. *Radiology* 1987;163:317-323
7. Balthazar EJ, Megibow AJ, Fazzini E, Opulencia JF, Engel I. Cytomegalovirus colitis in AIDS: radiographic findings in 11 patients. *Radiology* 1985;155:585-589
 8. Garcia F, Garan J, Sierra M, Marco U. Cytomegalovirus mononucleosis associated antral gastritis stimulating malignancy. *Arch Intern Med* 1987;147:787-788

Case 3: Hemorrhagic Cholecystitis

A 37-year-old man with a history of chronic alcohol abuse had a fever and sharp, constant, midepigastic pain radiating to the back for 4 days. The patient denied nausea, vomiting, or melena. On physical examination the patient was anicteric and febrile (body temperature, 102°F). The abdomen was tender with guarding in the midepigastrium and right upper quadrant. There was a suggestion of a subhepatic mass. The stool was positive for occult blood. Laboratory findings included a hematocrit of 36% and a WBC count of 14,500.

Sonographic evaluation of the abdomen (Figs. 3A and 3B) showed an enlarged, irregularly thickened gallbladder wall with a small amount of pericholecystic fluid. Multiple small echogenic foci with shadowing, which represented stones, were seen in the gallbladder. The lumen of the gallbladder was filled with heterogeneous material. No intrahepatic or extrahepatic biliary duct abnormalities were found. Subsequently, abdominal CT (Fig. 3C) showed a superficial, distended, 9 × 6 × 5 cm gallbladder with surrounding inflammatory changes extending to overlying soft tissues. The gallbladder wall was irregularly thickened and measured 1 cm. In the lumen of the gallbladder there was a fluid-fluid interface with a dependent, high-attenuation component. The liver showed diffuse fatty infiltration. There was no abdominal lymphadenopathy. A hepatobiliary scan was indeterminate for

cholecystitis because of poor excretion of the agent consistent with the patient's known cirrhosis. At cholecystectomy, the gallbladder was noted to be markedly inflamed, with areas of gangrene and adhesions but no perforation. Inside the gallbladder were numerous large blood clots and multiple small stones. The patient had an uneventful postoperative course.

Nontraumatic hemorrhagic cholecystitis is a rare complication of biliary tract disease [1, 2]. Most commonly associated with cholelithiasis, hemorrhagic cholecystitis has a high mortality rate. Biliary colic, jaundice, hematemesis, and melena make up the classic syndrome. Forty percent have a palpable mass in the right upper quadrant [3]. Other presentations include massive upper gastrointestinal bleeding, hydrops of the gallbladder, hemoperitoneum, or obstruction of the common bile duct [1]. In hemorrhagic cholecystitis, blood may clot in the gallbladder, especially after cystic duct obstruction, producing marked distention and possibly rupture. By passing through the common bile duct into the duodenum, blood may cause hematemesis or melena. Alternatively, if the blood clots in the common bile duct, obstructive jaundice will ensue [3, 4]. The mechanism is thought to be hemorrhage due to local inflammation caused by stones forming mucosal ulcerations or necrosis [3, 5], possibly more likely in patients with arteriosclerotic vascular changes [6]. Several reports describe diffuse oozing of blood from the gallbladder mucosa [1, 3, 6, 7]. Acute inflammation of mucosa in the stomach, colon, and bladder often produces hemorrhage, but this finding is distinctly uncommon in the gallbladder [7]. Other causes of hemobilia producing gross blood in the gallbladder include biliary neoplasms, trauma, vascular diseases (including aneurysms that rupture into the biliary tract), anticoagulation, parasites, and ectopic gastric or pancreatic mucosa [2, 8]. Correlation with chronic alcohol abuse has been noted in several patients with hemorrhagic cholecystitis [3, 8].

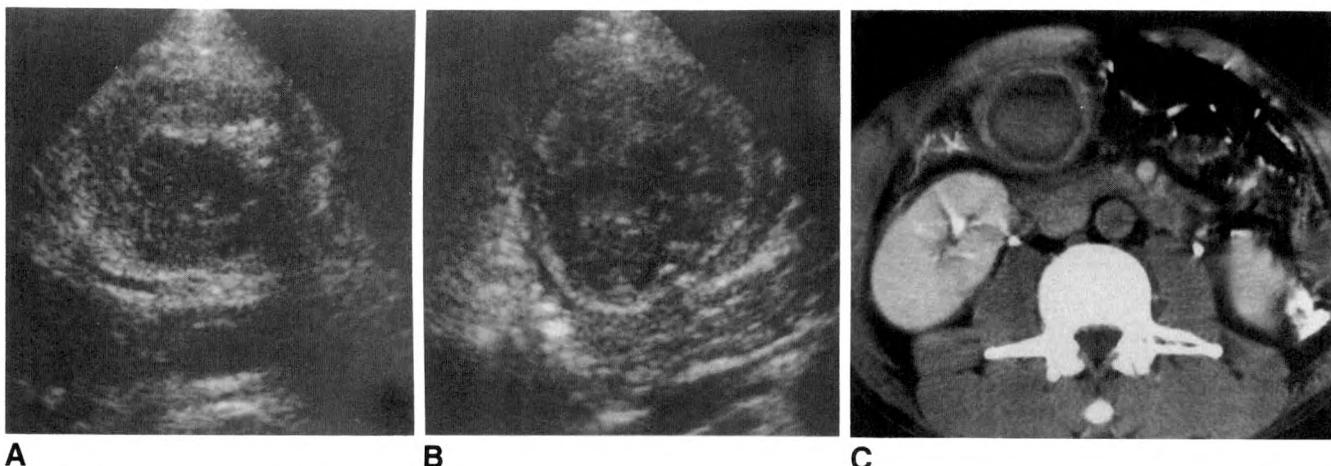


Fig. 3.—Case 3: Hemorrhagic cholecystitis.
A, Transverse sonogram reveals gallbladder filled with heterogeneous material. Several bright echogenic foci produce shadowing. Borders are poorly defined.
B, Transverse sonogram shows a small amount of pericholecystic fluid.
C, Contrast-enhanced CT scan shows a distended gallbladder containing high-attenuation material. Gallbladder wall is markedly thickened without nodularity. Inflammatory changes involve surrounding soft tissues. This study was done just before surgery, which revealed a large clot filling gallbladder lumen.

Jenkins et al. [2] discuss the differential diagnosis of hemorrhagic cholecystitis by use of CT and sonography. Blood in the gallbladder lumen appears echogenic, similar to thick sludge or pus. Although sludge normally layers to a dependent position, very thick sludge in an obstructed gallbladder may form echogenic clumps adherent to the wall, mimicking a carcinoma. Blood clots in the lumen may be seen as fixed, nonshadowing echogenic clumps. However, these solid structures may become a complex, cystic mass as the clots undergo lysis and liquefaction [2, 8]. High-attenuation bile in the gallbladder usually results from recent IV administration of contrast material or "milk of calcium" bile; neither of these is echogenic. Likewise, sludge, pus, or a gallbladder carcinoma does not have as high an attenuation on CT as blood in the gallbladder does [2].

In conclusion, the prompt diagnosis of hemorrhagic cholecystitis is important because of its high mortality rate. Although historically the diagnosis is rarely made preoperatively [3, 4], the combination of findings on CT and sonography should suggest this very unusual diagnosis.

Margo M. Moskos
David J. Eschelman

REFERENCES

1. Polse S, Stoney RJ, Baldwin JN. Hemorrhage from the gallbladder. *Calif Med* 1967;107:51-53
2. Jenkins M, Golding RH, Cooperberg PL. Sonography and computed tomography of hemorrhagic cholecystitis. *AJR* 1983;140:1197-1198
3. Butterfield WC, Choi U. Hemobilia associated with hemorrhagic cholecystitis in a patient with alcoholic cirrhosis. *Conn Med* 1971;35:295-299
4. Shah VR, Clegg JF. Haemorrhagic cholecystitis. *Br J Surg* 1979;66:404-405
5. Stahl WM. Gastrointestinal-tract hemorrhage due to gallbladder disease. *N Engl J Med* 1959;260:471-474
6. Hudson PB, Johnson PP. Hemorrhage from the gallbladder. *N Engl J Med* 1946;234:438-441
7. Horsburgh GA, Levi AJ. Haematocele of the gall-bladder. *Br J Surg* 1963;50:844-845
8. Yiu-Chiu VS, Chiu LC, Wedel VJ. Acalculous hemorrhagic cholecystitis. *CT* 1980;4:201-206

Case 4: Ovarian Luteinized Thecoma

This 73-year-old, previously healthy, woman experienced 2 weeks of lower abdominal pain and a small amount of vaginal bleeding. On physical examination the abdomen was moderately distended, and a 4-cm right adnexal mass was found. No signs of virilism were seen.

Endovaginal pelvic sonography (Figs. 4A-4C) showed an enlarged uterus with a $5.4 \times 6.3 \times 5.6$ cm hypoechoic, solid, right adnexal mass immediately adjacent to the body of the uterus. No fluid was present in the cul-de-sac. MR images of the pelvis (Figs. 4D and 4E) showed the mass to be separate from the uterus. The signal was isointense to muscle on T1-weighted (571/16) images and heterogeneously increased on T2-weighted (2000/60) images.

An exploratory laparotomy with hysterectomy and bilateral salpingo-oophorectomy was performed, and histologic examination of the right adnexal mass revealed a luteinized thecoma. The uterus contained an intramural leiomyoma and

endometrial hyperplasia. No evidence of malignancy was found.

Primary tumors of the ovary arise from one of three ovarian components. The surface coelomic epithelium accounts for 75% of tumors and gives rise to serous and mucinous adenomas or adenocarcinomas, along with clear cell, endometrioid, and undifferentiated carcinomas. Totipotential germ cells account for 15% of tumors and give rise to teratomas, dysgerminomas, choriocarcinomas, and embryonal cell carcinomas. The stroma of the ovary, including the sex cords, accounts for 10% of tumors and gives rise to granulosa cell tumors, thecomas, fibromas, luteomas, and Sertoli-Leydig cell tumors [1].

The stromal tumors exist in a great variety of cell combinations, as well as pure forms. It is suggested that the fibroma, fibrothecoma, thecoma, luteinized thecoma, and luteoma form a continuum of related stromatogenous tumors. This series of tumors becomes less estrogenic and more androgenic with progression toward the pure luteoma and acquisition of more steroid-hormone secreting cells [2].

The luteinized thecoma was first described in 1954 as a fibromatous ovarian tumor containing lutein (steroid-hormone secreting) cells. It is usually estrogenic or nonfunctioning, but may be androgenic [3]. In one large review of 50 luteinized thecomas, Zhang et al. [4] found estrogenic manifestations in 50% and androgenic manifestations in 11%. The remainder showed no evidence of hormone production. The average age of the patients was 46 years, and the most common presentation was vaginal bleeding.

The theca cell tumors are important for two reasons. First, they can elaborate large quantities of estrogen and may subsequently lead to endometrial carcinoma. Second, they may have an inherent malignant potential of their own. A malignant thecoma has been postulated to exist, but some suggest it actually is a fibrosarcoma. These tumors tend to have associated peritoneal and mesenteric implants that recur after excision [4, 5].

Sonograms of ovarian thecomas classically show a hyperechoic solid adnexal mass with posterior acoustic shadowing. Athey and Malone [6], suggest that a broader spectrum of findings exists, including an echogenic mass with or without septa and a hypoechoic mass with a well-defined back wall.

According to Lupetin [7], MR imaging of pure ovarian thecomas shows decreased signal relative to muscle on both T1- and T2-weighted images. They have also found that the granulosa cell tumors and corpus luteum cysts, which contain a higher content of steroid-hormone secreting cells, have increased signal on T2-weighted images. The current case shows increased signal on T2-weighted images, and we postulate that it is due to the luteinized cells.

The differential diagnosis in this case includes a granulosa cell tumor, luteoma, and a degenerating pedunculated leiomyoma of the uterus.

Lisa C. Martin

ACKNOWLEDGMENT

The author thanks Ewa Kuligowska for her guidance in the preparation of this case.

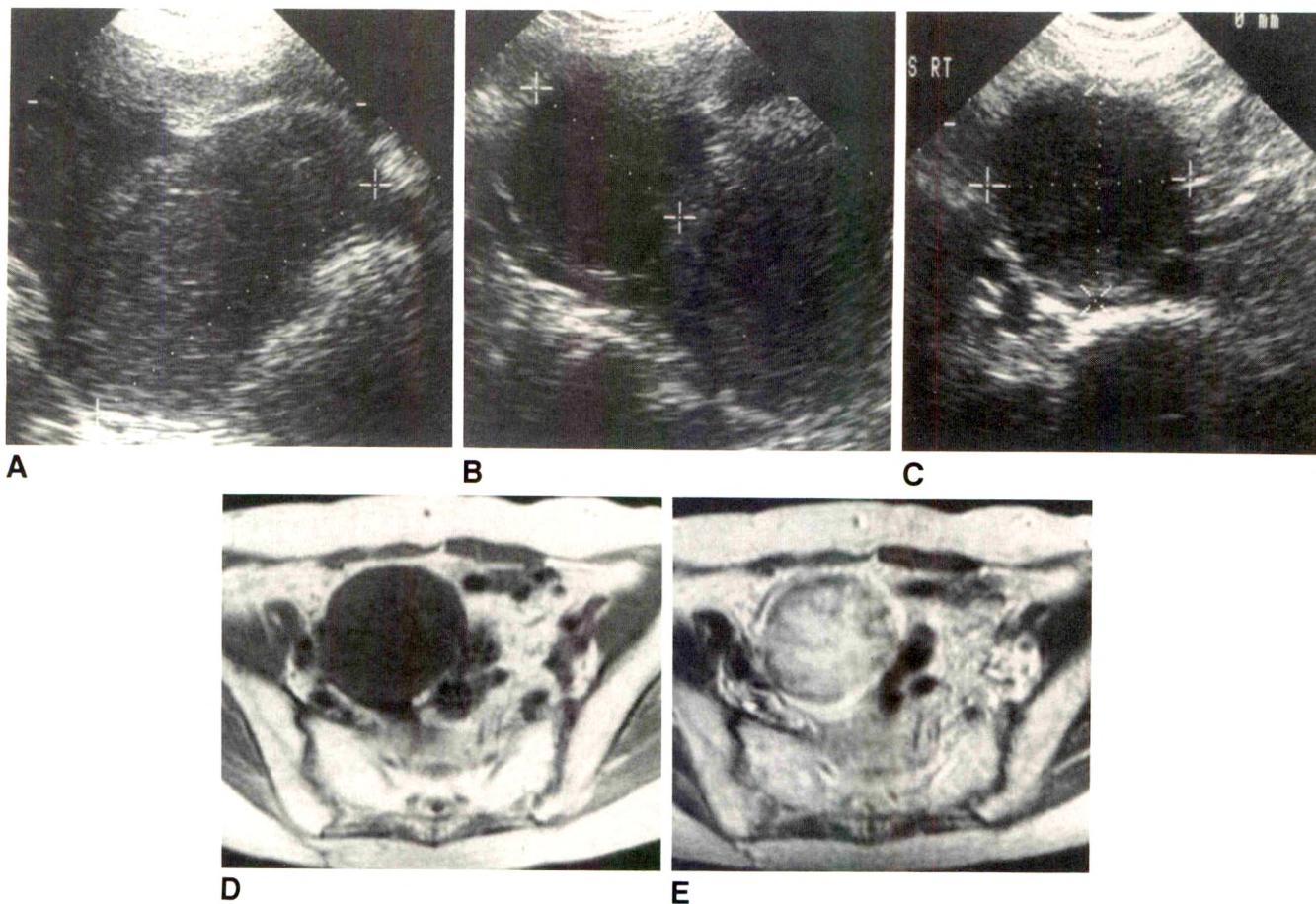


Fig. 4.—Case 4: Ovarian luteinized thecoma.

A, Longitudinal, endovaginal sonogram of mid pelvis shows an enlarged uterus measuring 10.5 cm.

B, Longitudinal, endovaginal sonogram of right adnexal region shows a hypoechoic mass (5.4 cm) with a well-defined back wall immediately adjacent to uterus.

C, Transverse, endovaginal sonogram shows hypoechoic mass (6.3 × 5.6 cm) in right adnexal region.

D, Axial T1-weighted (571/16) MR image of mid pelvis shows mass isointense to muscle. It is well circumscribed and separate from uterus.

E, Axial T2-weighted (2000/60) MR image of mid pelvis shows heterogeneous increased signal.

REFERENCES

1. Robbins S, Cotran R, Kumar V. The female genital tract. In: *Pathologic basis of disease*, 3rd ed. Philadelphia: Saunders, 1984:1142–1155
2. Hugesdon P. Lipid cell thecomas of the ovary. *Histopathology* 1983;7:681–692
3. Young R, Scully R. Ovarian sex cord-stromal tumors: recent progress. *Int J Gynecol Pathol* 1982;1:101–123
4. Zhang J, Young RH, Arseneau J, Scully RE. Ovarian stromal tumors containing lutein or Leydig cells: analysis of fifty cases. *Int J Gynecol Pathol* 1982;1:270–285
5. Dudzinski M, Cohen M, Ducatman B. Ovarian malignant luteinized thecoma: an unusual tumor in an adolescent. *Gynecol Pathol* 1989;35:104–109
6. Athey P, Malone R. Sonography of ovarian fibromas/thecomas. *J Ultrasound Med* 1987;6:431–436
7. Lupetin A. Female pelvis. In: Stark D, Bradley W. *Magnetic resonance imaging*. St. Louis: Mosby, 1988:1272–1296

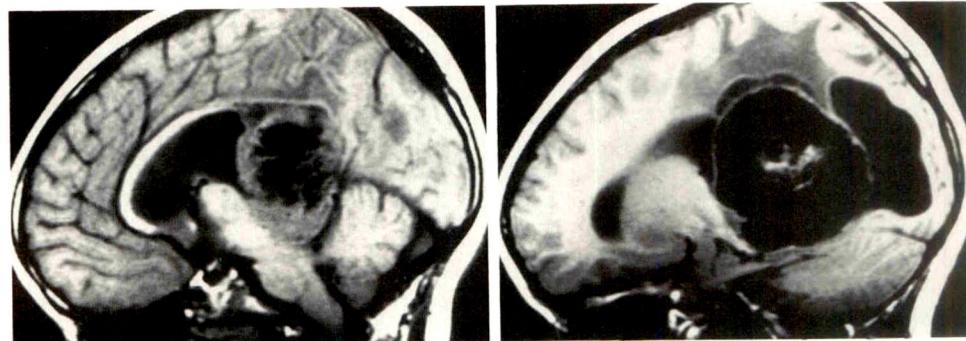
Neuroradiology Case of the Day

Daryl R. Parker,¹ David J. Eschelman, Douglas T. Gibbens, James D. Rabinov, and John F. O'Connor

Case 1: Intraventricular Meningioma

This 6-year-old girl came to the emergency department with a headache and increasing lethargy for 1 week. Physical examination revealed a mild ataxia. An unenhanced CT scan of the head (not shown) showed a densely calcified left-sided intraventricular mass with surrounding edema. MR images

(Figs. 1A–1D) displayed the large calcified mass as a well-defined area of signal void with few internal soft-tissue structures, arising from the trigone of the left lateral ventricle. Compression of the third ventricle produced an obstructive hydrocephalus. White matter edema with mild left-to-right midline shift was also shown. Resection of the mass revealed an intraventricular meningioma.



A

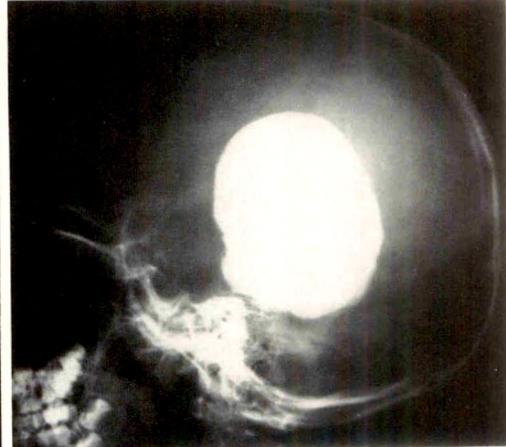
B



C



D



E

Fig. 1.—Case 1: Intraventricular meningioma.

A and B, Sagittal T1-weighted (600/15) MR images, midline (A) and left of midline (B), show a large intraventricular mass arising from trigone of left lateral ventricle. Some soft-tissue structure is evident, but predominant signal void results from dense calcification.

C and D, Axial T2-weighted (2000/80) MR images show extensive white matter edema surrounding large calcified mass. Compression of third ventricle produces obstructive hydrocephalus. There is mild left-to-right midline shift.

E, Lateral skull radiograph reveals large, densely calcified mass. Erosion of sella turcica is evidence of increased intracranial pressure.

¹ All authors: Department of Radiology, Boston University Medical Center, 88 E. Newton St., Boston, MA 02118. Address reprint requests to J. F. O'Connor.

Although meningiomas make up 15% of adult intracranial neoplasms, they account for only 1–2% of brain tumors in children [1, 2]. An intraventricular location is unusual in adults, accounting for three (1%) of 295 intracranial meningiomas studied by Cushing and Eisenhardt and seven (0.5%) of 1454 intracranial meningiomas in the Mayo Clinic series [2–4]. Although meningiomas are uncommon in children, 15–17% are within the ventricular system [1, 3]. Most commonly seen in the third and fourth decades of life, intraventricular meningiomas have been reported in patients from 3.5 to 72 years old [3]. A female preponderance of 2:1 is noted with intracranial meningiomas in adults, but no sex predilection has been described in meningiomas in children [2, 5]. Neurofibromatosis-2 is reported to have a prevalence of 24% in children with meningiomas, especially when the meningiomas are multiple or intraventricular [1–3].

Intraventricular meningiomas arise from groups of arachnoid fibroblasts in the tela choroidea, which is the vascular core of the choroid, continuous with the pia mater [6]. The trigone of the lateral ventricle is the most common site for intraventricular meningiomas [3, 4]. The left lateral ventricle is affected at least 50% more often than the right one [3–5, 7]. These tumors tend to be quite large at presentation because of the late onset of symptoms. Tumors located anteriorly in the lateral ventricles near the foramen of Monro and the very rare third and fourth ventricular meningiomas tend to present as smaller lesions because of the early onset of hydrocephalus [1, 3]. The most common signs and symptoms are headache, hemiparesis, visual changes, and seizures [5]. The clinical presentation of lateral ventricular meningiomas often mimics that of posterior fossa masses [4]. Skull radiographs (Fig. 1E) reveal changes of longstanding increased intracranial pressure in 64%, as shown by enlargement and/or destruction of the sella turcica [5].

Whereas approximately 10% of intracranial meningiomas calcify, 45–68% of intraventricular meningiomas have calcifications [1, 6]. The pattern is similar to that of meningiomas elsewhere, ranging from well-defined speckled calcifications to homogeneous amorphous areas. The calcification may be isolated to one portion of the tumor or the periphery. As demonstrated in the present case, the entire tumor may be densely calcified [3].

Choroid plexus papillomas and ependymomas occur commonly at the trigone of the lateral ventricles, but this large, densely calcified mass presenting with an insidious onset makes intraventricular meningioma the most likely diagnosis. Other childhood intraventricular masses include oligodendroglomas, astrocytomas, primitive neuroectodermal tumors, teratomas, and subependymal giant-cell astrocytomas [8].

David J. Eschelman
Douglas T. Gibbons

REFERENCES

- Merten DF, Gooding CA, Newton TH, Malamud N. Meningiomas of childhood and adolescence. *J Pediatr* 1974;84:696–700
- Deen HG, Scheithauer BW, Ebersold MJ. Clinical and pathological study of meningiomas of the first two decades of life. *J Neurosurg* 1982;56:317–322
- Batitzky S. Case 27: intraventricular meningioma. In: Weinberg PE, ed. *Neuroradiology (part 2) test and syllabus*. Reston, VA: American College of Radiology. 1990:715–743
- Kobayashi S, Okazaki H, MacCarty CS. Intraventricular meningiomas. *Mayo Clin Proc* 1971;46:735–741
- Mani RL, Hedcock MW, Mass SI, Gilmor RL, Enzmann DR, Eisenberg RL. Radiographic diagnosis of meningioma in the lateral ventricle: review of 22 cases. *J Neurosurg* 1978;49:249–255
- Perry RD, Parker GD, Hallinan JM. CT and MR imaging of fourth ventricular meningiomas. *J Comput Assist Tomogr* 1990;14:276–280
- Abbott KH, Courville CB. Intraventricular meningiomas: review of the literature and report of two cases. *Bull LA Neurol Soc* 1942;7:12–28
- Jelinek J, Smirniotopoulos JG, Parisi JE, Kanzer M. Lateral ventricular neoplasms of the brain: differential diagnosis based on clinical, CT, and MR findings. *AJR* 1990;155:365–372

Case 2: Recurrent Meningeal Hemangiopericytoma

This 57-year-old man initially presented 5 years earlier with sudden onset of a severe headache and blurry vision, followed by loss of consciousness. He underwent surgical excision of a mass in the left posterior fossa via left occipital craniotomy. Pathologic diagnosis was meningeal hemangiopericytoma. Postoperative CT revealed bilateral occipital lobe infarction. Two years later, CT showed a recurrent left cerebellar mass. The patient received 4000 cGy of whole-brain irradiation. A right-sided ventriculoperitoneal shunt was placed.

At the time of these studies, the patient had a 6-month progressive history of vomiting, lethargy, and ataxia. Cerebral MR imaging (Figs. 2A–2E) showed a 4 × 5 cm heterogeneous left cerebellar mass, compressing the fourth ventricle and brainstem. The tumor had a broad base abutting the tentorium. The mass was predominantly isointense to cortex on T1-weighted images and hyperintense on T2-weighted images. After administration of gadopentetate dimeglumine, heterogeneous tumor enhancement with marked peripheral enhancement was shown. A digital subtraction angiogram (Fig. 2F) of the left vertebral artery displayed a hypovascular mass with a small region of tumor blush supplied by the left superior cerebellar artery. The clinicopathologic diagnosis was recurrent meningeal hemangiopericytoma.

Meningiomas make up approximately 15% of all intracranial tumors [1, 2]. There are four basic types: fibroblastic, transitional, syncytial, and angioblastic. Mixed varieties exist. Meningeal hemangiopericytomas are considered by some to be a hemangiopericytic subtype of angioblastic meningiomas [3], and they are considered as such in this discussion. However, the question of whether the meningeal hemangiopericytoma is actually a meningioma remains controversial. Some have separated angioblastic meningiomas from the rest of meningiomas because they do not arise from archetypal meningotheelial cells [4]. Hemangiopericytomas arise from the pericytes of blood vessels. They adhere to the meninges with a smooth but unencapsulated surface and contain areas of hypocellularity, necrosis, and cyst formation.

Meningeal hemangiopericytomas account for 2.4% of all meningiomas and less than 1% of all CNS tumors [3]. The distribution of meningeal hemangiopericytomas is similar to that of other meningiomas, with 61% supratentorial, 13% tentorial, 13% posterior fossa, 5% torcular, and 5% spinal [3]. In contrast to the female preponderance in meningiomas as a whole, meningeal hemangiopericytomas display a slight male preponderance (55%) [3]. The average age of onset is 42 years compared with the early fifties for patients with other meningiomas [3]. For supratentorial tumors, the most common symptoms and signs are headache (68%), papilledema (50%), and hemiparesis (40%), whereas for infratentorial tumors, gait disturbance (56%), ataxia (44%), headache (44%), and papilledema (44%) are most common [3]. Before diagnosis, the average duration of symptoms is 11 months [3].

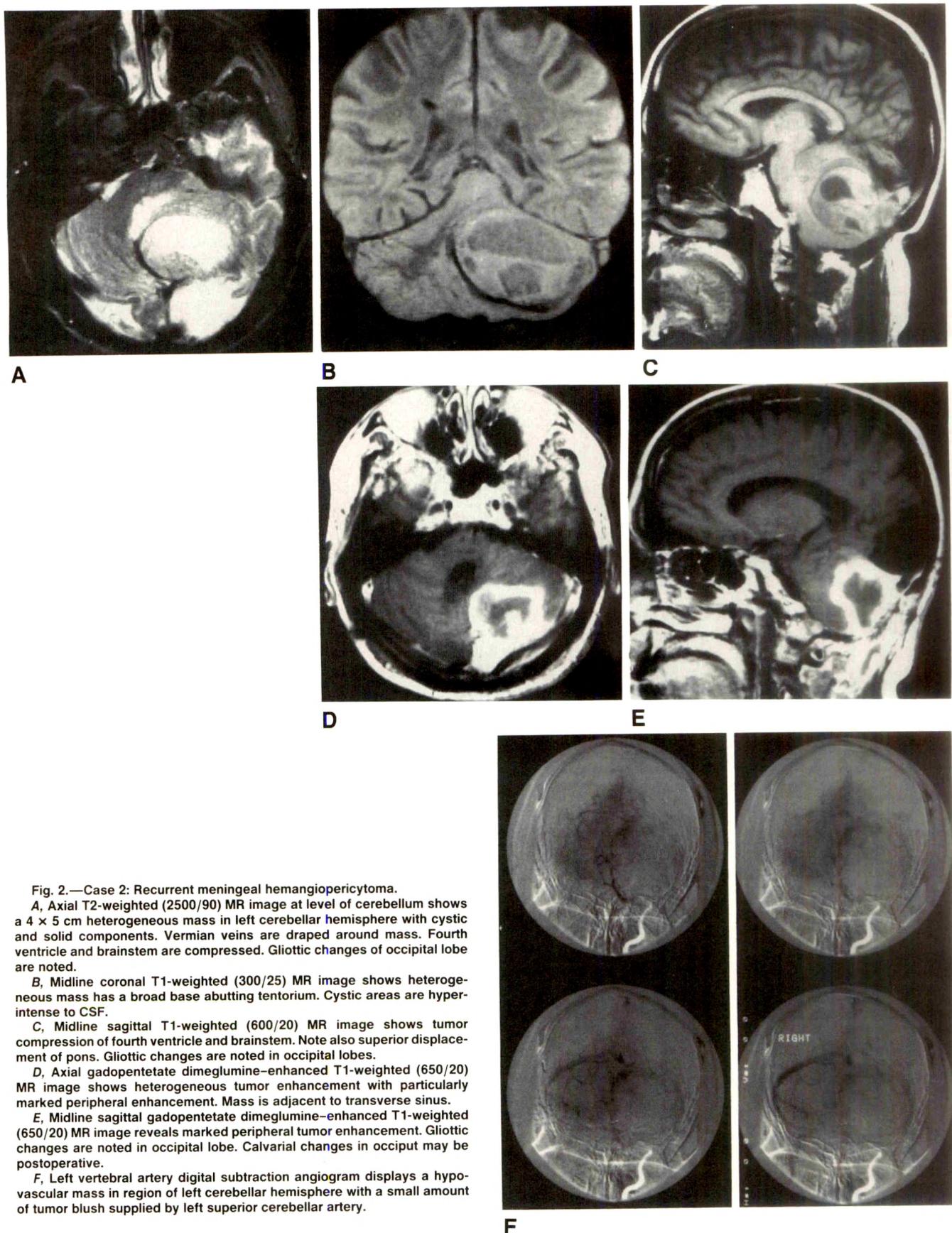


Fig. 2.—Case 2: Recurrent meningeal hemangiopericytoma.

A, Axial T2-weighted (2500/90) MR image at level of cerebellum shows a 4 × 5 cm heterogeneous mass in left cerebellar hemisphere with cystic and solid components. Vermian veins are draped around mass. Fourth ventricle and brainstem are compressed. Gliotic changes of occipital lobe are noted.

B, Midline coronal T1-weighted (300/25) MR image shows heterogeneous mass has a broad base abutting tentorium. Cystic areas are hyperintense to CSF.

C, Midline sagittal T1-weighted (600/20) MR image shows tumor compression of fourth ventricle and brainstem. Note also superior displacement of pons. Gliotic changes are noted in occipital lobes.

D, Axial gadopentetate dimeglumine-enhanced T1-weighted (650/20) MR image shows heterogeneous tumor enhancement with particularly marked peripheral enhancement. Mass is adjacent to transverse sinus.

E, Midline sagittal gadopentetate dimeglumine-enhanced T1-weighted (650/20) MR image reveals marked peripheral tumor enhancement. Gliotic changes are noted in occipital lobe. Calvarial changes in occiput may be postoperative.

F, Left vertebral artery digital subtraction angiogram displays a hypovascular mass in region of left cerebellar hemisphere with a small amount of tumor blush supplied by left superior cerebellar artery.

Meningeal hemangiopericytomas recur at greater frequency and more commonly have extraneurial metastases than do other meningiomas [3]. After initial surgery, hemangiopericytomas have recurrence rates of 15% at 1 year, 65% at 5 years, and 85% at 10 years [3]. Metastases, most commonly to lung and bone or rarely to liver, brain, and retroperitoneum, occur in 13% at 5 years, 33% at 10 years, and 64% at 15 years [3]. The 5-, 10-, and 15-year survival rates are 67%, 40%, and 23%, respectively [3]. Posterior fossa location, incomplete surgical resection, and metastases suggest a worse prognosis [3]. Complete tumor excision is recommended. Radiation therapy with doses greater than 5100 cGy after initial surgical resection prolongs length of survival by 50% [3].

Radiologically, the appearance of meningeal hemangiopericytomas varies. They are included among the angioblastic meningiomas in this discussion. Meningiomas usually have average attenuation equal to or greater than cortex on unenhanced CT scans. CT features used to differentiate the various types of meningiomas include definition of tumor margins, degree of peritumoral edema, presence of calcium aggregates, and tumor homogeneity before and after contrast administration [1]. Unlike fibroblastic and transitional meningiomas, angioblastic and syncytial meningiomas display heterogeneous attenuation with low-density cystic areas, poorly defined tumor margins, marked peritumoral edema, absence of calcium aggregates, and heterogeneous enhancement with nonenhancing cystic areas [1]. Angioblastic meningiomas, including meningeal hemangiopericytomas, are generally larger and more heterogeneous, with more cystic areas than the syncytial type [1].

On MR, meningiomas have an interface with brain consisting of a CSF cleft, vascular rim, or broad dural margin [2, 5]. The appearance of angioblastic meningiomas, including meningeal hemangiopericytomas, varies. T1-weighted images are not generally useful in differentiating types of meningioma. On T1-weighted images, 62% of meningiomas are isointense and 38% are hypointense when compared with the cortex [2, 6]. Rarely, angioblastic meningiomas may show hyperintensity on T1-weighted images due to intratumoral hemorrhage [6]. As opposed to T1-weighted images, the signal characteristics of T2-weighted images have been correlated with histopathologic findings in more than 75% of cases [6]. On T2-weighted images, hypointense lesions indicate predominantly fibroblastic or transitional elements, whereas hyperintense lesions indicate syncytial or angioblastic types of meningiomas [6]. Meningeal hemangiopericytomas less commonly are isointense on T2-weighted images [3]. Secondary criteria, including presence and severity of edema, cysts, and presence of calcium, are also helpful in differentiating the histologic type of meningioma [6]. Angioblastic meningiomas and syncytial meningiomas are associated with severe edema, central necrosis, and cyst formation, with heterogeneous internal signal before and after administration of gadopentetate dimeglumine [6].

Angiography of meningeal hemangiopericytomas usually reveals a vascular mass with a persistent vascular stain [3]. The tumor may have intradural or mixed intradural and extradural blood supply. The internal carotid artery is a major supplier of blood in most cases; it is the only arterial supply for half of the cases [3]. The majority of meningeal hemangiopericytomas fill rapidly and drain slowly [3].

In conclusion, the meningeal hemangiopericytoma is a rare cerebral neoplasm. Alternatively known as an angioblastic meningioma, hemangiopericytic type, this tumor has been considered a meningioma despite controversy surrounding this classification. Radiologically, the appearance of meningeal hemangiopericytomas may vary. CT shows a large heterogeneous mass with average attenuation greater than cortex with poorly defined tumor margins, marked peritumoral edema, absence of calcifications, and heterogeneous enhancement with nonenhanced cystic areas. MR imaging usually shows these tumors to be isointense to cortex on T1-weighted images and significantly hyperintense to cortex on T2-weighted images. A large amount of peritumoral edema, central necrosis, and cyst formation giving rise to heterogeneous signal also is associated with the tumor. Because of the risk of tumor recurrence and metastases, rigorous clinical and radiologic monitoring is necessary after initial treatment.

Daryl R. Parker
James D. Rabinov

ACKNOWLEDGMENT

The authors thank Jorge Delgado for his guidance in the preparation of this case.

REFERENCES

1. Vasilouthis J, Ambrose J. Computerized tomography scanning appearance of intracranial meningiomas. *J Neurosurg* 1979;50:320-327
2. Spagnoli M, Goldberg HI, Grossman RI, et al. Intracranial meningiomas: high-field MR imaging. *Radiology* 1986;161:369-375
3. Guthrie BL, Ebersold MJ, Scheithauer BW, Shaw EG. Meningeal hemangiopericytoma: histopathological features, treatment, and long-term follow-up of 44 cases. *Neurosurgery* 1989;25:514-521
4. Burger PC, Vogel FS. *The intracranial meninges: surgical pathology of the nervous system and its coverings*, 2nd ed. New York: Wiley Medical, 1982:92
5. Aoki S, Susaki J, Machida T, Tanioka H. Contrast enhanced MR images in patients with meningioma: Importance of enhancement of the dura adjacent to the tumor. *AJNR* 1990;11:935-938
6. Elster AD, Challa VR, Gilbert TH, Richardson DN, Contento JC. Meningiomas: MR and histopathologic features. *Radiology* 1989;170:857-862

Case 3: Acute Cerebral Arterial Thrombosis

A 25-year-old woman institutionalized for depression was found pulseless after hanging herself with a bedsheet between routine 15-min checks. After cardiopulmonary resuscitation was started, her blood pressure and pulse returned. When she arrived in the emergency department, she was unresponsive, with dilated pupils. Unenhanced CT of the head (Figs. 3A-3C) revealed cerebral edema and linear high-attenuation foci representing thrombosis of major intracerebral vessels, including the internal carotid arteries, anterior cerebral arteries, middle cerebral arteries, circle of Willis, posterior cerebral arteries, and basilar artery. After 36 hr, the patient had no brainstem functions, and a brain flow scan (Fig. 3D) revealed no cerebral blood flow.

Several recent reports [1-5] have described the homogeneous, high-attenuation appearance of structures corresponding to the contour and location of intracranial arteries in acute cerebral arterial thrombosis. This finding is generally noted in patients with thrombotic or embolic strokes, and the dense artery is often associated with hypodense ischemic areas in its distribution.

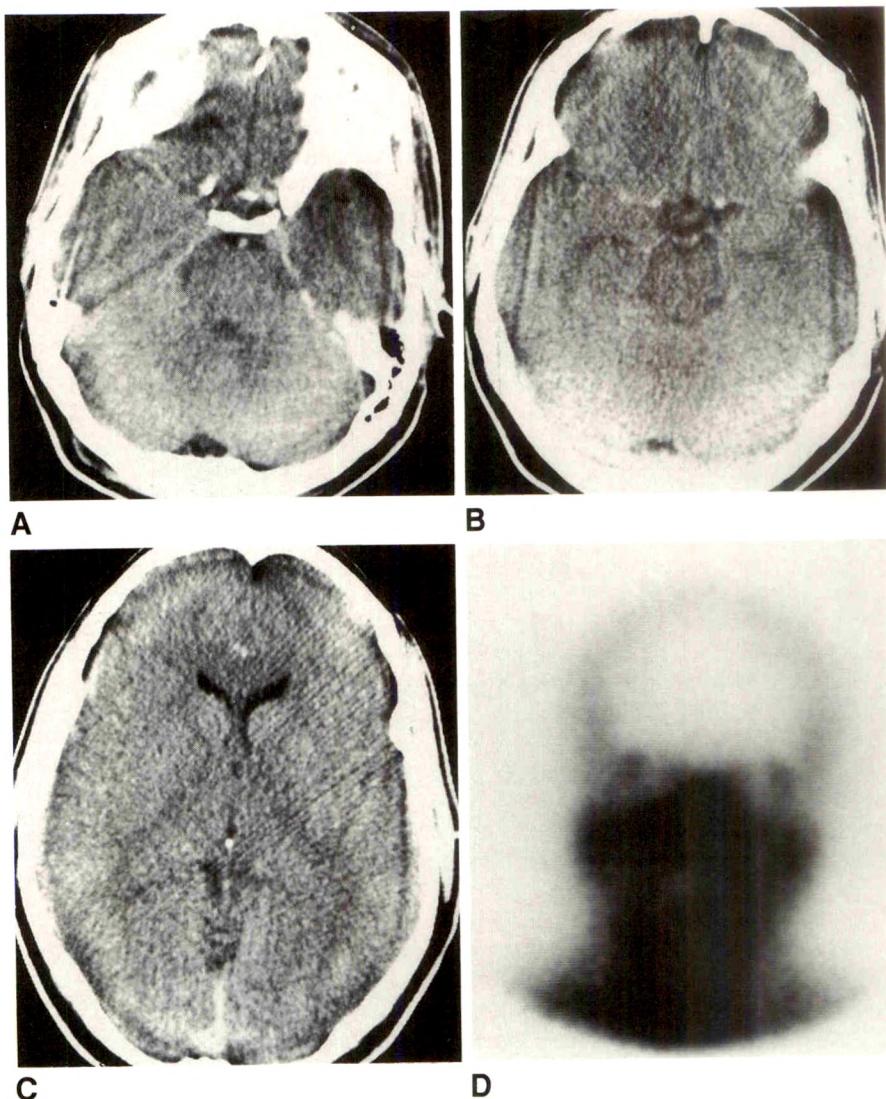
Fig. 3.—Case 3: Acute cerebral arterial thrombosis.

A, Axial unenhanced CT scan shows high-attenuation basilar artery representing thrombosis and cerebral edema.

B, Axial unenhanced CT scan reveals high-attenuation structures corresponding to thrombosis of several cerebral vessels: internal carotid arteries, anterior cerebral arteries, middle cerebral arteries, and circle of Willis.

C, Axial unenhanced CT scan reveals thrombosis in anterior cerebral arteries and cerebral edema.

D, Brain flow study, static image, shows no intracerebral blood flow.



Other causes of nonenhanced high-attenuation arteries have been delineated. For example, high-density arteries on unenhanced CT may be seen in patients with advanced arteriosclerotic disease, but arterial wall calcifications are usually irregular and patchy, as opposed to the homogeneous appearance of fresh thrombus. A normal cerebral artery surrounded by low-attenuation ischemic brain tissue or neoplasm may falsely appear hyperdense, but these arteries would still enhance with IV administration of contrast material [1]. Subintimal hemorrhage from dissection could also produce high-attenuation arteries [2]. In cerebrovascular accidents, clotted vessels should become less dense in several days as the thrombus matures [2, 5].

Because a limited distribution of high-attenuation cerebral arteries may be seen with acute thrombus or embolus causing cerebral infarction, this case is unusual because of the extensive thrombosis of cerebral arteries.

David J. Eschelman

REFERENCES

- Sasiadek M, Wasik A, Marcinak R. CT appearance of bilateral, acute thrombosis of the main cerebral arteries. *Comput Med Imaging Graph* 1990;14:89-90
- Pressman BD, Tourje EJ, Thompson JR. An early CT sign of ischemic infarction: increased density in a cerebral artery. *AJR* 1987;8:645-648
- Schuierer G, Huk W. The unilateral hyperdense middle cerebral artery: an early CT-sign of embolism or thrombosis. *Neuroradiology* 1988;30:120-122
- Tomsick TA, Brott TG, Chambers AA, et al. Hyperdense middle cerebral artery sign on CT: efficacy in detecting middle cerebral artery thrombosis. *AJR* 1990;11:473-477
- Hankey GJ, Khangure MS, Stewart-Wynne EG. Detection of basilar artery thrombosis by computed tomography. *Clin Radiol* 1988;39:140-143

Case 4: Central Neurocytoma

This 26-year-old Chinese man had a 3-month history of progressively blurred vision and difficulty differentiating colors. Seven years earlier, in China, he reportedly had a subarachnoid hemorrhage and a right hemispheric arteriovenous malformation shown by CT without subsequent surgery. Ophthalmologic examination now revealed optic atrophy and bilateral papilledema with decreased peripheral vision. CT of the head (Figs. 4A-4D) showed a heterogeneous intraventric-

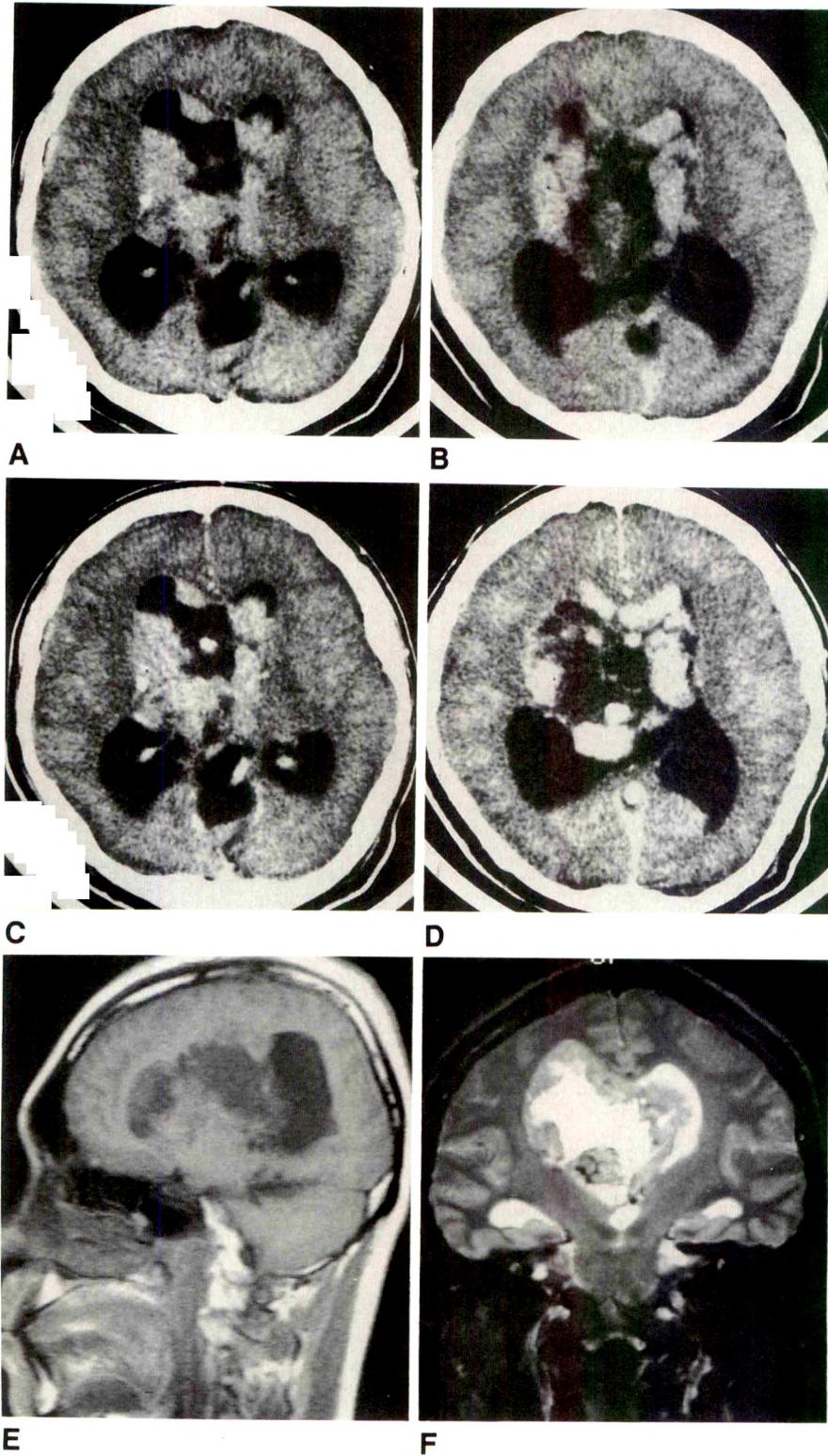


Fig. 4.—Case 4: Central neurocytoma.

A and **B**, Unenhanced CT scans of head at level of lateral ventricles reveal a $7 \times 6 \times 6$ cm heterogeneous intraventricular mass arising from body of lateral ventricles and extending around third ventricle. Mass is hyperdense relative to cerebral cortex and contains calcifications and low-attenuation areas. Note obstructive hydrocephalus. A 3-cm cystic lesion is seen between occipital horns.

C and **D**, Contrast-enhanced CT scans of head at level of lateral ventricles show heterogeneous tumor enhancement.

E, Midline sagittal T1-weighted (200/10) MR image shows $7 \times 6 \times 6$ cm heterogeneous intraventricular mass of lateral ventricles as predominantly hypointense to cerebral cortex. Mass extends into corpus callosum.

F, Coronal T2-weighted (3000/90) MR image reveals mass to be heterogeneous but predominantly hypointense relative to cortex. Mass displaces third ventricle inferiorly. Dilated temporal horns are well visualized.

G, Axial gadopentetate dimeglumine-enhanced T1-weighted (800/15) MR image at level of lateral ventricles shows heterogeneous mass enhancement.

ular mass, hyperdense relative to cerebral cortex, arising from the body of the lateral ventricles and extending around the third ventricle. There was obstructive hydrocephalus. The mass contained focal calcifications and showed heterogeneous contrast enhancement. A 3-cm cystic lesion was seen incidentally between the occipital horns.

Cerebral MR (Figs. 4E–4G) displayed a $7 \times 6 \times 6$ cm heterogeneous intraventricular mass of the lateral ventricles

with inferior displacement of the third ventricle. The tumor extended into the corpus callosum and right caudate nucleus. On T1-weighted images, the mass was predominantly hypointense to cortex and on T2-weighted images, largely hyperintense. The mass displayed heterogeneous enhancement after administration of gadopentetate dimeglumine. A cerebral angiogram (not shown) revealed a large hypovascular intraaxial mass in the region of the corpus callosum. Biopsy results

were diagnostic for central neurocytoma. Despite radiation therapy, the patient's symptoms have progressed.

Central neurocytoma is a rare, slowly growing neuroepithelial neoplasm of young adults arising from the lateral ventricles, with the third ventricle also commonly involved. Hydrocephalus is almost inevitably associated with these tumors. The age at presentation has ranged from 15 to 66 years with a peak in the midthirties [1-7]. There is no sex predilection [4]. Common presenting symptoms include headache, nausea, vomiting, blurred vision, dizziness, memory loss, and rarely paresis. Symptoms are related to progressive development of obstructive hydrocephalus. Duration of clinical symptoms before diagnosis is usually less than 6 months [5]. Common presenting signs include papilledema, decreased visual acuity, and rarely paresis.

Pathologically, immunocytochemical staining for neuron-specific enolase and the ultrastructural presence of neurosecretory granules and synapses are characteristic findings of central neurocytomas [1, 3, 5-7]. Data on management of central neurocytomas are limited. Prognosis is related to tumor resectability and is favorable if the bulk of the tumor can be removed [1, 4, 6]. Central neurocytomas have a better prognosis than primary cerebral neuroblastoma occurring in the hemispheres [1]. In one study, five of six patients with central neurocytoma were disease-free 15-227 months after total or partial tumor resection [4]. In addition, Tsujita et al. [7] have reported subtotal resection and 6000-cGy whole-brain radiation therapy as treatment with good results.

CT is helpful in showing the intraventricular location of these tumors and in showing focal calcifications. On unenhanced CT scans, the tumors are usually large with irregular margins and heterogeneous attenuation [4]. Neurocytomas are predominantly isodense to hyperdense as compared with cortex on unenhanced scans [1-7]. Focal calcifications are usually seen [1-3, 5-7]. Contrast enhancement varies, with some neurocytomas displaying no enhancement [3, 5], but the majority have slight to moderate enhancement [1, 4, 6]. Unilateral or bilateral ventricular dilatation due to obstruction at the foramen of Monro is commonly seen. Draining veins may be shown [5].

MR is helpful in better defining the extent of a neurocytoma, especially in sagittal and coronal planes. Intraventricular location, variable signal characteristics, and serpiginous flow void are the MR features of central neurocytomas [1, 5]. Neurocytomas tend to be isointense with cerebral cortex on T1-weighted images, with areas of intratumoral diminished signal representing focal calcifications [1, 5]. The appearance of central neurocytomas varies on T2-weighted images; some have been found to be isointense with cortex [5] and others, predominantly hyperintense [1]. Areas of focal hyperintensity on T2-weighted images may be due to focal necrosis [5]. The tumor signal is modified by large serpiginous signal flow voids resulting from intratumoral vessels and characteristic large draining veins [1, 5]. Neurocytomas usually do not enhance with gadopentetate dimeglumine.

Angiographic findings in central neurocytomas have been reported rarely [1, 6]. In these cases, the tumor has been relatively avascular.

Radiologic differential diagnosis of intraventricular neo-

plasms is dependent on the patient's age and the tumor location within the lateral ventricles (foramen of Monro, trigone, or body of the lateral ventricles), as well as the CT attenuation before contrast administration [8]. All intraventricular tumor types (except subependymoma) show contrast enhancement. MR is most useful in evaluating tumor location, size, and extent. However, MR findings of intraventricular tumors are not specific and usually are hypointense or isointense with cortex on T1-weighted images and hyperintense on T2-weighted images [8].

In patients between 6 and 30 years old, more than 85% of intraventricular tumors are low-grade gliomas, including subependymal giant-cell astrocytomas (SGCA), pilocytic astrocytomas, oligodendrogliomas, ependymomas, and mixed gliomas [8]. Choroid plexus papillomas and intraventricular meningiomas are less common [5, 8]. SGCA tend to arise in the region of the foramen of Monro, appearing partially calcified and hyperdense on unenhanced CT [8]. Calcification is a feature of ependymomas, SGCA, and less commonly oligodendrogliomas [1, 8]. Homogeneous enhancement is found in SGCA, meningiomas, choroid plexus papillomas, and oligodendrogliomas, whereas pilocytic astrocytomas and ependymomas display irregular enhancement [5, 8]. Unfortunately, neither CT nor MR provide distinctive findings that allow differentiation of central neurocytomas from other ventricular neoplasms.

In conclusion, central neurocytomas are rare, slowly growing neoplasms that arise in the lateral and/or third ventricles of young adults and are often associated with symptoms and signs of increased intracranial pressure. Radiologically, the appearance of neurocytomas varies. CT shows location and focal calcifications, and MR is helpful in defining tumor extent. However, neither imaging technique provides specific findings. Although central neurocytoma is a relatively rare lesion, it should be considered in the differential diagnosis of intraventricular lesions.

Daryl R. Parker

ACKNOWLEDGMENT

The author thanks Jorge Delgado for his guidance in the preparation of this case.

REFERENCES

1. Bolen JW Jr, Lipper MH, Caccamo D. Intraventricular central neurocytoma: CT and MR findings. *J Comput Assist Tomogr* 1989;13:495-497
2. Ferrell E, Sawaya R, deCourten-Myers GM. Primary cerebral neuroblastoma (neurocytoma) in adults. *J Neurooncol* 1989;7:121-128
3. Hassoun J, Gambarelli D, Grisoli F, et al. Central neurocytoma. *Acta Neuropathol (Berl)* 1982;56:151-156
4. Nishio S, Takatoshi T, Takeshita I, Fukui M. Intraventricular neurocytoma: clinicopathological features of six cases. *J Neural* 1988;68:665-670
5. Patil AA, McComb RD, Gerber B, McConnell J, Sasse S. Intraventricular neurocytoma: a report of two cases. *Neurosurgery* 1990;26:140-144
6. Townsend JJ, Seaman JP. Central neurocytoma: a rare benign intraventricular tumor. *Acta Neuropathol (Berl)* 1986;71:167-170
7. Tsujita Y, Nagashima K, Takakura K. A clinicopathological study of central neurocytoma. *No To Shinkei* 1989;41:547-548
8. Jelinek J, Smirniotopoulos JG, Parisi JE, Kanzer M. Lateral ventricular neoplasms of the brain: differential diagnosis based on clinical, CT, and MR findings. *AJR* 1990;155:365-372

Pediatric Case of the Day

John F. O'Connor,¹ Lisa C. Martin, Henry Chen, Bonnie L. Dobkin, Eric J. Sax, Oliver H. Pomeroy, and David J. Eschelman

Case 1: Ewing Sarcoma of Pubic Bone

This 15-year-old girl complained of intermittent left-sided groin pain for 2 years. She had no history of trauma, infection, or constitutional symptoms. Physical examination revealed fullness in the left inguinal region, but no discrete mass could be palpated.

The plain radiograph of the pelvis (Fig. 1A) revealed bony destruction of the left superior ramus and symphysis with a lamellated periosteal reaction. The bladder was displaced to the right by a large soft-tissue mass. A bone scan (Fig. 1B) showed markedly increased uptake in the left superior and inferior rami, symphysis, and acetabulum. The extent of the tumor mass was then evaluated by MR imaging. T1-weighted coronal (450/20) and axial (700/20) images (Figs. 1C, 1D, and 1F) and T2-weighted axial (3000/80) images (Figs. 1E and 1G) showed a large soft-tissue mass encasing the left superior ramus with extension into the pelvis. The mass was isointense to muscle on T1-weighted images and heterogeneously increased on T2-weighted images. Bladder wall invasion and bone marrow signal change in the left acetabulum were noted. An open biopsy was performed, and the histologic diagnosis was Ewing sarcoma.

Ewing sarcoma is a malignant bone tumor usually seen in patients between the ages of 5 and 14, rarely seen in patients over the age of 30 [1]. Overall, it is the second most common primary malignant tumor of bone in children and accounts for 10% of all primary bone tumors. In the pelvic bones, it is the most common primary malignant tumor [2]. The cell of origin is unknown, but it is thought by some to arise from a stem-cell precursor [3].

Clinically, there is a well-known delay in diagnosis. Patients will often have constitutional symptoms of malaise and fever with a leukocytosis suggesting an infection. When the pelvic bones are involved, poorly localized pain and a progressive limp are common [2]. Twenty percent of patients have metastases at the time of diagnosis, generally involving the lungs and other bones [4].

Plain radiography is the best imaging method for assessing the tumor and predicting the histologic diagnosis [1, 5]. There are four types of radiographic changes: diffuse sclerosis, diffuse osteolysis, mixed sclerosis and osteolysis, and per-

meative osteolysis [2]. The periosteal reaction may be lamellated or sunburst, and there may be a Codman's triangle. The tumor can occur at any skeletal site, occurring more often in the diaphyseal region of long tubular bones in patients younger than 18 years old and in the flat bones in older patients [1].

MR imaging is most useful in evaluating the extent of bone and soft-tissue involvement for preoperative and pretreatment planning [5]. The tumor is characteristically of decreased signal on T1-weighted images and increased signal on T2-weighted images [6]. After surgery or radiotherapy, a decreased signal on T2-weighted images has a high sensitivity for tumor sterilization. Continued increased signal on T2-weighted images may indicate residual tumor, inflammatory changes from radiation, or postoperative hematoma. Gadopentetate dimeglumine induces a signal enhancement of both active tumor and inflammatory changes, adding little to long-term follow-up [5].

The differential diagnosis of this tumor should include osteomyelitis, osteosarcoma, eosinophilic granuloma, non-Hodgkin lymphoma, and metastatic disease [2].

Survival rates have improved with aggressive adjunctive chemotherapy and megavoltage irradiation. The estimated 5-year survival rate is currently 15%. The most important predictor of prognosis is the primary site. Primary tumors of the pelvic bone have the lowest survival rate [1].

Lisa C. Martin

REFERENCES

1. Edeiken J, Dalinka M, Karasick D. Bone tumors and tumorlike conditions. In: *Roentgen diagnosis of diseases of bone*. Baltimore: Williams and Wilkins, 1990:395-421
2. Kozlowski K, Campbell J, Beluffi G, et al. Primary bone tumors of the pelvis in childhood: Ewing's sarcoma of the ilium, pubis and ischium. *Australas Radiol* 1989;33:354-358
3. Reinus W, Gilula L. Ewing's sarcoma. In: Taveras J, Ferrucci J. *Radiology*, vol. 5. Philadelphia: Lippincott, 1989;95:1-9
4. Simpson R, Bruner JM, Leavens ME. Metastatic Ewing's sarcoma to the brain: case report and review of treatment. *Surg Neurol* 1989;31:234-238
5. Frouge C, Vanel D, Coffre C, Couanet D, Cantesso G, Sarrazin D. The role of magnetic resonance imaging in the evaluation of Ewing Sarcoma. *Skeletal Radiol* 1988;17:387-392
6. Bloem J, Bluemm RG, Taminius AHM, Van Oosterom AT, Stoik J, Doorn-

¹ All authors: Department of Radiology, Boston University Medical Center, 88 E. Newton St., Boston, MA 02118. Address reprint requests to J. F. O'Connor.

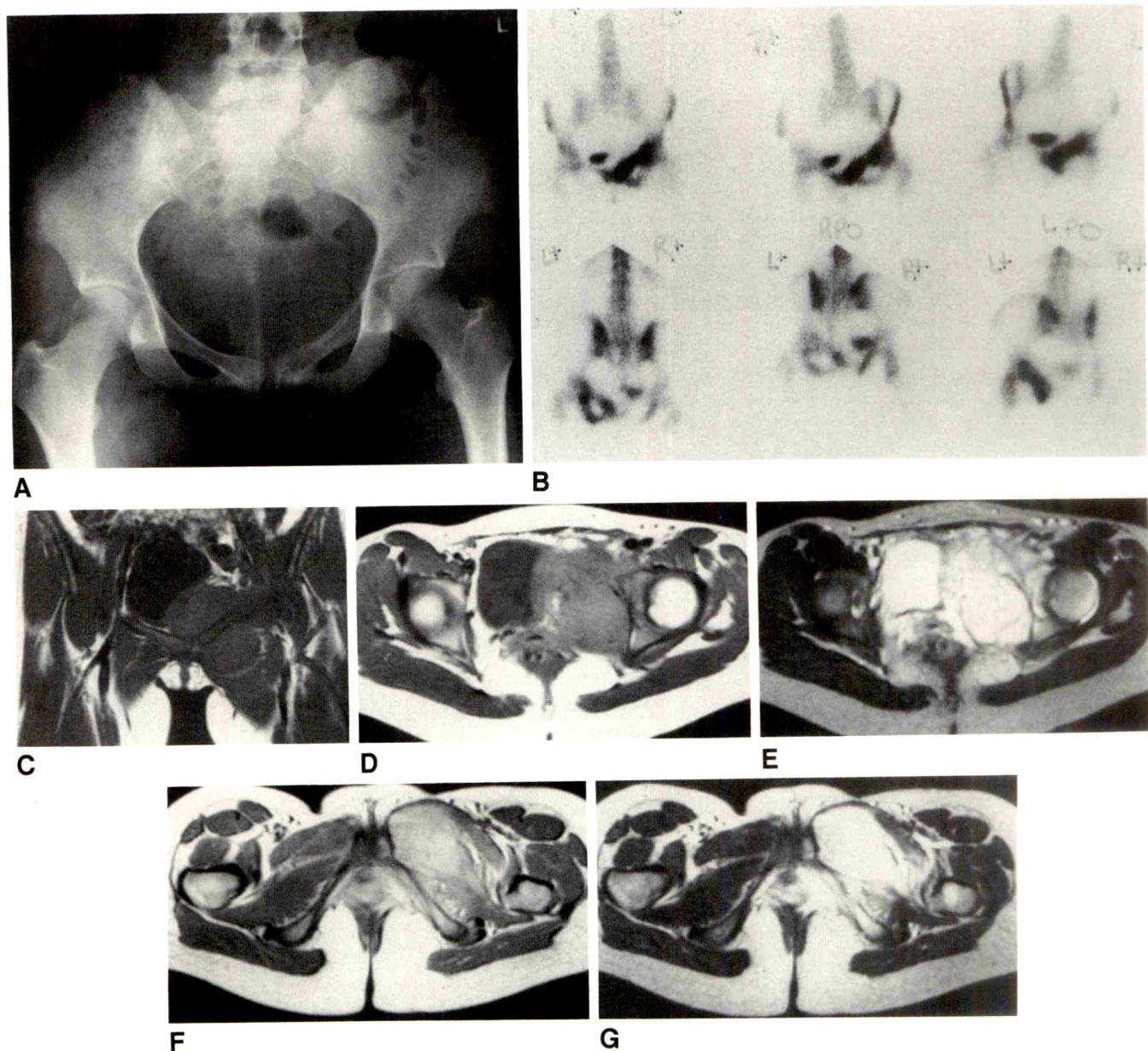


Fig. 1.—Case 1: Ewing sarcoma of the pubic bone.

A, Anteroposterior radiograph of pelvis shows permeative bony destruction of left superior pubic ramus and symphysis with lamellated periosteal reaction. Bladder is displaced by a large soft-tissue mass.

B, 99m Tc-methylene diphosphonate scintigram shows increased uptake in left superior and inferior pubic rami, symphysis, and acetabulum.

C, Coronal T1-weighted (450/20) MR image shows a large soft-tissue mass encasing left superior ramus with extension into pelvis. Bladder wall invasion is also seen.

D and **F**, Axial T1-weighted (700/20) MR images of pelvis show that soft-tissue mass is isointense to muscle.

E and **G**, Axial T2-weighted (3000/80) MR images of pelvis show heterogeneously increased signal in soft-tissue mass and bone-marrow signal changes in left acetabulum.

bos J. Magnetic resonance imaging of primary malignant bone tumors. *RadioGraphics* 1987;7:425-445

Case 2: Congenital Colonic Stenosis

After a normal delivery, a full-term girl passed meconium and was discharged from the nursery. On day two she returned with abdominal distension, emesis, and poor tolera-

tion of feedings. A plain abdominal radiograph showed a transverse colon massively dilated to 6 cm and containing feces mottled with gas (Fig. 2A). There were gas-fluid levels on the upright abdominal radiograph (Fig. 2B) and on the cross-table lateral radiograph (Fig. 2C), which also revealed an abrupt caliber change in the sigmoid colon. A barium enema showed the sigmoid colon and rectum narrowed to less than 1.5 cm (Fig. 2D). At the junction of the sigmoid and

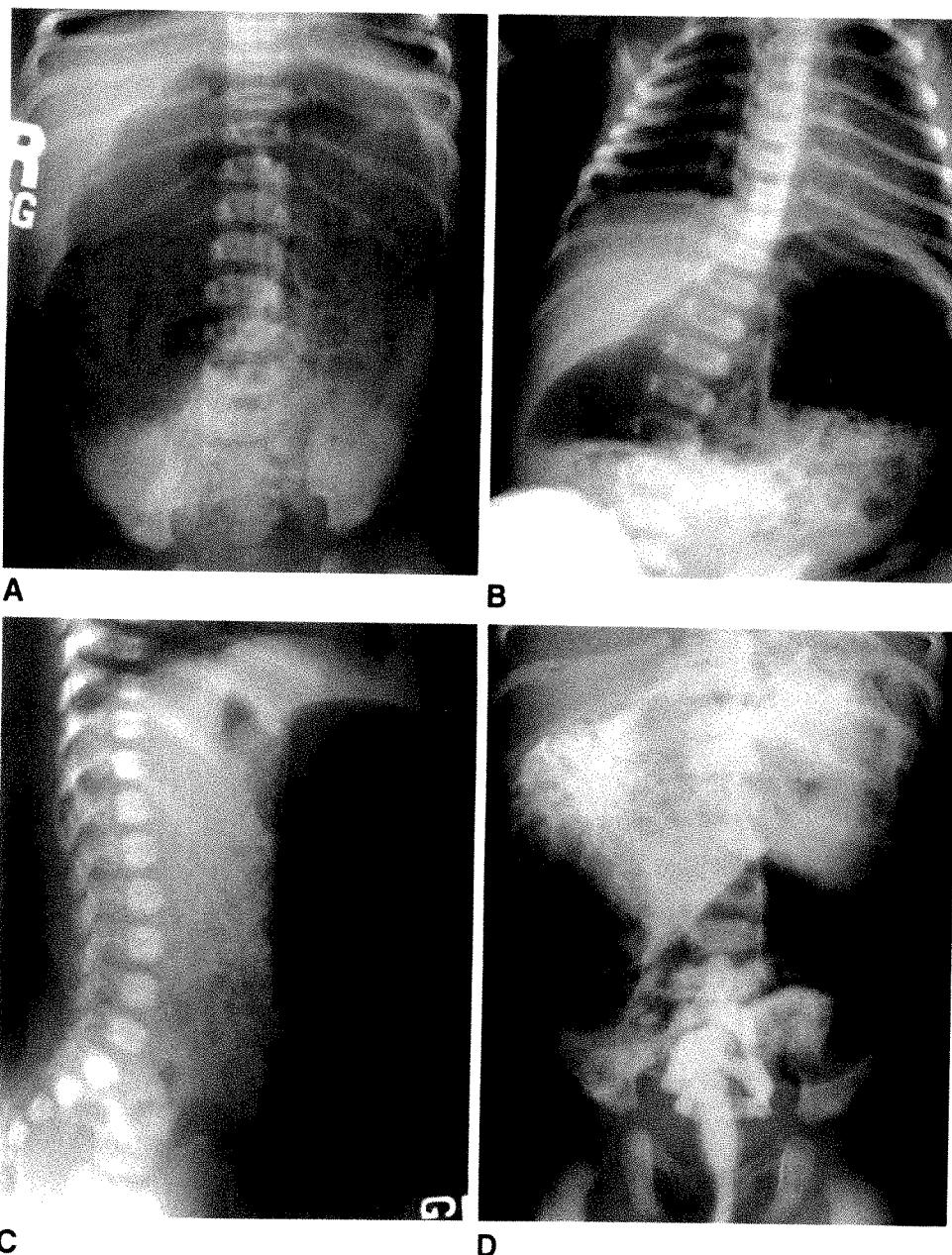


Fig. 2.—Case 2: Congenital colonic stenosis.

A. Abdominal radiograph of supine patient shows severe colonic dilatation. Colon contains mottled feces and gas.

B. Abdominal radiograph of upright patient shows marked colonic dilatation with gas-fluid levels.

C. Cross-table lateral radiograph reveals dilatation of proximal colon and relative narrowing of sigmoid colon distal to stenosis.

D. Barium enema shows a narrowed rectum and sigmoid colon. Colon is severely dilated proximal to congenital stenosis, located at junction of descending colon and sigmoid colon.

descending colon, a marked narrowing of 5 mm was encountered through which barium passed slowly. The differential diagnosis included colonic volvulus, congenital colonic stenosis, and Hirschsprung disease.

During surgery on the third day after birth, a sharp transition in bowel diameter was identified, changing from 2.5 cm in the distal descending colon to 5 mm in the proximal sigmoid colon. There were several corkscrewlike vessels from aberrant mesenteric locations at this site. The distal bowel was markedly kinked and quite narrow in caliber. The stenotic segment was resected with 1-cm margins, forming a Hartman pouch and a colostomy. Pathologic examination of the resected colon showed a 3-mm lumen at the stenosis. Ganglion

cells were present throughout the specimen, establishing the diagnosis of congenital colonic stenosis.

The colon is the least common site of congenital intestinal stenosis and atresia. It accounts for 5–15% [1] of intestinal stenoses and atresias, occurring in one in 40,000 births [2]. The theory of incomplete recanalization [3] applies to the duodenum but not the more distal small and large bowel. It is thought that atresias in these regions are the result of a vascular insult in utero [4]. Multiple intestinal atresias may be the result of an in utero inflammatory process of the bowel of unknown origin [5]. Louw [4] classified atresias in three groups as follows: type 1, one or more septa or diaphragms occluding the lumen; type 2, proximal and distal blind ends

joined by a threadlike structure, with or without a mesenteric defect; and type 3, proximal and distal blind ends that are completely separated with a V-shaped mesenteric defect.

Patients present clinically with vomiting and progressive abdominal distension. Physical examination often reveals abdominal distension, palpable intestinal loops, and dehydration. With complete colonic atresia, failure to pass meconium and absence of meconium in the rectal vault are noted. In congenital stenosis, passage of meconium may occur.

Abdominal radiographs show distended bowel with air-fluid levels. Rectal air may be absent in colonic atresias. A contrast enema typically demonstrates a small-caliber colon (microcolon) distal to an atresia without proximal flow, or a narrow segment of stenotic colon in congenital stenosis. In type 3 atresias, a characteristic "hooking" of the contrast column proximal to where retrograde flow is halted has been described in association with "recoiling" of the proximal portion of the distal atretic segment, which is free by virtue of its mesenteric defect [6].

Early surgical resection is imperative. Lesions proximal to the splenic flexure are treated with resection of the dilated proximal segment and primary ileocolostomy. Lesions distal to the splenic flexure are usually treated with diverting loop colostomy followed by staged resection of the atretic or stenotic segment and subsequent restoration of colonic continuity. Complications may require a staged repair regardless of the site of obstruction [7].

Eric J. Sax

ACKNOWLEDGMENT

The author thanks Kerry Bergman of the Boston Floating Hospital for surgical and pathologic follow-up in this case.

REFERENCES

1. Powell RW, Raffensperger JG. Congenital colonic atresia. *J Pediatr Surg* 1982;17:163-164
2. Franken EA Jr, ed. *Gastrointestinal imaging in pediatrics*, 2nd ed. New York: Harper Row, 1982:286-287
3. Tandler J. Zur Entwicklungsgeschichte des menschlichen Duodenum in fruhen embryonalstadien. *Morphol Jahrb* 1900;29:187-216
4. Louw JH. Congenital intestinal atresia and stenosis in the newborn: observations on its pathogenesis and treatment. *Ann R Coll Surg Engl* 1959;25:209-234
5. Puri P, Fujimoto T. New observations on the pathogenesis of multiple intestinal atresias. *J Pediatr Surg* 1988;23:221-225
6. Selke AC Jr, Jona JZ. The hook sign in type 3 colonic atresia. *AJR* 1978;131:350-351
7. Before NW Jr, Garcia-Rinaldi R, Mattox KL, Harberg FJ. Surgical management of colon atresia. *Surg Gynecol Obstet* 1976;143:767-769

Case 3: Diffuse Aseptic Bone Infarcts in a Child with Sickle Cell Disease

This case involved a 15-month-old Nigerian girl with sickle cell disease (Hb SS) who was brought to the emergency department with fever. In the course of her evaluation, a chest radiograph (Fig. 3A) that was obtained to exclude pneumonia showed bilateral cortical destruction and periosteal reaction in the humeri. A complete radiographic bone survey (Figs. 3B-3D) revealed symmetric abnormalities involving the long bones of the extremities. The findings consisted of cortical destruction, often full-thickness, and symmetric periosteal

reaction in the metadiaphyseal segment of the long bones. Similar changes also were noted in the metacarpals and phalanges of the right hand. At this point, the differential diagnosis included bone infarction and osteomyelitis. Radioisotope studies, both a technetium bone scan (Fig. 3E) and gallium imaging (Fig. 3F), had inconclusive results. Open bone biopsies of the proximal tibiae showed aseptic bone infarction.

When subjected to low oxygen tension, RBCs containing Hb SS become deformed into a sickle shape and block small blood vessels, preferentially at branching points, causing tissue ischemia and infarction if there is inadequate collateral circulation. In the neonate with Hb SS disease, the RBCs have a high concentration of fetal hemoglobin so that sickling does not occur. During the first year of life, Hb SS gradually replaces the fetal hemoglobin, and tissue ischemia and infarction occur [1].

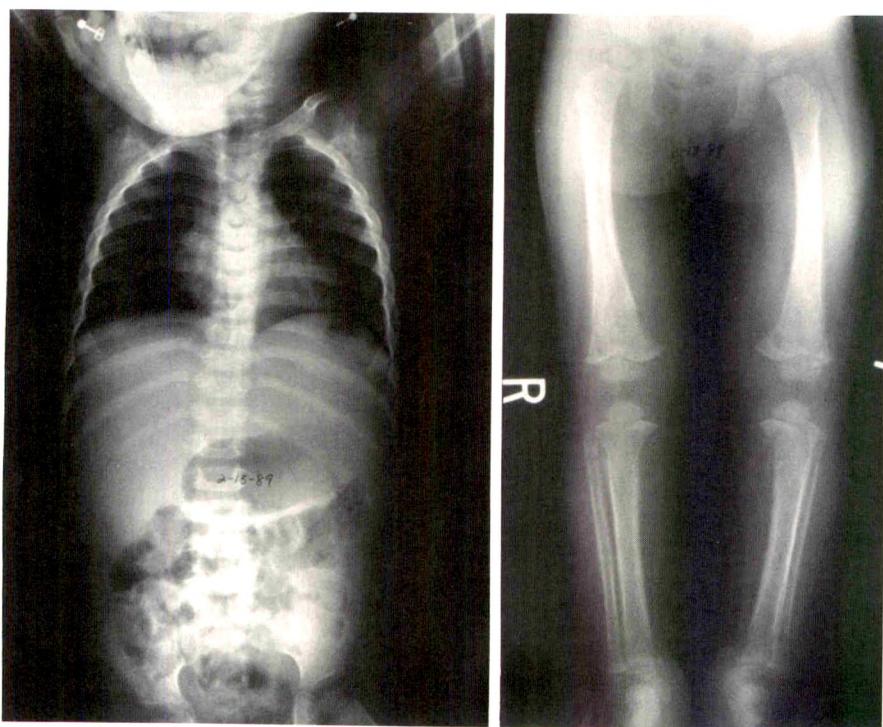
The main blood vessel to a long or short tubular bone is the nutrient artery that enters through the diaphyseal cortex, nourishing the medullary cavity and the inner portion of the cortex. Multiple periosteal vessels support the outer diaphyseal cortex. Both of these vascular sources must be compromised before cortical infarction is produced. This occurs more readily in the very young, in whom the periosteum is loosely attached to the cortex and can easily be separated by inflammatory edema. Separate vessels supply the epiphysis and metaphysis [1].

The first ischemic manifestation of Hb SS is usually dactylitis, also known as hand-foot syndrome. This may appear any time after 3 months of age, but more often occurs at 6-18 months. It often recurs but is uncommon after age 6, when red marrow recedes from the tubular bones of the hands and feet. Radiographs may show only soft-tissue swelling or a fine periosteal reaction when infarction is confined to the medullary cavity. If periosteal circulation becomes compromised, diaphyseal cortical bone infarction results, with areas of bone destruction and patchy areas of new bone formation. The destruction may be confined to the metadiaphyseal region, or the entire diaphysis may be involved. The epiphyses and metaphyses are usually spared because of their separate blood supply [1].

In the young, long bones undergo acute infarction just as do the short tubular bones of the hands and feet. This usually begins a few years later and may occur in association with dactylitis. When the long bone involvement is not severe, there may be no radiologic changes or only periosteal reaction. In these cases, infarction is confined primarily to the medullary cavity [1].

When involvement is more severe and the periosteal circulation is compromised, full thickness cortical destruction occurs. Single or layered periosteal reaction may be seen in association with cortical destruction. In children about 8 years old and older, the periosteum is more firmly attached to the diaphyseal cortex, and it is more difficult to compromise the periosteal circulation of the outer portion of the cortex. Acute diaphyseal involvement in these children is usually limited to the medullary cavity and adjacent inner half of the cortex, with splitting of the cortex into necrotic bone centrally and viable bone peripherally. Eventually this process can result in a "bone-in-a-bone" or "tram line" appearance [1].

Bone infarcts tend to spare the metaphyses because of extensive collateral circulation in the region of the growth plate. In the young, the epiphyses are not commonly infarcted;



A

B

Fig. 3.—Case 3: Diffuse aseptic bone infarcts in a child with sickle cell disease.

A, Radiograph of chest and abdomen shows cortical destruction and periosteal reaction involving both proximal humeri. Note enlarged spleen and heart.

B, Radiograph of both legs shows symmetric cortical destruction and extensive periosteal reaction in metadiaphyseal portion of distal femurs and proximal and distal tibias.

C and D, Radiographs of both arms show symmetric periosteal reaction and some cortical destruction in metadiaphyseal portion of long bones. Note also patchy destruction and periosteal reaction in metacarpals and phalanges of right hand.

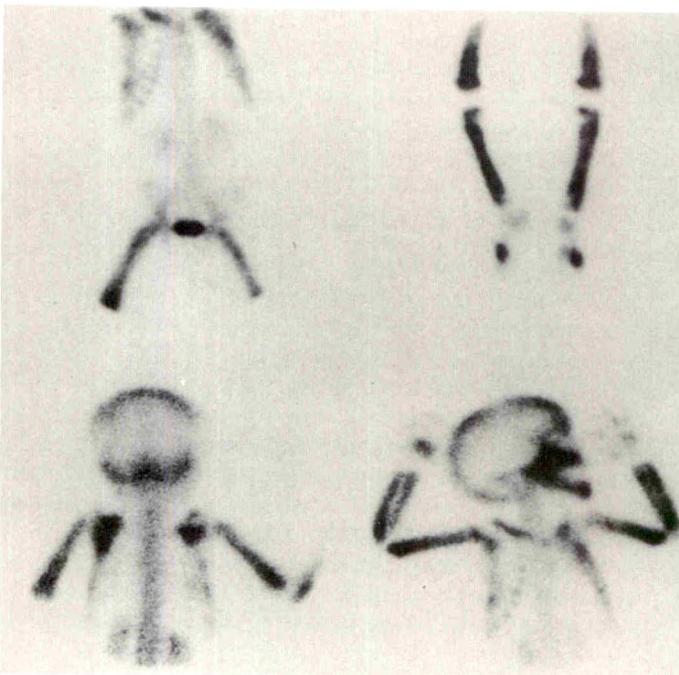
E, 99m Tc-methylene diphosphonate scan shows symmetric, abnormally increased uptake in long bones of arms and legs. Note increased uptake in right hand and both feet also.

F, Gallium scan, 48 hr after injection, shows symmetric, abnormally increased uptake in bones of arms, legs, feet, and right hand. Pattern is identical to that seen in bone scan.



C

D



E

F

it is rare for them to be involved before the growth plate fuses. The classic site for long bone infarcts is the metadiaphyseal segment of the shaft. The metadiaphyseal location is helpful in distinguishing Hb SS infarcts from primary hematogenous osteomyelitis, which classically begins at the metaphysis [1]. Bilateral, symmetric involvement is very frequent in Africa, of moderate frequency in Jamaica, and less common in the United States [1].

The classic sign of Hb SS in the spine is the H-shaped vertebra, which is virtually pathognomonic. In the skull, multiple episodes of infarction and periosteal reaction yield a distinctive "hair-on-end" appearance. Coarse granular osteopenia and focal lucencies also can be seen. Facial bone infarcts have been reported as well [2].

Infarcted bone is a fertile site for secondary infection. Furthermore, Hb SS patients have immunologic deficiencies, in part related to associated autosplenectomy. For these reasons, there is a high prevalence of secondary osteomyelitis at the site of acute bone infarcts. *Staphylococcus aureus* and *Salmonella* organisms are the most common offenders.

Radiologically and clinically, septic infarcts and sterile infarcts may be indistinguishable. This is understandable, because the mechanism of bone destruction in both is avascular necrosis [1]. Radionuclide studies have been suggested as a good method for distinguishing septic from sterile infarcts.

In this particular case, technetium-99m bone imaging and gallium-67 imaging were performed. In the study by Amundsen et al. [3], when osteomyelitis was present, ⁶⁷Ga uptake was abnormally increased. Sterile infarction usually resulted in normal or decreased ⁶⁷Ga uptake. However, when both ^{99m}Tc and ⁶⁷Ga uptake were increased, the result was indeterminate. Our patient demonstrated this pattern, and a biopsy was necessary for diagnosis. The final diagnosis was aseptic bone infarction.

Other radionuclide studies offer promise. ¹¹¹In-labeled leukocytes and technetium-sulfur colloid bone marrow imaging have been studied in conjunction with bone and gallium scans, with reports of increased sensitivity and specificity [4–6]. MR imaging will undoubtedly play a greater role in the evaluation of Hb SS bone disease.

Henry Chen

REFERENCES

- Bohrer SP. Bone changes in the extremities in sickle cell anemia. *Semin Roentgenol* 1987;22:176–185
- Royal JE, Harris VJ, Sansi PK. Facial bone infarcts in sickle cell syndromes. *Radiology* 1988;169:529–531
- Amundsen TR, Siegel MJ, Siegel BA. Osteomyelitis and infarction in sickle cell hemoglobinopathies: differentiation by combined technetium and gallium scintigraphy. *Radiology* 1984;153:807–812
- Schauwecker DS, Park HM, Mock BH, et al. Evaluation of complicated osteomyelitis with Tc-99m MDP, In-111 granulocytes, and Ga-67 citrate. *J Nucl Med* 1984;25:849–853
- Kahn CK, Ryan JW, Hatfield MK, Martin WB. Combined bone marrow and gallium imaging: differentiation of osteomyelitis and infarction in sickle hemoglobinopathy. *Clin Nucl Med* 1988;13:443–449
- Rao S, Solomon N, Miller S, Dunn E. Scintigraphic differentiation of bone infarction from osteomyelitis in children with sickle cell disease. *J Pediatr* 1985;107:685–688

Case 4: Neurocysticercosis

This 16-month-old girl, born in the United States to Cape Verdean parents, was brought to the emergency department with an afebrile generalized seizure. Unenhanced CT studies (Fig. 4A, top row) showed foci of decreased attenuation in the left parietal, left frontal, and right parietal lobes. A small focal calcification was noted in the left frontal and right parietal lesions. Contrast-enhanced CT (Fig. 4A, bottom row) showed enhancement of these lesions with associated surrounding edema. MR imaging (Figs. 4B and 4C) showed the calcifications as three foci of decreased signal in the subcortical gray/white matter junction on T2-weighted (3000/90) images, surrounded by irregular areas of increased signal representing white matter edema. Serologic testing of serum and CSF were positive for cysticercosis. Ova of *Taenia solium* were isolated from the stool of the patient's father.

Neurocysticercosis represents infestation of the CNS by the pork tapeworm, *Taenia solium*, in its larval stage. Neurocysticercosis is most prevalent in less-developed countries; however, its prevalence in the United States is increasing because of the influx of immigrants from endemic areas [1].

Infection occurs by ingesting ova from undercooked pork or by the fecal-oral route from an infected host. The larvae penetrate the intestinal wall and are distributed hematogenously to multiple sites that include the CNS, muscle, skin, and heart. Once established in the target organ, the larval cells proliferate, eventually producing cysts 1 cm or less in size. A small invagination develops along one margin of the cyst and proliferates to become a scolex measuring 2–3 mm. Without treatment, the natural history is for the parasite to die in approximately 1–5 years, resulting in cyst degeneration with a striking inflammatory and gliotic reaction in the host. Symptoms develop when cyst degeneration begins [2]. The end of the degenerative process is represented by cyst calcification. Clinical symptoms referable to CNS infection include seizures, intracranial hypertension, focal neurologic deficits, and dementia. The diagnosis of neurocysticercosis may be made by either CSF or radiologic findings. Examination of the CSF may reveal nonspecific findings of pleocytosis, eosinophilia, protein elevation, and glucose depression. Serologic tests for cysticercosis can be performed by specialized laboratories such as the Centers for Disease Control.

CT and MR imaging are the current imaging techniques of choice for the diagnosis of neurocysticercosis [1, 3]. The CT changes reflect the natural history of the disease and may be used to distinguish between viable, dying, and dead cysticerci. Three patterns of neurocysticercosis, either alone or in combination, may be observed on CT scans [4]. The parenchymal form is the most common and may be acute or chronic [5]. The acute phase looks like encephalitis because of compression, destruction, or irritation of brain tissue. During this stage, low-density cysts, measuring 1 cm or less in diameter, may be visualized. The cysts display ring enhancement or contain hyperdense nodules and are often associated with surrounding edema. In the chronic phase, which may occur within 1 year of onset, the cysts die and calcify, showing hyperdense foci on unenhanced CT scans and areas of signal void on MR images. The second form consists of intraventricular cysts.

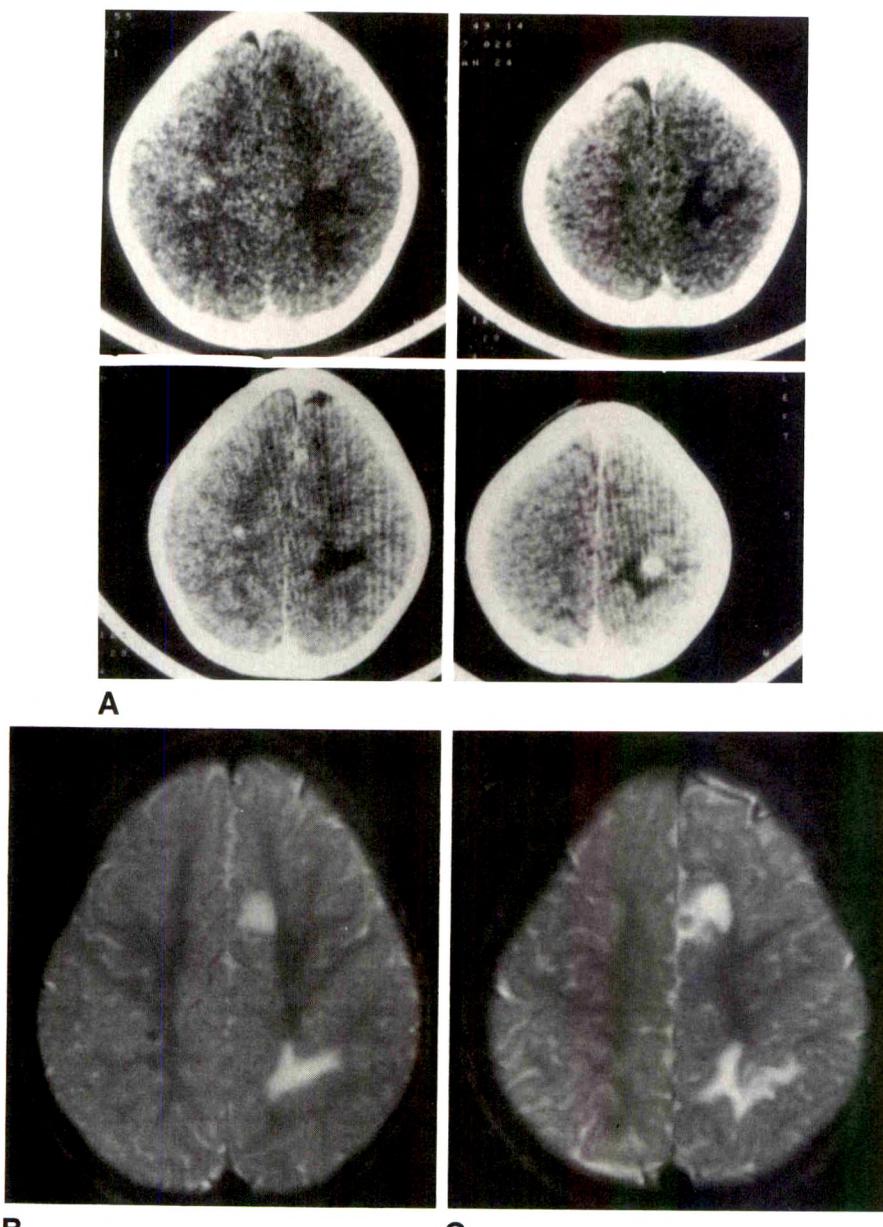


Fig. 4.—Case 4: Neurocysticercosis.

A, Unenhanced CT scans (*top row*) show low-attenuation areas of edema in left parietal, left frontal, and right parietal lobes. A small focal calcification is noted in left frontal and right parietal lesions. Enhanced CT scans (*bottom row*) show round, well-defined, enhancing foci within small areas of edema.

B and **C**, Axial T2-weighted (3000/90) MR images of head reveal irregular areas of increased signal representing white matter edema. Calcifications appear as well-defined foci of decreased signal.

B

C

These are asymptomatic unless there is obstruction to CSF flow, which may be fatal if onset is sudden, or result in intermittent intracranial hypertension. Finally, cysticerci within the subarachnoid space may be free-floating or adherent to the pia. Groups of cysts tend to aggregate in the basilar cisterns, forming structures up to several centimeters in diameter. These often produce a clinical picture of chronic aseptic meningitis.

Neurocysticercosis is rare in infancy, and its presentation as new-onset seizures in this 16-month-old infant is another warning to the medical community that immigrant populations may have a surprisingly wide range of underlying abnormalities. The large numbers of imaging studies performed for new-onset seizures that have normal findings may be vindicated by finding such a rare and unusual cause of seizures.

Therapy for neurocysticercosis may be surgical or medical. The ventricular form is treated either by resection of acces-

sible cysts or shunting. Medical treatment consists of anti-parasitic medication, either alone or in combination with steroids and antiepileptics.

Bonnie L. Dobkin
Oliver H. Pomeroy

REFERENCES

- Teitelbaum G, Otto R, Lin M, et al. MR imaging of neurocysticercosis. *AJNR* 1989;10:709-718
- Shanley JD, Jordan MC. Clinical aspects of CNS cysticercosis. *Arch Intern Med* 1980;140:1309-1313
- Suss R, Maravilla K, Thompson J. MR imaging of intracranial cysticercosis: comparison with CT and anatomicopathologic features. *AJNR* 1986;7:235-242
- Lotz J, Hewlett R, Alheit B, Bowen R. Neurocysticercosis: correlative pathomorphology and MR imaging. *Neuroradiology* 1988;30:35-41
- Mervis B, Lotz JW. Computed tomography (CT) in parenchymatous cerebral cysticercosis. *Clin Radiol* 1980;31:521-528

Letters

Breast Traction Mammography

Breast lesions seen adjacent to the chest wall on lateral views are often difficult to visualize on craniocaudal views, even after additional medially and laterally rotated views have been obtained. A number of techniques to solve this problem have emerged, such as tangential views, parallax techniques, breast sonography, and breast CT [1]. The advantages and disadvantages of these have been described in the literature [2]. Unfortunately, some of these require three-dimensional geometric calculations and are often difficult to conceptualize and apply clinically. We describe a simple, readily available technique that does not require special equipment to help identify mammographic abnormalities in the orthogonal plane.

Our technique involves applying additional traction on the breast on the craniocaudal view in order to visualize a greater amount of tissue near the chest wall (Fig. 1). Tegaderm (3M, St. Paul, MN), a transparent adhesive dressing, 10 × 12 cm, is placed on the superior and inferior surfaces of the breast. These two sheets then are apposed, leaving several centimeters of the two adherent sheets beyond the nipple. The breast is placed on the film cassette, and traction is applied to the Tegaderm until the breast is stretched maximally. The apposed ends of the sheets then are taped to the cassette, compression is applied, and the craniocaudal view is obtained.

We have used this technique in 28 patients. It was successful in depicting five deep lesions on the craniocaudal view, two of which biopsy subsequently proved were carcinomas. On average, 0.9 cm (range, 0.0–2.3 cm) more breast tissue was visualized when compared with the standard craniocaudal views. This was equivalent to approximately 12% more tissue imaged (range, 0.0–24%). This technique also has reduced the number of exposures required to localize lesions, thus diminishing radiation to the breast.

In addition to the advantages in detecting deep lesions, we have found this technique useful in maximizing the amount of breast tissue visible in small-breasted women. Although it is difficult to quantify this added benefit, we now routinely use Tegaderm in these women to improve traction. None of our patients has noted any increased discomfort when this procedure is used.

Commonly, the Tegaderm may produce anterior wrinkling of the skin as visualized mammographically, but this usually is not a major interpretive problem because the breast tissue is not distorted significantly, and the anterior tissue already has been imaged optimally on the routine craniocaudal view.

Judith M. Yancey
G. Farrell McNeely
Richard E. Kinard
*North Florida Regional Medical Center
Gainesville, FL 32605*

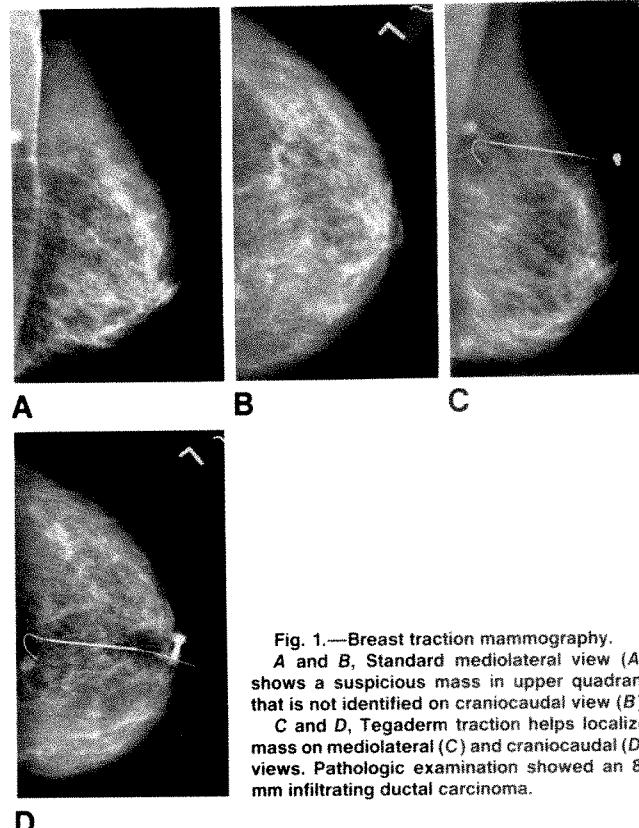


Fig. 1.—Breast traction mammography.
A and B, Standard mediolateral view (A) shows a suspicious mass in upper quadrant that is not identified on craniocaudal view (B).

C and D, Tegaderm traction helps localize mass on mediolateral (C) and craniocaudal (D) views. Pathologic examination showed an 8-mm infiltrating ductal carcinoma.

D

REFERENCES

1. Sickles EA. Practical solutions to common mammographic problems: tailoring the examination. *AJR* 1988;151:31–39
2. Yagan R, Weisen E, Bellon EM. Mammographic needle localization of lesions seen in only one view. *AJR* 1985;144:911–916

Adenoid Cystic Carcinoma of the Airway: MR Findings

Adenoid cystic carcinoma is the second most common primary tracheal tumor and accounts for the majority of tracheobronchial gland neoplasms [1]. Characteristically seen at bronchoscopy as a submucosal mass protruding into and obstructing the larger airways, the tumor tends to grow along the submucosa and invade the

adjacent mediastinal structures. Evaluation with conventional tomography and CT is limited because these techniques cannot be used to define accurately the extent of submucosal infiltration and involvement of adjacent mediastinal structures [2]. Multiplanar MR imaging with variably weighted sequences can overcome these limitations, thereby providing important diagnostic information.

A 34-year-old man had had intermittent cough and hemoptysis for 3 years and recently had had two episodes of respiratory distress. Chest radiograph at admission showed narrowing of the left main bronchus and areas of atelectasis and cystic change in the left lower lobe (Fig. 1A). Bronchoscopy showed occlusion of the left main bronchus just distal to the carina. Biopsies of this area confirmed a diagnosis of adenoid cystic carcinoma. Preoperative axial and coronal MR imaging at 1.5 T with various sequences showed invasion through the proximal left main bronchus and extension into the subcarinal and left paratracheal regions. The tumor mass had low signal intensity on T1-weighted images, higher signal on balanced images, and bright signal on T2-weighted images (Figs. 1B and 1C). Comparison with the preoperative CT scan clearly showed the superiority of MR for depicting the extent of submucosal infiltration and mediastinal involvement. The patient subsequently had a left pneumonectomy and carinal resection with reconstruction of the airway.

Most adenoid cystic carcinomas arise centrally within the trachea or main bronchi and gradually occlude the airway. Patients are usually in their fourth or fifth decade of life and have a prolonged clinical course of recurrent respiratory complaints. The insidious obstruction of the airway leads to recurrent episodes of pneumonitis, atelectasis,

and infection. No significant sex predilection or relationship to smoking has been found.

Conventional tomography, CT, or MR at the time of diagnosis usually shows a large mass obstructing the lumen of the airway. The ability of MR to provide images from multiple anatomic planes allows more accurate determination of tumor size and better definition of its relationship to other mediastinal structures. Tumor characterization with MR with variably weighted sequences can define the extent of submucosal infiltration and local invasion better, findings that may influence resectability.

Dean J. Shanley
Robin Daum-Kowalski
Ronald L. Embry
*Tripler Army Medical Center
Honolulu, HI 96859*

REFERENCES

1. Cleveland RH, Nice CM, Ziskind J. Primary adenoid cystic carcinoma (cylindroma) of the trachea. *Radiology* 1977;122:597-600
2. Spizarny DL, Shepard JO, McLoud TC, Grillo HC, Dedrick CG. CT of adenoid cystic carcinoma of the trachea. *AJR* 1986;146:1129-1132

Emphysematous Modification of Diffuse Centrilobular Lesions Due to Staphylococcal Pneumonia

In patients with preexisting pulmonary emphysema, the affected areas of the lungs have a sparse capillary bed, absence of the pores of Kohn, and distorted bronchiolar structure [1]. When pneumonia involves an emphysematous lobe, the dilated air spaces rarely are filled, and the exudate is confined to the relatively normal areas of lung that surround the emphysematous foci. Thus, with emphysema, the pattern of consolidation becomes disorganized [1]. We reported previously that high-resolution CT of immunocompromised patients with *Staphylococcus aureus* pneumonia showed widespread centrilobular lesions [2]. Here we describe a case of staphylococcal pneumonia that had an atypical pattern of diffuse centrilobular lesions that was due to preexisting pulmonary emphysema.

A 70-year-old man had shortness of breath, low-grade fever, cough, and yellowish-green sputum. He had smoked at least two packs of cigarettes each day for more than 30 years. He had received

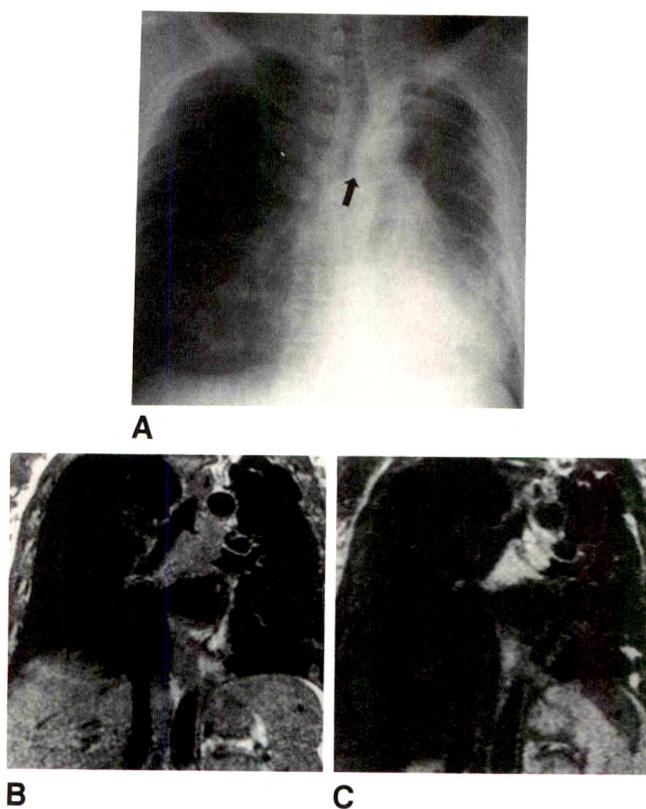


Fig. 1.—Adenoid cystic carcinoma of the airway.

A, Chest radiograph shows narrowing of left main bronchus (arrow) and evidence of volume loss in left hemithorax.

B and **C**, T1-weighted (882/18, **B**) and T2-weighted (2903/180, **C**) coronal MR images show a large tumor mass causing nearly complete obstruction of left main bronchus.

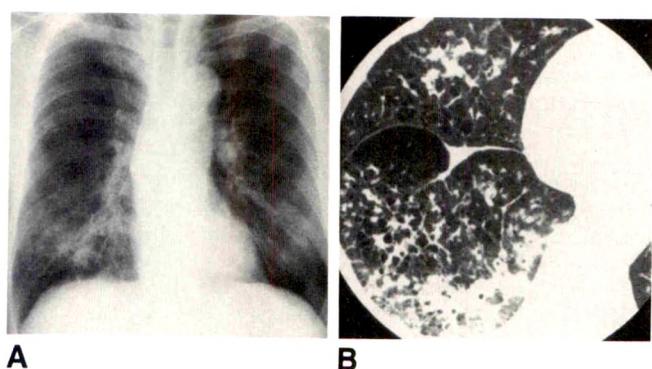


Fig. 1.—Staphylococcal pneumonia in a 70-year-old man with preexisting pulmonary emphysema.

A, Chest radiograph shows nodular or patchy consolidation, especially in right lower lobe of lung.

B, High-resolution CT scan shows widespread rounded, poorly defined nodules interrupted by air-filled spaces and smaller emphysematous foci outlined by consolidation.

interferon gamma because of pulmonary metastases from renal cell carcinoma (clear cell type). The WBC count was 10,800 cells/ μ l, with 74% neutrophils, 17% lymphocytes, 8% monocytes, and 1% eosinophils. The level of C-reactive protein was 25.0 mg/dl. A specimen of arterial blood, drawn while the patient was breathing oxygen (3 l/min, nasally), showed that the partial pressure of oxygen was 55 mm Hg, the partial pressure of carbon dioxide was 27 mm Hg, and the pH was 7.55. Plain chest radiography showed nodular or patchy consolidation, especially in the right lower lobe (Fig. 1A). High-resolution CT showed widespread rounded, poorly defined nodules interrupted by air-filled spaces and smaller emphysematous foci outlined by consolidation (Fig. 1B). Culture of sputum resulted in pure and heavy growth of *S. aureus*. Antibiotic therapy was started, and later radiographs showed improvement in the patient's condition.

In the differential diagnosis of certain parenchymal lung diseases, accurate localization of pathologic changes within the lobules can be helpful [3]. Although conventional chest radiography and standard CT provide little such information, high-resolution permits the localization of disease processes within the lobule [3]. We reported previously that staphylococcal pneumonia was associated with a uniform dissemination of less confluent opacities throughout the affected lung parenchyma [2]. However, as we report here, although the findings on plain chest radiographs were similar to those seen when emphysema was not present, the findings on high-resolution CT scans were quite different from the typical pattern of diffuse centrilobular lesions. Because the central portions of the lung lobule and respiratory bronchiole are destroyed in centrilobular emphysema (panlobular emphysema is extremely rare in Japan), diffuse centrilobular lesions caused by staphylococcal pneumonia should be interrupted. In conclusion, our case suggests that on high-resolution CT, the pattern of diffuse centrilobular lesions of the lung caused by *S. aureus* may be distorted by underlying emphysema, because emphysematous foci interfere with centrilobular lesions.

Jiro Fujita
Katashi Sato
Shozo Irino
and colleagues
Kagawa Medical School
Kagawa, 761-07, Japan

REFERENCES

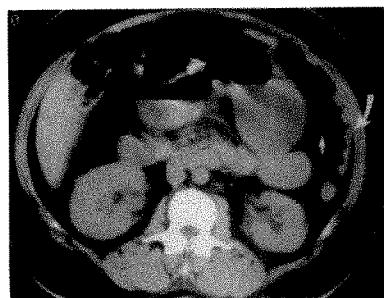
- Ziskind MM, Schwarz MI, George RB, et al. Incomplete consolidation in pneumococcal lobar pneumonia complicating pulmonary emphysema. *Ann Intern Med* 1970;72:835-839.
- Fujita J, Sato K, Hata Y, et al. Diffuse centrilobular lesions of the lung caused by *Staphylococcus aureus* in two immunocompromized patients (letter). *AJR* 1990;155:652-653.
- Murata K, Itoh H, Todo G, et al. Centrilobular lesions of the lung: demonstration by high-resolution CT and pathologic correlation. *Radiology* 1986;161:641-645.

Abdominal Brucellosis: CT Findings

Human brucellosis is a major health problem worldwide [1]. I report the CT findings of abdominal brucellosis in a patient with brucellar peritonitis.

A 53-year-old woman had severe abdominal pain, fever, and vomiting. She had diabetes and previously had had a laparotomy for a pancreatic cyst and a splenectomy. CT of the abdomen showed dilated loops of small intestine with fluid levels, ascites, and nodular plaques on the left peritoneal margin (Fig. 1). An exploratory laparotomy was performed because of small-bowel obstruction, and a band of adhesions was divided. Postoperatively, the patient's fever and vomiting persisted. On readmission 1 month after surgery, she had

Fig. 1.—Abdominal brucellosis. CT scan shows dilated loops of small bowel with fluid levels, ascites (straight arrow), and nodular plaques (curved arrow) on peritoneum.



persistent fever, repeated vomiting, headache, confusion, lethargy, pain in the right side of the neck, anorexia, and loss of weight. Physical examination showed abdominal tenderness and stiffness of the neck. Laboratory studies showed WBCs and proteins in the CSF, and microagglutination tests of blood and CSF and enzyme-linked immunosorbent assays of CSF were positive for brucellosis. Antibruceellosis chemotherapy led to a complete recovery. Follow-up CT after 1 month of therapy showed no ascites and no nodular plaques.

Human brucellosis usually is associated with consumption of unpasteurized goat's milk or cheese [2]. The systemic manifestations of the disease usually predominate over the gastrointestinal complaints despite the ease with which brucellosis is transmitted via the oral route. Limited reports [3, 4] on the gastrointestinal manifestations and complications have been published. To my knowledge, peritonitis associated with brucellosis has not been described before. The CT scan showed ascites and nodular plaques on the peritoneal surface. Low-density masses in the peritoneum associated with tuberculosis have been described. Irregular masses with nodular configurations have been described in malignant mesothelioma of the peritoneum and in peritoneal metastases, but the CT features of each of these are distinctly different from those of the case described here.

Fareed Mohamed Denath
Kuwait University
Safat, 13110 Kuwait

REFERENCES

- Matyas Z, Fujikura T. Brucellosis as a world problem. *Dev Biol Stand* 1989;56:3-20.
- Williams E. Brucellosis. *BMJ* 1969;1:612-614.
- Young EJ. Human brucellosis. *Rev Infect Dis* 1983;5:821-842.
- Mohamed AS, Madkour MM, Talukder MS, Al-Karawi MA. Alimentary tract presentation of brucellosis. *Ann Saudi Med* 1986;6:27-31.

Use of a Condom to Cover the Balloon of a Barium Enema Rectal Tip

Because of increasing concern about serious allergic reactions associated with the use of rectal tips with latex balloons, radiologists have been forced to abandon the use of such tips for barium enema examinations. Evidence reviewed by the Food and Drug Administration (FDA) and one of the major manufacturers of barium enema equipment (E-Z-EM, Inc., Westbury, NY) suggests that a possible source of these reactions is the soluble proteins present in the latex in the retention cuff. Thus far, nine deaths and about 150 complications, many of which were anaphylactic reactions, have been reported to the FDA (personal communication, Center for Devices and Radiological Health).

To avoid this problem, we use a condom to cover the retention cuff of the barium enema tip to prevent direct contact between the cuff and the rectal mucosa. Flexi-Cuff, a commercial barium enema

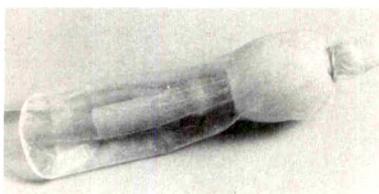


Fig. 1.—Condom is placed over retention cuff of barium enema tip to prevent direct contact between latex cuff and rectal mucosa.

retention tip (E-Z-EM, Inc.) is covered with a condom as follows. The reservoir tip of the condom is cut off, and a rubberband is used to secure the condom firmly in place over the rectal tip. The other end of the condom is inverted over the inflatable cuff (Fig. 1). This modified tip is lubricated with a standard commercial gel and inserted into the rectum, and the balloon cuff is inflated. We have used this technique in more than 30 patients and have observed no adverse reactions or complications. The condom has remained in place in every case.

This technique is based on the assumption that condoms, which are made of latex, do not cause serious allergic reactions. About half a billion condoms are manufactured each year in the United States and are used at the rate of 12 per second (personal communication with condom manufacturer).

A number of reports suggest that condoms can cause contact dermatitis and urticaria [1, 2]. One report [3] suggests that a condom caused an anaphylactic reaction after vaginal and oral intercourse. However, no deaths associated with the use of condoms have been reported.

J. Jamshidian
K. Sadriah

Veterans Affairs Medical Center, Wadsworth Division
Los Angeles, CA 90073

REFERENCES

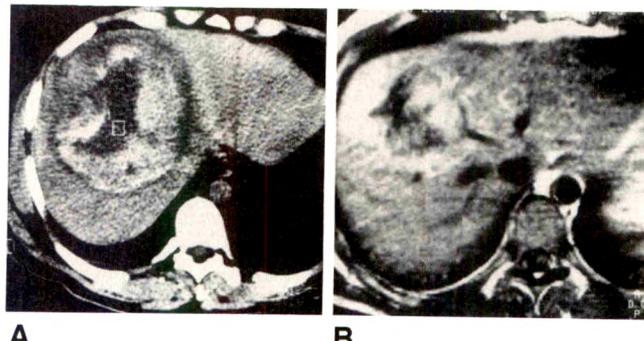
- Turjanmaa K, Reunala T. Condoms as a source of latex allergen and cause of contact urticaria. *Contact Dermatitis* 1989;20:360-364
- Rademaker M, Forsyth A. Allergic reactions to rubber condoms. *Genitourin Med* 1989;65:194-195
- Taylor JS, Cassettari J, Wagner W, Helm T. Contact urticaria and anaphylaxis to latex. *J Am Acad Dermatol* 1989;21:874-877

Liver Cell Adenoma Discovered After Blunt Hepatic Injury

Trauma-induced hemorrhage into a tumor may make it difficult to establish an accurate diagnosis of the lesion.

A 32-year-old man complained of pain in the right upper quadrant 2 days after a skiing accident caused severe closed abdominal injury. Sonography and CT showed a 13-cm heterogeneous mass in the right lobe of the liver (Fig. 1A). The diagnosis was intrahepatic hematoma. The patient was clinically stable and was treated conservatively. Sonographically guided biopsy performed 2 months later showed only necrotic cells. CT performed 6 months after the injury showed that the mass was still present but smaller. MR showed that the lesion was composed of tissue and blood (Fig. 1B). A partial hepatectomy was performed 7 months after the initial injury. Histologic examination showed a liver cell adenoma. The patient's recovery has been unremarkable.

Liver cell adenomas are rare benign tumors seen mainly in young women. The tumor often is discovered when hemorrhage into the tumor causes pain [1]. In our case, hemorrhage into the lesion



A

B

Fig. 1.—Liver cell adenoma discovered after blunt hepatic injury. *A*, Initial enhanced CT scan shows large blood-containing mass in liver. *B*, Gadolinium-enhanced T1-weighted spin-echo MR image shows mass in liver 6 months after injury.

probably was caused by trauma. The diagnosis was delayed because the appearance of the tumor was similar to that of a hematoma [2].

J. L. Bouillot

A. Hernigou

M. Ch. Plainfosse

J. H. Alexandre

Université Paris VI, Hôpital Broussais
Paris 75014, France

REFERENCES

- Leese T, Farges O, Bismuth H. Liver cell adenomas: a 12-year surgical experience from a specialist hepatobiliary unit. *Ann Surg* 1988;208:558-564
- Foley WD, Cates JD, Kellman GM, et al. Treatment of blunt hepatic injuries: role of CT. *Radiology* 1987;164:635-638

Hepatic Sarcoidosis: MR Findings

One case report [1] describing the CT appearance of hepatic sarcoidosis has been published. However, to our knowledge, the MR findings in this liver disease have not been described. A 43-year-old black woman with stage II sarcoidosis requiring no therapy was admitted because of recent onset of dyspnea, fatigue, and jaundice. Physical examination showed moderate hepatomegaly and slight jaundice. A sonogram showed a normal gallbladder and common bile duct and a diffusely heterogeneous liver with poorly defined interlacing hyper- and hypoechoic areas. CT showed an enlarged liver with diffuse, small, irregular hypodense foci amid preserved areas of normal-appearing parenchyma. Axial proton-density (2000/20 [TR/TE]) and T2-weighted (2000/120) MR images were obtained with a 1.5-T MR unit. The proton-density images showed multiple, small, closely packed nodular foci throughout the liver, with normal to slightly increased signal intensity (Fig. 1A). T2-weighted images showed that all areas of liver were decreased in signal (Fig. 1B). No foci of increased signal were seen on T2-weighted images. A percutaneous liver biopsy showed the cholestatic form of hepatic sarcoidosis.

Sarcoidosis has many different manifestations. The acute form of the disease, frequently limited to the thorax, has a high prevalence of spontaneous remission. Chronic sarcoidosis has a highly variable clinical course and can be insidiously progressive. Some reports indicate that in nearly two thirds of patients who have chronic sarcoidosis, the disease eventually is cured either spontaneously or with the use of corticosteroid therapy; approximately 3% of patients die of their disease [2]. Hepatic involvement of clinical significance

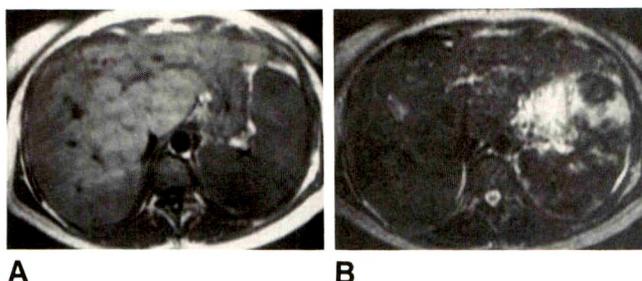


Fig. 1.—Hepatic sarcoidosis.

A, Proton-density MR image shows liver has diffuse nodular appearance and normal to increased intensity.

B, T2-weighted MR image shows decreased intensity throughout liver parenchyma. Note heterogeneity of spleen.

occurs in less than 5% of cases. Hepatic failure occurs rarely. The CT findings in this case are similar to those in the previously published case [1]: multiple, small, irregular, diffusely scattered, hypodense foci throughout the liver. These findings are relatively nonspecific and suggest diffuse metastases, widespread inflammatory disease, or, possibly, regions of scarring in a nodular, regenerating liver. MR in our case was useful in the differential diagnosis because the liver had multiple, diffuse, densely packed islands of isointense or slightly hyperintense parenchyma on proton-density images and corresponding foci of hypointensity on T2-weighted images. We think the finding on T2-weighted images effectively excludes metastases or inflammatory disease because these diseases have hyperintense signal on such images.

Fred W. Flickinger
Eric A. Pfeifer
Medical College of Georgia
Augusta, GA 30912-3910

REFERENCES

- Nakata K, Iwata K, Kojima K, Kanai K. Computed tomography of liver sarcoidosis. *J Comput Assist Tomogr* 1989;13:707-708
- Israel H, Karlan P, Menduke H, DeLisser O. Factors affecting the outcome of sarcoidosis: influence of race, extrathoracic involvement, and initial radiographic lung lesions. *Ann NY Acad Sci* 1986;465:609-617

A New Sign of Ascites

While performing a small-bowel examination, my colleagues and I observed a new, previously undescribed fluoroscopic sign for the presence of ascites.

A 55-year-old man with a history of unexplained gastrointestinal bleeding had a double-contrast enteroclysis examination of the small bowel. During instillation of the methylcellulose, marked cyclic, to-and-fro movement of the barium-filled loops of bowel was observed. Subsequently, a history of cirrhosis and concomitant ascites was obtained. The latter was confirmed with sonography (Fig. 1).

Conventional imaging of ascites usually is based on the secondary effects of the ascites on the bowel and adjacent organs. These may include bulging flanks, obscuration of organ outlines, separation of the liver from the lateral abdominal wall, separation of opacified bowel loops, and central gathering of the small-bowel loops floating in the ascites [1]. In malignant ascites, the loops of small bowel may be tethered [2].

In our case, exaggerated movement of the barium-filled loops of small bowel occurred during the instillation of methylcellulose for a double-contrast examination. The range of the movement was 5-7

Fig. 1.—Transverse sonogram of mid abdomen shows multiple fluid-filled loops of small bowel floating in large amounts of ascitic fluid.



cm, and it occurred without external compression being applied and with the patient at rest. The to-and-fro movement was cyclical, mimicking the bobbing of an object floating on ocean waves.

The most likely explanation for this movement was the rapid filling with methylcellulose (approximately 100 ml/min) of the previously partially collapsed small bowel. This filling displaced a similar amount of ascitic fluid in the somewhat elastic peritoneal cavity. The displaced fluid hit the lateral abdominal wall and rebounded, setting up a wavelike motion. This fluid wave markedly displaced the small bowel floating on the ascitic fluid.

Bruce R. Javors

North Shore University Hospital
Cornell University Medical College
Manhasset, NY 11030

REFERENCES

- Frimann-Dahl J. *Roentgen examinations in acute abdominal diseases*, 3rd ed. Springfield, IL: Thomas, 1974:59-77
- Hulnick DH, Megibow AJ. Computed tomography of the small bowel. In: Herlinger H, Maglinte D, eds. *Clinical radiology of the small intestine*. Philadelphia: Saunders, 1989:190

Stage D2 Transitional Cell Carcinoma of the Bladder in a 36-Year-Old Woman

A 36-year-old woman had had right-sided flank pain and dysuria for 1 week and had been having episodes of gross hematuria intermittently for 1 month. She had no history of cigarette smoking or exposure to chemical carcinogens. Pelvic examination showed an indurated palpable mass anterior to the vagina. Urinalysis showed 25-50 WBC/μl. An excretory urogram showed a dilated right collecting system consistent with obstruction. Delayed films showed a large, irregular, bladder filling defect (Fig. 1A). Cystoscopy showed an extensive papillary lesion involving the trigone with extension to the posterior and lateral walls. Both ureteral orifices were obscured, and the mass extended distally into the mid urethra. A limited transurethral resection was performed, and pathologic examination of the specimen showed grade 1-2 transitional cell carcinoma with invasion of the lamina propria. Technetium-99m bone scan showed findings compatible with metastatic disease (Fig. 1B). One month after treatment, the patient died.

Bladder carcinoma is uncommon in patients who are less than 40 years old. It accounts for an estimated 1% of bladder tumors. In the majority of patients, hematuria is the initial complaint. Male predominance is the usual finding, with male to female ratios as high as 8:1. More than 50% have a history of cigarette smoking [1].

Accurate staging is important in defining the management and assessing the prognosis of bladder carcinoma. At the time of diagnosis, transitional cell carcinoma is localized to the mucosa in 48%,

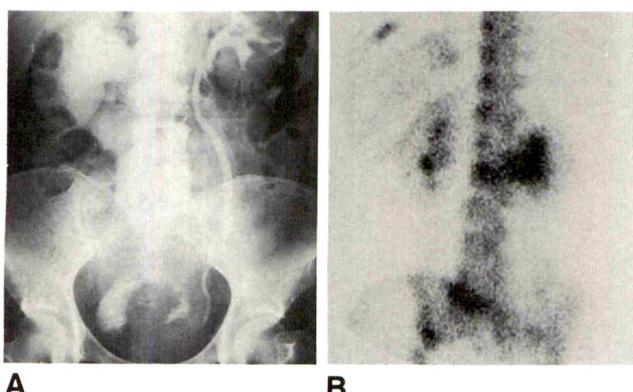


Fig. 1.—Transitional cell carcinoma of bladder in a 36-year-old woman.
A, Excretory urogram shows irregular defect in bladder and hydronephrosis of right kidney.
B, Bone scan shows areas of abnormal uptake of radionuclide and hydronephrosis.

to the lamina propria in 31%, and to the muscle in 21% of cases [2]. Current imaging techniques may not show accurately the degree of invasion into the muscle layer of the bladder wall. These studies are subject to errors in understaging, with rates between 40% and 50%.

Excretory urography can detect bladder tumors in only 45–60% of cases, and the postvoid film provides the most information. The finding of ureteral obstruction implies that the stage of the disease is at least T3 [3]. Ureteral obstruction has the same poor prognostic significance as an abnormal lymphangiogram. CT has limited usefulness in staging because the normal bladder wall, muscular hypertrophy, and infiltrating tumor may have similar attenuations. CT is helpful in showing nodal metastasis. MR is not significantly better than CT, but it may detect invasion of perivesical fat more readily. Transurethral sonography can be used to assess local tumor invasion and to provide follow-up information after resection. Metastases from transitional cell carcinoma of the bladder may involve lung, bone, mediastinum, liver, brain, urethra, abdominal nodes, and extrapleural space.

Ronald G. Frank
Perry S. Gerard
Gilbert J. Wise
and colleagues
*Maimonides Medical Center
Brooklyn, NY 11219*

REFERENCES

- Cherrie, RJ, Lindner A, deKernion JB. Transitional cell carcinoma of the bladder in the first four decades of life. *Urology* 1982;20:582–584
- Choyke PL, Thickman D, Kressel HY, et al. Controversies in the radiologic diagnosis of pelvic malignancies. *Radiol Clin North Am* 1985;23:531–549
- Greiner R, Skaleric C, Veraguth P. The prognostic significance of ureteral obstruction in carcinoma of the bladder. *Int J Radiat Oncol Biol Phys* 1977;2:1095–1100

Intra- and Interobserver Variations in Determining Blood-Flow Indexes with Doppler Sonography

Several authors have suggested that renal blood-flow indexes based on analysis of Doppler spectra are useful in determining the presence of renal parenchymal disease, particularly in the differential diagnosis of renal transplant dysfunction. However, recent reports on this issue have been more critical. Changes in Doppler curves and

increased resistive index may indicate renal disease, but they do not permit any differential diagnosis between various causes of renal dysfunction.

We reviewed eight recent reports on the use of Doppler sonography and the resistive index in the evaluation of kidneys (seven reports on transplanted kidneys and one on native kidneys) and found that only two of these [1, 2] consider possible intra- or interobserver errors. The errors reported were less than 10% or 6.5–12.0%, respectively. In no report were the errors determined by using color Doppler equipment.

For this reason and because, in our own experimental studies, we found that the range of interobserver error was $\pm 7.5\%$ and the range of intraobserver error was $\pm 7\%$ [3], we undertook a test with our color Doppler equipment (Quad 1, Quantum, Issaquah, WA). One volunteer who had no history of renal disease was the test subject. Each of four experienced sonographers used the 3-mHz transducer at medium flow level (7 mm/sec, according to the manufacturer's specifications), and made 10 determinations of the Pourcelot index (five on each kidney). The indexes in randomly selected intrarenal vessels were between 0.5 and 0.8; 34 of 40 measurements were 0.6 or 0.7.

The analysis of these values according to statistical variance gave the following results: interobserver variation, 6.4%; intraobserver variation, 9.6%; total variation, 11.5%. To this variation, the transducer/vessel angle error should be added, which according to our experimental study may vary up to $\pm 8\%$ in the angle range of 40° to 80° [3]. Even assuming no or minimal inherent error for equipment software calculations, we may face a total error of 15–20% in index determinations. This error may change many borderline cases from normal to abnormal, or vice versa, making the resistive index even less reliable. At least, the error factors must be taken into consideration whenever the index is used for evaluation of renal disease.

Larry S. Kessler

Janice C. Honeyman

Juri V. Kaude

Jeffrey A. Longmate

*University of Florida College of Medicine
Gainesville, FL 32610-0374*

REFERENCES

- Schwaighofer B, Kainberger F, Fruehwald F, et al. Duplex sonography of normal renal allografts. *Acta Radiol* 1989;30:53–56
- Townsend RR, Tomlanovich SJ, Goldstein RB, Filly RA. Combined Doppler and morphologic sonographic evaluation of renal transplant rejection. *J Ultrasound Med* 1990;9:199–206
- Cazenave CT, Sievers KW, Kaude JV, Williams JL, Bush D, Wright PG. Pulsatile flow index for qualitative measurements of blood flow with duplex ultrasound: an experimental study. *Eur J Radiol* 1989;9:42–43

Broadband Ultrasound Attenuation Measurements in Osteoporosis

Resch et al. [1] report that broadband ultrasound attenuation measurements of the calcaneus have "relatively low sensitivity" in the diagnosis of osteoporosis. In contrast, my colleagues and I [2–4] and others [5, 6] have shown that broadband ultrasound attenuation is a sensitive and specific discriminator of axial osteopenia, is predictive of hip fracture [7], and has the added advantages of being radiation-free and inexpensive. The discrepancy between the findings arises from inappropriate use of the term "normal range" by Resch et al. For quantities that vary with age, a normal range refers to the 95% confidence limits for a population of a given age (e.g., women who all are 63 years old). Resch et al. studied either 23 (according to the

text in [1]) or 21 (according to the figures) "normal" women whose mean age was 63 years and whose age range was approximately 45–81 years (my calculation, based on the standard error). The age-specific normal range of this population can be computed by using a linear regression analysis of bone density as a function of age; the 95% confidence limits for the line so obtained are calculated after removing variation due to age. Reporting the mean \pm 2 SD for a small group of women with a mean age of 63 years and an age range of four decades as the normal range will mislead many. Resch et al. simply should have stated that they were calculating the means \pm 2 SD of their populations of control subjects and patients. If this is done, all three techniques, single-photon absorptiometry, quantitative CT, and broadband ultrasound attenuation, give values that are significantly lower in patients who have osteoporosis. I suggest that Resch et al. use all three techniques on separate groups of women (50 women per group) from each decade from 40 to 80 years, determine the linear regression, and calculate the decade-specific 95% confidence limits. The added precision will remove the discrepancies between their results [1] and the results of others [2–7].

Daniel T. Baran

*University of Massachusetts Medical Center
Worcester, MA 01655*

REFERENCES

- Resch H, Pietschmann P, Bernecker P, Krexner E, Willvonseder R. Broadband ultrasound attenuation: a new diagnostic method in osteoporosis. *AJR* 1990;155:825–828
- Baran DT, Kelly AM, Karella A, et al. Ultrasound attenuation of the os calcis in women with osteoporosis and hip fractures. *Calcif Tissue Int* 1988;43:138–142
- Agren M, Karella A, Leahy D, Marks S, Baran D. Ultrasound attenuation of the calcaneus: a sensitive and specific discriminator of osteopenia in postmenopausal women. *Calcif Tissue Int* 1991;48:240–244
- Baran DT, McCarthy CK, Leahy D, Lew R. Broadband ultrasound attenuation of the calcaneus predicts lumbar and femoral neck density in Caucasian women: a preliminary study. *Osteoporos Int* 1991;1:110–113
- Poll V, Cooper C, Crawley MI. Broadband ultrasonic attenuation in the os calcis and single photon absorptiometry in the distal forearm: a comparative study. *Clin Phys Physiol Meas* 1986;7:375–379
- McCloskey EV, Murray SA, Miller C, et al. Broadband ultrasound attenuation in the os calcis: relationship to bone mineral at other skeletal sites. *Clin Sci* 1990;78:227–233
- Porter RW, Miller CG, Grainger D, Palmer SB. Prediction of hip fracture in elderly women: a prospective study. *BMJ* 1990;301:638–641

Reply

Dr. Baran suggests that we increase the number of broadband ultrasound attenuation measurements in normal subjects. Unfortunately, the ultrasonic device used in our study [1] was a prototype and is no longer available to us.

We are well aware of some divergent conclusions regarding the sensitivity of broadband ultrasonic attenuation measurements [2–5]. In our opinion, in clinical practice, the usefulness of a diagnostic procedure depends on its ability to discriminate between normal and pathologic conditions. Usually a normal range is defined in healthy subjects as the 5th to 95th percentile or, alternatively, the mean \pm 2 SD. In our study, we tried to investigate the clinical usefulness of an ultrasonic technique in defining a "normal range" and in assessing the number of osteoporotic patients outside the normal range. As we did not find a correlation between age and broadband ultrasound attenuation values in the normal subjects ($r = 0.08$, $p < .060$), we did not establish normal values for each decade. We are well aware that when compared with the numbers in published studies [2–4], our number of control subjects is far too small to define generally

applicable normal values. As we gave a clear description of how we obtained our normal range in our Patients and Methods section, we do not think that our conclusion will mislead the readers of AJR.

In contrast to other studies [2–5] that used broadband ultrasound attenuation in osteoporotic patients, we presented scattergrams in our report, allowing a direct comparison of individual measurements in the patients and the control subjects. Defining a normal range as the mean \pm 2 SD and using the values for the normal subjects studied by Baran et al. [2], we established the normal range as 35–90.2 dB/MHz. Although in this study no data on individuals are presented, the mean broadband ultrasound attenuation value for "osteoporotics" is given as 40.3 dB/MHz, and the mean value of hip fracture patients is given as 32.3 dB/MHz. When these values are related to the normal range as defined previously, a considerable overlap between the values of the control subjects and those of the patients seems to be evident. In this context, it should be emphasized that a similar overlap has been reported [6] between patients with osteoporosis when single-photon absorptiometry and quantitative CT were used to measure bone density. In conclusion, we think that broadband ultrasound attenuation may become an interesting tool in the clinical management of osteoporosis. However, further technical improvements are necessary before this method can be recommended for general clinical practice.

H. Resch

and colleagues

*Krankenhaus der Barmherzigen Brüder
A-1020 Wien, Austria*

REFERENCES

- Resch H, Pietschmann P, Bernecker P, Krexner E, Willvonseder R. Broadband ultrasound attenuation: a new diagnostic method in osteoporosis. *AJR* 1990;155:825–828
- Baran DT, Kelly AM, Karella A, et al. Ultrasound attenuation of the os calcis in women with osteoporosis and hip fractures. *Calcif Tissue Int* 1988;43:138–142
- Poll V, Cooper C, Crawley MI. Broadband ultrasonic attenuation in the os calcis and single photon absorptiometry in the distal forearm: a comparative study. *Clin Phys Physiol Meas* 1986;7:375–379
- McCloskey EV, Murray SA, Miller C, et al. Broadband ultrasound attenuation in the os calcis: relationship to bone mineral at other skeletal sites. *Clin Sci* 1990;78:227–233
- Porter RW, Miller CG, Grainger D, Palmer SB. Prediction of hip fracture in elderly women: a prospective study. *BMJ* 1990;301:638–641
- Hluck AF, Block J, Glueer CC, Steiger P, Genant HK. Mild versus definite osteoporosis: comparison of bone densitometry techniques using different statistical models. *J Bone Min Res* 1989;4:891–900

Dysbaric Osteonecrosis

We read with interest the article by Van Blarcom et al. [1] on follow-up radiographs of patients with dysbaric osteonecrosis that were obtained a minimum of 10 years after the patients' last exposure to hyperbaric pressures. We report a case of dysbaric osteonecrosis of the humeral and femoral heads that occurred 10 years after exposure to hyperbaric pressures.

A 50-year-old man had a painful right shoulder. Three months earlier, he suddenly had pain in his right shoulder. This had been followed, 10 days later, by pain in the right side of the groin, which induced limping. The patient had been a skin diver for 20 years, but it had been 10 years since his last exposure to hyperbaric pressures. He had no significant medical history. On physical examination, the right hip and shoulder were restricted and painful. The results of laboratory tests were normal. Radiographs showed osteonecrosis of the right humeral and femoral heads (Fig. 1). Scintigrams showed only a fixation of those bones. The patient had a total hip arthroplasty.

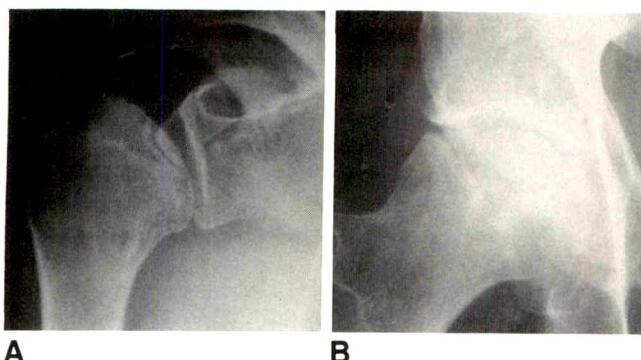


Fig. 1.—A and B, Radiographs show dysbaric osteonecrosis of right humeral (A) and femoral (B) heads 10 years after patient's last exposure to hyperbaric pressures.

The article by Van Blarcom and al. [1] is remarkable, and we would like to make some comments: (1) The number and severity of the osteonecrotic lesions are influenced not only by the frequency and severity of the exposure to a hyperbaric environment but also by the depth of the dive, the antecedents of bends, and the participation in experimental dives [2]. (2) Van Blarcom et al. have compared original and follow-up radiographs, but we cannot know when the lesions seen on the radiographs became worse because only 29.4% of the lesions of dysbaric osteonecrosis are symptomatic [2]. (3) Classically, lesions caused by caisson disease of bone are not seen on radiographs until late in the course of the disease. The earliest a lesion was seen was 10 months after exposure to hyperbaric pressures [3]. These lesions are uncommon in the early years after the exposure and are 10 times more likely to be seen if the radiographs are obtained more than 5 years after exposure. (4) The course of the disease is unpredictable. Scintigrams obtained more than 10 years after a patient's exposure to hyperbaric pressures may show fixations without radiologic lesions. Among those who have lesions seen on scintigrams, radiologic lesions develop in only 18% 5 years later [4].

Philippe Goupille
Bernard Fouquet
Philippe Cotté
Jean-Pierre Valat
C. H. U. Trousseau
37044 Tours, France

REFERENCES

- Van Blarcom ST, Czarnecki DJ, Fueredi GA, Wenzel MS. Does dysbaric osteonecrosis progress in the absence of further hyperbaric exposure? A 10-year radiologic follow-up of 15 patients. *AJR* 1990;155:95-97
- Amako T, Kawashima M, Torisu T, Hayashi K. Bone and joint lesions in decompression sickness. *Semin Arthritis Rheum* 1974;4:151-190
- Gregg PJ, Walder DN. Caisson disease of bone. *Clin Orthop* 1986;210:43-54
- MacLeod MA, McEwan AJB, Pearson RR, Houston AS. Functional imaging in the early diagnosis of dysbaric osteonecrosis. *Br J Radiol* 1982;55:497-500

Reply

The case reported by Dr. Goupille et al. is noted with interest. The delayed changes in dysbaric osteonecrosis seen in their patient are directly comparable to those seen in the patients in our study [1]. Many of our patients also were asymptomatic for many years until either articular fracture or associated osteoarthritic changes occurred.

The case reported by Goupille et al. is a further example of the latent morbidity associated with dysbaric osteonecrosis despite the decade-earlier cessation of exposure to hyperbaric pressures. Further prospective study of persons with exposure to hyperbaric pressures is needed because of the asymptomatic nature of the early stages of this disease.

Stephen T. Van Blarcom
St. Luke's Medical Center
Milwaukee, WI 53215

REFERENCE

- Van Blarcom ST, Czarnecki DJ, Fueredi GA, Wenzel MS. Does dysbaric osteonecrosis progress in the absence of further hyperbaric exposure? A 10-year radiologic follow-up of 15 patients. *AJR* 1990;155:95-97

Primary Squamous Cell Carcinoma of the Base of the Tongue with Liver and Bone Metastases

Distant metastases from oropharyngeal carcinomas are less common than metastases from most other head and neck primary tumors [1-4]. When metastases occur, the lungs are the most common site [1-4]. We present a case of bone and liver metastases from a primary oropharyngeal poorly differentiated squamous cell carcinoma.

A 42-year-old man had had weight loss, general malaise, progressive neck swelling, and pain in the right hip and knee over several months. Physical examination showed bilateral matted adenopathy of the anterior and posterior chains of lymph nodes. Laryngoscopy showed an extensive tumor of the tongue base extending down to the vallecula, the lingual and laryngeal surfaces of the epiglottis, and the right lateral pharyngeal wall. CT of the neck (Fig. 1A) showed an ulcerating mass at the base of the tongue, involving the right vallecula and base of the epiglottis. The right aryepiglottic fold was thickened. Extensive bilateral necrotic matted adenopathy throughout the entire jugular chain of nodes was noted. CT of the pelvis showed a 12 × 7 × 10 cm expansile, lytic, necrotic soft-tissue mass of the right iliac wing (Fig. 1B). CT of the abdomen showed a 6 × 4 × 6 cm necrotic mass in the right lobe of the liver. No lung or mediastinal lesions were seen on CT scans of the chest. Biopsy of the right lateral pharyngeal wall, the left side of the base of the tongue, and the iliac crest showed invasive poorly differentiated squamous cell carcinoma. According to

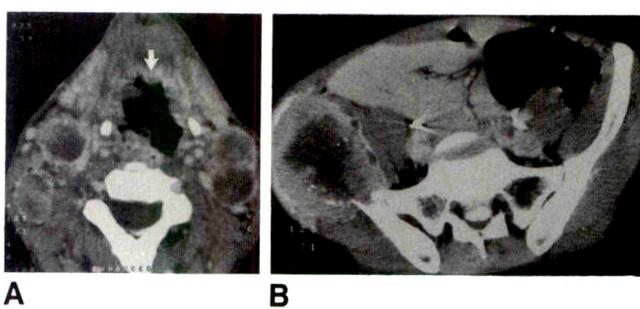


Fig. 1.—Squamous cell carcinoma of base of the tongue with liver and bone metastases.

A, Enhanced CT scan at level of oropharynx shows an irregular, ulcerated mass at base of tongue (arrow) extending into right oropharyngeal wall.

B, Enhanced CT scan of pelvis shows large, expansile, lytic, necrotic soft-tissue mass of right iliac wing, which biopsy showed was a metastasis of squamous cell carcinoma of base of tongue shown in A.

the TNM system of the International Union Against Cancer, this was a T3N2cM1, or stage IV, lesion.

Clinical detection of metastases from head and neck carcinoma occurs in only 5–25% of cases [1–4]. Most studies agree that nasopharyngeal, laryngeal (excluding vocal cord), and hypopharyngeal areas are the most likely sites of metastases from primary head and neck squamous cell carcinomas [1–4]. This case of an oropharyngeal carcinoma with disseminated disease illustrates one of the less likely of the head and neck carcinomas to metastasize.

The rate of distant metastases directly correlates with the stage of the neoplasm [2]. Studies [1, 3, 4] have shown that the more locally extensive (T3, T4) lesions are more likely to metastasize. Though a positive correlation of cervical adenopathy with distant metastases has been suggested, the relationship is more equivocal [1–3]. This case was a higher T and N stage neoplasm. It also was unusual in having liver and bone metastases without detectable lung metastases, as several studies have shown that lung metastases are more common than bone and liver metastases [1–4].

The stage of the disease or the histologic features of this particular carcinoma may have been the more important factors in determining its metastatic status at presentation. In cases reported in the literature, it often is difficult to determine if the stage of the primary neoplasm or the histologic findings differed significantly between

primary sites. This may have a significant impact on which primary site is more likely to be associated with disseminated disease. A more extensive evaluation of the prevalence of distant metastases from oropharyngeal and other head and neck carcinomas that includes the stage of disease and histologic information on the primary tumor would be of interest.

Dale N. Estes

University of Tennessee

Memphis, TN 38163

Jorge Salazar

University of Tennessee

Veterans Affairs Medical Center

Memphis, TN 38104

REFERENCES

1. Probert JC, Thompson RW, Bugshaw MA. Pattern of spread of distant metastases in head and neck cancer. *Cancer* 1974;33:127–133
2. Merino OR, Lindberg RD, Fletcher GH. An analysis of distant metastases from squamous cell carcinoma of the upper respiratory and digestive tracts. *Cancer* 1977;40:145–151
3. Dennington ML, Carter DR, Meyers AD. Distant metastases in head and neck epidermoid carcinoma. *Laryngoscope* 1980;90:196–201
4. Papac RJ. Distant metastases from head and neck cancer. *Cancer* 1984;53:342–345

Letters are published at the discretion of the Editor and are subject to editing.

Letters to the Editor must not be more than two double-spaced, typewritten pages. One or two figures may be included. Abbreviations should not be used. See Author Guidelines, page A5.

Material being submitted or published elsewhere should not be duplicated in letters, and authors of letters must disclose financial associations or other possible conflicts of interest.

Letters concerning a paper published in the AJR will be sent to the authors of the paper for a reply to be published in the same issue. Opinions expressed in the Letters to the Editor do not necessarily reflect the opinions of the Editor.

Review of Current Literature

Initials and addresses of corresponding authors are provided in parentheses for each article so that the reader can obtain reprints directly. Abstracts are printed verbatim from each journal.

The New England Journal of Medicine

Familial occurrence of inflammatory bowel disease. Orholm M, Munkholm P, Langholz E, Nielsen OH, Sørensen TIA, Binder V (MO, Dept. of Infectious Diseases 7721, Rigshospitalet, Tagensvej 20, DK-2200, Copenhagen N, Denmark). *N Engl J Med* 324:84-88, Jan. 1991

Background and Methods. We assessed the familial occurrence of inflammatory bowel disease in Copenhagen County, where there has been a long-term interest in the epidemiology of such disorders. In 1987 we interviewed 662 patients in whom inflammatory bowel disease had been diagnosed before 1979, asking whether their first- and second-degree relatives had this disorder. Ninety-six percent of the patients (504 with ulcerative colitis and 133 with Crohn's disease) provided adequate information.

Results. As compared with the general population, the first-degree relatives of the 637 patients with ulcerative colitis or Crohn's disease had a 10-fold increase in the risk of having the same disease as the patients, after standardization for age and sex. The risk of having the other of the two diseases was also increased, but less so, and the increase in the risk of having Crohn's disease was not significant in the relatives of patients with ulcerative colitis. The risk of ulcerative colitis in first-degree relatives of patients with ulcerative colitis appeared to be virtually independent of the generation to which the first-degree relative belonged and of the sex of the patient and the relative. The risk of ulcerative colitis in first-degree relatives tended to be higher if the disease had been diagnosed in the patient before the age of 50, but the risk seemed to be independent of the current age of the relatives. The prevalence of the same disease as that of the patient (either ulcerative colitis or Crohn's disease) among second-degree relatives was increased; the prevalence of the other disease was not increased.

Conclusions. The 10-fold increase in the familial risk of ulcerative colitis and Crohn's disease strongly suggests that these disorders have a genetic cause.

Efficacy and cost effectiveness of adjuvant chemotherapy in women with node-negative breast cancer: a decision-analysis model. Hillner BE, Smith TJ (BEH, Division of General Internal Medicine, Box 170, MCV Station, Richmond, VA 23298). *N Engl J Med* 324:160-168, Jan. 1991

Background. In 1988 the National Cancer Institute issued a Clinical Alert that has been widely interpreted as recommending that all women with node-negative breast cancer receive adjuvant chemotherapy. Acceptance of this recommendation is controversial, since many women who would not have a recurrence would be treated.

Methods. Using a decision-analysis model, we studied the cost effectiveness of chemotherapy in cohorts of 45-year-old and 60-year-old women with node-negative breast cancer by calculating life expectancy as adjusted for quality of life. The analysis evaluated different scenarios of the benefit of therapy: improved disease-free survival for five years, with a lesser effect on overall survival (base line); a lifelong benefit from chemotherapy; and a benefit in disease-free survival with no change in overall survival by year 10. The base-line analysis assumed a 30 percent reduction in the relative risk of recurrence for five years after treatment.

Results. For the 45-year-old woman, the base-line analysis found an average lifetime benefit from chemotherapy of 5.1 quality-months at a cost of \$15,400 per quality-year. The 60-year-old women gained 4.0 quality-months at a cost of \$18,800 per quality-year. Under the more and less optimistic scenarios, the benefit of chemotherapy varied from 1.4 to 14.0 quality-months for both groups.

Conclusions. Chemotherapy substantially increases the quality-adjusted life expectancy of an average woman at a cost comparable to that of other widely accepted therapies. This benefit decreases markedly if the changes in long-term survival are less than in disease-free survival. Given its uncertain duration, the benefit may be too small for many women to choose chemotherapy. Selective use of chemotherapy to maximize the benefit to individual patients may be possible with refinements in risk stratification and explicit assessment of the patients' risk preferences.

Chest

Magnetic resonance imaging in the diagnosis of pulmonary infarction. Kessler R, Fraisse P, Krause D, Veillon F, Vandevenne A (RK, Service de Pneumologie, Hôpital de Hautepierre, Centre Hospitalier Régional Universitaire, Strasbourg, France). *Chest* 99(2):298-300, Feb. 1991

We report for the first time, to our knowledge, MRI features which could differentiate noninvasively pulmonary infarction from pneumonia. Three subjects with angiographically proven pulmonary infarction showed high T₁ weighted MRI signals located in the embolic territory. Three patients with pneumonia and one patient with emboli, but without infarction, did not have these T₁ weighted images.

Gastroenterology

Impairment of esophageal emptying with hiatal hernia. Sloan S, Kahrilas PJ (SS, Dept. of Medicine, Northwestern University, Chicago, IL). *Gastroenterology* 100:596-605, 1991

Concurrent videofluoroscopy and manometry were used to analyze esophageal emptying during barium swallows in 22 patients with axial hiatal hernias and in 14 volunteers. Subjects were divided into three

groups: (a) volunteers with maximal phrenic ampullary length <2 cm (controls); (b) patients or volunteers with maximal ampullary/hiatal hernia length ≥ 2 cm that reduced between swallows (reducing-hernia group); and (c) patients with hernias that did not reduce between swallows. Complete esophageal emptying without retrograde flow was achieved in 86% of test swallows in the controls, 66% in the reducing-hernia group, and 32% in the nonreducing hernia group ($P < 0.05$). Impaired emptying in the reducing-hernia group was attributable to "late retrograde flow," whereby barium squirted retrograde from the hernia during emptying. Impaired emptying in the nonreducing-hernia group was attributable to "early retrograde flow" that occurred immediately after LES relaxation. The nonreducing hernia group also had longer acid clearance times than the controls ($P < 0.05$). We conclude that gastroesophageal junction competence is severely impaired in patients with nonreducing hiatal hernias, suggesting a mechanism whereby this subgroup of hiatal hernia is involved in the pathogenesis of reflux disease.

Reprinted with permission by the American Gastroenterological Association.

Digestive Diseases and Sciences

Medical dissolution of gallstones: clinical experience of d-limonene as a simple, safe, and effective solvent. Igimi H, Tamura R, Toraishi K, et al. (HI, Shionogi Research Laboratories, Shionogi & Co., Ltd., Fukushima-ku, Osaka 553, Japan). *Dig Dis Sci* 36(2):200-208, Feb. 1991.

Retained gallstones in the bile ducts account for 60–70% of all the cases of postcholecystectomy syndromes. A solvent *d*-limonene preparation was injected directly to the biliary system of 200 patients to dissolve or disintegrate the retained gallstones. The outcomes were: retained stones completely disappeared in 96 cases (48%); partial dissolution in 29 (14.5%); chelating agent was also used with partial dissolution in 16 (8%); ineffective in 59 (24.5%). To make this method more effective, several guidelines should be observed including an *in vitro* trial dissolution test. Cautious observation for possible side effects and frequent hepatic and pancreatic function tests during the treatment with this preparation also should be performed.

Achalasia in the elderly: effects of aging on clinical presentation and outcome. Clouse RE, Abramson BK, Todorcek JR (REC, Digestive Disease Clinical Center, One Barnes Hospital Plaza, St. Louis, MO 63110). *Dig Dis Sci* 36(2):225-228, Feb. 1991.

Clinical and manometric data from 13 elderly subjects with idiopathic achalasia (mean age 79 ± 2 years) were compared with findings from younger subjects with the same disease ($n = 79$) to see if aging altered the presentation and outcome of this motor disorder. Fewer elderly subjects complained of chest pain (27% vs 53%), and the pain was significantly less severe ($P < 0.01$). Other presenting features (including sex, duration of symptoms, and presence and severity of dysphagia) did not differ between the groups. Across all patients, age weakly and inversely correlated with residual postdeglutitive lower esophageal sphincter (LES) pressure ($R = -0.34$) and residual pressure was significantly lower in the older subjects (8.0 ± 1.3 mm Hg vs 11.9 ± 0.8 mm Hg; $P = 0.02$). No differences in basal LES pressure or esophageal-body contraction amplitudes were present between the groups. Initial success with pneumatic dilation was similar in the two subject groups, but the number of older subjects available for analysis was too small to draw strong conclusions. These results indicate that aging decreases the elevation of LES residual pressure that occurs with achalasia. As elderly achalasia patients also present with less chest pain, the findings may be interrelated.

Prevalence of *Helicobacter pylori* in specific forms of gastritis: further evidence supporting a pathogenic role for *H. pylori* in chronic nonspecific gastritis. Ormand JE, Talley NJ, Shorter RG, et al. (NJT, Gastroenterology Unit, Mayo Clinic, Rochester, MN 55902). *Dig Dis Sci* 36(2):142-145, Feb. 1991.

Helicobacter pylori colonization of the gastric mucosa is strongly associated with chronic nonspecific gastritis; moreover, there is evi-

dence to suggest that *H. pylori* may cause this form of gastritis. However, there is little or no information on the prevalence of *H. pylori* in specific forms of gastritis. Our hypothesis was that if *H. pylori* was pathogenic in chronic nonspecific gastritis, organisms would be found frequently in this type of gastritis but infrequently in specific forms of gastritis. Prevalence rates of *H. pylori* were determined independently in patients with eosinophilic and Crohn's gastritis, Menetrier's disease, and chronic nonspecific gastritis. The prevalence of *H. pylori* in patients with chronic nonspecific gastritis was 71%, whereas the organism was not identified in patients with any form of specific gastritis. This finding further supports the accumulating evidence that *H. pylori* is a primary pathogenic factor in chronic nonspecific gastritis.

Gastrointestinal Endoscopy

Laparoscopic cholecystectomy: an initial report. Salky BA, Bauer JJ, Kreel I, Gelernt IM, Gorfine SR (BAS, 25 E. 69 St., New York, NY 10021). *Gastrointest Endosc* 37(1):1-4, Jan. 1991

Sixty consecutive patients underwent an elective attempt at laparoscopic cholecystectomy between March 15 and July 31, 1990 at the Mount Sinai Hospital in New York. Fifty-two patients had successful completion of the laparoscopic cholecystectomy (87%). The reasons for conversion to open cholecystectomy were acute cholecystitis (four patients), inability to define the cystic duct-common duct junction (three patients), and one patient with an unexpected choledochal cyst variant. Forty patients (77%) were discharged on the first post-operative day, and the remaining 12 patients on the second post-operative day. Thirty-three patients (63%) required only oral pain medication, and 11 patients (21%) needed no pain medication post-operatively. Fifty-one patients (98%) had resumed normal activities by the seventh post-operative day. Cholecystectomy remains the treatment of choice for biliary colic. Laparoscopic cholecystectomy minimizes length of stay in the hospital, lessens post-operative pain, allows quicker return to normal activities, and has a superior cosmetic result.

Small bowel enteroscopy: an early experience in gastrointestinal bleeding of unknown origin. Gostout CJ, Schroeder KW, Burton DD (CJG, Mayo Clinic, 200 First St., S.W., Rochester, MN 55905). *Gastrointest Endosc* 37(1):5-8, Jan. 1991

Peroral small intestinal enteroscopy was performed in 35 consecutive patients with gastrointestinal bleeding of unknown origin by using a prototypic Sonde-type enteroscope. The median value for patient age was 69 years; duration of bleeding, 2 years (range, 2 months to 9 years); and transfusion requirements, 9 units. Bleeding was occult in 54% of these patients. Placement and passage of the enteroscope was performed by a gastrointestinal endoscopy assistant. Mean passage time was 4.3 hours. Complete passage was obtained in 14% of the patients, passage into the mid-distal ileum in 69%, and passage only into the jejunum in 17%. The diagnostic yield was 26%, with the majority of lesions encountered being mucosal vascular malformations. Small intestinal enteroscopy is a reasonable diagnostic procedure before embarking on visceral angiography and surgical exploration when standard endoscopic and radiologic methods fail to disclose a diagnosis.

Percutaneous cholangioscopic or transpapillary insertion of self-expanding biliary metal stents. Neuhaus H, Hagenmüller F, Griebel M, Classen M (HN, Dept. of Internal Medicine II, Technical University of Munich, Klinikum Rechts der Isar, Ismaninger Str. 22, D-8000 Munich 80, Germany). *Gastrointest Endosc* 37(1):31-37, Jan. 1991

Fifty-two self-expanding metal stents were implanted in 39 patients with malignant (35 patients) or benign (4 patients) biliary stenoses. The stents were inserted and properly released by means of a 7 or 9 French gauge delivery catheter via the percutaneous (20 patients) or transpapillary (19 patients) route. In all cases the endoprostheses expanded to a diameter of 7 to 10 mm and achieved complete biliary tract drainage. Jaundice disappeared in 36 of the 39 patients. No

early complication was observed. After a median follow-up of 121 days (range, 30 to 422 days), 19 of 36 patients are still alive and 17 died of non-procedure-related causes. Biliary re-obstruction occurred in five patients due to tumor overgrowth above or below the prosthesis (four patients) or bile encrustation (one patient). In patients with malignant stenoses, the probability of stent patency is 78% after 200 days. We conclude that large-bore metal stents are safe, effective, and provide better long-term patency than conventional endoprotheses.

Endoscopic treatment of biliary tract strictures in sclerosing cholangitis: a larger series and recommendations for treatment. Johnson GK, Geenen JE, Venu RP, Schmalz MJ, Hogan WJ (GKJ, 1333 College Ave., Racine, WI 53403). *Gastrointest Endosc* 37(1):38-43, Jan. 1991

We report a group of 35 patients with primary sclerosing cholangitis who had long-term follow-up after endoscopic treatment of major ductal strictures in the primary or secondary biliary ducts. Our patients were all symptomatic with ascending cholangitis or jaundice. There was significant improvement as measured by clinical parameters of hospitalization rates and laboratory data and comparable radiography. Long-term follow-up averaged 24 (± 2.8 months). We believe endoscopic treatment of sclerosing cholangitis should be attempted in selected symptomatic cases with major ductal strictures before liver transplantation.

The Journal of Bone and Joint Surgery

Osteoarthritis and congenital dysplasia of the hip in family members of children who have congenital dysplasia of the hip. Hoaglund FT, Healey JH (FTH, Dept. of Orthopaedic Surgery, Rm. U471, University of California, San Francisco, San Francisco, CA 94143-0728). *J Bone Joint Surg [Am]* 72-A(10):1510-1518, Dec. 1990

Four hundred and eight siblings, parents, and grandparents of seventy-eight children from the New England area who had congenital dysplasia of the hip were evaluated, by clinical examination and by measurements of the acetabulum on pelvic radiographs, for the signs and sequelae of congenital dysplasia of the hip. Six siblings and four mothers (representing seven of seventy-eight families) had been diagnosed with congenital dysplasia of the hip during childhood. The other ninety-one siblings were asymptomatic and had no radiographic evidence of dysplasia of the hip.

In the adults in these families, acetabular coverage (as measured by the center-edge angle of Wiberg) was no different from that in the control subjects. There was no difference between the study group and the control subjects in the prevalence of osteoarthritis of the hip or of osteoarthritis that could be considered secondary to congenital dysplasia of the hip.

The results indicate that children born to families that have a history of congenital dysplasia of the hip have a greater prevalence of this problem compared with the general population, but also that examinations of the hip in newborns are effective in detecting congenital dysplasia of the hip in such families. The greater prevalence of congenital disease of the hip among the siblings and mothers in these families is consistent with a multifactorial inheritance. The fact that acetabular development in the family members who did not have congenital dysplasia of the hip was no different from that in the control subjects suggests that acetabular dysplasia, rather than being an inherited abnormality, is secondary to subluxation or dislocation.

Clinical Orthopaedics and Related Research

Ultrasound in the diagnosis of congenital dysplasia and dislocation of the hip joints in children older than two years. Terjesen T, Runden TØ, Johnsen HM (TT, Dept. of Orthopaedic Surgery, Trondheim University Hospital, N-7006 Trondheim, Norway). *Clin Orthop* 262:159-169, Jan. 1991

To evaluate the use of ultrasound in the diagnosis of congenital dysplasia and dislocation of the hip (CDH) in children older than two years of age, 64 patients with normal hip joints and 47 patients with present or previous CDH were examined. Lateral and anterior ultrasound scanning was employed, and the coverage of the femoral head by the acetabular roof was assessed. The ultrasound measurements were compared with standard roentgenography, and a good accordance between the methods was found. A lateral projection of the femoral head in relation to the bony acetabular rim of more than 8 mm in children younger than ten years of age indicated subluxation and more than 15 mm at age two to four years indicated dislocation. Reliable images were obtained by ultrasound at any age between two and 18 years. Ultrasound is recommended as the primary imaging technique in the evaluation of hip joints, even in older children, and ultrasound should replace roentgenography in most of the follow-up examinations of children with previous CDH.

The Journal of Urology

Management of primary nonrenal parenchymal malignancies with vena caval thrombus. Concepcion RS, Koch MO, McDougal WS, Stewart JR, Merrill WH (WSM, Dept. of Urology, Vanderbilt University Medical Center, Nashville, TN 37232-2765). *J Urol* 145:243-247, Feb. 1991

We report our experience with the management of 7 primary nonrenal parenchymal malignancies with vena caval tumor thrombus. Included are 3 cases of adrenal cortical carcinoma and 1 each of transitional cell carcinoma, embryonal cell testicular carcinoma, pheochromocytoma and primary small cell carcinoma of the lung with metastases to the kidney. Surgical treatment and followup are presented, as well as a review of the literature. An aggressive surgical approach is warranted because prolonged survival free of disease are possible.

Pediatrics

Diagnostic utility of lower extremity radiographs of young children with gait disturbance. Blatt SD, Rosenthal BM, Barnhart DC (SDB, Dept. of Pediatrics, State University of New York Health Science Center at Syracuse, 750 E. Adams St., Syracuse, NY 13210). *Pediatrics* 87(2):138-140, Feb. 1991

The diagnostic utility of lower extremity radiographs was evaluated using 84 outpatients 1 to 5 years of age with gait disturbance whose lower extremities appeared physically normal. Chief complaints included limp (65 children [77%]), refusal to walk or stand (37 children [44%]), and frequent falling (6 children [7%]). A total of 43 children (51%) had more than one complaint. The mean age of patients was 26 months and the median duration of symptoms was 1 day. Trauma was reported in 43 (51%) cases and fever in 14 (17%). Results of radiographical studies appeared normal in 81 children (96%), demonstrated soft tissue swelling in 2 children, and revealed a bony island in 1 child. In 1 patient admitted to the hospital for failure to thrive and irritability, and whose radiographic results appeared normal, findings consistent with osteomyelitis later developed. Of the remaining children, 68 (81%) were available for follow-up observation 4 to 28 months after the initial visit and all reported spontaneous resolution of the initial complaint. It was concluded that in a well-appearing child with an otherwise normal physical examination results, an acute gait disturbance is likely to be a self-limiting condition and radiographs are unlikely to contribute to the diagnosis.

Reprinted by permission of PEDIATRICS © 1991.

The Journal of Pediatrics

Treatment of childhood angiomatous diseases with recombinant interferon alfa-2a. White CW, Wolf SJ, Korones DN, Sondheimer HM, Tosi MF, Yu A (CWW, Division of Pulmonary and Critical Care Medicine, National Jewish Center for Immunology and Respiratory Medicine, 1400 Jackson St., Denver, CO 80206). *J Pediatr* 118:59-66, Jan. 1991

A heterogeneous group of five patients with progressive, invasive angiomatic diseases including pulmonary hemangiomatosis, angiosarcoma, or massive hemangioma with associated consumptive coagulopathy were treated with interferon alfa-2a for periods of 17 to 33 months. One patient with a large thoracic hemangioma, cardiorespiratory failure, and consumptive coagulopathy died after less than 2 months of treatment. The remaining four patients have shown beneficial responses, including (1) regression of abnormal vessels on pulmonary angiogram and improved exercise tolerance in pulmonary hemangiomatosis (two patients), (2) decreased corticosteroid and/or platelet transfusion requirements in consumptive coagulopathy (two patients), and (3) decreased size and number of tumor nodules in the one patient with angiosarcoma arising in preexisting angiomatic lesions. Responses occurred during periods of 2 to 20 months of treatment. There was no measurable progression of angiomatic lesions in any patient receiving interferon at the therapeutic dose, except possibly in the one who died. Each of the four surviving patients had improved linear growth and weight gain during interferon treatment.

Asymmetric growth of the lateral cerebral ventricle in infants with posthemorrhagic ventricular dilation. Brann BS IV, Qualis C, Wells L, Papile L (BSB, Dept. of Pediatrics, Children's Hospital of New Mexico, University of New Mexico School of Medicine, 2211 Lomas Blvd., Albuquerque, NM 87131). *J Pediatr* 118:108-112, Jan. 1991

Lateral cerebral ventricular volume in 36 preterm infants with or without an intraventricular hemorrhage, and with or without posthemorrhagic hydrocephalus, was measured longitudinally and compared with the ventricular index measurements of the same ventricles. A poor correlation was found ($r^2 = 0.67$). To determine a reason for this poor relationship, we analyzed the volumes of the regions of the ventricles by a segmental volume analysis. The occipital region of the lateral cerebral ventricle enlarged at a much faster rate (1.904 ± 0.477 ml/day) than either the anterior region (0.546 ± 0.253 ml/day; $p < 0.01$) or the middle region (-0.209 ± 0.334 ml/day; $p < 0.01$) in infants with posthemorrhagic hydrocephalus. The rate of growth of the middle region of the lateral cerebral ventricles was the same for all infants. Linear indexes, such as the ventricular index and the lateral ventricular ratio, do not allow for accurate serial estimates of ventricular size in posthemorrhagic hydrocephalus because of asymmetric growth of the lateral cerebral ventricle. We conclude that sequential volume measurements are more useful than ventricular index measurements to follow ventricular size sequentially in infants with posthemorrhagic hydrocephalus.

Decreased mortality rate among small premature infants treated at birth with a single dose of synthetic surfactant: a multicenter controlled trial. Corbet A, Buccarelli R, Goldman S, et al. (AC, Dept. of Pediatrics, Baylor College of Medicine, Texas Medical Center, Houston, TX 77030). *J Pediatr* 118:277-284, Feb. 1991

To determine whether a single prophylactic dose of synthetic surfactant would reduce mortality and morbidity rates, we performed a randomized, controlled trial of Exosurf Neonatal at 19 hospitals in the United States. The Exosurf preparation (5 ml/kg) was instilled into the endotracheal tube of premature infants weighing 700 to 1100 gm during mechanical ventilation, as soon as practical after birth. Control infants were treated with air (5 ml/kg). Dose administration was performed in secrecy by clinicians who did not reveal for 2 years what they had instilled. A total of 222 infants received air and 224 received the synthetic surfactant; 36 infants with congenital pneumonia or malformations were excluded from the primary efficacy analysis. By the age of 28 days, there were 44 deaths in the air group and 27 deaths in the surfactant group ($p = 0.022$). By the age of 1 year after term there were 61 deaths in the air group and 35 deaths in the surfactant group ($p = 0.002$). Although there was no reduction in the incidence of respiratory distress syndrome, a significant reduction in the number of deaths attributed to respiratory distress syndrome, a significant reduction in the incidence of pulmonary air leaks, and significantly lower requirements for oxygen and mean airway

pressure indicated that lung disease was less severe in the Exosurf-treated infants. There were no significant differences in the incidence of complications such as bronchopulmonary dysplasia, intraventricular hemorrhage, patent ductus arteriosus, necrotizing enterocolitis, and infection. The results indicate that a single prophylactic dose of Exosurf, in high-risk premature infants treated soon after birth, reduces the number of deaths from respiratory distress syndrome and the overall mortality rate.

Journal of Ultrasound in Medicine

Prospective comparison of vaginal and abdominal sonography in normal early pregnancy. Pennell RG, Needleman L, Pajak T, et al. (LN, Division of Diagnostic Ultrasound, 10th and Sansom Sts., 7th Fl., Main Bldg., Philadelphia, PA 19107). *J Ultrasound Med* 10:63-67, Feb 1991

Vaginal and abdominal sonography were prospectively compared in 309 consecutive pregnancies of which 175 were normal. Two sonographic criteria of normal were analyzed: (1) the presence of an embryo compared with average gestational sac size and (2) the presence of embryonic cardiac activity compared with crown-rump length. Vaginally, 100% (160/160) of embryos were visualized when the average sac diameter was ≥ 12 mm. Abdominally, an embryo was noted in 99.2% (123/124) of gestational sacs ≥ 27 mm. Vaginal sonography revealed cardiac motion in all embryos of ≥ 5 mm (149/149 cases); abdominal sonography revealed cardiac activity in 100% (132/132) of embryos with a crown-rump length of ≥ 9 mm. One-third of normal embryos < 5 mm crown-rump length did not demonstrate cardiac activity. The study demonstrates through objective comparison that vaginal sonography is superior to abdominal sonography for detection of an intrauterine embryo and its cardiac activity before 8 menstrual weeks. The diagnosis of embryonic demise should not be made by vaginal sonography in embryos measuring < 5 mm crown-rump length without a heartbeat, and an empty gestational sac of < 12 mm average diameter should not be diagnosed as blighted ovum by vaginal scans. In these cases follow-up vaginal sonography is suggested.

Reprinted with permission by the American Institute of Ultrasound in Medicine.

Journal of Computer Assisted Tomography

MR imaging of septic sacroiliitis. Klein MA, Winalski CS, Wax MR, Piwnica-Worms DR (MAK, Medical College of Wisconsin, Dept. of Radiology, 8700 W. Wisconsin Ave., Milwaukee, WI 53226). *J Comput Assist Tomogr* 15(1):126-132, Jan./Feb. 1991

Septic sacroiliitis is difficult to diagnose, causing delayed treatment and increased morbidity. The traditional imaging techniques for diagnosis have been CT and nuclear medicine. Our purpose was to determine the ability of MR imaging to detect septic sacroiliitis, to evaluate the features of septic sacroiliitis with MR, and to compare the relative detection rate of MR, CT, and nuclear medicine. All patients with a discharge diagnosis of septic sacroiliitis who were evaluated by MR imaging of the pelvis were retrospectively evaluated. Five patients were collected with six septic sacroiliac joints, which were also evaluated with CT, ^{99m}Tc -methylene diphosphonate bone scans, and ^{67}Ga -citrate scans. Abnormalities consistent with sacroiliitis were seen in all sacroiliac joints both prospectively (impression from the initial report) and retrospectively on MR. In addition to the nonspecific MR findings of inflammation and/or fluid in the sacroiliac joint space, bone marrow of the sacrum and/or ilium, and iliopsoas muscle, fluid/inflammation was uniquely identified tracking posterior to the iliopsoas muscle in each of these patients with septic sacroiliitis. Even in retrospect, a definite diagnosis of sacroiliitis could be made in only five of six joints by ^{67}Ga -citrate scans, three of six joints by CT scans, and one of six joints by ^{99m}Tc -methylene diphosphonate bone scans. These results suggest MR imaging may be a sensitive modality in the early diagnosis of septic sacroiliitis.

News

Preceptorships in Ultrasound at Johns Hopkins

The Division of Ultrasound, Dept. of Radiology, The Johns Hopkins Hospital, Baltimore, is sponsoring visiting preceptorships in ultrasound, times to be arranged. The program is designed for physicians or sonographers who have been practicing ultrasound for at least 6 months. Participants will attend ultrasound reporting sessions and will observe obstetric, gynecologic, and abdominal studies and new or unusual techniques. Category 1 credit: 40 hr. Fee: \$500. Information: Program Coordinator, The Johns Hopkins Medical Institutions, Office of Continuing Education, Turner Bldg., 720 Rutland Ave., Baltimore, MD 21205; (301) 955-2959.

Obstetrics & Gynecology Ultrasound

The Dept. of Radiology, Division of Diagnostic Ultrasound, Thomas Jefferson University Hospital, Philadelphia, will present Obstetrics & Gynecology Ultrasound June 3-7 and July 22-26. Course director: Alfred B. Kurtz. Category 1 credit: 31 hr. Fee: \$675. Information: Judith Kaneff, Education Coordinator, Division of Diagnostic Ultrasound, Thomas Jefferson University Hospital, Rm. 792-B, Main Bldg., Philadelphia, PA 19107; (215) 955-8533.

Canadian Association of Radiologists Annual Meeting

The 54th annual meeting of the Canadian Association of Radiologists will be held June 9-13 at the Hamilton Convention Centre, Hamilton, Ontario. Guest lecturers will be Michel Osteaux, Anthony Proto, Gordon Guyatt, and Alec Megibow. The meeting will include a special symposium, Professional and Health Care Facilities, and three minisymposia: Gastrointestinal Tract Imaging, Pediatric Imaging, and Obstetrical and Gynecologic Ultrasound. Information: The Canadian Association of Radiologists, 5101 Buchan St., Ste. 510, Montreal, Quebec, Canada H4P 2R9; telephone: (514) 738-3111; fax: (514) 738-5199.

Workshop on New Devices for Cardiac and Peripheral Vascular Laboratories

The Pittsburgh Vascular Institute and Pittsburgh Heart Institute of Shadyside Hospital, Pittsburgh, are sponsoring New Devices for the Cardiac and Peripheral Vascular Laboratories: An Advanced Work-

shop, July 1-3, at Disney's Yacht and Beach Club Resorts, Walt Disney World, Lake Buena Vista, FL. Leading cardiologists, radiologists, cardiovascular surgeons, and biomedical engineers will teach and demonstrate how they use the new third-wave devices in their own laboratories. Topics will include angioscopy, complex multilevel angioplasty, intravascular stents, intravascular sonography, lasers, percutaneous atherectomy, and thrombolytics. Course directors: James D. O'Toole and Mark H. Wholey. Category 1 credit: 13 hr. Fee: physicians, \$500; nurses and technologists, \$300. Information: Shadyside Hospital, New Devices Technology Workshop, 5230 Centre Ave., Pittsburgh, PA 15232; (412) 623-1051.

Physics and Instrumentation

The Dept. of Radiology, Division of Diagnostic Ultrasound, Thomas Jefferson University Hospital, Philadelphia, will present Physics and Instrumentation July 8-12. Course director: Peter N. Burns. Category 1 credit: 31 hr. Fee: \$675. Information: Judith Kaneff, Education Coordinator, Division of Diagnostic Ultrasound, Thomas Jefferson University Hospital, Rm. 792-B, Main Bldg., Philadelphia, PA 19107; (215) 955-8533.

Cross Sectional Anatomy

The Dept. of Radiology, Division of Diagnostic Ultrasound, Thomas Jefferson University Hospital, Philadelphia, will present Cross Sectional Anatomy July 15-19. Course director: Carol Williams. Category 1 credit: 31 hr. Fee: \$675. Information: Judith Kaneff, Education Coordinator, Division of Diagnostic Ultrasound, Thomas Jefferson University Hospital, Rm. 792-B, Main Bldg., Philadelphia, PA 19107; (215) 955-8533.

Imaging on Lake Coeur d'Alene

The Depts. of Radiology, University of Washington, Seattle, and Sacred Heart Medical Center, Spokane, will cosponsor the 5th annual Imaging on Lake Coeur d'Alene: A Summer Radiology Meeting, July 25-27, at the Coeur d'Alene Resort, Coeur d'Alene, ID. The course is designed for practicing general diagnostic radiologists. It will include sessions on diagnostic oncology; thoracic, abdominal, and pelvic imaging; and diagnostic sonography. Category 1 credit: 20 hr. Fee: through July 15, \$400; after July 15, \$450. Information: Kathy Fischer, Course Secretary, Dept. of Radiology, Sacred Heart Medical Center, TAF-C9, Spokane, WA 99220; (509) 455-3352 or (509) 455-3330.

Abdominal Ultrasound

The Dept. of Radiology, Division of Diagnostic Ultrasound, Thomas Jefferson University Hospital, Philadelphia, will present Abdominal Ultrasound July 29-Aug. 1. Course director: Rick Feld. Category 1 credit: 27 hr. Fee: \$600. Information: Judith Kaneff, Education Coordinator, Division of Diagnostic Ultrasound, Thomas Jefferson University Hospital, Rm. 792-B, Main Bldg., Philadelphia, PA 19107; (215) 955-8533.

Prostate Ultrasound

The Dept. of Radiology, Division of Diagnostic Ultrasound, Thomas Jefferson University Hospital, Philadelphia, will present Prostate Ultrasound Aug. 2. Course director: Matthew D. Rifkin. Category 1 credit: 9 hr. Fee: \$375. Information: Judith Kaneff, Education Coordinator, Division of Diagnostic Ultrasound, Thomas Jefferson University Hospital, Rm. 792-B, Main Bldg., Philadelphia, PA 19107; (215) 955-8533.

Napa Valley Imaging Update

The Office of Continuing Medical Education and the Dept. of Radiology, University of California, Davis Medical Center, are sponsoring Napa Valley Imaging Update: MRI 1991, Aug. 4-8, at the Silverado Country Club, Napa, CA. Guest faculty: C. A. Helms, W. Kelly, R. F. Mattrey, and W. R. Webb. Category 1 credit: 17 hr. Fee (approximately): physicians, \$465; others, \$365. Information: Karen Buckman, Publicity Representative, Office of Continuing Medical Education, UC Davis Medical Center, 2701 Stockton Blvd., Sacramento, CA 95817; telephone: (916) 734-5390; fax: (916) 736-0188.

Symposium on Diagnostic Imaging

The Dept. of Diagnostic Imaging, Rhode Island Hospital and Brown University School of Medicine, will present their 12th annual symposium on diagnostic imaging Aug. 12-15 at the Sheraton Islander Inn, Newport, RI. The course will be presented in two parts. The first day will be a symposium on the economic and political aspects of radiologic practice. Faculty will include F. Graefe, G. Price, J. H. Chafee, L. Rogers, A. E. James, Jr., and B. Katzen. The remaining three days will concentrate on the radiology of trauma and on oncologic radiology. Guest faculty will include C. Ravin, J. Haaga, and D. Kopans. Category 1 credit: 16 hr. Fee: physicians, through July 1, \$550; after July 1, \$575; residents, fellows, and technologists, \$400 (letter required). Information: Mrs. Gayle Pascetta, Rhode Island Hospital, Dept. of Diagnostic Imaging, Main—3rd Fl., 593 Eddy St., Providence, RI 02903; (401) 277-5184.

Pacific Northwest Diagnostic Ultrasound Symposium

The American Institute of Ultrasound in Medicine and Swedish Hospital Medical Center, Seattle, are cosponsoring Pacific Northwest Diagnostic Ultrasound Symposium: OB/Gyn Update, Sept. 6-8, at the Westin Hotel, Seattle. The course will provide timely and useful information on obstetric and gynecologic sonography and Doppler imaging. Course directors: David A. Nyberg and Barry S. Mahony. Guest faculty: B. Benacerraf, R. Filly, F. Hadlock, L. Hill, F. Laing, L. Mack, and D. Pretorius. Category 1 credit: 16 hr. Fee: physicians, \$350; sonographers and residents, \$200; a surcharge of \$50 will be added to the fee for those who register after Aug. 1. Information:

Renée Durnell, Seattle Ultrasound Associates, 1229 Madison, #1150, Seattle, WA 98104; telephone: (206) 386-6300; fax: (206) 386-6312.

Diagnostic Ultrasound in Gynecology and Obstetrics and Abdomen

The Dept. of Radiology and Radiological Science, The Johns Hopkins Medical Institutions, is sponsoring the 20th annual Diagnostic Ultrasound in Gynecology and Obstetrics and Abdomen, Sept. 13-15, at the Marriott Inner Harbor Hotel, Baltimore. World-renowned experts will discuss clinical problems in diagnostic ultrasound. Participants will have the opportunity to ask questions and discuss general concerns. An exhibit area will be available where participants can test the latest ultrasonic equipment. Category 1 credit: 16.5 hr. Fee (3 days/2 days/1 day): physicians, \$400/\$300/\$150; sonographers, nurses, and allied health professionals, \$300/\$225/\$125. Information: Program Coordinator, The Johns Hopkins Medical Institutions, Office of Continuing Education, Turner Bldg., 720 Rutland Ave., Baltimore, MD 21205; (301) 955-2959.

Diagnostic Uses of Radiolabeled Monoclonal Antibodies

The American College of Nuclear Physicians and the U. S. Dept. of Energy, Office of Health and Environmental Research, Office of Energy Research, are sponsoring Diagnostic Uses of Radiolabeled Monoclonal Antibodies, Sept. 26-27, at the Loews L'Enfant Plaza Hotel, Washington, DC. This will be the fifth symposium in the six-part series Frontiers in Nuclear Medicine. The emphasis will be on use of monoclonal antibodies for detection of cancer and on nononcologic applications, including myocardial infarction and thrombus imaging. Program chair: Michael K. Haseman. Information: American College of Nuclear Physicians, 1101 Connecticut Ave., N.W., Ste. 700, Washington, DC 20036; (202) 857-1135.

Annual International Body Imaging Congress

The 16th annual International Body Imaging Congress will be held Oct. 5-12 at the Grand Hyatt Wailea, Maui, HI. Presentations will include topics in CT, sonography, MR, interventional radiology, and correlative techniques. A special section on breast imaging will be part of the program. Program director: Ronald J. Friedman. Guest faculty: W. D. Boswell, J. Crues, D. Hahn, V. Jackson, B. Jeffrey, L. Mack, M. L. Manco-Johnson, M. McSweeney-Kossoff, G. Kossoff, P. Ralls, J. Simon, P. F. G. M. van Waes, and J. Weinreb. Category 1 credit will be awarded. Fee (through June 30/after June 30): physicians, \$525/\$560; residents, interns, technologists, and nurses, \$425/\$460 (letter required). Information: Annual Body Imaging Congress, c/o Medical Seminars International, Inc., 18981 Ventura Blvd., Ste. 303, Tarzana, CA 91356; telephone: (818) 774-9077; fax: (818) 774-0244.

Neuroradiology Update: Emphasis on MRI

The Dept. of Radiology, University of Alabama at Birmingham, will offer Neuroradiology Update: Emphasis on MRI, Oct. 7-11, at the Westin Hotel, Hilton Head, SC. The course is designed to highlight the most clinically useful and practical applications of new developments in neuroradiology, with emphasis on MR imaging. The program will include a review of fundamentals of MR physics and MR contrast

agents, selected brain and spinal cord topics, and an update on the status of cerebrovascular Doppler imaging and MR angiography. Program director: Taher El Gammal. Information: Dawne Ryals, Ryals and Associates, P. O. Box 1925, Roswell, GA 30077-1925; telephone: (404) 641-9773; fax: (404) 552-9859.

Western Neuroradiological Society Annual Meeting

The Western Neuroradiological Society will hold its annual meeting Oct. 17-20 at the Ritz-Carlton Resort Hotel, Laguna Niguel, CA. The meeting will include detailed presentations on new developments and basic concepts in neuroradiologic imaging and intervention. Program director: Joachim F. Seeger. Information: Dawne Ryals, Ryals and Associates, P. O. Box 1925, Roswell, GA 30077-1925; telephone: (404) 641-9773; fax: (404) 552-9859.

Progress in Magnetic Resonance Imaging

The European Workshop on Magnetic Resonance in Medicine, European Magnetic Resonance Forum, will present Progress in Magnetic Resonance Imaging, Oct. 24-25, at the Hotel Maritim, Cologne, Germany. Program chairmen: Robert N. Muller and Peter A. Rinck. Guest faculty: B. Bongartz, G. M. Bydder, S. Felber, D. H. W. Grönemeyer, W. Kaiser, G. P. Krestin, D. B. Longmore, P. Lukas, R. N. Muller, J. M. Pennock, R. G. Ramsey, M. Reiser, P. A. Rinck, R. M. Seibel, D. D. Stark, F. Wehrli, and I. Young. Deadline for registration is Aug. 14. Category 1 credit is pending. Fee: DM 550. Information: European Magnetic Resonance Forum, P. O. Box 161, CH 1807 Blonay, Switzerland; telephone: +41-21-943 3834; fax: +41-21-943 3593.

Neuroradiologic and Musculoskeletal Seminars

The Depts. of Radiology, The Tampa General Hospital and the University of South Florida College of Medicine, are sponsoring the 9th annual Advanced Neuroradiology Seminar and the 1st annual Seminar on Musculoskeletal MRI, Oct. 24-27, at the Hyatt Regency Grand Cypress Resort, Orlando, FL. The neuroradiology seminar (Oct. 24-26) will emphasize recent advances in MR imaging, interventional neuroradiology, positron emission tomography, CT, new surgical techniques, and stereotactic radiosurgery. The musculoskeletal seminar (Oct. 26-27) will discuss spinal imaging and interventions; MR imaging of soft-tissue and bone neoplasms; and MR imaging of the knee, ankle, foot, shoulder, and wrist. These will be nonprofit meetings. The proceeds will go to the Radiology Resident Fund at The Tampa General Hospital. The fund is used as needed for medical books, slides, videos, visiting professors, and so forth. Program directors: Charles H. Fisher and Carlos R. Martinez. Guest faculty: G. Duckwiler, E. Eikman, R. M. Quencer, J. S. Ross, G. Sze, and M. B. Zlatkin. Category 1 credit: 22 hr. Fee: entire course: physicians, \$495; residents and fellows, \$400; neuroradiology seminar only, \$395; musculoskeletal seminar only, \$295. Information: Agnes Bridges, Radiological Services, The Tampa General Hospital, P. O. Box 1289, Tampa, FL 33601; (813) 251-7778.

Advanced Imaging of the Musculoskeletal System

The Dept. of Radiology, University of California, San Diego School of Medicine, will present Advanced Imaging of the Musculoskeletal System, Oct. 26-27, at the Hotel Del Coronado, Coronado (San Diego), CA. The course will review the basics of MR imaging and will address newer MR applications available for imaging the musculo-

skeletal system. Program director: Sevil Kursunoglu-Brahme. Fee: physicians, \$225; residents, fellows, and technologists, \$150. Information: Dawne Ryals, Ryals and Associates, P. O. Box 1925, Roswell, GA 30077-1925; telephone (404) 641-9773; fax: (404) 552-9859.

San Diego Postgraduate Radiology Course

The Dept. of Radiology, University of California, San Diego School of Medicine, will present the 16th annual San Diego Postgraduate Radiology Course, Oct. 28-Nov. 1, at the Hotel Del Coronado, Coronado (San Diego), CA. The faculty will discuss current concepts and recent advances in diagnostic radiology. Program director: David S. Feigin. Fee: physicians, \$550; residents, fellows, and technologists, \$375. Information: Dawne Ryals, Ryals and Associates, P. O. Box 1925, Roswell, GA 30077-1925; telephone (404) 641-9773; fax: (404) 552-9859.

International Symposium on Recent Advances in Diagnostic Imaging and Radiation Oncology

Baylor College of Medicine, Houston, TX, and the Institute of Medicine, Tribhuvan University, Kathmandu, Nepal, are cosponsoring International Symposium on Recent Advances in Diagnostic Imaging and Radiation Oncology, March 24-27, 1992, at Kathmandu, Nepal. The principal goal of the symposium is to review and update the latest principles and techniques in (1) diagnostic imaging, including MR imaging, CT, sonography, and positron emission tomography, and (2) radiation oncology in combination with other techniques. Program directors: Naresh Prasad and Gopal P. Acharya. Category 1 credit: 21 hr. Fee: \$250. Information: Dr. Naresh Prasad, Dept. of Radiology, Baylor College of Medicine, Houston, TX 77030; telephone: (713) 798-4415; fax: (713) 798-5556.

The American Board of Radiology Examinations

Written examinations for the American Board of Radiology (ABR) are scheduled for Oct. 3-4, 1991; Oct. 1-2, 1992; and Oct. 14-15, 1993. Oral examinations will be held at the Executive West Hotel in Louisville, KY, June 3-7, 1991; June 1-5, 1992; and May 31-June 4, 1993. The ABR will accept applications for admission to the examinations after July 1, but not later than Sept. 30, in the year preceding the year in which the examination is to be taken. For application forms and further information: Office of the Secretary, The American Board of Radiology, 300 Park, Ste. 440, Birmingham, MI 48009.

Meeting and Course Review

For the reader's convenience, a summary of upcoming meetings and courses is provided. Detailed listings are given in the AJR issue given in parentheses.

Cyanoacrylate Embolization Course, times arranged, Baltimore (July 1991)

Visiting Fellowships in International Radiology, times arranged, Baltimore (Oct 1991)

Swallowing Center Preceptorship, times arranged, Baltimore (Jan) **Imaging Fellowship**, times arranged, Miami Beach, FL (Jan)

MR Imaging Fellowships at LAC/USC Imaging Science Center, June 3-7, Aug. 5-9, Sept. 16-20, Oct. 7-11, and Nov. 4-8, Los Angeles (Feb)

- American College of Cryosurgery Annual Meeting**, June 6–10, La Jolla, CA (March)
- MRI Fellowships at Johns Hopkins**, June 17–21, Baltimore (Oct 1990)
- Contemporary Medical Imaging VIII**, June 19–23, Destin, FL (Feb)
- Advanced Techniques in MRI**, June 22–28, Kiawah Island, SC (March)
- Leeds Gastroenterology Course for Radiologists**, July 1–5, Leeds, England (Dec 1990)
- International Congress of Radiation Research**, July 7–12, Toronto (May 1990)
- Neuroradiology in the Rockies**, July 7–12, Snowmass at Aspen, CO (Feb)
- Mackinac Island Imaging Conference**, July 8–11, Mackinac Island, MI (May)
- Mammography and the Search for Breast Cancer**, July 12–13, Rochester, NY (April)
- Alaska 91—Cruise the Inland Passage—Magnetic Resonance Imaging at Sea**, July 14–21 (April)
- Advances in Gastroenterology**, July 15–19, Coronado (San Diego), CA (March)
- Radiology for the Non-Radiologist**, July 18–21, Coronado (San Diego), CA (March)
- Evaluation & Treatment of the Injured Athlete**, July 22–26, Chatham (Cape Cod), MA (May)
- Issues in Musculoskeletal Imaging and Magnetic Resonance Imaging**, July 22–27, Laguna Niguel, CA (March)
- Contemporary Diagnostic Imaging**, July 29–Aug. 2, Aspen, CO (April)
- Pittsburgh Breast Imaging Seminar**, Aug. 1–4, Pittsburgh (May)
- Body Imaging**, Aug. 5–9, Santa Fe, NM (April)
- Imaging of the Head, Spine, and Musculoskeletal System**, Aug. 12–16, Whistler, B.C. (April)
- Radiology for Clinicians**, Aug. 12–16, Coronado (San Diego), CA (April)
- Society of Computed Body Tomography Summer Practicum**, Aug. 18–22, Keystone, CO (April)
- Diagnostic Imaging Update**, Aug. 26–30, Vancouver, B.C. (April)
- Radiation, Physics, and Biology**, Aug. 26–30, New York City (May)
- World Congress in Ultrasound**, Sept. 1–6, Copenhagen (Sept 1990)
- International Workshop on Hypertrophic Osteoarthropathy**, Sept. 8–11, Dubrovnik, Yugoslavia (Jan)
- European Society of Gastrointestinal Radiologists Annual Meeting**, Sept. 8–11, Oxford, England (March)
- Sonography Update Conference and Exhibit**, Sept. 11–13, Coronado (San Diego), CA (May)
- Mallinckrodt Institute's 60th Anniversary Celebration**, Sept. 12–14, St. Louis (May)
- Transrectal Ultrasound in the Diagnosis and Management of Prostate Cancer**, Sept. 13–14, Chicago (May)
- Sonography Registry Review**, Sept. 14–15, Coronado (San Diego), CA (May)
- European Congress of Radiology 1991**, Sept. 15–20, Vienna, Austria (Oct 1990)
- Mammographic Interpretation: A Practical Approach**, Sept. 23–26 and Oct. 28–31, Boston (March)
- Applied Ultrasound: Accent on Doppler**, Sept. 23–26, Laguna Niguel, CA (May)
- Diagnosis of Musculoskeletal Disorders**, Sept. 25–28, Coronado (San Diego), CA (May)
- Diagnosis and Treatment of Bone and Soft-Tissue Tumors**, Nov. 21–23, Sacramento, CA (May)

AJR carries announcements of courses, symposia, and meetings of interest to its readers if received a minimum of 5 months before the event. There is no charge; receipt of items by the AJR Editorial Office is not acknowledged. Submit items for publication typed double-spaced. Provide title, date, location, brief description, sponsor, course directors, fees, category I credit, and address and telephone number for additional information. Faculty from the host institution will not be listed. Guest faculty names will appear **only** if initials are provided. Mail news items to AJR Editorial Office, 2223 Avenida de la Playa, Suite 103, La Jolla, CA 92037-3218.

American Roentgen Ray Society 92nd Annual Meeting

May 10-15, 1992, Orlando, FL

Marriott's Orlando World Center

Registration and Hotel Reservations

Forms for advance registration and hotel reservations will be in the February and March 1992 issues of the *AJR*.

Scientific Program

Abstracts of papers to be considered for the program must be submitted by November 1, 1991. Forms on which to submit abstracts are in this issue of the *AJR*. The ARRS Program Committee will select papers and notify authors in early January. The *AJR* has first rights to all papers accepted for presentation at the ARRS meeting. Mail original and five copies to

ARRS President-Elect
c/o Paul R. Fullager
American Roentgen Ray Society
1891 Preston White Dr.
Reston, VA 22091

Scientific Exhibits

Proposals for scientific exhibits must reach the Chairman of Exhibits by November 1, 1991. Forms, which may be photocopied, are in this issue of the *AJR*. Send completed form to

N. Reed Dunnick, M.D.
c/o Paul Fullager
American Roentgen Ray Society
1891 Preston White Drive
Reston, VA 22091
Telephone (703) 648-8992

Refresher Course Program

A summary of the refresher courses will appear in the *AJR* in February along with advance registration forms. Early registration is an advantage in ensuring preferred courses in this popular program.

Local Program

A program of sightseeing, shopping, and entertainment will be developed by the Local Arrangements Chairman. Information and advance registration forms will be in the February issue of the *AJR*.

Residents' Award Papers

The society offers several cash awards for the best scientific papers prepared by residents in radiology. The President's Award has a \$2000 prize. There are two Executive Council awards of \$1000 each. All are presented at the annual meeting. Papers should be submitted by February 15, 1992, for consideration in this competition. Send entries to

Nancy O. Whitley, M.D.
Dept. of Radiology
University of Maryland Medical Systems Hospital
22 S. Greene St.
Baltimore, MD 21201

Deadlines

Abstracts of papers: November 1, 1991
Scientific exhibit proposals: November 1, 1991
Residents' Award papers: February 14, 1992

Call for Papers

American Roentgen Ray Society 1992 Annual Meeting: May 10-15, 1992, Orlando, FL

ADDRESS OF PRESENTING AUTHOR

Department _____

Institution _____

Street _____

City, State _____ Zip _____

Phone: _____

Type title, authors, and abstract in the space provided below. (Instructions are on reverse side of this page. Abstract should not exceed 300 words.)

Select one category: Angio/Interventional Breast Chest CT Gastrointestinal Tract Genitourinary Tract
MR Neuroradiology Skeletal Sonography

Projection Requirements: 35 mm, single or double (circle one) 16 mm silent film 1/2" VHS 3/4"

Has this been presented elsewhere? yes no. If yes, please describe on reverse side of this page.

Instructions for Scientific Abstracts

1. Type the information single-spaced. Underline the name of the presenting author. Append as a last line of the abstract any research grant support, if applicable (e.g., Supported by USPHS Grant HE-80144). If the abstract is accepted, it will not be proofread; it will appear exactly as typed. Use the following format:

MR IMAGING OF THE SPINE AND NECK
F. S. Lau, M.D., A. N. Kirk, M.D., and R. A. Beck, Ph.D.
University of California, Bakersfield, Bakersfield, CA 92338

2. Abstracts should include four paragraphs devoted sequentially to the following topics: (1) object or purpose of the study, (2) materials, methods, and procedures, (3) results, (4) significance of the results and conclusions. The text should not exceed 300 words. Specific data are essential. The abstract should be a succinct summary of work done rather than a promissory note.
3. The Program Committee will grade each abstract and determine acceptance. Further information will be forwarded to those whose abstracts are accepted for presentation.

Deadline for submission of abstract is November 1, 1991. Mail abstract and four copies to

ARRS President-Elect
c/o Paul R. Fullagar
American Roentgen Ray Society
1891 Preston White Dr.
Reston, VA 22091

Call for Scientific Exhibits

**American Roentgen Ray Society
1992 Annual Meeting:
May 10-15, 1992, Orlando, FL**

FOR COMMITTEE USE ONLY

Date Received _____ Application No. _____
Subject _____ Score _____
Rejected _____ Accepted _____
Assigned _____ Space No. _____

Principal Exhibitor's Mailing Address

Name _____ Institution _____

Department _____ Street Address _____ City _____

State _____ Zip Code _____ Telephone: office (_____) home (_____)

Names of Exhibitors (List principal exhibitor first and telephone number of each person.)

Last	First	Middle	Telephone	Degree (one only)	Member ARRS?
------	-------	--------	-----------	----------------------	--------------

Title of Exhibit

Type abstract single-spaced in the space provided below. (See instructions on the reverse side of this page.)

Instructions for Abstract

The abstract should be a brief paragraph that states the purpose, principal information, and conclusions of the exhibit. Promissory statements are not acceptable. Type single-spaced in the space provided on the reverse side. Brevity is desirable but not at the expense of specific information. **The abstract will appear in the program book as submitted.** Please use typewriter and complete the application form on both sides. List space requirements.

What Type of Exhibit Is Proposed? (Check one and fill in all appropriate blanks.)

- Free-standing.** This is a self-contained display created in total by the exhibitor. It may be a fold-open unit, a unit shipped in cases and assembled on site, or a tabletop unit. Linear feet required _____.
- Poster Board (backboard panels).** Backboard panels are 4 × 8 ft. (1.2 × 2.5 m). Number of panels required _____. If two panels are needed, there will be a ¼-in. frame separating the panels, thus requiring a separation in the presentation.
- Viewbox.** Mounted materials (radiographs and other transparencies) for display on the society's illuminators. Each illuminator is 39.5 × 59.5 in. (100 × 151 cm). Number of illuminators required _____. Materials should not be glass mounted.

Please Indicate Most Appropriate Category.

Bone Cardiovascular Chest Gastrointestinal Genitourinary Breast Medical physics
 Neuroradiology Nuclear medicine Pediatric Radiation oncology Sonography

Exhibits will be chosen on the basis of the quality of the abstract and space available. Poster board exhibits are encouraged, as they do not require a viewbox or electricity.

Signature of Principal Exhibitor _____

Exhibitors will receive instructions for exhibit preparation.

Applications must be received no later than November 1, 1991. Mail original and five copies to

N. Reed Dunnick, M.D.
c/o Paul R. Fullagar
American Roentgen Ray Society
1891 Preston White Dr.
Reston, VA 22091
Telephone: (703) 648-8992

Classified Advertisements

Positions Available

LOCUMS TENENS—Earn top dollar. Don't work for an agency. Work for yourself. For details, send name and address to Dr. Monroe, 7035 Hwy. 6 South, Ste. R 175, Houston, TX 77083. 6ap

PEDIATRIC RADIOLOGIST—The Massachusetts General Hospital, Dept. of Radiology, is recruiting a radiologist to join the Division of Pediatric Radiology. Qualifications include board certification in diagnostic radiology and completion of at least 1 yr in pediatric radiology fellowship. Responsibilities include clinical, teaching, and research activities. The applicant must be versed in the imaging of children including CT, MRI, ultrasound, fluoroscopy, and plain film interpretation. ECFMG requirements must be fulfilled in order to be eligible for this position. Send a current CV and letter of inquiry to Johan G. Blickman, M.D., Division of Pediatric Radiology, Massachusetts General Hospital, Boston, MA 02114. The Massachusetts General Hospital is an equal opportunity employer/affirmative action employer. 6ap

LOCUM TENENS, 1 YR—I will be taking a yr of sabbatical and need a BC/BE radiologist to cover my hospital practice in a northern California summer and winter recreational area. Practice includes routine radiography, CT, ultrasound, mammography, and nuclear medicine. Please reply to Box M32, AJR (see address this section). 6-7ap

RADIOLOGIST/NUCLEAR MEDICINE—A 25-person radiology group in central New Jersey seeks a board-certified radiologist with additional nuclear medicine boards or ABR special competency to share responsibilities in nuclear medicine and some general radiology. Cardiac, nuclear, and SPECT experience required. Practice includes 2 450-bed hospitals, 3 offices, a radiology residency, and medical student teaching. Send CV to Richard Feinstein, M.D., c/o Kathy McGrath, Radiology Group of New Brunswick, 230 Old Bridge Tpk., South River, NJ 08882. 6-7a

APPLICATIONS ARE BEING ACCEPTED for the position of GI/general radiologist, Dept. of Diagnostic Radiology, Oregon Health Sciences University, Portland, OR. Faculty position opens on or about July 1, 1991. Minimum of 5 yr experience and board certification required. Send CV to William Weidner, M.D., Diagnostic Radiology, UHN 72, Oregon Health Sciences University, Portland, OR 97201-3098; (503) 494-4498. OHSU is an affirmative action, equal opportunity employer. 6a

PHYSICIAN/RADIOLOGIST—Full-time opening for board-certified radiologist in a desirable southern New Jersey shore location. This is an active, challenging, expanding hospital- and office-based practice. Must have training in CT, ultrasound, and MRI. Send CV to RABC, P.O. Box 729, Mt. Holly, NJ 08060. 6-8ap

DIAGNOSTIC RADIOLOGIST—Position for a board-certified radiologist to provide sole coverage for a 27-bed hospital in a southeast Idaho community of 20,000. Immediate potential for a \$220,000 practice while still having time to enjoy geographical amenities. Contract available. Please call or write Randall G. Holom, 1224 8th St., Rupert, ID 83350; (208) 436-0481. 6-8a

RADIATION ONCOLOGIST—A 320-bed community hospital is looking for a board-certified/eligible radiation oncologist to help open a new dept. Hospital-based practice. We are located in Englewood, CO, a south suburb of Denver. Interested applicants should send CV to Physician Services, 501 E. Hampden Ave., P.O. Box 2901, Englewood, CO 80150-0101. 6a

RADIOLOGIST/ANGIOGRAPHER—There is an opportunity to join a progressive group of 11 board-certified radiologists practicing at the Lehigh Valley Hospital Center, a 500-bed, university-affiliated hospital. The position requires angiographic/interventional skills and an interest in general radiology including CT and ultrasound. The radiology dept. has state-of-the-art equipment including 2 angiographic suites, 3 CT scanners, color flow Doppler, and MRI. The hospital is an acute-care facility and a state-designated Level 1 Trauma Center, located 1 hr from Philadelphia and 1½ hr from New York. The radiology dept. offers a postresidency fellowship program that includes training in angiography. The position offers a competitive salary and benefit package that leads to full partnership. For further information, contact Robert Kricun, M.D., Dept. of Radiology, Lehigh Valley Hospital Center, P.O. Box 689, Allentown, PA 18105; (215) 776-8088. 6-8ap

ANGIOGRAPHY/INTERVENTIONAL RADIOLOGIST needed to join the staff at William Beaumont Hospital, a modern, major, tertiary-care, teaching medical center in southeastern Michigan with residency and fellowship programs in diagnostic radiology. The dept. is expanding its state-of-the-art facilities to accommodate increasing demands on patient care. Fellowship in angiography/interventional radiology is required. Past experience in academic institutions is desirable. Area offers 1 of the best educational and recreational facilities. Excellent compensation. Write to Jalil Farah, M.D., Chairman, Diagnostic Radiology, William Beaumont Hospital, 3601 W. 13 Mile Rd., Royal Oak, MI 48073. 6-8ap

RADIOLOGY SERVICE VACANCIES—The VA Medical Center, Long Beach, CA, is seeking academically oriented, board-certified radiologists for staff appointments. Positions available are head, CT/Ultrasound Section; head, Neuroradiology Section; and general radiology, including interventional procedures. The medical center is a tertiary-care facility affiliated with the College of Medicine, University of California, Irvine. A significant interest in research and demonstrated teaching experience is necessary. The successful candidates will qualify for academic appointment at the University of California, Irvine, College of Medicine. The VA is an equal opportunity employer. U.S. citizenship is required. All interested candidates should submit CV and names of 3 references to Malcolm D. Jones, M.D., Chief, Radiology Service (114), 5901 E. 7th St., Long Beach, CA 90822. 6a

BC/BE BREAST IMAGING RADIOLOGIST needed part/full-time to join 2 member group for outpatient women's diagnostic center. Mammography and OB/GYN sonography expertise required. Flexible hr/no call. Ideal for radiologist with family responsibilities or semiretired. Immediate availability. Contact Frankie Weir, Director, Women's Center for Radiology, 615 E. Princeton St., Ste. 101, Orlando, FL 32803; (407) 894-2466. 6-7ap

CHEST RADIOLOGIST, CLEVELAND CLINIC FOUNDATION—The Cleveland Clinic Foundation has an opening for a staff position in the Section of Thoracic Imaging. The foundation is a 1000-bed hospital with a large outpatient population and an international referral base. Successful applicants will be involved in all diagnostic modalities, including CT, MRI, and interventional procedures. A strong interest in teaching, research, and patient care is required. Applicants should be board-certified, fellowship-trained, or have equivalent experience. Excellent salary and benefit package. Send CV to Moulay A. Meziane, M.D., Head, Section of Thoracic Imaging, Cleveland Clinic Foundation, One Clinic Center Dr., Cleveland, OH 44195-5021. The Cleveland Clinic Foundation is an equal opportunity employer. 5-10ap

NUCLEAR MEDICINE—The UCLA Dept. of Radiological Sciences is seeking a board-certified radiologist in nuclear medicine and/or radiology at the assistant professor level with extensive experience in positron emission tomography and related imaging methods. Added experience in imaging processing and mathematical modeling is desirable. Send application, CV, and names and addresses of 3 references or inquiries to Hooshang Kangarloo, M.D., Chairman, Dept. of Radiological Sciences, UCLA Medical Center, Los Angeles, CA 90024-1721. An EO/A employer. 5-7a

CHIEF, RADIOLOGY SERVICE—The VA Medical Center, Long Beach, CA, is seeking an academically oriented, board-certified radiologist for the position of Chief, Radiology Service. The medical center is a tertiary-care medical center affiliated with the College of Medicine, University of California, Irvine. Candidates should have a strong background in clinical radiology, a significant record of research accomplishments, and should possess demonstrated teaching and management skills. The successful candidate will qualify for academic appointment at the University of California, Irvine College of Medicine. The VA is an equal opportunity employer. U.S. citizenship is required. All interested candidates should submit a CV and the names of 3 references to David Webb, M.D., Acting Chief of Staff, VA Medical Center, 5901 E. 7th St., Long Beach, CA 90822. 5-6a

SUPERB PARTNERSHIP POSITION IN LAS VEGAS, NV—Rapidly expanding, 7-member group practice covering 2 full-service imaging centers and a small hospital has an immediate opening. We are looking for an additional board-certified radiologist with an uncommon dedication to excellence in patient care. Our outpatient facilities include 2 MR, 2 CT, angi with a 4-bed recovery area, 5 ultrasound, 5 mammography, 2 SPECT, plus R & F. This is an excellent opportunity for a partnership position with a well-respected group in a growing community. Please send CV to Dr. Mark Winkler, SDMI, 2950 S. Maryland Pkwy., Las Vegas, NV 89109. 5-10a

NEURORADIOLOGIST—Join the current staff of 2 neuroradiologists at William Beaumont Hospital, a modern, tertiary-care medical center in southeastern Michigan with residency and fellowship programs in diagnostic radiology. The dept. is expanding its state-of-the-art facilities to accommodate increasing demands on patient care. Area offers 1 of the best educational and recreational facilities. Excellent compensation. Write to Jalil Farah, M.D., Chairman, Diagnostic Radiology, William Beaumont Hospital, 3601 W. 13 Mile Rd., Royal Oak, MI 48073. 5-7a

DIRECTOR OF NEURORADIOLOGY—Position available for Director of Neuroradiology in 700-bed, university-affiliated teaching hospital with fully approved residency program. Modern equipment includes digital subtraction angiography, 2 CT, and 1 MRI. Staff of 12 full-time radiologists. Excellent salary and fringe package. Send CV to David Bryk, M.D., Maimonides Radiology Associates, P.C., 4802 Tenth Ave., Brooklyn, NY 11219. 5-7ap

DIAGNOSTIC RADIOLOGIST, EL PASO, TX—BE/BC radiologist with special competence in body imaging sought to join busy hospital radiology practice at a community medical center with a total of 330 beds. Modern imaging dept. with 1.5-T GE MR, CT, nuclear medicine with SPECT, ultrasound, angiography with DSA, mammography, and diagnostic radiography. Excellent salary, vacation, and benefits leading to early partnership. Send inquiries with CV to Roy K. Poth, M.D., 1625 Medical Center Dr., El Paso, TX 79902. 5-8ap

BC/BE RADIOLOGIST, SOUTHEASTERN MICHIGAN—Seven radiologists covering a 350-bed community hospital with a new women's center seek a radiologist with a fellowship in ultrasound and special interest in OB ultrasound. Practice involves all aspects of imaging modalities including MRI. Competitive compensation package leading to partnership. Send inquiries and a CV with references to Bhaskar U. Shenai, M.D., Professional X-Ray Center, 67 Cass Ave., Mt. Clemens, MI 48043. 5-7ap

DIAGNOSTIC RADIOLOGIST / PARTNERSHIP POTENTIAL—Well-established, multioffice practice offers an outstanding opportunity for growth to a BC/BE radiologist. Procedures include standard radiography and fluoroscopy, mammography, nuclear medicine, and ultrasound. IVF-associated procedures are a key specialty. Large referral base. Physician has 25+ yr experience and needs to share the burden of a still-expanding practice. Collateral earnings potential by reading for other medical groups with imaging capability. We are located in the Boston area near major roadways; you can live in any of Boston's beautiful suburbs. First-class equipment and excellent technologists will support your efforts. Please send your current CV and a cover letter to Box L21, AJR (see address this section). 5-7ap

DIAGNOSTIC RADIOLOGIST with skills in CT, MR, interventional, ultrasound, and nuclear medicine needed to join group of 8 board-certified radiologists. Growing practice in eastern Washington at a 228-bed hospital, a new multimodality imaging center, and 2 private offices. Potential for long-term practice is excellent. Top-notch school system, including 3 first-rate universities. Excellent hunting, fishing, boating, and skiing. Contact L. E. Crecelius, M.D., N. 5901 Lidgerwood, Ste. 18B, Spokane, WA 99207; (509) 482-2385. 5-10ap

DENVER, CO—The University of Colorado Health Sciences Center, Dept. of Radiology, Denver, CO, is continuing its expansion and is recruiting for full-time academic faculty positions in skeletal radiology, chest radiology, mammography, and general radiology. The level of faculty appointment will depend on the applicant's previous relevant experience. Applicants should demonstrate devotion to patient care, dedication to teaching, and interest in independent or collaborative research. Candidates interested in working in a stimulating academic and exciting clinical environment are encouraged to send their CV to Michael L. Manco-Johnson, M.D., Professor and Chairman, Dept. of Radiology, Box C277, University of Colorado Health Sciences Center, 4200 E. 9th Ave., Denver, CO 80262; (303) 270-7719. The University of Colorado Health Sciences Center is committed to equal opportunity and affirmative action. 5-6a

IMMEDIATE OPENING—BC diagnostic radiologist, imaging fellowship preferred, with experience in general radiology and expertise in interventional procedures and angiography, sought to join a group of 4 active, university-trained radiologists. Modern, 220-bed hospital in south suburb of Chicago with active ER and outpatient services. State-of-the-art equipment includes MRI, CT, ultrasound, nuclear medicine, and mammography. Attractive and competitive benefits package leading to early partnership. Contact John M. Nayden, M.D., South Suburban Hospital, 17800 S. Kedzie Ave., Hazel Crest, IL 60429; (708) 799-8010, ext. 3276. 5-7ap

LOCUMS NATIONWIDE—BC or BE diagnostic radiologists needed for nationwide locums. Opportunities range from 1 wk to several mo. Exceptional compensation and all travel expenses. Call Professional Temporary Services, Inc., 790 Cardinal Rd., P.O. Box 2702, New Bern, NC 28561; (800) 872-4534. 5-8a

MAMMOGRAPHY, UNIVERSITY OF PENNSYLVANIA, HALF- OR FULL-TIME POSITION

Exceptional opportunity in academic mammography within a high-volume, rapidly expanding, breast imaging section. Ongoing screening and problem-solving mammography, breast ultrasound, and collaborative projects. Academic rank and salary commensurate with credentials. Resident and student teaching responsibilities along with negotiable participation in bone and chest outpatient radiology. Position available immediately. Applicant must be ABR-certified and able to obtain license in Pennsylvania. U of P is an affirmative action, equal opportunity employer, and specifically encourages applications from women and minorities. Send letter and CV to Rosalind H. Troupin, M.D., Dept. of Radiology, H.U.P., 3400 Spruce St., Philadelphia, PA 19104. 5-7ap

DIAGNOSTIC RADIOLOGIST — BC/BE with expertise in general radiology including CT and ultrasound sought for 85-physician, multispecialty group practice in southern California community. Close to the ocean, with easy access to city and recreational areas, and excellent schools. Contact David B. Luce, M.D., Medical Director, Bay Shores Medical Group, Inc., 3625 Del Amo Blvd., Ste. #270, Torrance, CA 90503; (213) 371-6551. 5-6a

NEURORADIOLOGIST—The University of Louisville, Dept. of Diagnostic Radiology, is seeking a BC/BE diagnostic radiologist to fill a full-time faculty position as chief of neuroradiology. The candidate must have had additional training in neuroradiology and be willing to participate in undergraduate and graduate teaching and in research activities. This is a fine opportunity in a growing and busy dept. with excellent equipment. Tenure- and non-tenure-track appointments available; academic rank commensurate with training and experience; and compensation negotiable and competitive. Send inquiries with CV and 3 references to Hollis A. Thomas, M.D., Professor and Chairman, Dept. of Diagnostic Radiology, Humana Hospital-University of Louisville, 530 S. Jackson St., Louisville, KY 40202. The University of Louisville is an equal opportunity/affirmative action employer and encourages women and minority candidates to apply. 5-6ap

BROAD SPECTRUM RADIOLOGIST/UPSTATE NEW YORK — Radiologist wanted for hospital-based practice 90 mi. northwest of New York City. Excellent recreational activities and easy access to metropolis. All modalities available. Excellent salary and benefits leading to early partnership. Immediate availability, but can wait for right applicant. Call G. Bilick; (914) 794-3300, ext. 2216 or send CV to P.O. Box 144, Harris, NY 12742. 3-6ap

THE DEPT. OF RADIOLOGY AT TRIPLEX ARMY MEDICAL CENTER, HONOLULU, HI, is recruiting academic radiologists for several divisions of the dept. including ultrasound, chest, skeletal, neuro, and general diagnostic radiology. Our dept. offers a fully accredited residency program with 20 residents and 16 attending full-time staff. Numerous consultants from across the country lecture on a continuing and regular basis. The hospital is a modern, tertiary-care center serving Hawaii and the entire Pacific Basin. A strong residency program, diverse and interesting patient population, excellent equipment, and a tropical lifestyle are positive aspects of the practice. Academic credentials and/or experience are necessary. Recently graduated fellows are encouraged to apply. Board certification is mandatory. Candidates should be particularly interested in patient care, teaching, and research. Salary and benefits are competitive and generous. Tripler is an EO/EEO employer. Please contact Mark F. Hansen, M.D., Col., MC, Chief, Dept. of Radiology, TAMC, HI 96859-5000; (808) 433-6393. 8-7a

DIAGNOSTIC RADIOLOGIST—Immediate opening leading to partnership in expanding, 4-member, hospital-based practice near Boston. Seeking recently trained BC/BE radiologist with skills and experience in general radiology, ultrasound, mammography, CT, and angio/interventional. Interested persons should contact Steven Sitzman, M.D., The Malden Hospital, One Hospital Rd., Malden, MA 02148; (617) 322-7560. 5-7ap

THE UNIVERSITY OF MASSACHUSETTS MEDICAL CENTER, a tertiary-care hospital situated 40 mi. from Boston, is seeking a third pediatric radiologist. The pediatric dept. services central and eastern Massachusetts as well as southern New Hampshire and northern Connecticut. All medical and surgical pediatric subspecialties are represented and a broad range of pediatric pathology is encountered. Pediatric radiologists have the primary responsibility in ultrasound, CT, MRI, and interventional procedures in general radiologic exams. Competitive salaries and generous benefits are provided. For further information, contact Paul K. Kleinman, M.D., Dept. of Radiology, University of Massachusetts Medical Center, 55 Lake Ave., N., Worcester, MA 01655; (508) 856-3124, fax (508) 856-4669. 6xa

PRACTICE OPPORTUNITY IN FAST-GROWING LAS VEGAS, NV—Expanding, 6-member radiology group is seeking 2 additional BE/BC radiologists for July 1991 and Jan. 1992. We currently serve 2 hospitals with an outpatient imaging center to open in Jan. 1992. Outstanding salary and benefits package leading to full partnership in 2 yr. Send CV or contact Marc Pomerantz, M.D., Head of Search Committee, 1925 Spode Ave., Henderson, NV 89014; (702) 388-4640. 5-9ap

POSITION AVAILABLE IN MIDATLANTIC SMALL TOWN WITH COUNTRY LIVING, progressive medical community, easy access to major metropolitan regions, and a university hospital. Unique, diverse, academically oriented MR, CT, and conventional radiology practice that leaves time for family, reflection, or other interests. Direct an independent CT facility, read MR images at same site, and read conventional radiographs nearby if desired. Night call minimal. Compensation flexible and negotiable. Share duties with 2 other physicians. Write Box L25, AJR (see address this section). 5-6ap

BC/BE RADIOLOGIST—Full-time staff radiologist sought for active, tertiary-care medical center. Duties include interpreting general diagnostic films (excluding mammography), performing radiologic procedures and fluoroscopy, and supervising and training residents with affiliated medical center. Additional subspecialty skills or training in ultrasound/CT, and/or angiography and interventional procedures are beneficial. Candidate should be qualified to hold a faculty position with Yale University School of Medicine, and must be a U.S. citizen or qualify as a permanent resident of the United States. CV and letters of reference should be sent to Caroline Taylor, M.D., Chief, Radiology, Dept. of Veterans Affairs Medical Center, West Haven, CT 06516. The DVA Medical Center and Yale University are equal opportunity/affirmative action employers. Applications from women and minority group members are encouraged. Application deadline is Aug. 1, 1991. 5-7a

STAFF RADIOLOGIST—Miami Veterans Affairs Medical Center is seeking 1 full-time and 1 part-time staff radiologist for its teaching hospital affiliated with the University of Miami Medical School. Candidates must be board-eligible or certified. Interested physicians should send CV and list of references to Personnel Service (05C3/Jean Little), Veterans Affairs Medical Center, 1201 N.W. 16 St., Miami, FL 33125; (305) 324-4455, ext. 3617. Equal opportunity employer. 5-6a

IMAGING RADIOLOGIST—Join the current staff of 5 imaging radiologists (MR/CT/ultrasound) at William Beaumont Hospital, a modern, tertiary-care medical center in southeastern Michigan with residency and fellowship programs in diagnostic radiology. The dept. is expanding its state-of-the-art facilities to accommodate increasing demands on patient care. Area offers 1 of the best educational and recreational facilities. Excellent compensation. Write to Jalil Farah, M.D., Chairman, Diagnostic Radiology, William Beaumont Hospital, 3601 W. 13 Mile Rd., Royal Oak, MI 48073. 5-7a

FULL/PART-TIME BC/BE RADIOLOGIST wanted for 187-bed GM&S VA Medical Center. Excellent GE equipment, duplex Doppler ultrasound, diagnostic, and fluoroscopic. CT interpretation desirable. 18,000 procedures/yr. State university city amid hills and lakes in northwest Arkansas with cultural and recreational attractions. Competitive salary and excellent benefits/retirement. Call chief of staff; (501) 444-5050. 6xa

GOOD LIFE, GOOD MONEY—Radiologist needed for growing practice that covers 2 hospitals as well as 2 free-standing clinics. Modalities include R&F, general, mammography, CT, MRI, nuclear medicine, SPECT, and special procedures. Denton, population 60,000, located 30 mi. north of Dallas/Fort Worth, has 2 recreational lakes within 15 mi. and 2 major universities. Attractive financial and benefit packages with early partnership are offered. Contact Family Radiology with CV at 1614 Scripture, Ste. 2, Denton, TX 76201; (817) 387-6159. 5-6a

DIAGNOSTIC RADIOLOGIST—Due to the recent merger of residency programs with St. Luke's Hospital and Truman Medical Center, UMKC, School of Medicine, we are expanding the number of staff positions at the academic rank of assistant or associate professor level. The dept. currently performs 87,000 exams/yr. Strong teaching background required. Compensation commensurate with qualifications and experience. Send letter of interest and CV to Fong Tsai, M.D., Professor and Chairman, University of Missouri-Kansas City, Radiology Dept., 2301 Holmes, Kansas City, MO 64108. 4-6ap

DIAGNOSTIC RADIOLOGIST, IMMEDIATE OPENING—Ten-person radiology group seeks a diagnostic radiologist with fellowship training, including body MRI/body imaging, to join a busy, hospital-based practice located in rapidly growing north Dallas. GE 1.5-T magnet, Toshiba midfield magnet, 2 GE 9800 scanners, Acuson 128 with color flow Doppler, and new special procedures suite with DSA. Please send CV to Box K54, AJR (see address this section). 6xa

UTMB, GALVESTON, TX—The Dept. of Radiology of the University of Texas Medical Branch in Galveston has openings for persons trained and experienced in ultrasonography and mammography. The opportunity for academic advancement is great and benefits are generous. Salaries are competitive and living conditions are desirable. Interested persons should contact Melvyn H. Schreiber, M.D., Chairman, Dept. of Radiology, UTMB, Galveston, TX 77550; (409) 761-1823. UTMB is an equal opportunity M/F/H/V affirmative action employer. UTMB hires only individuals authorized to work in the United States. 4-9a

PEDIATRIC RADIOLOGIST—Division of Pediatric Radiology, OHSU, Portland, OR, invites applications for a faculty position available on or about July 1, 1991. Completion of approved fellowship in pediatric radiology and ABR certification required. Send CV to William Weidner, M.D., Diagnostic Radiology, UHN-72, Oregon Health Sciences University, Portland, OR 97201-3098; (503) 494-4498. Equal opportunity, affirmative action employer. 3-6a

RADIOLOGIST—Immediate opening for a qualified, board-certified/eligible radiologist to work in an outpatient imaging center located 40 mi. north of El Paso, TX. Must have knowledge of general radiology and experience with ultrasound, CT, and nuclear medicine. Interested doctors should send CV to Sun View Imaging Services, P.O. Box 8624, Las Cruces, NM 88006. 6-7ap

CHEST RADIOLOGIST, THOMAS JEFFERSON UNIVERSITY HOSPITAL—The Dept. of Radiology at Jefferson has an opening for a thoracic radiologist at either the junior or senior level. The position encompasses plain film radiography, CT, and percutaneous thoracic interventions. Involvement in mammography, other general diagnostic areas, and ultrasound can also be incorporated, depending on the interests of the candidate. Dedicated, nonclinical research time is provided, and the dept. has excellent research facilities and support. Our chest radiology practice is expanding rapidly and close working relationships are maintained with pulmonary medicine and thoracic surgery. Teaching is also emphasized, with a large residency program and a thoracic radiology fellowship. Excellent faculty income and benefits. This is a fine opportunity for a radiologist with academic interests to join a dynamic and rapidly growing dept. Interested candidates should contact David C. Levin, M.D., Chairman, Dept. of Radiology, Thomas Jefferson University Hospital, Philadelphia, PA 19107; (215) 955-7264. Jefferson is an equal opportunity/affirmative action employer. 4-6a

CHIEF OF DIAGNOSTIC RADIOLOGY—The Louis A. Weiss Memorial Hospital is a 275-bed, expanding affiliate of The University of Chicago that performs approximately 65,000 radiologic exams/yr. Applicants should have broad experience in general diagnostic radiology and administrative skills. An interest in teaching or research would be advantageous. The successful applicant will be appointed to the faculty at The University of Chicago. Academic rank and compensation commensurate with experience. Candidate should be board-certified and licensed to practice in Illinois. Interested parties should send their CVs to Heber MacMahon, M.D., Chairman, Weiss Search Committee, Dept. of Radiology, The University of Chicago, 5841 S. Maryland, Box 429, Chicago, IL 60637; (312) 702-1604, fax (312) 702-1161. Affirmative action/equal opportunity employer. 4-6ap

ANGIOGRAPHER/INTERVENTIONAL RADIOLOGIST, TOLEDO, OH—Quality-oriented, 22-radiologist group is seeking a board-certified, university-trained radiologist with angiography/interventional fellowship experience. Group covers 850-bed tertiary hospital, 350-bed suburban hospital, 3 outpatient offices, and performs 240,000 exams/yr. Position leads to equal partnership and combines excellent salary with very generous vacation time. All practice locations within 15 min of each other and are situated in an area of superb, family-oriented living with excellent schools. Send CV to Drs. David Parker or Keith Wilson, Roemer Bldg., 3912 Sunforest Ct., Toledo, OH 43623; (419) 471-4438 days. 4-6ap

DALLAS, TX—A 12-member, subspecialty group seeks a board-certified, general radiologist for an immediate opening. Fellowship training preferred, but will consider qualified individual with special expertise. CT/ultrasound, MRI, nuclear medicine, or angiography background particularly helpful. All imaging modalities available (state-of-the-art CT, angio, ultrasound, R & F, SPECT nuclear medicine, and MRI center). Salary and bonuses are excellent. Health and malpractice paid. No buy-in to partnership. Send CV to H. Stuart Peake, M.D., P.O. Box 814129, Dallas, TX 75381; (214) 888-7055. 4-9ap

RADIOLOGIST—The Elko Regional Medical Center seeks a board-certified/eligible diagnostic radiologist to work at the medical center as well as the local community hospital. CT, mammography, ultrasound, nuclear medicine, and some interventional training or experience required. Guaranteed salary for 6 mo leading to full partnership. Excellent benefit package including malpractice insurance. Elko is a thriving community surrounded by mountains and wilderness areas. Recreation yr round. Please send CV to Cherie Atwood, Administrator, Elko Regional Medical Center, 782 14th St., Elko, NV 89801; (702) 738-3111. 4-6ap

TEN-PERSON RADIOLOGY GROUP located in Corpus Christi is seeking a new associate to start July 1990 or as late as July 1991. Must be board-certified or eligible. Will perform all diagnostic studies, including interventional, CT, MRI, nuclear medicine, and ultrasound. Please send CV to Search Committee, P.O. Box 5608, Corpus Christi, TX 78465-5608. 6xa

RADIOLOGIST—Large, private-practice group in upstate New York seeks board-certified radiologist with general interests and preferably with fellowship training. Practice includes mix of private and teaching hospitals, offices, urban and rural settings. All modalities including 3 MRI units. This is an extremely high-quality practice offering excellent benefits and an opportunity for long-term security through shareholder status. Send CV to Box K50, AJR (see address this section). 4-6a

SENIOR FACULTY POSITION IN GI/GU RADIOLOGY—Dartmouth-Hitchcock Medical Center is seeking a senior faculty member at the associate or full professor level with experience and interest in GI/GU radiology. Clinical responsibility will be in an entirely new, 400-bed, clinical facility opening Sept. 1991, with state-of-the-art instrumentation. Position will involve responsibility for residency training in GI/GU area. Proven record of academic performance including research and teaching with an interest in providing academic guidance for energetic staff of younger radiologists necessary. Interested candidates write with CV to P. K. Spiegel, M.D., Chairman, Dept. of Diagnostic Radiology, Dartmouth-Hitchcock Medical Center, Hanover, NH 03756. AA/EOE. 6xa

IMMEDIATE OPENING FOR BC/BE GENERAL RADIOLOGIST with experience in interventional and vascular radiology. Join a group of 4 radiologists in a 160-bed hospital located in Allentown, PA, about 60 mi. northwest of Philadelphia. The daily practice includes all aspects of general radiology, CT, ultrasound, and nuclear medicine. Please call or send CV to Asad Shohadai, M.D., Allentown Osteopathic Medical Center, 1736 Hamilton St., Allentown, PA 18104; (215) 770-8700. 6xa

RADIOLOGISTS—A 4-member, rapidly growing practice in McAllen, TX needs 2 general, BC/BE radiologists. Hospital-based practice plus imaging center with 1.5-T GE MRI, 9800 GE CT, Sophy SPECT camera, color Doppler ultrasound, mammography, and fluoroscopy. Early partnership, excellent salary/opportunity. Contact William Martin, M.D.; (512) 682-0888. 4-6ap

DIRECTOR, DIAGNOSTIC RADIOLOGY—Applications accepted for Director, Diagnostic Radiology, OHSU, Portland, OR. Faculty position opens on or about July 1, 1991. Associate or full professor based on experience. Musculoskeletal radiology fellowship, minimum of 5 yr as Vice-Chairman or Director of Diagnostic Radiology required. Send CV to William Weidner, M.D., Diagnostic Radiology, UHN-72, Oregon Health Sciences University, Portland, OR 97201-3098; (503) 494-4498. Equal opportunity, affirmative action employer. 3-6a

MUSCULOSKELETAL RADIOLOGIST, MALLINCKRODT INSTITUTE OF RADIOLOGY/WASHINGTON UNIVERSITY—The musculoskeletal section is enlarging and has need for an additional person at the instructor, assistant professor, or associate professor level. The section performs all aspects of musculoskeletal imaging including CT, MRI, bone biopsy, and arthrography of all joints. The section also performs all diagnostic and screening mammography and breast procedures and directs emergency dept. radiology. The volume of clinical material is large. Teaching, academic, and working conditions are well-supported. Send CV to Louis A. Gilula, M.D., or William A. Murphy, M.D., Mallinckrodt Institute of Radiology, Barnes Hospital, 510 S. Kingshighway Blvd., St. Louis, MO 63110. 3-6a

RADIOLOGIST, CAPITOL DISTRICT, NEW YORK STATE—Well-established, hospital-based group practice in upstate New York seeks a board-certified, general diagnostic radiologist with special competence and interest in nuclear medicine and MRI. Angiography and interventional experience will be helpful. This will be an additional opening to a 5-person group currently performing all aspects of radiology. Salary first yr leading to full partnership. Please send CV to John J. Gorman, M.D., Dept. of Medical Imaging, St. Clare's Hospital, 600 McClellan St., Schenectady, NY 12304; (518) 382-2310. 4-7ap

HEAD, CROSS-SECTIONAL IMAGING SECTION
The Dept. of Radiology, University of Rochester Medical Center, Strong Memorial Hospital, Rochester, NY, is seeking a board-certified radiologist with subspecialty experience in body imaging for a faculty position as Head of Cross-Sectional Imaging Section, including ultrasound, CT, MRI, and body interventional. Strong Memorial Hospital is a 750-bed, tertiary-care hospital. State-of-the-art MRI, CT, and ultrasound equipment is available. Teaching of medical students, radiology residents, and fellows and the opportunity for developing research projects are afforded. Rank and salary are commensurate with experience. Interested candidates should forward CV to Robert E. O'Mara, M.D., Chair, Dept. of Radiology, Box 648, University of Rochester Medical Center, Rochester, NY 14642; (716) 275-2733. EO/AAM-F employer. 3-6ap

DIAGNOSTIC RADIOLOGIST needed in Conway Hospital, a community hospital located 10 mi. west of the resort/seaside community of Myrtle Beach, SC. The dept. performs 44,000 exams/yr including CT, MRI, nuclear medicine, ultrasound, mammography, and special procedures. All exams are done on state-of-the-art equipment. Our 3-person group offers a very strong financial package with all benefits including 17-wk vacation. Lovely, rapidly growing resort area includes 60 mi. of sandy beaches, 70 golf courses, and beautiful seaside homes. Contact Gary Rike, M.D., P.O. Box 917, Conway, SC 29526; (803) 347-7277. 6-8ap

NO-CALL RADIOLOGIST FOR SOUTHERN CALIFORNIA BEACHES—Position is now available with premier, 21-member group to help staff a growing number of outpatient facilities. Fellowship training in mammography/ultrasound is required. The group operates 5 Acuson imagers and 8 dedicated mammography units. Please send CV to Robert Hurwitz, M.D., 355 Placentia Ave., Ste. 207, Newport Beach, CA 92663. For faster reply, please call our dept. secretary, Denise, at (714) 645-9500. 4-6ap

BOSTON, IMMEDIATE OPENING—Radiologist wanted to join busy, well-established, private-practice group with 4 outpatient facilities. Expertise in ultrasound and mammography. No evening or weekend call. Excellent life-style, partnership opportunity. Send letter and CV to Box E49, AJR (see address this section). 6-11ap

FACULTY OPENING IN THORACIC IMAGING

The Johns Hopkins University Hospital has an opening at the junior faculty level in the Division of Thoracic Imaging. The division is fully integrated across all modalities including MRI, CT, and interventional procedures. Research opportunities are exceptional with protected research time available to rapidly establish an academic career. Academic rank and salaries will be determined by previous experience. The candidate must be board-certified. Contact Elias A. Zerhouni, M.D., Director, Thoracic Imaging & MRI Divisions, Dept. of Radiology, Johns Hopkins Hospital, Baltimore, MD 21205; (301) 955-4062. 1-6a

CROSS-SECTIONAL IMAGING/MRI, CT, ULTRASOUND

The Dept. of Radiology, Strong Memorial Hospital, University of Rochester, Rochester, NY, is seeking a board-eligible/certified radiologist for its body imaging section. An appointment as assistant professor or higher is available at a level appropriate to experience. One yr fellowship training or equivalent experience is required. Research and teaching opportunities are afforded in a strong academic dept. with state-of-the-art radiologic equipment. Send letter of inquiry to Robert E. O'Mara, M.D., Chair, Dept. of Radiology, Box 648, University of Rochester Medical Center, Rochester, NY 14642; (716) 275-2733. EO/AAM-F employer. 3-6ap

NEURORADIOLOGIST, BIG SKY COUNTRY

Group of 5 radiologists seek a BC, fellowship-trained colleague. Hospital and busy clinical practice. Must be a capable, general diagnostic radiologist. One yr to partnership. Send letter/CV to Bruce Pinkerton, M.D., Dept. of Diagnostic Radiology, Deaconess Medical Center, P.O. Box 2547, Billings, MT 59103. 2-7ap

DUKE UNIVERSITY MEDICAL CENTER/STAFF

RADIOLOGISTS—Duke University Medical Center is seeking qualified candidates for staff positions in the Dept. of Diagnostic Radiology. A limited number of staff positions currently are available in the following sections: general diagnostic, pediatric, chest, vascular/interventional, and musculoskeletal radiology. We offer an excellent salary and benefits package. The radiology dept. is state-of-the-art in diagnostic imaging with diverse resources available for clinical, teaching, and academic pursuits. Staff members have guaranteed academic time and research support. Interested board-certified radiologists with appropriate experience should phone Robert Vandemark, M.D. at (919) 681-2711 ext. 5233, for additional information. Letters of inquiry should be sent to Carl E. Ravin, M.D., Dept. of Radiology, Box 3808, Duke University Medical Center, Erwin Rd., Durham, NC 27710. AA/EOE. 2-7a

COME TO CALIFORNIA WITH A LICENSE

FROM ANY STATE—Loma Linda VA Hospital has a vacancy for a board-certified radiologist. A current license from any state is acceptable. Loma Linda is located 70 mi. east of Los Angeles near beaches, mountain ski resorts, and southland theme parks. This is a 500-bed, full-service hospital with a comprehensive diagnostic facility including ultrasound, CT, and MRI integrated with the Loma Linda University Medical Center residency training program. Opportunities exist to pursue clinical or academic interests. For additional information, contact Peter Dure-Smith, M.D., Chief, Radiology (114), Jerry L. Pettis Memorial Veterans Hospital, 11201 Benton St., Loma Linda, CA 92357; (714) 422-3069, fax (714) 422-4106. Equal opportunity employer. 3-8ap

SAN ANTONIO, TX—Group covering multiple hospitals and clinics seeks radiologists with imaging and angiography skills. Send CV to Search Committee, M & S X-Ray Associates, P.O. Box 15920, San Antonio, TX 78212-9510. 3-8ap

MAMMOGRAPHY FACULTY POSITION—The Dept. of Radiology at Johns Hopkins University Hospital has a faculty position available in mammography. The mammography section is part of the thoracic imaging division. The section offers a strong potential for academic growth with emphasis on original research and teaching. Protected academic time is available for candidates interested in developing a strong academic career. Support, resources, and opportunities are available for creative research. The candidate can also participate in all other aspects of diagnostic imaging as desired. Academic rank and salary will be determined by previous experience. Candidate must be board-certified. Contact Elias A. Zerhouni, M.D., Director, Thoracic Imaging and MRI Divisions, Dept. of Radiology, Johns Hopkins Hospital, Baltimore, MD 21205; (301) 955-4062. 1-6a

DIAGNOSTIC RADIOLOGIST—BC/BE radiologist wanted to join expanding practice of 12 radiologists in northeastern Pennsylvania. Practice includes 3 hospitals (720 beds) and free-standing MRI. Candidate must have experience in angiography and interventional radiology, and be willing to cover other areas of diagnostic imaging. Contact Paul M. Leiman, M.D., Dept. of Radiology, Moses Taylor Hospital, 700 Quincy Ave., Scranton, PA 18501; (717) 963-2601. 6ap

RADIOLOGIST NEEDED with experience in CT, ultrasound, nuclear medicine, mammography, and general radiology to provide vacation coverage for 2 practices in rural western Montana. One practice requires some traveling. Position would be excellent for person who wishes to semiretire in a pleasant scenic area. Great opportunity for recreational activities. Send inquiries to Tyler H. Gill, M.D., 1200 Westwood Dr., Hamilton, MT 59840; (406) 363-2211. 2-6a

Positions Desired

JULY 1991 RADIOLOGY RESIDENCY POSITION SOUGHT—Radiology resident currently in second yr seeks to transfer into the third yr of an academic university program. Also interested in programs offering 1 yr of research with faculty member(s) before beginning third yr. Plan a career in academic radiology. Have training in all modalities. Research experience in diagnostic imaging. Excellent references. 6bp

Fellowships and Residencies

MGH MR FELLOWSHIP—NIH fellowship positions are available for board-eligible/certified radiologists. Opportunities are available for clinical and/or basic research and include MRI (e.g., echo-planar, perfusion, diffusion, microscopy, other nuclei, and contrast agent studies), and MRS (e.g., CSI, metabolite quantitation, and oxygen consumption). The center contains about 20,000 sq. ft. of space, which includes 5 dedicated research magnets (1.5-T whole body, 2.0-T 18 cm, 4.7-T 33 cm, 6.0-T 5 cm, and 9.4-T 9 cm), a clinical/research system (1.5-T May 1991), and a clinical system (1.5-T). The dedicated, whole-body research magnet is a prototype GE Hyper-scan system with conventional Signa capabilities and resonant coils for real-time (EPI) acquisition (16 images/sec). In addition, the center contains support laboratories (biochemistry, computer, electronics, and surgery), conference rooms, and seating for 20 graduate students and fellows. The Center staff consists of 2 M.D., 6 MD/Ph.D., and 9 Ph.D. investigators with significant expertise in NMR and related biomedical fields. Individuals interested in a position should contact Thomas J. Brady, M.D., Director, MGH-NMR Center, Bldg. 149, 13 St., Charlestown, MA 02129. 6c

RADIOLOGY RESIDENCY—Unexpected opening for a third-yr resident. For further information, contact Francesca D'Abate, Education Assistant, The University of Connecticut Health Center, Dept. of Radiology, 263 Farmington Ave., Farmington, CT 06030; (203) 679-2345 or fax (203) 679-3145. 6c

FELLOWSHIP POSITIONS—The Dept. of Radiology, University of Arkansas for Medical Sciences, Little Rock, AR, has openings for fellowships to begin July 1992. Positions are available in body imaging/intervention, neuroradiology, vascular and interventional radiology, and pediatric radiology. Eligible candidates must be board-certified or eligible for certification in diagnostic radiology and should be eligible for licensing in the state of Arkansas. Interested candidates should contact the program directors: imaging/intervention — Teresita L. Angtuaco, M.D., or Steven K. Teplick, M.D.; neuroradiology — Edgardo J. C. Angtuaco, M.D.; vascular and interventional radiology — Ernest J. Ferris, M.D.; pediatric radiology — Joanna J. Siebert, M.D. All program directors listed above can be contacted at the Dept. of Radiology, University of Arkansas for Medical Sciences, Slot 556, 4301 W. Markham St., Little Rock, AR 72205; (501) 686-5740. The University of Arkansas for Medical Sciences is an affirmative action/equal opportunity employer. 6c

IMAGING FELLOWSHIP—A 1-yr fellowship in ultrasound, MRI, and body CT is available July 1, 1992–June 30, 1993, at a 576-bed teaching hospital. The Dept. of Radiology performs more than 140,000 exams with state-of-the-art equipment. The ultrasound section is responsible for all aspects of sonography including OB-GYN, pediatric, abdominal, and small parts. Extensive training in color flow imaging, duplex Doppler, transvaginal, transrectal techniques, and sonographically guided procedures. Two GE MRI scanners and 2 GE 9800 Quick CT units provide high-volume caseloads in these areas. Opportunities are available for participation in imaging research. For further information, please contact Marcela Bohm-Velez, M.D., Imaging Fellowship Director, West Penn Hospital, 4800 Friendship Ave., Pittsburgh, PA 15224. 5–10c

FELLOWSHIP IN BODY CT/MRI AND ULTRASOUND—The Dept. of Radiology of New York Medical College has an unexpected opening for 1-yr imaging fellowship starting in July 1991. Westchester County Medical Center is a 650-bed, tertiary-care facility offering advanced training with state-of-the-art equipment including 2 Siemens Hi-Q CT scanners, GE Signa 1.5-T MR, ISG 3D reconstruction console, and 6 ultrasound imagers (Acuson and Diasonics). Applicants must have completed an approved residency in diagnostic radiology and must be board-eligible or certified. Please contact Andrew Schechter, M.D., Director, MRI, Dept. of Radiology, New York Medical College, Valhalla, NY 10595; (914) 285-8550. 5–6cp

CARDIOVASCULAR-INTERVENTIONAL RADIOLOGY FELLOWSHIP—Unexpected opening available July 1, 1991, for a 1-yr fellowship program at a 750-bed teaching hospital. Extensive clinical experience involving all aspects of cardiovascular imaging, interventional vascular and nonvascular procedures, and availability for clinical or animal research. Send CV and inquiries to Oscar H. Gutierrez, M.D., Dept. of Radiology, Box 648, University of Rochester, Rochester, NY 14642-8648. An equal opportunity employer (M/F). 5–8c

FELLOWSHIP IN CALIFORNIA, JULY 1991—Interventional, cross-sectional imaging (MRI, CT, ultrasound) at a large trauma center. Send CV to Dr. Levan, Dept. of Radiology, St. Mary Medical Center, 1050 Linden Ave., Long Beach, CA 90813 or call (213) 491-9900 for information. 5–7cp

FELLOWSHIPS IN PEDIATRIC RADIOLOGY AND PEDIATRIC NEURORADIOLOGY—The Dept. of Radiology, Children's Hospital Medical Center, Cincinnati, OH, offers 1- or 2-yr fellowships in pediatric radiology beginning July 1, 1993. A 1-yr pediatric neuroradiology fellowship program is also offered and may be taken separately or combined with 1 yr of adult neuroradiology fellowship at the University of Cincinnati Medical Center. Children's Hospital Medical Center (CHMC) is a 355-bed institution. The dept. performs over 105,000 radiologic exams annually in the largest children's hospital and ambulatory practice in the U.S. The dept. has 14 full-time faculty pediatric radiologists, 6 fellows, and many resident trainees. Five pediatric radiology and 1 pediatric neuroradiology fellowship positions are available annually. Training includes all aspects of pediatric imaging: neonatal radiology, neuroimaging, musculoskeletal radiology, cardiovascular and thoracic imaging, abdominal imaging, oncologic imaging, ultrasonography, nuclear medicine, CT, MRI, and vascular/interventional procedures. The dept. has an active clinical service with state-of-the-art equipment as follows: digital fluoroscopy; Acuson, Al, and ATL ultrasound units with Doppler and color flow Doppler capabilities; planar SPECT gamma cameras; GE 9800 Quick CT scanner; 1.5-T GE MRI with spectroscopy; and cardiac catheterization/angiographic suite with digital vascular imaging. The fellowship provides a broad clinical experience in pediatric radiology as well as numerous opportunities to participate in both clinical and basic research. Candidates must be board-certified or board-qualified in diagnostic radiology and must be able to obtain an Ohio medical license. Salary and fringe benefits are highly competitive. Applications are due before Jan. 1992, with interviews scheduled during the fall and winter of 1991–1992. There are numerous career opportunities in pediatric radiology in academic and private practice settings. To receive more information about the fellowships at CHMC or careers in pediatric radiology, please contact Donald R. Kirks, M.D., Director, Dept. of Radiology, Children's Hospital Medical Center, Cincinnati, OH 45229-2899; (513) 559-8058. Children's Hospital Medical Center and the University of Cincinnati College of Medicine are affirmative action/equal opportunity employers. 5–4cp

FELLOWSHIP IN ULTRASOUND/CT/ANGIO/INTERVENTIONAL—A 1-yr fellowship program available beginning July 1992 at Lehigh Valley Hospital Center in Allentown, PA. LVHC is a 492-bed, acute-care, university-affiliated hospital. The fellowship program offers training in CT (head and body), ultrasound, angiography (neuro and visceral), and interventional radiography. MRI experience is also available. For further information, contact Robert Kricun, M.D., Dept. of Radiology, Lehigh Valley Hospital Center, P.O. Box 689, Allentown, PA 18105. 2–7c

ABDOMINAL IMAGING FELLOWSHIP—The Dept. of Radiology at the University of Florida is offering 1-yr fellowships in abdominal imaging beginning July 1, 1991, and July 1, 1992. Minimum requirements include successful completion of an accredited radiology residency. The fellowship includes training in all aspects of abdominal imaging (gastrointestinal and genitourinary radiology, CT, ultrasound, and MRI) by a 3-person subspecialty faculty. The program offers full clinical experience and research opportunities. Applicants must be eligible to obtain a license in the state of Florida. For additional information, contact Pablo R. Ros, M.D., Professor, Dept. of Radiology, Box J-374, Gainesville, FL 32610-0374; (904) 395-0288. The University of Florida is an equal opportunity/affirmative action employer and encourages applications from women and minorities. 10–6c

FELLOWSHIP IN BODY CT/MRI AND ULTRASOUND—The Dept. of Radiology of New York Medical College has 2 openings for a 1-yr imaging fellowship starting in July 1992. Westchester County Medical Center is a 650-bed, tertiary-care facility offering advanced training with state-of-the-art equipment. Equipment includes 2 Siemens Hi-Q CT scanners, GE Signa 1.5-T MR, ISG 3D reconstruction console, and 6 ultrasound imagers (Acuson and Diasonics). Applicants must have completed an approved residency in diagnostic radiology and must be board-eligible or certified. Please contact Andrew Schechter, M.D., Director, MRI, Dept. of Radiology, New York Medical College, Valhalla, NY 10595; (914) 285-8550. 5–6cp

INTEGRATED CHEST RADIOLOGY FELLOWSHIP AT JOHNS HOPKINS UNIVERSITY HOSPITAL—The Dept. of Radiology, Division of Thoracic Imaging, Johns Hopkins University is offering a 1- to 2-yr academically oriented fellowship in chest radiology. The fellowship offers an integrated experience in cross-sectional imaging, including over 4000 chest CT and 1000 thoracic MRI exams/yr. Strong research interests in high-resolution CT, MRI, digital imaging methods, and interventional thoracic radiology offer the candidate an exciting environment to work in. The fellowship is available starting July 1, 1991. Contact Elias A. Zerhouni, M.D., Director of Thoracic Imaging and MRI, Dept. of Radiology, Johns Hopkins Hospital, Baltimore, MD 21205; (301) 955-4062. 1–6c

FELLOWSHIPS AT THOMAS JEFFERSON UNIVERSITY HOSPITAL—The Dept. of Radiology at Thomas Jefferson University Hospital in Philadelphia offers the following fellowship programs each yr. Ultrasound/CT/MRI — Jefferson's ultrasound division is 1 of the largest in the world and performs all currently available exams including obstetric, vascular, lithotripsy, invasive, and endoluminal. We also operate 4 GE 1.5-T MRI units and 3 CT scanners. Contact Barry Goldberg, M.D., regarding this program. Cardiovascular/interventional — this division is housed in a new suite containing Philips angio units with DSA and performs the full range of vascular and non-vascular interventional procedures. Contact Geoffrey Gardiner, Jr., M.D. Neuro/ENT radiology — very active clinical services supply a wealth of material to this division, which is housed in a neurosciences imaging center containing all imaging modalities. Contact Carlos Gonzalez, M.D. Breast Imaging — Jefferson's new breast imaging center performs approximately 85 studies/day including ultrasound and needle localizations. Contact Stephen Feig, M.D. Chest — includes biopsies and CT. Contact Robert Steiner, M.D. MRI — a dedicated body MRI program including excellent research opportunities in addition to a large clinical case load. Contact Matthew Rifkin, M.D. Ultrasound — a dedicated ultrasound program. Contact Barry Goldberg, M.D. Musculoskeletal — includes MRI of the musculoskeletal system. Contact David Karasick, M.D. All program directors listed above can be contacted at the Dept. of Radiology, Thomas Jefferson University Hospital, Philadelphia, PA 19107. Jefferson is an equal opportunity/affirmative action employer. 6xc

WOMEN'S IMAGING FELLOWSHIP—A 1-yr fellowship is available at Oregon Health Sciences University, Portland, OR. Training includes hysterosalpingography, fallopian tube recanalization, mammography and breast procedures, obstetrical ultrasound, pelvic ultrasound including vaginal ultrasound, and pelvic and breast MRI. Please contact Amy Thurmond, M.D., Director of Women's Imaging, Oregon Health Sciences University, L340, 3181 S.W. Sam Jackson Park Rd., Portland, OR 97201; (503) 494-7576. 4–6c

FELLOWSHIPS AT MEMORIAL SLOAN-KETTERING CANCER CENTER—The Dept. of Medical Imaging at the Memorial-Sloan Kettering Cancer Center (MSKCC), a Cornell University Medical College affiliate, in New York City, has fellowships available beginning July 1, 1991. This is an excellent opportunity for intensive clinical training and research with a competitive salary and benefits. Send inquiries regarding cross-sectional imaging to J. Caravelli, M.D., or R. Castellino, M.D.; breast imaging to D. Dershaw, M.D.; and nuclear medicine to S. Larson, M.D., Memorial Sloan-Kettering Cancer Center, 1275 York Ave., New York, NY 10021. Integrated fellowships also are available, based at both New York Hospital (NYH) and MSKCC, during which the fellows rotate between the 2 institutions. Applicants are selected conjointly. Inquiries to New York Hospital should be addressed to Dept. of Radiology, 525 E. 68th St., New York, NY 10021. Send inquiries regarding neuroradiology to G. Krol, M.D., at MSKCC or R. Zimmerman, M.D., at NYH; and vascular/interventional to J. Botet, M.D., at MSKCC or T. Sos, M.D., at NYH. 5-6cp

MUSCULOSKELETAL RADIOLOGY FELLOWSHIP—Applications are now being accepted for a musculoskeletal fellow position for 1992 at the Cleveland Clinic Foundation (CCF). CCF is a 1000-bed, tertiary-care, teaching medical center with a large radiology residency program. Local, national, and international patients provide an interesting and varied mix of bone pathology. Training includes all aspects of musculoskeletal radiology including MR, CT, arthrography, biopsy, bone densitometry, and a large plain film experience. Fellowship includes patient care, teaching, and research. There is a close working relationship with the orthopedic, rheumatology, and endocrinology depts. There are presently 4 musculoskeletal staff in the section. For further information, please contact Bradford J. Richmond, M.D., Head, Section of Musculoskeletal Radiology, Desk A-21, 9500 Euclid Ave., Cleveland, OH 44195; (216) 444-3931. 5-10c

IMMEDIATE OPENING, FELLOWSHIP IN PEDIATRIC RADIOLOGY—Position available for fellowship in pediatric radiology, 1- or 2-yr, beginning July 1, 1992, or July 1, 1993. Full training with abundant hands-on experience with all imaging modalities. Supported by strong Dept. of Pediatrics with a good mixture of patient material. Excellent teaching on a 1-to-1 basis and ample opportunity for pursuing academic interests. Apply to Leonard E. Swischuk, M.D., Dept. of Radiology, The University of Texas Medical Branch, Child Health Center, C-65, Galveston, TX 77550; (409) 761-2096. UTMB is an equal opportunity M/F/H/V affirmative action employer. UTMB hires only persons authorized to work in the United States. 5-7c

FELLOWSHIPS AT ALBANY MEDICAL CENTER—The Dept. of Radiology at the Albany Medical Center offers the following fellowship programs each yr with openings available July 1992: ultrasound and body CT/MR — Wide variety of exams with state-of-the-art equipment including Acuson ultrasound, 3 GE CT scanners, and GE Signa 1.5-T MR. Contact James Peters, M.D.; neuro-radiology — regional referral center for neurosciences with extensive exposure to MR, CT, and angiography. Abundant research opportunities. Contact William Wagle, M.D.; angiography/interventional — busy, clinical service with in-depth experience in arteriography, lymphangiography, angioplasty, and interventional procedures. Contact Mohammad Sarrafizadeh, M.D. All program directors can be reached at the Dept. of Radiology, A-113, Albany Medical Center, 43 New Scotland Ave., Albany, NY 12208; (518) 445-3277. AMC is an equal opportunity, affirmative action employer. 4-6cp

FELLOWSHIP IN CARDIOVASCULAR/INTERVENTIONAL RADIOLOGY—A 1-yr fellowship in cardiovascular/interventional radiology is available at the Dartmouth-Hitchcock Medical Center in Hanover, NH, beginning July 1992. DHMC is the major teaching component of Dartmouth Medical School and is situated in a classic northern New England town. Training includes all aspects of diagnostic angiography (including neuro and pulmonary), vascular and nonvascular interventional techniques. This includes IVC filter placement, atherectomy, thrombolysis, biliary and urologic interventions, as well as biopsy and drainage procedures using multiple imaging modalities. We have a close working relationship with the depts. of vascular and general surgery. Approximately 2000 diagnostic and interventional procedures are performed/yr. The dept. will be moving to a new, tertiary-care, 429-bed hospital, in fall 1991, equipped with 2 new, state-of-the-art digital interventional suites and a 4-bed recovery room. Candidates must have completed an accredited diagnostic radiology residency program, must be certified or eligible by the ABR, and must be eligible for medical licensure in the state of New Hampshire. For further information, please contact Louis I. Juravsky, M.D., FRCPC, Dept. of Diagnostic Radiology, Dartmouth-Hitchcock Medical Center, 2 Maynard St., Hanover, NH 03756. Dartmouth College is an equal opportunity/affirmative action educator and employer. 6xcp

IMAGING FELLOWSHIP (CT, ULTRASOUND, MRI)—William Beaumont Hospital, a 970-bed, modern, tertiary-care teaching and academic institution in southeast Michigan, offers a 1-yr fellowship in sectional body imaging. The fellowship will provide extensive clinical experience in body CT, ultrasound, and MRI including CT and ultrasound-guided procedures, conventional and color-flow Doppler exams, prostatic and endovaginal sonography. Ample elective time is also provided for other rotations of individual interest. Candidates must be board-certified or eligible in diagnostic radiology and have a valid Michigan medical license. Four positions are available for July 1992. Salary and fringe benefits are highly competitive. For further information, write to Ali Shirkhoda, M.D., Chief, Imaging Division, William Beaumont Hospital, 3601 W. 13 Mile Rd., Royal Oak, MI 48073; (313) 551-1001. 4-6c

FELLOWSHIP IN CARDIOVASCULAR/INTERVENTIONAL RADIOLOGY—A 1-yr fellowship in cardiovascular/interventional radiology is available at the Dartmouth-Hitchcock Medical Center in Hanover, NH, beginning July 1991. DHMC is the major teaching component of Dartmouth Medical School and is situated in a classic northern New England town. Training includes all aspects of diagnostic angiography (including neuro and pulmonary), vascular and nonvascular interventional techniques. This includes IVC filter placement, atherectomy, thrombolysis, biliary and urologic interventions, as well as biopsy and drainage procedures using multiple imaging modalities. We have a close working relationship with the depts. of vascular and general surgery. Approximately 2000 diagnostic and interventional procedures are performed/yr. The dept. will be moving to a new, tertiary-care, 429-bed hospital, in fall 1991, equipped with 2 new, state-of-the-art digital interventional suites and a 4-bed recovery room. Candidates must have completed an accredited diagnostic radiology residency program, must be certified or eligible by the ABR, and must be eligible for medical licensure in the state of New Hampshire. For further information, please contact Louis I. Juravsky, M.D., FRCPC, Dept. of Diagnostic Radiology, Dartmouth-Hitchcock Medical Center, 2 Maynard St., Hanover, NH 03756. Dartmouth College is an equal opportunity/affirmative action educator and employer. 6xcp

UNIVERSITY OF WASHINGTON FELLOWSHIP IN DIAGNOSTIC IMAGING SCIENCES—The Diagnostic Imaging Sciences Center of the Dept. of Radiology at the University of Washington in Seattle is recruiting for 2 fellowship positions in radiology science research. The research fellowship program is funded by NCI Training Grant T32 CA 096552 and combines a 2-yr, fully funded, laboratory-based, educational and research program with a guaranteed clinical fellowship after successful completion of the radiology science program. Candidates should have successfully completed 2 or 3 yr of a diagnostic radiology residency and must have a strong interest and commitment to a career in academic radiology. The research fellowship program will combine academic courses and a thesis project that will lead to a masters degree in biomedical imaging at the University of Washington. A portion of each fellow's time will be spent in clinical subspecialty radiology training to keep the fellows clinically astute and to provide additional clinical experience. The Radiology Imaging Research Laboratory at the University of Washington consists of over 20,000 sq. ft. of dedicated research space and includes more than 25 full-time scientists, state-of-the-art equipment in MRI, NMR spectroscopy, PET, SPECT, DIN/PACS, angiography, ultrasound, and image processing. Four MRI instruments, including a GE Signa system, are dedicated to research use. Candidates interested in the Radiology Research Sciences Program should contact James A. Nelson, M.D., Dept. of Radiology, SB-05, University of Washington, Seattle, WA 98195; (206) 543-3757. The University of Washington is an equal opportunity employer. 5-6c

CARDIOVASCULAR AND INTERVENTIONAL RADIOLOGY—The Harvard Medical School and Brigham and Women's Hospital, Dept. of Radiology, is offering a 2-yr fellowship starting July 1, 1992, in cardiovascular and interventional radiology including peripheral and coronary angiography, cardiac catheterization, digital vascular imaging, all types of interventional procedures, noninvasive vascular techniques, and cardiovascular MRI. Research time available for participation in original or ongoing clinical and/or laboratory projects. Please send CV to B. Leonard Holman, M.D., Chairman, Dept. of Radiology, Brigham and Women's Hospital, 75 Francis St., Boston, MA 02115. Brigham and Women's Hospital/Harvard Medical School is an affirmative action/equal opportunity educator and employer. 3-8c

DUKE UNIVERSITY MEDICAL CENTER FELLOWSHIP POSITIONS—Duke University Medical Center is seeking qualified candidates for fellowship positions in the Dept. of Diagnostic Radiology. Currently there are positions available in the following areas: chest, musculoskeletal, and vascular/interventional radiology, ultrasound, advanced diagnostic imaging, MRI, neuroradiology, abdominal imaging, mammography, and research fellowships. The radiology dept. is state-of-the-art in diagnostic imaging with diverse resources available for clinical, teaching, and academic pursuits. Fellowship training is generally organized by organ systems, although experience can be individualized to accommodate special interests. Salary and benefits are competitive and academic time is guaranteed. For additional information, please phone Richard Leder, M.D. at (919) 681-2711 ext. 5310. Applications are due Feb. 1 of the preceding yr and can be obtained by writing to N. Reed Dunnick, M.D., Dept. of Radiology, Duke University Medical Center, Erwin Rd., Box 3808, Durham, NC 27710. AA/EOE. 2-7c

NEURORADIOLOGY FELLOWSHIP—The Dept. of Radiology, Strong Memorial Hospital, University of Rochester School of Medicine and Dentistry offers a 1- or 2-yr neuroradiology fellowship to begin July 1, 1991. Training is offered in MRI, CT, and special procedures, with the opportunity to perform both pediatric and carotid ultrasound. Assistance in teaching of medical students and residents is expected. Additional training in maxillofacial, dental, and ENT radiology also is available, as is the opportunity to perform both clinical and laboratory research. A very strong neuroscience community exists. The dept. consists of 25 radiologist faculty, 16 residents, and 3–5 fellows. State-of-the-art equipment is available in all modalities including new single and biplane angiographic systems, 3 third-generation CT, a 1.5-T MRI, and a midfield MR. Strong Memorial Hospital is a 750-bed, tertiary-care hospital with 100 beds dedicated to pediatric diseases. Candidates must have completed an accredited diagnostic radiology residency program, be board-certified or eligible, and have a New York state medical license by July 1, 1991. Send inquiries to Robert E. O'Mara, M.D., Box 648, University of Rochester Medical Center, Rochester, NY 14642; (716) 275-2733. EO/AA/M-F employer. 1–6c

FELLOWSHIP IN CROSS-SECTIONAL IMAGING The Dept. of Radiology, Dartmouth-Hitchcock Medical Center, has an opening for July 1992 for a 1-yr fellowship in MRI/CT/ultrasound. Training includes experience in all aspects of MRI, including neuro and body, CT, and ultrasound, including obstetric and vascular imaging. Imaging-guided biopsies and drainage procedures will be an integral part of the program. The Medical Center has a completely new 420-bed, tertiary-care hospital with state-of-the-art imaging equipment opening in the fall of 1991. Protected research time will be available for the fellow. There is ample opportunity for clinical radiologic research as well as technology assessment and outcome analysis in collaboration with Dartmouth Medical School Center for Evaluative Sciences. For further information, contact Robert D. Harris, M.D., Dept. of Radiology, Dartmouth-Hitchcock Medical Center, Hanover, NH 03756; (603) 646-5686. 6xc

Tutorials/Courses

MAUI, HAWAII 1991—16th Annual Body Imaging Congress, October 5–12, 1991. CME I, Grand Hyatt Wailea. Medical Seminars International, Inc., 18981 Ventura Blvd., Ste. 303, Tarzana, CA 91356; (818) 774-9077, fax (818) 774-0244. 6–9d

ALASKA 1991-CRUISE THE INLAND PASSAGE, BREAST IMAGING AT SEA, JULY 7–14, 1991, AND MRI AT SEA, JULY 14–21, 1991—Medical Seminars International, Inc., 18981 Ventura Blvd., Ste. 303, Tarzana, CA 91356; (818) 774-9077, fax (818) 774-0244. 3–6d

AJR Classified Advertisements Information

Box Responses and Address for Ad Placement

Write Box _____, AJR, 2223 Avenida de la Playa, Suite 103, La Jolla, CA 92037-3218; Phone: (619) 459-2229; FAX: (619) 459-8814.

Other

VISITING PROFESSORSHIPS, THOMAS JEFFERSON UNIVERSITY HOSPITAL—The Dept. of Radiology at Thomas Jefferson University Hospital in Philadelphia is offering visiting professorships over the next several yr, while some of our faculty members are on sabbatical leave. These positions can have either a 6-mo or 1-yr term. In particular, we are seeking candidates with expertise in either ultrasound or general diagnostic radiology, but emphasis in other areas may be acceptable as well. Funding for these positions is appropriate for a senior faculty member from another institution on sabbatical with partial funding of his/her own, or for a junior faculty member. These positions are also open to highly qualified foreign radiologists with current academic appointments at prestigious foreign medical schools. Visiting faculty members will do some clinical work in our dept. and also have access, for research or educational purposes, to state-of-the-art imaging modalities of all types, as well as well-equipped physics and physiology research laboratories. Interested persons should contact David C. Levin, M.D., Chairman, Dept. of Radiology, Thomas Jefferson University Hospital, Philadelphia, PA 19107. Jefferson is an equal opportunity/affirmative action employer. 6xe

Author Index Volume 156

Authors of *AJR* articles are also included in the 5-year cumulative index published in *Radiology*.

A

- Abécassis J-P, **156**:981
 Abeler V, **156**:1191
 Aberle DR, **156**:833
 Ablin DS, **156**:635
 Abrahams JJ, **156**:599
 Abu-Yousef MM, **156**:79
 Achong D, **156**:407
 Acuña B, **156**:751
 Acuña G, **156**:751
 Adam A, **156**:321
 Adam G, **156**:125
 Adams HG, **156**:198
 Agatston S, **156**:467
 Agildere AM, **156**:1113
 Aizpuru R, **156**:1007
 Akhan O, **156**:1113
 Akins EW, **156**:875, **156**:1155
 Alegret X, **156**:931
 Alexander A, **156**:99
 Alexandre JH, **156**:1324
 Allard JC, **156**:875
 Allen B, **156**:471
 Allison JW, **156**:255
 Alper A, **156**:751
 Alperin JB, **156**:1189
 Alpern MB, **156**:1113
 Amplatz K, **156**:1007, **156**:1087
 Anderson DJ, **156**:405
 Antonucci F, **156**:389
 Applegate G, **156**:307
 Argy N, **156**:849, **156**:1295
 Arno LJ, **156**:1110
 Aronson D, **156**:527
 Aronson FR, **156**:281
 Aronson J, **156**:353
 Atlas SW, **156**:1229

B

- Bach DB, **156**:520
 Baert AL, **156**:640
 Bagley D, **156**:99
 Baillie J, **156**:975
 Baker LL, **156**:1133
 Baker S, **156**:345
 Balduini FC, **156**:769
 Balthazar EJ, **156**:23
 Bar MH, **156**:281
 Baran DT, **156**:1326
 Barboriak D, **156**:474
 Barkovich AJ, **156**:587, **156**:791
 Barloon TJ, **156**:579
 Barnes DA, **156**:785
 Baron RL, **156**:945
 Barone GW, **156**:639
 Barreda R, **156**:199
 Barron PT, **156**:1261

- Bartiroli G, **156**:341
 Bassett LW, **156**:59, **156**:449
 Batnitzky S, **156**:1052, **156**:1279
 Beam CA, **156**:1209
 Beatrous TE, **156**:407
 Becker C, **156**:345
 Becker JM, **156**:769
 Belanger PL, **156**:775, **156**:781
 Bell DG, **156**:1081
 Belldegrun A, **156**:833
 Bellon EM, **156**:807
 Belloni C, **156**:753
 Beltran J, **156**:457
 Benenati JF, **156**:327
 Benigno SJ, **156**:1263
 Benjamin IS, **156**:321
 Ben-Menachem Y, **156**:1101
 Benson JE, **156**:807
 Benson RC, **156**:1205
 Benzel EC, **156**:801
 Berbaum KS, **156**:177
 Beres RA, **156**:823
 Berkowitz JE, **156**:638
 Bernardino ME, **156**:1171
 Bernstein RM, **156**:864
 Bero L, **156**:1109
 Berquist TH, **156**:337
 Berry M, **156**:1112
 Bertino RE, **156**:404
 Bertrand Y, **156**:1037
 Bessette JC, **156**:823
 Beyissen B, **156**:389
 Bigler SA, **156**:945
 Bisceglia M, **156**:351
 Biscesi MA, **156**:475
 Blanc P, **156**:281
 Bland PH, **156**:511
 Blaser SI, **156**:807
 Blebea JS, **156**:343
 Blinkhorn RJ, **156**:870
 Bloem JL, **156**:1017
 Blomlie V, **156**:1191
 Blum JE, **156**:58, **156**:806
 Boal DKB, **156**:1219
 Bohndorf K, **156**:125
 Bonni A, **156**:981
 Bood B, **156**:198
 Bookstein JJ, **156**:617
 Bornman PC, **156**:1263
 Botet JF, **156**:63
 Bouillot JL, **156**:1324
 Boulware SD, **156**:599
 Bower BL, **156**:385
 Boxt LM, **156**:1154
 Boyko OB, **156**:1053
 Brady TM, **156**:404
 Brahme FJ, **156**:1244
 Brandon JC, **156**:471

- Brandser E, **156**:201
 Brant WE, **156**:636
 Braun IF, **156**:373
 Braunstein EM, **156**:545
 Braverman RM, **156**:365
 Brenner RJ, **156**:719
 Brill PW, **156**:561
 Brink JA, **156**:1163
 Brisson LJ, **156**:639
 Brogan M, **156**:161
 Brooks BS, **156**:1075
 Brown CEL, **156**:523
 Brown DE, **156**:333
 Brown WE, **156**:871
 Browning M, **156**:1155
 Brown-Jones C, **156**:141
 Buchbinder SS, **156**:866
 Buck JL, **156**:481
 Buckley KM, **156**:467
 Buckner CB, **156**:255
 Bulas DI, **156**:155, **156**:571
 Burger PC, **156**:1053
 Burhenne HJ, **156**:73
 Burton DJ, **156**:555
 Buxton R, **156**:307

C

- Caballero-Saez A, **156**:769
 Cáceres J, **156**:931
 Cameron JL, **156**:327
 Campeau RJ, **156**:406
 Capello W, **156**:545
 Cardozo JD, **156**:725
 Caro JJ, **156**:825
 Carpenter RJ Jr, **156**:636
 Carrera GF, **156**:131
 Carty H, **156**:635
 Casas JM, **156**:1113
 Caskey CI, **156**:711
 Cassidy CI, **156**:59
 Castañeda-Zúñiga WR, **156**:1007, **156**:1087
 Cataldo MF, **156**:403
 Catena LM, **156**:141
 Cavallino RP, **156**:1253
 Cazenave FL, **156**:395
 Çelik L, **156**:751
 Cerqueira MD, **156**:44
 Chakeres DW, **156**:161
 Chandnani V, **156**:457
 Chapuis Y, **156**:981
 Charboneau JW, **156**:1081
 Charles HC, **156**:105
 Charnsangavej C, **156**:1025
 Chen HH, **156**:858, **156**:1314
 Chen YM, **156**:303
 Chetty N, **156**:321
 Chew FS, **156**:200, **156**:474,

D

- Daffner RH, **156**:332
 Dail DH, **156**:985
 Damiano MA, **156**:381
 Dammer M, **156**:125
 Dang H, **156**:471
 Daniel TB, **156**:875
 Darcy MD, **156**:385, **156**:623
 Daum-Kowalski R, **156**:1321
 Davey DD, **156**:287
 David CL, **156**:1159
 Davis GB, **156**:617
 Davis LM, **156**:917
 Davis PC, **156**:1039, **156**:1237
 Davis S, **156**:345
 Davros WJ, **156**:493
 Dee PM, **156**:539
 DeLaPaz RL, **156**:579
 Del Buono EA, **156**:511
 DelMaschio A, **156**:753
 De Marcos JA, **156**:931
 Demas B, **156**:989
 Denath FM, **156**:1322
 deSouza NM, **156**:507

- Deutsch L-S, **156**:471
 Dillon WP, **156**:689
 Disler DG, **156**:1016
 Dobben RL, **156**:757
 Dobkin BL, **156**:858, **156**:1314
 Doi O, **156**:921
 Dolenz K, **156**:757
 Donaldson JS, **156**:351
 Donoso L, **156**:1114
 Doppman JL, **156**:39
 Douek P, **156**:1037
 Downey DB, **156**:404
 Downey PR, **156**:1199
 Doyle TB, **156**:313
 Draganic M, **156**:408
 Drane WE, **156**:199
 Duberg A, **156**:1245
 DuBrow RA, **156**:1159
 Dunham CM, **156**:273
 Dunn RS, **156**:1116
 Dupuy D, **156**:1167
 Duva-Frissona AD, **156**:852,
 156:1301
 Dwyer AJ, **156**:39
 Dwyer SJ III, **156**:1279
- E**
- Edgerton VR, **156**:765
 Edwards MSB, **156**:587, **156**:791
 Effmann EL, **156**:1209
 Eggleston DE, **156**:345
 Ehara S, **156**:1110
 Ehrlich SM, **156**:367
 Eidelman EM, **156**:611
 Eidt JF, **156**:639
 Eisenberg RL, **156**:944
 Ekberg O, **156**:293, **156**:1181
 El Gammal T, **156**:1075
 Elkadi T, **156**:14
 El-Khoury GY, **156**:1199
 Ellis JH, **156**:995
 Ellis K, **156**:669
 Elster AD, **156**:157, **156**:605
 Embry RL, **156**:1321
 Engeler CE, **156**:1087
 Erickson SJ, **156**:3, **156**:131,
 156:539
 Eschelman DJ, **156**:846, **156**:849,
 156:852, **156**:854, **156**:858,
 156:1288, **156**:1295, **156**:1301,
 156:1307, **156**:1314
 Essinger A, **156**:389
 Estes DN, **156**:1328
 Evens RG, **156**:400
 Ezaki T, **156**:868
- F**
- Fagien M, **156**:199
 Fatouros PP, **156**:373
 Fava M, **156**:405
 Fay J, **156**:467
 Feigin DS, **156**:280
 Feinberg MJ, **156**:293, **156**:1181
 Feinstein KA, **156**:1215
 Feld R, **156**:737
 Feldman F, **156**:121
 Fenke F, **156**:125
 Fernandez MdP, **156**:1171
 Fernbach SK, **156**:137, **156**:1215
 Ferrucci JT, **156**:317, **156**:867,
 156:869
 Feuerstein IM, **156**:39
 Fielding JR, **156**:849, **156**:1295
 Figley MM, **156**:1100
 Figlin RA, **156**:833
 Filly RA, **156**:555
 Finberg HJ, **156**:359
 Findling JW, **156**:39
 Fishman EK, **156**:517, **156**:711,
 156:715
- Fishman JE, **156**:833
 Fishman M, **156**:1005
 Fitz CR, **156**:571
 Fitzgerald SW, **156**:131
 Flickinger FW, **156**:1324
 Flower CDR, **156**:1145
 Foley WD, **156**:3
 Foradori G, **156**:405
 Formanek AG, **156**:1033
 Forrest JV, **156**:1277
 Forsberg DA, **156**:200
 Fouquet B, **156**:1327
 Francis IR, **156**:1113
 Frank JA, **156**:407
 Frank R, **156**:865
 Frank RG, **156**:1325
 Franken EA, **156**:177
 Franquet T, **156**:1113
 Freeny PC, **156**:326
 Friedman AC, **156**:104
 Friedman M, **156**:1253
 Friloux L, **156**:307
 Fuchigami T, **156**:741
 Fukushima M, **156**:741, **156**:965
 Fujita J, **156**:1322
 Fujita M, **156**:921
 Fukunaga T, **156**:765
 Futerman C, **156**:471
- G**
- Gaeta M, **156**:341
 Galvin JR, **156**:15
 Gamsu G, **156**:281
 Garra BS, **156**:493
 Garvin KL, **156**:333
 Gatewood OMB, **156**:638
 Gaux JC, **156**:389
 Gebarski SS, **156**:790, **156**:1218
 Gelfand DW, **156**:1, **156**:303,
 156:939
 Geller SC, **156**:97
 Gelman R, **156**:51
 Gens D, **156**:51
 Gerard PS, **156**:865, **156**:1325
 Gerard-McFarland EL, **156**:724
 Gerscovich E, **156**:1011
 Ghose R, **156**:1112
 Gianturco C, **156**:757
 Giardina PJ, **156**:561
 Gibbons DT, **156**:849, **156**:852,
 156:854, **156**:1295, **156**:1301,
 156:1307
 Gikas PW, **156**:511
 Ginalski JM, **156**:872
 Gindre T, **156**:866
 Glass P, **156**:571
 Glass-Royal MC, **156**:395, **156**:493
 Glazer GM, **156**:511
 Glazer HS, **156**:45, **156**:405
 Glick SN, **156**:961
 Glover JR, **156**:197
 Goerg C, **156**:949, **156**:1185
 Goerg K, **156**:949
 Gokmen E, **156**:751
 Gold RH, **156**:59
 Goldberg BB, **156**:99
 Goldberg HI, **156**:1229
 Golebiowski P, **156**:916
 Good BC, **156**:1107
 Goodman P, **156**:1189
 Goodman PC, **156**:944
 Goupille P, **156**:1327
 Gramm HF, **156**:748
 Grantham JJ, **156**:501
 Grantmyre EB, **156**:149
 Grassi CJ, **156**:813
 Grattan-Smith JD, **156**:785
 Greene R, **156**:467
 Greensite F, **156**:307
 Greenspan A, **156**:635, **156**:1011
- Griscom NT, **156**:371
 Grist TM, **156**:105
 Grix A, **156**:635
 Groskin SA, **156**:680, **156**:960
 Gross GW, **156**:367
 Grossman HB, **156**:511
 Grossman RI, **156**:1229
 Gulliver DJ, **156**:975
 Gunther RW, **156**:125, **156**:389
 Gupta AK, **156**:1257
 Gur D, **156**:198, **156**:1107
 Guzman S, **156**:405
 Gyepes MT, **156**:1208
- H**
- Hackbarth DA, **156**:539
 Hackney DB, **156**:1074
 Hadden TA, **156**:801
 Hagler NG, **156**:871
 Hahn PF, **156**:235, **156**:252,
 156:317, **156**:1163
 Hallioglu M, **156**:1113
 Hall FM, **156**:200, **156**:637, **156**:867,
 156:872
 Hamilton PA, **156**:745
 Hamm B, **156**:235, **156**:245,
 156:317
 Hammerman AM, **156**:313
 Hamper UM, **156**:401
 Hanafee W, **156**:1068
 Harada K, **156**:297
 Harms GF, **156**:925
 Harned RK, **156**:481
 Harrell RS, **156**:523
 Harris HS, **156**:875
 Harris MN, **156**:866
 Hata K, **156**:1115
 Hata T, **156**:408, **156**:636, **156**:1115
 Hattery RR, **156**:1081
 Hawkins IF Jr, **156**:875
 Hayashi T, **156**:1177
 Hazebroucq V, **156**:981
 Heberger R, **156**:343
 Hebrang A, **156**:1091
 Heitmiller RF, **156**:715
 Helms CA, **156**:531
 Hendee WR, **156**:176, **156**:1283
 Hennerici M, **156**:873
 Herlinger H, **156**:731
 Herman TE, **156**:151, **156**:799
 Hernandez RJ, **156**:1029
 Hernigou A, **156**:1324
 Hesselink JR, **156**:1059, **156**:1245
 Hessler C, **156**:543
 Hicks ME, **156**:385, **156**:623
 Higashiyama M, **156**:921
 Hillman BJ, **156**:443
 Hilsenrath PE, **156**:177
 Hoefs J, **156**:307
 Hofer HO, **156**:113
 Hoffman AD, **156**:1081
 Hoffman JC Jr, **156**:1039, **156**:1237
 Hoffmann G, **156**:265
 Hogg JC, **156**:225
 Holder JC, **156**:639
 Honeyman JC, **156**:1326
 Hopper KD, **156**:1219
 Houwer OW, **156**:1081
 Houssin D, **156**:981
 Hricak H, **156**:989
 Huang HK, **156**:835
 Hudgins PA, **156**:1039, **156**:1237
 Hull JE, **156**:403
 Hung W, **156**:141
 Hunter DW, **156**:1007, **156**:1087
- I**
- Idvall I, **156**:634
 Iida M, **156**:965
- Ikezoe J, **156**:297
 Ingram JD, **156**:571
 Inoue E, **156**:921
 Irino S, **156**:1322
 Irwin GAL, **156**:486
 Irwin RS, **156**:917
 Iwashita A, **156**:741
- J
- Jaeger Ph, **156**:872
 Jain R, **156**:1112
 Jamshidian J, **156**:1323
 Javors BR, **156**:1325
 Jeffrey RB Jr, **156**:725, **156**:749
 Jendrisak M, **156**:623
 Jenkins R, **156**:1167
 Joffre F, **156**:389
 Johnson CD, **156**:93
 Johnson JE, **156**:131
 Johnson MB, **156**:85
 Johnston GS, **156**:865
 Jones B, **156**:517
 Joseph S, **156**:1257
- K
- Kaalhus O, **156**:1191
 Kamenica S, **156**:408
 Kamino K, **156**:1177
 Kaneko M, **156**:868
 Kanel GC, **156**:91, **156**:307
 Kang YS, **156**:517
 Kaplan AS, **156**:1109
 Kaplan PA, **156**:333, **156**:353
 Karella A, **156**:781
 Karnik S, **156**:406
 Karchner ZA, **156**:406
 Kathol MH, **156**:1199
 Kattan M, **156**:866
 Katz RL, **156**:199
 Kaude JV, **156**:199, **156**:1326
 Kazerrooni E, **156**:543
 Keefe B, **156**:1195
 Kehler M, **156**:345
 Kelsch RC, **156**:1029
 Kerut T, **156**:367
 Kessler LS, **156**:1326
 Kier R, **156**:527
 Kiernan H, **156**:121
 Kim D, **156**:173
 Kim EE, **156**:780, **156**:1025
 Kimme-Smith C, **156**:234, **156**:449,
 156:954
 Kimura Y, **156**:965
 Kinard RE, **156**:1321
 King AR, **156**:1199
 King BF, **156**:1081
 King JG, **156**:287
 Kinoshita T, **156**:69
 Kipper MS, **156**:500
 Kirchhoff R, **156**:874
 Kirk IR, **156**:199
 Kirshenbaum GL, **156**:1253
 Kirshenbaum KJ, **156**:1253
 Kitao M, **156**:1115
 Kjorstad K, **156**:1191
 Klein DS, **156**:633
 Kleinholffer MA, **156**:385, **156**:623
 Klein JS, **156**:281
 Kleinman PK, **156**:576, **156**:775,
 156:781
 Klukowicz A, **156**:1110
 Kneeland JB, **156**:131
 Knudson GJ, **156**:539
 Kobayashi K, **156**:297
 Koch E, **156**:113
 Koch P, **156**:265
 Koch SR, **156**:1001
 Kochhar R, **156**:1111
 Kodama K, **156**:921

Koffman CG, **156**:507
 Kogutt MS, **156**:634
 Kolin A, **156**:745
 Korobkin M, **156**:1113
 Korula J, **156**:85
 Kosuge T, **156**:69
 Kotlyarov E, **156**:865
 Kotner LM Jr, **156**:313
 Kozuka T, **156**:297
 Kraft KA, **156**:373
 Krauthamer R, **156**:763
 Kricheff II, **156**:611, **156**:1110
 Krige JEJ, **156**:1263
 Kroll SS, **156**:1159
 Kromhout J, **156**:202
 Kronthal AJ, **156**:517, **156**:715
 Kucharczyk J, **156**:1133
 Kuhlman JE, **156**:517, **156**:715
 Kuipers D, **156**:1017
 Kumar R, **156**:1189
 Kumar S, **156**:1257
 Kuriyama K, **156**:921
 Kuroda C, **156**:921
 Kursunoglu-Brahme S, **156**:457
 Kurtz AB, **156**:99, **156**:737
 Kushner DC, **156**:141

L

Lachman RS, **156**:149
 Laine FJ, **156**:373
 Lamb MN, **156**:1261
 Lang EK, **156**:870
 Lang EV, **156**:1225
 Lantz PE, **156**:1033
 Laufer I, **156**:731, **156**:955
 Lebowitz RL, **156**:365, **156**:407
 Leeba J, **156**:636
 Lee G, **156**:917
 Lee KF, **156**:1252
 Lee KP, **156**:85
 Lee MJ, **156**:97, **156**:317, **156**:1163
 Leithiser RE, **156**:255
 Leopold GR, **156**:867
 Letourneau JG, **156**:1087
 Levenson H, **156**:307
 Levine E, **156**:501
 Levine MS, **156**:731, **156**:955
 Levy IM, **156**:117
 Lew R, **156**:917
 Lewis D, **156**:1167
 Lewis ER, **156**:711
 Libshitz HI, **156**:199, **156**:1159
 Lida M, **156**:741
 Lieberman JM, **156**:870
 Lien MD, **156**:769
 Lien HH, **156**:1191
 Lightdale C, **156**:63
 Lillington GA, **156**:404
 Ling A, **156**:39
 Lipchik EO, **156**:823
 Litt AW, **156**:611
 Liu J-B, **156**:99
 Llewellyn HJ, **156**:467
 Loes DJ, **156**:579
 Longmaid HE III, **156**:492
 Longmate JA, **156**:1326
 Loriaux DL, **156**:39
 Lou SL, **156**:835
 Loyer EM, **156**:1159
 Lucas D, **156**:77
 Luethke JM, **156**:381
 Lycke G, **156**:77

M

MacEwan DW, **156**:1188
 Mack LA, **156**:359
 Macken MB, **156**:149
 Magaram DL, **156**:863
 Makuuchi M, **156**:69

Malik AK, **156**:1111
 Mandell SH, **156**:511
 Marchand T, **156**:493
 Marcus ML, **156**:15
 Marder DM, **156**:636
 Mari G, **156**:408, **156**:636
 Marincek B, **156**:113
 Marks SC Jr, **156**:775
 Marks TI, **156**:1029
 Martin LC, **156**:852, **156**:858, **156**:1301, **156**:1314
 Martin TD, **156**:1155
 Martineau BS, **156**:863
 Martinez S, **156**:200
 Martinez-Noguera A, **156**:1114
 Marx M, **156**:864
 Maskovic J, **156**:1091
 Mata J, **156**:931
 Mathiesen TI, **156**:634
 Matsuda M, **156**:1110
 Matsui T, **156**:741
 Matsumoto T, **156**:965
 Matthews JW II, **156**:1011
 Mayfield WR, **156**:1155
 McClellan BL, **156**:841, **156**:866
 McClure RD, **156**:989
 McCullough J, **156**:903
 McDowell J, **156**:870
 McGahan JP, **156**:547, **156**:636
 McGeady SJ, **156**:367
 McGhee RA Jr, **156**:457
 McGregor M, **156**:825
 McLachlan SJ, **156**:611
 McLellan GL, **156**:397
 McLeod RA, **156**:337
 McLoud TC, **156**:1145
 McNeely GF, **156**:1321
 Merchant S, **156**:406
 Merton DA, **156**:99
 Mewissen MW, **156**:823
 Miers JF, **156**:567
 Miller DL, **156**:638
 Miller R, **156**:343
 Miller RA, **156**:1110
 Millward SF, **156**:1261
 Milner LB, **156**:948
 Mink JH, **156**:765
 Mintorovich J, **156**:1133
 Minutoli A, **156**:341
 Mirfakhraee M, **156**:801
 Mirvis SE, **156**:51, **156**:273, **156**:865
 Mirza W, **156**:605
 Mitchell SE, **156**:327
 Mitchell SP, **156**:404
 Mitnick JS, **156**:866
 Mittelstaedt CA, **156**:1195
 Miura K, **156**:1177
 Miura T, **156**:1177
 Mizushima A, **156**:807
 Mochizuki T, **156**:868
 Modic MT, **156**:235, **156**:239
 Moldawer NP, **156**:833
 Molina PL, **156**:45, **156**:405
 Molpus WM, **156**:353
 Moore TE, **156**:1199
 Morehouse HT, **156**:117
 Morimoto S, **156**:297
 Morin LRM, **156**:1115
 Morin RL, **156**:925
 Morin de Finfe C-H, **156**:866
 Morparia H, **156**:406
 Morrison MC, **156**:1163
 Morton MJ, **156**:337
 Moseley HS, **156**:539
 Moseley ME, **156**:1133
 Moser RP, **156**:481, **156**:1010
 Moskos MM, **156**:852, **156**:1301
 Mrose HE, **156**:467
 Muellenaa AA Jr, **156**:1209
 Mueller PR, **156**:97, **156**:1163

Mulligan SA, **156**:930
 Myers JL, **156**:925
 N

Nabhani HA, **156**:871
 Nadel L, **156**:373
 Nadel S, **156**:957
 Nadimpalli SR, **156**:1253
 Nagi B, **156**:1111
 Nakao N, **156**:1177
 Narumi Y, **156**:921
 Nathan MH, **156**:633
 Nelson NL, **156**:333
 Newell JD II, **156**:381
 Neylan JF, **156**:1171
 Nieman LK, **156**:39
 Nikolic G, **156**:408
 Nishimura T, **156**:868
 Nomura F, **156**:707
 Norman A, **156**:116
 Norman G, **156**:198
 Northington FJ, **156**:567
 Northway WH Jr, **156**:681
 Novy SB, **156**:774
 Nowels K, **156**:77
 Nuruddin RN, **156**:989

O

Oakes WJ, **156**:1053
 Oates E, **156**:407
 O'Brien MJ, **156**:968
 O'Connor JF, **156**:845, **156**:846, **156**:849, **156**:852, **156**:854, **156**:858, **156**:1287, **156**:1288, **156**:1295, **156**:1301, **156**:1307, **156**:1314
 Ohnishi M, **156**:1177
 Okamoto E, **156**:1177
 O'Keefe FN, **156**:145
 Olcott EW, **156**:725
 Olmsted WW, **156**:481
 Olson RA, **156**:1171
 Onik G, **156**:531
 Osterman FA Jr, **156**:327
 Oteo JA, **156**:1113
 Ott DJ, **156**:303, **156**:939
 Ott R, **156**:471
 Owen DA, **156**:177
 Ownby DR, **156**:903
 Ozaki H, **156**:69
 Ozonoff MB, **156**:154

P

Palmer R, **156**:1199
 Palmer WE, **156**:724, **156**:1144
 Panageas E, **156**:846, **156**:1288
 Pandolfo I, **156**:341
 Parienté D, **156**:981
 Parker DR, **156**:849, **156**:852, **156**:854, **156**:858, **156**:1295, **156**:1301, **156**:1307
 Parsa MB, **156**:1095
 Pashu-Cerecina V, **156**:408
 Pass HI, **156**:39
 Patel V, **156**:406
 Patet JD, **156**:1037
 Patriquin H, **156**:364
 Patten RM, **156**:359, **156**:1101
 Patterson SK, **156**:995
 Peck WW, **156**:586
 Peene P, **156**:640
 Peix J-L, **156**:866
 Penn-Jones K, **156**:403
 Pervulov S, **156**:408
 Peterman SB, **156**:1039
 Peters JJM, **156**:202
 Peters PE, **156**:265
 Pfeifer EA, **156**:1324
 Philippe N, **156**:1037

R

Rabinov JD, **156**:854, **156**:1307
 Radin DR, **156**:91, **156**:487
 Rak KM, **156**:381
 Ralls PW, **156**:85, **156**:874, **156**:1205, **156**:874 Marinelli DL
 Ramsey RG, **156**:181
 Rao AS, **156**:1257
 Rao VRK, **156**:1257
 Rappaport DC, **156**:1227
 Raptopoulos V, **156**:917
 Rattner D, **156**:1163
 Ravimandalam K, **156**:1257
 Rawat B, **156**:73
 Raynaud A, **156**:389
 Reaman G, **156**:155
 Reidy JF, **156**:507
 Reinhart M, **156**:635
 Reiter AA, **156**:408
 Remley K, **156**:1069
 Rennie D, **156**:1109
 Resch H, **156**:1327
 Revenis ME, **156**:571
 Rice S, **156**:85
 Richardson DN, **156**:157
 Richardson P, **156**:273
 Richli WR, **156**:1025
 Richmond JM, **156**:775
 Riles TS, **156**:611
 Rimoin DL, **156**:149
 Roberts AC, **156**:617
 Roddie M, **156**:321
 Rollins ES, **156**:385
 Romo LV, **156**:846, **156**:849, **156**:1288, **156**:1295
 Ros PR, **156**:481, **156**:1227
 Rose BS, **156**:201
 Rosen MP, **156**:846, **156**:1288
 Rosenberg MA, **156**:456
 Rothstein RD, **156**:955
 Rousseau H, **156**:389
 Rozanes I, **156**:751
 Rubens DJ, **156**:343
 Rubens JR, **156**:467
 Rubesin SE, **156**:731
 Rubin GD, **156**:749
 Ruiz ME, **156**:131
 Rummeny E, **156**:265
 Ryan T, **156**:717

S

Sacks D, **156**:873
 Sadriah K, **156**:1323

- Safirstein BH, **156**:1110
 Sagel SS, **156**:45, **156**:181, **156**:405
 Sahn DJ, **156**:14, **156**:916
 Saini S, **156**:97, **156**:235, **156**:236,
156:317, **156**:1163
 Saka H, **156**:707
 Sakai S, **156**:707
 Sakai T, **156**:965
 Salazar J, **156**:1328
 Sammons N, **156**:903
 Samuels BI, **156**:1025
 Sargent SK, **156**:559
 Sarr MG, **156**:93
 Sartoris DJ, **156**:130, **156**:784
 Sato K, **156**:1322
 Sato Y, **156**:579
 Savader BL, **156**:401
 Savader SJ, **156**:327
 Sawhney S, **156**:1112
 Sax EJ, **156**:858, **156**:1314
 Saxon RR, **156**:281
 Scanlan KA, **156**:1267
 Schaefer KM, **156**:467
 Schatzki SC, **156**:554, **156**:1024,
156:1180
 Scheiner JD, **156**:731
 Schlesinger AE, **156**:1029
 Schmalbrock P, **156**:161
 Schultz DS, **156**:199
 Schuttevaer HM, **156**:1017
 Schwartzenberg St, **156**:611
 Schwerk WB, **156**:949, **156**:1185
 Scorpio R, **156**:273
 Secaf E, **156**:989
 Seibert JJ, **156**:353, **156**:567
 Seneterre E, **156**:317
 Setiawan AT, **156**:523
 Sevick RJ, **156**:1133
 Shanley DJ, **156**:1321
 Sharma B, **156**:870
 Sheffner SE, **156**:995
 Shellcock FG, **156**:765
 Shreff MJ, **156**:131
 Sherman JL, **156**:1219
 Sheth S, **156**:401
 Shimokata K, **156**:707
 Shiozaki H, **156**:297
 Shogen K, **156**:297
 Sialer G, **156**:113
 Siegel EL, **156**:1095
 Siegel HA, **156**:316
 Siegel JB, **156**:173
 Siegel ME, **156**:762
 Siegel MJ, **156**:45, **156**:151,
156:799
 Sierra AE, **156**:475
 Silva E, **156**:307
 Silverman PM, **156**:395
 Silverstone DZ, **156**:173
 Simeone JF, **156**:1163
 Sim FH, **156**:337
 Simpson W, **156**:559
 Singson RD, **156**:121
 Sironi S, **156**:753
- T
- Taccagni GL, **156**:753
 Tada S, **156**:741
 Takahashi M, **156**:868
 Takashima S, **156**:297
 Takayama T, **156**:69
 Takayasu Y, **156**:1177
 Takehara Y, **156**:868
 Takeuchi N, **156**:297
 Talner LB, **156**:985, **156**:1005
 Tampas JP, **156**:938
 Tarr RW, **156**:807
 Tart RP, **156**:863
 Tarver RD, **156**:717
 Tateishi R, **156**:921
 Taupitz M, **156**:317
 Taylor BJ, **156**:567
- Sivit CJ, **156**:141
 Skolnick ML, **156**:984
 Skorton DJ, **156**:15
 Skucas J, **156**:730
 Slifer KJ, **156**:403
 Sline RM, **156**:863, **156**:1155
 Slusher SL, **156**:501
 Smith AS, **156**:807
 Smith C, **156**:201
 Smith JA, **156**:345
 Smith JW, **156**:131
 Smith PL, **156**:474
 Smith WL, **156**:177
 Solomon SL, **156**:405
 Soloway RD, **156**:493
 Someshwar R, **156**:406
 Sonda LP, **156**:995
 Sostman HD, **156**:105
 Soto B, **156**:930
 Souillet G, **156**:1037
 Spencer RP, **156**:798
 Spevak MR, **156**:775, **156**:781
 Stafford SA, **156**:822
 Stanford W, **156**:15
 Stanley MD, **156**:403
 Stanley RJ, **156**:1266
 Stanojevic M, **156**:408
 Stansberry SD, **156**:145
 Staron R, **156**:121
 Steinke W, **156**:873
 Stelling CB, **156**:287
 Stephens DH, **156**:93
 Stewart BK, **156**:835
 Stigers KB, **156**:287
 Storella JM, **156**:173
 Straub WH, **156**:1107
 Sugisawa M, **156**:1110
 Surratt RS, **156**:623
 Susman N, **156**:400
 Swan JS, **156**:545
 Swanson D, **156**:77
 Swensen SJ, **156**:925
 Swischuk LE, **156**:145
 Szabo RM, **156**:1011
 Szymowski J, **156**:1059
- U
- Umalic C, **156**:917
 Unger JM, **156**:1111
 Unni KK, **156**:337
 Unni M, **156**:1257
 Usselman JA, **156**:394
- V
- Valat J-P, **156**:1327
 Valji K, **156**:617
 Valk PE, **156**:689
 Van Barcom ST, **156**:1328
 Vandemark RM, **156**:638
 van der Heul RO, **156**:1017
 Vandemark P, **156**:587
 Van Erp JS, **156**:511
 Varma DGK, **156**:406, **156**:1025
 Vassallo P, **156**:265
 Vazquez MF, **156**:866
 Vellet AD, **156**:520
 Venbrux AC, **156**:327
 Verbeeten B Jr, **156**:202
 Vine HS, **156**:154
 Volta S, **156**:341
 von Schultheiss GK, **156**:113
 Vorwerk D, **156**:389
- W
- Wack JP, **156**:864
 Wagner ML, **156**:785
 Walker CW, **156**:255, **156**:353
 Wallace S, **156**:757, **156**:1025
 Walling A, **156**:539
 Walmsley S, **156**:745
 Walter JF, **156**:749
 Walter R, **156**:77
 Warshauer DM, **156**:1195
 Warshaw AL, **156**:97
 Watanabe A, **156**:707
 Webb JAW, **156**:985
 Webb WR, **156**:281
 Weber A, **156**:957
 Weinreb JC, **156**:611
 Weisner KM, **156**:1033
 Weiss KL, **156**:117
 Weissman BN, **156**:120, **156**:1036
 Wernecke K, **156**:265
 Wetzel LH, **156**:501
 Whalen E, **156**:189
 White KS, **156**:1209
 White SJ, **156**:345
 Widius DM, **156**:327
 Wiechmann BN, **156**:1155
 Wiener SN, **156**:1116
 Wiley C, **156**:1245
 Willing SJ, **156**:1001
 Wilms G, **156**:640
 Winchester P, **156**:561
 Wise GJ, **156**:1325
 Withers CE, **156**:745
 Wittenberg J, **156**:1273
 Wittich GR, **156**:77
 Wolber R, **156**:73
 Wong WK, **156**:835
 Woolsey EJ, **156**:995
 Wootton P, **156**:688
 Wright KC, **156**:757
- Y
- Yakes WF, **156**:381
 Yamamoto J, **156**:69
 Yancey JM, **156**:1321
 Yao T, **156**:741
 Yedlicka JW Jr, **156**:1007, **156**:1087
 Yeung E, **156**:321
 Young JWR, **156**:1198
 Young W, **156**:559
 Yousem DM, **156**:1229
 Yuan C, **156**:161
 Yuh WTC, **156**:579
- Z
- Zafaranooc S, **156**:865
 Zegel HG, **156**:639, **156**:769
 Zeman RK, **156**:395, **156**:493,
156:737
 Zerhouni EA, **156**:403
 Zerin JM, **156**:407, **156**:1029
 Zollikofer ChL, **156**:389
 Zuurbier R, **156**:395

Subject Index Volume 156

AJR articles are also included in the 5-year cumulative index published in *Radiology*.

Index Key: a = abstract, b = book review, e = editorial, l = letter, m = memorial, p = pictorial essay, v = videotape review

Subjects in this index are cataloged by body part where possible. Disease entities unique to a body part are listed by that part; other more general diseases have separate listings by name. Technical procedures are also listed by part, as appropriate. Because of general interest, subjects dealing with CT, MR imaging, sonography, radionuclide imaging, and pediatric radiology are listed under those headings as well as under appropriate body part and/or disease.

A

Abdominal aorta, coarctation, malignant hypertension and collateral mesenteric circulation (l), 156:201

Abscess, see specific organ or site

Achalasia, elderly patients (a), 156:1331

Achilles tendon, rupture, polylactic acid implant for repair of, 156:769

Acquired immunodeficiency syndrome

benign lymphoepithelial parotid tumors in, CT and MR, 156:1253

intraabdominal *Mycobacterium tuberculosis* vs *Mycobacterium avium-intracellulare*, CT, 156:487

lymphoma related to

CT (p), 156:969

infant, 156:1037

Pneumocystis carinii pneumonia

aerosolized pentamidine against (a), 156:409

oral therapy (a), 156:409

visceral calcification and, 156:745

Acquired renal cystic disease, dialysis patients, 156:501

Adamantinoma, vs fibrous dysplasia, tibia, 156:1017

Adenoid cystic carcinoma, airway, MR (l), 156:1321

Adenomatous polyposis syndromes, extracolonic manifestations (p), 156:481

Adrenal hyperplasia, neonatal congenital, sonography, 156:141

Adrenal myelolipoma, 156:724

Adrenocorticotrophic hormone, bronchial carcinoid tumors produced by, MR vs CT, 156:39

Airway, adenoid cystic carcinoma, MR (l), 156:1321

Allergic reaction, Gd-DTPA and (a), 156:646

Alpha-1-antitrypsin, deficiency, liver disease (a), 156:882

Alpha-fetoprotein, maternal serum, elevated, normal sonography and (a), 156:410

American College of Radiology, summit meeting—1990, 156:841, 156:1273 commentary, 156:1277

American Roentgen Ray Society

information and application for membership, 156:214, 156:432

1991 meeting, Boston, MA, 156:211

instructional courses and symposium, 156:423, 156:659, 156:885

introduction to research seminar, 156:1266

invitation, 156:419, 156:651

local activities and tennis and golf tournaments, 156:425

scientific program, 156:888

summary, 156:213, 156:421, 156:654, 156:884

1992 meeting, Orlando, FL, 156:1338

call for papers, 156:1339

call for scientific exhibits, 156:1341

officers, committees and membership information, 156:210, 156:428, 156:653, 156:894, 156:1124

Amiodarone, lung, CT-pathology correlation (a), 156:206

Amniography, monoamniotic pair in a triplet pregnancy, 156:559

Amniotic band syndrome, sonography (p), 156:555

Amyloidosis, small intestine

barium meal study (a), 156:205

double-contrast radiographs, 156:741

systemic, scintigraphy evaluation (a), 156:410

Anaphylaxis

barium enemas and latex balloons, 156:1

Gd-DTPA and (a), 156:646

latex allergy and, during barium studies, 156:903

Angiocardiography, congenital heart malformations (b), 156:1208

Angiography

coronary, predicting the appropriate use of (a), 156:642

enhanced 3-D MR, venous anatomy of brain, 156:161

gastrointestinal bleeding, obscure origin, 156:385

MR, cerebrovascular disease in sickle cell anemia (a), 156:645

MR and contrast, diagnosis of carotid artery stenosis, 156:611

need for, mediastinal hemorrhage, 156:273

Angioplasty

balloon

infrarenal portion of abdominal aorta, 156:1257

unsuccessful, iliac artery stenosis after, 156:389

kissing-balloon technique for, popliteal artery trifurcation, 156:823

percutaneous transluminal, subclavian arteries, 156:1091

Ankle, lateral collateral ligament, MR (p), 156:131

Anorectal tuberculosis, CT (l), 156:870

Anorexia nervosa, adolescent girls, decreased bone density in (a), 156:205

Anterior spinal artery syndrome, infarction of conus medullaris (l), 156:1115

Antroduodenal motility, real-time sonography (a), 156:880

Aorta

abdominal, coarctation, malignant hypertension and collateral mesenteric circulation (l), 156:201

infrarenal portion, balloon angioplasty, 156:1257

descending, anomaly of, pediatric, 156:1033

translumbar access, CT, 156:395

Aortic thrombosis, after umbilical artery catheterization, neonate, 156:567

Aortitis, nonaneurysmal bacterial, impending rupture of, CT (a), 156:645

Aortography, translumbar, uncommon complication of (l), 156:408

Arterial puncture technique, standard, modification of (l), 156:864

Arteriography, coronary, techniques other than, 156:15

Arteriosclerosis, intravascular sonography in detection of, 156:1087

Arteriovenous fistulas, biopsy of renal allografts and, 156:507

Arthritis

rheumatoid, knee, enhanced MR, 156:125

septic, hip, infant (a), 156:412

Arthroplasty, girdlestone, aspiration of hip in, 156:545

Artifacts

magnetic susceptibility, MR, spine, 156:1069

sonography, origins (p), 156:1267

Ascites

new sign of (l), 156:1325

peritoneal carcinomatosis with (p), 156:1185

Aspiration, elderly patients, videofluoroscopy, 156:293

Aspirin, low-dose, heparin comparison, myocardial infarction (a), 156:1117

Atherectomy, facilitated by long vascular sheaths, 156:173

Atrial septal defect, surgical repair, long-term outcome (a), 156:1118

Audiovisual presentations, effective, 156:181

Azygos lobe, imaging (p), 156:931

B

Balloon, latex

barium enema

- anaphylactic reactions and, 156:1
rectal tip, condom coverage of (l), 156:1323
- Barium studies**
air contrast, inverted colonic diverticulum, 156:961
amyloidosis, small intestine (a), 156:205
enema rectal tip, condom coverage of (l), 156:1323
E-Z-EM balloon-retaining (l), 156:869
gastrointestinal iohexol comparison, infants and children, 156:345
latex balloons, anaphylactic reactions and, 156:1, 903
- Bile duct**
malignant obstruction, self-expandable stainless steel endoprosthesis for, 156:321
obstruction, sialogram-aided sonography (a), 156:412
papillomatosis, ampillary carcinoma and (l), 156:405
stones, endoscopic laser lithotripsy (a), 156:204
- Bile-plug syndrome**, spontaneous resolution, 156:1225
- Biliary duct**, strictures, percutaneous transluminal biopsy, 156:77
- Biliary endoprostheses**, self-expandable stainless steel, malignant obstruction of bile duct, 156:321
- Biliary stents**, metal, cholangioscopic or transpillary insertion (a), 156:1331
- Biopsy**
breast, abnormalities caused by, mammographic findings (p), 156:287
fine-needle aspiration
breast carcinoma (a), 156:206
breast lesions (a), 156:643
small hepatocarcinoma, fatal bleeding after (l), 156:1114
percutaneous, CT-guided (l), 156:639
percutaneous needle aspiration, nonfluoroscopic, lung, patient with pneumonia (a), 156:410
renal allografts, arteriovenous fistulas and, 156:507
stereotactic, breast (l), 156:634
transluminal, biliary strictures, biptome, 156:77
vs phase-contrast MR, fatty infiltration of liver, 156:307
- Biptome**, percutaneous transluminal biopsy with, biliary strictures, 156:77
- Bladder**, transitional cell carcinoma, stage D2 (l), 156:1325
- Blood supply**, systemic, lung, developmental abnormalities, 156:669
- Body coil**, MR imaging with, prostate carcinoma, 156:511
- Bone**
diseases (b), 156:120
dysplasia, deferoxamine-induced, 156:561
loss, spinal, ovulatory disturbances and (a), 156:642
radionuclide imaging, stress injury of anterior iliac crest (a), 156:413
scan, radioisotope, metastatic prostatic cancer patients (a), 156:203
scintigraphy, pelvic pain (l), 156:407
- Book reviews**
aids to radiological differential diagnosis, 156:316
angiography of congenital heart malformations, 156:1208
cancer imaging with radiolabeled antibodies, 156:798
cardiovascular application of Doppler ultrasound, 156:930
Christensen's physics of diagnostic radiology, 4th ed, 156:234
clinical profiles of diffuse interstitial pulmonary disease, 156:680
computed tomography, anatomy, and morphology of the lower extremity, 156:1198
computed tomography of the trunk, 156:326
congenital heart disease, 156:1154
control of radon in houses, 156:968
CT and MRI of the liver and biliary system, 156:492
CT review, 156:486
- disorders of the patellofemoral joint, 2nd ed, 156:332
Dr. Susan Love's breast book, 156:286
duplex scanning in vascular disorders, 156:984
Edeiken's roentgen diagnosis of diseases of bone, 4th ed, 156:120
Fuchs's principles of radiography exposure, processing and quality control, 156:954
imaging anatomy of the head and spine, 156:586
maxillofacial imaging, 156:1068
MRI, Central nervous system, 156:790
MRI, Musculoskeletal system, 156:784
MRI of the musculoskeletal system, 156:456
nuclear cardiovascular imaging, 156:44
nuclear medicine annual 1990, 156:780
optimization of image quality and patient exposure in diagnostic radiology, 156:176
osteoporosis, 156:130
pocket atlas of normal CT anatomy of the head and brain, 156:1244
pocket atlas of pediatric ultrasound, 156:364
practical echocardiography and Doppler, 156:916
practical nuclear medicine, 156:394
primer of sectional anatomy with MRI and CT correlation, 156:570
quantitative imaging, 156:762
radiation protection, 156:688
radiologic clinics of North America
imaging the lymphomas, 156:748
lung cancer, 156:280
radiology of renal failure, 2nd ed, 156:104
radiology of the eye and orbit, 156:1218
radionuclides in nephro-urology, 156:500
review of radiology, 156:58
skeletal radiology, 156:116
the abdominal plain film, 156:730
the year book of diagnostic radiology, 1990, 156:806
trauma of the spine, 156:1036
trauma radiology, 156:774
two-dimensional echocardiography and cardiac Doppler, 156:14
- Bowel**
inflammatory disease
epidemiology of (a), 156:1118
familial (a), 156:1330
small, enteroscopy (a), 156:1331
- Brain**
intracranial vascular abnormalities, MR phase imaging, 156:373
metastases, diagnosis, CT vs MR, 156:1039
paranasal sinus mucosal thickening, MR images, 156:381
radiation injury, 156:689
venous anatomy, enhanced 3-D MR angiography, 156:161
white matter disease (v), 156:1074
- Brain stem**, MR (v), 156:1052
- Breast**
biopsy, abnormalities caused by, mammography (p), 156:287
carcinoma
tumor angiogenesis and metastasis in (a), 156:1117
ultrasound-guided fine-needle aspiration biopsy (a), 156:206
imaging, medicolegal aspects of, 156:719
lesion
fine-needle aspiration biopsy (a), 156:643
nonpalpable, transected wire localization (l), 156:877
mucocele of, 156:199
node-negative cancer, adjuvant chemotherapy in (a), 156:1330
reconstruction, mammographic and CT findings after (p), 156:1159
sonography, 156:449
stereotactic biopsy (l), 156:634
- Bronchograms**, air, small peripheral carcinoma of the lung, CT, 156:921
- Bronchopulmonary dysplasia**
late pulmonary sequelae of (a), 156:1117
research in diagnostic radiology, 156:681
- Brucellosis**, abdominal, CT (l), 156:1323
- C**
- Calcium**, supplementation, postmenopausal women (a), 156:409
- Caliceal diverticula**, renal, stones and infection in, 156:995
- Cancer**
see also specific type or site
radiolabeled antibodies (b), 156:798
- Carcinomatosis**, peritoneal, with ascites (p), 156:1185
- Carotid artery**
retrieval of 4-French diagnostic catheter fragment from, 156:1105
stenosis, angiography comparison, 156:611
- Case of the day**
abdominal, 156:852, 156:1301
chest, 156:846, 156:1295
general diagnosis, 156:846, 156:1288
neuroradiology, 156:854, 156:1307
pediatric, 156:859, 156:1314
- Catheter**
balloon, hemorrhage from subclavian artery after catheter removal, 156:1261
4-French, retrieval from common carotid artery, 156:1105
5-French, high-velocity jets from (l), 156:874
- Cat-scratch disease**, disseminated hepatic and splenic lesions, imaging of, 156:1227
- Celiac axis**, ligamentous compression, CT, 156:1101
- Centrilobular lesions**, staphylococcal pneumonia (l), 156:1322
- Cerebral ischemia**, MR/spectroscopy, 156:1133
- Cerebral ventricles**, asymmetric growth of, posthemorrhagic ventricular dilation, infant (a), 156:1333
- Cerebrospinal fluid**, shunt function, evaluation, 156:801
- Cervix**
carcinoma, MR, 156:753
clinical stage I carcinoma, degree of invasiveness, MR, 156:1191
uterine, third-trimester, translabial sonography (a), 156:883
- Chemotherapy**, adjuvant, node-negative breast cancer (a), 156:1330
- Child abuse**
healing fractures
extension of growth plate cartilage into metaphysis, 156:775
normal metaphysial radiologic variants confused with (p), 156:781
osteogenesis imperfecta differentiation (l), 156:634
- Cholangiography**
choledochal cyst appearance (p), 156:327
intraoperative, serum diatrizoate during (a), 156:204
- Cholangiopancreatography**, endoscopic retrograde, asymptomatic pancreatitis after (a), 156:206
- Cholangioscopy**, percutaneous, insertion of biliary metal stents (a), 156:1331
- Cholangitis**, sclerosing, biliary tract strictures in (a), 156:1332
- Cholecystectomy**, laparoscopic (a), 156:1331
- Cholecystostomy**, percutaneous, sepsis of unknown cause, 156:1163
- Choledochal cyst**, appearance, cholangiography (p), 156:327
- Cholelithiasis**
fragmentation, biliary lithotripsy, 156:493
medical dissolution of (a), 156:1331
- Cholescintigraphy**, gallbladder perforation (a), 156:1120
- Cholestasis**, severe, scintigraphic assessment (a), 156:643
- Cholesterol**, gallstone disease, gallbladder motility and (a), 156:643
- Chondrodysplasia**, Schmid-like metaphysial, simulating child abuse, 156:576
- Chondrosarcoma**, MR, 156:1016
- Claustrophobia**, MR-induced, alprazolam and (l), 156:633
- Clavicle**, condensing osteitis, 156:1011

Clinoril, esophageal ulcer due to, 156:955
Colitis, ulcerative, colorectal cancer and (a), 156:641
Collateral mesenteric circulation, malignant hypertension and, coarctation of abdominal aorta associated with (l), 156:201
Colon, cancer, radiologic screening, economic implications, 156:939
 inverted diverticulum, air contrast barium findings, 156:961
 neoplasms, radiologic detection of, 156:303
Colonoscopy, screening, asymptomatic persons (a), 156:880
Colorectal cancer, cross-sectional imaging, 156:909
 ulcerative colitis and (a), 156:641
Contrast media, atypical reactions, interleukin-2 therapy, 156:833
 CSF shunt function, 156:801
 Gd-DTPA, anaphylaxis and allergic reaction (a), 156:646
 high- vs low-osmolality, risks, 156:825
 MR advances in, 156:235
 gastrointestinal agents, 156:252
 nonionic, guidelines for (l), 156:865
 vomiting induced by, prevention (l), 156:633
Coronary artery, bypass graft, patency, 156:15
 disease, intensive lipid-lowering therapy and (a), 156:641
Cricopharyngeal bars, biomechanics (a), 156:411
Crohn's disease, predictability of (a), 156:204
Cryptococciosis, intracranial, immunocompromised patients, CT and MR, 156:1245
CT, AIDS-related lymphoma (p), 156:969
 pyelonephritis (a), 156:204
 review (b), 156:486
 sectional anatomy (b), 156:570
CT, abdomen, active intraabdominal arterial hemorrhage, 156:725
 acute pancreatitis, 156:93
 after liver transplantation, 156:1167
 AIDS patient, intraabdominal *Mycobacterium tuberculosis* vs *Mycobacterium avium-intracellulare*, 156:487
 anorectal tuberculosis (l), 156:870
 aorta-bifurcation prosthesis, intrasigmoidal (l), 156:202
 brucellosis (l), 156:1323
 celiac axis, ligamentous compression of, 156:1101
 gastrointestinal tract, principles and interpretation, 156:23
 hepatic and splenic lesions, cat-scratch disease, 156:1227
 peliosis hepatitis, HIV infection and, 156:91
 rectal intussusception (l), 156:870
 retrograde jejunoduodenogastric intussusception, complication of gastrostomy tubes, 156:957
CT, body, CT of trunk (b), 156:326
CT, bone, idiopathic myelofibrosis, diffuse intraabdominal lymphoma complicating, 156:1189
CT, breast, after breast reconstruction (p), 156:1159
CT, cranium, benign lymphoepithelial parotid tumors, AIDS patients, 156:1253
 congenital nasal masses, 156:587
 double-dose delayed, cerebral metastases, 156:1039
 hamartomas of the tuber cinereum, 156:1053
 intracranial cryptococciosis, immunocompromised patients, 156:1245
 limited slice of paranasal sinus, children, 156:367
 orbit and its contents, children (p), 156:1219
 pocket atlas of anatomy (b), 156:1244
 ruptured intracranial dermoid cyst, 156:807
CT, esophagus, carcinoma, vs MR, 156:297

mediastinal seroma, after esophagogastrectomy, 156:715
 perforation (a), 156:643
CT, extremities, angiosarcoma, associated with chronic lymphedema, 156:543
CT, fetal, amniography, monoamniotic pair in a triplet pregnancy, 156:559
CT, head and neck, tubes, alimentary and respiratory tracts (p), 156:1047
CT, hip, iliopsoas bursal distension (a), 156:206
CT, kidney, lymphoma (a), 156:645
CT, liver, biliary system and (b), 156:492
 choledochojejunostomy, liver transplantation (a), 156:883
 hydatid cyst, 156:751
 imaging of tumors (l), 156:867
 periportal contrast enhancement, 156:313
 subcapsular hepatic necrosis, 156:981
CT, pancreas, after secretin provocation, pancreas divisum (a), 156:643
 asymptomatic pancreatitis, following endoscopic retrograde cholangiopancreatography (a), 156:206
 microcystic adenoma, presenting with acute hemoperitoneum, 156:749
CT, pelvis, after cesarean section, 156:523
 pelvimetry, 156:527
CT, scrotum, perforated retroperitoneal appendix, Fournier gangrene caused by, 156:341
CT, spleen, acute splenic torsion, children with wandering spleen, 156:151
CT, thorax, amiodarone lung (a), 156:206
 aorta and inferior vena cava, translumbar access, 156:395
 aortic aneurysms and dissections (a), 156:645
 artificial pneumothorax and, origin and extent of tumor, 156:707
 bronchial carcinoid tumors, adrenocorticotrophic hormone-induced, 156:39
 calcification, ligamentum arteriosum, pediatric, 156:351
 collateral venous channels (a), 156:206
 lymphoma, lung, 156:711
 mediastinal hemorrhage on chest radiographs and, 156:273
 mediastinal lymphoma, therapeutic response, 156:265
 mediastinal masses, high-attenuation, 156:45
 nonaneurysmal bacterial aortitis, impending rupture (a), 156:645
 pleura, 156:1145
 small peripheral carcinoma of lung, air bronchograms in, 156:921
 solitary pulmonary nodules, 156:925
 ventricular myocardium, noncompaction of, 156:717
CT, trachea, measurement of tracheal lumen, children and adolescents, 156:371
CT, ureter, occult ectopic, girls with urinary incontinence, 156:365
CT, vagina, reconstruction, rectus abdominis myocutaneous flap, 156:1001
Cyst, see specific organ or site
Cystadenocarcinoma, biliary (l), 156:1113
Cystadenoma, biliary (l), 156:1113
Cystinosis, nephropathic, swallowing dysfunction in (a), 156:410
Cystography, vaginal filling during, detection (l), 156:406
Cytology, endoscopic retrograde brush (a), 156:411

D

Deferoxamine, bone dysplasia induced by, thalassemia major with, 156:561
Dermoid cyst, intracranial, ruptured, CT and MR, 156:807
Dialysis, access planning, preoperative evaluation of subclavian vein, 156:623
 acquired renal cystic disease in, 156:501

Diaphragm, rupture, blunt trauma and, 156:51
Diskectomy, lumbar, automated percutaneous, 156:531
Diverticulitis, jejunum (a), 156:882
Down syndrome, arthropathy of (a), 156:882
Drug abuse, lung disorders and (a), 156:1120
Duodenal hematoma, percutaneous management of (l), 156:1112
Dysphagia, elderly patients without, altered swallowing function, 156:1181

E

Echocardiography, practical (b), 156:916
 two-dimensional, cardiac Doppler and (b), 156:14
Endarterectomy, carotid, predicting the appropriate use of (a), 156:642
Endocarditis, bacterial, perivalvular pseudoaneurysm, MR detection, 156:1155
Endometriosis, periumbilical, imaging of (l), 156:636
Endoscopy, gallbladder carcinoma (a), 156:881
 insertion, expandable biliary metal stents for malignancies (a), 156:412
 retrograde cannulation cytology (a), 156:411
 gallbladder (a), 156:412
 sonography, upper GI tract (p), 156:63
 sphincterotomy, bile duct diameter after (a), 156:883
 upper gastrointestinal, predicting the appropriate use of (a), 156:642
Yersinia enterocolitica enterocolitis (a), 156:881
Endotracheal tube, location, preterm and term neonates (a), 156:1120
Enteroclysis, inverted Meckel diverticulum (l), 156:1111
Enterocolitis, *Yersinia enterocolitica*, endoscopy in (a), 156:881
Enteroscopy, small bowel, gastrointestinal bleeding (a), 156:1331
Epilepsy, chronic partial, contrast-enhanced MR, 156:605
ERCP, anatomic variants and artifacts in interpretation (p), 156:975
Erythromycin, intravenous, gastric emptying in gastroparesis diabeticorum (a), 156:413
Esophagogastrectomy, mediastinal seroma after, CT, 156:715
Esophagus, Barrett's, prevalence of (a), 156:204
 carcinoma, CT vs MR, 156:297
 emptying, hiatal hernia and (a), 156:1330
 evaluation, marshmallow bolus (a), 156:882
 foreign body, childproof cap on medicine bottle (l), 156:201
 perforation, CT (a), 156:643
 squamous cell carcinoma, MR (a), 156:205
 ulcer, Clinoril-induced, 156:955
ESWL, see Extracorporeal shock-wave lithotripsy
Exercise, acute effects on skeletal muscle, MR, 156:765
Extracorporeal membrane oxygenation, posterior fossa intracranial hemorrhage with, infant, sonography, 156:571
Extracorporeal shock-wave lithotripsy, assessment of patients (a), 156:1119
 long-term soft-tissue effects of, 156:73
 ursodiol effects, gallstones (a), 156:641

F

Fallopian tubes, recanalization, selective salpingography and, 156:33
Fetus, anomalies, MR (p), 156:1205
 death, Doppler assessment of circulation in (l), 156:636
Fibromatosis, aggressive, MR (a), 156:646
 MR imaging, 156:539
Fibrous dysplasia, adamantinoma of the tibia vs, 156:1017
Filters, inferior vena caval, 156:813

Fluoride, therapy, osteoporosis, bone fragility during (a), 156:1119
Fournier gangrene, perforated retroperitoneal appendix, CT, 156:341
Functional residual capacity, determination, digital radiography, neonatal chest, 156:1209

G**Gadopentetate dimeglumine**

enhancement
 MR after brain tumor surgery, children, 156:1237
 MR of musculoskeletal system, 156:457
 pancreatic transplant dysfunction, 156:1171

Gallbladder

carcinoma, endoscopic sonography (a), 156:881
 contraction, ursodeoxycholic acid effects, gallstone patients (a), 156:203
 endoscopic retrograde cannulation (a), 156:412
 imaging (p), 156:737
 motility, cholesterol gallstone disease (a), 156:643
 perforation, cholescintigraphic and sonographic findings (a), 156:1120
 striated thickening of wall, sonography, 156:945

Gallstone, see Cholelithiasis**Gastric emptying**, measurement (a), 156:644**Gastritis**

Campylobacter pylori, diagnosis (a), 156:1119
Helicobacter pylori (a), 156:1331

Gastrointestinal bleeding

obscure origin
 angiography in detection, 156:385
 small bowel enteroscopy (a), 156:1331

Gastrointestinal tract

CT, 156:23
 endoscopic sonography (p), 156:63
 lesions, long-distance running and (a), 156:412
 polyposis syndromes, familial (p), 156:481

Gastroparesis diabetorum, gastric emptying in, intravenous erythromycin in (a), 156:413**Gastrostomy tube**, retrograde jejunoduodenogastric intussusception, CT, 156:957**Geiger, Andrew H** (m), 156:822**Goiter**, non toxic, hypervascularity of, color Doppler sonography (l), 156:199**Granuloma**, giant-cell reparative, hand and foot bones (a), 156:881**Growth hormone**, idiopathic deficiency, MR, 156:599**Growth plate**, cartilage, extension into metaphysis, healing fracture in abused infant, 156:775**H****Heart**

congenital disease (b), 156:1154
 sonography, fetal, four-chamber view, 156:547
 transvenous pacing lead perforation, percutaneous removal, 156:471

Hemobilia, control by embolization, hepatic artery, 156:1263**Hemoperitoneum**, acute, pancreatic microcystic adenoma presenting with, 156:749**Heparin**, low-dose aspirin comparison, myocardial infarction (a), 156:1117**Hepatectomy**, partial, recurrent hepatocellular carcinoma after, 156:1177**Hepatic artery**, false aneurysm and arteriopertobilary fistula, hemobilia in, control by embolization, 156:1263**Hepatic vein**, duplex Doppler sonography, tricuspid regurgitation, 156:79**Hepatitis**, peliosis, HIV and, 156:91**Hepatocarcinoma**, small, fine-needle aspiration biopsy, fatal bleeding (l), 156:1114**Hepatocellular carcinoma**

recurrent, after partial hepatectomy, 156:1177
 regression of (l), 156:868

screening methods (l), 156:869

Hip

aspiration, girdlestone arthroplasty, 156:545
 congenital dysplasia

osteoarthritis and (a), 156:1332

sonography diagnosis in children (a), 156:1332

Human immunodeficiency virus

peliosis hepatitis with, 156:91
 prevalence among university students (a), 156:880
 type 1, pulmonary tuberculosis patients (a), 156:1118

Hydrocephalus, congenital, prenatal sonography, 156:359**Hydronephrosis**, ureteral compression and, splenosis, scintigraphic diagnosis (l), 156:406**Hypertension**, malignant, coarctation of abdominal aorta associated with (l), 156:201**Hypothalamus**, anatomy and pathology, MR, 156:579**Hyslop, Charles P.** (m), 156:622**I****Ileitis**, *Yersinia terminal*, sonography, 156:965**Iliac artery**, stenosis, unsuccessful balloon angioplasty and, 156:389**Iliopsoas bursa**, distended, hip, MR (p), 156:1025**Infertility**, selective salpingography, Fallopian tube recanalization and, 156:33**Interferon- α 2a**, recombinant, treatment of childhood angiomatic diseases (a), 156:1332**Interleukin-2**, systemic therapy, atypical contrast reactions, 156:833

therapy, pulmonary edema during, 156:281

Intestine, small, amyloidosis, double-contrast radiographs, 156:741**Intraabdominal hemorrhage**, arterial, CT, 156:725**Intracranial hemorrhage**, posterior fossa, extracorporeal membrane oxygenation treatment and, 156:571**Intrathoracic cyst**, transbronchial aspiration of (l), 156:1110**Iohexol**

gastrointestinal studies, barium comparison, infants and children, 156:345

intrathecal, reaction to (l), 156:403

oral, hypersensitivity reaction (l), 156:197

Ischemia, cerebral, MR/spectroscopy, 156:1133**J****Jejunum**, diverticulitis (a), 156:882**K****Kidney**

allograft, biopsy of, arteriovenous fistulas and, 156:507

autosomal dominant polycystic disease (a), 156:642

caliceal diverticula, stones and infection in, 156:995

failure, radiology of (b), 156:104

lymphoma, CT (a), 156:645

medullary sponge, benign tubular ectasia (l), 156:872

oncocytoma, 156:1144

transplantation, rejection, ^{31}P MR spectroscopy, 156:105

Knee

arthroplastics, painful or infected, indium 111 leukocyte scanning in (a), 156:644

buckled meniscus (l), 156:200

displaced bucket-handle tear, medial meniscus, sagittal MR images, 156:117, 156:121

high signal in meniscus, MR, 156:333

rheumatoid arthritis, enhanced MR, 156:125

L**Lacunae**, urographic finding, chronic obstructive uropathy, 156:985**Lambdoid synostosis**, new plain film sign, infant, 156:1215**Lee, John Joonjae** (m), 156:1252**Leukemia**

lymphoblastic, acute bone pain, children (a), 156:205

myelogenous, splenic activity (a), 156:413

Ligamentum arteriosum, calcification, CT, pediatric, 156:351**Limb-lengthening procedures**, radiology of (p), 156:353

d-Limonene, medical dissolution of gallstones (a), 156:1331

Lithotripsy

biliary

gallstone fragmentation during, 156:493

physicochemical determinants (a), 156:881

shock-wave pressures (a), 156:411

endoscopic laser, large bile duct stones (a), 156:204

piezoelectric, symptomatic gallbladder stones (a), 156:411

Liver

blunt injury, liver cell adenoma discovered after (l), 156:1324

detection of tumors

CT vs MR (l), 156:867

sonography (l), 156:867

disease, alpha-1-antitrypsin deficiency (a), 156:882

fatty infiltration, phase-contrast MR vs biopsy, 156:307

focal nodular hyperplasia, MR, 156:317

hydatid cyst, CT, 156:751

peripheral contrast enhanced CT, 156:313

sarcoidosis, MR (l), 156:1324

transplantation

abdominal CT findings after, 156:1167

choledochojejunostomy in (a), 156:883

subcapsular hepatic necrosis in, 156:981

Liver cell adenoma, discovered after blunt hepatic injury (l), 156:1324**Loop, John Wickwire** (m), 156:1100**Lumbar disk**, herniated, automated percutaneous lumbar discectomy, 156:531**Lung**

amiodarone, CT-pathology correlation (a), 156:206

bullous disease, digital storage phosphor radiography, 156:467

cancer, chest CT combined with artificial pneumothorax in determination of, 156:707

disorders, drug abuse and (a), 156:1120

interstitial disease, unknown cause, 156:225

lymphoma, CT, 156:711

nonfluoroscopic percutaneous needle aspiration, patient with pneumonia (a), 156:410

open biopsy, critically ill newborn (a), 156:412

small peripheral carcinoma, air bronchograms, CT, 156:921

systemic blood supply, developmental abnormalities, 156:669

Lymphedema, chronic, angiosarcoma associated with, CT, 156:543**Lymphoma**

AIDS-related

CT (p), 156:969

infant, 156:1037

diffuse intraabdominal, complicating idiopathic

myelofibrosis, CT, 156:1189

kidney, CT (a), 156:645

lung, CT, 156:711

mediastinal sonography, CT, and chest radiography compared, 156:265

M**MacPherson, Robert Alexander** (m), 156:1188**Malpractice**, mammography and, 156:475**Mammography**

after breast reconstruction (p), 156:1159

breast abnormalities, caused by biopsy (p), 156:287

breast traction (l), 156:1321

malpractice and, 156:475

medicolegal aspects, 156:719

residency training in, 156:59

McCune-Albright syndrome, scintigraphic abnormality pattern (a), 156:413**Meckel diverticulum**, inverted, enterocolysis (l), 156:1111**Meckel syndrome**, fetal renal artery blood flow, Doppler velocity waveforms (l), 156:408**Mediastinum**

hemorrhage, angiography, 156:273

lymphoma, sonography, CT, and chest radiography compared, 156:265

masses, high-attenuation on unenhanced CT, 156:45
pseudomass, neonates with anterior pneumothorax, 156:145
Medical decision making, defining terms for (I), 156:198
Medicine in American art, 156:554, 156:1180
Memorials
Andrew H. Geiger, 1956–1990, 156:822
Andrew N. Schwartz, 1950–1989, 156:154
Charles P. Hyslop, 1924–1990, 156:622
Hyman R. Senteria, 1909–1990, 156:400
John Joonjae Lee, 1940–1990, 156:1252
John Wickwire Loop, 1924–1990, 156:1100
Robert Alexander MacPherson, 1903–1990, 156:1188
Meniscus
buckled (I), 156:200
high signal, MR, 156:333
medial, displaced bucket-handle tear, MR, 156:117, 156:121
Metaphysis
healing injury
infant abuse, 156:775
normal metaphyseal radiologic variants confused with infant abuse (p), 156:781
Midbrain, enlarged perivascular spaces, focal high signal on MR, 156:157
MR imaging
central nervous system (b), 156:790
claustrophobia induced by, alprazolam and (I), 156:633
contrast-enhanced, advances in, 156:235
musculoskeletal system (b), 156:784
patient comfort, music enhancement of (I), 156:403
sectional anatomy (b), 156:570
seminal vesicles (p), 156:989
two-piece wrist surface coil, 156:343
vena cava tumor thrombi (a), 156:882
MR imaging, abdomen
contrast-enhanced, gastrointestinal agents, 156:252
pancreatic transplant dysfunction, 156:1171
MR imaging, ankle, lateral collateral ligament (p), 156:131
MR imaging, bone, septic sacroiliitis (a), 156:1333
MR imaging, cervix
carcinoma, 156:753
clinical stage I carcinoma, degree of invasiveness, 156:1191
MR imaging, cranium
benign lymphoepithelial parotid tumors, AIDS patients, 156:1253
brain tumor surgery, gadopentetate dimegline-enhanced MR after, 156:1237
cerebral ischemia, 156:1133
congenital nasal masses, 156:587
contrast-enhanced
cerebral metastases, 156:1039
chronic partial epilepsy, 156:605
neurologic applications, 156:239
nonneurologic applications, 156:245
conventional neuroangiography (p), 156:1075
hamartomas of the tuber cinereum, 156:1053
hypothalamus, anatomy and pathology, 156:579
idiopathic growth hormone deficiency, 156:599
intra- and paraorbital lesions, paramagnetic contrast enhanced, 156:1059
intracranial cryptococcosis, immunocompromised patients, 156:1245
midbrain, focal high signal caused by enlarged perivascular spaces, 156:157
orbit and its contents, children (p), 156:1219
phase imaging
intracranial vascular abnormalities, 156:373
paranasal sinuses, mucosal thickening, 156:381
ruptured intracranial dermoid cyst, 156:807
MR imaging, esophagus
carcinoma, vs CT, 156:297
squamous cell carcinoma (a), 156:205
MR imaging, extremities, reflex sympathetic dystrophy, 156:113
MR imaging, fetus, anomalies (p), 156:1205

MR imaging, heart, bacterial endocarditis, perivalvular pseudoaneurysm, 156:1155
MR imaging, hip
distended iliopsoas bursa (p), 156:1025
iliopsoas bursal distension (a), 156:206
MR imaging, knee
gadopentetate dimegline-enhanced, rheumatoid arthritis, 156:125
high signal in meniscus, 156:333
sagittal images, displaced bucket-handle tear, 156:117, 156:121
MR imaging, leg, Achilles tendon rupture, polylactic acid implant for repair of, 156:769
MR imaging, liver
biliary system and (b), 156:492
focal nodular hyperplasia, 156:317
phase-contrast, vs biopsy, fatty infiltration, 156:307
sarcoidosis (I), 156:1324
tumors (I), 156:867
MR imaging, mesentery, sclerosing mesenteritis, 156:517
MR imaging, muscle, exercise effects, concentric vs eccentric actions, 156:765
MR imaging, musculoskeletal system
contrast-enhanced, gadopentetate dimegline, 156:457
teaching file (b), 156:456
MR imaging, prostate, carcinoma, tumor volume, 156:511
MR imaging, soft tissue
fibromatosis, 156:539
synovial sarcoma (p), 156:337
MR imaging, spine
dermal sinus tracts, children, 156:791
infection, gadolinium-enhanced (a), 156:206
magnetic susceptibility artifacts and motion effects, cervical neural foramina, 156:1069
neural foramina, degenerative narrowing, 156:1229
MR imaging, thorax
anterior chest wall, flat coil use in (I), 156:1110
bronchial carcinoid tumors, adrenocorticotrophic hormone-induced, 156:39
pleura, 156:1145
pulmonary infarction (a), 156:1330
vascular ring, infant (I), 156:1111
Mucocoele, breast, 156:199
Mycobacterial infections, changing epidemiology, United States, 156:255
Mycobacterium tuberculosis, vs *Mycobacterium avium-intracellulare*, AIDS patient, 156:487
Myelofibrosis, idiopathic, diffuse intraabdominal lymphoma and, CT, 156:1189
Myocardium
infarction, heparin and low-dose aspirin for (a), 156:1117
ventricular, noncompaction of, CT, 156:717
N
Nasal masses, congenital, CT and MR, 156:587
Nephro-urology, radionuclides in (b), 156:500
Neuroangiography, conventional (p), 156:1075
Neuroblastoma, screening, infant (a), 156:644
Nuclear medicine
annual 1990 (b), 156:780
practical (b), 156:394
O
Oncocytoma, renal, 156:1144
Orbit, fat-suppression MR, paramagnetic contrast enhanced, 156:1059
Oropharyngeal dysfunction, elderly patients, videofluoroscopy, 156:293
Osteitis, condensing, clavicle, 156:1011
Osteoarthritis, congenital dysplasia of hip and (a), 156:1332
Osteogenesis imperfecta, child abuse differentiation from (I), 156:634
Osteomyelitis, talus, limping in childhood and, 156:785
Osteonecrosis, dysbaric (I), 156:1327
Osteoporosis
broadband attenuation measurements, sonography (I), 156:1326
fluoride therapy for, bone fragility during (a), 156:1119
physiological basis (b), 156:130
Ovary, torsion, pregnancy and (I), 156:871
P
Pacemaker, nonfunctioning lead, percutaneous removal, 156:471
Paget disease, bone, sarcoma in, 156:1199
Pancreas
cancer, superior mesenteric artery involvement, sonography, 156:69
congenital short, polysplenia syndrome with, pediatric, 156:799
cystic tumors, sonography and CT (a), 156:883
microcystic adenoma, presenting with acute hemoperitoneum, 156:749
necrosis, lack of contrast enhancement in CT, 156:93
transplantation, dysfunction, MR, 156:1171
Pancreatitis
acute
CT, 156:93
leukocyte infiltration in (a), 156:1119
focal calcification, 156:1005
pseudoaneurysm formation and, interventional radiology, 156:97
Papillomatosis, common bile duct, ampullary carcinoma and (I), 156:405
Paranasal sinus
limited-slice CT, children, 156:367
mucosal thickening, MR images of brain, 156:381
Parotid gland, lymphoepithelial tumors, AIDS patients, CT and MR, 156:1253
Patellectomy, partial, displaced patellar fractures (a), 156:644
Patellofemoral joint, disorders (b), 156:332
Pediatric radiology
angiomatic disease, recombinant interferon alfa-2a (a), 156:1332
anorexia nervosa, decreased bone density in, adolescent girls (a), 156:205
aortic thrombosis, after umbilical artery catheterization, neonate, 156:567
childproof cap on medicine bottle, esophageal foreign body (I), 156:201
congenital dysplasia of hip, sonography diagnosis in children (a), 156:1332
congenital nasal masses, CT and MR, 156:587
congenital short pancreas, polysplenia syndrome with, 156:799
deferoxamine-induced bone dysplasia, thalassemia major, 156:561
descending aorta, anomaly of, 156:1033
Down syndrome, arthropathy of (a), 156:882
endotracheal tube location, preterm and term neonates (a), 156:1120
functional residual capacity, digital radiography, neonatal chest, 156:1209
gadopentetate dimegline-enhanced MR, brain tumor surgery, 156:1237
gait disturbance, radiology of lower extremities (a), 156:1332
gastrointestinal studies, barium compared with iohexol, 156:345
lambdoid synostosis, new plain film sign, infant, 156:1215
ligamentum arteriosum, calcification of, CT, 156:351
lung biopsy, open, critically ill newborn (a), 156:412
lymphoblastic leukemia, acute bone pain in (a), 156:205
mediastinal pseudomass, neonates with anterior pneumothorax, 156:145
neonatal congenital adrenal hyperplasia, sonography, 156:141
neuroblastoma, screening, infant (a), 156:644
occult ectopic ureter, girls with urinary incontinence, CT, 156:365
orbit and contents, children, CT and MR (p), 156:1219
osteomyelitis of the talus, limping and, 156:785
paranasal sinus, limited-slice CT, 156:367
pocket atlas of pediatric ultrasound (b), 156:364

- posterior fossa intracranial hemorrhage, extracorporeal membrane oxygenation treatment and, 156:571
- posthemorrhagic ventricular dilation, asymmetric growth of cerebral ventricle with, infant (a), 156:1333
- primary lymphoma, CNS, infant with AIDS, 156:1037
- reflex sympathetic dystrophy (a), 156:204
- renal length measurements, sonography, 156:1029
- Schmid-like metaphyseal chondrodysplasia, simulating child abuse, 156:576
- septic arthritis, hip, infant (a), 156:412
- sickle cell anemia, cerebrovascular disease in, MR angiography (a), 156:645
- spinal dermal sinus tracts, MR, 156:791
- synthetic surfactant, mortality in infants treated with (a), 156:1333
- thanatophoric dwarf variant fetus, sonography, 156:149
- tracheal lumen, CT measurement, 156:371
- unilateral hydrocephalus, sonography, 156:359
- urethral abnormalities, male neonates with VATER association, 156:137
- vascular ring, infant, MR (l), 156:1111
- wandering spleen, acute splenic torsion in, 156:151
- Pelvimetry**, CT, level of ischial spines, 156:527
- Pelvis**, after cesarean section, CT appearance, 156:523
- Pentamidine**, aerosolized, *Pneumocystis carinii* pneumonia and (a), 156:409, 880
- Peptic disease**, pyloric deformation (a), 156:881
- Pericardium**, transvenous pacing lead perforation, percutaneous removal, 156:471
- Perivalvular pseudoaneurysm**, bacterial endocarditis and, MR detection, 156:1155
- Petrous bone**, deformed, new plain film sign, infant, 156:1215
- Picture archiving and communications systems (PACS)**
- cost-effectiveness, 156:177
 - ultrafast network for, 156:835
- Pleura**
- sonography, CT and MR, 156:1145
 - transvenous pacing lead perforation, percutaneous removal, 156:471
- Pneumocystis carinii pneumonia**
- aerosolized pentamidine against (a), 156:409
 - AIDS patient, visceral calcification and, 156:745
 - atypical presentations, patients receiving inhaled pentamidine prophylaxis (a), 156:880
 - oral therapy for (a), 156:409
- Pneumonia**, staphylococcal, centrilobular lesions due to (l), 156:1322
- Pneumoperitoneum**, supine abdominal radiography, 156:731
- Pneumothorax**
- anterior, neonate, mediastinal pseudomass in, 156:145
 - artificial, chest CT combined with, 156:707
 - catamenial, pneumoperitoneum and (l), 156:404
 - development of, thoracentesis and, 156:917
- Polylactic acid**, implant, Achilles tendon rupture repair, 156:769
- Polypsindrome**, congenital short pancreas, pediatric, 156:799
- Popliteal artery**, trifurcation, kissing-balloon technique for angioplasty, 156:823
- Pregnancy**
- early, vaginal and abdominal sonography (a), 156:1333
 - ovarian torsion and (l), 156:871
- Prostate**
- cancer, radioisotope bone scan limitations in (a), 156:203
 - carcinoma, MR, 156:511
- Pseudoaneurysm**, formation, pancreatitis with, interventional radiology, 156:97
- Pulmonary disease**, interstitial (b), 156:680
- Pulmonary edema**, during interleukin-2 therapy, 156:281
- Pulmonary emboli**, Wilms tumor and, 156:155
- Pulmonary nodules**, solitary, CT, 156:925
- Pyelonephritis**, acute, CT (a), 156:204
- R**
- Radiation**
- injury of the brain, 156:689
 - protection (b), 156:688
- Radiography, technique**
- chest
 - functional residual capacity, neonate, 156:1209
 - history and interpretation (l), 156:197
 - digital storage phosphor, bullous lung disease, 156:467
 - double-contrast, amyloidosis, small intestine, 156:741
 - exposure, Fuchs's principles (b), 156:954
 - lower extremities, children with gait disturbance (a), 156:1332
 - supine abdominal, pneumoperitoneum, 156:731
 - **Radiologists**, visual acuity testing, commentary, 156:1107
- Radiology**
- communication of images, 156:835
 - diagnostic
 - aids (b), 156:316
 - bronchopulmonary dysplasia, 156:681
 - Christensen's physics of (b), 156:234
 - environment and (l), 156:863
 - information overload and management in, 156:1283
 - interventional
 - pancreatitis with pseudoaneurysm formation, 156:97
 - percutaneous access set, 156:397
 - orthopedic (v), 156:1010
 - residency training, mammography, 156:59
 - trauma (b), 156:774
 - whose turf is imaging, 156:443
 - **Radiology, technique**
 - colon cancer screening, economic implications, 156:939
 - colonic neoplasms, 156:303
 - eye and orbit (b), 156:1218
 - limb-lengthening procedures (p), 156:353
- Radiology Centennial, Inc. (RCI)**, 156:938, 156:944
- Radiology journalism**, 1991 Figley Fellows, 156:448
- Radiology residents**, recommended textbooks (l), 156:863
- Radon**, control (b), 156:968
- Rectal intussusception**, CT (l), 156:870
- Rectosigmoid cancer**, local recurrence (a), 156:205
- Rectus abdominis musculocutaneous flap**, breast reconstruction with, mammographic and CT findings after (p), 156:1159
- Rectus abdominis myocutaneous flap**, vaginal reconstruction with, CT, 156:1001
- Reflex sympathetic dystrophy**
- children (a), 156:204
 - extremities, MR imaging in, 156:113
- Renal artery**, stenosis, Wallstent treatment of (l), 156:640
- Renal cell carcinoma**
- intratumoral fat in (l), 156:871
 - vena cava, surgical management (a), 156:1119
- Residency**, training, mammography, 156:59
- Retropertitoneal hematoma**, percutaneous management of (l), 156:1112
- S**
- Sacrococcygeal teratoma**, antenatal diagnosis, Doppler sonography and MR (l), 156:1115
- Sacrolitis**, septic, MR (a), 156:1333
- Salpingography**, selective, Fallopian tube recanalization and, 156:33
- Sarcoidosis**
- gallium-67 distribution in (a), 156:1120
 - hepatic, MR (l), 156:1324
 - multinodular splenic, CT and sonography (l), 156:1113
 - retroperitoneal, 156:520
- Sarcoma**, Paget disease of bone, 156:1199
- Schwartz, Andrew N.** (m), 156:154
- Sclerosing mesenteritis**, MR, 156:517
- Sclerotherapy**, endoscopic, portosystemic shunts of, portal venous system after, 156:85
- Seminal vesicles**
- MR (p), 156:989
 - transrectal ultrasound (a), 156:1120
- Senturia, Hyman R.** (m), 156:400
- Sepsis**, unknown cause, percutaneous cholecystostomy, 156:1163
- Shuntography**, functional positive-contrast, 156:801
- Sickle cell anemia**, cerebrovascular disease in, MR angiography (a), 156:645
- Society of uroradiology**, tenth meeting and post-graduate course, meeting news, 156:189
- Soft tissue**, long term effects of ESWL, 156:73
- Sonography**
- artifacts and their origins (p), 156:1267
 - color Doppler
 - hypervascularity of nontoxic goiter (l), 156:199
 - improved needle-tip visualization by, 156:401
 - intrascrotal pathology (a), 156:644
 - performance requirements and operational parameters, 156:3
 - Doppler
 - blood-flow indexes (l), 156:1326
 - cardiac (b), 156:14
 - circulation in case of fetal death (l), 156:636
 - duplex (b), 156:984
 - nomenclature (l), 156:874
 - polycystic renal disease (l), 156:408
 - **Sonography, abdomen**
 - antroduodenal motility studied by (a), 156:880
 - duplex Doppler, hepatic vein in tricuspid regurgitation, 156:79
 - early pregnancy (a), 156:1333
 - endoscopic, gallbladder carcinoma (a), 156:881
 - gallbladder
 - perforation (a), 156:1120
 - striated thickening of wall, 156:945
 - gastrointestinal tract, endoscopic (p), 156:63
 - sinalde-aided, common bile duct (a), 156:412
 - *Yersinia* terminal ileitis, 156:965
 - **Sonography, adrenal**, congenital hyperplasia, neonate, 156:141
 - **Sonography, bone**, broadband attenuation measurements, osteoporosis (l), 156:1326
 - **Sonography, breast**
 - equipment and review, 156:449
 - fine-needle aspiration biopsy, carcinoma (a), 156:206
 - **Sonography, carotid artery**, color Doppler conventional (l), 156:873
 - **Sonography, cranium**
 - posterior fossa intracranial hemorrhage, extracorporeal membrane oxygenation treatment and, 156:571
 - unilateral hydrocephalus, prenatal, 156:359
 - **Sonography, endorectal**, surgical glove and (l), 156:865
 - **Sonography, esophagus**, duplex Doppler, portal venous system, 156:85
 - **Sonography, fetal**
 - amniotic band syndrome, 156:555
 - heart, four-chamber view, 156:547
 - thanatophoric dwarf variant fetus, 156:149
 - **Sonography, intravascular**, arteriosclerosis detection, 156:1087
 - **Sonography, kidney**, length measurements, children, 156:1029
 - **Sonography, liver**, detection of tumors (l), 156:867
 - **Sonography, pancreas**, superior mesenteric artery thickening, cancer, 156:69
 - **Sonography, spleen**, focal lesions (p), 156:949
 - **Sonography, thorax**
 - Doppler, cardiovascular application (b), 156:930
 - mediastinal lymphoma, therapeutic response, 156:265
 - pleura, 156:1145
 - Takayasu's arteritis (a), 156:645
 - thoracentesis, pneumothorax associated with, 156:917

Sonography, transesophageal, mediastinal lymph node metastases, lung cancer (a), 156:203
Sonography, translabial, third-trimester uterine cervix (a), 156:883
Sonography, transperineal, urethra, diverticula of, female, 156:1195
Sonography, transrectal, seminal vesicles (a), 156:1120
Sonography, umbilical cord, hematoma (l), 156:1115
Sonography, urinary tract, endoluminal, 156:99
Spectroscopy
 cerebral ischemia, 156:1133
³¹P MR, renal transplant rejection, 156:105
Sphincterotomy, endoscopic, bile duct diameter after (a), 156:883
Spine
 cervical, neural foramina, degenerative narrowing, MR, 156:1229
 dermal sinus tracts, MR, children, 156:791
 magnetic susceptibility artifacts and motion effects, cervical neural foramina, MR, 156:1069
 radiology, trauma patients (l), 156:638
 trauma (b), 156:1036
Spleen
 candidal abscesses, 156:474
 focal lesions, sonography (p), 156:949
 wandering, acute splenic torsion in, children, 156:151
Splenosis, scintigraphic detection, ureteral compression and hydronephrosis (l), 156:406
Spondylolisthesis, cervical, CT (l), 156:200
Squamous cell carcinoma, base of tongue, liver and bone metastases (l), 156:1328
Subcapsular hepatic necrosis, liver transplantation, CT, 156:981
Subclavian artery
 hemorrhage after removal of catheter, balloon catheter control, 156:1261
 percutaneous transluminal angioplasty in, 156:1091
Subclavian vein, preoperative evaluation, dialysis access planning and, 156:623
Surfactant, synthetic, infants treated with (a), 156:1333
Surgical glove, endorectal sonography and (l), 156:865
Swallowing, altered function, elderly patients without dysphagia, 156:1181
Synovial sarcoma, MR (p), 156:337
Syphilis, congenital, hepatic calcifications caused by (l), 156:634

T

Takayasu's arteritis, carotid duplex sonography (a), 156:645
Talus, osteomyelitis, limping in childhood and, 156:785
Teleradiology, hardware and communications, 156:1279
Thalassemia major, bone dysplasia, deferoxamine-induced, 156:561
Thallium-201, reinjection, following delayed imaging (a), 156:882
Thoracentesis, pneumothorax associated with, 156:917
Thoracic vent, Tru-Close, different opinion (l), 156:404
Thrombolysis, pulsed-spray, arterial and bypass graft occlusions, 156:617
Thrombosis, left-sided vena cava (l), 156:875
Tibia, adamantinoma, fibrous dysplasia vs, 156:1017
Tongue, primary squamous cell carcinoma, liver and bone metastases (l), 156:1328
Transcatheter arterial chemoembolization, recurrent hepatocellular carcinoma, after partial hepatectomy, 156:1177
Transitional cell carcinoma, stage D2, bladder (l), 156:1325
Trauma
 blunt, diaphragmatic rupture, 156:51
 radiology of cervical spine (l), 156:638
 thoracic, CT screening, 156:273
Tricuspid regurgitation, duplex Doppler sonography, hepatic vein, 156:79
Tuber cinereum, hamartomas of, CT, MR, and pathologic findings, 156:1053
Tuberculosis
 changing epidemiology, United States, 156:255
 pulmonary, HIV type 1 in (a), 156:1118
Tuberous sclerosis, imaging characteristics (p), 156:1081
Tubes, alimentary and respiratory tracts, CT appearance in head and neck (p), 156:1047

U

Umbilical artery, catheterization, aortic thrombosis after, neonate, 156:567
Umbilical cord, hematoma, sonography (l), 156:1115
Ureter, calculi, oblique plain radiographs (l), 156:637
Ureteral stent

V

VATER association, male neonates, urethral abnormalities with, 156:137
Vena cava
 inferior filters, 156:813
 membranous stenosis of (l), 156:639
 translumbar access, CT, 156:395
 left-sided, isolated thrombosis (l), 156:875
 thrombus, nonrenal parenchymal malignancy with (a), 156:1332
 tumor thrombi, MR (a), 156:882
Venography, lower extremity, conventional vs phosphorus plate venograms, 156:1095
Videofluoroscopy, aspiration, elderly patients, 156:293
Videotape reviews
 MRI of MS and white matter disease, 156:1074
 MRI of the brain stem, 156:1052
 orthopedic radiology, 156:1010
 RSNA today, vol. 4, no. 2, 156:96
 RSNA today, vol. 4, no. 3, 156:948
 Wolf-Heidegger's atlas of human anatomy, 156:960

W

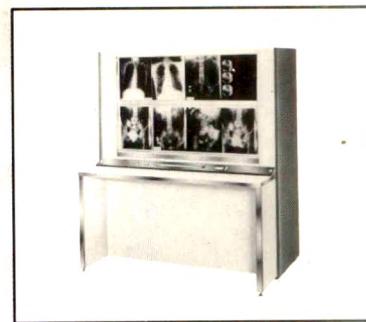
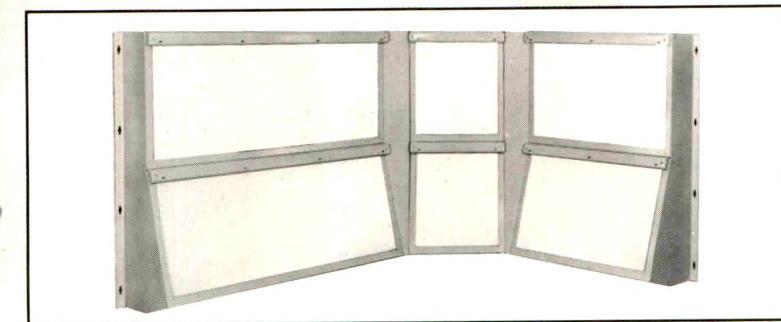
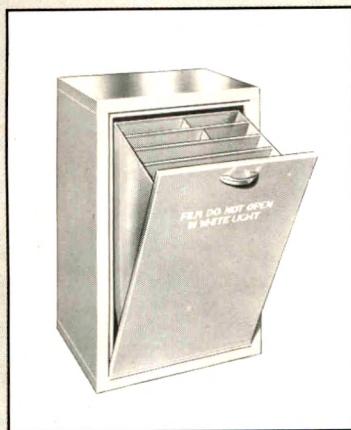
Wilms tumor, pulmonary emboli and, 156:155
Wrist surface coil, two-piece, 156:343

Z

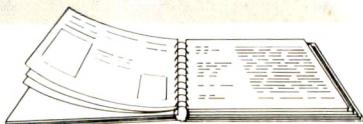
Zollinger-Ellison syndrome, peptic ulcer perforation (a), 156:1118

X-RAY ACCESSORIES

The Difference is Clear



For a FREE copy of our fully illustrated, 100+ page catalog, contact S & S directly or your local x-ray dealer.



Phone: 718/649-8500
FAX: 718/257-0219
Toll Free: 800/347-XRAY

- X-RAY Film Viewers
- X-RAY Protection
- X-RAY Files
- X-RAY Darkroom Equipment
- X-RAY Cabinets
- X-RAY Accessories

1101 Linwood Street
Brooklyn, N.Y. 11208



REVIEW ARTICLE

- 1133 Recent advances in MR imaging/spectroscopy of cerebral ischemia. Baker LL, Kucharczyk J, Sevick RJ, Mintorovitch J, Moseley ME
- 1145 Imaging the pleura: sonography, CT, and MR imaging. McLoud TC, Flower CDR

CARDIOVASCULAR RADIOLOGY

- 1155 Perivalvular pseudoaneurysm complicating bacterial endocarditis: MR detection in five cases. Akins EW, Sloane RM, Wiechmann BN, Browning M, Martin TD, Mayfield WR

BREAST RADIOLOGY

- 1159 Pictorial essay. Mammographic and CT findings after breast reconstruction with a rectus abdominis musculocutaneous flap. Loyer EM, Kroll SS, David CL, Dubrow RA, Libshitz HI

GASTROINTESTINAL RADIOLOGY

- 1163 Treatment of critically ill patients with sepsis of unknown cause: value of percutaneous cholecystostomy. Lee MJ, Saini S, Brink JA, et al.
- 1167 Abdominal CT findings after liver transplantation in 66 patients. Dupuy D, Costello P, Lewis D, Jenkins R
- 1171 Diagnosis of pancreatic transplant dysfunction: value of gadopentate dimeglumine-enhanced MR imaging. Fernandez MdP, Bernardino ME, Neylan JF, Olson RA
- 1177 Recurrent hepatocellular carcinoma after partial hepatectomy: value of treatment with transcatheter arterial chemoembolization. Nakao N, Kamino K, Miura K, et al.
- 1181 Altered swallowing function in elderly patients without dysphagia: radiologic findings in 56 cases. Ekberg O, Feinberg MJ
- 1185 Pictorial essay. Peritoneal carcinomatosis with ascites. Goerg C, Schwerk W-B
- 1189 Case report. Diffuse intraabdominal lymphoma complicating idiopathic myelofibrosis: CT demonstration. Goodman P, Kumar R, Alperin JB

GENITOURINARY RADIOLOGY

- 1191 Clinical stage I carcinoma of the cervix: value of MR imaging in determining degree of invasiveness. Lien HH, Blomlie V, Kjørstad K, Abeler V, Kaalhus O
- 1195 Diverticula of the female urethra: diagnosis by endovaginal and transperineal sonography. Keefe B, Warshauer DM, Tucker MS, Mittelstaedt CA

SKELETAL RADIOLOGY

- 1199 Sarcoma in Paget disease of bone: clinical, radiologic, and pathologic features in 22 cases. Moore TE, King AR, Kathol MH, El-Khoury GY, Palmer R, Downey PR

PEDIATRIC AND FETAL RADIOLOGY

- 1205 Pictorial essay. MR imaging of fetal anomalies. Benson RC, Colletti PM, Platt LD, Ralls PW
- 1209 Determination of functional residual capacity from digital radiographs of the normal neonatal chest: studies in a rabbit model. White KS, Muelenaer AA Jr, Beam CA, Effmann EL
- 1215 The deformed petrous bone: a new plain film sign of premature lambdoid synostosis. Fernbach SK, Feinstein KA
- 1219 Pictorial essay. Abnormalities of the orbit and its contents in children: CT and MR imaging findings. Hopper KD, Sherman JL, Boal DK
- 1225 Case report. Spontaneous resolution of bile-plug syndrome. Lang EV, Pinckney LE
- 1227 Case report. Disseminated hepatic and splenic lesions in cat-scratch disease: imaging features. Rappaport DC, Cumming WA, Ros PR

NEURORADIOLOGY

- 1229 Degenerative narrowing of the cervical spine neural foramina: evaluation with high-resolution 3DFT gradient-echo MR imaging. Yousem DM, Atlas SW, Goldberg HI, Grossman RI
- 1237 Gadopentetate dimeglumine-enhanced MR imaging in children following surgery for brain tumor: spectrum of meningeal findings. Hudgins PA, Davis PC, Hoffman JC Jr
- 1245 Intracranial cryptococcosis in immunocompromised patients: CT and MR findings in 29 cases. Tien RD, Chu PK, Hesselink JR, Duberg A, Wiley C
- 1253 Benign lymphoepithelial parotid tumors in AIDS patients: CT and MR findings in nine cases. Kirshenbaum KJ, Nadimpalli SR, Friedman M, Kirshenbaum GL, Cavallino RP

VASCULAR RADIOLOGY

- 1257 Obstruction of the infrarenal portion of the abdominal aorta: results of treatment with balloon angioplasty. Ravimandalam K, Rao VRK, Kumar S, et al.
- 1261 Case report. Use of a balloon catheter to control hemorrhage from the subclavian artery after removal of an inadvertently placed catheter. Millward SF, Lamb MN, Barron PT
- 1263 Case report. Control of hemobilia by embolization of a false aneurysm and arterioportobilary fistula of the hepatic artery. Beningfield SJ, Bornman PC, Krige JEJ, Terblanche J

SONOGRAPHY

- 1267 Pictorial essay. Sonographic artifacts and their origins. Scanlan KA

PERSPECTIVES

- 1273 Radiology Summit 1990: Specialization in radiology—trends, implications, and recommendations. Thrall JH, Wittenberg J
- 1277 Commentary. Generalists vs specialists: time to decide. Forrest JV
- 1279 Teleradiology: costs of hardware and communications. Dwyer SJ III, Templeton AW, Batnitzky S
- 1283 Information overload and management in radiology. Hendee WR

ARRS 1991 MEETING CASE OF THE DAY ANSWERS

- 1287 Introduction. O'Connor JF
- 1288 General diagnosis case of the day. Eschelman DJ, Panageas E, Rosen MP, Romo LV, O'Connor JF
- 1295 Chest case of the day. Eschelman DJ, Gibbens DT, Fielding JR, et al.
- 1301 Abdominal case of the day. Eschelman DJ, Duva-Frisson AD, Martin LC, et al.
- 1307 Neuroradiology case of the day. Parker DR, Eschelman DJ, Gibbens DT, Rabinov JD, O'Connor JF
- 1314 Pediatric case of the day. O'Connor JF, Martin LC, Chen H, et al.

OTHER CONTENT

- Book reviews 1154, 1198, 1208, 1218, 1244
- 1144 Radiologic-pathologic conference
- 1180 Medicine in American art
- 1188 Memorial, Robert A. MacPherson
- 1214 ARRS 1992 resident award papers information
- 1252 Memorial, John J. Lee
- 1266 Introduction to Research Seminar. Stanley AJ
- 1286 Forthcoming articles
- 1321 Letters
- 1330 Review of current literature
- 1334 News
- 1338 ARRS 1992 meeting announcement, calls for papers and exhibits
- 1343 Classified advertisements
- 1350 Index, Volume 156
- A13 Guidelines for authors
- A33 AJR business and subscriber information